

**A Deterministic and Random Propagation Study with the Design of an
Open Path 320 GHz to 340 GHz Transmissometer**

by

Lawrence J. Scally

B.E.E., Villanova University, 1983

M.E.E., Villanova University, 1985

M.B.A., Villanova University, 2006

A thesis submitted to the

Faculty of the Graduate School of the

University of Colorado in partial fulfillment

of the requirements for the degree of

Doctor of Philosophy

Department of Electrical and Computer Engineering

2017

This thesis entitled:
A Deterministic and Random Propagation Study with Design of an Open Path
THz Transmissometer from 320 GHz to 340 GHz

written by Lawrence J. Scally

has been approved for the Department of Electrical and Computer Engineering

Albin J. Gasiewski, Ph.D.

Henry Everitt, Ph.D.

Date _____

The final copy of this thesis has been examined by the signatories, and we find that both the content and the form meet acceptable presentation standards of scholarly work in the above mentioned discipline.

Lawrence J. Scally (Ph.D., Electromagnetics/Remote Sensing)

A Deterministic and Random Propagation Study with the Design of an Open Path THz 320 GHz to 340 GHz Transmissometer

Thesis directed by Prof. Albin J. Gasiewski

This program was implemented by Lawrence J. Scally for a Ph.D. under the EECE department at the University of Colorado at Boulder with most funding provided by the U.S. Army. Professor Gasiewski is the advisor and guider for the entire program; he has a strong history decades ago in this type of program. This program is developing a more advanced than previous years transmissometer, called Terahertz Atmospheric and Ionospheric Propagation, Absorption and Scattering System (TAIPAS), on an open path between the University of Colorado EE building roof and the mesa on owned by National Institute of Standards and Technology (NIST); NIST has invested money, location and support for the program. Besides designing and building the transmissometer, that has never be accomplished at this level, the system also analyzes the atmospheric propagation of frequencies by scanning between 320 GHz and 340 GHz, which includes the peak absorption frequency at 325.1529 GHz due to water absorption. The processing and characterization of the deterministic and random propagation characteristics of the atmosphere in the real world was significantly started; this will be executed with varies aerosols for decades on the permanently mounted system that is accessible 24/7 via a network over the CU Virtual Private Network (VPN).

To my wife, Nancy

To my son, Lawrence, Jr.

To my daughter, Brittan

To my son, Matthew

To my son, Preston

To my father, James

Acknowledgements

I would like to express my sincere gratitude to my advisor, Prof. Albin J. Gasiewski, for his dedication, guidance, and support throughout my Ph.D. studies at the University of Colorado, Boulder. I am indebted to him for sharing his talent, extensive and versatile expertise, drive, discipline, and rigor in the study of science and engineering. As my doctoral work concludes, I am excited to continue learning from him as a friend and colleague; especially on more co-funding programs.

I'm grateful to Dr. Dejan Filipovic, Dr. Henry Everitt, Dr. Edward Kuester, Dr. Andreas Muschinski, and Dr. Alexander Voronovich for serving on my Dissertation Committee and for their teaching and guidance over the years.

The contributions of the National Institute of Standards Technology / National Telecommunications and Information Administration (NIST/NTIA) were critical to enabling and supporting the installation of the transmissometer system at the Green Mesa site. I would like to specifically thank Dr. Paul McKenna and Mike Cotton.

The Colorado Engineering Inc. team of Dean Pizio, Ali Ghorashi, Ken Moore, Matt Scally, and Matt Williamson were key contributors in helping me translate the transmissometer vision into a working system. I greatly appreciate their inputs and efforts. David Kraft from the University of Colorado contributed significantly over years to the system's mechanical design and deserves my significant gratitude.

In addition, I would like to thank and acknowledge the United State Army, Redstone Army Research Lab for the financial support under project W31P4Q-11-C-0054 to develop a "Terahertz Atmospheric and Ionospheric Propagation, Absorption and Scattering System (TAIPAS)".

I would like to thank and acknowledge the contribution by Mike Bonato, Brian Gaffney, Ph.D., and Julie Howell for their extensive editing.

Last but foremost, I would like to thank my wife Nancy; without her love, encouragement and support, I would not have been able to complete this journey.

CONTENTS

Chapter 1.....	1
Introduction.....	1
1.1 Focus.....	1
1.2 Vision.....	2
1.3 Instrument	3
1.4 Motivations	4
1.5 Propagation Model.....	7
1.6 Model Verification.....	12
1.7 An Absorptive Model for Radiative Transfer.....	18
1.8 TAI PAS Transmissometer Development	21
1.9 Thesis Description	24
Chapter 2.....	27
Transmissometer Design	27
2.1 Introduction.....	27
2.2 Propagation Link Design	29
2.3 Transmissometer Hardware Design.....	38
2.4 Coho Link	81
2.5 Coherent (Coho) Link Hardware	92
2.6 Anemometer	96
2.7 Hygrometer	98
2.8 Data Link	100
2.9 Scintillometer.....	105

2.10 Calibration – Alignment	140
2.11 DSP	142
2.12 Software / Control.....	144
2.13 Systems Design.....	152
2.14 System Phase Noise.....	168
2.15 Meteorological Truth.....	178
2.16 Hallway Testing.....	178
2.17 Summary.....	182
Chapter 3.....	184
Propagation Statistics.....	184
3.1 Propagation	184
3.2 Atmosphere Turbulence Structure.....	187
3.3 Prediction.....	192
3.4 EM	194
3.5 Polarization	202
3.6 Aperture Averaging	202
3.7 Phase Amplitude Cross Correlation.....	203
3.8 MCF.....	203
3.9 Covariance Matrix	205
3.10 Permittivity	207
3.11 Construction Constants.....	208
3.12 Experiments	216
3.13 Predicted Variance Analysis.....	221

3.14 LEEDR Model	250
3.15 MATLAB Analysis	255
3.16 Hallway 40 m Path Analysis.....	258
3.17 Final Open Path 1924 m Analysis	316
Chapter 4.....	501
Propagation in Aerosols.....	501
4.1 Introduction.....	501
4.2 Aerosol Scattering and Absorption.....	502
4.3 LEEDR Model	514
Chapter 5.....	522
Corroboration of Manning Beam Wave Complex Refractive Model	522
5.1 Introduction.....	522
5.2 Lorentz	523
5.3 Spatial Wave Types	528
5.4 Manning.....	530
Chapter 6.....	536
Anomalous Refractivity Validation.....	536
6.1 Introduction.....	536
6.2 Lorentz / Kramers-Kronig	538
6.3 TAIPAS Hallway – 40 m Indoor Path.....	540
6.4 TAIPAS 1924 m Open Path	566
Chapter 7.....	596
IR/Thz Beam Co-Propagation	596

7.1 Introduction.....	596
7.2 Co-Collimation Theory.....	599
7.3 Structure Functions.....	604
7.4 Ray Path / Phase / AoA	609
7.5 Conclusion.....	619
Chapter 8.....	620
Conclusions.....	620
References.....	623
Appendix A: MATLAB Diffraction Source Code	630
Appendix B: Datasheets	655
Appendix C: XML Code	679
Appendix D: MATLAB LEEDR Source Code	691
Appendix E: MATLAB TAIPAS Source Code.....	697

TABLES

Table 2.1. Laser siting system performance calculations.....	57
Table 2.2. TAIPAS bulkhead connectors and functions.....	61
Table 2.3. Propagation Analysis for Coho Link.....	92
Table 2.4. Key Data on Hygrometer.....	100
Table 2.5. Hygrometer Vapor Density Categories.....	100
Table 2.6. Communication Link Friis for CA.....	102
Table 2.7. AirGrid Power vs. Data Rates.....	102
Table 2.8. Communication Link Beam Characteristics and Alignment.....	103
Table 2.9. Communication Link Friis for Rain.....	103
Table 2.10. Communication Link Friis for Snow.....	104
Table 2.11. Scintillometer Telescope and LED Characteristics.....	111
Table 2.12. Dual LED Characteristics at Colorado Springs Airport.....	121
Table 2.13. Dual Led Spread vs. Touching at Various Ranges.....	122
Table 2.14. Results with a Three-point Fitted Curve.....	122
Table 2.15. Image Intensity and Sampling Rate.....	137
Table 2.16. Alignment Laser Calculations.....	141
Table 2.17. IP Network Addresses.....	149
Table 2.18. TAIPAS CA Friis – 40 m Path.....	157
Table 2.19. TAIPAS CA Friis – 1924 m Path.....	158
Table 2.20. Tx Calibration Table.....	159
Table 2.21. Tx and Rx Lens Effective Aperture Size.....	160
Table 2.22. Path 1024 m SNR.....	162

Table 2.23. Path 1024 m THz Beam Characteristics.....	163
Table 2.24. Path 1024 m THz Beam Alignment.	163
Table 2.25. TAIPAS Rain Friis – 1924 m Path.....	164
Table 2.26. TAIPAS Rain SNR – 1924 m Path.....	166
Table 2.27. TAIPAS Snow Friis – 1924 m Path.....	166
Table 2. 28. TAIPAS Snow SNR – 1924 m path.	168
Table 2.29. TAIPAS Detailed Path Calculations for Coho.	169
Table 2.30. TAIPAS Phase Noise Analysis with MLS Synthesizer.....	172
Table 2.31. TAIPAS Phase Noise Analysis with Ideal Synthesizer.....	174
Table 2.32. TAIPAS Phase Noise Analysis with OE Waves Synthesizer.....	175
Table 2.33. TAIPAS Phase Noise Analysis Requirements for Synthesizer.....	177
Table 3.1. WB Frequency Scan.	219
Table 3.2. Narrow Band, LWL Frequency Scan.	220
Table 3.3. Narrow Band, UWL Frequency Scan.....	220
Table 3.4. Amplitude Plane Wave Prediction.	224
Table 3.5. Amplitude Plane Outer Scale Adjustment Prediction.	226
Table 3.6. Amplitude Spherical Wave Prediction.	229
Table 3.7. Amplitude Spatial Covariance with and without Aperture Averaging.....	232
Table 3.8. Power Spectrum of Amplitude Fluctuations – Rytov.....	235
Table 3.9. Phase Prediction – GO.....	238
Table 3.10. Phase Diffraction for Plane Wave – Rytov.	240
Table 3.11. Phase Diffraction for Spherical Wave – Rytov.	241

Table 3.12. AoA with / without Aperture Averaging - Spherical – GO.....	243
Table 3.13. AoA with / without Aperture Averaging – Planar – GO.....	244
Table 3.14. AoA with / without Aperture Averaging – Collimated – GO.	244
Table 3.15. Spot Variance – Collimated Beam – GO.....	245
Table 3.16. AoA – Plane Wave – Rytov.	246
Table 3.17. AoA – Spherical Wave – Rytov.	247
Table 3.18. Power Spectrum – Spherical / Plane Wave – Rytov.	248
Table 3.19. Cross Correlation of Amp/Phase – Planar / Spherical Waves – Rytov.	249
Table 3.20. LEEDR Example Configuration.....	254
Table 4.1. TAIPAS Rain Friis – 1924 m Path.	513
Table 4.2. TAIPAS Rain SNR – 1924 m Path.....	513
Table 4.3. TAIPAS Snow Friis – 1924 m path.....	513
Table 4.4. TAIPAS Snow SNR – 1924 m Path.	514
Table 4.5. LEEDR Sand Tabular Inputs and Results.	518
Table 4.6. LEEDR Sand Tabular Inputs and Results with Increased Concentration.	520
Table 6.1. Narrow Band, Absorption LWL Frequency Scan.	537
Table 6.2. Narrow Band, Absorption UWL Frequency Scan.....	538

FIGURES

Figure 1.1. (a) Clear-air (CA) attenuation versus frequency, and (b,c) HAS components of the currently-used MRT propagation model for (b) rain and (c) ice [39].	20
Figure 2.1. Paths for five accessible line-of-site transmissometer links each with transmitter based at the CU CET ECEE rooftop observatory: 1) CU Gamow Tower (520 m), 2) NIST Green Mesa radio site (1.90 km), 3) NCAR Table Mesa site (3.37 km), 4) NOAA BAO tower (22.57 km), and 5) DoC Table Mountain site (6.52 km). The Phase I study focused on the use of the Green Mesa site (1.90 km).	31
Figure 2.2. NIST Green Mesa site propagation path topography illustrating key atmospheric outer scale distances and cutoff wavenumbers.	32
Figure 2.3. Photos of the CU rooftop observatory platform and NIST Green Mesa sites. A clear elevated line-of-site exists between the CU deck platform and Green Mesa site. Note the occurrence of haze in some of these pictures. (The bottom center view is a sixth candidate link of approximate the same distance as Green Mesa to the CU dormitory towers.)	33
Figure 2.4. Fresnel link efficiency η_l for the TAIPAS path showing the impact of propagation through a circular aperture of radius a located a distance z_a along the 1924 m path. Nominal TAIPAS beam parameters for Gaussian transmit and receive beams are assumed.	37
Figure 2.5. Clearance radii for a diffractive circular aperture impacting the TAIPAS link budget by less than the -20, -40, and -60 dB. The estimated TAIPAS path clearance to building tops or other ground-located scatters is shown for comparison.	38
Figure 2.6. THz Transmissometer System.	41
Figure 2.7. Rendering of the TAIPAS transmitter and receiver housing.	42

Figure 2.8. TAIPAS receiver wind resistant shells at the Mesa site.....	44
Figure 2.9. TAIPAS transmitter wind resistant shell at CU rooftop site along with inner and outer I-beams.	45
Figure 2.10. TAIPAS housing and shell mechanical isolation plate system.	45
Figure 2.11. TAIPAS receivers as viewed from behind looking toward the transmitter.	46
Figure 2.12. TAIPAS receivers as viewed behind looking toward the transmitter.	47
Figure 2.13. TAIPAS Rx2 viewed from the front showing the 320-340 GHz aperture (upper left) and optical telescope aperture (lower right).....	48
Figure 2.14. View along the TAIPAS path from the Mesa receiver site to the CU rooftop transmitter.	49
Figure 2.15. Photo of TAIPAS transmitter system on the CU ECEE rooftop.....	50
Figure 2.16. TAIPAS transmitter site communication and environmental sensing package.	51
Figure 2.17. TAIPAS Mesa receiver site as viewed from the CU rooftop transmitter site. ..	52
Figure 2.18. Zoomed image of the TAIPAS Mesa receiver site.	53
Figure 2.19. TAIPAS Rx1 receiver with shell face painted black to minimize sun reflections. Also shown is the C-band network link antenna.	54
Figure 2.20. Satellite images of TAIPAS path and vicinity of the receiver and transmitter sites.	55
Figure 2.21. TAIPAS laser alignment system components.	57
Figure 2.22. TAIPAS laser siting system shimming.	58
Figure 2.23. TAIPAS laser siting source located on CU rooftop as viewed from the Mesa site.....	58
Figure 2.24. TAIPAS transceiver housing interior.	59

Figure 2.25. TAIPAS 3-axis feedhorn/lens position adjustment system.	60
Figure 2.26. TAIPAS bulkhead feedthrough for the hygrometer and anemometer.	62
Figure 2.27. THz solid state amplifier transition frequency advancements.	64
Figure 2.28. THz output power versus frequency from various sources [55].	64
Figure 2.29. VDI Supplied Technologies for TAIPAS [53].	66
Figure 2.30. VDI Supplied Transmitter Top View and Block Diagram.	68
Figure 2.31. VDI Supplied Transmitter Side View.	69
Figure 2.32. TAIPAS THz Receiver Block Diagram and Photo.	71
Figure 2.33. TAIPAS THz Receiver Photo.	72
Figure 2.34. Receiver IF Signal Conditioning.	73
Figure 2.35. TAIPAS IF Receiver Conditioner Box.	74
Figure 2.36. TAIPAS Receiver Gain and Filter Systems.	75
Figure 2.37. TAIPAS IF Receiver Conditioner Connectorized Component Circuit.	75
Figure 2.38. IF Anti-Aliasing BPF Circuit.	76
Figure 2.39. Polarization of Output.	76
Figure 2.40. WR.2.8 Receiver Input.	77
Figure 2.41. WR.2.8 Receiver Diagonal Horn Photo.	77
Figure 2.42. WR.2.8 Receiver Diagonal Horn Diagram.	78
Figure 2.43. Lens Photos.	79
Figure 2.44. Lens / Horn Configuration Control.	80
Figure 2.45. Tx and Rx Lenses.	81
Figure 2.46. Coho Link Block Diagram.	82
Figure 2.47. RHCP Cross Dipole Antenna.	84

Figure 2.48. RHCP Transmitter and LHCP Receiver.....	85
Figure 2.49. RHCP Transmitter and RHCP Receiver.	85
Figure 2.50. Horizontal Polarization Transmitter and Vertical Polarization Receiver.....	86
Figure 2.51. Vertical Polarization Transmitter and Vertical Polarization Receiver.....	86
Figure 2.52. Horizontal Polarization Transmitter and Horizontal Polarization Receiver.	87
Figure 2.53. Incident Angle on the Horizontal Axis - Reflection Coefficients for Varying Polarization and Dielectric of Ground.	91
Figure 2.54. Coho Link Transmitter VSS Model Block Diagram.....	93
Figure 2.55. Coho Link Receiver VSS Model Block Diagram.	94
Figure 2.56. Coho Link Transmitter Block Diagram.	94
Figure 2.57. Coho Link Receiver Block Diagram.	95
Figure 2.58. Coho Link Transmitter Photos.	95
Figure 2.59. Coho Link Receiver Photos.....	96
Figure 2.60. Anemometer.	97
Figure 2.61. Hygrometer.....	99
Figure 2.62. ADC.	100
Figure 2.63. C Band Communication/Network Link.	101
Figure 2.64. Rain Attenuation and Scattering Plot [39].	104
Figure 2.65. Snow Attenuation and Scattering Plot [39].....	105
Figure 2.66. Custom Scintillometer Block Diagram.	107
Figure 2.67. Scintillometer Equipment Photos.....	107
Figure 2.68. Example 7-bit Barker Convolution.	110
Figure 2.69. Dual LED Photo – 1960 m.....	124

Figure 2.70. Dual LED Photo – Multiple Frames.	125
Figure 2.71. Dual LED Photo – 1000 m.....	126
Figure 2.72. Dual LED Photo – 300 m.....	126
Figure 2.73. Single LED Photo – 1900 m – 0.25ms Shutter.	128
Figure 2.74. Single LED Photo – 1900 m – 0.12 ms Shutter.	129
Figure 2.75. Barker LED System – 7 chips – 0.12 ms Shutter.....	130
Figure 2.76. Multiple Barker Cross LED Photo – 760 m – 0.12 ms Shutter.....	131
Figure 2.77. Barker Cross Picture.....	132
Figure 2.78. Barker Cross Picture Tracked.	132
Figure 2.79. Barker Cross Picture Tracked on Mountain.....	133
Figure 2.80. Barker Cross Picture Tracked Above Trailers.	134
Figure 2.81. Barker Cross Picture Tracked Above and on Trailers.....	134
Figure 2.82. Barker Cross Picture Short Range Picture.	135
Figure 2.83. Barker Cross Template.....	135
Figure 2.84. Final Single LED/Barker Cross Configuration.	136
Figure 2.85. Current Single LED Configuration	138
Figure 2.86. NIST Scintillometer Photo.....	139
Figure 2.87. Example Day Photo of Telescope for Scintillometer.....	140
Figure 2.88. ADC Photo and Block Diagram.....	143
Figure 2.89. DSP: Digital Down Converter (DDC).	143
Figure 2.90. Receiver Controller.	144
Figure 2.91. Transmitter Controller.....	145
Figure 2.92. Linux Software Threads Block Diagram.	145

Figure 2.93. Timing Diagram of the Multi-Threaded Program.	146
Figure 2.94. Connections to the CU CET and CEI Labs.	147
Figure 2.95. Network Block Diagram.	149
Figure 2.96. Friis Derivation.	154
Figure 2.97. CA Attenuation Plot.	155
Figure 2.98. Tx Power vs. Frequency Plot.	158
Figure 2.99. Rx1 and Rx2 Receiver Conversion Losses.	161
Figure 2.100. Rx1 and Rx2 Receiver Noise Temperatures.	162
Figure 2.101. Rain Absorption and Scattering [38].	165
Figure 2.102. Snow Absorption and Scattering [38].	167
Figure 2.103. Picture of System at CEI Lab.	178
Figure 2.104. Picture of Outer Tx System at CEI Lab.	179
Figure 2.105. Picture of Inner Tx System at CEI Lab.	180
Figure 2.106. Picture of Outer Rx1 System at CEI Lab.	181
Figure 2.107. Picture of Inner Rx1 System at CEI Lab.	182
Figure 3.1. Eddies and Measurements.	188
Figure 3.2. Kolomogorov Turbulent Refractive Index Spectrum [31].	189
Figure 3.3. Structure Functions for Common Refractive Turbulence Models [31].	190
Figure 3.4. Phase Structure Functions [31].	198
Figure 3.5. Phase Structure Functions (radians) [31].	199
Figure 3.6. Phase Autocorrelation vs Time Lags [31].	200
Figure 3.7. MCF for Differing Phase Shapes.	205

Figure 3.8. Anomalous Real (solid) and Imaginary Refraction (dashed).....	209
Figure 3.9. Vertical Profiles of C_n^2 - Wheelon [32].	211
Figure 3.10. Resonant Frequency and Damping Dependence of the Spectral Line Width [62].....	214
Figure 3.11. Voigt Absorption Profiles [6].....	215
Figure 3.12. High Level TAIPAS Transmissometer System Block Diagram.	217
Figure 3.13. TAIPAS Transmissometer Frequencies (Janssen [38]).	219
Figure 3.14. Outer Scale Factors for Amplitude Variance [32].	226
Figure 3.15. LEEDR Location Map and Tabs.	251
Figure 3.16. LEEDR Attenuation.	252
Figure 3.17. LEEDR C_n^2	253
Figure 3.18. LEEDR TAIPAS Configuration.....	253
Figure 3.19. TAIPAS Tx and Rx1 Hallway Experiments Photo.	260
Figure 3.20. TAIPAS Tx vs Rx Computer Synchronization.	261
Figure 3.21. TAIPAS Tx vs Rx Computer Synchronization Enlargement.....	262
Figure 3.22. TAIPAS Tx vs Rx Computer Synchronization Error.....	262
Figure 3.23. TAIPAS Raw Data Received Across Two Scans (66 frequencies).	263
Figure 3.24. TAIPAS Raw Data Received UWL 11 Frequencies.....	264
Figure 3.25. Example LWL - TAIPAS Raw Data Received LWL 11 Frequencies.....	264
Figure 3.26. TAIPAS Raw Data Received WB 11 Frequencies.	265
Figure 3.27. TAIPAS Filtered Data Received WB 11 Frequencies.	266
Figure 3.28. TAIPAS Single Scan FFT of Tuned Data.....	267
Figure 3.29. TAIPAS Single Scan Histogram of Tuned Data.....	267

Figure 3.30. TAIPAS WB Hallway Scan.	268
Figure 3.31. TAIPAS WB Hallway Scan with Friis.....	269
Figure 3.32. TAIPAS WB Hallway Scan Normalized with Friis.....	269
Figure 3.33. TAIPAS LWL Hallway Scan.	270
Figure 3.34. TAIPAS LWL Hallway Scan with Friis.	270
Figure 3.35. TAIPAS up LWL Hallway Scan Normalized with Friis.....	271
Figure 3.36. TAIPAS UWL Hallway Scan.	271
Figure 3.37. TAIPAS UWL Hallway Scan with Friis.	272
Figure 3.38. TAIPAS LWL Hallway Scan Normalized with Friis.....	272
Figure 3.39. TAIPAS LWL and UWL Flipped Hallway Scan Normalized with Friis.	273
Figure 3.40. TAIPAS C_n^2 Example Collection.....	274
Figure 3.41. TAIPAS FFT C_n^2 Example Collection.....	274
Figure 3.42. Hallway Temperature from Anemometers.....	275
Figure 3.43. Hallway Wind U from Anemometers.	276
Figure 3.44. Hallway Wind V from Anemometers.	276
Figure 3.45. Hallway Wind W from Anemometers.	277
Figure 3.46. Hallway Humidity from Hygrometers.	277
Figure 3.47. Hallway WB and Friis Extinction Plots.	278
Figure 3.48. Hallway LWL and Friis Extinction Plots.....	279
Figure 3.49. Hallway UWL and Friis Extinction Plots.	279
Figure 3.50. Hallway LWL, Flipped UWL and Friis Extinction Plots.....	280
Figure 3.51. Hallway WB and Friis SNR Plots.	281
Figure 3.52. Hallway LWL and Friis SNR Plots.....	281

Figure 3.53. Hallway UWL and Friis SNR Plots.	282
Figure 3.54. WB MCF/Structure Function Plots.	283
Figure 3.55. LWL MCF/Structure Function Plots.	283
Figure 3.56. UWL MCF/Structure Function Plots.	284
Figure 3.57. WB Amplitude Scintillation with Outer Scale Factor Prediction.	285
Figure 3.58. LWL Amplitude Scintillation with Outer Scale Factor Prediction.	285
Figure 3.59. UWL Amplitude Scintillation with Outer Scale Factor Prediction.	286
Figure 3.60. WB Phase Scintillation with Prediction.	287
Figure 3.61. WB Phase Scintillation.	287
Figure 3.62. LWL Phase Scintillation with Prediction.	288
Figure 3.63. LWL Phase Scintillation.	288
Figure 3.64. UWL Phase Scintillation with Prediction.	289
Figure 3.65. UWL Phase Scintillation.	289
Figure 3.66. WB Phase Scintillation STD Degrees.	290
Figure 3.67. WB Phase Scintillation STD Prediction Degrees.	290
Figure 3.68. LWL Phase Scintillation STD Degrees.	291
Figure 3.69. LWL Phase Scintillation STD Prediction Degrees.	291
Figure 3.70. UWL Phase Scintillation STD Degrees.	292
Figure 3.71. UWL Phase Scintillation STD Prediction Degrees.	292
Figure 3.72. WB Phase Scintillation STD Millimeters.	293
Figure 3.73. WB Phase Scintillation STD Prediction Millimeters.	293
Figure 3.74. LWL Phase Scintillation STD Millimeters.	294
Figure 3.75. LWL Phase Scintillation STD Prediction Millimeters.	294

Figure 3.76. UWL Phase Scintillation STD Millimeters.....	295
Figure 3.77. UWL Phase Scintillation STD Prediction Millimeters.	295
Figure 3.78. WB Phase Scintillation STD Picoseconds.	296
Figure 3.79. WB Phase Scintillation STD Prediction Picoseconds.....	296
Figure 3.80. LWL Phase Scintillation STD Picoseconds.....	297
Figure 3.81. LWL Phase Scintillation STD Prediction Picoseconds.....	297
Figure 3.82. UWL Phase Scintillation STD Picoseconds.....	298
Figure 3.83. UWL Phase Scintillation STD Prediction Picoseconds.	298
Figure 3.84. WB Amplitude/Phase Scintillation Cross Correlation with Prediction.	299
Figure 3.85. WB Amplitude/Phase Scintillation Cross Correlation Prediction.....	300
Figure 3.86. WB Amplitude/Phase Scintillation Cross Correlation Hallway Data.	300
Figure 3.87. LWL Amplitude/Phase Scintillation Cross Correlation with Prediction.	301
Figure 3.88. LWL Amplitude/Phase Scintillation Cross Correlation Prediction Data.....	301
Figure 3.89. LWL Amplitude/Phase Scintillation Cross Correlation Hallway Data.....	302
Figure 3.90. UWL Amplitude/Phase Scintillation Cross Correlation with Prediction.....	302
Figure 3.91. UWL Amplitude/Phase Scintillation Cross Correlation Prediction Data.	303
Figure 3.92. UWL Amplitude/Phase Scintillation Cross Correlation Hallway Data.	303
Figure 3.93. C_T^2 Hallway Data.	304
Figure 3.94. C_Q^2 Hallway Data.....	305
Figure 3.95. C_{TQ} Hallway Data.....	305
Figure 3.96. Amplitude Scintillation Correlated with C_N^2 Hallway Data.....	306
Figure 3.97. Amplitude Scintillation Correlated with C_T^2 Hallway Data.	307
Figure 3.98. Amplitude Scintillation Correlated with C_Q^2 Hallway Data.	308

Figure 3.99. Phase Scintillation Correlated with C_n^2 Hallway Data.....	309
Figure 3.100. Phase Scintillation Correlated with C_n^2 Hallway Data.....	310
Figure 3.101. Phase Scintillation Correlated with C_Q^2 Hallway Data.	311
Figure 3.102. $C_T^2 C_n^2$ Correlation with C_n^2 Hallway Data.	312
Figure 3.103. C_Q^2 Correlation with C_n^2 Hallway Data.	313
Figure 3.104. C_T^2 Correlation with C_Q^2 Hallway Data.....	314
Figure 3.105. Phase Scint. and Amplitude Scint. Correlation with Receiver U-Wind Hallway Data.	315
Figure 3.106. Phase Scint. and Amplitude Scint. Correlation with Receiver V-Wind Hallway Data.	315
Figure 3.107. Phase Scint. and Amplitude Scint. Correlation with Receiver W-Wind Hallway Data.	316
Figure 3.108. Data Acquisition Camera 10142016_193175.	317
Figure 3.109. Timing Synchronization – 10142016_193175.....	318
Figure 3.110. Tracking of the Delta Time between Tx and Rx – 10142016_193175.....	318
Figure 3.111. Raw Data after DDC for Rx1 – 10142016_193175.....	320
Figure 3.112. Averaged Filtered (80 Tap) Data after DDC for Rx1 – 10142016_193175.	320
Figure 3.113. FFT of First WB Frequency (320 GHz) after DDC for Rx1 – 10142016_193175.....	321
Figure 3.114. Histogram of First WB Frequency (320 GHz) after DDC for Rx1 – 10142016_193175. It is also important to note for the plots below, the light blue bubbles at the points are the standard deviation divided by the square root of the number of points. The closer these are to the existing dark blue circles, the better the accuracy.	321

Figure 3.115. WB Scan 1 for Rx1 – 10142016_193175.	323
Figure 3.116. WB/Friis Scan 1 for Rx1 – 10142016_193175.....	323
Figure 3.117. WB/Friis Normalized Scan 1 for Rx1 – 10142016_193175.....	324
Figure 3.118. LWL Absorption Scan 2 for Rx1 – 10142016_193175.....	325
Figure 3.119. LWL / Friis Absorption Scan 2 for Rx1 – 10142016_193175.....	325
Figure 3.120. LWL / Friis Normalized Absorption Scan 2 for Rx1 – 10142016_193175..	326
Figure 3.121. UWL Absorption Scan 3 for Rx1 – 10142016_193175.....	327
Figure 3.122. UWL / Friis Absorption Scan 3 for Rx1 – 10142016_193175.	327
Figure 3.123. UWL / Friis Normalized Absorption Scan 3 for Rx1 – 10142016_193175.	328
Figure 3.124. WB Scan 4 for Rx1 – 10142016_193175.	329
Figure 3.125. WB/Friis Normalized Scan 4 for Rx1 – 10142016_193175.....	329
Figure 3.126. WB Absorption Scan 4 for Rx1 – 10142016_193175.	330
Figure 3.127. LWL / Friis Absorption Scan 5 for Rx1 – 10142016_193175.....	330
Figure 3.128. LWL / Friis Normalized Absorption Scan 5 for Rx1 – 10142016_193175..	331
Figure 3.129. LWL Absorption Scan 3 for Rx1 – 10142016_193175.....	331
Figure 3.130. UWL / Friis Absorption Scan 6 for Rx1 – 10142016_193175.	332
Figure 3.131. UWL / Friis Normalized Absorption Scan 6 for Rx1 – 10142016_193175.	332
Figure 3.132. UWL / Friis Normalized Absorption Scan 6 for Rx1 – 10142016_193175.	333
Figure 3.133. LWL & UWL Flipped Amp / Friis Normalized Absorption – 10142016_193175.....	334
Figure 3.134. WB SNR and Predicted Friis – 10142016_193175.	335
Figure 3.135. LWL SNR and Predicted Friis – 10142016_193175.....	335
Figure 3.136. UWL SNR and Predicted Friis – 10142016_193175.....	336

Figure 3.137. $C_n^2 - 10142016_193175$	337
Figure 3.138. FFT of $C_n^2 - 10142016_193175$	337
Figure 3.139. Transmit & Receiver Temp – 10142016_193175.....	338
Figure 3.140. Wind U Transmit & Receiver – 10142016_193175.	339
Figure 3.141. Wind V Transmit & Receiver – 10142016_193175.	339
Figure 3.142. Wind W Transmit & Receiver – 10142016_193175.	340
Figure 3.143. Humidity Transmit, Receiver & Mean – 10142016_193175.....	341
Figure 3.144. WB Amplitude Scintillation Variance and Predicted – 10142016_193175.	342
Figure 3.145. Enlarge of WB Amplitude Scintillation Variance and Predicted – 10142016_193175.....	342
Figure 3.146. LWL Amplitude Scintillation Variance and Predicted – 10142016_193175.	343
Figure 3.147. Enlarge LWL Amplitude Scintillation Variance and Predicted – 10142016_193175.....	344
Figure 3.148. UWL Amplitude Scintillation Variance and Predicted – 10142016_193175.	345
Figure 3.149. Enlarged UWL Amplitude Scintillation Variance and Predicted – 10142016_193175.....	345
Figure 3.150. WB Amplitude Scintillation and Predicted – 10142016_193175.....	346
Figure 3.151. Enlarged WB Amplitude Scintillation and Predicted – 10142016_193175.	347
Figure 3.152. LWL Amplitude Scintillation and Predicted – 10142016_193175.....	348
Figure 3.153. Enlarged LWL Amplitude Scintillation and Predicted – 10142016_193175.	348

Figure 3.154. UWL Amplitude Scintillation and Predicted – 10142016_193175.	349
Figure 3.155. Enlarged UWL Amplitude Scintillation and Predicted – 10142016_193175.	350
Figure 3.156. WB Phase Scintillation Variance and Predicted – 10142016_193175.	351
Figure 3.157. Enlarged WB Phase Scintillation Variance and Predicted – 10142016_193175.	351
Figure 3.158. LWL Phase Scintillation Variance and Predicted – 10142016_193175.	352
Figure 3.159. Enlarged LWL Phase Scintillation Variance and Predicted – 10142016_193175.....	353
Figure 3.160. UWL Phase Scintillation Variance and Predicted – 10142016_193175.....	354
Figure 3.161. Enlarged UWL Phase Scintillation Variance and Predicted – 10142016_193175.....	354
Figure 3.162. WB Phase Scintillation STD and Predicted Deg. – 10142016_193175.	355
Figure 3.163. Enlarged WB Phase Scintillation STD and Predicted Deg. – 10142016_193175.....	356
Figure 3.164. LWL Phase Scintillation STD and Predicted Deg. – 10142016_193175.	357
Figure 3.165. Enlarged LWL Phase Scintillation STD and Predicted Deg. – 10142016_193175.....	357
Figure 3.166. UWL Phase Scintillation STD and Predicted Deg. – 10142016_193175.....	358
Figure 3.167. Enlarged UWL Phase Scintillation STD and Predicted Deg. – 10142016_193175.....	359
Figure 3.168. WB Phase Scintillation STD and Predicted MM – 10142016_193175.....	360

Figure 3.169. Enlarged WB Phase Scintillation STD and Predicted MM – 10142016_193175.....	360
Figure 3.170. LWL Phase Scintillation STD and Predicted MM – 10142016_193175.....	361
Figure 3.171. Enlarged LWL Phase Scintillation STD and Predicted MM – 10142016_193175.....	362
Figure 3.172. UWL Phase Scintillation STD and Predicted MM – 10142016_193175.	363
Figure 3.173. UWL Phase Scintillation STD and Predicted MM – 10142016_193175.	363
Figure 3.174. WB Phase Scintillation STD and Predicted ps – 10142016_193175.....	364
Figure 3.175. Enlarged WB Phase Scintillation STD and Predicted ps – 10142016_193175.	365
Figure 3.176. LWL Phase Scintillation STD and Predicted ps – 10142016_193175.	366
Figure 3.177. LWL Phase Scintillation STD and Predicted ps – 10142016_193175.	366
Figure 3.178. UWL Phase Scintillation STD and Predicted ps – 10142016_193175.....	367
Figure 3.179. Enlarged UWL Phase Scintillation STD and Predicted ps – 10142016_193175.....	368
Figure 3.180. WB Amp/Phase Scintillation Correlation and Predicted – 10142016_193175.	369
Figure 3.181. LWL Amp/Phase Scintillation Correlation and Predicted – 10142016_193175.	369
Figure 3.182. UWL Amp/Phase Scintillation Correlation and Predicted – 10142016_193175.	370
Figure 3.183. C_T^2 – 10142016_193175.	371
Figure 3.184. C_Q^2 – 10142016_193175.....	371

Figure 3.185. C_{TQ} – 10142016_193175.....	372
Figure 3.186. $\langle C_n^2 \rangle$ Construction and $\langle X \rangle$ Amplitude – 10142016_193175.....	373
Figure 3.187. $\langle C_T^2 \rangle$ Temp Construction and Amplitude Variance – 10142016_193175.	374
Figure 3.188. $\langle C_Q^2 \rangle$ Construction Temp and Amplitude Variance – 10142016_193175.	375
Figure 3.189. $\langle C_n^2 \rangle$ Construction and Phase Variance – 10142016_193175.....	376
Figure 3.190. $\langle C_T^2 \rangle$ Temp Variance and Phase Variance – 10142016_193175.	376
Figure 3.191. $\langle C_Q^2 \rangle$ Humidity Variance and Phase Variance – 10142016_193175.	377
Figure 3.192. $\langle C_T^2 \rangle$ Variance and $\langle C_n^2 \rangle$ Variance – 10142016_193175.	378
Figure 3.193. $\langle C_Q^2 \rangle$ Variance and $\langle C_n^2 \rangle$ Construction Variance – 10142016_193175. ...	378
Figure 3.194. $\langle C_Q^2 \rangle$ Humidity Variance and $\langle C_T^2 \rangle$ Temp Variance – 10142016_193175.	379
Figure 3.195. Phase, U Wind and Amplitude Variance – 10142016_193175.	380
Figure 3.196. Phase, V Wind and Amplitude Variance – 10142016_193175.	381
Figure 3.197. Phase, W Wind and Amplitude Variance – 10142016_193175.....	382
Figure 3.198. Hardware Excluded Histogram – 10142016_193175.	383
Figure 3.199. WB Amplitude No Hardware – 10142016_193175.....	384
Figure 3.200. WB Amplitude No Hardware, Friis and Difference – 10142016_193175. ..	385
Figure 3.201. WB Normalized Amplitude No Hardware, Friis and Difference – 10142016_193175.....	386
Figure 3.202. LWL Amplitude No Hardware – 10142016_193175.	387
Figure 3.203. LWL Amplitude No Hardware, Friis and Difference – 10142016_193175.	388
Figure 3.204. LWL Normalized Amplitude No Hardware, Friis and Difference – 10142016_193175.....	389

Figure 3.205. UWL Amplitude No Hardware – 10142016_193175.....	390
Figure 3.206. UWL Amplitude No Hardware, Friis and Difference – 10142016_193175.	391
Figure 3.207. UWL Amplitude No Hardware, Friis and Difference – 10142016_193175.	392
Figure 3.208. WB Scan 4 Amplitude No Hardware – 10142016_193175.....	393
Figure 3.209. WB Scan 4 Amplitude No Hardware, Friis and Difference – 10142016_193175.....	393
Figure 3.210. WB Scan 4 Amplitude No Hardware, Friis and Difference – 10142016_193175.....	394
Figure 3.211. LWL Scan 5 Amplitude No Hardware – 10142016_193175.....	394
Figure 3.212. LWL Scan 5 Amplitude No Hardware, Friis and Difference – 10142016_193175.....	395
Figure 3.213. LWL Scan 5 Amplitude No Hardware, Friis and Difference – 10142016_193175.....	395
Figure 3.214. UWL Scan 6 Amplitude No Hardware – 10142016_193175.	396
Figure 3.215. UWL Scan 6 Amplitude No Hardware, Friis and Difference – 10142016_193175.....	396
Figure 3.216. UWL Scan 6 Amplitude No Hardware, Friis and Difference – 10142016_193175.....	397
Figure 3.217. LWL & UWL Flipped Mean Amplitude No Hardware – 10142016_193175.	398
Figure 3.218. WB Extinction with No Hardware – 10142016_193175.....	399
Figure 3.219. LWL Extinction with No Hardware – 10142016_193175.....	400
Figure 3.220. UWL Extinction with No Hardware – 10142016_193175.	401

Figure 3.221. LWL & UWL Flipped Mean Amplitude No Hardware – 10142016_193175.	402
Figure 3.222. Data Acquisition Camera – 11012016_145401.	403
Figure 3.223. Timing Synchronization – 11012016_145401.	404
Figure 3.224. Tracking of the Delta Time between Tx and Rx – 11012016_145401.	404
Figure 3.225. Raw Data after DDC for Rx1 – 11012016_145401.	406
Figure 3.226. Raw Data after DDC for Rx2 – 11012016_145401.	406
Figure 3.227. Averaged Filtered (80 Tap) Data after DDC for Rx1 – 11012016_145401.	407
Figure 3.228. Averaged Filtered (80 Tap) Data after DDC for Rx2 – 11012016_145401.	407
Figure 3.229. FFT of first WB Frequency (320 GHz) after DDC for Rx1 – 012016_145401.	408
Figure 3.230. FFT of first WB Frequency (320 GHz) after DDC for Rx2 – 1012016_145401.	408
Figure 3.231. Histogram of first WB Frequency (320 GHz) after DDC for Rx1 – 1012016_145401.	409
Figure 3.232. Histogram of first WB Frequency (320 GHz) after DDC for Rx 2 – 11012016_145401.	409
Figure 3.233. WB Scan 1 for Rx1 – 11012016_145401.	411
Figure 3.234. WB/Friis Scan 1 for Rx1 – 11012016_145401.	411
Figure 3.235. WB/Friis Normalized Scan 1 for Rx1 – 11012016_145401.	412
Figure 3.236. LWL Absorption Scan 2 for Rx1 – 11012016_145401.	413
Figure 3.237. LWL / Friis Absorption Scan 2 for Rx1 – 11012016_145401.	413
Figure 3.238. LWL / Friis Normalized Absorption Scan 2 for Rx1 – 11012016_145401..	414

Figure 3.239. UWL Absorption Scan 3 for Rx1 – 11012016_145401.....	415
Figure 3.240. UWL / Friis Absorption Scan 3 for Rx1 – 11012016_145401.	415
Figure 3.241. UWL / Friis Normalized Absorption Scan 3 for Rx1 – 11012016_145401.	416
Figure 3.242. WB Scan 4 for Rx1 – 11012016_145401.	417
Figure 3.243. WB/Friis Normalized Scan 4 for Rx1 – 11012016_145401.....	417
Figure 3.244. WB Absorption Scan 4 for Rx1 – 11012016_145401.	418
Figure 3.245. LWL / Friis Absorption Scan 5 for Rx1 – 11012016_145401.....	418
Figure 3.246. LWL / Friis Normalized Absorption Scan 5 for Rx1 – 11012016_145401..	419
Figure 3.247. LWL Absorption Scan 3 for Rx1 – 11012016_145401.....	419
Figure 3.248. UWL / Friis Absorption Scan 6 for Rx1 – 11012016_145401.	420
Figure 3.249. UWL / Friis Normalized Absorption Scan 6 for Rx1 – 11012016_145401.	420
Figure 3.250. UWL / Friis Normalized Absorption Scan 6 for Rx1 – 11012016_145401.	421
Figure 3.251. LWL & UWL Flipped Amp / Friis Normalized Absorption – 11012016_145401.....	422
Figure 3.252. WB Scan 1 for Rx2 – 11012016_145401.	423
Figure 3.253. WB/Friis Scan 1 for Rx2 – 11012016_145401.....	423
Figure 3.254. WB/Friis Normalized Scan 1 for Rx2 – 11012016_145401.....	424
Figure 3.255. LWL Absorption Scan 2 for Rx2 – 11012016_145401.....	425
Figure 3.256. LWL / Friis Absorption Scan 2 for RX2 – 11012016_145401.....	425
Figure 3.257. LWL / Friis Normalized Absorption Scan 2 for Rx2 – 11012016_145401..	426
Figure 3.258. UWL Absorption Scan 3 for Rx2 – 11012016_145401.....	427
Figure 3.259. UWL / Friis Absorption Scan 3 for Rx2 – 11012016_145401.	427
Figure 3.260. UWL / Friis Normalized Absorption Scan 3 for Rx2 – 11012016_145401.	428

Figure 3.261. WB Scan 4 for Rx2 – 11012016_145401.	429
Figure 3.262. WB/Friis Normalized Scan 4 for Rx2 – 11012016_145401.....	429
Figure 3.263. WB Absorption Scan 4 for Rx2 – 11012016_145401.	430
Figure 3.264. LWL / Friis Absorption Scan 5 for Rx2 – 11012016_145401.....	430
Figure 3.265. LWL / Friis Normalized Absorption Scan 5 for Rx2 – 11012016_145401..	431
Figure 3.266. LWL Absorption Scan 3 for Rx2 – 11012016_145401.	431
Figure 3.267. UWL / Friis Absorption Scan 6 for Rx2 – 11012016_145401.	432
Figure 3.268. UWL / Friis Normalized Absorption Scan 6 for Rx2 – 11012016_145401.	432
Figure 3.269. UWL / Friis Normalized Absorption Scan 6 for Rx2 – 11012016_145401.	433
Figure 3.270. LWL & UWL Flipped Amp / Friis Normalized Absorption – 11012016_145401.....	434
Figure 3.271. WB SNR and Predicted Friis – 11012016_145401.	435
Figure 3.272. LWL SNR and Predicted Friis – 11012016_145401.	435
Figure 3.273. UWL SNR and Predicted Friis – 11012016_145401.....	436
Figure 3.274. C_n^2 – 11012016_145401.....	437
Figure 3.275. FFT of C_n^2 – 11012016_145401.	437
Figure 3.276. Transmit & Receiver Temp – 11012016_145401.....	438
Figure 3.277. Wind U Transmit & Receiver - 11012016_145401.....	439
Figure 3.278. Wind V Transmit & Receiver – 11012016_145401.	439
Figure 3.279. Wind W Transmit & Receiver – 11012016_145401.	440
Figure 3.280. Humidity Transmit, Receiver & Mean – 11012016_145401.....	441
Figure 3.281. MCF – 11012016_145401.	442
Figure 3.282. MCF – 11012016_145401.	442

Figure 3.283. MCF – 11012016_145401.	443
Figure 3.284. WB Amplitude Scintillation Variance and Predicted – 11012016_145401.	444
Figure 3.285. LWL Amplitude Scintillation Variance and Predicted – 11012016_145401.	445
Figure 3.286. UWL Amplitude Scintillation Variance and Predicted – 11012016_145401.	446
Figure 3.287. WB Phase Scintillation Variance and Predicted – 11012016_145401.	447
Figure 3.288. LWL Phase Scintillation Variance and Predicted – 11012016_145401.	448
Figure 3.289. UWL Phase Scintillation Variance and Predicted – 11012016_145401.	449
Figure 3.290. WB Phase Scintillation STD and Predicted Deg. – 11012016_145401.	450
Figure 3.291. LWL Phase Scintillation STD and Predicted Deg. – 11012016_145401.	451
Figure 3.292. UWL Phase Scintillation STD and Predicted Deg. – 11012016_145401.	452
Figure 3.293. WB Phase Scintillation STD and Predicted MM – 11012016_145401.	453
Figure 3.294. LWL Phase Scintillation STD and Predicted MM – 11012016_145401.	454
Figure 3.295. UWL Phase Scintillation STD and Predicted MM – 11012016_145401.	455
Figure 3.296. WB Phase Scintillation STD and Predicted ps – 11012016_145401.	456
Figure 3.297. LWL Phase Scintillation STD and Predicted ps -- 11012016_145401.	456
Figure 3.298. UWL Phase Scintillation STD and Predicted ps – 11012016_145401.	457
Figure 3.299. WB Amp/Phase Scintillation Correlation and Predicted – 11012016_145401.	458
Figure 3.300. LWL Amp/Phase Scintillation Correlation and Predicted – 1012016_145401.	458

Figure 3.301. UWL Amp/Phase Scintillation Correlation and Predicted – 1012016_145401.	459
Figure 3.302. C_T^2 – 11012016_145401.	459
Figure 3.303. C_Q^2 – 11012016_145401.	460
Figure 3.304. C_{TQ} – 11012016_145401.....	461
Figure 3.305. $\langle C_n^2 \rangle$ Construction and $\langle X \rangle$ Amplitude – 11012016_145401.	462
Figure 3.306. $\langle C_n^2 \rangle$ Temp Construction and Amplitude Variance – 11012016_145401.	463
Figure 3.307. $\langle C_Q^2 \rangle$ Construction Temp and Amplitude Variance – 11012016_145401.	464
Figure 3.308. $\langle C_n^2 \rangle$ Temp Variance and Phase Variance – 11012016_145401.	465
Figure 3.309. $\langle C_T^2 \rangle$ Temp Variance and Phase Variance – 11012016_145401.	466
Figure 3.310. $\langle C_Q^2 \rangle$ Humidity Variance and Phase Variance – 11012016_145401.	467
Figure 3.311. $\langle C_n^2 \rangle$ and $\langle C_T^2 \rangle$ Variance – 11012016_145401.	467
Figure 3.312. $\langle C_Q^2 \rangle$ Humidity Variance and $\langle C_n^2 \rangle$ Construction Variance – 1012016_145401.....	468
Figure 3.313. $\langle C_Q^2 \rangle$ Humidity Variance and $\langle C_T^2 \rangle$ Temp Variance – 11012016_145401.	469
Figure 3.314. Phase, U Wind and Amplitude Variance – 11012016_145401.	470
Figure 3.315. Phase, V Wind and Amplitude Variance – 11012016_145401.	471
Figure 3.316. Phase, W Wind and Amplitude Variance – 11012016_145401.....	472
Figure 3.317. Hardware Excluded Histogram – 11012016_145401.	473
Figure 3.318. Hardware Excluded Histogram – 11012016_145401.	473
Figure 3.319. WB Amplitude No Hardware – 11012016_145401.....	474
Figure 3.320. WB Amplitude No Hardware, Friis and Difference – 11012016_145401. ..	475

Figure 3.321. WB Normalized Amplitude No Hardware, Friis and Difference – 11012016_145401.....	476
Figure 3.322. LWL Amplitude No Hardware – 11012016_145401.	477
Figure 3.323. LWL Amplitude No Hardware, Friis and Difference – 11012016_145401.	477
Figure 3.324. LWL Normalized Amplitude No Hardware, Friis and Difference – 11012016_145401.....	478
Figure 3.325. UWL Amplitude No Hardware – 11012016_145401.....	479
Figure 3.326. UWL Amplitude No Hardware, Friis and Difference – 11012016_145401.	479
Figure 3.327. UWL Amplitude No Hardware, Friis and Difference – 11012016_145401.	480
Figure 3.328. WB Scan 4 Amplitude No Hardware – 11012016_145401.....	481
Figure 3.329. WB Scan 4 Amplitude No Hardware, Friis and Difference – 11012016_145401.....	481
Figure 3.330. WB Scan 4 Amplitude No Hardware, Friis and Difference – 11012016_145401.....	482
Figure 3.331. LWL Scan 5 Amplitude No Hardware – 11012016_145401.....	482
Figure 3.332. LWL Scan 5 Amplitude No Hardware, Friis and Difference – 11012016_145401.....	483
Figure 3.333. LWL Scan 5 Amplitude No Hardware, Friis and Difference – 11012016_145401.....	483
Figure 3.334. UWL Scan 6 Amplitude No Hardware – 11012016_145401.	484
Figure 3.335. UWL Scan 6 Amplitude No Hardware, Friis and Difference – 11012016_145401.....	484

Figure 3.336. UWL Scan 6 Amplitude No Hardware, Friis and Difference – 11012016_145401.....	485
Figure 3.337. LWL & UWL Flipped Mean Amplitude No Hardware – 11012016_145401.	486
Figure 3.338. WB Amplitude No Hardware – 11012016_145401.....	487
Figure 3.339. WB Amplitude No Hardware, Friis and Difference – 11012016_145401. ..	487
Figure 3.340. WB Normalized Amplitude No Hardware, Friis and Difference – 11012016_145401.....	488
Figure 3.341. LWL Amplitude No Hardware – 11012016_145401.	488
Figure 3.342. LWL Amplitude No Hardware, Friis and Difference – 11012016_145401.	489
Figure 3.343. LWL Normalized Amplitude No Hardware, Friis and Difference – 11012016_145401.....	489
Figure 3.344. UWL Amplitude No Hardware – 11012016_145401.	490
Figure 3.345. UWL Amplitude No Hardware, Friis and Difference – 11012016_145401.	490
Figure 3.346. UWL Amplitude No Hardware, Friis and Difference – 11012016_145401.	491
Figure 3.347. WB Scan 4 Amplitude No Hardware – 11012016_145401.....	492
Figure 3.348. WB Scan 4 Amplitude No Hardware, Friis and Difference – 11012016_145401.....	492
Figure 3.349. WB Scan 4 Amplitude No Hardware, Friis and Difference - 11012016_145401.....	493
Figure 3.350. LWL Scan 5 Amplitude No Hardware – 11012016_145401.....	493
Figure 3.351. LWL Scan 5 Amplitude No Hardware, Friis and Difference – 11012016_145401.....	494

Figure 3.352. LWL Scan 5 Amplitude No Hardware, Friis and Difference – 11012016_145401.....	494
Figure 3.353. UWL Scan 6 Amplitude No Hardware – 11012016_145401.	495
Figure 3.354. UWL Scan 6 Amplitude No Hardware, Friis and Difference – 11012016_145401.....	495
Figure 3.355. UWL Scan 6 Amplitude No Hardware, Friis and Difference – 11012016_145401.....	496
Figure 3.356. LWL & UWL Flipped Mean Amplitude No Hardware – 11012016_145401.	496
Figure 3.357. WB Extinction with No Hardware – 11012016_145401.....	497
Figure 3.358. LWL Extinction with No Hardware – 11012016_145401.....	498
Figure 3.359. UWL Extinction with No Hardware – 11012016_145401.	499
Figure 3.360. LWL & UWL Flipped Mean Amplitude No Hardware – 11012016_145401.	500
Figure 4.1. Liquid and Ice Mono-dispersions Absorption and Scattering Plots [39].	503
Figure 4.2. Liquid and Ice Poly-dispersions Absorption and Scattering Plots [39].	504
Figure 4.3. Rain and Snow Absorption and Scattering Plots [39].	505
Figure 4.4. Smaller Diameter Aerosol Distributions with Wind Speeds [64].	506
Figure 4.5. Spherical Cross Section Plot [65].	508
Figure 4.6. TAIPAS Rain Extinction [39].	511
Figure 4.7. TAIPAS Snow Extinction [39].	512
Figure 4.8. LEEDR Rain Extinction.....	515

Figure 4.9. LEEDR Sand Extinction.	516
Figure 4.10. LEEDR Aerosol Input Selection.	517
Figure 4.11. LEEDR Sand Path Results.	519
Figure 4.12. LEEDR Sand Path Attenuation in dB/km.	519
Figure 4.13. LEEDR Sand Path Results with Increased Concentration.	521
Figure 4.14. LEEDR Sand Path Attenuation in dB/km with Increased Concentration.	521
Figure 5.1. Permittivity Real and Imaginary Components Including Resonance.	525
Figure 5.2. EM Wave Types [31].	529
Figure 6.1. Permittivity Real and Imaginary Components including Resonance.	537
Figure 6.2. TAIPAS LWL Hallway Scan.	541
Figure 6.3. TAIPAS LWL Hallway Scan with Friis.	542
Figure 6.4. TAIPAS LWL Hallway Scan Normalized with Friis.	542
Figure 6.5. TAIPAS UWL Hallway Scan.	543
Figure 6.6. TAIPAS UWL Hallway Scan with Friis.	543
Figure 6.7. TAIPAS UWL Hallway Scan Normalized with Friis.	544
Figure 6.8. TAIPAS LWL and UWL Flipped Hallway Scan Normalized with Friis.	544
Figure 6.9. Hallway LWL and Friis Extinction Plots.	545
Figure 6.10. Hallway UWL and Friis Extinction Plots.	546
Figure 6.11. Hallway LWL, Flipped UWL and Friis Extinction Plots.	546
Figure 6.12. WB MCF/Structure Function Plots.	547
Figure 6.13. LWL MCF/Structure Function Plots.	548

Figure 6.14. UWL MCF/Structure Function Plots.	548
Figure 6.15. WB Amplitude Scintillation with Outer Scale Factor Prediction.	549
Figure 6.16. LWL Amplitude Scintillation with Outer Scale Factor Prediction.	550
Figure 6.17. UWL Amplitude Scintillation with Outer Scale Factor Prediction.....	550
Figure 6.18. LWL Phase Scintillation with Prediction.....	551
Figure 6.19. LWL Phase Scintillation.	552
Figure 6.20. UWL Phase Scintillation with Prediction.	552
Figure 6.21. UWL Phase Scintillation.....	553
Figure 6.22. WB Phase Scintillation STD Degrees.....	553
Figure 6.23. WB Phase Scintillation STD Prediction Degrees.	554
Figure 6.24. LWL Phase Scintillation STD Degrees.....	554
Figure 6.25. LWL Phase Scintillation STD Prediction Degrees.	555
Figure 6.26. UWL Phase Scintillation STD Degrees.	555
Figure 6.27. UWL Phase Scintillation STD Prediction Degrees.....	556
Figure 6.28. LWL Phase Scintillation STD Millimeters.	556
Figure 6.29. LWL Phase Scintillation STD Prediction Millimeters.....	557
Figure 6.30. UWL Phase Scintillation STD Millimeters.....	557
Figure 6.31. UWL Phase Scintillation STD Prediction Millimeters.	558
Figure 6.32. LWL Phase Scintillation STD Picoseconds.....	558
Figure 6.33. LWL Phase Scintillation STD Prediction Picoseconds.....	559
Figure 6.34. UWL Phase Scintillation STD Picoseconds.....	559
Figure 6.35. UWL Phase Scintillation STD Prediction Picoseconds.	560
Figure 6.36. WB Amplitude/Phase Scintillation Cross Correlation with Prediction.	561

Figure 6.37. WB Amplitude/Phase Scintillation Cross Correlation with Prediction. 561

Figure 6.38. WB Amplitude/Phase Scintillation Cross Correlation Hallway Data. 562

Figure 6.39. LWL Amplitude/Phase Scintillation Cross Correlation with Prediction. 562

Figure 6.40. LWL Amplitude/Phase Scintillation Cross Correlation Prediction Data. 563

Figure 6.41. LWL Amplitude/Phase Scintillation Cross Correlation Hallway Data. 563

Figure 6.42. UWL Amplitude/Phase Scintillation Cross Correlation with Prediction. 564

Figure 6.43. UWL Amplitude/Phase Scintillation Cross Correlation Prediction Data. 564

Figure 6.44. TAI PAS Single Scan FFT of Tuned Data. 565

Figure 6.45. TAI PAS Single Scan Histogram of Tuned Data. 566

Figure 6.46. FFT of First WB Frequency (320 GHz) after DDC for Rx1 - 1012016_145401.
 567

Figure 6.47. FFT of first WB Frequency (320 GHz) after DDC for Rx2 - 1012016_145401.
 567

Figure 6.48. LWL Absorption Scan 2 for Rx1 - 11012016_145401. 568

Figure 6.49. LWL / Friis Absorption Scan 2 for Rx1 - 11012016_145401. 569

Figure 6.50. UWL Absorption Scan 3 for Rx1 - 11012016_145401. 570

Figure 6.51. UWL / Friis Absorption Scan 3 for Rx1 - 11012016_145401. 570

Figure 6.52. LWL / Friis Absorption Scan 5 for Rx1 - 11012016_145401. 571

Figure 6.53. LWL / Friis Normalized Absorption Scan 5 for Rx1 - 11012016_145401. ... 572

Figure 6.54. UWL / Friis Absorption Scan 6 for Rx1 - 11012016_145401. 573

Figure 6.55. UWL / Friis Normalized Absorption Scan 6 for Rx1 - 11012016_145401. 573

Figure 6.56. LWL Absorption Scan 2 for Rx2 - 11012016_145401. 574

Figure 6.57. LWL / Friis Absorption Scan 2 for Rx1 - 11012016_145401. 575

Figure 6.58. LWL / Friis Normalized Absorption Scan 2 for Rx1 - 11012016_145401. ...	575
Figure 6.59. UWL Absorption Scan 3 for Rx1 - 11012016_145401.	576
Figure 6.60. UWL / Friis Absorption Scan 3 for RX1 - 11012016_145401.	577
Figure 6.61. UWL / Friis Normalized Absorption Scan 3 for Rx1 - 11012016_145401....	577
Figure 6.62. LWL / Friis Absorption Scan 5 for Rx2 - 11012016_145401.	578
Figure 6.63. LWL / Friis Normalized Absorption Scan 5 for Rx2 - 11012016_145401. ...	579
Figure 6.64. LWL Absorption Scan 3 for Rx2 - 11012016_145401.....	579
Figure 6.65. UWL / Friis Absorption Scan 6 for Rx2 - 11012016_145401.....	580
Figure 6.66. UWL / Friis Normalized Absorption Scan 6 for Rx2 - 11012016_145401....	580
Figure 6.67. UWL / Friis Normalized Absorption Scan 6 for Rx2 - 11012016_145401....	581
Figure 6.68. LWL & UWL Flipped Amp / Friis Normalized Absorption - 11012016_145401.....	582
Figure 6.69. LWL SNR and Predicted Friis - 11012016_145401.....	583
Figure 6.70. UWL SNR and Predicted Friis - 11012016_145401.	583
Figure 6.71. MCF - 11012016_145401.	584
Figure 6.72. MCF - 11012016_145401.	585
Figure 6.73. LWL Amplitude Scintillation Variance and Predicted - 11012016_145401..	586
Figure 6.74. LWL Amplitude Scintillation Variance and Predicted - 11012016_145401..	587
Figure 6.75. LWL Phase Scintillation Variance and Predicted - 11012016_145401.....	588
Figure 6.76. UWL Phase Scintillation Variance and Predicted - 11012016_145401.	589
Figure 6.77. LWL Phase Scintillation STD and Predicted Deg. - 11012016_145401.....	590
Figure 6.78. UWL Phase Scintillation STD and Predicted Deg. - 11012016_145401.	590

Figure 6.79. LWL Amp/Phase Scintillation Correlation and Predicted - 11012016_145401.
..... 591

Figure 6.80. UWL Amp/Phase Scintillation Correlation and Predicted - 11012016_145401.
..... 592

Figure 6.81. LWL Extinction with No Hardware - 11012016_145401. 593

Figure 6.82. UWL Extinction with No Hardware - 11012016_145401. 594

Figure 6.83. LWL & UWL Flipped Mean Amplitude No Hardware- 11012016_145401.. 595

GLOSSARY

Acronym	Definition
1D	One-dimensional
2D	Two-dimensional
3D	Three-dimensional
A/D	Analog-to-Digital
ADC	Analog-to-Digital Converter
AFIT	Air Force Institute of Technology
AGC	Automatic Generation Control
AlGaAs	Aluminium Gallium Arsenide
ALMA	Atacama Large Millimeter Array
AMC	Amplifier-Multiplier Chain
AoA	Angle of Arrival
AREPS	Advanced Refractive Effects Prediction System
ARO	U.S. Army Research Office
BAO	Boulder Atmospheric Observatory
BPF	Band Pass Filter
CA	Clear-air
CAR	Clear Air Refraction
CCD	Charge Coupled Device
CEI	Colorado Engineering Inc.
CET	Center for Environmental Technology
CFLOS	Cloud Free Line of Sight
C/M	Clutter-to-Multipath
COTS	Commercial-off-the-Shelf
CU	University of Colorado
CW	Continuous Wave
CWRU	Case Western Reserve University
DARPA	Defense Advanced Research Projects Agency
DDC	Digital Down Converter

DDS	Direct Digital Synthesizers
DNS	Domain Name Server
DoC	Department of Commerce
DSP	Digital Signal Processing
ECEE	Electrical, Computer, and Energy Engineering
EIO	Extended Interaction Oscillator
EM	Electromagnetic
EMI	Electromagnetic interference
EO	Electro-optic
EPOCH	An operating system starting point that determines a computers time and date by counting the ticks from the epoch
FCC	Federal Communications Commission
FDDI	Fiber Distributed Data Interface
FFT	Fast Fourier Transform
FIR	Finite Impulse Response
FPGA	Field Programmable Gate Array
FWG	Folded Waveguide
GaAs	Gallium Arsenide
GaN	Gallium Nitride
GO	Geometric Optics
GTRI	Georgia Technology Research Institute
H	Horizontal Polarization
HAS	Hydrometeor Absorption and Scattering
HEMT	High Electron Mobility Transistor
HF	High Frequency
HiFIVE	High-Frequency Integrated Vacuum Electronics
HITRAN	High-Resolution Transmission Molecular Absorption
HPA	High Power Amplifier
IF	Intermediate Frequency
IMPATT	IMPact Avalanche Transit Time
InP	Indium Phosphide

InSb	Indium Antimonide
IP	Internet Protocol
IP	Ionospheric Propagation
I/Q	In-phase and Quadrature
IR	Infrared
ISIS-CTD	Integrated Sensor Is Structure Critical Technology Demonstration
ISM	Industrial, Scientific and Medical
JPL	Jet Propulsion Laboratory
KK	Kramers-Kronig
LCP	Left-Circular Polarization
LED	Light Emitting Diode
LEEDR	Laser Environmental Effects Definition and Reference
LHCP	Left Hand Circular Polarized
LNA	Low Noise Amplifier
LO	Local Oscillator
LoS	Line-of-Site
LPF	Low Pass Filter
LSB	Least Significant Bit
LWL	Lower Wing Line
MCF	Mutual Coherence Function
ME	Maxwell's Equations
MMIC	Monolithic Microwave Integrated Circuit
MMW	Millimeter Wave
MPSR	Multipath Propagation and Surface Reflection
MRT	Microwave Radiative Transfer
MSPS	Mega Samples Per Second
NAT	Network Address Translation
NCAR	National Center for Atmospheric Research
NICT	National Institute of Information and Communications Technology
NIST	National Institute of Standards Technology

NMMW	Near-Millimeter Wave
NOAA	National Oceanic and Atmospheric Administration
NOMADS	NOAA Operational Model Archive Distribution System
NPFV	Net Present Future Value
NRL	Naval Research Laboratory
NTIA	National Telecommunications and Information Administration
NTP	Network Time Protocol
OCXO	Oven Controlled Crystal Oscillator
OS	Operating System
PDF	Probability Distribution Function
PLL	Phase Locked Loop
PVC	<i>Poly</i> (Vinyl Chloride)
RF	Radio Frequency
RFI	Receiver Fixture Interface
RH	Relative Humidity
RHCP	Right Hand Circular Polarization
RP	Ray Path
RSA	Real-time Spectrum Analyzer
RTD	Resonant Tunneling Diodes
Rx1	Receiver 1
Rx2	Receiver 2
SMART	Scalable Millimeter Wave Architectures for Reconfigurable Transceivers
SMMW	Submillimeter Wave
SNR	Signal-to-Noise Ratio
SNTP	Simple Network Time Protocol
SPAWAR	Space and Naval Warfare Systems Command
SPT	South Pole Telescope
SSH	Secure Shell
STD	Standard Deviation
STTR	Small Business Technology Transfer

SWIFT	Sub-millimeter Wave Imaging Focal Plane Technology
TAIPAS	Terahertz Atmospheric and Ionospheric Propagation, Absorption and Scattering System
TDS	Time Domain Spectroscopy
TE	Transverse Electric
T-Gap	THz Gap
TIFT	Imaging Focal Plane Array Technology
TM	Transverse Magnetic
TP	Turbulent Propagation
T/R	Transmit/Receive
TWT	Traveling Wave Tube
Tx	Transmit
UAV	Unmanned Aerial Vehicle
UDP	User Datagram Protocol
UHF	Ultra-high Frequency
USB	Universal Serial Bus
UTC	Coordinated Universal Time
UWL	Upper Wing Line
V	Vertical Polarization
VDI	Virginia Diodes
VE	Vacuum Electronics
VHF	Very High Frequency
VPN	Virtual Private Network
VSWR	Voltage Standing Wave Ratio
WB	Wideband
WBFS-RF	Wide Band Gap Semiconductors for RF Applications
WRF	Weather Research and Forecasting
XML	eXtensible Markup Language

Chapter 1

Introduction

1.1 Focus

This thesis focused on the development of a transmissometer system that is capable of scanning from 320 GHz to 340 GHz to study and characterize the deterministic and random propagation characteristics of the atmosphere in a real world, open path environment. This band falls within a larger frequency range commonly referred to as the THz range, or THz Gap (T-Gap), which is defined as the radio spectrum from 100 GHz (millimeter-waves) to 10 THz (the far infrared). Even though the band covered by this thesis is only a small fraction of the THz range, it will be referred to as a THz frequency due to its representativeness of many of the spectral features within the larger THz range. The transmissometer system is referred as the Terahertz Atmospheric and Ionospheric Propagation, Absorption and Scattering System (TAIPAS) instrument, which is also synonymous with the propagation modeling system which is developed in this thesis based on data collected and analyzed from the transmissometer and other sources. This thesis focuses specifically on the atmospheric measurements available from the TAIPAS transmissometer over the aforementioned Submillimeter-Wavelength (SMMW) frequency band.

The transmitter is located on the University of Colorado (CU) Center for Environmental Technology (CET) rooftop observatory on the CU Boulder campus. Two phase coherent receivers with variable spacing of up to ~8 m apart were built to enable measurement of the Mutual Coherence Function (MCF) and transverse coherence length of the THz beam wave.

These receivers are located at the National Institute of Standards Technology/National Telecommunications and Information Administration (NIST/NTIA) Green Mesa site approximately 1.90 km from the transmitter along a nearly level Line-of-Site (LOS) open path. The receiver site is provided and maintained by NTIA, which supports this work as a means of improving the scientific understanding of SMMW/THz propagation and improved propagation model development.

1.2 Vision

TAIPAS was designed with the broader goal of developing an instrument and model relevant for understanding atmospheric propagation in the range of ~1-3000 GHz, along with understanding several intriguing aspects of SMMW propagation that have heretofore never been empirically characterized. Specifically, TAIPAS work is focused on: 1) the design of a baseline 320-340 GHz phase coherent transmissometer system coincident with an optical scintillometer to extend the measurements performed during the Army Research Office's 1983 Flatville near-millimeter wave (NMMW, 100-1000 GHz) field studies to higher SMMW/THz frequencies (~300-1000 GHz) under open path conditions, and 2) the integration of existing propagation models for absorption, refraction, and beam scintillation into a common modeling framework useful for image generation and link analysis from 1 to 1000 GHz. Future work on this program beyond this thesis will be focused on extending the TAIPAS instrument's spectral capabilities by adding a transmissometer at 620-670 GHz. This addition will provide unique, coherent multiband data at a relatively unexplored region of the THz spectrum, along with approximately two octaves separating THz frequency bands. The data will be valuable for studying the

coherence effects of co-propagating THz and optical beams in a randomly fluctuating and absorbing atmosphere.

1.3 Instrument

The immediate goal of the TAIPAS transmissometer design is to satisfy the scientific needs for new remote sensing concepts based on the potential to profile a variety of organic and inorganic trace gases using double resonance spectroscopy [1]. To accomplish this goal, an open path site suitable for ongoing, long-term propagation measurements in the SMMW/THz spectral range was identified in Boulder, Colorado (approximately 1655 m above sea level). The larger objective is to leverage the lessons learned in TAIPAS to begin building a propagation test range collocated at CU and NIST/NTIA that could function as a national propagation test facility. This site was only partly selected for convenience to educational and national institute facilities; Colorado's widely varying atmospheric conditions drove the site selection. The propagation link is expected to undergo widely ranging humidity, temperature, wind, clouds, fog, and aerosol conditions, including rain, snow, hail, dust and smoke during the span of a few years. The proximity of the site to the Front Range, the easternmost section of the Southern Rocky Mountains, is expected to result in desired and occasional high wind-induced turbulence caused by occasional gusts of up to 45 m/sec. The long-term product to be generated by this asset is a comprehensive software model that allows verified simulation of propagation, scattering and absorption statistics from the low radio range — 100 kHz — through the THz range applicable to a wide range of environmental conditions. The measurements are specifically expected to further validate and potentially improve upon existing propagation models by including the statistical variances and co-variances of beam amplitude and phase as calculated products.

1.4 Motivations

One of the chief motivations for co-locating two beams of widely separated frequency is to extend the current statistical modeling capabilities for waves propagating in a turbulent atmosphere allowing the prediction of the cross-band coherence properties of two co-propagating THz, infrared, or visible beams. The initial expectation assumes the effects of turbulence on phase and amplitude fluctuations will be common in so far as the same refractive sensitivity coefficients to temperature and humidity exist at the two bands. However, this conjecture has yet to be proven by observation in the THz range, where water vapor fluctuations have a strong impact on both refractivity and absorption, and, moreover, an impact that varies considerably with frequency from the THz to the visible range. It is thus an open question as to whether beams at two disparate THz frequencies, much less disparate bands of the spectrum, will co-propagate: exhibit similar instantaneous fluctuations in amplitude, phase, and Angle of Arrival (AoA) within a turbulent random atmosphere, or will be perturbed independently by the atmosphere.

The requirement of co-propagation is essential to the success of double resonance spectroscopy of the atmosphere in which an intense Infrared (IR) beam is used as a pump to selectively modulate the transition probabilities of specific THz resonances [1]. It is also important for high resolution THz and Electro-Optic (EO)/IR image fusion, wherein highly directional beams may be used to implement multiband imagery for improving standoff detection purposes [2]. Other applications of cross-band propagation coherence include multicarrier THz communication link diversity and wideband THz image stabilization in the presence of a fluctuating atmosphere, similar to multicolor optical stellar interferometry [3], and THz clock

signal distribution. Scientists working with data from radio-astronomy observatories such as the South Pole Telescope (SPT [4]) and Atacama Large Millimeter Array (ALMA [5]) could potentially benefit from the availability of a co-propagation model to support multiband phase correction and multiband seeing condition analysis.

In general, temperature and absolute humidity density variations perturb the down-range beam phase and amplitude characteristics differently near absorption line centers and line wings; this difference is evidenced by the following full Lorentzian model for the complex permittivity for a collection of lines [6] shown in Equation 1.1:

$$\epsilon_{g(\omega)} = \sum_{\text{species } k,n} \sum \left(\frac{n_o e^{-\frac{E_2}{kT}}}{Z} \left[1 - e^{-\frac{\hbar\omega_0}{kT}} \right] \left(\frac{|\bar{\mu}_{12}|^2}{3\hbar} \right) \right) \times \quad (1.1)$$

$$\left[\frac{\omega_0 - \omega}{(\omega_0 - \omega)^2 + (1/\tau)^2} + \frac{\omega_0 + \omega}{(\omega_0 + \omega)^2 + (1/\tau)^2} + i \left\{ \frac{1/\tau}{(\omega_0 - \omega)^2 + (1/\tau)^2} + \frac{1/\tau}{(\omega_0 + \omega)^2 + (1/\tau)^2} \right\} \right]$$

where the collisional broadening time constant $\tau \sim T^{0.8}$ [6]; ω_0 is the line center angular frequency for the $k \leftrightarrow n$ quantum transition, $\bar{\mu}_{12}$ is the associated dipole moment matrix element; E_2 is the final state energy level; T is the temperature in K; Z is the partition function; $k = 1.38 \times 10^{-23}$ J/K is Boltzmann's constant; $\hbar = 1.054 \times 10^{-34}$ J-s is Plank's constant; and n_o is the density of a specific atomic or molecular gaseous species (such as water vapor). Refractivity variations are due to the real part of the permittivity, whereas absorption variations are due to the imaginary part. As can be seen from Eq. 1.1, while neglecting the anti-resonant terms, refractivity

variations due to a strong absorption line will be an odd function of frequency about the line center, and, thus, density fluctuations will affect the beam phase and amplitude fluctuations more at a frequency offset just below the line center than they would for the same frequency offset just above the line center. In contrast, absorptions variations, due to this same line, are an even function of frequency about the line center, which causes fluctuations in the beam amplitude caused by density fluctuations to be equal below and above the line center. Microscale temperature and pressure variations affect the overall air density, which impacts both vapor density and dry air density.

The frequency tuning range of the TAIPAS transmissometer provides an important degree of observational freedom in this regard, permitting study of the relative impact of temperature and humidity variations on the measureable beam statistical quantities of phase variance, amplitude variance, AoA variance, and transverse mutual coherence by observing across a strong THz water vapor line simultaneously with the visible range. The cross-band coherence of these quantities between the THz and visible ranges provides a means for directly probing the validity of a spectroscopically-based, co-propagation model, and, ultimately, engineering communications and remote sensing systems based on cross-band coherence. The importance of studying cross-band coherence in the THz range is due to the strong impact of water vapor fluctuations on the aggregate index of refraction near THz line centers, along with the existence of a number of very strong water absorption lines. The impact's extent of humidity on the complex index-of-refraction can be studied by adjusting the frequency of these water absorption lines. Such a probing capability can also be obtained using both a THz and optical or IR beam —

wherein only temperature fluctuations are significant — although the phase information for the EO/IR beam is much harder to recover due to the need for a coherent reference at the receiver.

The relevant co-propagation effects can also be observed using two nearly identical transmissometer beams operating at closely located THz absorption resonances that derive their phase reference from a common pilot link, such as the High Frequency (HF) pilot link implemented in this thesis, or optical link. In either case, the correlation of water vapor and temperature fluctuations, as characterized by the structure parameter C_{TQ} , will be relevant in predicting cross-band coherence. This statistic is measured by the TAIPAS transmissometer using micrometeorological instrumentation at either end of the path.

1.5 Propagation Model

Radio wave propagation models have been steadily improved during the past several decades, producing what is widely recognized as a set of standard components for the attenuation, dispersion and nominal path trajectory of radio wave modes at frequencies within the spectrum from ~ 100 kHz to ~ 3 THz. Key components of these models can be categorized per the following essential propagation effects:

- Clear Air Refraction (CAR), including attenuation and dispersion caused by both major and trace gases (specifically O_3) and the Zeeman effect [7,8];
- Scattering and absorption by hydrometeors and aerosols, including the aggregate quantities of the phase matrix, propagation constants for the coherent wave within Foldy's approximation, and hydrometeor size and phase distribution models (Hydrometeor Absorption and Scattering (HAS)) [12];

- Turbulent Propagation (TP), the power spectrum of turbulence and its origins in atmospheric stability, and the effects of turbulence on the random index of refraction on Bragg scattering, wave amplitude fluctuations, phase fluctuations, AoA variations, transverse coherence, and the mutual coherences function [30, 31, 32];
- Mean Ray Path (RP), based on the Eikonal approximation and standard models for slowly varying vertical refractive variations in all regions of the atmosphere;
- Multipath Propagation and Surface Reflection (MPSR), including both land and water surfaces, and ionospheric reflection [11]; and
- Ionospheric Propagation (IP), including electron and ion density models, magnetic field models and the influence of charged particles on the propagating modes [13].

Each of these model components exists in commonly accepted analytical and/or semi-empirical analytical and associated software forms [7, 8, 9, 10, 11, 12, 13], although a standard and well validated numerical model covering 100 kHz up to 3 THz and incorporating all of these components in a comprehensive, applications-based, and numerically efficient form has never, to the author's knowledge, been made publicly available. The LOWTRAN 7 model [14] incorporates some of these features, but provides insufficient spectral resolution below 1 THz. The Japanese National Institute of Information and Communications Technology (NICT) model [15] attempts to reconcile the Jet Propulsion Laboratory (JPL) line-by-line [16] catalog with the High-Resolution Transmission Molecular Absorption (HITRAN) line database [17], but does not consider propagation through turbulence that can affect submillimeter wave communications, imaging, and remote sensing. Similar shortcomings as well as unique features of various models, can be enumerated. The Navy's Space and Naval Warfare Systems Command

(SPAWAR) division has a model called the Advanced Refractive Effects Prediction System (AREPS). For example, the current operational uses of this system include airborne and surface-based radar probability of detection, Very High Frequency/Ultra High Frequency (VHF)/(UHF) communication assessment, strike and electronic countermeasures assessment, early warning aircraft stationing, and HF ground / sky-wave assessment. This system's frequency range is 2 MHz to 57 GHz. It has built-in climatology and mesoscale meteorological models. It is government-owned and license-free.

Major developments in line-by-line modeling of strong rotational absorption features in the atmosphere have occurred since Van Vleck's seminal work on line shape [49]. Foremost among these for TAIPAS is the work of Liebe [7, 8, 18, 23] for modeling the absorption and refraction of water vapor and oxygen below 1000 GHz. Central to his work was the development of a continuum absorption model to accommodate the strong wings of water vapor absorption lines in the far infrared portion of the spectrum. Refinements of Liebe's basic reduced line base model continue to be made based upon careful radiometric measurements of atmospheric thermal emission [50], albeit with ever decreasing changes due to the good basic accuracy of the model for most applications.

Thus, there are elements of the above components that are either semi-empirical or purely empirical in nature, and therefore incomplete from a standpoint of their physical basis. For example, the wings of a number of strong absorption lines caused by rotational water vapor transitions in the far-infrared portion of the spectrum produce sizeable attenuation in the microwave window regions near and in between the microwave window bands at ~35, 90, 140,

220, and 340, 410, 670, 870, and 930 GHz. Attenuation within these window bands is modeled by semi-empirical continuum terms of a simple power law nature that are added to the attenuation spectrum, otherwise calculated using a partial set of resonant lines [18]. The challenge in modeling the attenuation caused by the wings of strong lines lies in the associated difficulty of modeling the distortion of the molecular structure of atmospheric gases during the brief interval of a collision. While the continuum correction provides necessary compensation for this un-modeled attenuation, it does not necessarily correct properly for refractive dispersion, nor does it necessarily follow the Kramers-Kronig causality conditions.

Other components of radio propagation models that incorporate semi-empirical elements include MPSR models for surface reflection, emission and scattering, ground wave propagation, and ocean wave / foam emission, HAS models for large ice-water-air conglomerates such as graupel or highly aspherical particles such as ice plates, needles, or snow aggregates, and TP models based on numerically simplified Born or Rytov solutions to the wave equation in a continuously varying random medium.

Overall, the inclusion of the effects of all relevant molecular transitions, trace gases, aerosol types, and hydrometeor effects into a rapidly computable model with tangent linear (or, Jacobian) capability is currently lacking. For the CAR component, while an infinite number of transitions exist for each of a large number of atmospheric species, only a finite set of transitions for each of a specific set of species produces a measurable impact on the spectrum below three THz. Accounting precisely for these and only these key transitions is critical to implementing a fast model. This finite set depends not only on altitude and frequency, but also required

precision, which can vary appreciably from application to application. For example, due to pressure broadening, upper atmospheric remote sensing of trace species typically requires greater precision in total path attenuation than does lower tropospheric image correction. In the HAS component, the Mie scattering model for spherical poly-dispersions are numerically intensive and look-up models can accelerate processing. Similar look-up models based on corrections to the Mie spherical, poly-dispersive model are also needed for aspherical hydrometeors. Finally, although aerosols are composed primarily of liquid water, the effects of varying ionic content — hence varying conductivity and absorption loss — need to be considered along with the distinct absorption and scattering effects of a catalogue of dry aerosols composed of biogenic material, sulfates, sea salt, or any of several types of mineral dust.

Basic propagation models are of immense value in point-to-point communications; remote sensing, both passive and active; precise time keeping; imaging through fog and haze; and geolocation. However, there is also an increasing need for tangent linear versions of these models to automate both tracking of the environmental state vector and improving state vector parameter estimation via remote sensing. Full and fast forward tangent linear propagation models are generally lacking, although this capability could readily be incorporated into a standardized and comprehensive propagation model, specifically if fast numerical spline libraries, which readily admit to fast tangent linear model development, are developed for the most numerically cumbersome elements. Fast tangent linear capabilities are thus considered basic requirements of the TAIPAS model.

1.6 Model Verification

A large amount of field work on propagation at centimeter and Millimeter-Wave (MMW) frequencies (<100 GHz) has been performed, mostly by U.S. and Russian investigators, and reliable, basic expressions for amplitude, phase, and AoA variations have been published. An excellent summary of such work has been compiled by Wheelon [31, 32]. If it is to have impact, experimental propagation model verification must be understood to be a complex task requiring careful hardware design, site selection, and implementation. It has been admirably furthered by a number of investigators, including groups at the Georgia Tech Research Institute (Gallagher, McMillan, Bohlander, and Wiltse [19]), Case Western Reserve University (CWRU) (Claspy, Merat, Manning, and Gasiewski [20, 21, 22]), National Bureau of Standards (Liebe, Gimestad, Hopponen and Hufford [7, 8, 18, 23]), Naval Oceans System Center (Anderson [24]), National Oceanic and Atmospheric Administration (NOAA), Clifford, Hill, Lataitis, Churnside, [25, 26, 27, 28]), and others. Notably, horizontal line-of-sight, near-surface propagation studies were performed in the early 1980s by Georgia Tech and CWRU under the support of the late Dr. Walter Flood of the U.S. Army Research Office (ARO). These experiments yielded a large empirical database of statistical information on propagation through attenuating and randomly refracting atmospheres at key MMW and SMMW frequencies: 116, 140, 173, 230, and 337 GHz. Importantly, this work was used to validate Liebe's model for attenuation at SMMW frequencies and to study and verify the Rytov phase perturbation method for propagation in random media [29, 30, 31, 32]. A very useful compendium of much of this work exists within a two-volume set of texts published by Wheelon [31, 32]. The basic theory for propagation through random media extends from earlier seminal studies by V. Tatarski [33].

The 1983 Flatville measurement campaign by MacMillan, Wiltse, Bohlander, Gallagher, and others [25, 47, 48] provided essential data on the propagation of beam waves over homogeneous flat terrain for near-surface (3.68 m high) propagation paths and in a variety of stable and unstable conditions. The conditions varied from hot surface-dominated convection over the plains during summertime to stable conditions characterized by the presence of fog, snow, and stratiform rain. Specifically, studies were conducted at 116, 140, 173, and 230 GHz. These key experiments illustrated the marked effects of turbulent refractive variations at NMMW frequencies as compared to either centimeter radio or optical frequencies [26], and served to validate the basic theory of spherical wave propagation at NMMW frequencies. However, these experiments were performed only for frequencies less than or equal to 230 GHz and significantly far from major water vapor absorption features. Absorption at frequencies above the 220 GHz window region becomes increasingly complex due to the plethora of strong dipole transitions between the vibrational states of water vapor and other trace gases. The absorption lines associated with these features result in strong refractive variations near line centers. The question of the impact of turbulence at SMMW/THz frequencies in the decade of frequencies above, and especially near the center of strong water vapor lines, was unable to be answered in the Flatville experiment. One reason for this limitation was the nascent technology available at the time for SMMW generation and detection. This technology has markedly advanced in the intervening years, thus providing new means of accurately measuring turbulent effects at frequencies up to and exceeding 1 THz on open paths.

These same rapid advances in transmitter and receiver technology are now making the SMMW/THz portion of the spectrum attractive for imaging, wideband communications, and

spectroscopy, albeit over limited path lengths or at high altitudes, due to the large absorption caused by water vapor. For example, new double-resonance spectroscopy techniques have been identified that may permit remote measurement of trace gas plumes. This technique uses an infrared pump beam from a CO₂ laser to non-thermally populate specific vibrational energy levels that can be observed using a SMMW probe beam. However, such spectroscopic techniques now require extending the Flatville observations to frequencies up to ~1 THz or higher with specific emphasis on accurate absorption, refraction, and scintillation models across broad regions of the SMMW/THz spectrum to accommodate the differential resonances hypothesized to be observable. Moreover, the 1983 Flatville study did not focus on the attenuation and scattering caused by aerosols, which are expected to become more important for both absorbers and scatterers at frequencies approaching and exceeding 1 THz. In limiting cases of high albedo, the scattering caused by aerosols may impact the utility of the double resonance method. Finally, the Flatville data considered only propagation on paths near the surface, and did not consider propagation on high open paths that would be typical of scenarios for which SMMW/THz imaging, remote sensing, and communication would likely occur. Accordingly, there is a need to observe propagation effects on open paths well above ground level, but without the cost, logistics, and technical challenges associated with airborne platforms.

Despite the extensiveness of these past field campaigns, the equipment used had several major deficiencies associated with the nascent state of millimeter-wave technology at the time. The Georgia Technology Research Institute (GTRI) experiments at Flatville relied on phase-locked, Extended Interaction Oscillators (EIOs) and super-heterodyne receivers that provided phase differences between up to four receiver elements. The CRWU experiments at the NASA

Plumbrook facility in Sandusky, Ohio, leveraged an optically-pumped, far infrared methanol laser and both incoherent pyroelectric and cooled Indium Antimonide (InSb) detectors. Although high power was obtained using the EIOs, the detection noise was much higher than could be obtained using harmonic, up-converted sources and heterodyne receivers built from solid state beam lead mixers. In addition, the reliability of this equipment limited the amount of total observation time that could be accrued. As a result, the system noise and range up-time were factors that limited the number and variety of cases that could be studied, and equipment limitations effectively precluded studies at higher SMMW/THz frequencies.

The amount of data collected was also extremely limited by the data collection and processing technology available at the time. Phase and amplitude sample rates were limited to 100 Hz for the Radio Frequency (RF) data, or less for the micrometeorological data. Three decades later, solid state phase locked sources, coherent down converting detectors and precision time-stamped data collected on moderately sized, field-hardened computers permit improvements in Signal-to-Noise Ratios (SNR) estimated to be ~20-40 dB higher than attainable during these early studies. Modern equipment also permits narrowband phase coherent heterodyne detection; increased sampling rates beyond the Nyquist rate caused by atmospheric dynamics; and larger data storage volumes - several orders of magnitude. Advances in digital processing hardware also permit digital sampling, and In-phase and Quadrature (I/Q) demodulation of received signal phase and amplitude from Intermediate Frequencies (IF) signals without the drift and inaccuracy associated with analog IF and sampling hardware.

Improvements in lidar remote sensing technology, while not part of this thesis, also permit greatly enhanced path characterization in all relevant variables, including temperature, moisture and aerosols, along with their short-term statistical variations. Past experiments relied upon point measurements of fluctuating meteorological quantities (temperature, humidity, and winds) obtained using fast response in-situ sensors, specifically, fine wire temperature probes, Lyman-alpha hygrometers, and sonic anemometers. While these point measurements still remain indispensable for measuring the structure parameters of a fluctuating atmosphere, characterization of the full path by mean water vapor, temperature, aerosol concentration, and hydrometeor state — water content, mean size, and phase — can now be obtained using lidar, either Raman or differential absorption lidar – DIAL, and polarimetric short wavelength radar. Instrumentation for such measurements has progressed markedly, and is now reliable and available off-the-shelf in some cases.

Scintillometer measurements of the refractive structure coefficient C_n^2 at optical or near-IR wavelengths remain one of the best means of characterizing the path-averaged value of temperature-induced refractive index variations. The turbulent spectrum of small-scale atmospheric index-of-refraction fluctuations under the Obukhov 2/3-power dissipation scaling law is shown in Equation 1.2:

$$\Phi_n(k) = 0.033C_n^2k^{-11/3} \quad (1.2)$$

where the structure parameter C_n^2 describes the level of fluctuations in the real part of the index-of-refraction due to turbulence and k is the spatial wavenumber [34, 31]. The above

Kolomogorov spectrum was extended to account for viscous inner scale and boundary-induced outer scale cutoffs by von Karman [31]. The relationships between C_n^2 and the associated meteorological structure parameters C_T^2 , C_Q^2 and C_{TQ} for temperature and water vapor variations, respectively, are determined from the relationship between the index of refraction n' and these variables, shown in Equation 1.3:

$$C_n^2(f) = A_T^2 C_T^2 + A_T A_Q C_{TQ} + A_Q^2 C_Q^2 \quad (1.3)$$

where the parameters A_T and A_Q are derivatives of the index of refraction with respect to temperature and humidity, respectively (Equation. 1.4):

$$\begin{aligned} A_T(f) &= \frac{\partial n'}{\partial T} = \frac{1}{2} \frac{\partial \Re\{\epsilon_g\}}{\partial T} \\ A_Q(f) &= \frac{\partial n'}{\partial Q} = \frac{1}{2} \frac{\partial \Re\{\epsilon_g\}}{\partial Q} \end{aligned} \quad (1.4)$$

These parameters can be considered to be the Jacobian elements relating temperature and absolute humidity variations to variations in the real part of the index of refraction, and are thus strong functions of frequency. Differing A_T and A_Q at different bands — e.g., between optical and THz, or between one THz band to another, or between the center of a THz resonance and wings of the resonance — leads to cross-band de-coherence, which, in turn, places limits on the co-propagation of beams of differing frequencies.

A similar Jacobian relationship with parameters B_T and B_Q holds for relating the structure parameter of the imaginary part of the index of refraction to the meteorological structure parameters (Equation. 1.5).

$$C_{n''}{}^2(f) = B_T{}^2 C_T{}^2 + B_T B_Q C_{TQ} + B_Q{}^2 C_Q{}^2 \quad (1.5)$$

where:

$$B_T(f) = \frac{\partial n''}{\partial T} = \frac{1}{2} \frac{\partial \Im m \{ \epsilon_g \}}{\partial T} \quad (1.6)$$

$$B_Q(f) = \frac{\partial n''}{\partial Q} = \frac{1}{2} \frac{\partial \Im m \{ \epsilon_g \}}{\partial Q}$$

Therefore, it is generally recognized that the index of refraction $n = n' + in''$ exhibits a spatio-temporal spectrum of fluctuations in both its real and imaginary parts, and that these fluctuations are correlated by the complex refractivity model (Equation. 1.6).

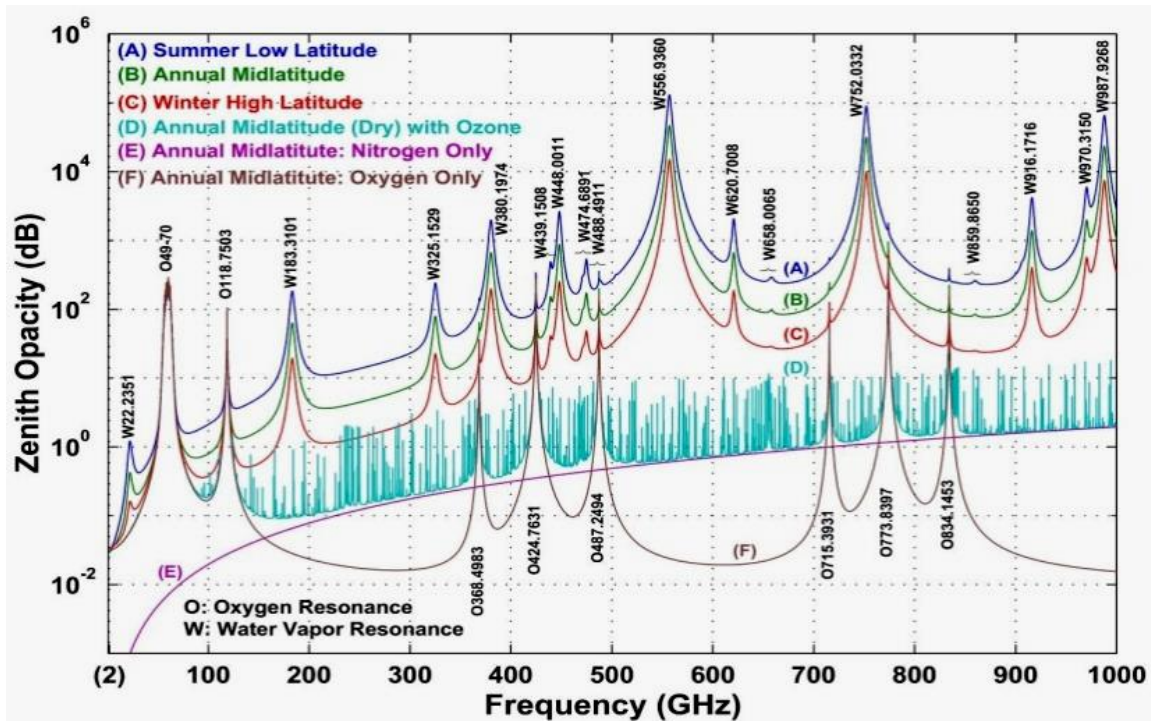
Overall, much more extensive and accurate propagation model validation can now be performed, specifically for the CAR, HAS, and TP components, and at lower inflation-adjusted cost than incurred for past experiments. Accordingly, this thesis focuses on the design and fielding of the hardware needed for advanced propagation measurements and atmospheric characterization in both deterministic and random atmospheres.

1.7 An Absorptive Model for Radiative Transfer

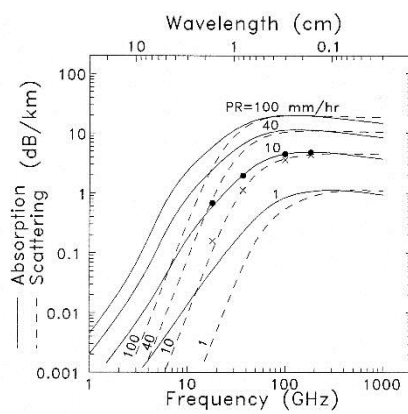
An example of a versatile and useful standardized propagation model for absorption and radiative transfer calculations is the Microwave Radiative Transfer (MRT) program developed by Gasiewski in 1987-88 at MIT [35], extended to THz frequencies at Georgia Tech [36], and later revised to support a GUI interface at NOAA [37]. The MRT is currently maintained and used today within the NOAA-CU Center for Environmental Technology (CET) for remote

sensing, communication, and propagation studies. The MRT model is based on the Liebe [7,8] and Rosenkranz [38] models for clear-atmosphere absorption; a full Mie series integration over a gamma hydrometeor size distribution for the HAS component; and full integration over a user-defined multiple sub-band passband and arbitrary length, slant propagation path for computing the atmospheric emission and path loss. Sample output from the CAR and HAS components of the model are illustrated in Figure 1.1. This model is based on the Liebe MPM absorption line model. It is well referenced and validated and is the current culmination of ~25 years of effort and experience by Prof. Gasiewski and his students. There are additional components lacking by the MRT model, specifically and most importantly for this project, the TP and RP components, along with a user interface more suited for point-to-point communications. An ongoing effort at CET is to extend MRT to accommodate arbitrary paths; compute results for the full Stokes vector; provide a full tangent linear capability; accommodate multiple hydrometeor types; and provide multiple data type I/O to facilitate a “plug-and-play” compatible system with standard operational data sources, including Weather Research and Forecasting (WRF) output.

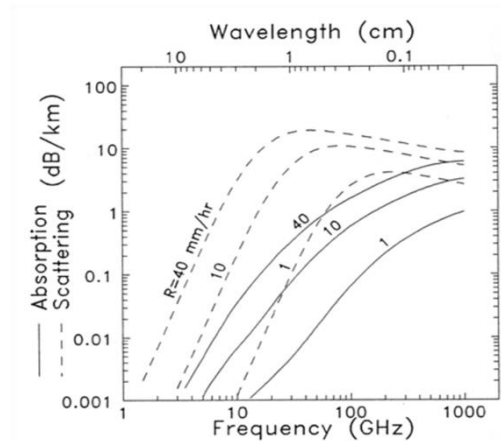
Figure 1.1 also illustrates an important shortcoming that exists in all currently available propagation models. The curves provide no indication of the variance in the expected path attenuation and how this variance relates to season, location, meteorological conditions, and frequency. In many cases, the amount of such variability, whether in path attenuation, phased delay, AoA, or other beam parameters, can be critical to making communications channel decisions based on the model output and to the interpretation of remotely sensed data. Beam fluctuation statistics can provide this important additional component and are thus a focus, beyond this thesis, of the TAIPAS study.



(a)



(b)



(c)

Figure 1.1. (a) Clear-air (CA) attenuation versus frequency, and (b,c) HAS components of the currently-used MRT propagation model for (b) rain and (c) ice [39].

Development of fast, stable version of MRT that incorporates both complex aspherical hydrometeors and calculation of the full Stokes vector in horizontally inhomogeneous scattering

and absorbing clouds is currently under development at CU. This model includes a fast Jacobian capability for computing the sensitivity of brightness temperatures with respect to the basic meteorological variables.

1.8 TAIPAS Transmissometer Development

The design of the TAIPAS open-path transmissometer was based on the need to measure fluctuations in absorption and refraction at THz and visible wavelengths under conditions ranging from dry and clear air to precipitation, aerosol, and fog-laden. The SNR, phase stability, and sample rate of the system were determined to permit quantitative measurement of relative path attenuation and instantaneous phase and amplitude variations coherently sampled using two THz receivers over a band of frequencies ranging from the moderately strong water line center at 325.153 GHz to the minimum of attenuation in the 340 GHz spectral window. Mechanical stability and many environmental issues were also considered in the hardware development to ensure that the basic measurements would be able to be performed.

TAIPAS was implemented as part of a Phase I and Phase II Small Business Technology Transfer (STTR) program of study with Colorado Engineering, Inc. (CEI) and CU funded by the Army Research Office from 2011-2016. The TAIPAS effort identified, through an engineering design study, and later procured, assembled, and tested the basic hardware down to the component level and associated remote sensing equipment necessary to implement a single-band 320-340 GHz coherent transmissometer with optical scintillometer for the CU-Green Mesa link.

Consideration was focused on the following major experiment design issues, which had been traded off against system cost:

1) Frequency Selection. Ultimately, it is envisioned that up to four key bands may be required for model verification of the effects of water vapor, rain, snow, fog, aerosols, and turbulence, which are the primary variables to be studied for TAIPAS validation. A set of window-channel frequencies spanning nearly a decade in frequency, but weighted toward the unexplored submillimeter wave bands — frequencies of 140, 325-340, 495, 670, and 870 GHz — were originally of interest. These bands were selected on a scientific basis due to their minimum attenuation; overall span of the spectrum up to ~1 THz; and, in the case of 320-340 GHz, their inclusion of a weak water line to study the effects of enhanced refractive variation caused by water vapor fluctuations. The TAIPAS project, specifically this thesis, focused on the 320-340 GHz band to extend the Flatville measurements almost one octave higher in frequency.

2) THz Beam Variables. The baseline transmissometer variables to be measured were wavefront relative amplitude, or equivalently, intensity; wavefront relative phase and phase variance; wavefront AoA; wavefront transverse coherence; and wavefront MCF. The AoA variance will be obtained using the covariance statistics of the wavefront phases measured by two closely spaced antennas. A pair of aperture antennas with variable spacing and coherent downconversion and sampling provides measurements of the MCF and associated transverse coherence length of the beam wavefront. A long enough path length to observe meaningful fluctuations was identified to be in the ~km range, thus leading to the specific 1.92 km path between the CU CET rooftop observatory and Green Mesa site.

A beam wave generated and received using a set of $\sim 100\lambda$ lens antennas was the most practical for the transmitters and both receivers. This size of aperture permits tight collimation during the portion of the path over one nearby the CU building rooftop, but with suitable beam waist expansion to ~ 25 meters diameter at the Green Mesa site, to provide a meaningful measure of expected transverse coherence length. Far zone 3 dB beam-widths for this aperture size are ~ 0.8 degrees — large enough to permit straightforward beam alignment. Protection of the lenses by hoods to preclude accrual of hydrometers; attenuation of mechanical vibration caused by wind induced gusts; and thermal stabilization of transmitter and receiver equipment were considered requirements.

3) Site Selection. Key design issues studied included transmitted power, bandwidth, phase stability, phase reference accuracy, transmitter/receiver aperture size, sampling rate, receiver noise, and required Analog-to-Digital (A/D) sampling precision. For example, the value of the received SNR with $\sim 10\lambda$ apertures at 1920 meters and using a 1 mW (0 dBm) 620-670 GHz transmitter/receiver with < 12 dB DSB noise figure, and 10 kHz IF bandwidth is ~ 13 dB. Similar large values hold for the other bands referenced above. Extension of the propagation path to longer distances would seriously degrade the SNR for the higher SMMW bands, thus underscoring the optimum choice of the 1.92 km CU-Green Mesa link.

4) Link Architecture. The architecture of the transmitter/receiver and system hardware specifications is based on the ability to coherently measure the above radio variables with

excellent SNR and within sampling intervals of ~ 0.1 msec. This sampling time is smaller than the frozen time of the atmosphere for electromagnetic wave propagation consideration.

Provision of a reliable phase reference at the far-end of the link was a key design challenge that was addressed using a 40 MHz, HF carrier wave as a pilot or, “coho” — link, along with phase locking of this receiver carrier signal. For a given value of C_n^2 , the phase fluctuation variance, due to atmospheric turbulence, is expected to scale roughly with frequency [31]; hence, phase fluctuation noise is expected on this received carrier. However, this noise is heavily filtered using a phase locked loop with long time loop filter constant at the receiver end. This scheme provides an effectively precluded introduction of atmospheric induced phase noise over time scales shorter than the loop filter time constant.

5) Meteorological Truth. Fast Lyman- α hygrometers and sonic anemometers and cameras are utilized to measure 1 ms samples of temperature, humidity and three-axis winds, as well as visual conditions at both the transmitter and receiver ends of the site. While characterization of these variables along the entire path length would be desirable, any more than two such stations are cost and deployment impractical. To compensate for the lack of along-path information, an optical, camera-based scintillometer is used to measure the integrated optical C_n^2 along the path.

1.9 Thesis Description

This thesis describes the detailed design, implementation, and initial performance of the TAIPAS transmissometer instrument. The following are brief descriptions of the chapters of this thesis along with key research points made within each chapter:

Chapter 1) Introduction and Background. Discussion of past work in development of statistical beam wave propagation models in the THz range, field experiments used to validate THz propagation models, and the basic constraints on the design of the TAIPAS transmissometer.

Chapter 2) Transmissometer. Discussion of the design a state-of-the-art 320 GHz – 340 GHz coherent transmissometer for analysis of amplitude scintillation, phase scintillation and angle-of-arrival (AoA) fluctuations around the 325.1529 GHz water absorption resonance. This also includes the design of a custom scintillometer leveraging LEDs and telescopes.

Chapter 3) Propagation. Discussion of measurements and analysis of AoA, phase and amplitude scintillations and for varying transverse coherence length distances at 320-340 GHz to empirically characterize these statistics of a beam wave propagating through a turbulent medium. Measured statistics will be used in conjunction with the Rytov approximation to verify expected values of inner- and outer scale parameters, or, to study the applicability of beamwave models (versus plane or spherical wave models) in calculating wavefront statistics.

Chapter 4) Aerosols. Discussion of the area of study and analysis of THz propagation through naturally generated aerosols and hydrometeors. The data was not available at the time of this thesis publication.

Chapter 5) Manning Beamwave. Discussion of Manning's beamwave, complex refractive model. SMMW signals, unlike optical, are effected heavily by both temperature and humidity, the first of which affects phase and the latter of which cause attenuation. This area of study will entail an investigation into the use of the Manning beamwave statistical propagation model [3] for complex refracting and absorbing media and its corroboration over a band encompassing the 325 GHz water vapor resonance and the 340 GHz transmission window.

Chapter 6) Refractivity. Discussion about the anomalous refractivity validation. The THz frequency band has a significant absorption peak at the 325.1529 GHz water vapor resonance. This task investigates the hypotheses that there can be anomalous (negative trending) refractivity's required by the Kramers-Kronig (KK) relations, around this large absorption peak.

Chapter 7) Co-Propagation. Discussion of "Under what conditions can a THz IR and SMMW beam co-propagate closely enough to satisfy double resonance sensing criteria?"; co-collimation of a temperature sensitive IR beam wave and a temperature and humidity dependent THz beam wave is critical to the implementation of the double resonance remote sensing technique.

Chapter 8) Conclusion. Implements a summary for each chapter.

Chapter 2

Transmissometer Design

2.1 Introduction

This chapter details the design of the TAIPAS open path tropospheric transmissometer for measurement of THz radio propagation path statistics. The transmissometer path is 1.924 km long between the Electrical, Computer, and Energy Engineering (ECEE) building at CU and the NTIA Mesa site at the NOAA-NIST campus. It gradually ascends rising terrain containing a range of suburban features, including trees, fields, houses and buildings – none of height exceeding 55 ft. The path slope from transmitter to receivers is 3.62° . The transmissometer consists of a state-of-the-art 320 GHz – 340 GHz transmitter with two-phase coherent receivers designed for measurements of amplitude scintillation, phase scintillation and AoA fluctuations around the 325.1529 GHz water absorption resonance. The TAIPAS system uses a unidirectional transmitter with 9 cm diameter lens aperture antenna and two phase-coherent receivers each with 9 cm diameter lens aperture antennas and an adjustable transverse separation of up to 8 meters. Coherency is achieved utilizing a 40.7 MHz Industrial, Scientific and Medical (ISM) band continuous wave (CW) signal phase locked with the transmitter Local Oscillator (LO) utilizing a Phase Locked Loop (PLL) at the receivers. The system can measure long range, coherent THz propagation statistics during continuous long-duration studies of turbulent atmospheric propagation effects over an extensive array of atmospheric conditions in a realistic operational environment.

The transmitter and receivers are designed with sufficient phase and amplitude coherence and stability to measure the effects of a turbulent atmosphere on the received signal phase and amplitude. In order to accurately measure these effects, analysis of potential sources of phase and amplitude error was performed to ensure requisite levels of system phase accuracy, system multipath effects on phase, transverse coherence measurement accuracy, system mechanical stability, and crosstalk of AoA and amplitude fluctuation signatures. Sources of phase and amplitude error in the transmissometer include the THz receivers and transmitter chain as well as the low frequency RF coherent pilot link.

Initial tests of the transmissometer used a short (~10 m) level indoor propagation path in the CEI and CET laboratory environments. This path was ~1 to 1.5 meters above a smooth floor, and otherwise unobstructed. Paths of this length permitted phase locking the transmitter and receiver LOs using a coaxial cable to preclude coherent link phase and amplitude noise. The cable was critical to verifying inherent system phase error variances. This short-range configuration, similar to that of the Flatville experiment [25, 48, 51] but on a shorter indoor path with negligible turbulence, permitted characterization of system phase and amplitude statistics, thus yielding a baseline set of transmissometer performance specifications.

The system was subsequently configured for long term measurements on the full 1.92 km elevated path. Measurement of phase and amplitude performance on this outdoor THz link was studied vis-à-vis the anticipated theoretical performance based on the Rytov approximation [29, 52].

2.2 Propagation Link Design

The goal for the experiment was driven by the desire to have an above-ground, free space SMMW link representing a typical urban scenario. Several near-horizontal open propagation paths with varying distances were identified in Boulder, Colorado. There were several factors in selecting Boulder. This location has a range of dry-to-precipitating conditions which provide the wide range of moisture environments ($\sim 2\text{-}15\text{ g/m}^3$ density) necessary for comprehensive SMMW/THz propagation studies. The nearby mountains also provide a wide range of wind speed conditions; the largest of which generate significant levels of turbulence pertinent to many applications of SMMW/THz radio propagation in remote sensing and imaging, including the important urban environment. Large-scale turbulent parcels originating by lee-generated Kelvin-Helmholtz rotors initiate dissipative processes producing a cascade of turbulent parcels with large and significant values of C_n^2 .

In addition to turbulence, hydrometeor states in Boulder during a typical year include clear air, fog, rain, wet/dry snow, and hail. Aerosol loading caused by forest fires and windborne dust is variable and can be at significant levels, as can aerosol loading by advected pollutants from automobile traffic. Accordingly, the effects of aerosols on SMMW/THz propagation can be potentially studied.

A set of paths with a principle, central transmitter on the rooftop observatory established by the NOAA-CU CET and receivers at any of several key limited- or protected-access sites in and around Boulder were identified to support continuous local operation of the equipment. Proximity to the CET lab was deemed essential for readily improving and maintaining the

experiment at moderate cost by taking advantage of established facilities, thus allowing reliable data to be collected on a year-round basis. In contrast, the efficacy of a propagation site, even if located only a few miles from a lab facility, incurs significant travel cost and reduced observation time, particularly in inclement weather. Finally, the propagation paths from CU to various other CU and government facilities over Boulder extend the measurements at Flatville to elevated open paths more representative of those anticipated in both defense and civilian applications.

Five candidate propagation paths with varying path lengths were identified and evaluated. These paths utilize six sites; all are accessible to CET for long term studies (Figure 2.1). Each leverages the NOAA-CU CET rooftop observation deck on the CU ECEE building. The CET observation deck provides power, high speed Internet, security, and grounding for lightning strike protection. It is in the same building as the CET laboratory and has excellent line-of-site views to the candidate receiver sites: 1) the roof of the CU Gamow Tower (520 m); 2) the NIST Green Mesa radio site (1.90 km); 3) the National Center for Atmospheric Research (NCAR) Mesa laboratory on Table Mesa (3.37 km); 4) the NOAA Boulder Atmospheric Observatory (BAO) in Erie, Colorado (22.57 km), and 5) the Department of Commerce (DoC) Table Mountain site (6.52 km). These distances do not include elevation gains.



Figure 2.1. Paths for five accessible line-of-site transmissometer links each with transmitter based at the CU CET ECEE rooftop observatory: 1) CU Gamow Tower (520 m), 2) NIST Green Mesa radio site (1.90 km), 3) NCAR Table Mesa site (3.37 km), 4) NOAA BAO tower (22.57 km), and 5) DoC Table Mountain site (6.52 km). The Phase I study focused on the use of the Green Mesa site (1.90 km).

The 1.92 km link to the NIST Mesa site (Path #2) was identified as optimal for initial testing based on the expected values of attenuation, wave-front fluctuation levels, and SNR for a wide range of SMMW frequencies and propagation conditions. The NTIA subsequently installed a power service to this site to support the project. A diagram of the path is shown in Figure 2.2; the elevation scale is exaggerated for readability. The transmitter elevation is 1650 m MSL and receiver location is 1771 m MSL, thus providing an elevation change over the entire path of ~121 m. Thus, the radio path length is $\sqrt{(121)^2 + (1900)^2} = 1924$ m to within an accuracy of

± 2 m. The minimum and maximum path elevations range from ~ 14 m — the ECEE building roof height — at the transmitter end, to 67 m maximum at a distance of $\sim 75\%$ to the receivers, to ~ 1.5 m just in front of the receivers. Turbulent outer scale lengths L_o based on Tatarski's approximation documented by Wheelon [31]:

$$L_o \approx .4 \times \text{height (m)} \quad (2.1)$$

thus range ~ 0.6 m to ~ 27 m. The associated low frequency spatial cutoff wavenumbers are:

$$\kappa_0 = \frac{2\pi}{L_o} \quad (2.2)$$

and range from $10.5 \text{ rad}\cdot\text{m}^{-1}$ at the transmitter on top of the CU building to $0.234 \text{ rad}\cdot\text{m}^{-1}$ at the largest height above the terrain. Figure 2.3 shows several views of the CU rooftop, Mesa site, and other paths studied.

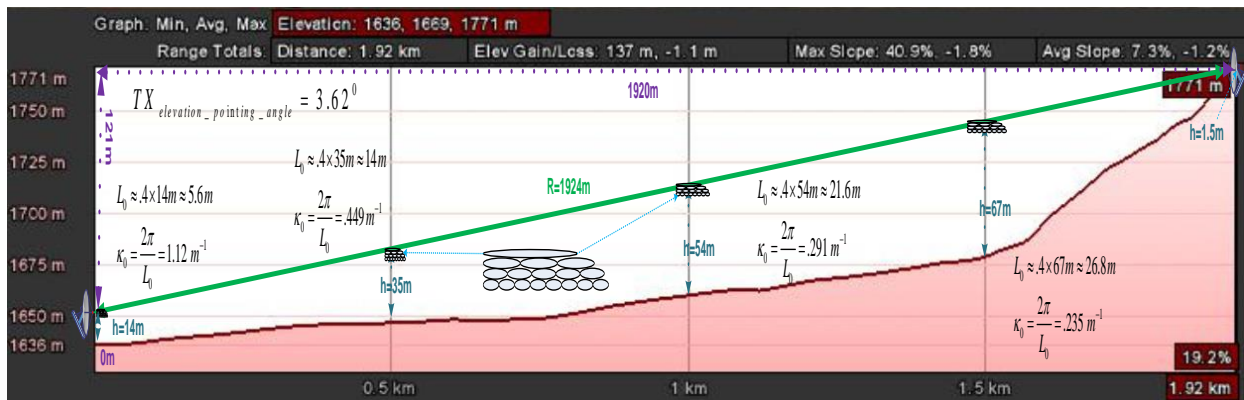


Figure 2.2. NIST Green Mesa site propagation path topography illustrating key atmospheric outer scale distances and cutoff wavenumbers.

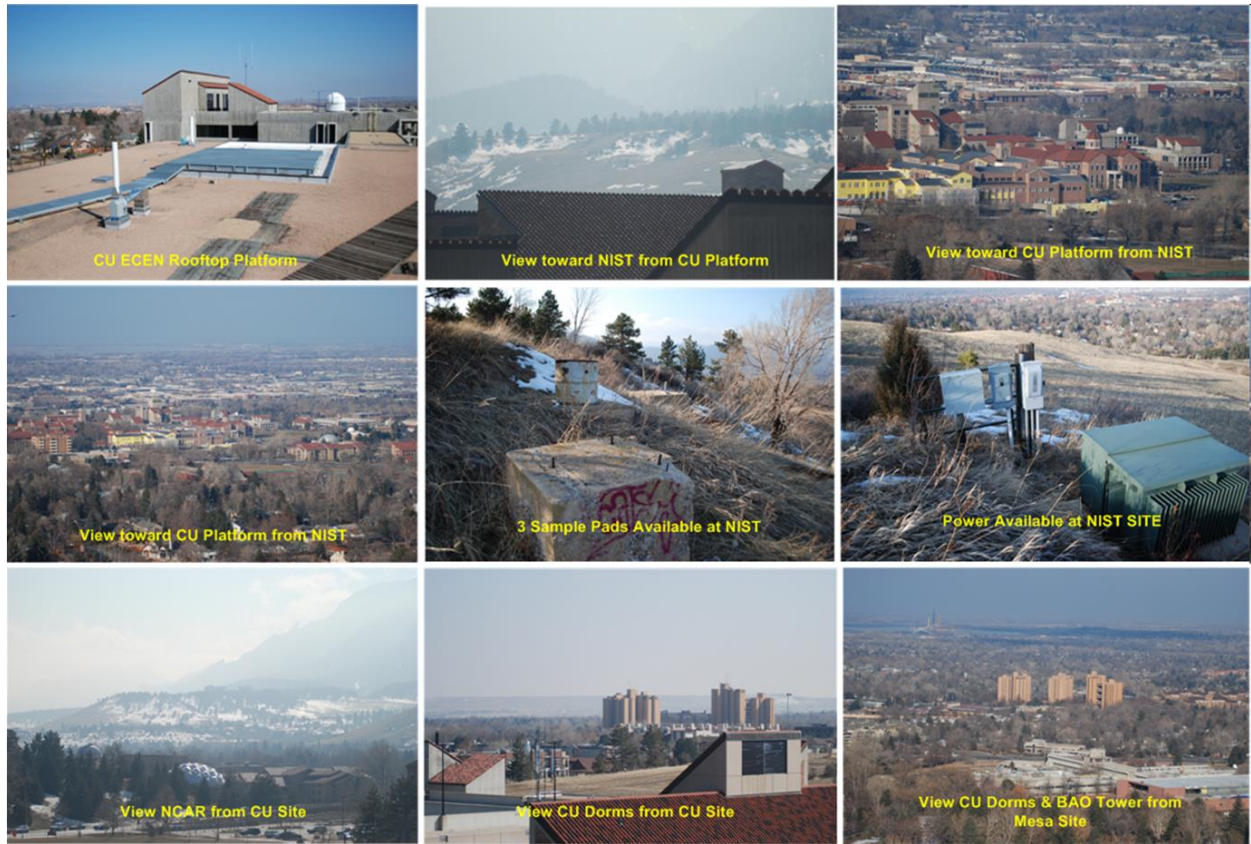


Figure 2.3. Photos of the CU rooftop observatory platform and NIST Green Mesa sites. A clear elevated line-of-sight exists between the CU deck platform and Green Mesa site. Note the occurrence of haze in some of these pictures. (The bottom center view is a sixth candidate link of approximate the same distance as Green Mesa to the CU dormitory towers.)

The propagation path topography profile provides a means of determining clearance at MMW/SMMW frequencies to obstacles located around the path boresight, both within the near zone of each of the transmitter and receiver antennas and along the length of the path over which divergence is occurring. For 9 cm diameter lens antennas at 340 GHz, divergence of the radiated power density with a uniform beamwidth occurs at the far zone distance R_f :

$$R_f = \frac{2D^2}{\lambda} = 18.3 \text{ m} \quad (2.3)$$

Thus, the beam is relatively well contained within a ~9 cm diameter flux tube and slightly affected by multipath scattering during passage over the ECEE building rooftop, which terminates ~20 m along the path from the transmitter aperture.

Beyond the rooftop edge, the beam expands with a half power beamwidth of ~0.73° resulting in a 3dB spot size at either end of the path of ~24 meters in diameter. For TAIPAS, scattering or absorbing objects of relevance on the ground along the path include buildings, houses, trees, vehicles, poles, and wires. It is important to be able to determine the potential impact of these objects on the received power in order to preclude their effect on the measured signal phase and amplitude statistics. Traditionally, and for most communications links, this analysis is done by a study of the Fresnel zone radii along the path. Fresnel zones are a series of non-confocal ellipses with their foci located between the transmitter and receiver. The Fresnel zone ellipse radii are defined by Equation 2.4, where R is the path length, z is the distance along the path of the circular Fresnel zone perpendicular to the path, and λ is the wavelength. The radii of these circular zones provide a general guideline on the perpendicular distance from the propagation path boresight, which must be clear of scattering or absorbing objects in order to close the propagation link budget without significant signal loss or multipath by wave diffraction from near-path objects. The first Fresnel zone radius (Equation 2.5) is a commonly used determinant of multipath propagation clearance for communication links.

$$F_n = \sqrt{n\lambda} \sqrt{\frac{z(R-z)}{R}} \quad (2.4)$$

$$F_1 = \sqrt{\frac{\lambda z(R-z)}{R}} \quad (2.5)$$

However, the Fresnel zone ellipses do not provide a quantitative determinant of the degree to which path blockage and near-path scattering objects can affect the received power across the link, and, thus, to what degree multipath-induced fluctuation effects can be precluded from the measured statistics of received phase and amplitude fluctuations. To better understand the potential impacts of near-path scatterers, the diffractive effects of a circular aperture of varying radii perpendicular to the path on the link signal power were analyzed. For this study, the transmitter and receiver fields are each modeled by Gaussian beams parametrized by waist radii $W_o=0.6435a$, where $a = 9$ cm is the TAIPAS aperture radius for the transmitter and receiver lenses. Infinite phase radii of curvature $R_o \rightarrow \infty$ are used to model properly focused lens-feedhorn antennas. This model shows [6] that the link efficiency $\eta_l(a, z_a)$ for Gaussian beam diffraction through a circular aperture of radius a located at distance z_a along the path relative to an unobstructed path can be computed as:

$$\eta_l(a, z_a) = |1 - e^{-Aa^2}|^2 \quad (2.6)$$

$$A = A' + jA'' = \frac{1}{\frac{1}{\alpha_t} - j\frac{2z_a}{k}} + \frac{1}{\frac{1}{\alpha_r} - j\frac{2(R - z_a)}{k}} \quad (2.7)$$

$$\alpha_{t,r} = \frac{1}{W_{o,t,r}^2} + j\frac{k}{2R_{o,t,r}} \quad (2.8)$$

where and $k = \frac{2\pi}{\lambda}$ is the wavenumber; the subscripts t and r represent the transmitter and receiver, respectively, and the full diffractive effects of the circular aperture are considered in the expression.

The closer the link efficiency parameter η_l is to unity the less potential diffractive effect an object at radius a and distance z_a will have on the link power budget (Figure 2.4); MATLAB code is in Appendix A. Aperture diffraction produces both reductions and increases in link signal power, but generally does not affect the path budget in the light blue areas. The diffraction-free zone typically lies several Fresnel zone radii from the path boresight. Calculating the difference of η_l from unity in decibels provides a conservative bound on how much link variation could be caused by diffracting objects near the path. This radial bound for various levels of link power variation is plotted in Figure 2.5, along with the actual measured path clearance distance. The calculations indicate the effects of individual diffracting objects adjacent to the TAIPAS path will be negligible to at least -60 dB. While these results do not conclusively preclude a significant impact by the collection of path-aggregated diffracting objects, the exponential decay of beam impact and proximity of scattering objects only below the path bore-site strongly support the hypothesis that collective effects will be negligible.

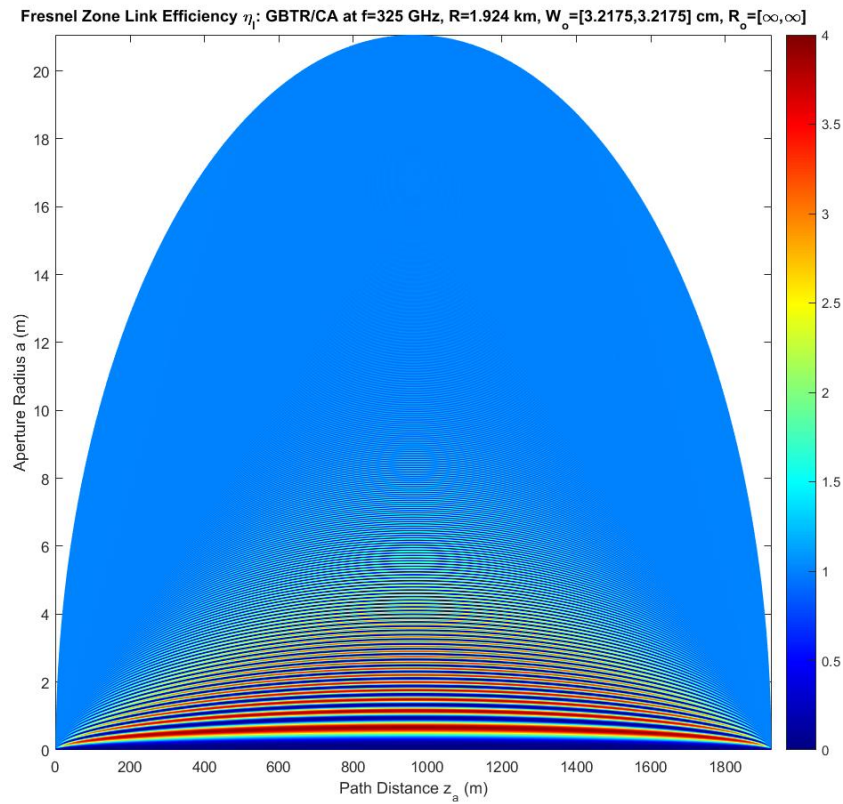


Figure 2.4. Fresnel link efficiency η_l for the TAIPAS path showing the impact of propagation through a circular aperture of radius a located a distance z_a along the 1924 m path. Nominal TAIPAS beam parameters for Gaussian transmit and receive beams are assumed.

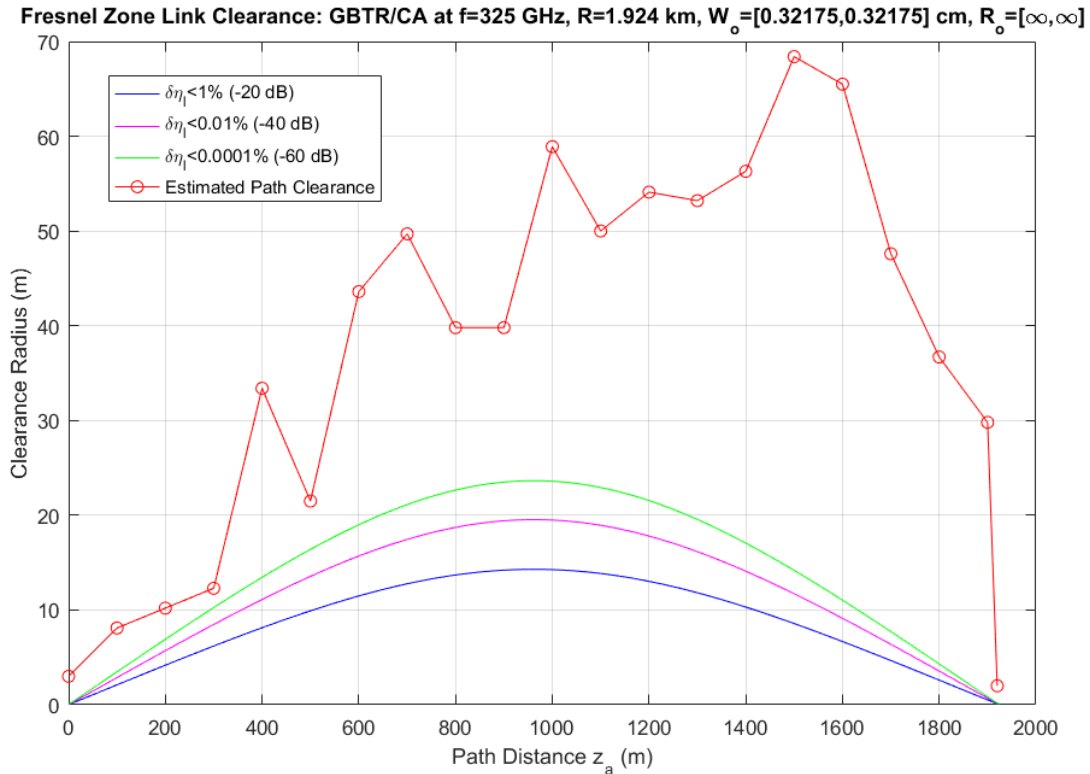


Figure 2.5. Clearance radii for a diffractive circular aperture impacting the TAIPAS link budget by less than the -20, -40, and -60 dB. The estimated TAIPAS path clearance to building tops or other ground-located scatters is shown for comparison.

2.3 Transmissometer Hardware Design

Improvements in the accuracy of propagation models by empirical measurement require attention to detail in hardware design, measurement, and data interpretation. The architecture of the transmitter/receiver and system hardware specifications must be based on the ability to measure the phase and amplitude of the received signal with excellent SNR within sampling time intervals during which the atmosphere can be considered frozen for SMMW propagation. Such a sampling interval is consistent with the Taylor frozen flow hypothesis [25] and is ~ 1 msec for typical TAIPAS path conditions. Key design issues that flow from this requirement include

transmitter power, bandwidth, phase stability, phase reference accuracy, transmitter/receiver aperture size, sampling rate, receiver noise, and required A/D sampling precision.

A phase coherent transmissometer operating over a frequency range approximately one octave higher than studied at Flatville, including both the lower and upper wings of the moderately strong water vapor resonance at 325.153 GHz and sampling greater than ~40 kHz, was deemed important to extend what was learned at Flatville. Specifically, identified hardware requirements included instantaneous phase fluctuations and the mutual coherence function over a band of frequencies ranging from the moderately strong water line lower wing at 320 GHz to the minimum of attenuation in the spectral window at 340 GHz and high phase receiver coherency and stability. Phase measurements are important in understanding refractive dispersion near water lines. Such dispersive effects are important in understanding the infrared radio dispersion with relevance to double resonance measurements of trace gases.

Overall, the innovations for which TAIPAS is capable, relative to the previous Flatville field work, thus include: 1) 40 KHz sample rates to capture temporal variations associated with above-ground, free space paths far above the 1 ms frozen time of the atmosphere; 2) high received signal-to-noise power ratios for observing low phase and amplitude standard deviations; 3) absolute receiver power calibration to a level of ~1 dB open loop; 4) preclusion of multipath from the ground by the use of high gain antennas; 5) receiver phase measurements referenced to the transmitter phase for long term total phase drift assessment; 6) an above-ground free space path representing a typical urban scenario; 7) a broad range of humidity and weather conditions;

and 8) a broad range of aerosol conditions. This section describes the hardware developments supporting these innovations.

2.3.1 Frequency Selection

Ultimately, it is envisioned that up to four frequency bands will be required for model verification of the effects of water vapor, rain, snow, fog, aerosols, and turbulence; the primary variables to be studied for future TAIPAS validation. To this end, a set of window-channel frequencies spanning nearly a decade in frequency but weighted toward the relatively unexplored SMMW bands were identified. The frequencies are, in order of interest: 320-340, 670, 495, 870, and 140 GHz. They have been selected due to their minimum attenuation, overall span of the spectrum up to ~ 1 THz, and (in the case of 320-340 GHz) their inclusion of a weak water line to study the effects of enhanced refractive variation caused by water vapor fluctuations.

2.3.2 Mechanical Design and Site Installation

The TAIPAS transmissometer is based on a single transmitter and two phase coherent receivers spaced up to ~ 8 m apart to enable measurement of the transverse coherence length (Figure 2.6). Beams are generated using a diagonal horn and lens combination on both the transmitter and receivers with approximately quadratic aperture illumination. The F-number of each antenna/lens is 1.5 (Equation 2.13). Required transmitter and receiver pointing precisions are comparable to the 3 dB beam-widths of 0.74° (Equation 2.14) and are facilitated using 3-axis caliper-adjustable micrometers with precisions exceeding 1.74 mm (Equation 2.15).

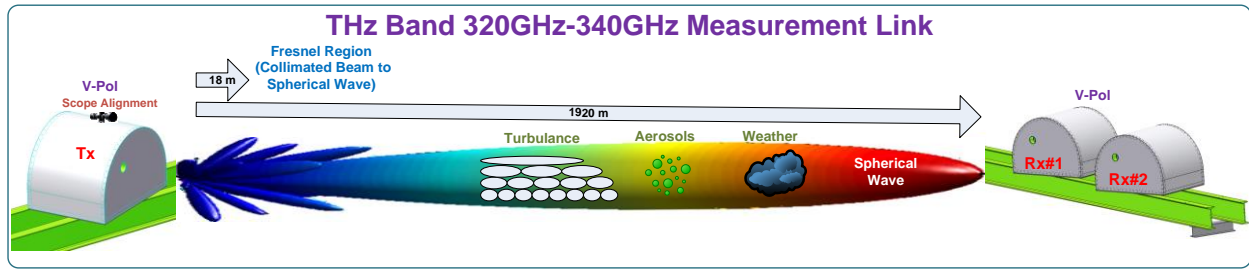


Figure 2.6. THz Transmissometer System.

$$\lambda_{center} = \frac{c}{f} = \frac{2.977 \times 10^8 \text{ m/s}}{332.5 \times 10^9 \text{ cycles/s}} = 0.9 \text{ mm} \quad (2.9)$$

$$R_{near_field} \leq \frac{2D^2}{\lambda} = 18 \text{ m} \quad (2.10)$$

$$BW_{3dB} = \frac{1.27\lambda}{D}; \text{ radians} \Rightarrow 0.75^\circ \quad (2.11)$$

$$SpotSize_{3dB} = (R - R_{far_field}) BW_{3dB} = 25 \text{ m} \quad (2.12)$$

$$F_D = \frac{f_{focal_length}}{D_{effective}} = 1.5 \quad (2.13)$$

$$TX_{pointing_precision} = \frac{Spot_Size_{3dB}}{R} = 0.74^\circ \quad (2.14)$$

$$TX_{FP_position} = TX_{point_prec.} \times Dia_t \times F_D = 1.74 \text{ mm} \quad (2.15)$$

Figure 2.7 depicts a mechanical block diagram of the housing scheme, which is designed with sufficient mechanical stiffness to preclude wind-driven dimensional variations in the path length as small as $\sim \lambda/100$ at the future frequency of 670 GHz (Equation 2.16 and Equation 2.17)

and thermal-induced variations. The housing system includes an aerodynamic outer shell which reduces wind loading on the inner housing, which contains the transceivers. The housing maintains a temperature and humidity-regulated environment for the transceivers along with protecting the equipment from rain, snow, large animals, and humans. The lenses are fixed to the housing body while the receiver, transmitter feeds and microwave hardware are mounted on a three-axis caliper, adjustable platform to allow proper alignment with the lens and limited beam steering. An air-conditioning unit regulates the temperature of the interior chamber and minimizes humidity. The A/C unit is remotely turned off during data collection to minimize the impact of compressor vibrations on the path length. The housing is clamped to heavy dual I-beams for mechanical stabilization. The outer shell is clamped to a separate set of beams for isolation purposes.

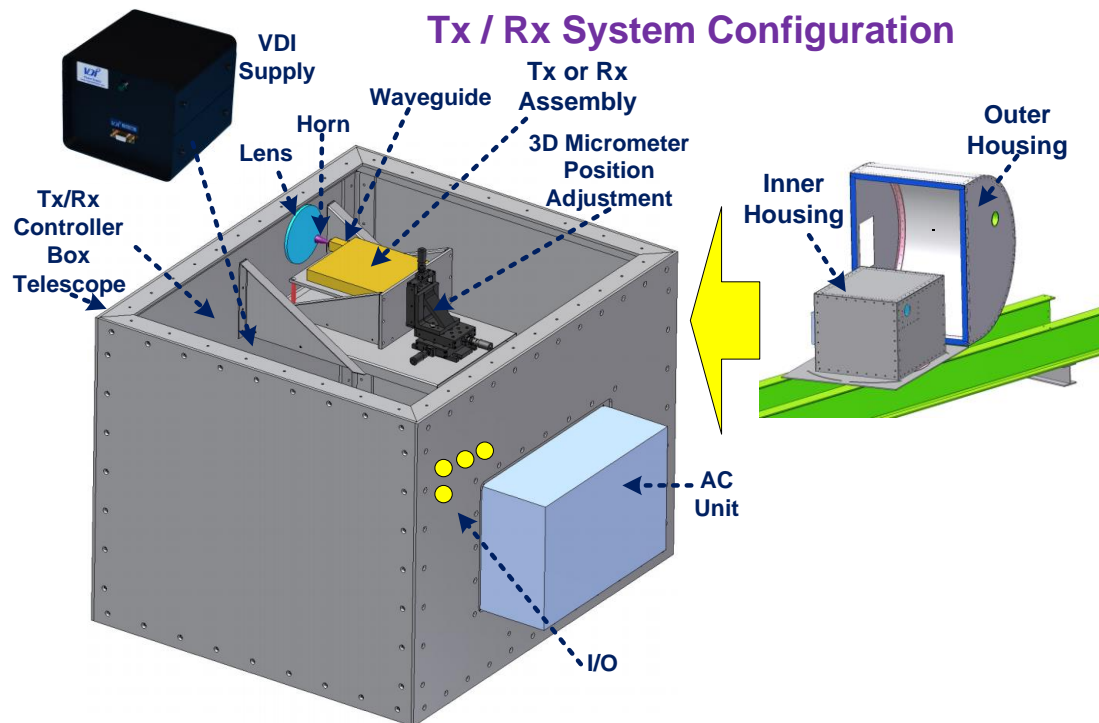


Figure 2.7. Rendering of the TAI PAS transmitter and receiver housing.

$$\text{Lens / Feedhorn Vib Limit} : \frac{\lambda}{100} = 4.5 \mu\text{m} \quad (2.16)$$

$$\lambda_{670\text{GHz}} = \frac{2.998 \times 10^8 \text{ m/s}}{670 \times 10^9 \text{ cycles/s}} = 0.45 \text{ mm (Future)} \quad (2.17)$$

The shell and housing structure were designed and fabricated to meet wind loads for gusts of up to 50 m/sec (~100 kts). Since the cross-sectional area of the box holding the equipment is ~ 1 square meter, the maximum gust force will be $\frac{1}{2} \rho v^2 \sim 1300 \text{ N}$ (~300 lbs.), where $\rho \cong 1.05 \text{ kg/m}^3$ is the air density in Boulder, Colorado. Using a lever arm of ~ 0.5 m, the resulting torque requirement on the outer beams is thus ~ 650 N-m or ~ 475 lb.-ft.

$$\text{Max_Gust_Torque} = \text{torque_lever} \times \frac{1}{2} \rho v^2 \times \text{Area} \quad (2.18)$$

This calculation drove the design of the system to have the housing supported on two inner I-beams and the shell to cover the housing, but supported on its own two outer I-beams; the shell was also designed with a small as possible wind cross section. Photos of the container components at the Mesa and CU sites are shown in Figure 2.8 and Figure 2.9, respectively. The Mesa receiver site utilized existing concrete pads while the CU site leveraged the CET metal grating deck for support of all equipment.



Figure 2.8. TAIPAS receiver wind resistant shells at the Mesa site.



Figure 2.9. TAI PAS transmitter wind resistant shell at CU rooftop site along with inner and outer I-beams.

Figure 2.10 shows the inner housing mounting baseplate. One of these plates exists at each of the CU rooftop and Mesa systems. For each plate, the slotted bolt circle is tied to the inner I-beams and can rotate in azimuth without mechanical connection to the outer shell. The outer plate is attached to the outer I-beams and rotates in azimuth independently.



Figure 2.10. TAI PAS housing and shell mechanical isolation plate system.

Figure 2.11 shows the receiver site at the top of the Mesa as seen from behind the receivers looking toward the transmitter. Precise phase referencing for coherent reception is achieved

using a line-of-site HF (40.7 MHz) coherent (“Coho”) link, for which the vertical dipole antenna is encased in Poly Vinyl Chloride (PVC) pipe. The Coho antenna is suspended with three ropes attached to anchors via springs to adjust the pull strength. Receiver 1 (Rx1) is on the left with Receiver 2 (Rx2) on the right. The two pairs of I-beams are tilted down toward the transmitter by 3.61° using standoffs to align the receivers along the downward sloping path. Figure 2.12 shows the NTIA power panel and high-voltage warning stickers used to discourage tampering by hikers.

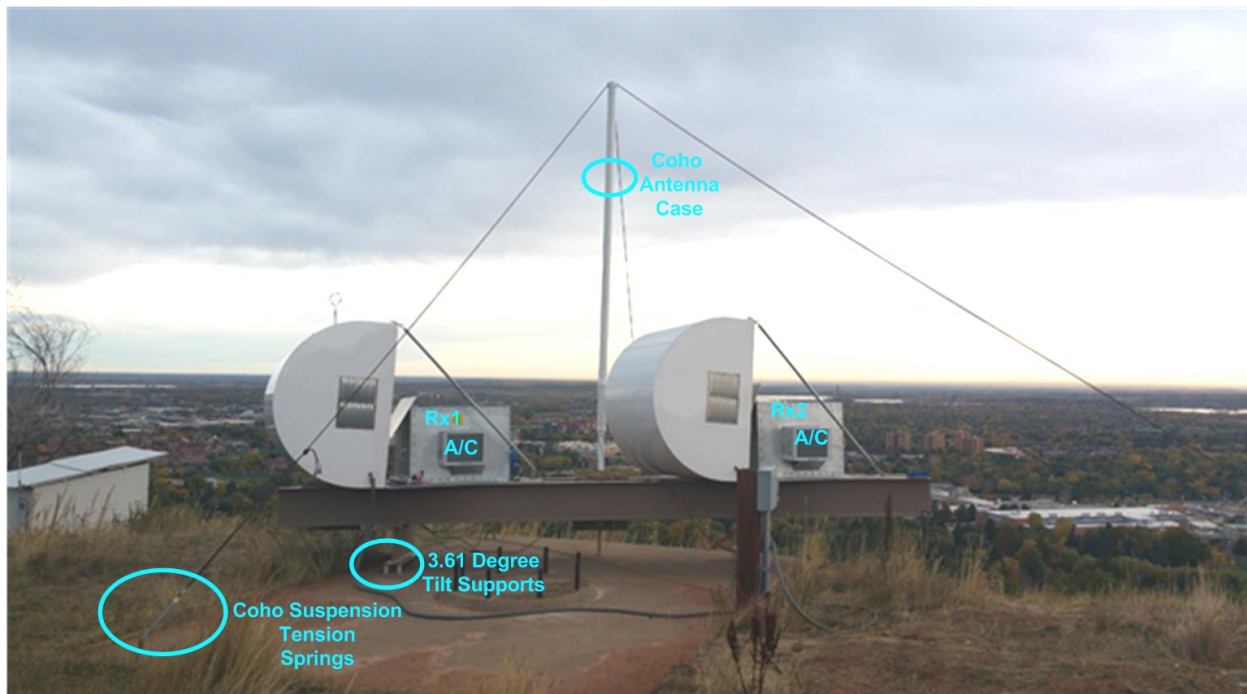


Figure 2.11. TAI PAS receivers as viewed from behind looking toward the transmitter.



Figure 2.12. TAIPAS receivers as viewed behind looking toward the transmitter.

Figure 2.13 shows a front view of the Rx2 shell. The 320-340 GHz lens antenna is located within a ~12 cm long PVC cone of full angle 30° that serves to preclude debris or small animals from entering the gap between the shell and housing. A ~20 cm (8") diameter optical telescope aperture used for the scintillometer is at the bottom right; foam is inserted to seal the telescope to the shell. Figure 2.14 shows a photo of the transmitter on the CU rooftop taken from the Mesa site.



Figure 2.13. TAIPAS Rx2 viewed from the front showing the 320-340 GHz aperture (upper left) and optical telescope aperture (lower right).



Figure 2.14. View along the TAIPAS path from the Mesa receiver site to the CU rooftop transmitter.

Figure 2.15 shows the transmitter system on the CU ECEE building rooftop. The aluminum standoffs in the front align the transmitter upward by 3.61° to be coincident with the TAIPAS path to the receivers. The suspension lines for the Coho transmitter antenna use springs to maintain proper tension. The rooftop seatainer houses a laptop PC that permits operating the system remotely. A photo of the network communications system antenna and meteorological sensor package at the transmitter site are shown in Figure 2.16. The upper sensor is the sonic anemometer with its open circles aligned axially toward the receivers so the U-component of wind speed is in the direction of the path. The next sensor down is the Lyman alpha hygrometer, mounted horizontally to limit the settling of dust on its optical surfaces. A commercial 802.11n wireless antenna and electronics package provides a C-band network communications link between the CU rooftop and Mesa sites. Figure 2.17 shows the Mesa receiver site as viewed

from the CU rooftop transmitter site, and Figure 2.18 shows a zoomed view of the receivers from the transmitter location.

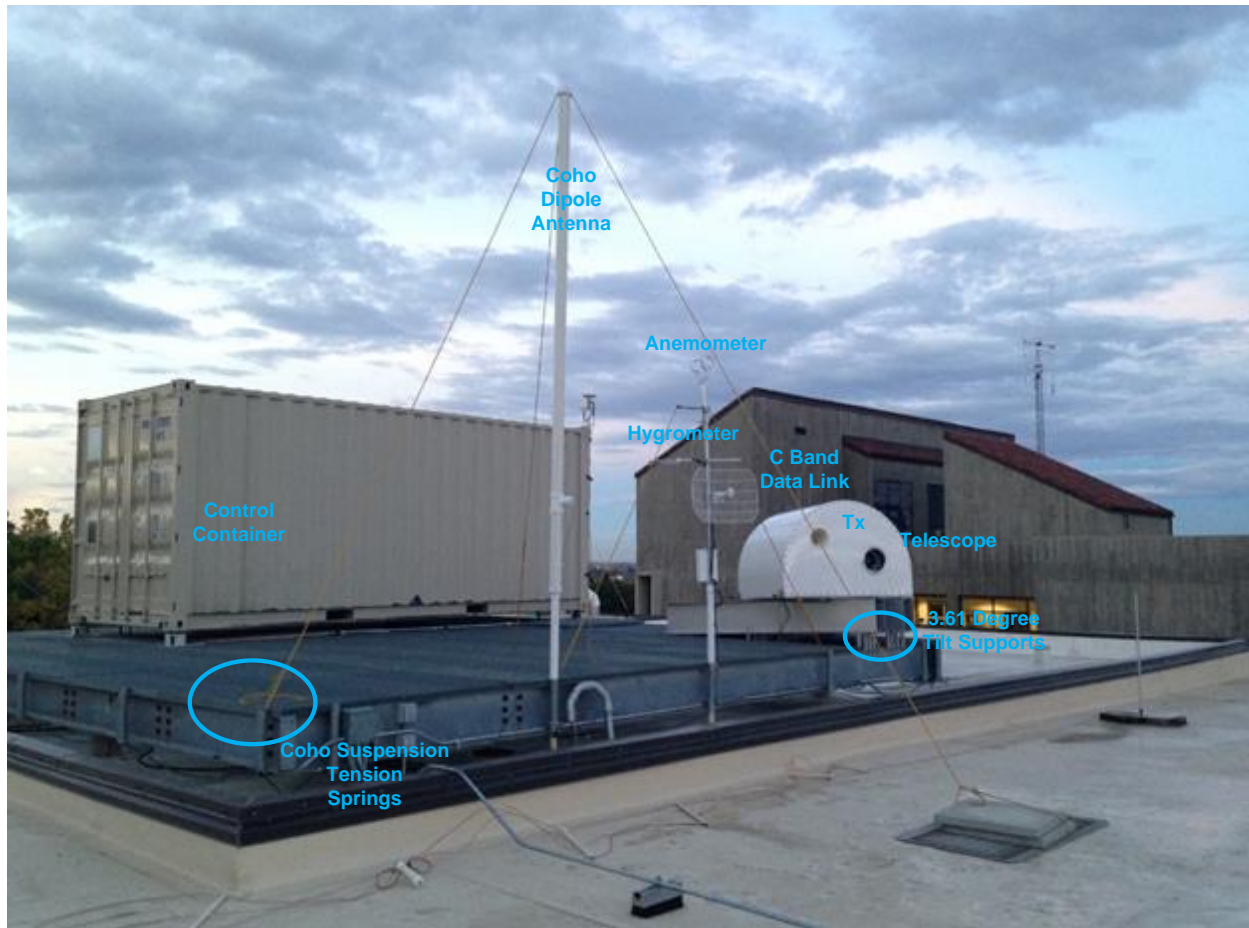


Figure 2.15. Photo of TAIPAS transmitter system on the CU ECEE rooftop.



Figure 2.16. TAIPAS transmitter site communication and environmental sensing package.



Figure 2.17. TAIPAS Mesa receiver site as viewed from the CU rooftop transmitter site.



Figure 2.18. Zoomed image of the TAIPAS Mesa receiver site.

Figure 2.19 illustrates black paint on the front face of the Rx1 shell to improve the contrast of the optical scintillometer. Observations of LEDs using the scintillometer telescope at the transmitter end were compromised by the early morning sun reflecting specularly from the initially white panel on which the LEDs were located. The non-reflective paint significantly improved scintillometer contrast and permitted continuous operation. The photos in Figure 2.20 show the general path, terrain, vegetation, and buildings near the transmitter and receiver.



Figure 2.19. TAIPAS Rx1 receiver with shell face painted black to minimize sun reflections. Also shown is the C-band network link antenna.



Figure 2.20. Satellite images of TAIPAS path and vicinity of the receiver and transmitter sites.

Figure 2.21 shows the battery-powered laser-siting system developed to validate the alignment of the TAIPAS housings. The beam from a red laser diode — VLM-635-01-LPA from Quarton, Inc. — mounted at the end of a 76 cm pipe is aligned along the pipe axis using a temporary pinhole aperture of diameter ~ 0.76 mm at the other end of the pipe. The pipe with the laser is subsequently aligned with the TAIPAS transmitter and receiver housings. Some shimming up to ~ 1.5 mm was used to facilitate precise alignment (Figure 2.22). The final precision of the beam alignment, with respect to the TAIPAS housing faceplate, was estimated as $\sim 0.06^\circ$, or about twice the specified laser beam divergence of 0.5 mrad and about one tenth of the TAIPAS SMMW antenna beamwidth. Table 2.1 provides performance calculations for the laser and siting system. At less than 5 m distance, long-term exposure from the 3 mW laser can damage the eye, however, it is eye-safe for direct long-exposure viewing at distances greater than 20 m. Along the 1924 m TAIPAS path, the viewer intensity using a 50 mm diameter scope is $\sim 2.7\%$ of the threshold power density for eye safety. However, during low sun brightness it is easily detectable at this range with the unaided eye.

During alignment, the laser was visible from the opposite end of the path as a point source across a ~ 3 -meter transverse horizontal range (Figure 2.23). Observation of the spot centroid was used to adjust the azimuth and elevation of the housings by rotating the housing on its mounting base plate or shimming the housing standoffs using washers; up to 3 mm of washer shim thickness was required for housing alignment.

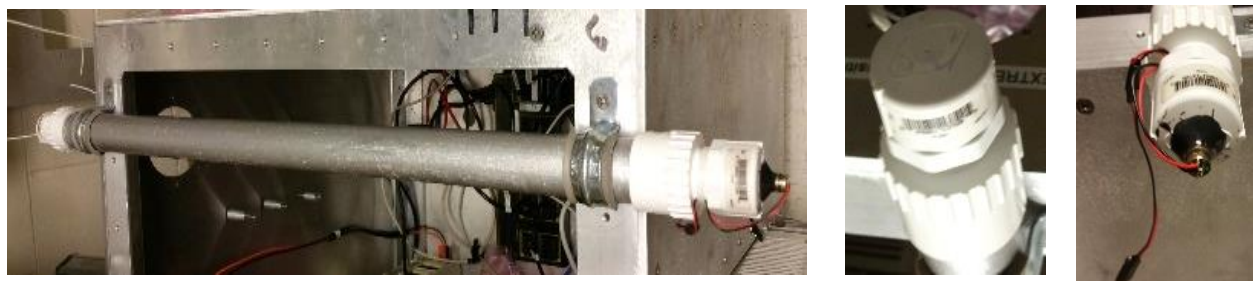


Figure 2.21. TAIPAS laser alignment system components.

Table 2.1. Laser siting system performance calculations.

Laser/Spotting scope performance/safety calculations			
Laser part number		VLM-635-01-LPA	Quarton, Inc.
Laser power	mW	3.0	
Laser wavelength	nm	635	
Beam divergence	mrad	0.5	
Spot size at 5 m	mm	5.00	
Voltage	V	4.00	
Current	mA	50	
Power (DC input)	mW	200	
Distance	km	1.90	
Spot size at distance	m	0.95	According to beam divergence spec
Spot size at distance	m	1.90	According to empirical beam spot size spec
Effective source aperture diam	mm	1.651	According to beam divergence spec
Far zone distance	m	8.59	
Laser siting tube length	inches	30.0	
	m	0.762	
Siting tube pinhole aperture di	mm	0.762	
	inches	0.030	
Power density at 5 meters	mW/cm ²	1.53E+01	According to empirical beam spot size spec.
Power density at 20 meters	mW/cm ²	9.55E-01	According to empirical beam spot size spec.
Power density at distance	mW/cm ²	4.23E-04	According to beam divergence spec.
Spotting scope aperture diame	mm	50.0	
Spotting scope received power	mW	8.31E-03	
Spotting scope magnification	(--)	8.0	
Spotting viewer's intensity	mW/cm ²	2.71E-02	
Maximum long duration expos	mW/cm ²	1.0	400-700 nm band long exposure power density limit for eye safety.

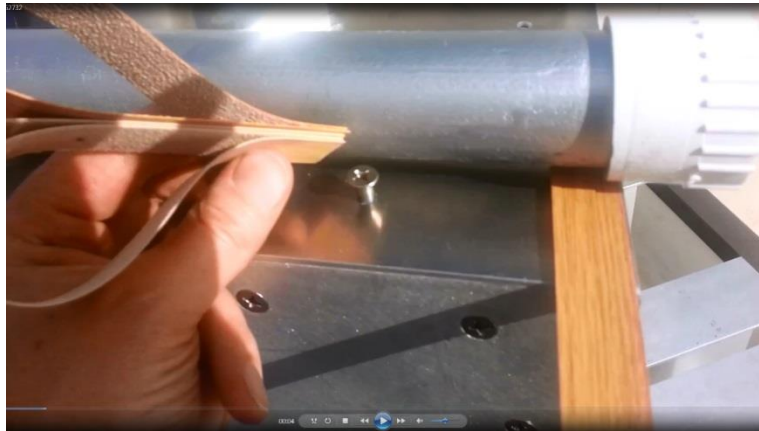


Figure 2.22. TAIPAS laser siting system shimming.

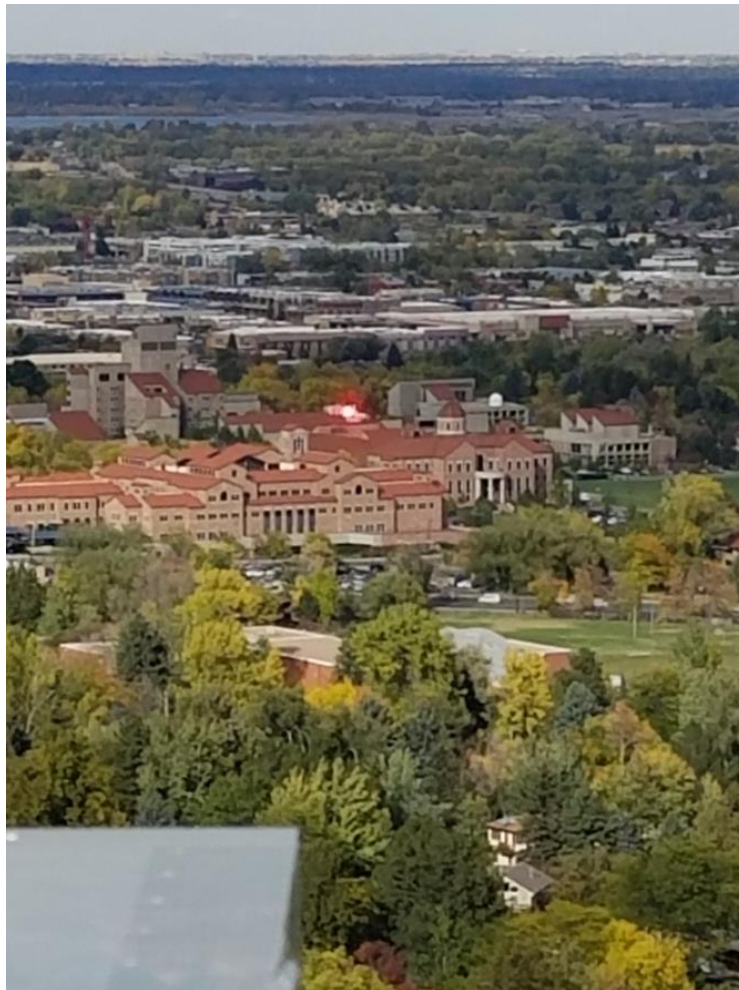


Figure 2.23. TAIPAS laser siting source located on CU rooftop as viewed from the Mesa site.

Figure 2.24 shows an inner housing with the air conditioning unit installed. The spacing of the screws that bolt all six sides of the container, shown on the right, is ~ 11 cm (4.3") or less. Using a $\lambda/8$ slot radiation criterion, this spacing precludes Radio Frequency Interference (RFI) leakage into the housing through wall gaps up to ~ 340 MHz. Other leakage paths through (e.g. power lines) exist, however, thus Electromagnetic Interference (EMI) decoupling of RF components within the housing was carefully practiced.



Figure 2.24. TAIPAS transceiver housing interior.

Figure 2.25 shows the feed-horn / lens antenna position adjustment system implemented for both the transmitter and receiver antennas. The system uses Vernier micrometers (Standa 7T38XYZ) with a total range of 15 mm on each axis and repeatable adjustment precision of 2 μm . For a focal length of 13.5 cm, the system provides ~ 13 μrad beam steering precision, or approximately one-thousandth of a beamwidth. One full micrometer turn steers the beam by ~ 0.5 3-dB beamwidths. Table 2.2 lists the input and output bulkhead connectors and their intended functions as installed on each housing. Figure 2.26 details the DB9 bulk head connector pins used to support the hygrometer and anemometer. The anemometer and hygrometer utilize a common DB9 feed through for power. A second DB9 feed through is utilized solely by the hygrometer.

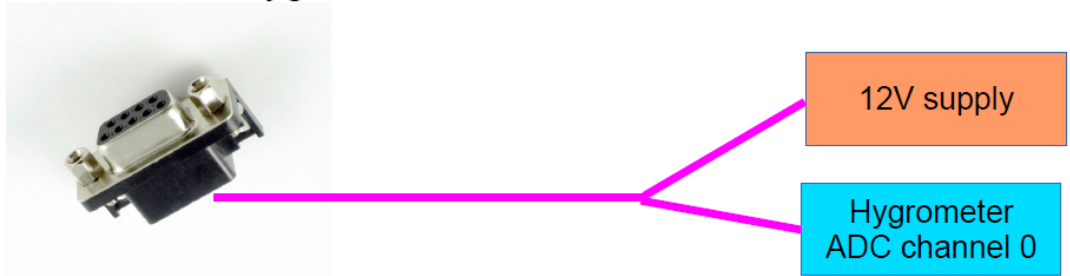


Figure 2.25. TAIPAS 3-axis feedhorn/lens position adjustment system.

Table 2.2. TAIPAS bulkhead connectors and functions.

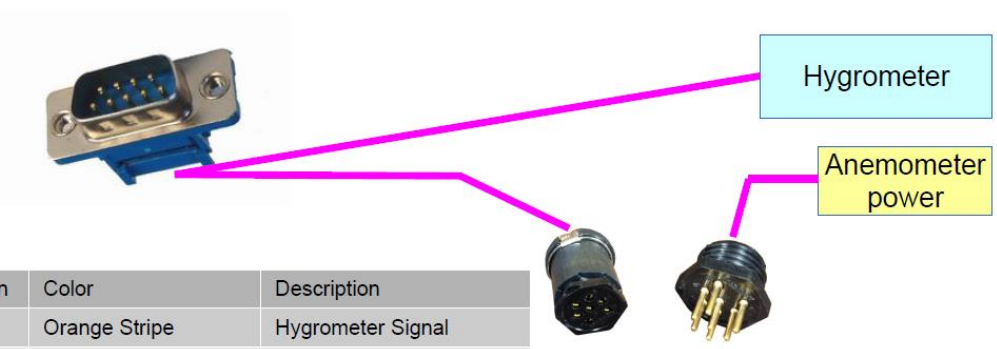
TAIPAS Bulk Head Connectors									
Transmitter Signals		Connector type							
120V		120V standard plug recepticle with switch (switch could be seprate if it is easier)							
Hygrometer		Four pin wire capable connector							
Anemometer		USB Gen-2							
Coho Dipole		SMA (2X) need expanzion to circular polarization							
1Gb Ethernet		RJ45 or similar to handle CAT6							
Data Link		USB Gen-2							
Snytehsizer Test point		SMA(1X)							
Video		VGA							
Keyboard/mouse		USB - Gen 2							
Camera		USB - Gen2							
Receiver #1 Signals		Connector type							
120V		120V standard plug recepticle with switch (switch could be seprate if it is easier)							
Hygrometer		Four pin wire capable connector							
Anemometer		USB Gen-2							
Coho Dipole		SMA (2X) need expanzion to circular polarization							
1Gb Ethernet		RJ45 or similar to handle CAT6							
Data Link		USB Gen-2							
Snytehsizer Test point		SMA(1X)							
Video		VGA							
Keyboard/mouse		USB - Gen 2							
Camera		USB - Gen2							
RF Clk to Rx2 - 10 MHz		SMA							
Synthesize Rx2 control		USB							
Scintillometer LED Pwer		Two pin power connetor that can supply low voltage (5V-14V)							
1 MHz IF Data from Rx2		SMA							
Receiver #2 Signals		Connector type							
120V		120V standard plug recepticle with switch (switch could be seprate if it is easier)							
Anemometer		connector in CET lab - check equipment							
Snytehsizer Test point		SMA(1X)							
RF Clk from Rx1 - 10 MHz		SMA							
Synthesize Rx2 control		USB - (prefer printer type USB, but any acceptable)							
1 MHz IF Data to Rx1		SMA							

Hygrometer Cable Inside of Box



Pin	Color	Description
1	Orange Stripe	Hygrometer Signal
2	N/C	
3	N/C	
4	White	+12 V for Hygrometer
5	White	+12 V for Anemometer
6	Blue Stripe	Hygrometer Return
7	Shield – Black Stripe	Hygrometer Shield
8	Green Stripe	Ground for Hygrometer
9	Green Stripe	Ground for Anemometer

Hygrometer Cable Outside of Box



Pin	Color	Description
1	Orange Stripe	Hygrometer Signal
2	N/C	
3	N/C	
4	White	+12 V for Hygrometer
5	White	+12 V for Anemometer
6	Blue Stripe	Hygrometer Return
7	Shield – Black Stripe	Hygrometer Shield
8	Green Stripe	Ground for Hygrometer
9	Green Stripe	Ground for Anemometer

Pin	Color	Description
A	N/C	
B	N/C	
C	N/C	
D	White	+12 V for Anemometer
E	Blue Stripe	Ground for Anemometer

Figure 2.26. TAIPAS bulkhead feedthrough for the hygrometer and anemometer.

2.3.3 RF Transceiver Hardware

Devices that provide THz gain and up/downconversion capabilities include active devices such as Indium Phosphide (InP) high electron mobility transistors (HEMTs) and passive devices such as Schottky barrier diodes. Schottky diodes are commonly used for square law power detection. It is difficult to develop transistors and diodes at TAIPAS frequencies due to parasitic losses and junction capacitances, both of which limit the transition frequencies of these devices. Improvements have been steadily increasing the transition frequency for Si CMOS, SiGe, and III-V HEMT devices since 2005 (Figure 2.27). IMPATT (IMPact Avalanche Transit Time) diodes, Gunn diodes and Resonant Tunneling Diodes (RTD) along with chains of nonlinear multipliers based on these diodes and amplifiers can generate THz signals. The technology for solid state THz signal generation exhibits a major “THz gap” (Figure 2.28) that remains as of this writing. The U.S. Defense Advanced Research Projects Agency (DARPA) has supported the development of THz InP-based Monolithic Microwave Integrated Circuit (MMIC) low noise amplifier (LNA) and heterodyne receiver and detector development at Teledyne Technologies, Inc. and the Northrop Grumman Corporation, but at this time, these devices are not readily available nor affordable for TAIPAS.

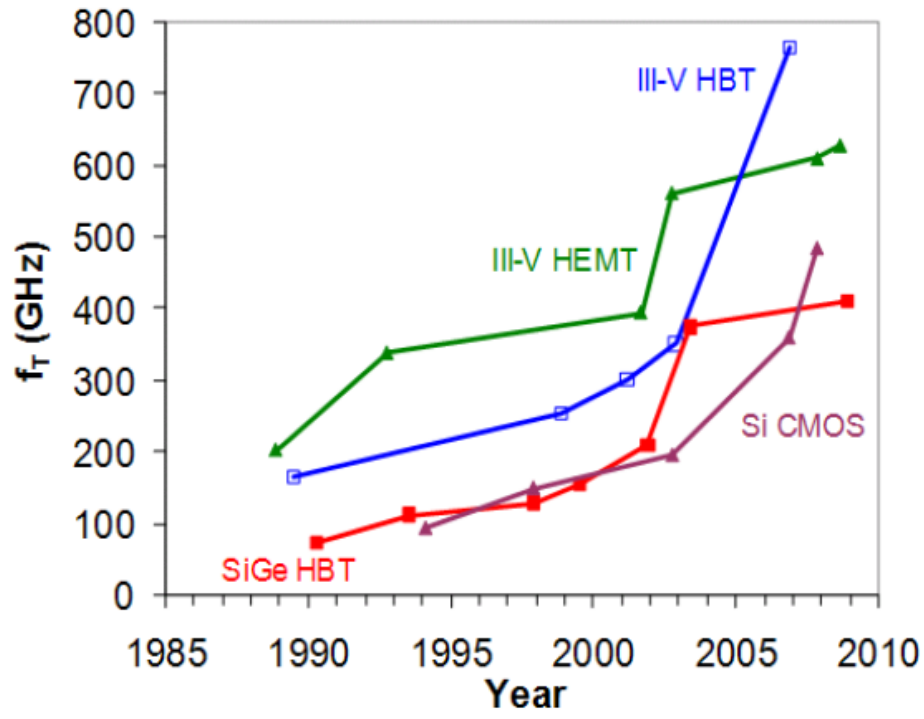


Figure 2.27. THz solid state amplifier transition frequency advancements.

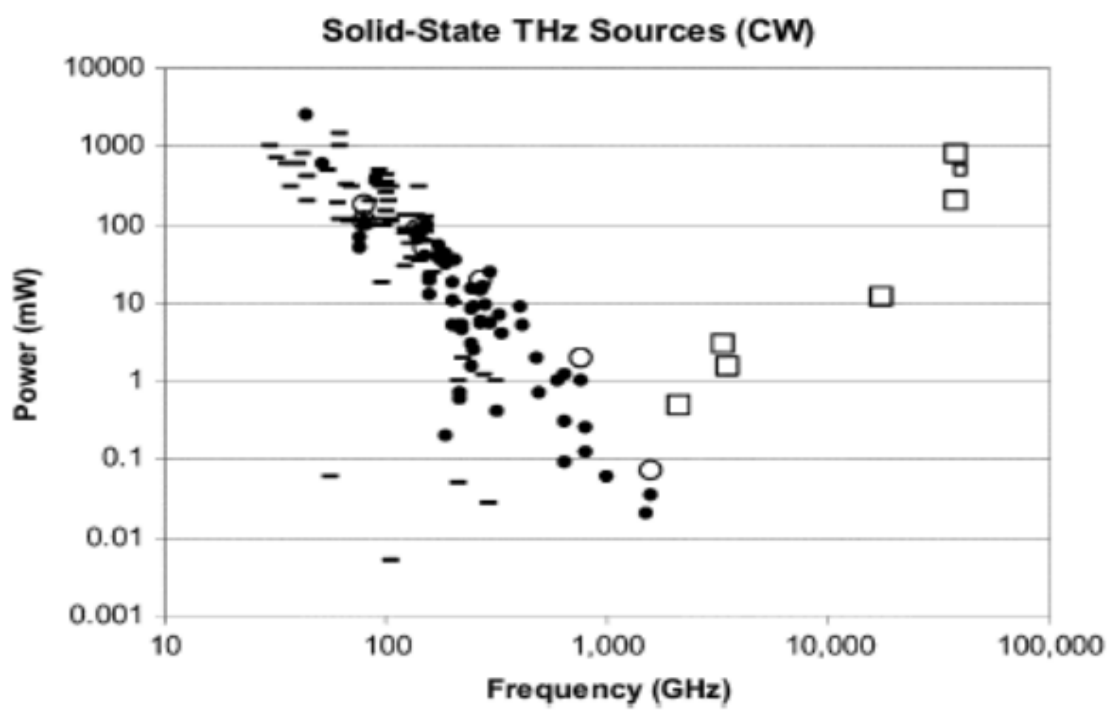


Figure 2.28. THz output power versus frequency from various sources [55].

Vacuum Electronics (VE) for THz had intense development in the last decade. DARPA funded the High-Frequency Integrated Vacuum Electronics (HiFIVE) 2005 program which resulted in a Traveling Wave Tube (TWT) amplifier with 3 - 5.5% efficiency over 30% bandwidth. In 2009, DARPA funded \$37M toward a Phase I THz electronics contract for development of active receivers and transmitters at 670 GHz — extension of the Sub-millimeter Wave Imaging Focal Plane Technology (SWIFT) program. Northrop Grumman has a VE THz source-based Folded Waveguide (FWG) as part of DARPA's THz Imaging Focal Plane Array Technology (TIFT) program; several sources from 0.605 and 0.675 THz are at RF power levels up to 52 mW at duty cycles of 3%. LEIDOS and the Naval Research Laboratory (NRL) are also developing these tubes; 50 W at 220 GHz has been demonstrated.

DARPA is funding a number of technologies for next generation Transmit/Receive (T/R) modules for sensor and communication systems: waferscale integration under Wide Band Gap Semiconductors for RF Applications (WBFS-RF) program; Scalable Millimeter Wave Architectures for Reconfigurable Transceivers (SMART) program; Integrated Sensor Is Structure Critical Technology Demonstration (ISIS-CTD); and SWIFT program using Gallium Nitride (GaN) and MMIC technologies. DARPA has also funded a sub 50 nm InP HEMT Device with $F_{\max} > 1$ THz: 1.1 THz with $f_T = 385$ GHz, which was demonstrated with a three-stage common source LNA MMIC amplifier with 18 dB gain at 300 GHz and 15 dB gain at 340 GHz [54].

A project called Nanoelectronic Initiative produced GHz and THz Amplifier and Oscillator Circuits with one-dimensional (1D) nanoscale devices for Multispectral Heterodyning Detector

Arrays and measured kinetic inductance and plasmonic waves of 1D conductor using carbon nanotubes and quantum wires and Gallium Arsenide (GaAs) / Aluminium Gallium Arsenide (AlGaAs) as the 1D conductor. The single-walled nanotube and on chip transmission lines exploited kinetic inductance and plasmonic waves to build amplifiers [54].

Due to funding and availability, it was required to develop TAIPAS utilizing Commercial-off-the-Shelf (COTS) THz technologies. Virginia Diodes (VDI) was selected since they are primarily the only game in town. There are other companies that integrate receivers and exciters at these frequencies, but they leverage VDI technologies; therefore, it was decided to go with VDI equipment, shown in Figure 2.29. The power supplies were provided with each component since they drive part of the calibration data provided. The cost of this package exceeded \$100K.

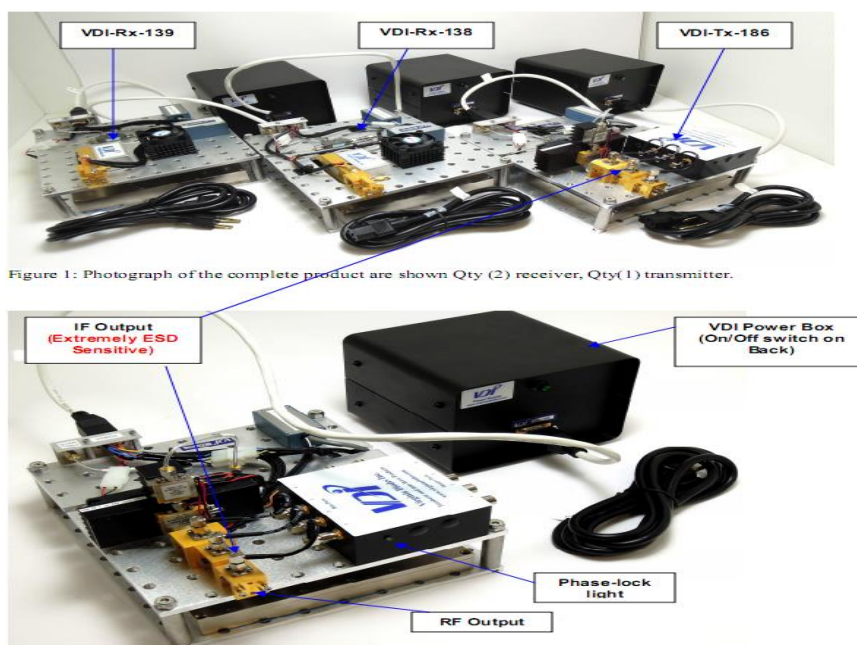


Figure 1: Photograph of the complete product are shown Qty (2) receiver, Qty(1) transmitter.

Figure 2.29. VDI Supplied Technologies for TAIPAS [53].

2.3.4 THz Transmitter

The transmitter portion of the radio link, purchased from VDI, is implemented using a state-of-the-art, coherent SMMW technology based on a precision synthesizer and multiplier / amplifier chain providing a high link SNR. The power across the frequency band varies in the 10 - 12 dBm range. The programmable synthesizer, driven by a 10 MHz signal from an Oven Controlled Crystal Oscillator (OCXO), produces a signal at the low end of Ku band (~13 GHz). In the future, utilizing a higher frequency OCXO will help reduce phase noise (e.g. 100 MHz). The system was designed to be capable of scanning from 320 - 340 GHz. Figure 2.30 shows a photo and block diagram of the transmissometer transmitter. Figure 2.31 shows a side view photo. The transmitter utilizes the 10 MHz Wenzel oscillator and a digitally controller frequency synthesizer to feed a 24X Amplifier-Multiplier Chain (AMC). The data sheets for these devices are in Appendix B. There is a coupler port provided to allow monitoring of the Ku band synthesizer signal. Attenuation control and modulation input are set by VDI. Universal Serial Bus (USB) is utilized to control the synthesizer; software developed controls the transmitter. The 10 MHz coupler provides the signal for the coherent (Coho) dipole transmitter, which in turn drives the receiver's synthesizer reference; the receiver OCXO was removed and the synthesizer reference is driven from the Coho receiver.

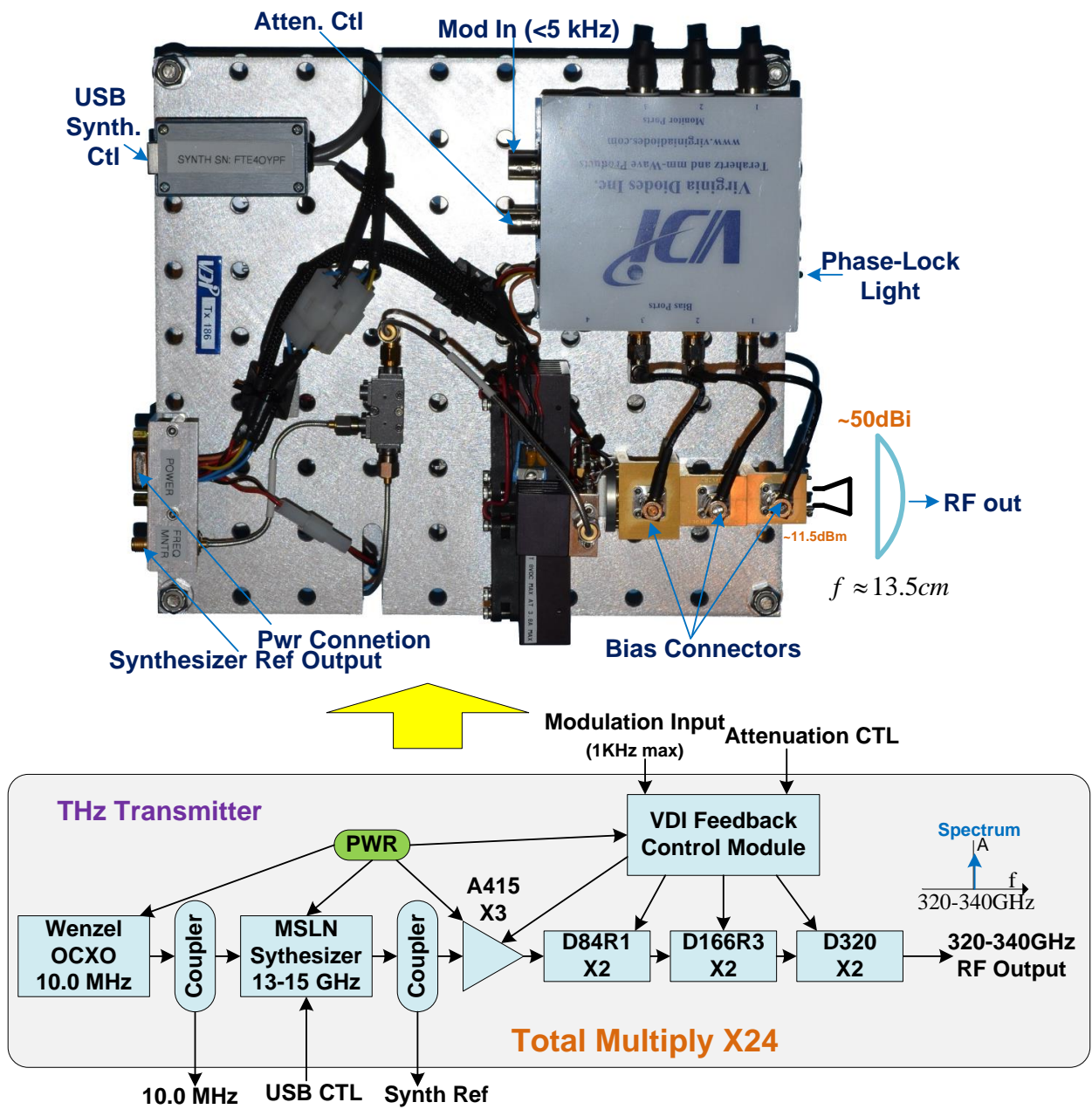


Figure 2.30. VDI Supplied Transmitter Top View and Block Diagram.

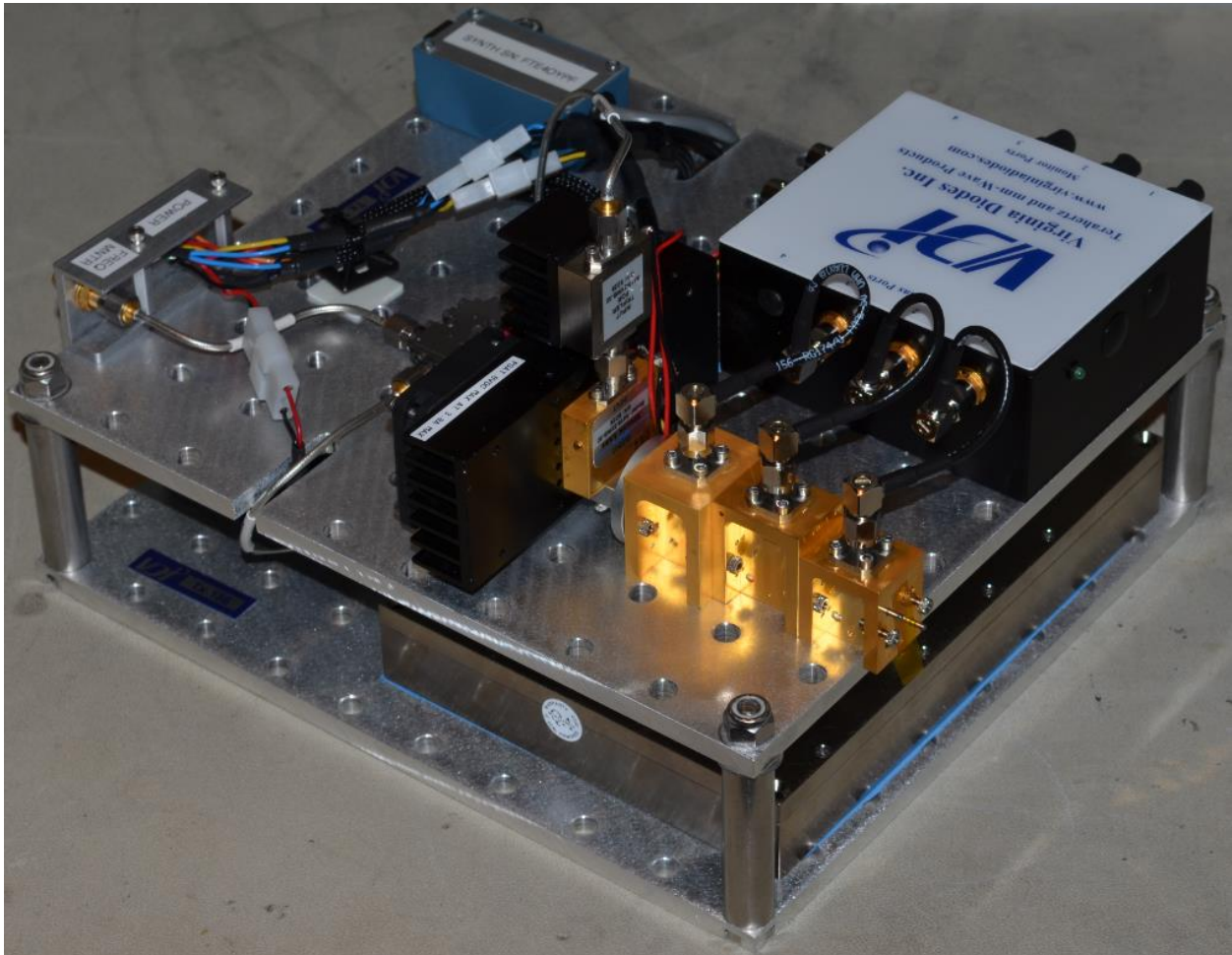


Figure 2.31. VDI Supplied Transmitter Side View.

Due to cost and available technology, the Micro Lambda MLSN-1214 digitally controlled synthesizers chosen have switching / tuning times of 10 - 12 ms, depending on the magnitude of frequency change; these are slower than the atmosphere frozen time of 1 ms. Advancements will be made in the next couple of years by utilizing new EM Research's Direct Digital Synthesizers (DDS) with 6 μ sec switching/tuning capability — ~\$14K cost. The MLSN synthesizers have a 1 Hz step size and phase noise of -102 dBc/Hz at 10 kHz offset. This is also improved with the new DDS synthesizers. TAIPAS utilizes a very small portion of the 12 - 14 GHz tuning range: 13.333 – 14.1666 GHz. The highest frequency generates 340 GHz and is

slightly over the specified frequency range; Micro Lambda stated this would work and was verified in the lab. The digital control of the synthesizer is implemented through an FTDI/FT245 chip that converts USB signals to a five-wire bus. This bus is driven through USB via TAIPAS software controller at a baud rate of 9600 b/s.

2.3.5 THz Receiver

Figure 2.32 and Figure 2.33 show photos and block diagrams of the transmissometer THz receiver. The receiver utilizes a coherent local 10 MHz signal from the transmitter as a reference to a digitally-controlled synthesizer that feeds an AMC and drives a sub-harmonic pumped mixer LO to convert the received IF to 1 MHz.

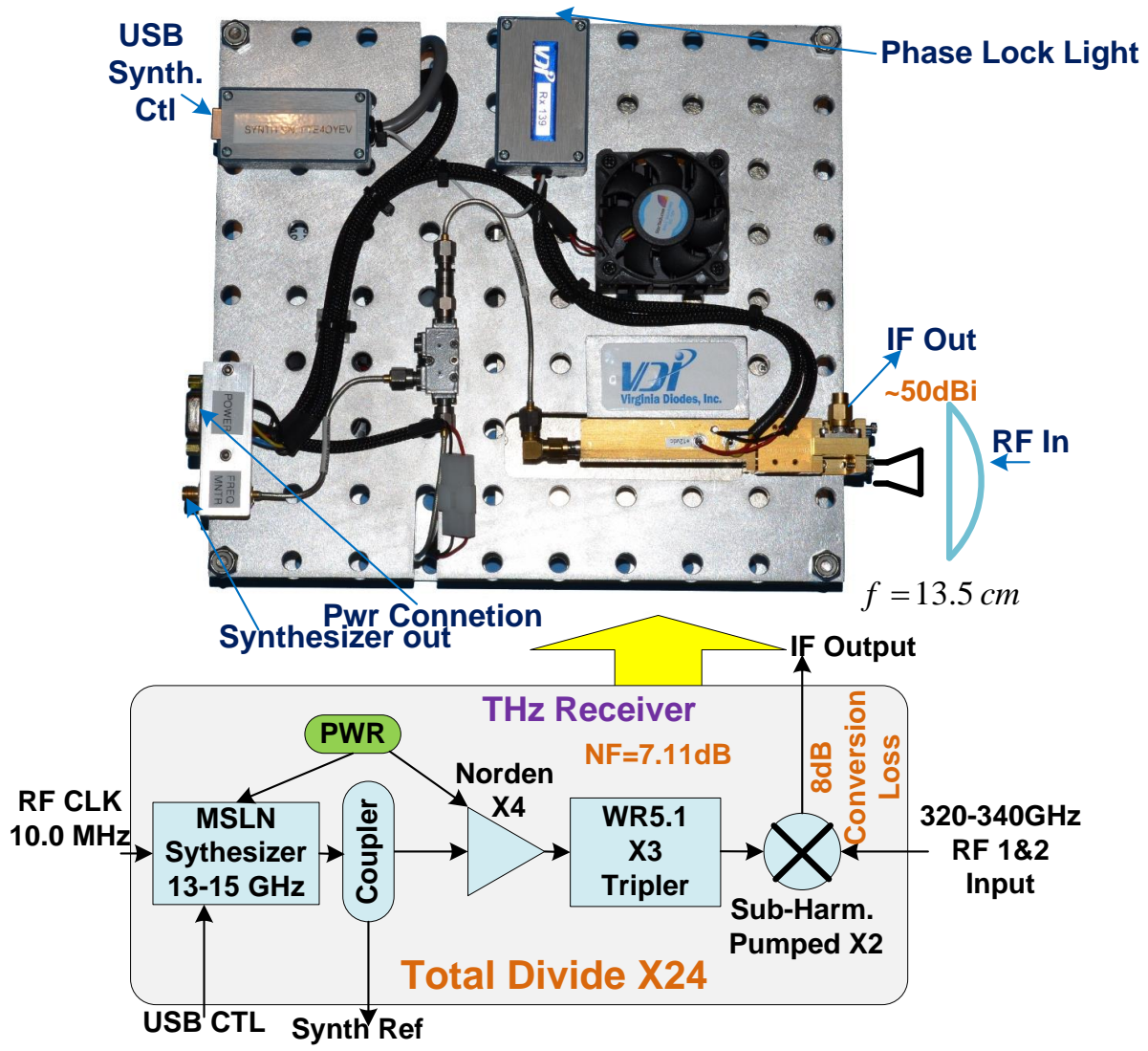


Figure 2.32. TAIPAS THz Receiver Block Diagram and Photo.

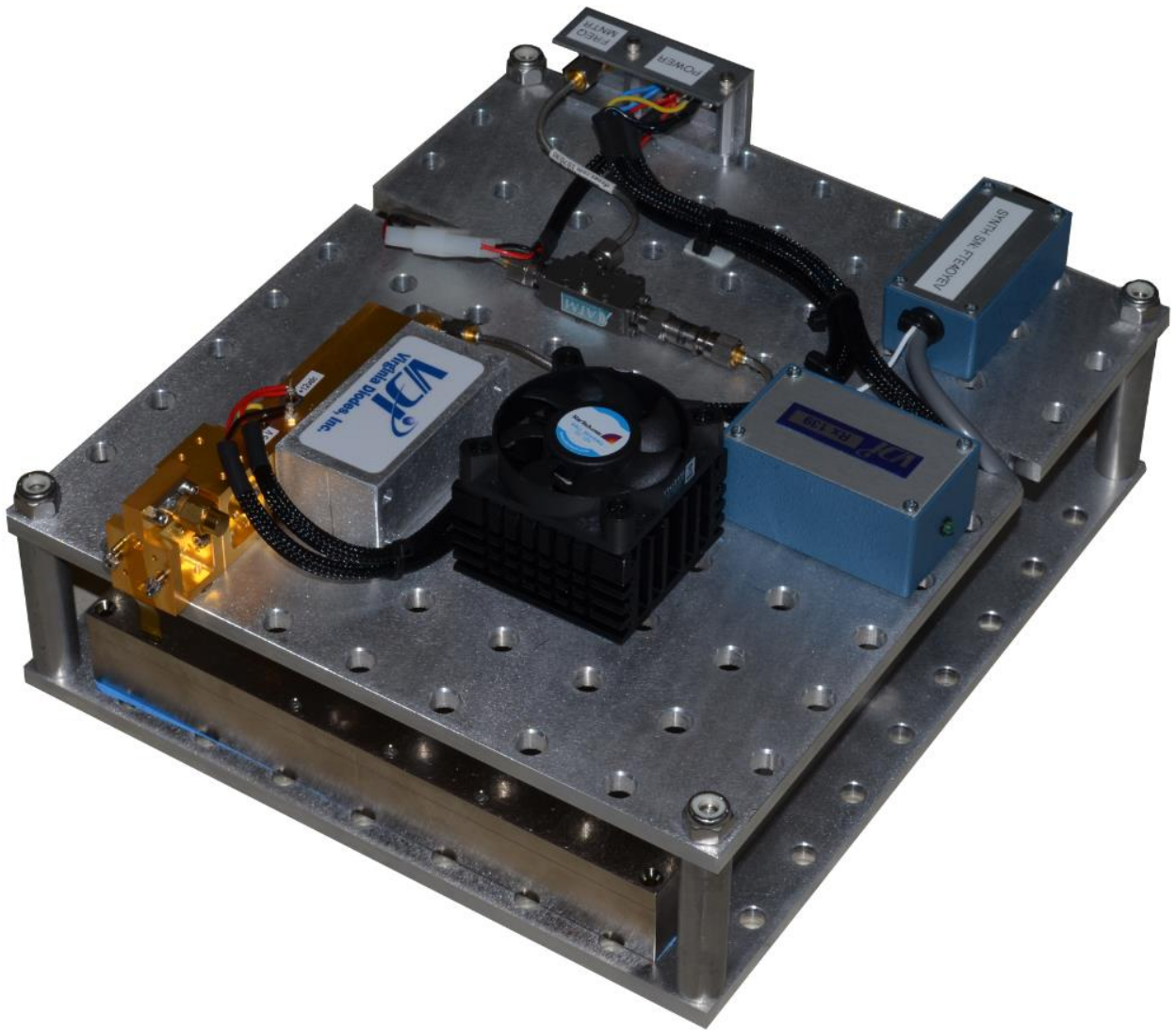


Figure 2.33. TAI PAS THz Receiver Photo.

Figure 2.34 shows a diagram of the signal conditioning from the THz receiver to the Analog-to-Digital Converter (ADC). A lumped element L-C Low Pass Filter (LPF) is utilized to remove the image frequency and noise above 2.3 MHz modeled — 1.9 MHz hardware; insertion loss, $(-20 \log(|S_{21}|))$ dB, of -0.3 dB. The LPF is followed by a 78.5 dB gain block; the gain is set to toggle the Least Significant Bits (LSBs) with the noise floor on a 16-bit ADC when a 50 Ohm

load is driven. The anti-aliasing Band Pass Filter (BPF) passes a 10 KHz bandwidth centered at 1 MHz with an insertion loss of -7 dB. The noise floor is made up of the thermal noise plus the noise figure (F). The noise temperature of the system ranges from 700 – 1100 K: noise figure as a function of temperature (Equation 2.19) and the thermal noise floor is shown in Equation 2.20. For example, the noise floor of the THz receiver only at 331 GHz is 3.4-3.7 dB. The total noise figure of the receiver is 13.3 dB.

$$F = \frac{T_{room} + T_{Rx}}{T_{room}} ; T \text{ in } K \quad (2.19)$$

$$\text{Thermal_Noise} = kTB \quad (2.20)$$

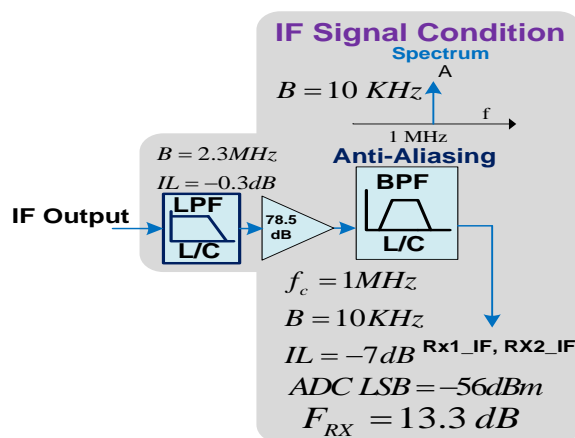


Figure 2.34. Receiver IF Signal Conditioning.

There are two ADCs — one for each receiver — therefore, there are two receiver conditioning boxes. The box holding the conditioning circuit is shown in Figure 2.35, with a block diagram in Figure 2.36. This block diagram shows, for both receivers, the total gain in the system that drives the ADCs. This includes a 6-dB pad at the sub-harmonic mixer for protection, gain per amplifier of 23 dB and 17 dBm compression. The final pads control the input into the

ADC and the filter implements the anti-aliasing. The filter also is narrowband, which reduces the noise floor. In the future, this gain box will need control as part of an Automatic Generation Control (AGC) system. Figure 2.37 and Figure 2.38 show the connectorized components and the filter (inductive and capacitive) design. The LED indicates the box has power. The IF conditioning circuit is made up of COTS connectorized components except for a custom BPF made by Lark Engineering. CEI specified the anti-aliasing filter circuit, after complete modeling in Microwave Office; the gain (S21) is made for pass of close to 1 MHz with a 30 KHz bandwidth.



Figure 2.35. TAIPAS IF Receiver Conditioner Box.



Figure 2.38. IF Anti-Aliasing BPF Circuit.

2.3.6 THz Antenna

The signal emitting from the waveguide is vertically polarized as shown in Figure 2.39. Figure 2.40 shows a photo of the WR2.8 format waveguide output. This example is the receiver waveguide opening; easily determined by the terminated SMA output connector on the sub-harmonic mixer.

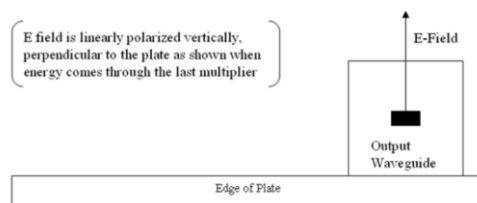


Figure 2.39. Polarization of Output.

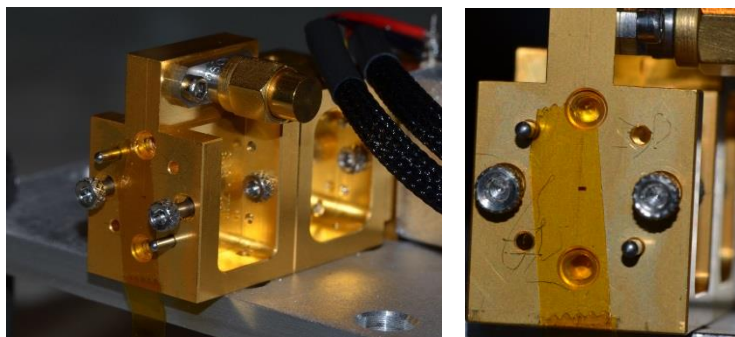


Figure 2.40. WR.2.8 Receiver Input.

A diagonal horn was made for TAIPAS by Custom Microwave in Colorado. Figure 2.41 shows the diagonal horn attached to the receiver. Figure 2.42 shows the Custom Microwave mechanical drawing of the horn. The horn length and width are 19 mm. The depth of the horn is 12.7 mm with a flare length of 6.5 mm and an aperture size of 1.3 mm. The elevation taper half-angle is 9 degrees and azimuth taper half-angle is 6 degrees, yielding a 3 dB beamwidth of 36.5 degrees. The horn design was driven by the focal length of the lens; at the focal length, the beam illuminates the entire lens area.

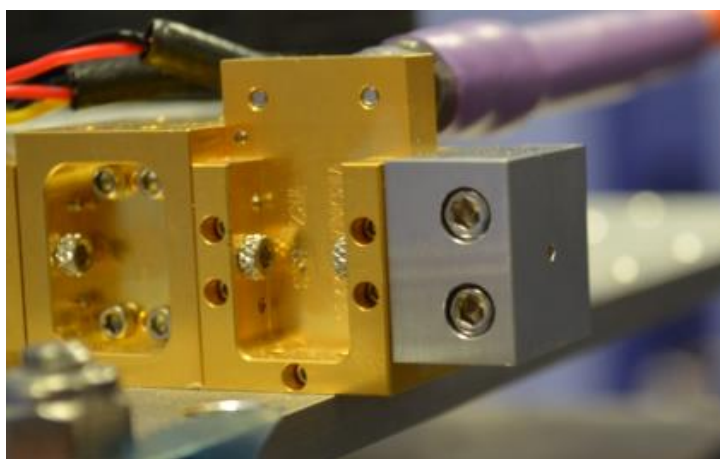


Figure 2.41. WR.2.8 Receiver Diagonal Horn Photo.

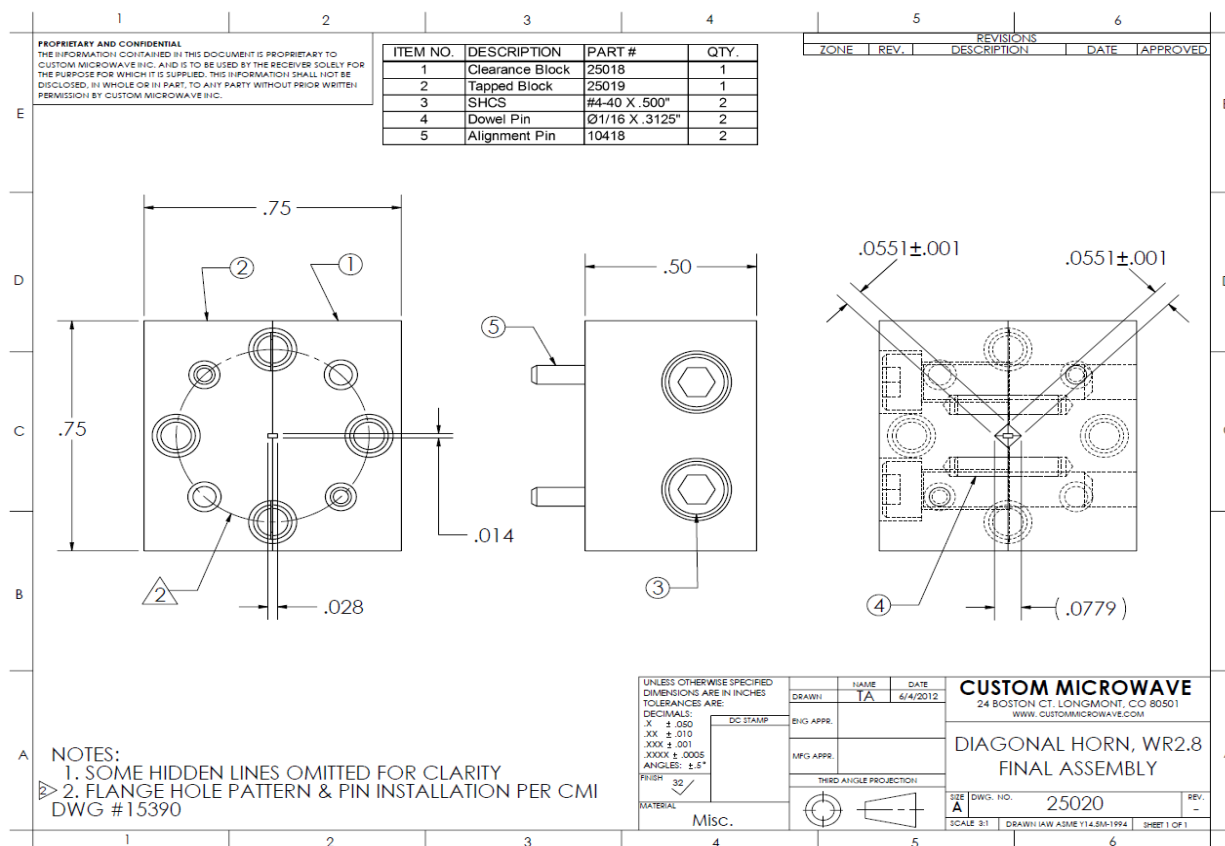


Figure 2.42. WR.2.8 Receiver Diagonal Horn Diagram.

There are two reasons the antenna needs to provide significant gain to the system: low power of the transmitter for a 1.92 km path length and to maintain a narrow beam to reduce multipath and diffraction, especially over the roof tops close to the transmitter. The total antenna for TAIPAS is configured of a horn and Rexolite 1422 lens at both the transmitter and receivers. The lens is plano-convex with a relative permittivity/dielectric constant of $2.535 - j.0013$. The lens size was determined by the approximate 100 factor of the wavelength; at 325 GHz, this yields a 9 cm lens diameter. The quadratically tapered lens has ribbing orthogonal to the electric field to reduce side-lobes; Figure 2.43 shows photos of the lens. The top left picture shows the back ribbing to reduce sidelobes. The combined antenna system yields tight collimation over the

portion of the path being traversed. The gain of the combined system, horn and lens, is approximately 50 dBi.



Figure 2.43. Lens Photos.

As shown in Figure 2.44, the entire receiver and transmitter are on x, y and z calipers that align the beam at the focal length with centered illumination on the lens: boresight beam – no steering. If the z dimension is even slightly off, the 50 dBi can drop significantly. Figure 2.44 shows a block diagram of the horn and lens configuration. The z adjustment controls the focal length. The x and y calipers allow the beam to be deflected or steered in azimuth and elevation, respectively; a positive increase in y or x causes a negative deflection in elevation or azimuth and vice versa. The deflection of the beam off boresight (Equation 2.18) is a function of the ratio of source (horn) displacement to the focal length. To achieve the look-up angle from the CU

building roof-top or the look-down angle of the Mesa receivers, the displacement would have to be .85 cm (Equation 2.21 – Equation 2.23). This displacement is more than the calipers can support, so the 3.63° look angle was produced by mechanically tilting the system in the most convenient place: box, box with dome, first tear I-beam or second tear I-beam.

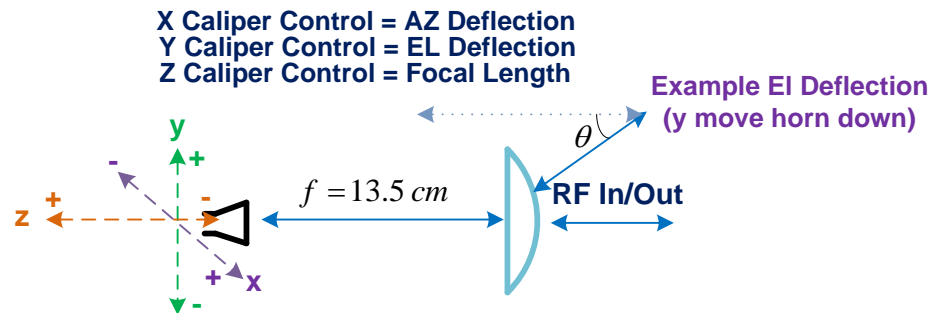


Figure 2.44. Lens / Horn Configuration Control.

$$\Delta\theta = -\frac{\Delta y}{f_L} \quad (2.21)$$

$$-3.6^\circ_y = +\frac{\Delta y}{13.5 \text{ cm}} \quad (2.22)$$

$$\Delta y = -.85 \text{ cm} \quad (2.23)$$

The two primary testing path lengths were the 40 m in the CU hallway and the 1924 m final open path. Figure 2.45 shows a diagram of the two-lens system: Tx and Rx. The relationship of the focal length to the range is shown in Equation 2.24 – Equation 2.28 for ranges of 40 m and 1924 m. The change in focal length due to a shorter path length of 40 m, shown in Equation 2.24 – Equation 2.26; this is only half a millimeter difference from the focal length of 1924 m shown in Equation 2.28. As the path length (R_2) goes to infinity, the focal length is equal to R_1 . The

focal length changes between the two paths did not require significant adjustment. By reciprocity, the same relationship is true for Tx and Rx.

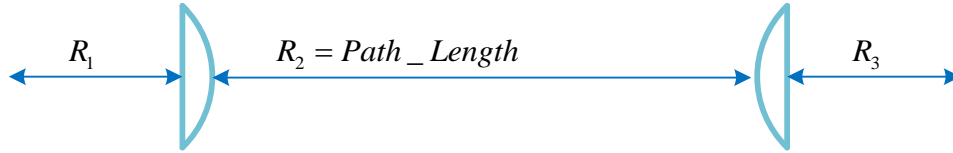


Figure 2.45. Tx and Rx Lenses.

$$\frac{1}{R_1} + \frac{1}{R_2} = \frac{1}{f_L} \quad (2.24)$$

$$\frac{1}{R_1} + \frac{1}{40} = \frac{1}{.135} \quad (2.25)$$

$$R_{1_{40m}} = 13.55 \text{ cm} \quad (2.26)$$

$$\frac{1}{R_1} + \frac{1}{1924} = \frac{1}{.135} \quad (2.27)$$

$$R_{1_{1924m}} = 13.50 \text{ cm} \quad (2.28)$$

2.4 Coho Link

Provision of a reliable phase reference at the far-end of the link was a key design driver addressed using a coherent VHF pilot link and phase locking of the receivers to this reference frequency. Note that phase fluctuation variance is expected to scale roughly with frequency [31]. However, since the values of C_n^2 are multiple orders of magnitude smaller at VHF versus the SMMW region, it was anticipated for no major receiver phase noise to occur as the result of the propagation of the pilot link. The loop bandwidth of the receiver PLL is readily reduced under

high SNR conditions to preclude introduction of atmospheric induced phase noise if the overall phase deviation of the pilot signal is small — slow PLL control-loop feedback time. As a result, the receiver oscillators were locked at the transmitter within a small fraction of a degree.

2.4.1 Multipath and Polarization Empirical

Since multipath is a large design constraint, the Coho system was thought to look like Figure 2.46. The 40.68 MHz +/- .2 MHz ISM band was chosen. The antennas would be crossed dipoles fed with a 90-degree phase difference to produce a circular polarization. Multipath would be reduced since only the even mode reflections would provide significant interference; if you transmit and receive Right Hand Circular Polarization (RHCP, the normal reflections off hard body objects causes the polarization to change to Left-CP (LCP), which will not provide significant power on an RHCP receiver / antenna. A PLL at the receiver locks the signal and utilizes the resultant signal for the synthesizer reference on both receivers. Since this antenna is very low gain, the Fresnel Zone will not come into play.

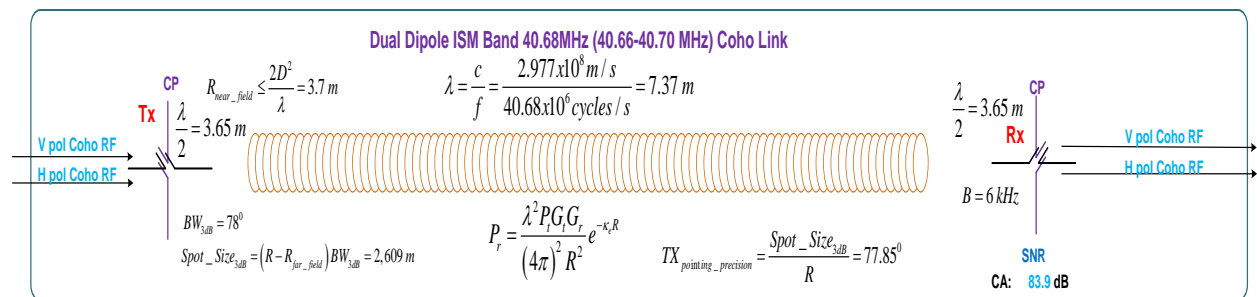


Figure 2.46. Coho Link Block Diagram.

Testing was implemented using the circularly polarized antenna. The goal was to determine if CP provided enough upside to warrant installing a large, cross-shaped antenna on both ends of the link that would have to withstand high wind conditions. Figure 2.47 shows a photo of the RHCP antenna configuration. Two antennas were spaced approximately 30 m in a high multipath environment: steep hill with trees on one side and brick building on the other side. Tests were run with all polarization configurations to determine if the polarization would be good enough for the TAIPAS path. Figure 2.48 - Figure 2.52 show the spectrum analyzer plot at the receiver for various polarization tests ran. The plots did not scintillate in amplitude and there was no visible phase noise difference. The polarizations versus receive power were RHCP to Left Hand Circular Polarized (LHCP)/-48.19 dBm, RHCP to RHCP/ - 47.65 dBm, H (Horizontal) to V (Vertical) / -43.91 dBm, V to V/-40.14 dBm, and H to H – 51.11 dBm. It should be noted that perfect orientation was not attempted or achieved in the experiment. The empirical data shows that the optimal polarization would be V-to-V. H-to-H is most likely not optimal due to the close proximity to the ground; horizontal waves are reversed when they hit the ground, which produces cancellation of the wave. It was also determined that CP should only be used if the PLL loses lock due to multipath; this was not the case. H-H on this short, close-to-the-ground path is only approximately 3.5 dB lower than V-V. The driving force for the polarization of the Coho link will most likely be the easiest mechanical configuration.



Figure 2.47. RHCP Cross Dipole Antenna.

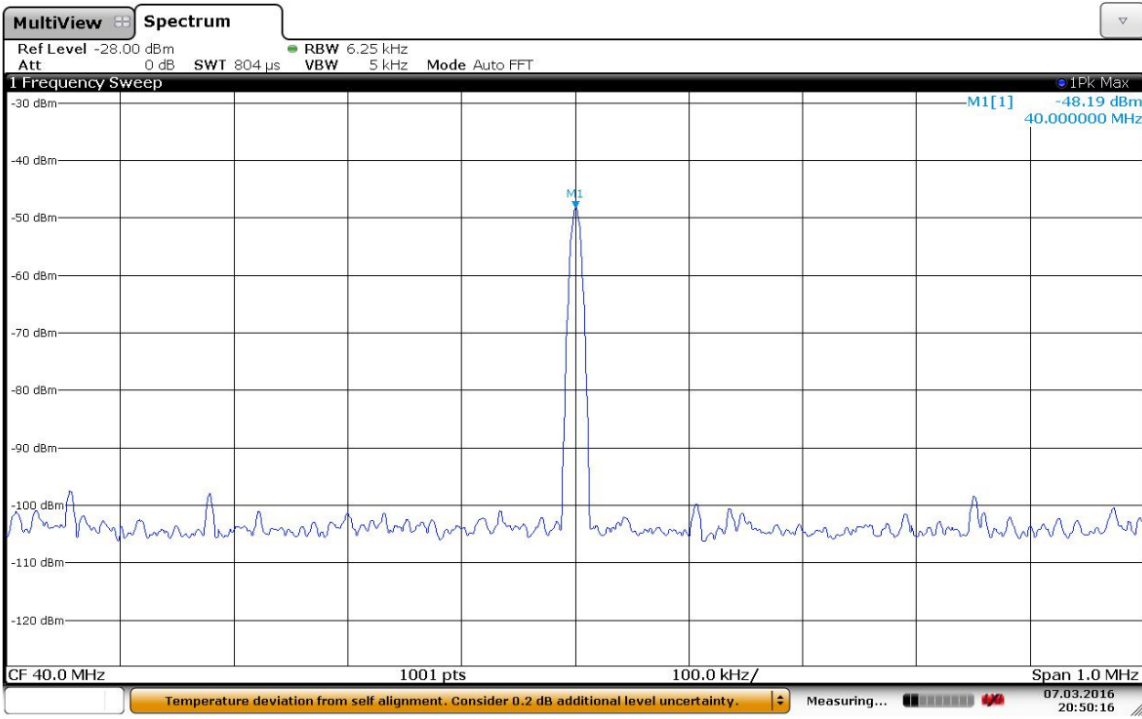


Figure 2.48. RHCP Transmitter and LHCP Receiver.

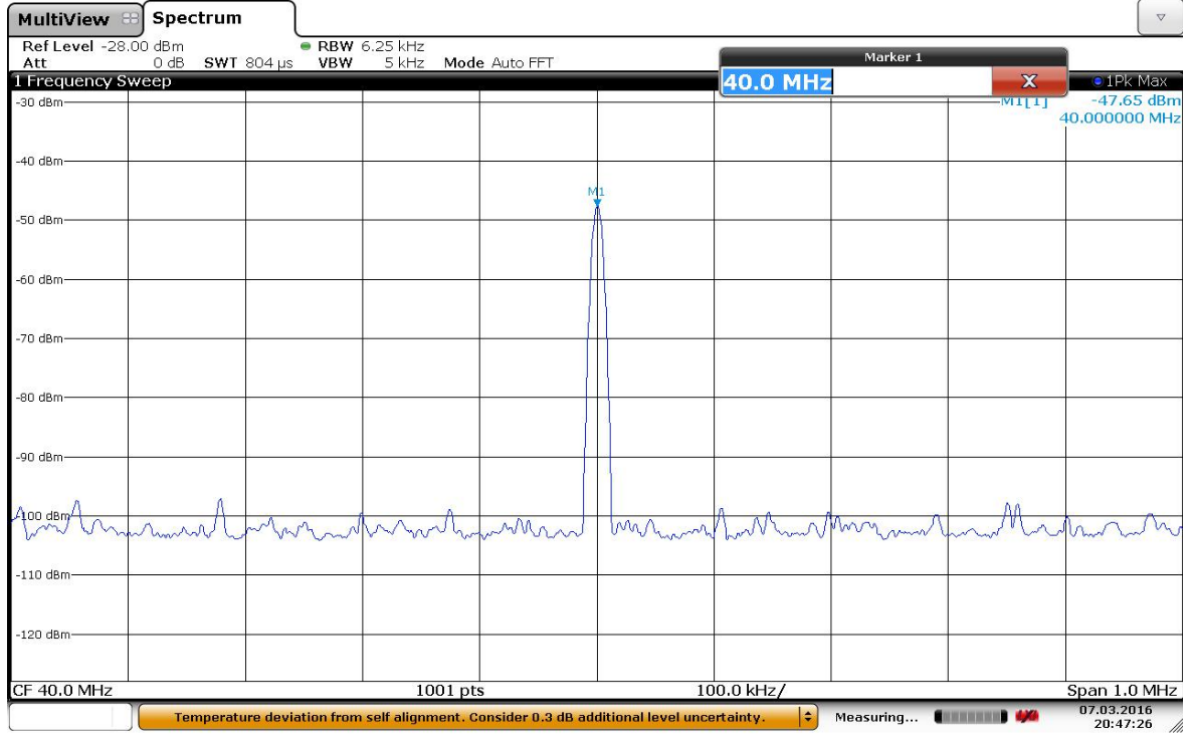


Figure 2.49. RHCP Transmitter and RHCP Receiver.

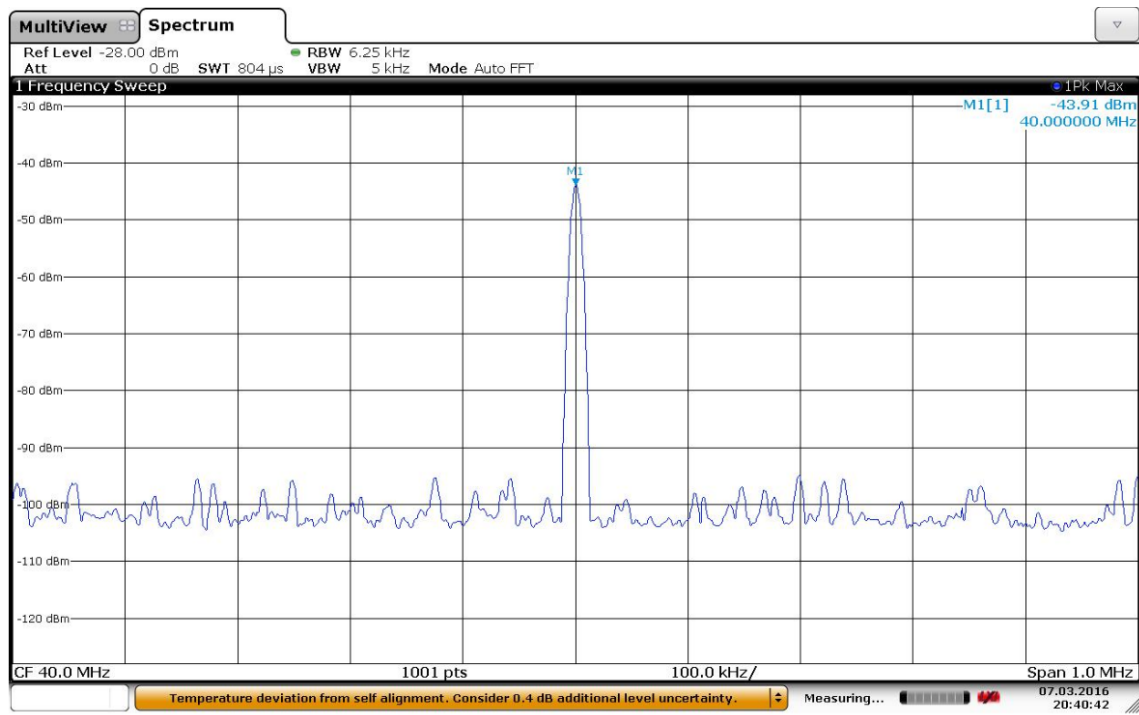


Figure 2.50. Horizontal Polarization Transmitter and Vertical Polarization Receiver.

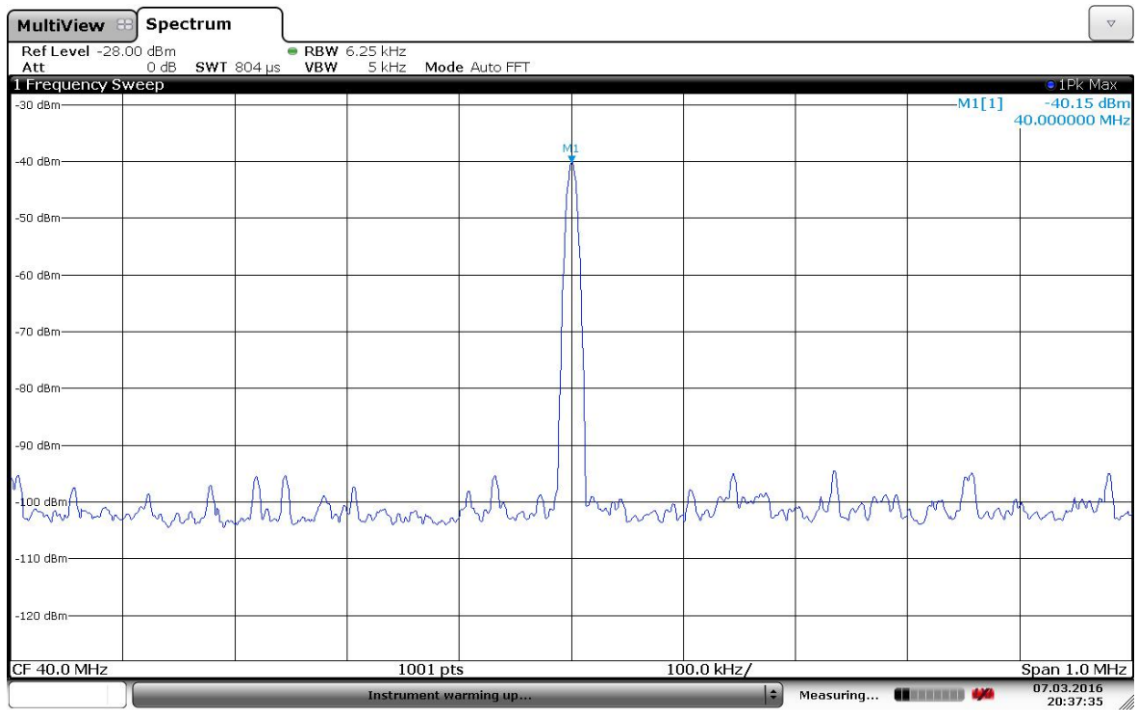


Figure 2.51. Vertical Polarization Transmitter and Vertical Polarization Receiver.

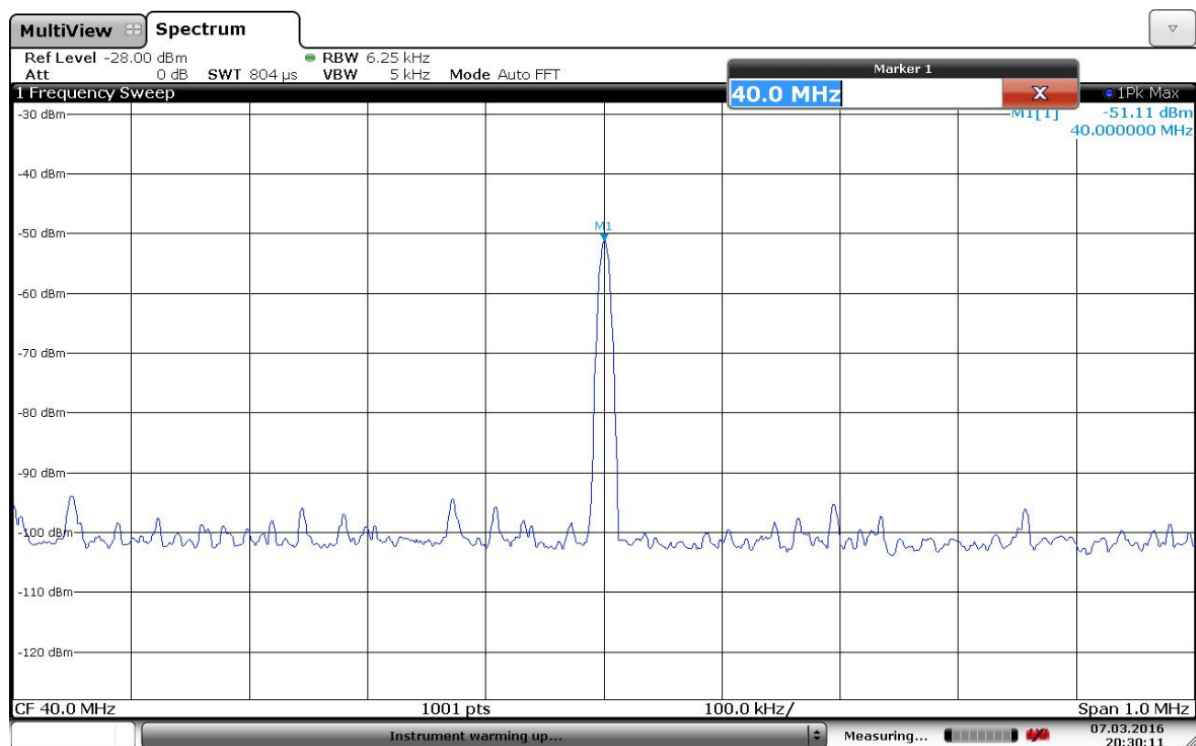


Figure 2.52. Horizontal Polarization Transmitter and Horizontal Polarization Receiver.

2.4.2 Multipath Theoretical

The receiver phase measurements referenced to transmitter phase drift assessment are critical due to the importance of understanding the effects on refractive dispersion near the 325.153 GHz water line. Such dispersive effects are expected to be important in understanding infrared radio dispersion with relevance to double resonance measurements of trace gases. Given the large Fresnel ellipse and broad beam / low directivity of the Coho link, there is a concern about the effects of multipath on phase jitter. These effects will be dominated by forward scatter from near-grazing incidence, and thus will not reverse polarization upon reflection; therefore, circular polarization will not add significant value from a forward-grazing perspective. The circular polarization would help with backscatter from the mountains that are past the receiver; backscatter from them will affect the link phase noise. On the upside, forward

scatter will not cause as much phase noise as backscatter and the backscatter from the mountains will be significantly attenuated. The phase jitter that forward scatter does introduce will be independent of that at 340 GHz, and thus will add to the received THz phase variance. It was discussed to use the 10 MHz GPS signal to study Coho link phase noise stability, but this was left to a future exercise for TAIPAS.

There has been significant work in applied mathematical algorithms to represent RF multipath / clutter in dynamic environments. Most of this has been driven by mobile communication systems and radars; especially radars on mobile platforms, with the primary focus of effects on received power for obvious reasons. They have also applied Rician probability distributions to the micro-cellular propagation channel, especially fixed and unblocked, to determine the likely received signal envelope. The channel will contain a dominant direct component with reflected waves adding or subtracting incoherently with this desired component. The Clark model predicts N plane waves with uniform azimuth distribution and identical amplitudes at the receiver; uniform arbitrary distributed phase. Most of this work is to determine the Clutter-to-Multipath (C/M) ratio.

The angle of the vertical and horizontal reflection coefficients for a lossy Earth depends strongly on the incidence angle near grazing. A calculation of Gamma probability distribution, which characterizes decay in space and time, would be a good fit to characterizing a multipath environment, especially since the path geometry is well understood. The channel response for TAIPAS will remain constant over time. Fast or short term variations are the only effects that matter.

The large trade for TAIPAS to minimize the multipath was driven by multiple factors. If the transmitter is on the roof at CU, there are adjacent rooftops within the first 30 m of propagation that will provide non-coherent forward scattering that could quickly combine with the primary signal. The transmitter for the Coho link at the NIST Mesa provides a quick drop off of forward reflectors, making it optimal for the transmit. The downside is that the receiver would be on the rooftop at CU mostly enclosed by building peaks that would provide backscatter phase distortions. The same rooftops prior to the CU ECEE building would also provide forward scattering. Under this configuration, with the length of the path and the power of the Coho link, both multipath effects would be at much lower power than the former configuration rooftop forward scattering.

The optimal approach to solving the multipath effects is to increase the gain of the transmit antenna. This could be done with an array of Vivaldi antenna elements or patches (End-Fire). Significant reduction in the amount of signal that is incident with the ground would be achieved. The transmit power could be reduced significantly due to the gain contributions to the SNR, which would also decrease the multipath effects. Further reductions could be achieved by placing nulls in the direction of the reflectors. Implementing this same array at the receiver could also improve C/M. Unfortunately, the 7.5 m wavelength would generate large antenna elements and spacing for this antenna. While the feasibility is low risk, the cost was prohibitive for this phase of TAIPAS.

2.4.3 Multipath Conclusion

Due to the cost constraint, it was decided that leveraging the plethora of multipath models for a significant amount of disparate scatterers at significantly lower altitude for most of the path would not generate any useful knowledge for the engineered design. The cost constraint on every engineering project also prohibited a high gain antenna approach; this should be considered in future development of TAIPAS. An empirical approach was taken by setting up the dipole antenna system on each end of the fixed path and measuring the phase noise on a spectrum analyzer before and after the extremely slow feedback loop PLL to optimize the configuration within the cost constraint of the program. The predicted optimized configuration was the vertical dipole transmitter at the mesa receiver site; besides the points made earlier, due to the steep in-range drop, the Brewster angle will work to reducing the multipath. Reflections decrease with incident angle with a minimum at the Brewster angle. Typical dielectric soil value reflection coefficients, as a function of incidence angle, are shown in Figure 2.53 [55]. As shown, vertical polarization (Transverse Magnetic (TM)) has a greater attenuation at all incidence angles compared to horizontal polarization (Transverse Electric (TE)).

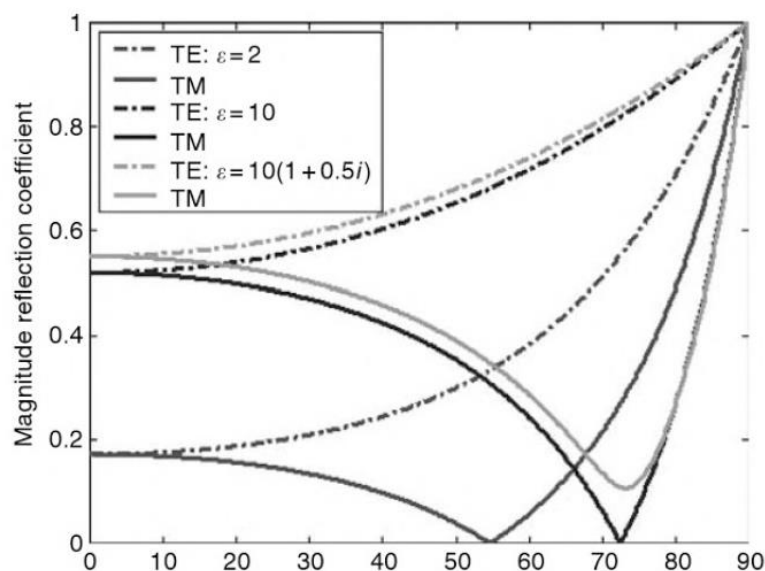


Figure 2.53. Incident Angle on the Horizontal Axis - Reflection Coefficients for Varying Polarization and Dielectric of Ground.

As shown in the next section, due to the significant frequency multiplication on the transmitter (24X) which will multiply the phase noise as well, the Coho transmitter will be placed at the transmitter sight. Like all engineering trades, you cannot just look at multipath optimization in a vacuum of the larger trade space; there is never a free lunch.

2.4.4 Coho Propagation Link Analysis

Table 2.3 contains all the analysis for the propagation of the Coho link. The Friis calculations show an extremely strong CA SNR of 84.9 dB. Due to the 7.5 m wavelength, the effects on the SNR in rain and snow will be negligible. The near field of the antenna is significantly shorter than the propagation path and the spot size due to the low gain, which makes alignment of the receive antenna trivial. The equations will be delineated in the THz Friis sections of this Chapter.

Table 2.3. Propagation Analysis for Coho Link.

TAIPAS ISM HF-Band Coho Link Clear Air System Calculations (40.68 MHz)										
					Available Test Site Ranges (m)					
					CU TWR	NIST	NCAR	DoC	NOAA	
					520	1920	3370	6520	22570	
					Range					
					1920 (m)					
Ref. Coef.										
0.3										
$\Gamma = \frac{Z_L - Z_A}{Z_L + Z_A}$										
$VSWR = \frac{1 + \Gamma }{1 - \Gamma }$										
$c = 2.998 \times 10^8 \text{ m/s}$										
$\lambda = \frac{c}{f}$										
Power Received					$P_r = \frac{\lambda^2 P_t G_t G_r}{(4\pi)^2 R^2} e^{-\kappa_e R}$					
f	λ	$P_{t_exciter}$	$P_{t_Antenna}$	$\kappa_e = \kappa_a + \kappa_s$	$1 Np = 4.3429 \text{ dB}$					
Frequencies	Wavelength	Tx Power	Tx Power	Absorpt.	Scatter.	Extict.	Extict.	Rx Power	Rx Power	
40 (MHz)	7.495 (m)	89.12509 (mw)	62.38757 (mw)	0 (dB/km)	0 (dB/km)	0 (dB/km)	0 (Np/km)	1.62E-05 (mW)	-47.90 (dBm)	
Plot #1										
Gain Transmit	SNR	B			NF			SNR		
2.150 (dBi)		0.006 (MHz)	3.44 (dB)	$NF = 10 \log \left(\frac{T_{rec}}{T_0} \right)$			84.9 (dB)			
		T_0	P_n	$P_n = kTB ; k = 1.38 \times 10^{-23} \text{ J/K}$			$SNR = 10 \log \left(\frac{P_r}{P_n} \right)$			
Gain Receive		290 (K)	5.30E-14 (mw)							
2.150 (dBi)		T_{rec}	-132.76 dBm							
		350 (K)								
Beam Characteristics										
Far zone		$R_{far_field} = \frac{2D^2}{\lambda}$			3-dB Beamwidth		3-dB spot size			
3.7 (m)					78.000 (deg)		2608.70 (m)			
$Spot_Size_{3dB} = (R - R_{far_field}) BW_{3dB}$										
$BW_{3dB_in_radians}$										
Alignment										
Required TX pointing precision										
77.848 (deg)										
$TX_{pointing_precision} = \frac{Spot_Size_{3dB}}{R}$										

2.5 Coherent (Coho) Link Hardware

The exciter/transmitter utilizes 1 W High Power Amplifier (HPA) on each polarization to generate a 19.5 dBm signal at a 6 kHz bandwidth to yield an SNR of ~80 dB in all weather conditions. The receiver implements a PLL design to lock the receiver’s reference.

Note that phase fluctuation variance is expected to scale roughly with frequency, but phase noise will scale back up with frequency multiplication, which is significant on the transmitter. For this reason, a PLL was implemented at the receiver end to preclude introduction of atmospheric induced phase noise on time scales smaller than ~1 second. As a result, it is

expected to be able to lock the receiver oscillators to the transmitter phase to within a small fraction of a degree at 320-340 GHz.

Figure 2.54 shows a VSS model block diagram of the Coho Transmitter. It is designed to drive a dipole CP configuration. The final system only utilized the in-phase component to drive a single vertical dipole. Figure 2.55 shows the receiver VSS model block diagram. Figure 2.56 - Figure 2.57 show block diagrams that are easier to read; exciter is the same as transmitter. Pictures of the Coho transmitter and receiver are shown in Figure 2.58 - Figure 2.59.

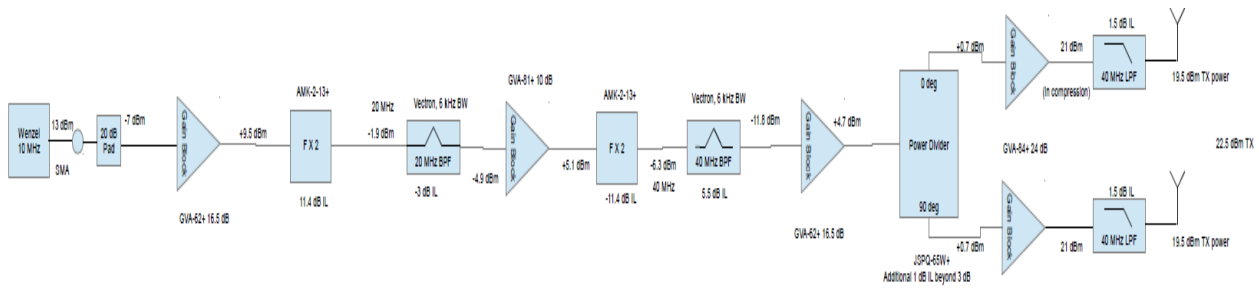


Figure 2.54. Coho Link Transmitter VSS Model Block Diagram.

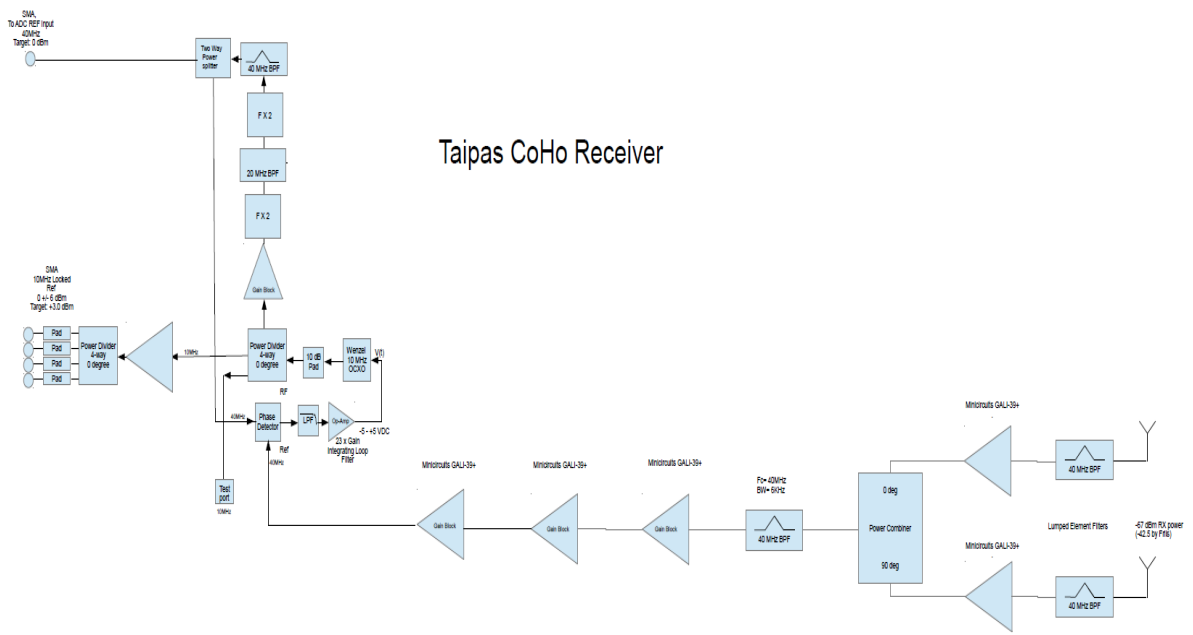


Figure 2.55. Coho Link Receiver VSS Model Block Diagram.

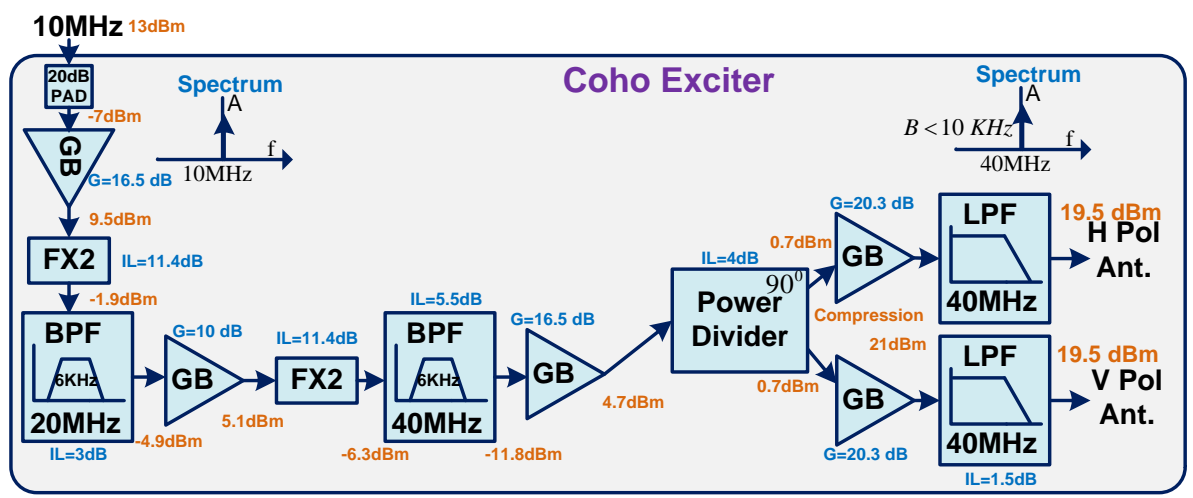


Figure 2.56. Coho Link Transmitter Block Diagram.

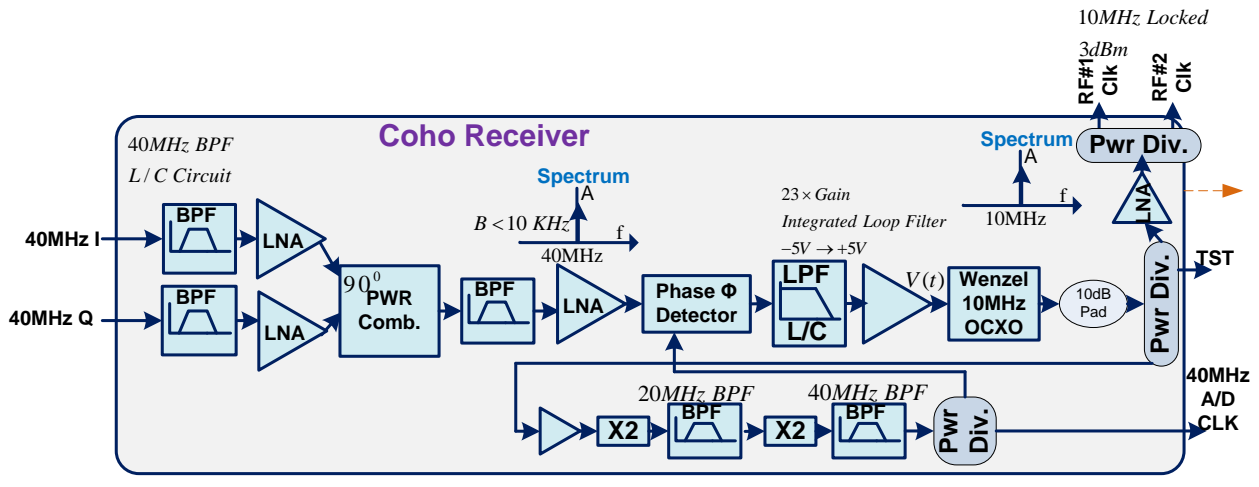


Figure 2.57. Coho Link Receiver Block Diagram.



Figure 2.58. Coho Link Transmitter Photos.

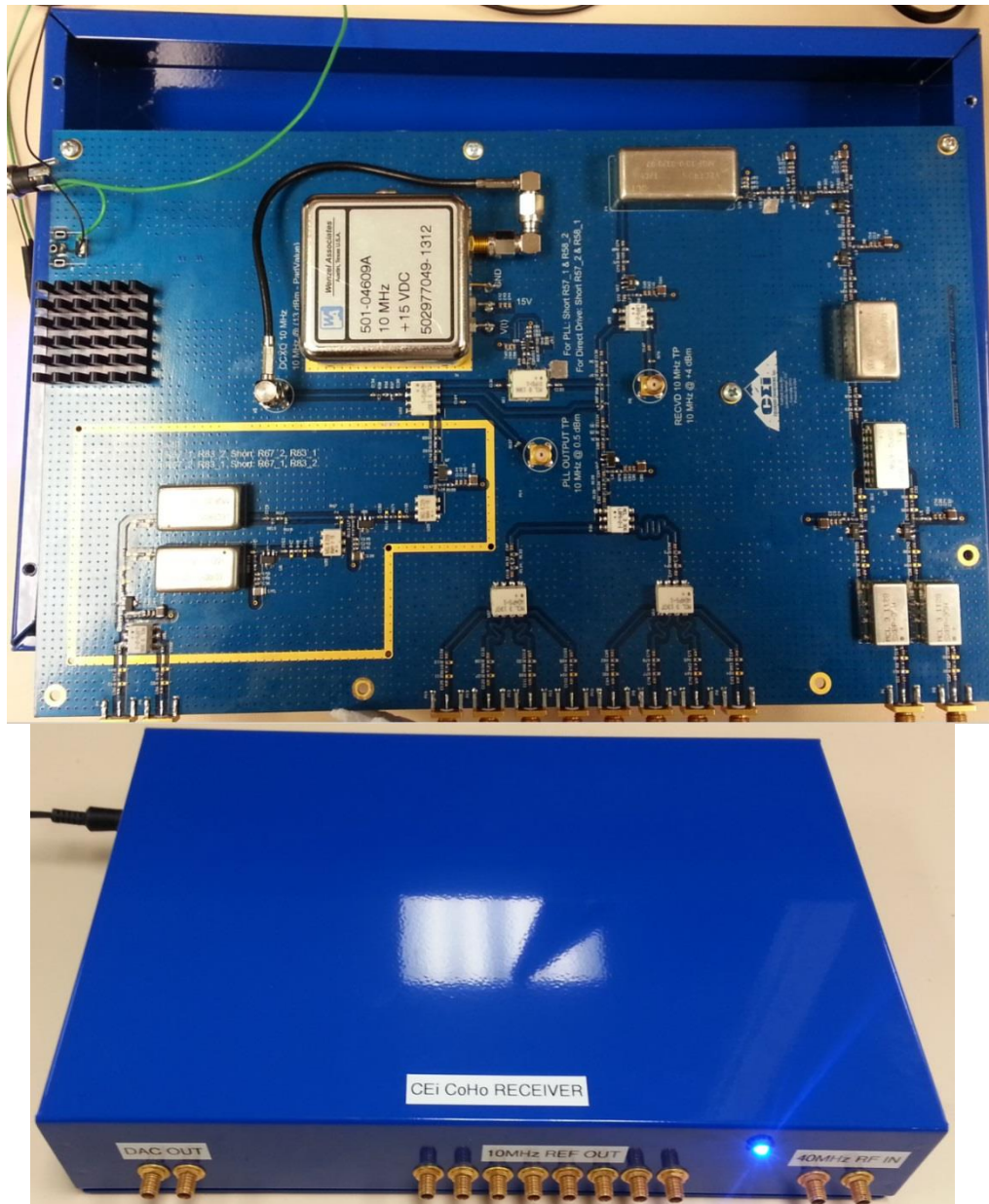


Figure 2.59. Coho Link Receiver Photos.

2.6 Anemometer

The ultrasonic anemometer measures a portion of the required meteorological truth: wind and temperature. There are two in the system located at the transmitter and receiver. While it would be beneficial to have sensors along the entire propagation path at the level of the beam, it

was not practical for cost and location drivers. Figure 2.60 shows a picture of one of the anemometers from Applied Technologies; it is a V-style ultrasonic anemometer. The two circular frames holding sensors will be orthogonal to the most important and probable wind direction: horizontal. This system gives the capability to characterize the atmospheric turbulence based on two path samples, beginning and end, in three dimensions. The anemometer samples at 5 ms (200 Hz) increments — average of five samples — which is the atmospheric frozen time. This is a significant improvement over earlier transmissometer weather sensors. The interface is over an RS232 serial port: 9600 bauds, data output in time stamp, U (parallel to x axis, m/s), V (parallel to y axis m/s), W and Temperature (C degrees). A flat surface at the top of the array allows for alignment to achieve .1-degree angle accuracy. A large portion of the data sheet is in Appendix B.

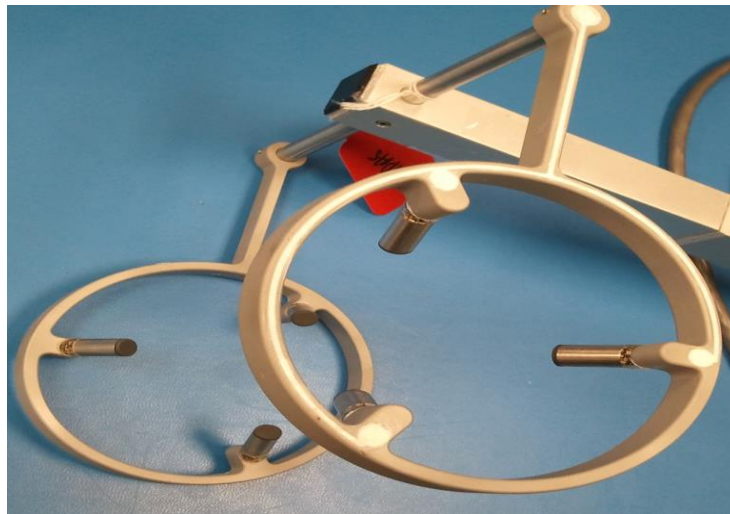


Figure 2.60. Anemometer.

2.7 Hygrometer

The humidity sensor from Campbell Scientific is a KH20 Krypton Hygrometer, shown in Figure 2.61 and described in Appendix B. It is a Lyman-alpha version, based on the absorption of the radiation by water vapor at the Lyman alpha emission line of atomic hydrogen. The KH20 sensor uses a krypton lamp that emits two absorption lines: major line at 123.58 nm and minor line at 116.49 nm. Both lines are absorbed by water vapor, and a small amount of the minor line is absorbed by oxygen. There are two hygrometers in the system: one each at the transmitter and receiver. The preferred configuration would be to distribute hygrometers in the open path, but this was cost and location prohibitive. The units were provided with calibration adjustment information that is applied in the TAIPAS software. The outputs are analog, so they run through an ADC, which samples the data and sends it out on a USB port: shown in Figure 2.62. The output format is shown in Table 2.4. The file format for output is as follows: time/EPOCH, Clean Full, Clean Dry, Clean Wet, Scaled Full, Scaled Dry and Scaled Wet; Table 2.5 shows the ranges. Due to the Colorado location, most of the time TAIPAS will utilize the Clean Dry Vapor range. The top of the file also includes data on the applied calibrations. All measurements are in g/m^3 .

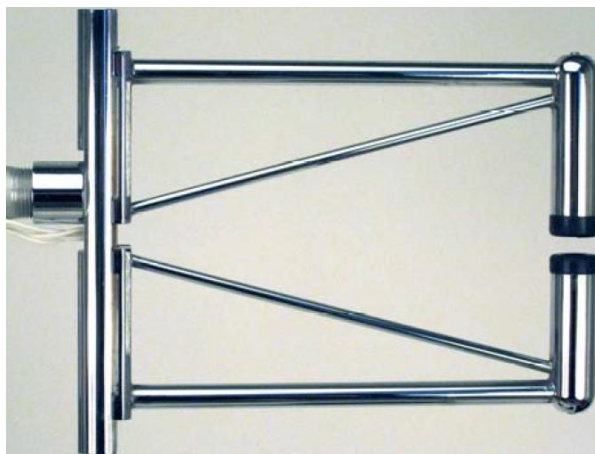


Figure 2.61. Hygrometer.



Figure 2.62. ADC.

Table 2.4. Key Data on Hygrometer.

Measurements	
Calibration Range:	1.7 to 19.5 g/m ³ (nominal)
Frequency Response:	100 Hz
Operating Temperature Range:	-30 to +50°C
Electrical	
Supply Voltage:	10 V to 16 Vdc
Current Consumption:	20 mA max at 12 Vdc
Power Consumption:	0.24 Watts
Output Signal Range:	0 to 5Vdc

Table 2.5. Hygrometer Vapor Density Categories.

Ranges	Vapor Density (g/m³)
Full Vapor Range	2 – 19
Dry Vapor Range	2 – 9.5
Wet Vapor Range	8.25 – 19

2.8 Data Link

Figure 2.63 illustrates the C-band, COTS, AirGrid, network communications link. The full data sheet is located in Appendix B. This system was required for TAIPAS to control the

receiver units at the Mesa and retrieve the received data. The password for the network is as follows: *ceirockstaipis*.

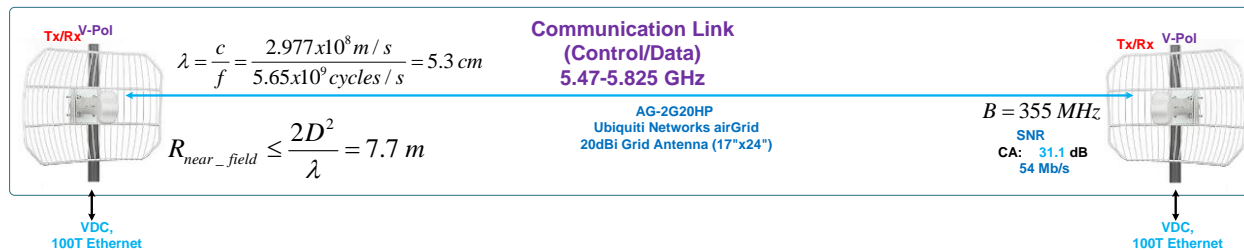


Figure 2.63. C Band Communication/Network Link.

Table 2.6 shows the Friis analysis of the AirGrid in CA with a bandwidth of 355 MHz and antenna gain of 20 dBi. The 31.6 dB SNR allows for data rates of 54 Mb/s, which is more than enough to support TAIPAS. Table 2.7 from the AirGrid Data sheet shows the -82 dBm with tolerance adjustment — minimum receive power required to achieve 54 Mb/s, the maximum data rate. Table 2.8 shows the beam will create a spot size on the Mesa with a 290 m diameter requiring a pointing precision of 8.7 degrees; allowing for easy alignment of the system. Table 2.9 shows the Friis analysis for varying rain rates; Figure 2.64 shows a plot of the rain attenuation due to absorption and scattering that was utilized to generate the extinction coefficients. Table 2.10 shows the Friis analysis for varying snow rates; Figure 2.65 shows a plot of the snow attenuation due to absorption and scattering that was utilized to generate the extinction coefficients. The minimum receive power of -45 dBm for rain and snow is more than enough to support the 54 Mb/s data rates. As shown by the rain and snow plots, rain absorption is higher than scattering and snow has higher scattering than absorption. The equations will be delineated in the THz Friis sections of this Chapter.

Table 2.6. Communication Link Friis for CA.

TAIPAS C-Band Comm Link Clear Air System Calculations (5.470GHz - 5.825GHz)									
		Ref. Coef.		Available Test Site Ranges (m)					
		0.316		CU TWR	NIST	NCAR	DoC	NOAA	
		$\Gamma = \frac{Z_L - Z_A}{Z_L + Z_A} = .316$		520	1920	3370	6520	22570	
		Plot #2		Range					
				1920 (m)					
$c = 2.998 \times 10^8 \text{ m/s}$		$\lambda = \frac{c}{f}$		$VSWR = \frac{1+ \Gamma }{1- \Gamma } = 1.926$		$K_e = K_a + K_s$		$1 Np = 4.3429 \text{ dB}$	
Power Received		$P_{t_exciter}$		P_{t_Horn}		K_e		$P_r = \frac{\lambda^2 P_t G_t G_r}{(4\pi)^2 R^2} e^{-\kappa_e R}$	
Frequencies	Wavelength	Tx Power	Tx Power	Absorpt.	Scatter.	Extict.	Extict.	Rx Power	Rx Power
5.65 (GHz)	53.062 (mm)	316 (mw)	216.144 (mw)	0 (dB/km)	0 (dB/km)	0 (dB/km)	0 (Np/km)	1.05E-05 (mW)	-49.81 (dBm)
Plot #1		SNR							
Gain Transmit		B	NF	$NF = 10 \log \left(\frac{T_{rec}}{T_0} \right)$		SNR		$SNR = 10 \log \left(\frac{P_r}{P_n} \right)$	
20,000 (dBi)		355 (MHz)	7.11 (dB)			31.6 (dB)			
		T_0	P_n	$P_n = kTB ; k = 1.38 \times 10^{-23} \text{ J/K}$					
		290 (K)	7.30E-09 (mw)						
Gain Receive		T_{rec}	-81.37 dBm						
20,000 (dBi)		1200 (K)							

Since this is a high gain antenna, the Fresnel zone comes into play. The communication link radius at 962 m distance is 5.4 m (Equation 2.4); this first zone is nowhere close to hitting the ground at this distance. The rooftops at 30 - 40 m are approximately 20 m below the direct LoS. The first Fresnel ellipse at 40 m distance is approximately 1.5 m (Equation 2.5); this is the distance from the LoS to the ellipse, so the penetration percentage would be zero since the building is way below the ellipse. Fresnel Ellipses 2 and 3 will have a distance at 2 m and 2.7 m, respectively. If an obstruction hits the Fresnel zone, a 20 - 40% penetration is required to have an effect.

Table 2.7. AirGrid Power vs. Data Rates.

AirGrid M5 HP - Operating Frequency 5470-5825 MHz*						
OUTPUT POWER: 25 dBm						
5 GHz TX POWER SPECIFICATIONS				5 GHz RX POWER SPECIFICATIONS		
	DataRate	Avg. TX	Tolerance		DataRate	Tolerance
11a	1-24 Mbps	25 dBm	+/- 2 dB	11a	1-24 Mbps	-97 dBm +/- 2 dB
	36 Mbps	24 dBm	+/- 2 dB		36 Mbps	-90 dBm +/- 2 dB
	48 Mbps	22 dBm	+/- 2 dB		48 Mbps	-86 dBm +/- 2 dB
	54 Mbps	21 dBm	+/- 2 dB		54 Mbps	-84 dBm +/- 2 dB

Table 2.8. Communication Link Beam Characteristics and Alignment.

Beam Characteristics	Far zone 7.7 (m) $R_{far_field} = \frac{2D^2}{\lambda}$	3-dB Beamwidth 8.683 (deg) $BW_{3dB} = \frac{74\lambda}{D}$	3-dB spot size 289.79 (m) $Spot_Size_{3dB} = (R - R_{far_field}) BW_{3dB}$ $BW_{3dB_in_radians}$
Alignment	Required TX pointing precision 8.648 (deg) $TX_{pointing_precision} = \frac{Spot_Size_{3dB}}{R}$		

Table 2.9. Communication Link Friis for Rain.

TAIPAS C-Band Comm Link Rain System Calculations (5.470GHz - 5.825GHz)

		Available Test Site Ranges (m)								
		Ref. Coef.	CU TWR	NIST	NCAR	DoC	NOAA			
		0.316	520	1920	3370	6520	22570			
		$\Gamma = \frac{Z_L - Z_0}{Z_L + Z_0} = .316$	Range		1920 (m)					
$c = 2.998 \times 10^8 \text{ m/s}$		$\lambda = \frac{c}{f}$	Plot #2		$VSWR = \frac{1+ \Gamma }{1- \Gamma } = 1.926$				$P_r = \frac{\lambda^2 P_t G_t G_r}{(4\pi)^2 R^2} e^{-\kappa_r R}$	
Power Received			$P_{t_exciter}$	P_{t_Horn}	Plot #3	Plot #3	$\kappa_e = \kappa_a + \kappa_s$	$1 Np = 4.3429 \text{ dB}$		
Rain Rate	f	Wavelength	Tx Power	Tx Power	Absorpt.	Scatter.	Extinct.	Extinct.	Rx Power	Rx Power
1 (mm/hr)	5.65 (GHz)	53.062 (mm)	316 (mw)	216.144 (mw)	0.004 (dB/km)	0 (dB/km)	0.004 (dB/km)	0.000921 (Np/km)	4.15E-05 (mW)	-43.81 (dBm)
10 (mm/hr)	5.65 (GHz)	53.062 (mm)	316 (mw)	216.144 (mw)	0.035 (dB/km)	0 (dB/km)	0.035 (dB/km)	0.008059 (Np/km)	4.10E-05 (mW)	-43.87 (dBm)
40 (mm/hr)	5.65 (GHz)	53.062 (mm)	316 (mw)	216.144 (mw)	0.2 (dB/km)	0.0065 (dB/km)	0.2065 (dB/km)	0.047548 (Np/km)	3.80E-05 (mW)	-44.20 (dBm)
100 (mm/hr)	5.65 (GHz)	53.062 (mm)	316 (mw)	216.144 (mw)	0.6 (dB/km)	0.025 (dB/km)	0.625 (dB/km)	0.143912 (Np/km)	3.16E-05 (mW)	-45.01 (dBm)

SNR	B	NF	SNR
	355 (MHz)	7.11 (dB)	37.6 (dB)
	T_0		37.5 (dB)
	290 (K)		37.2 (dB)
	T_{rec}		36.4 (dB)
	1200 (K)		
		$NF = 10 \log \left(\frac{T_{rec}}{T_0} \right)$	
		$P_n = kTB ; k = 1.38 \times 10^{-23} \text{ J/K}$	
			$SNR = 10 \log \left(\frac{P_r}{P_n} \right)$

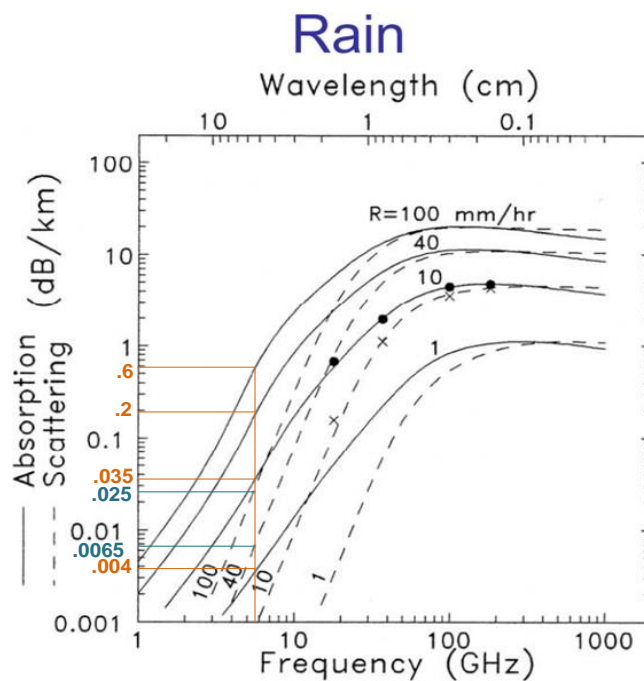


Figure 2.64. Rain Attenuation and Scattering Plot [39].

Table 2.10. Communication Link Friis for Snow.

TAIPAS C-Band Comm Link Snow System Calculations (5.470GHz - 5.825GHz)															
										Available Test Site Ranges (m)					
										CU TWR	NIST	NCAR	DoC	NOAA	
										520	1920	3370	6520	22570	
										Range					
										1920 (m)					
										Ref. Coef.					
										0.316					
										$\Gamma = \frac{Z_L - Z_A}{Z_L + Z_A} = .316$					
										Plot #2					
										$VSWR = \frac{1+ \Gamma }{1- \Gamma } = 1.926$					
										$\kappa_e = \kappa_a + \kappa_s$	$1 Np = 4.3429 dB$				
										$P_r = \frac{\lambda^2 P_t G_t G_r}{(4\pi)^2 R^2} e^{-\kappa_e R}$					
Rain Rate	Frequencies	Wavelength	$P_{t_exciter}$	P_{t_horn}	Plot #3 Absorpt.	Plot #3 Scatter.	κ_e Extinct.	κ_e Extinct.	P_r Rx Power	P_r Rx Power					
1 (mm/hr)	5.65 (GHz)	53.062 (mm)	316 (mw)	216.144 (mw)	0 (dB/km)	0 (dB/km)	0 (dB/km)	0 (Np/km)	4.16E-05 (mW)	-43.81 (dBm)					
10 (mm/hr)	5.65 (GHz)	53.062 (mm)	316 (mw)	216.144 (mw)	0.002 (dB/km)	0.022 (dB/km)	0.024 (dB/km)	0.005526 (Np/km)	4.12E-05 (mW)	-43.85 (dBm)					
40 (mm/hr)	5.65 (GHz)	53.062 (mm)	316 (mw)	216.144 (mw)	0.007 (dB/km)	0.45 (dB/km)	0.457 (dB/km)	0.105228 (Np/km)	3.40E-05 (mW)	-44.68 (dBm)					

SNR		NF		SNR	
B	355 (MHz)	NF	7.11 (dB)	SNR	37.6 (dB)
T_0	290 (K)	P_n	7.30E-09 (mw)	SNR	37.5 (dB)
T_{rec}	1200 (K)		-81.37 dBm	SNR	36.7 (dB)
		$NF = 10 \log \left(\frac{T_{rec}}{T_0} \right)$		$SNR = 10 \log \left(\frac{P_r}{P_n} \right)$	
		$P_n = kTB ; k = 1.38 \times 10^{-23} J/K$			

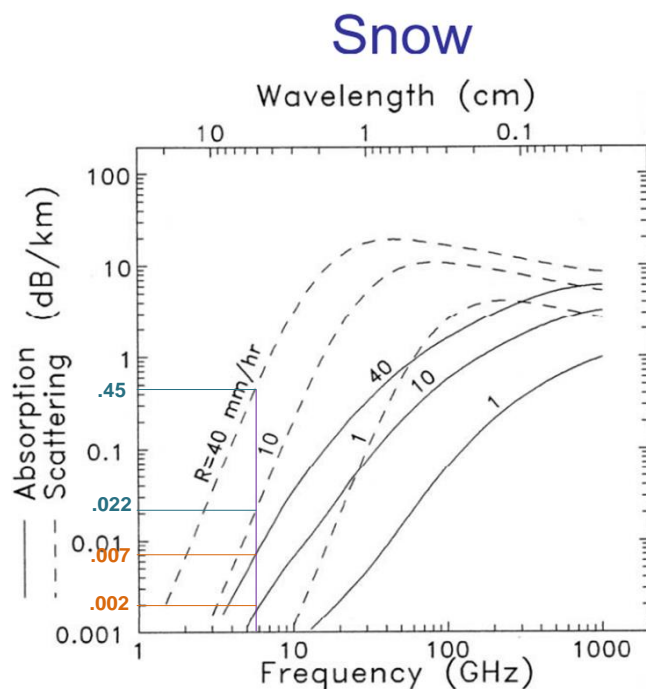


Figure 2.65. Snow Attenuation and Scattering Plot [39].

The system can be controlled by leveraging this extended network via a tablet left powered on a laptop in the container on the CU EECE roof top. A Virtual Private Network (VPN) is required to access the laptop and then all other systems in TAIPAS are accessible. The fixed Internet Protocol (IP) address is 128.138.248.122 with a subnet mask of 255.255.255.0 and gateway of 128.138.248.1. The Domain Name Server (DNS) addresses include 128.138.129.76 and 128.138.240.1. All this information allows the TAIPAS system to run 24/7 from anywhere.

2.9 Scintillometer

Scintillometer measurements of the optical refraction structure constant C_n^2 remain one of the best means of characterizing the path-averaged/integrated value of refractive index

variations. Overall, much more extensive and accurate propagation model validation can now be performed, specifically for the CAR, HAS, and TP components, and at lower inflation-adjusted cost than incurred for past experiments. What is required, however, is a broad understanding of the propagation models and their shortcomings along with experience in the design and fielding of the hardware needed for propagation measurements and atmospheric characterization.

A custom scintillometer is utilized to measure the index-of-refraction structure coefficient of the atmosphere (C_n^2). It is implemented with a telescope, red Light Emitting Diodes (LEDs), narrow red, band pass filter, and a black and white camera; the temperature in the chamber must be tightly controlled or else the mechanical tuning on the telescope focus will change with temperature. This system can function well over the required path length in the most desired environmental conditions. Figure 2.66 shows a diagram of the future system utilizing multiple telescopes and emitters. The configuration at the time of this thesis utilized a single telescope in the transmitter and the LED pattern in the vacant telescope hole located in Rx1. This configuration yielded a C_n^2 that was integrated over the entire path. In the future, multiple telescopes will be utilized to break this entire path integrated C_n^2 into multiple integrated sections. The single telescope configuration leverages the work implemented by Shiril Tichkule and Andreas Muschincki at CU [56]. The multiple telescope approach and LED encoding are extensions developed under this thesis. It should be noted that due to the open, un-level path, the Mohnin-Obukhov similarity theory for relating surface heat fluxes to C_T^2 , C_Q^2 , and C_{TQ} could not be applied. It was assumed that $C_{TQ} = +/- C_T C_Q$.

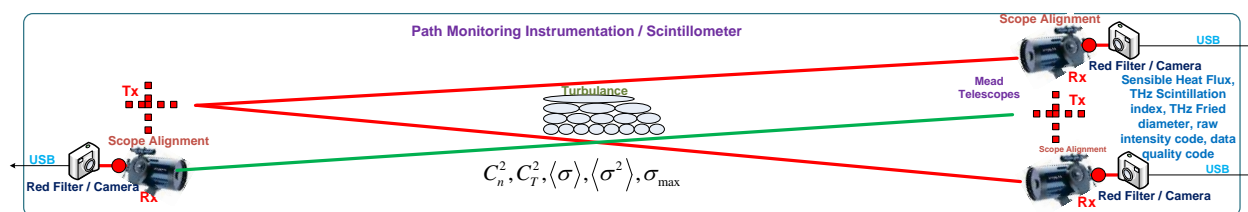


Figure 2.66. Custom Scintillometer Block Diagram.

The telescopes are Meade LX-80, 6", Schmidt-Cassegrain reflector models. The Edmund Optics, hard coated, band pass, red filter passes wavelengths of 625 nm. A PointGray Chameleon USB 2.0 black and white camera was utilized: Sony Exview ICX445 Charge Coupled Device (CCD), 1.3 MP (1296 x 964), 18 FPS and maximum shutter speed of 0.1 ms. Figure 2.67 shows pictures of the equipment. Applicable details for this equipment and the 627 nm LEDs with half intensity at $\pm 4^\circ$ are in Appendix B.



Figure 2.67. Scintillometer Equipment Photos.

There are two methods utilized to measure C_n^2 : area and encoded pattern displacement. Both methods leverage an AoA measurement to determine the index of refraction of the optical

path. The area method integrates many varying AoAs on the CCD; the exposure time is longer than the atmosphere frozen time (shutter slow) which allows many AoAs to generate a large integrated image. The area is bounded by pixel intensities that are within six standard deviations of the highest intensity pixel. The encoded pattern displacement requires a shutter speed that is faster than the atmospheric frozen time of ~ 1 ms. This allows the measurement of a single AoA displacement. While this is possible with a single or small group of LED(s), the accuracy can be significantly increased by encoding the LED pattern and implementing a matched filter to create a sinc-squared function. Further accuracy is achieved by implementing a spline curve fit. A Barker code was chosen since it yields constant sidelobes. As pointed out in Alquaddoomi and Scholtz [57], two-dimensional (2D) Barker codes are very limited. This design does not implement a multidimensional matched filter. The end results are a location on a 2D image; achieved with a linear convolution across the columns and another linear convolution across the rows. These two convolutions are lined up to determine the intersection point from the displacement referenced to the center of the CCD. This allows any size Barker code from the limited known set of codes.

The convolution implements a filtering operation when one signal, $f(t)$, is convolved with the filter impulse response, $h(t)$. Equation 2.29 shows the linear representation of convolution. Equation 2.30 shows the discrete version of the convolution which is circular over modulo N ; this is applied since the pixel image is digital and finite. The negative tau or m component can be implemented by taking the complex conjugate of the impulse response. If the signal is an even function, this step is not required and the convolution is equivalent to a correlation function. In the case of the Barker code, the function is an odd function, so the complex conjugation must

be implemented. The convolution is the time reversal/reflection of impulse response, conjugation, and sliding this weighting function through the signal integrating or summing. It is drilled into every undergraduate Electrical Engineer that convolution in the time domain is equivalent to multiplication in the frequency domain, and visa versa. This is usually taken advantage of when the number of taps in a filter are large; it is more efficient to implement the function in the frequency domain than using a Finite Impulse Response (FIR) in the time domain. In the case of the Barker code there is a small number of samples, so FIR is an optimal approach. However, a frequency domain convolution was implemented, usually called “Fast Convolution,” since it was easy to implement in software.

$$f(t) * h(t) = \int_{-\infty}^{\infty} f(\tau) h(t - \tau) d\tau \quad (2.29)$$

$$f(n) * h(n) = \sum_{m=0}^{N-1} f(m) h(n - m) \quad (2.30)$$

When implementing the convolution in either domain, the processing must go through the number of samples in the signal set plus the number of samples that represent the impulse response; this allows the convolution to complete the sliding of the impulse response through the entire signal of interest. This is implemented by zero padding in the time domain and implementing overlap add or overlap discard / overlap save. The convolution is implemented by taking the Fast Fourier Transform (FFT) of the input signal and multiplying it by the spectrum of the impulse response of the filter: the FFT of the Barker code zero filled in the time domain to match the length of the signal FFT to generate the transfer function. After the multiplication, the IFFT is taken to return to the time domain. The type of filter developed is a matched filter, so

before the spectrum of the impulse response is multiplied, it is conjugated; this turns the convolution of odd functions into a correlation. The output will be a triangular shaped peak with triangulate shaped equal size sidelobes. The sidelobes for a three-digit Barker code are at -9.5 dBc; a seven-digit code drives the sidelobes to -16.9 dBc (Figure 2.68). A lot of the theoretical work in this section assumes a seven-bit code; for the implementation, a three-bit code was used for reasons that will be described. All of the math for the correlation / matched filter is implemented on the PC located on Rx1 in C code.

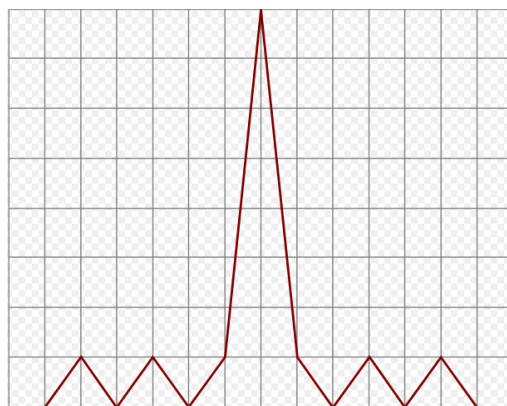


Figure 2.68. Example 7-bit Barker Convolution.

Table 2.11 shows the detailed specifications for the telescope and LEDs. The desired results developed are at the bottom of the table: C_n^2 as a function of pixel size and pixel area or pixel count. Both equations are for the area method for calculating C_n^2 . The specification's variable names in the table are presented in blue at the end of the row.

Table 2.11. Scintillometer Telescope and LED Characteristics.

TAIPAS Telescope Scintillometer Analysis			
AJG/ST/AM/LAS/LJS 022716	2292016		
Fundamental Constants			
Plank's constant	(J-s)	6.626E-34	
Speed of light	(m/sec)	2.998E+08	
Path Characteristics			
Path length	(m)	1920	L
Cn2	(m-2/3)	2.00E-12	C_n^2
Telescope and CCD			
Meade 6" LX80 SC			
Aperture diameter	(cm)	15.2	$D = 6" \times 2.54 \text{ cm / inch}$
Focal length	(m)	1.524	Telescope Data sheet F_L
CCD array size	H	1280	Lumenera 075M with Sony ICX424AL chip = # of active pixels $\#Pixels_H$
	V	960	Camera Data sheet (Actual pixels 1348 x 976, effective pixels 1296 x 966) - # of active pixels = 1280 x 960 $\#Pixels_V$
	H	6.26	Sony CCD Data Sheet CCD_Size_H
	V	5.01	Sony CCD Data Sheet CCD_Size_V
Pixel size	(um)	3.75	Square pixels on CCD chip - data sheet $Pixel_Size$
Angular resolution/pixel	H	3.21	$Angular_resolution_H$
	V	3.42	$Angular_resolution_V$
	(H+V)/2	3.32	$Average_Angular_resolution$
Resolution at source distance	(mm)	6.37	$Resolution\ at\ Source$
FOV at source distance	(m), H	7.89	FOV_H
	(m), V	6.31	FOV_V
Source			
LED intensity	(mcd)	84000	Peak on-axis intensity - array of bright LEDs (7 LEDs)
	(W/st)	1.23E-01	Radiation intensity toward telescope
Source LED separation	(m)	0.03	LED Separation of Chips in H and V dimensions ΔLed Tatarskii (1971) geometrical optics solution, also Cheon and Muschinski (2007), Tichkule comp exam (2013)
Centroid Determination Performance			
Angle of arrival variance	(rad^2)	2.04E-08	σ^2
AOA STD	(deg)	8.18E-03	σ
Centroid x-std	(um)	176.33	$Centroid_{x_std}$
1-sigma pixel std	(pixels)	47.02	$\#Pixel_{1x_std}$
6-sigma pixel std	(pixels)	282.13	$\#Pixel_{6x_std}$
Airy FP pattern width	(um)	6.46	ECEN 5264 Notes $Airy_FP_Pattern_width$
	(pixels)	1.72	for single LED $\#pixels_{single_LED}$
6-sigma+2*Airy Height percent	(% FS)	29.75%	Percent of full-screen Vertical CCD array single LED $\%_Height_{single_LED}$
6-sigma+2*Airy Width percent	(% FS)	22.31%	Percent of full-screen Horizontal CCD array single LED $\%_Width_{single_LED}$
Source LED FP separation H	(pixels)	6.35	$LED_FP_Separation_H_{\#pixels}$
	(% FS)	0.50%	Percent of full-screen CCD array width (H) Separation $\%LED_FP_Separation_H$
Source LED FP separation V	(pixels)	6.35	Note: LED separation is same for H and V $LED_FP_Separation_V_{\#pixels}$
	(% FS)	0.66%	Percent of full-screen CCD array width (V) separation $\%LED_FP_Separation_V$
Barker Code Discrimination	%		The above two % must be larger than 6 Sigma Area patter to distiquish (LEDs)
Max Path L to Desc. 2X LEDs	(m)	153	$L < .214 D^{1/3} F_L^{-1/3} \Delta Led^{2/3} (C_n^2)^{-1/3}$ See derivation
		Tst Cn2 Derivation	2.00004E-12
Total Pixel Count= $(\#Pixel_{6x_std})^2$		$C_n^2 = .009788 L^{-1} D^{1/3} F_L^{-1} (\#Pixel_{6x_std})^2 (Pixel_Size)^2$	See derivation
		OR	
Shape_Area (m)		$C_n^2 = .009788 L^{-1} D^{1/3} F_L^{-1} (Shape_Area)^{1/2} (Pixel_Size)$	See derivation

The equations utilized to derive values in Table 2.11 are shown in sequential order from Equation 2.31 through Equation 2.49. The angular resolution in the horizontal and vertical planes is developed from the equivalent pixel size, derived from the CCD size divided by the number of pixels and the focal length in Equation 2.31 - Equation 2.32. The average angular

resolution is the mean of the vertical and horizontal resolutions (Equation 2.33). The resolution at the source will be a function of the path length (L) and the average angular resolution (Equation 2.34). The field of view in the horizontal and vertical dimensions is a function of the path length, angular resolution and number of pixels (Equation 2.35 and Equation 2.36). The airy focal plane width is a function of focal length, diameter of the lens and lambda (Equation 2.37). The angular variance as it relates to path length, atmosphere structure constant and the diameter of the lens is described in the paragraphs below; it is presented here for completeness with respect to the table and represented as sigma squared (Equation 2.38). The standard deviation, sigma, is the square root of the angle variance (Equation 2.39). The centroid is a function of the variance and focal length (Equation 2.40). The single sigma, number of pixels is a function of the centroid and pixel size (Equation 2.41) — multiplying this by six yields the six-sigma quantity of pixels (Equation 2.42). The number of pixels represented by a single LED is determined by the airy pattern width and the pixel size (Equation 2.43). The percent height and width of the LED patterns is a function of the six-sigma pixel quantity: the number of pixels for a single LED and the number of pixels in the vertical or horizontal dimension (Equation 2.44 and Equation 2.45). The LED focal plane separation in vertical and horizontal are a function of LED separation, focal length, pixel size and path length (Equation 2.46 – Equation 2.47). The percent LED separation is a function of LED separation and the number of pixels in the vertical or horizontal dimension (Equation 2.48 – Equation 2.49).

$$Angular_resolution_H = \frac{Pixel_Size_{equivalent_H}}{F_L} = \frac{CCD_Size_H}{\#_Pixels_H F_L} \quad (2.31)$$

$$Angular_resolution_H = \frac{Pixel_Size_{equivalent_V}}{F_L} = \frac{CCD_Size_V}{\#_Pixels_H F_L} \quad (2.32)$$

$$Average_Angular_resolution = \frac{(Angular_resolution_H + Angular_resolution_V)}{2} \quad (2.33)$$

$$Resolution\ at\ Source = Angular_resolution_{Average} \times L \quad (2.34)$$

$$FOV_H = L \times Angular_resolution_H \times \#Pixels_H \quad (2.35)$$

$$FOV_V = L \times Angular_resolution_V \times \#Pixels_V \quad (2.36)$$

$$Airy_FP_Pattern_width = \frac{3.233\lambda}{\pi} \frac{F_L}{D} \quad (2.37)$$

$$\sigma^2 = 2.838C_n^2 LD^{-1/3} \quad (2.38)$$

$$\sigma = \sqrt{\sigma^2} \quad (2.39)$$

$$Centroid_{X-STD} = \sqrt{\sigma^2} F_L \quad (2.40)$$

$$\#Pixel_{1X_STD} = \frac{Centroid_{X-STD}}{Pixel_Size} \quad (2.41)$$

$$\#Pixel_{6X_STD} = 6 \times \#Pixel_{1X_STD} \quad (2.42)$$

$$\#pixels_{single_LED} = \frac{Airy_Pattern_width}{Pixel_Size} \quad (2.43)$$

$$\%_Height_{Single_LED} = \frac{(\#Pixel_{6X_STD} + 2 \times \#pixels_{single_LED})}{\#Pixels_V} \quad (2.44)$$

$$\%_Width_{Single_LED} = \frac{(\#Pixel_{6X_STD} + 2 \times \#pixels_{single_LED})}{\#Pixels_H} \quad (2.45)$$

$$LED_FP_Separation_{H_ \#Pixels} = \frac{LED_Separation_H}{L} \frac{F_L}{Pixel_Size} \quad (2.46)$$

$$LED_FP_Separation_{V_ \#Pixels} = \frac{LED_Separation_V}{L} \frac{F_L}{Pixel_Size} \quad (2.47)$$

$$\%LED_FP_Separation_H = \frac{LED_FP_Separation_{H_ \#Pixels}}{\#Pixels_H} \quad (2.48)$$

$$\%LED_FP_Separation_V = \frac{LED_Separation_{V_ \#Pixels}}{\#Pixels_V} \quad (2.49)$$

The following derives the equations relating area or displacement to C_n^2 ; their derivation's foundation is presented [31]. The AoA variations of an optical transmission are affected primarily by the inertial range of the atmospheric spectrum. In other words, the variance is related to the spatial variations in the atmosphere, caused by turbulence and structurally represented as outer scale large eddies at the energy input stage that decay to small inner scale eddies close to the ground where the remaining energy is dissipated as heat. For this reason, the Kolmogorov model is applied. From the Kolmogorov model, the wavenumber cutoffs, inner scale wavenumber ($2\pi/l_0$) to outer scale wavenumber ($2\pi/L_0$), are utilized for the integration duration for the AoA variance (Equation 2.50) to represent the inertial range. The denominators represent the lengths of the eddies at the energy insertion point, L_0 , and the energy dissipation point, l_0 ; these are represented in Figure 2.2 for the open path as a function of 0.4 x height, which is the Tatarski estimation. The variable R is the path length.

$$\langle \delta\theta^2 \rangle = \frac{2}{3} \pi^2 R \int_{\kappa_0}^{\kappa_m} \kappa^3 \frac{.033 C_n^2}{\kappa^{11/3}} d\kappa \quad (2.50)$$

When the outer scale length, L_0 , is much greater than the inner scale length, l_0 , which for all practical applications is the case, the AoA variance Equation 2.51 becomes Equation 2.52 for spherical waves.

$$\langle \delta\theta^2 \rangle = .651 R C_n^2 \kappa_m^{1/3} \quad (2.51)$$

$$\langle \delta\theta^2 \rangle = 2.837 R C_n^2 D_r^{-1/3} \quad (2.52)$$

The derivation would stop here if it were not for the effects of aperture averaging. This forces eddies that are smaller than the telescope lens radius size to have little to no effect; therefore, the inner scale length is replaced with the radius of the aperture (lens). As could be expected, deriving the new variance utilizes integrating a decaying function (Bessel Function) [31]. With the diverging rays and aperture size considered, not a point receiver as above, the AoA variance as a function of the diameter becomes Equation 2.52 for plane waves. This is the same as the above sigma denoted variable with L replaced by R.

The following derivation yields C_n^2 in terms of pixel count or area when utilizing a single LED. Solving for C_n^2 yields Equation 2.53. The centroid for a single standard deviation from Equation 2.49 is shown for completeness in Equation 2.55. Solving for the angle variance yields Equation 2.56, and substituting it into Equation 2.53 yields Equation 2.56. Leveraging Equation 2.41 and Equation 2.42, the number of six-sigma pixels is shown in Equation 2.57. Solving for the centroid standard deviation yields Equation 2.58. Substituting this into Equation 2.56 yields Equation 2.59 and then Equations 2.60 and 2.61. The final pixel count is Equation 2.62; this is

the equation utilized in the TAIPAS MATLAB code for determining C_n^2 for a single LED.

Subbing Equation 2.63 yields an equation as a function of area instead of pixel count.

$$C_n^2 = \frac{\langle \delta\theta^2 \rangle}{2.838RD^{-1/3}} \quad (2.53)$$

$$Centroid_{X-STD} = \sqrt{\langle \delta\theta^2 \rangle} F_L \quad (2.54)$$

$$\langle \delta\theta^2 \rangle = \frac{Centroid_{X-STD}^2}{F_L} \quad (2.55)$$

$$C_n^2 = \frac{Centroid_{X-STD}^2}{2.838RD^{-1/3} F_L} \quad (2.56)$$

$$\#Pixel_{6X-STD} = 6 \times \frac{Centroid_{X-STD}}{Pixel_Size} \quad (2.57)$$

$$Centroid_{X-STD} = \frac{\#Pixel_{6X-STD} Pixel_Size}{6} \quad (2.58)$$

$$C_n^2 = \frac{\left(\frac{\#Pixel_{6X-STD} Pixel_Size}{6} \right)^2}{2.838RD^{-1/3} F_L} \quad (2.59)$$

$$C_n^2 = \frac{\left(\frac{\#Pixel_{6X-STD}^2 Pixel_Size^2}{36} \right)}{2.838RD^{-1/3} F_L} \quad (2.60)$$

$$C_n^2 = \frac{\#Pixel_{6X-STD}^2 Pixel_Size^2}{102.17RD^{-1/3} F_L} \quad (2.61)$$

$$C_n^2 = .009788 R^{-1} D^{1/3} F_L^{-1} (\#Pixel_{6X-STD})^2 (Pixel_Size)^2 \quad (2.62)$$

$$\#Pixel_{6X-STD} = \left(\frac{Shape_Area}{Pixel_Size^2} \right)^{1/2} \quad (2.63)$$

$$C_n^2 = .009788 R^{-1} D^{1/3} F_L^{-1} (\text{Shape_Area})^{1/2} (\text{Pixel_Size}) \quad (2.64)$$

The following derivation is for the multi-LED pattern set up. For TAIPAS, Barker codes are utilized to increase precision measurement of the AoA displacement for a single capture faster than the frozen time of the atmosphere; no integration of multiple AoAs as in the single LED area case above. To distinguish the LEDs at a distance, the LED focal plane separation must be greater than the width of a single LED (Equation 2.65). Subbing in Equation 2.45 and Equation 2.48 yields Equation 2.66 with reduction implemented in Equation 2.67. Inequality Equation 2.68 is formed by subbing Equation 2.46 on the left side and Equation 2.43 with Equation 2.37 subbed for the aery pattern on the right side. Subbing in Equation 2.38 for the angular variance on the first fraction numerator on the right side of the inequality yields Equation 2.69. Equation 2.70 defines LED separation as a shorter variable name, resulting in Equation 2.71. Reducing the inequality is shown in Equation 2.72 and Equation 2.73. Finding a common denominator and adding the right-side yields Equation 2.74 with reduction produces Equation 2.75. The path length is isolated on the right side with further reduction in Equation 2.76 – Equation 2.84. Going from Equation 2.85 to Equation 2.87 assumes 3.233λ , since a small wavelength has very little effect; therefore, it can be eliminated. Equation 2.83 shows the range must be less than the amount determined by the LED separation, focal length, lens diameter and C_n^2 . Equation 2.84 - Equation 2.85 resolve the inequality for C_n^2 as a function of path length, LED separation, focal length and lens diameter. Equation 2.86 – Equation 2.87 solve for the required LED separation given the range of C_n^2 , given path length and optics information. Equation 2.83, Equation 2.85

and Equation 2.87 are very useful in the design of the scintillometer and for determining C_n^2 .

The vertical equations are the same as the horizontal with easy substitutions.

$$\%LED_FP_Separation_H > \%_Width_{Single_LED} \quad (2.65)$$

$$\frac{LED_FP_Separation_{H_#Pixels}}{\#Pixels_H} > \frac{(\#Pixel_{6X_STD} + 2 \times \#pixels_{single_LED})}{\#Pixels_H} \quad (2.66)$$

$$LED_FP_Separation_{H_#Pixels} > \#Pixel_{6X_STD} + 2 \times \#pixels_{single_LED} \quad (2.67)$$

$$\frac{LED_Separation_H}{R} \frac{F_L}{Pixel_Size} > 6 \times \frac{\sqrt{\sigma^2 F_L}}{Pixel_Size} + \frac{3.233\lambda}{\pi} \frac{F_L}{D} \quad (2.68)$$

$$\frac{LED_Separation_H}{R} \frac{F_L}{Pixel_Size} > 6 \times \frac{\sqrt{2.838C_n^2 R D^{-1/3} F_L}}{Pixel_Size} + \frac{3.233\lambda}{\pi} \frac{F_L}{D} \quad (2.69)$$

$$LED_Separation_H = \Delta Led_H \quad (2.70)$$

$$\frac{\Delta Led_H}{R} \frac{F_L}{Pixel_Size} > 6 \times \frac{\sqrt{2.838C_n^2 R D^{-1/3} F_L}}{Pixel_Size} + \frac{3.233\lambda}{\pi} \frac{F_L}{D} \quad (2.71)$$

$$\frac{\Delta Led_H}{R} \frac{F_L}{Pixel_Size} > 6 \sqrt{2.838C_n^2 R D^{-1/3} F_L} + \frac{3.233\lambda}{\pi} \frac{F_L}{D} \quad (2.72)$$

$$\frac{\Delta Led_H}{R} \frac{F_L}{Pixel_Size} > 10.12 \sqrt{C_n^2 R^{1/2} D^{-1/6} F_L^{1/2}} + \frac{3.233\lambda}{\pi} \frac{F_L}{D} \quad (2.73)$$

$$\frac{\Delta Led_H}{R} \frac{F_L}{Pixel_Size} > \frac{D \pi 10.12 \sqrt{C_n^2 R^{1/2} D^{-1/6} F_L^{1/2}} + 3.233\lambda F_L}{D \pi} \quad (2.74)$$

$$\frac{\Delta Led_H}{R} \frac{F_L}{Pixel_Size} > \frac{10.12\pi \sqrt{C_n^2 R^{1/2} D^{5/6} F_L^{1/2}} + 3.233\lambda F_L}{D \pi} \quad (2.75)$$

$$R < \frac{\Delta \text{Led}_H F_L D \pi}{10.12 \pi \sqrt{C_n^2 R^{1/2} D^{5/6} F_L^{1/2}} + 3.233 \lambda F_L} \quad (2.76)$$

$$R < \frac{\Delta \text{Led}_H D \pi}{10.12 \pi \sqrt{C_n^2 R^{1/2} D^{5/6} F_L^{-1/2}} + 3.233 \lambda} \quad (2.77)$$

$$R < \frac{\Delta \text{Led}_H D \pi}{10.12 \pi \sqrt{C_n^2 R^{1/2} D^{5/6} F_L^{-1/2}}} \quad (2.78)$$

$$R < \frac{\Delta \text{Led}_H D^{1/6} F_L^{1/2}}{10.12 \sqrt{C_n^2 R^{1/2}}} \quad (2.79)$$

$$R^{3/2} < \frac{\Delta \text{Led}_H D^{1/6} \pi F_L^{1/2}}{10.12 \sqrt{C_n^2}} \quad (2.80)$$

$$R < \left(\frac{\Delta \text{Led}_H D^{1/6} \pi F_L^{1/2}}{10.12 \sqrt{C_n^2}} \right)^{2/3} \quad (2.81)$$

$$R < \frac{\Delta \text{Led}_H^{2/3} F_L^{1/3} D^{1/9}}{4.68 (C_n^2)^{1/3}} \quad (2.82)$$

$$R < .214 D^{1/9} F_L^{1/3} \Delta \text{Led}_H^{2/3} (C_n^2)^{-1/3} \quad (2.83)$$

$$C_n^2 = \left(\frac{.214 D^{1/9} F_L^{1/3} \Delta \text{Led}_H^{2/3}}{R} \right)^3 \quad (2.84)$$

$$C_n^2 = .0098 D^{1/3} F_L \Delta \text{Led}_H^2 R^{-3} \quad (2.85)$$

$$\Delta \text{LED}_H = \left(\frac{R (C_n^2)^{1/3}}{.214 D^{1/9} F_L^{1/3}} \right)^{3/2} \quad (2.86)$$

$$\Delta \text{LED}_H = 10.10 R^{3/2} (C_n^2)^{1/2} D^{-1/6} F_L^{-1/2} \quad (2.87)$$

The ΔLED Equation 2.87 is useful in spacing the LEDs for the TAIPAS 1924 m path length for the range of C_n^2 . Equation 2.88 represents the anticipated range of C_n^2 for Boulder, Colorado. Equation 2.89 utilizes Equation 2.87 to show that there is a significant range of LED separation. Therefore, there needs to be a range of LED cross Barker code emitters to satisfy the index-of-refraction, structure constant range. This was not practical for the TAIPAS effort, primarily due to funding and schedule. The approach was to utilize a three chip Barker code inside the CU hallway with a path length of 40 m with a C_n^2 that will be very small due to the lack of wind and high temperature. The three-chip code was placed on a disk that fits in a circular hole on Rx1 — the same place the telescope is located on Tx1 and Rx2. In the future, the LEDs will be placed external to the box on both Tx and Rx, and Rx1 will contain a telescope. On the 40 m path and a reduced C_n^2 range, the LED separation is much more manageable on the 9” diameter hole. Equation 2.90 and Equation 2.91 show the range that can be handled in the hallway propagation link path.

$$10^{-17} < C_n^2 < 10^{-12} \quad (2.88)$$

$$9.7 \text{ cm} < \Delta LED_H < 30.83 \text{ m} \quad (2.89)$$

$$10^{-17.5} < C_n^2 < 10^{-16.5} \quad (2.90)$$

$$5.5 \text{ cm} < \Delta LED_H < 17.3 \text{ cm} \quad (2.91)$$

Table 2.12 utilizes Equation 2.85 to calculate C_n^2 based on rough estimates of two LED CCD patterns touching at the six-sigma point. This is not extremely accurate, but gives a good feel that the math is working and C_n^2 is in the expected ballpark, showing that the further the distance, the larger the delta LED variable. Since this experiment was executed at the Colorado

Springs Airport, the environmental data was taken from METAR/SPECL. The temperature was dropping, which caused the C_n^2 to drop, also due to LED pattern estimations. Table 2.13 shows the LED separation for spread and touching. Touching is when the LED patterns touch and spread is when the LED patterns are separated by the distance of an LED pattern. This allows for a zero chip to be present between the two chips to represent a Barker Code. Table 2.14 shows the results in tabular form and a three-point fitted curve. The spread has increased linearity, since estimating it is much easier than the LEDs touching.

Table 2.12. Dual LED Characteristics at Colorado Springs Airport.

Used for calculating the Cross chip separation							
Collected Data Testing (2 LEDs)							
Range (m)	Δ LED Touching (cm)	ToD	Date	Cn2 Dual LEDs	Δ Cn2	OGIMET Data	
300	6	3:41pm	8 12 2015	1.06368E-12		30C/8C/7KT/30.32"Hg	86F
1000	15	4:22pm	8 12 2015	1.79496E-13	8.84185E-13	28C/11C/7KT/30.31"Hg	82.4F
1960	18	4:46pm	8 12 2015	3.43281E-14	1.45168E-13	23C/14C/10KT/30.31"Hg	73.4F

Table 2.13. Dual Led Spread vs. Touching at Various Ranges.

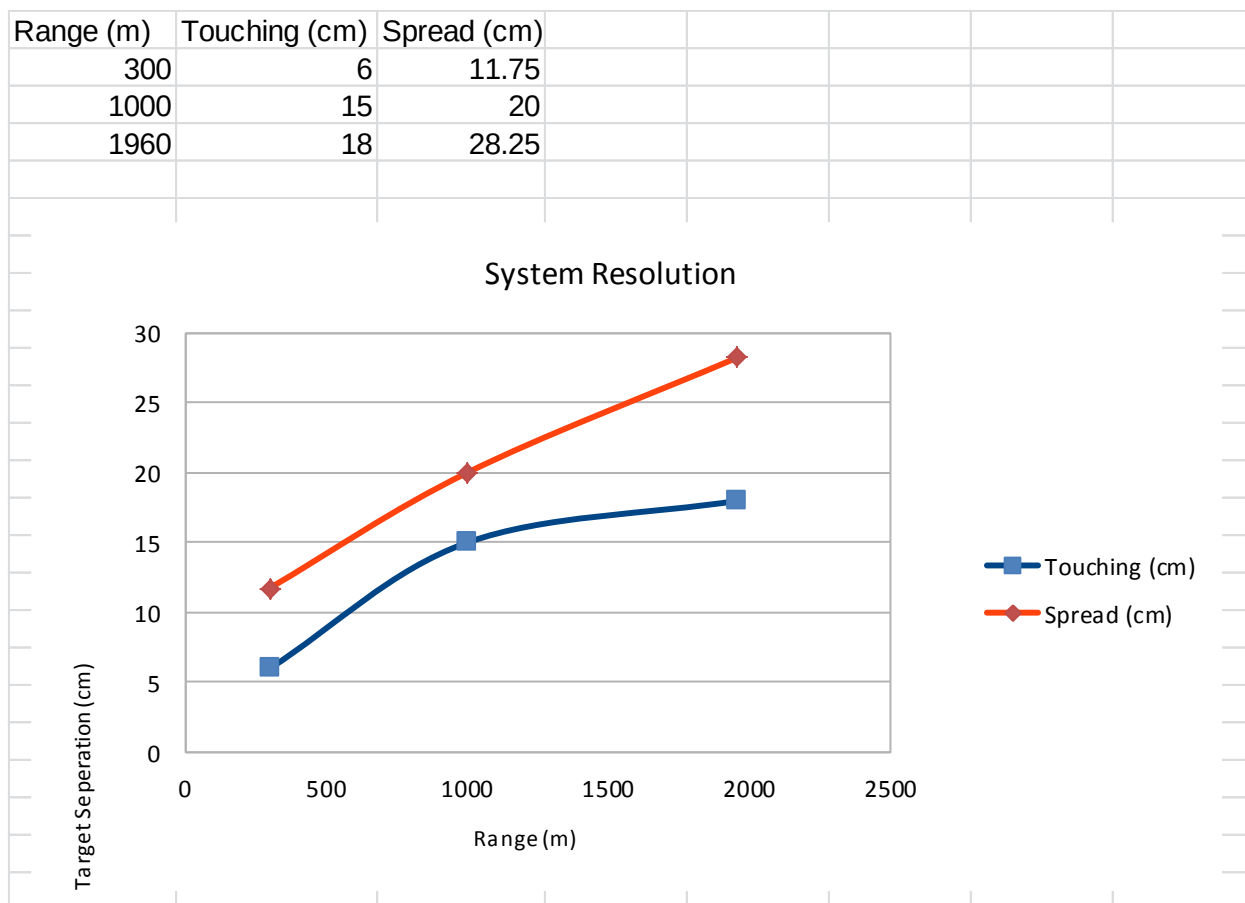


Table 2.14. Results with a Three-point Fitted Curve.

Cn2 Single LED	
3.55668E-14	$m^{(-2/3)}$

Cn2 Single LED	
1.13146E-12	$m^{(-2/3)}$

Cn2 Single LED		
1.65763E-13	$m^{(-2/3)}$	

Figure 2.69 shows a picture of the two LEDs at 1960 m. The C_n^2 is calculated leveraging Equation 2.45. Pixel count in the software is determined through a histogram and six standard deviations away from the primary value. For these examples, Gimp is utilized to draw an approximate six-sigma pixel count, delineated by the dotted line. This figure is a single snapshot of two LEDs. The scintillation on both LEDs is the same. The varying base shapes are due to the look angle of the telescope and the fit of the LED in the plastic mount for the four degree LED lens-generated beam. The offset in the x direction is a function of the cutting of the pixels and has nothing to do with the physics of the path. Figure 2.70 shows the multiple frames captured at different distances; it is easy to see the effects of atmospheric intensity scintillation. Figure 2.71 and Figure 2.72 show close-up views of the pixels for 1000 m and 300 m, respectively. The C_n^2 results are shown on the top of each photo. The variance is due to the time of day the photos were taken; the larger C_n^2 was taken during hotter times of the day.

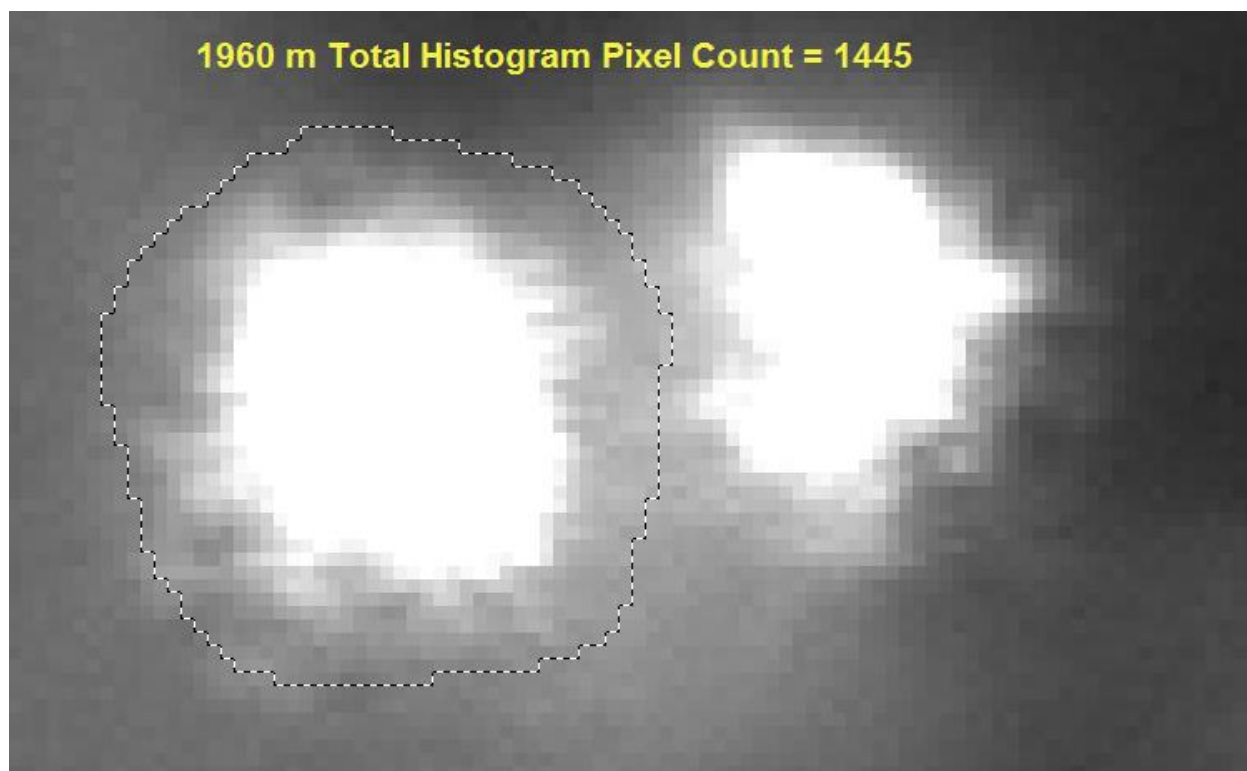


Figure 2.69. Dual LED Photo – 1960 m.

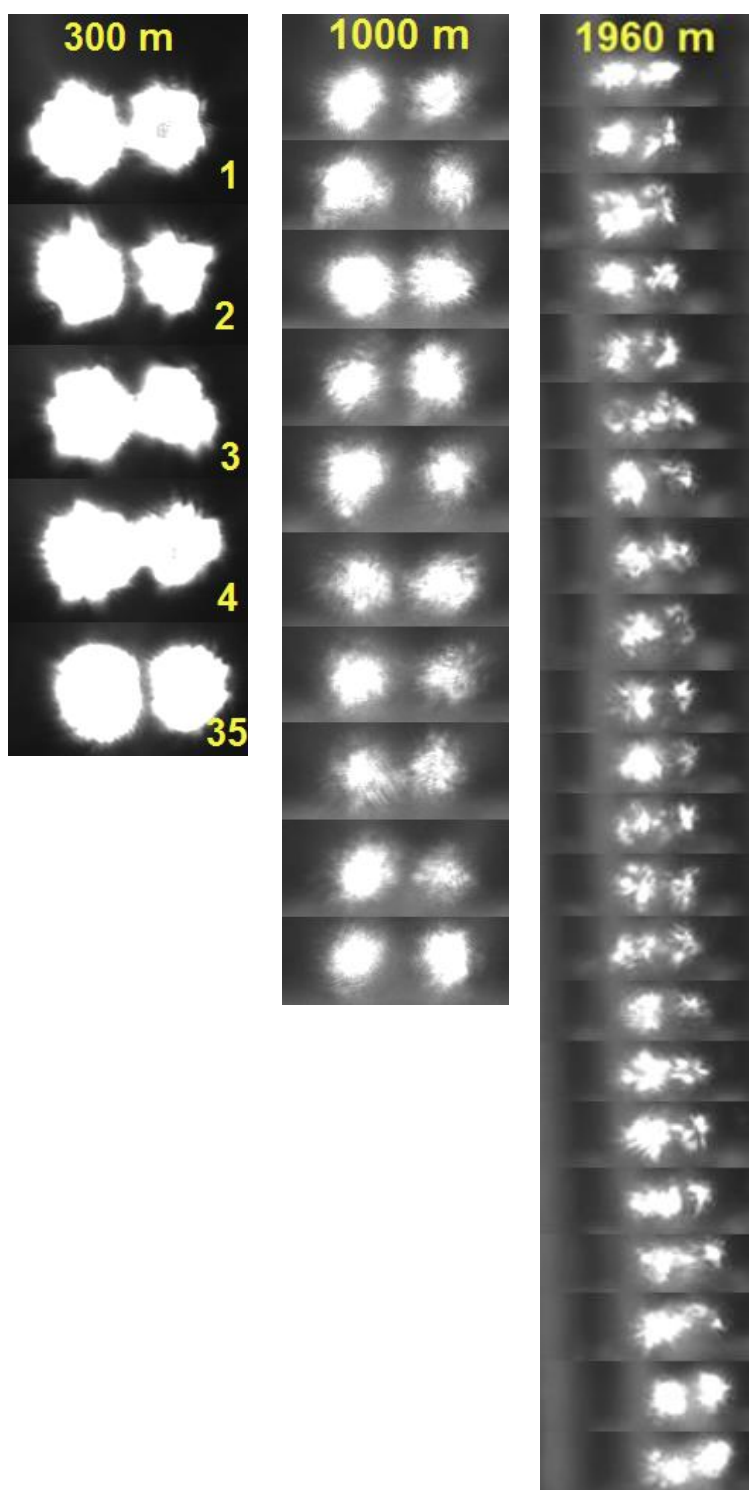


Figure 2.70. Dual LED Photo – Multiple Frames.

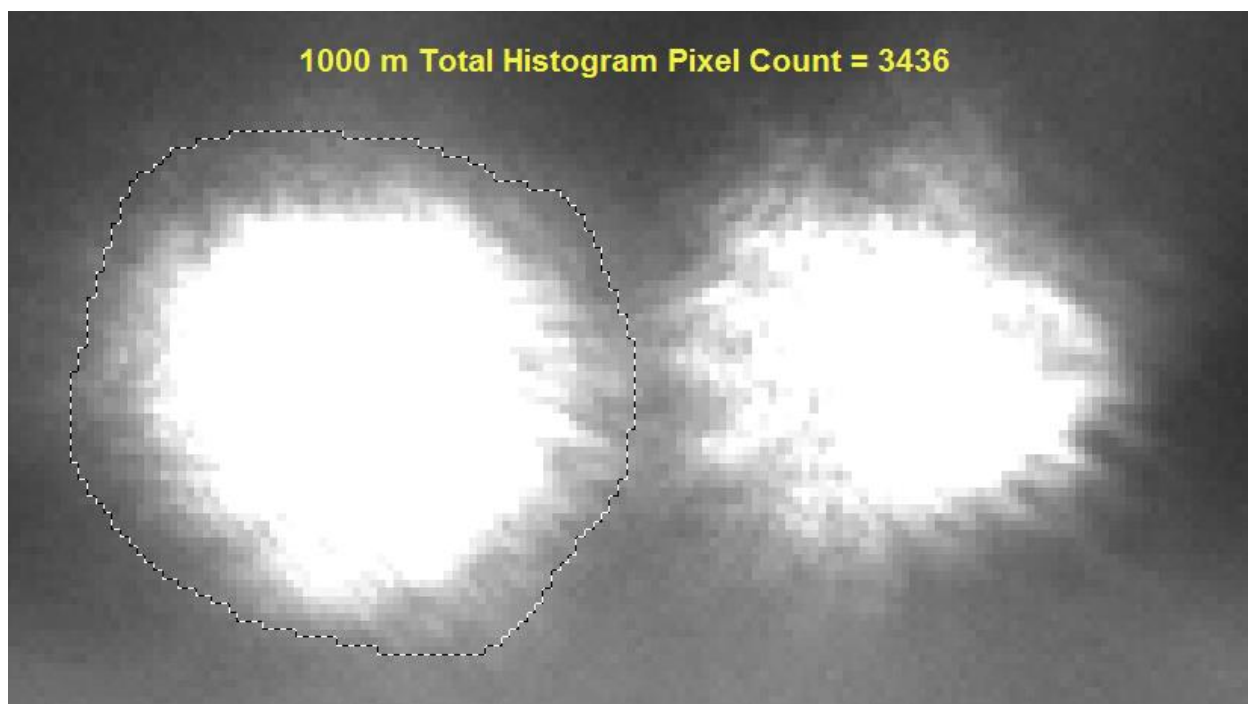


Figure 2.71. Dual LED Photo – 1000 m.

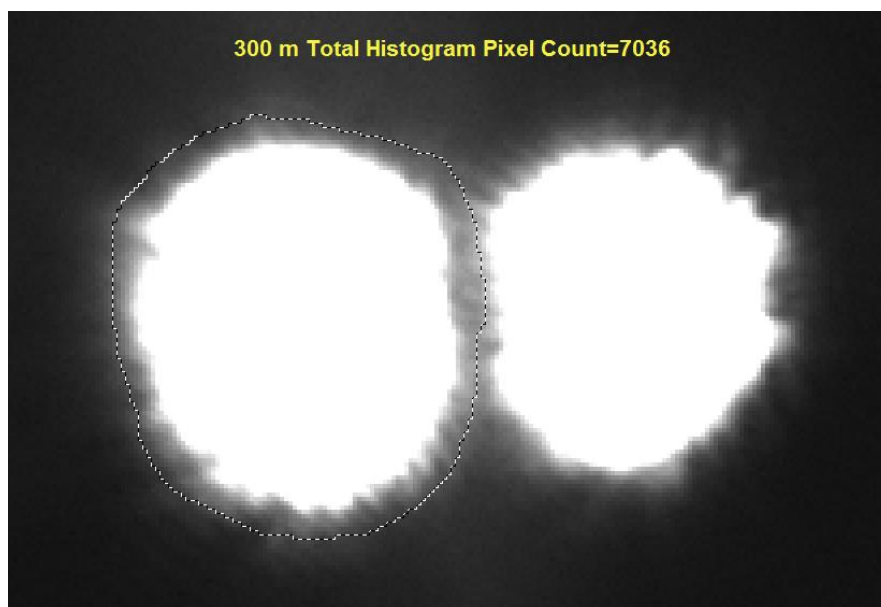


Figure 2.72. Dual LED Photo – 300 m.

The shutter speed on the camera had the capability to sample the images up to a 10 KHz rate: 0.1 ms per image. This is ten times faster than the theorized frozen time of the atmosphere of 1 ms. Theoretically, the frozen time of the atmosphere can be measured with the camera; look for consistency across multiple AoAs across frames. Figure 2.73 and Figure 2.74 show shutter speeds of 0.25 ms and 0.12 ms, respectively. In both pictures, the stability, for approximately the same C_n^2 , is significantly more stable than the slower shutter speeds shown in Figure 2.70. If the atmosphere is truly frozen at 1 ms increments, 0.25 ms samples should be consistent across four frames, and eight frames for the 0.12 ms speed. Figure 2.73 shows some samples that have 2 - 3 similar frames. Figure 2.74 shows that two frames are similar, but nothing close to eight frames. This only questions the hypothesis that the atmosphere is frozen at 1 ms increments if the camera's data port can keep up; this will be discussed later. Significantly more work needs to be focused in this area to come to a definitive conclusion, which is beyond the scope of this thesis.

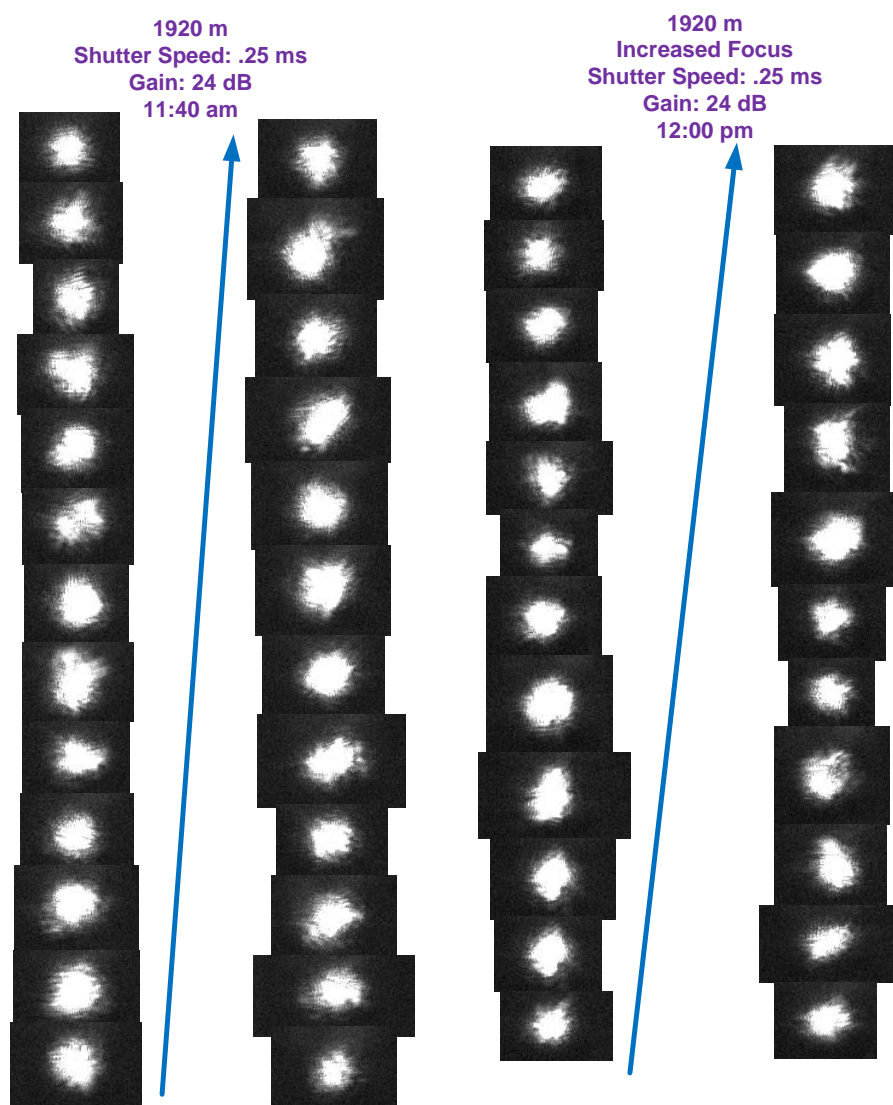


Figure 2.73. Single LED Photo – 1900 m – 0.25ms Shutter.

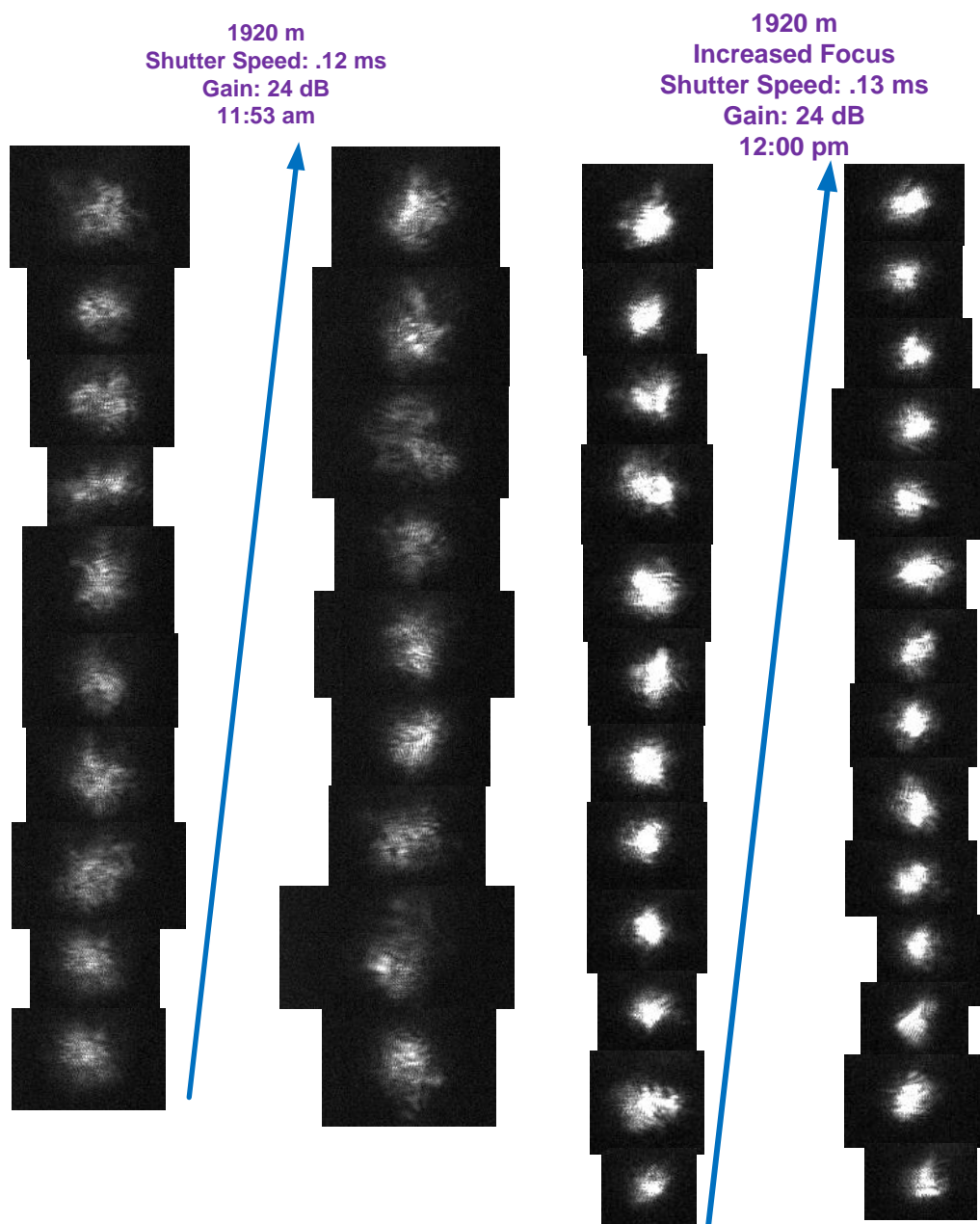


Figure 2.74. Single LED Photo – 1900 m – 0.12 ms Shutter.

The same scintillation that was trying to be measured by the Barker coded LED pattern was causing significant distortion in the Barker cross to a point of not being able to discriminate the chips. When the ~10 ms shutter speed was utilized, it was impossible to discriminate the cross at

any useful distance. Figure 2.75 shows the scintillometer emitter that was utilized for the experiment: four chip Barker code (1011). The codes are produced by the separation of two adjacent LEDs; a large separation is a one and short separation is a zero. There is also a single LED in the top corner for area testing C_n^2 . The results, with the shutter speed and the LEDs spaced closely, are shown in Figure 2.76. The chips are close to distinguishable. This definitely shows the atmosphere is getting more stable at higher sample rates. This also reduces the non-coherent integration that is taking place — less AoAs summed on the CCD. This shows promise that with multiple LED spacing for Barker patterns, multiple simultaneous emitters, and a fast shutter speed, measuring the displacement of close to a single AoA is feasible for a significant range of C_n^2 .

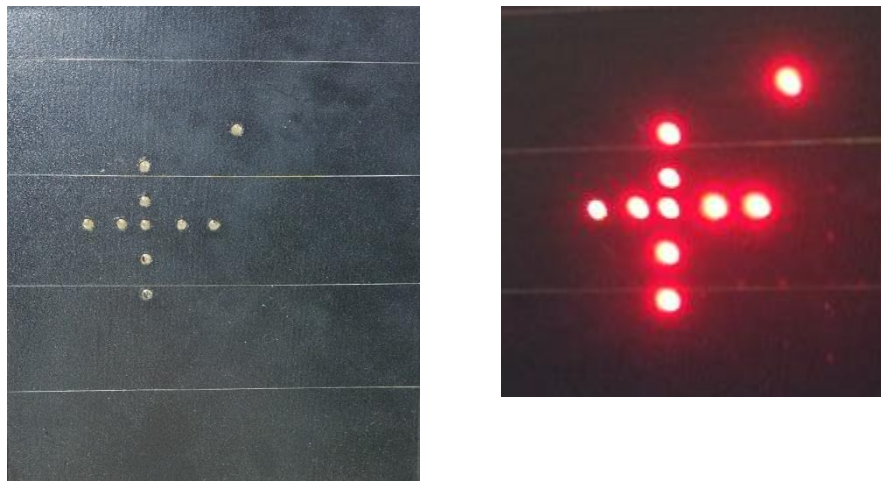


Figure 2.75. Barker LED System – 7 chips – 0.12 ms Shutter.

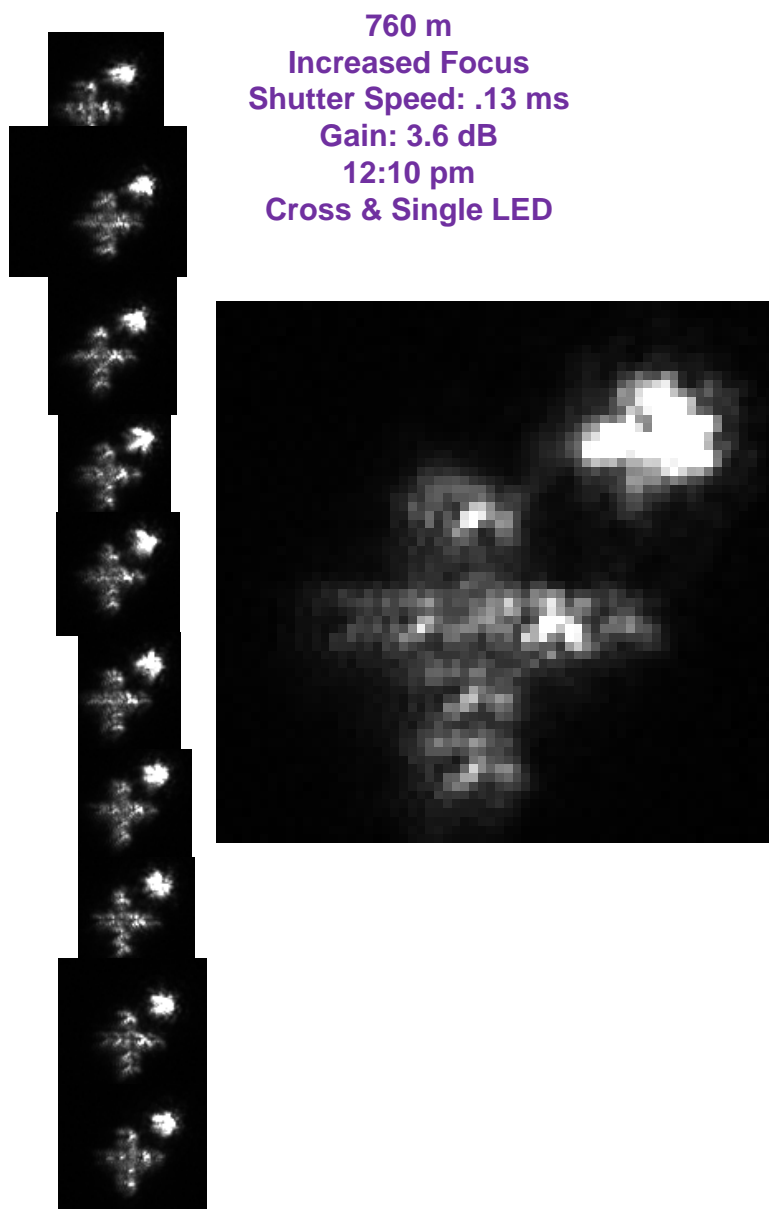


Figure 2.76. Multiple Barker Cross LED Photo – 760 m – 0.12 ms Shutter.

Early stages of testing Barker code compression to measure the displacement of AoA for a single frame were implemented with precise digital pictures for targets. The kernels utilized are shown in Figure 2.77; the kernel on the right is inverted. Figure 2.78 shows the CCD output looking at a picture through the telescope with the Barker cross on a Pikes Peak background.

The circles around the cross show a tight track on the correlated sync-squared outputs. From the slightest vibrations representing atmospheric scintillation to large telescope movement, the trackers remain locked on the targets. Figure 2.79 shows much smaller targets and fewer pixels on the treed background that is behind the mesa; the algorithm continued to lock on the targets. If the circles lose track, they rapidly wander all over the image searching for targets.

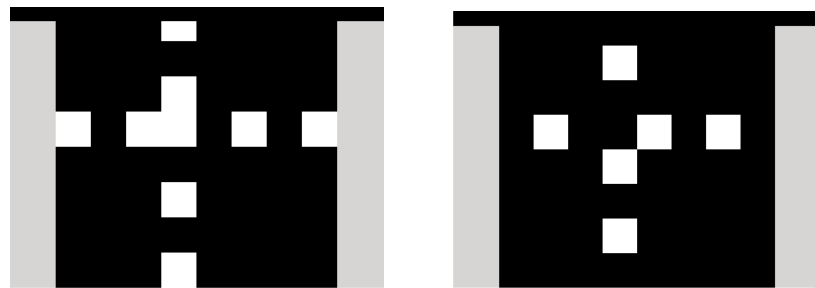


Figure 2.77. Barker Cross Picture.

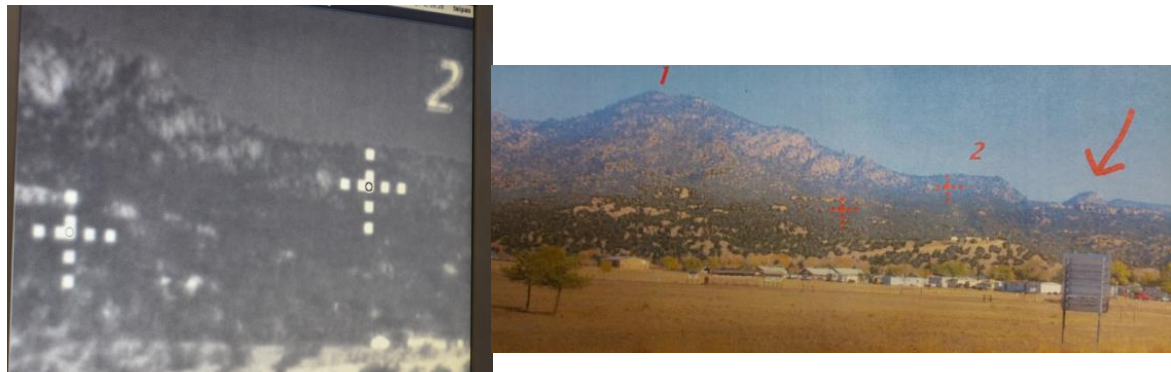


Figure 2.78. Barker Cross Picture Tracked.

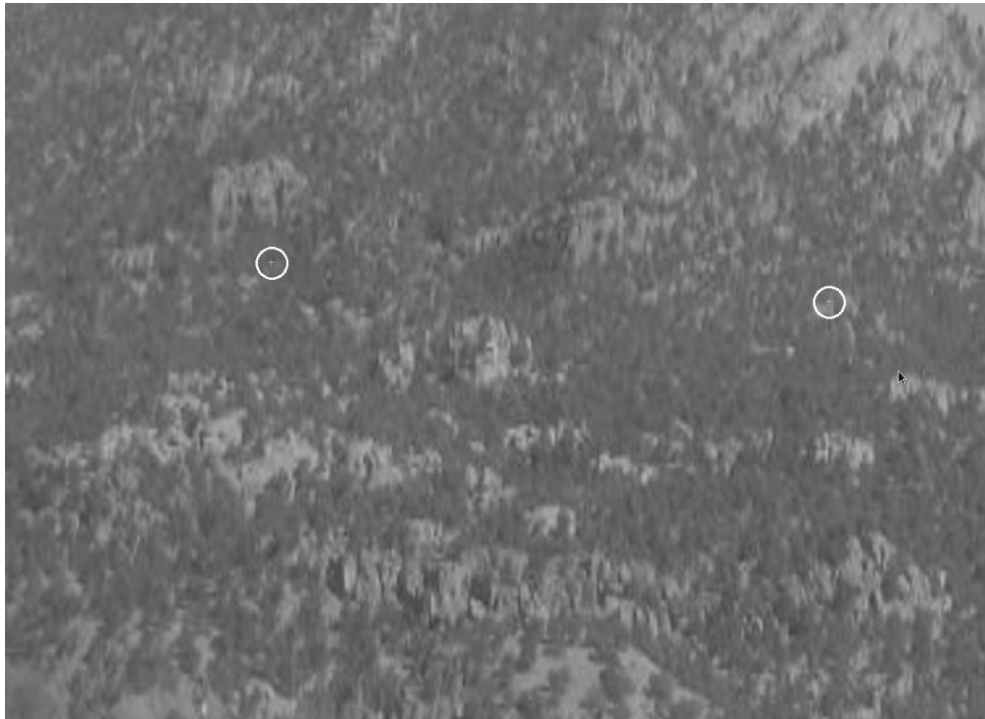


Figure 2.79. Barker Cross Picture Tracked on Mountain.

Since there are white trailers behind the TAIPAS receivers on the mesa, the same tests were run on this background. The chip colors could have been changed to a color that allowed better distinguishability, but they would be filtered out by the black and white camera. Figure 2.80 shows good lock on the targets just above the trailers. Figure 2.81 shows the right cross over on the trailer with track maintained.



Figure 2.80. Barker Cross Picture Tracked Above Trailers.



Figure 2.81. Barker Cross Picture Tracked Above and on Trailers.

Figure 2.82 shows the LED pattern up close and the issue of lining up the LEDs four-degree beams perfectly orthogonal with the telescope. There is more fine-tuning that needs to be implemented to developing the coding techniques. One possibility is to slide a template, like the one shown in Figure 2.83, to reduce the search volume and the chip variation.



Figure 2.82. Barker Cross Picture Short Range Picture.

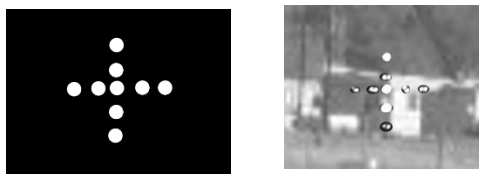


Figure 2.83. Barker Cross Template.

The final LED pattern is shown in Figure 2.84. The Barker cross was limited to a three-chip pattern due to the limited space inside the window on the Rx1 telescope window. For the 40 m path, the Barker was utilized, however, in the long run, the single LED was utilized with the area function determination of C_n^2 . The camera that is utilized to photographically catch the weather conditions during an acquisition is on this plate too and the bottom photo.

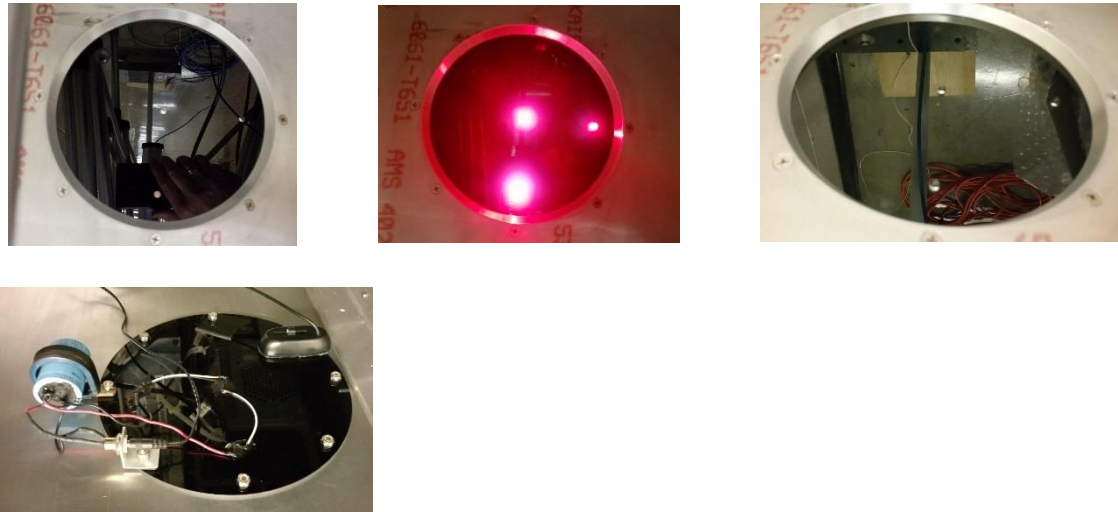


Figure 2.84. Final Single LED/Barker Cross Configuration.

The LED was selected utilizing the image intensity Equation 2.92 and Equation 2.93, shown in Table 2.15. Detected photons during exposure time exceed the daytime background light from the mesa, so the emitter should be distinguishable. The data rate calculations (Equation 2.94 – Equation 2.96) are shown in the bottom portion of the table; the 3.7 GB/s at 18 frames/s can be handled, but are too fast for USB 2.0, which can handle 480 Mb/s. PCIe X4 Gen 3 can handle these types of rates for continuous sampling, but this interface will not be on cameras that TAIPAS can afford during this phase of the program. For this reason, the variations seen in Figure 2.73, Figure 2.74 and Figure 2.75 are partially, if not totally, due to the contribution of the slow data rate.

$$Photon_E = \frac{hc}{\lambda} \quad (2.92)$$

$$\#Photons = \frac{P_r}{Photon_E} \frac{T}{e_{optical}} \quad (2.93)$$

$$B_{image} = \left(\#Pixels_H \#Pixels_V b_{pixel} \right) / 8 \quad (2.94)$$

$$D_{rate} = \frac{B_{image}}{F_{rate}} \tag{2.95}$$

$$Data / Measurement = D_{rate} t_{duration} \tag{2.96}$$

Table 2.15. Image Intensity and Sampling Rate

Image Intensity Performance			
Received power	(W)	6.09E-10	P_r
Wavelength	(um)	0.628	Red LEDs (www.superbrightleds.com)
Photon energy	(J)	3.16E-19	$Photon_E$
Exposure time	(msec)	1.00	T
Optical & quantum efficiency	(%)	70%	$e_{optical}$
Received photons	(--)	1.35E+06	Detected photons during exposure time - should exceed daytime background light from mesa. $\# Photons$
Sampling and Data Rate			
Frame rate	(fps)	18	F_{rate}
Bits per pixel	(b/pel)	12	b_{pixel}
Data per image	(Bytes)	1843200	B_{image}
Data rate	MB/sec	31.64	D_{rate}
Measurement duration	(min)	2.00	$t_{duration}$
Data per measurement	(GB)	3.71	Implication is that some preprocessing of each frame to determine centroids and widths should be developed.

For the direct measurement of C_Q^2 , from previous work [58], it has been theorized this can be achieved by synchronizing the sampling of the images with the THz link. This is far beyond current data rate technology hardware.

Figure 2.85 shows Rx1 with the dome tiled. Two of the LEDs are covered and taped; all scintillometer data is collected leveraging a single LED area. This plate also has a built-in camera to photo the path during collections.



Figure 2.85. Current Single LED Configuration

Figure 2.86 shows the NIST scintillometer pointed toward NIST on the campus. NIST has provided scintillometer data that is not in the exact azimuth direction, elevation or length, but it was leveraged to compare for the TAI PAS version. The white covered scope looks at a source on the closest buildings to the bottom right in the photo.



Figure 2.86. NIST Scintillometer Photo.

Figure 2.87 shows an example picture of the aligned telescope fixed on the receivers. This picture is viewed on the laptop display and shows the precision from the telescope at the distance.



Figure 2.87. Example Day Photo of Telescope for Scintillometer.

2.10 Calibration – Alignment

The primary alignments discussed earlier were made to keep the planar wave orthogonal at the receivers in both x and y planes. As discussed earlier, the systems at the mesa and on the roof at CU must be pointed at a 3.61-degree angle: roof up 3.61 degrees and mesa down 3.61 degrees. This is the coarse elevation alignment. The next layer of alignment was accomplished with a laser, as discussed earlier. Fine alignment was implemented with the Y calipers on both the Tx and Rx units after alignment of the boxes was implemented.

The boxes inside the domes are on swivels that allow alignment of the Tx and Rx systems in azimuth. The next layer of alignment was accomplished with a laser; discussed earlier. Fine

alignment was implemented with the X calipers on both the Tx and Rx units after alignment of the boxes was implemented.

An alignment laser was placed on the Tx and Rx1. The laser goes through a tube that allows alignment with the lens on the chassis. The object of the alignment is to see the spread beam in a circular laser spot; if it is elliptical, it is not aligned. During the night, the laser could be seen on the box after alignment, which was helpful. The data sheet for the laser is in Appendix B. Table 2.16 shows the calculations for the laser.

Table 2.16. Alignment Laser Calculations.

Laser power	mW	3.0	
Laser wavelength	nm	635	
Beam divergence	mrad	0.5	
Spot size at 5 m	mm	5.00	
Voltage	V	4.00	
Current	mA	50	
Power (DC input)	mW	200	
Distance	km	1.90	
Spot size at distance	m	0.95	According to beam divergence spec
Spot size at distance	m	1.90	According to empirical beam spot size spec
Effective source aperture diam	mm	1.651	According to beam divergence spec
Far zone distance	m	8.59	
Laser sitting tube length	inches	30.0	
	m	0.762	
Siting tube pinhole aperture di	mm	0.762	
	inches	0.030	
Power density at 5 meters	mW/cm ²	1.53E+01	According to empirical beam spot size spec. This is larger than the long term exposure power density, and thus could cause damage if the laser is directly viewed from a close in distance.
Power density at 20 meters	mW/cm ²	9.55E-01	According to empirical beam spot size spec. This needs to be less than long term exposure power density for safety.
Power density at distance	mW/cm ²	4.23E-04	According to beam divergence spec. This needs to be less than long term exposure power density for safety.
Spotting scope aperture diame	mm	50.0	
Spotting scope received power	mW	8.31E-03	
Spotting scope magnification	(-)	8.0	
Spotting viewer's intensity	mW/cm ²	2.71E-02	Needs to be less than long term exposure power density for safety, but reasonably large for detectability. In this case, ~2.7% of the long-term exposure limit is acceptable without use of neutral density filters.
Maximum long duration expos	mW/cm ²	1.0	400-700 nm band long exposure power density limit for eye safety.
The above study indicates that given laser is eye-safe for long exposure beyond 20 meters range, but is readily detectable without eye risk at 2 km range with the spotting scope.			
The laser is also likely detectable with the unaided eye at 2 km range, but perhaps not during full daylight.			

All alignments were accomplished with personnel in communication on both sides of the link. The engineers at the Rx looked at the signal on a Real-time Spectrum Analyzer (RSA) to optimize the magnitude while talking to the engineers at the Tx.

To measure the exact black body temperature of the receivers, a splash plate could be put in front of the receivers at night to point directly up. This was not implemented during this phase. Also, the entire system parameters, including phase noise, should be measured over temperature. This was not implemented due to cost and time.

2.11 DSP

Control systems are at either end of the transmissometer. These systems handle the data management and command/status through an Ethernet communication connection to the CET laboratory. Weather stations utilizing anemometer for temperature and wind, Hygrometer for humidity, and video cameras for monitoring are also part of these systems. EPOCH-based time stamping of all measurements (radio and meteorological) are used to ensure proper time referencing to an accuracy well within the time scale of the atmosphere.

TAIPAS utilizes a four channel, 12 bit, 40 Mega Samples Per Second (MSPS) ADC (DAS4020): Figure 2.88. The input was converted to 50 Ω with modification to the card. Two of the channels are utilized for the two receivers: 20 MSPS each. The data is transferred out of the PCI bus that supports up to 132 MB/s. The Field Programmable Gate Array (FPGA) on the ADC card implements the front end Digital Signal Processing (DSP). Figure 2.89 shows a block diagram of the Digital Down Converter (DDC) circuit that converts the 1 MHz-wide IF signal to

baseband by defining the complex plane with I/Q components. The FIR filters are 20 taps at baseband; 3dB at +/- 600 KHz. Decimation is implemented at baseband allowing lower data rates: 40 kSPS.

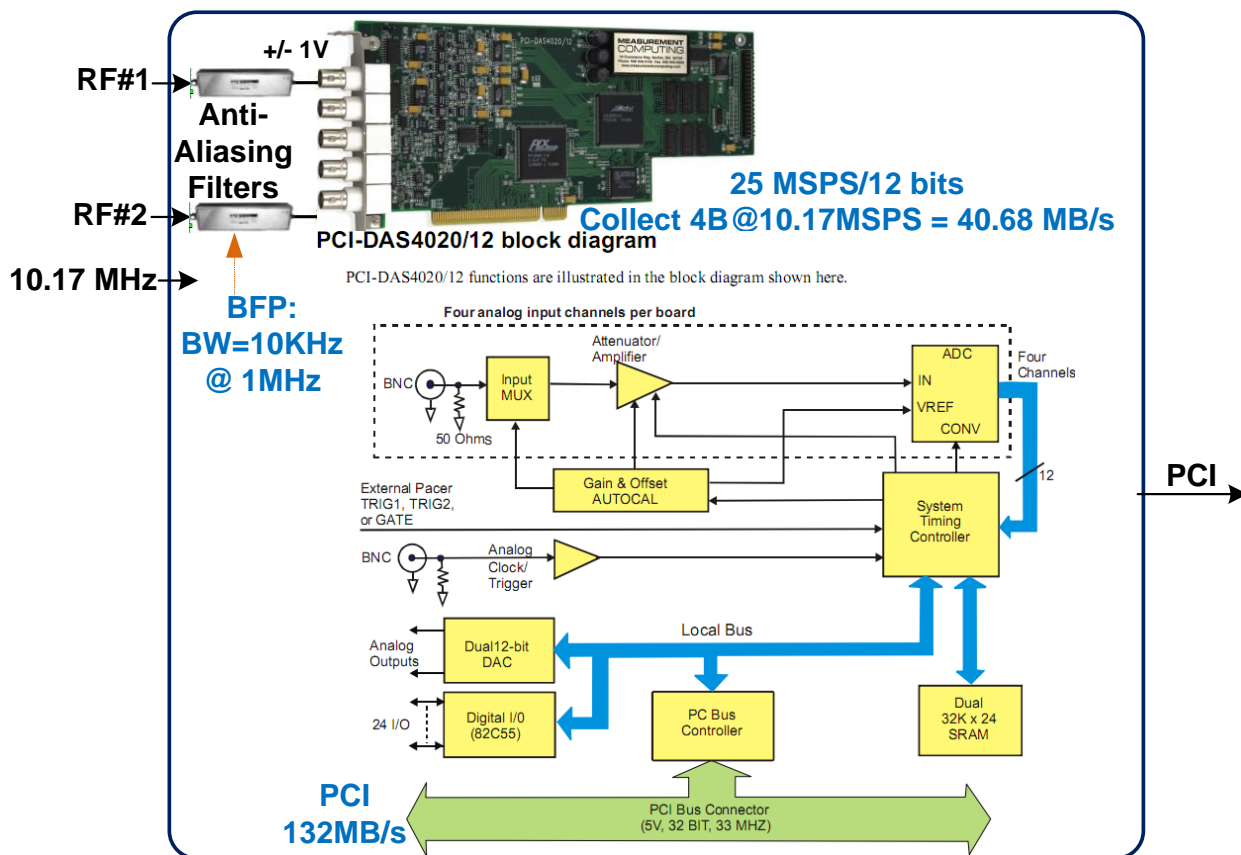


Figure 2.88. ADC Photo and Block Diagram.

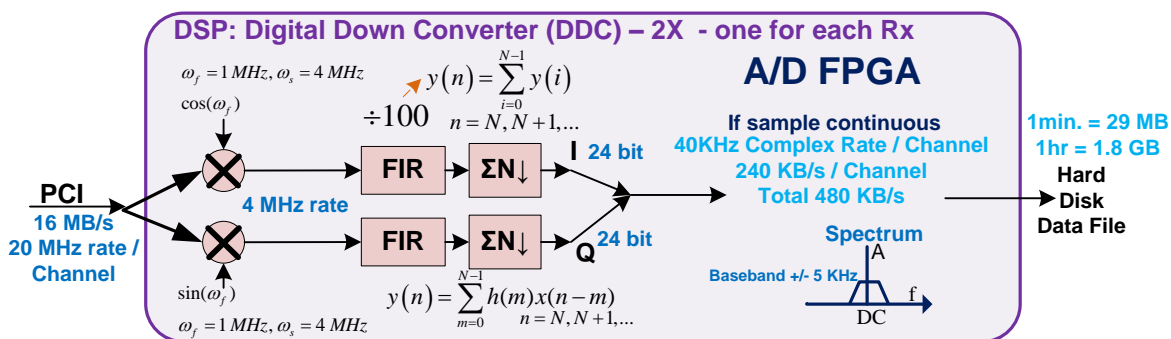


Figure 2.89. DSP: Digital Down Converter (DDC).

2.12 Software / Control

Figure 2.90 and Figure 2.91 are the high-level block diagrams of the TAIPAS receivers and transmitters, respectively. The C-band coherent pilot link will provide the synchronous 10 MHz clock, which will be sourced by the CEI clock distribution board. The Tx computer runs a Linux Operating System (OS); multi-threads allow real-time programming of the system. An Ethernet-controlled power switch allows the control of bringing the system up and turning the air conditioning unit off during data collections; the locations of system plugs are programmed into the outlet strip and can be seen on its LCD display. The strip has eight programmable and two permanent power outlets. The strips are fed by a UPS unit for protection. The OCXO requires a minimum of five minutes after power up to stabilize on both sides of the Coho link. The receiver contains all the data acquisition hardware. Rx1 contains all the functionality and Rx2 is sparse; all controls and data acquisition are implemented in Rx1. Figure 2.92 shows a diagram of the threads of the Linux software application.

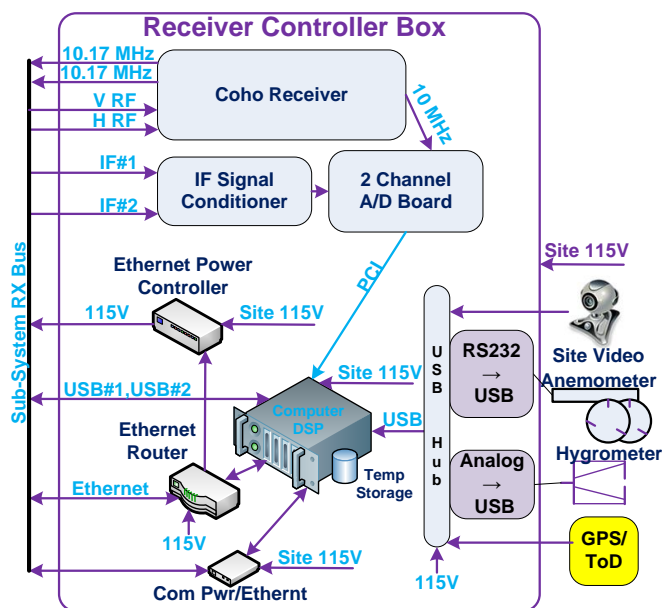


Figure 2.90. Receiver Controller.

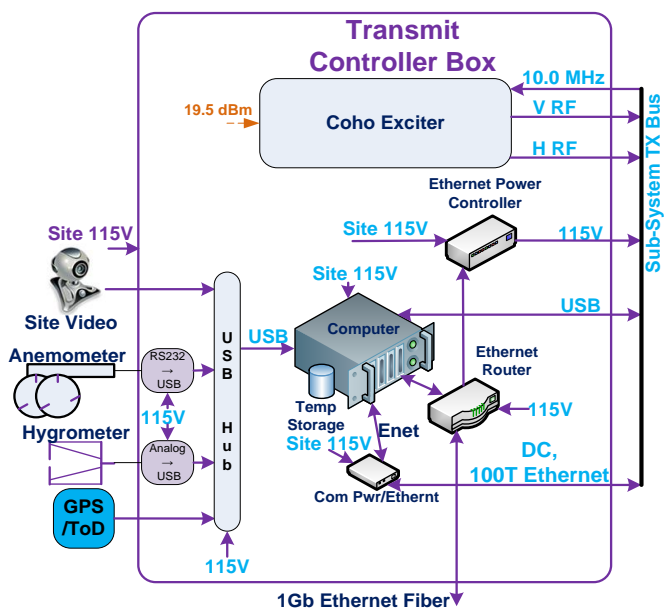


Figure 2.91. Transmitter Controller.

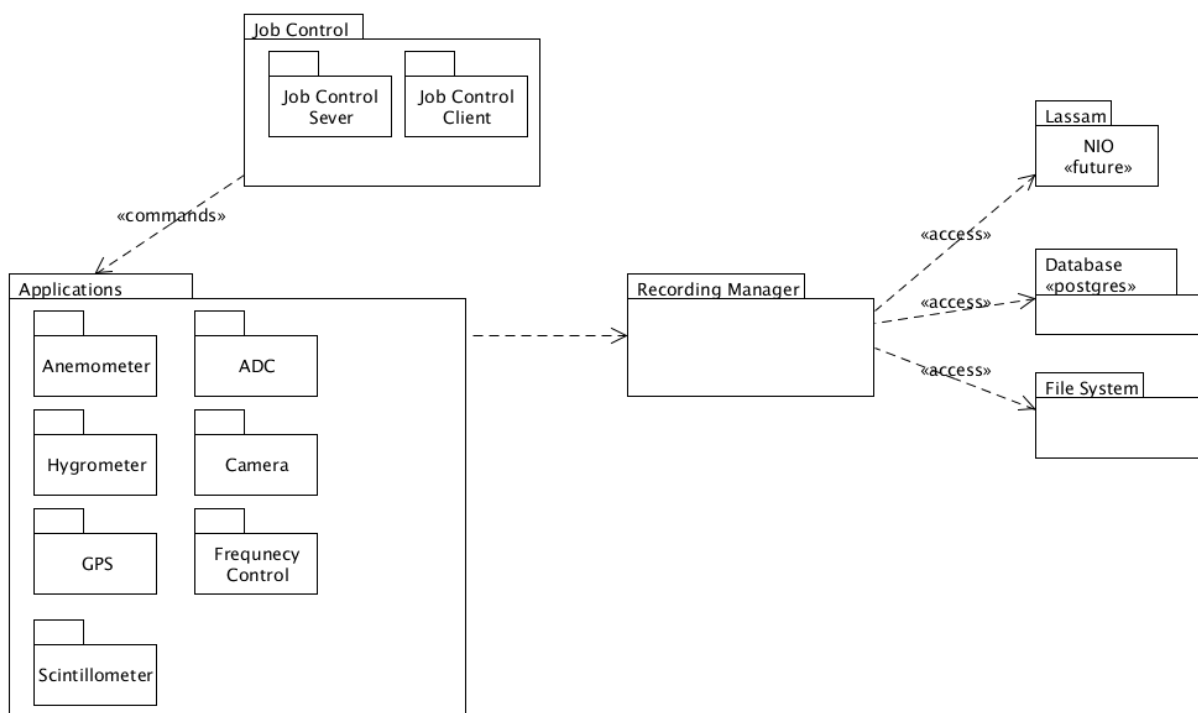


Figure 2.92. Linux Software Threads Block Diagram.

Figure 2.93 shows a timing diagram of the multi-threaded program. The long-term goal is to change frequencies on a 20 ms timeframe, but this could not be achieved due to the few milliseconds lock of the Tx and Rx1 systems via EPOCH. This diagram shows the data collection timing for the THz link across frequency switching times, as well as environmental sensors.

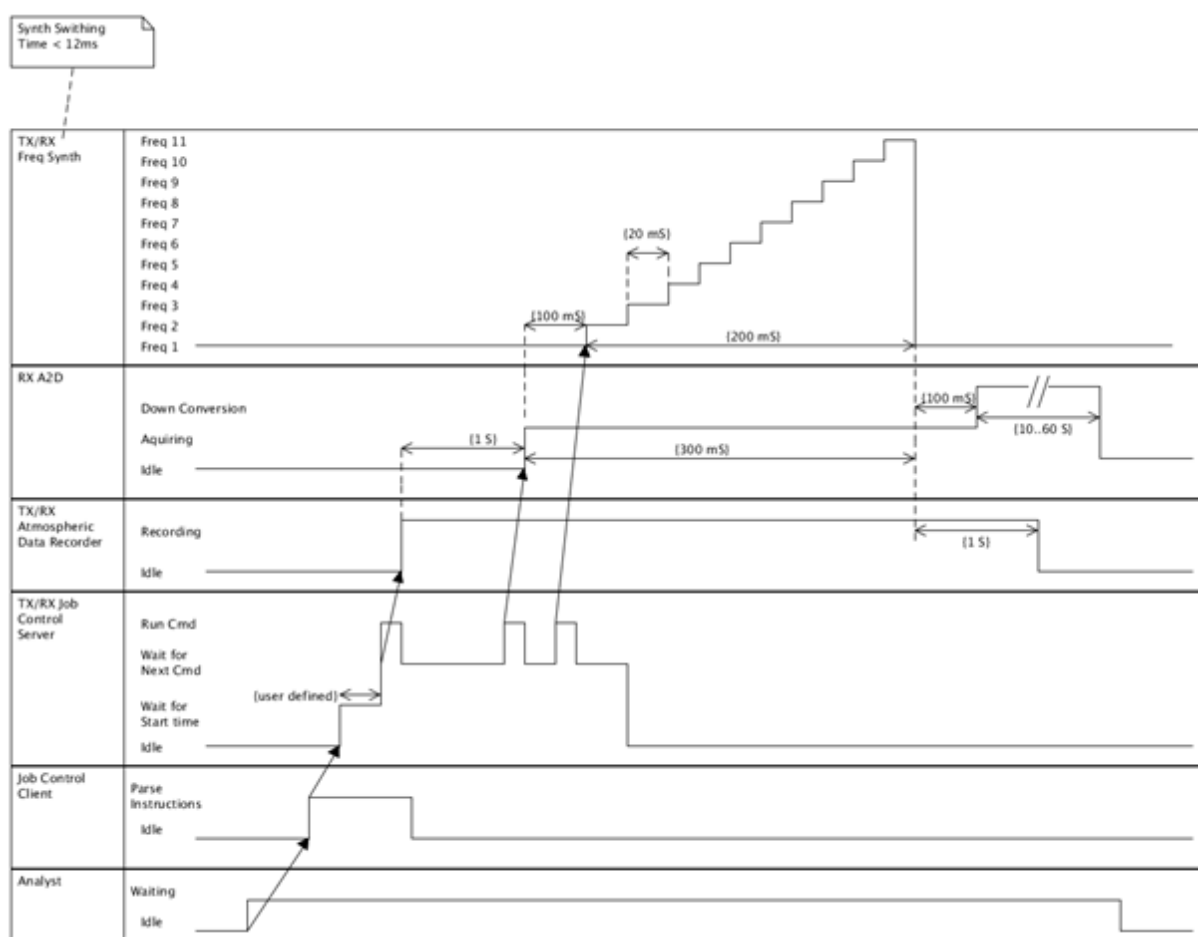


Figure 2.93. Timing Diagram of the Multi-Threaded Program.

Figure 2.94 shows the connections to the CU CET and CEI labs. The Tx on the roof of the CU engineering building is connected to the CET lab via Ethernet over fiber. The CEI lab can remotely log into the system from Colorado Springs.

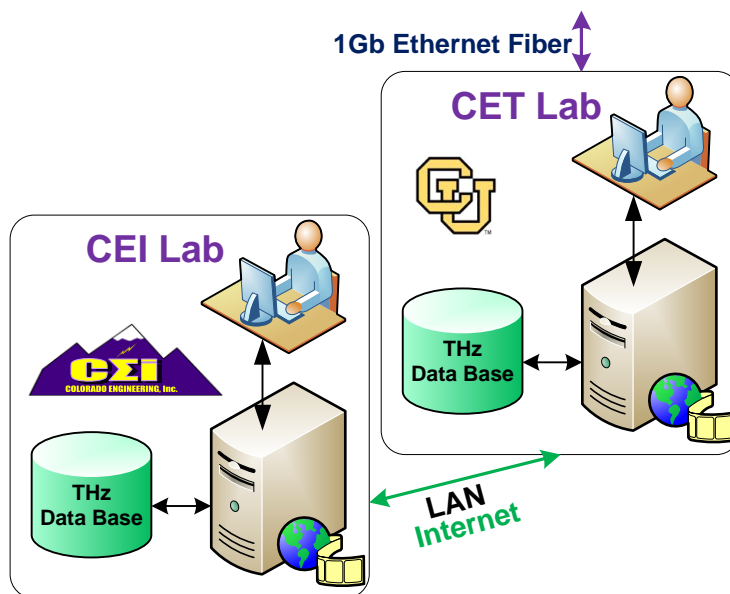


Figure 2.94. Connections to the CU CET and CEI Labs.

The Tx and Rx1 control systems handle all the data management and command/status through an Ethernet communication connection to the CET laboratory. The Ethernet IP network connection between these two boxes is handled over the C-band Air Grid. The Air Grids are bi-directional links that allow data and control to be passed. These devices are configured with fixed IP addresses and routing information for the network.

The Network Time Protocol (NTP) is the most commonly used Internet time protocol, and the one that provides the best performance. Large computers and workstations often include NTP software with their operating systems. The client software runs continuously as a background

task that periodically gets updates from one or more servers. The client software ignores responses from servers that appear to be sending the wrong time, and averages the results from those that appear to be correct. Many of the available NTP software clients for personal computers don't do any averaging at all. Instead, they make a single timing request to a signal server (just like a Daytime or Time client) and then use this information to set their computer's clock. The proper name for this type of client is Simple Network Time Protocol (SNTP). The NIST servers listen for an NTP request on port 123, and respond by sending a User Datagram Protocol (UDP)/IP data packet in the NTP format. The data packet includes a 64-bit timestamp containing the time in Coordinated Universal Time (UTC) seconds since January 1, 1900, with a resolution of 200 ps. Most of the NIST time servers do not require any authentication when requesting the time in NTP format, and no keys or passwords are needed to use this service. In addition to this standard NTP service — which was not modified — an authenticated version of NTP using a single time server that implements the symmetric key encryption method defined in the NTP documentation was implemented. To use this server, a NIST encryption key must be leveraged, which was linked to the network address of the system. This service is being offered on an experimental basis only, and it may not be continued after the initial testing period.

Figure 2.95 shows the network layout of TAIPAS. The Airgrid links are configured as transparent bridges. The Tx workstation is setup as a Network Address Translation (NAT) and bridges the 200.x and the CU network. It also forwards its port 2222 to port 22 of the Rx station. This way, external addresses on the CU network can access the Rx workstation directly via the Tx station. All fixed IP addresses are defined in this diagram. Table 2.17 shows the fixed IP addresses and masks that allow access over VPN from anywhere.

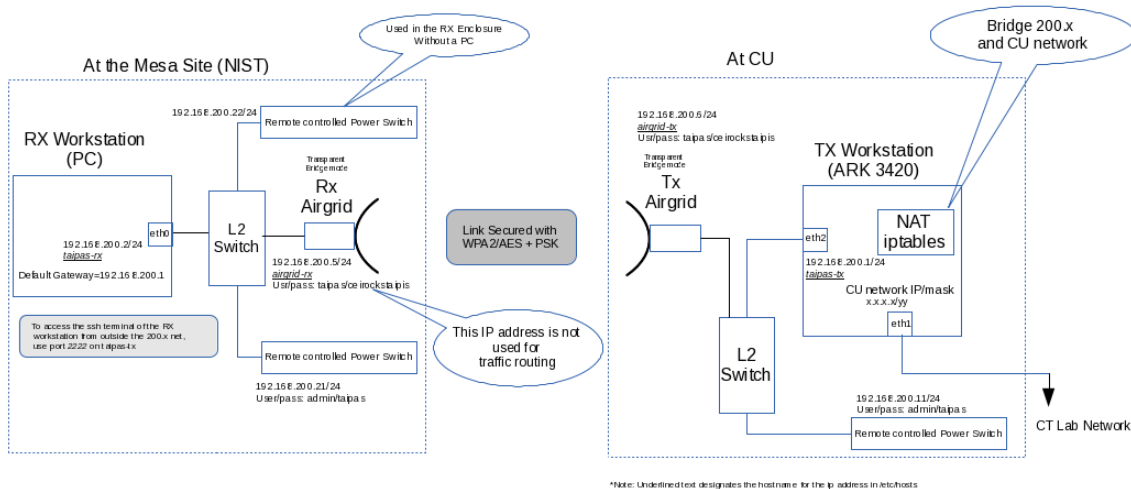


Figure 2.95. Network Block Diagram.

Table 2.17. IP Network Addresses.

Component Name	IP Address	Netmask Address	Default Route
Ubiquity AirGrid Tx Endpoint	10.1.1.2	255.255.255.0	10.1.1.1
Ubiquity AirGrid Rx Endpoint	10.1.1.3	255.255.255.0	10.1.1.1
Rx Control Workstation	10.1.1.4	255.255.255.0	10.1.1.1
Tx Control Workstation	10.1.1.5	255.255.255.0	10.1.1.1
NAT Router LAN IF	10.1.1.1	255.255.255.0	
NAT Router WAN IF	128.138.248.207	255.255.255.192	128.138.248.200
NAT Router DNS	128.138.130.30		

From the system terminal in the CET lab, Secure Shell (SSH) is utilized to log into each computer with the following login information: User – taipas, Password – taipas. In Linux, to remote into another computer, select Applications → System Tools → Terminal. Then SSH taipas-tx or SSH taipas-rx is input. There must be two terminal windows open to operate the system: Tx and Rx1. Both the Tx and Rx1 require JobController_server followed by two returns to run; two returns start the job server and continue in the background to allow access to the terminal. The & symbol will allow the JobController_server to run in the background. On the Tx side, navigation to the /home/taipas/tmp directory is required; clear the data in the tmp directory to allow new data to be captured. The acquisition is initiated by navigating to the 0_RunTaipas directory and running ./005_connect_internet_and_clocks.sh; “taipas” is the password. This connects the Tx computer to the Internet and gives the clock access for synching time — NTP. A delay of at least 15 minutes is required for this computer's clock to synchronize with the NTP server. This wait is required so that the Tx computer can act as an NTP server for the Rx computer. When the 005_connect_internet_and_clocks.sh command is executed, the contents of the /etc/resolv.conf file will be displayed.

The Rx side runs ./010_synch_computer_times.sh. This script brute forces time synchronization 100 times between the Rx and Tx computers. If the above script indicates “no server suitable for synchronization found,” the system must wait another 10 minutes to allow the Tx computer to synchronize its clock and become an NTP server.

The time delta shown as a long number offset 0.000123123123123 (can be positive or negative -0.04012312312) should be observed. Ideally, at least three zeros to the right of the

decimal point will be displayed indicating the two computer clocks are synchronized to under 1 ms; this has been difficult to achieve. The best synchronization over the entire capture period has been 3 ms. This varies and will be addressed in a future phase, and slows the switching of the frequencies.

On the Rx side, in the `\home\taipas\directory`, typing “mount data,” is required, which maps the Rx data directory to the Tx computer `\home\taipas\data_store\Rx` path. As a result, all the data collected will be in the `\home\taipas\data_store\` and can be downloaded in one operation.

The data collection process on both the Rx and Tx side requires navigations to the `\home\taipas\0_RunTaipas\directory`. This directory contains all the `.xml` and `.sh` files for execution. On the Rx side, the user must enter without executing `./010_synch_computer_times.sh`. On the Tx side, the user must enter without executing the following: `JobController_client -f 020_collect_data.xml`. These files have two versions that allow collection on one or two receivers. To collect data, the computers must be synchronized to at least 3 ms. The Rx side execution is started first to execute time synchronization script. As it runs, if the time offset changes signs, the Tx can start execution of data collection once the time synchronization script has completed. While the `020_collect-data.xml` script is executing "Opening `.dev/Video0`" and "Corrupt JPEG data" errors, a few extraneous bytes may be referenced; this can be ignored. After running this data collection twice, the `JobController_server` programs must be killed on both Tx and Rx sides and started again. If this is not completed, the `JobController_server` will run out of timers and crash — roughly on timer instance #104. Since the collect data routine uses roughly 40 timers, data can only be collected

twice. All data is initially placed in the /tmp folder on the Rx and Tx computers, followed by data being moved to the /data folder. The /data folder on the Tx side is mapped to the Tx hard drive directory: /home/taipas/data_store/tx/. The data folder on the Rx side is mapped to the Tx hard drive directory: /home/taipas/data_store/Rx/. All files are named by their data source and time stamped for each data collection iteration, except for the file that logs the times the frequency synthesizer changes frequencies; this is just continuously appended with new data for each data collection cycle.

The synthesizers on Tx and Rx1 are programmed through a USB interface that converts to a Fiber Distributed Data Interface (FDDI) interface with the following addresses: Tx - SN FTE40YFP, Rx1 - SN FTE40YEV, Rx2 - SN FTE40YF6. These are marked on the block diagrams and are critical for controlling the timing of the system. The frequencies are programmed in eXtensible Markup Language (XML) format. An example file and file format instructions are shown in Appendix C.

2.13 Systems Design

There are three frequency scan modes for the system: 320-340 GHz, 324.153-325.153 GHz and 325.153 GHz – 326.153 GHz. The synthesizers on the transmitter are programmed with the frequencies in low Ku band to generate the precise offsets needed for transmission at the absorption peak at 325.153 GHz. The synthesizers ultimately determine the scan time by virtue of their 15 ms settle time, as well as system phase noise; they significantly overweight the phase noise from the OCXO, which makes the need for such a high end, expensive oscillator questionable. Note that the settling time of the transceiver is much slower than the 1 ms

coherence time of the atmosphere. While this is far faster than any transmissometer implemented to date, improvement to sub-millisecond tuning is proposed in the next phase to provide observations at more than a single frequency within the coherence time of the atmosphere.

2.13.1 System THz CA Friis

The Friis equation, utilized for SNR calculations, is shown in Equation 2.97; the derivation from the pointing vector is shown in Figure 2.96. Equation 2.98 shows the calculations for the effective diameter of the lens for a given frequency; the 9 cm was implemented for a 325 GHz frequency. Figure 2.97 shows a plot of clear air absorption for the frequencies of interest. This plot was utilized to calculate the extinction coefficient (K_e), sum of absorption and scattering coefficients, in Np/km at a relative humidity of 20%.

$$P_{r_Circ_Aperture} = \frac{\pi^2 P_t Dia_t^2 Dia_r^2}{(4R\lambda)^2} e^{-K_e R} \quad (2.97)$$

$$Dia_{Effective@XGHz} = (Dia_{@325GHz}) \left(\frac{325 GHz}{X GHz} \right) \quad (2.98)$$

TAIPAS Transmissometer Friis Equations

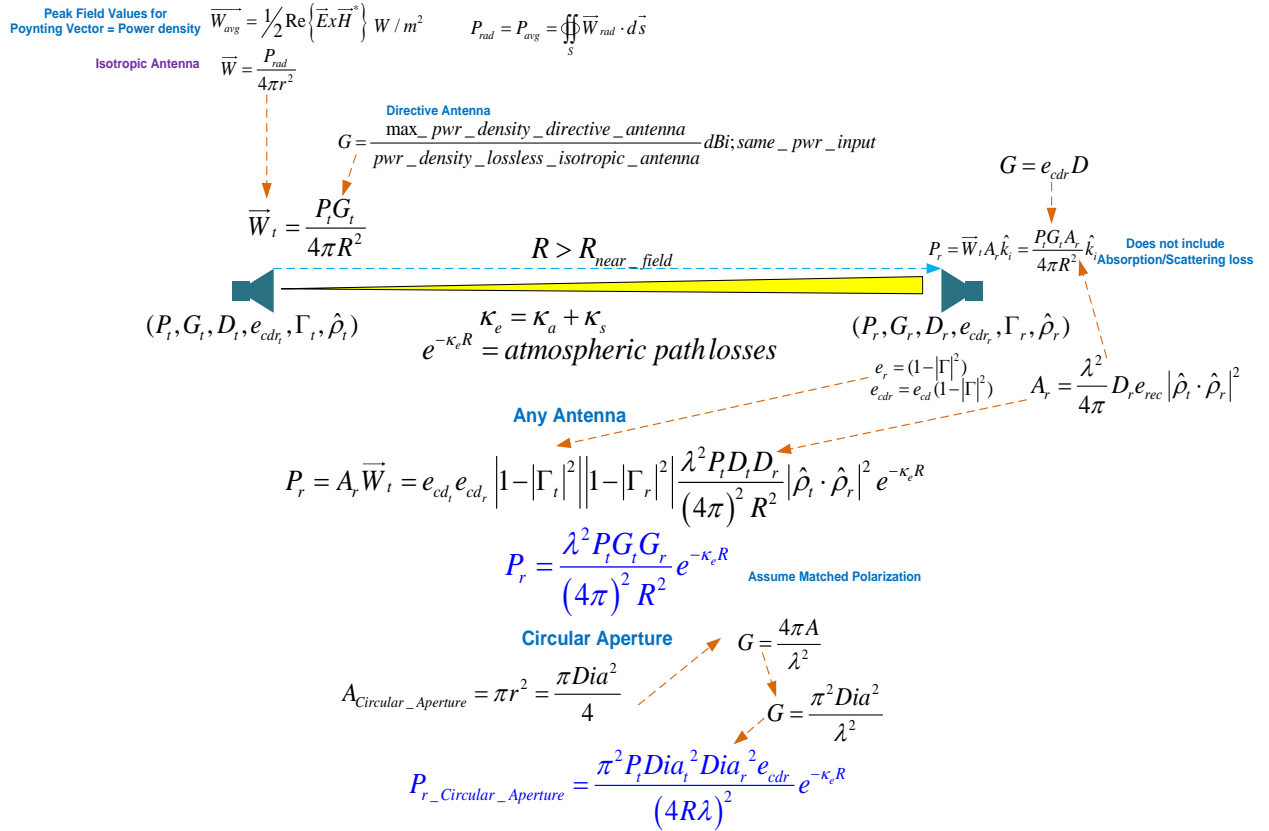


Figure 2.96. Friis Derivation.

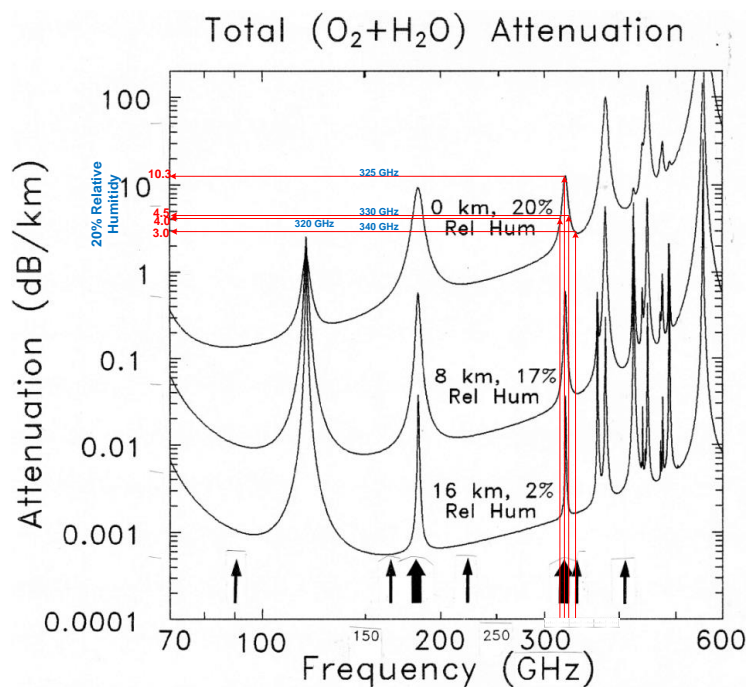


Figure 2.97. CA Attenuation Plot.

Table 2.18 and Table 2.19 show the wideband scan CA Friis calculation with embedded equations for the indoor hallway 40 m path and the final path of 1924 m, respectively; the equations utilized in Excel are adjacent to the applicable column and inputs highlighted in yellow. Equation 2.99 - Equation 2.102 show new equations leveraged in the spreadsheet. For the design to be valid, the wide band scan was utilized. The exciter power column varies with frequency; the plot and table for the hardware are shown in Figure 2.98 and Table 2.20, respectively. This power calibration has significant variance across the frequency band of interest and is shown in the third column from the left. The horn transmit power column takes into consideration a Voltage Standing Wave Ratio (VSWR) of 1.904; a reflection coefficient of .316. Absorption in CA is taken off Figure 2.97; due to CA, the scattering is assumed to be negligible, therefore the extinction coefficient equals the absorption. The second to last column shows the received power in dBm and the final column in dBm, representing the received power

after the necessary calibrations for Tx power and receive insertion loss. The effective size of the antenna aperture at each frequency is calculated using Equation 2.98 and shown in Table 2.21; the lens antenna diameter was designed for 325 GHz. The receive frequency calibrations are shown in Figure 2.99. Since the plot represents a double sideband case, additional 3 dB of loss needs to be added for single sideband.

$$\Gamma = \frac{Z_L - Z_A}{Z_L + Z_A} \quad (2.99)$$

$$VSWR = \frac{1 + |\Gamma|}{1 - |\Gamma|} \quad (2.100)$$

$$K_e = K_a + K_s \quad (2.101)$$

$$1 \text{ Np} = \frac{1}{e} = 4.3429 \text{ dB} \quad (2.102)$$

Table 2.18. TAIPAS CA Friis – 40 m Path

TAIPAS THz Clear Air Wide Band 20 GHz Scan(320GHz - 340GHz) - Entire Absorption Peak (EAP) System Calculations																			
Ind of Ref Struct Const		Available Test Site Ranges (m)																	
2.00E-12 m ⁴ -(2/3)	C_n^2	CU TWR	NIST	NCAR	DoC	NOAA													
Innerscale Length		520	1924	3370	6520	22570													
0.001 m	ℓ_0	Range																	
		40 (m)																	
$\Gamma = \frac{Z_t - Z_A}{Z_t + Z_A}$ Ref. Coef. 0.316 $VSWR = \frac{1+ \Gamma }{1- \Gamma }$ VSWR 1.924						LENS - Antenna $Dia_{Tx\&Rx@XGHz} = \left(\frac{325GHz}{XGHz} \right) Dia_{Tx\&Rx@325GHz}$ $Dia_{Tx\&Rx@325GHz} = 0.09 \text{ m}$													
$T \approx 3ps$ $c = 2.998 \times 10^8 \text{ m/s}$ $\lambda = \frac{c}{f}$						$P_{r_Circ_Aperture} = \frac{\pi^2 P_t Dia_t^2 Dia_r^2}{(4R\lambda)^2} e^{-\kappa_e R}$													
Power Received f λ $P_{t_exciter}$ P_{t_Hom} 20% rel hum Plot#1 Plot#2						$1Np = \frac{1}{e} = 4.3429 \text{ dB/level}$													
						$\kappa_e = \kappa_a + \kappa_s$		κ_e		κ_e		$P_r @_{antenna}$		$P_r @_{After_Hom}$		$P_r @_{no_CAL}$		Adjust for Tx and Rx Cal $P_r @_{Rx_139}$ $P_r @_{Rx_138}$	
Frequencies	Wavelength	Tx Power	Tx Power	Tx Power	Absorpt.	Scatter.	Extict.	Extict.	Extict.	Rx Power	Rx Power	Rx Power	Rx Power	Rx Power	Rx Power	Rx Power	Rx Power	Rx Power	Rx Power
320.000 (GHz)	0.937 (mm)	17.5 (mw)	11.97 (mw)	10.8 (dBm)	4 (dB/km)	0 (dB/km)	4 (dB/km)	0.921034 (Np/km)	3.54E-01 (mW)	2.42E-01 (mW)	-6.15 (dBm)	-14.65 (dBm)	-15.15 (dBm)						
323.153 (GHz)	0.928 (mm)	21.9 (mw)	14.9796 (mw)	11.8 (dBm)	5 (dB/km)	0 (dB/km)	5 (dB/km)	1.151293 (Np/km)	4.31E-01 (mW)	2.95E-01 (mW)	-5.31 (dBm)	-14.78 (dBm)	-15.28 (dBm)						
324.153 (GHz)	0.925 (mm)	21.1 (mw)	14.4324 (mw)	11.6 (dBm)	9.5 (dB/km)	0 (dB/km)	9.5 (dB/km)	2.187456 (Np/km)	3.96E-01 (mW)	2.71E-01 (mW)	-5.67 (dBm)	-14.99 (dBm)	-15.49 (dBm)						
324.653 (GHz)	0.923 (mm)	21.49 (mw)	14.69916 (mw)	11.7 (dBm)	10 (dB/km)	0 (dB/km)	10 (dB/km)	2.302585 (Np/km)	4.00E-01 (mW)	2.74E-01 (mW)	-5.63 (dBm)	-15.02 (dBm)	-15.52 (dBm)						
325.153 (GHz)	0.922 (mm)	22.57 (mw)	15.43788 (mw)	11.9 (dBm)	10.3 (dB/km)	0 (dB/km)	10.3 (dB/km)	2.371663 (Np/km)	4.18E-01 (mW)	2.86E-01 (mW)	-5.44 (dBm)	-15.05 (dBm)	-15.55 (dBm)						
325.653 (GHz)	0.921 (mm)	25.05 (mw)	17.1342 (mw)	12.3 (dBm)	10 (dB/km)	0 (dB/km)	10 (dB/km)	2.302585 (Np/km)	4.64E-01 (mW)	3.17E-01 (mW)	-4.99 (dBm)	-15.05 (dBm)	-15.55 (dBm)						
326.153 (GHz)	0.919 (mm)	22.85 (mw)	15.6294 (mw)	11.9 (dBm)	9.5 (dB/km)	0 (dB/km)	9.5 (dB/km)	2.187456 (Np/km)	4.23E-01 (mW)	2.90E-01 (mW)	-5.38 (dBm)	-15.04 (dBm)	-15.54 (dBm)						
327.153 (GHz)	0.916 (mm)	17.43 (mw)	11.92212 (mw)	10.8 (dBm)	7 (dB/km)	0 (dB/km)	7 (dB/km)	1.61181 (Np/km)	3.29E-01 (mW)	2.25E-01 (mW)	-6.48 (dBm)	-14.97 (dBm)	-15.47 (dBm)						
330.000 (GHz)	0.908 (mm)	20.19 (mw)	13.80996 (mw)	11.4 (dBm)	4.5 (dB/km)	0 (dB/km)	4.5 (dB/km)	1.036163 (Np/km)	3.83E-01 (mW)	2.62E-01 (mW)	-5.82 (dBm)	-14.94 (dBm)	-15.44 (dBm)						
335.000 (GHz)	0.895 (mm)	22.83 (mw)	15.61572 (mw)	11.9 (dBm)	3.4 (dB/km)	0 (dB/km)	3.4 (dB/km)	0.782879 (Np/km)	4.24E-01 (mW)	2.90E-01 (mW)	-5.37 (dBm)	-15.03 (dBm)	-15.53 (dBm)						
340.000 (GHz)	0.882 (mm)	17.92 (mw)	12.25728 (mw)	10.9 (dBm)	3 (dB/km)	0 (dB/km)	3 (dB/km)	0.690776 (Np/km)	3.24E-01 (mW)	2.22E-01 (mW)	-6.54 (dBm)	-15.14 (dBm)	-15.64 (dBm)						

Table 2.19. TAIPAS CA Friis – 1924 m Path

TAIPAS THz Clear Air Wide Band 20 GHz Scan(320GHz - 340GHz) - Entire Absorption Peak (EAP) System Calculations

Ind of Ref Struct Const		Available Test Site Ranges (m)				
2.00E-12 m ⁴ ·(2/3)	C_n^2	CU TWR	NIST	NCAR	DoC	NOAA
Innerscale Length	0.001 m ℓ_0	520	1924	3370	6520	22570
		Range				
		1924 (m)				

Ref. Coef.	VSWR
0.316	1.924

$T \approx 3ps$
 $c = 2.998 \times 10^8 m/s$
 $\lambda = \frac{c}{f}$

Table #1
Plot #1

Power Received
 f
 λ
 $P_{Tx_exciter}$
 P_{Tx_Horn}
 $P_{Tx_antenna}$
 $P_{Tx_After_Horn}$
 $P_{Tx_no_CAL}$
 $P_{r@Rx_139}$
 $P_{r@Rx_138}$

20% rel hum
Plot #2
 $K_e = K_a + K_s$
 $1Np = \frac{1}{e} = 4.3429 dB/level$
Adjust for Tx and Rx Cal

LENS - Antenna
 $Dia_{Tx\&Rx@325GHz} = \left(\frac{325GHz}{X GHz} \right) Dia_{Tx\&Rx@325GHz}$
 0.09 m

$P_{r_Circ_Aperture} = \frac{\pi^2 P_i Dia_i^2 Dia_r^2}{(4R\lambda)^2} e^{-\kappa_e R}$

Frequencies	Wavelength	Tx Power	Tx Power	Tx Power	Absorpt.	Scatter.	Extict.	Extict.	Rx Power	Rx Power	Rx Power	Rx Power	Rx Power
320.000 (GHz)	0.937 (mm)	17.5 (mw)	11.97 (mw)	10.8 (dBm)	4 (dB/km)	0 (dB/km)	4 (dB/km)	0.921034 (Np/km)	2.70E-05 (mW)	1.85E-05 (mW)	-47.33 (dBm)	-55.83 (dBm)	-56.33 (dBm)
323.153 (GHz)	0.928 (mm)	21.9 (mw)	14.9796 (mw)	11.8 (dBm)	5 (dB/km)	0 (dB/km)	5 (dB/km)	1.151293 (Np/km)	2.13E-05 (mW)	1.46E-05 (mW)	-48.37 (dBm)	-57.84 (dBm)	-58.34 (dBm)
324.153 (GHz)	0.925 (mm)	21.1 (mw)	14.4324 (mw)	11.6 (dBm)	9.5 (dB/km)	0 (dB/km)	9.5 (dB/km)	2.187456 (Np/km)	2.78E-06 (mW)	1.90E-06 (mW)	-57.21 (dBm)	-66.53 (dBm)	-67.03 (dBm)
324.653 (GHz)	0.923 (mm)	21.49 (mw)	14.69916 (mw)	11.7 (dBm)	10 (dB/km)	0 (dB/km)	10 (dB/km)	2.302585 (Np/km)	2.26E-06 (mW)	1.55E-06 (mW)	-58.11 (dBm)	-67.50 (dBm)	-68.00 (dBm)
325.153 (GHz)	0.922 (mm)	22.57 (mw)	15.43788 (mw)	11.9 (dBm)	10.3 (dB/km)	0 (dB/km)	10.3 (dB/km)	2.371663 (Np/km)	2.07E-06 (mW)	1.42E-06 (mW)	-58.49 (dBm)	-68.09 (dBm)	-68.59 (dBm)
325.653 (GHz)	0.921 (mm)	25.05 (mw)	17.1342 (mw)	12.3 (dBm)	10 (dB/km)	0 (dB/km)	10 (dB/km)	2.302585 (Np/km)	2.62E-06 (mW)	1.79E-06 (mW)	-57.47 (dBm)	-67.53 (dBm)	-68.03 (dBm)
326.153 (GHz)	0.919 (mm)	22.85 (mw)	15.6294 (mw)	11.9 (dBm)	9.5 (dB/km)	0 (dB/km)	9.5 (dB/km)	2.187456 (Np/km)	2.97E-06 (mW)	2.03E-06 (mW)	-56.92 (dBm)	-66.58 (dBm)	-67.08 (dBm)
327.153 (GHz)	0.916 (mm)	17.43 (mw)	11.92212 (mw)	10.8 (dBm)	7 (dB/km)	0 (dB/km)	7 (dB/km)	1.61181 (Np/km)	6.82E-06 (mW)	4.66E-06 (mW)	-53.31 (dBm)	-61.80 (dBm)	-62.30 (dBm)
330.000 (GHz)	0.908 (mm)	20.19 (mw)	13.80996 (mw)	11.4 (dBm)	4.5 (dB/km)	0 (dB/km)	4.5 (dB/km)	1.036163 (Np/km)	2.35E-05 (mW)	1.61E-05 (mW)	-47.94 (dBm)	-57.06 (dBm)	-57.56 (dBm)
335.000 (GHz)	0.895 (mm)	22.83 (mw)	15.61572 (mw)	11.9 (dBm)	3.4 (dB/km)	0 (dB/km)	3.4 (dB/km)	0.782879 (Np/km)	4.20E-05 (mW)	2.87E-05 (mW)	-45.42 (dBm)	-55.08 (dBm)	-55.58 (dBm)
340.000 (GHz)	0.882 (mm)	17.92 (mw)	12.25728 (mw)	10.9 (dBm)	3 (dB/km)	0 (dB/km)	3 (dB/km)	0.690776 (Np/km)	3.82E-05 (mW)	2.61E-05 (mW)	-45.83 (dBm)	-54.44 (dBm)	-54.94 (dBm)

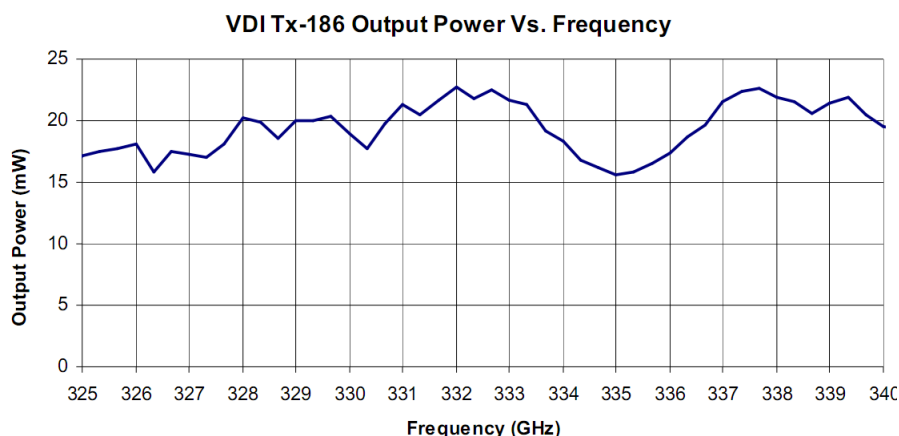


Figure 2.98. Tx Power vs. Frequency Plot.

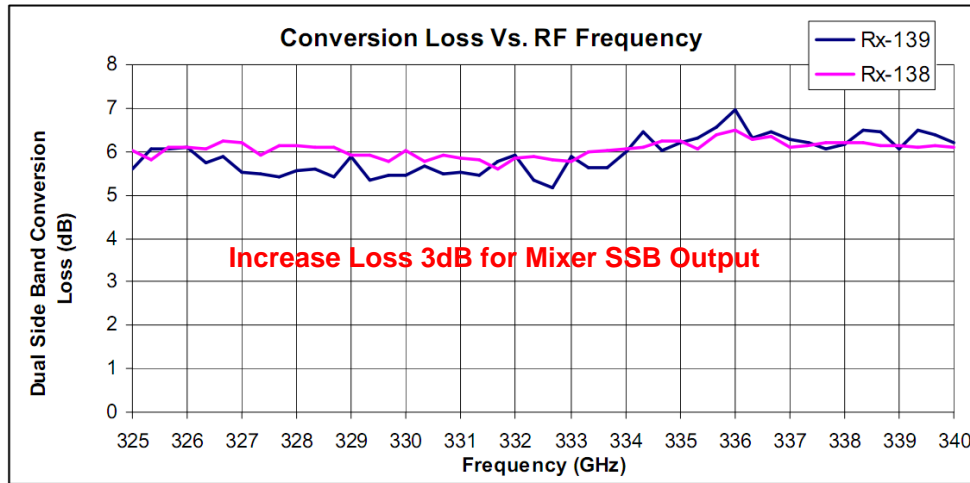
Table 2.20. Tx Calibration Table.**Reference Tables**

Table #1	<i>VDI</i>		
Frequency (GHz)	Power		Power (dBm)
	(mW)		
319.22	15.16		11.80658
319.50	15.74		11.96943
320.00	17.50		12.43091
320.50	18.55		12.68237
321.00	21.77		13.37777
321.50	26.18		14.18024
322.00	24.71		13.92896
322.50	22.73		13.56524
323.00	22.16		13.45626
323.50	21.19		13.26227
324.00	21.07		13.23596
324.50	21.35		13.29355
325.00	21.89		13.40304
325.50	25.03		13.98451
326.00	23.47		13.70521
326.50	21.21		13.26484
327.00	17.50		12.43067
327.50	19.12		12.81579
328.00	20.68		13.15508
330.00	20.19		13.05076
330.50	18.50		12.67183
331.00	20.89		13.19999
331.50	19.30		12.85658
332.00	20.85		13.19149
332.50	20.65		13.14968
333.00	20.89		13.19931
333.50	21.24		13.27227
334.00	24.43		13.87956
334.50	26.16		14.177
335.00	22.83		13.58428
335.50	22.62		13.5453
336.00	19.26		12.84547
336.50	22.11		13.44498
337.00	22.75		13.57048

337.50	21.42	13.30828
338.00	21.03	13.22906
338.50	23.04	13.62407
339.00	21.65	13.35362
339.50	20.04	13.01951
340.00	17.92	12.53422
340.50	19.46	12.89231
341.00	19.97	13.00363
341.50	19.73	12.95167
342.00	18.68	12.71288
342.50	17.81	12.50716
343.00	19.52	12.90453
343.50	17.39	12.40251
344.00	15.92	12.01862
344.50	14.23	11.53314
345.00	12.14	10.84197

Table 2.21. Tx and Rx Lens Effective Aperture Size.

	Transmitter Dt	Receiver Dr
320.000	0.09145 (m)	0.091 (m)
323.153	0.09056 (m)	0.091 (m)
324.153	0.09028 (m)	0.090 (m)
324.653	0.09014 (m)	0.090 (m)
325.153	0.090 (m)	0.090 (m)
325.653	0.08986 (m)	0.090 (m)
326.153	0.08972 (m)	0.090 (m)
327.153	0.08945 (m)	0.089 (m)
330.000	0.08868 (m)	0.089 (m)
335.000	0.08735 (m)	0.087 (m)
340.000	0.08607 (m)	0.086 (m)



The DSB conversion loss for the systems is shown

Figure 2.99. Rx1 and Rx2 Receiver Conversion Losses.

Table 2.22 shows the calculations for SNR over the 1924 m path length; yellow represents inputs. The noise temperature of the receivers was taken from Figure 2.100. The SNRs shown are sufficient for the experiment. The math is delineated in the table collocated by the answers as well as Equation 2.103 through Equation 2.107.

$$NF = 10 \log \left(\frac{T_{rec}}{T_0} \right) \quad (2.103)$$

$$F_n = \frac{S_{IN} / N_{IN}}{S_{OUT} / N_{OUT}} \quad (2.104)$$

$$P_n = kTB ; k = 1.38 \times 10^{-23} \text{ J/K} \quad (2.105)$$

$$\delta T_{rms} = \frac{T}{\sqrt{B\tau_{int}}} \quad (2.106)$$

$$SNR = 10 \log \left(\frac{P_{r-rec}}{P_n} \right) \quad (2.107)$$

Table 2.22. Path 1024 m SNR.

B	NF	$NF = 10 \log \left(\frac{T_{rec}}{T_0} \right) F_n = \frac{S_{IN} / N_{IN}}{S_{OUT} / N_{OUT}}$	$SNR = 10 \log \left(\frac{P_{r-rec}}{P_n} \right)$	
0.01 (MHz)	7.11 (dB)		SNR Rx 139	SNR Rx 138
T_0	P_n	$P_n = kTB ; k = 1.38 \times 10^{-23} \text{ J/K}$	71.0 (dB)	70.5 (dB)
290 (K)	2.06E-13 (mw)		69.0 (dB)	68.5 (dB)
τ_{int}		$\partial T_{rms} = \frac{T}{\sqrt{B\tau_{int}}}$	60.3 (dB)	59.8 (dB)
1 (sec)	-126.87 dBm		59.4 (dB)	58.9 (dB)
τ_{c_peak} Plot #4	∂T_{rms}		58.8 (dB)	58.3 (dB)
1200 (K)	2.910 K		59.3 (dB)	58.8 (dB)
			60.3 (dB)	59.8 (dB)
			65.1 (dB)	64.6 (dB)
			69.8 (dB)	69.3 (dB)
			71.8 (dB)	71.3 (dB)
			72.4 (dB)	71.9 (dB)

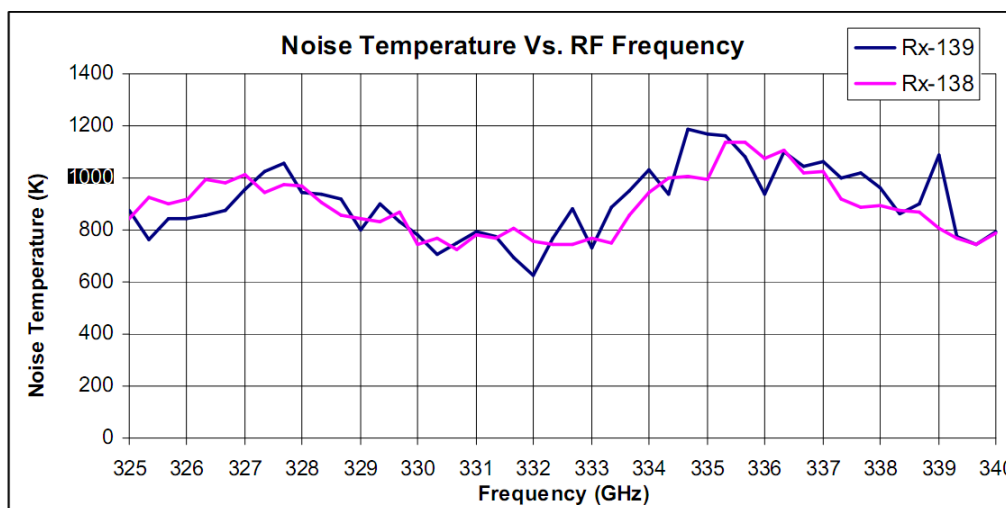


Figure 2.100. Rx1 and Rx2 Receiver Noise Temperatures.

Table 2.23 shows the features of the of the THz beam. The spot size, 24.8 m, is large enough to fit the two receivers, spread 8 m, simultaneously in the beam for the MCF. The math embedded in the table is Equation 2.108 through Equation 2.111.

$$R_{far_field} = \frac{2D^2}{\lambda} \tag{2.108}$$

$$BW_{3dB} = \frac{1.27\lambda}{D}; \text{radians} \quad (2.109)$$

$$P_n = kTB; k = 1.38 \times 10^{-23} \text{ J/K} \quad (2.110)$$

$$Spot_Size_{3dB} = (R - R_{far_field}) BW_{3dB}; BW_{3dB} \text{ in radians} \quad (2.111)$$

Table 2.23. Path 1024 m THz Beam Characteristics.

Beam Characteristics	Far zone	3-dB Beamwidth	3-dB spot size
325GHz	17.6 (m)	0.745 (deg)	24.80 (m)
	$R_{far_field} = \frac{2D^2}{\lambda}$	$BW_{3dB} = \frac{1.27\lambda}{D}; \text{radians}$	$Spot_Size_{3dB} = (R - R_{far_field}) BW_{3dB}$ $BW_{3dB} \text{ in radians}$

Table 2.24 shows the required alignment of the THz beam. The math is embedded and shown in Equations 2.112 through 2.114.

$$F_D = \frac{f_{focal_length}}{D_{effective}} \quad (2.112)$$

$$TX_{pointing_precision} = \frac{Spot_Size_{3dB}}{R} \quad (2.113)$$

$$TX_{FP_positioning} = TX_{pointing_precision} \times Dia_t \times F_D \quad (2.114)$$

Table 2.24. Path 1024 m THz Beam Alignment.

Alignment	f_{focal_length} 0.135 (m)	Required TX pointing precision	Required TX focal plane positioning
F_D 1.5	$F_D = \frac{f_{focal_length}}{D_{effective}}$	0.739 (deg) $TX_{pointing_precision} = \frac{Spot_Size_{3dB}}{R}$	1.74 (mm) $TX_{FP_positioning} = TX_{pointing_precision} \times Dia_t \times F_D$

2.13.2 System THz Friis Rain

Table 2.25 shows the rain Friis analysis utilizing the same equations from CA; they are also embedded in the table. The rain rates covered include 1, 10, 40 and 100 mm/hr. The absorption and scattering numbers to form the extinction coefficient were taken from Figure 2.101 [38]. Rain is usually dominated by absorption, but at the TAIPAS frequencies, scattering and absorption are equal contributors; this is on the horizontal / limit portion of the curve.

Table 2.25. TAIPAS Rain Friis – 1924 m Path.

TAIPAS THz Rain System Calculations (340GHz)										
				Available Test Site Ranges (m)						
				CU TWR	NIST	NCAR	DoC	NOAA		
				520	1920	3370	6520	22570		
				Range						
				1920 (m)						
				Ref. Coef.						
				0.316						
				$\Gamma = \frac{Z_L - Z_A}{Z_L + Z_A} = .316$						
				Plot #1						
				VSWR = $\frac{1+ \Gamma }{1- \Gamma } = 1.926$						
				$c = 2.998 \times 10^8 \text{ m/s}$						
				$\lambda = \frac{c}{f}$						
				$P_{t_exciter}$						
				P_{t_Horn}						
				Plot #2						
				Plot #2						
				$K_e = K_a + K_s$						
				$1 Np = 4.3429 \text{ dB}$						
				$P_{r_Circ_Aperture} = \frac{\pi^2 P_t \text{Dia}_t^2 \text{Dia}_r^2}{(4R\lambda)^2} e^{-K_e R}$						
Power Recieved	f	λ	$P_{t_exciter}$	P_{t_Horn}	Plot #2	Plot #2	K_e	K_e	P_r	P_r
Rain Rate	Frequencies	Wavelength	Tx Power	Tx Power	Absorpt.	Scatter.	Extict.	Extict.	Rx Power	Rx Power
1 (mm/hr)	340 (GHz)	0.882 (mm)	19 (mw)	12.996 (mw)	1.2 (dB/km)	1.2 (dB/km)	2.4 (dB/km)	0.5526 (Np/km)	6.35E-05 (mW)	-41.97 (dBm)
10 (mm/hr)	340 (GHz)	0.882 (mm)	19 (mw)	12.996 (mw)	5 (dB/km)	5 (dB/km)	10 (dB/km)	2.3026 (Np/km)	2.21E-06 (mW)	-56.56 (dBm)
40 (mm/hr)	340 (GHz)	0.882 (mm)	19 (mw)	12.996 (mw)	10 (dB/km)	10 (dB/km)	20 (dB/km)	4.6052 (Np/km)	2.65E-08 (mW)	-75.76 (dBm)
100 (mm/hr)	340 (GHz)	0.882 (mm)	19 (mw)	12.996 (mw)	20 (dB/km)	20 (dB/km)	40 (dB/km)	9.2103 (Np/km)	3.83E-12 (mW)	-114.16 (dBm)

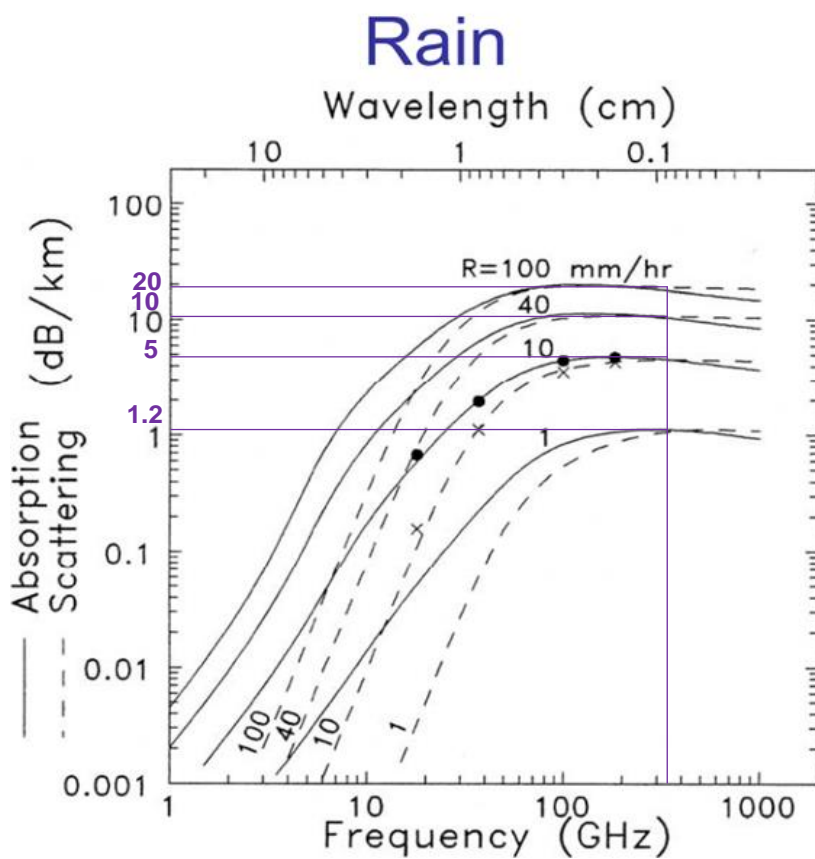


Figure 2.101. Rain Absorption and Scattering [38].

Table 2. 26 shows the SNR for the varying rain rates using the same equations for CA; they are also embedded in the table. The SNR is significantly down at 100 mm/hr. (12.7 dB).

Table 2. 26. TAIPAS Rain SNR – 1924 m Path

SNR	B	NF	$NF = 10 \log \left(\frac{T_{rec}}{T_0} \right)$	SNR
	0.01 (MHz)	7.11 (dB)		84.9 (dB)
	T_0	P_n	$P_n = kTB ; k = 1.38 \times 10^{-23} J/K$	70.3 (dB) $SNR = 10 \log \left(\frac{P_r}{P_n} \right)$
	290 (K)	2.06E-13 (mw)		51.1 (dB)
	τ_{int}	-126.87 dBm		12.7 (dB)
	1 (sec)		$\partial T_{rms} = \frac{T}{\sqrt{B\tau_{int}}}$	
	T_{rec}	∂T_{rms}		
	1200 (K)	2.910 K		

2.13.3 System THz Friis Snow

Table 2.27 shows the snow Friis analysis utilizing the same equations from CA; equations are also embedded in the table. The snow rates covered include 1, 10 and 40 mm/hr. The absorption and scattering numbers to form the extinction coefficient were taken from Figure 2.102 [38]. Snow is dominated by scattering, but at these frequencies absorption plays a significant role as well.

Table 2.27. TAIPAS Snow Friis – 1924 m Path.

TAIPAS THz Snow System Calculations (340GHz)											
				Available Test Site Ranges (m)							
				CU TWR	NIST	NCAR	DoC	NOAA			
				520	1924	3370	6520	22570			
				Ref. Coef.	Range						
				0.316	1924 (m)						
				$\Gamma = \frac{Z_L - Z_A}{Z_L + Z_A} = .316$					$P_{r_Circ_Aperture} = \frac{\pi^2 P_t Dia_t^2 Dia_r^2}{(4R\lambda)^2} e^{-\kappa_e R}$		
				$c = 2.998 \times 10^8 m/s$	$\lambda = \frac{c}{f}$					$1 Np = 4.3429 dB$	
				Plot #1	$VSWR = \frac{1+ \Gamma }{1- \Gamma } = 1.926$					$\kappa_e = \kappa_a + \kappa_s$	
				$P_{t_exciter}$	P_{t_Horn}	Plot #2	Plot #2	κ_e	κ_e	P_r	P_r
Rain Rate	Frequencies	Wavelength	Tx Power	Tx Power	Absorpt.	Scatter.	Extict.	Extict.	Rx Power	Rx Power	
1 (mm/hr)	340 (GHz)	0.882 (mm)	19 (mw)	12.996 (mw)	0.45 (dB/km)	4 (dB/km)	4.45 (dB/km)	1.0247 (Np/km)	2.54E-05 (mW)	-45.94 (dBm)	
10 (mm/hr)	340 (GHz)	0.882 (mm)	19 (mw)	12.996 (mw)	2 (dB/km)	8 (dB/km)	10 (dB/km)	2.3026 (Np/km)	2.18E-06 (mW)	-56.62 (dBm)	
40 (mm/hr)	340 (GHz)	0.882 (mm)	19 (mw)	12.996 (mw)	4.5 (dB/km)	12 (dB/km)	16.5 (dB/km)	3.7993 (Np/km)	1.22E-07 (mW)	-69.13 (dBm)	

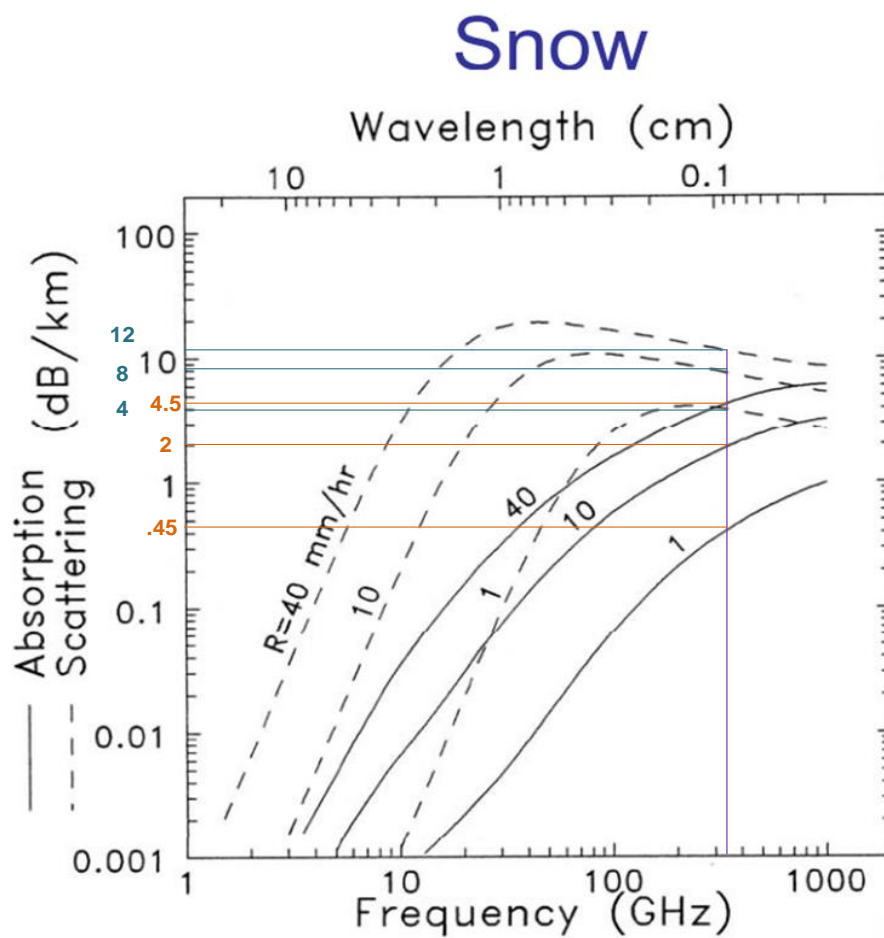


Figure 2.102. Snow Absorption and Scattering [38].

Table 2. 28 shows the SNR with for the varying snow using the same equations for CA; they are also embedded in the table.

Table 2. 28. TAIPAS Snow SNR – 1924 m path.

SNR				SNR	
B	NF	$NF = 10 \log \left(\frac{T_{rec}}{T_0} \right)$		80.9 (dB)	$SNR = 10 \log \left(\frac{P_r}{P_n} \right)$
0.01 (MHz)	7.11 (dB)			70.2 (dB)	
T_0	P_n	$P_n = kTB ; k = 1.38 \times 10^{-23} J/K$		57.7 (dB)	
290 (K)	2.06E-13 (mw)				
τ_{int}		$\partial T_{rms} = \frac{T}{\sqrt{B\tau_{int}}}$			
1 (sec)	-126.87 dBm				
T_{rec}	∂T_{rms}				
1200 (K)	2.910 K				

2.14 System Phase Noise

2.14.1 Coho Fresnel Zone Analysis

Table 2.29 shows a detailed accounting of the slope and the first Fresnel zone clearance for the Coho link; the yellow cells are inputs. The analysis considers the transmitter height on top of the CU building, the receiver height at the mesa and topographical changes of urban buildings, houses and fields. The math utilized is shown in Equation 2.115 through Equation 2.120; they are also embedded in the table.

$$Path \text{ Avg. Slope} = \frac{Total \text{ Rise}}{Total \text{ Run}} \times 100 \quad (2.115)$$

$$H_{sfc_bld} = Surface \text{ Height} + Building \text{ Height} \quad (2.116)$$

$$Path \text{ _ Elevation} = R_{current} + H_{Tx} + \left(\frac{R_{current} - R_{min}}{R_{max} - R_{min}} \right) \left((Surface \text{ _ El}_{max} + H_{Rx}) - (Surface \text{ _ El}_{min} + H_{Tx}) \right) \quad (2.117)$$

$$Fresnel \text{ _ Radii}_{1st} = \lambda_{coho} R_{current} \left(\frac{R_{max} - R_{current}}{R_{max} - R_{current-1}} \right) \quad (2.118)$$

2.14.2 Phase Noise Analysis

Phase noise analysis was implemented with the existing Wenzel OCXO and MLS synthesizer; Table 2.30 shows the analysis. The math utilized for the current synthesizer phase noise analysis and ones that utilize future synthesizers is delineated in Equation 2.121 through Equation 2.131. The offsets utilized for dBc/Hz included 100 Hz, 1 kHz and 10 kHz. Multipath generated phase noise is not included in this analysis — not on the THz link or the Coho link — since the Fresnel zone analysis in the above sections showed there would be no conservable effect. If the Coho link generates more multipath than expected, the slow closure time on the PLL of the Coho link will filter the generated phase variations. The yellow, filled in blocks on the table were taken from component data sheets. The total induced phase noise ranges from -81 dBc/Hz to -110 dBc/Hz. The THz link multiplies by 24; utilizing Equation 2.122, the range converts to -53 dBc to -82 dBc/Hz. The Coho link phase noise is very low (< -155 dBc/Hz); this was added, but has little effect. The Rx phase noise is low, since it subtracts the log of the divider of 24X (Equation 2.123). The total THz link phase noise for the Tx and Rx (Equation 2.124) ranges from -50 dBc/Hz to -79 dBc/Hz. The next few equations convert this to the time domain to compare to phase jitter, due to variations of the speed of light, caused by the atmosphere. The conversion requires the integration under the spread of the tone. First, the data is converted to the linear domain (Equation 2.125). The first box utilizes the trapezoid method to approximate the area. The total jitter comes out to 98 ms, which is far too much. The second method leverages the frequency method to estimate the area under the curve. This method yields phase jitter in the 500 ms range, which is unacceptable as well.

$$\phi_{noise_total(dBc)_OCXO} = 10\text{Log} \left(10^{\frac{\phi_{noise\#1(dBc)}}{10}} + 10^{\frac{\phi_{noise\#2(dBc)}}{10}} \right) \quad (2.121)$$

$$\phi_{noise_total(dBc)_Tx} = \phi_{noise_initial(dBc)} + 20\text{Log} \left(N_{Multiplier} \right) \quad (2.122)$$

$$\phi_{noise_total(dBc)_Rx} = \phi_{noise_initial(dBc)} - 20\text{Log} \left(N_{Divider} \right) \quad (2.123)$$

$$\phi_{noise_total(dBc)_Tx_Rx} = 10\text{Log} \left(10^{\frac{\phi_{noise\#Tx(dBc)}}{10}} + 10^{\frac{\phi_{noise\#Rx(dBc)}}{10}} \right) \quad (2.124)$$

$$\phi_{noise_raw} = 10^{\frac{\phi_{noise(dBc)}}{10}} \quad (2.125)$$

$$A_{Total_Trap} = \sum A_{Partial} \quad (2.126)$$

$$\phi_{jitter_rms_radians} = \sqrt{2A_{Total}} \quad (2.127)$$

$$\phi_{jitter_rms_sec_trap} = \frac{\phi_{jitter_rms_rad}}{2\pi f_{carrier}} \quad (2.128)$$

$$\text{Trapazoidal Sub-Area} = .5 \left(f_{offset_n} - f_{offset_(n-1)} \right) \left(\phi_{noise_raw_n} + \phi_{noise_raw_(n-1)} \right) \quad (2.129)$$

$$A_{Total_Freq} = \phi_{noise_dBc} + 10\text{Log} \left(2f_0 \right) \quad (2.130)$$

$$\phi_{jitter_rms_radians_freq} = \sqrt{2 \times 10^{A_{total}/10}} \quad (2.131)$$

Table 2.30. TAIPAS Phase Noise Analysis with MLS Synthesizer

Current Configuration with 1Hz step Synthesizer			
Note: EMI / Multipath generated phase noise is not included ; A/D clock circuit is passive so adds no phase jitter; assuming all impedances are matched (no reflections)			
Component Phase Noise			
Wenzel Oscillator Phase Noise			
offset	Phase Noise		
10 (Hz)	-120 (dBc/Hz)		
100 (Hz)	-155 (dBc/Hz)		
1000 (Hz)	-165 (dBc/Hz)		
10000 (Hz)	-165 (dBc/Hz)		
$\phi_{noise_total}(dBc) = 10\text{Log} \left(10^{\frac{\phi_{noise\#1}(dBc)}{10}} + 10^{\frac{\phi_{noise\#2}(dBc)}{10}} \right)$			
MLS Synthesizer Phase Noise			
offset	Phase Noise		
100 (Hz)	-81 (dBc/Hz)		
1000 (Hz)	-104 (dBc/Hz)		
10000 (Hz)	-110 (dBc/Hz)		
100000 (Hz)	-113 (dBc/Hz)		
1000000 (Hz)	-144 (dBc/Hz)		
$\phi_{noise_total}(dBc) = 10\text{Log} \left(10^{\frac{\phi_{noise\#1}(dBc)}{10}} + 10^{\frac{\phi_{noise\#2}(dBc)}{10}} \right)$			
Total Component Induced Phase Noise			
offset	Phase Noise		
100 (Hz)	-81 (dBc/Hz)		
1000 (Hz)	-104 (dBc/Hz)		
10000 (Hz)	-110 (dBc/Hz)		
High fidelity Wenzel Oscillator wasted			
THz Link Tx			
offset	Mult	Phase Noise	
100 (Hz)	24	-53.395775 (dBc/Hz)	
1000 (Hz)	24	-76.3957717 (dBc/Hz)	
10000 (Hz)	24	-82.3957614 (dBc/Hz)	
$\phi_{noise_total}(dBc) = \phi_{noise_initial}(dBc) + 20\text{Log}(N_{Multiplier})$			
Coho Link Tx			
offset	Mult	Phase Noise	
100 (Hz)	4	-142.9588 (dBc/Hz)	
1000 (Hz)	4	-152.9588 (dBc/Hz)	
10000 (Hz)	4	-152.9588 (dBc/Hz)	
$\phi_{noise_total}(dBc) = \phi_{noise_initial}(dBc) + 20\text{Log}(N_{Multiplier})$			
Coho Link Rx			
offset	Mult	Phase Noise	
100 (Hz)	4	-155 (dBc/Hz)	
1000 (Hz)	4	-165 (dBc/Hz)	
10000 (Hz)	4	-165 (dBc/Hz)	
$\phi_{noise_total}(dBc) = \phi_{noise_initial}(dBc) - 20\text{Log}(N_{Divider})$			
THz Link Rx (same Tx phase noise fed to mixer from both inputs (Tx and Rx chain noise))			
offset	Phase Noise		
100 (Hz)	-50.3855 (dBc/Hz)		
1000 (Hz)	-73.3855 (dBc/Hz)		
10000 (Hz)	-79.3855 (dBc/Hz)		
$\phi_{noise_total}(dBc) = 10\text{Log} \left(10^{\frac{\phi_{noise\#Tx}(dBc)}{10}} + 10^{\frac{\phi_{noise\#Rx}(dBc)}{10}} \right)$			
Total Jitter at A/D Converter Trapezoidal Method (Note: Coho Link Jitter generating A/D clock is so low will have no effect as seen above in component noise)			
offset	Phase Noise	Phase Noise Raw	$A_{Trapezoid_partial}$
10 (kHz)	-50.3855 (dBc/Hz)	9.15066E-06	
1000 (kHz)	-73.3855 (dBc/Hz)	4.5862E-08	0.004552
10000 (kHz)	-79.3855 (dBc/Hz)	1.152E-08	0.000258
A_{Total}			
$\phi_{jitter_rms_radians}$			
$\phi_{jitter_rms_sec}$			
A= Area=Integrated Phase Noise Power			
$\phi_{noise_raw} = 10^{\frac{\phi_{noise}(dBc)}{10}} \quad A_{Total} = \sum A_{Partial} \quad \phi_{jitter_rms_radians} = \sqrt{2A_{Total}} \quad \phi_{jitter_rms_sec} = \frac{\phi_{jitter_rms_rad}}{2\pi f_{carrier}}$			
$\text{Trapezoidal Sub-Area} = .5(f_{offset_n} - f_{offset_(n-1)}) (\phi_{noise_raw_n} + \phi_{noise_raw_(n-1)})$			
Does not meet requirement!!!!			
Total Jitter at f0 frequency method (Note: Coho Link Jitter generating A/D clock is so low will have no effect as seen above in component noise)			
f_0	A_{Total}	$\phi_{jitter_rms_radians}$	$\phi_{jitter_rms_sec}$
0.01 (MHz)	-7.37518	0.605001	96288.9333 ps
1 (MHz)	-10.3752	0.428308	68167.3701 ps
10 (MHz)	-6.37516	0.678824	108038.129 ps
$A_{Total} = \phi_{noise_dBc} + 10\text{Log}(2f_0)$			
$\phi_{jitter_rms_radians} = \sqrt{2 \times 10^{A_{Total}/10}}$			

A second approach was taken to test a limit of the ideal situation: the synthesizer had equal phase noise to the OCXO; Table 2.31 shows the calculations and results. The time phase jitter gets down in single digit picoseconds using the trapezoid method.

Table 2.31. TAIPAS Phase Noise Analysis with Ideal Synthesizer.

Ideal Configuration Phase Noise equal to Oscillator							
Component Phase Noise							
Wenzel Oscillator Phase Noise							
offset	Phase Noise						
10 (Hz)	-120	(dBc/Hz)					
100 (Hz)	-155	(dBc/Hz)					
1000 (Hz)	-165	(dBc/Hz)					
10000 (Hz)	-165	(dBc/Hz)					
			$\phi_{noise_total}(dBc) = 10\text{Log} \left(10^{\frac{\phi_{noise\#1}(dBc)}{10}} + 10^{\frac{\phi_{noise\#2}(dBc)}{10}} \right)$				
MLS Synthesizer Phase Noise							
offset	Phase Noise						
100 (Hz)	-155	(dBc/Hz)					
1000 (Hz)	-165	(dBc/Hz)					
10000 (Hz)	-165	(dBc/Hz)					
100000 (Hz)	-165	(dBc/Hz)					
1000000 (Hz)	-165	(dBc/Hz)					
			Total Component Induced Phase Noise				
offset	Phase Noise						
100 (Hz)	-152	(dBc/Hz)					
1000 (Hz)	-162	(dBc/Hz)					
10000 (Hz)	-162	(dBc/Hz)					
$\phi_{noise_total}(dBc) = \phi_{noise_initial}(dBc) + 20\text{Log}(N_{Multiplier})$							
THz Link Tx							
offset	Mult	Phase Noise					
100 (Hz)	24	-124.385475 (dBc/Hz)					
1000 (Hz)	24	-134.385475 (dBc/Hz)					
10000 (Hz)	24	-134.385475 (dBc/Hz)					
$\phi_{noise_total}(dBc) = \phi_{noise_initial}(dBc) + 20\text{Log}(N_{Multiplier})$							
Coho Link Tx							
offset	Mult	Phase Noise					
100 (Hz)	4	-142.9588 (dBc/Hz)					
1000 (Hz)	4	-152.9588 (dBc/Hz)					
10000 (Hz)	4	-152.9588 (dBc/Hz)					
$\phi_{noise_total}(dBc) = \phi_{noise_initial}(dBc) + 20\text{Log}(N_{Multiplier})$							
Coho Link Rx							
offset	Mult	Phase Noise					
100 (Hz)	4	-155 (dBc/Hz)					
1000 (Hz)	4	-165 (dBc/Hz)					
10000 (Hz)	4	-165 (dBc/Hz)					
$\phi_{noise_total}(dBc) = \phi_{noise_initial}(dBc) - 20\text{Log}(N_{Divider})$							
THz Link Rx (same Tx phase noise fed to mixer from both inputs)							
offset	Phase Noise						
100 (Hz)	-121.375	(dBc/Hz)					
1000 (Hz)	-131.375	(dBc/Hz)					
10000 (Hz)	-131.375	(dBc/Hz)					
			$\phi_{noise_total}(dBc) = 10\text{Log} \left(10^{\frac{\phi_{noise\#Tx}(dBc)}{10}} + 10^{\frac{\phi_{noise\#Tx}(dBc)}{10}} \right)$				
Total Jitter at A/D Converter Trapezoidal Method (Note: Coho Link Jitter generating A/D clock is so low will have no effect as seen above in component noise)							
offset	Phase Noise	Phase Noise Raw	$A_{Trapezoid_partial}$	A_{Total}	$\phi_{jitter_rms_radians}$	$\phi_{jitter_rms_sec}$	A= Area=Integrated Phase Noise Power
10 (kHz)	-121.375 (dBc/Hz)	7.28589E-13					
1000 (kHz)	-131.375 (dBc/Hz)	7.28589E-14	3.97E-10	1.05E-09	4.59E-05	7.30188754 ps	
10000 (kHz)	-131.375 (dBc/Hz)	7.28589E-14	6.56E-10				
$\phi_{noise_raw} = 10^{\frac{\phi_{noise}(dBc)}{10}}$ $A_{Total} = \sum A_{Partial}$ $\phi_{jitter_rms_radians} = \sqrt{2A_{Total}}$ $\phi_{jitter_rms_sec} = \frac{\phi_{jitter_rms_rad}}{2\pi f_{carrier}}$ $Trapezoidal\ Sub-Area = 5(f_{offset_n} - f_{offset_(n-1)}) (\phi_{noise_raw_n} + \phi_{noise_raw_(n-1)})$							
Total Jitter at f0 frequency method (Note: Coho Link Jitter generating A/D clock is so low will have no effect as seen above in component noise)							
f_0	A_{Total}	$\phi_{jitter_rms_radians}$	$\phi_{jitter_rms_sec}$	A= Area=Integrated Phase Noise Power			
0.01 (MHz)	-78.3649	0.000171	27.170108 ps				
1 (MHz)	-68.3649	0.00054	85.9194255 ps				
10 (MHz)	-58.3649	0.001707	271.70108 ps				
$A_{Total} = \phi_{noise_dBc} + 10\text{Log}(2f_0)$ $\phi_{jitter_rms_radians} = \sqrt{2 \times 10^{A_{Total}/10}}$							

A third approach was taken to test a limit using an expensive — \$150K — OEwaves narrow band Synthesizer. Table 2.32 shows the calculations and results. The time phase jitter gets down in 500 picoseconds using the trapezoid method.

Table 2.32. TAIPAS Phase Noise Analysis with OE Waves Synthesizer.

OEwaves Configuration Narrow Band Synthesizer

Component Phase Noise
Wenzel Oscillator Phase Noise

offset	Phase Noise
10 (Hz)	-128 (dBc/Hz)
100 (Hz)	-159 (dBc/Hz)
1000 (Hz)	-165 (dBc/Hz)
10000 (Hz)	-165 (dBc/Hz)

MLS Synthesizer Phase Noise

offset	Phase Noise
100 (Hz)	-110 (dBc/Hz)
1000 (Hz)	-140 (dBc/Hz)
10000 (Hz)	-160 (dBc/Hz)
100000 (Hz)	-160 (dBc/Hz)
1000000 (Hz)	-160 (dBc/Hz)

THz Link Tx $\phi_{noise_total(dBc)} = \phi_{noise_initial(dBc)} + 20\text{Log}(N_{Multipler})$

offset	Phase Noise
100 (Hz)	-82.3956378 (dBc/Hz)
1000 (Hz)	-112.382063 (dBc/Hz)
10000 (Hz)	-131.202465 (dBc/Hz)

Coho Link Tx $\phi_{noise_total(dBc)} = \phi_{noise_initial(dBc)} + 20\text{Log}(N_{Multipler})$

offset	Phase Noise
100 (Hz)	-142.9588 (dBc/Hz)
1000 (Hz)	-152.9588 (dBc/Hz)
10000 (Hz)	-152.9588 (dBc/Hz)

Coho Link Rx $\phi_{noise_total(dBc)} = \phi_{noise_initial(dBc)} - 20\text{Log}(N_{Divider})$

offset	Phase Noise
100 (Hz)	-155 (dBc/Hz)
1000 (Hz)	-165 (dBc/Hz)
10000 (Hz)	-165 (dBc/Hz)

THz Link Rx (same Tx phase noise fed to mixer from both inputs)

offset	Phase Noise
100 (Hz)	-79.3853 (dBc/Hz)
1000 (Hz)	-109.372 (dBc/Hz)
10000 (Hz)	-128.192 (dBc/Hz)

Total Jitter at A/D Converter Trapezoidal Method (Note: Coho Link Jitter generating A/D clock is so low will have no effect as seen above in component noise)

offset	Phase Noise	Phase Noise Row	$A_{Trapezoid_partial}$	A_{Total}	$\phi_{jitter_rms_radians}$	$\phi_{jitter_rms_sec}$	A=Area=Integrated Phase Noise Power
10 (kHz)	-79.3853 (dBc/Hz)	1.15204E-08	5.71E-06	5.76E-06	0.003394	540.236071 ps	
1000 (kHz)	-109.372 (dBc/Hz)	1.15564E-11	5.27E-08				
10000 (kHz)	-128.192 (dBc/Hz)	1.51629E-13					

$$\phi_{noise_row} = 10^{-\frac{\phi_{noise_dBc}}{10}}$$

$$A_{Total} = \sum A_{Partial} \quad \phi_{jitter_rms_radians} = \sqrt{2A_{Total}} \quad \phi_{jitter_rms_sec} = \frac{\phi_{jitter_rms_rad}}{2\pi f_{carrier}}$$

Trapezoidal Sub-Area $= .5(f_{offset_n} - f_{offset_(n-1)})(\phi_{noise_row_n} + \phi_{noise_row_(n-1)})$

Total Jitter at f0 frequency method (Note: Coho Link Jitter generating A/D clock is so low will have no effect as seen above in component noise)

f_c	A_{Total}	$\phi_{jitter_rms_radians}$	$\phi_{jitter_rms_sec}$	A=Area=Integrated Phase Noise Power
0.01 (MHz)	-36.375	0.021467	9416.51423 ps	
1 (MHz)	-46.3615	0.006799	1082.08646 ps	
10 (MHz)	-55.1819	0.002463	391.960128 ps	

$$A_{Total} = \phi_{noise_dBc} + 10\text{Log}(2f_0) \quad \phi_{jitter_rms_radians} = \sqrt{2 \times 10^{A_{Total}/10}}$$

OEwaves: Advanced Opto-Electronic Oscillator (OEO) \$150K

ITT EXELIS Direct Digital Synthesizer (DDS): Required Configuration with sub 1Hz step Synthesizer

Component Phase Noise
Wenzel Oscillator Phase Noise

offset	Phase Noise
10 (Hz)	-120 (dBc/Hz)
100 (Hz)	-155 (dBc/Hz)
1000 (Hz)	-165 (dBc/Hz)
10000 (Hz)	-165 (dBc/Hz)

MLS Synthesizer Phase Noise

offset	Phase Noise
100 (Hz)	-105 (dBc/Hz)
1000 (Hz)	-125 (dBc/Hz)
10000 (Hz)	-137 (dBc/Hz)
100000 (Hz)	-138 (dBc/Hz)
1000000 (Hz)	-138 (dBc/Hz)

THz Link Tx $\phi_{noise_total(dBc)} = \phi_{noise_initial(dBc)} + 20\text{Log}(N_{Multipler})$

offset	Phase Noise
100 (Hz)	-77.3957317 (dBc/Hz)
1000 (Hz)	-97.3953409 (dBc/Hz)
10000 (Hz)	-109.388898 (dBc/Hz)

Coho Link Tx $\phi_{noise_total(dBc)} = \phi_{noise_initial(dBc)} + 20\text{Log}(N_{Multipler})$

offset	Phase Noise
100 (Hz)	-142.9588 (dBc/Hz)
1000 (Hz)	-152.9588 (dBc/Hz)
10000 (Hz)	-152.9588 (dBc/Hz)

Coho Link Rx $\phi_{noise_total(dBc)} = \phi_{noise_initial(dBc)} - 20\text{Log}(N_{Divider})$

offset	Phase Noise
100 (Hz)	-155 (dBc/Hz)
1000 (Hz)	-165 (dBc/Hz)
10000 (Hz)	-165 (dBc/Hz)

THz Link Rx (same Tx phase noise fed to mixer from both inputs)

offset	Phase Noise
100 (Hz)	-74.3854 (dBc/Hz)
1000 (Hz)	-94.385 (dBc/Hz)
10000 (Hz)	-106.379 (dBc/Hz)

Total Jitter at A/D Converter Trapezoidal Method (Note: Coho Link Jitter generating A/D clock is so low will have no effect as seen above in component noise)

offset	Phase Noise	Phase Noise Row	$A_{Trapezoid_partial}$	A_{Total}	$\phi_{jitter_rms_radians}$	$\phi_{jitter_rms_sec}$	A=Area=Integrated Phase Noise Power
10 (kHz)	-74.3854 (dBc/Hz)	3.64299E-08	1.82E-05	2E-05	0.006318	1005.48101 ps	
1000 (kHz)	-94.385 (dBc/Hz)	3.64331E-10	1.74E-06				
10000 (kHz)	-106.379 (dBc/Hz)	2.30219E-11					

$$\phi_{noise_row} = 10^{-\frac{\phi_{noise_dBc}}{10}}$$

$$A_{Total} = \sum A_{Partial} \quad \phi_{jitter_rms_radians} = \sqrt{2A_{Total}} \quad \phi_{jitter_rms_sec} = \frac{\phi_{jitter_rms_rad}}{2\pi f_{carrier}}$$

Trapezoidal Sub-Area $= .5(f_{offset_n} - f_{offset_(n-1)})(\phi_{noise_row_n} + \phi_{noise_row_(n-1)})$

Total Jitter at f0 frequency method (Note: Coho Link Jitter generating A/D clock is so low will have no effect as seen above in component noise)

f_c	A_{Total}	$\phi_{jitter_rms_radians}$	$\phi_{jitter_rms_sec}$	A=Area=Integrated Phase Noise Power
0.01 (MHz)	-31.3751	0.038173	6076.45122 ps	
1 (MHz)	-31.3747	0.038175	6075.72461 ps	
10 (MHz)	-33.3683	0.030346	4829.70105 ps	

$$A_{Total} = \phi_{noise_dBc} + 10\text{Log}(2f_0) \quad \phi_{jitter_rms_radians} = \sqrt{2 \times 10^{A_{Total}/10}}$$

A fourth approach was taken to do a bottoms-up calculation: required synthesizer phase noise to achieve acceptable measurements on the TAIPAS 1924 m path. This phase variance is shown in the propagation chapter (Chapter 3). The time phase jitter required was assumed to be in the 50 ps range. Table 2.33 shows the requisite synthesizer phase noise is -130 dBc/Hz at 100 Hz, -155 dBc/Hz at 1 kHz, and -162 dBc/ Hz at 10 kHz – 100 kHz.

Table 2.33. TAIPAS Phase Noise Analysis Requirements for Synthesizer.

Required Configuration with Synthesizer Phase Noise							
Component Phase Noise							
Wenzel Oscillator Phase Noise							
<i>offset</i>	<i>Phase Noise</i>						
10 (Hz)	-120	(dBc/Hz)					
100 (Hz)	-155	(dBc/Hz)					
1000 (Hz)	-165	(dBc/Hz)					
10000 (Hz)	-165	(dBc/Hz)					
$\phi_{noise_total}(dBc) = 10\text{Log} \left(10^{\frac{\phi_{noise\#1}(dBc)}{10}} + 10^{\frac{\phi_{noise\#2}(dBc)}{10}} \right)$							
MLS Synthesizer Phase Noise							
<i>offset</i>	<i>Phase Noise</i>						
100 (Hz)	-130	(dBc/Hz)					
1000 (Hz)	-155	(dBc/Hz)					
10000 (Hz)	-162	(dBc/Hz)					
100000 (Hz)	-162	(dBc/Hz)					
1000000 (Hz)	-162	(dBc/Hz)					
$\phi_{noise_total}(dBc) = \phi_{noise_initial}(dBc) + 20\text{Log}(N_{Multiplier})$							
THz Link Tx							
<i>offset</i>	<i>Mult</i>	<i>Phase Noise</i>					
100 (Hz)	24	-102.382063 (dBc/Hz)					
1000 (Hz)	24	-126.981848 (dBc/Hz)					
10000 (Hz)	24	-132.631427 (dBc/Hz)					
$\phi_{noise_total}(dBc) = \phi_{noise_initial}(dBc) + 20\text{Log}(N_{Multiplier})$							
Coho Link Tx							
<i>offset</i>	<i>Mult</i>	<i>Phase Noise</i>					
100 (Hz)	4	-142.9588 (dBc/Hz)					
1000 (Hz)	4	-152.9588 (dBc/Hz)					
10000 (Hz)	4	-152.9588 (dBc/Hz)					
$\phi_{noise_total}(dBc) = \phi_{noise_initial}(dBc) + 20\text{Log}(N_{Multiplier})$							
Coho Link Rx							
<i>offset</i>	<i>Mult</i>	<i>Phase Noise</i>					
100 (Hz)	4	-155 (dBc/Hz)					
1000 (Hz)	4	-165 (dBc/Hz)					
10000 (Hz)	4	-165 (dBc/Hz)					
$\phi_{noise_total}(dBc) = \phi_{noise_initial}(dBc) - 20\text{Log}(N_{Divider})$							
THz Link Rx (same Tx phase noise fed to mixer from both inputs)							
<i>offset</i>	<i>Phase Noise</i>						
100 (Hz)	-99.3718 (dBc/Hz)						
1000 (Hz)	-123.972 (dBc/Hz)						
10000 (Hz)	-129.621 (dBc/Hz)						
$\phi_{noise_total}(dBc) = 10\text{Log} \left(10^{\frac{\phi_{noise\#Tx}(dBc)}{10}} + 10^{\frac{\phi_{noise\#Tx}(dBc)}{10}} \right)$							
Total Jitter at A/D Converter Trapezoidal Method (Note: Coho Link Jitter generating A/D clock is so low will have no effect as seen above in component noise)							
<i>offset</i>	<i>Phase Noise</i>	<i>Phase Noise Raw</i>	$A_{Trapezoid_partial}$	A_{Total}	$\phi_{jitter_rms_radians}$	$\phi_{jitter_rms_sec}$	A= Area=Integrated Phase Noise Power
10 (kHz)	-99.3718 (dBc/Hz)	1.15564E-10	5.74E-08	5.97E-08	0.000346	54.9934853 ps	
1000 (kHz)	-123.972 (dBc/Hz)	4.00724E-13	2.29E-09				
10000 (kHz)	-129.621 (dBc/Hz)	1.09116E-13					
$\phi_{noise_raw} = 10^{\frac{\phi_{noise}(dBc)}{10}} \quad A_{Total} = \sum A_{Partial} \quad \phi_{jitter_rms_radians} = \sqrt{2A_{Total}} \quad \phi_{jitter_rms_sec} = \frac{\phi_{jitter_rms_rad}}{2\pi f_{carrier}}$							
$Trapezoidal\ Sub - Area = .5(f_{offset_n} - f_{offset_(n-1)}) (\phi_{noise_raw_n} + \phi_{noise_raw_(n-1)})$							
Total Jitter at f0 frequency method (Note: Coho Link Jitter generating A/D clock is so low will have no effect as seen above in component noise)							
f_0	A_{Total}	$\phi_{jitter_rms_radians}$	$\phi_{jitter_rms_sec}$	A= Area=Integrated Phase Noise Power			
0.01 (MHz)	-56.3615	0.00215	342.185784 ps				
1 (MHz)	-60.9612	0.001266	201.498914 ps				
10 (MHz)	-56.6108	0.002089	332.501645 ps				
$A_{Total} = \phi_{noise_dBc} + 10\text{Log}(2f_0) \quad \phi_{jitter_rms_radians} = \sqrt{2 \times 10^{A_{Total}/10}}$							

2.15 Meteorological Truth

The identification of key meteorological variables along the path drives the design of a meteorological truth system that has the capability to observe profiles of hydrometers and aerosols, and path integrated values of turbulence variables. TAIPAS, under this phase of the program, fell significantly short for hydrometers and aerosols. These would require radar and lidar, which were left to future modifications due to cost. Even the values of turbulence are left short; temperature, wind and humidity are only measured at the end points. Ideally, many samples of these variables would be taken along the path. This is cost prohibitive and, possibly, location prohibitive.

2.16 Hallway Testing

Figure 2.103 illustrates the C-band Internet communications link, Pilot signal dipole, sonic anemometer, hygrometer, and rugged Tx inner housing; there are two more of these housings for the receive site. The box at the time of this picture did not have the scintillometer telescope or emitters mounted.

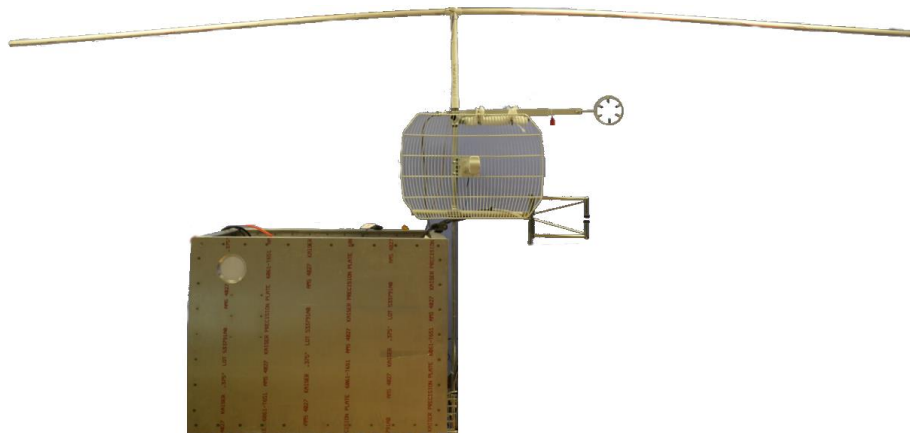


Figure 2.103. Picture of System at CEI Lab.

Pictures of the system implemented for testing in the hallway outside of the CET lab at CU are shown in Figure 2.104 - Figure 2.107. The hygrometer and anemometer were temporarily mounted on tripods. The telescope and emitters were installed and the insides were nearly complete, missing UPS and cleanup.



Figure 2.104. Picture of Outer Tx System at CEI Lab.

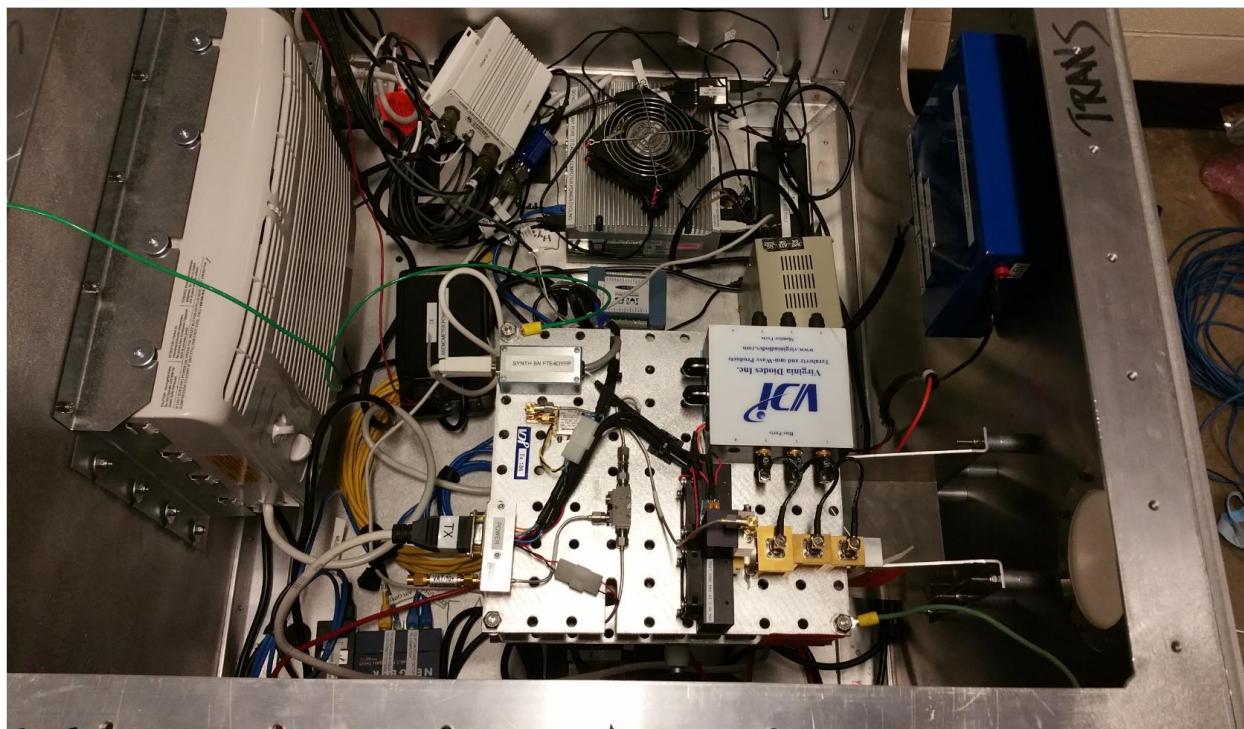


Figure 2.105. Picture of Inner Tx System at CEI Lab.



Figure 2.106. Picture of Outer Rx1 System at CEI Lab.

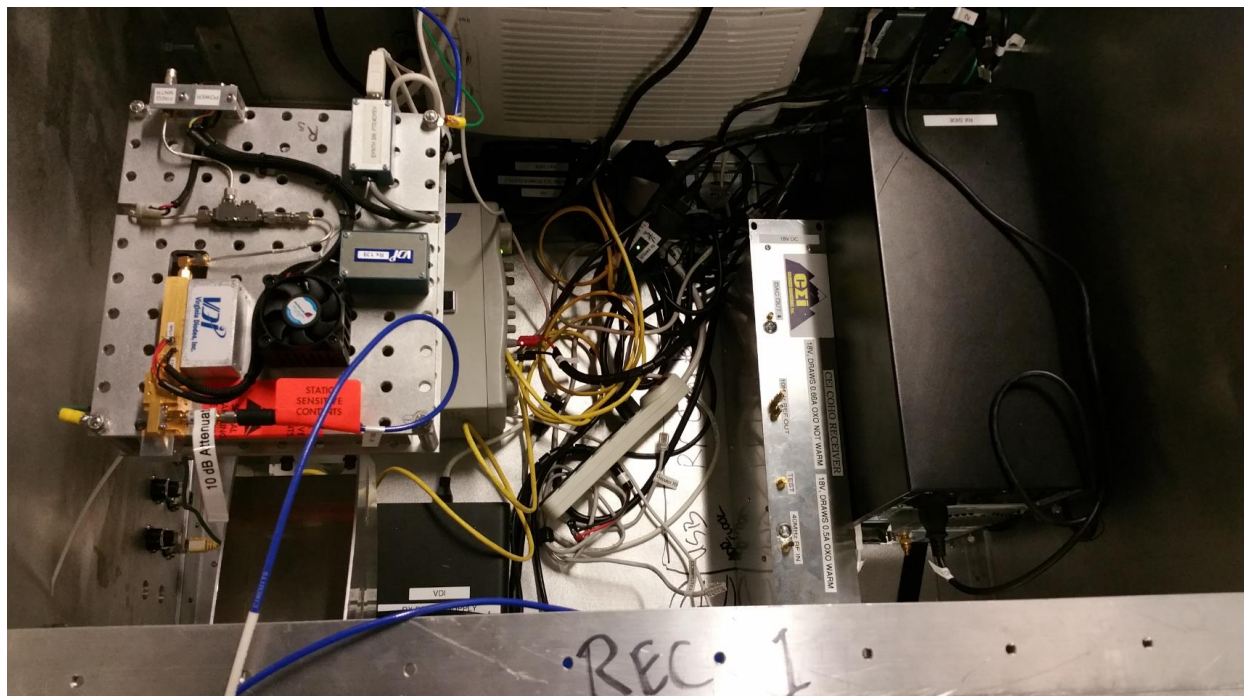


Figure 2.107. Picture of Inner Rx1 System at CEI Lab.

2.17 Summary

The TAIPAS project presented here supports electromagnetic propagation experiments and 24/7 data collection at a critical water absorption line; the volume and fidelity of data collected at this absorption line have never been implemented before. The first phase of short range testing began in early 2016. The system and experiment design accounts for the associated risk to assure success. The experimental data will be used to refine and enhance atmospheric propagation models in the TAIPAS modeling framework. One of the goals of TAIPAS is to make these models, and the data, available to the scientific and defense communities in order to aid in the design and production of future THz systems for a wide variety of applications including remote sensing, imaging, security, communications, biomedical and others that have yet to be

considered. Data at these frequencies are very sparse and under limited conditions, so the contributions of TAIPAS could be invaluable.

Planned future research and development activity includes additional data collection systems and propagation experiments at 495, 670 and 870 GHz; the existing housing can handle all but 870 GHz without modification. Meteorological truth improvements will be implemented as well. Identification of key meteorological variables along the path will drive the design of the meteorological truth subsystem, which will include capability to observe path profiles of hydrometers and aerosols and path integrated values of turbulence variables. The path profiles of hydrometeors will be measured using the dual-polarized Ka-band (35 GHz) radar. This unit will be located at the CU observation deck and trained along the line of site. An eye-safe modulated laser will provide total path optical refractivity and aerosol load variations. A bi-static CCD camera located at the NOAA site underneath the path and sensitive to this laser wavelength will be considered to measure side-scattering caused by aerosols. Local microwave water vapor profilers and wind lidars at NOAA and other sites in the Boulder area will be used for collecting additional data on stability on an as-available basis. All of these additions, however, will require more collaboration and funding from other organizations.

Chapter 3

Propagation Statistics

3.1 Propagation

This chapter explores how attenuation is altered by aerosol scattering and trace gas absorption, or how attenuation varies temporally and spatially because of turbulence; including the spatio-temporal effects of wind- and terrain-induced turbulence. The contribution of “continuum absorption” has been empirically modeled well [23]; this chapter extensively explores the effects of attenuation path loss at the 325.153 GHz water absorption peak. SMMW refractivity $N=N'-jN''$, unlike optical refractivity, is affected heavily by both temperature and humidity, the first of which affects phase through N' and the latter of which causes attenuation through N'' . The interaction of photons with water vapor at SMMW frequencies occurs strong through rotational quantum state transitions. Such strong transitions are weaker at optical frequencies. To understand the quantitative influence of water vapor absorption on the statistics of an SMMW beam wave, Manning’s statistical propagation model [59, 60] for complex refracting and absorbing media over a band encompassing the 325.153 GHz water vapor resonance and the 340 GHz transmission window is used. Observations to be made using the TAIPAS link include the effects caused by temperature fluctuations (C_T^2) and humidity fluctuations (C_Q^2), correlations between temperature and humidity (C_{TQ}) and on- and off-line measurements of the relevant fluctuation statistics of the beam wave.

While Wheelon [31, 32] discusses several key aspects of beam propagation in a random medium, his analysis focuses on optical propagation for which fluctuations in the imaginary part

of the index-of-refraction for which C_n^2 depends only on C_T^2 . At SMMW frequencies, analysis utilizing the full Lorentzian line shape, shown in Chapter 1, is needed to determine how both temperature and moisture fluctuations affect the real and imaginary components of the index-of-refraction. This section thus re-derives Manning's [60] solution for a beam wave propagating in a complex turbulence medium and applies Manning's solution [60] to complex refracting and absorbing atmospheres over the 320 GHz to 340 GHz band.

Measurements. Observable fluctuating quantities of an EM wave are driven by random permittivity fluctuations caused by atmospheric turbulence. The statistics describing these quantities include variances of the logarithm of the wave amplitude (σ_χ^2), wave phase (σ_ϕ^2), and wave AoA (σ_α^2), and the complex MCF of the complex wave amplitude at two points located transverse to the path boresight. These quantities are related to spectrum of fluctuation of the permittivity (ϵ) of the atmosphere. The complex nature of the permittivity and permeability (μ) can be thought of as due to a lag in the induced polarization of the medium with respect to the applied E and H fields. Classically, it takes non-zero time for atomic and molecular charges to move, in other words polarize, in response to an external oscillating field stimulus. Quantum mechanically, and, quite precisely, the complex part of the dielectric constant, describe the physical process of absorption and re-emission of photons due to energy level transitions. An out-of-phase condition between the applied field and induced polarization vectors leads to a transfer of energy from the fields to the medium for atoms and molecules in thermal equilibrium. For atoms and molecules pumped by an external means to exhibit a population inversion, the phase condition is of opposite sign, thus leading to emission of radiation. This is the basis of

lasers, masers, and fiber optic amplifiers. Refractivity varies with moisture and temperature, but within turbulent parcel sizes that exhibit remarkably well-understood size spectra.

The refractivity can be considered to have both a mean value related to average pressure, temperature, and humidity, and a fluctuating part driven by small perturbations in these quantities (Equation 3.1).

$$N = \langle N \rangle + \delta N = \langle N' \rangle + \delta N' - j(\langle N'' \rangle + \delta N'') \quad (3.1)$$

Random scattering, due to random spatial and temporal fluctuations in permittivity, is caused by random fluctuations in temperature, pressure and humidity and thus randomness in the stochastic component of complex permittivity. AoA and the phase variations speeding up and slowing down of propagation due to the dielectric — primarily permittivity — of the atmosphere changes the phase. The bunching and spreading of the ray lines, caused by diffraction, that make up the beam cause the amplitude scintillation. Evaporation at the surface causes cooling, making the humidity increase and temperature decrease. The ideal gas law states that as temperature increases, the density of air drops. Also, heat capacity changes with humidity, and water in the vapor phase has different thermal conductivity.

Measurable EM quantities vary with the following independent variables: frequency, distance, transmitter and receiver aperture size, separation between receivers, temperature, humidity and zenith angle. Unlike optical frequencies, RF refractivity is affected by both temperature and humidity. An FFT of the received and down-converted signal allows the measurement of coherence and spectral spreading.

3.2 Atmosphere Turbulence Structure

The description of a random atmospheric medium is based on the spatial autocorrelation function of the refractive-index fluctuations at two distinct points; the MCF is the resulting spatial coherence function. The atmosphere near the surface is simplified by assuming that it is both homogeneous in its statistics and isotropic: statistical averages don't depend on position, and measured scale lengths in vertical and horizontal dimensions are equal, respectively. The assumption of isotropy does not apply to turbulence at all scales; correlation lengths are generally larger horizontally than vertically for large turbulent parcels.

In developing a structure function for the lower atmosphere, based on temperature and humidity using the refractive-index, the square root of the permittivity is considered exclusively, with the permeability being effectively unity. This overall level of turbulence is proportional to the refractive-index structure constant, C_n^2 , which is the strength of the turbulence refractive-index irregularities.

The spectrum of turbulence in the atmosphere is a result of sub-dividing eddies that begin as large inertially generated parcels and eventually dissipate into heat, shown in Figure 3.1 [31]. In characterizing the size of the eddies, there is thus an outer scale length L_0 describing the largest eddy and an inner scale length l_0 describing the size when just prior to viscous dissipation. As eddies decay closer to the inner scale length, they become more symmetric (i.e., spherical). The spatial frequency of eddies is often described using the wavenumber k (Equation 3.2 - Equation

3.5). The scaled refractive-index spectrum (Equation 3.4) is shown in Figure 3.2; this represents the three phases of the atmosphere structure as a function of wavenumber.

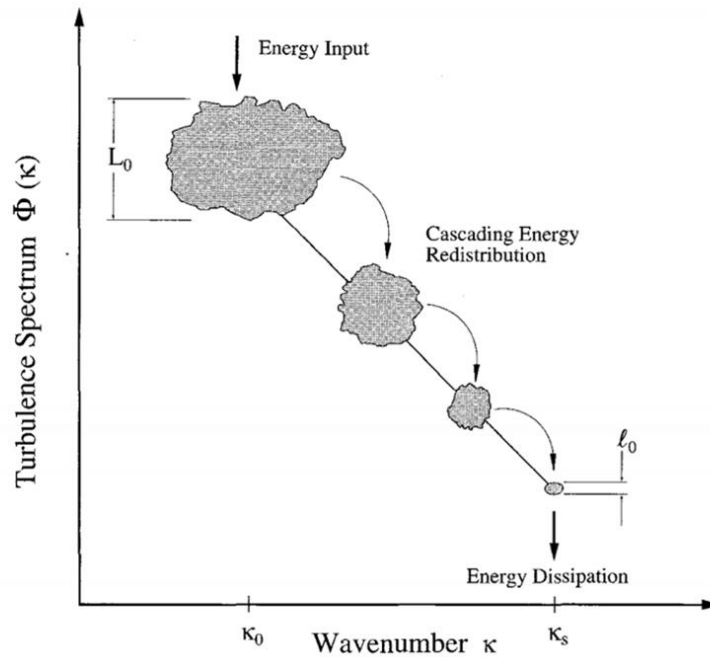


Figure 3.1. Eddies and Measurements.

$$\kappa_0 = \frac{2\pi}{L_0} ; \textit{outerscale} \quad (3.2)$$

$$\kappa_s = \frac{2\pi}{\ell_0} ; \textit{innerscale} \quad (3.3)$$

$$\Phi_n(\kappa) = \frac{.033C^2}{\kappa^{11/3}} ; \textit{average Length Eddie}; \frac{2\pi}{L_0} < \kappa < \frac{2\pi}{\ell_0} = \textit{inertial range} \quad (3.4)$$

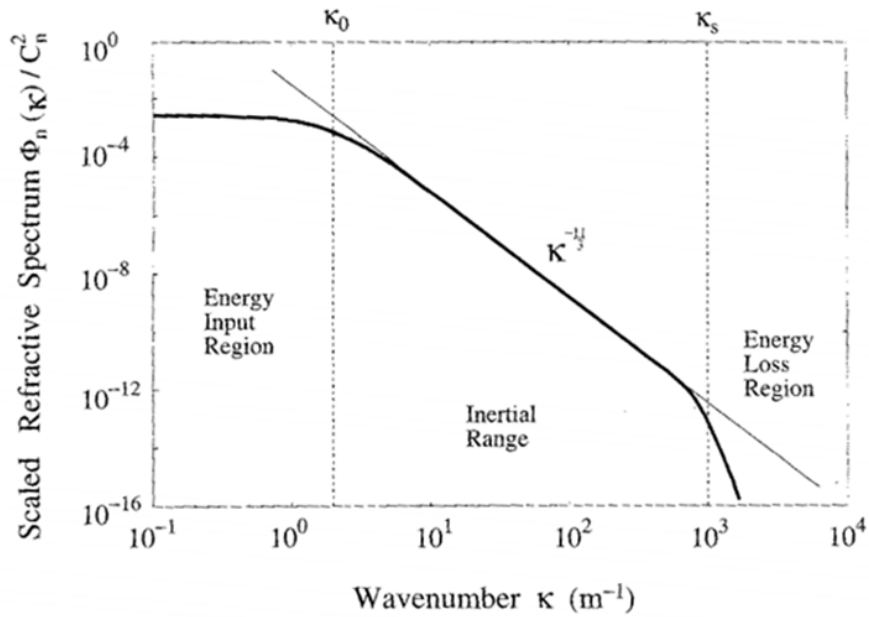


Figure 3.2. Kolmogorov Turbulent Refractive Index Spectrum [31].

The Kolmogorov refractive-index spectral model (Equation 3.5) considers the inertial region. The Von Karman model (Equation 3.6) cut off the Kolmogorov spectrum at both small and large wavenumbers, excluding the dissipative region at high wavenumbers and the large scale eddy region at low wavenumbers (Equation 3.7). The associated structure functions are shown in Figure 3.3 where ρ is the distance between the two receivers whose ratio eliminates C_n^2 .

$$\langle \delta n^2 \rangle = .622 C_n^2 (\kappa_0)^{-2/3} \quad (3.5)$$

$$\langle \delta n^2 \rangle = .523 C_n^2 (\kappa_0)^{-2/3} \quad (3.6)$$

$$\Phi_n(\kappa) = .033 C_n^2 (\kappa^2 + \kappa_0^2)^{-11/6} ; 0 < \kappa < \kappa_s \quad (3.7)$$

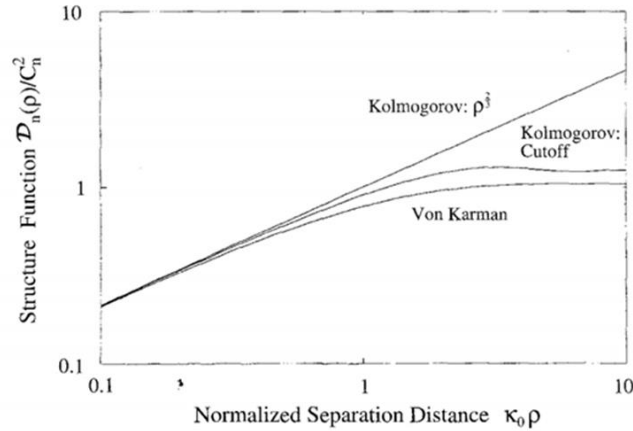


Figure 3.3. Structure Functions for Common Refractive Turbulence Models [31].

The Navier-Stokes equations of hydrodynamics are fundamentally nonlinear, and solutions to them exhibit chaotic behavior. The turbulent velocity stirs up the scalars temperature and humidity, which create the random structures. The fundamental length scale for diffraction is the Fresnel length (Equation 3.8); for the TAIPAS path and frequency the maximum Fresnel length at mid-path equals ~ 1.33 m. The inner scale length is of order millimeters, and is always much smaller than the Fresnel length.

$$Fresnel_length = \sqrt{\lambda R} \quad (3.8)$$

Phase variations depend primarily on large eddies where refraction at eddy boundaries must be considered, but diffraction can be ignored; proportional to path length and the first moment of turbulent irregularities. The amplitude variance, bunching and diverging of energy bearing rays, is driven by the smaller eddies, generated by the spectrum's third moment, which emphasizes the energy dissipation region; diffraction plays a major role. Aperture averaging effects will be discussed later and can deplete that dependence. The AoA is in-between amplitude and phase

and is dependent on the path length and third moment; for small apertures, this is dominated in the dissipation range. If the energy loss section drives the inclusion of kinematic velocity and diffusion, the turbulence spectrum needs to be adapted by the Hill bump model. Since TAIPAS Tx is on a multistory roof and a steep hill on Rx, this will not be required. The energy input section drives the large eddies into the decaying process; the first two moments drive the average scale length and refractive-index. The model that includes this input region is the Von Karman Model, but for close to the ground the Kolmogorov is optimal for optical, which is best for refractive-index and temperature fluctuations. RF is better represented by the Von Karman Model, but it is close enough to leverage the Kolmogorov.

Understanding the atmospheric turbulence state is critical to predicting the amplitude, phase and AoA variances; this requires understanding of the wind, temperature, humidity and refractive-index. Since TAIPAS is deployed in an environment that is usually very dry, sometimes temperature will be the primary factor, similar to high altitude. The Taylor hypothesis states that the eddies are frozen and wind is constant during the samples; Tatarski proved this is true for the inertial and energy dissipation phases. Tatarski also introduced the locally frozen medium which eliminates assumptions by recognizing the wind variation component. Since TAIPAS is leveraging a 6" aperture scintillometer — which is much larger than the inner scale length — the influence of small eddies on C_n^2 can be removed, which decreases with altitude; this will be discussed in more detail in the scintillometer section. If convection occurs in high enough columns (> 10 m) for the TAIPAS's location, then intermittency will be prominent in the turbulence characteristics; these events input energy into the eddy decay process which is described in Navier-Stokes equations.

3.3 Prediction

Characterization of the changes in Electromagnetic (EM) propagation in a turbulent medium has many components. One driver is the consideration of the beam shape at the receiver, which can be driven by the beam shape or gain, receiver gain and range. There are three primary shapes the EM field can have at the receiver: spherical Gaussian beam; planar Gaussian beam; and beam wave, proselytized by Manning [60] and discussed in more detail in Chapter 5. This thesis will approach looking at the beam from all spatial perspectives. There are also many views in predicting the scintillation of amplitude/intensity, phase and AoA; all will be leveraged. Many look at all of these with an “or” perspective; an “and” holistic view will be compared to measure data.

Geometric Optics (GO) does a good job of describing RF propagation for phase and AoA [31]; amplitude/intensity variations are described by the Rytov approximation, which includes diffraction effects and provides for weak scattering conditions. Strong scattering breaks the first order Rytov approximation; it requires the utilization of second order Rytov, or the Markov approximation, based on differential equations for the moments of the electric field strengths or adaptation of the path and diffraction widening of the beam - integral for use in quantum physics or a Monte Carlo Simulation. The Rytov approximation is a method of smooth perturbations and it will be the primary model utilized for TAIPAS; if GO is easily available, it can be used for comparison. Rytov takes Geometric Optics (GO) to the level of including diffraction effects. The Born approximation model is a building block for Rytov. Rytov requires amplitude variance to be less than one. Unlike GO, Rytov can predict amplitude and phase variations.

Kolmogorov describes, through the structure function, important features of turbulent behavior of temperature and humidity that influence EM waves. The anisotropy of the atmosphere cannot be avoided. In a vertically polarized system like TAIPAS, turbulence is characterized as elongated in the direction of the magnetic field. Troposphere aberrations near the surface are correlated over longer distances in the horizontal component with disparities increasing quickly in the shorter vertical direction. This is true over the TAIPAS open path that climbs 124 m. There are three phases of turbulence: energy entry, inertial and energy dissipation. Kolmogorov is utilized to model the atmospheric structure during the inertial range. It would be optimal to utilize radar to verify and understand the structure of the atmosphere, but TAIPAS was limited by cost for this feature.

In TAIPAS's LoS propagation, the predicted phase variance is proportional to the path length and the first moment — expectation (mean) — of the spectrum of turbulent irregularities; the moments describe the nature of a distribution of samples. While the expectation is important, higher order central moments about the mean describe the shape of the distribution. The second central moment is the variance — width of the distribution — which is a statistical value utilized many times in this chapter; standard deviation is the positive square root. The normal moments are divided by the standard deviation to the power of the moment number. The third central moment is the lopsidedness of the Probability Distribution Function (PDF); if symmetric, it equals zero and normalized yields skew left and right. The fourth central moment measures tallness or squatness; if a normal distribution, it measures Kurtosis. The more data, the better, in determining all the useful PDF descriptors.

3.4 EM

Maxwell's Equations (ME) in random media states that the divergence of the induction/magnetic field vanishes, since there is no magnetic charge; circular lines return to the origin. Outside of the source antenna, the electric flux density or displacement field diverges to zero. The magnetic flux (B) and magnetic field (H) are approximately equal, since the permeability is approximately one in the atmosphere. The permittivity is the complex portion with a mean($\bar{\epsilon}$) and small stochastic part($\epsilon(r,t)$); both are a function of position with the latter also a function of time. The stochastic component causes the EM scintillation. Therefore, the vector wave equation, away from the antenna, is a stochastic function of position and time (Equation 3.9). The permittivity fluctuation is slow compared to the frequency, so the only factors are spatial and temporal variation of permittivity. The wind is the major turbulence generator and only the horizontal needs to be considered, so the wave equation becomes scalar; ignore polarization changes. Prediction is dependent on integration of the delta permittivity over the entire path.

$$\nabla^2 E(\vec{r}) + k^2 [1 + \Delta\epsilon(\vec{r}, t)] E(\vec{r}) = 0 \quad (3.9)$$

GO is an approximate solution for EM field equations assuming the wavelength is much less than the dimensions; boundary conditions and dielectric constant change much slower than lambda. This is not optimal for high scattering environment caused by aerosols. The plane wave is far from the antenna, which fits TAIPAS on the long open path, with an infinite array of parallel rays. A spherical wave has diverging rays while focused beams have converging rays.

Collimated beams are a spatially limited bundle of parallel rays bounded by the beamwidth; beam wave from Manning [60].

The phase can be described if the average dielectric depends only on height. Phase shift is separated in the mean value and stochastic component. Using integrals along the ray path, total phase shift is derived. GO predicts the phase variance second moment well. Variations in the permittivity along the average trajectory cause the ray path to wander / oscillate. Angle error is an integration of these bendings along the path; GO is not optimal for this measurement at the long TAIPAS path length. The receiver for TAIPAS must be large enough to get the largest displacement of the beam or spot size. Amplitude requires multiple ray paths, defined as close spacing of rays. This assumes the ray spacing cannot change significantly compared to λ . Amplitude variance of log amp is proportional to the fifth moment of the wavenumber spectrum; small eddies affect the most. Since this is not true for SMMW, GO cannot be utilized. All variance measurements are also sensitive to non-stationary processes in the atmosphere, sample length, filtering and DSP; shown in Chapter 2, TAIPAS overkills everything but non-stationary conditions. Aperture averaging will have a minimal effect. SMMW path variations equate to virtual changes in the path length, which is millions of wavelengths in length. This is one of the reasons that TAIPAS transmitters and receivers must be on very stable structures. It is very important to note that most transmissometer experiments are extremely close and parallel to a flat ground surface and, therefore, smaller eddies are present and the atmosphere is closer to isotropic. TAIPAS is expanded into a new territory with an elevated, heterogeneous and slanted path, as shown in Chapter 2. It will have much longer outer scale lengths, but if these are

significantly shorter than the path length, the current structure functions can be utilized. The von Karman model for phase variance is usable for TAIPAS (Equation 3.10).

$$\langle \varphi^2 \rangle = .782 R k^2 C_n^2 \kappa_0^{-5/3}; \text{ von Karman Model} \quad (3.10)$$

Transmissometers have sampled the phase influence by random variations of refractive-index and gradual changes with statistics over long periods of time, then applying a linear regression or polynomial fit of the running average phase. This results in the stationary process results. If a finite sample is utilized, large Eddie effects and gradual changes can't be distinguished.

TAIPAS is designed with two receivers to measure the phase structure function with a basic interferometer. This requires taking the phase difference between two receivers to cancel out the slow changes and the remainder is the desired stationary process if the large scale inhomogeneities and intermittent structures enclose both paths, which is especially true for TAIPAS's elevated path. TAIPAS also has the capability of varying the spacing of the two receivers up to 8 m; obviously, they should be no closer than a Fresnel length. Unfortunately, changes in distance are manual at the restricted NIST site. In the future, it would be nice to install a motor driven system to be commanded to separate the receivers at a much higher rate. The Phase correlation between the two receivers differs with the EM shape: planar, spherical or beam.

Spherical waves (zero focal length) are usually considered at microwave frequencies. TAIPAS is SMMW and has 50 dBi of gain each on transmit and receive apertures. TAIPAS requires a normal LoS to optimize the gain. Therefore, the transmitter is tilted up 3.6 degrees and receivers are pointed down the same amount. It is unlikely that the TAIPAS waveforms are spherical. Plane waves near the surface are difficult to produce at microwave frequencies, but TAIPAS is elevated with high gain at a long distance; this will also fit into the collimated / infinite focal length category since they are LoS lined up. Usually, optical waves are the only frequencies that are considered beam waves; Manning [60] has a different view. These are represented by straight rays traversing the transmitter aperture to a focal point.

Covariance between the receiver's phase utilizes the wavenumber, which represents the spatial correlation. The separation of the receivers is ρ (Equation 3.11) and is much less than the path length R , which also causes the separation angle to be small. This designates the waves with homogeneous, isotropic irregularities, so Kolmogorov's model can be utilized. The phase structure function verses receiver separation is shown in Figure 3.4; inner scale and outer scale lengths are marked. Figure 3.5 shows the close to linear responses to the phase structure function parallel to a line $\rho^{5/3}$ with different y intercepts for different times of the day. This was measured by Hill, McMillan, Priestley and Sheonfeld [26] at 173 GHz. For small separations less than the inner scale length, which is impossible for TAIPAS due to receiver and aperture size, structure is shown in Equation 3.13. For large separations greater than the outer scale length — also impossible for TAIPAS — Equation 3.14 structure is applied. The inertial region is represented by Equation 3.14 and has no dependency on inner scale or outer scale lengths. These assume

spherical waves for the structure function. For plane waves, the structure is larger than spherical; with the Kolmogorov spectrum, the constants get larger: (Equation 3.15 – Equation 3.17).

$$\rho = R\theta \quad (3.11)$$

$$D_\varphi(\rho) = \rho^2 \left(.651 R k^2 C_n^2 \kappa_s^{1/3} \right); \kappa_s \rho < 1 \quad (3.12)$$

$$D_\varphi(\rho) = .073 R k^2 C_n^2 L_0^{5/3}; \kappa_0 \rho > 1 \quad (3.13)$$

$$D_\varphi(\rho) = \rho^{5/3} \left(1.093 R k^2 C_n^2 \right) \quad (3.14)$$

$$D_\varphi(\rho) = \rho^2 \left(1.953 R k^2 C_n^2 \kappa_s^{1/3} \right); \kappa_s \rho < 1 \quad (3.15)$$

$$D_\varphi(\rho) = \rho^{5/3} \left(2.914 R k^2 C_n^2 \right) \quad (3.16)$$

$$D_\varphi(\rho) = .073 R k^2 C_n^2 L_0^{5/3}; \kappa_0 \rho > 1 \quad (3.17)$$

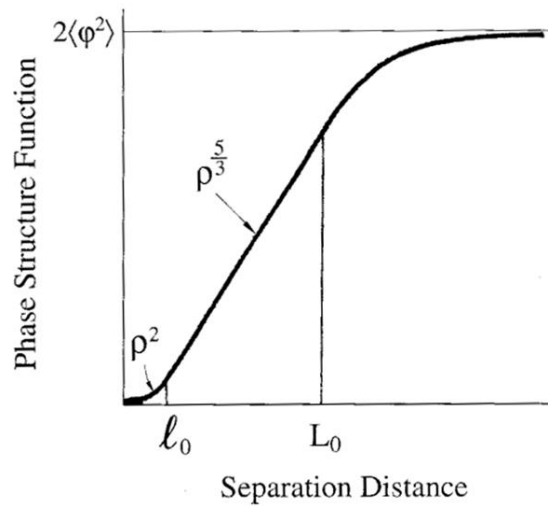


Figure 3.4. Phase Structure Functions [31].

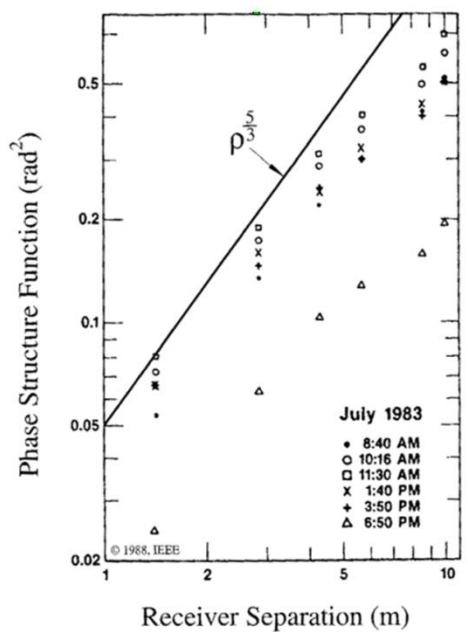


Figure 3.5. Phase Structure Functions (radians) [31].

In the lower atmosphere, the permittivity is equal to two times the refractive index with variability driven by winds. If no wind is present, self-motion, driven by convection, is the driving factor: $C_n^2 \sim 0$. Time shifted phase covariance is the basic measurement of single receiver phase variance — temp and water driven and both scalars. Less than 10% of wind variation is converted to turbulence. The autocorrelation function is a way to describe the variability of phase fluctuations: phase variance divided by the magnitude of the mean squared. Phase covariance is primarily influenced by normal wind. Figure 3.6, measured at 9.4 GHz by Norton et al., shows the autocorrelation verses time lag; as expected the more lag in time, the less correlation. The power spectrum, related to the autocorrelation via the Wiener-Khintchine theorem, is important for understanding phase perturbations. TAIPAS MATLAB code generates spectral plots of all frequencies in the scan. TAIPAS, later in this chapter, looks at many versions of phase variance and AoA prediction: GO, Rytov, spherical, planar, etc.

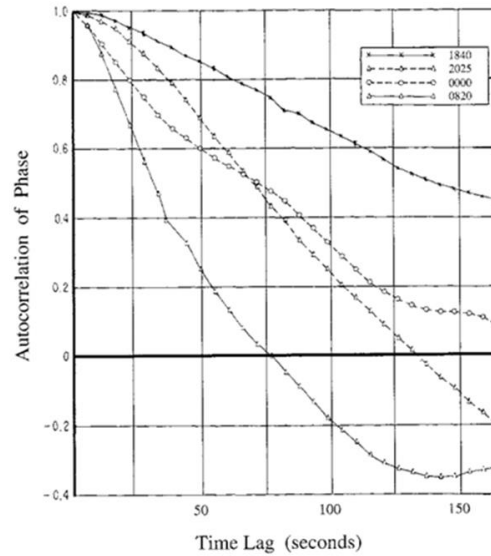


Figure 3.6. Phase Autocorrelation vs Time Lags [31].

TAIPAS utilized two receivers, not to prove earlier scientific work on phase variances but to measure the second order statistical moment, the MCF; it takes the average of a field strength at one spatial location and multiplies by the complex conjugate at a different point. Phase differences and trends cancel out when the receivers are close. Since the phase fluctuations are Gaussian random variables, functions derived from them are Gaussian: central limit theorem. MCF describes the correlation of the E field at different points; coherency exists only if the phase structure function (D) is less than one. This applies to real work communication applications to define the maximum available bandwidth for information to determine the frequency separation at which the field strength becomes de-correlated. The bandwidth is equal to the carrier frequency divided by the square root of the phase variance (Equation 3.18 – Equation 3.20). The MCF is shown in Equation 3.20.

$$B = \frac{f_c}{\sqrt{\langle \varphi^2 \rangle}} \quad (3.18)$$

$$\text{Microwave_Link} : B \approx 10\text{GHz} \quad (3.19)$$

$$\langle E_1(f_1)E^*(f_2) \rangle = |E_0|^2 \exp\left(-\frac{(f_1 - f_2)^2}{2B^2}\right) \quad (3.20)$$

Manning [60] drives for a beam wave utilizing the von Karman spectrum / model; this is applicable to SMMW. Both absorptive fluctuations, the imaginary part of permittivity, non-ionizing atmosphere, aerosol free, and 1 mm wavelength or smaller allow beam wave spatial characteristics. Manning considers the beam wave nature of the field due to the finite size of the transmitter aperture and the shape of the phase front at the aperture. He assumes the wavelength is much less than the inner scale length due to the aperture size; this is true for TAIPAS. Manning also shows that it is reasonable to ignore the second order effects of Rytov; only first order is required. Manning derives a single mode Gaussian beam wave propagation source; representation changes a variable to include a focusing effect with a radius of curvature of the wavefront at the aperture. This allows him to cover a divergent/spherical beam wave, focused beam wave and collimated beam wave. Since the Rytov approximation is only single scattering, correlation will only occur in the plane transverse to the direction of propagation. The wave is a beam wave with a complex radius of curvature. A deeper discussion will take place in Chapter 5. Wheelon only thinks of beam wave with respect to a laser. The type of wave radiated depends on the transmitter design: plane wave, spherical wave or beam wave. There are significant differences in scintillations. Many references assume spherical waves to start since the waves are divergent requiring a small transmitter aperture. Planewaves must be simulated by collimated beams.

It is important to note that the surface over this open path should have little effect on the propagation of the THz signal; this was seen in the calculations of the Fresnel zones in Chapter 2. Therefore, the ground and buildings do not come into play with respect to the amplitude variance. All the amplitude scintillation will increase as it relates to the carrier frequency square of the distance traveled.

There are two primary regions of propagation: Fresnel and Fraunhofer. The latter takes the outer scale effect on amplitude variance into consideration. The Fresnel region is the lower limit and Fraunhofer is the upper regime. Equations are presented in the sections below where TAIPAS calculations are implemented for both.

3.5 Polarization

LoS propagation is dominated by forward scattering with very small angles, therefore, the polarization does not change. TAIPAS is vertically polarized on transmit and receive. This allows the propagation to be described with scalar quantities.

3.6 Aperture Averaging

To this point, the amplitude variation was described at a discrete point. In the TAIPAS transmissometer, significant gain is implemented to increase the SNR and decrease multipath. The absolute mean-square result of the aperture averaged field depends on the MCF. The wavenumber generated due to the aperture averaging weights both spherical and plane waves. On TAIPAS, the Fresnel length defined above is approximately 1.4 m. Since the aperture size is 9 cm, the weighting function will be approximately one.

3.7 Phase Amplitude Cross Correlation

Correlation of the phase and amplitude is a third measure of the EM field behavior and plays an important role in propagation research; phase distribution depends on this cross correlation. As stated above, the validity conditions for the Rytov approximation depends on cross correlation inequalities. The amplitude variance is dependent on the inner scale lengths — small eddies — and the phase variance is dependent on the outer scale length — large eddies. This measurement links the two within the full turbulence spectrum; the two measurements are inverse cross variations from a spatial perspective. This allows the outer scale region to be researched in a way that could not be done independently, since the cross correlation is more sensitive to large eddies than small eddies close to dissipation. This shows one example of the power of the complete covariance matrix.

3.8 MCF

The MCF of a propagating EM wave describes the cross correlation of the complex field in a plane that is transverse to the direction of propagation. It describes the degree of coherence of the field at two separated points: angular distribution of the field and main energy density. The transverse coherent length is the distance an EM wave maintains specific amount of coherence. The approximate coherence length is shown in Equation 3.21, where n is the refractive-index and B is the RF bandwidth. The MCF measurements drove the requirement of two receivers with coherent LOs.

$$L = \frac{c}{nB} \quad (3.21)$$

Plotting shows more rapid temporal fluctuations in intensity than the phase differences because the Fresnel zone size is much smaller than the transverse coherence length of the phase. The phase difference for the minimum antenna spacing shows more rapid fluctuations than for the maximum spacing. Since phase is more dependent on the outer scale lengths, both receivers have the same phase scintillation. The MCF is the sum of the structure functions of the log-amplitude and phase with the imaginary part being much smaller than the real part. The phase structure function shows a large decay at larger receiver distances due to the outer scale turbulence dependence. MCF by definition is the measurement of phase correlation as a function of the separation distance of the receivers. The equations for the MCF are shown in Equation 3.22 – Equation 3.24.

$$\langle \mathbf{E}_1 \mathbf{E}_2^* \rangle = |\mathbf{E}_0|^2 e^{j(\varphi_1 - \varphi_2)} \quad (3.22)$$

$$\langle \mathbf{E}_1 \mathbf{E}_2^* \rangle = |\mathbf{E}_0|^2 e^{-\frac{1}{2} \langle (\varphi_1 - \varphi_2)^2 \rangle} \quad (3.23)$$

$$\langle \mathbf{E}_1 \mathbf{E}_2^* \rangle = |\mathbf{E}_0|^2 e^{-\frac{1}{2} D_\phi(\rho)} \quad (3.24)$$

Manning [60] derives the wave structure function and MCF relations for a plane wave for phase distribution (Equation 3.25). If the inner scale length goes to zero and imaginary portion of C_n^2 goes to zero, then the equation reduces to Equation 3.26.

$$D_\phi(R, \rho) = k^2 R (2.915 \rho^{5/3} - 8.704 \kappa_m^{-5/3}) (C_{n_r}^2 + C_{n_t}^2) ; \rho \gg \ell_0 \quad (3.25)$$

$$D_\phi(R, \rho) = 2.915 k^2 R C_{n_r}^2 \rho^{5/3} ; \rho \gg \ell_0 \quad (3.26)$$

Figure 3.7 [31] shows the MCF for varying EM propagation spatial shapes for phase. It is plotted against the squared ratio of the receiver separation and the Fresnel length, and normalized. For TAIPAS, the x-axis $.0033\rho^2$ m; with the maximum separation of 8 m, the x-axis maximum will be .21 m. Therefore, due to cost constraints for stability of the separation, it will stay in the coherence range (MCF ~ 1) for all beam phase shape cases. To cover this range, a 50 m separation would be required.

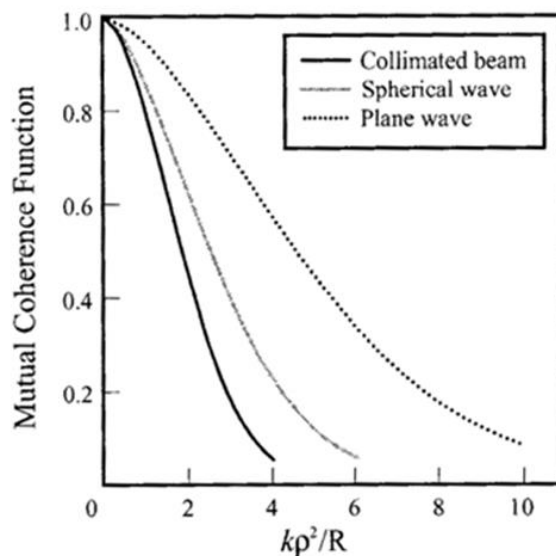


Figure 3.7. MCF for Differing Phase Shapes.

3.9 Covariance Matrix

The covariance of two quantities describes the level of correlation, the capability of predicting the second quantity when knowing the first. Temporal coherence is the measure of the average correlation between two wave points separated by a delay. The quicker the quantities de-correlate results in a smaller delay, and the larger the range of frequencies the quantity contains. The covariance matrix represents all inner correlations of all applicable variables for propagation.

AoA requires the management through movement and/or size of small aperture phase measurements compared with larger aperture AoA requirements and measurements. This will most likely be future work as it requires blocking the lens apertures that make up the TAIPAS receivers; produce a small aperture. Obviously, this will significantly reduce the SNR over the long open path link. This experiment will allow phase, AoA and amplitude biases, separate amplitude and AoA. Phase and amplitude are best measured with a small aperture, but a long open path does not provide an optimal experimental platform to perform these smaller aperture measurements and the experiment will require key hardware innovations. The AoA part of the matrix is a future addition to the matrix and highlighted in blue; equations are below.

One of the goals of the TAIPAS measurements is to fill in, as much as possible, the covariance matrix (Equation 3.27) made up of amplitude/intensity, phase and AoA. This matrix will be filled in three ways: theoretically, 40 m indoor path and 1924 m open path. Each value will be implemented as a series of comparative plots.

$$\Sigma = \begin{bmatrix} \langle \chi^2 \rangle & \langle \chi\varphi \rangle & \langle \chi\phi \rangle \\ \langle \varphi\chi \rangle & \langle \varphi^2 \rangle & \langle \varphi\phi \rangle \\ \langle \phi\chi \rangle & \langle \phi\varphi \rangle & \langle \phi^2 \rangle \end{bmatrix} \quad (3.27)$$

χ =intensity, φ = phase, ϕ =AoA

The matrix can grow significantly when including temperature and humidity. The objective is to determine the influence of the variance of temperature, humidity and refraction on the variances of amplitude, phase and AoA; this is a very important extension to propagation

analysis. This extends the covariance/correlation matrix to a 6 x 6 matrix (Equation 3.28). The variables are defined as follows: intensity/amplitude = χ ; φ = phase; ϕ = AoA; temperature structure constant = C_T^2 ; humidity structure constant = C_Q^2 ; and the index-of-refraction structure constant = C_n^2 .

$$\Sigma = \begin{bmatrix} \langle \chi^2 \rangle & \langle \chi\varphi \rangle & \langle \chi\phi \rangle & \langle \chi C_n^2 \rangle & \langle \chi C_T \rangle & \langle \chi C_Q \rangle \\ \langle \varphi\chi \rangle & \langle \varphi^2 \rangle & \langle \varphi\phi \rangle & \langle \varphi C_n^2 \rangle & \langle \varphi C_T \rangle & \langle \varphi C_Q \rangle \\ \langle \phi\chi \rangle & \langle \phi\varphi \rangle & \langle \phi^2 \rangle & \langle \phi C_n^2 \rangle & \langle \phi C_T \rangle & \langle \phi C_Q \rangle \\ \langle C_n^2 \chi \rangle & \langle C_n^2 \varphi \rangle & \langle C_n^2 \phi \rangle & \langle C_n^2 \rangle & \langle C_n^2 C_T \rangle & \langle C_n^2 C_Q \rangle \\ \langle C_T \chi \rangle & \langle C_T \varphi \rangle & \langle C_T \phi \rangle & \langle C_T C_n^2 \rangle & \langle C_T^2 \rangle & \langle C_T C_Q \rangle \\ \langle C_Q \chi \rangle & \langle C_Q \varphi \rangle & \langle C_Q \phi \rangle & \langle C_Q C_n^2 \rangle & \langle C_Q C_T \rangle & \langle C_Q^2 \rangle \end{bmatrix} \quad (3.28)$$

3.10 Permittivity

Temperature and absolute humidity density variations perturb the down-range beam phase and amplitude characteristics differently near absorption line centers and line wings, as evidenced by the following full Lorentzian model for the complex permittivity for a collection of lines (Equation 3.29):

$$\epsilon_g(\omega) = \sum_{species} \sum_{k,n} \left(\frac{n_o e^{\frac{E_2}{kT}}}{Z} \left[1 - e^{-\frac{\hbar\omega_0}{kT}} \right] \left(\frac{|\bar{\mu}_{12}|^2}{3\hbar} \right) \right) \times \quad (3.29)$$

$$\left[\frac{\omega_0 - \omega}{(\omega_0 - \omega)^2 + (1/\tau)^2} + \frac{\omega_0 + \omega}{(\omega_0 + \omega)^2 + (1/\tau)^2} + i \left\{ \frac{1/\tau}{(\omega_0 - \omega)^2 + (1/\tau)^2} + \frac{1/\tau}{(\omega_0 + \omega)^2 + (1/\tau)^2} \right\} \right]$$

where $\tau \sim T^{0.8}$ [6]. In addition, microscale temperature variations affect the overall air density, which impacts both vapor density and dry air density. Finally, the effects of absorption fluctuations caused by absolute humidity variations also affect the down-range beam characteristics, particularly near strong water vapor line centers. TAIPAS will be implementing many sample scans up and down the water absorption peak to measure the continuity and symmetry of the wings.

3.11 Construction Constants

The index-of-refraction — measure of speed relative to the speed of light — is driven by frequency, temperature, pressure and humidity. Pressure related to altitude drives temperature and humidity. The real part is due to the speed variations during EM propagation and the imaginary part is a function of energy absorption. Frequency is a driver of the index-of-refraction when transitioning from nominal refraction to anomalous driven refraction; the latter occurs at strong absorption lines. TAIPAS is measuring across a strong absorption line, therefore anomalous components of refraction are a driver. Anomalous dispersion occurs when the index-of-refraction increases with decreasing frequency with the real part decreasing significantly and

the imaginary absorption component peaking (Figure 3.8); peak absorption drives increased anomalous dispersion. The group delay is phase velocity, so it is not showing that it travels faster than the speed of light. This can be seen in the Lorentz equation for permittivity; repeated here from Chapter 1 (Equation 3.29), due to its importance. This is the opposite of normal dispersion or non-absorption peak lines.

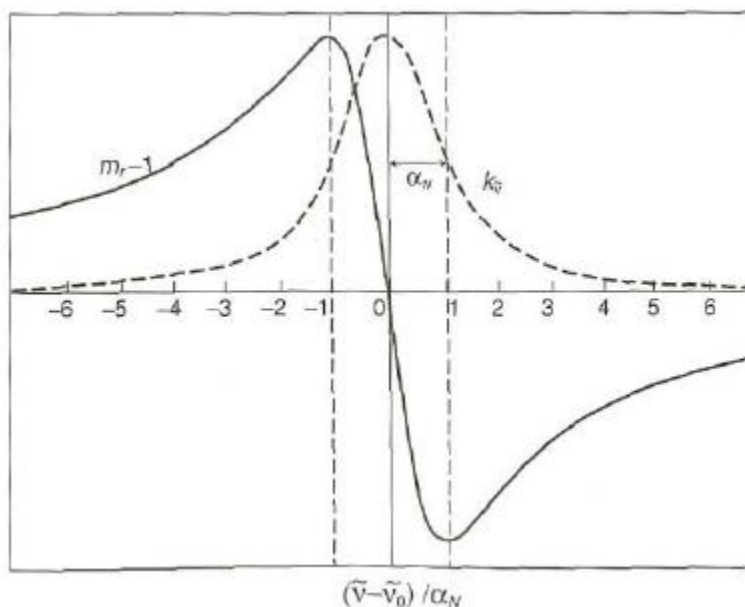


Figure 3.8. Anomalous Real (solid) and Imaginary Refraction (dashed).

The relationship between all three construction contacts and their covariance are shown in Equation 3.30 – Equation 3.32. These three equations can be solved simultaneously to derive C_T^2 and C_Q^2 ; then the covariance C_{TQ} can easily be determined [26]. A_T and A_Q are derivatives of the real part of the refractive index with respect to the logarithm of T and Q, absolute temperature and absolute humidity, respectively. At RF frequencies, both temperature and humidity play an important role in the refractive-index. For TAIPAS, when using an optical scintillometer, temperature alone plays the dominant role.

$$C_n^2(\lambda) = A_T^2 C_T^2 + A_T A_Q C_{TQ} + A_Q^2 C_Q^2 \quad (3.30)$$

$$C_n^2(\lambda) = \frac{A_T^2(\lambda)}{T^2} C_T^2 + \frac{A_Q^2(\lambda)}{Q^2} C_Q^2 + \frac{2A_T(\lambda)A_Q(\lambda)}{TQ} C_{TQ} \quad (3.31)$$

$$C_{TQ} = \pm \sqrt{C_T^2 C_Q^2} \quad ; \text{ day+}, \text{ night-} \quad (3.32)$$

The vertical profile of C_n^2 , Figure 3.9, was determined using a 49.25 MHz Doppler radar by Eaton, Pearson, Hines, Peterman, Good, Beland and Brown [61]. The solid line represents the microwave version and the dashed line is the optical. As the equations above show, these are the combined contributions of temperature and humidity. Humidity was removed from the dashed optical line. The two are extremely correlated after an altitude of 10 km. This is approximately 33 K feet, where the humidity is very low. TAIPAS is at an altitude of 1771 m (5,810 ft.); this is at the bottom of the scale, since the altitudes are relative to New Mexico, which averages ~5 K feet. The lowest reading available variation of optical is $10^{-19} < C_n^2 < 10^{-16} \text{ m}^{-2/3}$ and microwave is $10^{-15.2} < C_n^2 < 10^{-14.8} \text{ m}^{-2/3}$; these are about 2 km above New Mexico, which is approximately 11K feet. The data was derived in New Mexico in August 1985 with 15 minute averages. TAIPAS utilizes the custom optical scintillometer to measure C_n^2 ; it has been proven that C_n^2 is frequency agnostic, especially above 10 km.

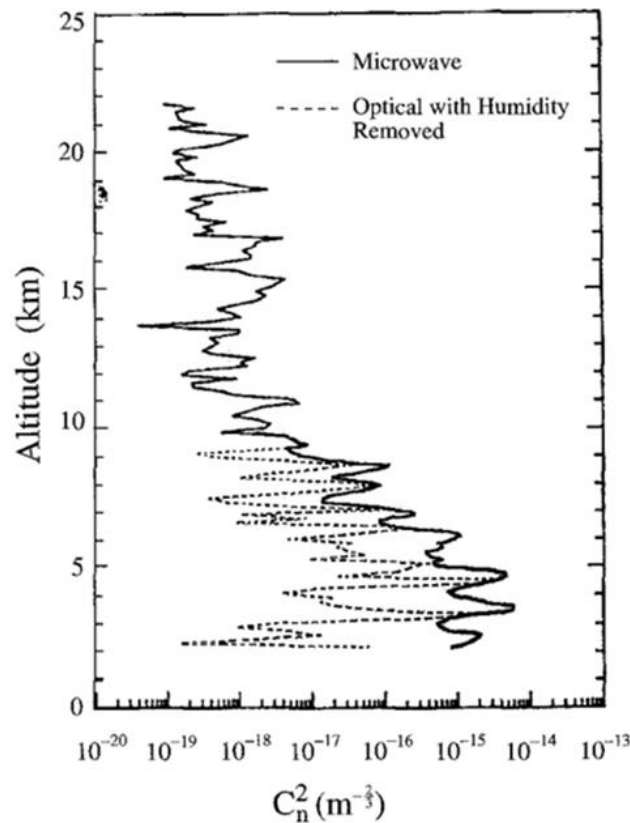


Figure 3.9. Vertical Profiles of C_n^2 - Wheelon [32].

The refractive-index construction constant over large sample sets and longer periods is important to understand for such an important constant for variances. Equation 3.33 – Equation 3.34 are refractometer readings over large samples sets over long periods. Equation 3.35 was taken in February at dawn for one month. Equation 3.36 was taken during the ascent and decent of an aircraft staying at a height of 100 m to remain isotropic at two altitude extremes: Colorado and Florida. It is important to note that these are averages over long periods of time, so the number can be larger or smaller than the ranges.

The structure function for temperature is shown in Equation 3.37 [31], derived from empirical data. The variable ρ is the separation distance of the temperature measurements. Many low level transmissometer tests have many equally spaced temperature sensors along the path. For TAIPAS, since it is an open path at higher altitudes, this was not practical with the funding; therefore, the samples are assumed to be a straight line between the transmitter temperature sample and receiver temperature sample. In the future, flying Unmanned Aerial Vehicles (UAVs) could provide a reasonable cost of getting more temperature sample points along the path. Solving for C_T^2 , the equation becomes Equation 3.38. The structure function of temperature is shown in Equation 3.39. The two-point equations for TAIPAS (Equation 3.40 and Equation 3.41) state that at a given series of samples at time t during the stable tuned time of the synthesizers, take the ΔT between the transmitter and receiver, square it, and divide the mean of this value by the separation, which for this path equals 1924 m, to the $2/3$ power. The construction constant for humidity follows the same derivation (Equation 3.42).

$$\text{Microwave } 36\text{GHz} - \text{avg. Stable Conditions} : \bar{C}_n^2 = 1.2 \times 10^{-14} \text{ m}^{-2/3} \quad (3.33)$$

$$\text{Microwave } 36\text{GHz} - \text{avg. Convective Conditions} : \bar{C}_n^2 = 6.6 \times 10^{-14} \text{ m}^{-2/3} \quad (3.34)$$

$$\text{Optical} - \text{avg. Stable Conditions} : \bar{C}_n^2 = 1.0 \times 10^{-14} \text{ m}^{-2/3} \quad (3.35)$$

$$\text{Microwave} - \text{plane} - \text{ascend / descend} : 10^{-17} \text{ m}^{-2/3} < C_n^2 < 3.0 \times 10^{-13} \text{ m}^{-2/3} \quad (3.36)$$

$$D_T(\rho) = C_T^2 |\rho|^{2/3} \quad (3.37)$$

$$C_T^2 = \frac{D_T(\rho)}{|\rho|^{2/3}} \quad (3.38)$$

$$D_T(\rho) = \left\langle \left[\delta\Gamma(r, t) - \delta\Gamma(r + \rho, t) \right]^2 \right\rangle \quad (3.39)$$

$$C_T^2 = \frac{\left\langle \left[T_{Tx}(t) - T_{Rx}(t) \right]^2 \right\rangle}{|\rho|^{2/3}} \quad (3.40)$$

$$C_T^2 = \frac{\left\langle \left[\Delta T_{TxRx}(t) \right]^2 \right\rangle}{|\rho|^{2/3}} \quad (3.41)$$

$$C_Q^2 = \frac{\left\langle \left[\Delta Q_{TxRx}(t) \right]^2 \right\rangle}{|\rho|^{2/3}} \quad (3.42)$$

Line Broadening: Another goal of TAIPAS is to understand the shape of the absorption peak at 325.153 GHz. TAIPAS has much faster frequency changing capabilities with more programmability than experiments implemented in the 1980s. It is important to understand what forms the width of this absorption peak: line broadening. Line broadening at an absorption peak is driven by pressure and Doppler, and still requires advances in characterization; as these drivers increase, lines broaden. The broadening occurs across frequency and there can also be a shift in center frequency. The tropospheric atmosphere pressure will broaden in the 5 GHz region. TAIPAS will be taking a close look at these wings with fine frequency step scans; this is an important investigation for TAIPAS. Doppler limited line broadening is in the 1 MHz region and is due to gas atom distribution of velocities and rotations as perceived from the LoS; increased temperature widens this Gaussian distribution. The line broadens due to the lower probability of reabsorption of photons at the line wings than at the center line peak; this peak can sometimes become inverted due to significant intensity of reabsorption called self-absorption. Also,

different line broadening contributors can act in unison; collision effects and Doppler shifts can have coherency, which could cause line narrowing.

Figure 3.10 shows the resonant frequency and damping dependence of the spectral line width. Γ_n represents the effective damping from photon emissions as the electrons return to the non-excited state and ν is frequency [62]; shape is a Lorentzian with thickness dependent on Γ_n . The larger the Γ_n , the broader the spectral line — related to the quantum state transitions — which is governed by Fermi's Golden Rule and is related to the initial and final energy states and perturbing Hamiltonian. The total absorption is the sum over all transitions in the molecule: absorption coefficient.

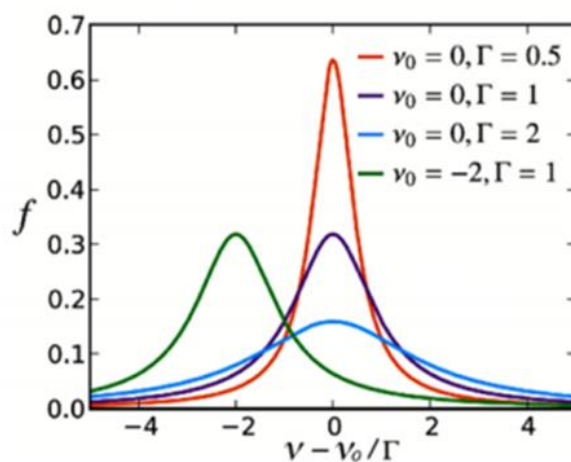


Figure 3.10. Resonant Frequency and Damping Dependence of the Spectral Line Width [62].

Pressure broadening, the dominant broadening driver, is caused by molecules colliding, which produces a damping effect by transferring energy and shortening the excited state lifetime. An increase in pressure broadens the lines; since Colorado is at higher altitude, the pressure will

be less, so the broadening will be less. Doppler broadening, much less of a driver, occurs by photons colliding with random velocity direction molecules; half are moving toward and half away. The molecules moving toward cause a positive frequency shift and negative for away. This adds a Gaussian shape to the absorption line. A temperature increase causes the molecules to become more active, which increases the Doppler broadening effect.

Voigt profiles are utilized by simulation to combine pressure and Doppler broadening effects. Figure 3.11 shows the Voigt combination for absorption lines. These profiles are close to Gaussian at resonance ($\nu = \nu_0$) and Lorentzian shape far from resonance. Near the surface, where collision broadening can dominate, they will be more Lorentzian in shape. When Doppler broadening dominates at higher altitudes, the absorption line shape is more Gaussian. Each Voigt profile describes a single molecular transition in an absorption feature, which does not work well in weak absorption areas.

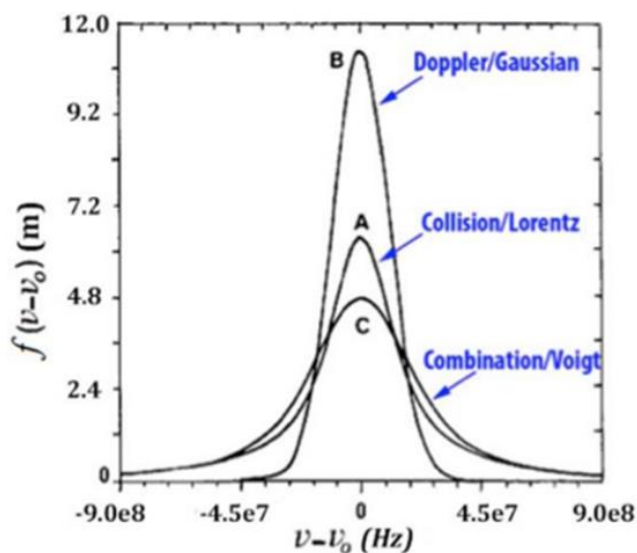


Figure 3.11. Voigt Absorption Profiles [6].

3.12 Experiments

TAIPAS extends the Flatville measurements [25, 28, 51] and analysis for phase, amplitude scintillations and varying transverse coherence length distances for a range of turbulence conditions at 320-340 GHz to empirically characterize these statistics of a beam wave propagating through a turbulent medium. Measured statistics in conjunction with the Rytov approximation are leveraged to verify expected values of inner and outer scale parameters; study the applicability of beam wave models (versus plane or spherical wave models) in calculating wave-front statistics. The measurements are useful for analysis of open propagation paths with longer range, more variable terrain slope and higher altitude than those obtained at Flatville [25, 48, 51]; this fits applications that will soon require this type of data. EM propagation at THz bands exhibits significant and measurable fluctuations in amplitude and phase over distances of 1.924 km; full characterization of scintillation parameters will provide insight into the propagation behavior. Unlike a level path, C_T^2 and C_Q^2 are not easily derived from C_n^2 . Figure 3.12 shows a high-level block diagram of the system. The only section that was not completely implemented was the path monitoring instrumentation; the only part of this section that was implemented was the custom scintillometer.

The left side of Figure 3.12 represents the Green Mesa receive site and the right side is the CU engineering roof-top transmit site. The top box is the C-band pilot link that will provide a coherent 10 MHz reference signal between the two sites; this was implemented in the 40.7 MHz ISM band to ease Federal Communications Commission (FCC) licensing requirements. The measurement link is made up of a single transmitter and dual receivers as discussed above. The site measurement / communications / control block contains weather stations, video cameras for

monitoring purposes, and control computers at both sites with an Internet connection. The Green Mesa site will support the PC that controls the entire receiver system.

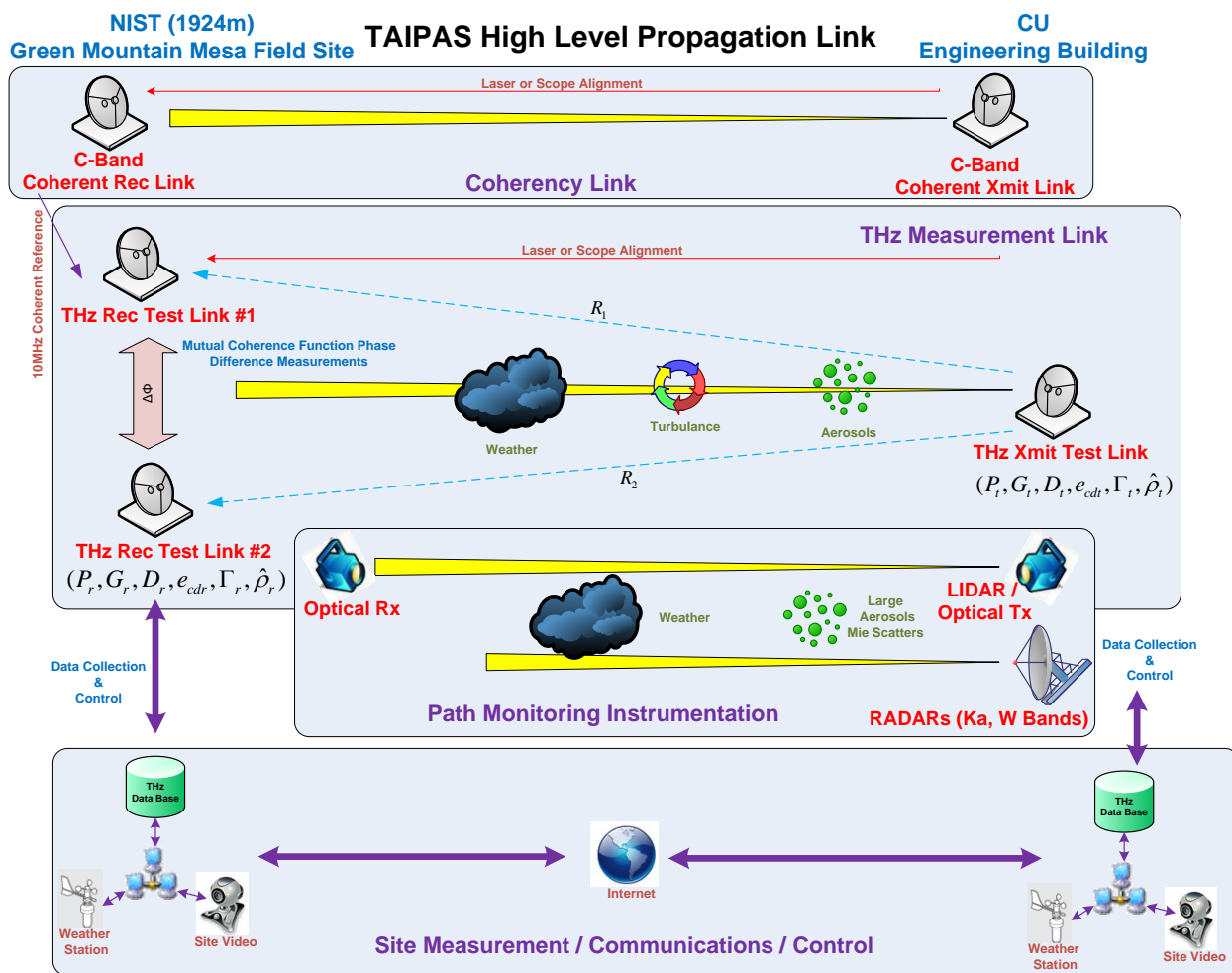


Figure 3.12. High Level TAIPAS Transmissometer System Block Diagram.

There are three frequency scan modes for the system: 320-340 GHz called Wideband (WB), 324.153-325.153 GHz called Lower Wing Line (LWL) of absorption resonance and 325.153 GHz – 326.153 GHz called Upper Wing Line (UWL) of absorption resonance. Figure 3.13 shows the peak relationship to frequency. It is important to note that the vertical absorption scale

is logarithmic and the units are in dB; the size of the absorption peak is much larger relative to other absorptions on a linear scale. These scans are shown in Table 3.1, Table 3.2 and Table 3.3 with three columns that represent Ku synthesizer frequency, RF frequency and offset from absorption peak (325.153 GHz). The receiver synthesizer is offset by 41.67 kHz, which offsets the RF to provide a 1 MHz IF into the ADCs. Each scan consists of 11 frequencies which are dwelled on 200 ms. This is much slower than the frozen time of the atmosphere, due to the 15 ms synthesizer tuning and the locking of the clocks between the transmitter and receiver. Ideally, all 11 frequencies in a scan would be sampled in less than 1 ms, less than the frozen time of the atmosphere for SMMW propagation, which is consistent with the Taylor frozen flow hypothesis [46]. Statistics must be utilized and are homogeneous. The XML file that currently controls the systems implements three scans (WB, LWL and UWL) twice for a total of 66 frequencies.

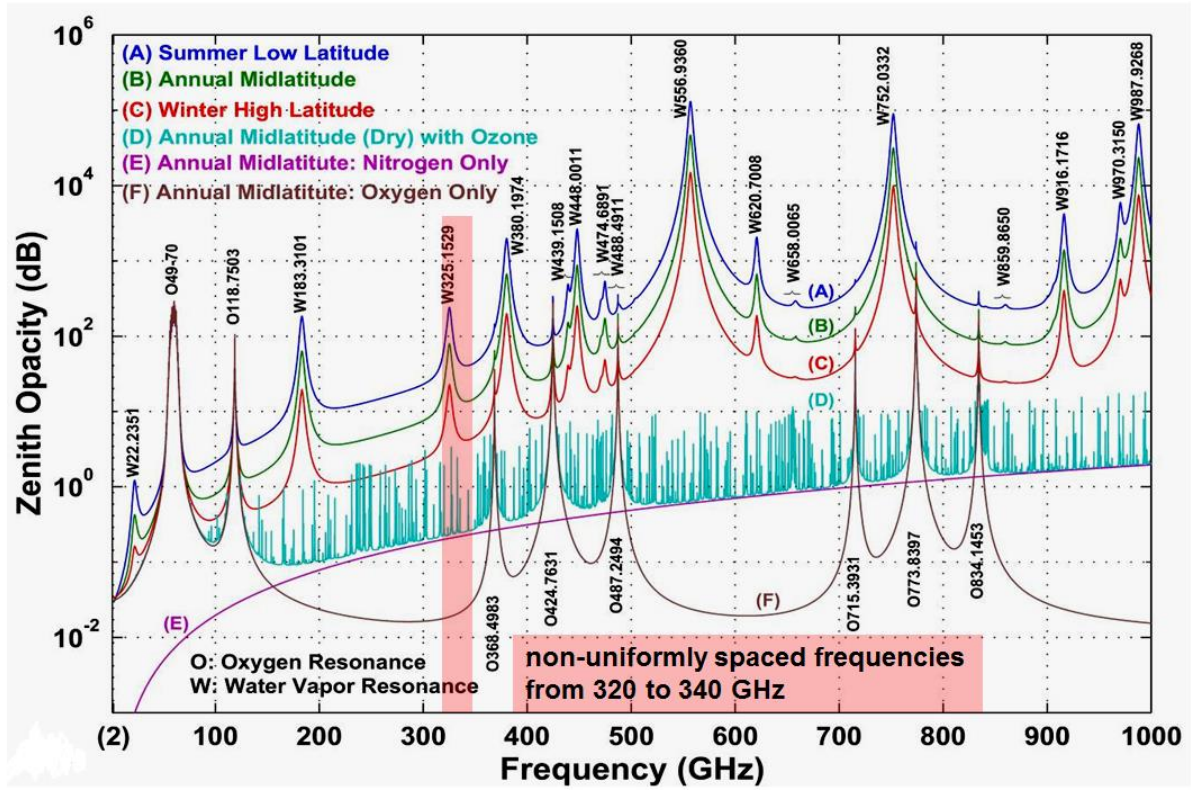


Figure 3.13. TAI PAS Transmissometer Frequencies (Janssen [38]).

Table 3.1. WB Frequency Scan.

Wide Band (WB) Scan (20 GHz)
Entire Absorption Peak (EAP)

<i>Freq Name</i> →	<i>Synth Freq</i> →	<i>RF</i> →	<i>Peak Offset</i>
f_1	13.333333333	320.000	-5.153
f_2	13.464708333	323.153	-2
f_3	13.506375000	324.153	-1
f_4	13.527208333	324.653	-0.5
f_5	13.548041667	325.153	0 H_2O Line Center
f_6	13.568875000	325.653	.5
f_7	13.589708333	326.153	1
f_8	13.631375000	327.153	2
f_9	13.750000000	330.000	4.847
f_{10}	13.958333333	335.000	9.847
f_{11}	14.166666667	340.000	14.847

Table 3.2. Narrow Band, LWL Frequency Scan.

Narrow Band (NB) Scan (5 GHz)			
LWL of Absorption Peak (USAP)			
<i>Freq Name</i> →	<i>Synth Freq</i> →	<i>RF</i> →	<i>Peak Offset</i>
f_1	13.506375000	324.153	−1.000
f_2	13.510541667	324.253	−.900
f_3	13.514708333	324.353	−.800
f_4	13.518875000	324.453	−.700
f_5	13.523041667	324.553	−.600
f_6	13.527208333	324.653	−.500
f_7	13.531375000	324.753	−.400
f_8	13.535541667	324.853	−.300
f_9	13.539708333	324.953	−.200
f_{10}	13.543875000	325.053	−.100
f_{11}	13.548041667	325.153	0.000 <i>H₂O Line Center</i>

Table 3.3. Narrow Band, UWL Frequency Scan.

Narrow Band (NB) Scan (5 GHz)			
UWL of Absorption Peak (DSAP)			
<i>Freq Name</i> →	<i>Synth Freq</i> →	<i>RF</i> →	<i>Peak Offset</i>
f_1	13.548041667	325.153	0.000 <i>H₂O Line Center</i>
f_2	13.552208333	325.253	.100
f_3	13.556375000	325.353	.200
f_4	13.560541667	325.453	.300
f_5	13.564708333	325.553	.400
f_6	13.568875000	325.653	.500
f_7	13.573041667	325.753	.600
f_8	13.577208333	325.853	.700
f_9	13.581375000	325.953	.800
f_{10}	13.585541667	326.053	.900
f_{11}	13.589708333	326.153	1.000

3.13 Predicted Variance Analysis

The prediction section is implemented in an Excel spreadsheet along with the TAIPAS Friis analysis. Most of these predictions were taken from Wheelon, Volumes I and II [31, 32]; therefore, the predictions in phase are looked at from a GO and Rytov standpoint. The approach was to calculate any prediction from any point of view to compare to the actual results.

Wide ranges were considered for real and imaginary components of the complex C_n^2 (Equation 3.43 – Equation 3.44), since all possible combinations cannot be displayed in this thesis, $2 \times 10^{-12} \text{ m}^{-2/3}$ was utilized for the real part. The hallway testing was not predicted as it was a very short path (~ 40 m) with no wind; the path length utilized was the open path length of 1924 m. All calculations assume weak scattering (Equation 3.45) to allow usage of GO and the first order Rytov amplitude variance; no aerosols are modeled where a second order Rytov amplitude variance would be required. All data utilizes the WB frequency scan to cover the broadest range for comparison. The equations utilized proceed each table, but they are also embedded near the applied calculation in the table.

$$\text{Real – part Microwave : } 10^{-17} \text{ m}^{-2/3} < C_n^2 < 1.0 \times 10^{-11} \text{ m}^{-2/3} \quad (3.43)$$

$$\text{Imaginary – part Microwave : } 10^{-23} \text{ m}^{-2/3} < C_n^2 < 1.0 \times 10^{-16} \text{ m}^{-2/3} \quad (3.44)$$

$$\langle \chi^2 \rangle < 1 \quad (3.45)$$

Table 3.4 shows calculations for the amplitude plane wave leveraging Manning [59], Wheelon Vol II [32], and Brussard and Watson [63]. The first column calculates the angular wavenumber (Equation 3.46). All further calculations yield units in Nepers; conversion to dB is

implemented (Equation 3.47). The amplitude variance (Equation 3.48) leveraged the Rytov first approximation from Kolomorov for the inertial turbulence region. For the special case where the propagation link has the inner scale length going to zero and the inner scale wavenumber going to infinity, then C_{ni}^2 and $C_{ni_{nr}}$ both are zero (Equation 3.49). This drives the reduced equation that is only a function of the real portion of C_n^2 (Equation 3.50); the amplitude variance is in the 0.02 Np^2 range: approximately 1.5 dB. The standard deviation column shows a region around 1.2 dB (Equation 3.51).

$$k = \frac{2\pi}{\lambda} \quad (3.46)$$

$$1 \text{ } Np^2 = 75.44 \text{ dB}^2; \text{int} \quad (3.47)$$

$$\langle \chi^2 \rangle = k^{7/6} R^{11/6} \left[.307(C_{n_R}^2 - C_{n_I}^2) - 2.293C_{n_R n_I} \right] - 2.176k^2 R \kappa_m^{-5/3} (C_{n_R}^2 + C_{n_I}^2) \quad (3.48)$$

$$\text{special_case: } C_{n_R n_I} = C_{n_I}^2 = 0 \text{ and } \ell_0 \rightarrow 0 \text{ (ie. } \kappa_m \rightarrow \infty) \quad (3.49)$$

$$\langle \chi^2 \rangle = .307k^{7/6} R^{11/6} C_{n_R}^2 \quad (3.50)$$

$$\chi = \sqrt{\chi^2} \quad (3.51)$$

The bottom of Table 3.4 shows the amplitude plane wave inner scale adjustment (Equation 3.52); this multiplies the amplitude variance (Equation 3.50) by the adjustment. With an inner scale length of approximately 1 mm (Equation 3.53), the inner scale factor (Equation 3.54) equals the Fresnel length divided by the inner scale length, which is 1,332. All inner scale models yield an inner scale factor of one, so the adjustment — looking at the embedded graph from Wheelon Vol. II, which was taken from Hill and Clifford [26] and based on the Hill bump

model for the spectrum in the energy-loss region — is approximately 1.3 in the Hill Plane curve, an increase for the variance of 30%.

$$\langle \chi^2 \rangle_{inner_scale} = (.307k^{7/6}R^{11/6}C_{n_R}^2) \mathfrak{S}_{pl} \left(\frac{R\kappa_m}{k} \right) \quad (3.52)$$

$$\ell_0 \approx 1 \text{ mm} \quad (3.53)$$

$$\text{Inner_Scale_factor_Parameter: } \frac{\sqrt{R\lambda}}{\ell_0} \quad (3.54)$$

Table 3.4. Amplitude Plane Wave Prediction.

Fluctuations	
Combined range real – part Microwave: $10^{-17} m^{-7/3} < C_n^2 < 1.0 \times 10^{-11} m^{-7/3}$	First Fresnel Zone
Combined range imaginary – part Microwave: $10^{-23} m^{-2/3} < C_n^2 < 1.0 \times 10^{-16} m^{-2/3}$	1.33 (m) Fresnel_Length = $\sqrt{R\lambda}$
$\langle \chi^2 \rangle < 1$ Amplitude Weak Scattering	

Amplitude Plane Wave		Manning/Wheelon Vol II /Brussard, Watson			$1 Np^2 = 75.44 dB^2; int$	
Cn2	Frequency	Angular Wavenumber k	Amplitude Variance	Derived from first Rytov Approx Kolmogorov; inertial	Amplitude STD	Amplitude STD
		$k = \frac{2\pi}{\lambda}$			$\chi = \sqrt{\chi^2}$	
2.00E-12 m ^{-2/3}	320.000 (GHz)	6.707 (rad/mm)	0.0188 Np ²		13.7%	1.1900 dB
	323.153 (GHz)	6.773 (rad/mm)	0.0190 Np ²		13.8%	1.1968 dB
	324.153 (GHz)	6.794 (rad/mm)	0.0191 Np ²		13.8%	1.1989 dB
	324.653 (GHz)	6.804 (rad/mm)	0.0191 Np ²		13.8%	1.2000 dB
	325.153 (GHz)	6.815 (rad/mm)	0.0191 Np ²		13.8%	1.2011 dB
	325.653 (GHz)	6.825 (rad/mm)	0.0192 Np ²		13.8%	1.2022 dB
	326.153 (GHz)	6.835 (rad/mm)	0.0192 Np ²		13.9%	1.2032 dB
	327.153 (GHz)	6.856 (rad/mm)	0.0193 Np ²		13.9%	1.2054 dB
	330.000 (GHz)	6.916 (rad/mm)	0.0195 Np ²		13.9%	1.2115 dB
	335.000 (GHz)	7.021 (rad/mm)	0.0198 Np ²		14.1%	1.2222 dB
	340.000 (GHz)	7.126 (rad/mm)	0.0201 Np ²		14.2%	1.2328 dB

$\langle \chi^2 \rangle = k^{7/6} R^{11/6} [.307(C_{n_r}^2 - C_{n_t}^2) - 2.293 C_{n_r n_t}] - 2.176 k^2 R \kappa_m^{-5/3} (C_{n_r}^2 + C_{n_t}^2)$
special_case: $C_{n_r n_t} = C_{n_t}^2 = 0$ and $\ell_0 \rightarrow 0$ (ie. $\kappa_m \rightarrow \infty$)
 $\langle \chi^2 \rangle = .307 k^{7/6} R^{11/6} C_{n_r}^2$

Amplitude Plane Wave Inner Scale Adjustment		Wheelon Vol II
$\langle \chi^2 \rangle_{inner_scale} = (.307 k^{7/6} R^{11/6} C_{n_r}^2) \mathfrak{S}_{pl} \left(\frac{R \kappa_m}{k} \right) \quad \ell_0 \approx 1 mm$		
Inner Scale Factor Parameter		
Inner_Scale_factor_Parameter: $\frac{\sqrt{R\lambda}}{\ell_0}$	1331.91	Plot #5
All Inner Scale models yield Inner Scale Factor = 1		

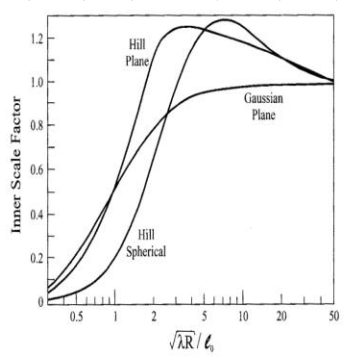


Figure 3.5: The inner scale factor for plane and spherical waves computed by Hill and Clifford [15]. These curves are based on the Hill bump model for the spectrum in the energy-loss region. The curve for a plane wave with a Gaussian dissipation function is shown for reference.

Table 3.5 shows the amplitude plane variance wave outer scale adjustment (Equation 3.55). The outer scale correction is shown in Figure 3.14 from Wheelon Vol II [32] for Kolmogorov and von Karman; the former was utilized in this table. The outer scale factor parameter on the horizontal axis (Equation 3.56) is leveraged to find the outer scale factor from the plot. The value is calculated for many predictions of outer scale length (Equation 3.57 – Equation 3.59). The outer scale length predicted by Kolmogorov is about two times what Tatarski refined and three times Brussaard's calculations. All three of these predictions are carried in most tables, but, when needed, Tatarski is the default. The amplitude standard deviation is significantly less than the one in Table 3.5 without the adjustment: for the varying heights across the TAIPAS open propagation path, shown in yellow (inputs), the standard deviation will range for Tatarski from .71 dB and short heights to .06 dB at close to 70 m. These are samples along the path; the TAIPAS numbers will be the integrated versions that should fall in this range.

$$\langle \chi^2 \rangle_{outer_scale} = (.307k^{7/6}R^{1/6}C_{nr}^2)O\left(\frac{2\pi R\lambda}{L_0^2}\right) \quad (3.55)$$

$$outer_scale_factor_parameter = \left(\frac{2\pi R\lambda}{L_0^2}\right) \quad (3.56)$$

$$L_0 \approx h \quad (3.57)$$

$$L_0 \approx .4h ; Tatarski \quad (3.58)$$

$$L_0 \approx \frac{h}{3} ; Brussaard \quad (3.59)$$

If the outer scale length is much larger than the Fresnel Length, inner scale regime, then Fresnel Scattering persists. If this is not true, then Fraunhofer Scattering applies in the outer scale regime; microwave falls between the two. For the case of the TAIPAS open path, it is more Fraunhofer Scattering in the early path length at lower altitudes and transitions to Fresnel Scattering. This can be seen in Table 3.5. Fresnel scattering is also more applicable for long range MMW (Tatarski). The Fraunhofer amplitude variance utilizes the inner scale wavenumber (Equation 3.60).

Table 3.6 shows amplitude variance for spherical waves, which is the top half of the table. The amplitude variance for spherical decreases the numerical constant by more than two times plane waves; the standard deviation is approximately .77 dB as compared to 1.2 dB for planar. The middle section of the table leverages work by Wheelon [31, 32] to calculate the Log variance for a spherical wave (Equation 3.62). The variance is considered four times the amplitude variations above; the numerical constant out front becomes 0.496 (Equation 3.63).

$$\langle \chi^2 \rangle_{Fraunhofer} = (.391k^2RC_{nR}^2)(\kappa_0)^{-5/3} \quad (3.60)$$

$$\langle \chi^2 \rangle_{spherical} = .124C_n^2k^{7/6}R^{11/6} \quad (3.61)$$

$$\sigma_{\log_I}^2 = 4\langle \chi^2 \rangle \quad (3.62)$$

$$\langle \sigma^2 \rangle_{Spherical} = .496C_n^2k^{7/6}R^{11/6} \quad (3.63)$$

The bottom section of Table 3.6 covers the amplitude wave aperture gain factor adjustment for both spherical and planar waves. It leverages the embedded plot from Wheelon Vol II [32]. The aperture averaging gain factor parameter (Equation 3.64) is leveraged for the horizontal scale. The result is a very small number making both receiver gains from the plot equal to one (Equation 3.65). A quick test for adjustment can be implemented by comparing the aperture radius to the Fresnel length: 0.045 m is less than 1.33 m, so the receiver gain factor is one.

$$\text{Aperture - Averaging - Gain - Factor - Parameter} = \left(a_r \sqrt{\frac{2\pi}{R\lambda}} \right) \quad (3.64)$$

$$a_r < \sqrt{R\lambda} \quad (3.65)$$

Table 3.6. Amplitude Spherical Wave Prediction.

Amplitude Spherical Wave		Wheelon Vol. II		$1 Np^2 = 75.44 \text{ dB}^2; \text{int}$	
Frequency	Angular Wavenumber k	Amplitude Variance	Amplitude STD	Amplitude STD	Amplitude STD
Cn2	320.000 (GHz)	6.707 (rad/mm)	0.0076 Np ²	8.7%	0.7563 dB
2.00E-12 m ⁻² (-2/3)	323.153 (GHz)	6.773 (rad/mm)	0.0077 Np ²	8.8%	0.7606 dB
	324.153 (GHz)	6.794 (rad/mm)	0.0077 Np ²	8.8%	0.7620 dB
	324.653 (GHz)	6.804 (rad/mm)	0.0077 Np ²	8.8%	0.7627 dB
	325.153 (GHz)	6.815 (rad/mm)	0.0077 Np ²	8.8%	0.7633 dB
	325.653 (GHz)	6.825 (rad/mm)	0.0077 Np ²	8.8%	0.7640 dB
	326.153 (GHz)	6.835 (rad/mm)	0.0078 Np ²	8.8%	0.7647 dB
	327.153 (GHz)	6.856 (rad/mm)	0.0078 Np ²	8.8%	0.7661 dB
	330.000 (GHz)	6.916 (rad/mm)	0.0079 Np ²	8.9%	0.7700 dB
	335.000 (GHz)	7.021 (rad/mm)	0.0080 Np ²	8.9%	0.7767 dB
	340.000 (GHz)	7.126 (rad/mm)	0.0081 Np ²	9.0%	0.7835 dB

Amplitude Spherical Wave		Gasiewski		$1 Np^2 = 75.44 \text{ dB}^2; \text{int}$	
Frequency	Angular Wavenumber k	Intensity Variance (Log Amp)	Intensity STD	Intensity STD	Intensity STD
Cn2	320.000 (GHz)	6.707 (rad/mm)	0.0303 Np ²	17.4%	1.5125 dB
2.00E-12 m ⁻² (-2/3)	323.153 (GHz)	6.773 (rad/mm)	0.0307 Np ²	17.5%	1.5212 dB
	324.153 (GHz)	6.794 (rad/mm)	0.0308 Np ²	17.5%	1.5239 dB
	324.653 (GHz)	6.804 (rad/mm)	0.0308 Np ²	17.6%	1.5253 dB
	325.153 (GHz)	6.815 (rad/mm)	0.0309 Np ²	17.6%	1.5267 dB
	325.653 (GHz)	6.825 (rad/mm)	0.0310 Np ²	17.6%	1.5281 dB
	326.153 (GHz)	6.835 (rad/mm)	0.0310 Np ²	17.6%	1.5294 dB
	327.153 (GHz)	6.856 (rad/mm)	0.0311 Np ²	17.6%	1.5322 dB
	330.000 (GHz)	6.916 (rad/mm)	0.0314 Np ²	17.7%	1.5399 dB
	335.000 (GHz)	7.021 (rad/mm)	0.0320 Np ²	17.9%	1.5535 dB
	340.000 (GHz)	7.126 (rad/mm)	0.0325 Np ²	18.0%	1.5670 dB

Innerscale Adjustment yield the same correction as plane waves = 1

Amplitude Wave Aperture Averaging Gain Factor Adjustment (Plane and Spherical) Wheelon Vol. II

Aperture Gain Factor Parameter = 8.469E-05 Quick Test for Adjustment =1

Aperture – Averaging _ Gain _ Factor _ Parameter = $\left(a_r \sqrt{\frac{2\pi}{R\lambda}} \right)$ $a_r < \sqrt{R\lambda}$ Fresnel Length

0.045 m < 1.33 m

Valid expression therefore Adjustment =1

Plot #7
Yields Aperture Averaging Gain Factor = 1

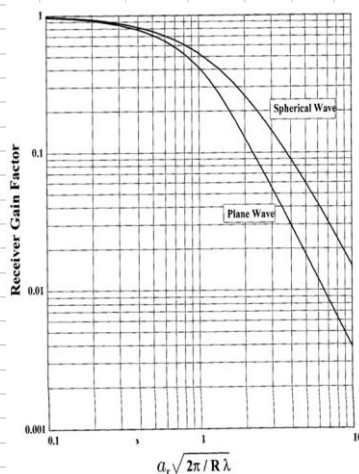


Figure 3.9: Receiver gain factors for plane and spherical waves.

Plot #7 Wheelon Vol II

The frequency correlations for comparison of detailed variations at two wavelengths is important for this chapter, but significantly important for the Co-Propagation Chapter 4, where the frequency difference is significant; calculating medium bandwidth frequency separation over which signals behave in the same manner. Wide bandwidth correlations with weak scattering can also be considered; two simultaneous frequencies for microwave and optical correlate enough to characterize the lower atmosphere. Two simultaneous frequencies on the same path are independent from C_n^2 (Equation 3.66 - Equation 3.67), dependent on the outer scale length to the Fresnel length. For most of the open path, TAIPAS's outer scale length is greater than the Fresnel length (Equation 3.66) making it very close to a wavelength ratio equivalent to amplitude variance ratio. This drives the amplitude scintillation frequency correlation constant (Equation 3.69), with "r" (3.68) substituted.

$$\frac{\langle \chi_1^2 \rangle}{\langle \chi_2^2 \rangle} = \left(\frac{\lambda_2}{\lambda_1} \right)^{\frac{7}{6}} ; \sqrt{R\lambda} < L_0 ; L_0 \approx .4h \quad (3.66)$$

$$\frac{\langle \chi_1^2 \rangle}{\langle \chi_2^2 \rangle} = \left(\frac{\lambda_2}{\lambda_1} \right)^2 ; \sqrt{R\lambda} > L_0 ; L_0 \approx .4h \quad (3.67)$$

$$r = \frac{k_2}{k_1} = \frac{f_2}{f_1} = \frac{\lambda_1}{\lambda_2} \quad (3.68)$$

$$C(k_1, k_2) = \frac{1}{r^{5/12}} \left[\left(\frac{r+1}{2} \right)^{5/6} - \left(\frac{r-1}{2} \right)^{5/6} \right] \quad (3.69)$$

Until now, for amplitude variance, the atmosphere was assumed to be isotropic. This is a reasonable assumption since the variance is primarily dependent on the inner scale lengths,

which are close to equal near the ground; eddies are more spherical. They are unlikely to be perfectly spherical, so an adjustment can be made; this is good for understanding the anisotropic effects. The scaling parameters for the dimensions of the inner scale length Eddie size need to be applied (Equation 3.70). The relation of the anisotropic to the isotropic with the adjustments is shown in Equation 3.71. If $L_z < L_y$, then $c < a$, which drives the axial ratio range to Equation 3.72; if $c = a$, the adjustment is one, therefore the atmosphere is isotropic at the inner scale length.

$$L_x = aL_0 ; L_y = bL_0 ; L_z = cL_0 ; a = b ; \text{Scaling_Parameters} \quad (3.70)$$

$$\langle \chi^2 \rangle_{anisotropic} = \langle \chi^2 \rangle_{isotropic} \left\{ \frac{a}{c^{5/3}} \frac{1}{2\pi} \int_0^{2\pi} d\omega \left[1 - \left(1 - \frac{c^2}{a^2} \right) \cos^2 \omega \right]^{5/6} \right\} \quad (3.71)$$

$$L_z < L_y \therefore c < a \rightarrow \text{axial_ratio_range} : 0 < 1 - \frac{c^2}{a^2} < 1 \quad (3.72)$$

The spatial covariance for two receivers separated by ρ , like TAIPAS, shows the similarity of signals measured on adjacent receivers. The first section of Table 3.7 shows the amplitude spatial covariance with and without aperture averaging. The correlation parameter (Equation 3.73) increases with separation. This number is utilized in the embedded plots from Wheelon [31, 32]. The aperture adjustment (Equation 3.74) is constant, since it is not a function of separation. The special correlation without aperture adjustment varies from 1 to 0.92 over the 2.5 m separation. The special correlation with aperture averaging shows that the correlation decreases with separation: 1 down to 0.88 in a 2.5 m separation. The last block shows the case where the Fresnel length is greater than seven times the inner scale length (Equation 3.75), which

yields the case where the inner scale influence can be ignored. For the plot on the left, the plane waves spatial correlation is found by dividing the covariance by the amplitude variance. For spherical waves, the spatial correlation is close to one if the receivers have a relatively small separation.

$$\text{Amplitude_Spatial_Correlation_Parameter} = \rho \sqrt{\frac{2\pi}{\lambda R}} \tag{3.73}$$

$$\eta = a_r \sqrt{\frac{2\pi}{\lambda R}} \tag{3.74}$$

$$\sqrt{\lambda R} > 7\ell_0 \tag{3.75}$$

Table 3.7. Amplitude Spatial Covariance with and without Aperture Averaging.

Amplitude Spatial Covariance with and without Aperture Averaging		Wheelon Vol II	Plot #8		Plot #9
σ - receiver separation		Correlation Param.	Spatial Correlation	$\eta = a_r \sqrt{\frac{2\pi}{\lambda R}}$	Spatial Correlation w/ Apert. Avg.
0.5 (m)	$\text{Amplitude_Spatial_Correlation_Parameter} = \rho \sqrt{\frac{2\pi}{\lambda R}}$	0.0298	1	0.0027	1
1 (m)		0.0595	1	0.0027	0.99
2 (m)		0.1190	0.98	0.0027	0.94
3 (m)		0.1785	0.92	0.0027	0.88

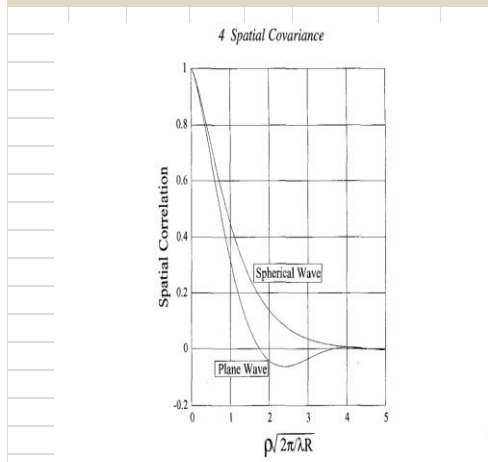


Figure 4.2: Spatial correlation of intensity fluctuations for plane and spherical waves predicted by the Kolmogorov model. These curves do not include aperture averaging or inner-scale effects.

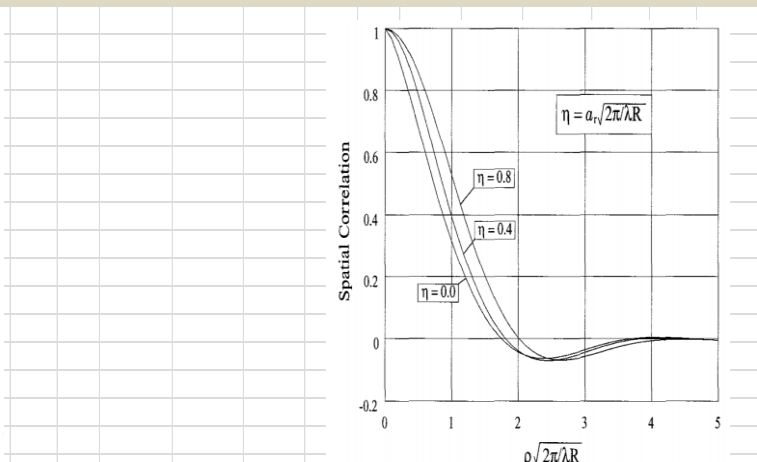


Figure 4.7: The influence of aperture averaging on the spatial correlation for a plane wave.

Plot #8	Wheelon Vol II	Plot #9	Wheelon Vol II
---------	----------------	---------	----------------

Amplitude Spatial Covariance with Inner -Scale Influence	Wheelon Vol II
Test for significance $\sqrt{\lambda R} > 7\ell_0$	Fresnel Length
$\ell_0 \approx 1 \text{ mm}$	7x innerscale
	1.3319 m > 0.0070 m
	Ignore Inner Scale Influence

The Rytov terrestrial links spherical and planar power spectrum of amplitude fluctuations are shown in Table 3.8. The temporal covariance is related to the spatial covariance by the wind vector. The power spectrum and autocorrelation, or covariance of the same data stream, are related by the Wiener-Khintchine theorem. The power spectrum and autocorrelation can ignore large eddies; they are inertial range dependent. The autocorrelation is equivalent to the lateral displacement of receivers. The autocorrelation is preferred since it is normalized to unity when $\Delta t=0$. Power spectrum is based on amplitude fluctuations and the FFT of the temporal covariance; usually normalize the power spectrum to DC – low frequency behavior. The variable ω is the scintillation frequency. The Fresnel scintillation frequency is related to the wind (Equation 3.76). Utilizing the wind speed inputs highlighted in yellow and converting to m/s, the Fresnel frequency is calculated in rad/s. Equation 3.77 shows the ratio of the frequency of the amplitude scintillation to the Fresnel frequency; Equation 3.78 depicts the range. Ranges of the normalized scintillation are derived. The inversion of scintillation times 2π yields the range of the smallest period. Taking this value in seconds, inverting it and multiplying by the increased Nyquist rate (Equation 3.79) shows the last column on the top right. The minimum sampling frequency is not to alias, which maxes out for a 30 mph wind of 31.8 Hz with TAIPAS sampling at 40 kHz (Equation 3.80). The planar power spectrum equations for the amplitude scintillation are Equation 3.81- Equation 3.82; the latter in terms of the amplitude variance. The normalized version is shown in Equation 3.83. Pointing arrows show the column each equation creates. The spherical power spectra are shown in Equation 3.84 – Equation 3.85 with the latter normalized. The planar normalized is comparable to the spherical normalized; the latter has smaller power as expected. The planar amplitude power is shown in the last column for the max

wind speed of 30 mph. Converting this to log shows the power levels are down in the -125 dBm range. The embedded plot shows the normalized curves of the spherical and plane waves that begin to have an effect at the Fresnel frequency.

$$Fresnel_freq: \omega_F = v \sqrt{\frac{2\pi}{\lambda R}} \quad (3.76)$$

$$\xi = \frac{\omega}{\omega_F}; Scaled_Scnt_Freq \quad (3.77)$$

$$.01 < \frac{\omega}{\omega_F} < 100 \quad (3.78)$$

$$f_s > 2.5 f_{\max} \quad (3.79)$$

$$f_{s_TAIPAS} = 40 \text{ kHz} \quad (3.80)$$

$$W_{x_Plane_Wave_Power_Spectrum}(\omega) = 1.096 \frac{RC_n^2 k^2 v^{5/3}}{\omega^{8/3}}; \omega \gg \omega_F \quad (3.81)$$

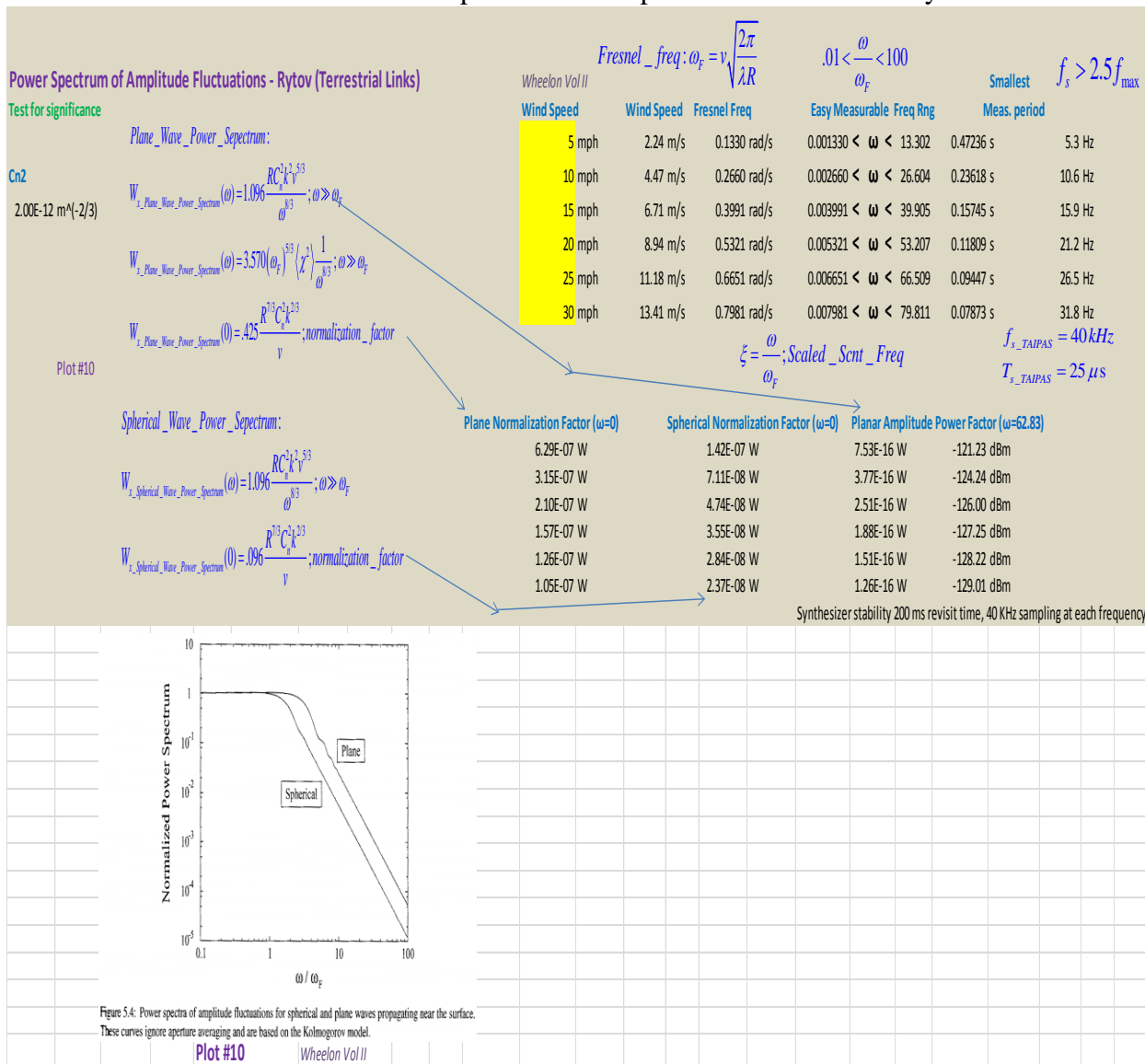
$$W_{x_Plane_Wave_Power_Spectrum}(\omega) = 3.570 (\omega_F)^{5/3} \langle \chi^2 \rangle \frac{1}{\omega^{8/3}}; \omega \gg \omega_F \quad (3.82)$$

$$W_{x_Plane_Wave_Power_Spectrum}(0) = .425 \frac{R^{7/3} C_n^2 k^{2/3}}{v}; normalization_factor \quad (3.83)$$

$$W_{x_Spherical_Wave_Power_Spectrum}(\omega) = 1.096 \frac{RC_n^2 k^2 v^{5/3}}{\omega^{8/3}}; \omega \gg \omega_F \quad (3.84)$$

$$W_{x_Spherical_Wave_Power_Spectrum}(0) = .096 \frac{R^{7/3} C_n^2 k^{2/3}}{v}; normalization_factor \quad (3.85)$$

Table 3.8. Power Spectrum of Amplitude Fluctuations – Rytov.



This section explores the single path phase variance that is proportional to the first moment of the spectrum of irregularities: large eddies or the small portion of the outer scale wave number spectrum - energy being fed into the turbulent cascade process. The measurements are sensitive to trends in the data caused by non-stationary processes; sample length, filtering or aperture smoothing have no significant affect. Phase fluctuation is a stochastic function of time, since it

is a linear function of the stochastic delta permittivity ($\Delta\epsilon$). It is described in moments and correlations functions; take the ensemble average over all possible configurations of the medium and phase variance is determined by squaring and averaging the equation over the path. Single path phase variations are equivalent to changes in the electric path length — looking for fractional changes in wavelength. This forces the transmitter and receiver to be mechanically very stable. The von Karman model is a good place to start since it includes the energy entry and large eddies. If a finite data set is leveraged, distinguishing between large eddy effects from secular trends is not possible; small sample sets will exaggerate phase fluctuations.

The phase structure function is critical to understanding phase variances. This requires the measurement of phase difference between two adjacent receivers, which is important in a transmissometer design. Since TAIPAS has phased locked receivers to the transmitter, the difference of the two paths will cancel out trends. The phase variation is different for planar and spherical waves: eddies larger than the receiver separation affect planar and all eddies affect spherical waves. The ideal situation would be to have the same height on the transmitter and receivers, but TAIPAS breaks this desire to yield an open path LoS system. The covariance of the two receivers vs. time is the desired calculation.

Phase varies in a temporal fashion due to the dielectric constant changing along the path, temperature and humidity changing the refractive-index. The wind vector causes a turbulent motion of humidity and temperature with a 10% or less energy transfer to turbulence. Phase fluctuation can be measured with covariance/autocorrelation in a single path via a time structure function. The phase power spectrum can be related to temporal covariance by the Wiener-

Khintchine theorem; the covariance and power spectrum provide equivalent descriptions of the phase fluctuations with power spectrum having the advantage that phase noise is not correlated. Spectral energy drives lower in frequency as horizontal wind increases, and when wind velocities are zero, self-motion is the major turbulence driver; refractive irregularity changes with vertical convection driven by temperature gradients. Phase measurement issues are eased in a dual receiver system with focus on the structure function; convert from temporal structure function to spatial structure function. Just like the amplitude variations, covariance of phase difference between two receivers is an effective measurement technique.

Table 3.9 shows single path phase variance calculations for various outer scale lengths — inputs in yellow. The outer scale wavenumber (Equation 3.86) is calculated first to plug into the GO phase variance equation (Equation 3.87) derived from the von Karman turbulence model. The standard deviation fraction of lambda (Equation 3.88) is calculated by taking the square root of the variance. The phase standard deviation, in mm, is derived by multiplying lambda times the phase standard deviation. This is converted to seconds in the last column (Equation 3.89). There are three sections for differing outer length calculations; they all yield fractions of picosecond numbers. Tatarski values range from 165 to 479 fs.

$$\kappa_0 = \frac{2\pi}{L_0} \quad (3.86)$$

$$\langle \phi_0^2 \rangle_{GO_von_Karman} = .782R k^2 C_n^2 \kappa_0^{-5/3} \quad (3.87)$$

$$\phi = \sqrt{\phi^2} \quad (3.88)$$

$$T = \frac{\text{phase_shift}}{c} \tag{3.89}$$

Table 3.9. Phase Prediction – GO.

Single Path Phase Variance										
Phase Geometric Optics		$L_0 \approx h$	Wheelon Vol.I	Phase Variance		Phase STD	Phase STD	Phase STD	$T = \frac{\text{phase_shift}}{c}$	Phase STD
Cn2	Outerscale Length	Outerscale Wavenumber		Phase Variance	$\langle \phi^2 \rangle = .782R k^2 C_n^2 \kappa_0^{-5/3}$	Phase STD	Phase STD	Phase STD		Phase STD
2.00E-12 m ⁻⁴ ·(-2/3)	14 (m)	0.449 (1/m)	$\kappa_0 = \frac{2\pi}{L_0}$	0.5279 rad ²	von Karman Model	41.63 deg	0.115637 λ	0.106620 mm	$\phi = \sqrt{\phi^2}$	0.3556 ps
	25 (m)	0.251 (1/m)		1.3875 rad ²		67.49 deg	0.187473 λ	0.172856 mm		0.5766 ps
	40 (m)	0.157 (1/m)		3.0370 rad ²		99.85 deg	0.277357 λ	0.255731 mm		0.8530 ps
	50 (m)	0.126 (1/m)		4.4051 rad ²		120.25 deg	0.334039 λ	0.307994 mm		1.0273 ps
Phase Geometric Optics		$L_0 \approx .4h$	Tatarski	Wheelon Vol.I	Phase Variance		Phase STD	Phase STD	Phase STD	$T = \frac{\text{phase_shift}}{c}$
Cn2	Outerscale Length	Outerscale Wavenumber		Phase Variance	$\langle \phi^2 \rangle = .782R k^2 C_n^2 \kappa_0^{-5/3}$	Phase STD	Phase STD	Phase STD		Phase STD
2.00E-12 m ⁻⁴ ·(-2/3)	5.6 (m)	1.122 (1/m)	$\kappa_0 = \frac{2\pi}{L_0}$	0.1146 rad ²	von Karman Model	19.40 deg	0.053886 λ	0.049685 mm	$\phi = \sqrt{\phi^2}$	0.1657 ps
	10 (m)	0.628 (1/m)		0.3013 rad ²		31.45 deg	0.087362 λ	0.080550 mm		0.2687 ps
	16 (m)	0.393 (1/m)		0.6595 rad ²		46.53 deg	0.129248 λ	0.119170 mm		0.3975 ps
	20 (m)	0.314 (1/m)		0.9566 rad ²		56.04 deg	0.155661 λ	0.143524 mm		0.4787 ps
Phase Geometric Optics		$L_0 \approx \frac{h}{3}$	Brussaard	Wheelon Vol.I	Phase Variance		Phase STD	Phase STD	Phase STD	$T = \frac{\text{phase_shift}}{c}$
Cn2	Outerscale Length	Outerscale Wavenumber		Phase Variance	$\langle \phi^2 \rangle = .782R k^2 C_n^2 \kappa_0^{-5/3}$	Phase STD	Phase STD	Phase STD		Phase STD
2.00E-12 m ⁻⁴ ·(-2/3)	4.67 (m)	1.346 (1/m)	$\kappa_0 = \frac{2\pi}{L_0}$	0.0846 rad ²	von Karman Model	16.66 deg	0.046291 λ	0.042681 mm	$\phi = \sqrt{\phi^2}$	0.1424 ps
	8.33 (m)	0.754 (1/m)		0.2223 rad ²		27.02 deg	0.075048 λ	0.069196 mm		0.2308 ps
	13.33 (m)	0.471 (1/m)		0.4867 rad ²		39.97 deg	0.111029 λ	0.102372 mm		0.3415 ps
	16.67 (m)	0.377 (1/m)		0.7059 rad ²		48.14 deg	0.133720 λ	0.123294 mm		0.4113 ps

Table 3.10 shows the phase diffraction in a weak scattering environment for a planar wave leveraging Rytov, which modifies the GO very slightly. Fraunhofer is required when the eddy sizes are larger than the Fresnel length. The Rytov planar amplitude variance (Equation 3.50) is the adjustment that is made to the GO (Equation 3.90). The Fresnel phase variance (Equation 3.91) is calculated in the second column. The Fraunhofer phase variance equates to half the GO, which equates to amplitude variance (Equation 3.92). The intermediate test is shown in Equation 3.93, which equates to the variable portion of the Fresnel phase variance. The phase standard deviation in seconds for Tatarski outer scale length prediction ranges from 151 fs to 473 fs; these are not far off from the GO calculations above.

$$\langle \varphi^2 \rangle = \langle \varphi_0^2 \rangle_{GO} - \langle \chi^2 \rangle_{Rytov} \quad (3.90)$$

$$\langle \varphi^2 \rangle_{Fresnel} = \langle \varphi_0^2 \rangle \left[1 - .393 \left(\frac{Rk_0^2}{k} \right)^{5/6} \right] \quad (3.91)$$

$$\langle \varphi^2 \rangle_{Fraunhofer} = \frac{1}{2} \langle \varphi_0^2 \rangle_{GO} = \langle \chi^2 \rangle_{Rytov} \quad (3.92)$$

$$Intermediate_Test : \zeta = \frac{2\pi\lambda R}{L_0^2} \quad (3.93)$$

Table 3.10. Phase Diffraction for Plane Wave – Rytov.

Phase Diffraction (Weak Scat./Rytov) - Plane	Outer Scale Scatt.	Wheeler Vol II	$L_0 \approx h$	Phase Variance	Phase STD	Phase STD	Phase STD	Phase STD
Plane_Phase_Variance:	Parameter Test	Rtyov Correction						
$\langle \phi_0^2 \rangle_{GO} = .782R k^2 C_n^2 \kappa_0^{-5/3}$; von Karman Model	0.0569	0.9640		0.5089 rad ²	40.87 deg	0.11 λ	0.10 mm	0.3492 ps
$\langle \chi^2 \rangle_{Rytov} = .307k^{7/6} R^{11/6} C_n^2$	0.0178	0.9863		1.3685 rad ²	67.03 deg	0.19 λ	0.17 mm	0.5726 ps
Amp_depends_scatt./wavelgth=two_regions	0.0070	0.9937		3.0179 rad ²	99.54 deg	0.28 λ	0.25 mm	0.8503 ps
$\langle \phi^2 \rangle = \langle \phi_0^2 \rangle_{GO} - \langle \chi^2 \rangle_{Rytov}$	0.0045	0.9957		4.3861 rad ²	119.99 deg	0.33 λ	0.31 mm	1.0251 ps
Fresnel: $\langle \phi^2 \rangle = \langle \phi_0^2 \rangle \left[1 - .393 \left(\frac{R \kappa_0^2}{k} \right)^{5/6} \right]$	All Small = Fresnel							
Fraunhofer: $\langle \phi^2 \rangle = \frac{1}{2} \langle \phi_0^2 \rangle_{GO} = \langle \chi^2 \rangle_{Rytov}$	Outer Scale Scatt.	Rtyov Correction	$L_0 \approx 4h$	Phase Variance	Phase STD	Phase STD	Phase STD	Phase STD
Intermediate_Test: $\zeta = \frac{2\pi\lambda R}{L_0^2}$	Parameter Test							
Neither weak or strong scattering need adjustment	0.3554	0.8340		0.0956 rad ²	17.72 deg	0.05 λ	0.05 mm	0.1514 ps
	0.1115	0.9369		0.2823 rad ²	30.44 deg	0.08 λ	0.08 mm	0.2601 ps
	0.0435	0.9712		0.6405 rad ²	45.85 deg	0.13 λ	0.12 mm	0.3917 ps
	0.0279	0.9801		0.9376 rad ²	55.48 deg	0.15 λ	0.14 mm	0.4739 ps
	All Small = Fresnel							
	Outer Scale Scatt.	Rtyov Correction	$L_0 \approx \frac{h}{3}$	Phase Variance	Phase STD	Phase STD	Phase STD	Phase STD
	Parameter Test							
	0.5118	0.7751		0.0656 rad ²	14.67 deg	0.04 λ	0.04 mm	0.1253 ps
	0.1605	0.9144		0.2033 rad ²	25.84 deg	0.07 λ	0.07 mm	0.2207 ps
	0.0627	0.9609		0.4676 rad ²	39.18 deg	0.11 λ	0.10 mm	0.3347 ps
	0.0401	0.9730		0.6869 rad ²	47.49 deg	0.13 λ	0.12 mm	0.4057 ps
	All Small = Fresnel							

Table 3.11 shows the phase diffraction in a weak scattering environment for a spherical wave leveraging the Rytov model. The amplitude variance (Equation 3.61) drives the Fresnel calculation, which reduces the constant from the intermediate value by approximately a factor of two. The Tatarski range in time shift changes from 160 fs to 477 fs, which is relatively small differences. The bandwidth around the carrier frequency is calculated using Equation 3.94.

$$B = \frac{f_c}{\sqrt{\langle \phi^2 \rangle}} \tag{3.94}$$

Table 3.11. Phase Diffraction for Spherical Wave – Rytov.

Phase Diffraction (Weak Scat./Rytov) - Spherical		Outer Scale Scatt.	Wheeler Vol II	$L_0 \approx h$	Phase Variance	Phase STD	Phase STD	Phase STD	Phase STD
<i>Spherical_Phase_Variance:</i>		Parameter Test	Rytov Correction						
$\langle \phi_0^2 \rangle_{GO} = .782R k^2 C_n^2 K_0^{-5/3}; \text{ von Karman Model}$		0.0569	0.9849		0.5199 rad ²	41.31 deg	0.11 λ	0.11 mm	0.3529 ps
		0.0178	0.9942		1.3795 rad ²	67.30 deg	0.19 λ	0.17 mm	0.5749 ps
		0.0070	0.9974		3.0290 rad ²	99.72 deg	0.28 λ	0.26 mm	0.8519 ps
		0.0045	0.9982		4.3971 rad ²	120.15 deg	0.33 λ	0.31 mm	1.0264 ps
<i>Amp_depends_scatt./ wavelength = two_regions</i>		All Small = Fresnel							
<i>Fresnel:</i> $\langle \phi^2 \rangle = \langle \phi_0^2 \rangle_{GO} - \langle \chi^2 \rangle_{Rytov}$		Outer Scale Scatt.	Rytov Correction	$L_0 \approx 4h$	Phase Variance	Phase STD	Phase STD	Phase STD	Phase STD
$\langle \chi^2 \rangle_{Rytov} = .124C_n^2 k^{7/6} R^{11/6}$		Parameter Test							
		0.3554	0.9303		0.1066 rad ²	18.71 deg	0.05 λ	0.05 mm	0.1598 ps
		0.1115	0.9735		0.2933 rad ²	31.03 deg	0.09 λ	0.08 mm	0.2651 ps
		0.0435	0.9879		0.6515 rad ²	46.25 deg	0.13 λ	0.12 mm	0.3951 ps
	0.0279	0.9916		0.9486 rad ²	55.80 deg	0.16 λ	0.14 mm	0.4767 ps	
<i>Fraunhofer:</i> $\langle \phi^2 \rangle = \frac{1}{2} \langle \phi_0^2 \rangle_{GO} = \langle \chi^2 \rangle_{Rytov}$		All Small = Fresnel							
<i>Intermediate_Test:</i> $\zeta = \frac{2\pi\lambda R}{L_0^2}$		Outer Scale Scatt.	Rytov Correction	$L_0 \approx \frac{h}{3}$	Phase Variance	Phase STD	Phase STD	Phase STD	Phase STD
		Parameter Test							
		0.5118	0.9056		0.0766 rad ²	15.86 deg	0.04 λ	0.04 mm	0.1355 ps
		0.1605	0.9641		0.2144 rad ²	26.53 deg	0.07 λ	0.07 mm	0.2266 ps
		0.0627	0.9836		0.4787 rad ²	39.64 deg	0.11 λ	0.10 mm	0.3387 ps
		0.0401	0.9887		0.6979 rad ²	47.87 deg	0.13 λ	0.12 mm	0.4089 ps
		All Small = Fresnel							

The AoA fluctuations will not be calculated in this thesis due to the time and cost constraint, so this feature of the covariance matrix will utilize the predicted values below. These fluctuations equate to a jitter of the beam. The angular fluctuations are proportional to the lateral gradients of the permittivity variations. The wave front tilt is proportional to the phase difference between displaced receivers and, thus, the variance is proportional to the phase structure function — third moment of the turbulence spectrum which increases linearly with the path length. The AoA is affected by both larger and smaller eddies, between amplitude and phase variance. The angular error on spherical waves will be approximately three times more than planar.

Table 3.12 shows the GO AoA spherical wave variances. The GO spherical with aperture averaging (Equation 3.95) is in the first section. The AoA standard deviations are very small even over larger ranges: from 0.0019 degrees at 240 m to 0.0055 degrees at 1924 m. Using the equation without aperture averaging leveraging, the inner scale wave number (Equation 3.96) can convert to the outer scale wave number (Equation 3.97), and major amplification (Equation 3.98). This is shown in the second section of the table. The angle standard deviation ranges from .0043 degrees at 240 m to 0.0122 degrees at 1924 m. This shows that the aperture significantly dampens the AoA, and is size dependent.

$$\left\langle \delta\theta^2 \right\rangle_{GO_Spherical_with_Aperture_Avg.} = 1.064RC_n^2 D_{rec}^{-1/3} \quad (3.95)$$

$$\kappa_s = \frac{2\pi}{\ell_0} \quad (3.96)$$

$$\kappa_m = .942\kappa_s \quad (3.97)$$

$$\left\langle \delta\theta^2 \right\rangle_{GO_Spherical_w/o_Aperture_Avg.} = .651RC_n^2 (\kappa_m)^{1/3} \quad (3.98)$$

Table 3.12. AoA with / without Aperture Averaging - Spherical – GO.

Angle of Arrival with Aperture Averaging - Spherical Wave - GO				Wheelon Vol.1	
	Range		AoA Variance	AoA STD	
Cn2	240.5 (m)	$\langle \delta\theta^2 \rangle_{\text{spherical}} = 1.064 RC_n^2 D_{\text{rec}}^{-1/3}$	1.1420E-09 rad^2	0.0019 deg	$\theta = \sqrt{\theta^2}$
2.00E-12 m^(-2/3)	481 (m)		2.2840E-09 rad^2	0.0027 deg	
	962 (m)		4.5681E-09 rad^2	0.0039 deg	
	1924 (m)		9.1361E-09 rad^2	0.0055 deg	
Angle of Arrival without Aperture Averaging - Spherical Wave - GO				Wheelon Vol.1	
	Range	Innerscale Length	Innerscale Wavenumber	AoA Variance	AoA STD
Cn2	240.5 (m)	0.001 (m)	6283.185 (1/m)	5.6642E-09 rad^2	0.0043 deg
2.00E-12 m^(-2/3)	481 (m)	0.001 (m)	6283.185 (1/m)	1.1328E-08 rad^2	0.0061 deg
	962 (m)	0.001 (m)	6283.185 (1/m)	2.2657E-08 rad^2	0.0086 deg
	1924 (m)	0.001 (m)	6283.185 (1/m)	4.5313E-08 rad^2	0.0122 deg

The equations for the planar measurement are amplified compared to spherical (Equation 3.99 - Equation 3.100) with increased constants out front: factor of approximately three times. Table 3.13 shows the two sections with and without aperture. With aperture, the AoA standard deviation ranges from 0.0075 degrees at 240 m to 0.0211 at 1924 m. Without the aperture, the AoA varies from 0.0044 to 0.0125 degrees.

$$\langle \delta\theta^2 \rangle_{GO_Planar_with_Aperture_Avg.} = 2.837 RC_n^2 D_{\text{rec}}^{-1/3} \quad (3.99)$$

$$\langle \delta\theta^2 \rangle_{GO_Planar_w/o_Aperture_Avg.} = 1.95 RC_n^2 (\kappa_m)^{1/3} \quad (3.100)$$

Table 3.13. AoA with / without Aperture Averaging – Planar – GO.

Angle of Arrival with Aperture Averaging - Plane Wave - GO		Wheelon Vol.I	
Range		AoA Variance	AoA STD
Cn2	240.5 (m)	3.0450E-09 rad^2	0.0032 deg
2.00E-12 m^(-2/3)	481 (m)	6.0900E-09 rad^2	0.0045 deg
	962 (m)	1.2180E-08 rad^2	0.0063 deg
	1924 (m)	2.4360E-08 rad^2	0.0089 deg

$$\langle \delta\theta^2 \rangle_{plane} = 2.837RC_n^2 D_{rec}^{-1/3}$$

$$\theta = \sqrt{\theta^2}$$

Angle of Arrival without Aperture Averaging - Plane Wave - GO		Wheelon Vol.I			
Range	Innerscale Length	Innerscale Wavenumber	AoA Variance	AoA STD	
Cn2	240.5 (m)	0.001 (m)	6283.185 (1/m)	1.6966E-08 rad^2	0.0075 deg
2.00E-12 m^(-2/3)	481 (m)	0.001 (m)	6283.185 (1/m)	3.3933E-08 rad^2	0.0106 deg
	962 (m)	0.001 (m)	6283.185 (1/m)	6.7866E-08 rad^2	0.0149 deg
	1924 (m)	0.001 (m)	6283.185 (1/m)	1.3573E-07 rad^2	0.0211 deg

$$\kappa_m = .942\kappa_s$$

$$\kappa_s = \frac{2\pi}{\ell_0}$$

$$\langle \delta\theta^2 \rangle_{plane} = 1.95RC_n^2 (\kappa_m)^{1/3}$$

$$\theta = \sqrt{\theta^2}$$

Table 3.14 shows the AoA variance with a collimated beam (Equation 3.101 – Equation 3.102) using GO. The standard deviation is close to the spherical with GO.

$$\langle \delta\theta^2 \rangle_{col_beam} = 2.914RC_n^2 (\omega_0)^{-1/3} \tag{3.101}$$

$$\omega_0 = xmit\ initial\ beam\ diameter\ (m) \tag{3.102}$$

Table 3.14. AoA with / without Aperture Averaging – Collimated – GO.

Angle of Arrival without Aperture Averaging - Collimated Beam - GO		Wheelon Vol.I	
Range	Beamwidth 3 dB	AoA Variance	AoA STD
Cn2	240.5 (m)	5.9594E-09 rad^2	0.0044 deg
2.00E-12 m^(-2/3)	481 (m)	1.1919E-08 rad^2	0.0063 deg
	962 (m)	2.3837E-08 rad^2	0.0088 deg
	1924 (m)	4.7675E-08 rad^2	0.0125 deg

$$\langle \delta\theta^2 \rangle_{col_beam} = 2.914RC_n^2 (\omega_0)^{-1/3}$$

$$\omega_0 = xmit\ initial\ beam\ diameter\ (m)$$

$$\theta = \sqrt{\theta^2}$$

The spot variance for the collimated beam leveraging GO is shown using Equation 3.103 in Table 3.15. The standard deviation ranges from 0.6° at 240 m to 13.9 degrees at 1924 m. It is important to demonstrate that the beam wave requires small apertures on both receivers for AoA variance measurements.

$$\langle P^2 \rangle_{GO_Col-Beam_w/o_Aperture_Avg.} = .971R^3 C_n^2 (\omega_0)^{-1/3} \tag{3.103}$$

Table 3.15. Spot Variance – Collimated Beam – GO.

Spot Variance - Collimated Beam - GO <i>Wheelon Vol.1</i>					
	Range	Beamwidth 3 dB	Spot Variance	Spot STD	
Cn2	240.5 (m)	0.745 (deg)	1.1486E-04 rad ²	$\langle p^2 \rangle_{col_beam} = .971R^3 C_n^2 (\omega_0)^{-1/3}$	0.6140 deg
2.00E-12 m ^{-2/3}	481 (m)	0.745 (deg)	9.1886E-04 rad ²	$\omega_0 = \text{initial xmit beam diameter}$	1.7368 deg
	962 (m)	0.745 (deg)	7.3509E-03 rad ²		4.9124 deg
	1924 (m)	0.745 (deg)	5.8807E-02 rad ²		13.8943 deg

$p = \sqrt{p^2}$

The AoA with no aperture adjustment for a plane wave, leveraging the Rytov Model, is shown in Table 3.16. This is implemented with the phase structure function and two receivers (Equation 3.104). The equations selected are dependent on the comparison of the receiver separation to the Fresnel length (Equation 3.105 – Equation 3.106). The AoA standard deviation ranges from 0.0048 to 0.0068°; these are very small changes without even considering the damping of the aperture.

$$\langle \delta\theta^2 \rangle_{Rytov} = \frac{1}{k^2 \rho^2} D_\phi(\rho) \tag{3.104}$$

$$D_\phi(\rho)_{GO_Planar_no_adj_Rytov} = 1.457R k^2 C_n^2 \rho^{5/3} ; \ell_0 < \rho < \sqrt{\lambda R} \tag{3.105}$$

$$D_{\varphi}(\rho)_{GO_Planar_no_adj_Rytov} = 2.914R k^2 C_n^2 \rho^{5/3} ; \sqrt{\lambda R} < \rho < L_0 \quad (3.106)$$

Table 3.16. AoA – Plane Wave – Rytov.

Angle of Arrival - no adj- Plane Wave - Rytov			Wheelon Vol.II	Wheelon Vol.II	AoA STD
Cn2	Rec Separation			AoA Variance	
	0.5 (m)	<Fresnel Length		7.0638E-09 rad^2	0.0048 deg
2.00E-12 m^(-2/3)	1 (m)	<Fresnel Length		5.6065E-09 rad^2	0.0043 deg
	2 (m)	>Fresnel length		1.7800E-08 rad^2	0.0076 deg
	4 (m)	>Fresnel length		1.4128E-08 rad^2	0.0068 deg

Rytov _ Plane _ Phase _ Structure _ Function / AoA-no _ adjustments:

$$\langle \delta\theta^2 \rangle = \frac{1}{k^2 \rho^2} D_{\varphi}(\rho)$$

$$D_{\varphi}(\rho) = 1.457R k^2 C_n^2 \rho^{5/3} ; \ell_0 < \rho < \sqrt{\lambda R}$$

$$D_{\varphi}(\rho) = 2.914R k^2 C_n^2 \rho^{5/3} ; \sqrt{\lambda R} < \rho < L_0$$

2X _ factor _ at _ Fresnel _ length _ Break

The AoA with no aperture adjustment for a spherical wave leveraging the Rytov Model is shown in Table 3.17. This is implemented with the phase structure functions and two receivers (Equation 3.107 – Equation 3.108). There are very small changes in the constant from the planar version. The AoA standard deviation varies from 0.0046 to 0.0062°; these are very small changes without even considering the damping of the aperture. This is lower from planar by approximately 0.0002°.

$$D_{\varphi}(\rho)_{GO_Spherical_no_adj_Rytov} = 1.353R k^2 C_n^2 \rho^{5/3} ; \ell_0 < \rho < \sqrt{\lambda R} \quad (3.107)$$

$$D_{\varphi}(\rho)_{GO_Spherical_no_adj_Rytov} = 2.706R k^2 C_n^2 \rho^{5/3} ; \sqrt{\lambda R} < \rho < L_0 \quad (3.108)$$

Table 3.17. AoA – Spherical Wave – Rytov.

Angle of Arrival - no adj- Spherical Wave - Rytov		Wheelon Vol.II	Wheelon Vol.II	AoA STD
Cn2	Rec Separation		AoA Variance	
	0.5 (m)	<Fresnel Length	6.5596E-09 rad^2	0.0046 deg
2.00E-12 m^(-2/3)	1 (m)	<Fresnel Length	5.2063E-09 rad^2	$\theta = \sqrt{\theta^2}$ 0.0041 deg
	2 (m)	>Fresnel length	1.6529E-08 rad^2	0.0074 deg
	4 (m)	>Fresnel length	1.3119E-08 rad^2	0.0066 deg
<i>Rytov_Spherical_Phase_Structure_Function / AoA-no_adjustments:</i>				
$\langle \delta\theta^2 \rangle = \frac{1}{k^2 \rho^2} D_\varphi(\rho)$				
$D_\varphi(\rho) = 1.353R k^2 C_n^2 \rho^{5/3}; \ell_0 < \rho < \sqrt{\lambda R}$				
$D_\varphi(\rho) = 2.706R k^2 C_n^2 \rho^{5/3}; \sqrt{\lambda R} < \rho < L_0$				
<i>2X_factor_at_Fresnel_length_Break</i>				

The Rytov phase power spectrum (Equation 3.109), which is a common description of phase fluctuations, is shown in Table 3.18. By Wiener-Khintchine, the inverse FFT will yield the phase covariance. The plane and spherical waves are very similar. When diffraction comes into play, and when the angular frequency of the changes is larger than the Fresnel angular frequency, the spectrum is approximately cut in half (Equation 3.110). The Tatarski outer scale length is utilized in the table. The power in the diffraction region ranges from -121 dBm to 108 dBm; wind speeds range from 5 mph to 30 mph.

$$W_\varphi(\omega)_{\text{Rytov_Spherical\&Planar}} = 2.192 \frac{RC_n^2 k^2 v^{5/3}}{(\omega^2 + \kappa_0^2 v^2)^{4/3}} ; \omega \ll \omega_F \quad (3.109)$$

$$W_\varphi(\omega)_{\text{Rytov_Spherical\&Planar}} = 1.097 \frac{RC_n^2 k^2 v^{5/3}}{\omega^{8/3}} ; \omega \gg \omega_F \quad (3.110)$$

As discussed earlier, to get valid AoA information, the aperture needs to be scaled down as much as possible. This will significantly drive the SNR and requires much more time and funding, so it was left to a future test.

Table 3.18. Power Spectrum – Spherical / Plane Wave – Rytov.

Power Spectrum of Phase Fluctuations - Spherical / Plane - Rytov (Terrestrial Links)		Fresnel_freq: $\omega_F = v \sqrt{\frac{2\pi}{\lambda R}}$		$.01 < \frac{\omega}{\omega_F} < 100$	$f_s > 2.5 f_{max}$	
Test for significance		Wind Speed	Wind Speed	Fresnel Freq	Easy Measurable Freq Rng	Smallest Measurable Period
Cn2	Rytov_Spherical / Plane_Phase_Power_Spectrum: Fresnel_freq: $\omega_F = v \sqrt{\frac{2\pi}{\lambda R}}$ $W_\phi(\omega) = 2.192 \frac{RC_n^2 k^2 v^{5/3}}{(\omega^2 + k_0^2 v^2)^{4/3}}; \omega \ll \omega_F$ $W_\phi(\omega) = 1.097 \frac{RC_n^2 k^2 v^{5/3}}{\omega^{8/3}}; \omega \gg \omega_F$ $L_0 \approx 4h = 20 m$	5 mph	2.24 m/s	0.1330 rad/s	0.001330 < ω < 13.302	0.472356 s
2.00E-12 m ^{-2/3})		10 mph	4.47 m/s	0.2660 rad/s	0.002660 < ω < 26.604	0.236178 s
Plot #8		15 mph	6.71 m/s	0.3991 rad/s	0.003991 < ω < 39.905	0.157452 s
		20 mph	8.94 m/s	0.5321 rad/s	0.005321 < ω < 53.207	0.118089 s
		25 mph	11.18 m/s	0.6651 rad/s	0.006651 < ω < 66.509	0.094471 s
		30 mph	13.41 m/s	0.7981 rad/s	0.007981 < ω < 79.811	0.078726 s
				Synthesizer stability 100 ms revisit time		$f_s_{TAMPAS} = 40 kHz$ $T_s = 25 \mu s$
		Normalization Factor ($\omega=0$)	Power Spectrum (ω =above max)		Power Spectrum ($\omega=2\pi*80 Hz$)	
		3.84E-12 W	7.54E-16 W		-121.23 dBm	
		1.92E-12 W	2.39E-15 W		-116.21 dBm	
		1.28E-12 W	4.71E-15 W		-113.27 dBm	
		9.61E-13 W	7.60E-15 W		-111.19 dBm	
		7.68E-13 W	1.10E-14 W		-109.58 dBm	
		6.40E-13 W	1.49E-14 W		-108.26 dBm	

The Rytov planar and spherical cross correlation of amplitude and phase variance is shown in Table 3.19. These are complimentary EM characteristics in a random medium and are different for spherical and planar waves. There is a difference between Fresnel and the Fraunhofer regions. From Equation 3.111 – Equation 3.114, the math is a constant multiply times the amplitude variance for spherical and planar waves; the difference is approximately two times with planar, the larger cross correlation. The Rytov cross correlation in the Fraunhofer

regime, spherical (Equation 3.115) and planar (Equation 3.116), becomes very small due to scattering, driving to zero in the spherical case.

$$\langle \varphi\chi \rangle_{\text{Rytov_Planar_Fresnel}} = 1.146R^{11/6}k^{7/6}C_n^2 \quad (3.111)$$

$$\langle \varphi\chi \rangle_{\text{Rytov_Planar_Fresnel}} = 3.732 \langle \chi^2 \rangle_{\text{Planar}} \quad (3.112)$$

$$\langle \varphi\chi \rangle_{\text{Rytov_Spherical_Fresnel}} = .463R^{11/6}k^{7/6}C_n^2 \quad (3.113)$$

$$\langle \varphi\chi \rangle_{\text{Rytov_Spherical_Fresnel}} = 3.734 \langle \chi^2 \rangle_{\text{Spherical}} \quad (3.114)$$

$$\langle \varphi\chi \rangle \rightarrow 0; \text{Fraunhofer} \quad (3.115)$$

$$\langle \varphi\chi \rangle_{\text{Rytov_Fraunhofer_Planar_or_Spherical}} = .58 \langle \chi^2_{\text{Planar_or_Spherical}} \rangle \left(\frac{R\lambda\kappa_0^2}{2\pi} \right)^{-11/6} \quad (3.116)$$

Table 3.19. Cross Correlation of Amp/Phase – Planar / Spherical Waves – Rytov.

Cross Correlation of Amplitude and Phase Plane / Spherical - Rytov		Fresnel	Fraunhofer
Cn2	Rytov_Plane_Cross_Correlation: <small>Wheelon Vol II</small>	Plane Cross Correlation	Plane Cross Correlation
2.00E-12 m ⁴ (-2/3)	$\langle \varphi\chi \rangle_{PL} = 1.146R^{11/6}k^{7/6}C_n^2; \text{Fresnel}$	7.1384E-09	5.4345E-14
	$\langle \varphi\chi \rangle_{PL} = 3.732 \langle \chi^2 \rangle_{PL}; \text{Fresnel}$		
	Rytov_Spherical_Cross_Correlation:	Spherical Cross Correlation	
	$\langle \varphi\chi \rangle_{SPH} = .463R^{11/6}k^{7/6}C_n^2; \text{Fresnel}$	2.8840E-09	Spherical Cross Correlation
	$\langle \varphi\chi \rangle_{SPH} = 3.734 \langle \chi^2 \rangle_{SPH}; \text{Fresnel}$		2.1950E-14
	Ignore Outerscale Cutoff – Kolmogorov		
			Rytov_Cross_Correlation:
			$\langle \varphi\chi \rangle = .58 \langle \chi^2 \rangle \left(\frac{R\lambda\kappa_0^2}{2\pi} \right)^{-11/6}; \text{Fraunhofer}$
			$\langle \varphi\chi \rangle \rightarrow 0; \text{Fraunhofer}$
			Since Scattering Parameter Lrge in regime

3.14 LEEDR Model

The prediction model tool leveraged is the Laser Environmental Effects Definition and Reference (LEEDR) developed by the Air Force Institute of Technology (AFIT). The tool predicts atmospheric propagation based on location, time of day and relative humidity. Profiles of temperature, pressure, water vapor content, optical turbulence and aerosols (particulates and hydrometers) are implemented. The frequencies cover range from ultra-violet to RF. It includes air-to-ground, air-to-air and ground to space Cloud Free Line of Sight (CFLOS) calculator for 415 land sites. The NOAA Operational Model Archive Distribution System (NOMADS) data feed is incorporated to provide real-time weather. It includes refractive bending calculations and leverages the HITRAN data base.

Figure 3.15 shows the LEEDR location map; the latitude and longitude were provided for Boulder, CO. This also has a function to provide the sodium overlay (NaGS) which was not utilized for TAIPAS predictions. The tabs across the top of the software show the major sections. The simulation for attenuation in dB/km in CA leveraging LEEDR for varying Relative Humidity's (RH) is shown in Figure 3.16. The C_n^2 relative plots for varying RH are shown in Figure 3.17. Figure 3.18 shows the inputs for the TAIPAS configuration. The LEEDR configuration summary table is shown in MATLAB code for the plots is provided in Appendix D.

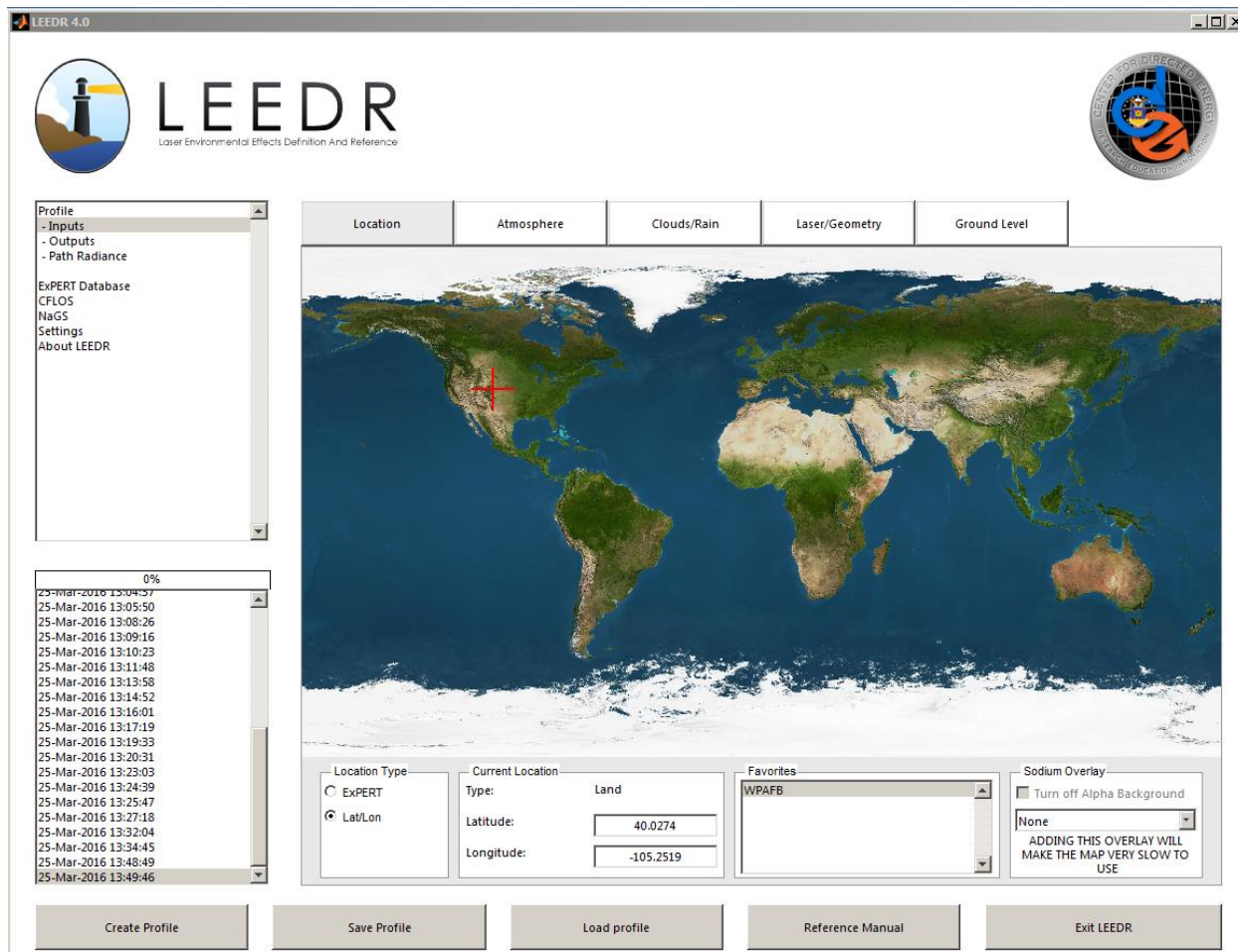


Figure 3.15. LEEDR Location Map and Tabs.

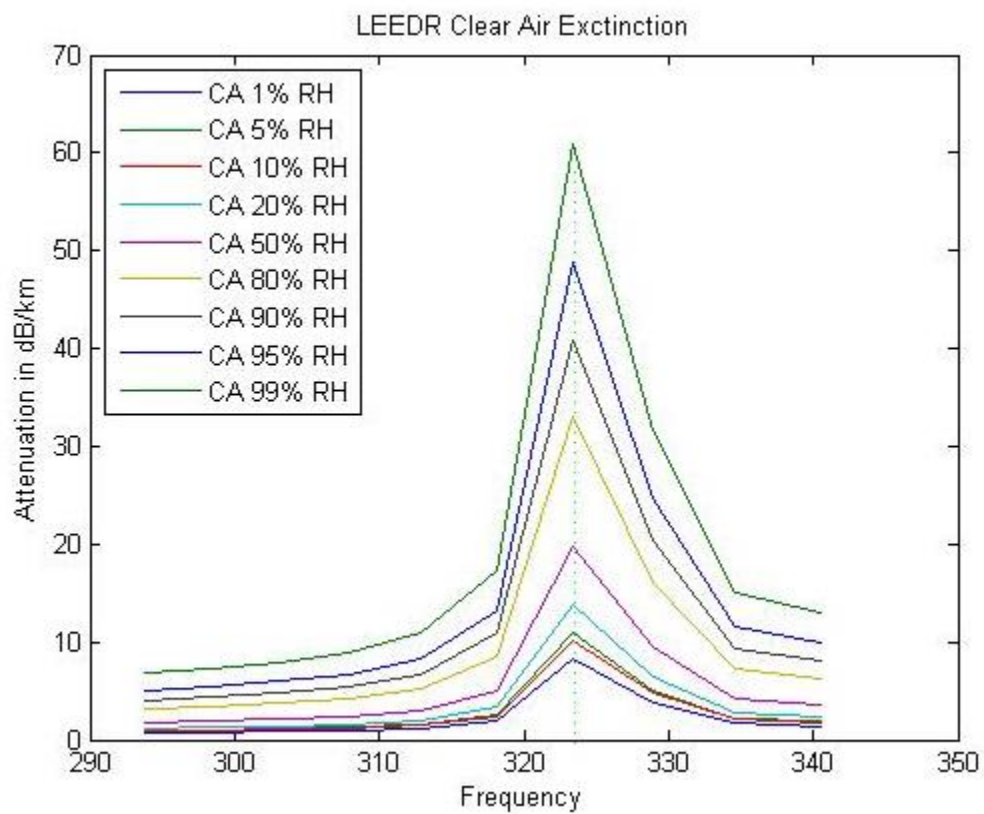


Figure 3.16. LEEDR Attenuation.

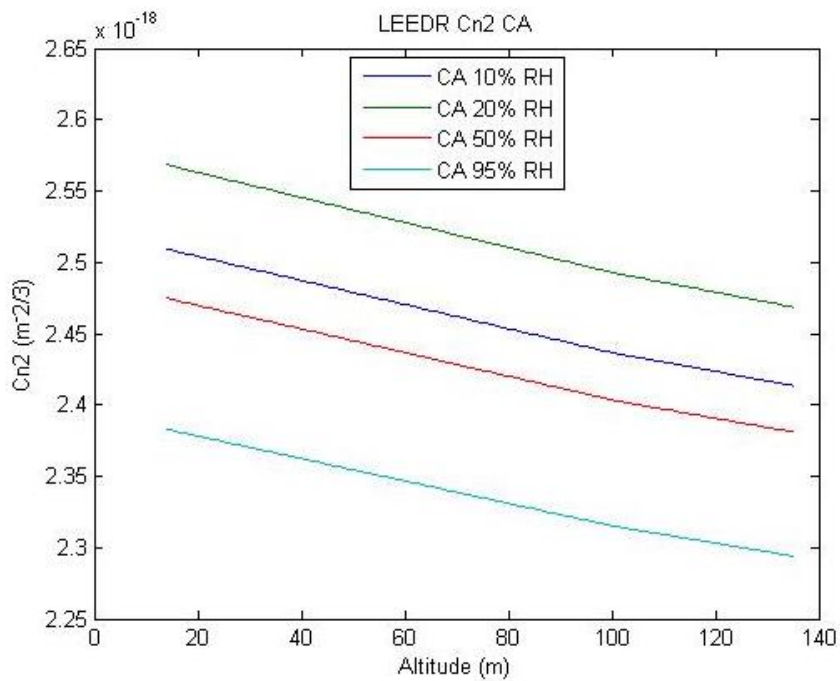


Figure 3.17. LEEDR C_n^2 .

Path Type

Slant Path

Slant Path

Platform Altitude (m): 14

Target Altitude (m): 135

Path Length (m): 1920

Layers

Path Resolution: 200

Wavelength

Wavelength (um): 1.31525

User Wavelength (m): 0.000922

.35e-6(m) -- 8.6(m)

Figure 3.18. LEEDR TAIPAS Configuration.

Table 3.20. LEEDR Example Configuration.

LEEDR Profile				
Time				3/12/2016 12:04
Name				3/12/2016 12:04
Wavelength (m)				0.000922
Latitude				40.0274
Longitude				-105.2519
PATH				
Path Type				Slant
Platform Altitude (m)				14
Target Altitude (m)				135
Path Length (m)				1920
Path Transmittance				1.26065E-07
Path Extinction (1/km)				8.274200128
Path Specific Attenuation (db/km)				35.9343547
Surface Visibility (km)				55.3813822
Slant Path Visibility (km)				55.09529834
ATMOSPHERE				
Atmosphere				ExPERT
- ExPERT Site				Boulder, CO
- Relative Humidity Percentile				50%
- Time of Day				12->15
- Atmosphere Standard Type				Midlatitude North
- Site Altitude				1769
- High Ozone Latitude				40.0274
Aerosols				Standard
- Aerosols Standard Type				Continental Average
Volcanic				None
Molecular				Calculation
Turbulence				Calculations - Tatarski
- Multiplier				1
Wind				Climatological
Season				Summer
Boundary Layer (m)				1524
GROUND LEVEL				
Name	Parts/cm^3	Rmin (um)	Rad (um)	Rmax (um)
Insoluable	0.010075171	0.005	0.471	20
Soot	209.0598021	0.005	0.0118	20
WaterSol	176.3154957	0.005	0.021200001	20.00000072

3.15 MATLAB Analysis

Appendix E contains the MATLAB code for analysis of the propagation. The general bullet description with the starting line number is below. The more detailed descriptions are in the code comments and in the detailed description of the hallway and open path data.

- Line 1 – Documents major change dates and thesis information.
- Line 26 – Implements upfront MATLAB set up and daylight vs. standard mountain times.
- Line 34 – Documentation for TAIPAS and MATLAB adjustments and delineators.
- Line 52 – Describes the naming file name format expected for the ADCs, hygrometers, anemometers, scintillometer and frequency timing control.
- Line 77 – Special system adjustment data is in 77 through 127. This includes gain adjustments in RF processing, calibration data, path length, absorption from plots, elevation, noise figure, etc.
- Line 129 – Special flags that allow disabling Rx2 when both receivers cannot be on the same run, for example, in the hallway or any short path. It also allows defining the amount of FFT plots to implement and if enabled. This stops too many plots from crashing MATLAB. There could be 66 plots of FFT.
- Line 159 – Constants utilized are defined.
- Line 165 – Request input middle name of files and define the file names.
- Line 191 – Sets up WB, LWL and UWL frequency scan, loads data and breaks into columns. If Rx2 is in disable mode, it disables, the processing duplicates Rx1 data to Rx2 with a randomly multiply of I by two, and Q to change the amplitude and phase.

Scintillometer, hygrometer and anemometer for Tx and Rx data is read in and parsed.

This also reads in the timing for the Tx and Rx controllers to verify synchronicity.

- Line 393 – Process EPOCH time and provide ms clocks.
- Line 441 – Process and plot the timing between the Tx and Rx computers for synchronicity.
- Line 575 – Design of a FIR filter when required.
- Line 604 – Converts the raw voltage data to dBm power, less the RF receiver gain, and plots the data.
- Line 706 – The raw data has a large noise floor for small signals, so this next section runs an 80-point running average filter to dampen the noise to see clear frequency transitions and then plots both channels.
- Line 848 – Separates out the good data for each tuned frequency and removes data that occurs during re-tuning/noise.
- Line 1245 – Shortens the data matrix to remove all bad data to the final data matrix for processing.
- Line 1271 – Implements spectral analysis of the data from each scan and plots. The number of frequencies implemented is defined in the set section at the top of the file.
- Line 1379 – Implements the calibration. Inputs the calibration points from VDI and applies to the Tx and Rx data. This section also figures means of each frequency sample set. This includes hardware.
- Line 1761 – Implements a histogram and plots. This, like frequency processing, allows for enabling which histograms get implemented. There would be too many — 66 — for

MATLAB to handle without crashing. This is defined in the beginning configuration section.

- Line 1848 – Implements the Friis prediction data; this is the expected result based on math.
- Line 1951 – Plots mean data with calibration adjustment from both receivers with Friis for all scans.
- Line 3699 – SNR calculation.
- Line 3875 – Calculates and plots turbulence structure constant C_n^2 ; this is based on the single diode area method. It has the Barker code implemented as well, but this was not possible with the available diode spacing dynamics required on the long path.
- Line 4052 – Processes the anemometers and plots.
- Line 4379 – Processes the hygrometer data and plots.
- Line 4574 – Implements the MCF calculation and plots. Requires both receivers operational.
- Line 4756 – Calculates and plots amplitude scintillation $\langle \chi^2 \rangle$ using plane wave math vs. real data.
- Line 5127 – Calculates phase scintillation $\langle \phi^2 \rangle$ using plane wave with GO math vs. real data.
- Line 5778 – Calculates Rytov Fresnel amp / phase cross correlation $\langle \chi \phi \rangle$.
- Line 6017 – Calculates and plots C_T^2 .
- Line 6059 – Calculates and plots C_Q^2 .
- Line 6100 – Calculates and plots $C_T C_Q$.
- Line 6145 – Calculates the correlation and plots $\langle \chi C_n^2 \rangle$.

- Line 6200 – Calculates the correlation and plots $\langle \chi C_T^2 \rangle$.
- Line 6252 – Calculates the correlation and plots $\langle \chi C_Q^2 \rangle$.
- Line 6301 – Calculates the correlation and plots $\langle \phi C_n^2 \rangle$.
- Line 6350 – Calculates the correlation and plots $\langle \phi C_T^2 \rangle$.
- Line 6395 – Calculates the correlation and plots $\langle \phi C_Q^2 \rangle$.
- Line 6440 – Calculates the correlation and plots $\langle C_n^2 C_T^2 \rangle$.
- Line 6484 – Calculates the correlation and plots $\langle C_n^2 C_Q^2 \rangle$.
- Line 6527 – Calculates the correlation and plots $\langle C_T^2 C_Q^2 \rangle$.
- Line 6569 – Amp and phase with U wind Calculations.
- Line 6621 – Amp and phase with V wind Calculations.
- Line 6670 – Amp and phase with W wind Calculations.
- Line 6725 – Calibration for special for eliminating hardware.
- Line 7088 – Histogram without hardware – atmosphere only.
- Line 7175 – Friis for atmosphere only – no hardware.
- Line 7310 – Mean data with calibration with hardware removed.
- Line 6569 – Amp and phase with U wind Calculations.
- Line 9079 – Calculates and plots the absorption / scattering loss – extinction.
- Lines 9257 – Plotting with flip of UML.

3.16 Hallway 40 m Path Analysis

Figure 3.19 is a picture of the hallway experiment from the transmitter looking down toward Rx1. The distance between the two systems is 40 m. Experiments with no lenses, horn-to-horn, matched Friis receive power calculations to within 1 dB. Early alignment experiments with

lenses achieved gain expectations to within 5 dB; this accounted for 95 dBi of gain with the lenses installed. This type of alignment takes a significant amount of time since the lenses work optimally when the plane of the EM wave is perfectly parallel to the lens. This takes a significant amount of shimming of both large containers. In the experiments below, alignment was achieved rapidly with the attached lasers to achieve gain of 75 dBi for both Tx and Rx antennas, down from the theoretical achievement of 100 dBi. Much more significant gains were achieved earlier and without the lenses. The gain of the horns was close to perfect; it was verified that the hardware was operational and ready for deployment to the open path. The hallway data was processed through the entire MATLAB set and is shown below. Even though this data on a very short path was not expected to show perfect, expected results due to noise and calibration, it was implemented and lightly analyzed as a starting point before attacking a much longer range of 1924 m on a slanted open path with dynamic environmental conditions.



Figure 3.19. TAIPAS Tx and Rx1 Hallway Experiments Photo.

Figure 3.20 shows the entire seven-second collection time synchronization between the transmitter controller and the receiver controller. The plot is time vs. frequency selection, so it also shows that the two complete scans of WB, LWL and UWL are working with synchronous EPOCH timing. The two WB scans are represented by the peaks. Figure 3.21 shows a blow up

of one of the peaks, which demonstrates that they are not in perfect synchronization. The more they are off, the slower the possible scans. Figure 3.22 shows the error ranging between -1 and -2 ms, varying error of 1 ms. This can get up to 8 ms and, due to the XML program timing for the scans, the data is still usable.

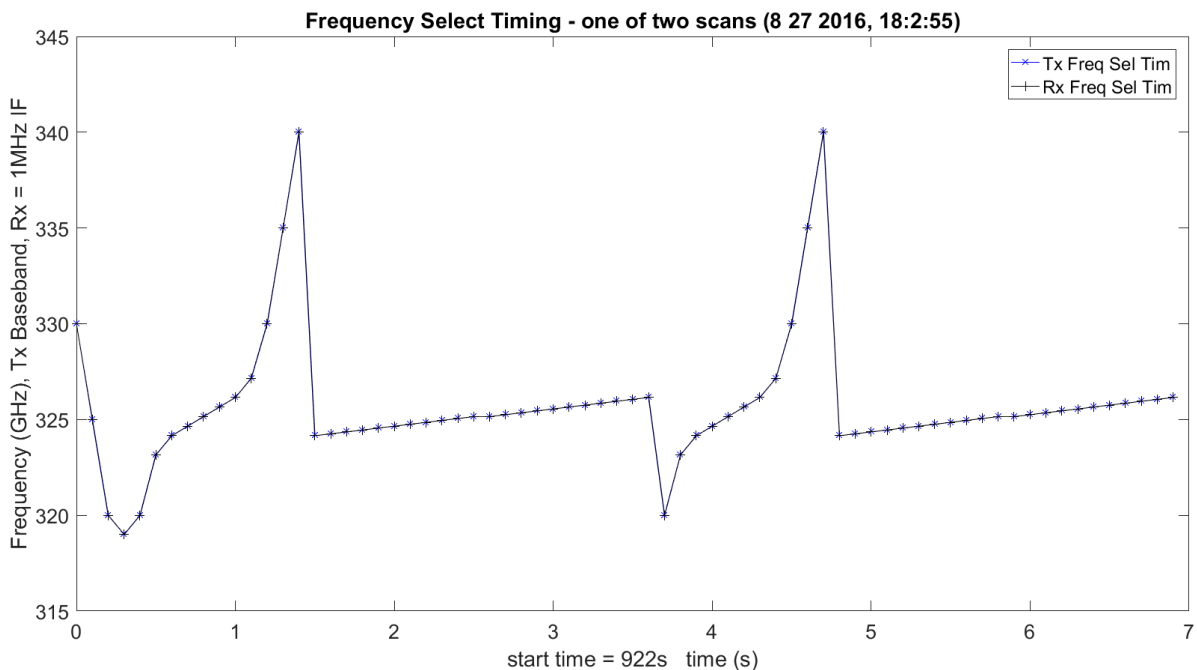


Figure 3.20. TAIPAS Tx vs Rx Computer Synchronization.

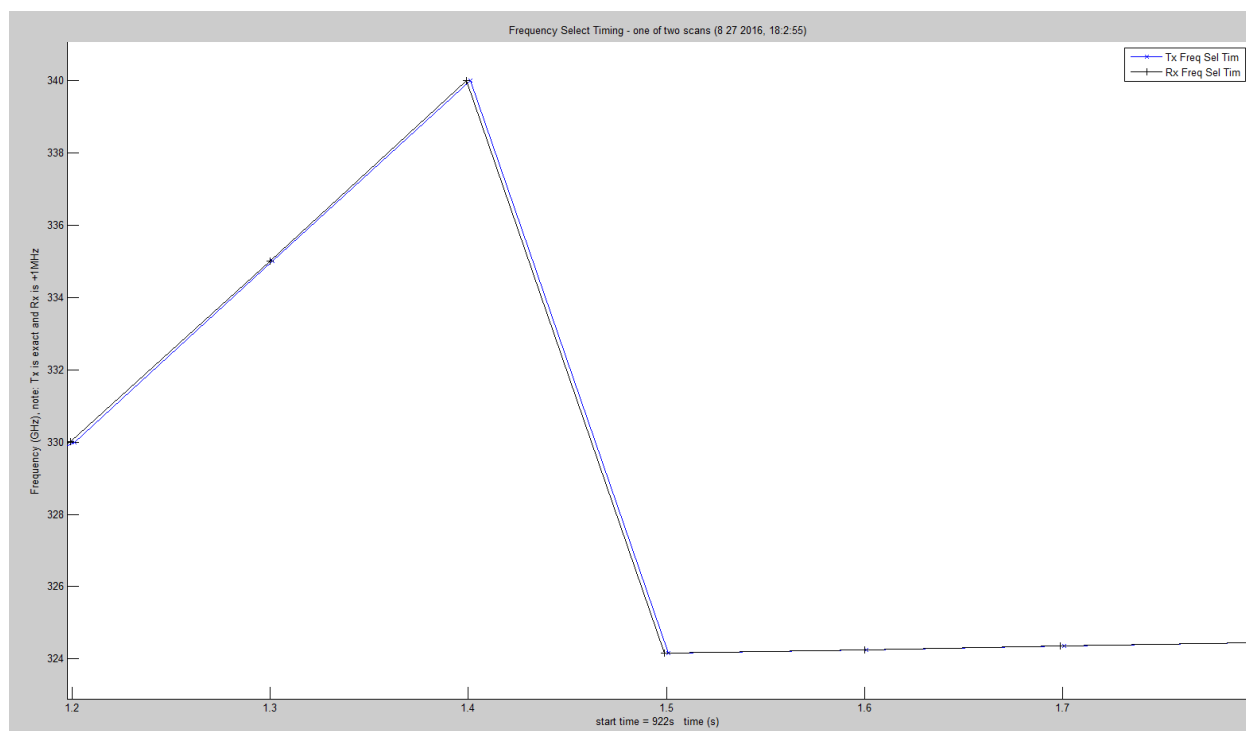


Figure 3.21. TAIPAS Tx vs Rx Computer Synchronization Enlargement.

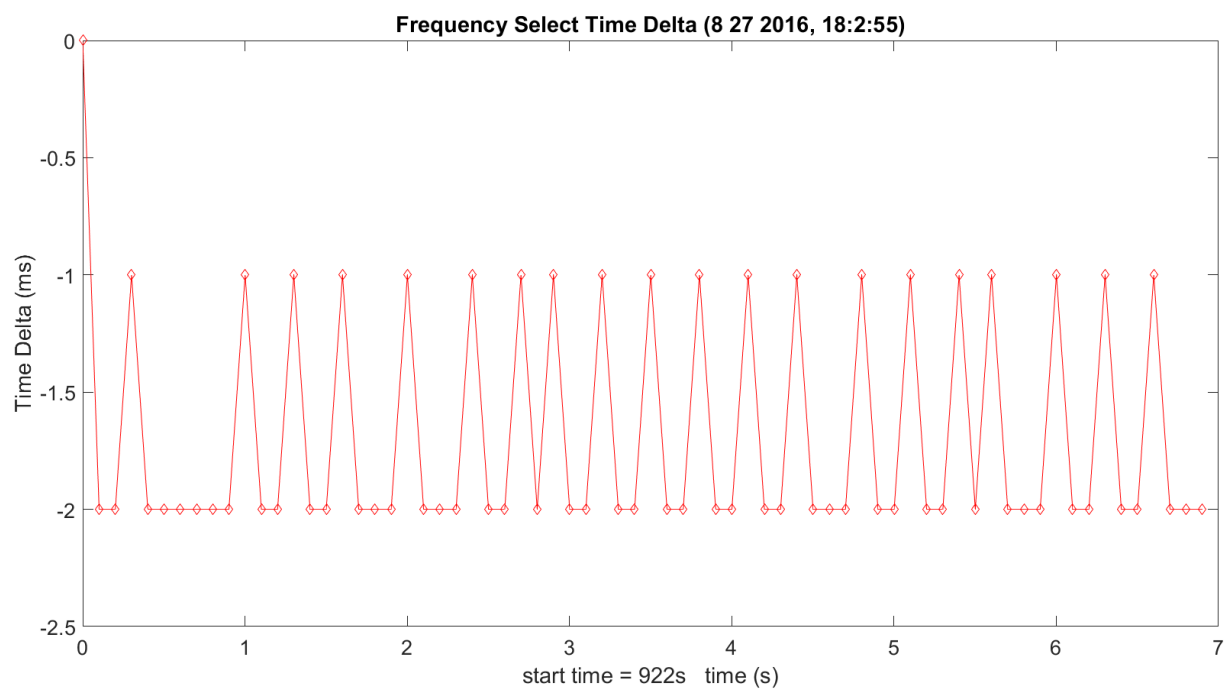


Figure 3.22. TAIPAS Tx vs Rx Computer Synchronization Error.

Figure 3.23 shows the entire three raw scans. The first five frequency selections — data not processed — ensure the system is in sync and then the following 66 frequencies that are processed data. The order of the three eleven-frequency scans is as follows: WB, LWL and UWL; this sequence is repeated twice. As expected, the WB scan has the maximum amplitude volatility. It is easy to see that the amplitudes of each of the two exact scans are similar. Figure 3.24, Figure 3.25 and Figure 3.26 show a blow up of each of the 11 frequencies per scan. The upfront portion of the scan with amplified noise is during the tuning process; the valid data is during the lower noise portion. The low power dip is when the tuners are asynchronous. As expected, due to the short path, these scans don't show the expected shape of the absorption peak.

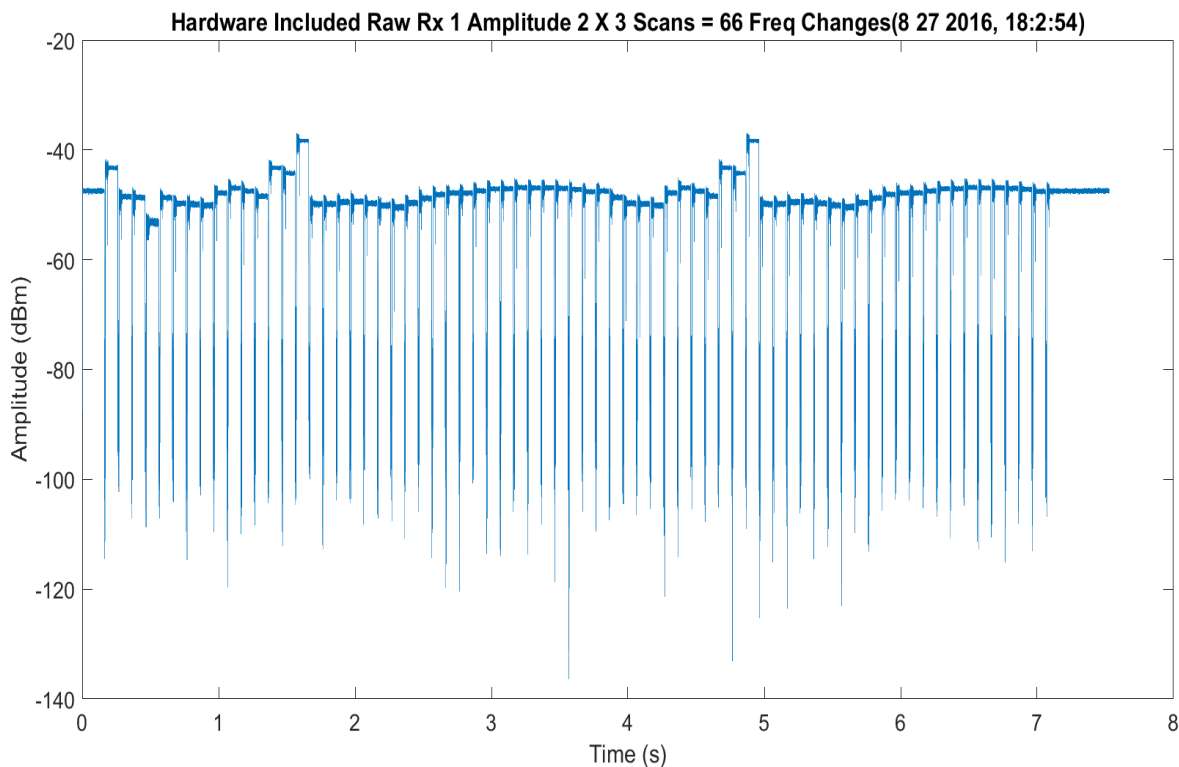


Figure 3.23. TAIPAS Raw Data Received Across Two Scans (66 frequencies).

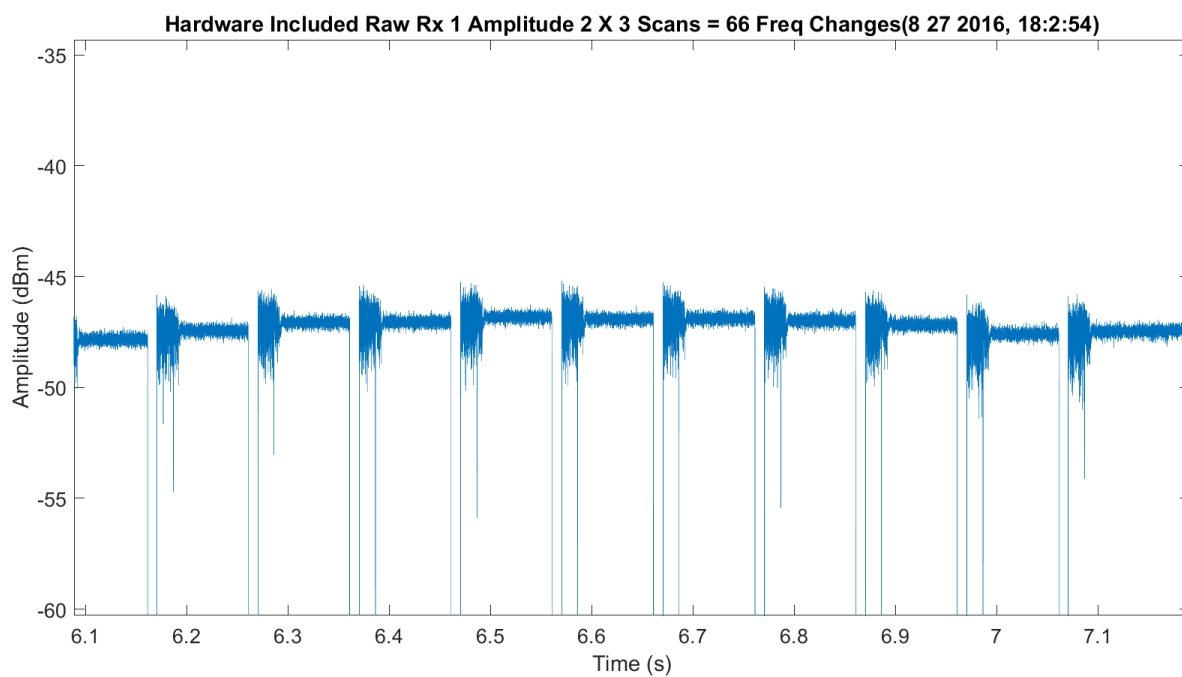


Figure 3.24. TAIPAS Raw Data Received UWL 11 Frequencies.

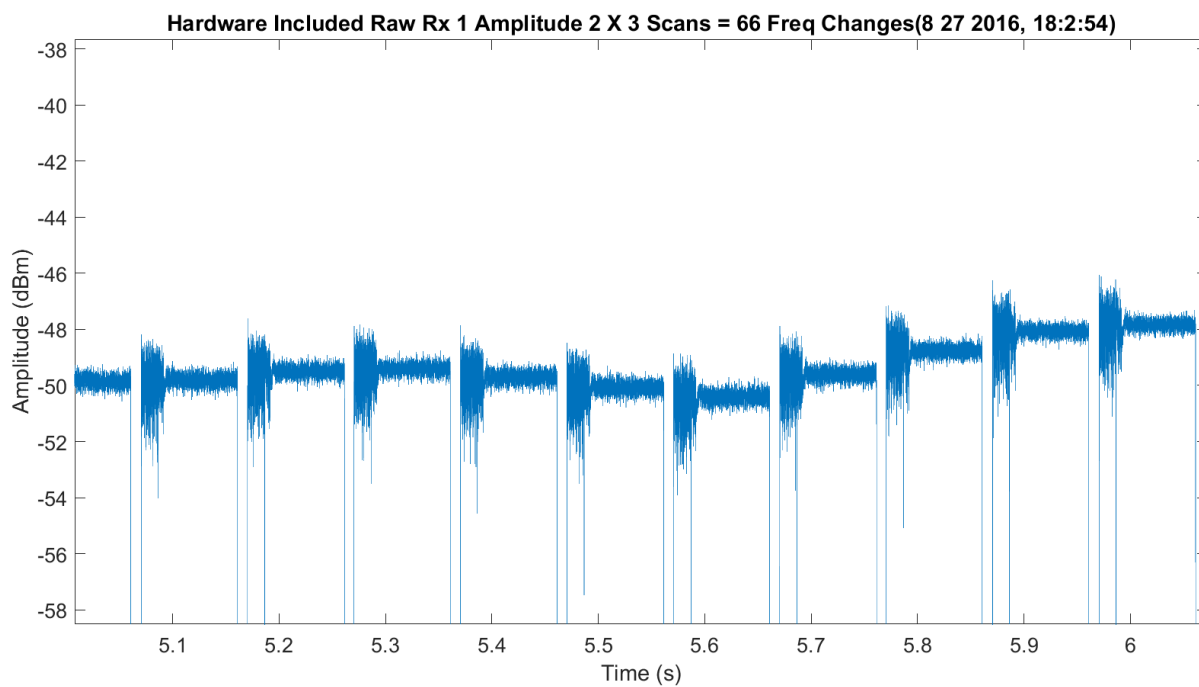


Figure 3.25. Example LWL - TAIPAS Raw Data Received LWL 11 Frequencies.

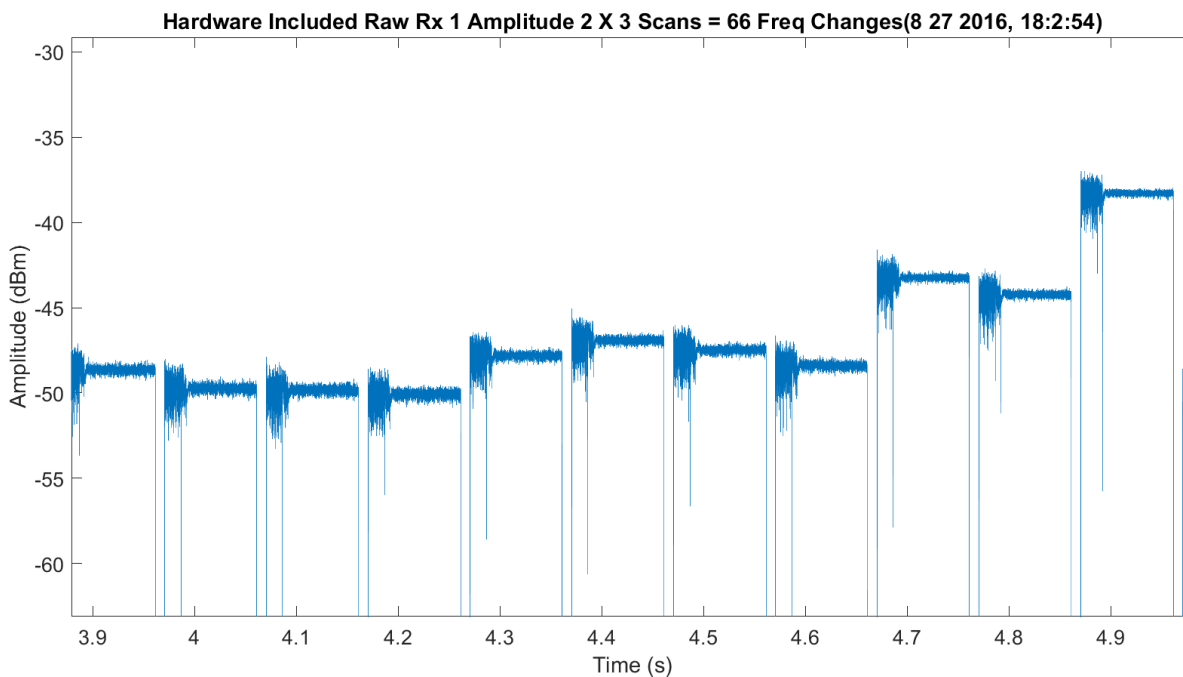


Figure 3.26. TAIPAS Raw Data Received WB 11 Frequencies.

Figure 3.27 shows the entire three raw scans with an 80-point sliding averaging filter applied. This was implemented purely to allow the MATLAB algorithm to easily find the boundaries of the good data versus the tuning or out-of-tune throw away portions. All future processing utilizes the raw data; this data is utilized for separation only.

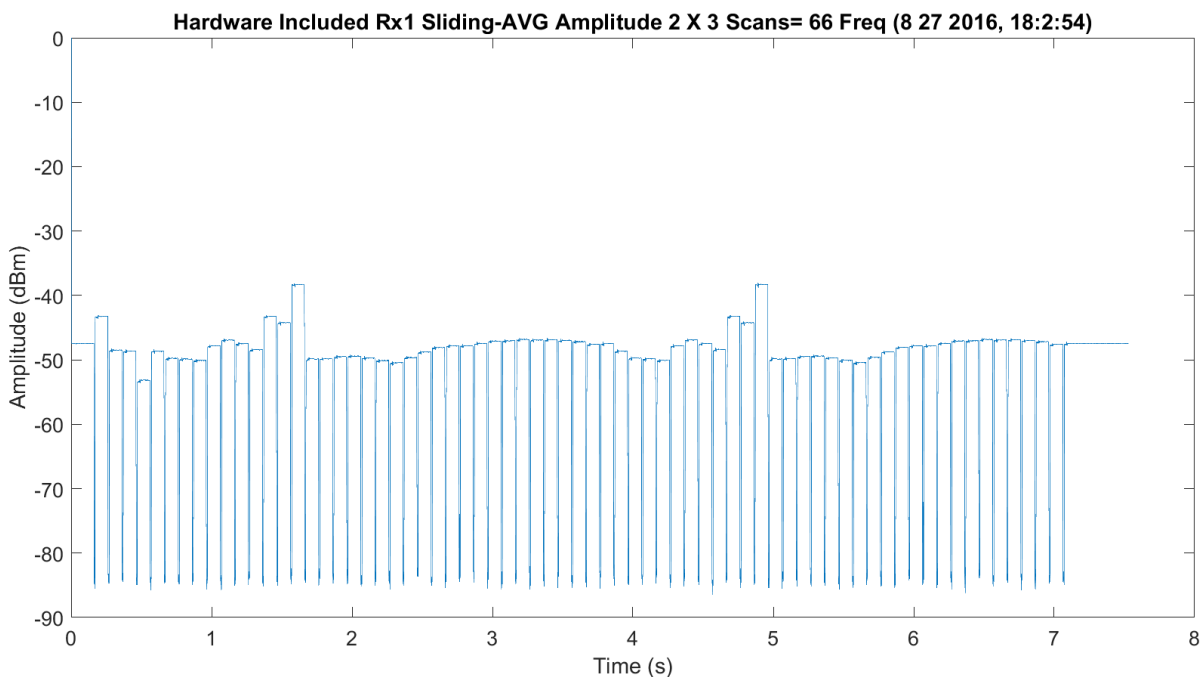


Figure 3.27. TAIPAS Filtered Data Received WB 11 Frequencies.

Figure 3.28 shows an FFT of a single tuned frequency. It is in the 15 kHz carrier range due to the offset of the synthesizers on the transmitter and receiver. The receiver is tuned 1 MHz off of the desired frequency to keep the output of the sub-harmonic mixer off of baseband for sampling in the ADC. This offset is not exact, so when the I/Q DDC is implemented after the sampling, there is still a 15-kHz offset. The sampling after the DDC is 40 kHz; this is the limit on the FFT plot scale. The broadening of the frequency's base is due to phase noise, atmospheric effects of phase and the fact it is in the hallway and the Coho phase lock is not implemented. Figure 3.29 shows a histogram of the single frequency.

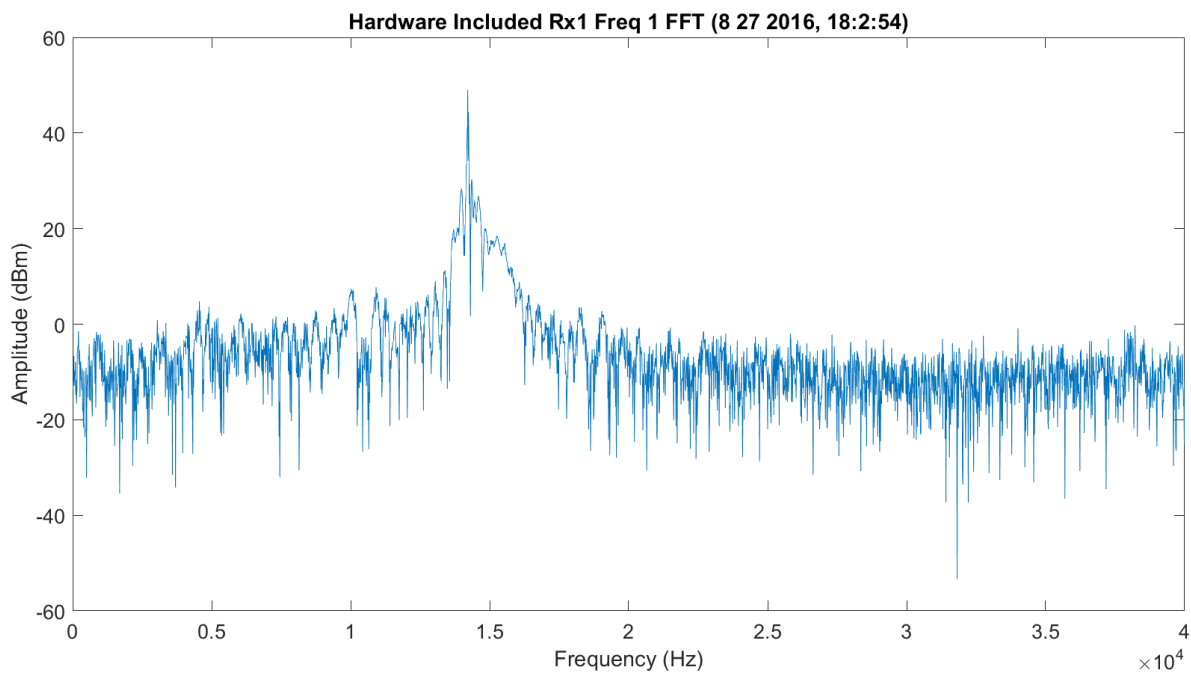


Figure 3.28. TAIPAS Single Scan FFT of Tuned Data.

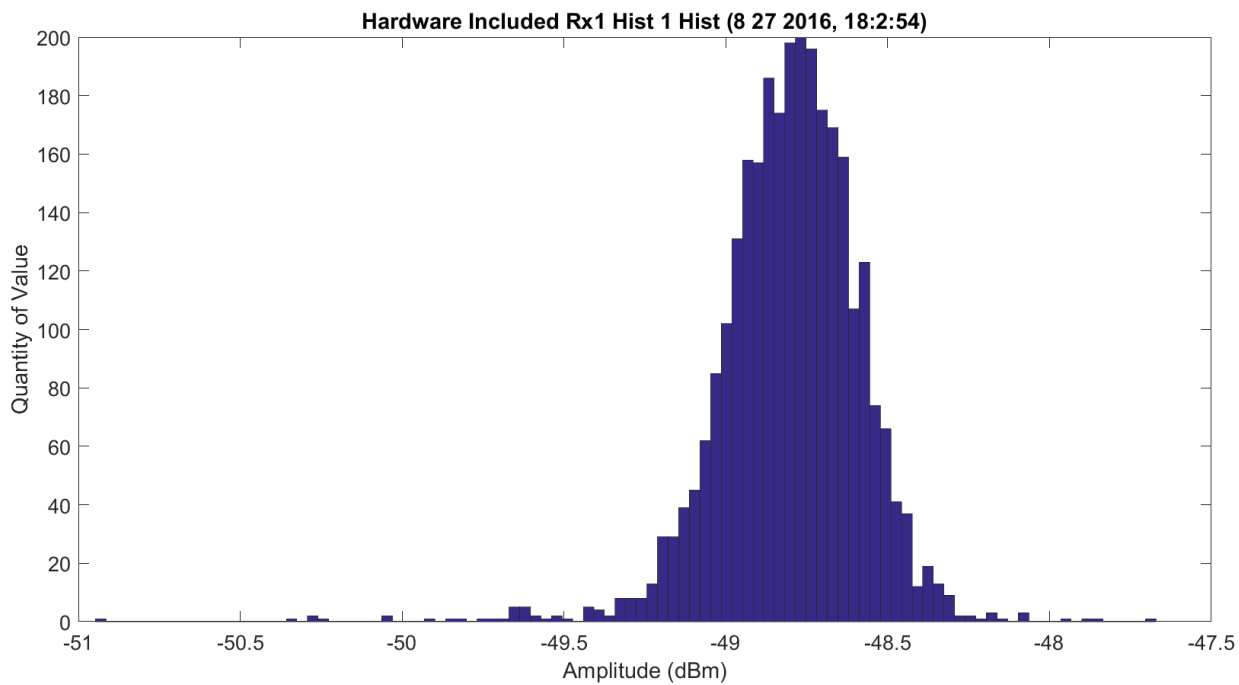


Figure 3.29. TAIPAS Single Scan Histogram of Tuned Data.

Figure 3.30 - Figure 3.32, Figure 3.33 - Figure 3.35 and Figure 3.36 - Figure 3.38 show the three scans utilizing a mean amplitude value for each scan frequency; the consistent order is WB, LWL and UWL. The WB scan has more range on the vertical dBm scale. All three look off for the most attenuation, which should be at 325.153 GHz. This is due to errors in calibration and is not expected on the much longer path of the destination. Figure 3.31, Figure 3.34 and Figure 3.37 show the earlier plots with the Friis expectation plot in green and the difference in red. The amplitudes exaggerated are off due to the lack of tuning discussed earlier. Figure 3.32, Figure 3.35 and Figure 3.38 show a normalized received data with the Friis data to show a close shape relationship of the predicted data to the sampled data. Figure 3.39 shows the Friis, LWL and a flipped UWL; this allows them to overlap. The flipping of the UWL on future longer paths will allow comparison of the LWL vs. the UWL.

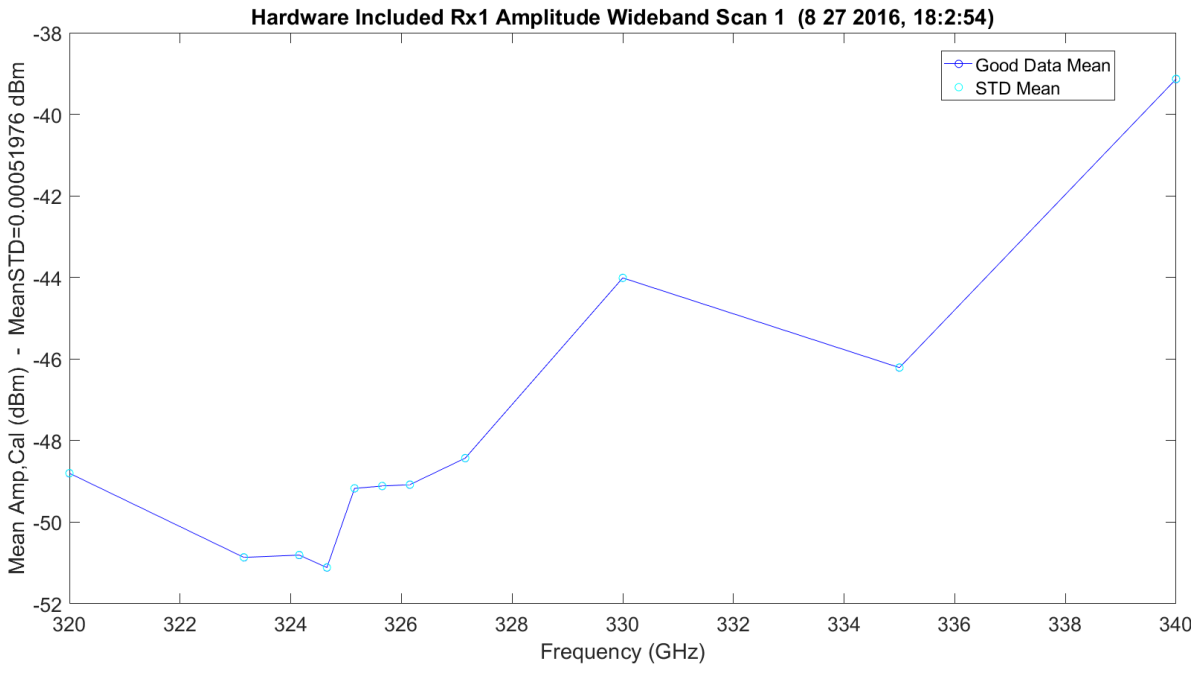


Figure 3.30. TAIPAS WB Hallway Scan.

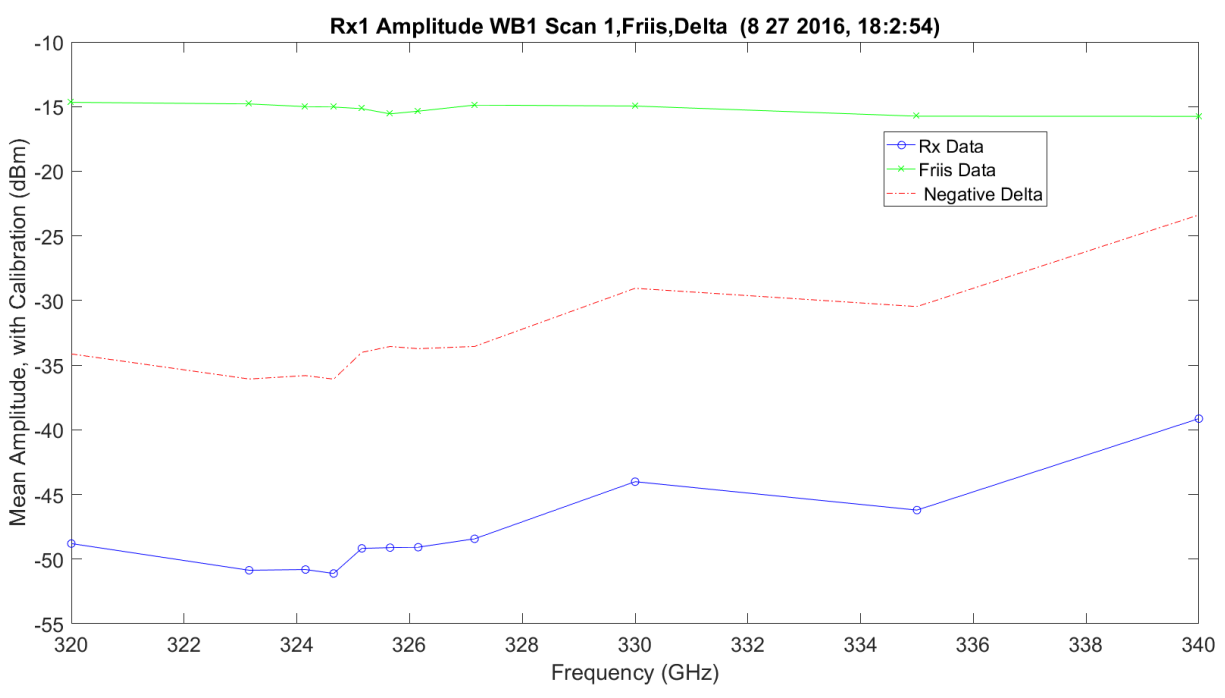


Figure 3.31. TAIPAS WB Hallway Scan with Friis.

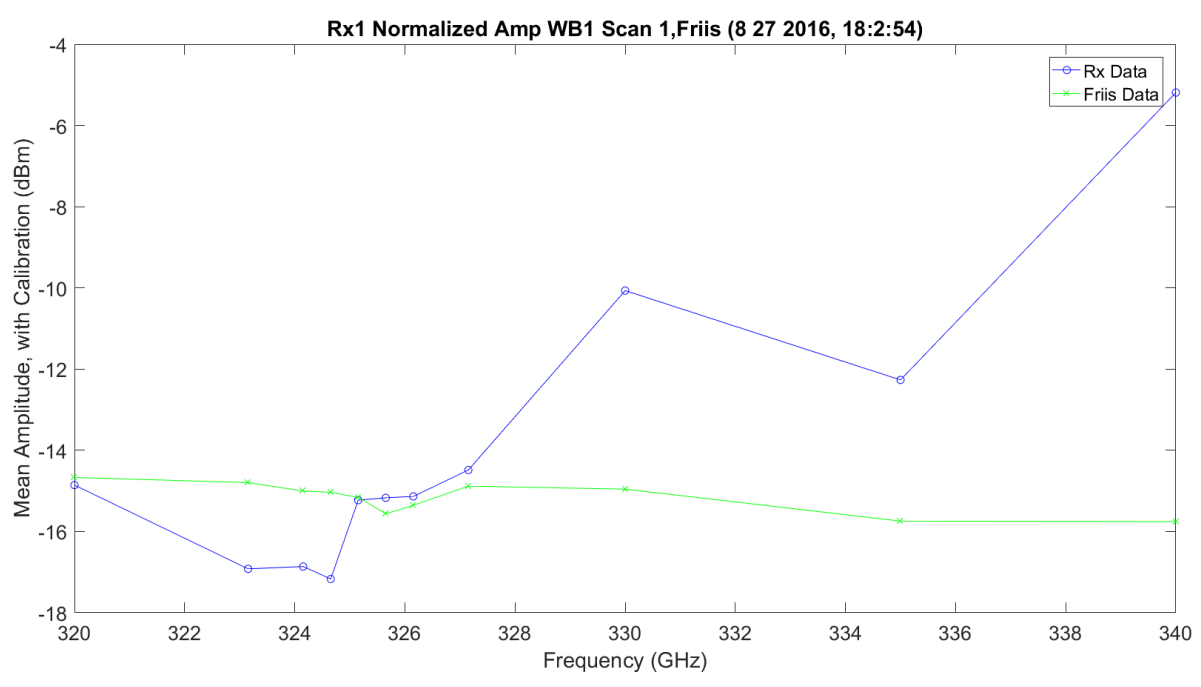


Figure 3.32. TAIPAS WB Hallway Scan Normalized with Friis.

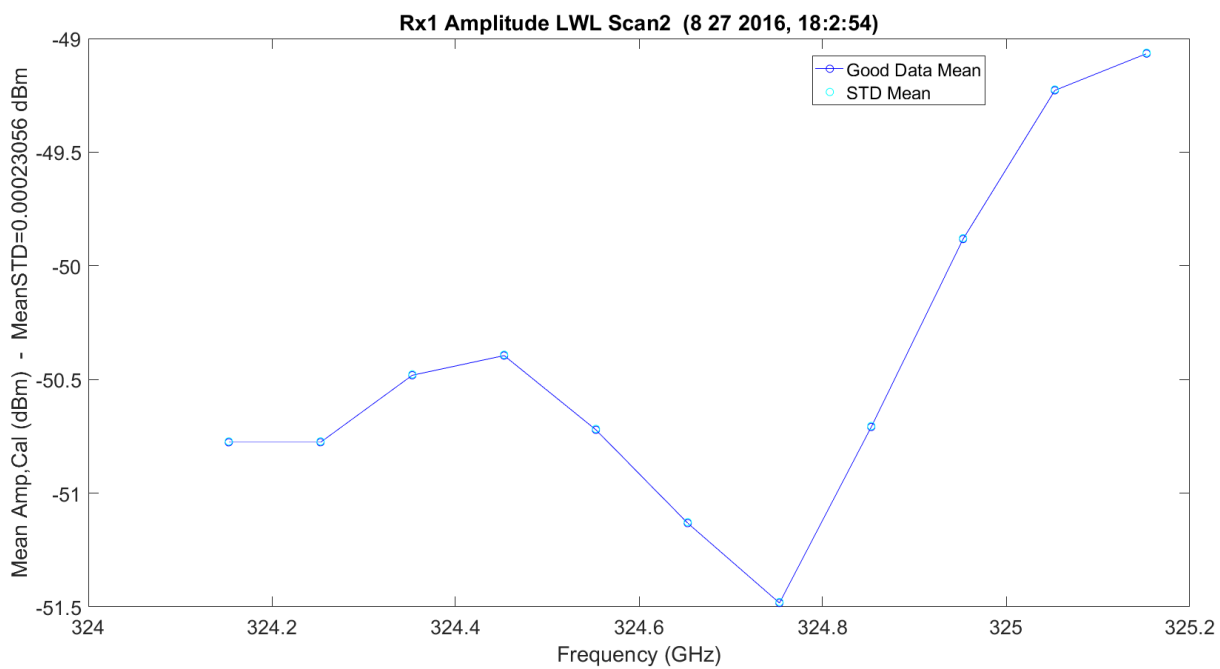


Figure 3.33. TAIPAS LWL Hallway Scan.

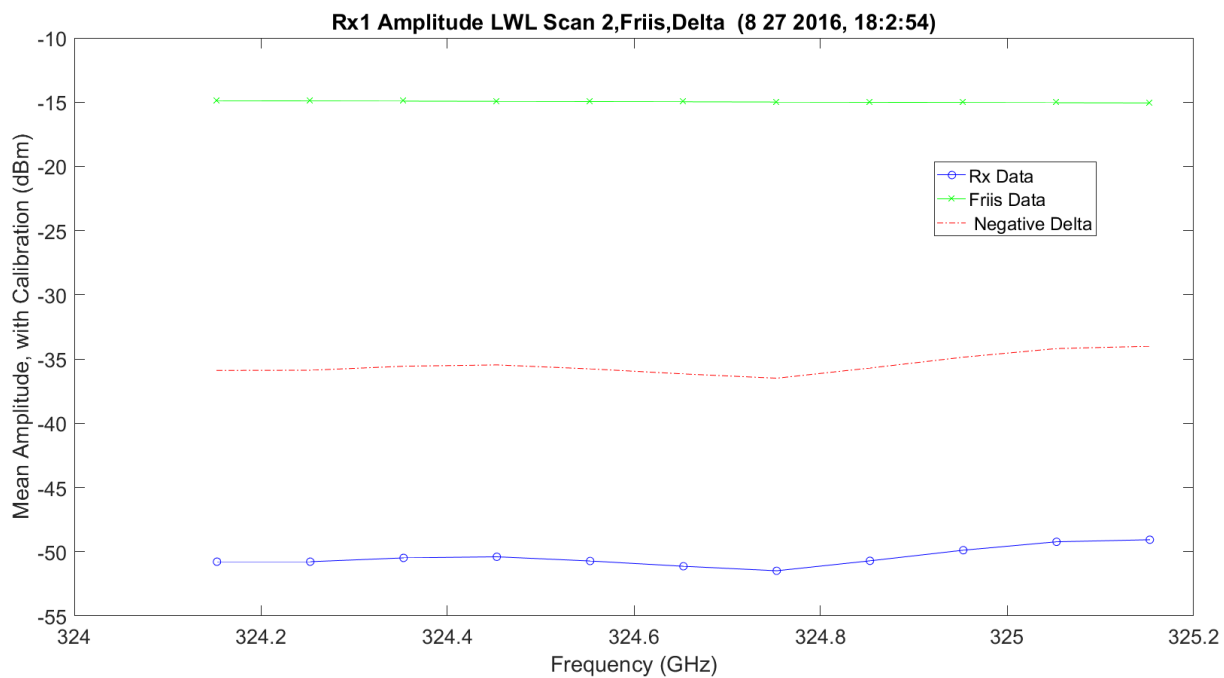


Figure 3.34. TAIPAS LWL Hallway Scan with Friis.

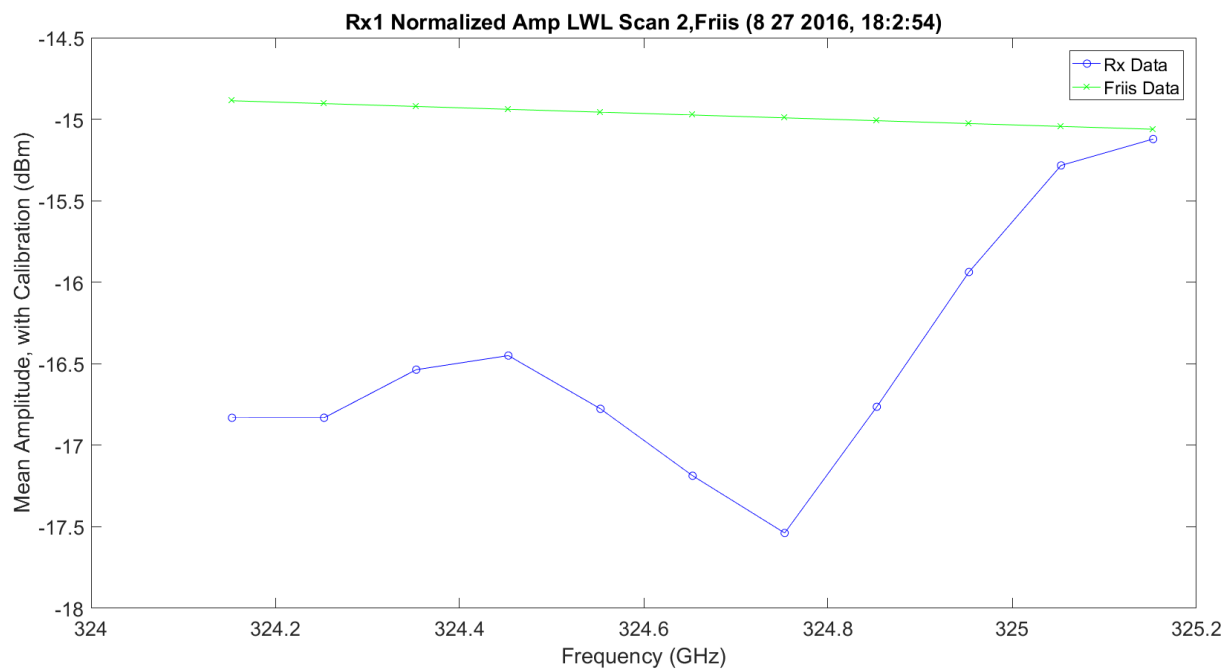


Figure 3.35. TAIPAS up LWL Hallway Scan Normalized with Friis.

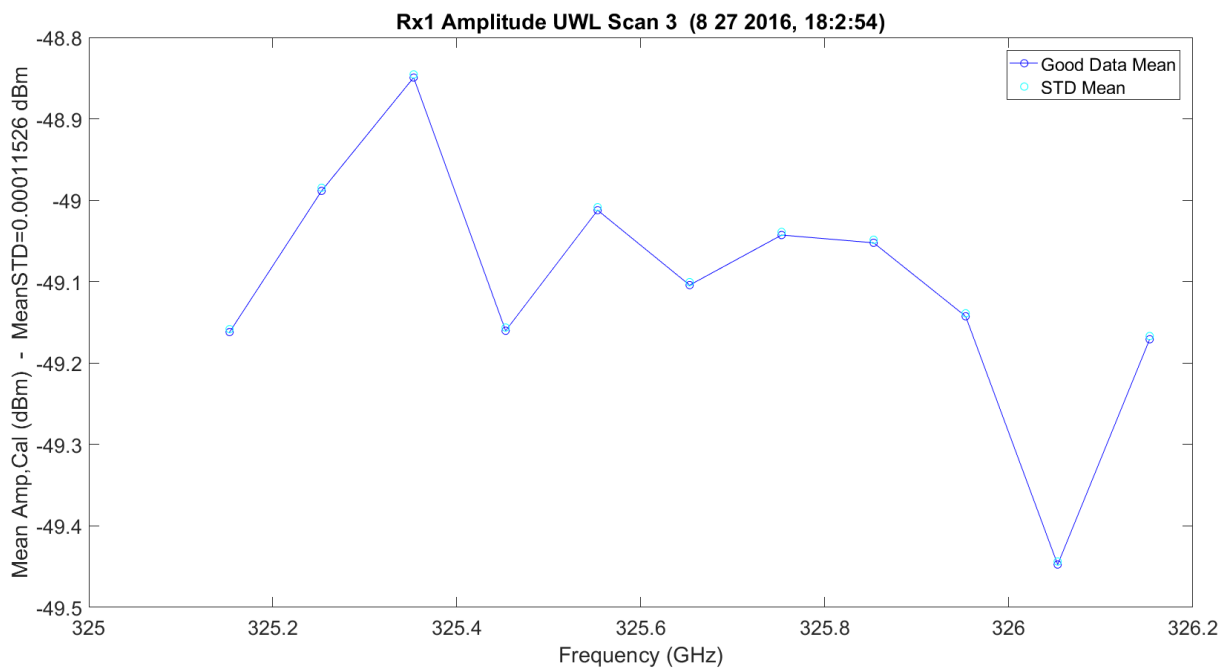


Figure 3.36. TAIPAS UWL Hallway Scan.

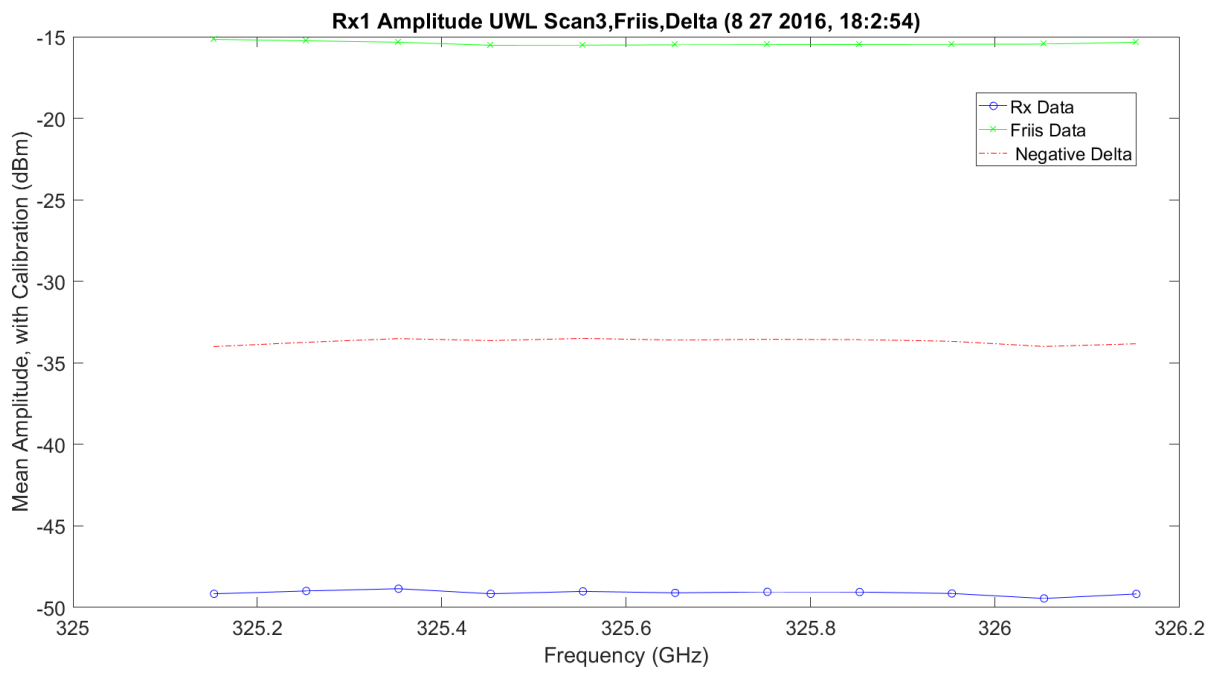


Figure 3.37. TAIPAS UWL Hallway Scan with Friis.

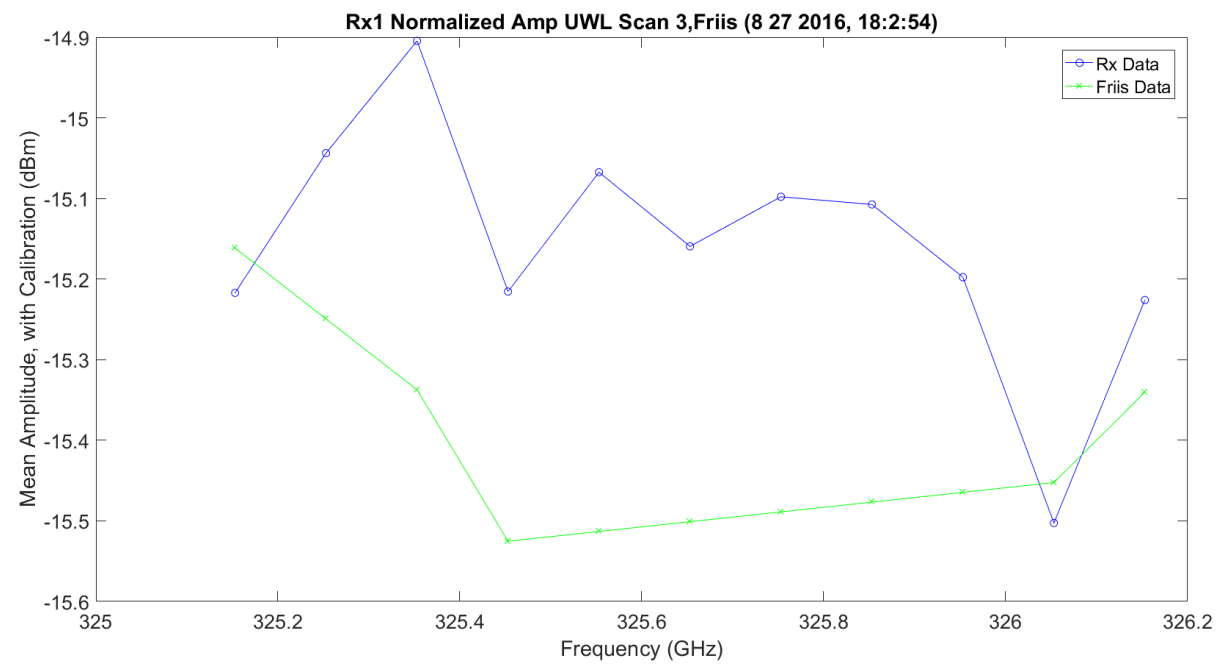


Figure 3.38. TAIPAS LWL Hallway Scan Normalized with Friis.

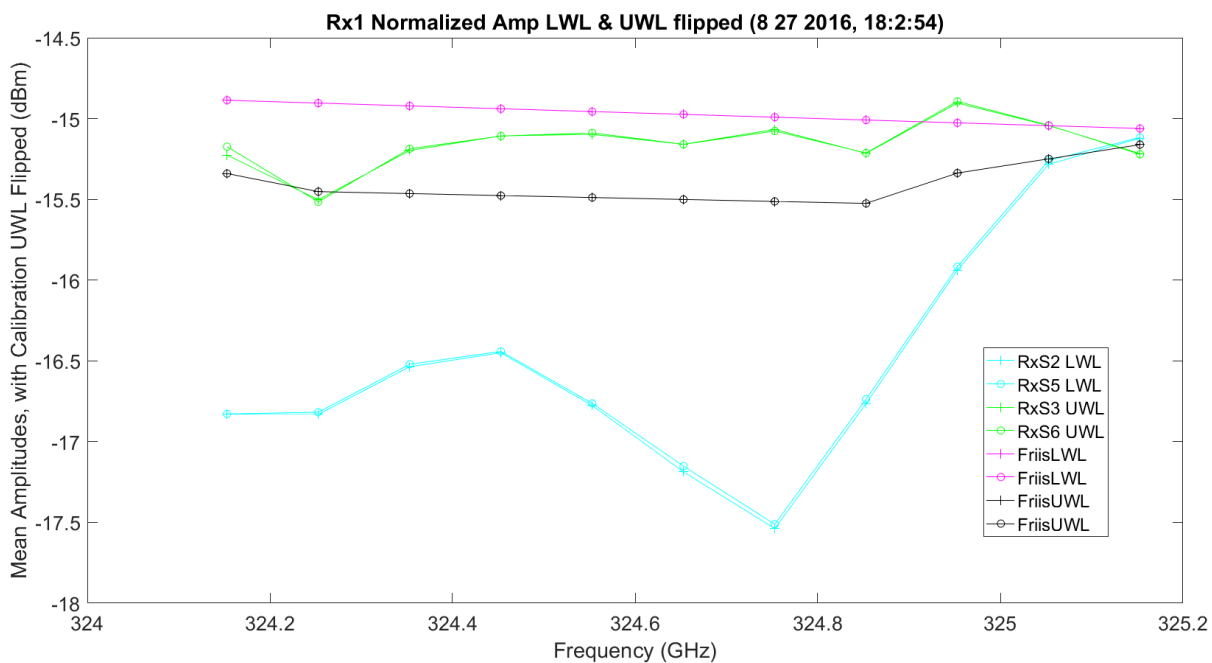


Figure 3.39. TAIPAS LWL and UWL Flipped Hallway Scan Normalized with Friis.

Figure 3.40 shows an example collection of C_n^2 ; this is not hallway data, it was taken on a longer path in Colorado Springs with a single LED and the area calculation method. The $\times 10^{-13}$ power was expected. Due to cost, the best that can be executed to calibrate the custom scintillometer is comparison to simulations and data obtained from NIST's scintillometer. Figure 3.41 shows an FFT of the plot with a dominant component in a one-cycle-per-second. The sample frequency was 40 kHz.

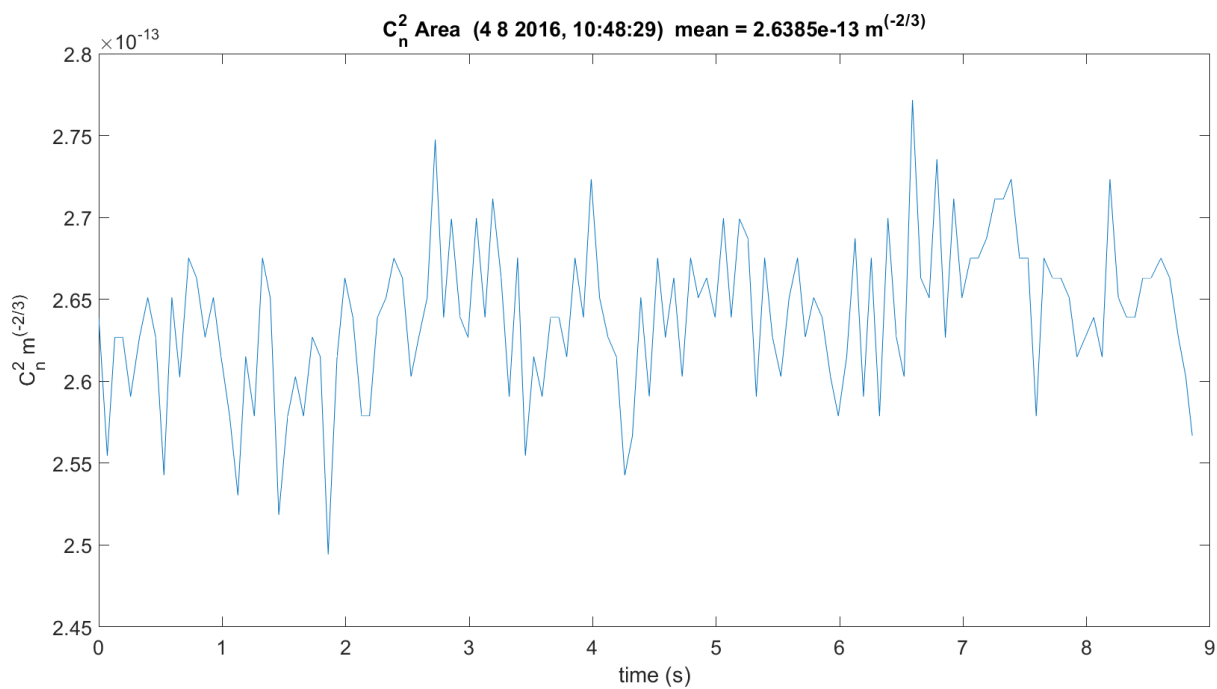


Figure 3.40. TAIPAS C_n^2 Example Collection.

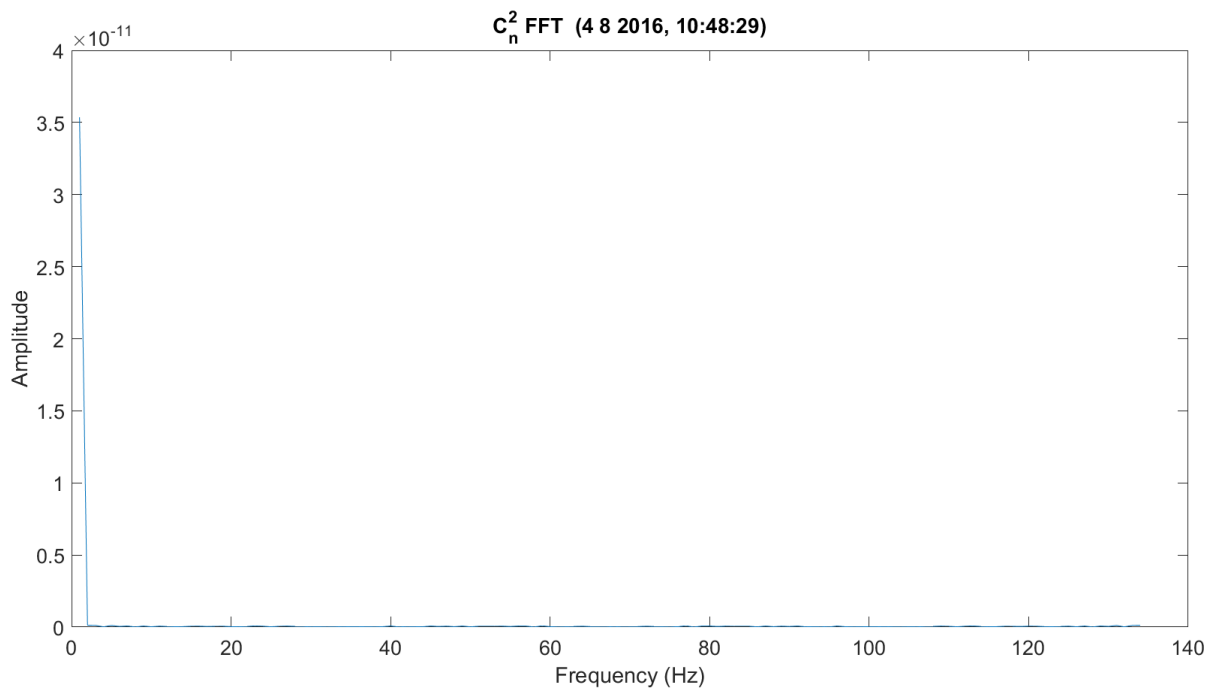


Figure 3.41. TAIPAS FFT C_n^2 Example Collection.

Figure 3.42 – Figure 3.44 show the transmit and receive anemometer results with the mean of the two. The U wind is the along the EM path wind component. The V wind is the across wind component. The W wind component is the vertical wind component. Obviously, there was not a lot of wind in the hallway. Figure 3.45 and Figure 3.46 show the wet and dry components of the transmitter and receiver hygrometers; the means are also plotted.

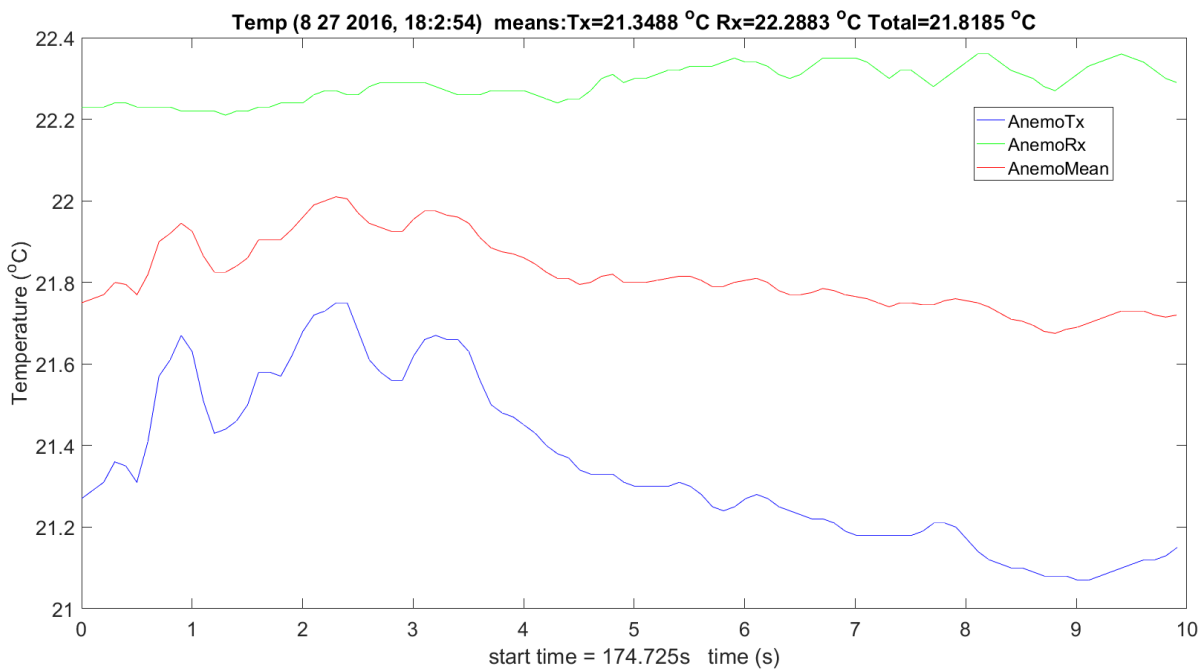


Figure 3.42. Hallway Temperature from Anemometers.

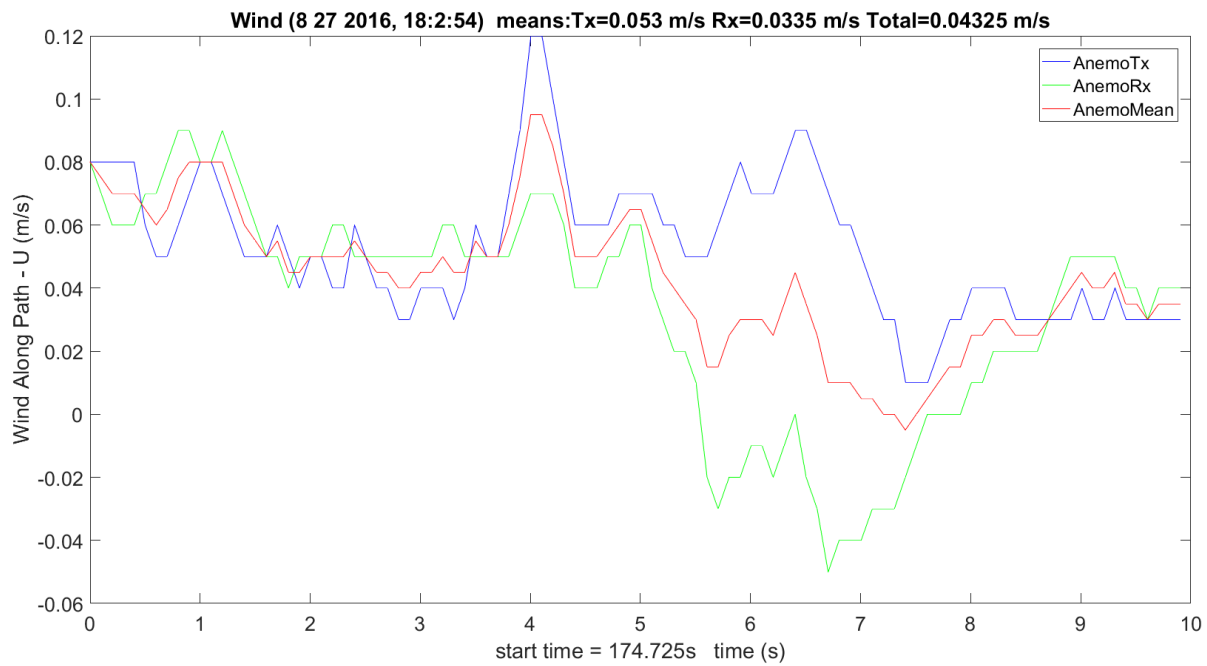


Figure 3.43. Hallway Wind U from Anemometers.

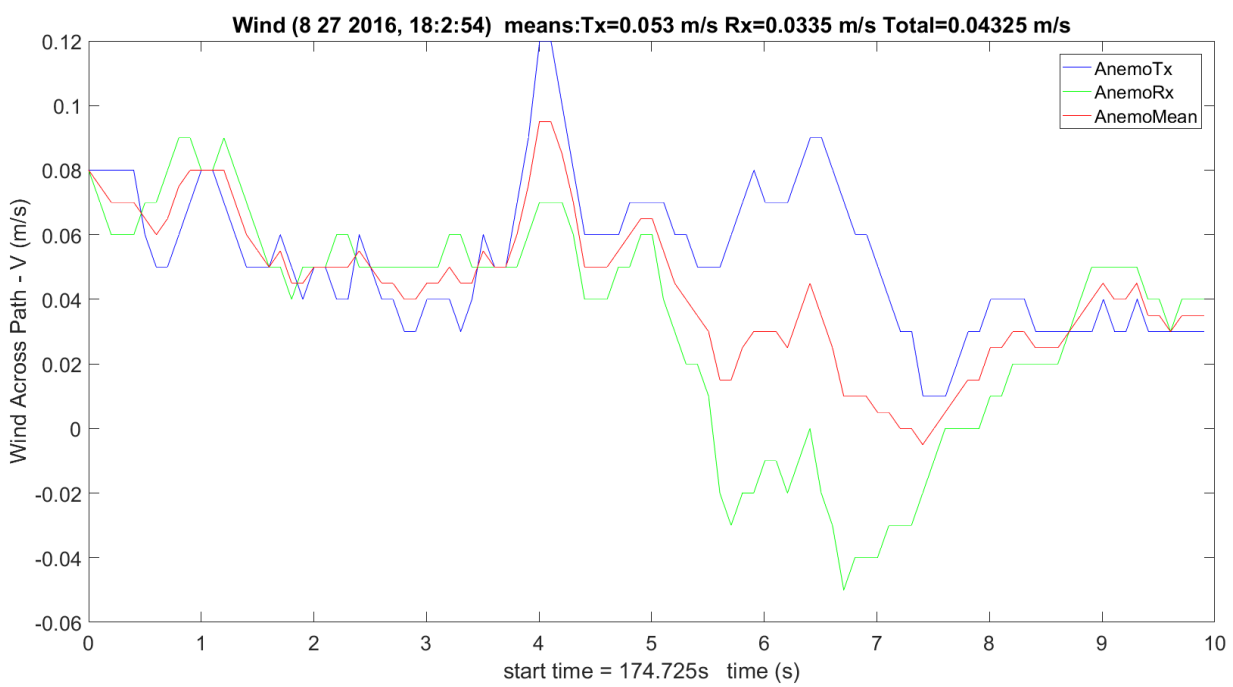


Figure 3.44. Hallway Wind V from Anemometers.

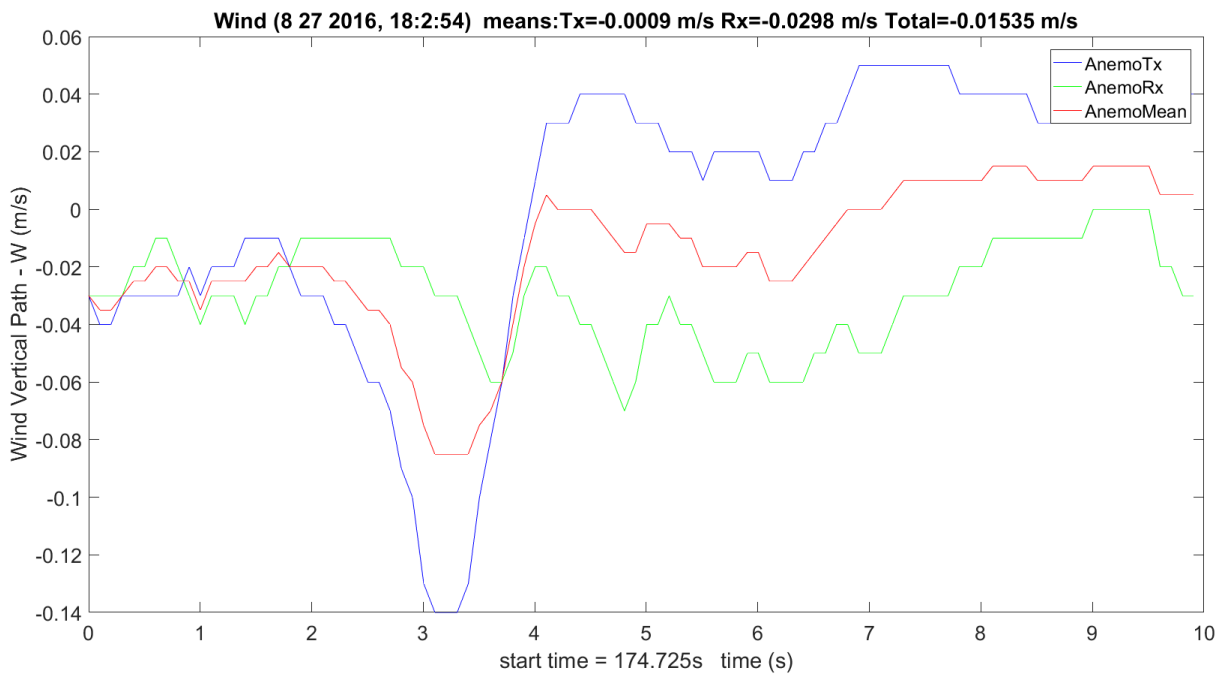


Figure 3.45. Hallway Wind W from Anemometers.

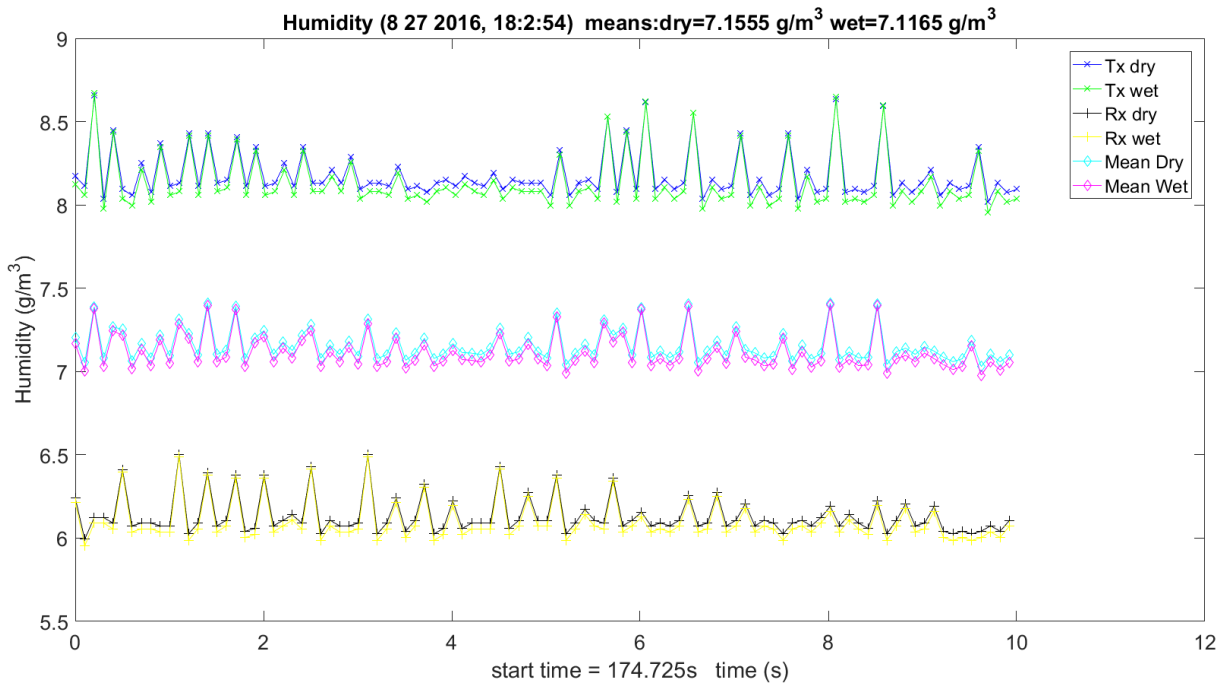


Figure 3.46. Hallway Humidity from Hygrometers.

Figure 3.47, Figure 3.48 and Figure 3.49 show the extinction plots for the WB, LWL and UWL scans. Since two receivers could not fit in the hallway, nor was the spot size large enough over 40 m to cover them, the Rx1 equals Rx2. As expected, the two WB scans are off due to the lack of alignment in the hallway. The Friis calculation is at the bottom of the plot. Figure 3.50 shows the same LWL and Friis plot with the UWL flipped. This allows comparison of the LWL and UWL absorption shapes.

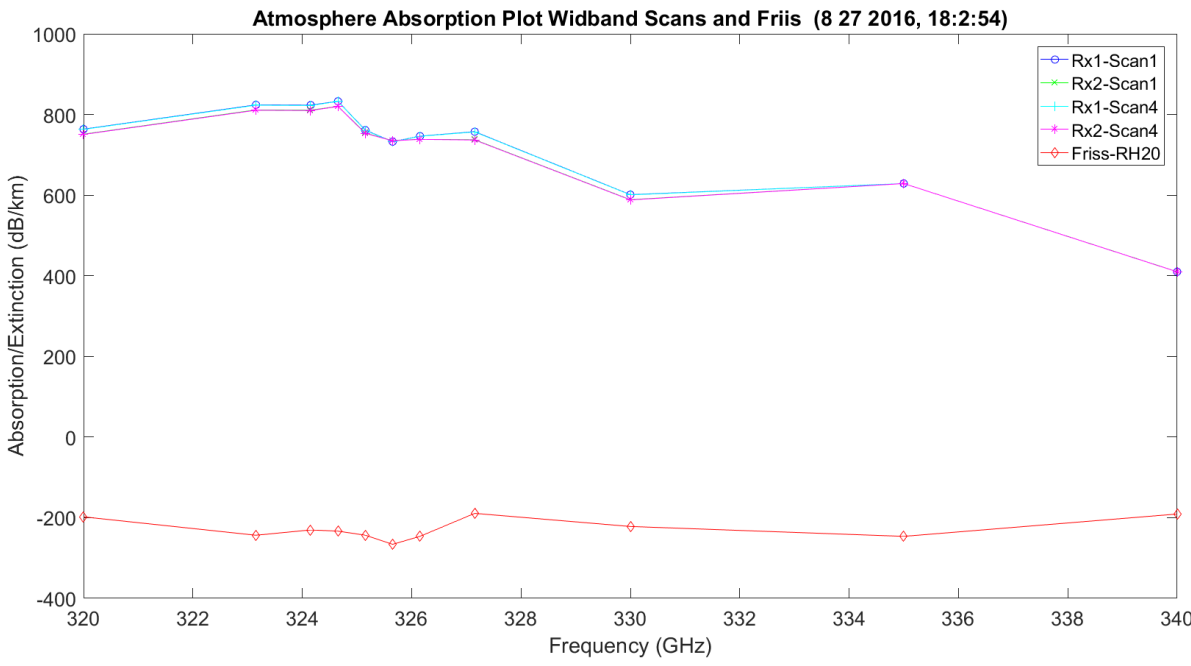


Figure 3.47. Hallway WB and Friis Extinction Plots.

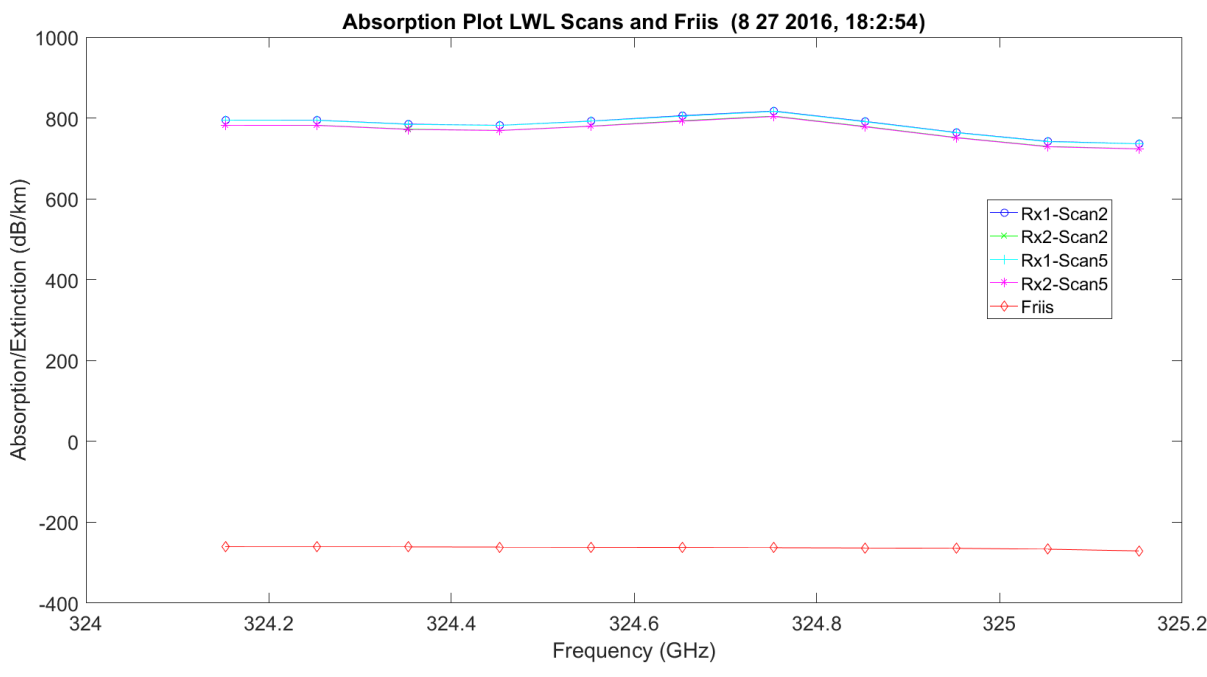


Figure 3.48. Hallway LWL and Friis Extinction Plots.

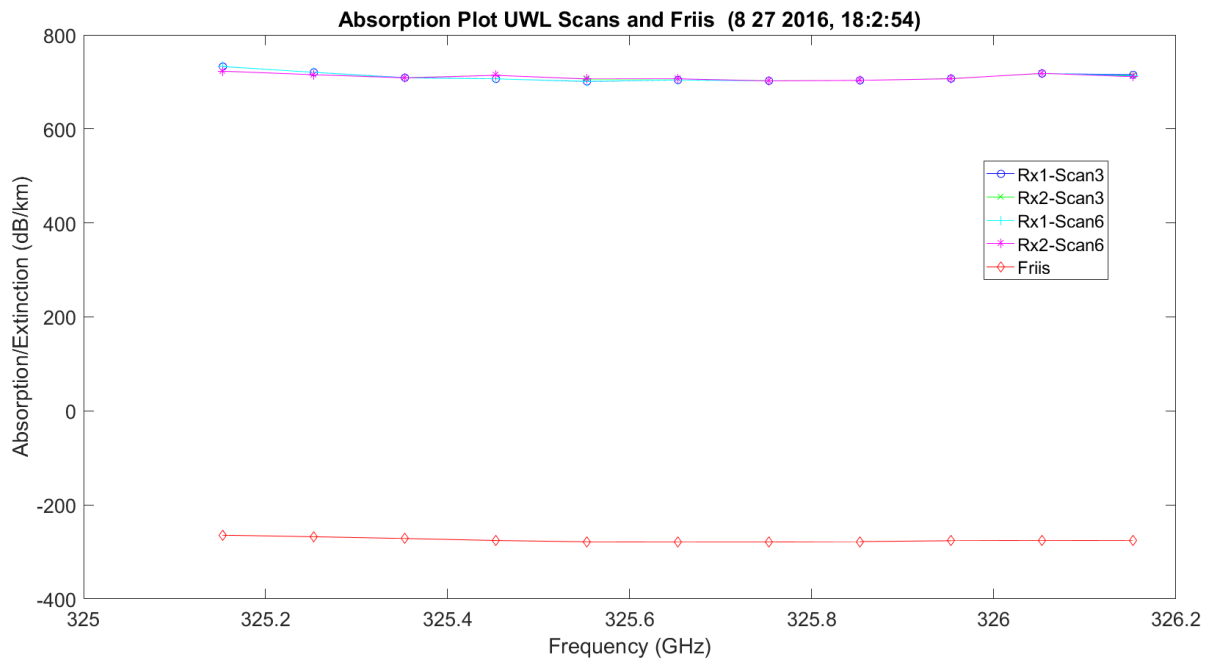


Figure 3.49. Hallway UWL and Friis Extinction Plots.

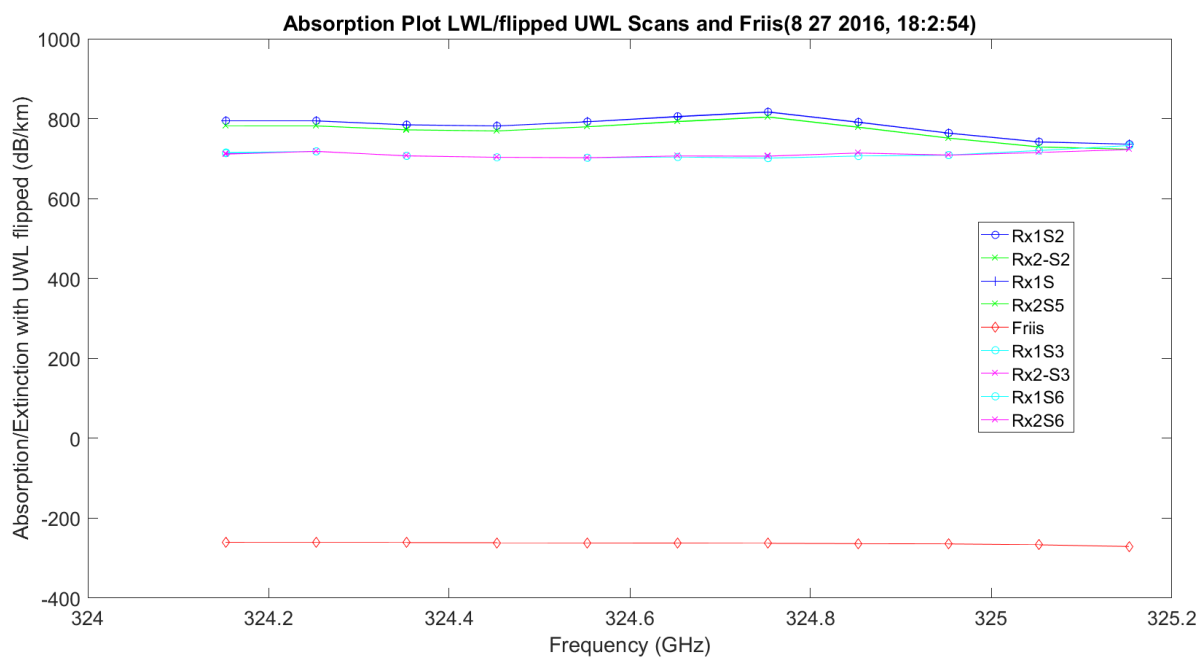


Figure 3.50. Hallway LWL, Flipped UWL and Friis Extinction Plots.

Figure 3.51 – Figure 3.53 show the SNR plots for the WB, LWL and UWL scans. They also show the expected Friis SNRs.

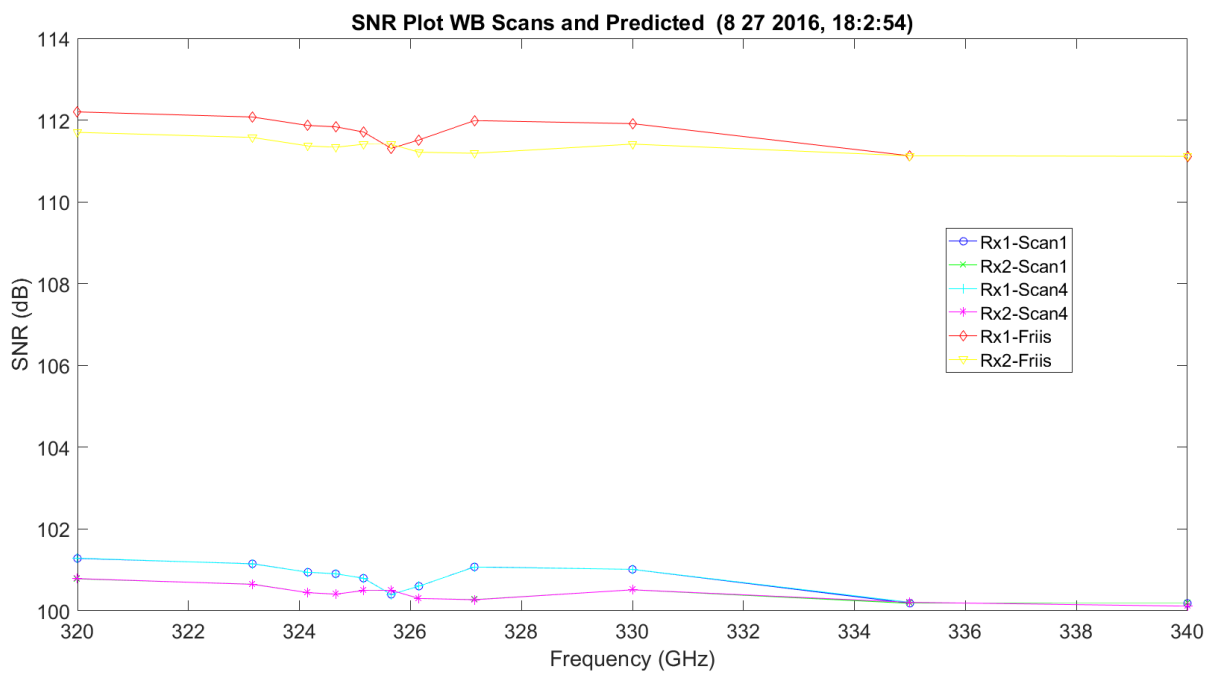


Figure 3.51. Hallway WB and Friis SNR Plots.

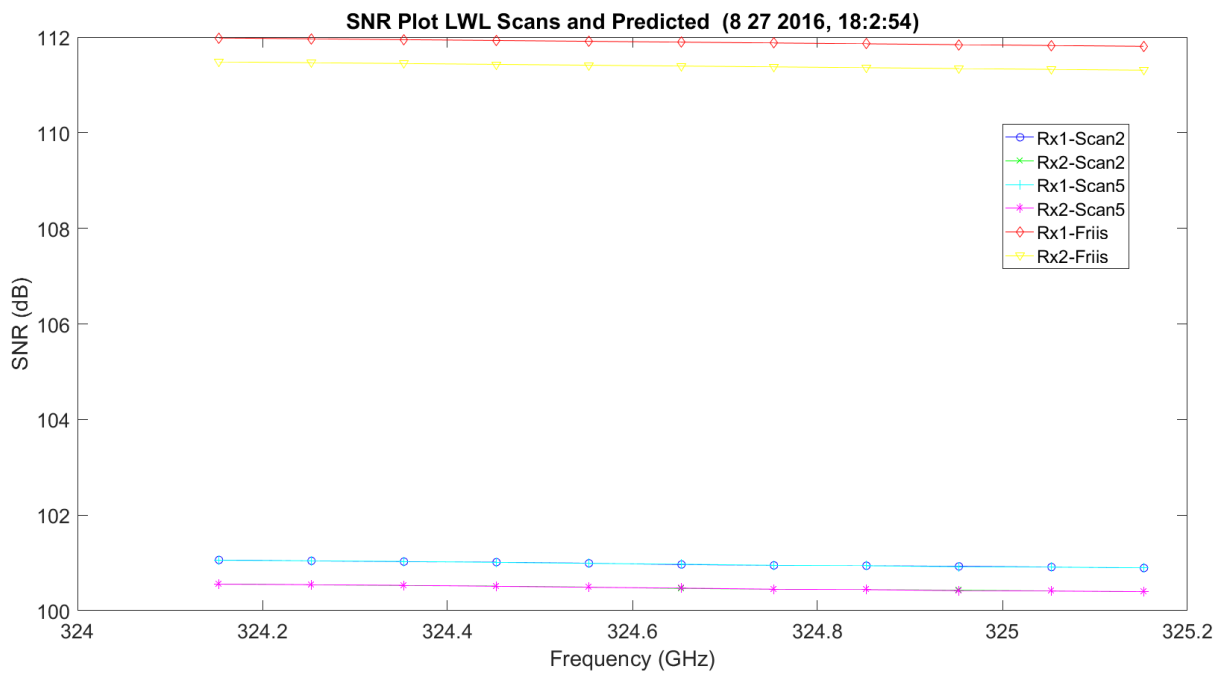


Figure 3.52. Hallway LWL and Friis SNR Plots.

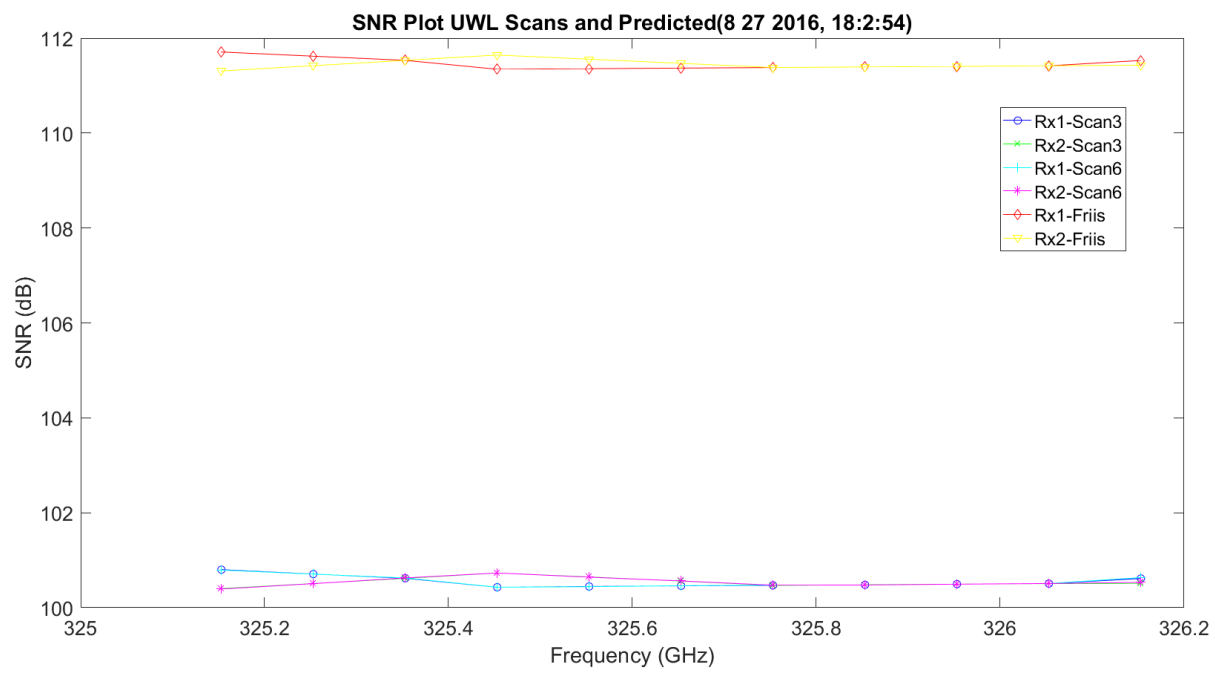


Figure 3.53. Hallway UWL and Friis SNR Plots.

Figure 3.54 – Figure 3.56 show the MCF and phase structure functions for the WB, LWL and UWL scans. The phase structure function is just minus two times the MCF. The blue plots in this case represent the two sets of identical frequency scans (e.g. WB 1 and 4). These are fairly close for all scans.

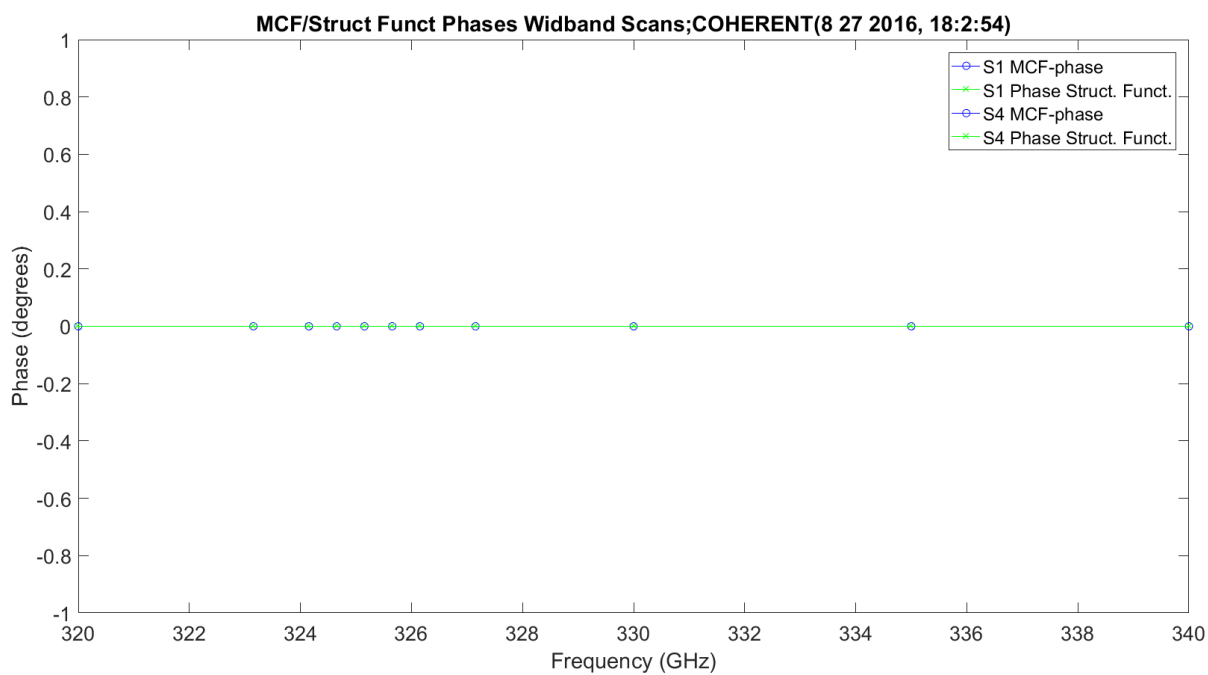


Figure 3.54. WB MCF/Structure Function Plots.

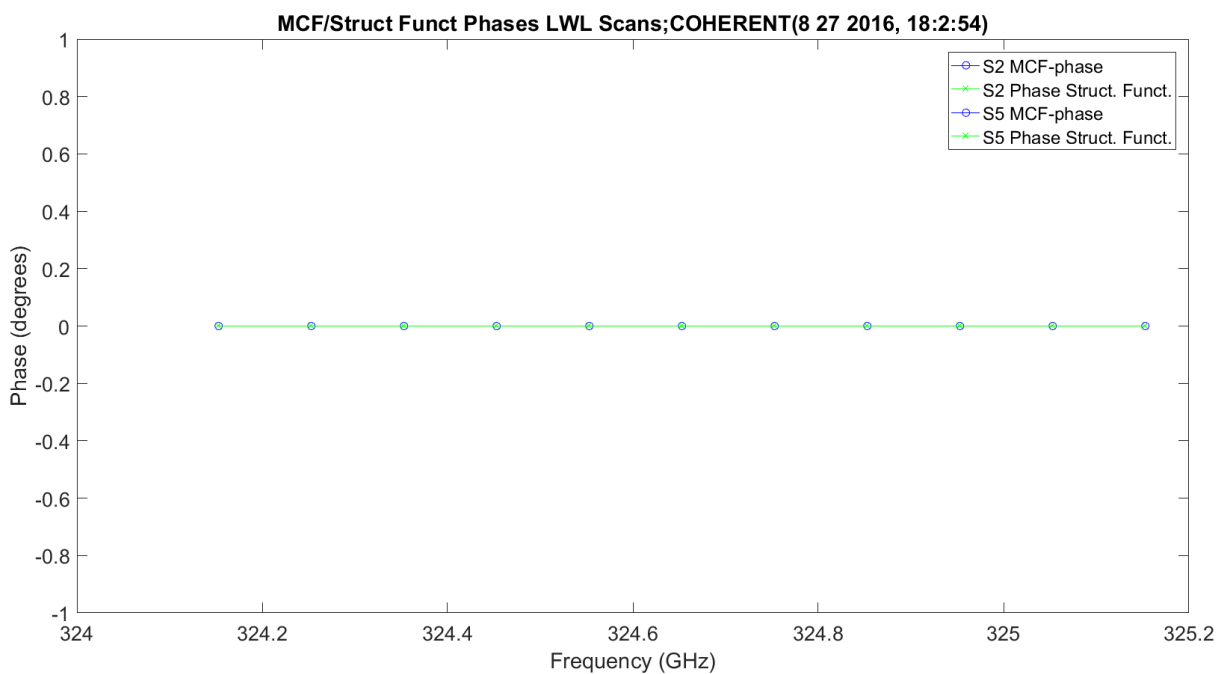


Figure 3.55. LWL MCF/Structure Function Plots.

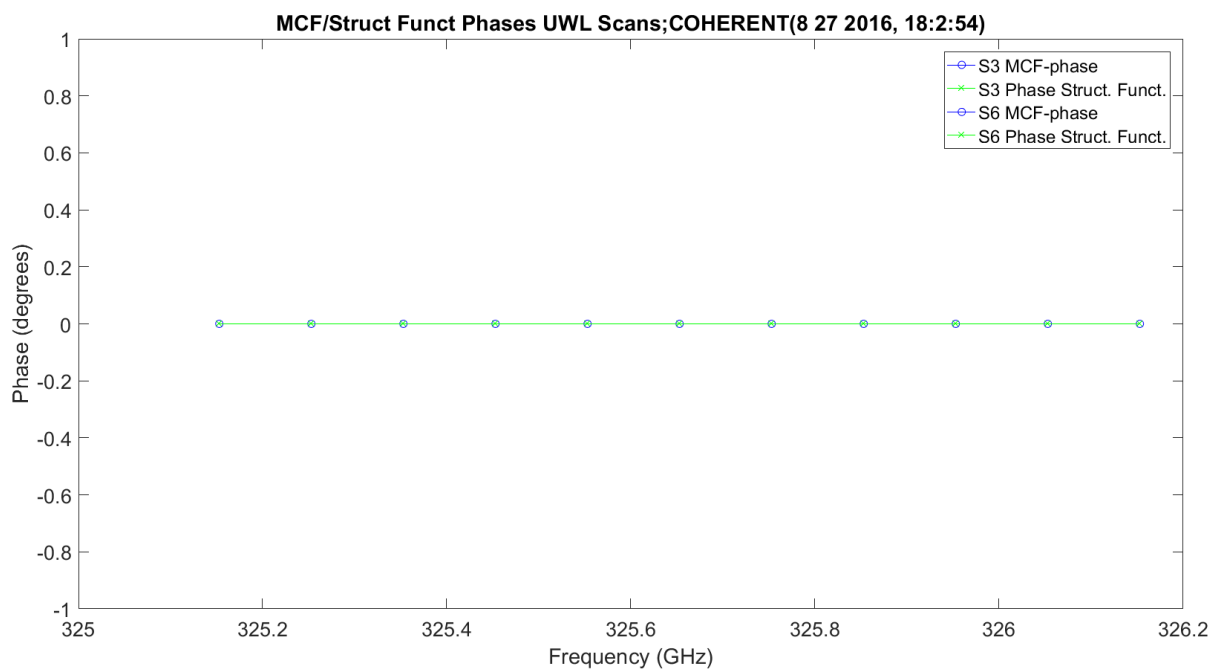


Figure 3.56. UWL MCF/Structure Function Plots.

Figure 3.57 – Figure 3.59 show the amplitude scintillation, $\langle \chi^2 \rangle$, for all the scans, two each, compared to the predicted value utilizing Kolmogorov with outer scale.

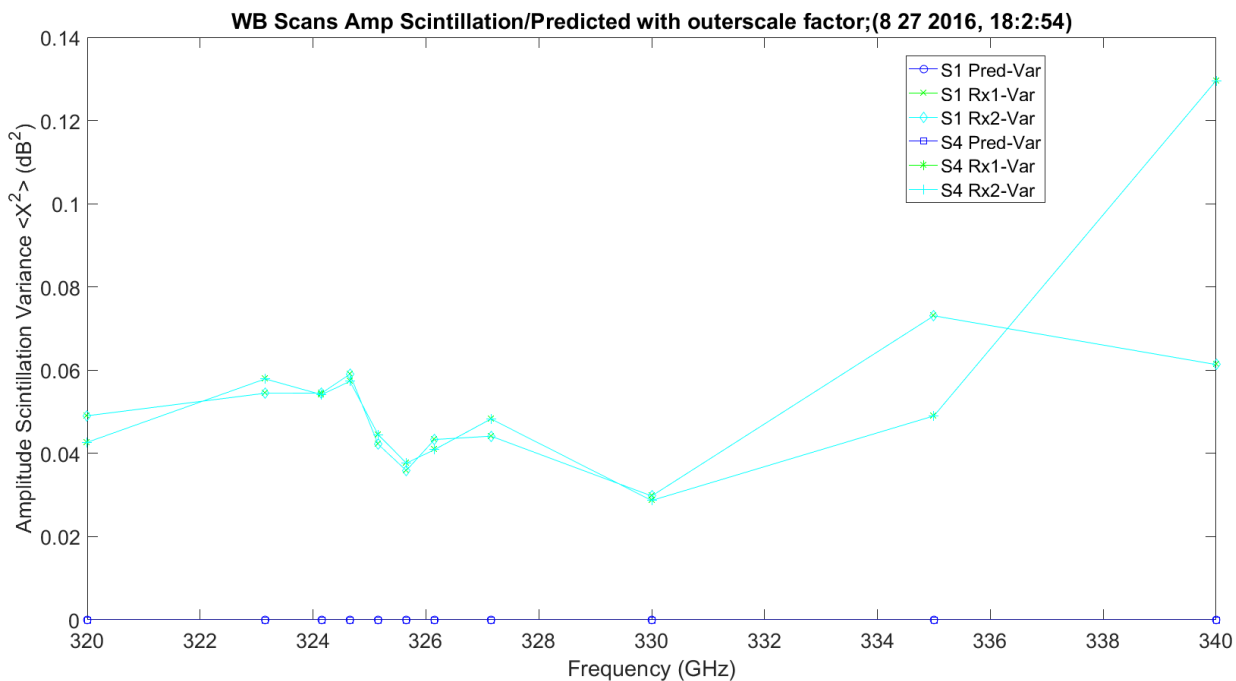


Figure 3.57. WB Amplitude Scintillation with Outer Scale Factor Prediction.

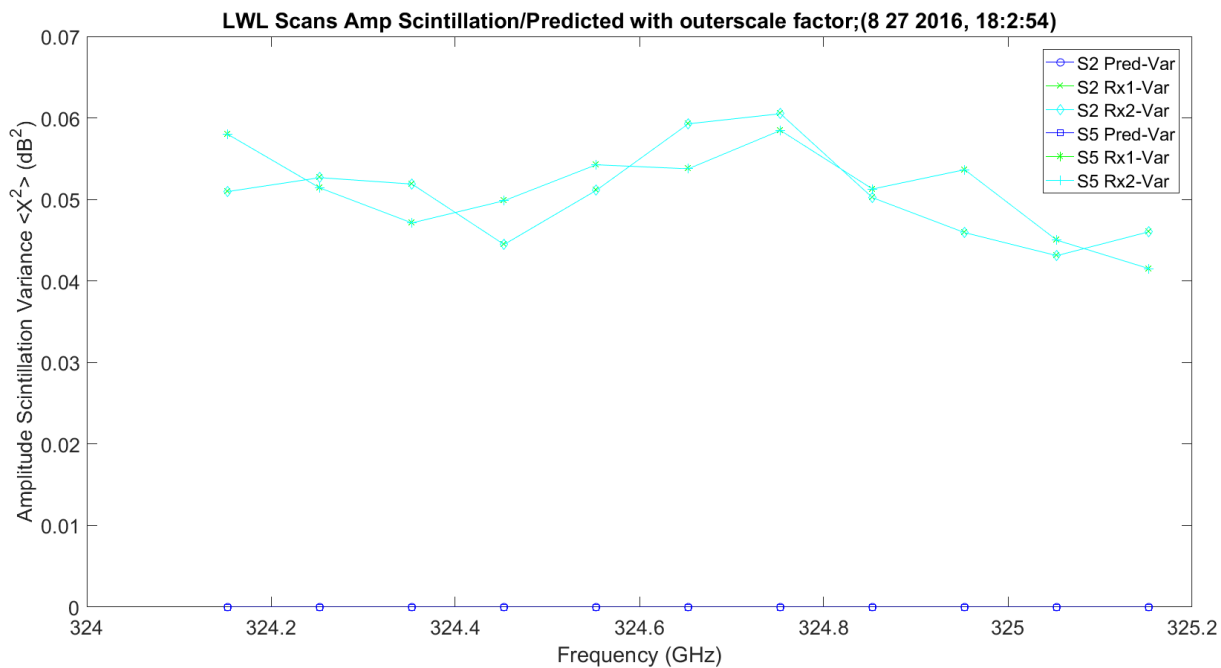


Figure 3.58. LWL Amplitude Scintillation with Outer Scale Factor Prediction.

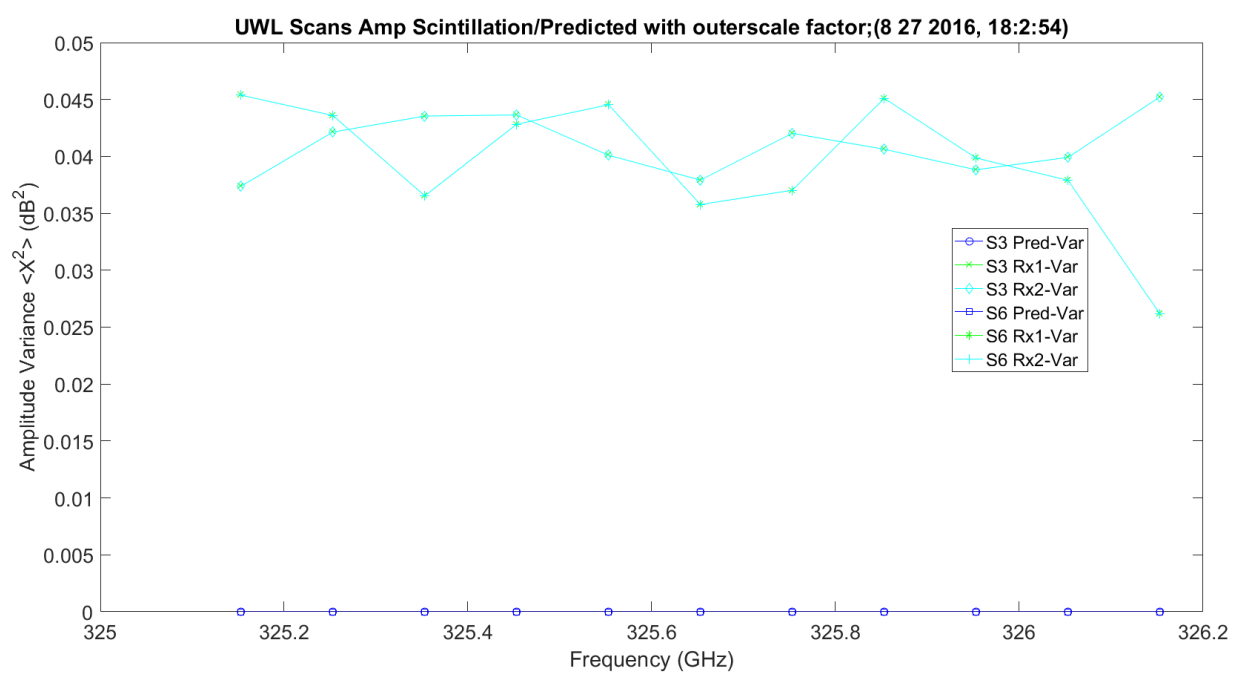


Figure 3.59. UWL Amplitude Scintillation with Outer Scale Factor Prediction.

Figure 3.60 – Figure 3.83 show the phase scintillation, $\langle \phi^2 \rangle$, for all the scans, two each, compared to the predicted valued utilizing GO, von Karman Model. Each set of plots shows the collected data for both receivers, with minor difference for both scans and the predicted value. This is repeated for all three types of scans for phase in degrees, millimeters and picoseconds.

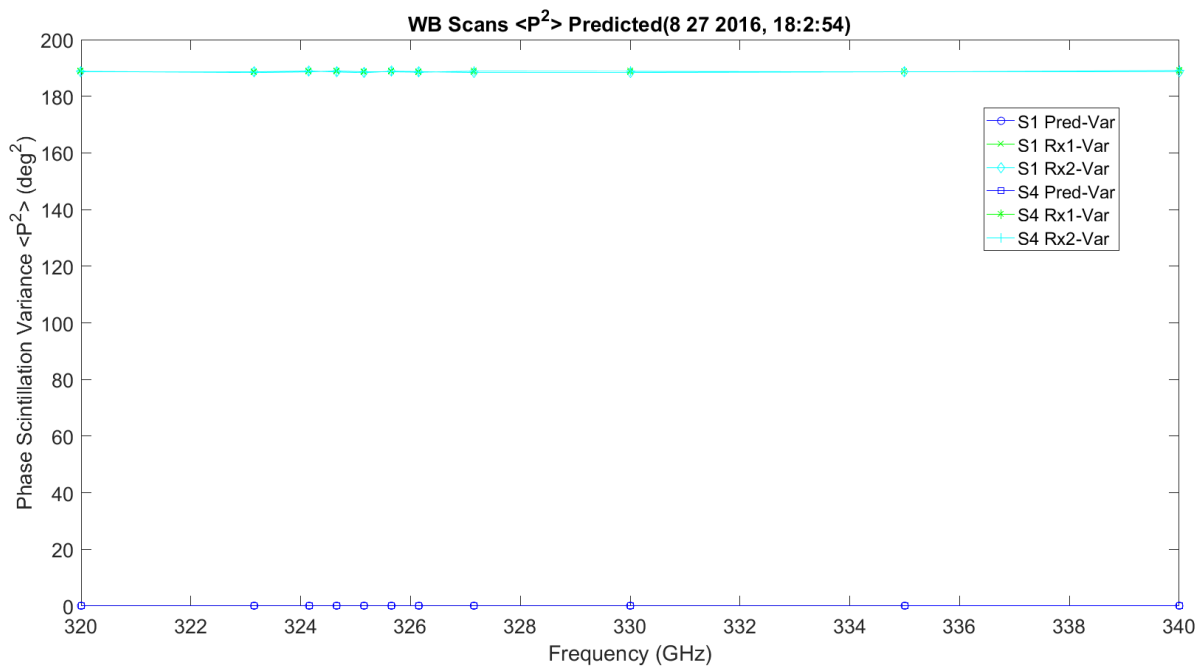


Figure 3.60. WB Phase Scintillation with Prediction.

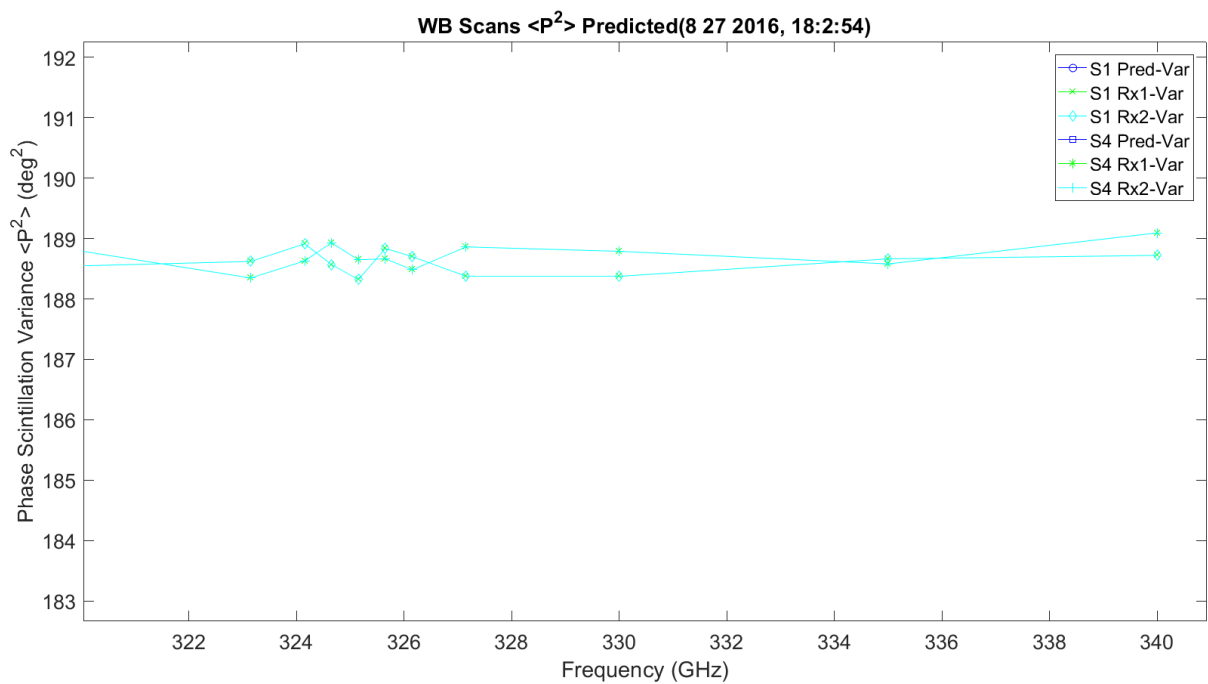


Figure 3.61. WB Phase Scintillation.

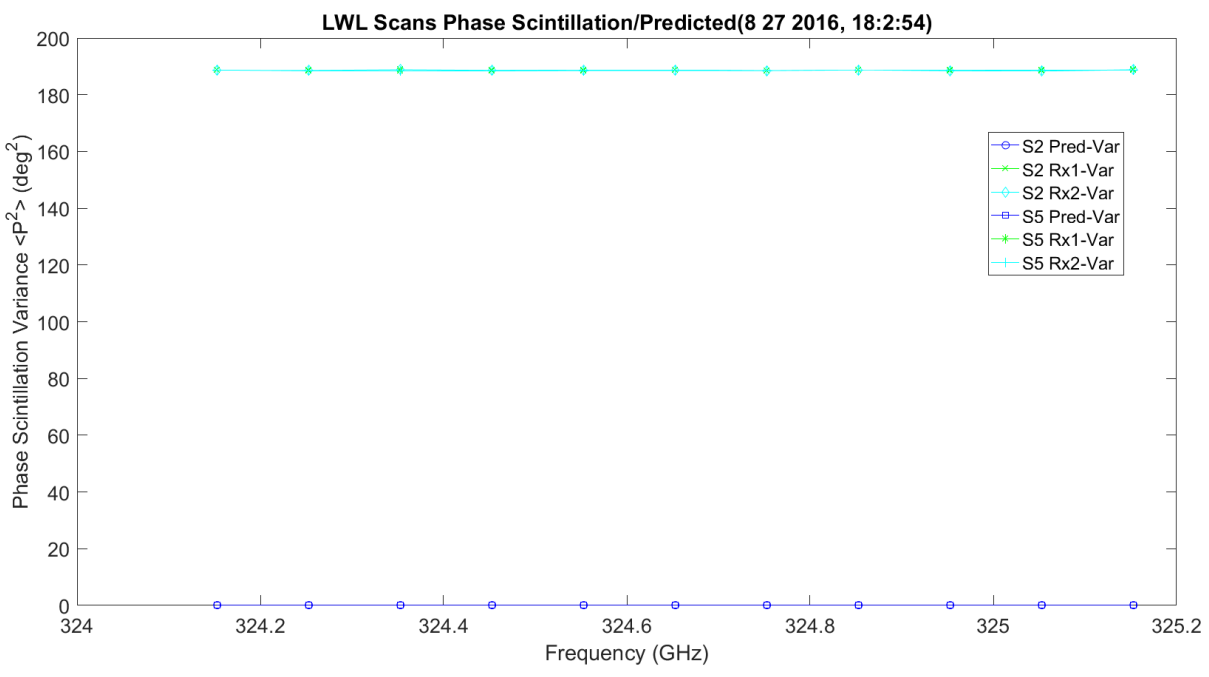


Figure 3.62. LWL Phase Scintillation with Prediction.

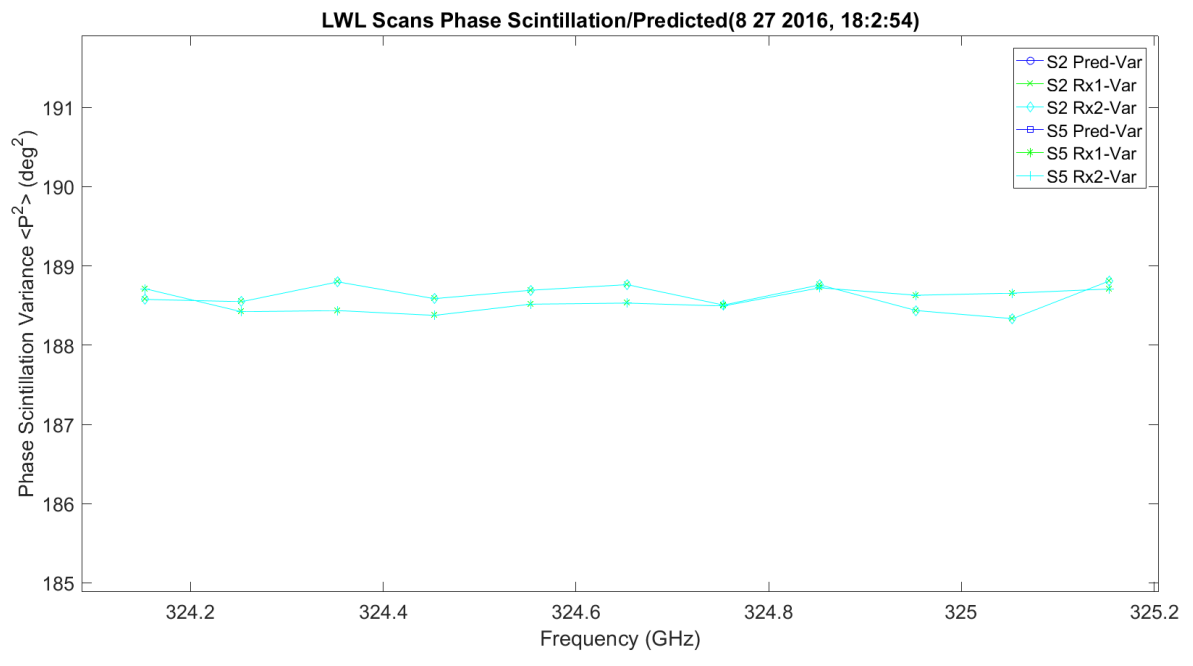


Figure 3.63. LWL Phase Scintillation.

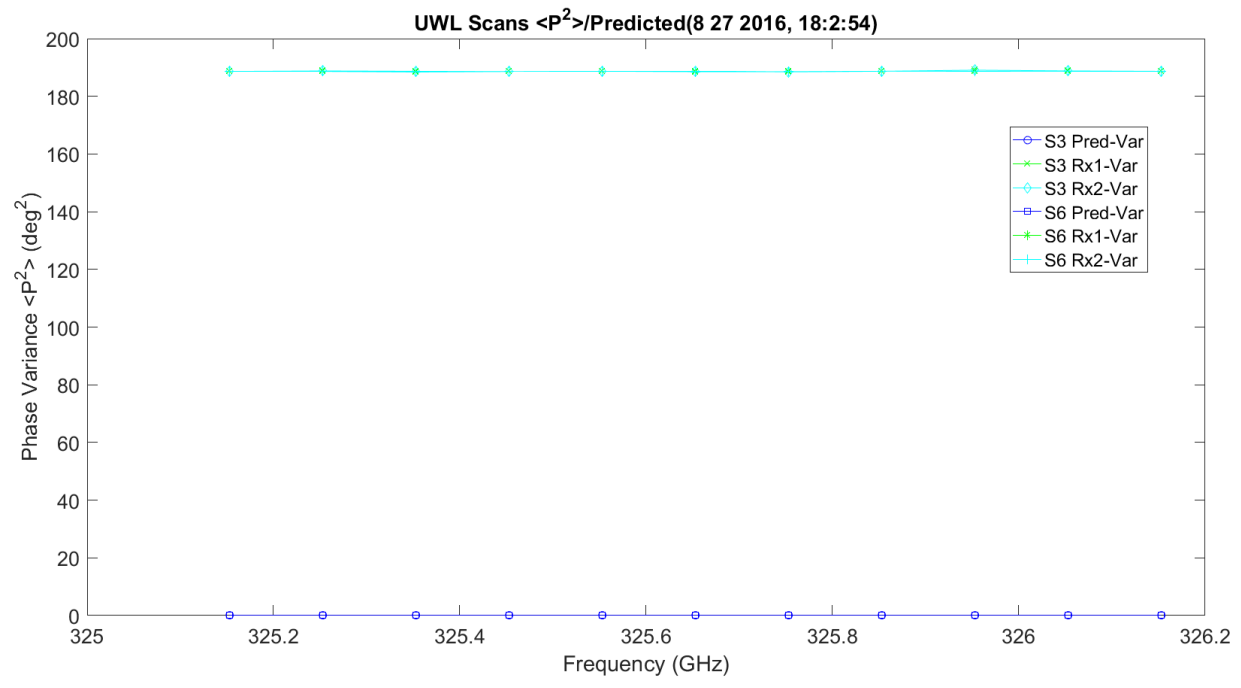


Figure 3.64. UWL Phase Scintillation with Prediction.

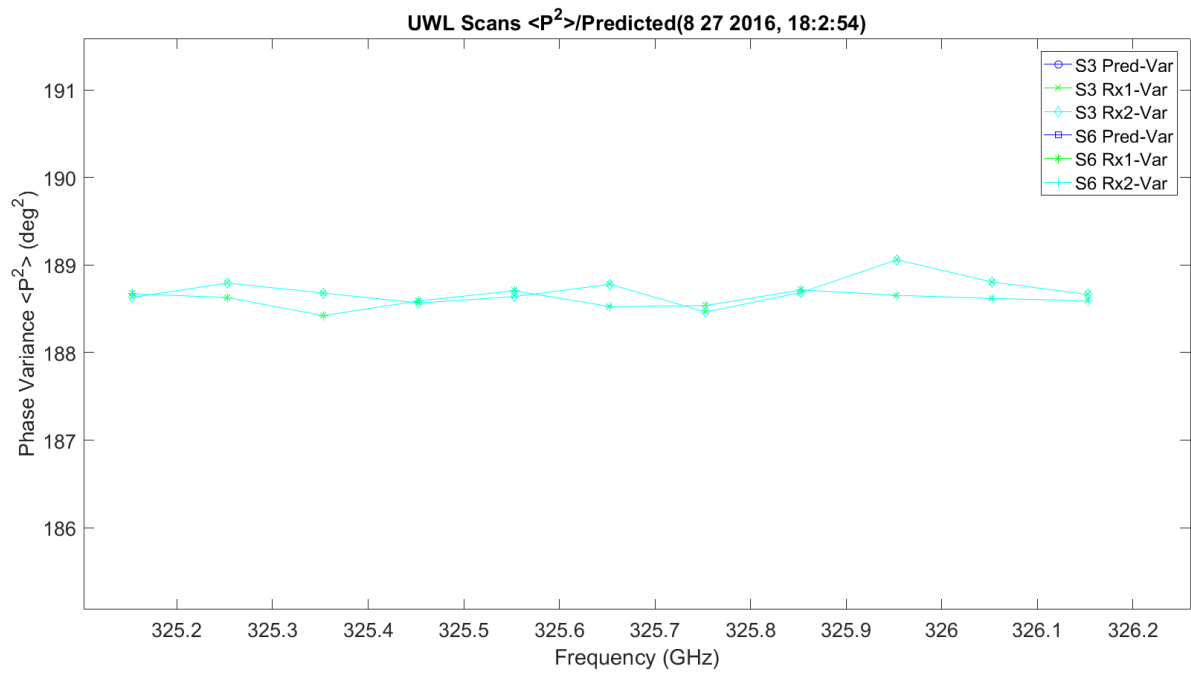


Figure 3.65. UWL Phase Scintillation.

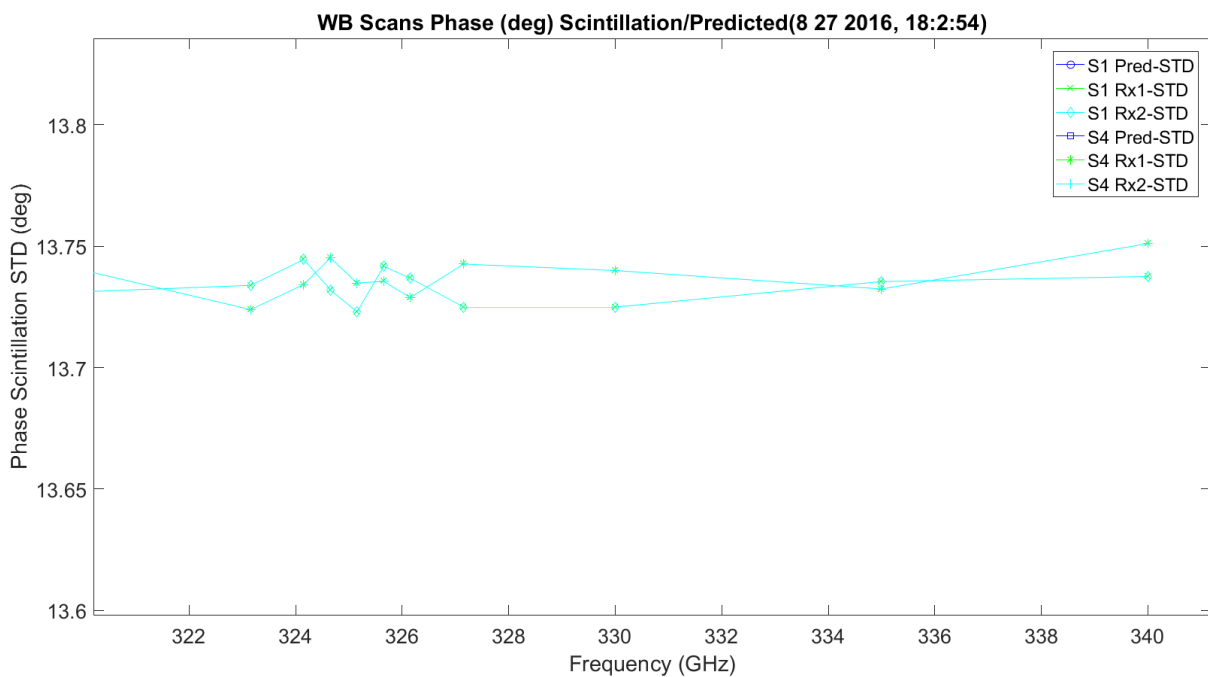


Figure 3.66. WB Phase Scintillation STD Degrees.

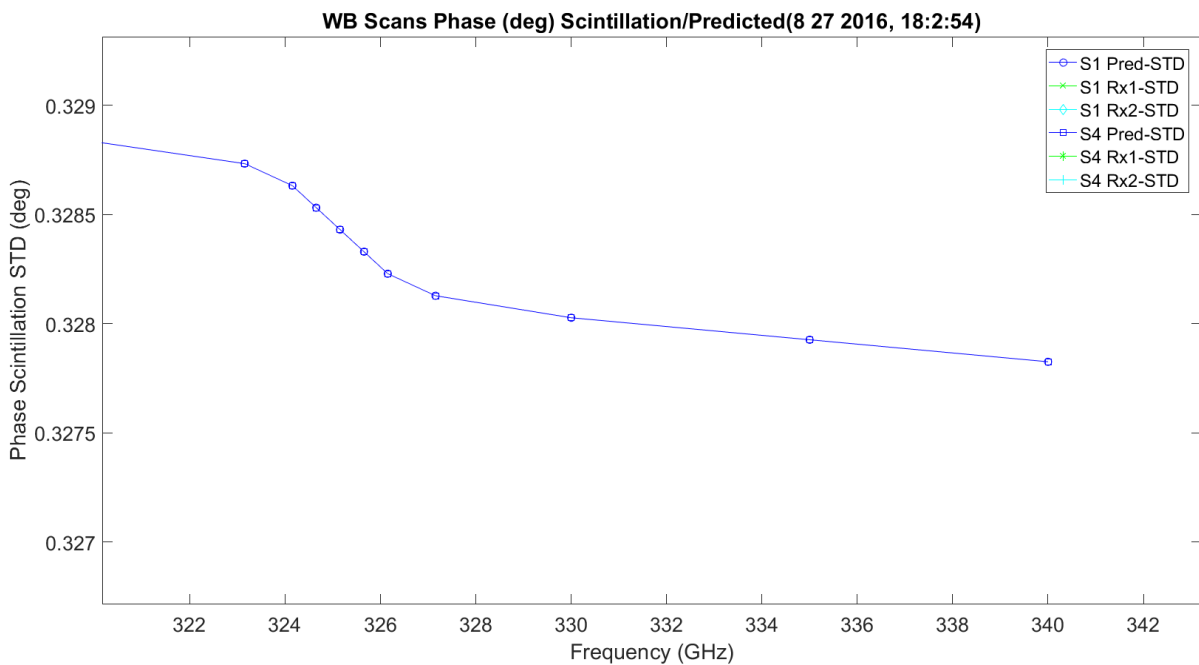


Figure 3.67. WB Phase Scintillation STD Prediction Degrees.

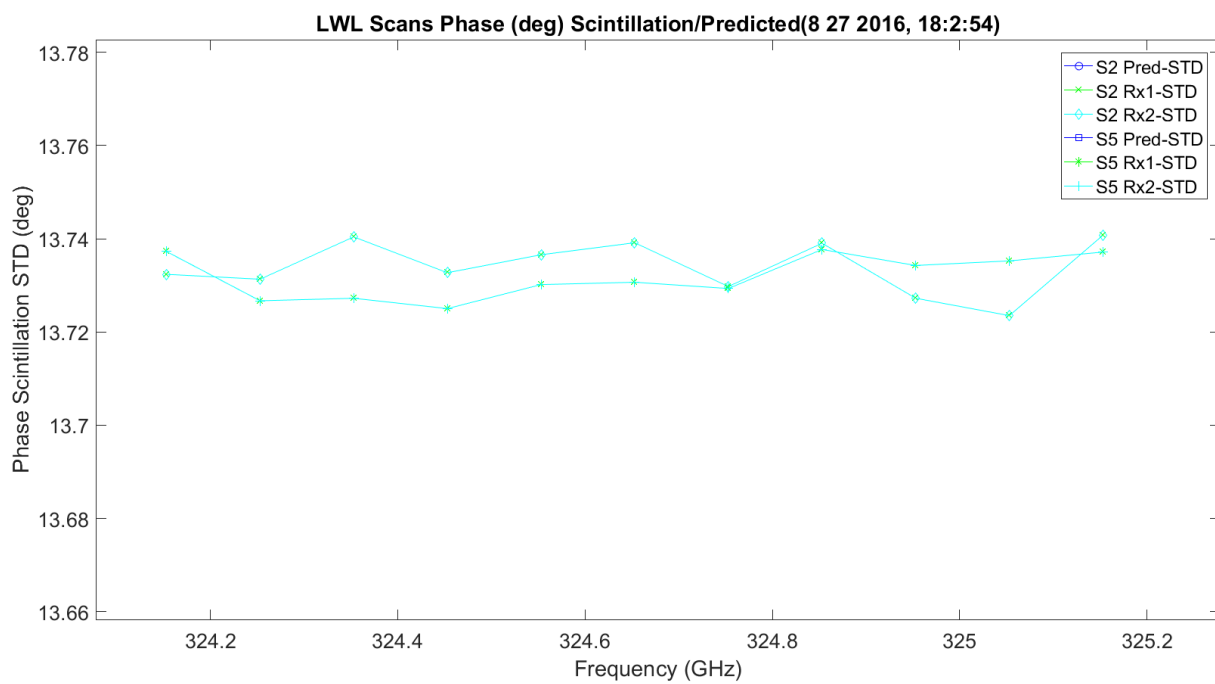


Figure 3.68. LWL Phase Scintillation STD Degrees.

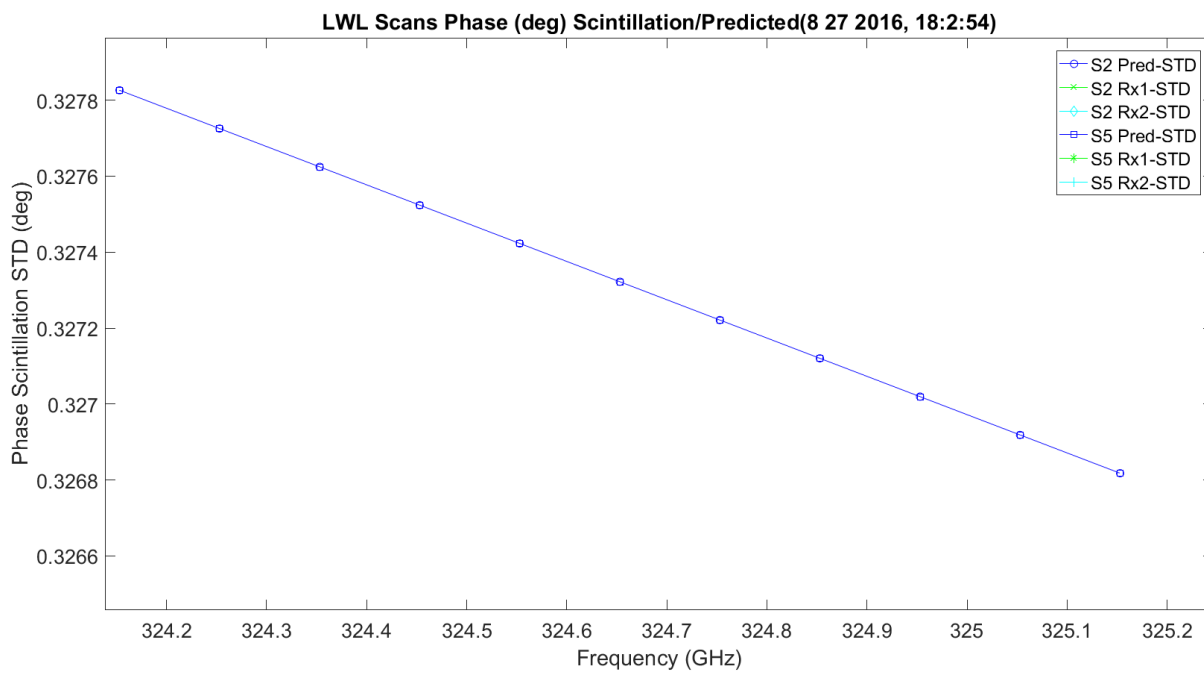


Figure 3.69. LWL Phase Scintillation STD Prediction Degrees.

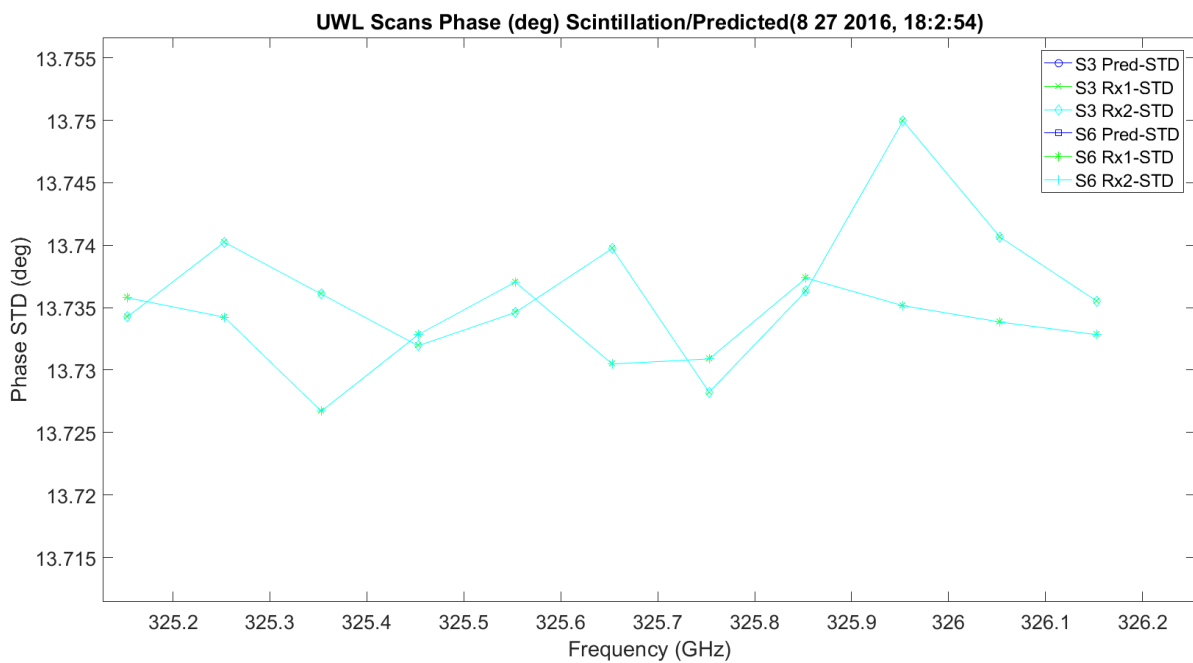


Figure 3.70. UWL Phase Scintillation STD Degrees.

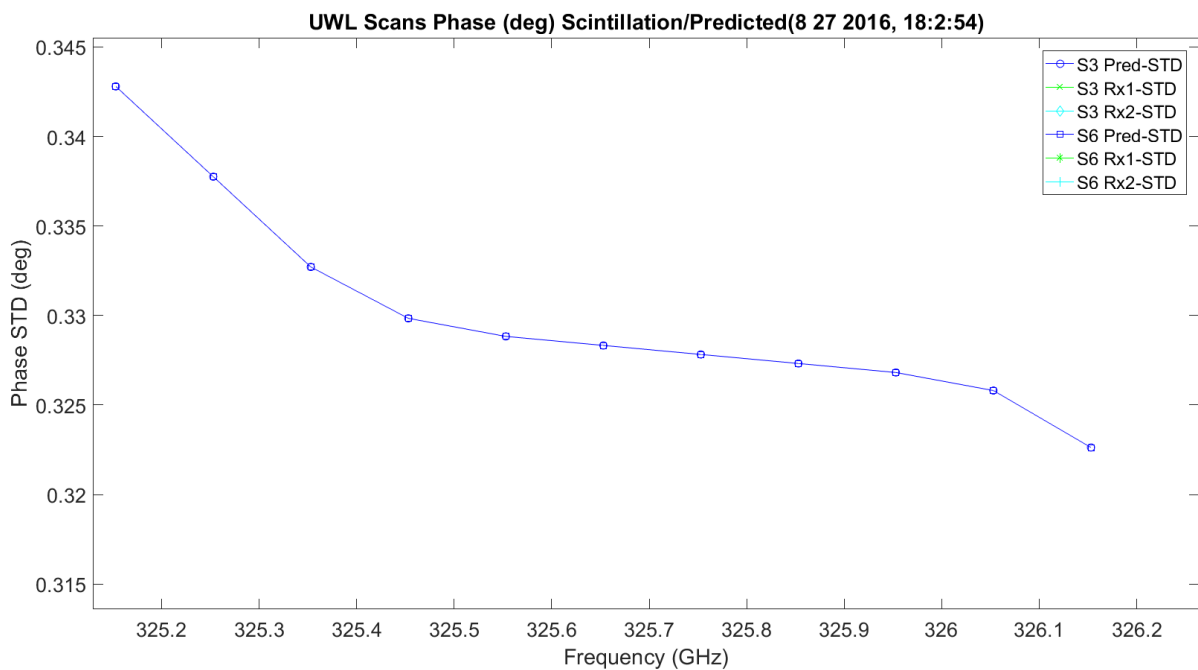


Figure 3.71. UWL Phase Scintillation STD Prediction Degrees.

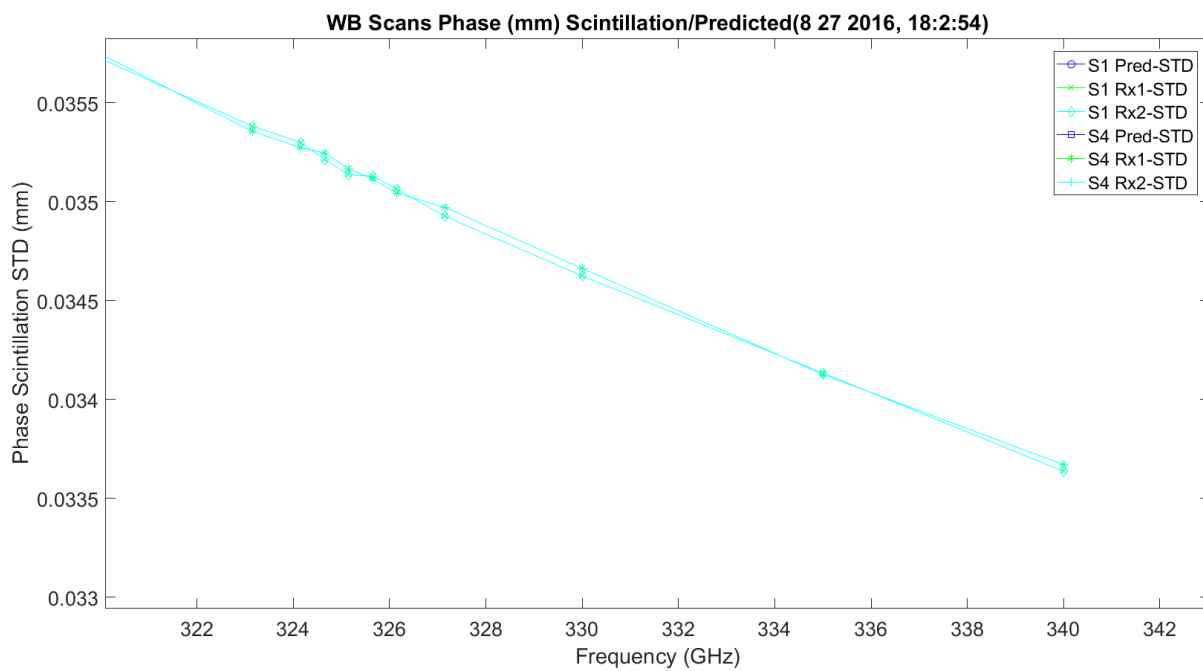


Figure 3.72. WB Phase Scintillation STD Millimeters.

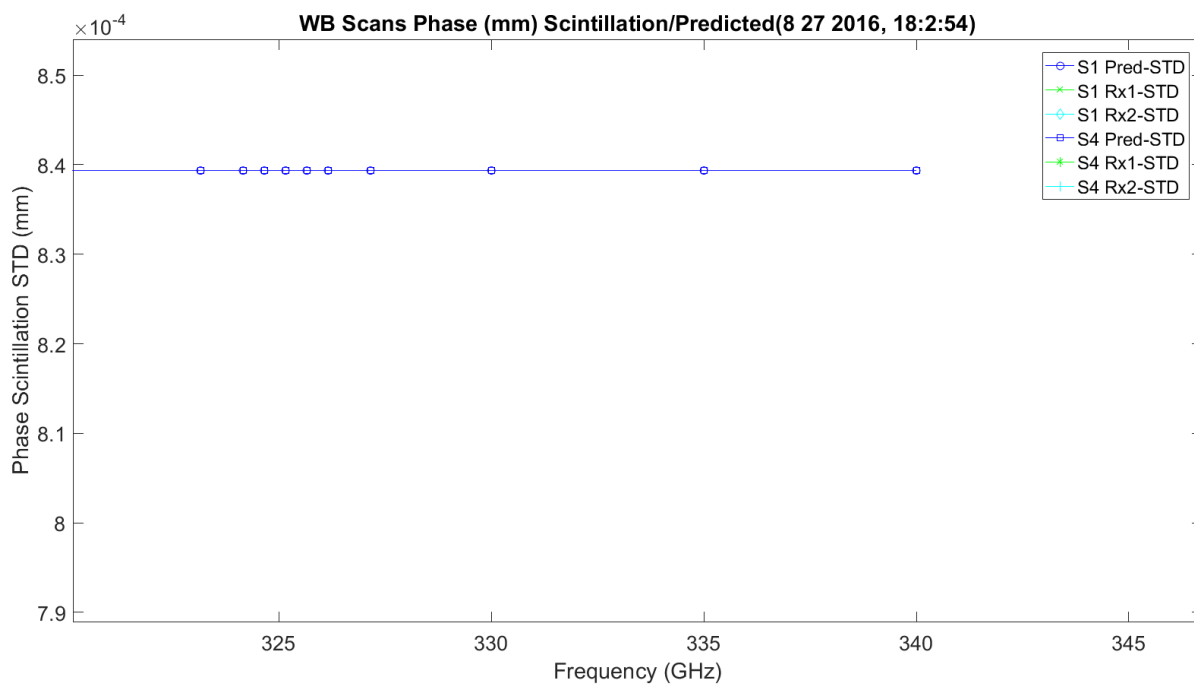


Figure 3.73. WB Phase Scintillation STD Prediction Millimeters.

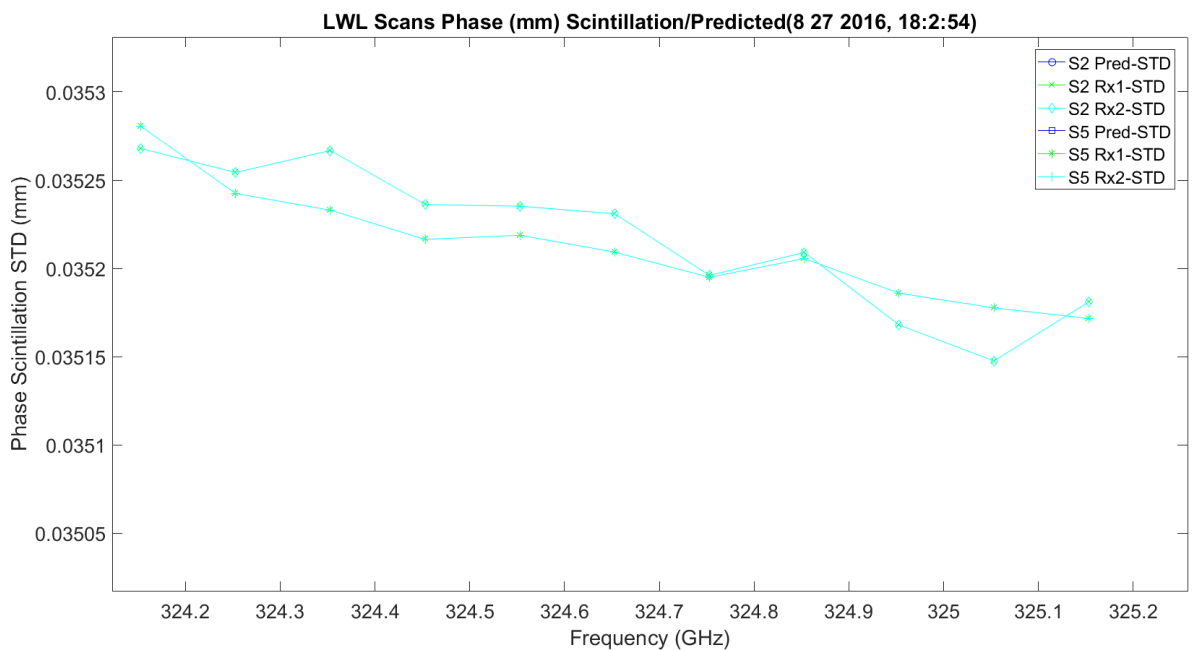


Figure 3.74. LWL Phase Scintillation STD Millimeters.

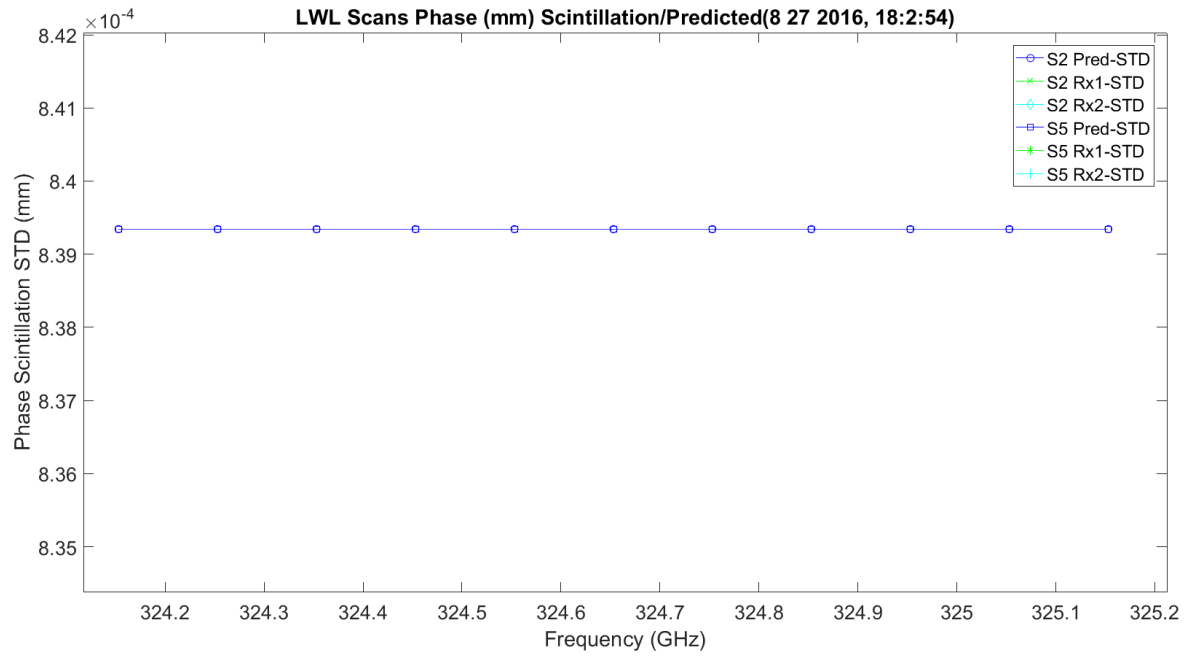


Figure 3.75. LWL Phase Scintillation STD Prediction Millimeters.

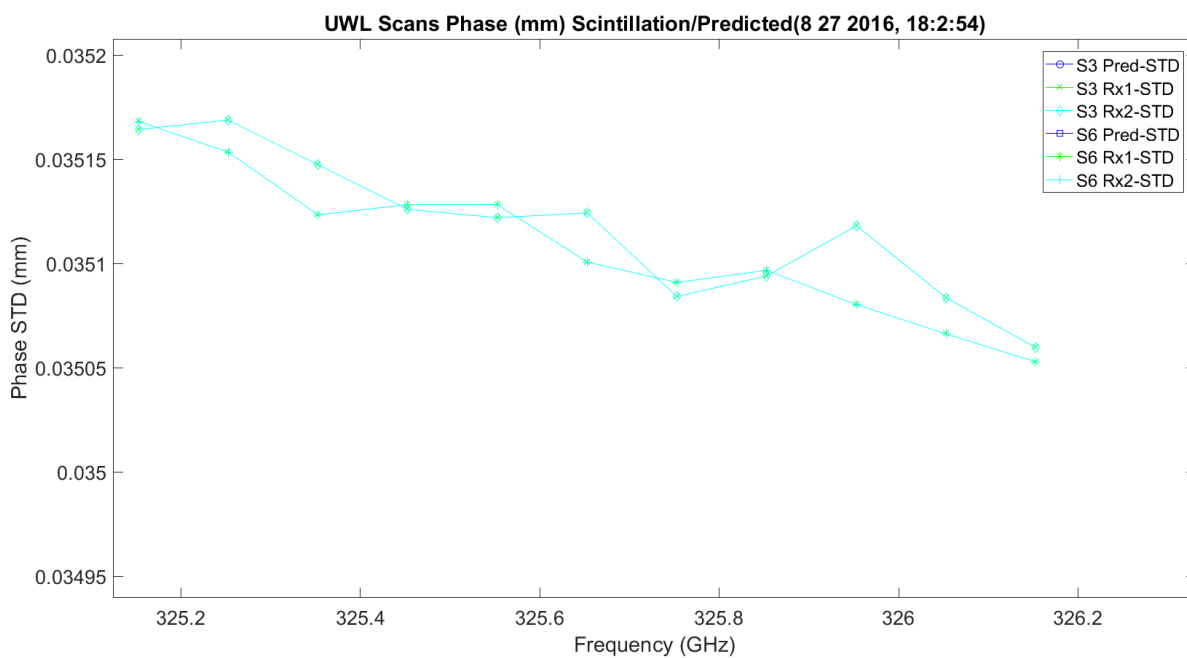


Figure 3.76. UWL Phase Scintillation STD Millimeters.

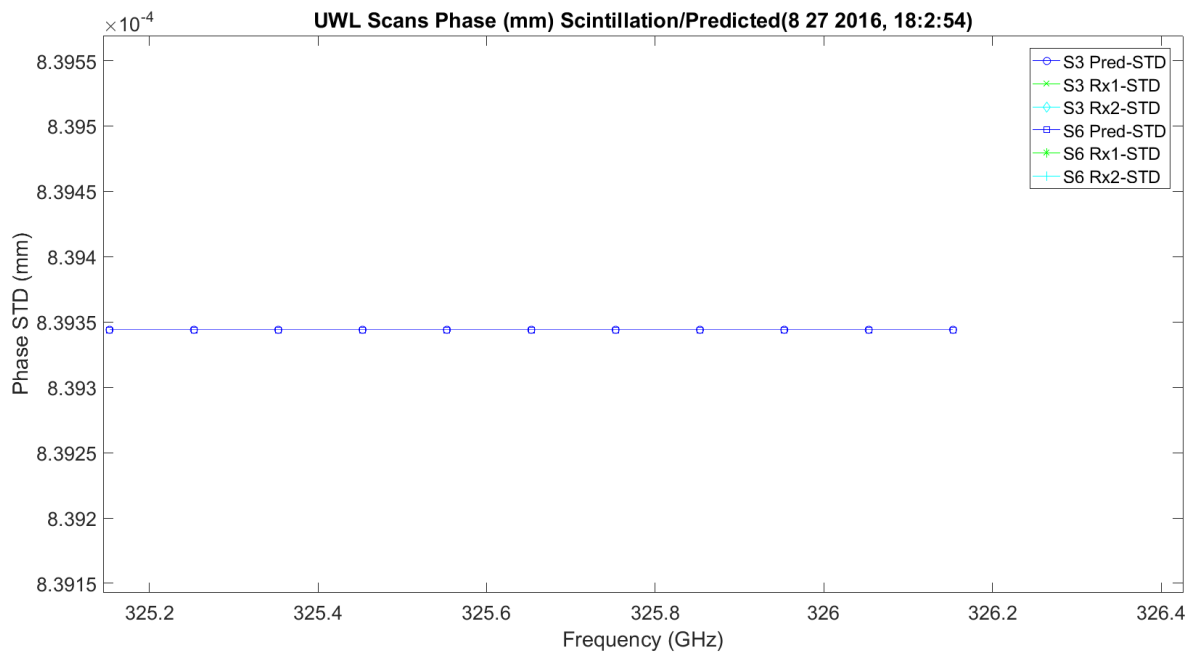


Figure 3.77. UWL Phase Scintillation STD Prediction Millimeters.

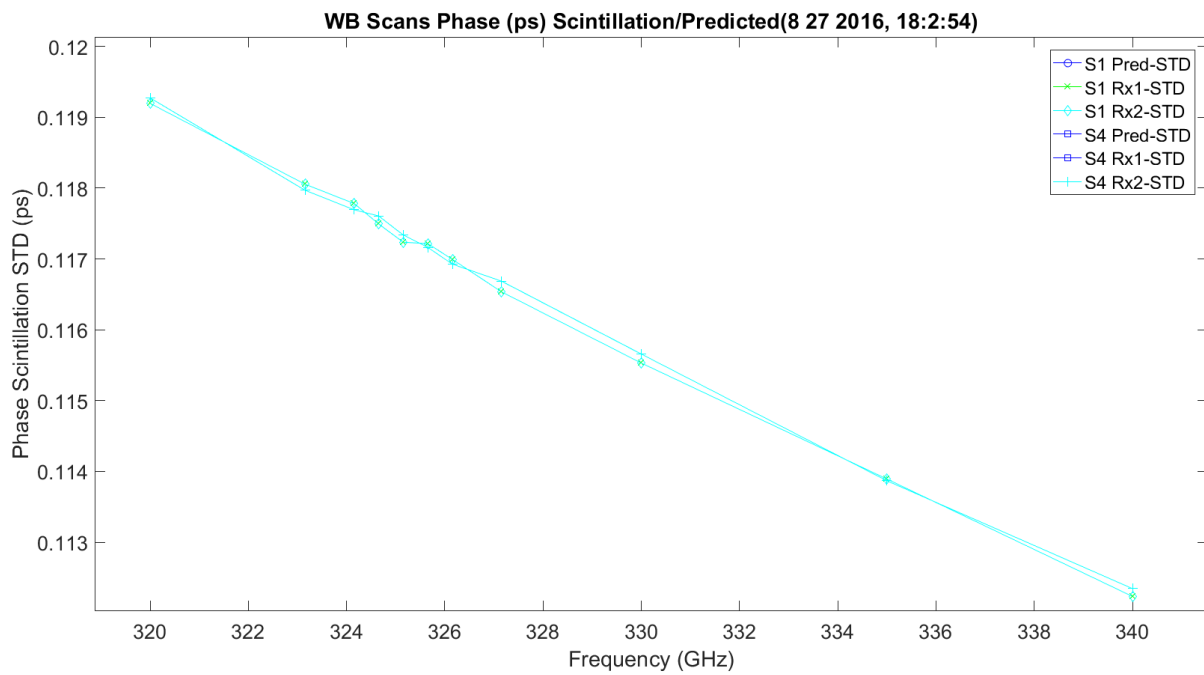


Figure 3.78. WB Phase Scintillation STD Picoseconds.

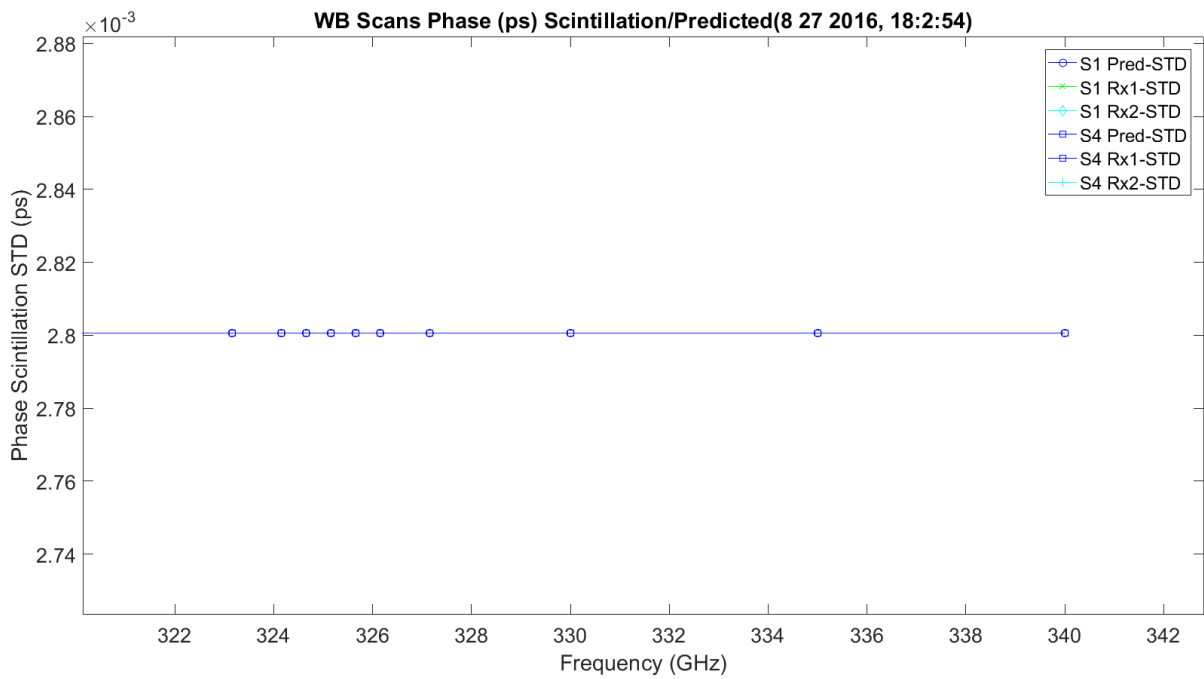


Figure 3.79. WB Phase Scintillation STD Prediction Picoseconds.

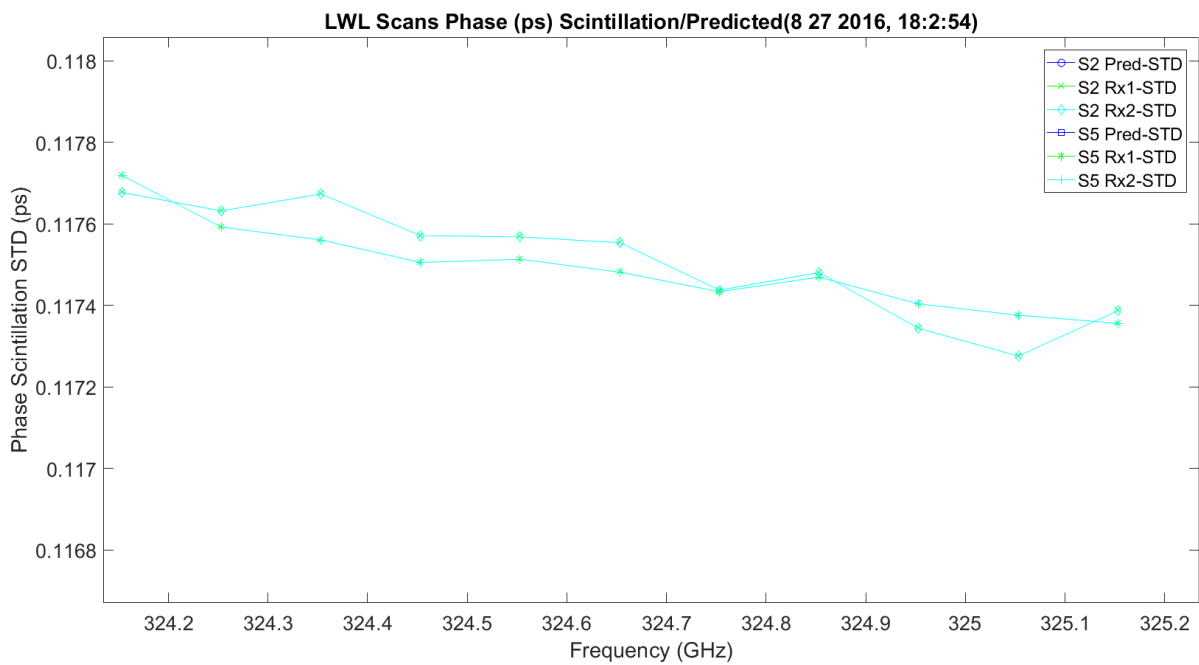


Figure 3.80. LWL Phase Scintillation STD Picoseconds.

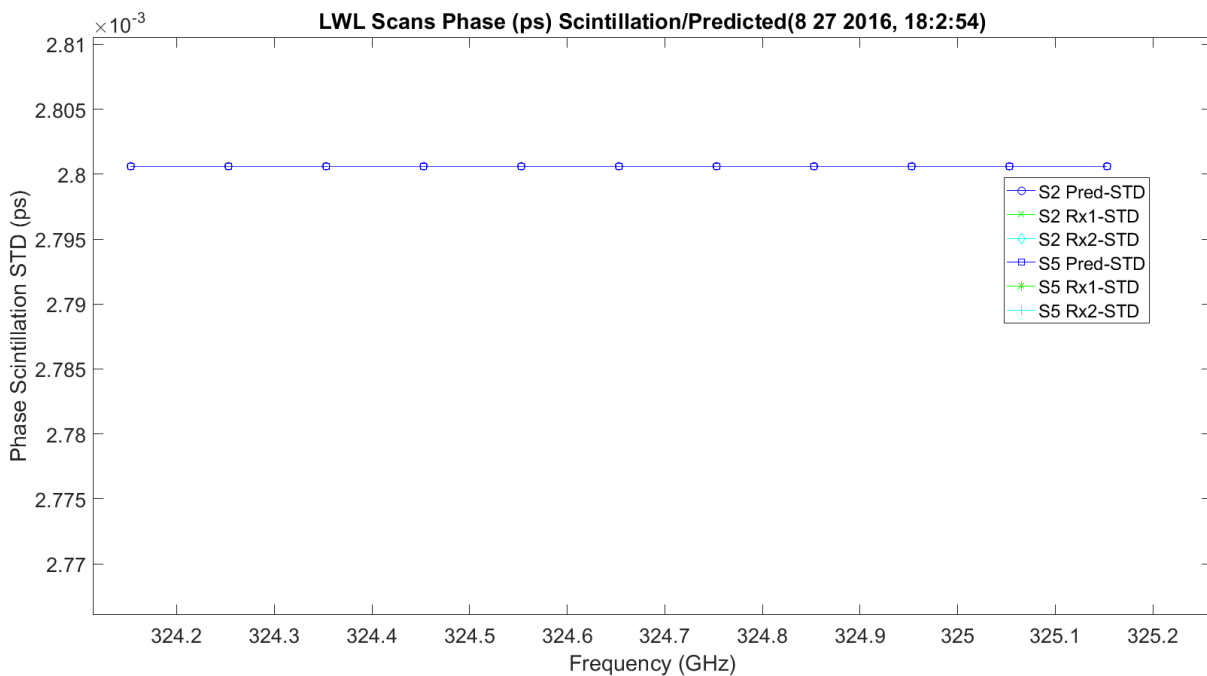


Figure 3.81. LWL Phase Scintillation STD Prediction Picoseconds.

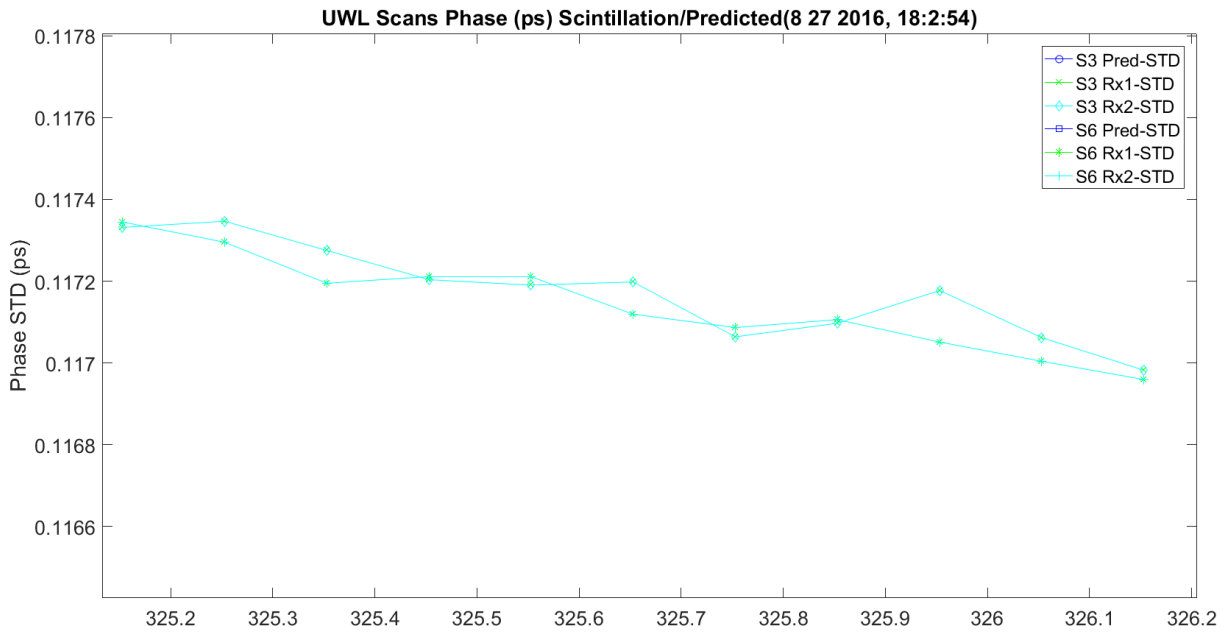


Figure 3.82. UWL Phase Scintillation STD Picoseconds.

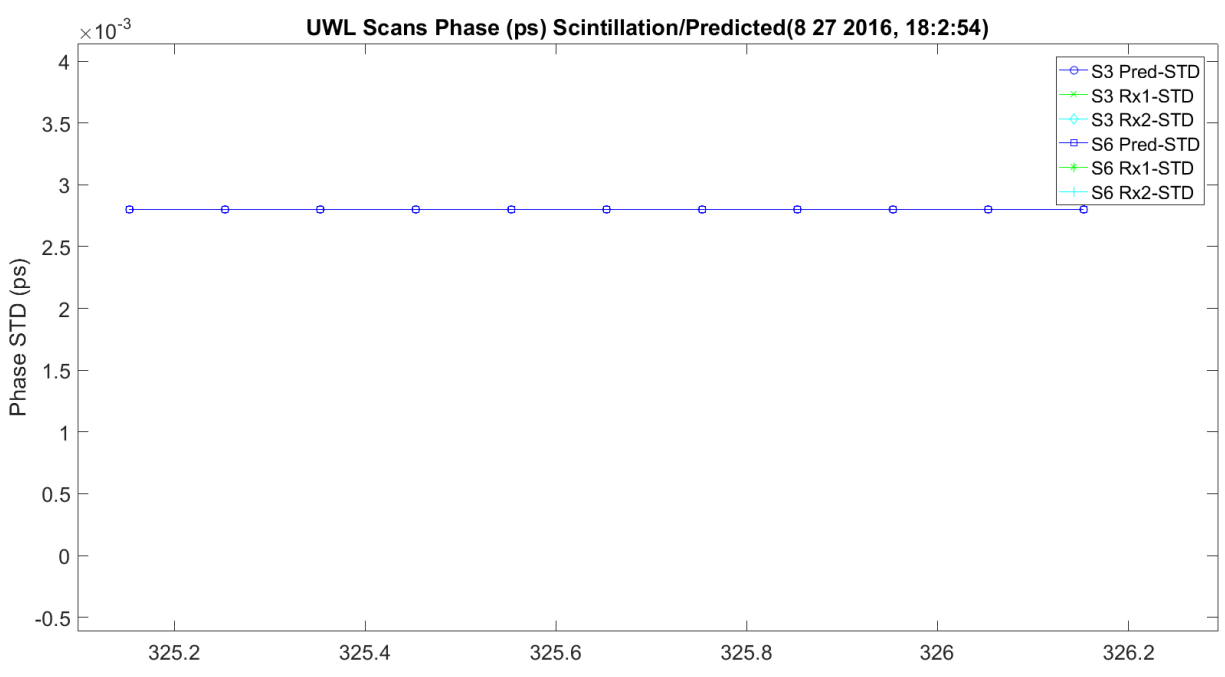


Figure 3.83. UWL Phase Scintillation STD Prediction Picoseconds.

Figure 3.84 – Figure 3.92 show the amplitude and phase scintillation correlation, $\langle \chi\phi \rangle$, for all the scans, three each: total view of predicted and hallway data; view of predicted data; and view of hallway data. The prediction utilizes the Rytov, Fresnel and Fruanhofer versions. In the case of the real data, the correlation becomes stronger as frequency is increased, especially around the absorption peak.

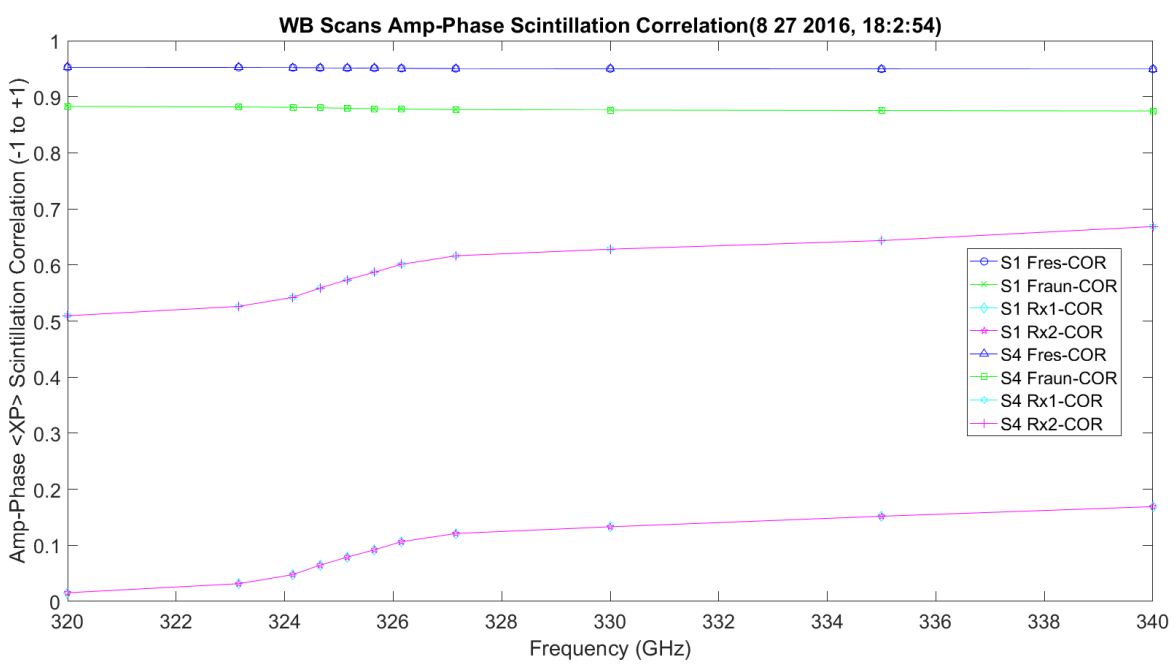


Figure 3.84. WB Amplitude/Phase Scintillation Cross Correlation with Prediction.

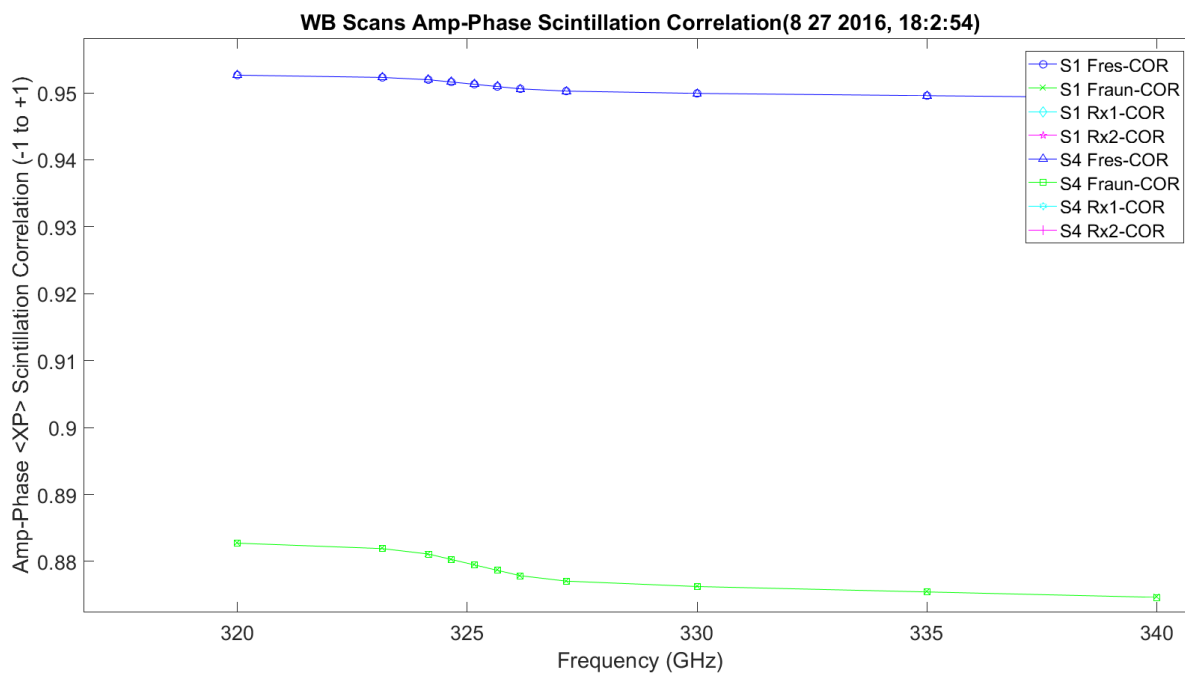


Figure 3.85. WB Amplitude/Phase Scintillation Cross Correlation Prediction.

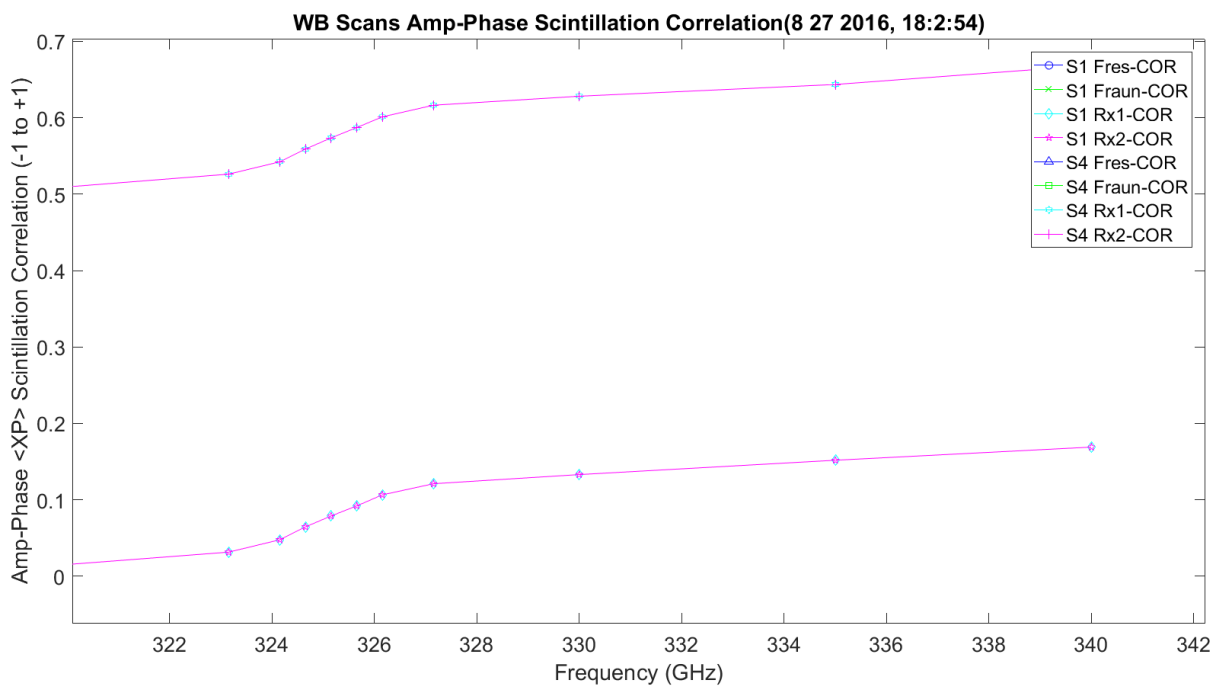


Figure 3.86. WB Amplitude/Phase Scintillation Cross Correlation Hallway Data.

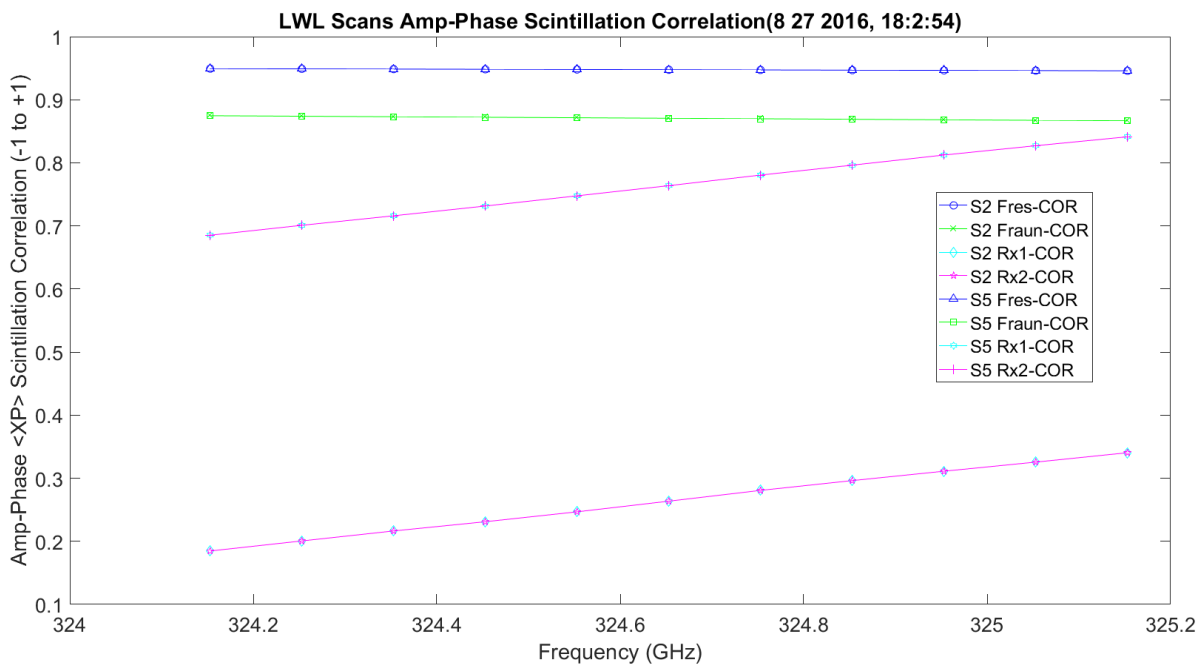


Figure 3.87. LWL Amplitude/Phase Scintillation Cross Correlation with Prediction.

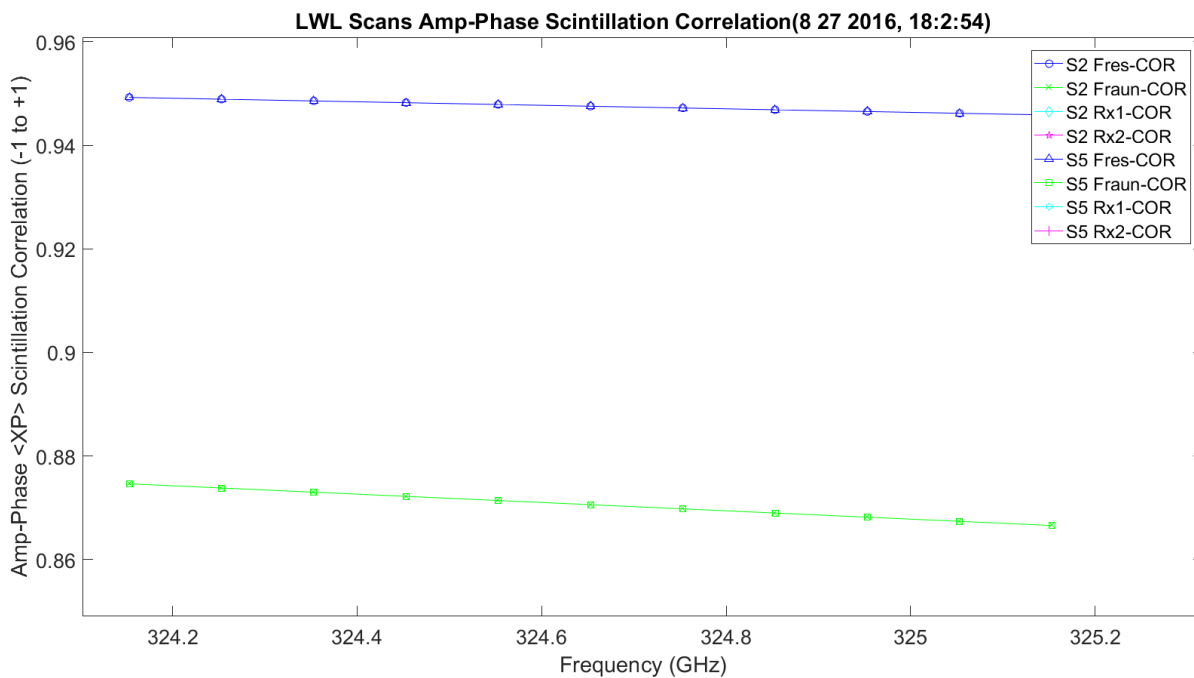


Figure 3.88. LWL Amplitude/Phase Scintillation Cross Correlation Prediction Data.

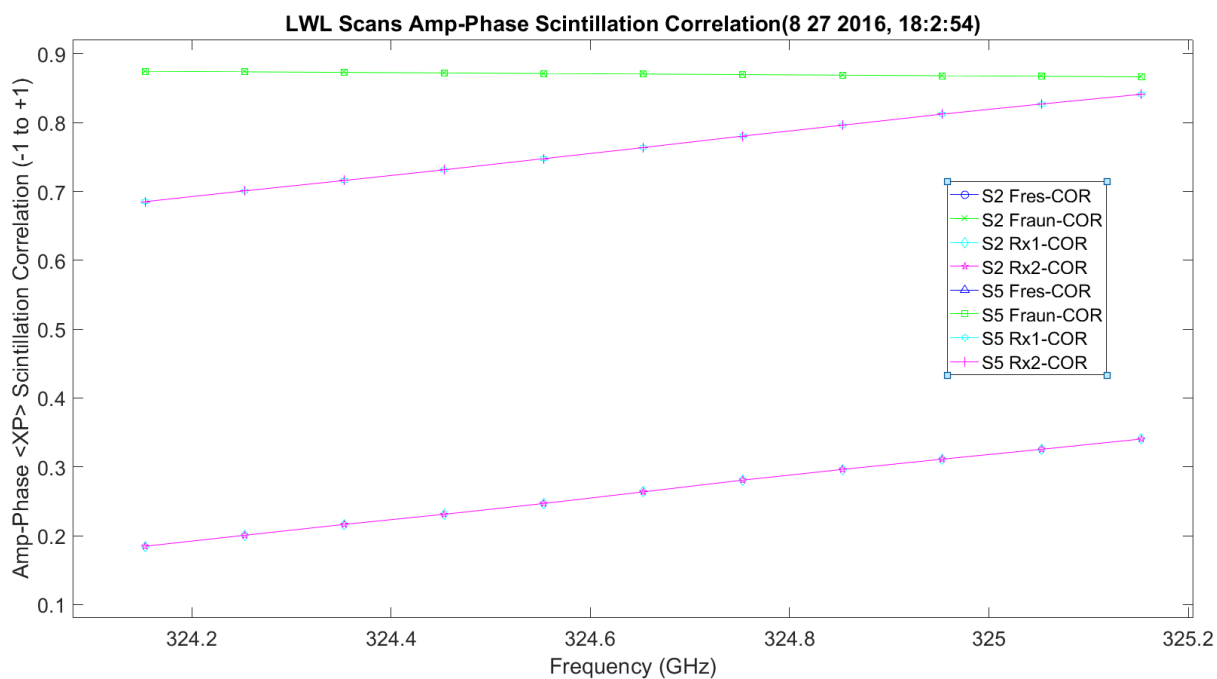


Figure 3.89. LWL Amplitude/Phase Scintillation Cross Correlation Hallway Data.

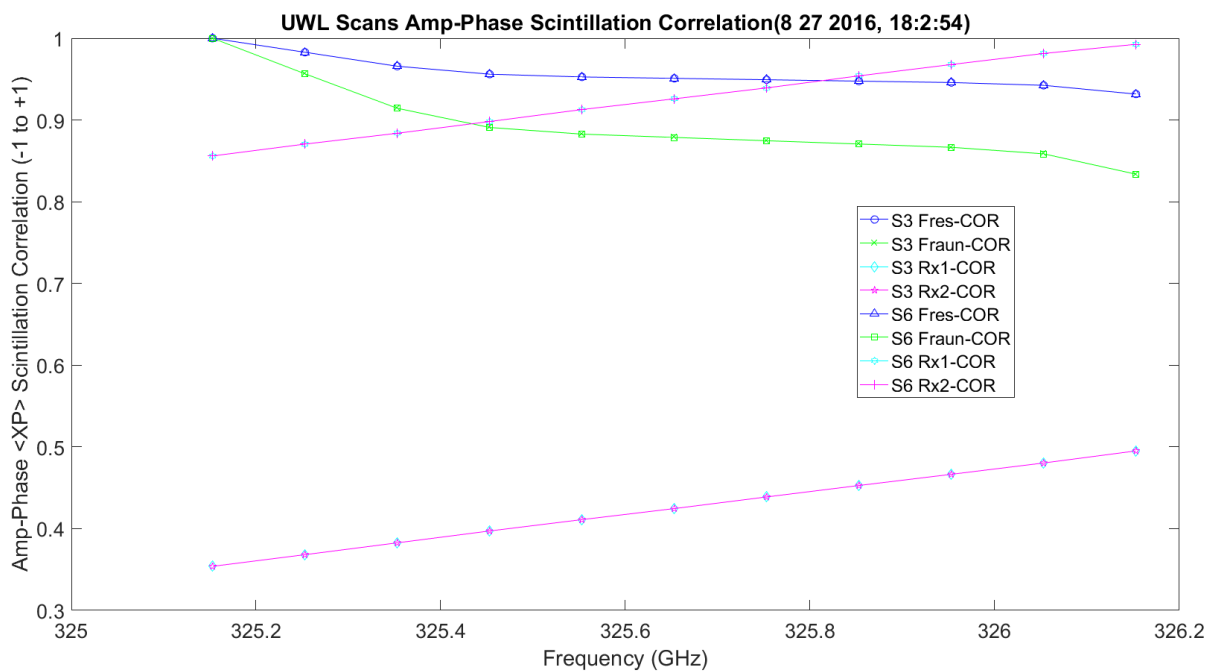


Figure 3.90. UWL Amplitude/Phase Scintillation Cross Correlation with Prediction.

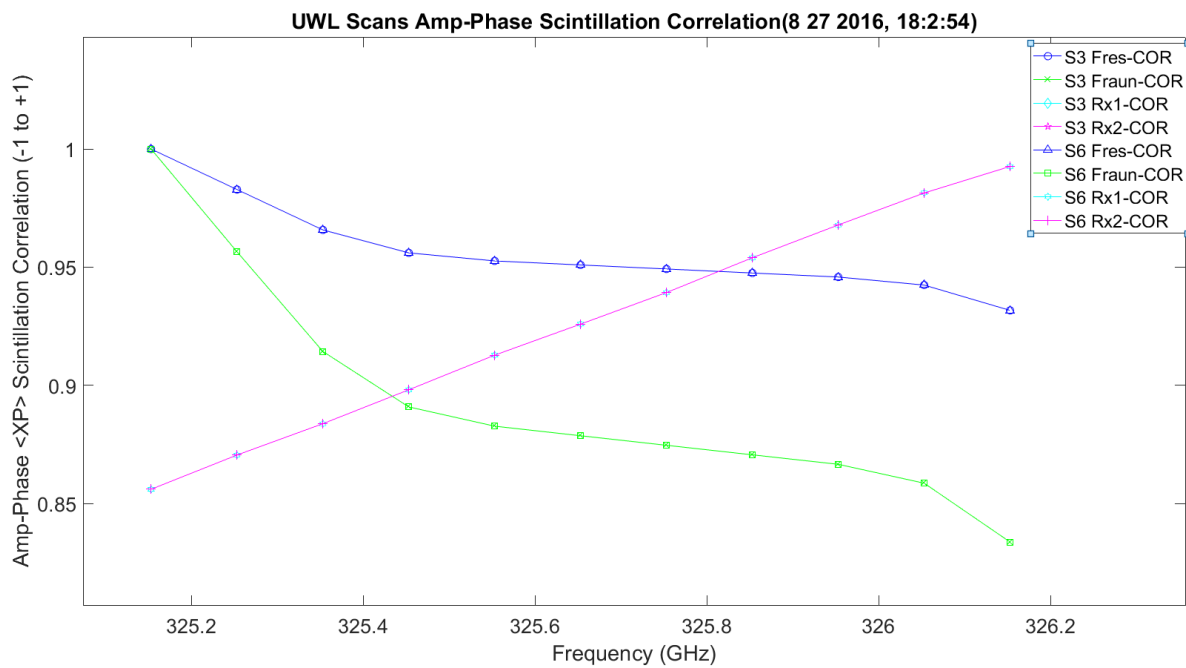


Figure 3.91. UWL Amplitude/Phase Scintillation Cross Correlation Prediction Data.

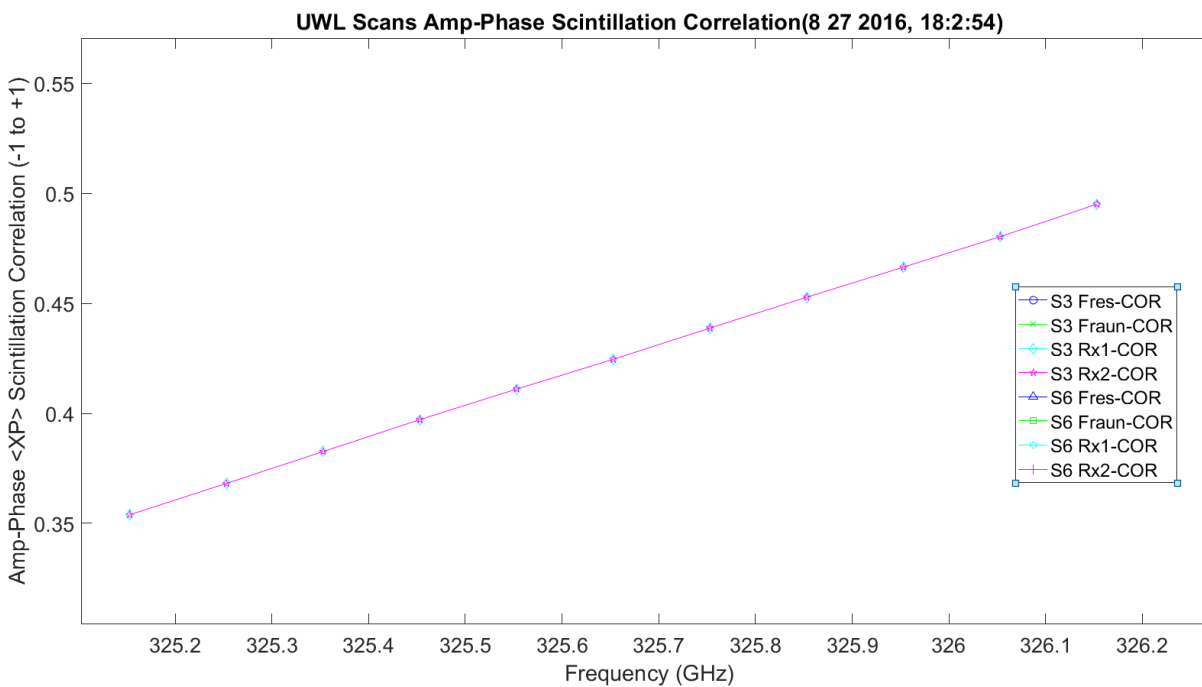


Figure 3.92. UWL Amplitude/Phase Scintillation Cross Correlation Hallway Data.

Figure 3.93 shows a plot of C_T^2 for the hallway experiment. Figure 3.94 shows a plot of C_Q^2 for the hallway experiment. Figure 3.95 shows a plot of C_{TQ} for the hallway experiment.

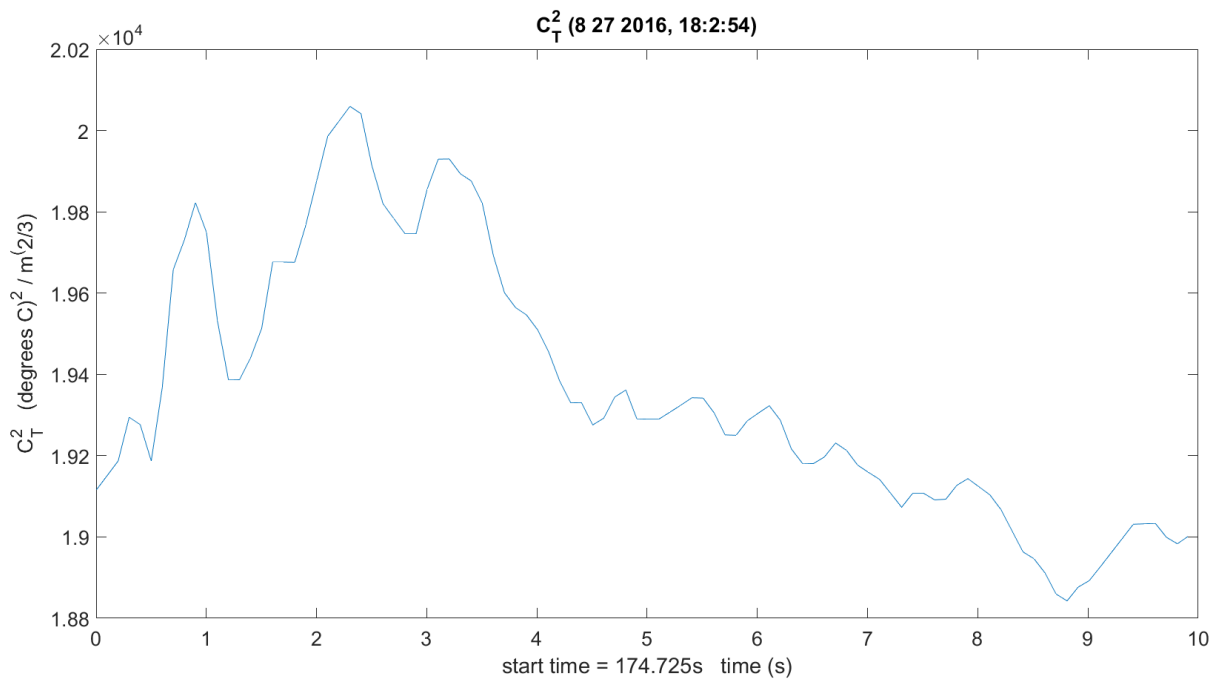


Figure 3.93. C_T^2 Hallway Data.

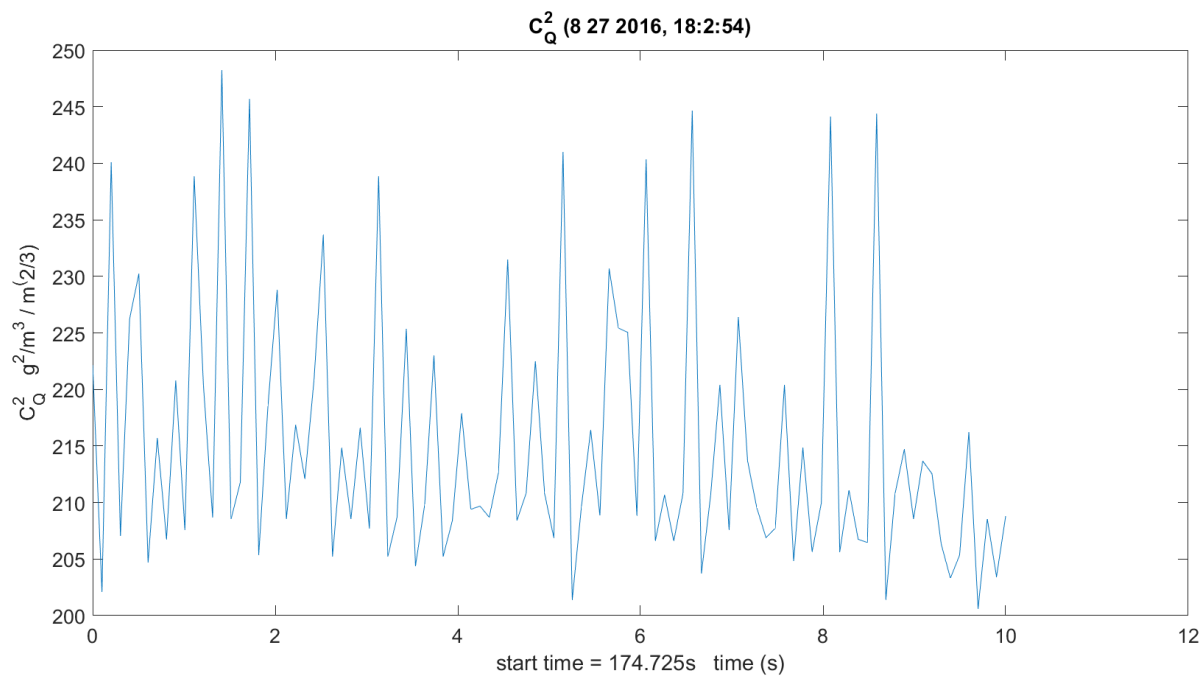


Figure 3.94. C_Q^2 Hallway Data.

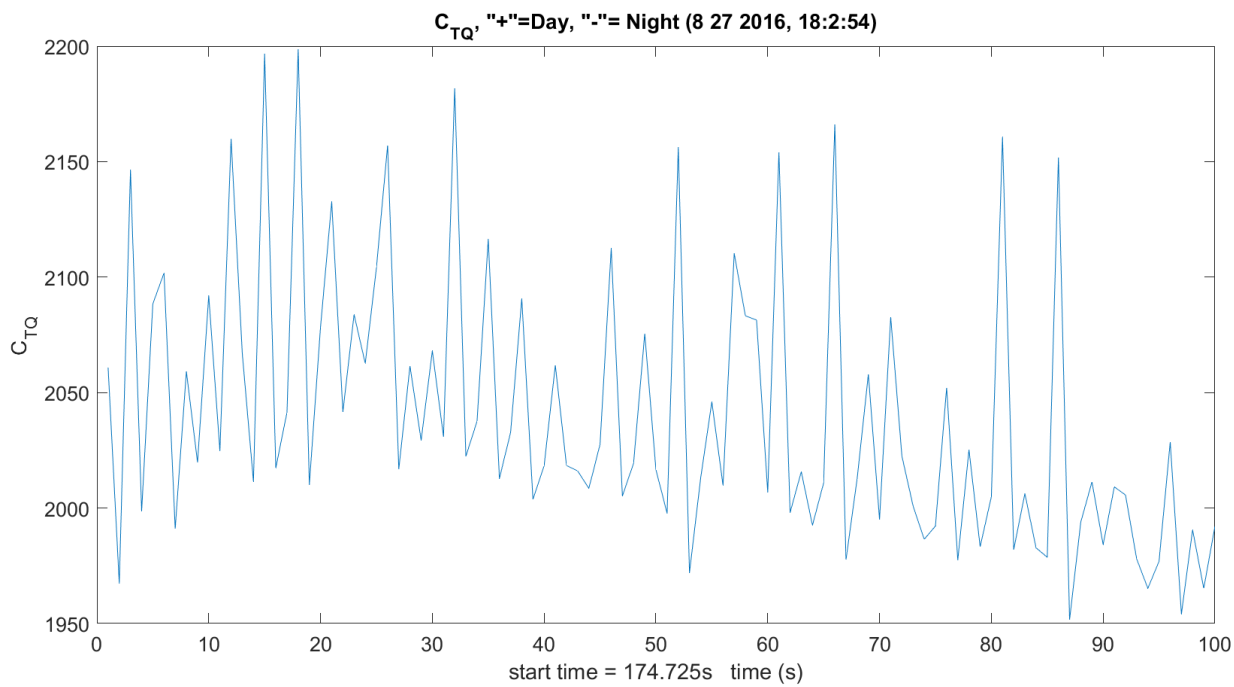


Figure 3.95. C_{TQ} Hallway Data.

Figure 3.96 shows a plot of C_n^2 correlated with amplitude scintillation. This is very low correlation. It should change over a longer path and when the scintillometer is collected at the same time on the identical path.

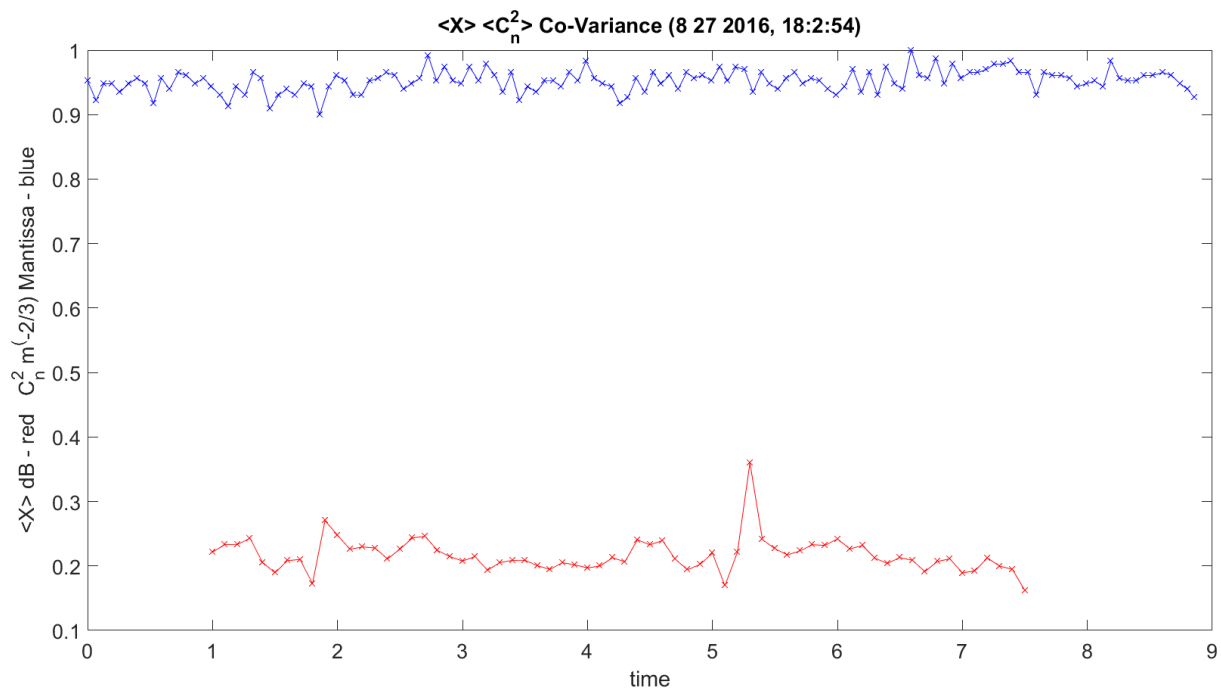


Figure 3.96. Amplitude Scintillation Correlated with C_n^2 Hallway Data.

Figure 3.97 shows a plot of C_T^2 correlated with amplitude scintillation. This data was collected at the same time on the identical path. This is very low correlation.

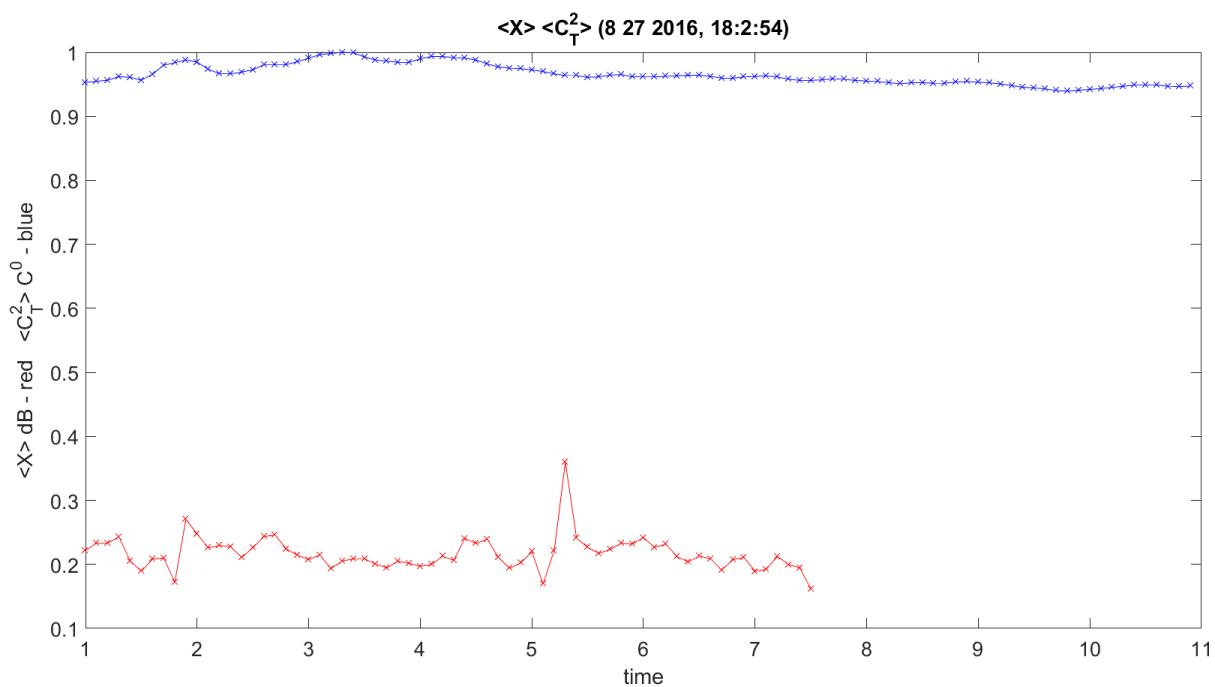


Figure 3.97. Amplitude Scintillation Correlated with C_T^2 Hallway Data.

Figure 3.98 shows a plot of C_Q^2 correlated with amplitude scintillation. This has very low correlation. This data was collected at the same time on the identical path.

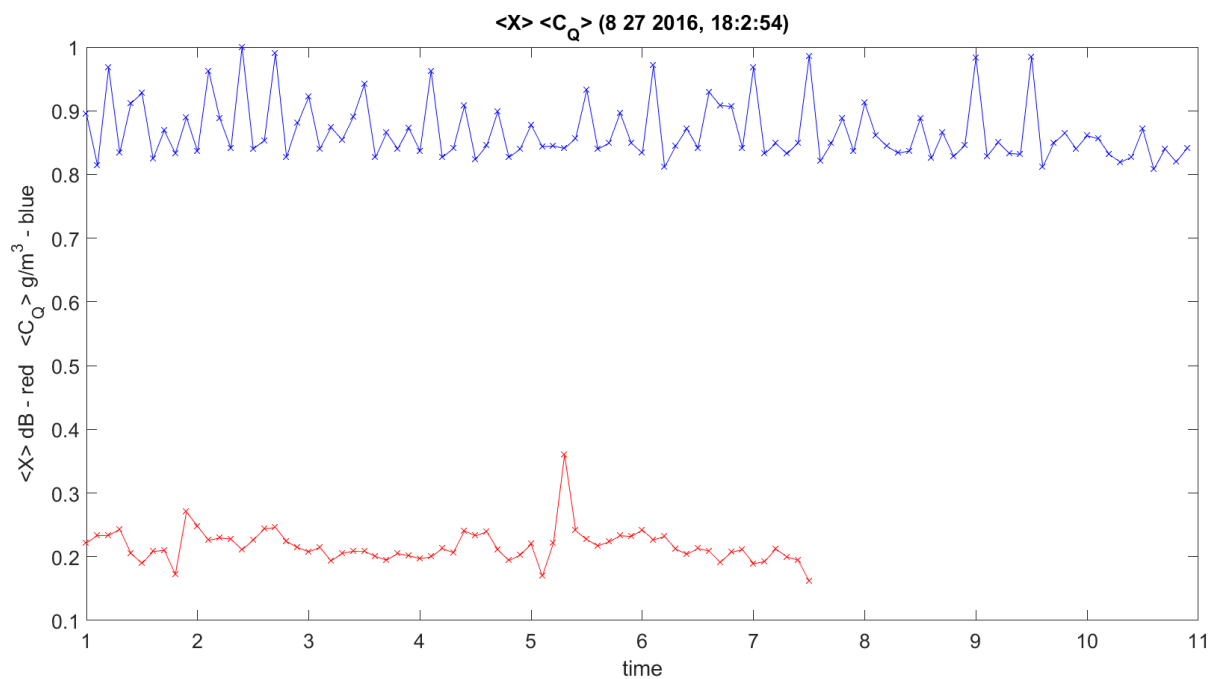


Figure 3.98. Amplitude Scintillation Correlated with C_Q^2 Hallway Data.

Figure 3.99 shows a plot of C_n^2 correlated with phase scintillation. This is higher correlation. This should change over a longer path and when the scintillometer is collected at the same time on the identical path.

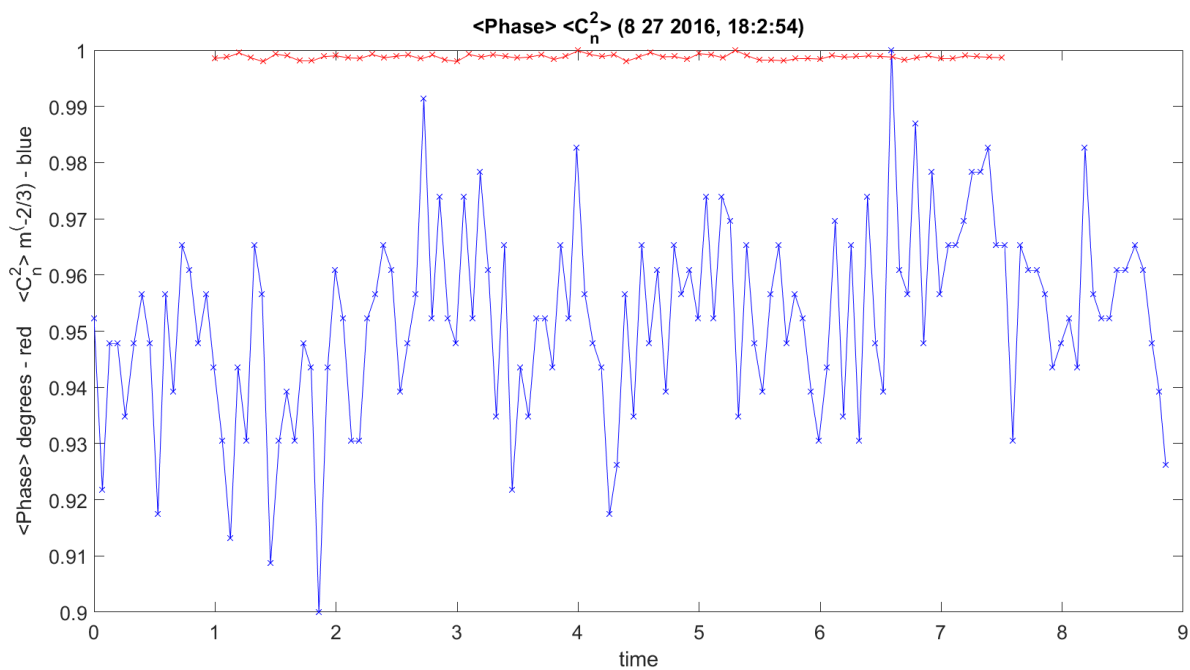


Figure 3.99. Phase Scintillation Correlated with C_n^2 Hallway Data.

Figure 3.100 shows a plot of C_n^2 correlated with phase scintillation. This has higher correlation.

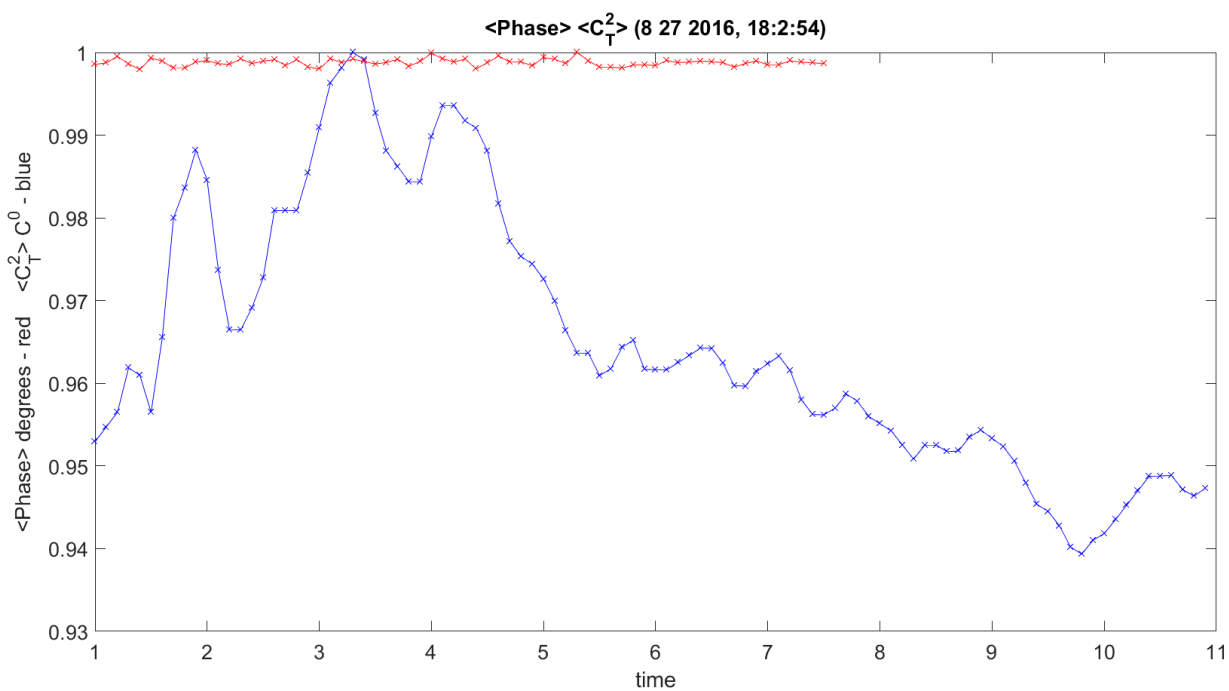


Figure 3.100. Phase Scintillation Correlated with C_n^2 Hallway Data.

Figure 3.101 shows a plot of C_Q^2 correlated with phase scintillation. This is higher correlation.

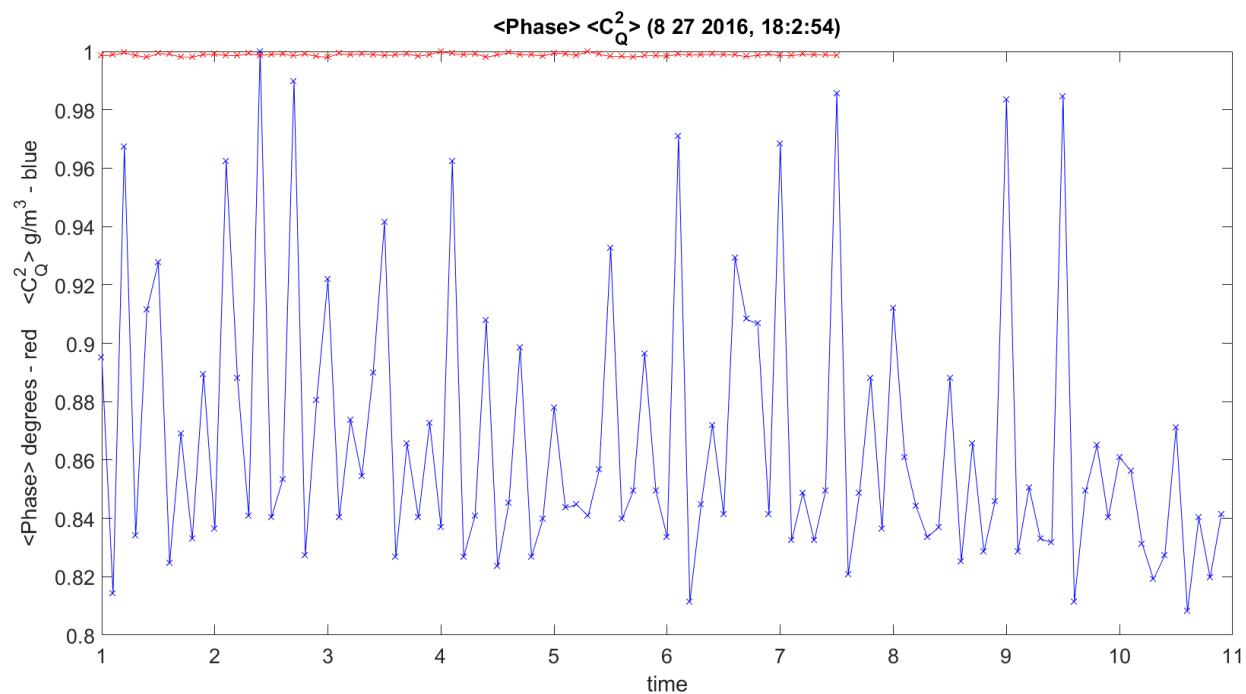


Figure 3.101. Phase Scintillation Correlated with C_Q^2 Hallway Data.

Figure 3.102 shows a plot of $C_T^2 C_n^2$ correlated with phase scintillation. This is higher correlation. This should change over a longer path and when the scintillometer is collected at the same time on the identical path.

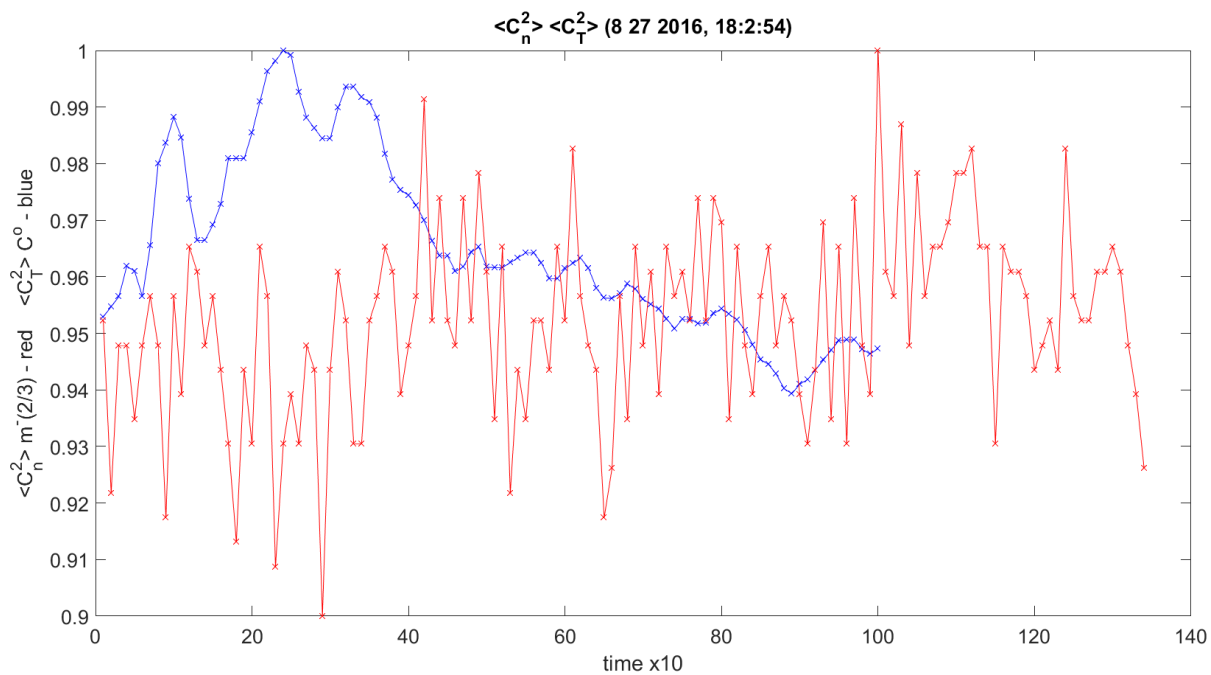


Figure 3.102. C_T^2 C_n^2 Correlation with C_n^2 Hallway Data.

Figure 3.103 shows a plot of C_Q^2 C_n^2 correlated with phase scintillation. This is higher correlation. It should change over a longer path and when the scintillometer is collected at the same time on the identical path.

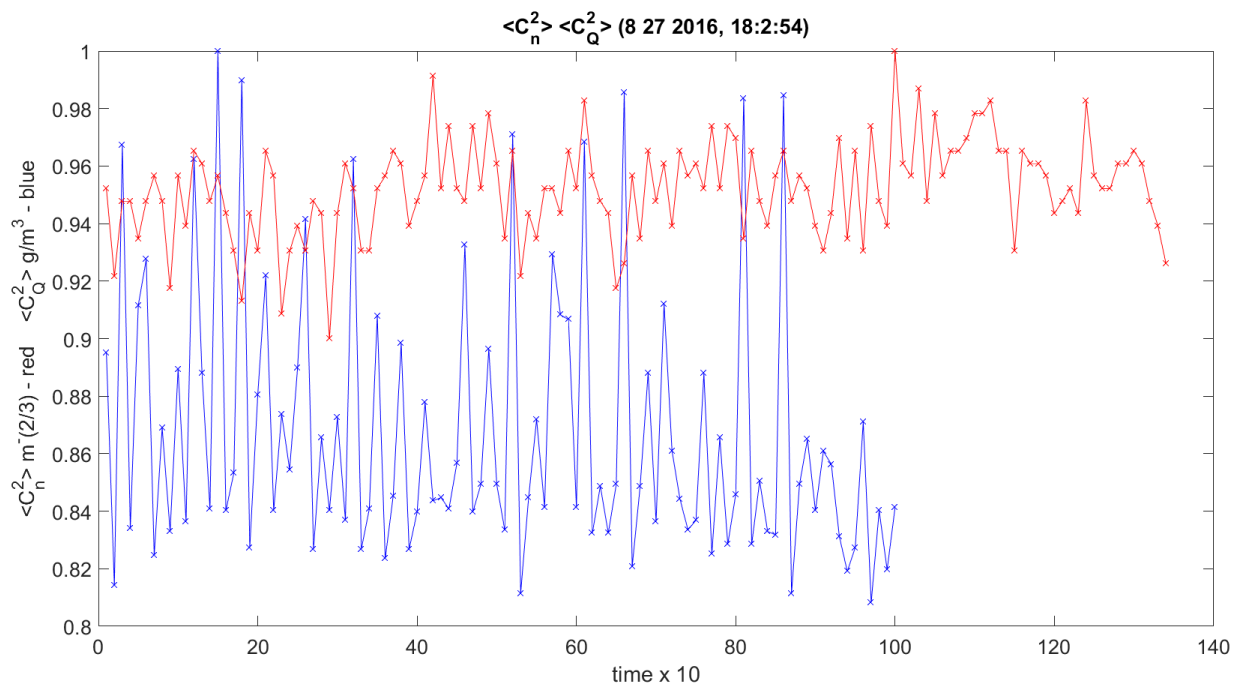


Figure 3.103. C_Q^2 Correlation with C_n^2 Hallway Data.

Figure 3.104 shows a plot of $C_T^2 C_Q^2$ correlated with phase scintillation. This is higher correlation.

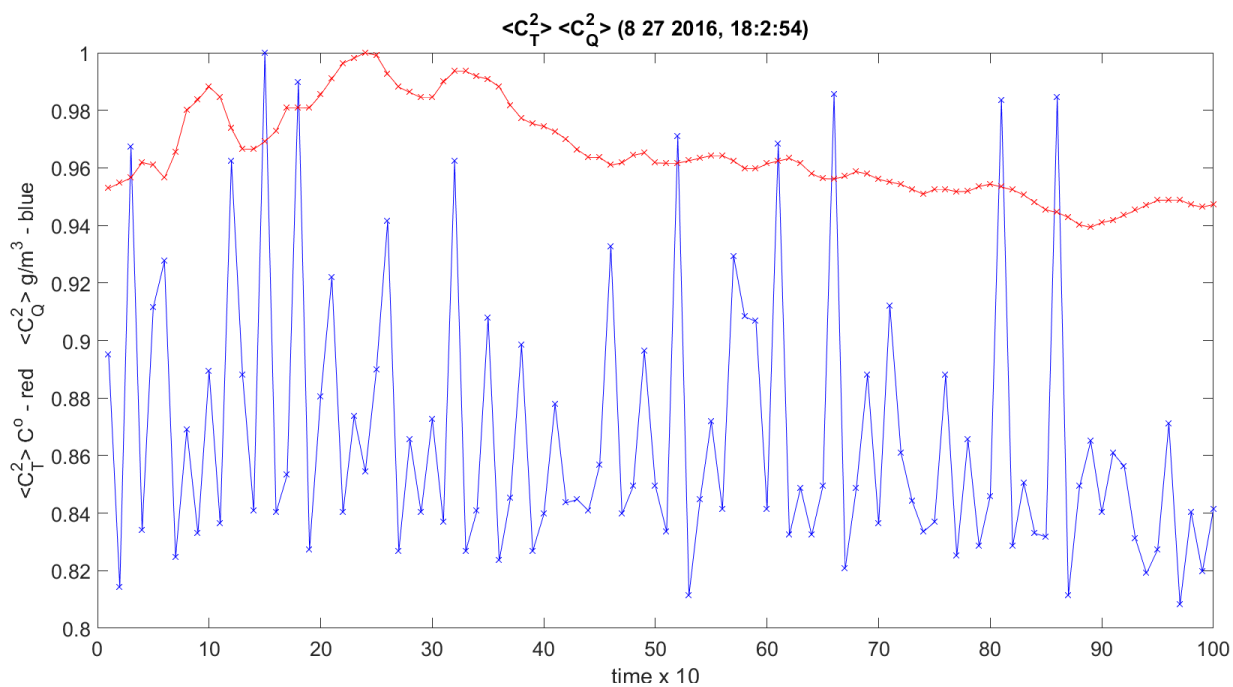


Figure 3.104. C_T^2 Correlation with C_Q^2 Hallway Data.

Figure 3.105 – Figure 3.107 show plots of amplitude scintillation and phase scintillation correlation with the different components of wind, just at the receiver for this path. Each set has a larger blow up of the phase correlation. The Phase is less correlated than the amplitude. The amplitude correlation to all three wind components is similar.

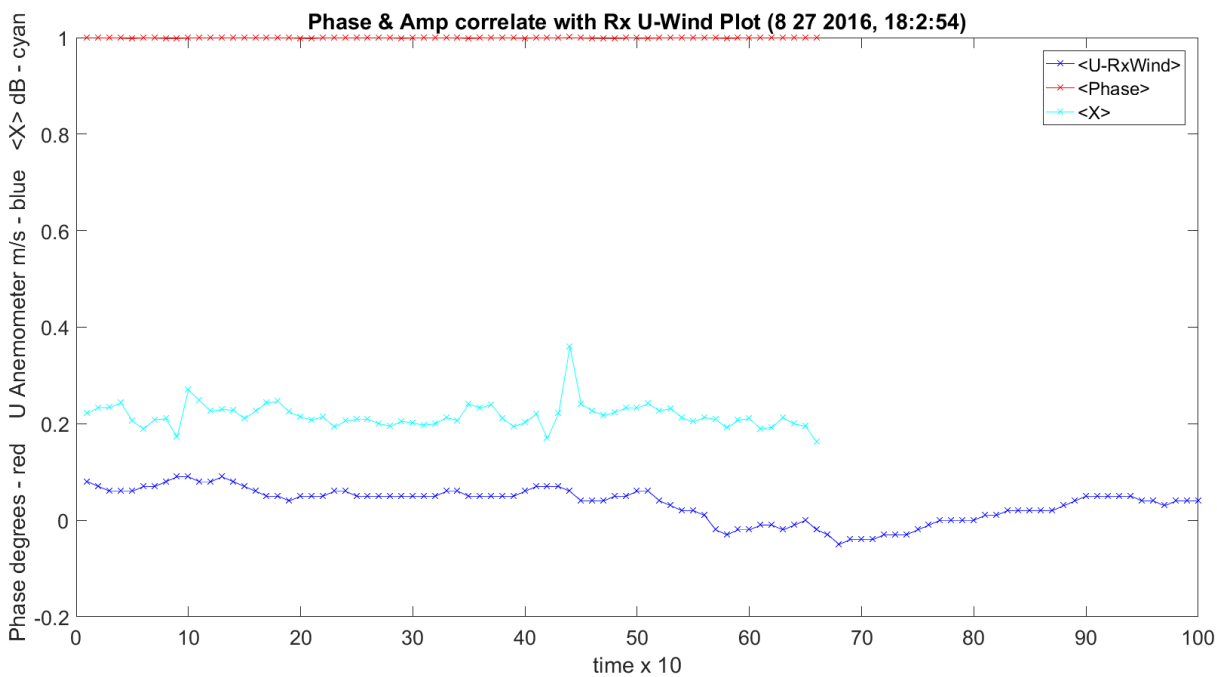


Figure 3.105. Phase Scint. and Amplitude Scint. Correlation with Receiver *U*-Wind Hallway Data.

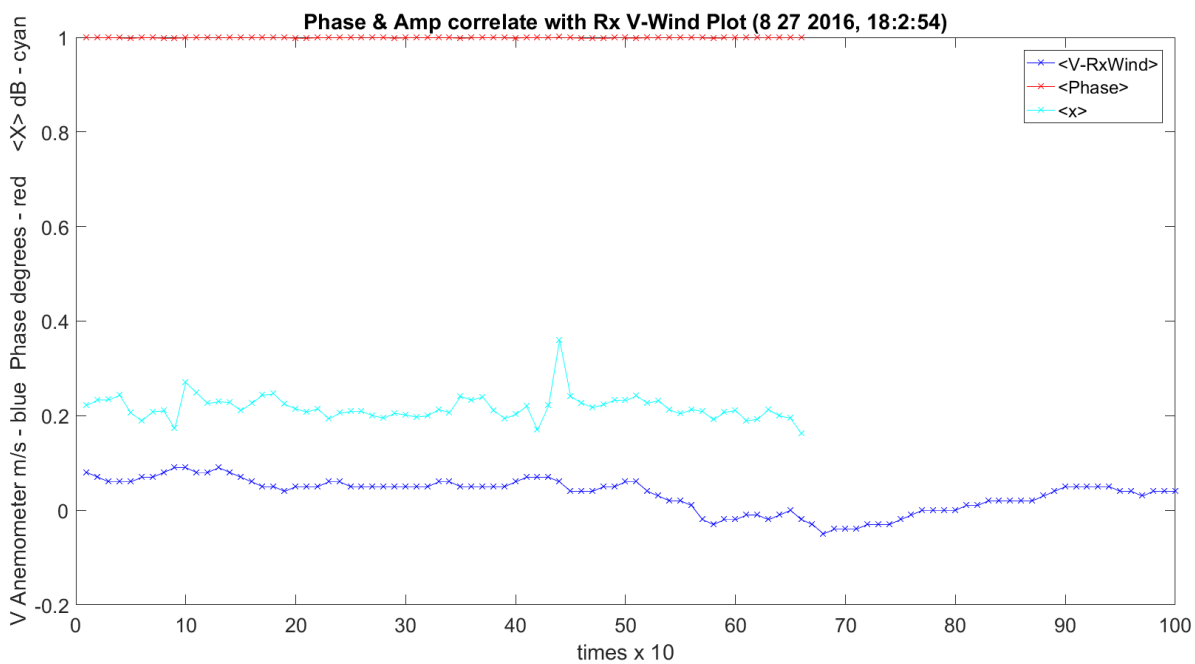


Figure 3.106. Phase Scint. and Amplitude Scint. Correlation with Receiver *V*-Wind Hallway Data.

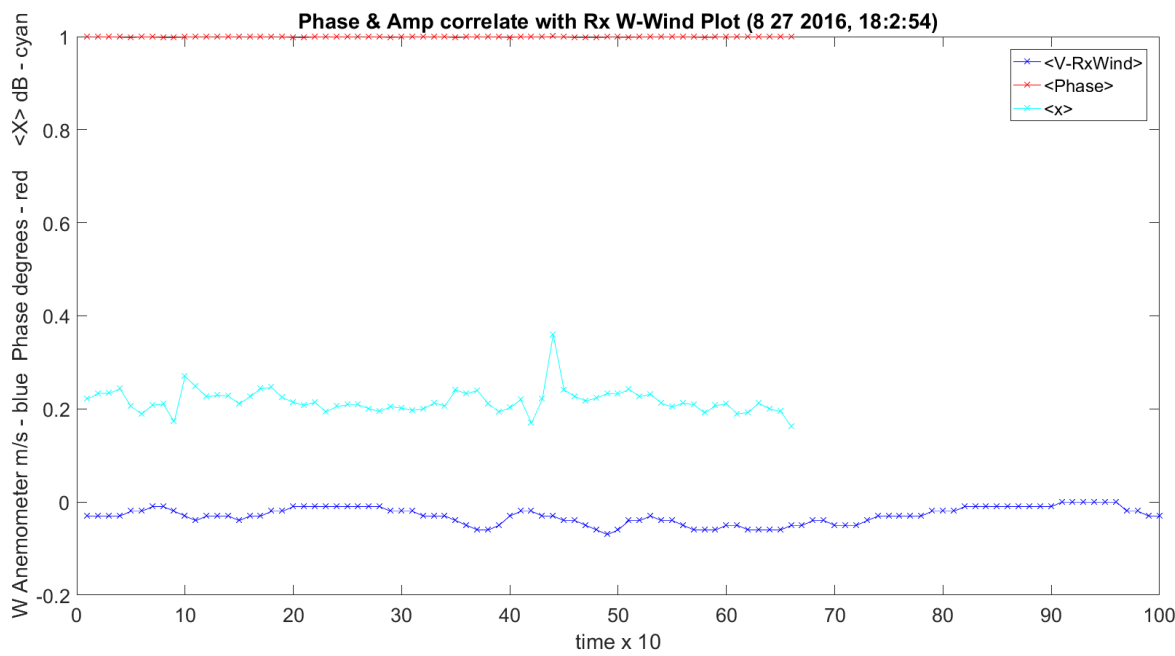


Figure 3.107. Phase Scint. and Amplitude Scint. Correlation with Receiver W-Wind Hallway Data.

3.17 Final Open Path 1924 m Analysis

This pass was run on 10142016_193175; the date is first and the time in ms is second. This was the first pass that was taken after a long, 17-hour day with no more clipping due to adding pads on the receiver prior to feeding the ADC. During this time, only Rx1 was working, so no Rx2 data or MCF will be covered. The only missing data was due to not turning on the anemometer on the transmitter side. This pass was taken at night and the picture from Rx1 on the mesa is in Figure 3.108. The reflection off the class in front of the camera and the scintillometer LED shows the operation and the weather are visible.

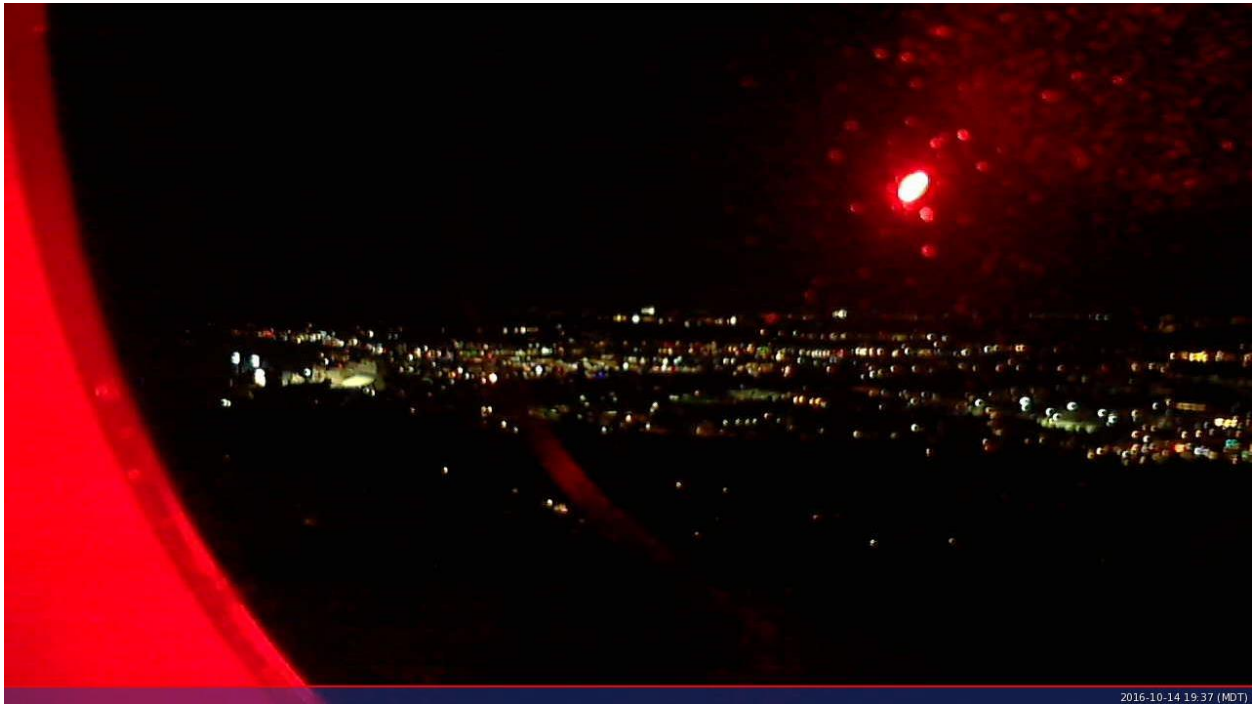


Figure 3.108. Data Acquisition Camera 10142016_193175.

Figure 3.109 shows the synchronization for the approximate seven-second duration of running the 66 frequency shifts. Figure 3.110 traces the exact offset of the times between the transmitter and the receivers. There is some acceptable straddling from scan-to-scan with a total worst case shift of 17 ms; the maximum time between scans was very acceptable at 2 ms.

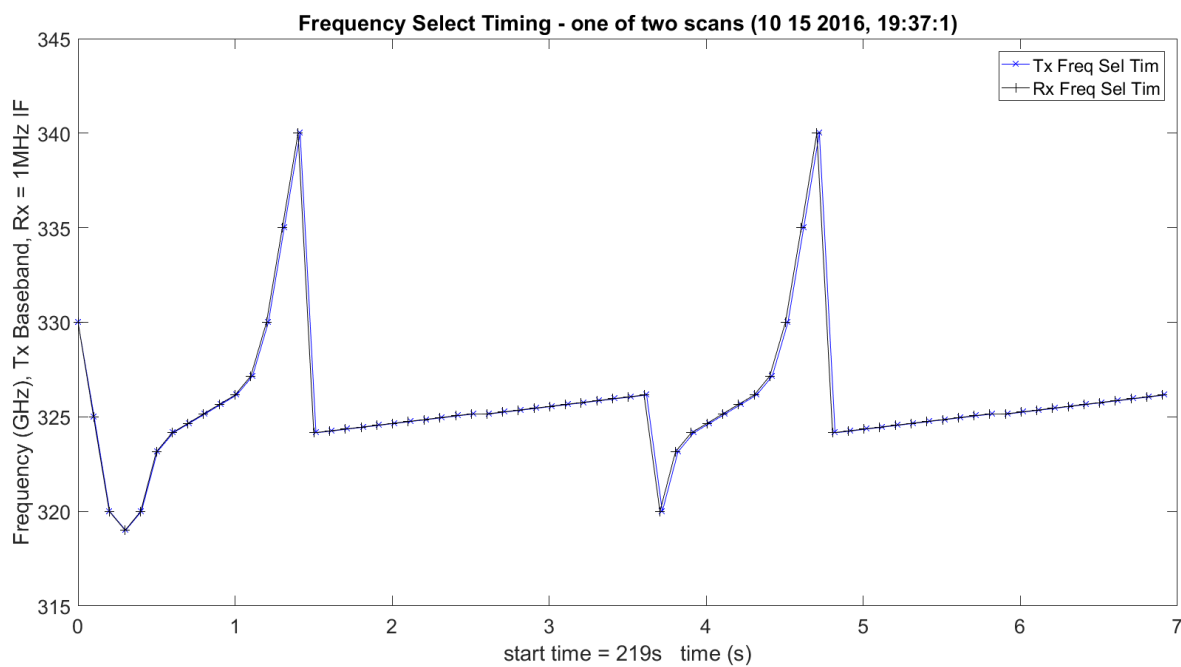


Figure 3.109. Timing Synchronization – 10142016_193175.

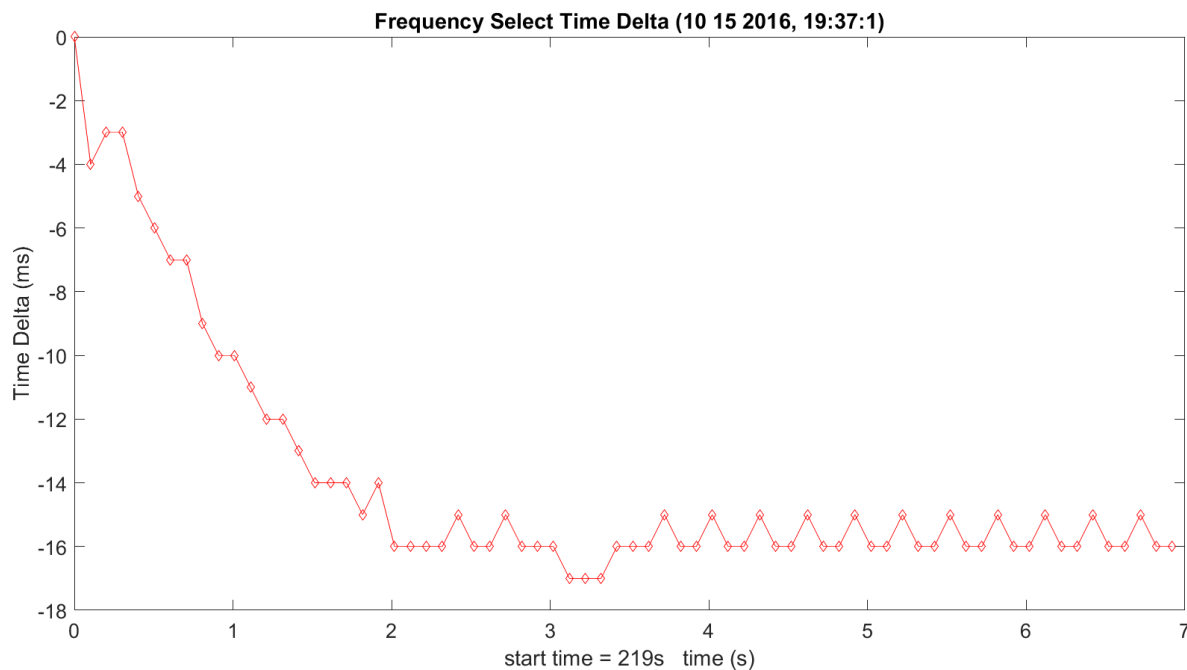


Figure 3.110. Tracking of the Delta Time between Tx and Rx – 10142016_193175.

Every scan is made up of 11 frequencies, with three sets covering WB, LWL and UWL (33 frequencies). The reason there are 66 total frequencies is due to implementing the scans twice for comparison.

Figure 3.111 shows the raw data from the ADC after the DDC to baseband is implemented. This showed very good results over the long open path; the WB scans, LWL absorption/UWL gain and UWL/LWL patterns looked good and identical for the two sets of scans. Figure 3.112 shows the same response, only filtering out the noise. This is needed to detect the edges of good data and bad data in MATLAB. The bad data occurs during the switching and scanning of the synthesizers as they stabilize and the delta in the clocks, discussed earlier. This, again, looks as expected. An FFT was taken on the first frequency (320 GHz) to see the conditions of the DDC (Figure 3.113); this can be done for every frequency but would crash MATLAB. This is utilized to verify functionality and debug when a failure occurs. The tone looks very close to baseband as expected. **Figure 3.114** shows the histogram of the same first frequency — 320 GHz — of the WB scan. This is implemented on the raw data and shows very good results and ranges in amplitude from approximately -82 dBm to 81.7 dBm.

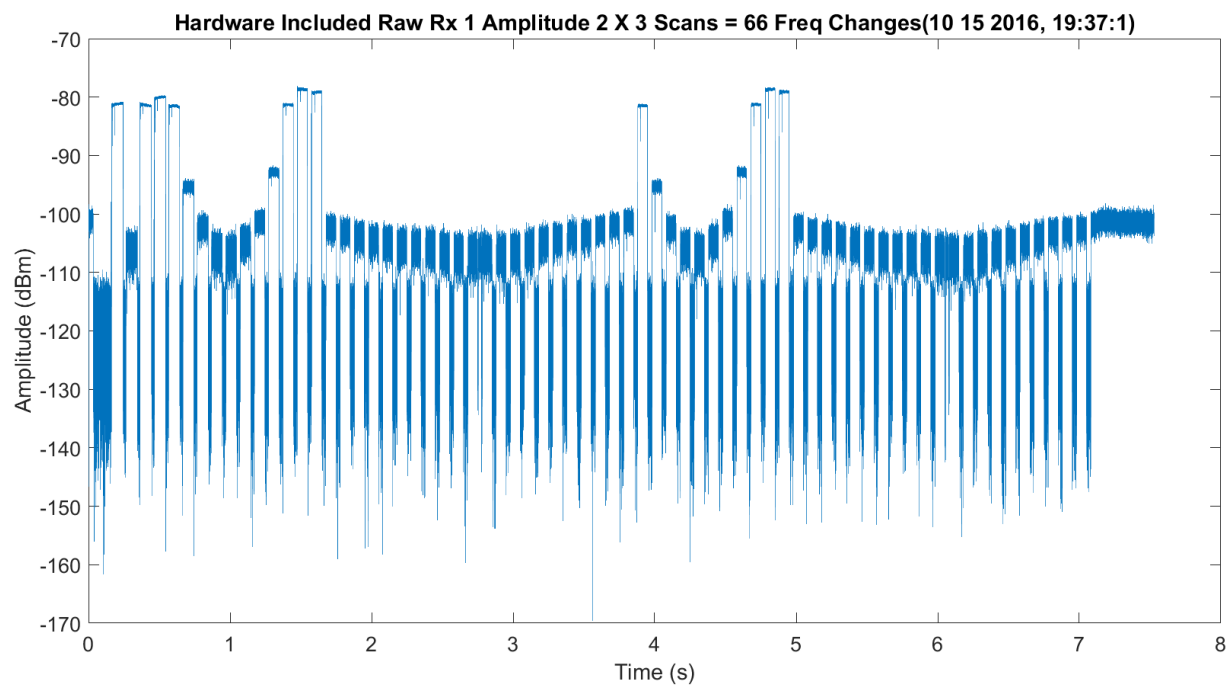


Figure 3.111. Raw Data after DDC for Rx1 – 10142016_193175.

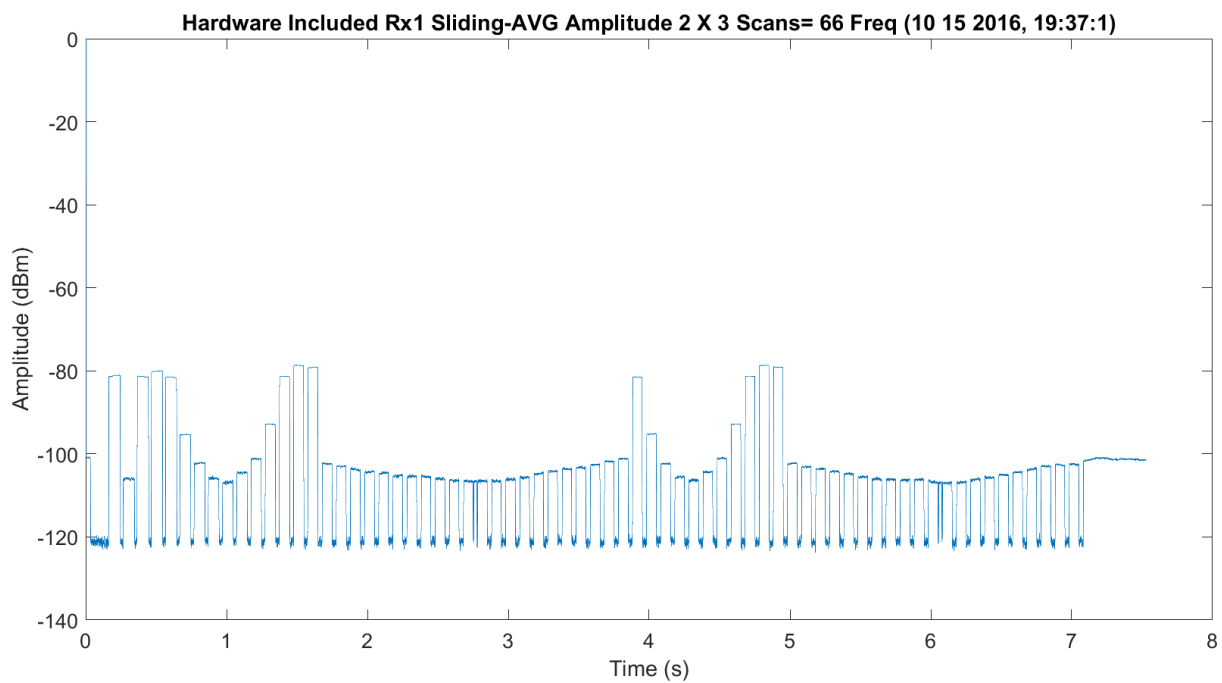


Figure 3.112. Averaged Filtered (80 Tap) Data after DDC for Rx1 – 10142016_193175.

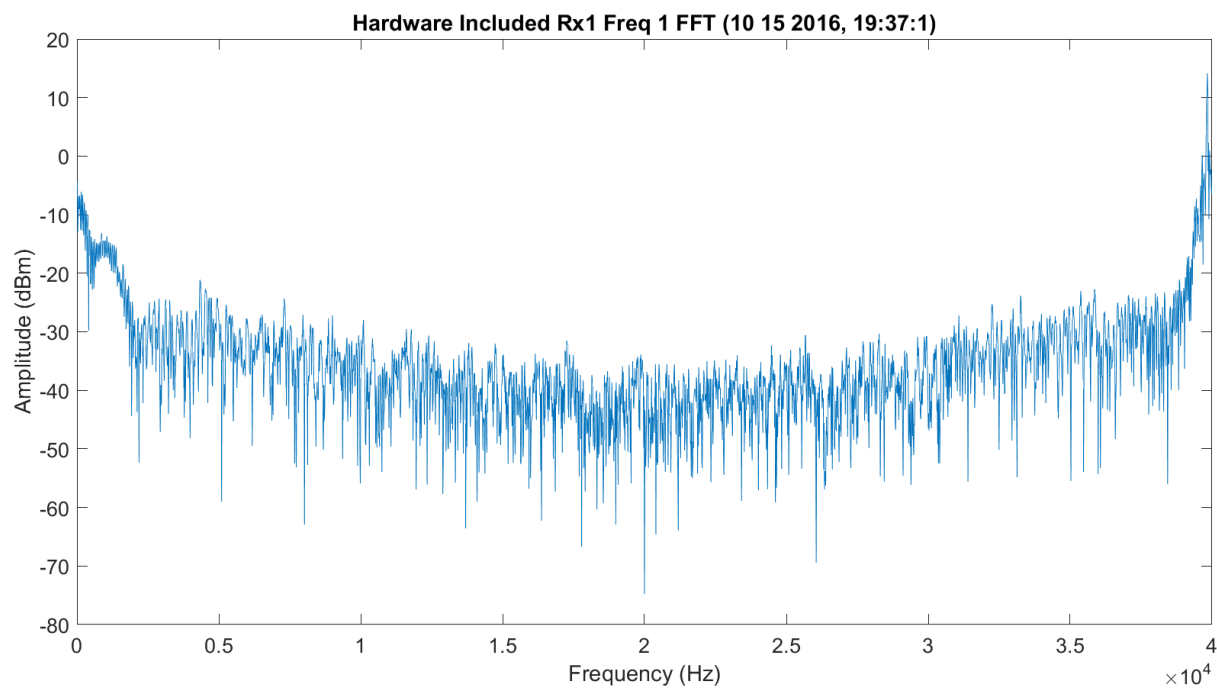


Figure 3.113. FFT of First WB Frequency (320 GHz) after DDC for Rx1 – 10142016_193175.

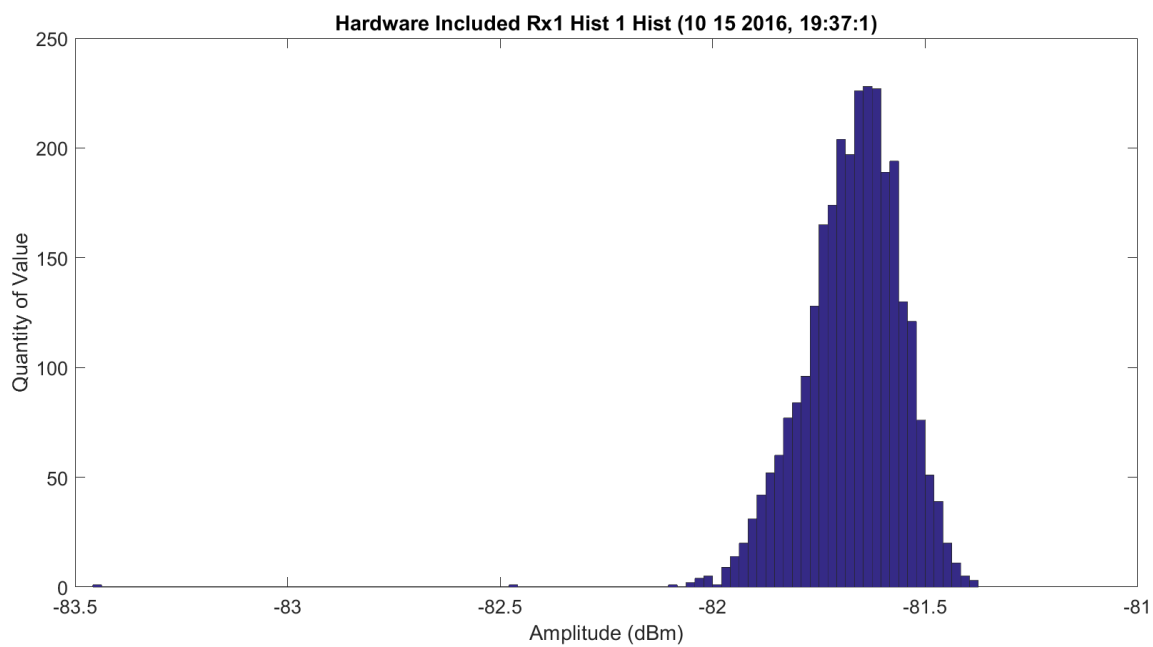


Figure 3.114. Histogram of First WB Frequency (320 GHz) after DDC for Rx1 – 10142016_193175.

It is also important to note for the plots below, the light blue bubbles at the points are the standard deviation divided by the square root of the number of points. The closer these are to the existing dark blue circles, the better the accuracy.

Figure 3.115 shows the amplitude scan over the first scan of the WB frequencies; these modes have hardware losses and gains that may not be known in the system. The amplitude ranges from approximately -106 dBm at 325.153 GHz to -82 dBm at 320 GHz, and 330 GHz through 340 GHz. The total difference in attenuation is approximately 24 dB, which seems higher than results in the 80s. The response looks as expected. Figure 3.116 shows the same data with the Friis. There is a significant offset in the traces, but the difference is approximately 10 dB. Figure 3.117 normalizes the data to have full overlap of the Friis prediction and the collected data to compare the shapes. The Friis is wider and not as close to a sharp peak as the TAIPAS collected data. It should be noted that Rx1 VDI failed the next time utilized and was sent back for repair. The sub-harmonic mixer failed. This failing could have affected the amount of the drop in power.

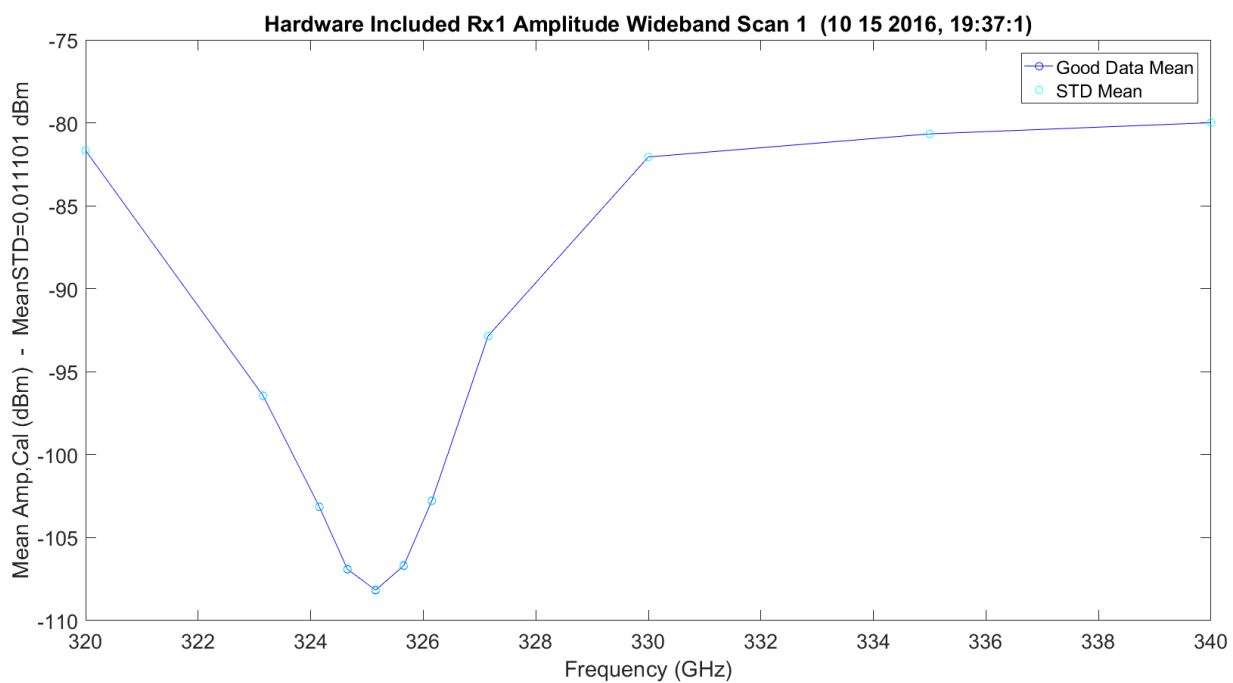


Figure 3.115. WB Scan 1 for Rx1 – 10142016_193175.

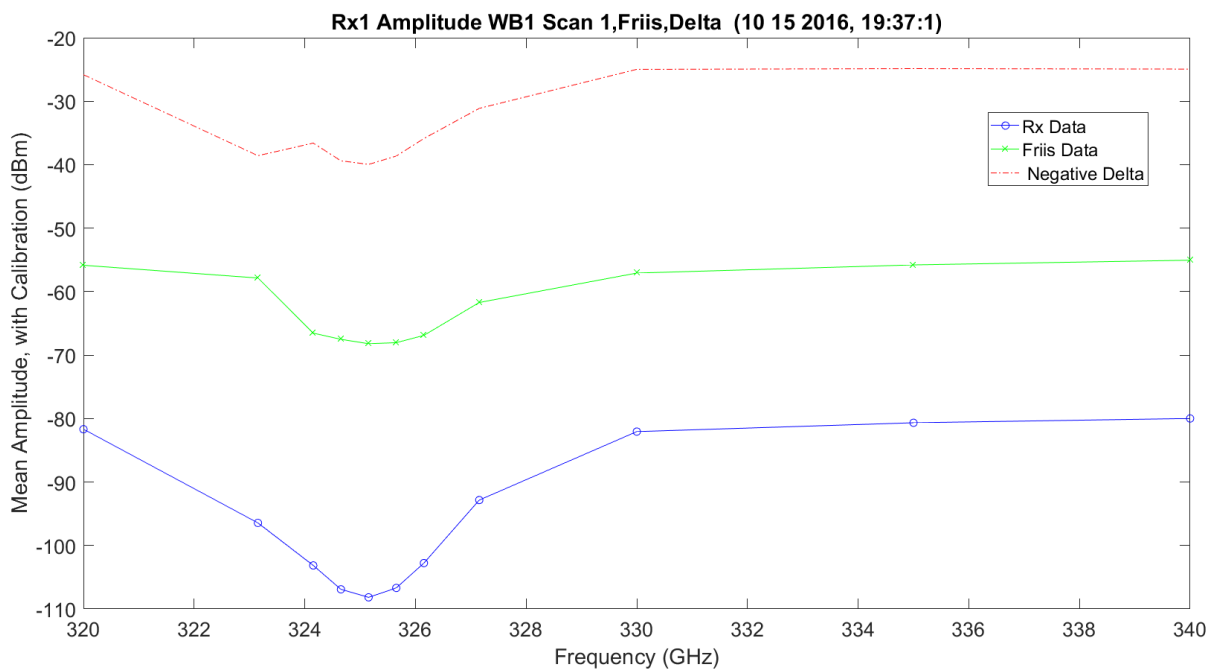


Figure 3.116. WB/Friis Scan 1 for Rx1 – 10142016_193175.

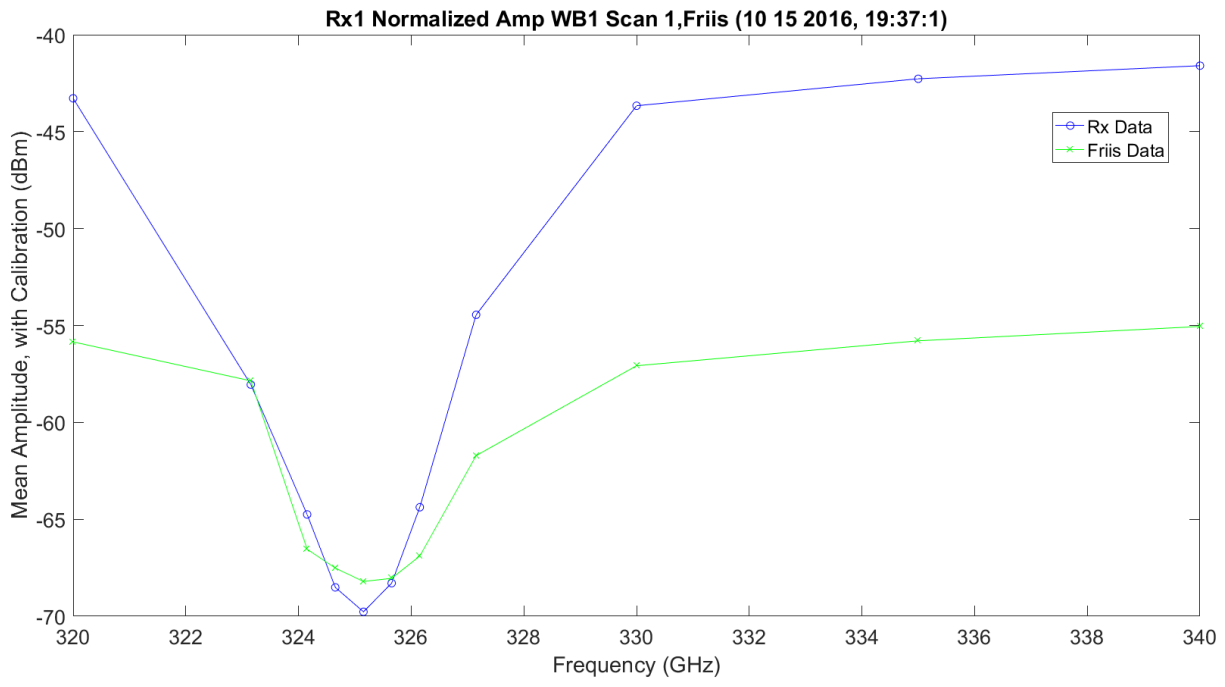


Figure 3.117. WB/Friis Normalized Scan 1 for Rx1 – 10142016_193175.

Figure 3.118 shows an absorption LWL scan 2 frequency. There is more ripple in the finally spaced frequencies of 100 MHz, which could be due to the calibration of the data on transmit and receive; the values can change in dB from point to point, especially on transmit. It looks like the high sample of the LWL does show some atmosphere ripples on the EM. Figure 3.119 shows the data with the Friis prediction and the difference. The ripples on the collected data become less obvious and the wings of the two look approximately the same, but they have approximately 40 dB of difference in amplitude. Figure 3.120 shows the normalization of the Friis and collected data. As expected, this shows the rippling on the collected, but the Friis response is flat. The real data is less flat and the wing is flatter than the Friis prediction. The two are not parallel.

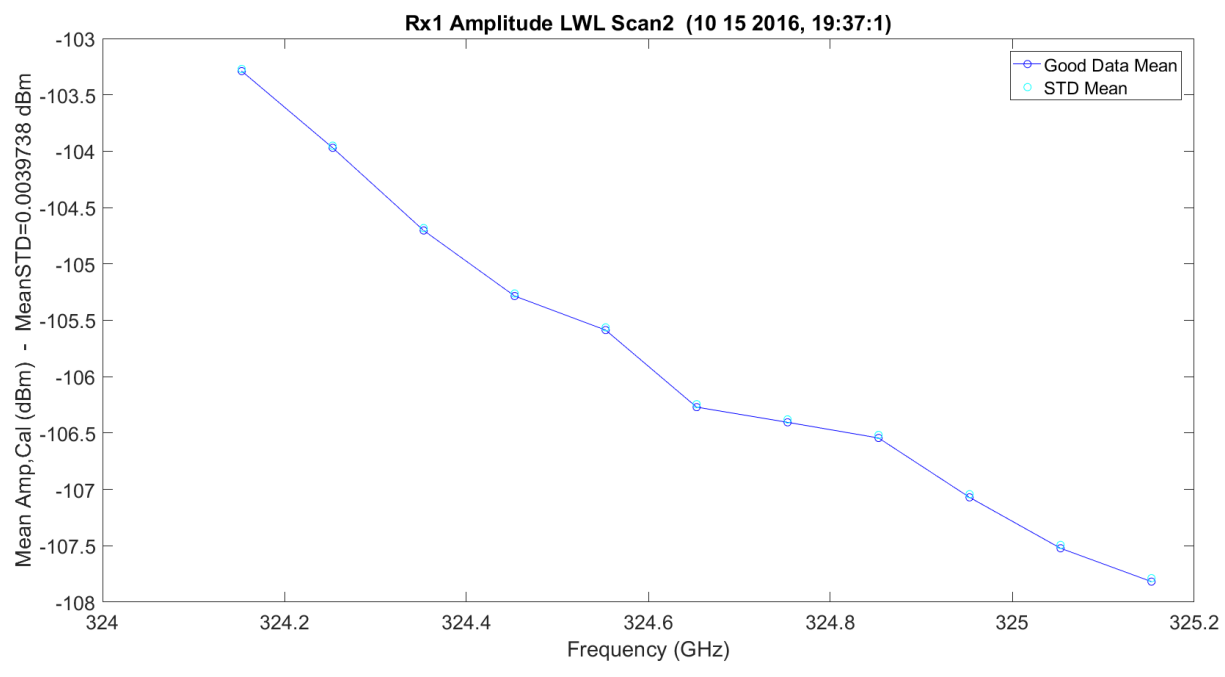


Figure 3.118. LWL Absorption Scan 2 for Rx1 – 10142016_193175.

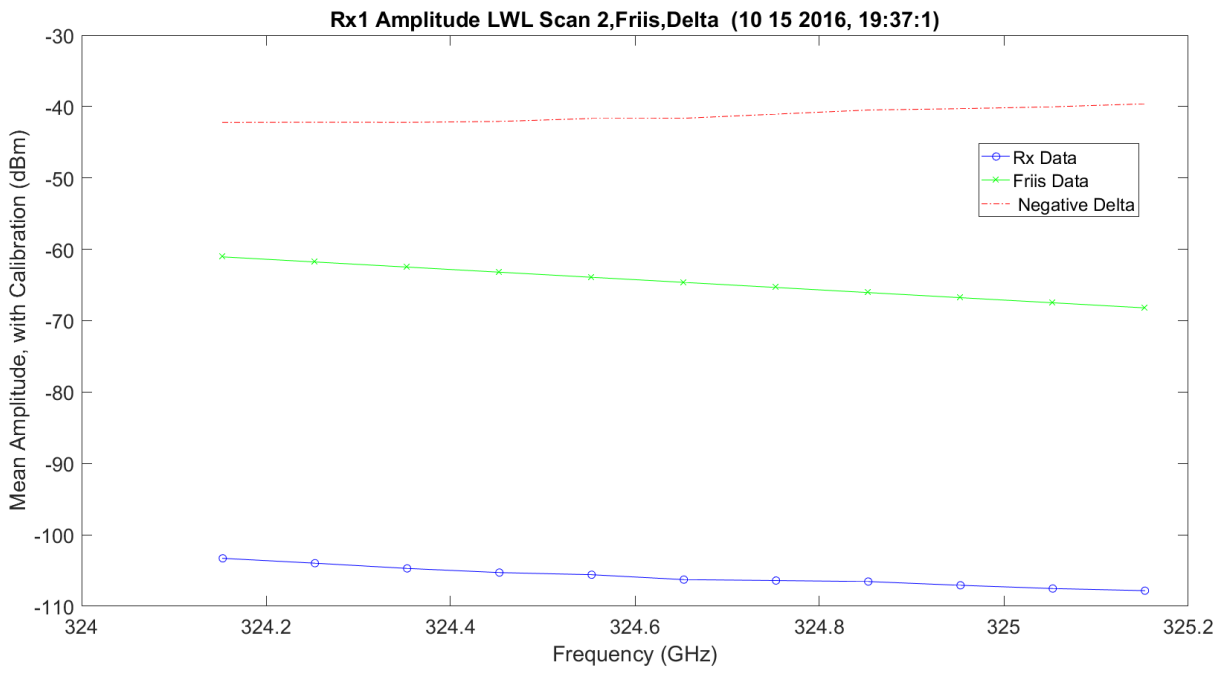


Figure 3.119. LWL / Friis Absorption Scan 2 for Rx1 – 10142016_193175.

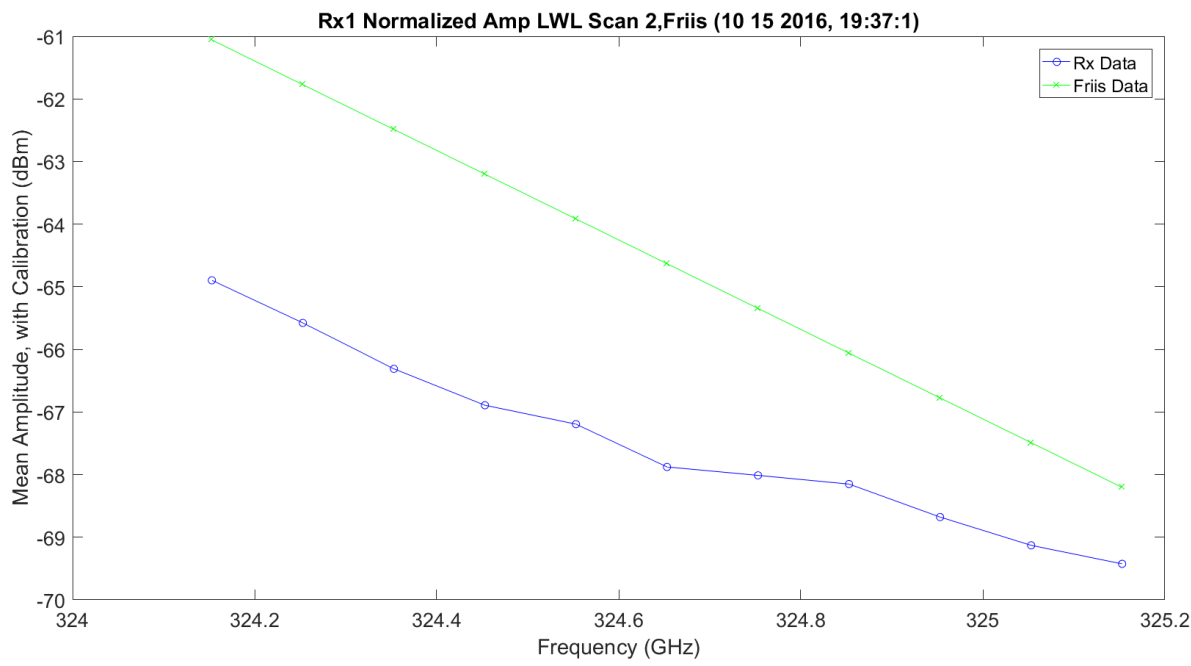


Figure 3.120. LWL / Friis Normalized Absorption Scan 2 for Rx1 – 10142016_193175.

Figure 3.121 shows an absorption UWL scan 3 frequency. There is more ripple in the finely spaced frequencies of 100 MHz, which could be due to the calibration of the data on transmit and receive; the values can change minor in dB from point-to-point. It looks like the high sample of the UWL does show some atmospheric ripples on the EM. Figure 3.122 shows the data with the Friis prediction and the difference. The ripples on the collected data become less obvious and the wings of the two look approximately the same, but they have approximately a 38 dB difference in amplitude. Figure 3.123 shows the normalization of the Friis and collected data. As expected, this shows the rippling on the collected, but the Friis response is flat. The real data is less flat and the wing is flatter than the Friis prediction. In this figure, the parallelization of the Friis and real data looks close, except the offset.

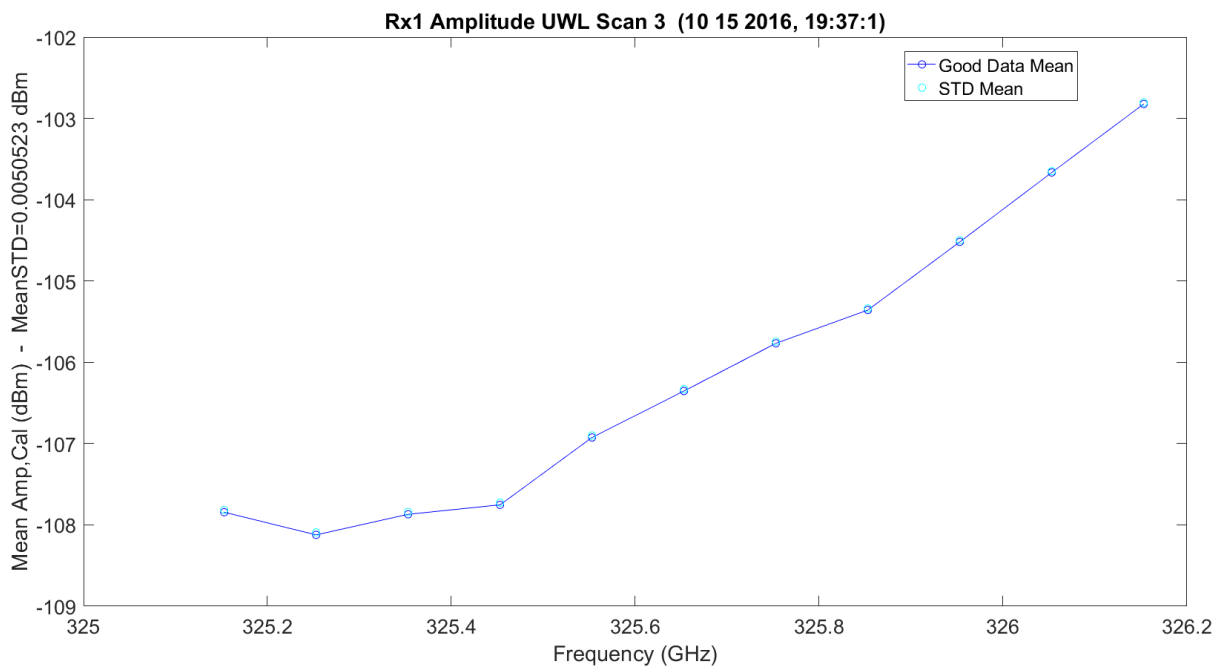


Figure 3.121. UWL Absorption Scan 3 for Rx1 – 10142016_193175.

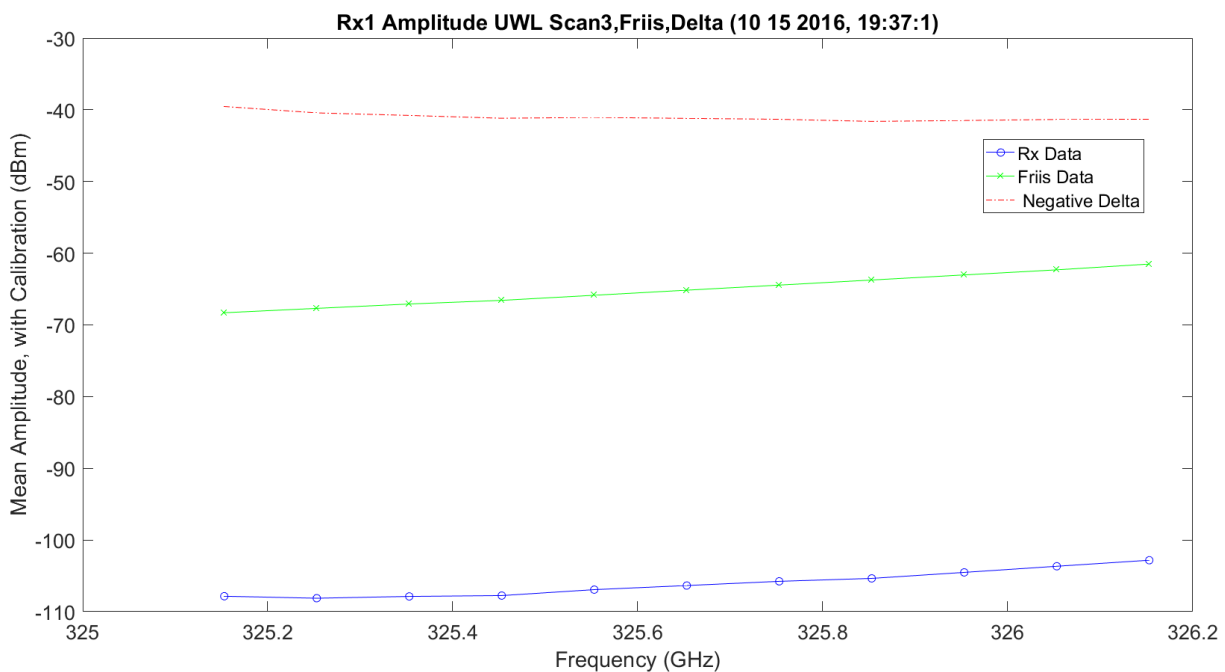


Figure 3.122. UWL / Friis Absorption Scan 3 for Rx1 – 10142016_193175.

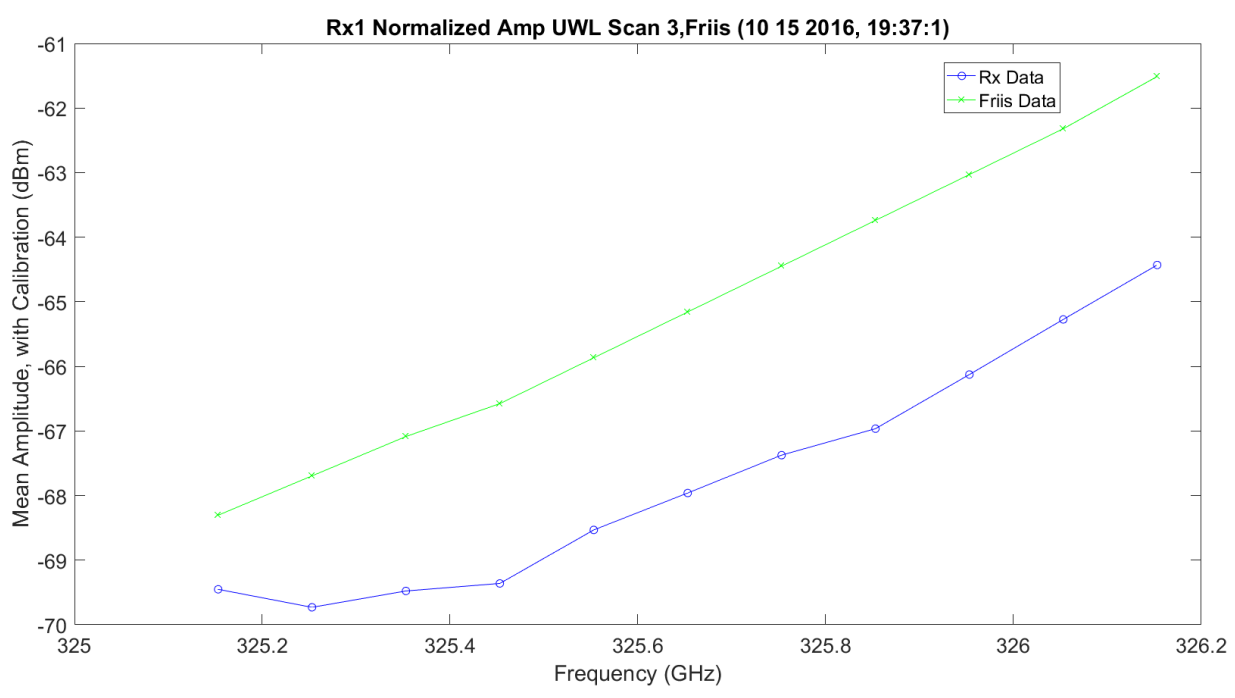


Figure 3.123. UWL / Friis Normalized Absorption Scan 3 for Rx1 – 10142016_193175.

The following images (Figure 3.124 – Figure 3.132) are the second set of identical scans: WB, LWL and UWL. They each scan 11 different frequencies. They are included for completeness, but they look identical to the first 33 scanned frequencies. The up and down wings have very different jugs than where assumed due to calibration on Tx and Rx. This may not be true; it could be an atmospheric effect, but much more data over a longer duration of time is required to come to a conclusion.

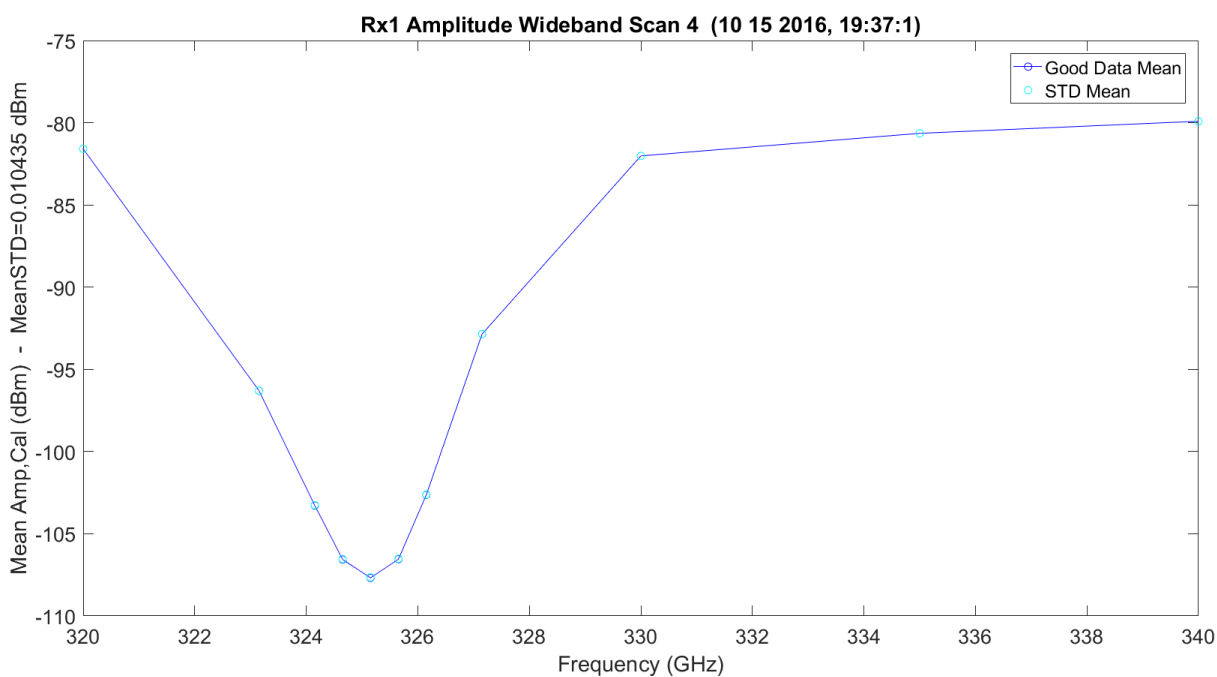


Figure 3.124. WB Scan 4 for Rx1 – 10142016_193175.

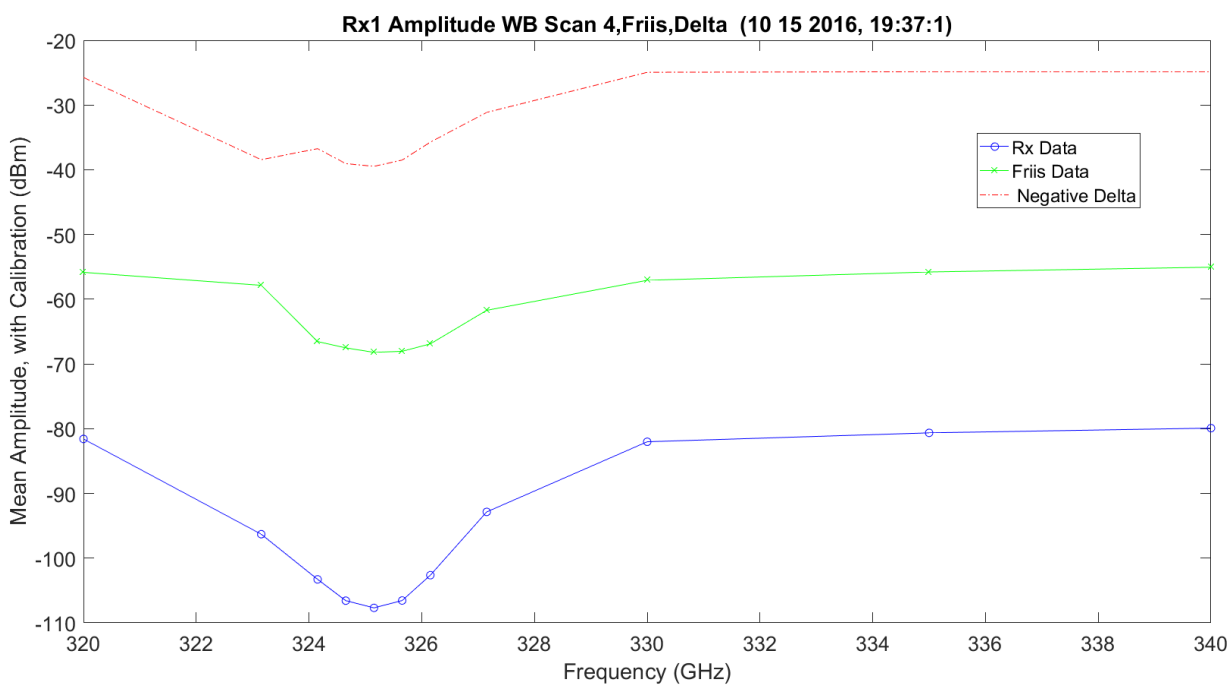


Figure 3.125. WB/Friis Normalized Scan 4 for Rx1 – 10142016_193175.

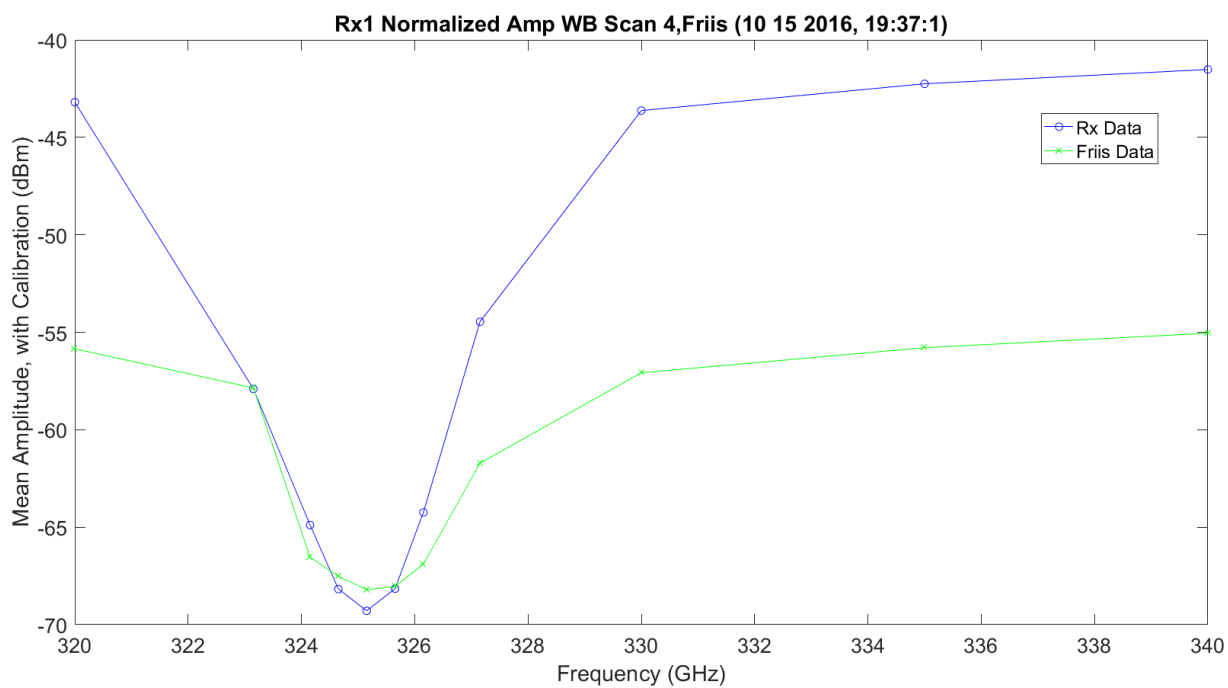


Figure 3.126. WB Absorption Scan 4 for Rx1 – 10142016_193175.

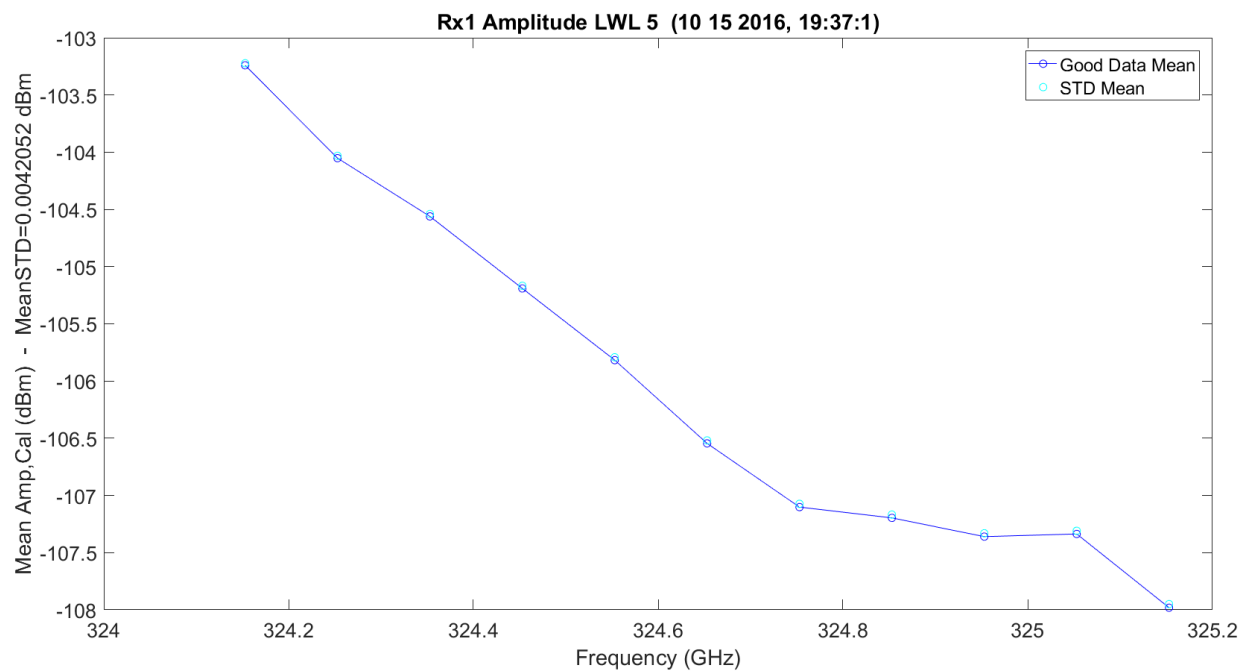


Figure 3.127. LWL / Friis Absorption Scan 5 for Rx1 – 10142016_193175.

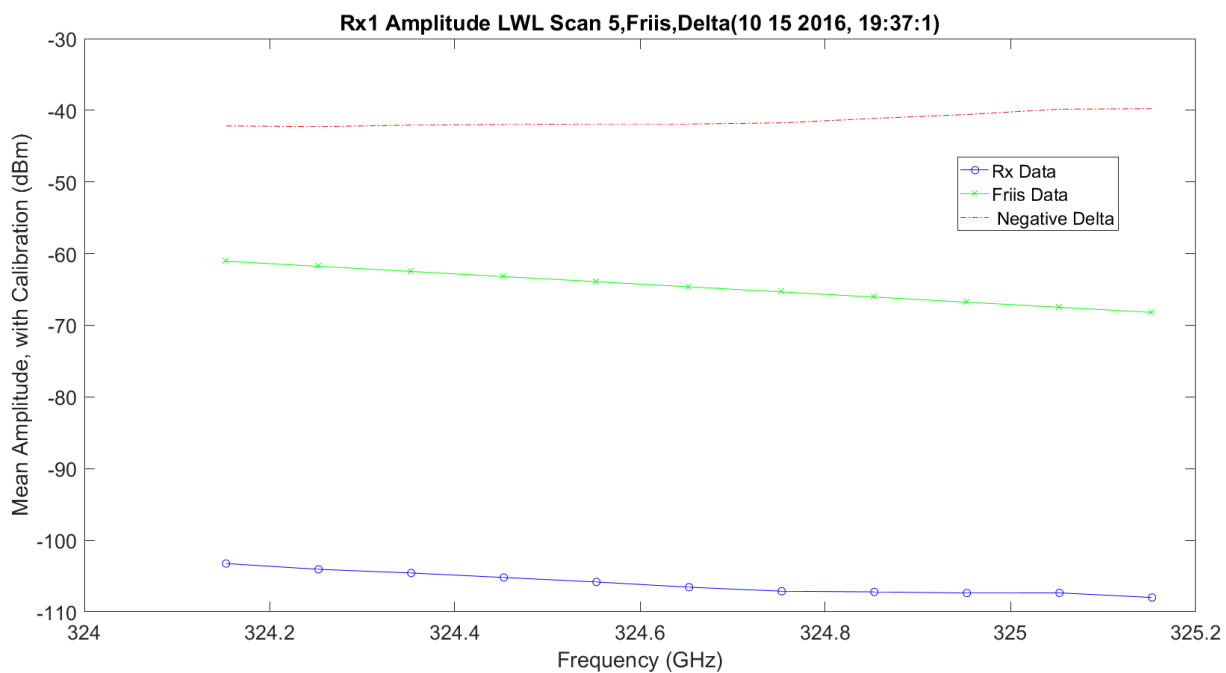


Figure 3.128. LWL / Friis Normalized Absorption Scan 5 for Rx1 – 10142016_193175.

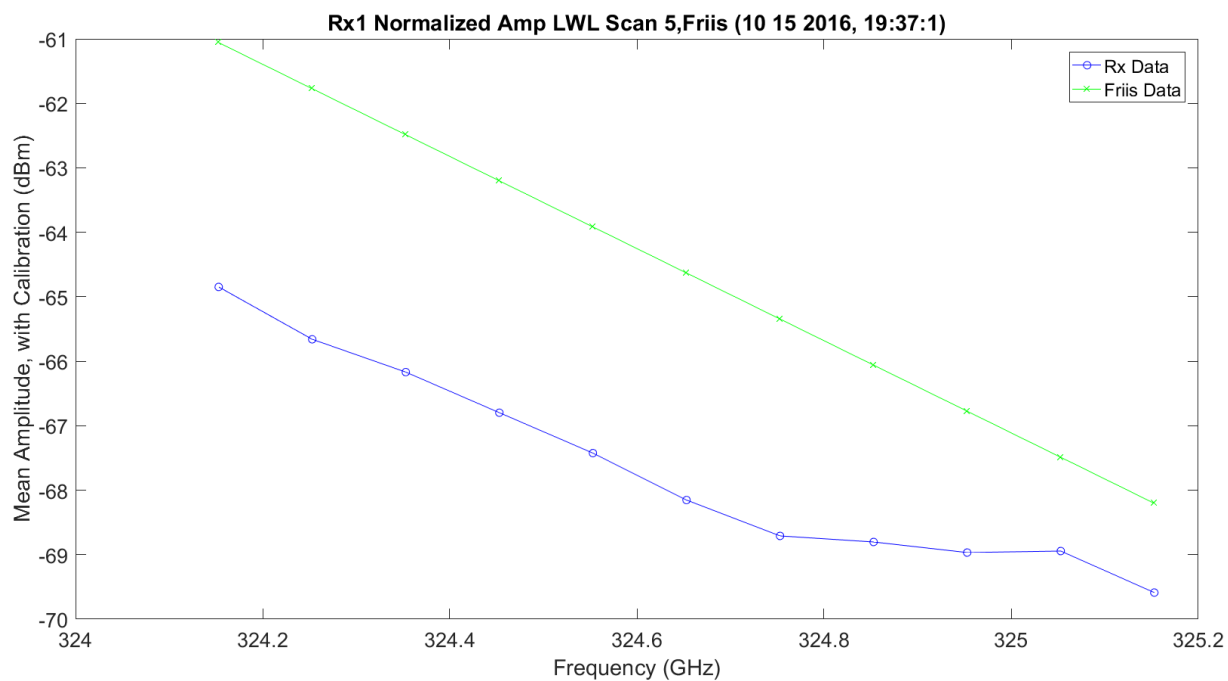


Figure 3.129. LWL Absorption Scan 3 for Rx1 – 10142016_193175.

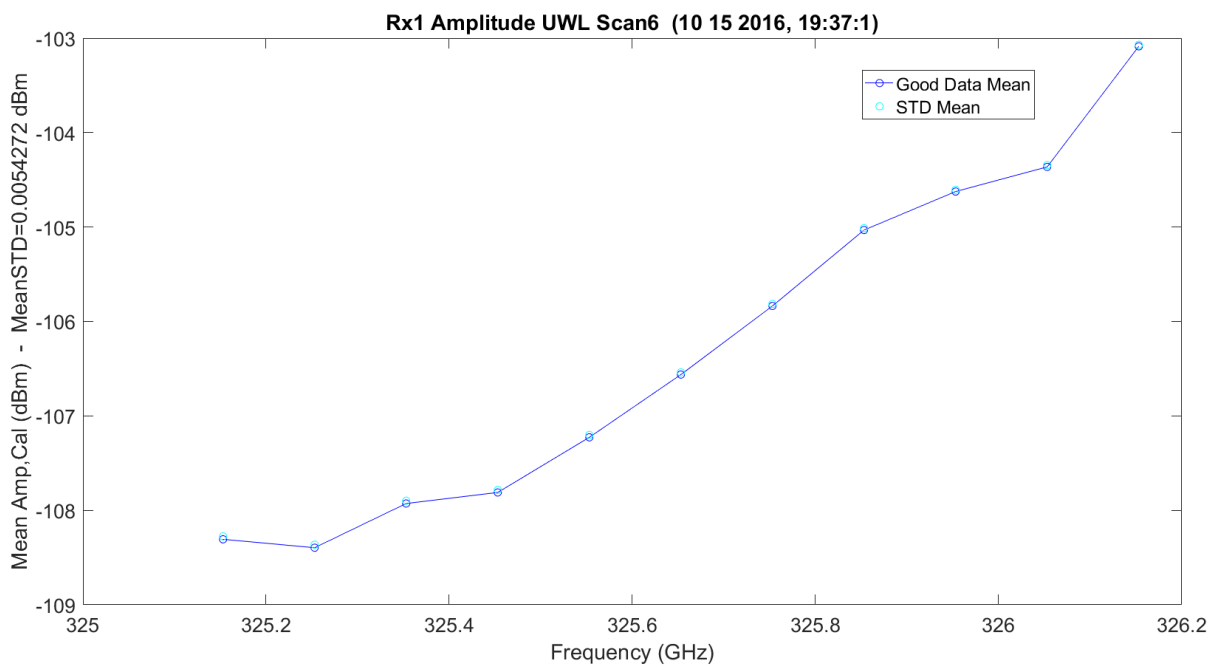


Figure 3.130. UWL / Friis Absorption Scan 6 for Rx1 – 10142016_193175.

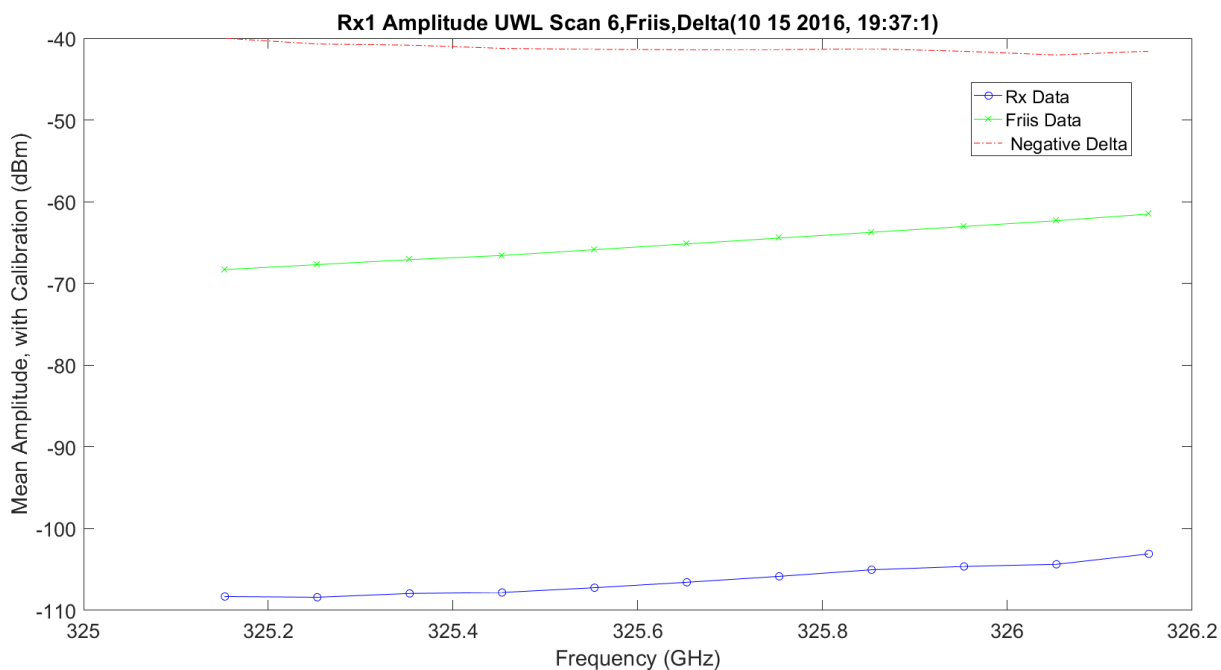


Figure 3.131. UWL / Friis Normalized Absorption Scan 6 for Rx1 – 10142016_193175.

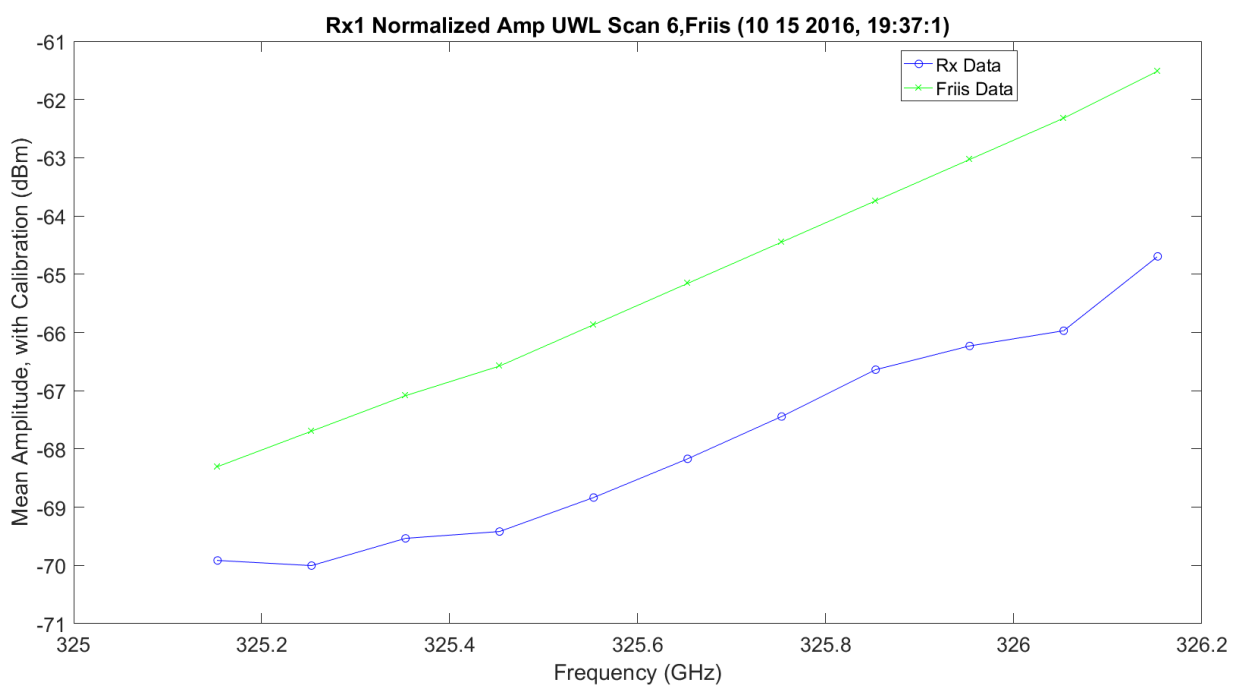


Figure 3.132. UWL / Friis Normalized Absorption Scan 6 for Rx1 – 10142016_193175.

Figure 3.133 shows both LWL and UWL, two scans each, on the same plot with the UWL reflected over the LWL to compare. The LWL and UWL are about 4-5 dB lower than the Friis. The two scans for UWL and LWL, compared to each, are similar. The UWL looks slightly higher by 1 dB and the shapes are slightly different from the LWL and UWL. The shape of the LWL vs. UWL is significantly different at approximately a frequency range of 324.9 GHz to 325 GHz.

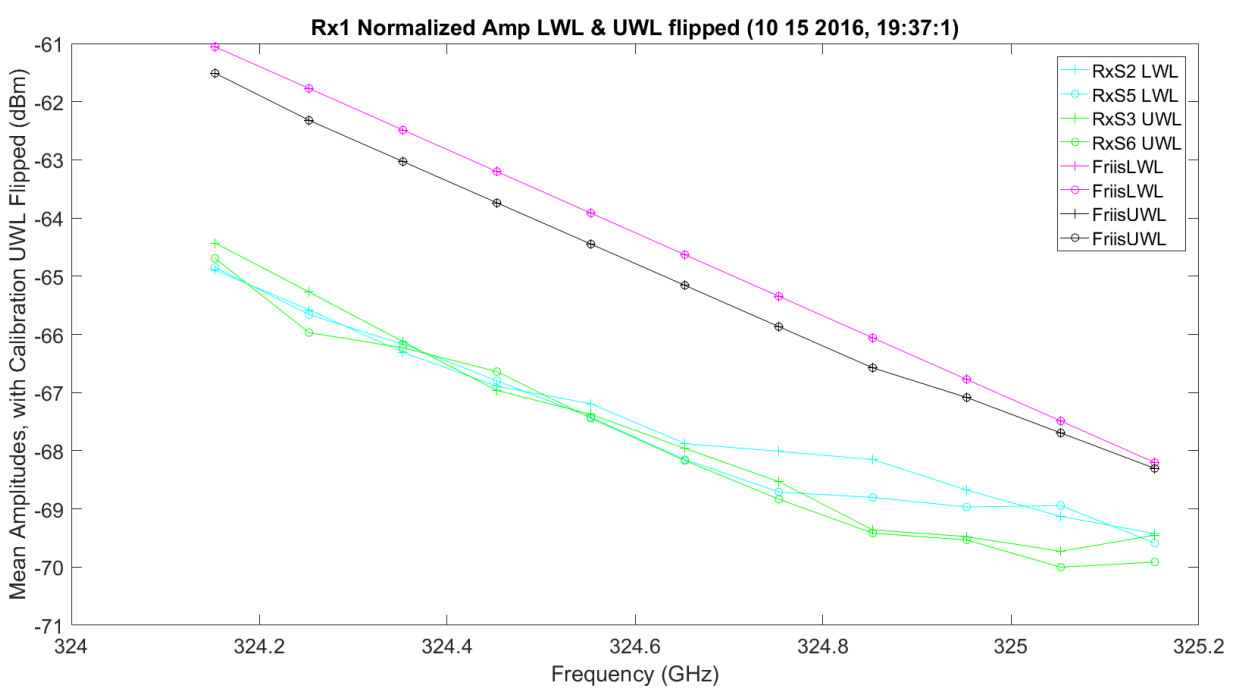


Figure 3.133. LWL & UWL Flipped Amp / Friis Normalized Absorption – 10142016_193175.

Figure 3.134 – Figure 3.134 show SNR plots for WB, LWL and UWL, respectively. The WB SNR drops 10 dB around the peak on both the Friis and real data. The simulation vs. the real data has much higher signals, but very similar SNR. The WB SNR shows that the shape of the SNR going down vs. up has different curves; the SNR gaining on the UWL is slower.

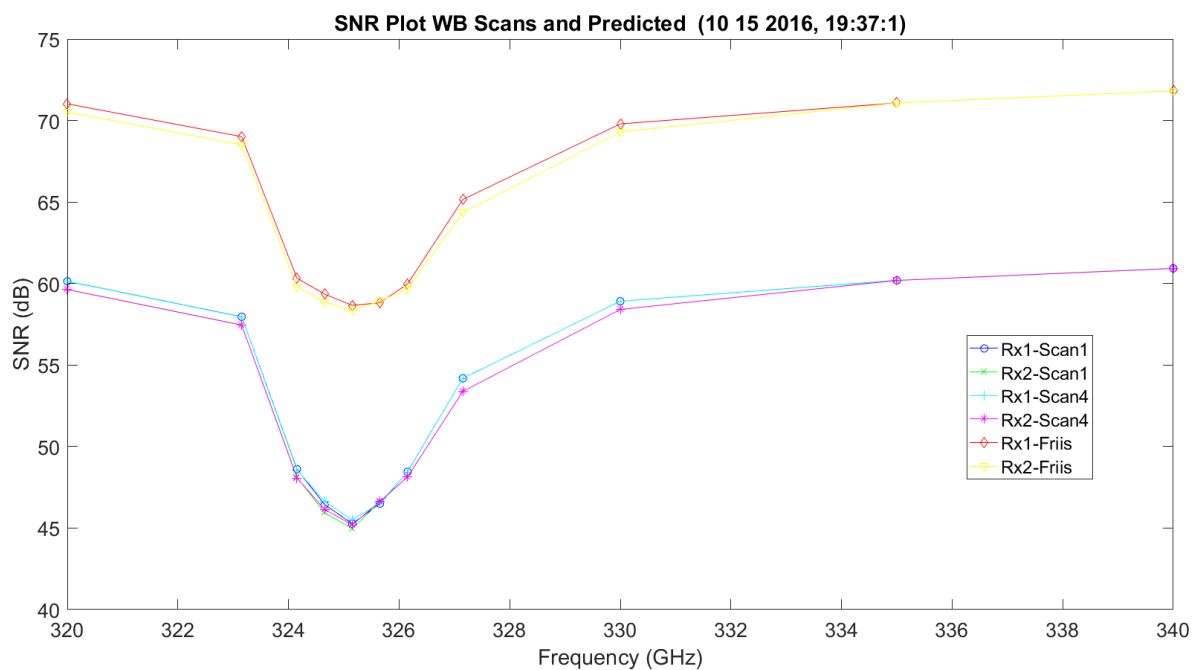


Figure 3.134. WB SNR and Predicted Friis – 10142016_193175.

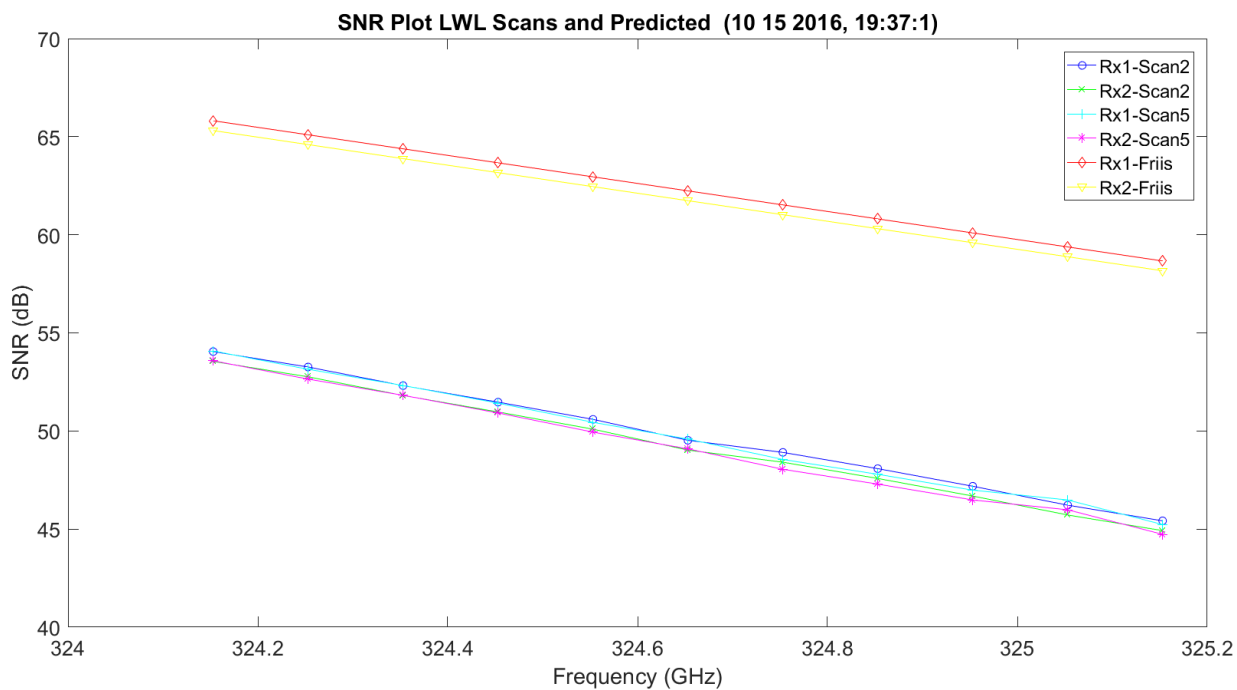


Figure 3.135. LWL SNR and Predicted Friis – 10142016_193175.

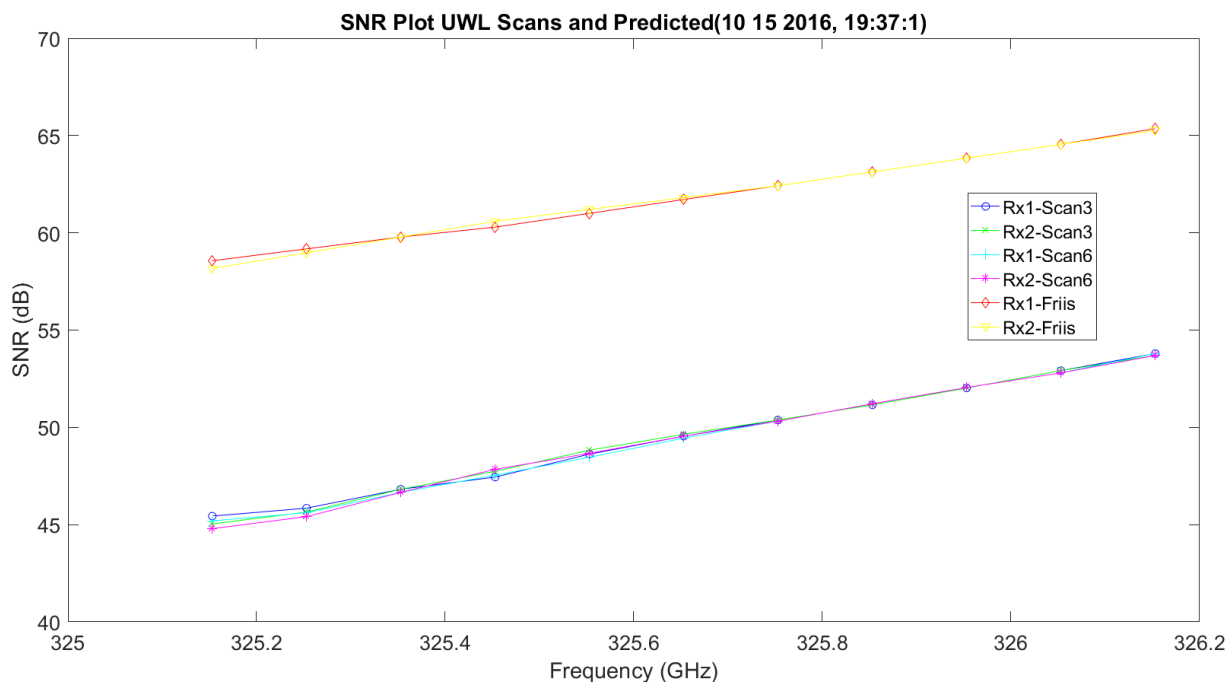


Figure 3.136. UWL SNR and Predicted Friis – 10142016_193175.

Figure 3.137 is a plot of C_n^2 . The $\times 10^{-13}$ is exactly what NIST was seeing that day. The variation of the mantissa is not significant: 1 to 1.5. The mean value is shown in the title. Figure 3.138 shows the FFT of the C_n^2 . This shows there is no significant distortion on the measurement.

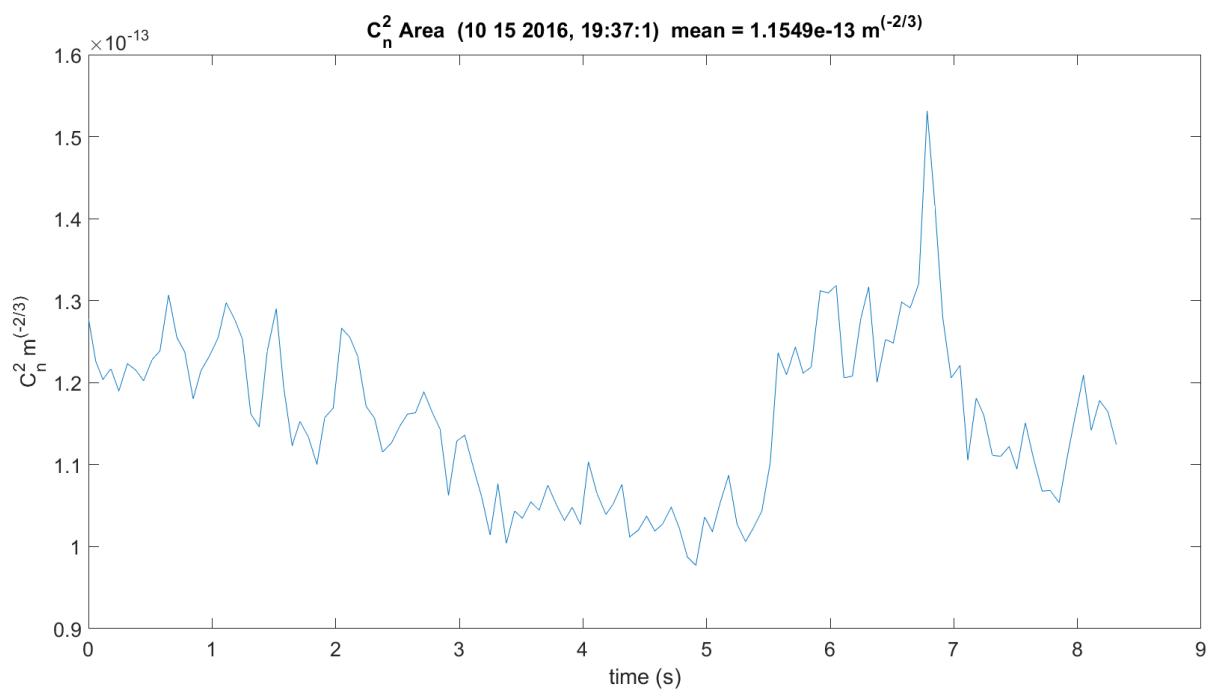


Figure 3.137. C_n^2 – 10142016_193175.

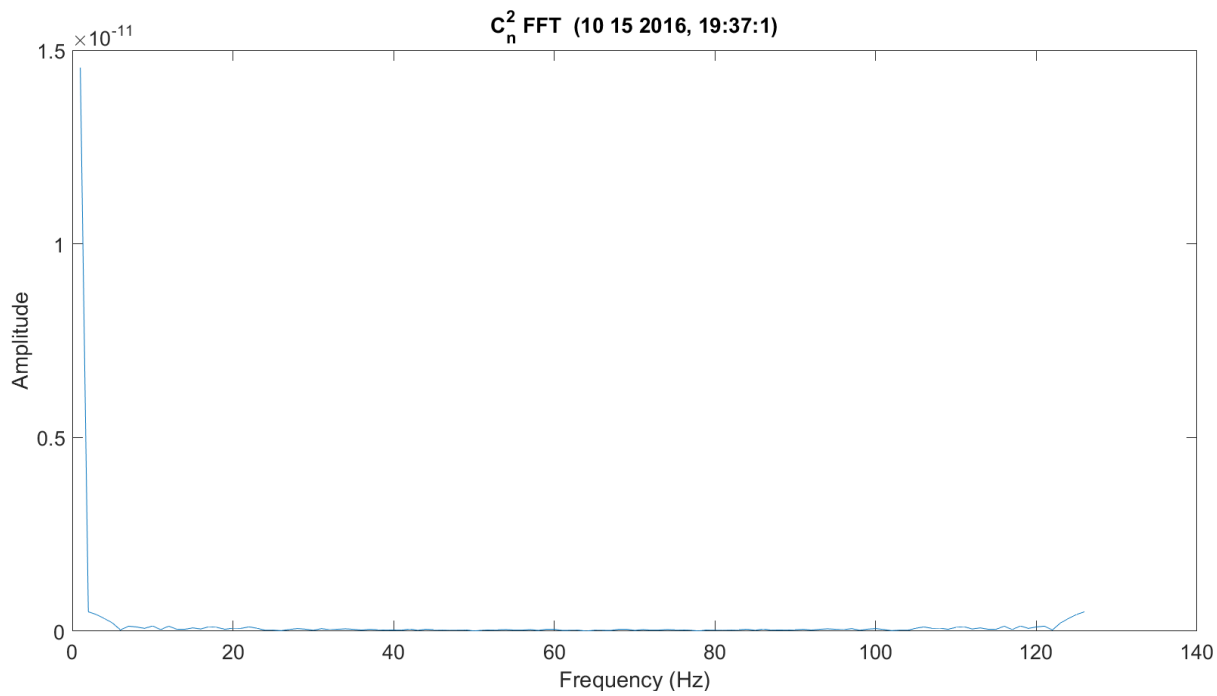


Figure 3.138. FFT of C_n^2 – 10142016_193175.

Figure 3.139 shows the transmit and receive anemometer temperatures. As expected, since the receiver is on the Mesa, the temperature would be lower. In this experiment, the Tx was not turned-on, so it shows as zero.

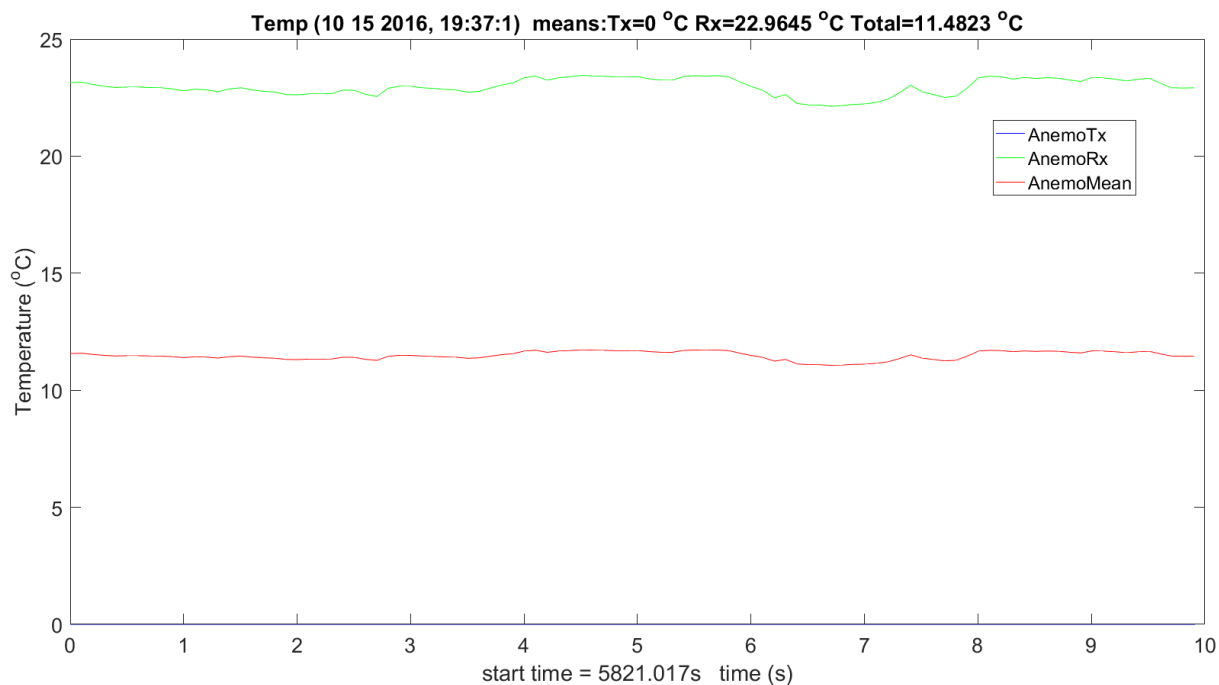


Figure 3.139. Transmit & Receiver Temp – 10142016_193175.

Figure 3.140 - Figure 3.140 show the wind information for U , V and W . U is the most critical for eddy formation. This, again, was zero on Tx, so the difference is low. At the Mesa high altitude, the wind is usually higher.

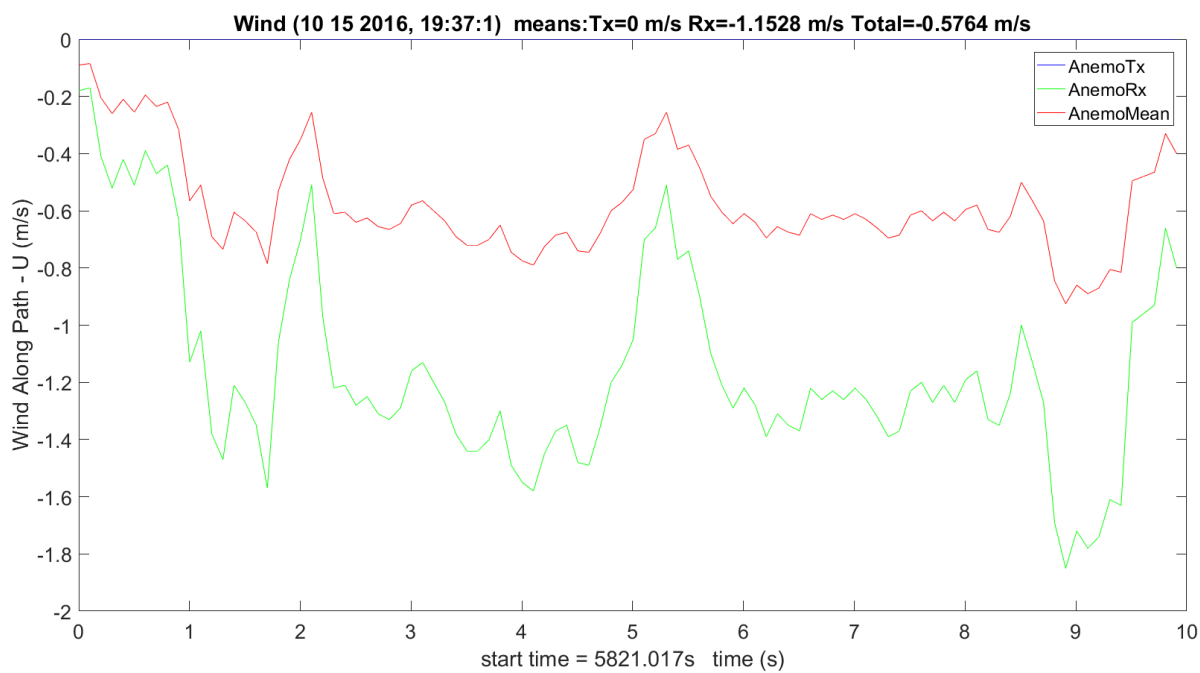


Figure 3.140. Wind *U* Transmit & Receiver – 10142016_193175.

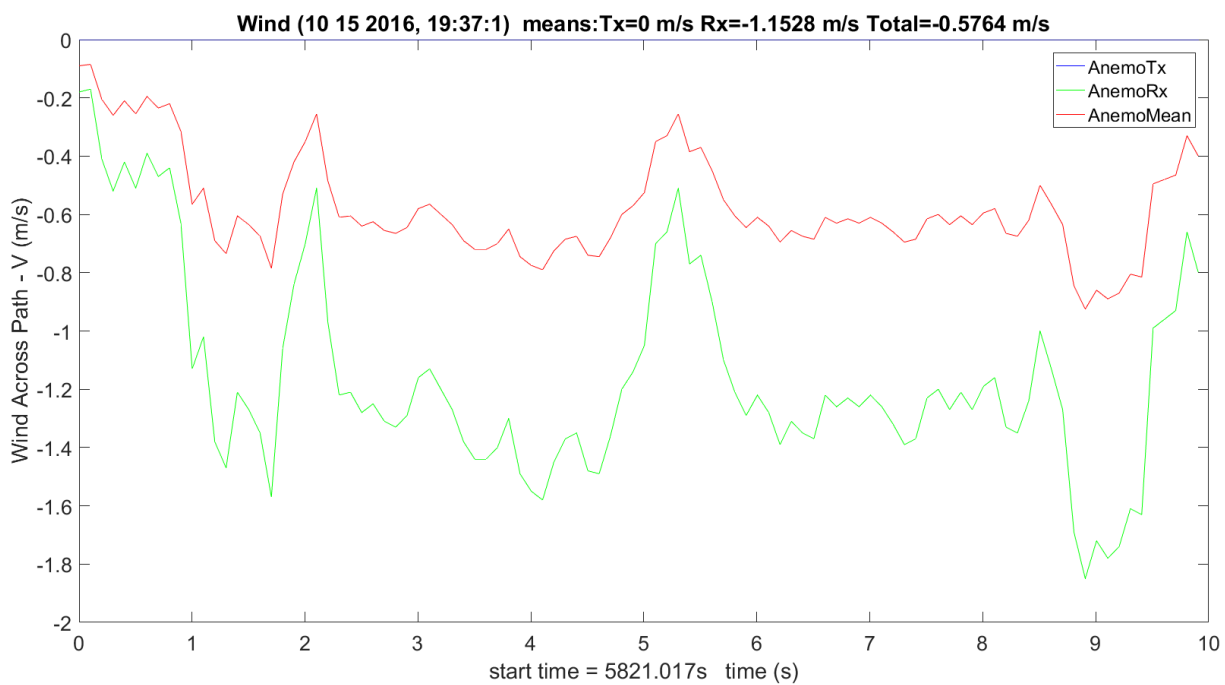


Figure 3.141. Wind *V* Transmit & Receiver – 10142016_193175.

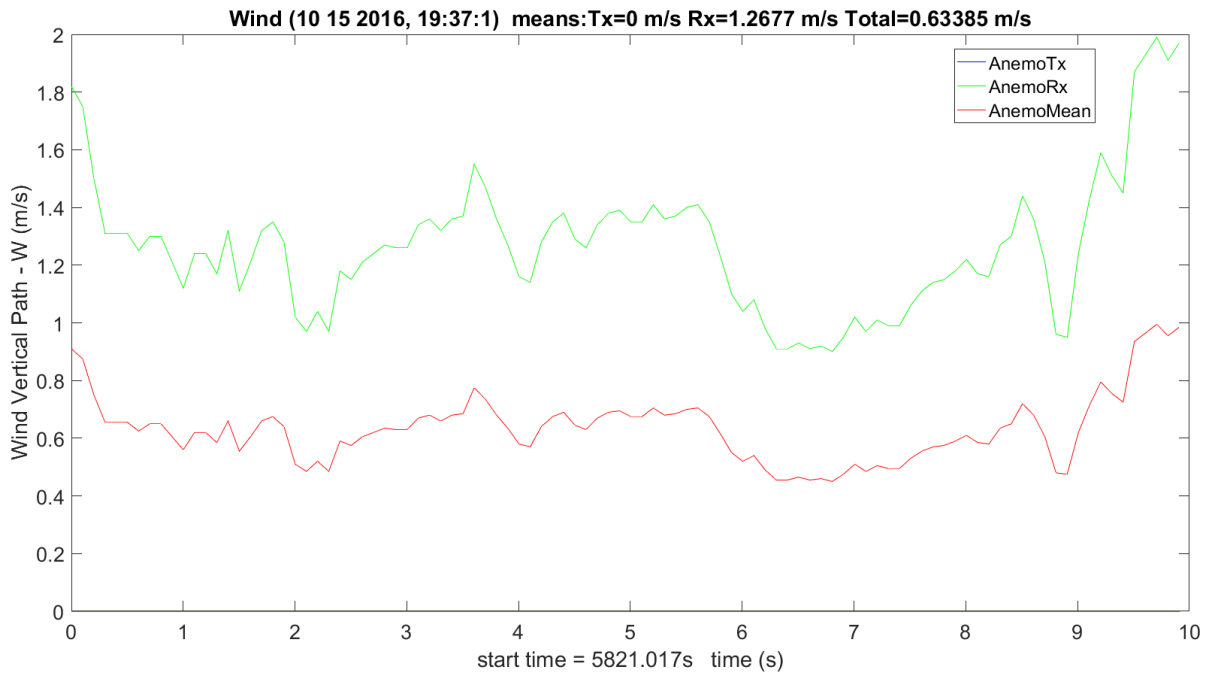


Figure 3.142. Wind W Transmit & Receiver – 10142016_193175.

Figure 3.143 shows the transmit and receive hygrometers. The dry and wet differences are small and the dry is utilized, since it is optimal for most Colorado weather conditions. The humidity at the Mesa is significantly lower than the transmit: about 2.5 g/m³ higher; this is expected under most weather conditions.

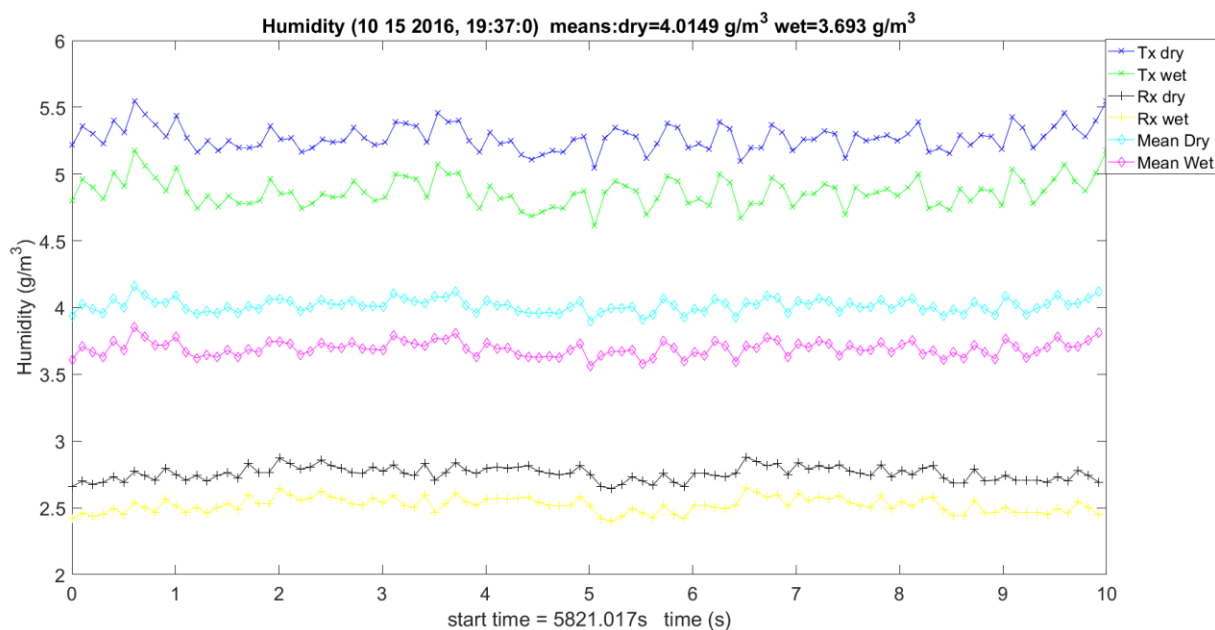


Figure 3.143. Humidity Transmit, Receiver & Mean – 10142016_193175.

Figure 3.144 shows the WB scans amplitude scintillation variance. It is easy to see how it peaks at the absorption peak; it is almost an identical shape. The total range is from zero to 2.5 dB^2 . Figure 3.145 is the predicted value magnified since it is much less.

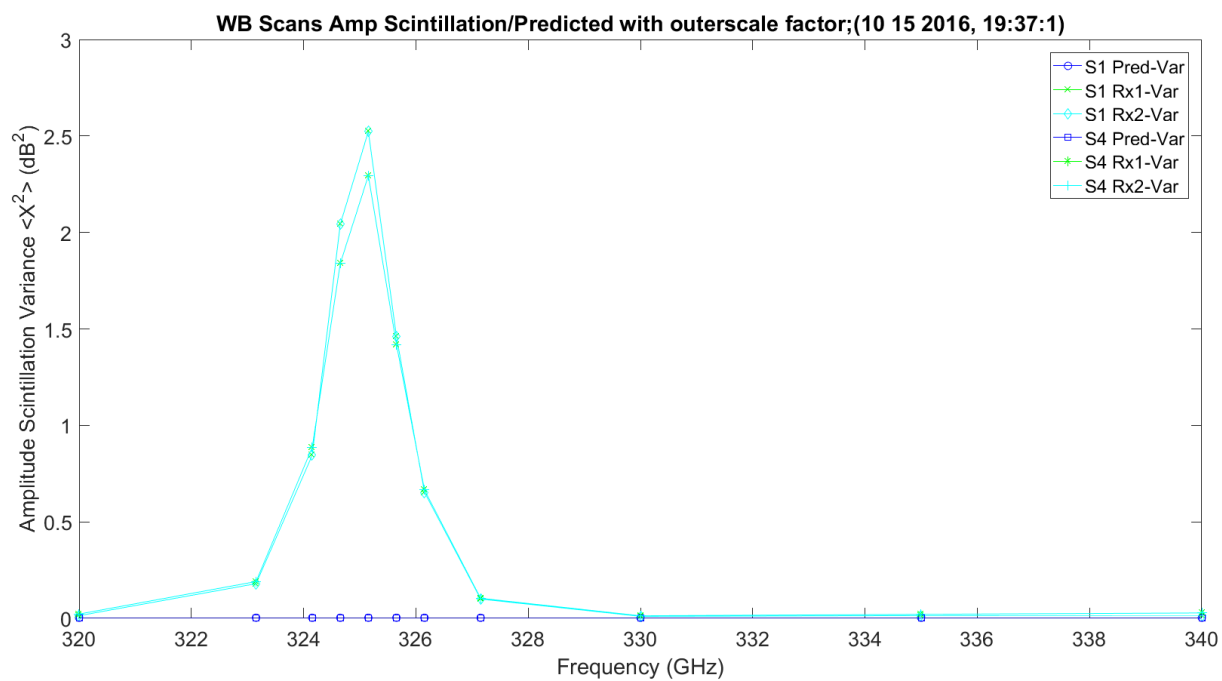


Figure 3.144. WB Amplitude Scintillation Variance and Predicted – 10142016_193175.

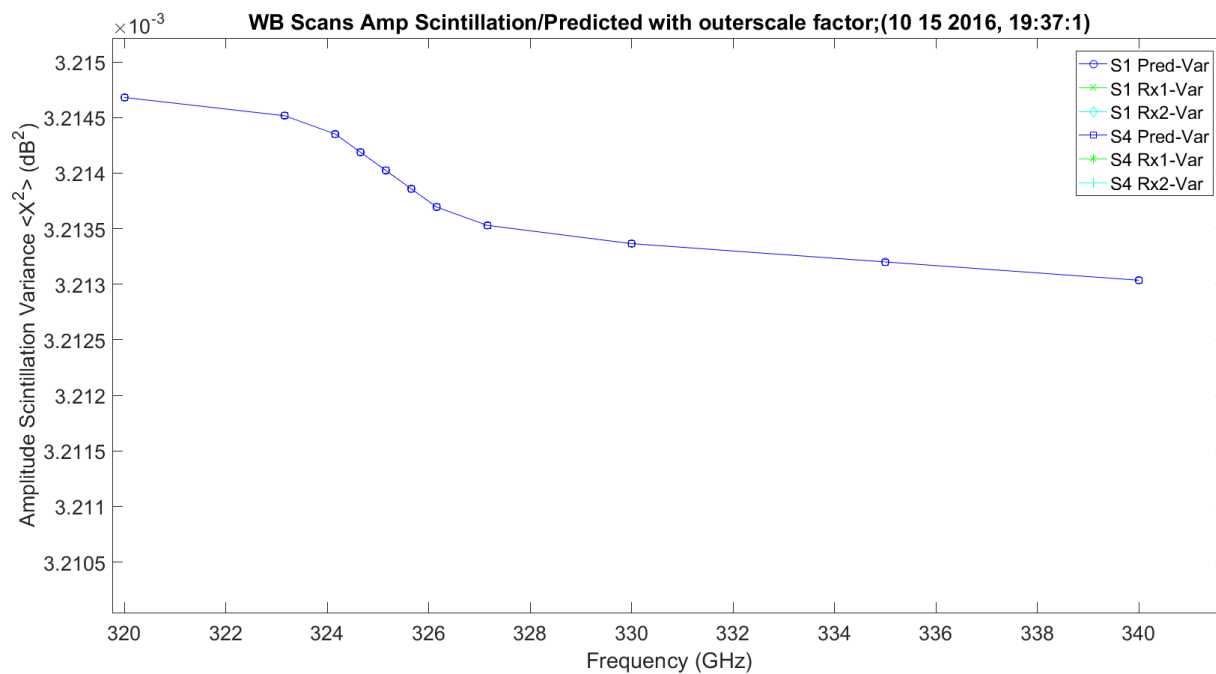


Figure 3.145. Enlarge of WB Amplitude Scintillation Variance and Predicted – 10142016_193175.

Figure 3.146 shows the LWL scans amplitude scintillation variance. It is a linear increase over frequency with a range of 1 to 2.5 dB². Figure 3.147 is the predicted value magnified since it is much less.

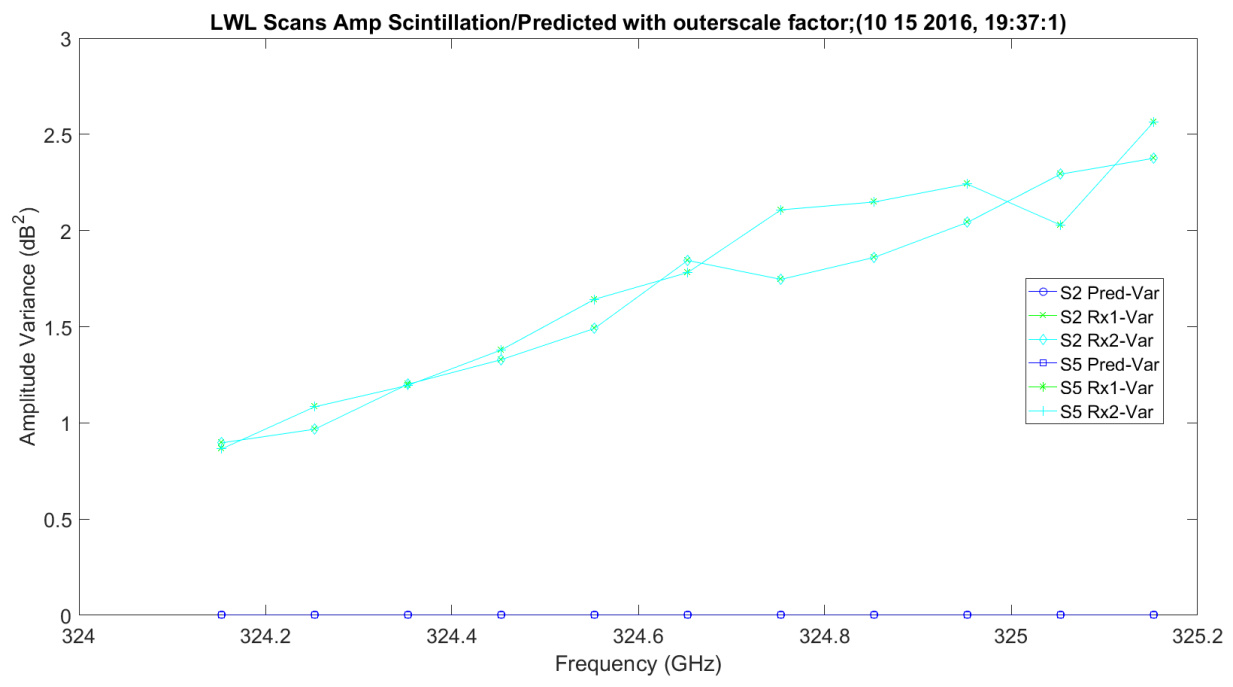


Figure 3.146. LWL Amplitude Scintillation Variance and Predicted – 10142016_193175.

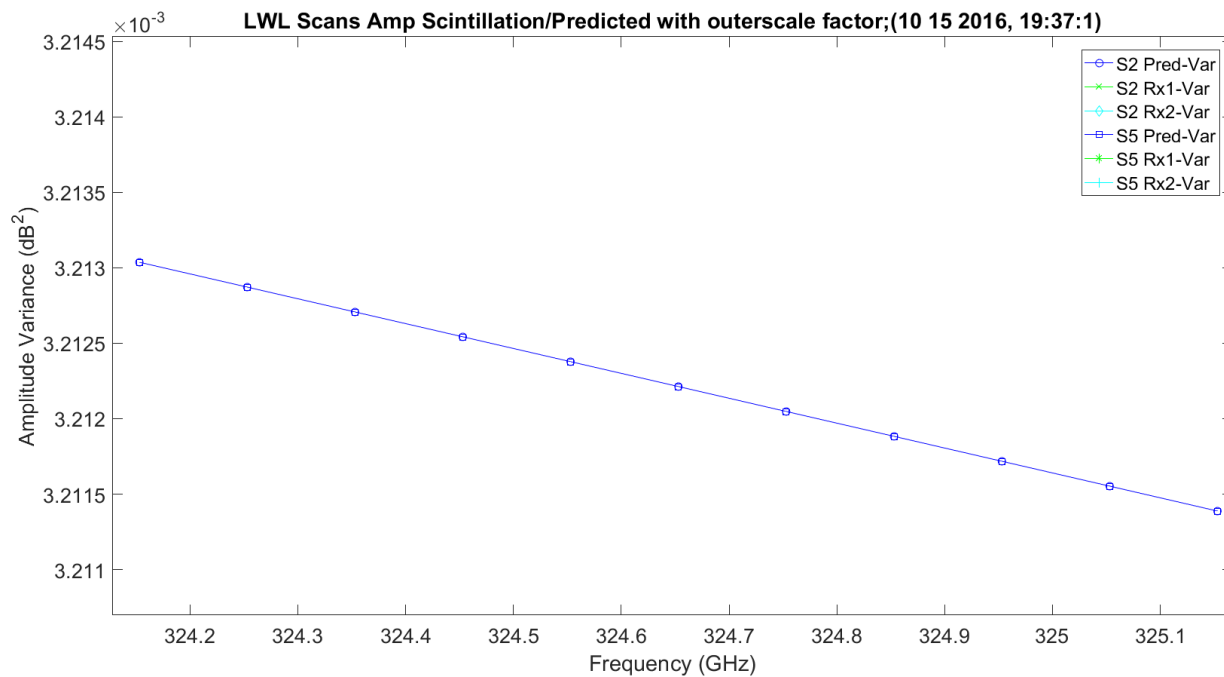


Figure 3.147. Enlarge LWL Amplitude Scintillation Variance and Predicted – 10142016_193175.

Figure 3.148 shows the UWL scans amplitude scintillation variance. It is a linear decrease over frequency with a range of 1 to 2.5 dB². Figure 3.149 is the predicted value magnified since it is much less.

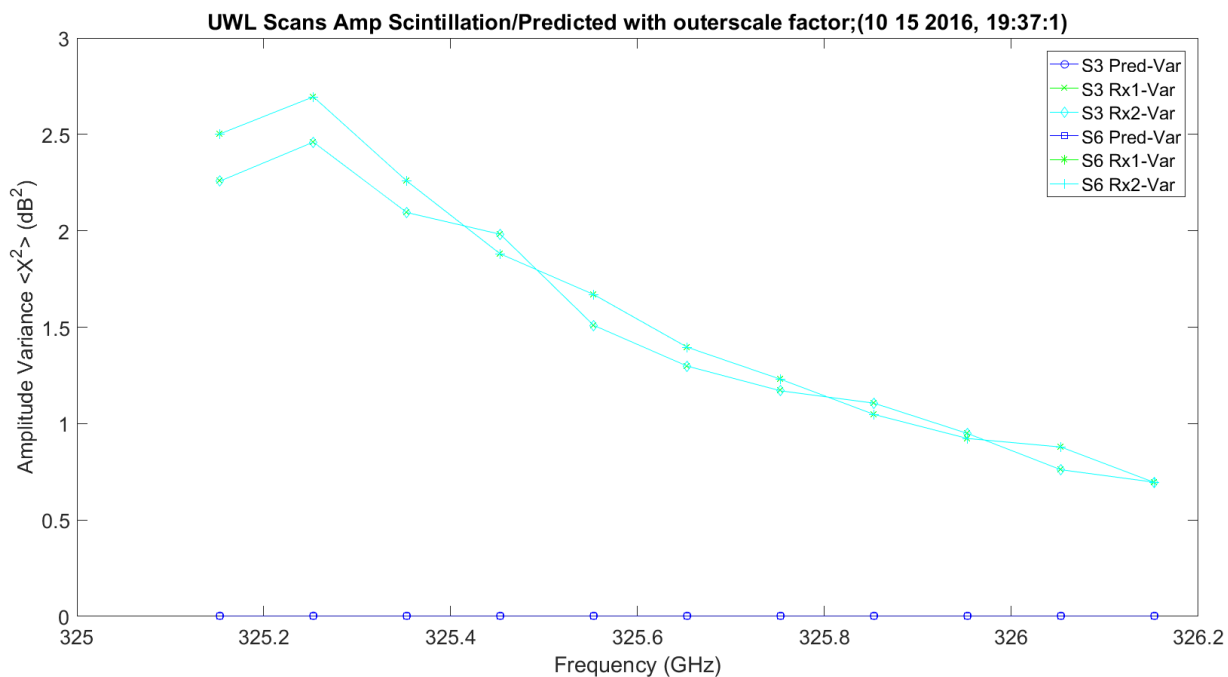


Figure 3.148. UWL Amplitude Scintillation Variance and Predicted – 10142016_193175.

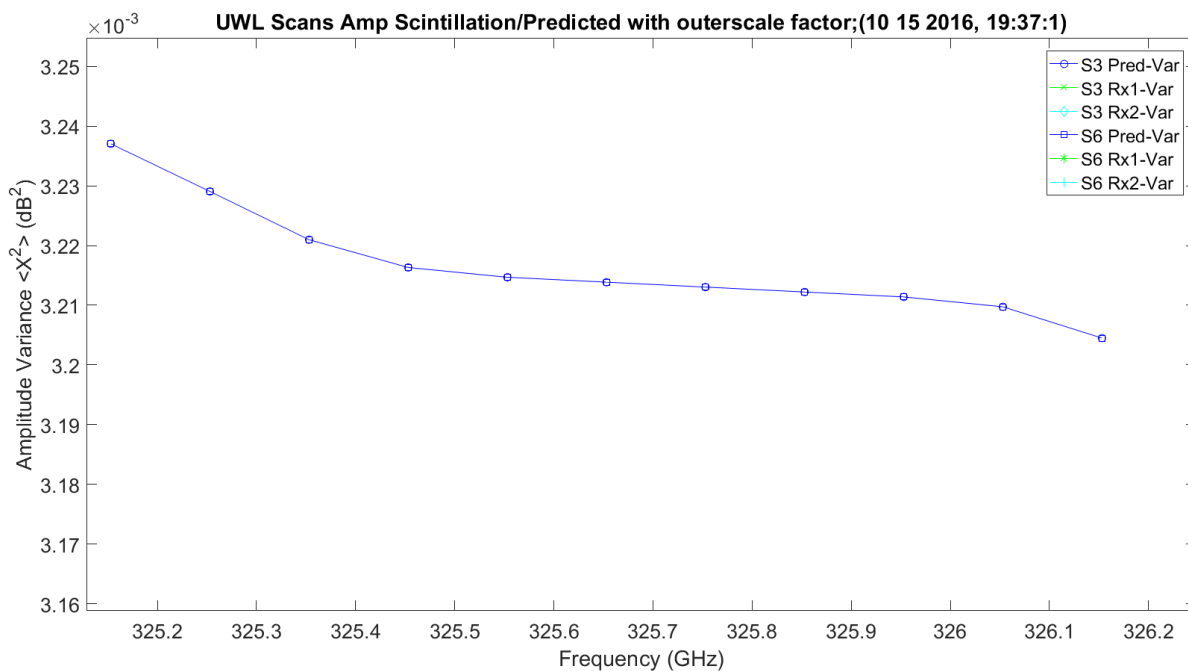


Figure 3.149. Enlarged UWL Amplitude Scintillation Variance and Predicted – 10142016_193175.

Figure 3.150 shows the WB scans amplitude scintillation Standard Deviation (STD). It obviously has similar characteristics to variance. It is a range over frequency with a range of 0.2 to 1.6 dB². Figure 3.151 is the predicted value magnified since it is much less.

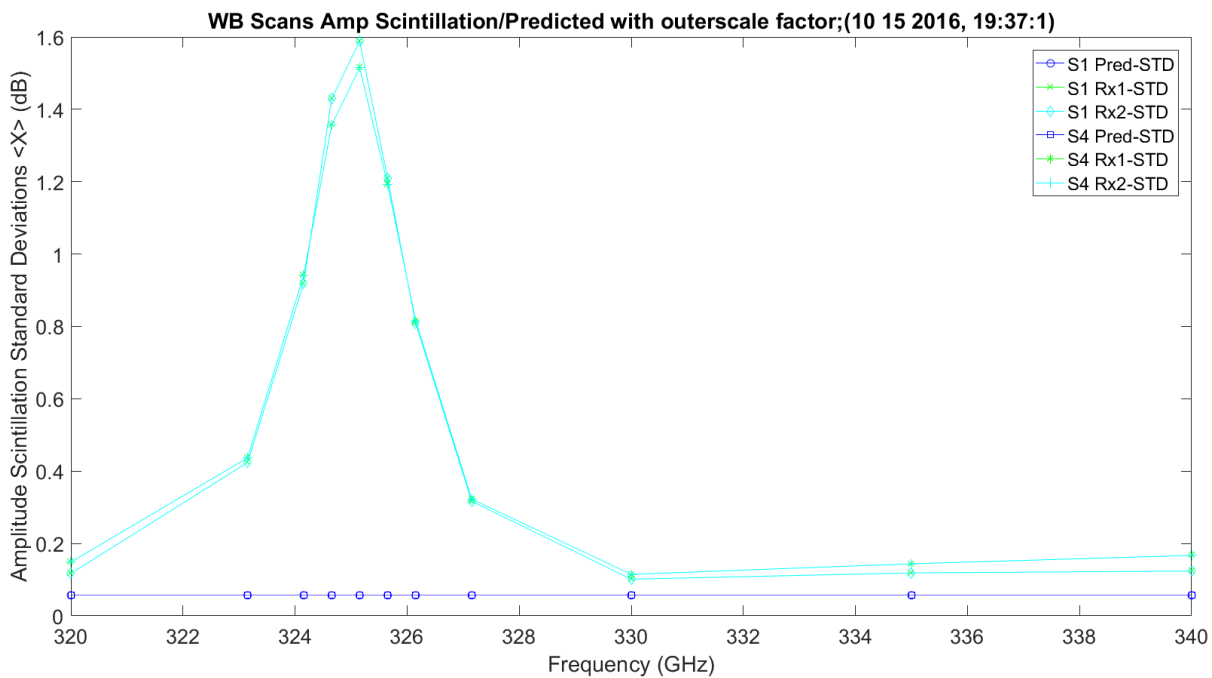


Figure 3.150. WB Amplitude Scintillation and Predicted – 10142016_193175.

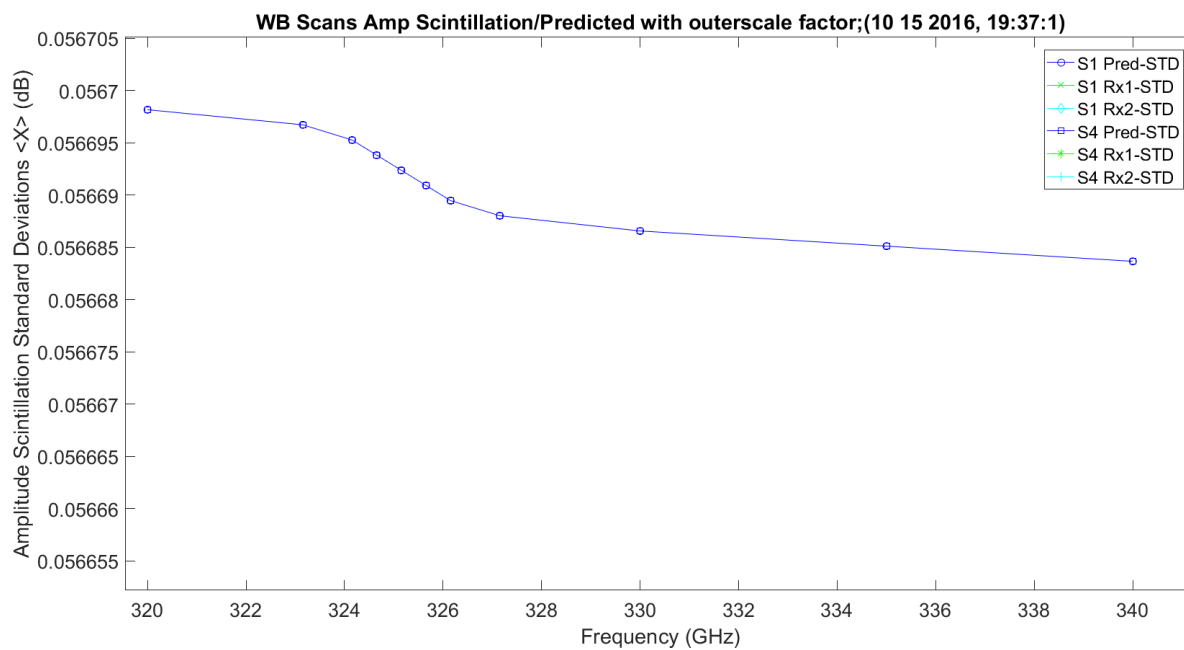


Figure 3.151. Enlarged WB Amplitude Scintillation and Predicted – 10142016_193175.

Figure 3.152 shows the LWL scans amplitude scintillation STD. It obviously has similar characteristics to variance. It is a range over frequency with a range of 0.9 to 1.6 dB². Figure 3.153 is the predicted value magnified since it is much less.

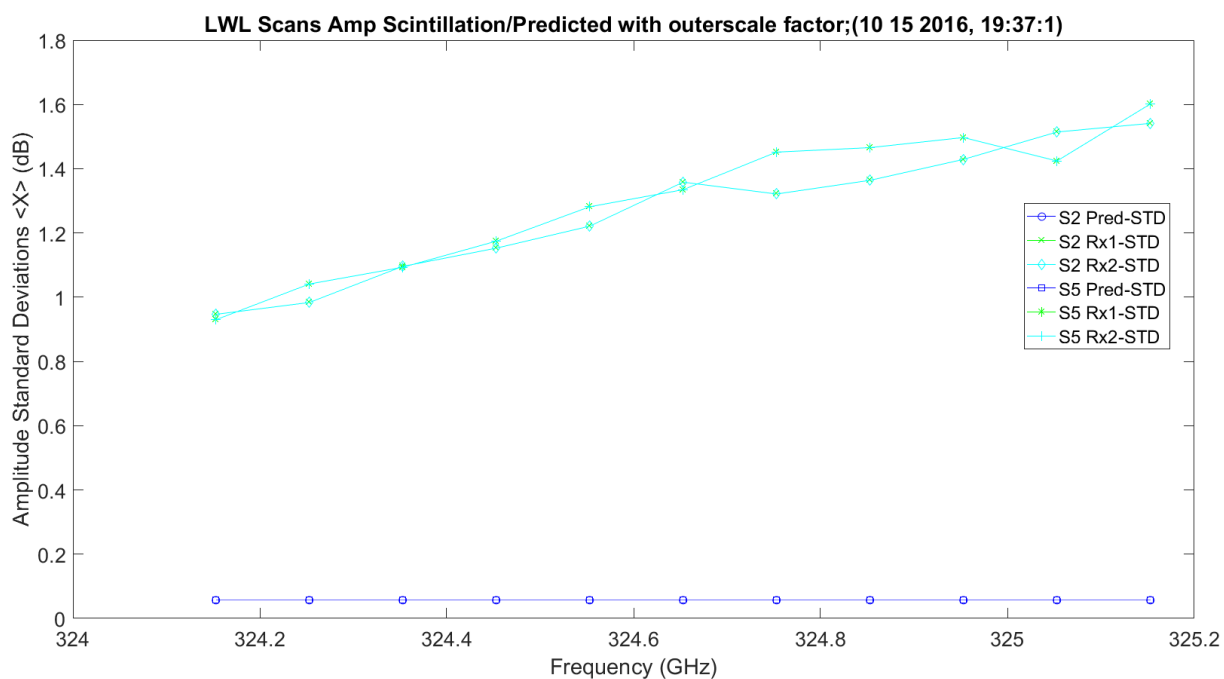


Figure 3.152. LWL Amplitude Scintillation and Predicted – 10142016_193175.

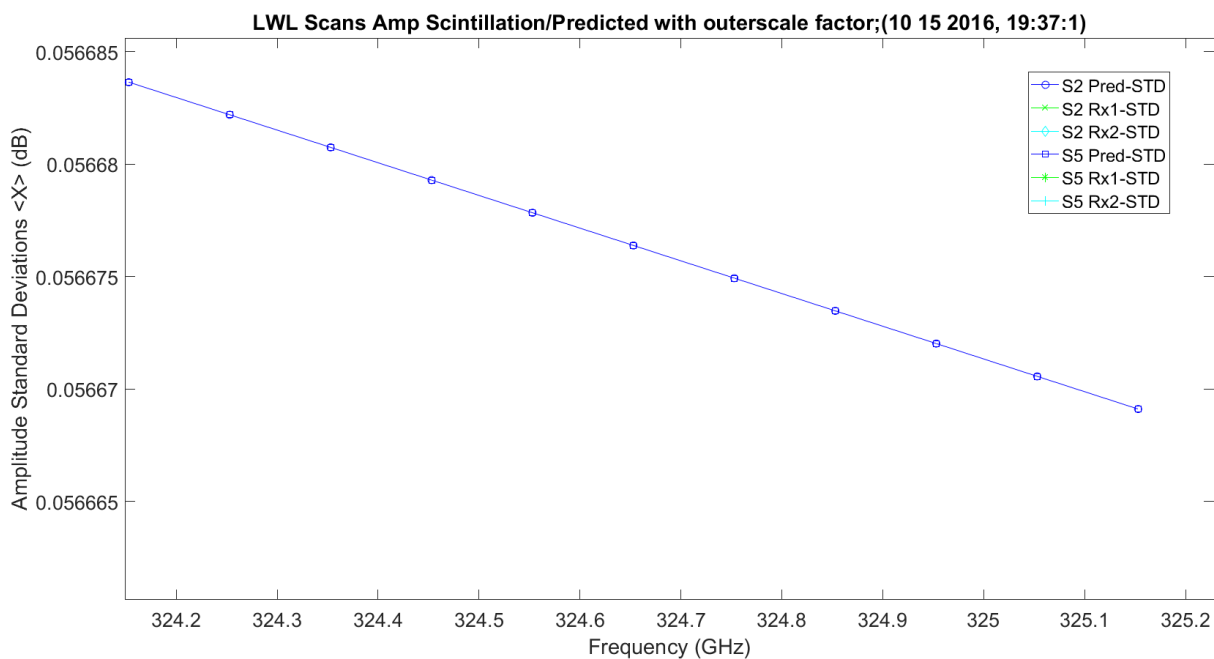


Figure 3.153. Enlarged LWL Amplitude Scintillation and Predicted – 10142016_193175.

Figure 3.154 shows the UWL scans amplitude scintillation STD. It obviously has similar characteristics to variance. It is a range over frequency with a range of 0.9 to 1.6 dB². Figure 3.155 is the predicted value magnified since it is much less.

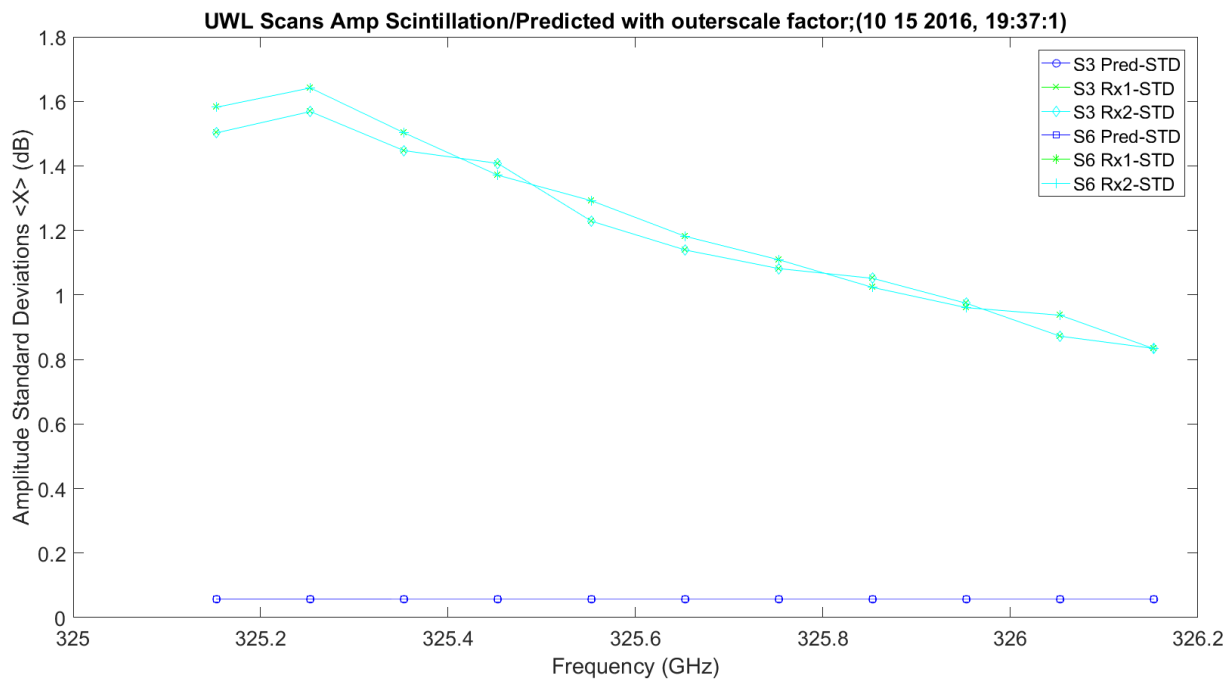


Figure 3.154. UWL Amplitude Scintillation and Predicted – 10142016_193175.

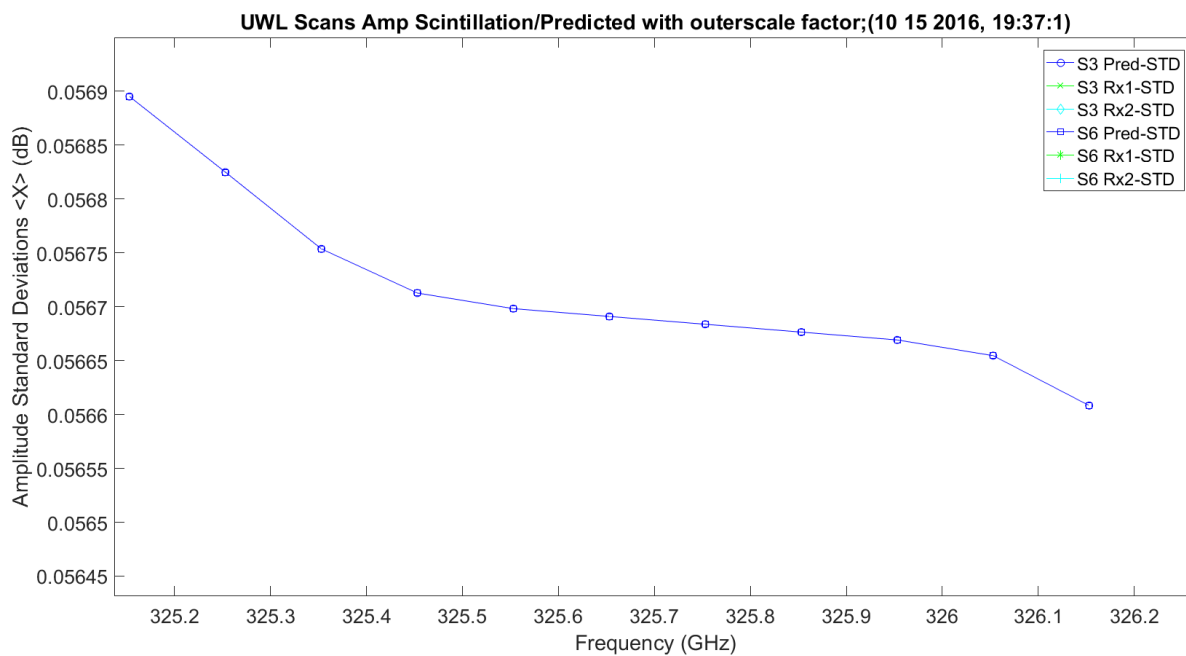


Figure 3.155. Enlarged UWL Amplitude Scintillation and Predicted – 10142016_193175.

Figure 3.156 shows the WB scans phase scintillation variance. The variance is around 180 degrees, much higher than the prediction which is shown in Figure 3.157. It has linear growth with frequency.

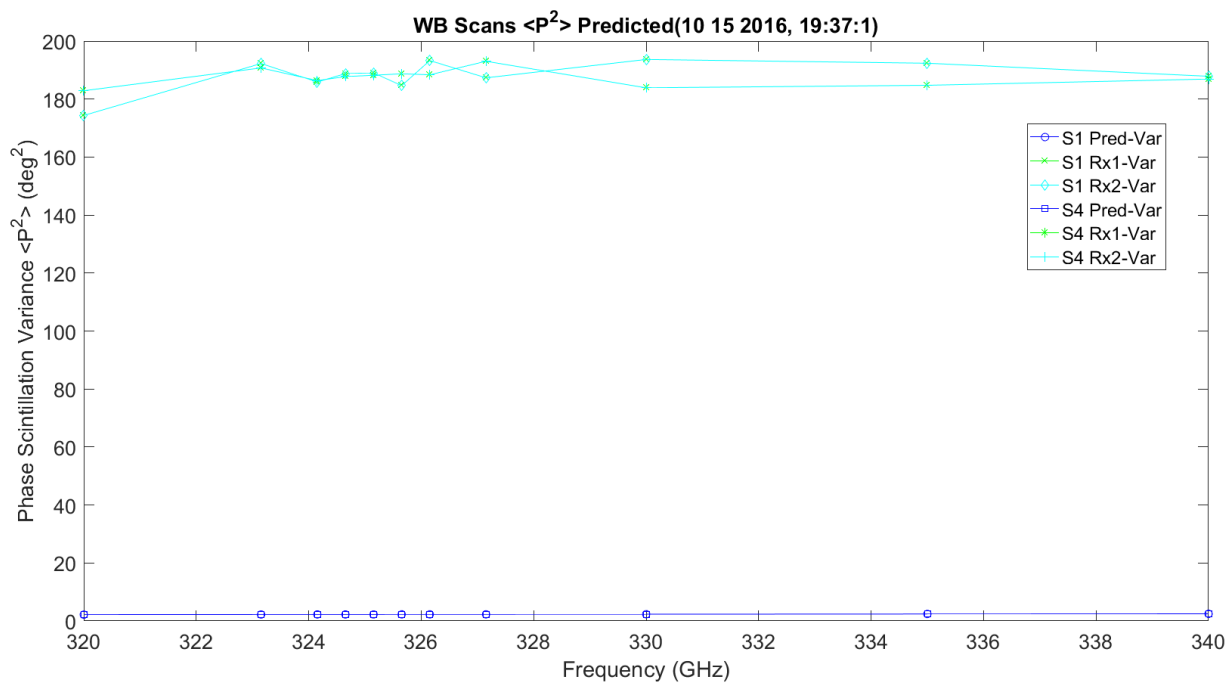


Figure 3.156. WB Phase Scintillation Variance and Predicted – 10142016_193175.

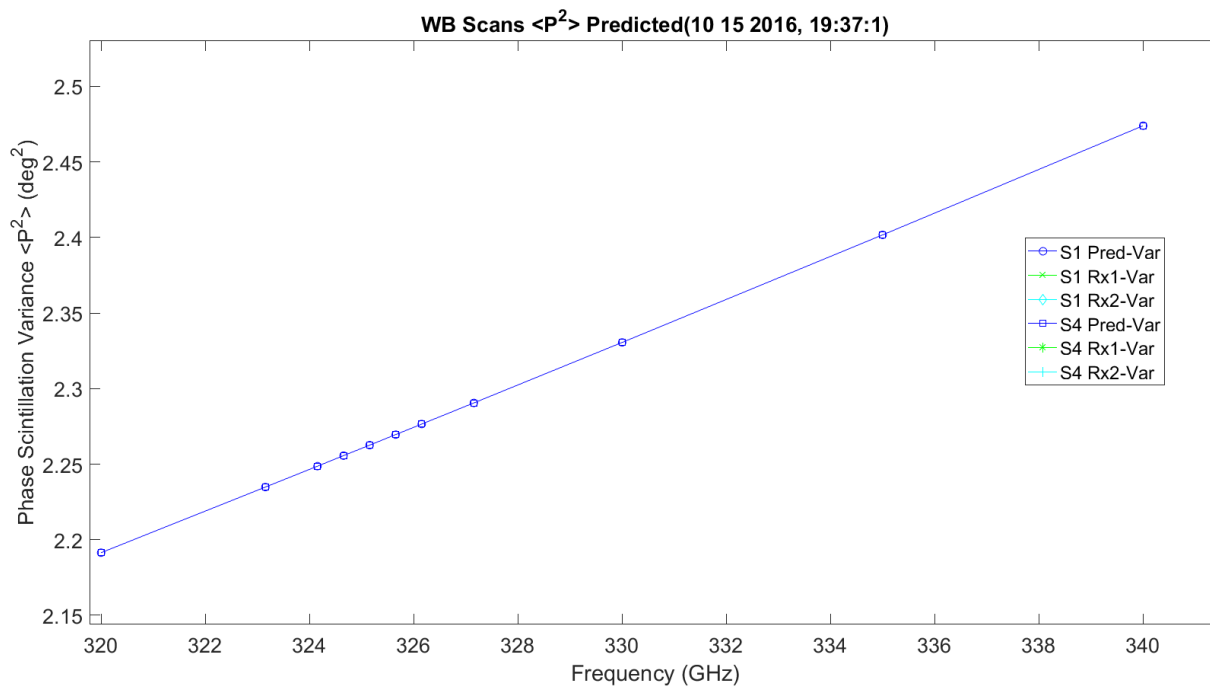


Figure 3.157. Enlarged WB Phase Scintillation Variance and Predicted – 10142016_193175.

Figure 3.158 shows the LWL scans phase scintillation variance. The variance is around 180 degrees, much higher than the prediction which is shown in Figure 3.159. It has linear growth with frequency.

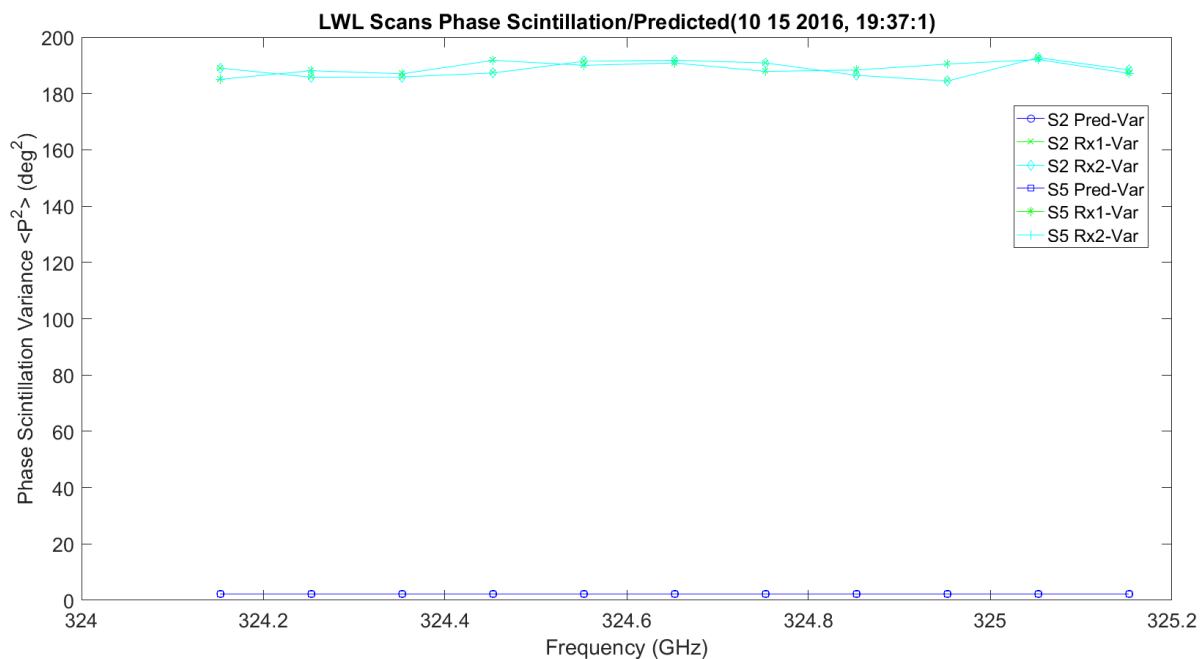


Figure 3.158. LWL Phase Scintillation Variance and Predicted – 10142016_193175.

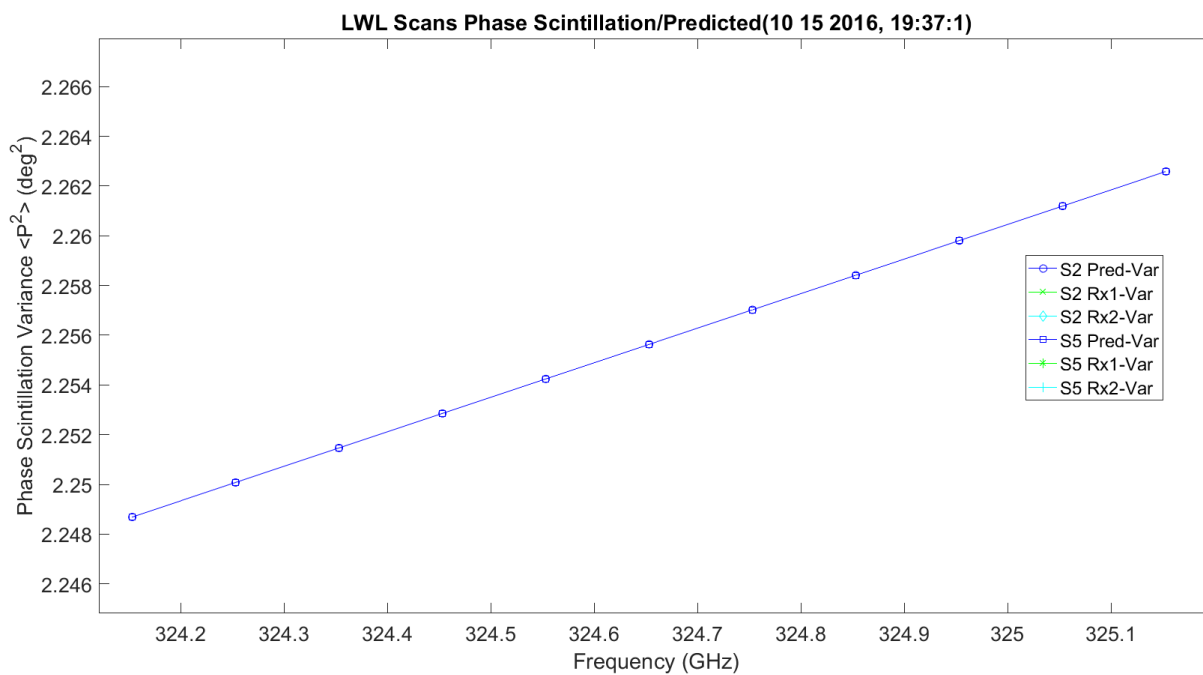


Figure 3.159. Enlarged LWL Phase Scintillation Variance and Predicted – 10142016_193175.

Figure 3.160 shows the UWL scans phase scintillation variance. The variance is around 180 degrees, much higher than the prediction which is shown in Figure 3.161. It has linear growth with frequency.

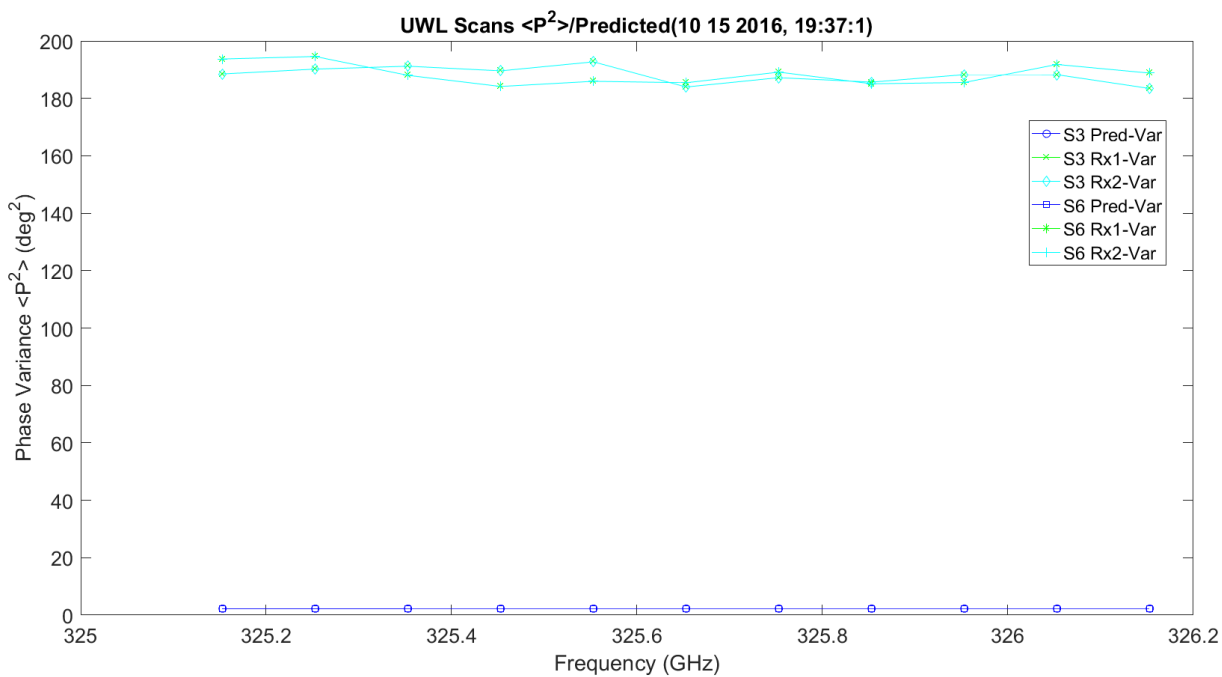


Figure 3.160. UWL Phase Scintillation Variance and Predicted – 10142016_193175.

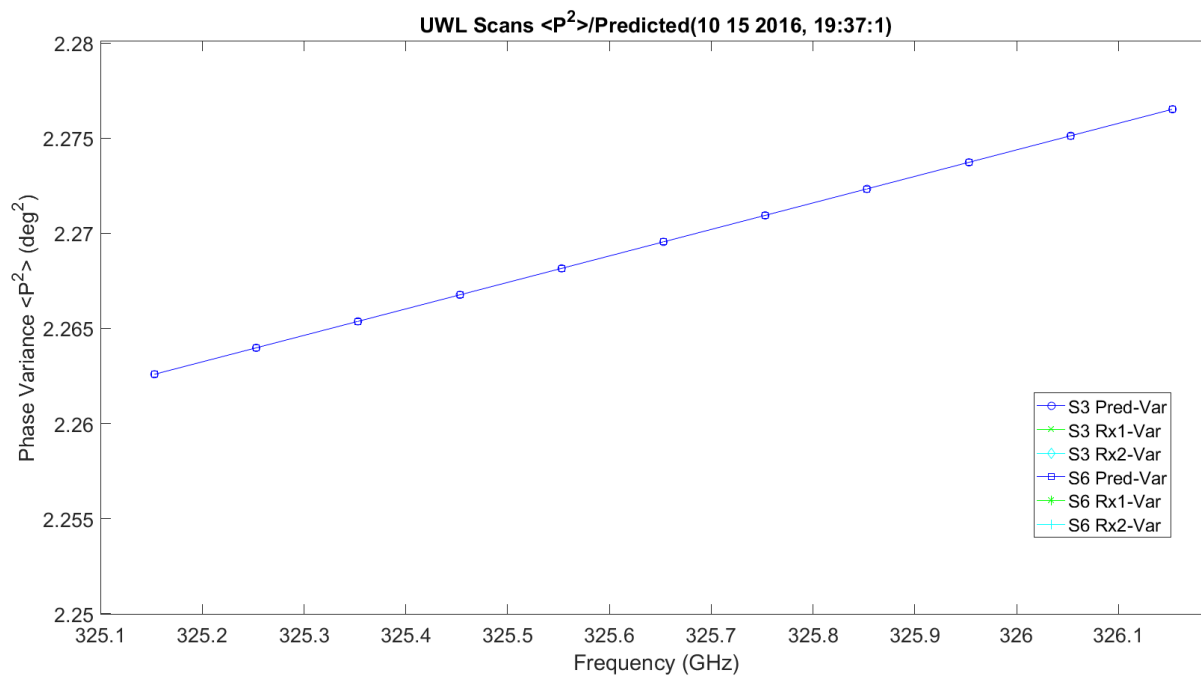


Figure 3.161. Enlarged UWL Phase Scintillation Variance and Predicted – 10142016_193175.

Figure 3.162 shows the WB scans phase scintillation STD. The STD variance is around 14 degrees, much higher than the prediction which is shown in Figure 3.163. It has linear growth with frequency.

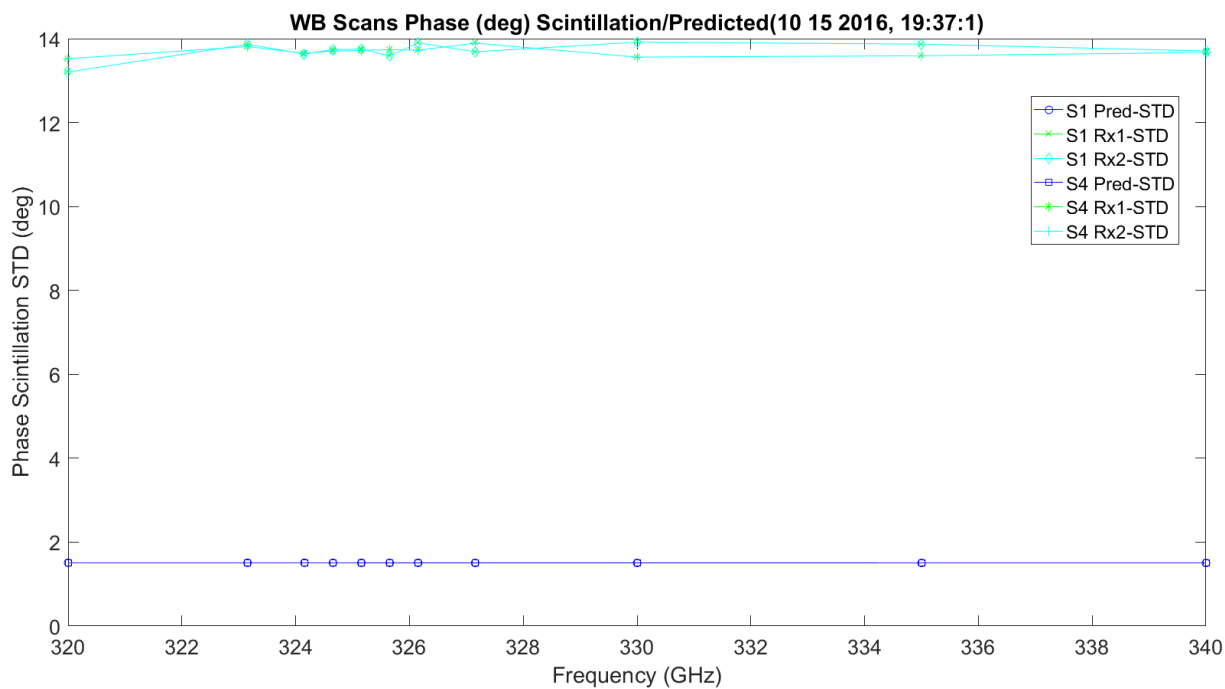


Figure 3.162. WB Phase Scintillation STD and Predicted Deg. – 10142016_193175.

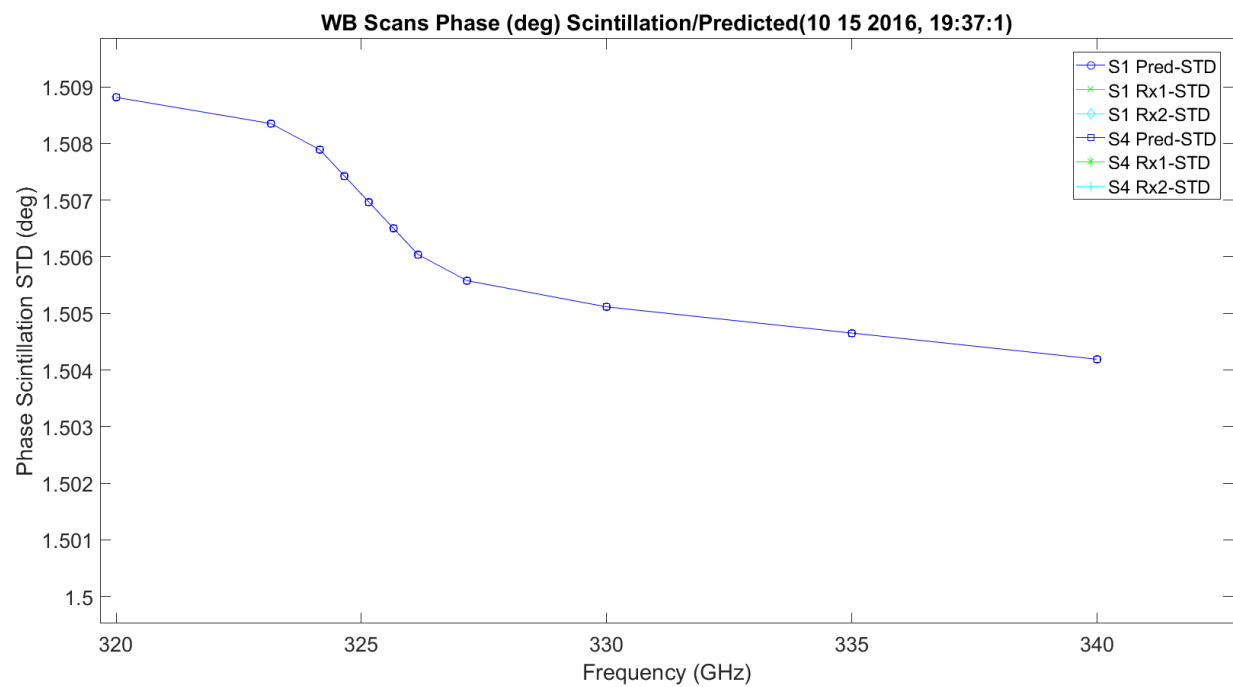


Figure 3.163. Enlarged WB Phase Scintillation STD and Predicted Deg. – 10142016_193175.

Figure 3.164 shows the LWL scans phase scintillation STD. The STD variance is around 14 degrees, much higher than the prediction which is shown in Figure 3.165. It has linear growth with frequency.

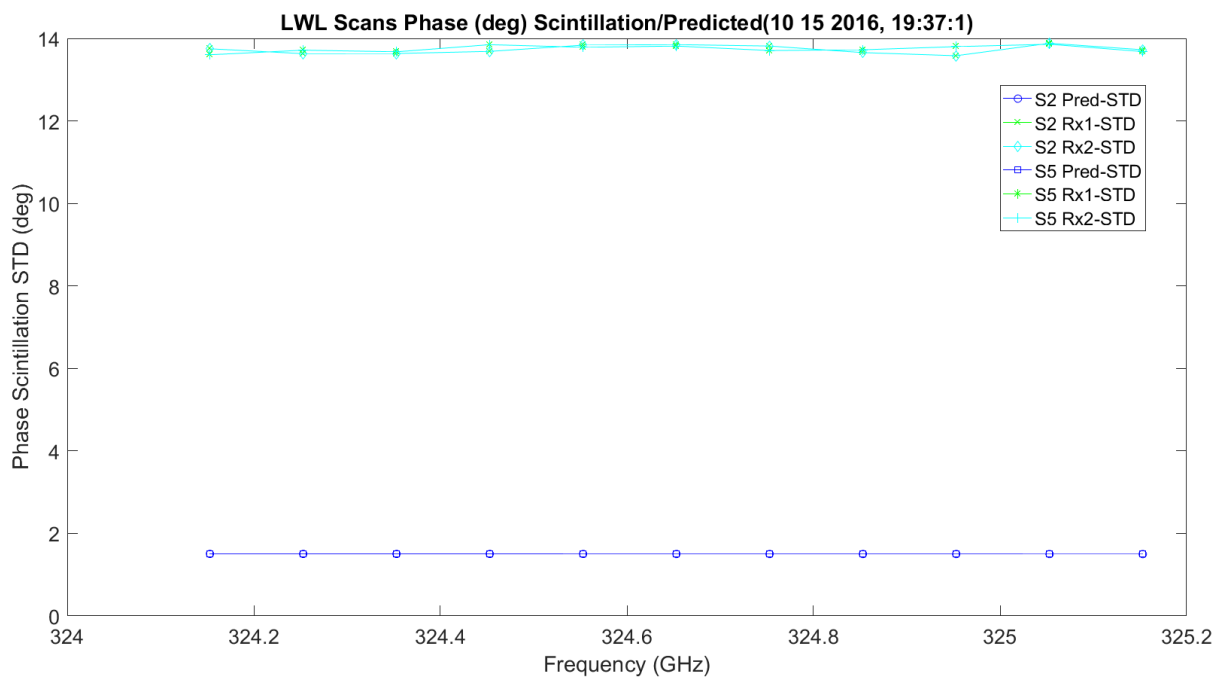


Figure 3.164. LWL Phase Scintillation STD and Predicted Deg. – 10142016_193175.

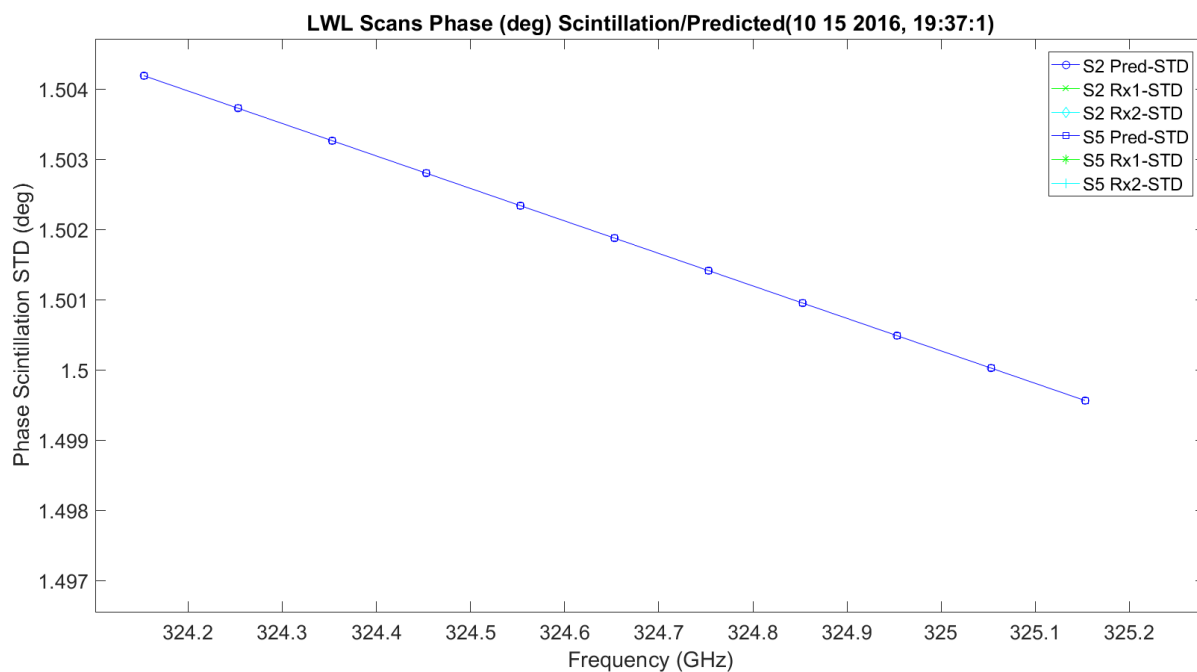


Figure 3.165. Enlarged LWL Phase Scintillation STD and Predicted Deg. – 10142016_193175.

Figure 3.166 shows the UWL scans phase scintillation STD. The STD variance is around 14 degrees, much higher than the prediction which is shown in Figure 3.167. It has linear growth with frequency.

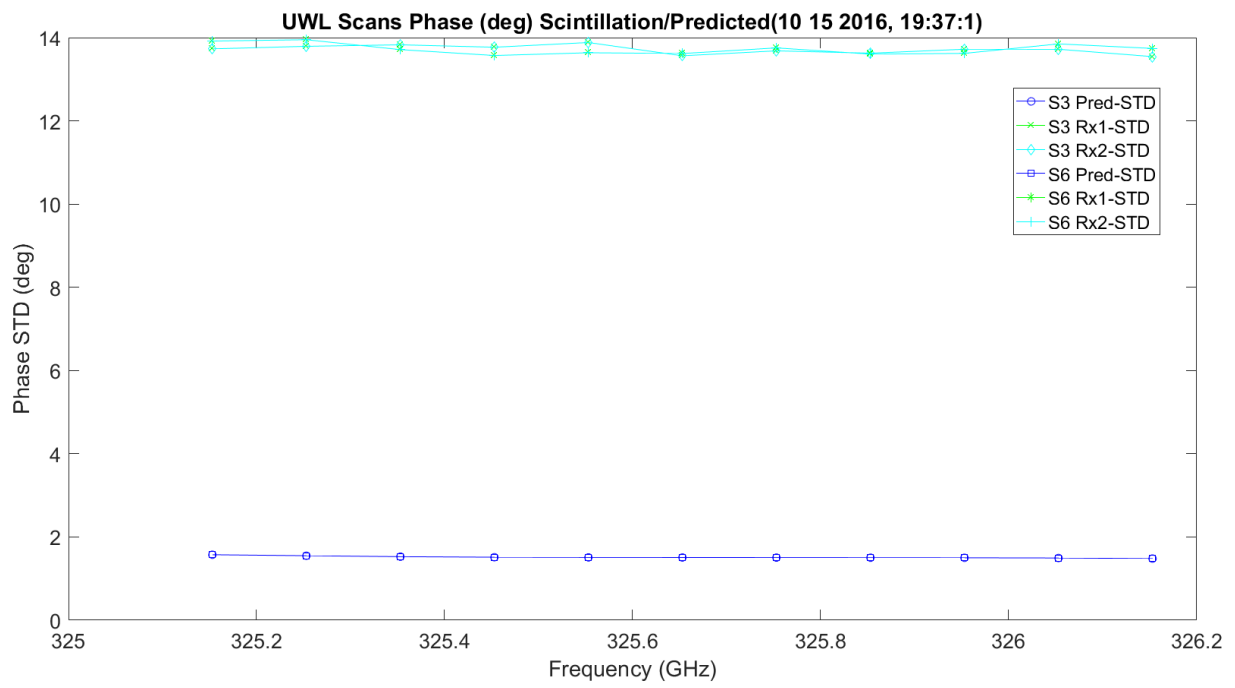


Figure 3.166. UWL Phase Scintillation STD and Predicted Deg. – 10142016_193175.

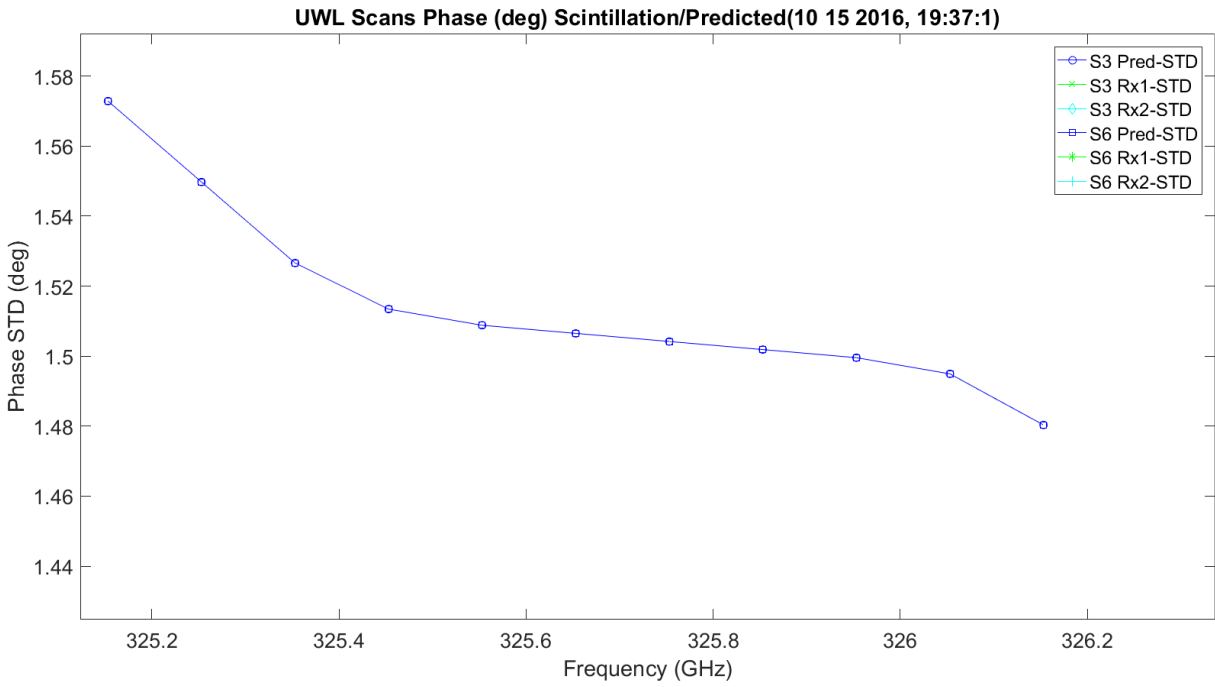


Figure 3.167. Enlarged UWL Phase Scintillation STD and Predicted Deg. – 10142016_193175.

Figure 3.168 shows the WB scans phase scintillation STD. The STD variance is around 0.035 millimeters, much higher than the prediction which is shown in Figure 3.169. It has linear growth with frequency.

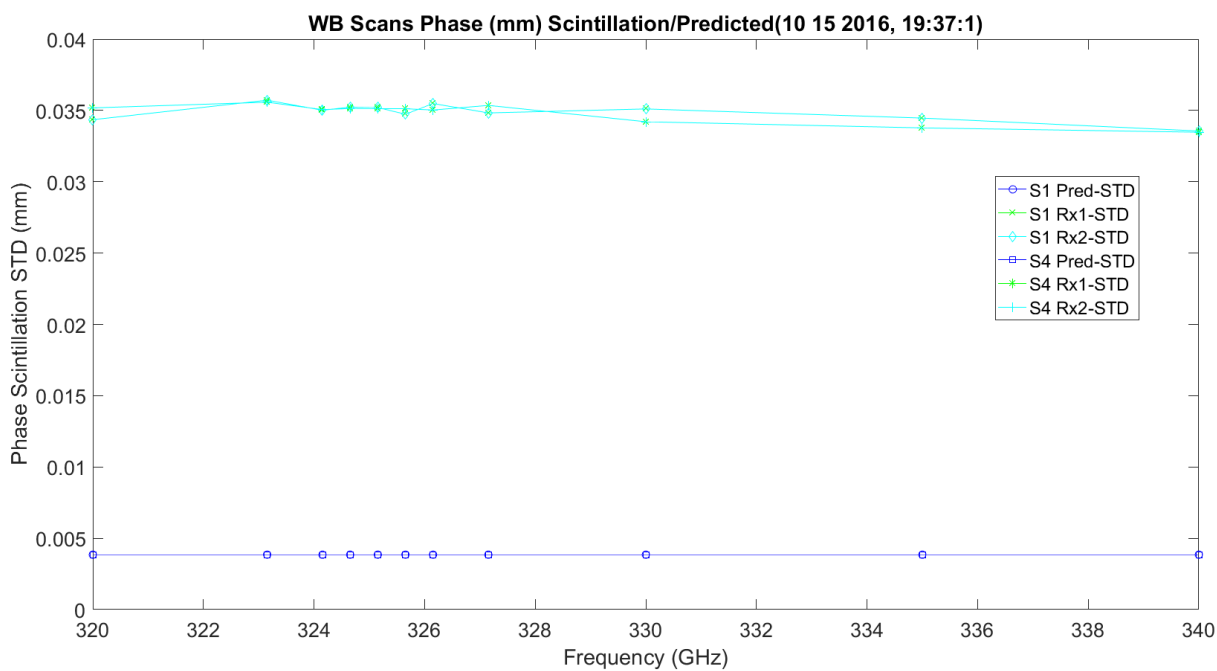


Figure 3.168. WB Phase Scintillation STD and Predicted MM – 10142016_193175.

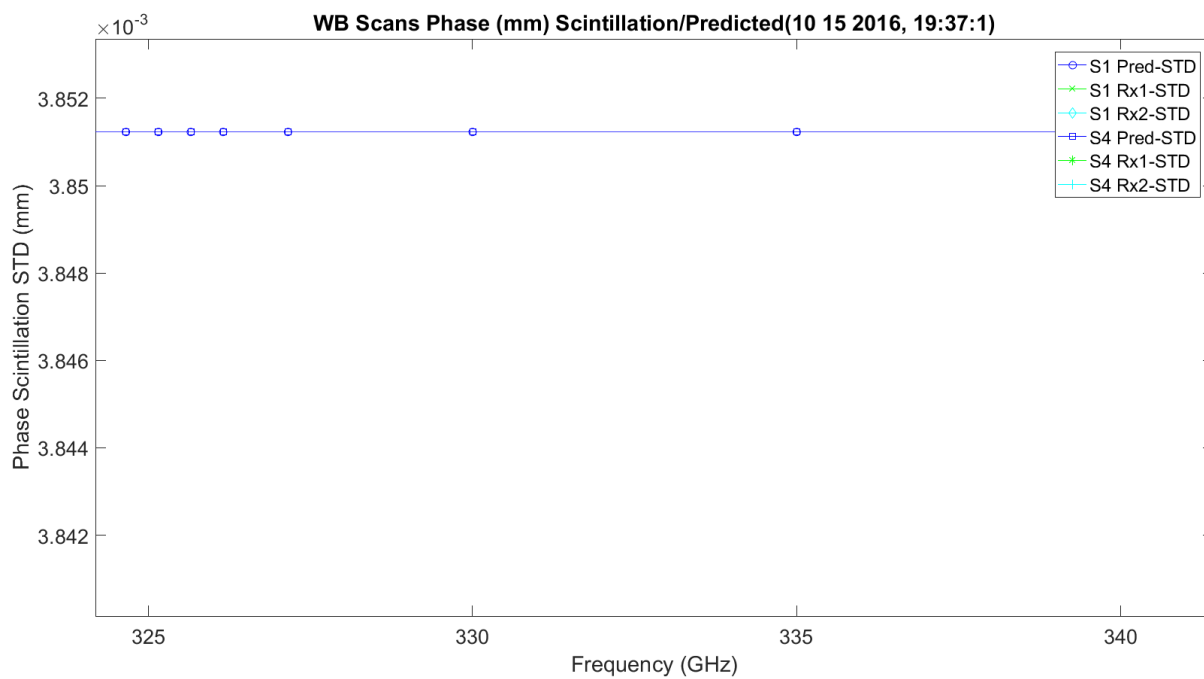


Figure 3.169. Enlarged WB Phase Scintillation STD and Predicted MM – 10142016_193175.

Figure 3.170 shows the LWL scans phase scintillation STD. The STD variance is around 0.035 millimeters, much higher than the prediction which is shown in Figure 3.171. It has linear growth with frequency.

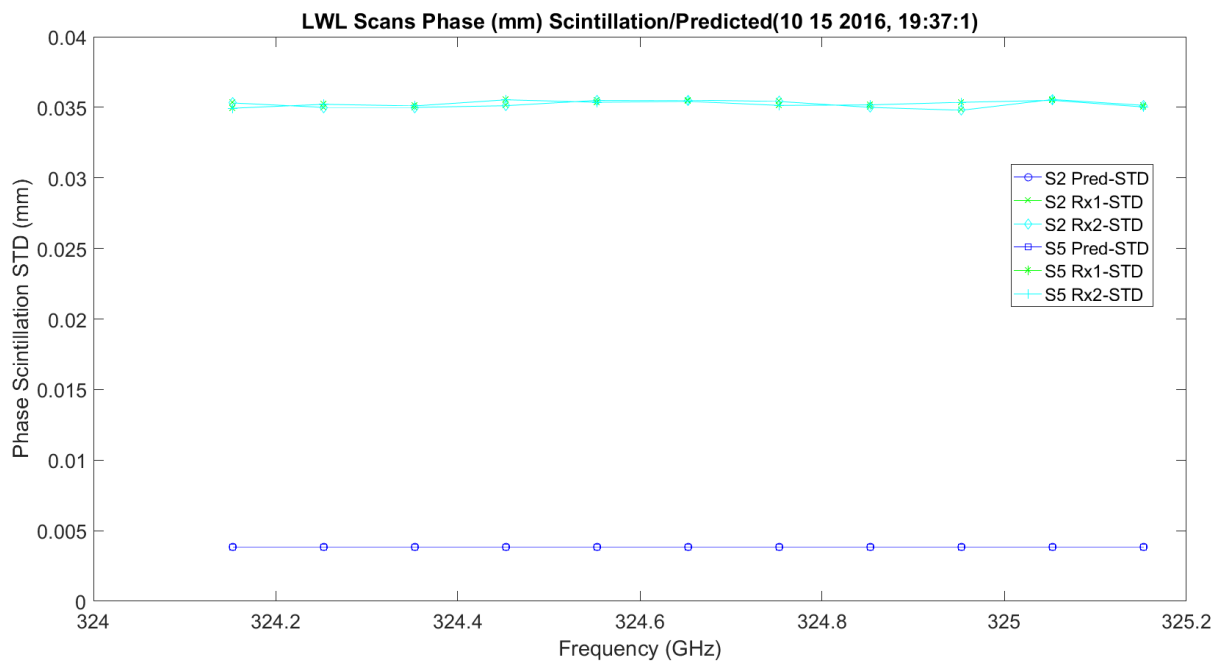


Figure 3.170. LWL Phase Scintillation STD and Predicted MM – 10142016_193175.

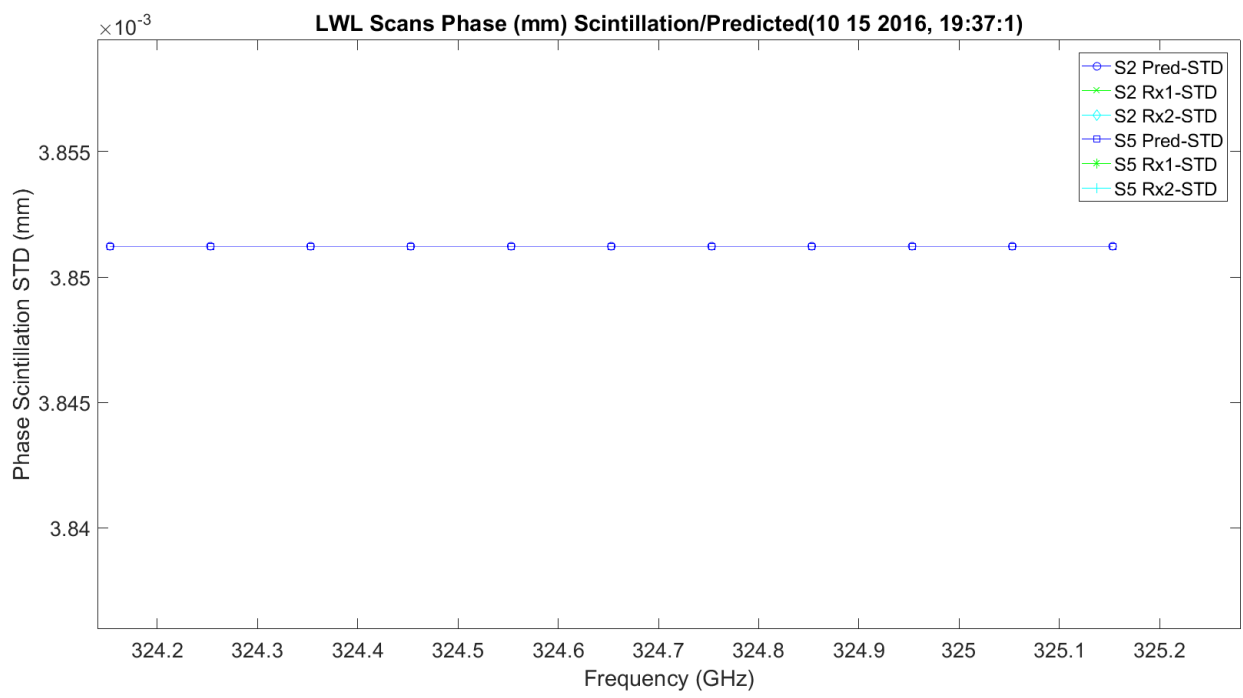


Figure 3.171. Enlarged LWL Phase Scintillation STD and Predicted MM – 10142016_193175.

Figure 3.172 shows the UWL scans phase scintillation STD. The STD variance is around 0.035 millimeters, much higher than the prediction which is shown in Figure 3.173. It has linear growth with frequency.

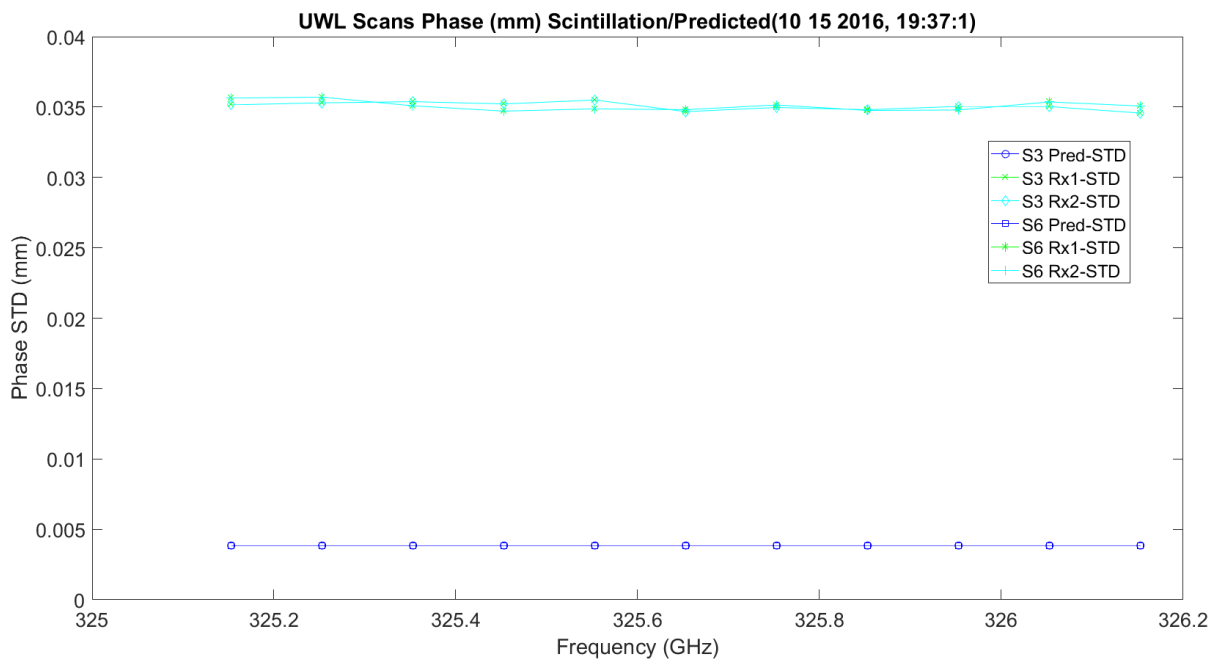


Figure 3.172. UWL Phase Scintillation STD and Predicted MM – 10142016_193175.

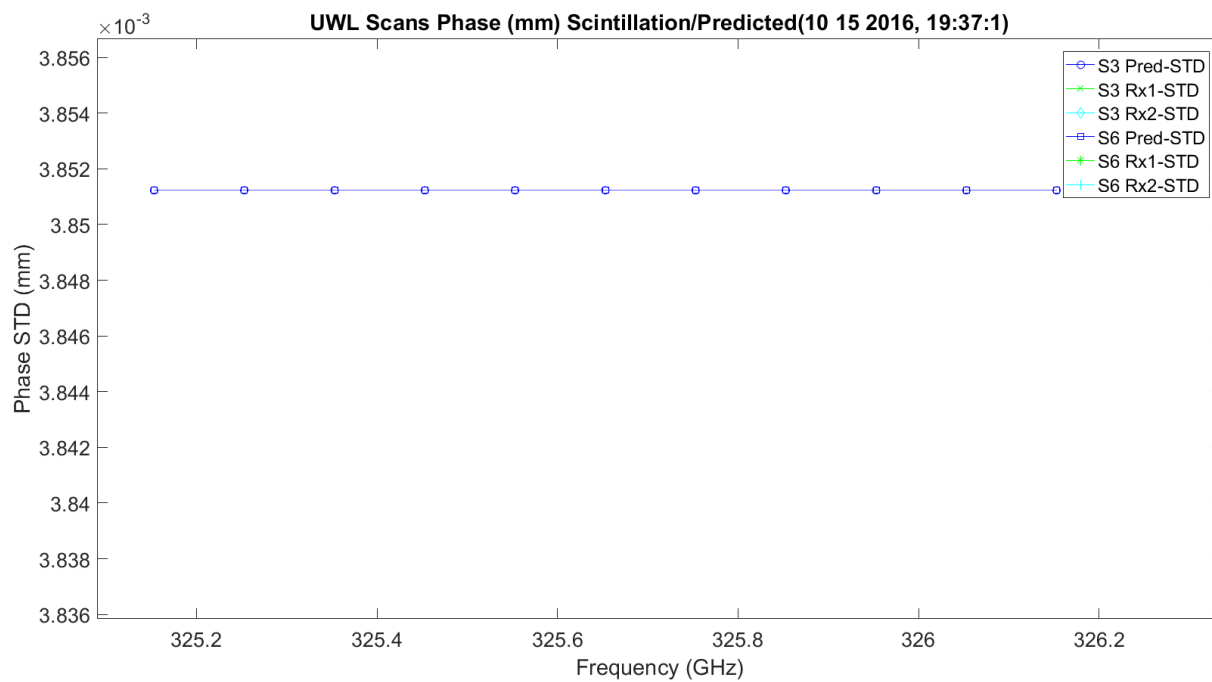


Figure 3.173. UWL Phase Scintillation STD and Predicted MM – 10142016_193175.

Figure 3.174 shows the WB scans phase scintillation STD. The STD variance is around 0.12 picoseconds, much higher than the prediction which is shown in Figure 3.175. It has linear growth with frequency.

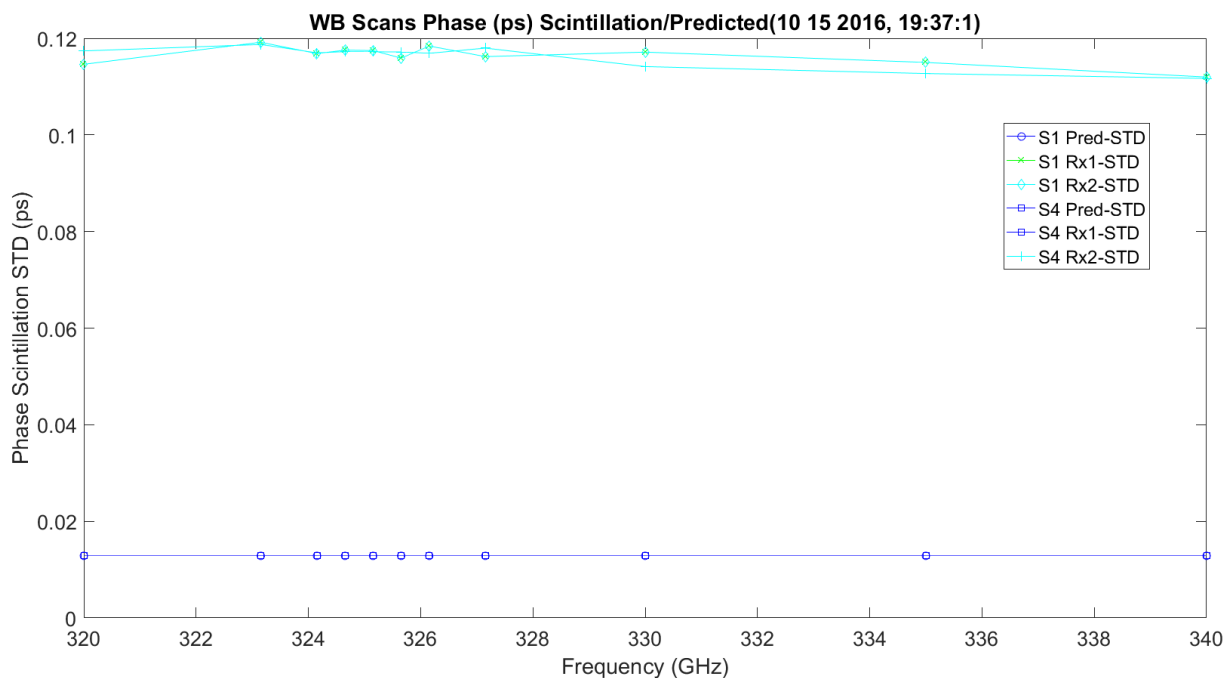


Figure 3.174. WB Phase Scintillation STD and Predicted ps – 10142016_193175.

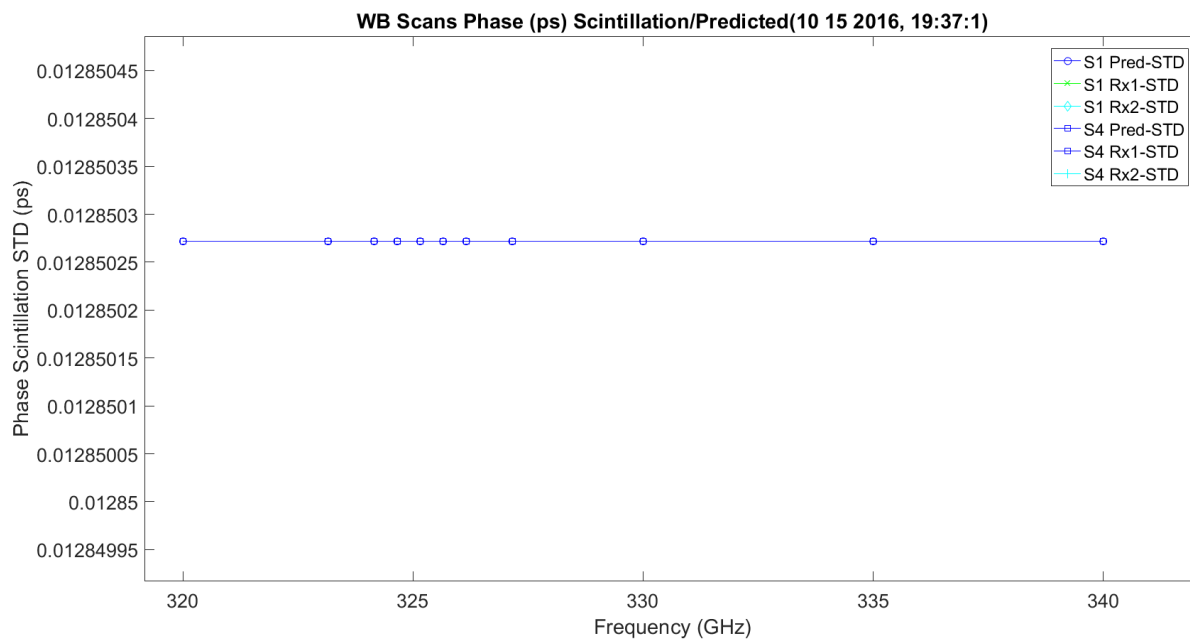


Figure 3.175. Enlarged WB Phase Scintillation STD and Predicted ps – 10142016_193175.

Figure 3.176 shows the LWL scans phase scintillation STD. The STD variance is around 0.12 picoseconds, much higher than the prediction which is shown in Figure 3.177. It has linear growth with frequency.

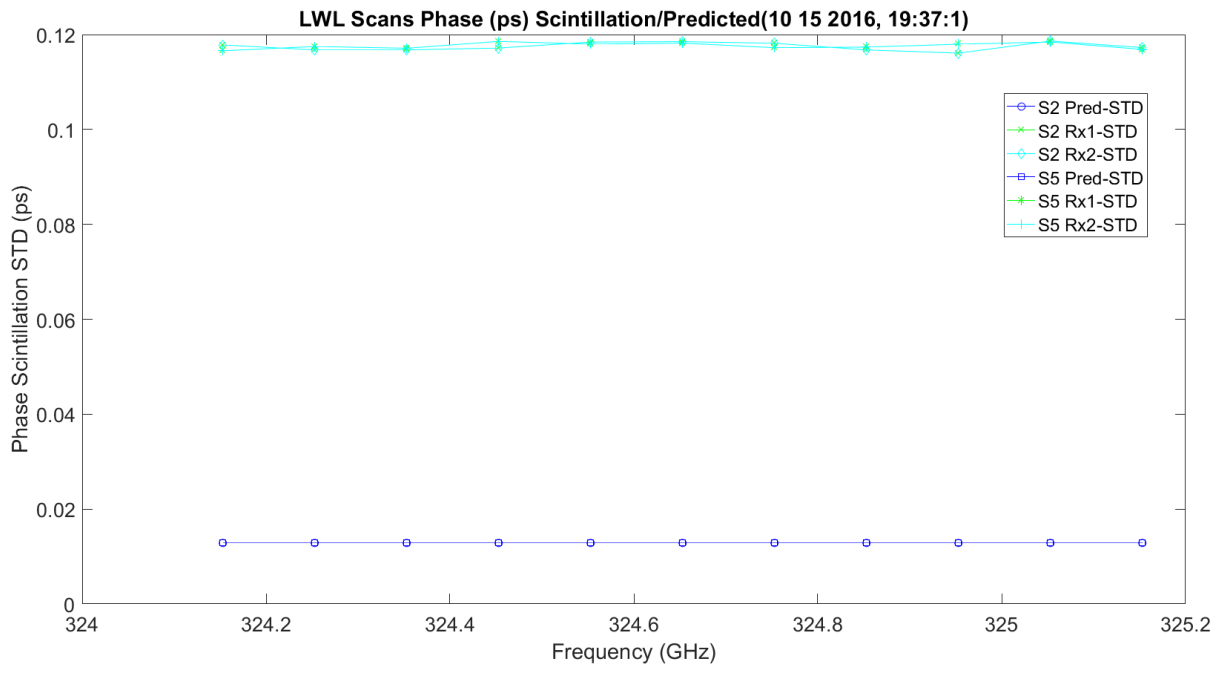


Figure 3.176. LWL Phase Scintillation STD and Predicted ps – 10142016_193175.

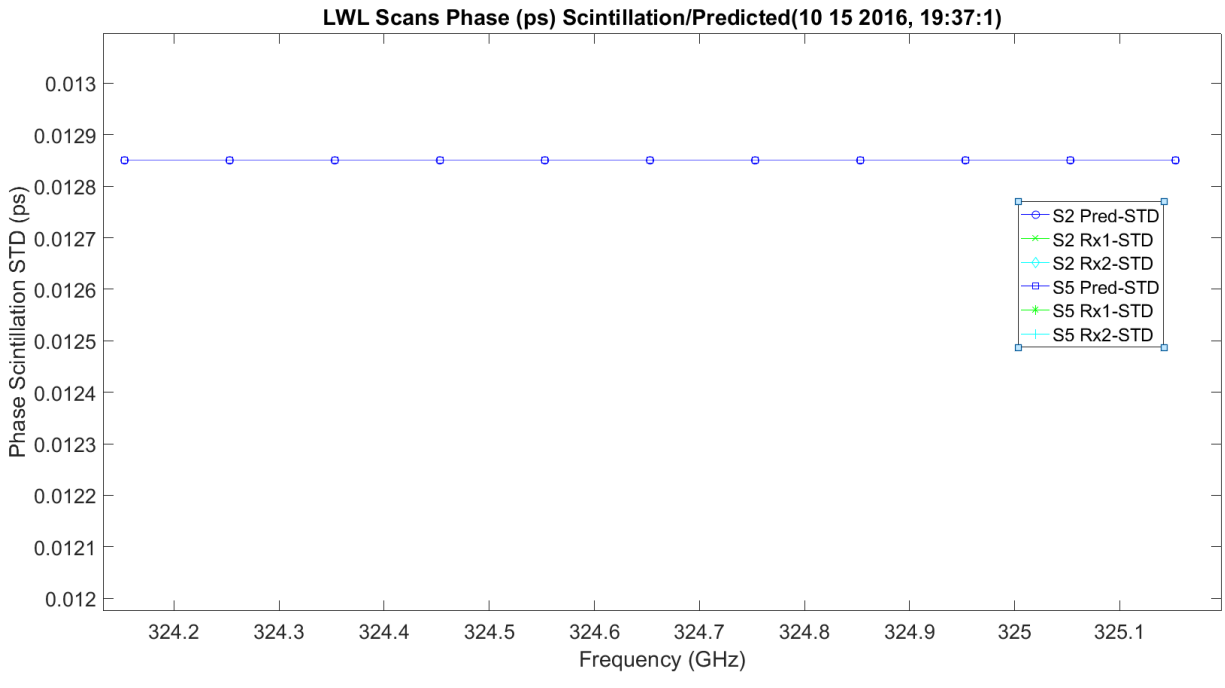


Figure 3.177. LWL Phase Scintillation STD and Predicted ps – 10142016_193175.

Figure 3.178 shows the UWL scans phase scintillation STD. The STD variance is around 0.12 picoseconds, much higher than the prediction which is shown in Figure 3.179. It has linear growth with frequency.

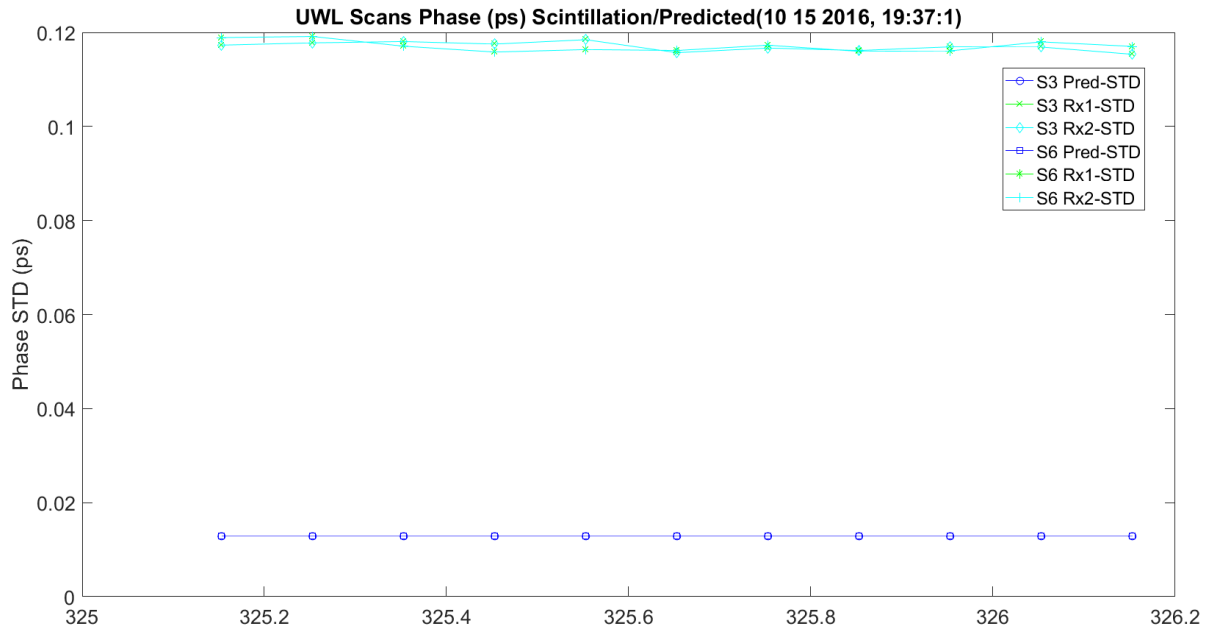


Figure 3.178. UWL Phase Scintillation STD and Predicted ps – 10142016_193175.

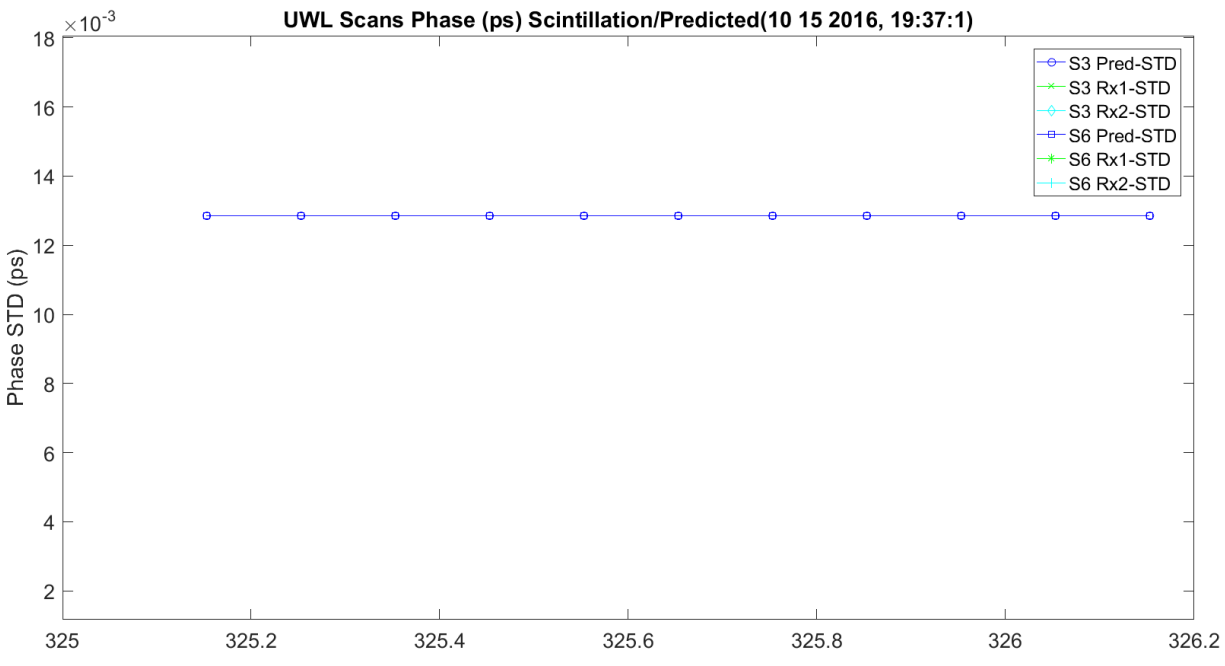


Figure 3.179. Enlarged UWL Phase Scintillation STD and Predicted ps – 10142016_193175.

Figure 3.180 shows the WB amplitude and phase scintillation correlation. This is compared to prediction by Fresnel and Fraunhofer; these have the most significant correlation. One pair is correlated higher than the later scan, which is around zero until it grows around the peak to 0.2. Figure 3.181 LWL shows the later scans are getting closer to theoretical. Figure 3.182 shows the same for UWL; the accuracy is very close to theoretical.

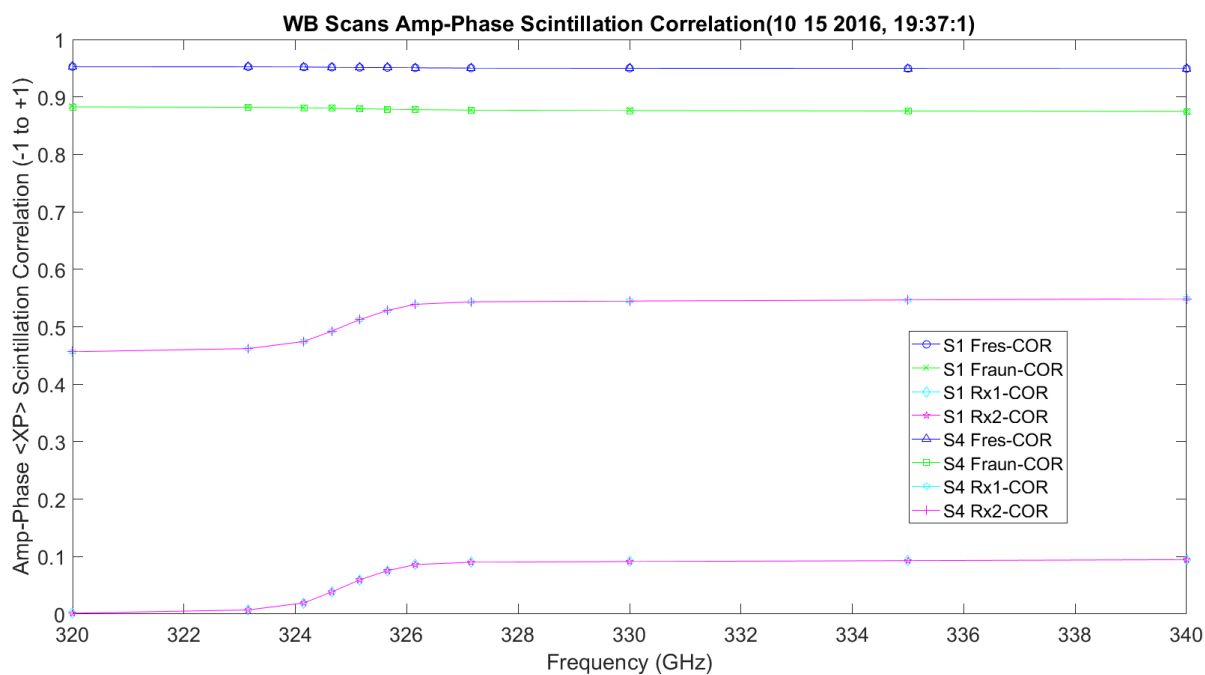


Figure 3.180. WB Amp/Phase Scintillation Correlation and Predicted – 10142016_193175.

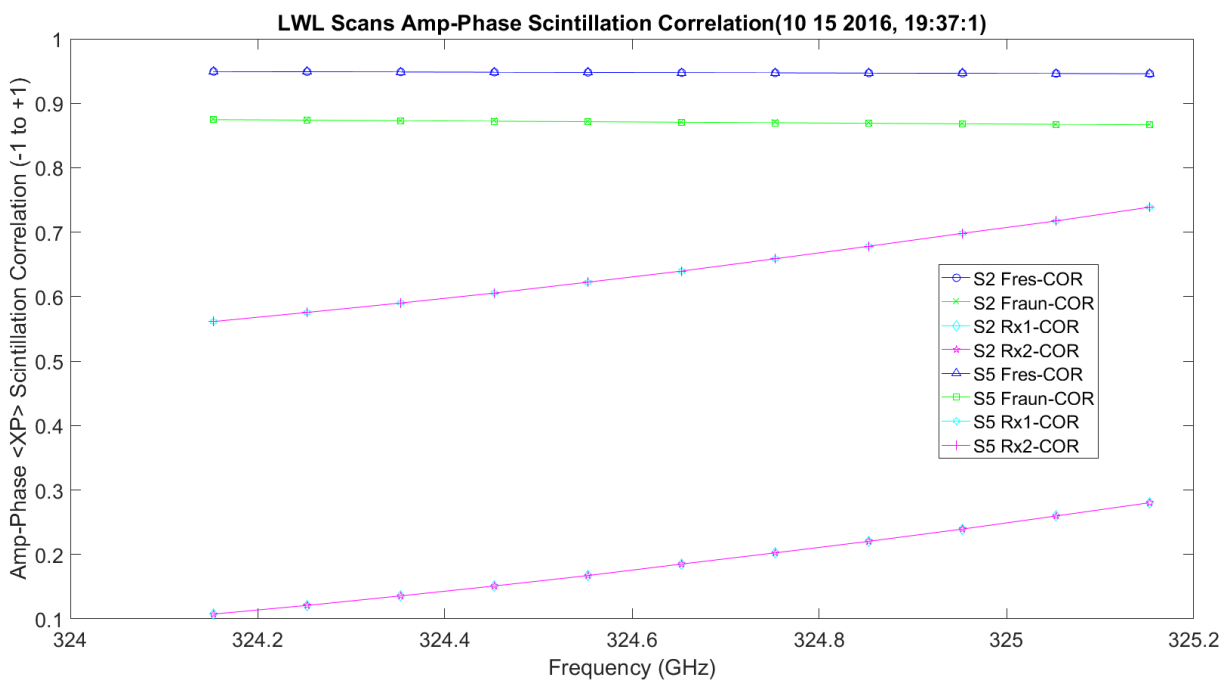


Figure 3.181. LWL Amp/Phase Scintillation Correlation and Predicted – 10142016_193175.

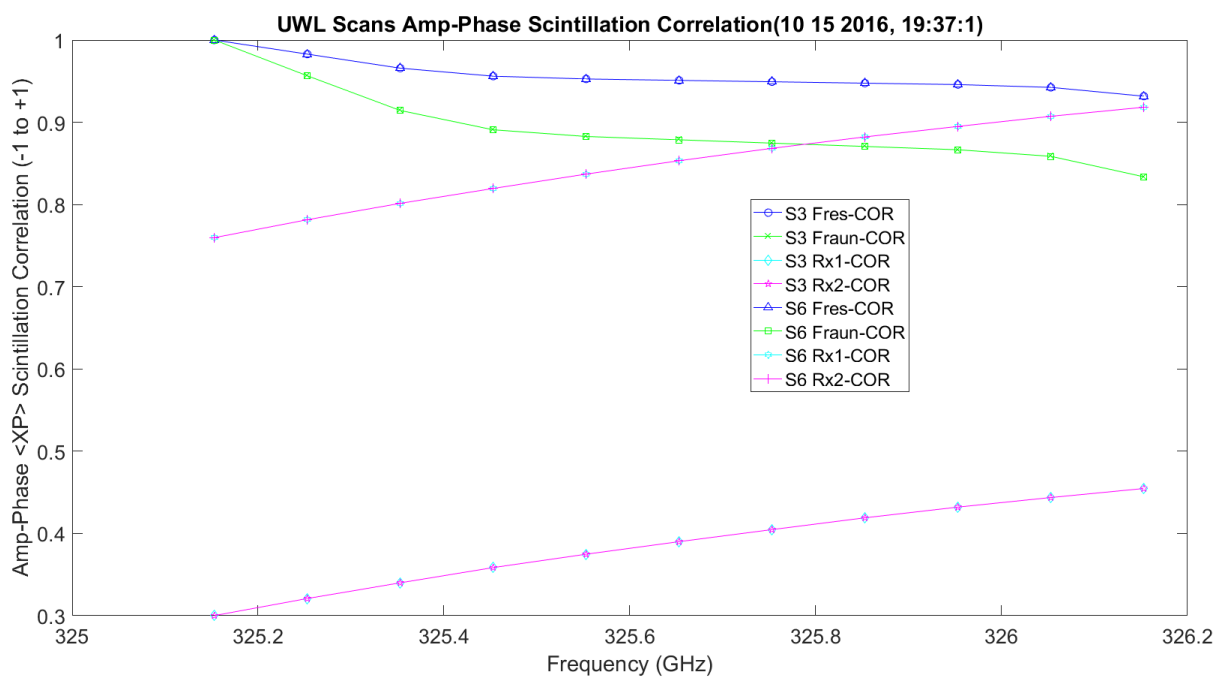


Figure 3.182. UWL Amp/Phase Scintillation Correlation and Predicted – 10142016_193175.

Figure 3.183 shows C_T^2 . The Tx anemometer was off, so the only one shown was on the receive, mesa, side.

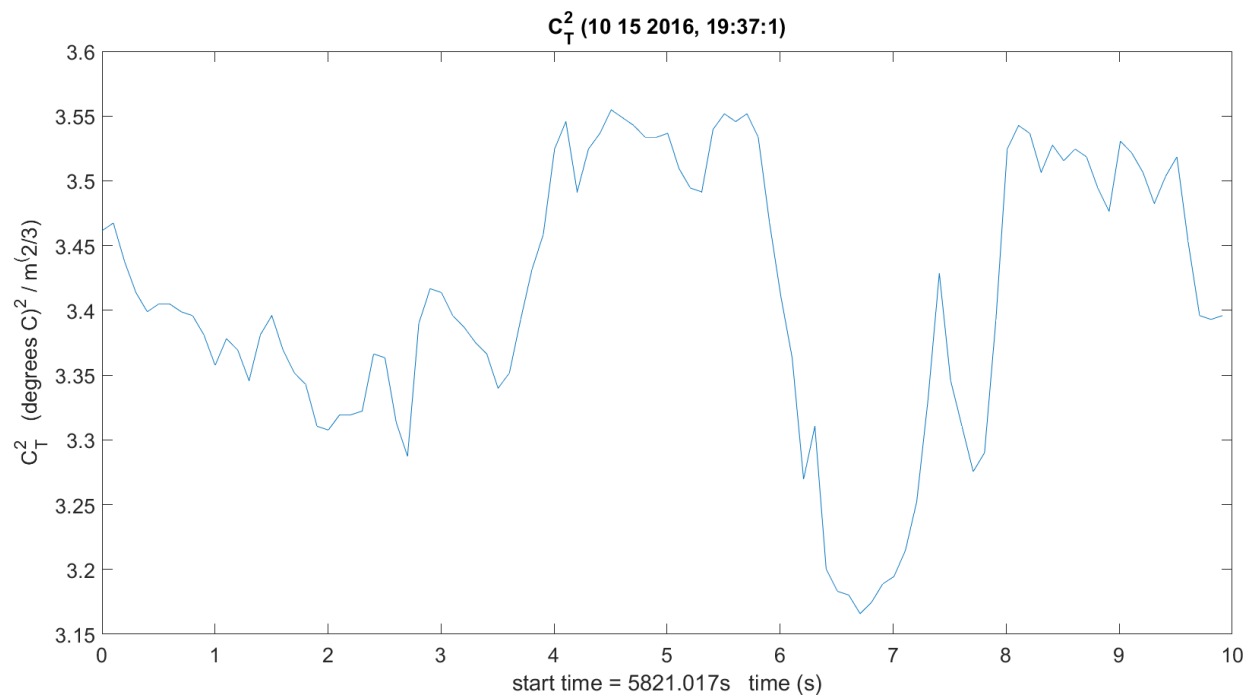


Figure 3.183. C_T^2 – 10142016_193175.

Figure 3.184 shows C_Q^2 . This includes transmit and receive hygrometer sensors averaged.

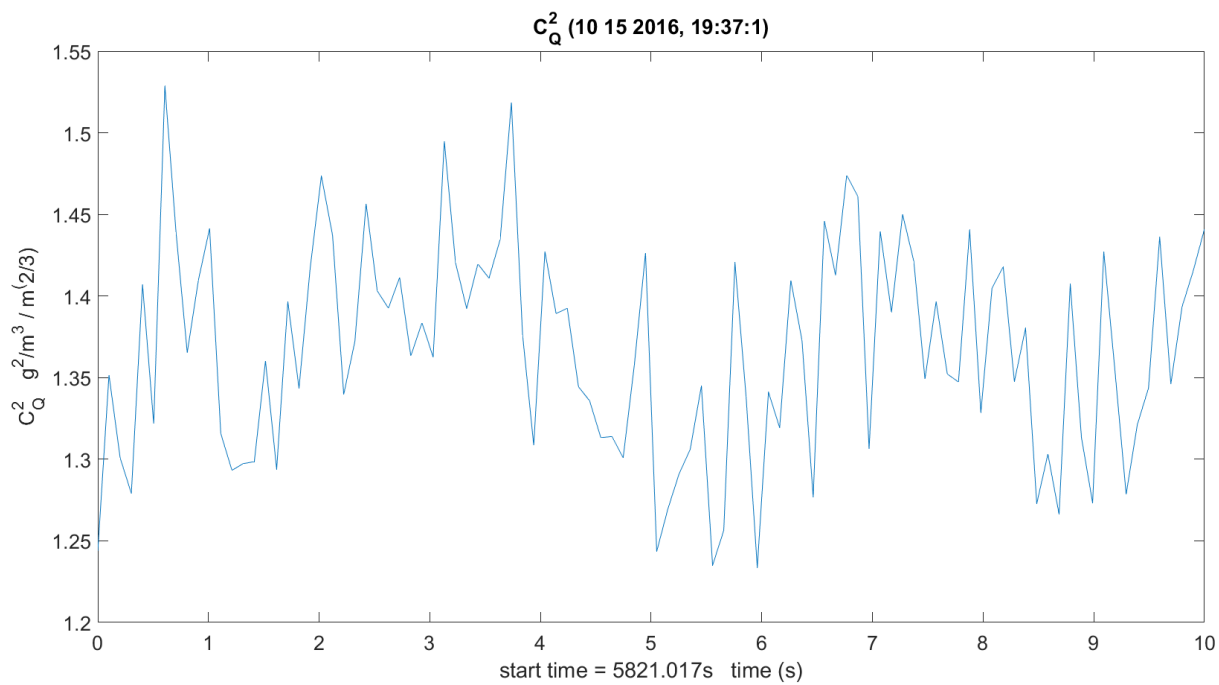


Figure 3.184. C_Q^2 – 10142016_193175.

Figure 3.185 shows C_{TQ} . This includes transmit and receive hygrometer sensors averaged and temperature on receive only.

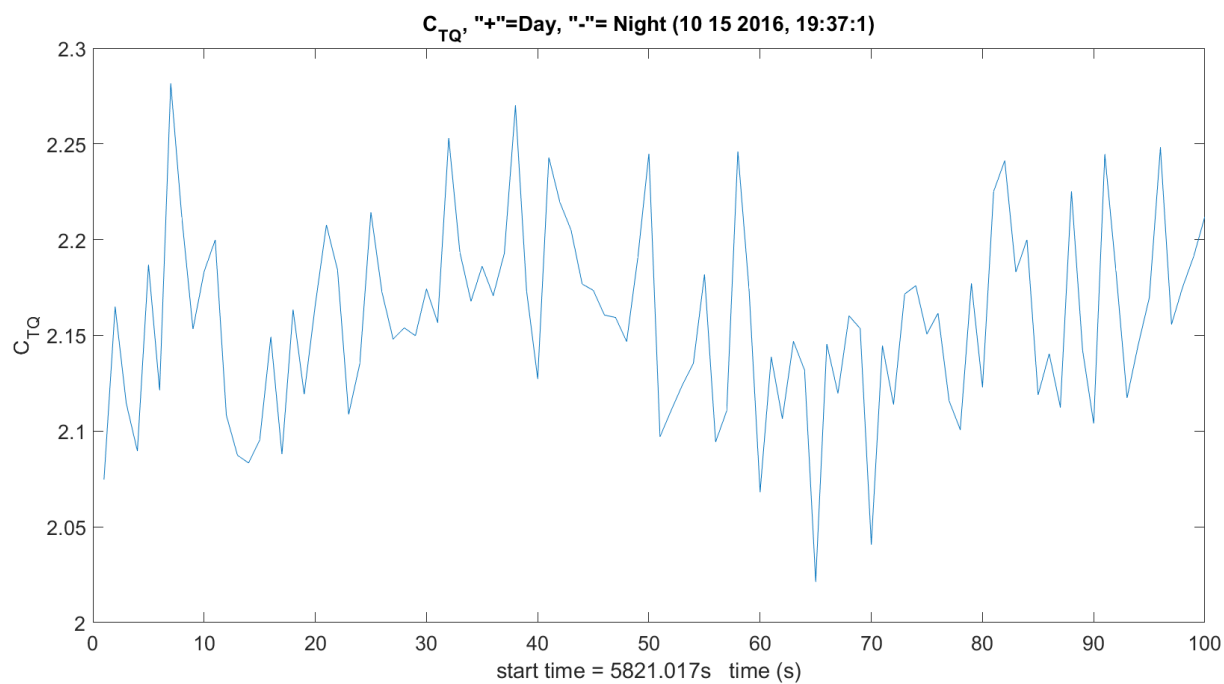


Figure 3.185. C_{TQ} – 10142016_193175.

Figure 3.186 shows amplitude STD and C_n^2 relation on two plots.

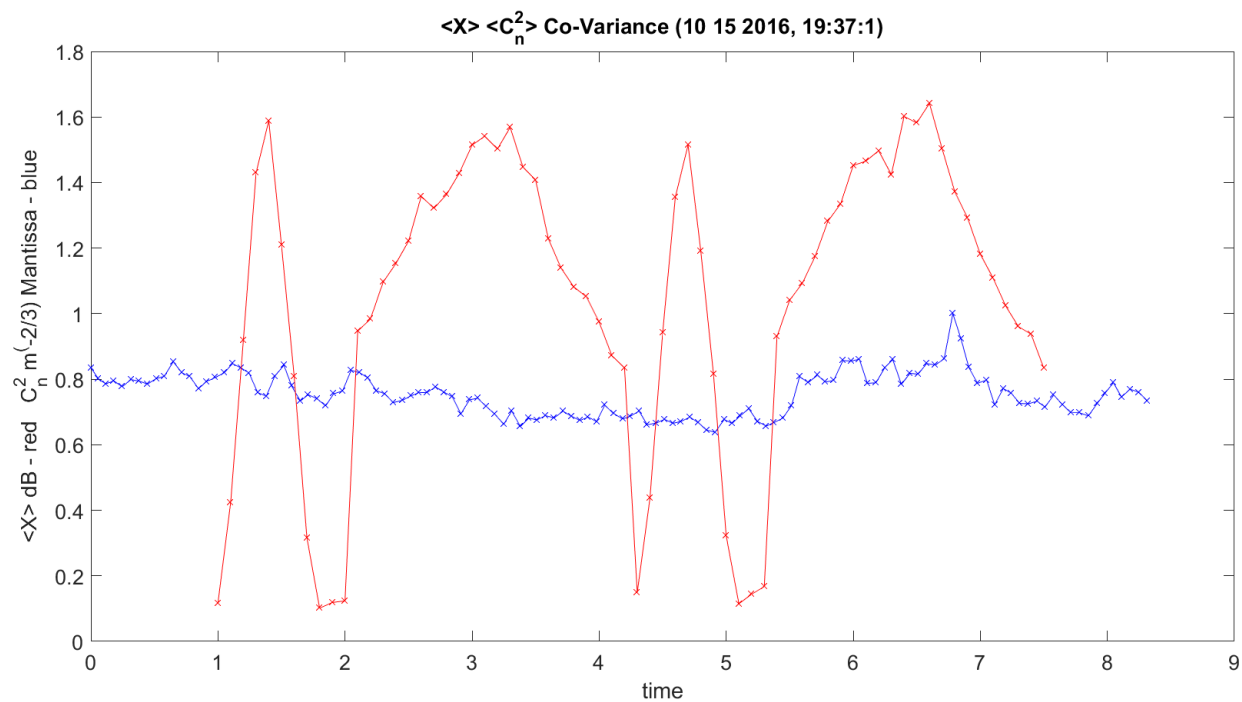


Figure 3.186. $\langle C_n^2 \rangle$ Construction and $\langle X \rangle$ Amplitude – 10142016_193175.

Figure 3.187 shows amplitude STD and C_T^2 relation on two plots.

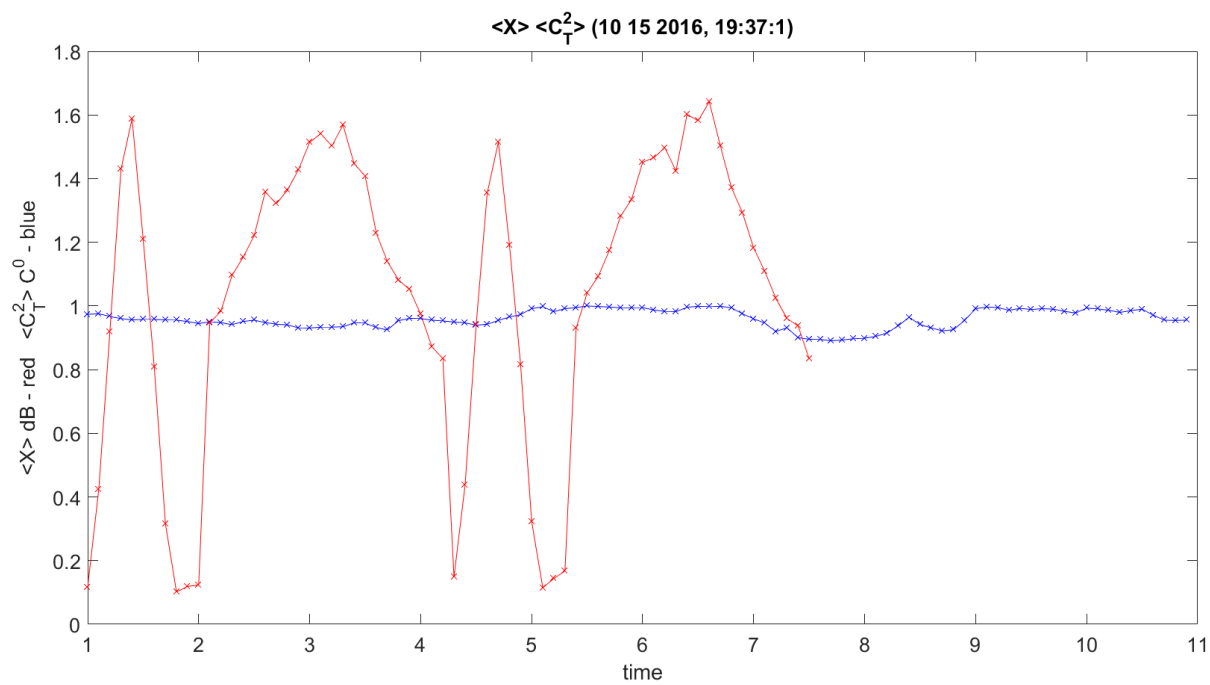


Figure 3.187. $\langle C_T^2 \rangle$ Temp Construction and Amplitude Variance – 10142016_193175.

Figure 3.188 shows amplitude STD and C_Q^2 relation on two plots.

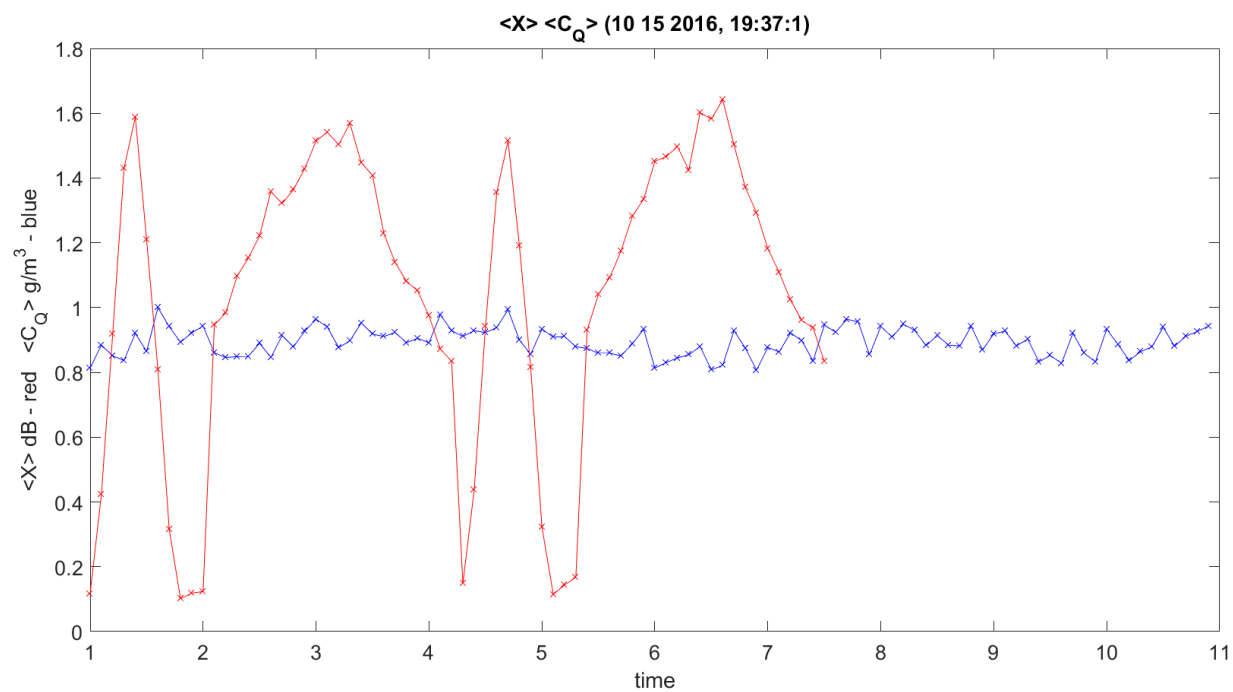


Figure 3.188. $\langle C_Q^2 \rangle$ Construction Temp and Amplitude Variance – 10142016_193175.

Figure 3.189 shows phase STD and $\langle C_n^2 \rangle$ relation on two plots.

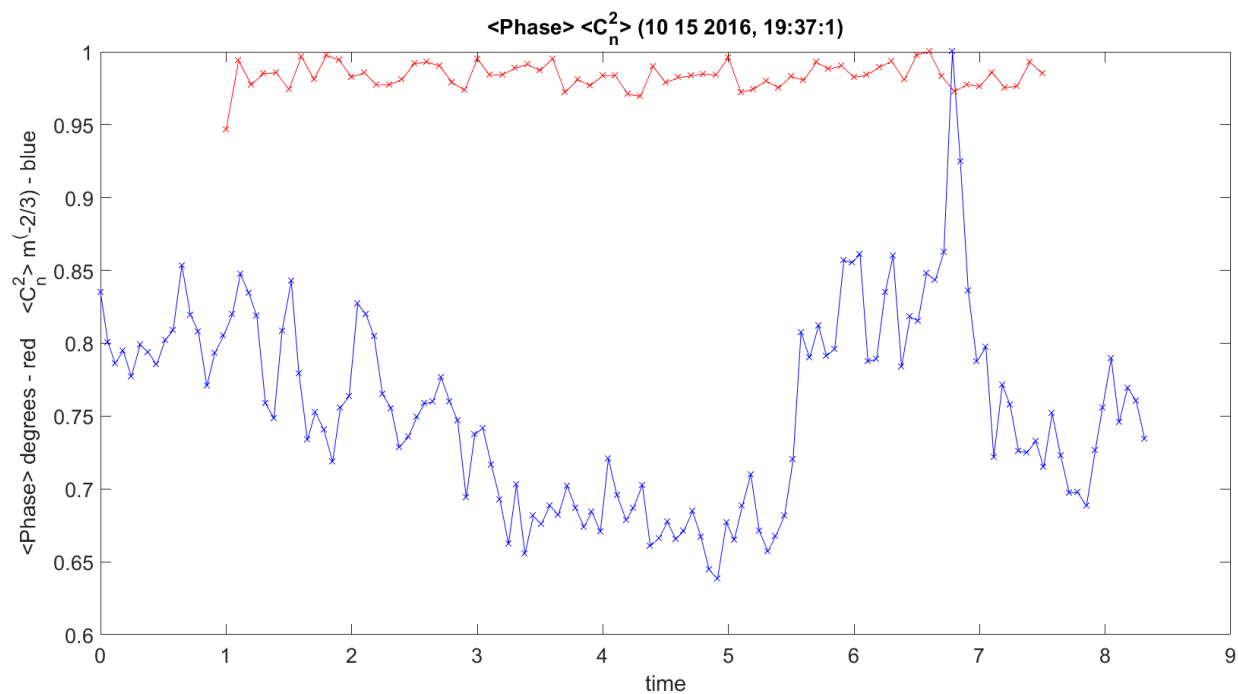


Figure 3.189. $\langle C_n^2 \rangle$ Construction and Phase Variance – 10142016_193175.

Figure 3.190 shows phase STD and $\langle C_T^2 \rangle$ relation on two plots.

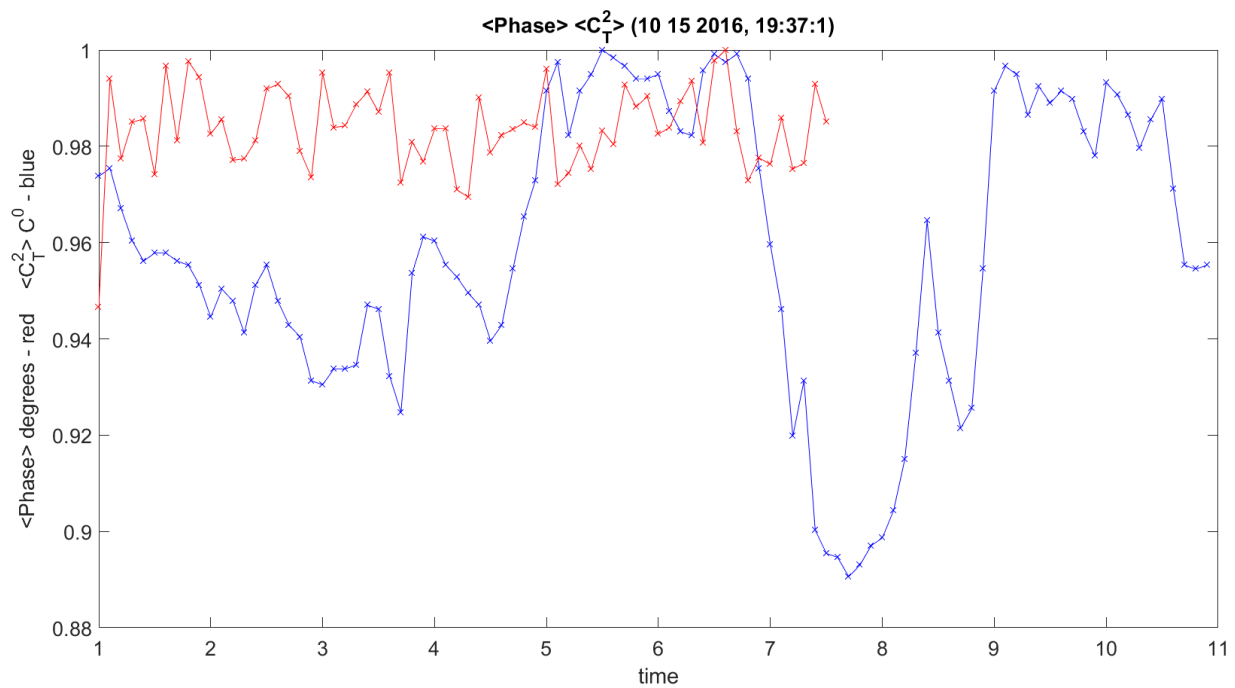


Figure 3.190. $\langle C_T^2 \rangle$ Temp Variance and Phase Variance – 10142016_193175.

Figure 3.191 shows phase STD and $\langle C_Q^2 \rangle$ relation on two plots.

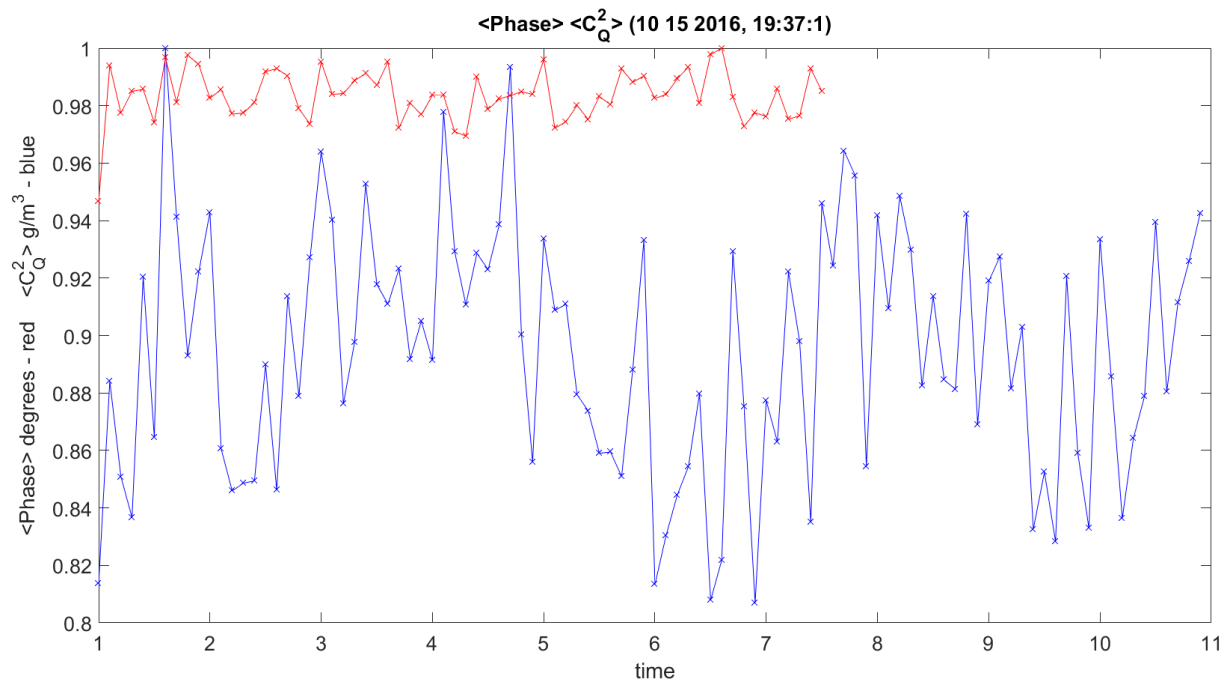


Figure 3.191. $\langle C_Q^2 \rangle$ Humidity Variance and Phase Variance – 10142016_193175.

Figure 3.192 shows $\langle C_T^2 \rangle$ and $\langle C_n^2 \rangle$ relation on two plots.

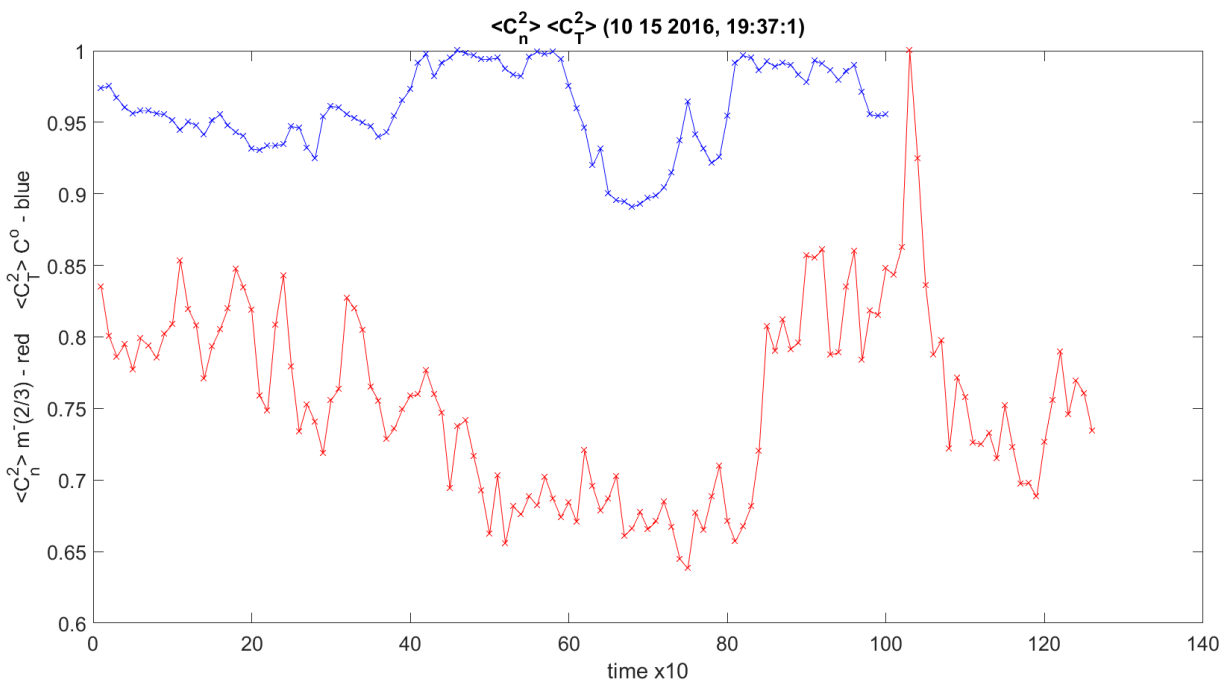


Figure 3.192. $\langle C_T^2 \rangle$ Variance and $\langle C_n^2 \rangle$ Variance – 10142016_193175.

Figure 3.193 shows $\langle C_Q^2 \rangle$ and $\langle C_n^2 \rangle$ relation on two plots.

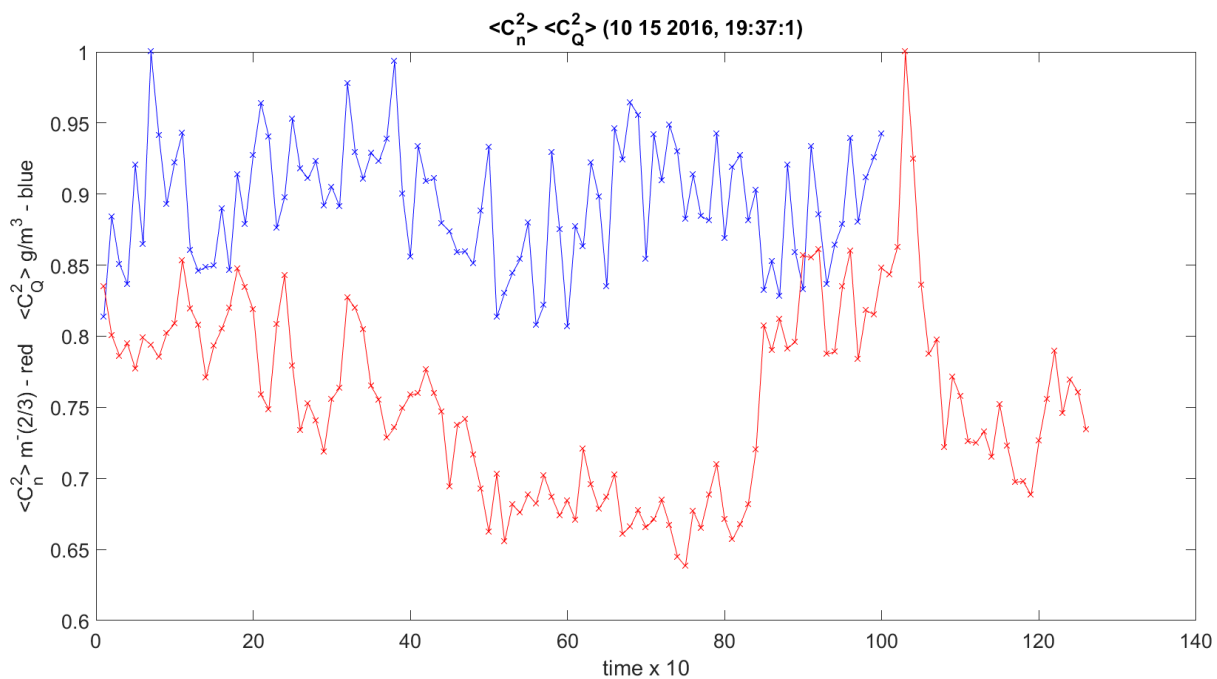


Figure 3.193. $\langle C_Q^2 \rangle$ Variance and $\langle C_n^2 \rangle$ Construction Variance – 10142016_193175.

Figure 3.194 shows $\langle C_T^2 \rangle$ and $\langle C_Q^2 \rangle$ relation on two plots.

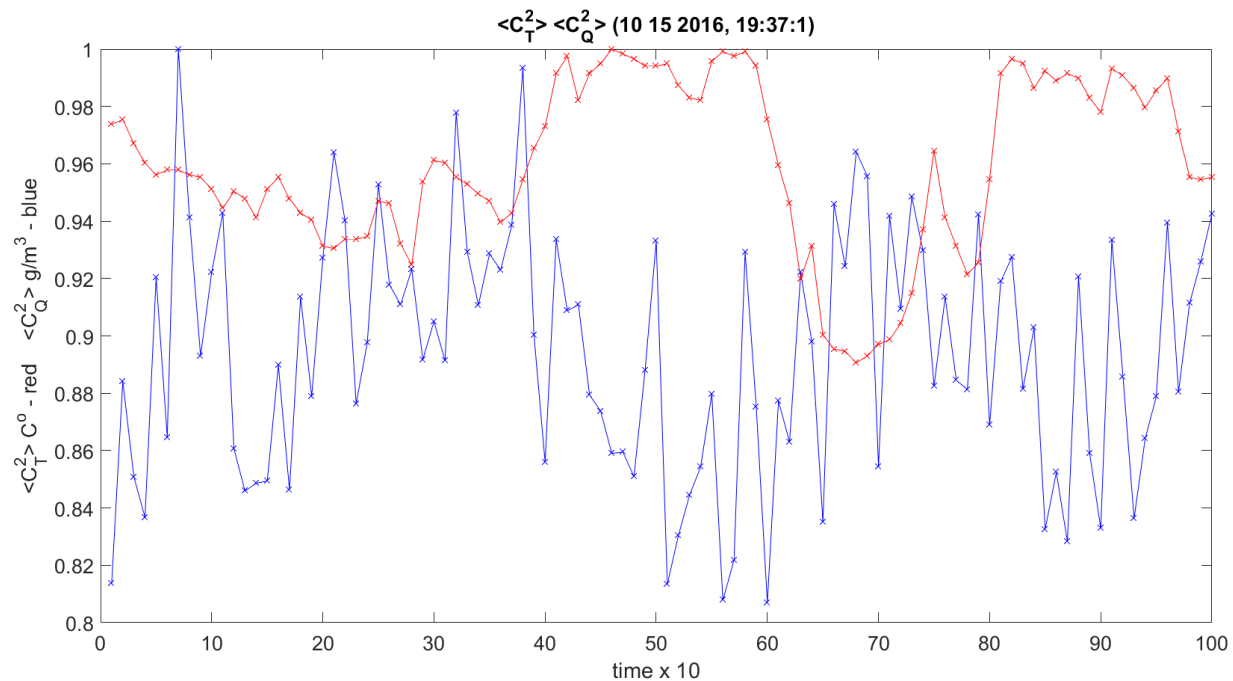


Figure 3.194. $\langle C_Q^2 \rangle$ Humidity Variance and $\langle C_T^2 \rangle$ Temp Variance – 10142016_193175.

Figure 3.195 shows amplitude/phase variance STD and U wind variance STD relation on two plots.

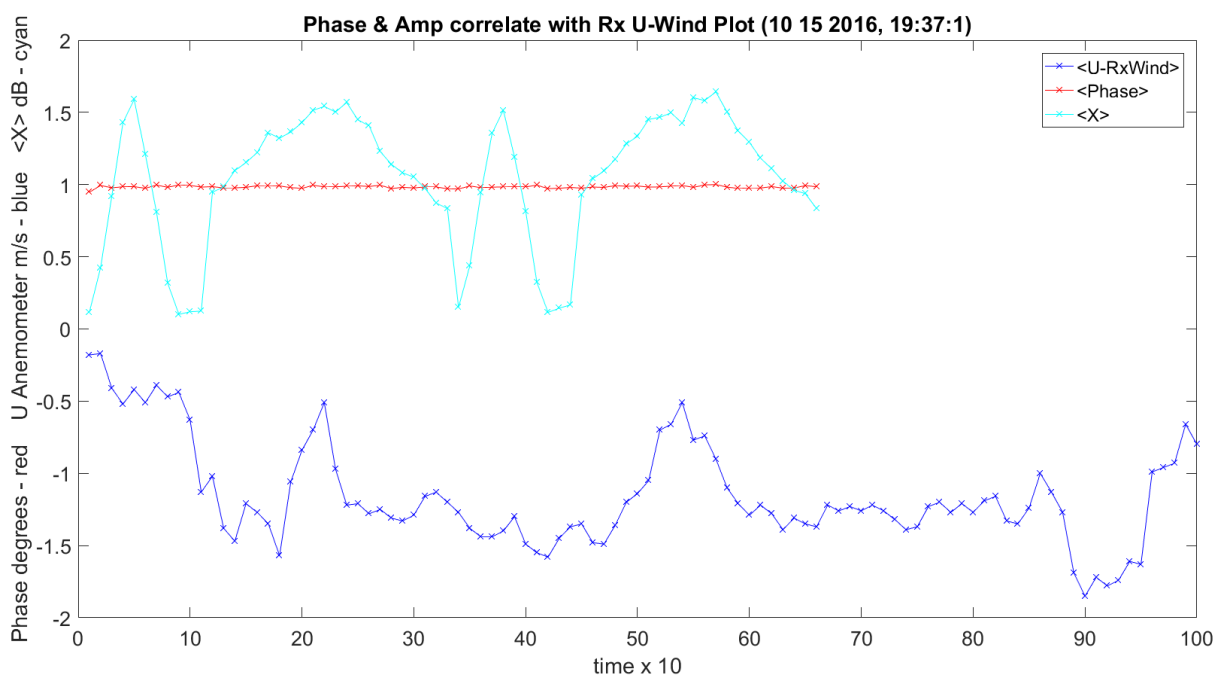


Figure 3.195. Phase, U Wind and Amplitude Variance – 10142016_193175.

Figure 3.196 shows amplitude/phase variance STD and V wind variance STD relation on two plots.

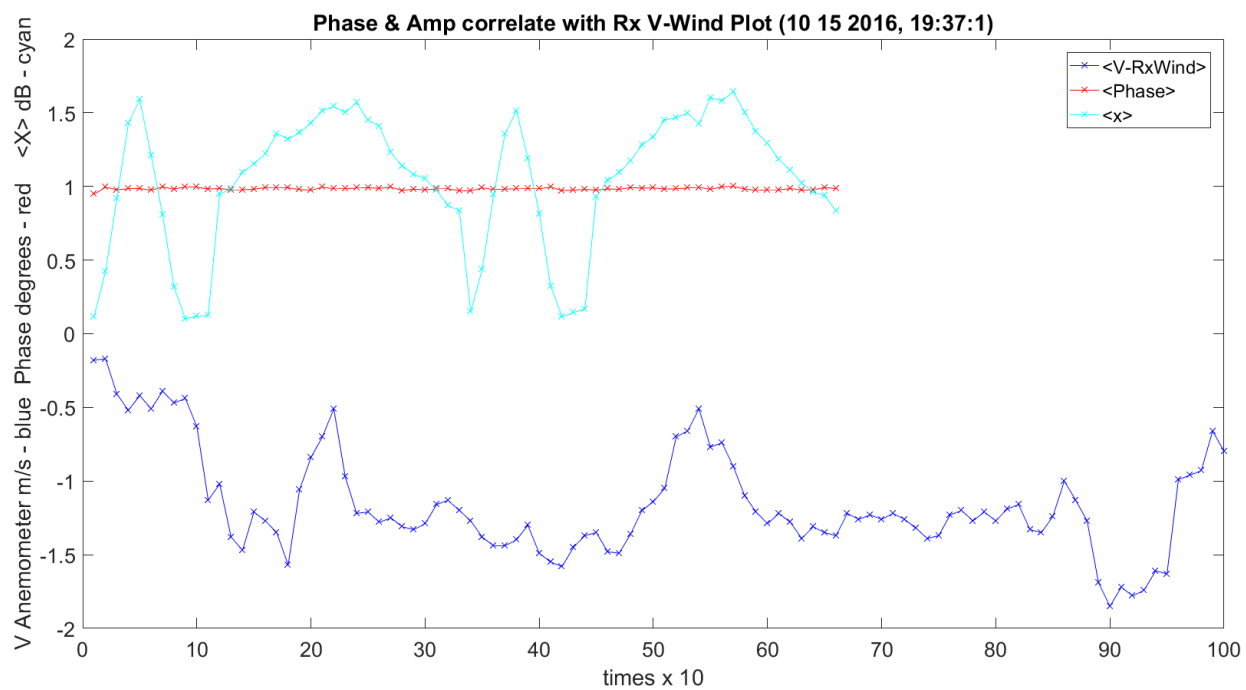


Figure 3.196. Phase, *V* Wind and Amplitude Variance – 10142016_193175.

Figure 3.197 shows amplitude/phase variance STD and *W* wind variance STD relation on two plots.

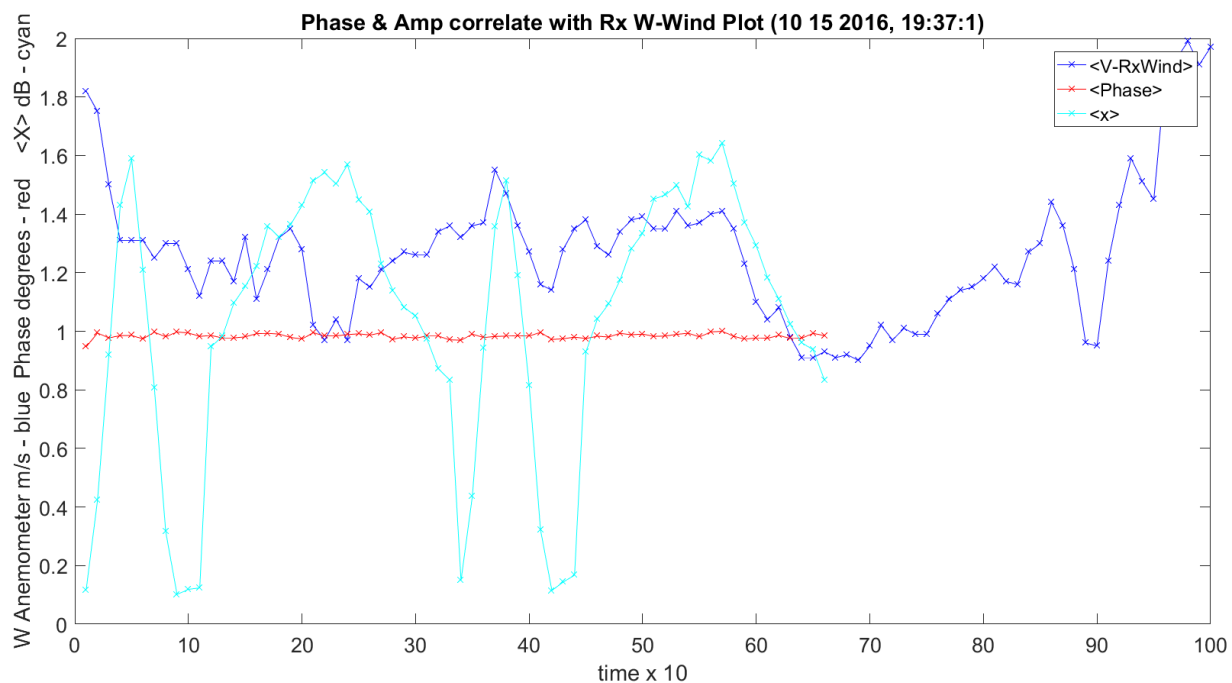


Figure 3.197. Phase, *W* Wind and Amplitude Variance – 10142016_193175.

Figure 3.198 shows the histogram for the 320 GHz frequency. This is better than presented before, since all hardware gain was removed; output of the Tx lens, through the atmosphere, and received at the receive lens.

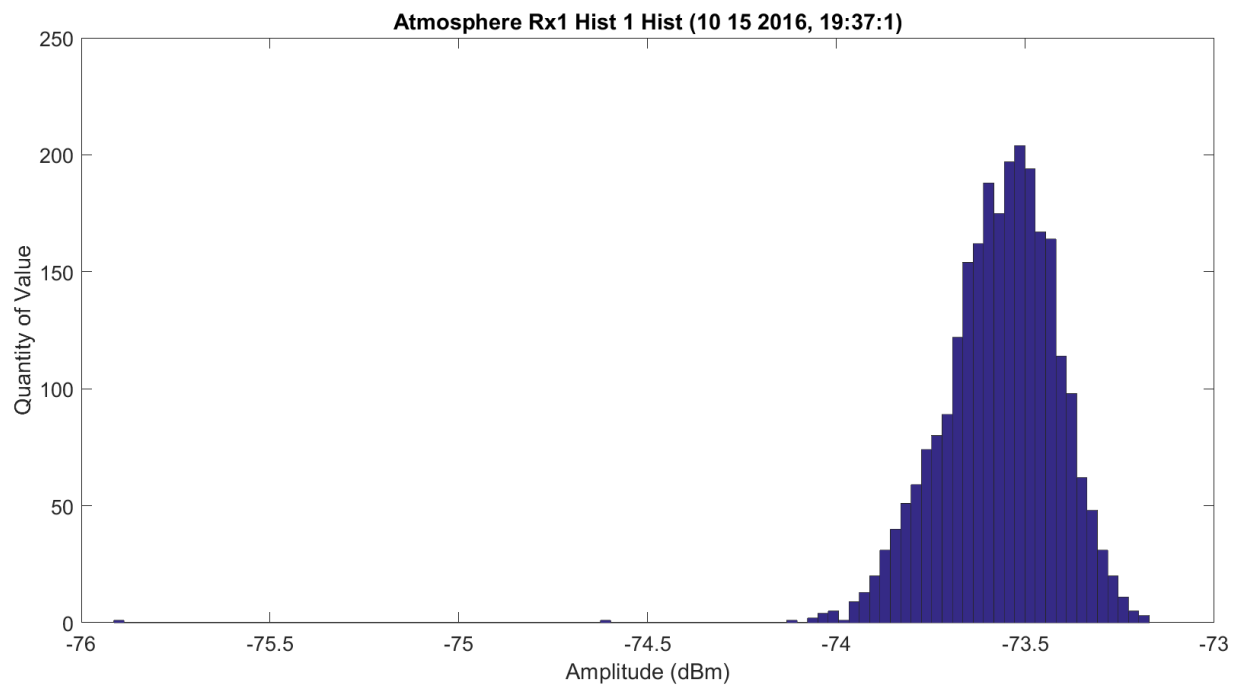


Figure 3.198. Hardware Excluded Histogram – 10142016_193175.

Figure 3.199 shows the WB mean amplitude for each frequency. The amplitude at 320 GHz is approximately 10 dB higher.

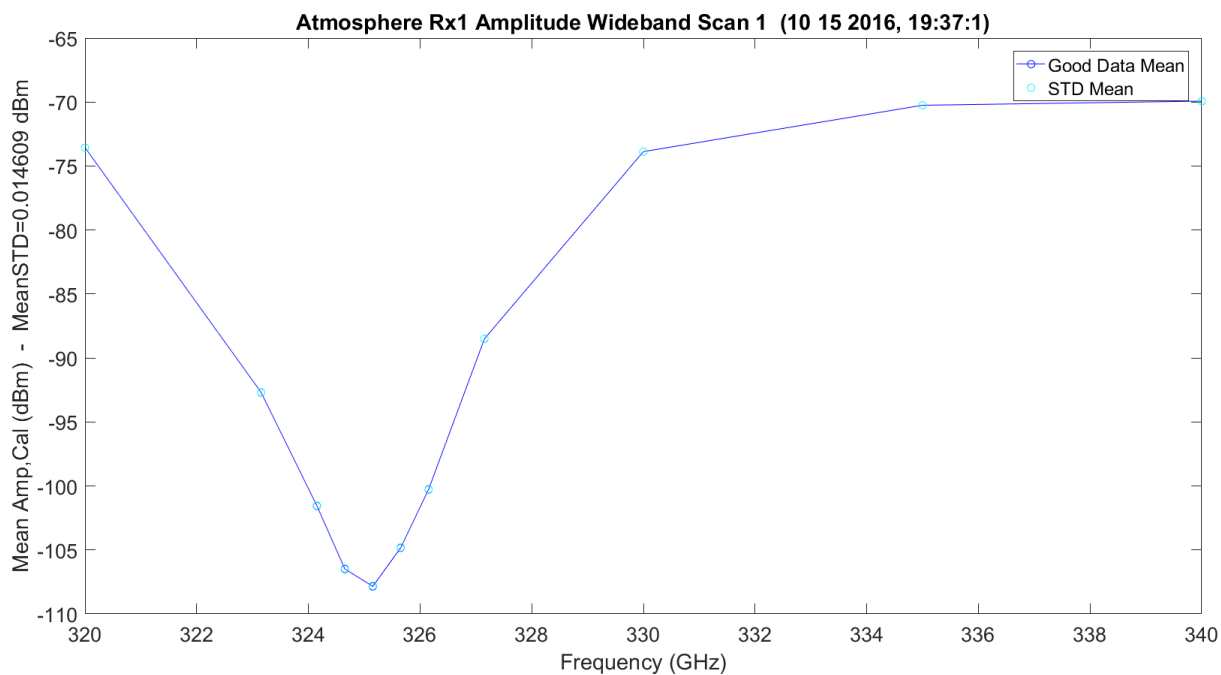


Figure 3.199. WB Amplitude No Hardware – 10142016_193175.

Figure 3.200 shows the WB mean amplitude with Friis and the difference for each frequency. The amplitude at 320 GHz is approximately 10 dB higher. The peaks are about 40 dB different.

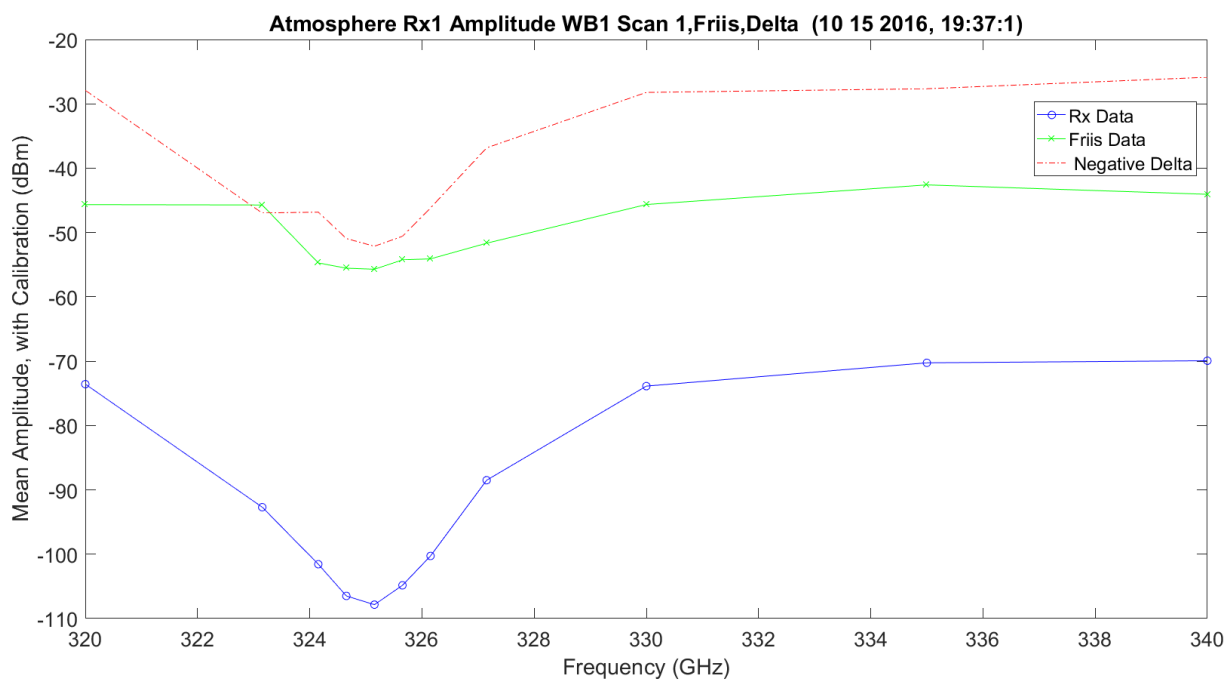


Figure 3.200. WB Amplitude No Hardware, Friis and Difference – 10142016_193175.

Figure 3.201 shows the WB mean amplitude normalized with Friis. The amplitude at 320 GHz is approximately 10 dB higher.

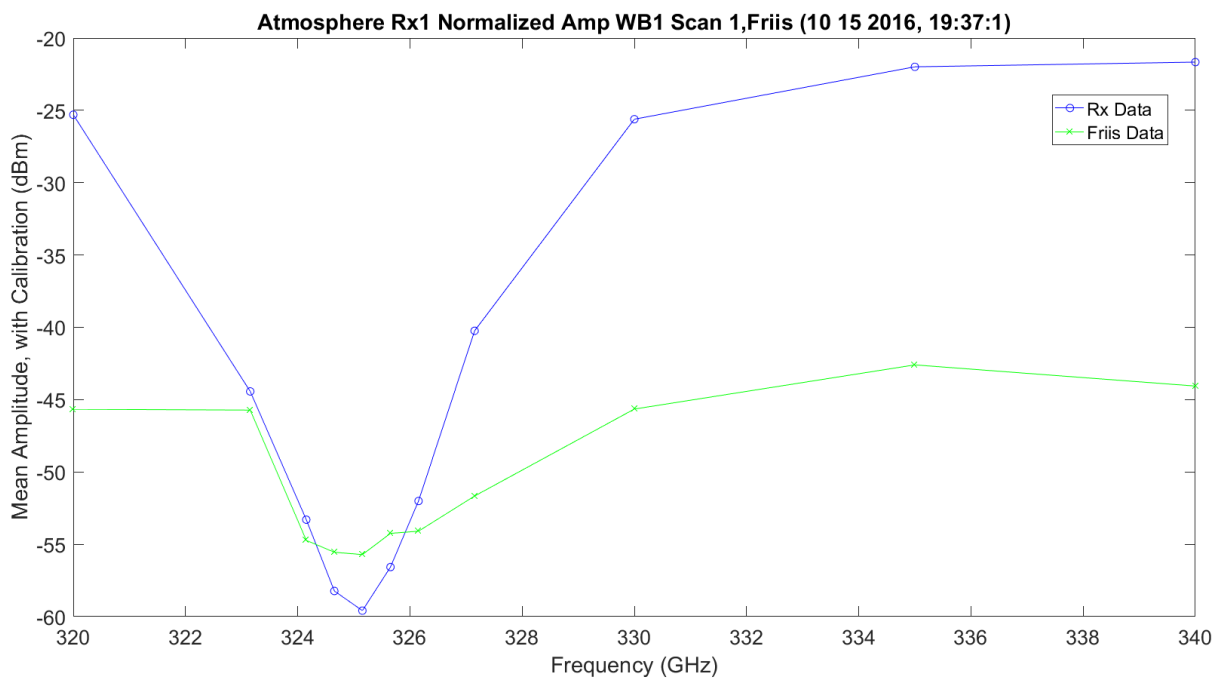


Figure 3.201. WB Normalized Amplitude No Hardware, Friis and Difference – 10142016_193175.

Figure 3.202 shows the LWL mean amplitude for each frequency.

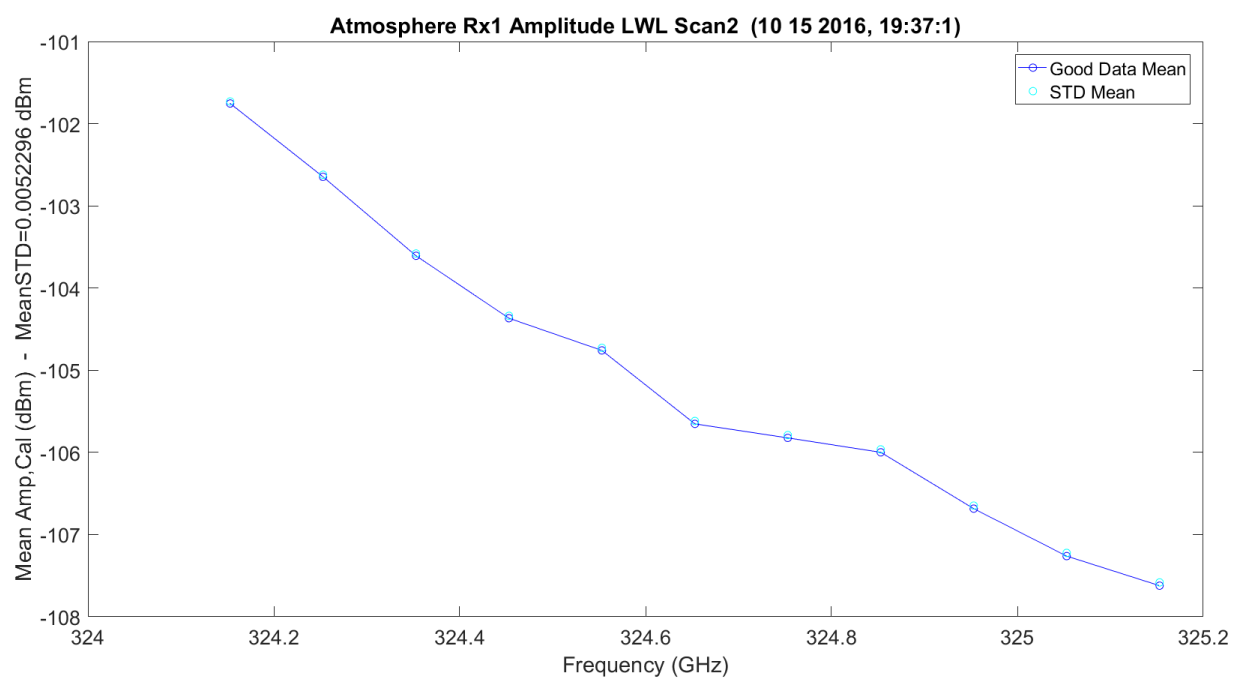


Figure 3.202. LWL Amplitude No Hardware – 10142016_193175.

Figure 3.203 shows the LWL mean amplitude with Friis and the difference for each frequency. The amplitude at 320 GHz is approximately 10 dB higher. This has a 50 dB difference over the linear slope.

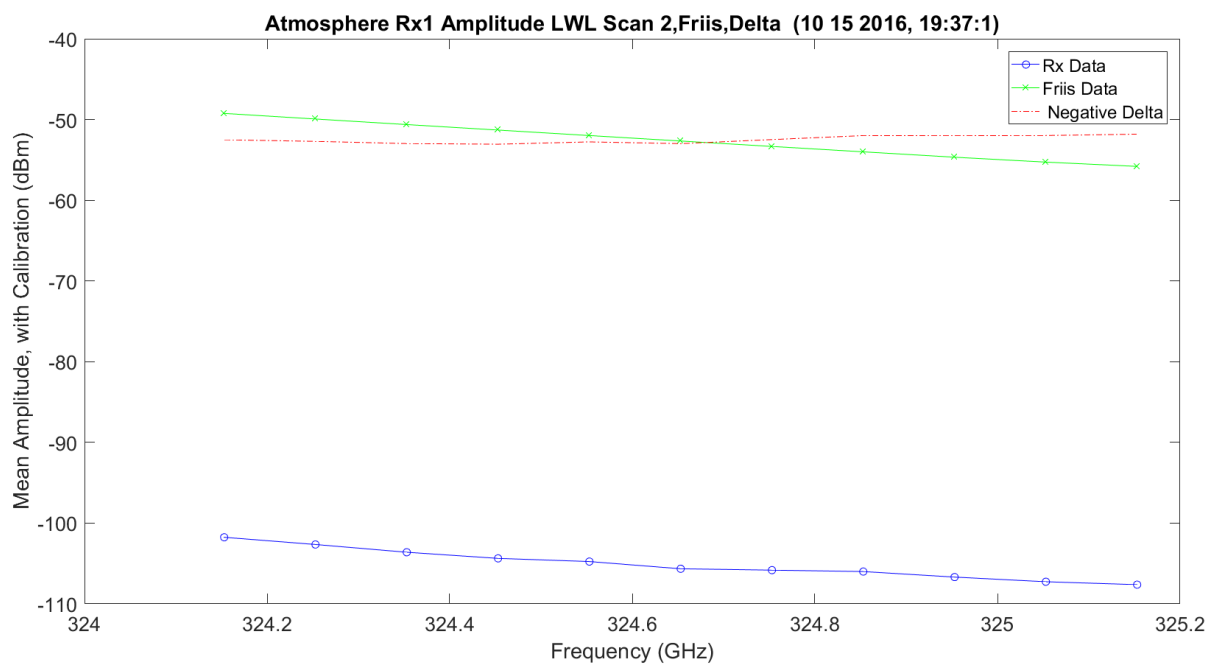


Figure 3.203. LWL Amplitude No Hardware, Friis and Difference – 10142016_193175.

Figure 3.204 shows the LWL mean amplitude normalized with Friis. The amplitude has a normalized linear difference.

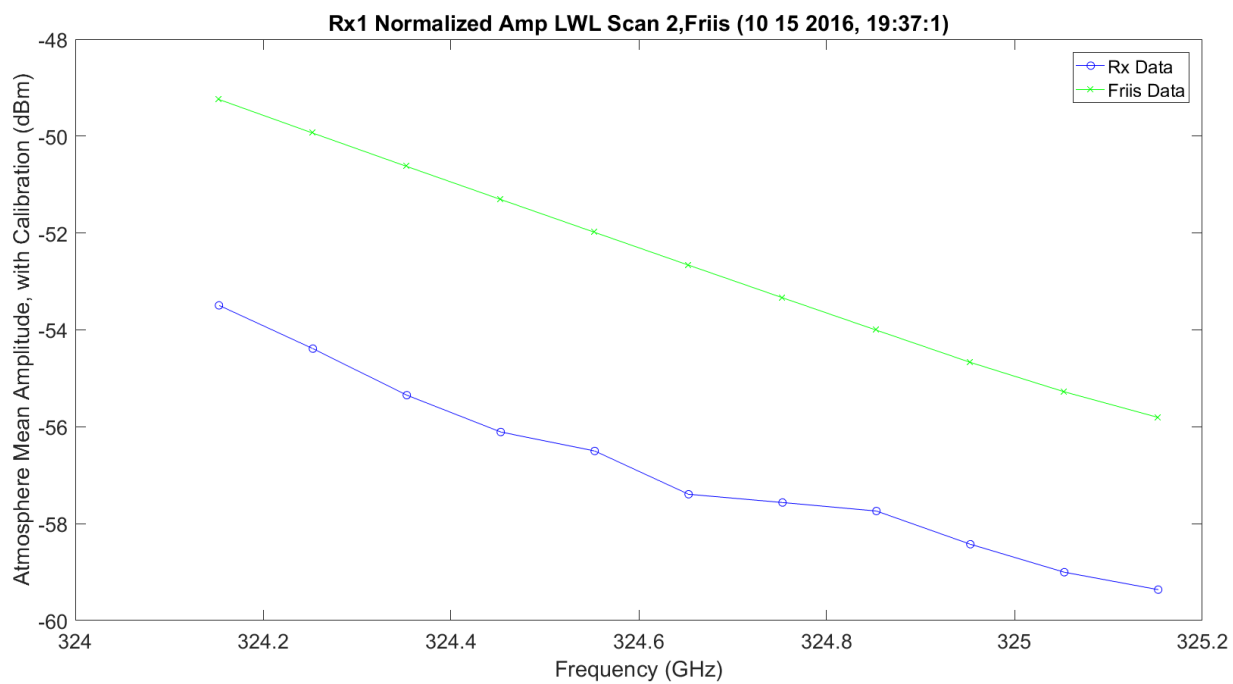


Figure 3.204. LWL Normalized Amplitude No Hardware, Friis and Difference – 10142016_193175.

Figure 3.205 shows the UWL mean amplitude for each frequency.

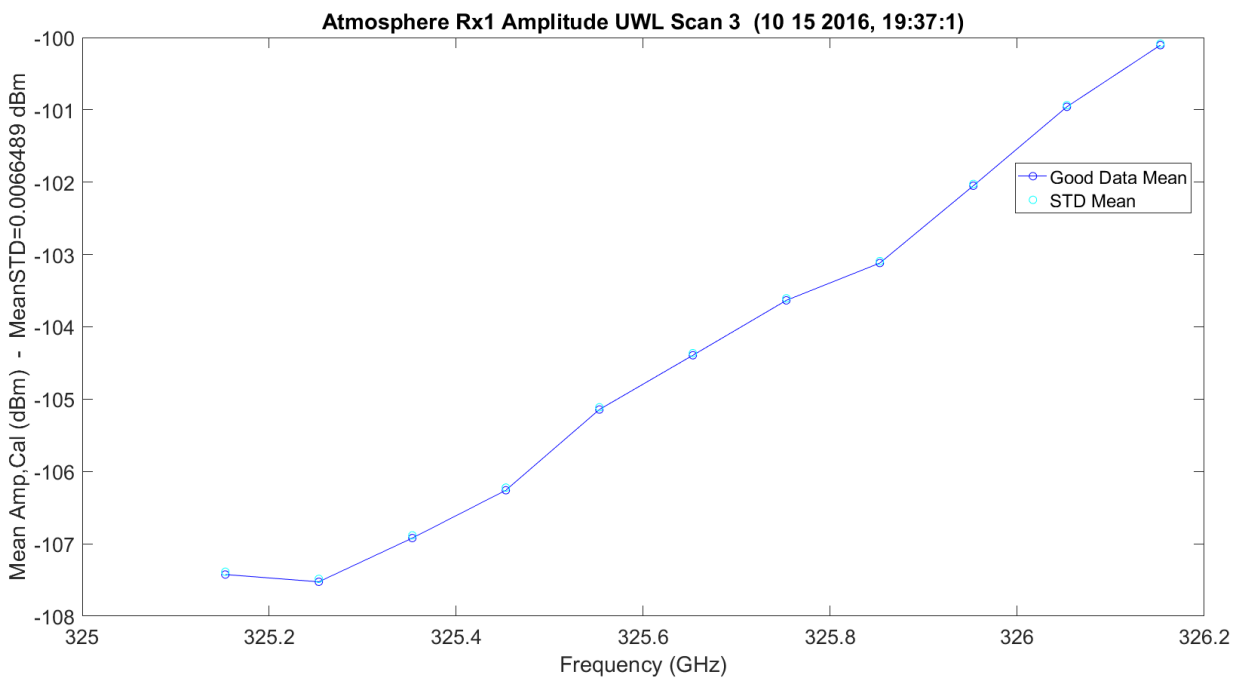


Figure 3.205. UWL Amplitude No Hardware – 10142016_193175.

Figure 3.206 shows the UWL mean amplitude with Friis and the difference for each frequency. This has a 50 dB difference over the linear slope.

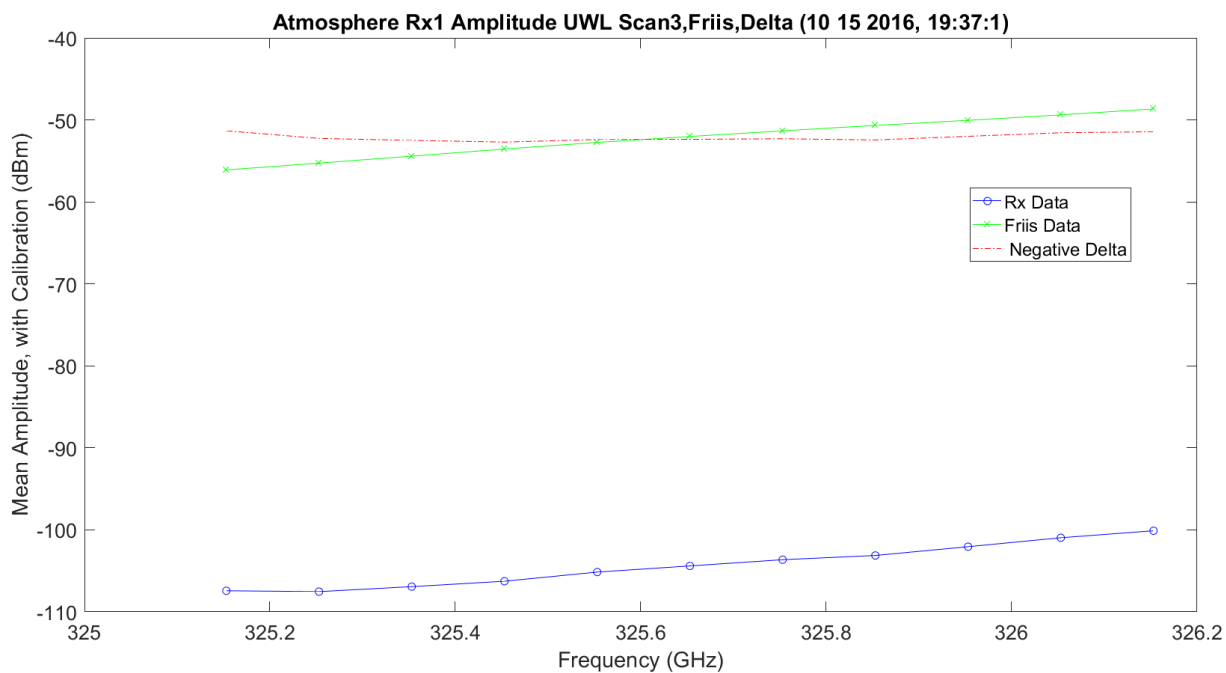


Figure 3.206. UWL Amplitude No Hardware, Friis and Difference – 10142016_193175.

Figure 3.207 shows the UWL mean amplitude normalized with Friis. The amplitude has a normalized linear difference.

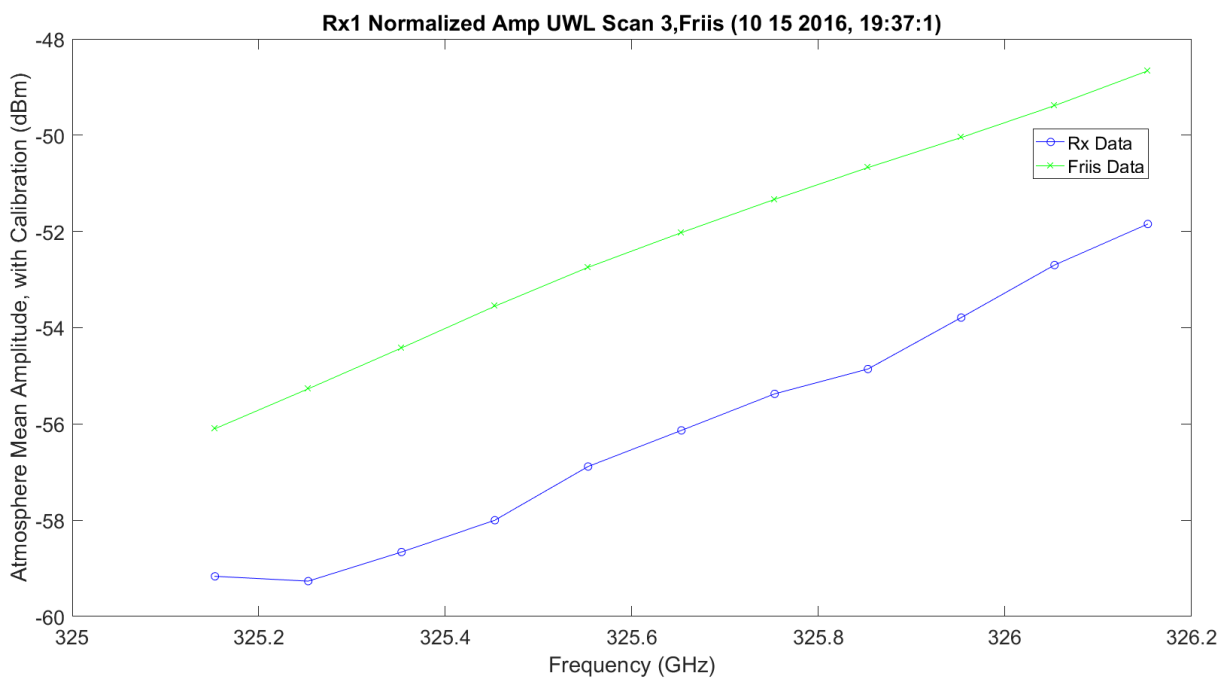


Figure 3.207. UWL Amplitude No Hardware, Friis and Difference – 10142016_193175.

Figure 3.208 – Figure 3.216 show the same plots for the second set of three-11 frequency scans: the last 33 frequency changes on the total 66 frequencies.

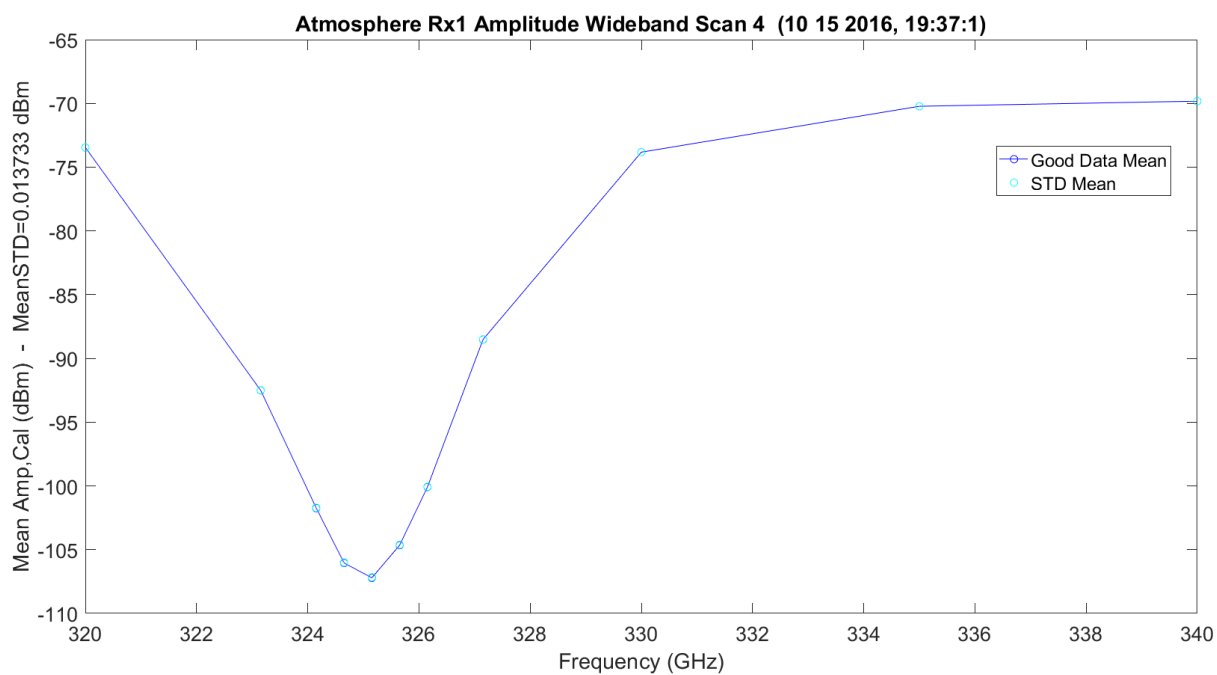


Figure 3.208. WB Scan 4 Amplitude No Hardware – 10142016_193175.

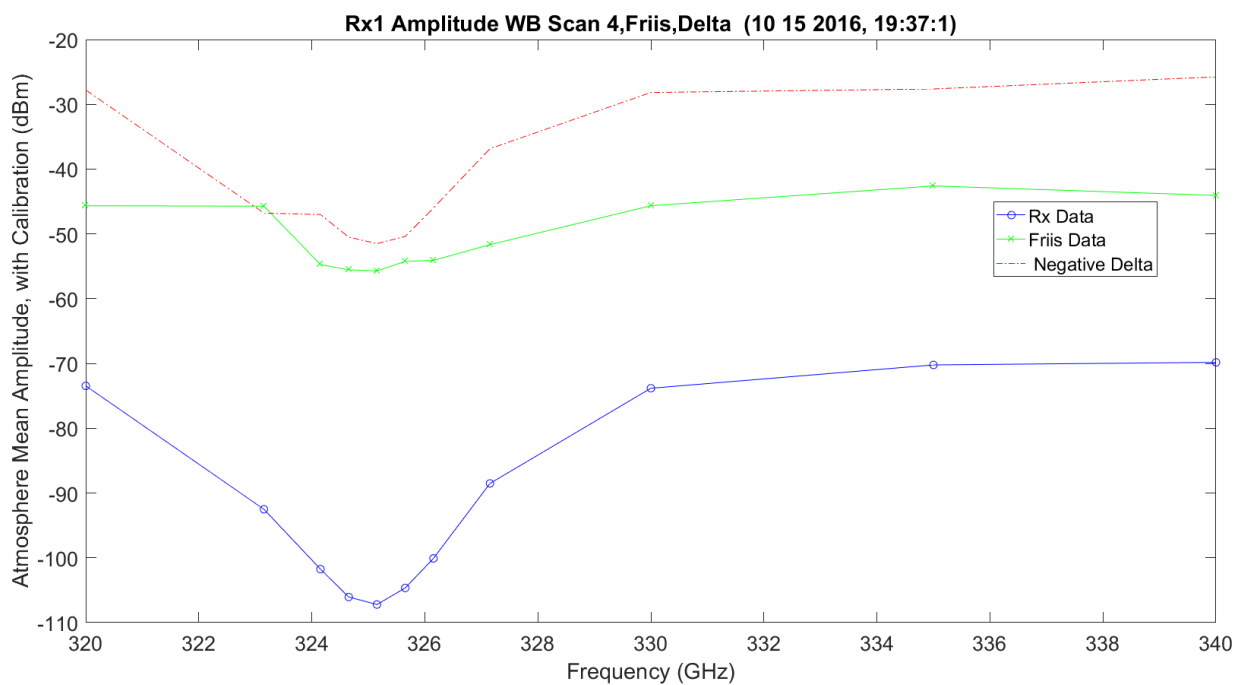


Figure 3.209. WB Scan 4 Amplitude No Hardware, Friis and Difference – 10142016_193175.

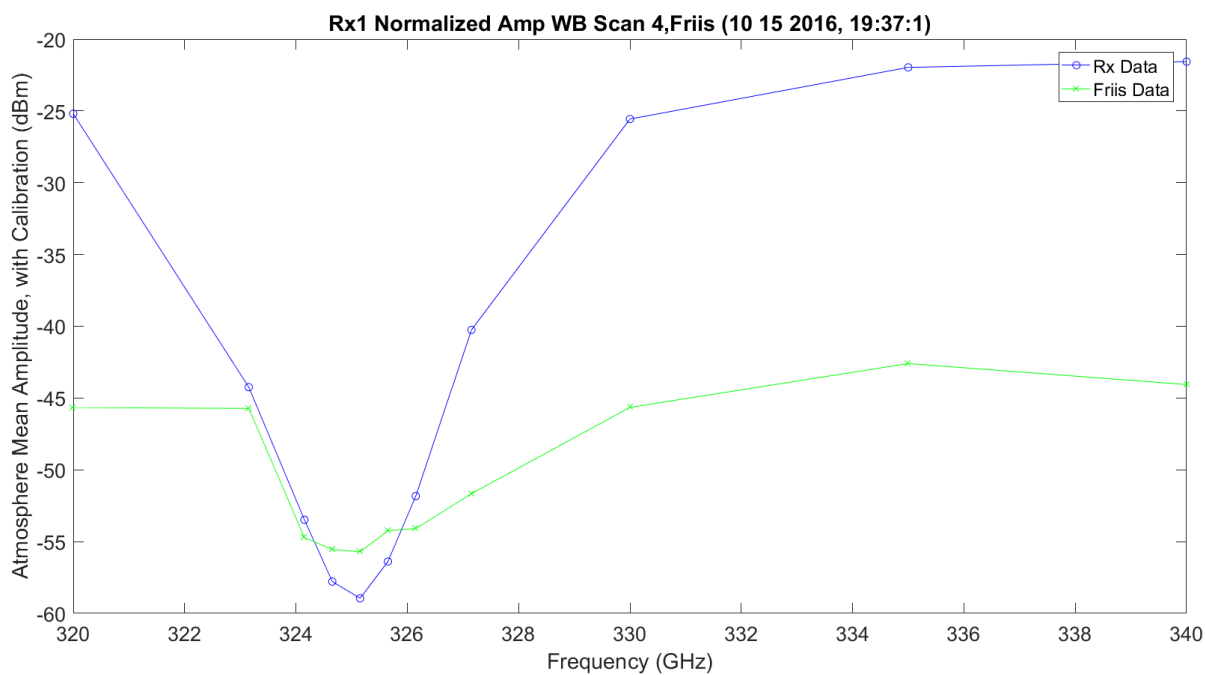


Figure 3.210. WB Scan 4 Amplitude No Hardware, Friis and Difference – 10142016_193175.

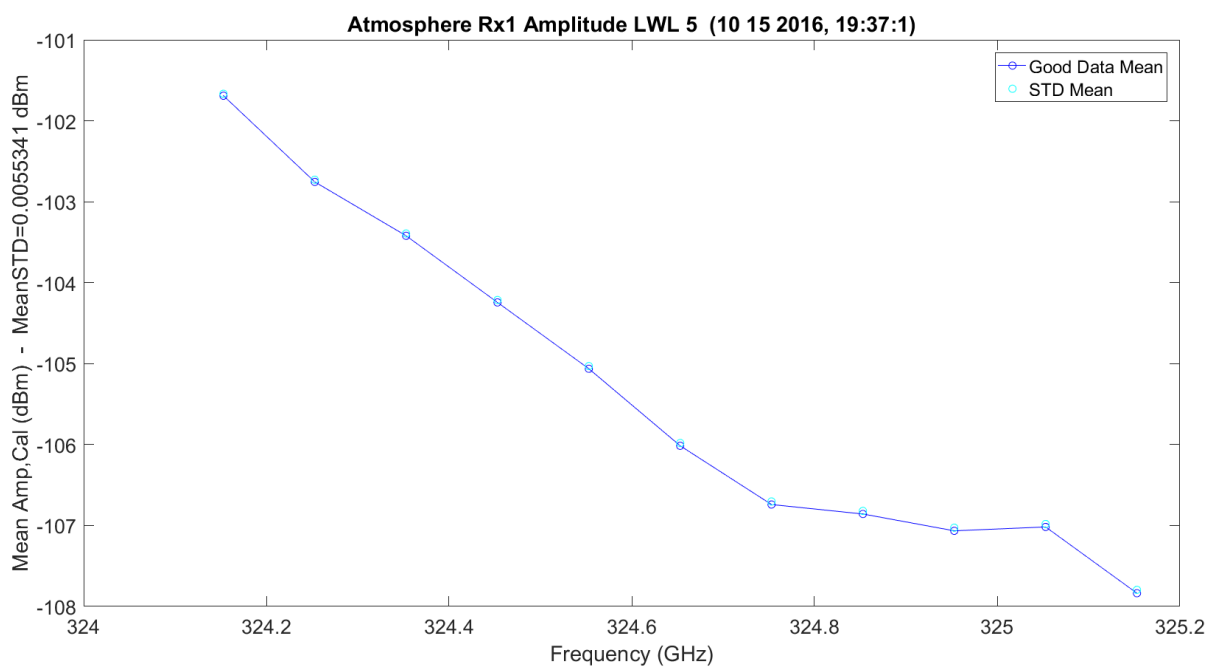


Figure 3.211. LWL Scan 5 Amplitude No Hardware – 10142016_193175.

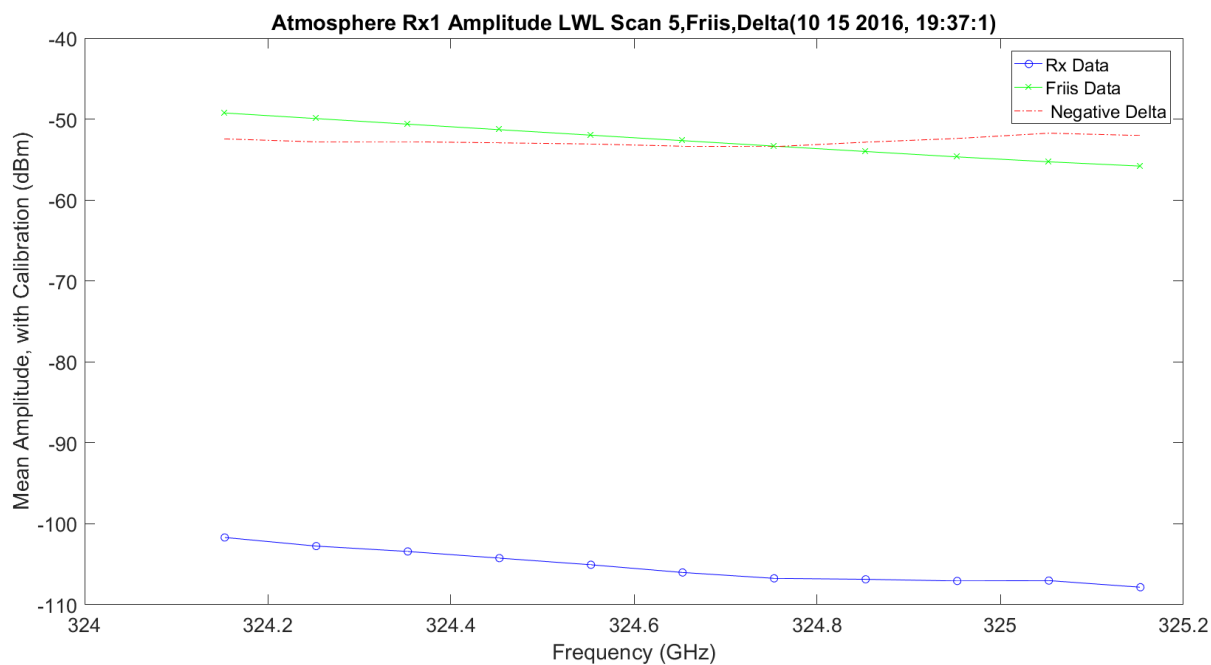


Figure 3.212. LWL Scan 5 Amplitude No Hardware, Friis and Difference – 10142016_193175.

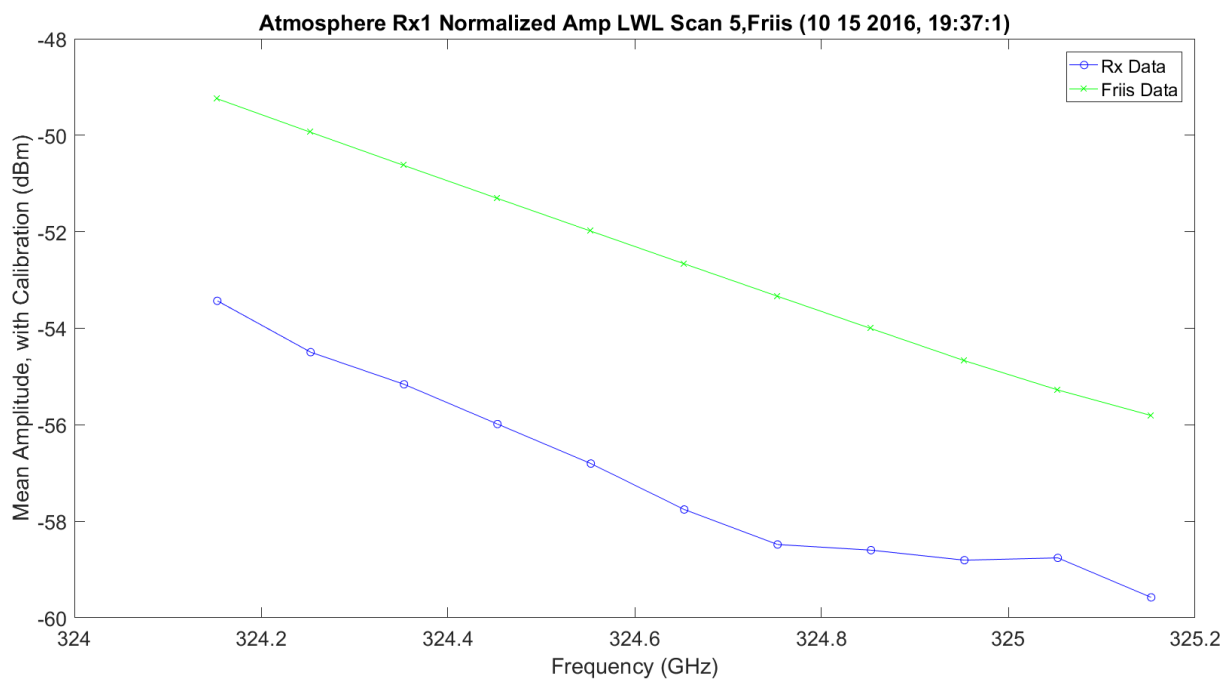


Figure 3.213. LWL Scan 5 Amplitude No Hardware, Friis and Difference – 10142016_193175.

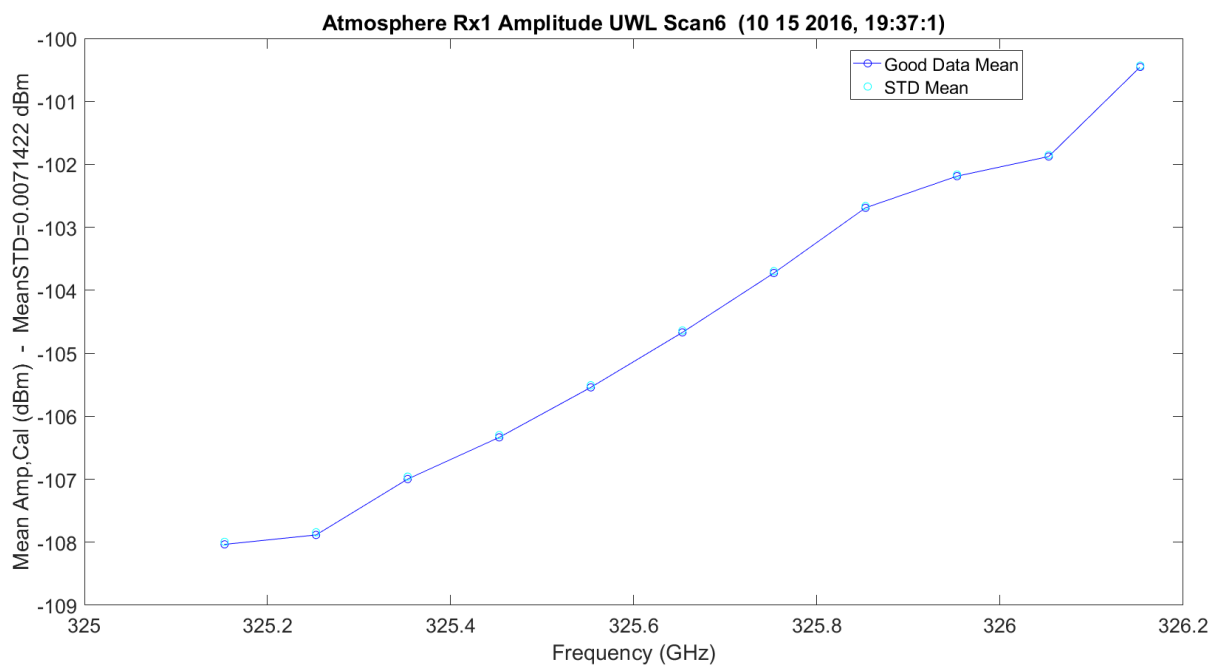


Figure 3.214. UWL Scan 6 Amplitude No Hardware – 10142016_193175.

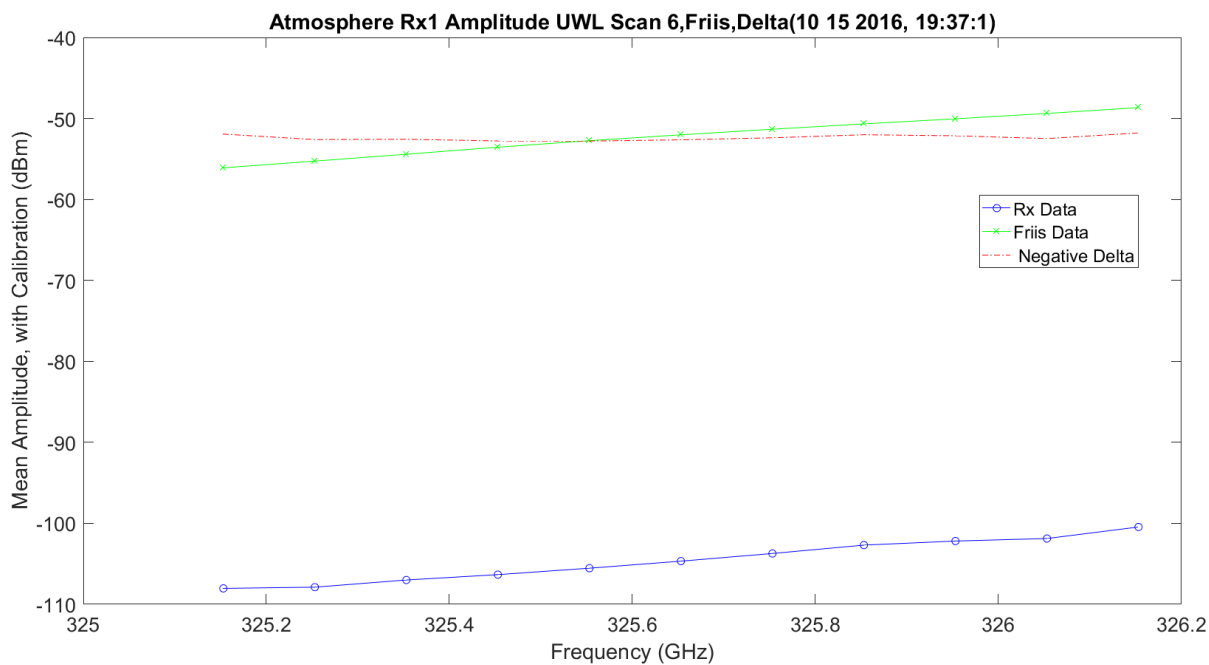


Figure 3.215. UWL Scan 6 Amplitude No Hardware, Friis and Difference – 10142016_193175.

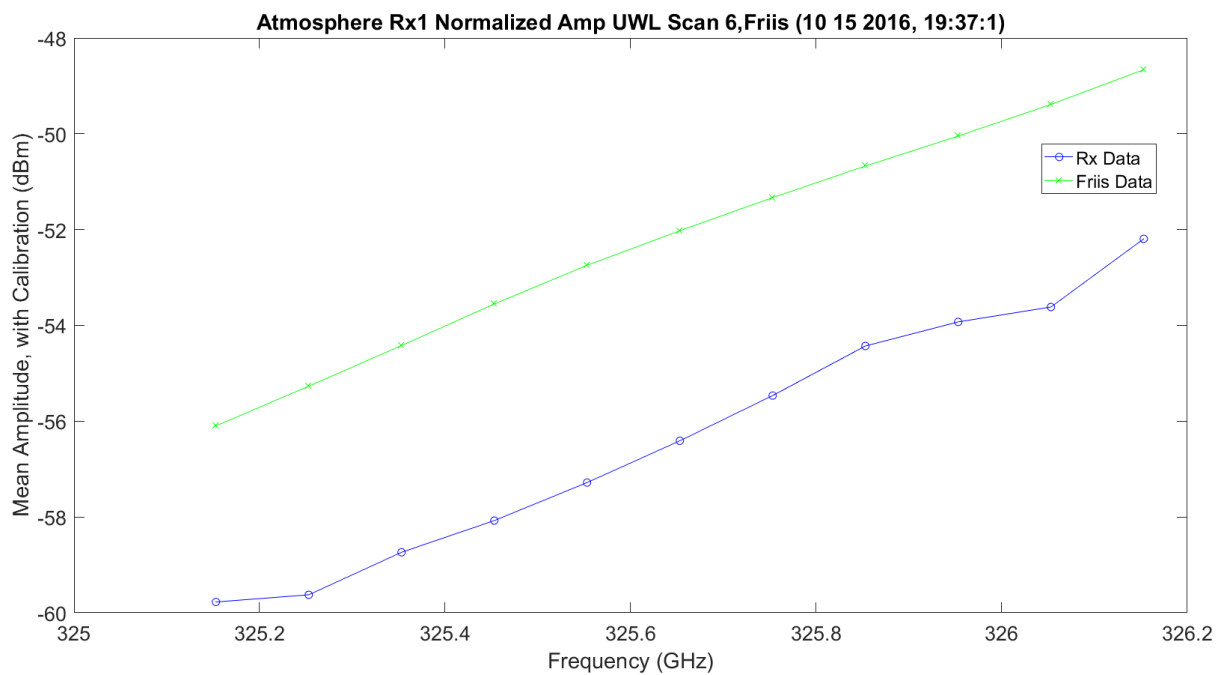


Figure 3.216. UWL Scan 6 Amplitude No Hardware, Friis and Difference – 10142016_193175.

Figure 3.217 shows the normalized and predicted with Friis vs. the LWL and UWL reflected to compare the two slopes. These are very similar to early plots.

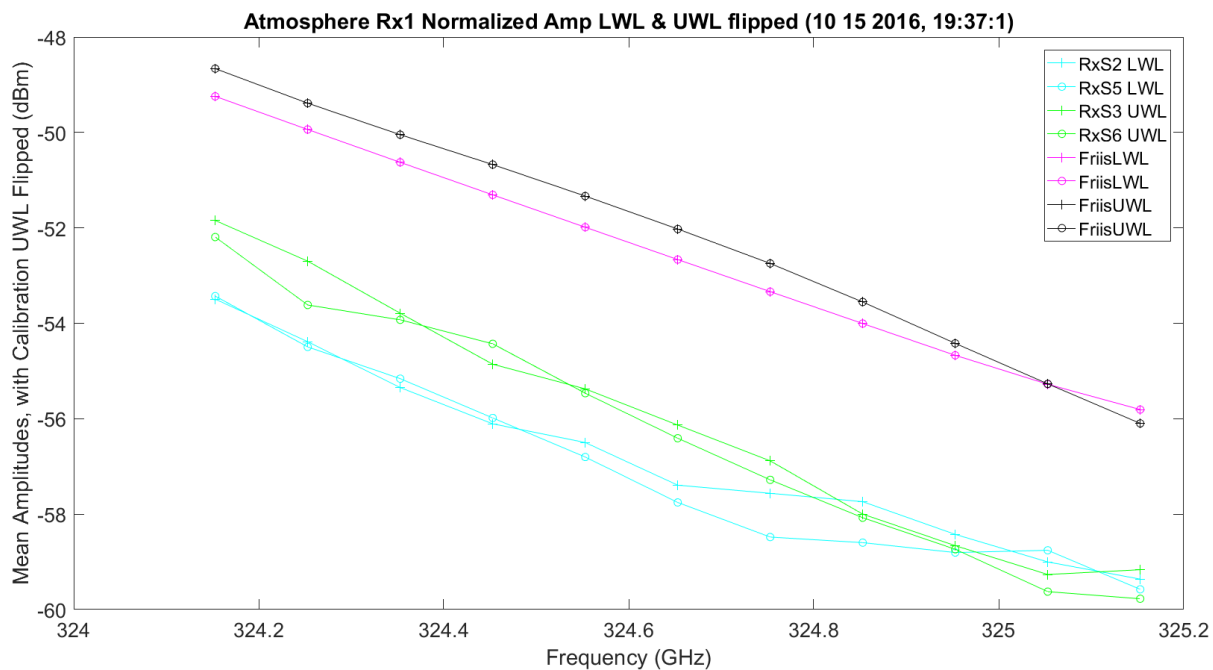


Figure 3.217. LWL & UWL Flipped Mean Amplitude No Hardware – 10142016_193175.

Figure 3.218 shows the WB absorption plot. The red plot represents the Friis view at a 20% RH. The data from TAIPAS was ~30% RH, but is still higher.

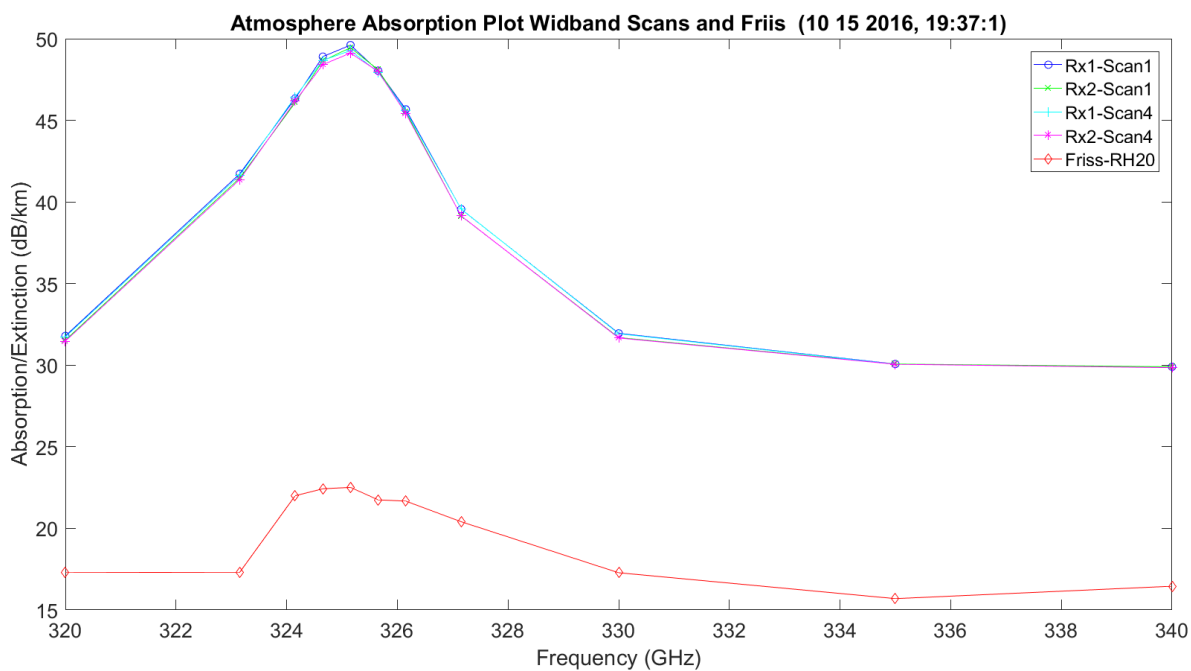


Figure 3.218. WB Extinction with No Hardware – 10142016_193175.

Figure 3.219 shows the LWL absorption plot. The red plot represents the Friis view at 20% RH. The data from TAIPAS was ~30% RH, but is still higher.

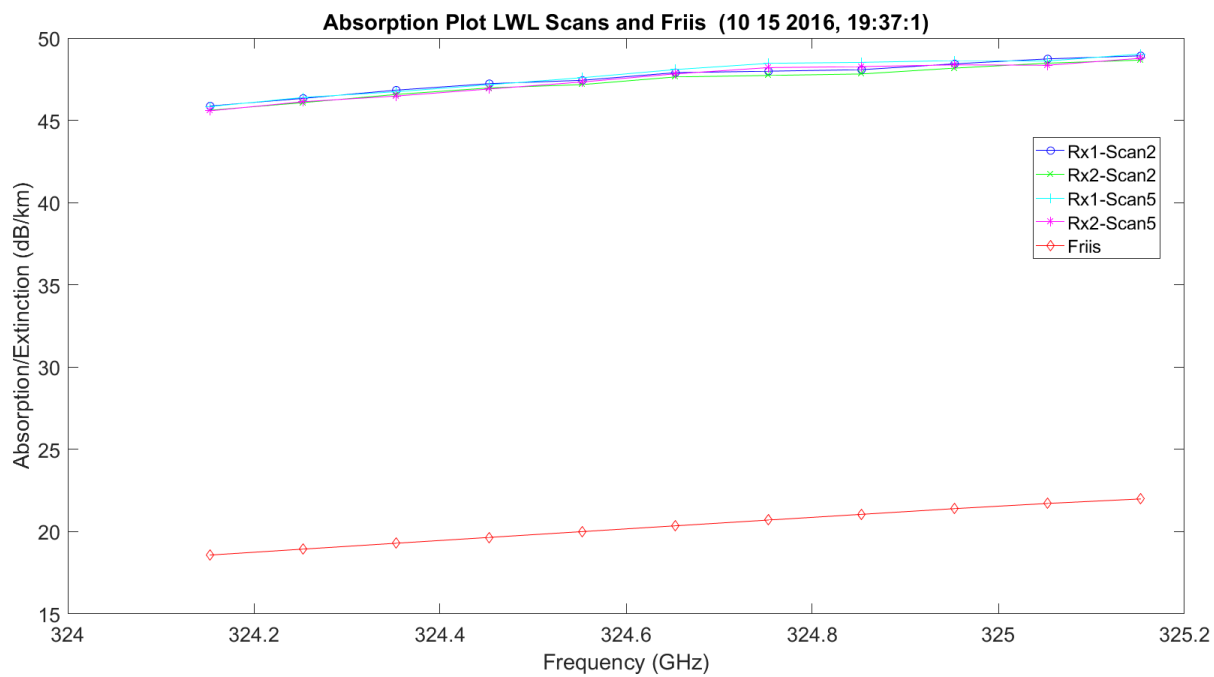


Figure 3.219. LWL Extinction with No Hardware – 10142016_193175.

Figure 3.220 shows the UWL absorption plot. The red plot represents the Friis view at 20% RH. The data from TAIPAS was ~ 30% RH, but is still higher.

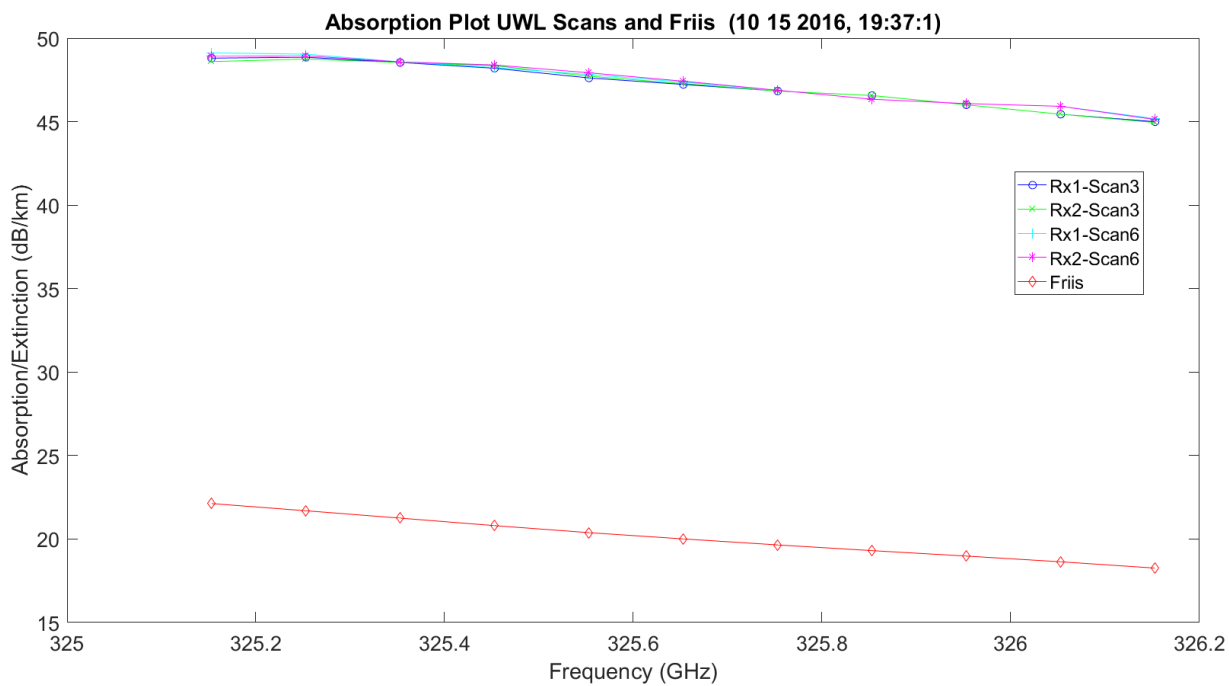


Figure 3.220. UWL Extinction with No Hardware – 10142016_193175.

Figure 3.221 shows the LWL and UWL flipped absorption plot. The red plot represents the Friis view at 20% RH. The data from TAIPAS was ~30% RH, but is still higher.

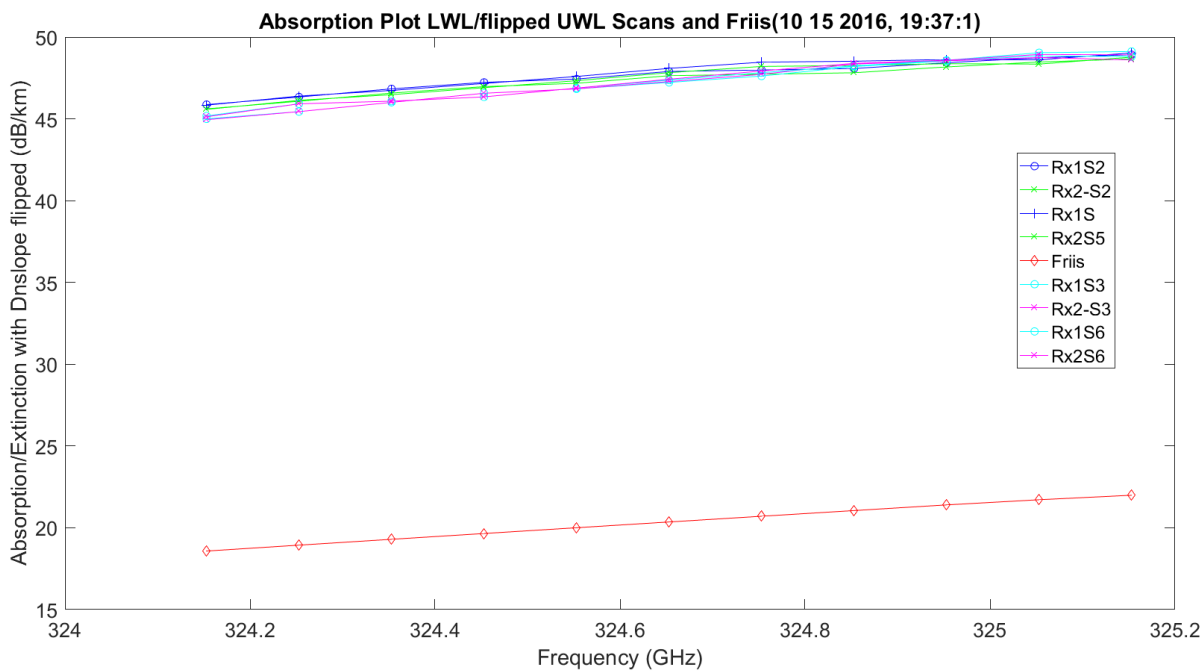


Figure 3.221. LWL & UWL Flipped Mean Amplitude No Hardware – 10142016_193175.

This pass was run on 11012016_145401; the date is first and the time in ms is second. During this time, both receivers were operational, but Rx1 had very low SNR. Due to the low receiver, the threshold from good data to the retuning synthesizer change was programmable in MATLAB with variables set up in dB: $Rx1_Threshold_Good_to_Bad_Data_dB = 2.595$ and $Rx2_Threshold_Good_to_Bad_Data_dB = 3$. Rx1 had the lowest SNR due to excessive padding. The normal threshold for both is 5 dB. This was the first full set of data for the transmitter and both receivers. This pass was taken during the day remotely from Colorado Springs and the picture from Rx1 on the mesa during the day is in Figure 3.222.



Figure 3.222. Data Acquisition Camera – 11012016_145401.

Figure 3.223 shows the synchronization for the entire approximate seven-second duration of running the 66 frequency shifts. Figure 3.224 traces the exact offset of the times between the transmitter and the receivers. There is some acceptable straddling from scan-to-scan with a total worst case shift of 1 ms; the maximum time between scans was very acceptable at 2 ms. This is improved over the earlier runs.

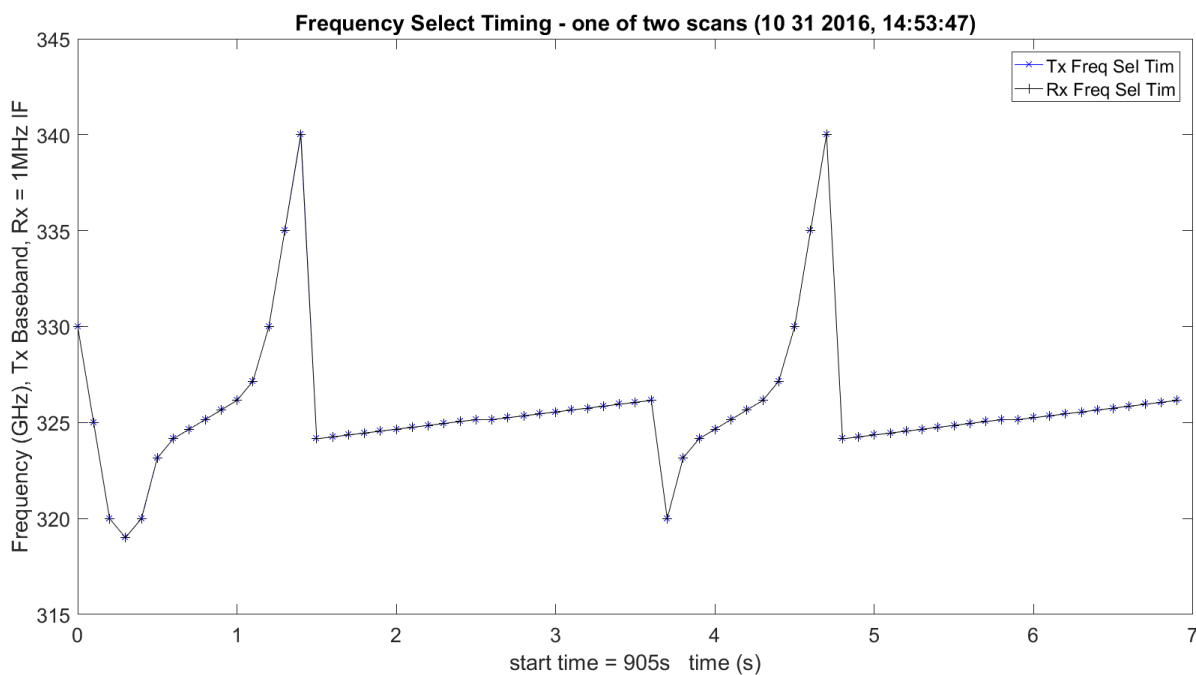


Figure 3.223. Timing Synchronization – 11012016_145401.

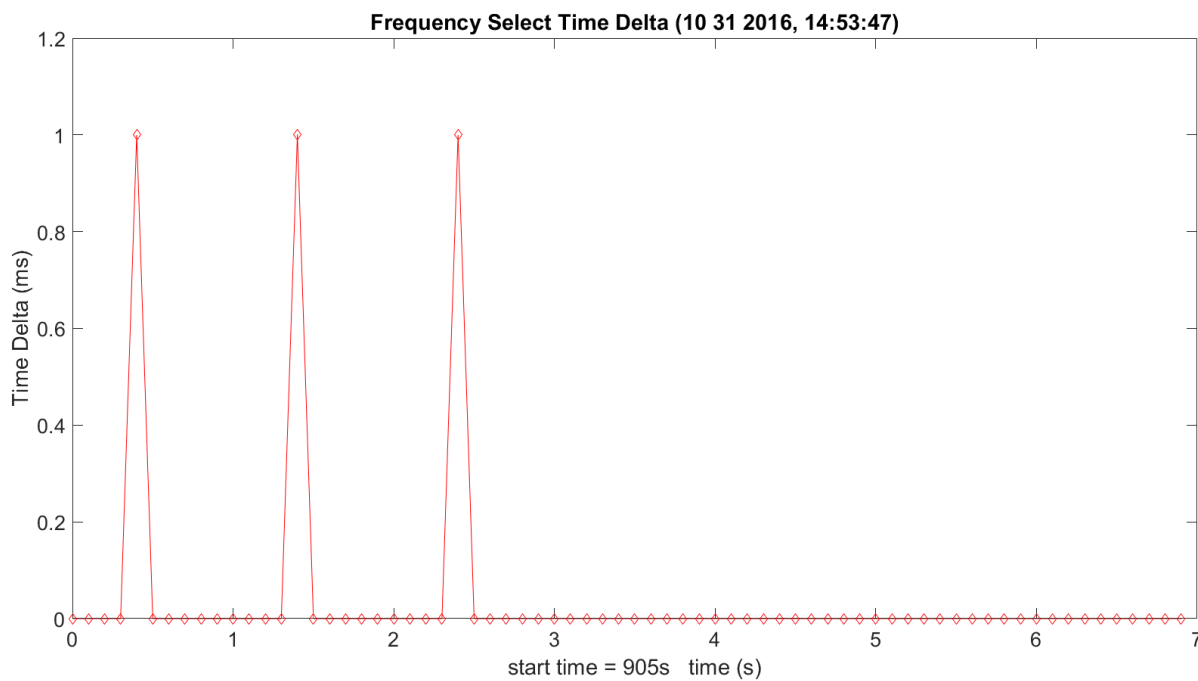


Figure 3.224. Tracking of the Delta Time between Tx and Rx – 11012016_145401.

Figure 3.225 and 3.226 shows the raw data from the ADC after the DDC to baseband was implemented for Rx1 and Rx2. This showed very good results over the long open path; both receivers to the naked eye look very similar. Figure 3.227 and 3.228 show the same response, only filtering out the noise. This is needed to detect the edges in MATLAB of good data and bad data. The bad data occurs during the switching and scanning of the synthesizers as they stabilize and the delta in the clocks discussed above. This, again, looks as expected. An FFT was taken on the first frequency (320 GHz) to see the conditions of the DDC (Figure 3.229 – Figure 3.230); this can be done for every frequency, but would crash MATLAB. This shows receiver SNR is ~20 dB greater than Rx1. This is utilized to verify functionality and debug when a failure occurs. The tones look very close to baseband as expected. Figure 3.231 and 3.232 show the histograms of the same first frequency (320 GHz) of the WB scan; the histogram for the first frequency of Rx1 is much lower. This is implemented on the raw data and shows very good results and ranges in amplitude from approximately -82 dBm to -81.7 dBm for Rx2.

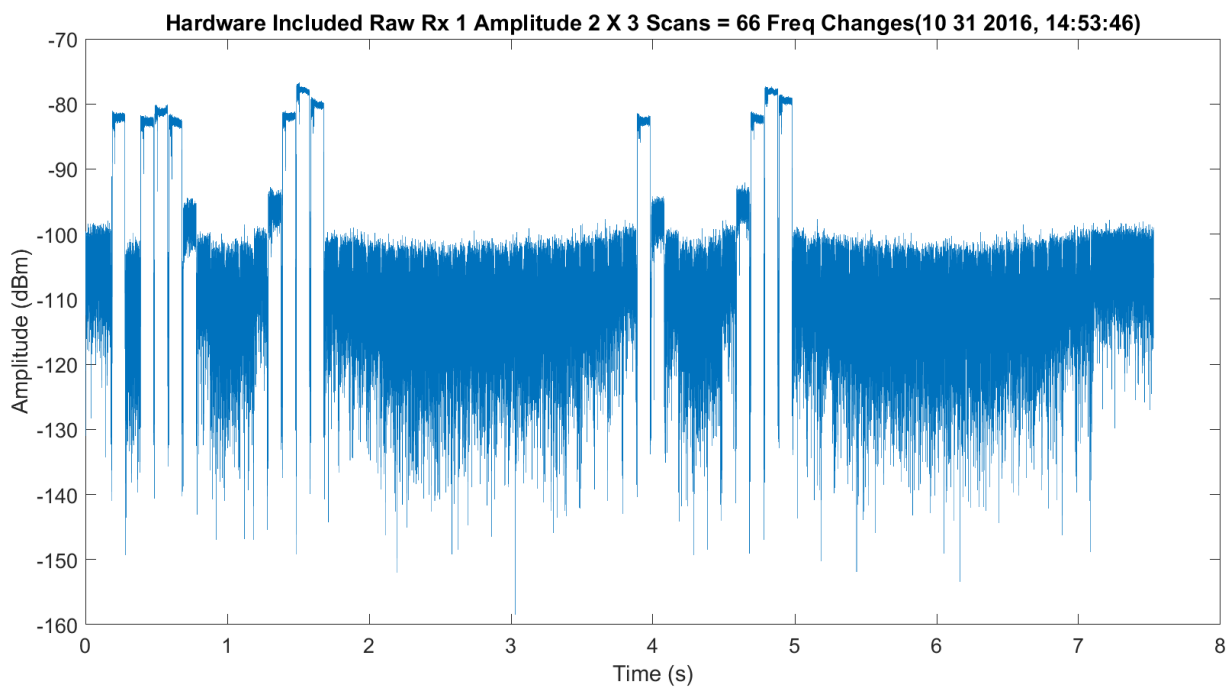


Figure 3.225. Raw Data after DDC for Rx1 – 11012016_145401.

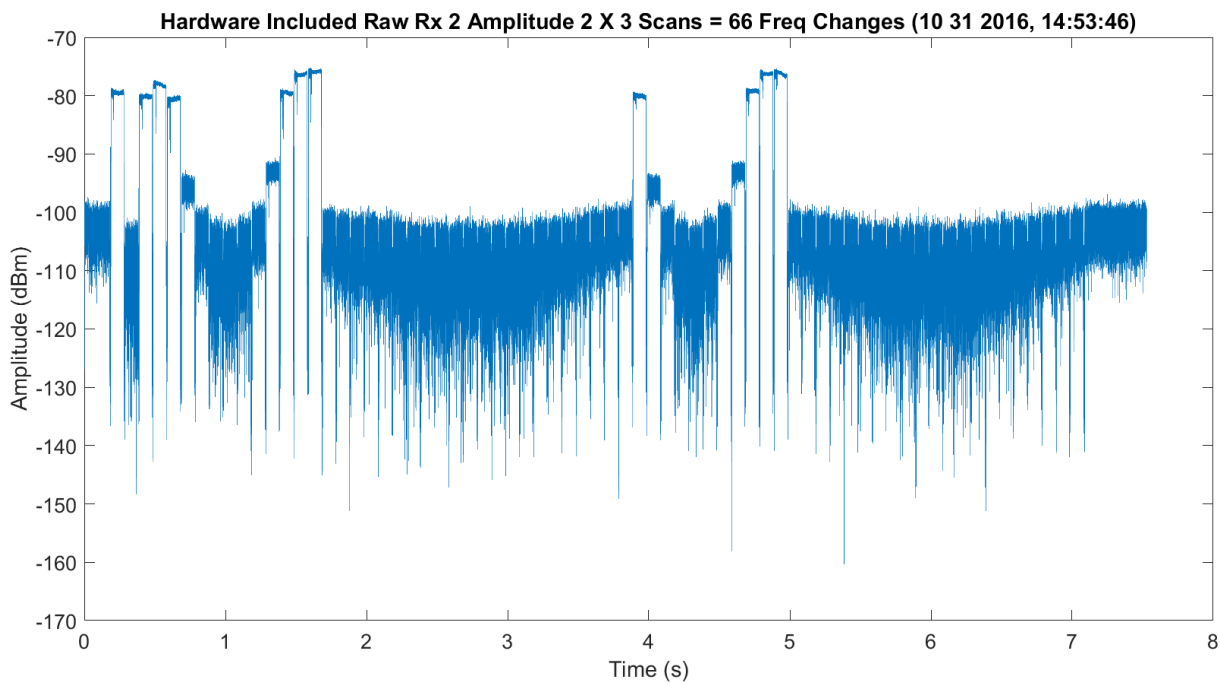


Figure 3.226. Raw Data after DDC for Rx2 – 11012016_145401.

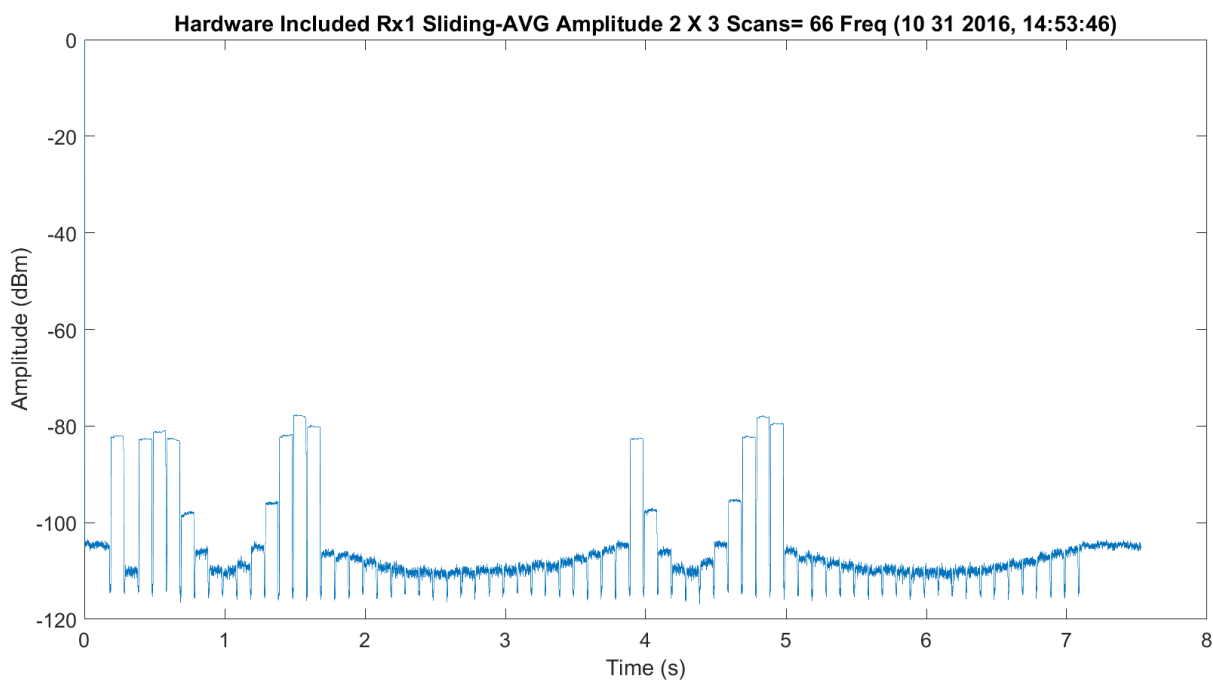


Figure 3.227. Averaged Filtered (80 Tap) Data after DDC for Rx1 – 11012016_145401.

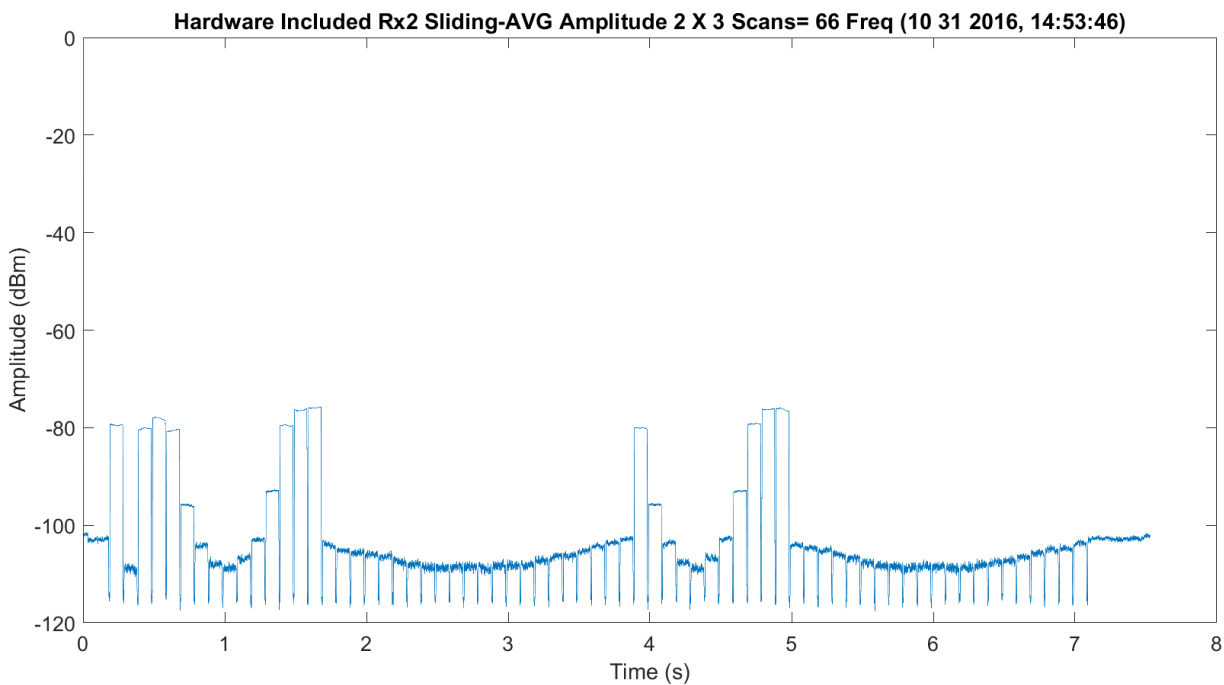


Figure 3.228. Averaged Filtered (80 Tap) Data after DDC for Rx2 – 11012016_145401.

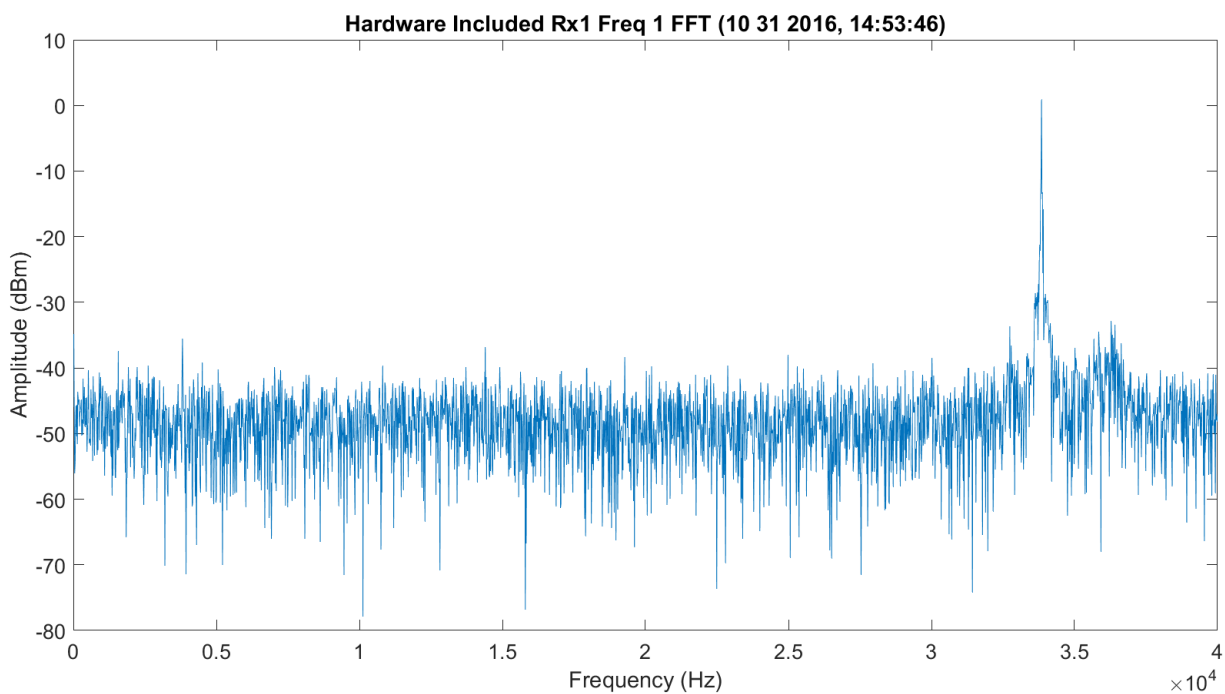


Figure 3.229. FFT of first WB Frequency (320 GHz) after DDC for Rx1 – 012016_145401.

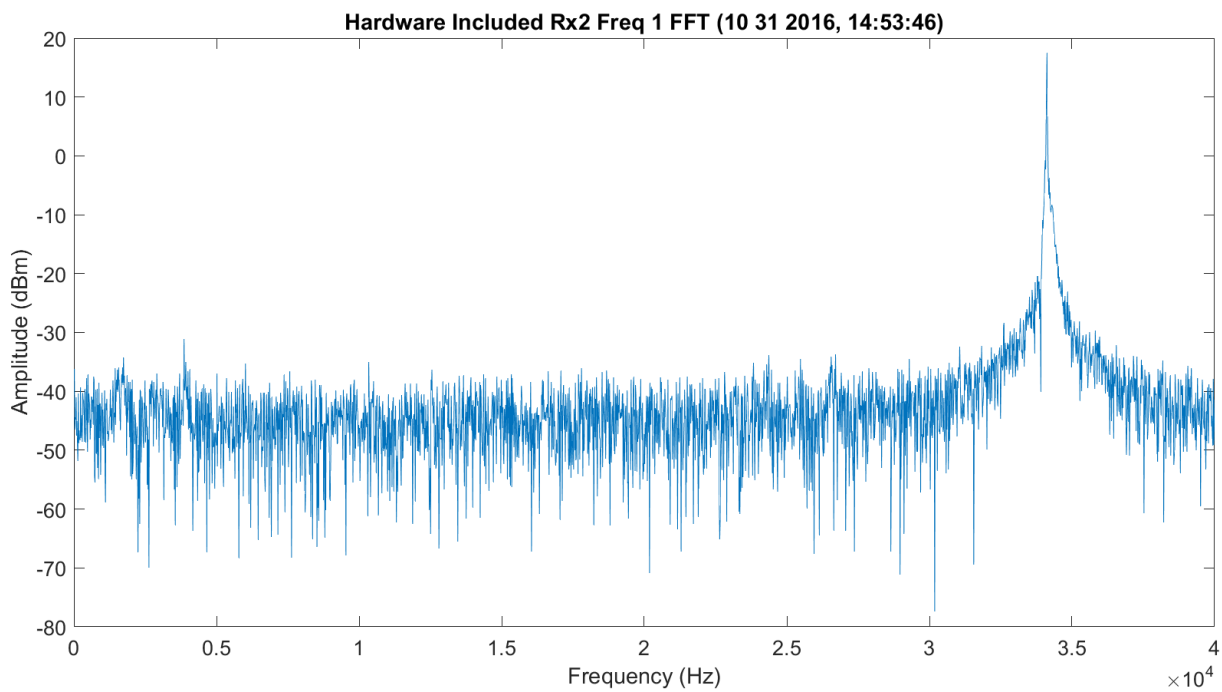


Figure 3.230. FFT of first WB Frequency (320 GHz) after DDC for Rx2 – 1012016_145401.

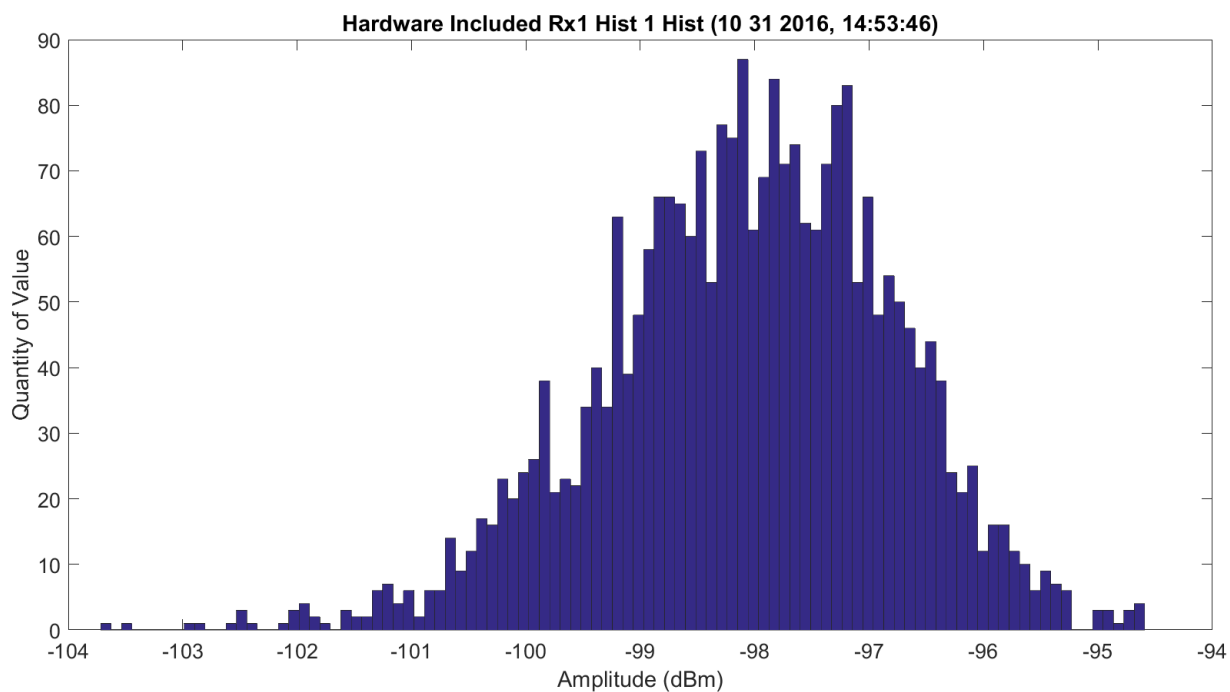


Figure 3.231. Histogram of first WB Frequency (320 GHz) after DDC for Rx1 – 1012016_145401.

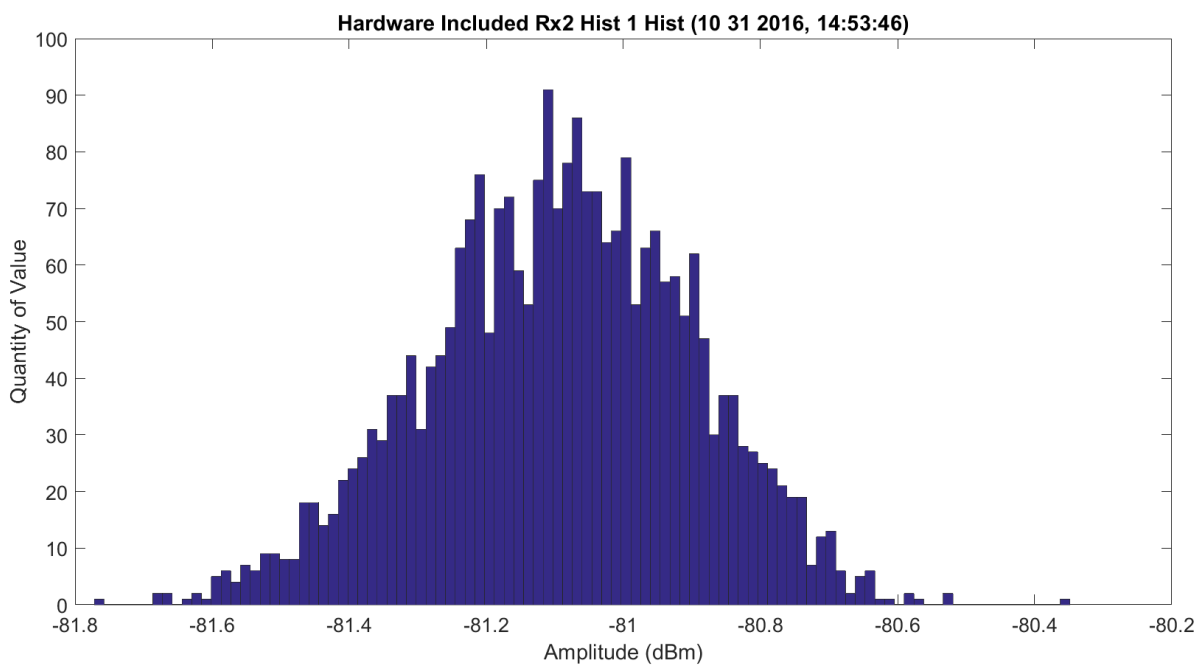


Figure 3.232. Histogram of first WB Frequency (320 GHz) after DDC for Rx 2 – 11012016_145401.

It is also important to note that the light blue bubbles at the sample points are the standard deviation divided by the square root of the number of points; this is on the plots. The closer these are to the existing dark blue circles, the better the accuracy.

Figure 3.233 shows the amplitude scan over the first scan of the WB frequencies; all these modes have hardware losses and gains that may not be known in the system. The amplitude ranges from approximately -109 dBm at 325.153 GHz to -97 dBm at 320 GHz and -82 dBm for 330 GHz through 340 GHz. The frontend looks distorted, due to the low SNR. The total difference in attenuation is approximately 24 dB, which seems higher than results in the 80s. The response looks as expected, very good. Figure 3.234 shows the same data with the Friis. There is a significant offset in the traces. Figure 3.235 normalizes the data to have full overlap of the Friis prediction and the collected data to compare the shapes; this only shows Friis due to the low SNR data on the signal. The Friis is wider and not as close to a sharp peak as the TAIPAS collected data.

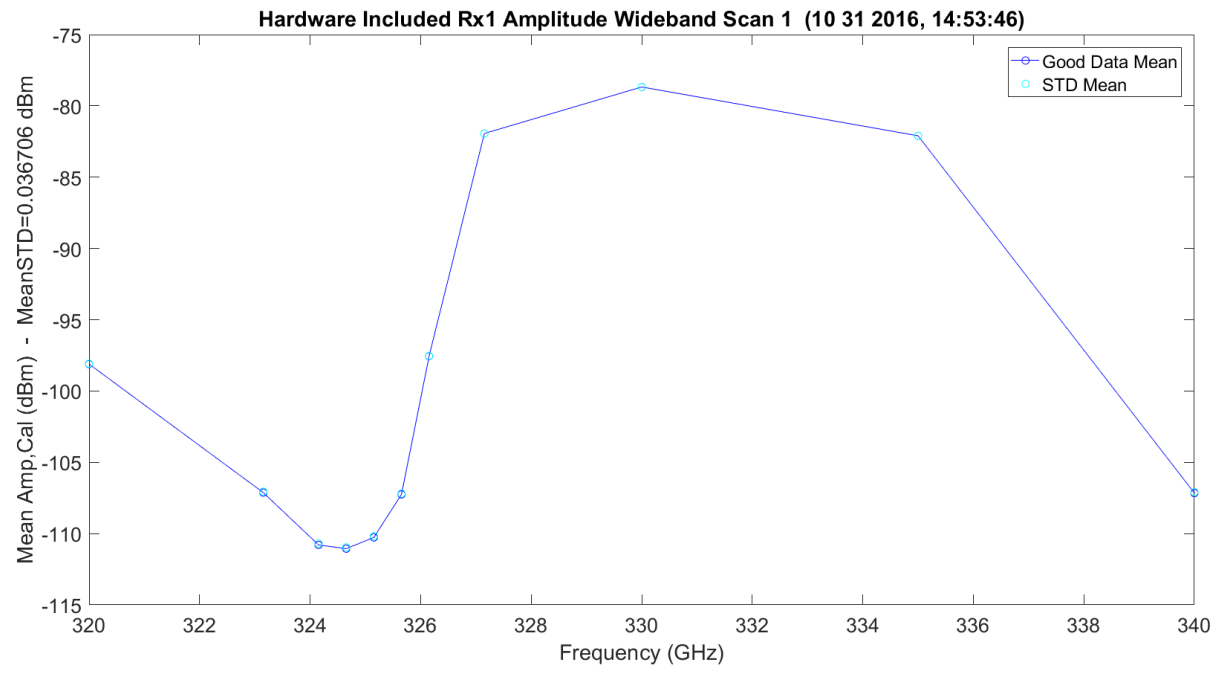


Figure 3.233. WB Scan 1 for Rx1 – 11012016_145401.

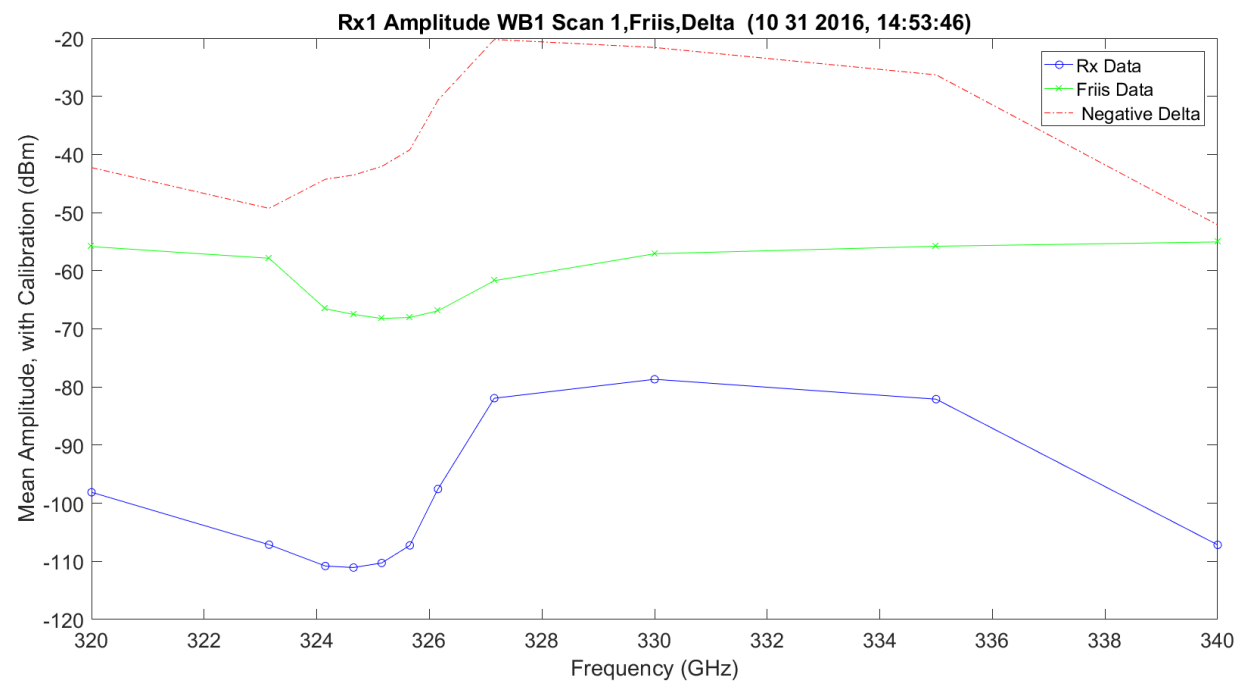


Figure 3.234. WB/Friis Scan 1 for Rx1 – 11012016_145401.

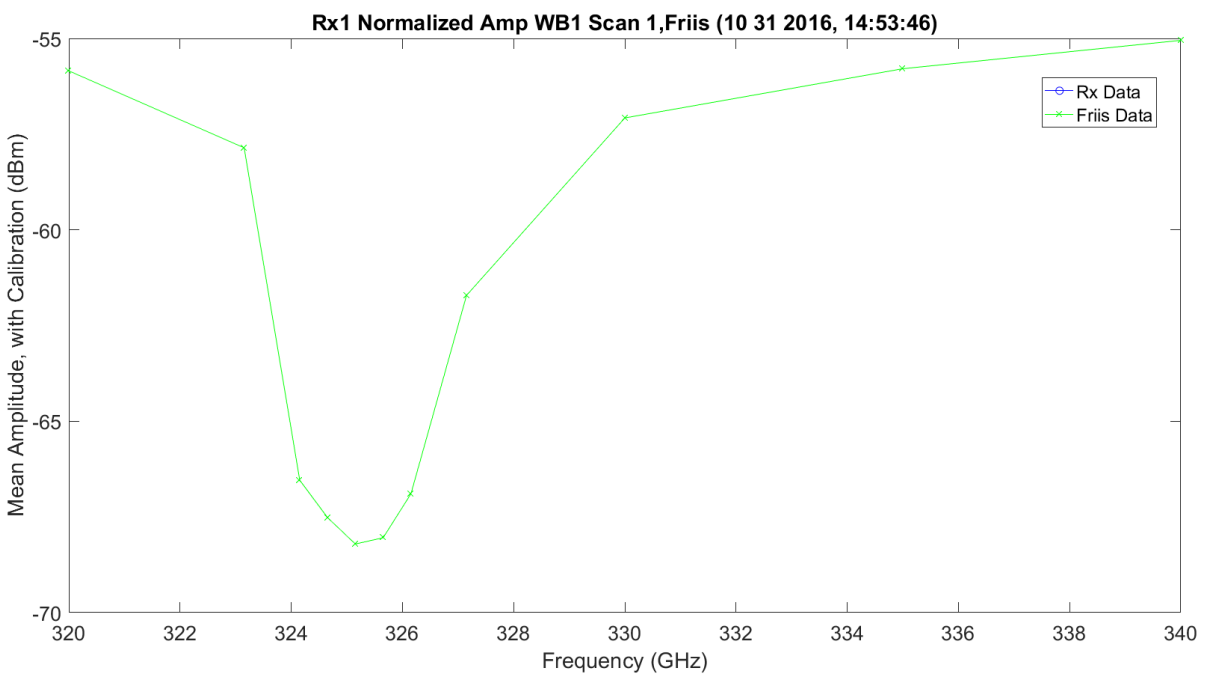


Figure 3.235. WB/Friis Normalized Scan 1 for Rx1 – 11012016_145401.

Figure 3.236 shows an absorption LWL scan 2 frequency. There is more ripple in the finely spaced frequencies of 100 MHz, which could be due to the calibration of the data on transmit and receive; the values can change minor in dB from point-to-point. It looks like the high sample of the LWL does show some atmosphere ripples on the EM. It also shows, for the low SNR, that some of the points were dropped. Figure 3.237 shows the data with the Friis prediction and the difference — missed points here as well. The ripples on the collected data become less obvious and the wings of the two look approximately the same, but they have approximately 40 dB of difference in amplitude. Figure 3.238 shows the normalization of the Friis and collected data; again, only Friis was shown.

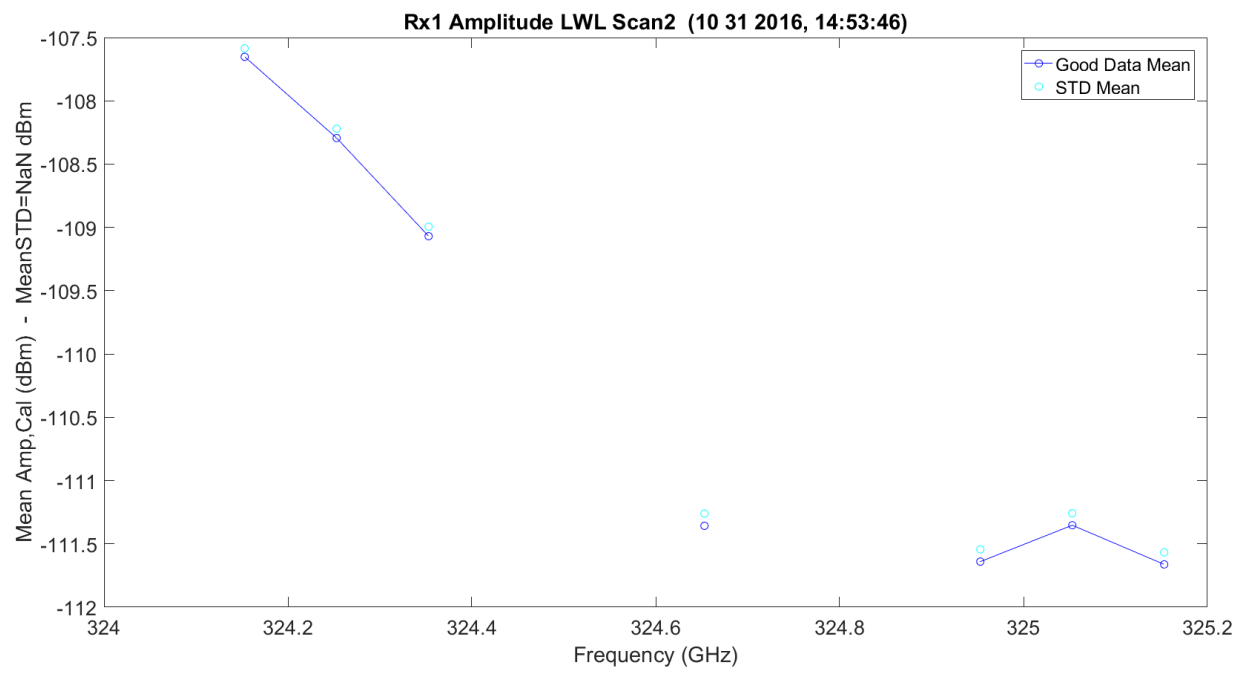


Figure 3.236. LWL Absorption Scan 2 for Rx1 – 11012016_145401.

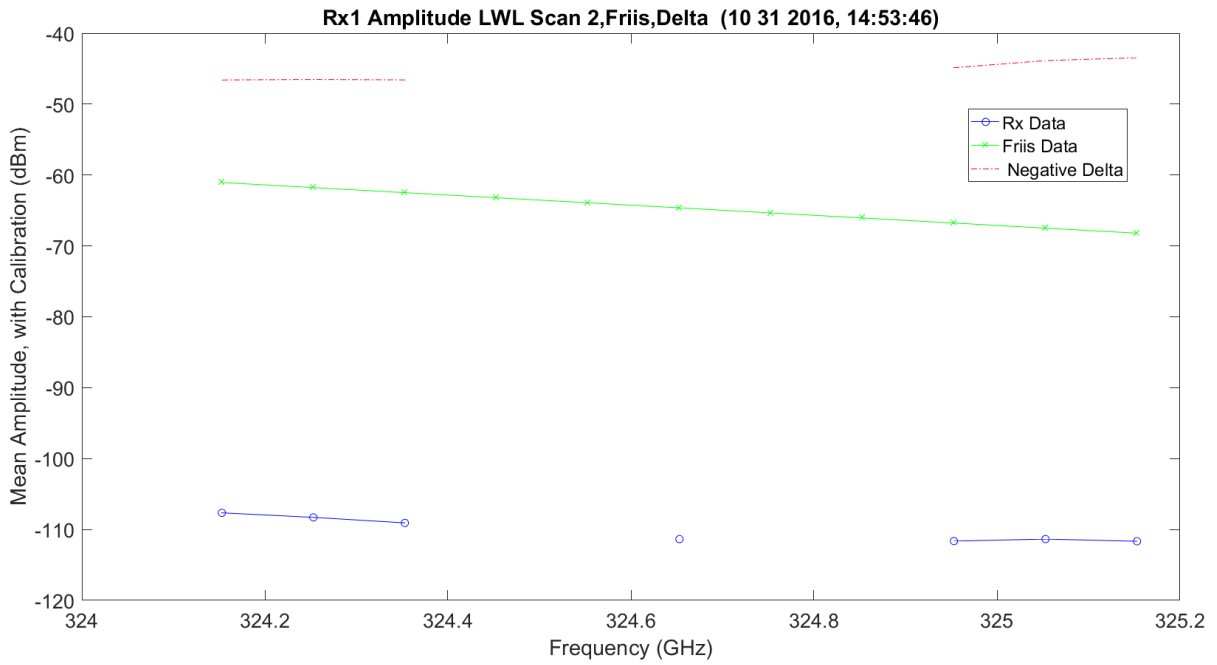


Figure 3.237. LWL / Friis Absorption Scan 2 for Rx1 – 11012016_145401.

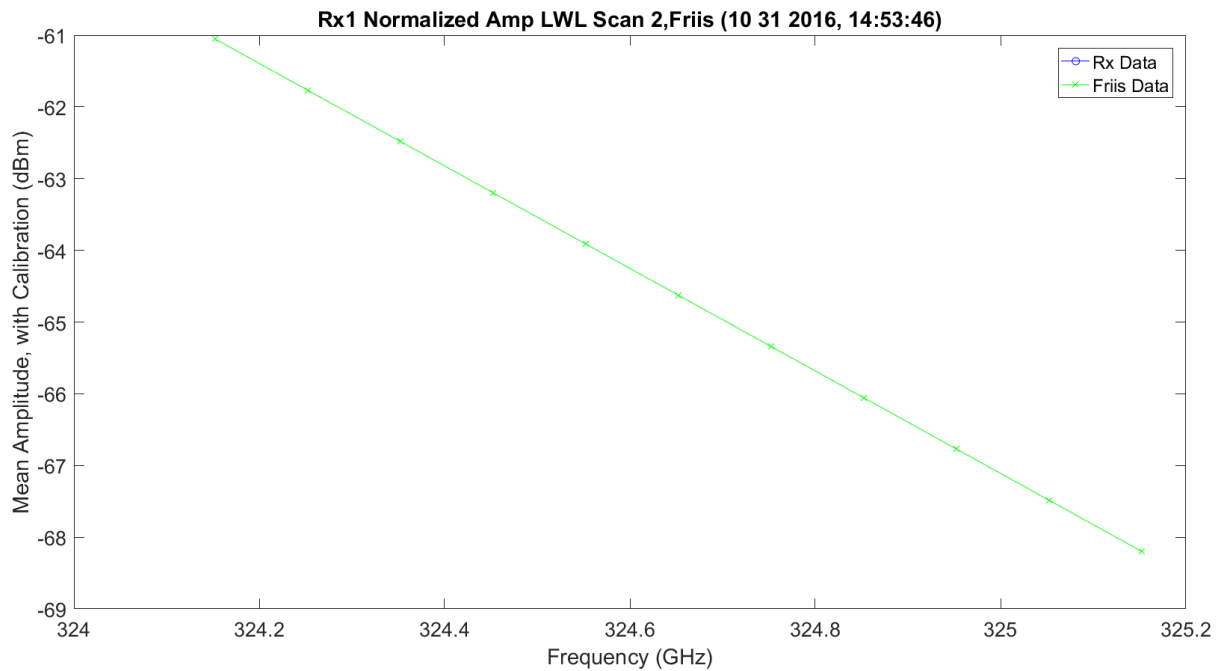


Figure 3.238. LWL / Friis Normalized Absorption Scan 2 for Rx1 – 11012016_145401.

Figure 3.239 shows an absorption UWL scan 3 frequency. There is more ripple in the finely spaced frequencies of 100 MHz, which could be due to the calibration of the data on transmit and receive; the values can change minor in dB from point-to-point. It looks like the high sample of the UWL does show some atmospheric ripples on the EM. Figure 3.240 shows the data with the Friis prediction and the difference. The ripples on the collected data become less obvious and the wings of the two look approximately the same, but they have approximately 48 dB of difference in amplitude. Figure 3.241 shows the normalization of the Friis and collected data; it is only Friis due to low SNR. This UWL performed much better than the above LWL.

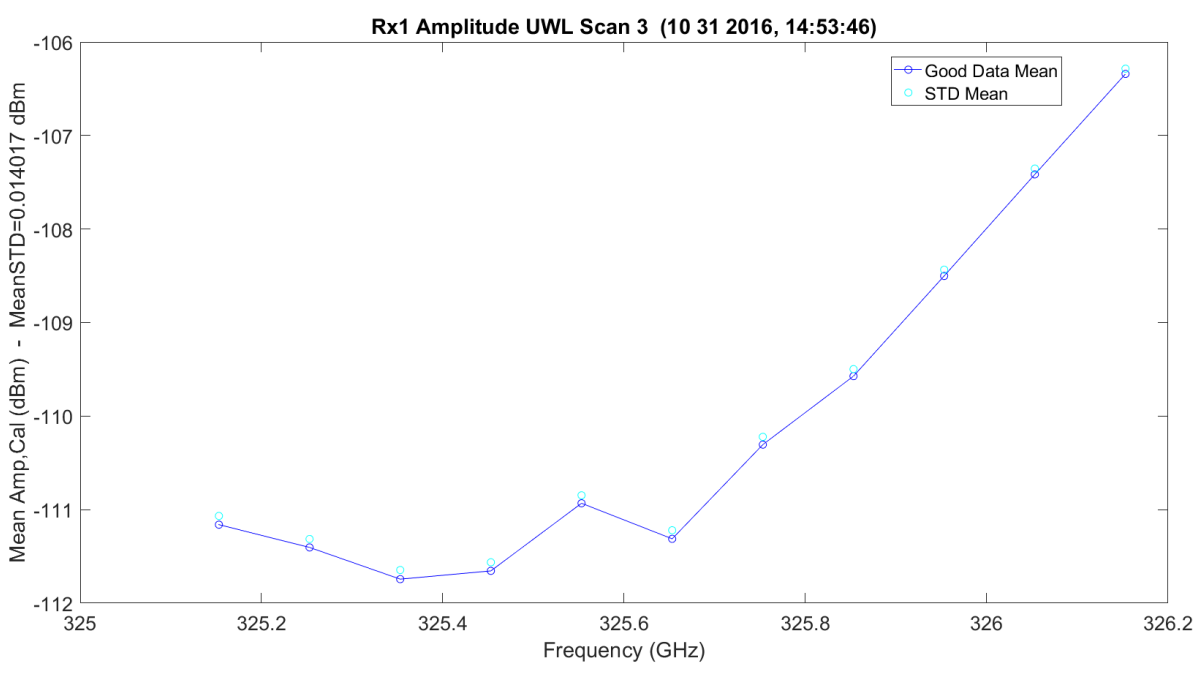


Figure 3.239. UWL Absorption Scan 3 for Rx1 – 11012016_145401.

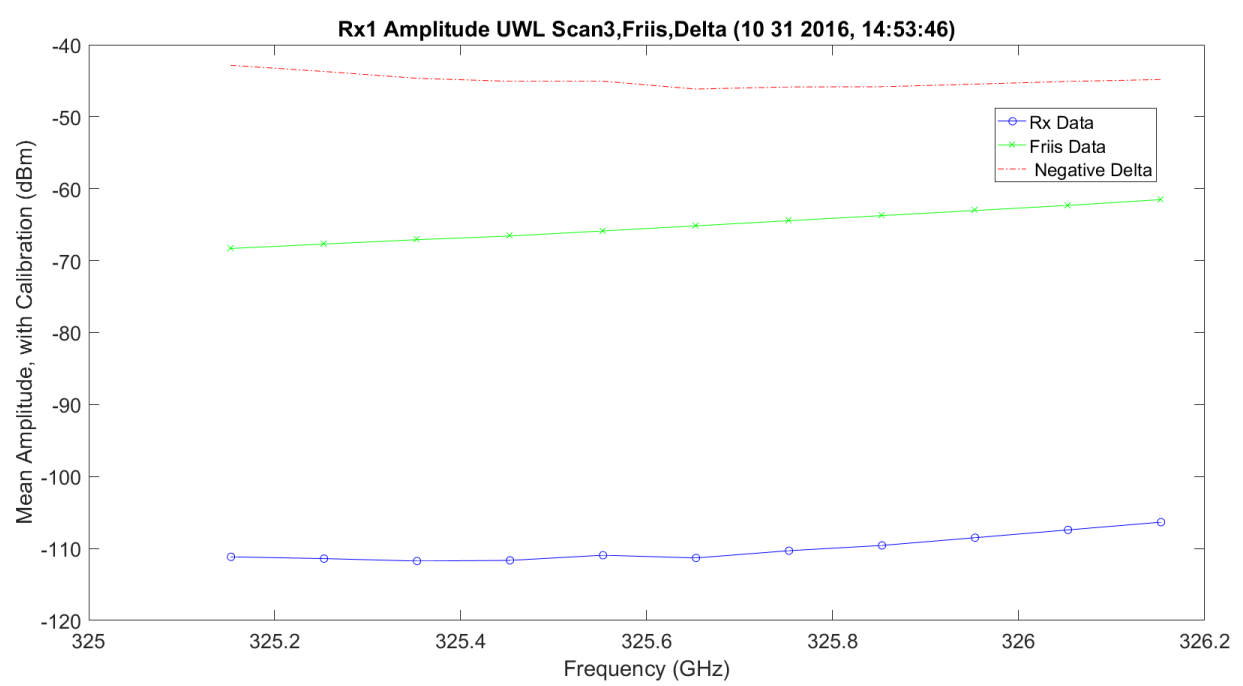


Figure 3.240. UWL / Friis Absorption Scan 3 for Rx1 – 11012016_145401.

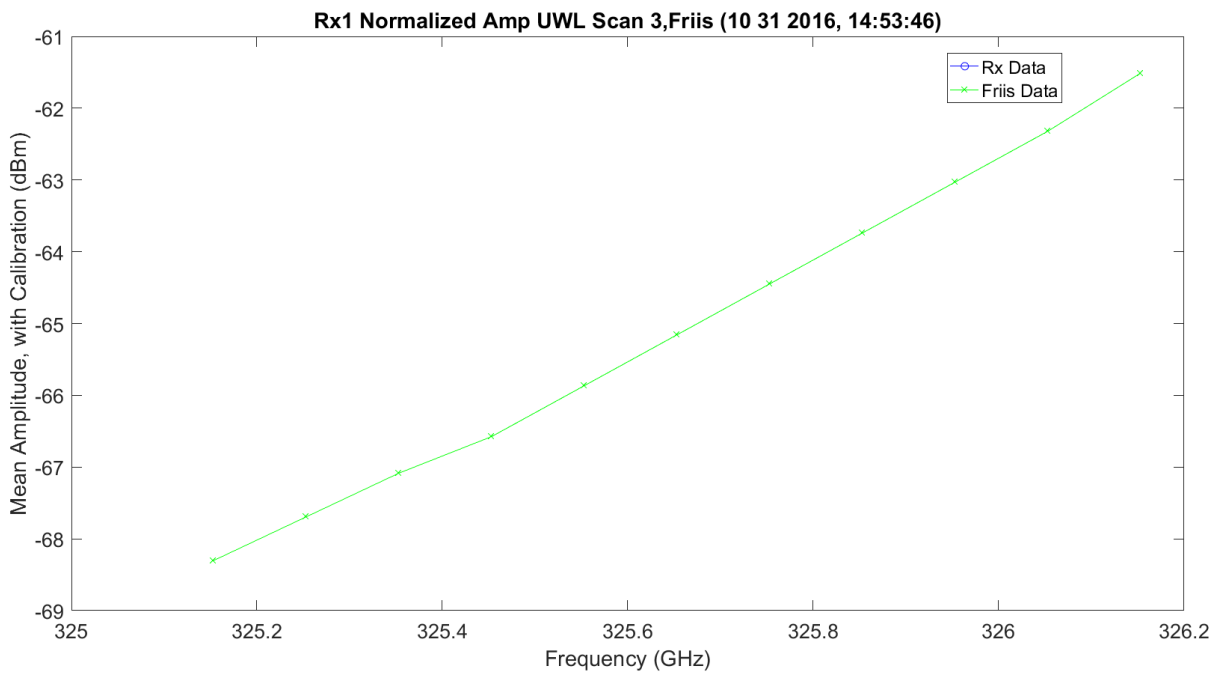


Figure 3.241. UWL / Friis Normalized Absorption Scan 3 for Rx1 – 11012016_145401.

The following plots (Figure 3.242-3.250) are the second set of identical scans: WB, LWL and UWL. They each scan 11 different frequencies. They are included for completeness, but they look better for the LWL than the first 33 scanned frequencies. The LWLs and UWLs have very different wing jugs.

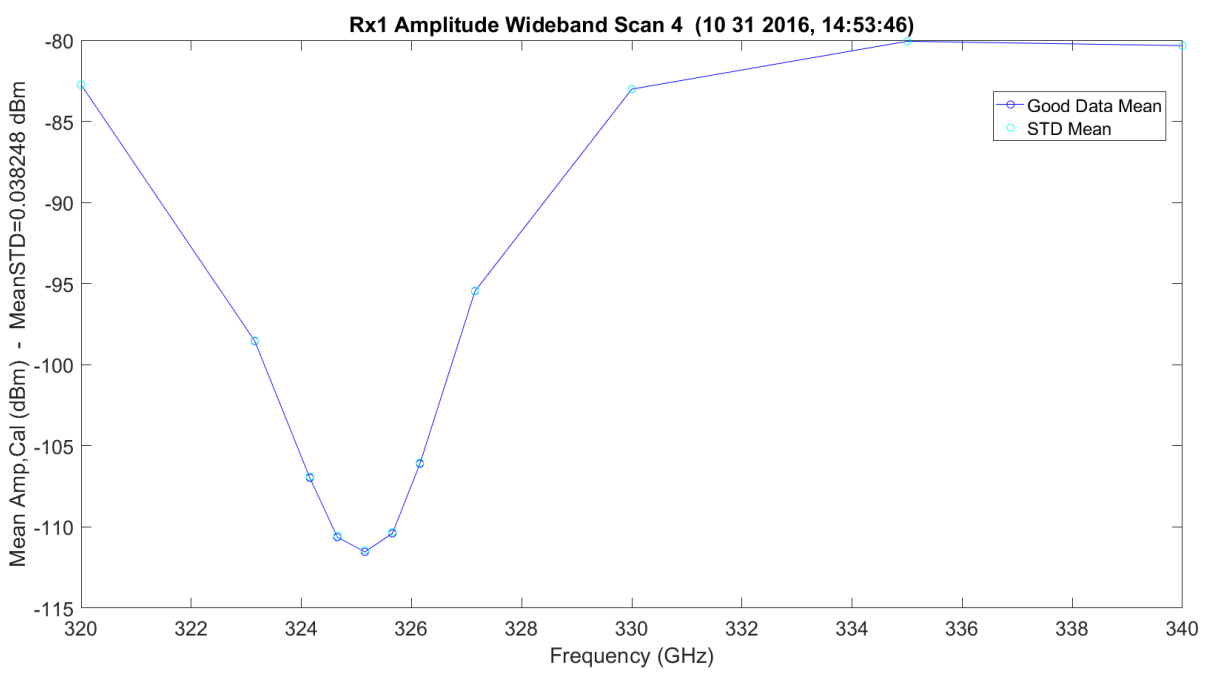


Figure 3.242. WB Scan 4 for Rx1 – 11012016_145401.

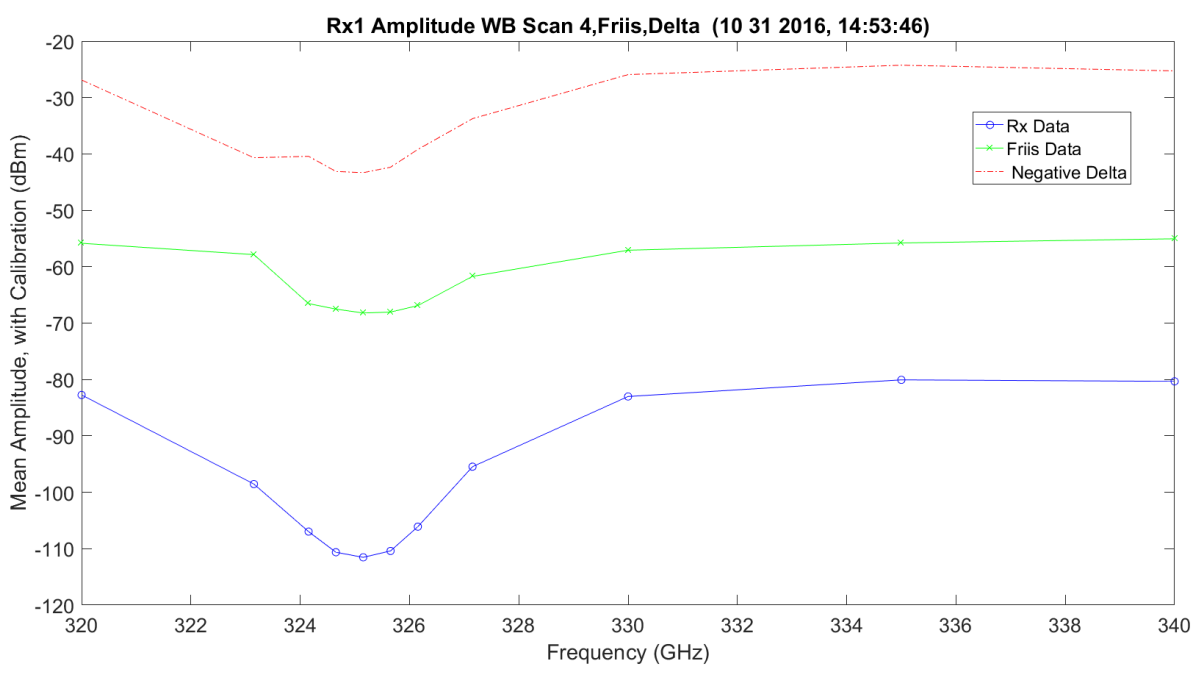


Figure 3.243. WB/Friis Normalized Scan 4 for Rx1 – 11012016_145401.

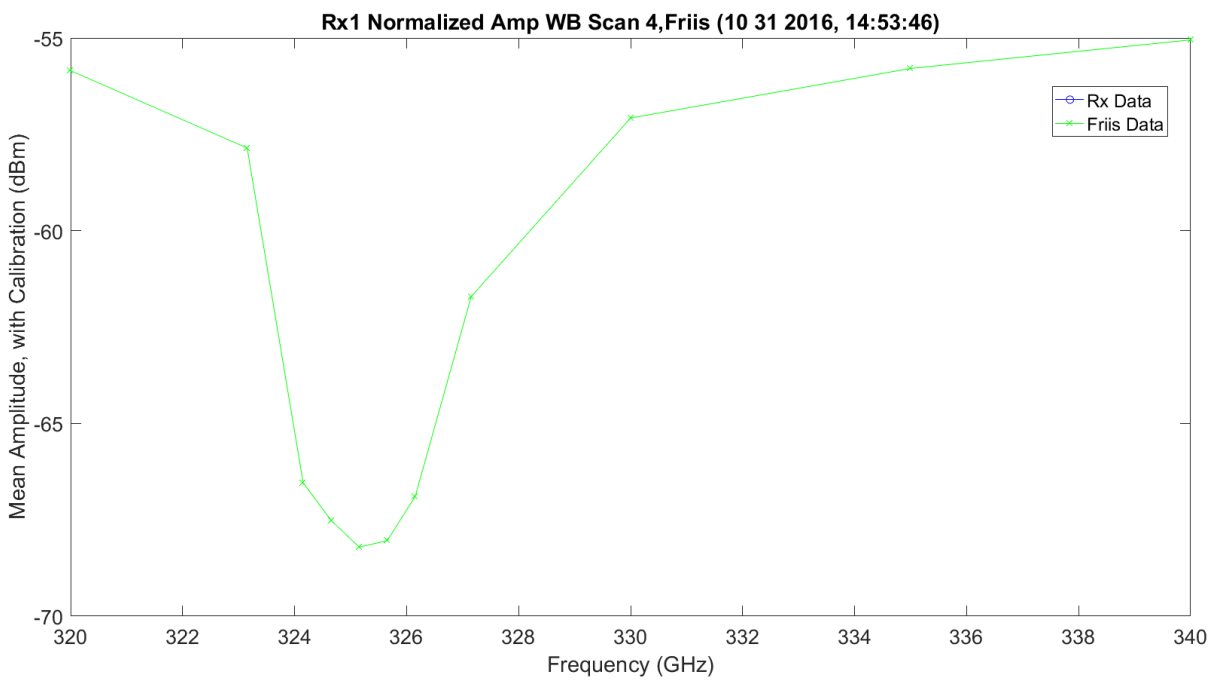


Figure 3.244. WB Absorption Scan 4 for Rx1 – 11012016_145401.

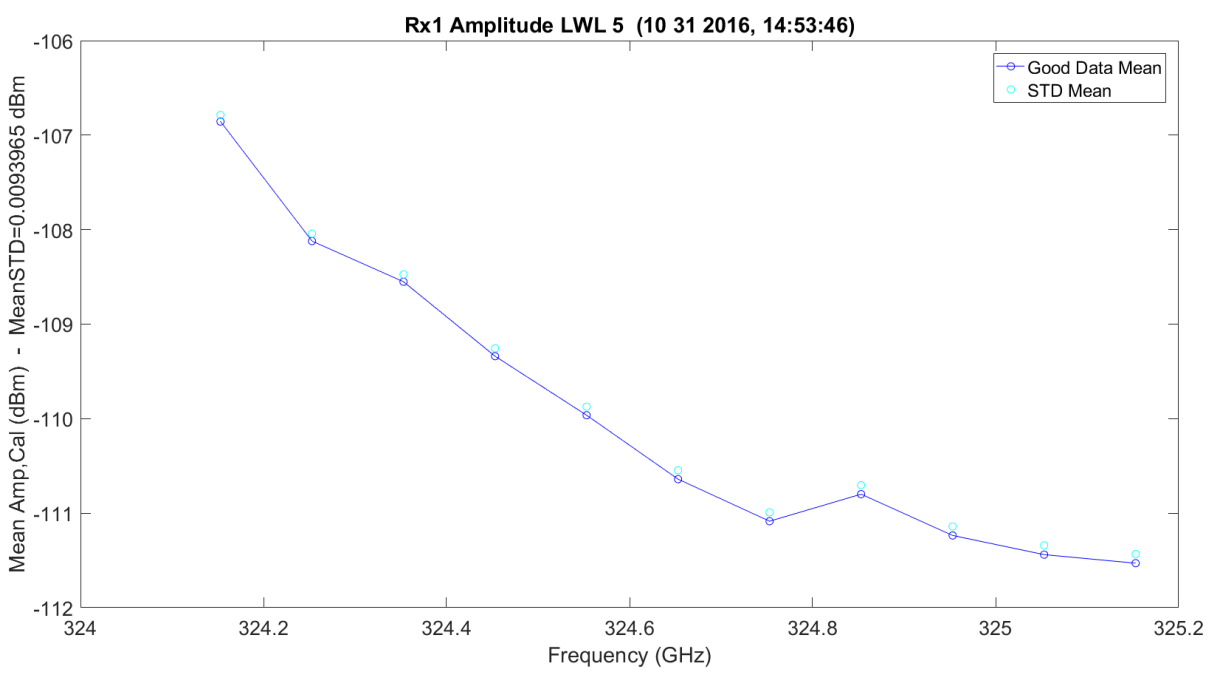


Figure 3.245. LWL / Friis Absorption Scan 5 for Rx1 – 11012016_145401.

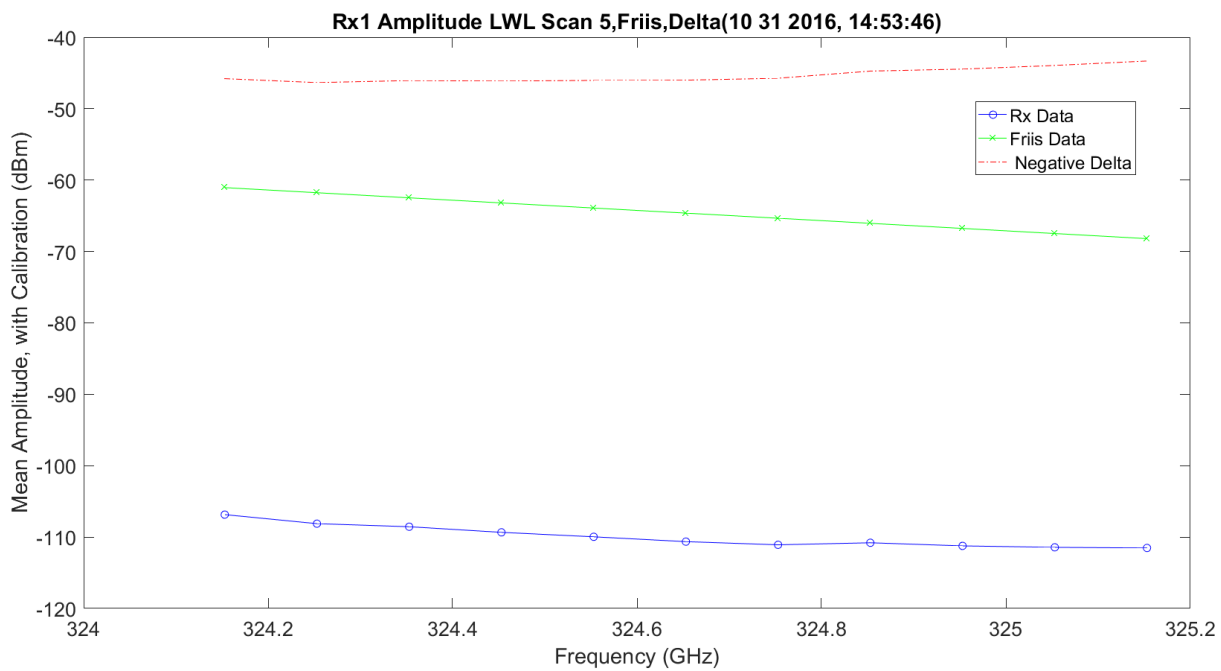


Figure 3.246. LWL / Friis Normalized Absorption Scan 5 for Rx1 – 11012016_145401.

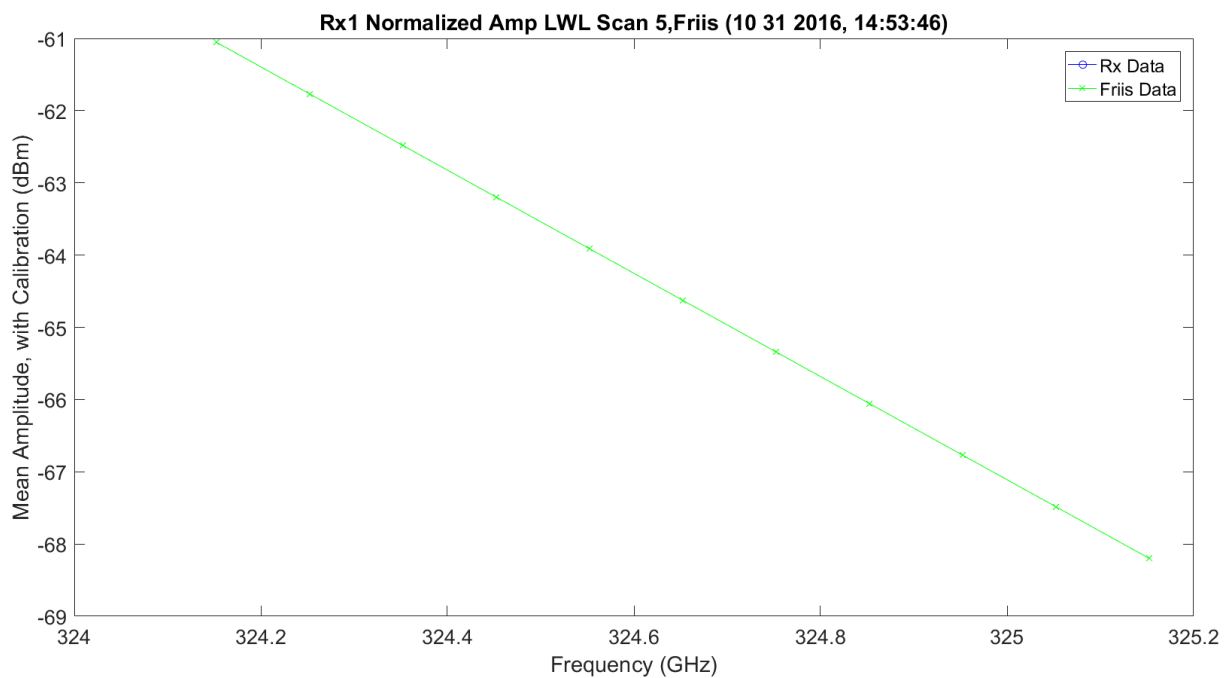


Figure 3.247. LWL Absorption Scan 3 for Rx1 – 11012016_145401.

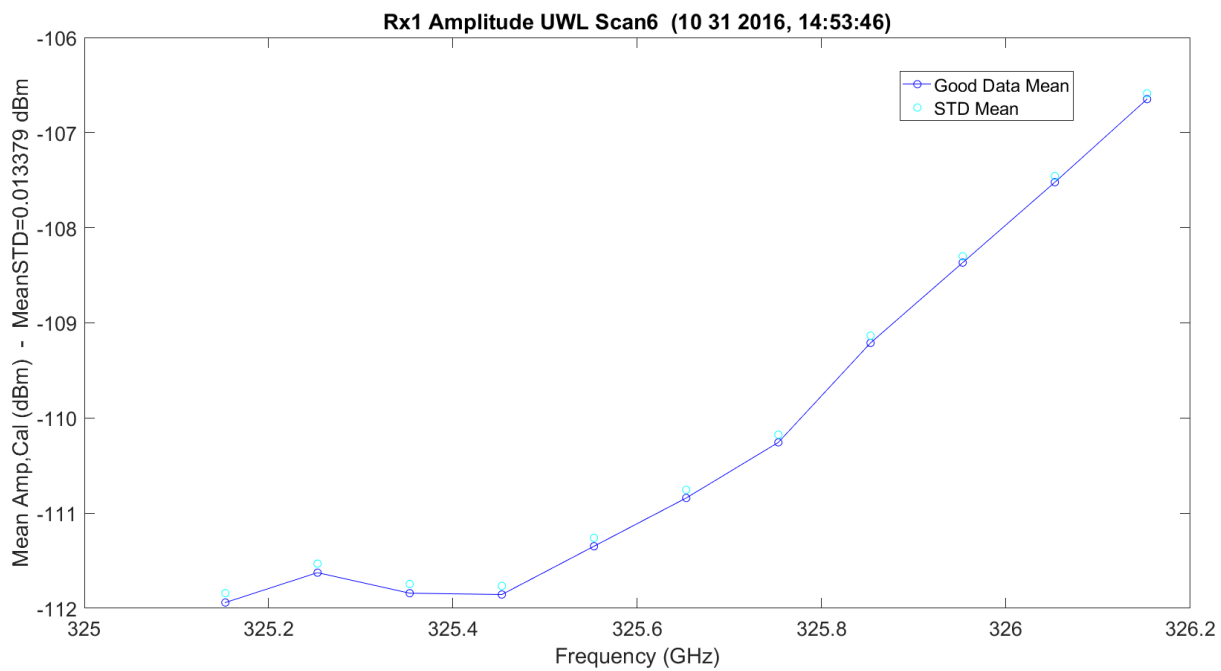


Figure 3.248. UWL / Friis Absorption Scan 6 for Rx1 – 11012016_145401.

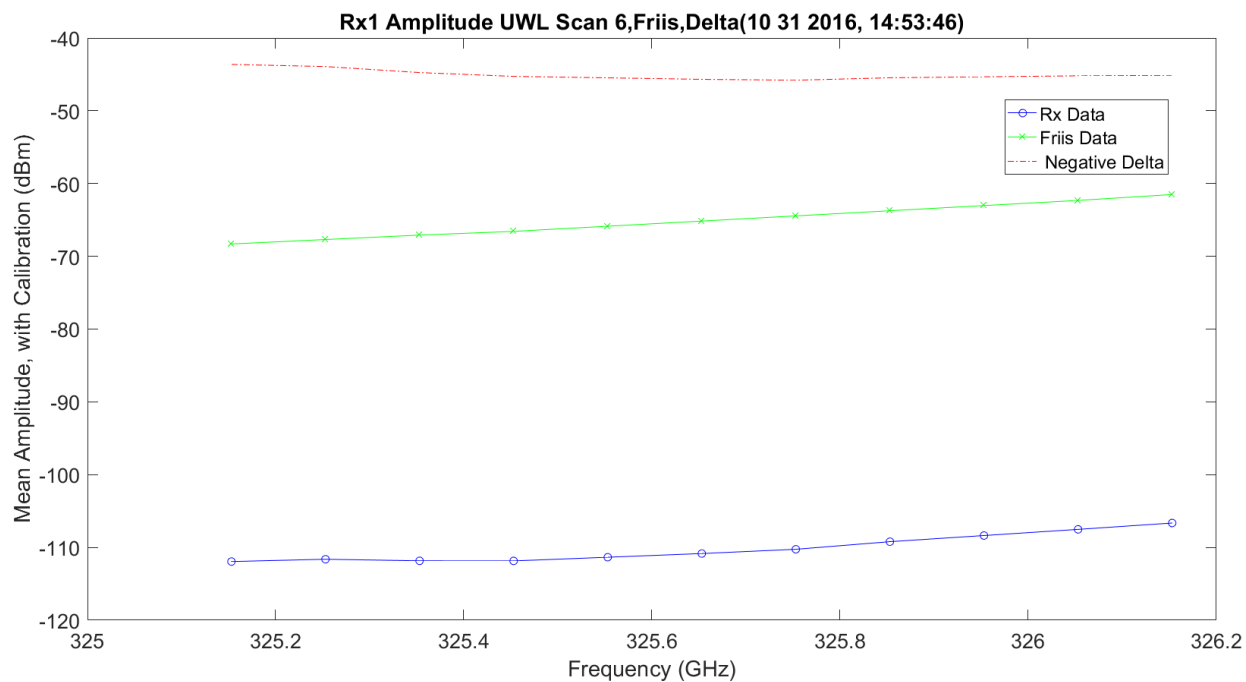


Figure 3.249. UWL / Friis Normalized Absorption Scan 6 for Rx1 – 11012016_145401.

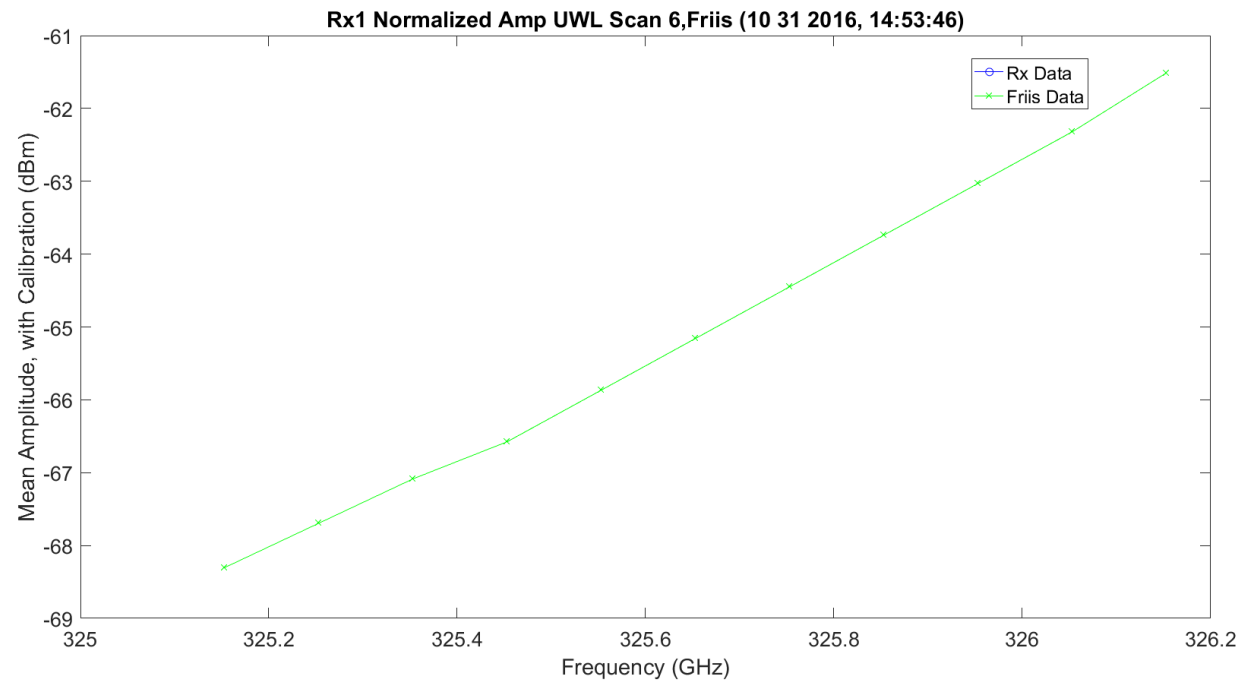


Figure 3.250. UWL / Friis Normalized Absorption Scan 6 for Rx1 – 11012016_145401.

Figure 3.251 shows both LWL and UWL, two scans each, on the same plot with the UWL reflected on top of the LWL to compare. Unfortunately, only Friis made the bar.

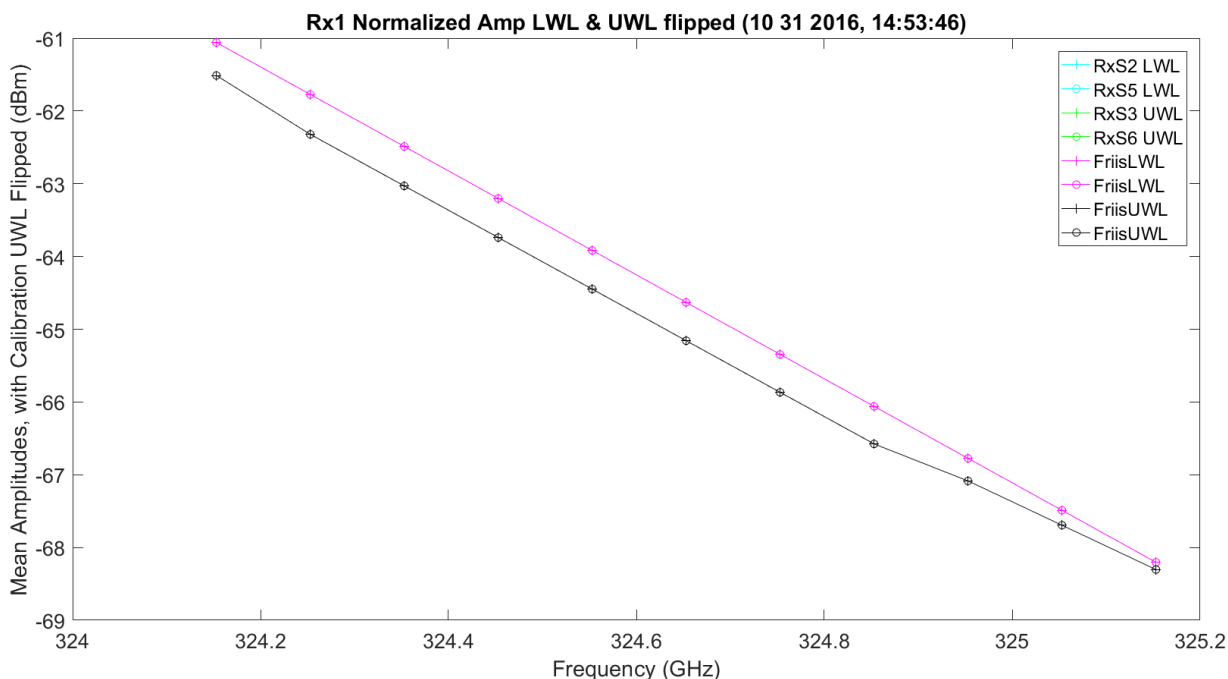


Figure 3.251. LWL & UWL Flipped Amp / Friis Normalized Absorption – 11012016_145401.

Figure 3.252 shows the amplitude scan over the first scan of the WB frequencies; these modes have hardware losses and gains that may not be known in the system. The amplitude ranges from approximately -108 dBm at 325.153 GHz to -83 dBm at 320 GHz, and 330 GHz through 340 GHz. The total difference in attenuation is approximately 27 dB, which seems higher than results in the 80s. The response looks, as expected, very good. Figure 3.253 shows the same data with the Friis. There is a significant offset in the traces; the difference is approximately 25 dB. Figure 3.254 normalizes the data to have full overlap of the Friis prediction and the collected data to compare the shapes. The Friis is wider and not as close to a sharp peak as the TAIPAS collected data.

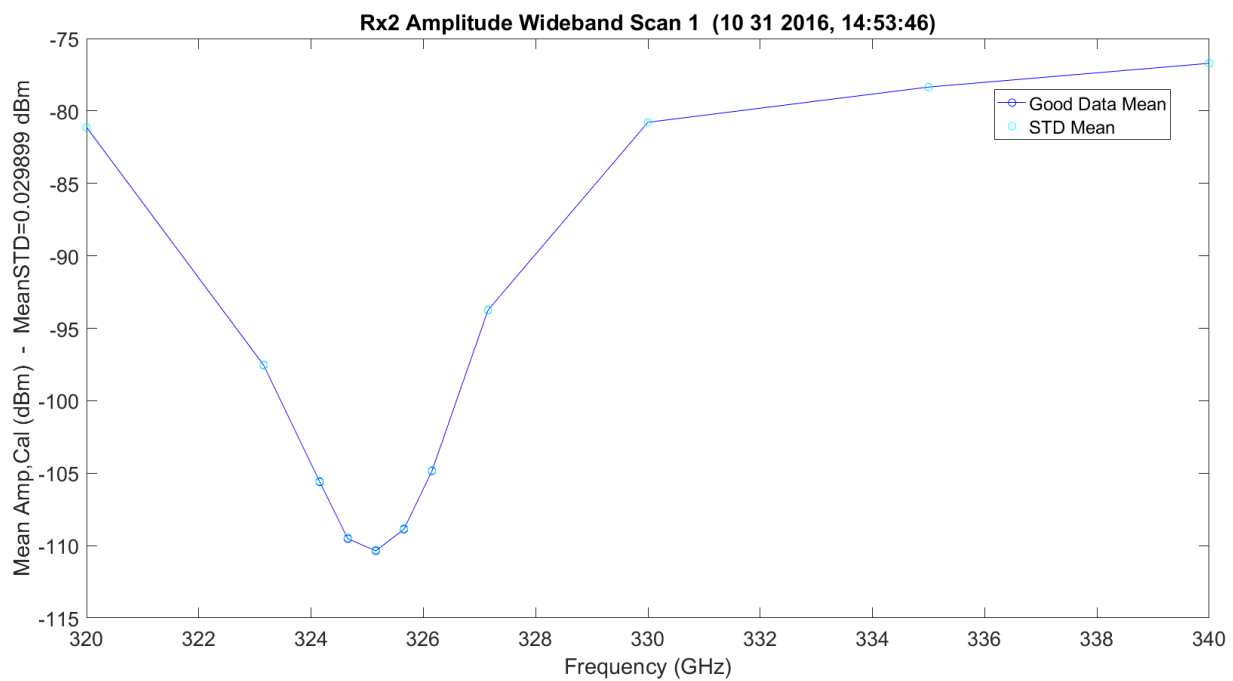


Figure 3.252. WB Scan 1 for Rx2 – 11012016_145401.

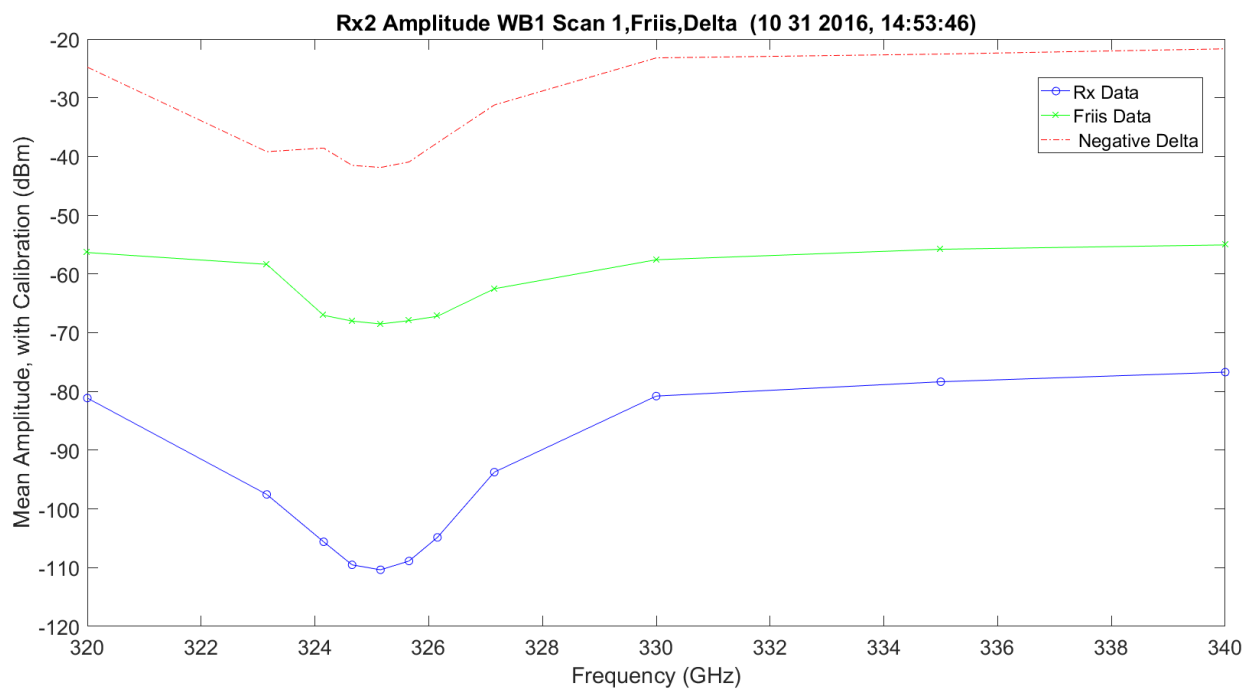


Figure 3.253. WB/Friis Scan 1 for Rx2 – 11012016_145401.

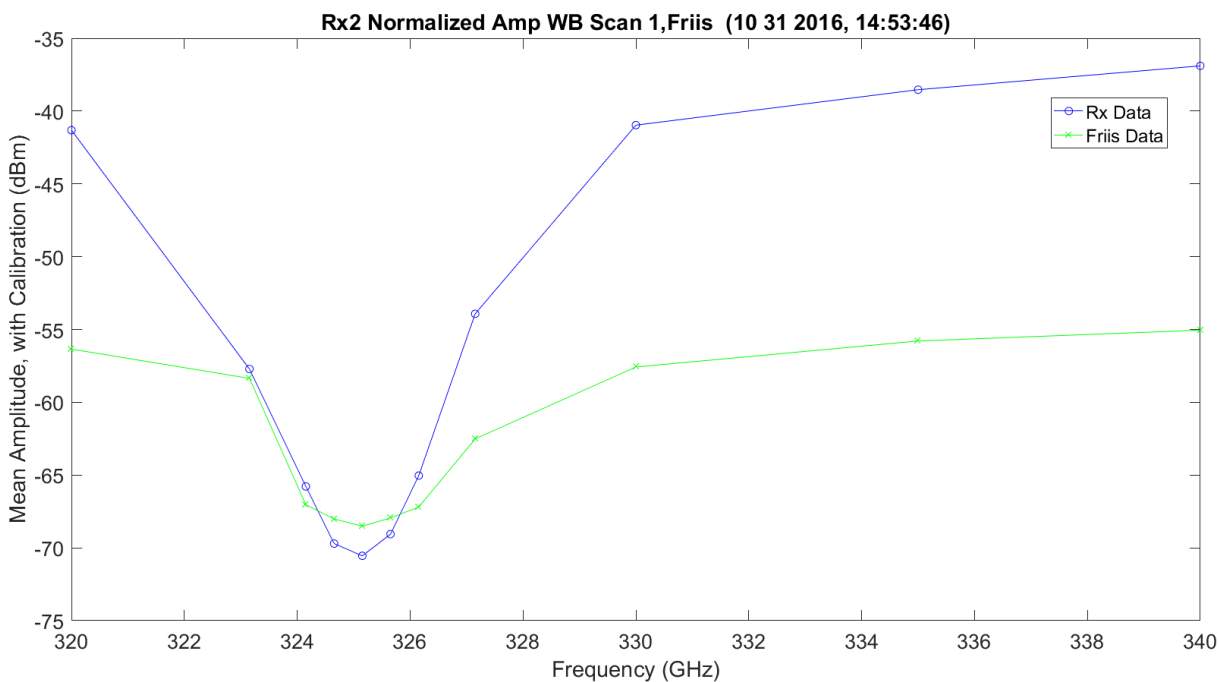


Figure 3.254. WB/Friis Normalized Scan 1 for Rx2 – 11012016_145401.

Figure 3.255 shows an absorption LWL scan 2 frequency. There is more ripple in the finely spaced frequencies of 100 MHz, which could be due to the calibration of the data on transmit and receive; the values can change minor in dB from point-to-point. It looks like the high sample of the LWL does show some atmospheric ripples on the EM. Figure 3.256 shows the data with the Friis prediction and the difference. The ripples on the collected data become less obvious and the wings of the two look approximately the same, but they have approximately 40 dB of difference in amplitude. Figure 3.257 shows the normalization of the Friis and collected data. As expected, this demonstrates the rippling on the collected, but the Friis response is flat. The real data is less flat and the wing is flatter than the Friis prediction.

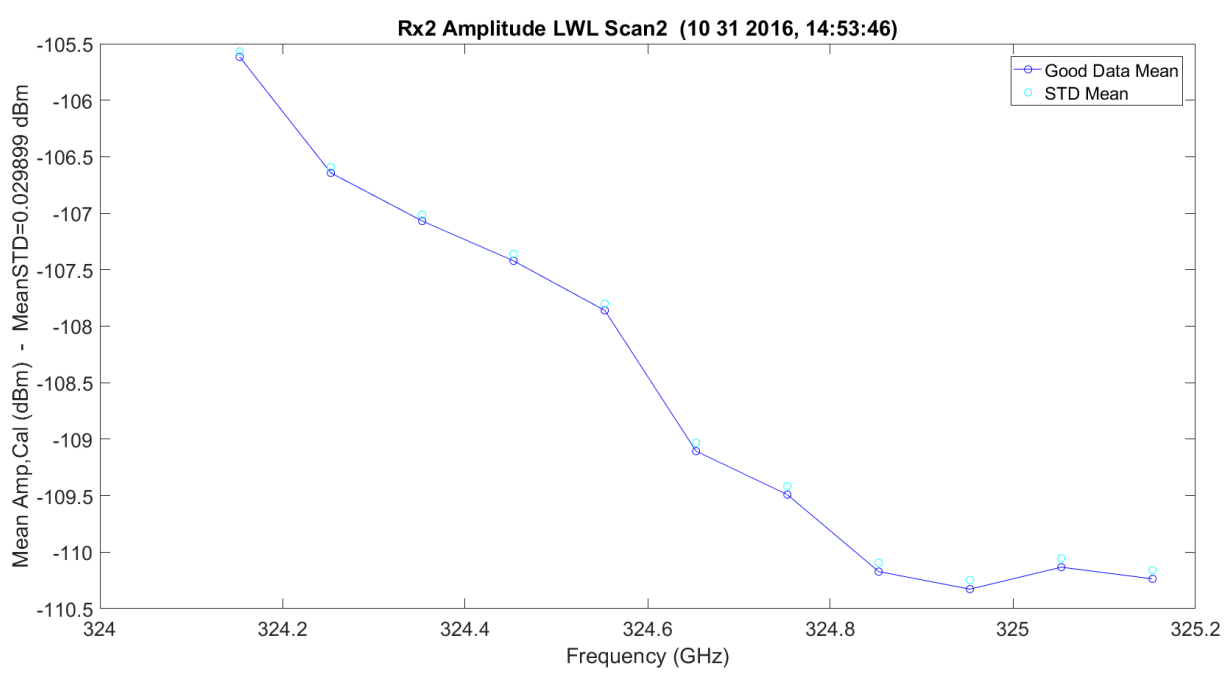


Figure 3.255. LWL Absorption Scan 2 for Rx2 – 11012016_145401.

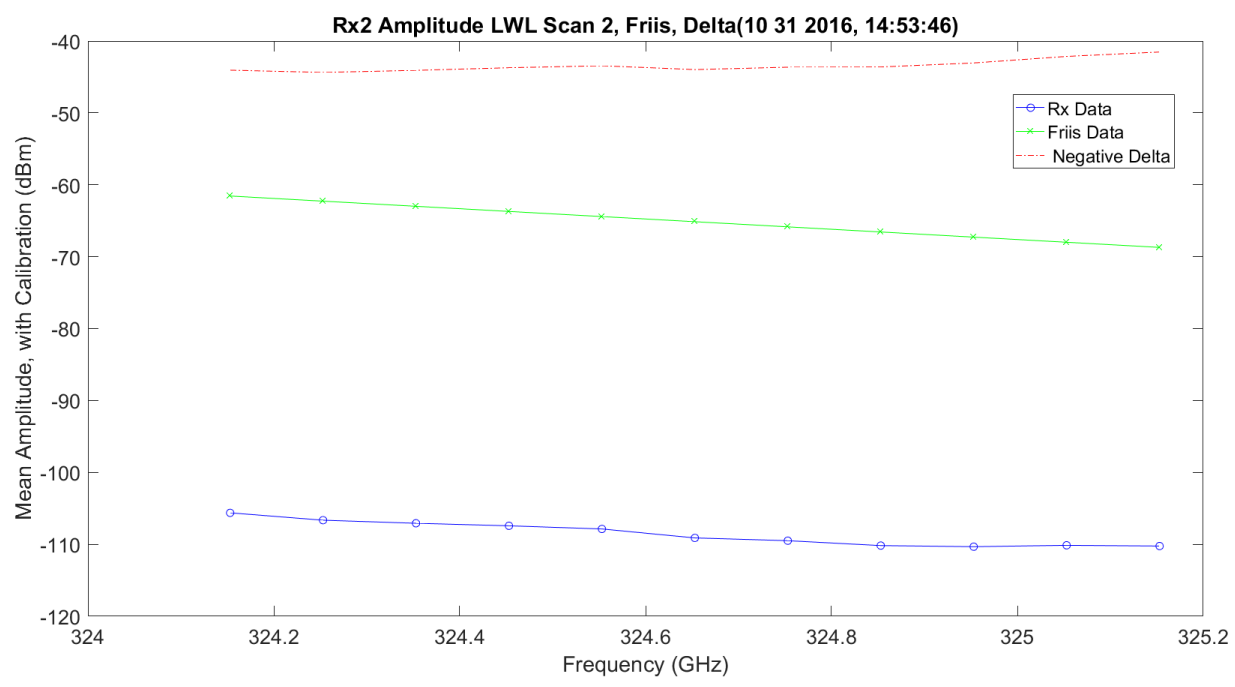


Figure 3.256. LWL / Friis Absorption Scan 2 for RX2 – 11012016_145401.

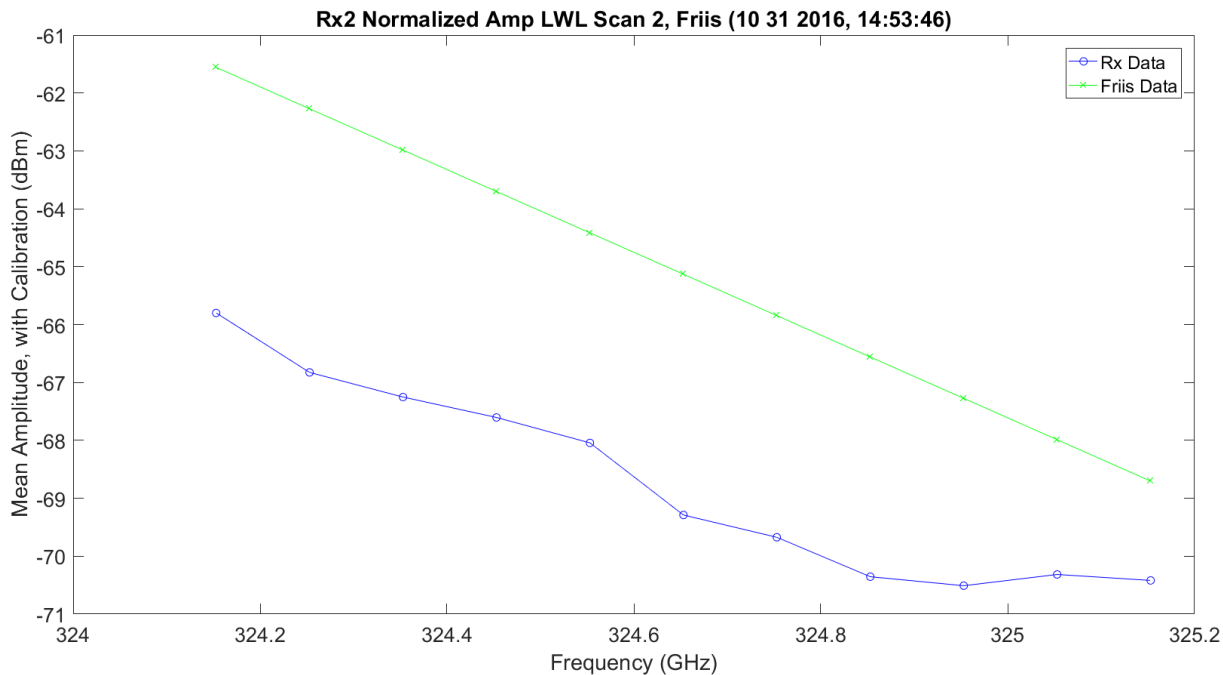


Figure 3.257. LWL / Friis Normalized Absorption Scan 2 for Rx2 – 11012016_145401.

Figure 3.258 plots an absorption UWL scan 3 frequency. There is more ripple in the finely spaced frequencies of 100 MHz, which could be due to the calibration of the data on transmit and receive; the values can change minor in dB from point-to-point. The high sample of the UWL does show some perceived atmospheric ripples on the EM. Figure 3.259 shows the data with the Friis prediction and the difference. The ripples on the collected data become less obvious and the wings of the two look approximately the same, but they have approximately 40 dB of difference in amplitude. Figure 3.260 shows the normalization of the Friis and collected data. As expected, this shows the rippling on the collected, but the Friis response is flat. The real data is less flat and the wing is flatter than the Friis prediction. In this figure, the parallelization of the Friis and real data look close.

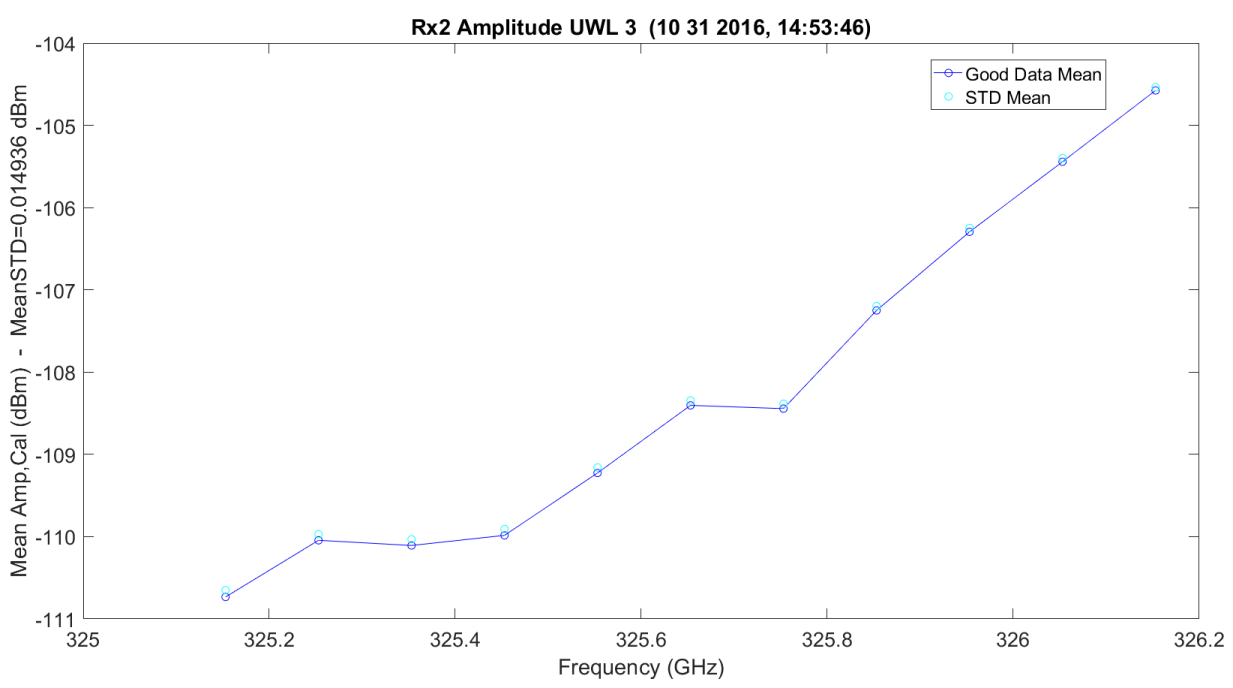


Figure 3.258. UWL Absorption Scan 3 for Rx2 – 11012016_145401.

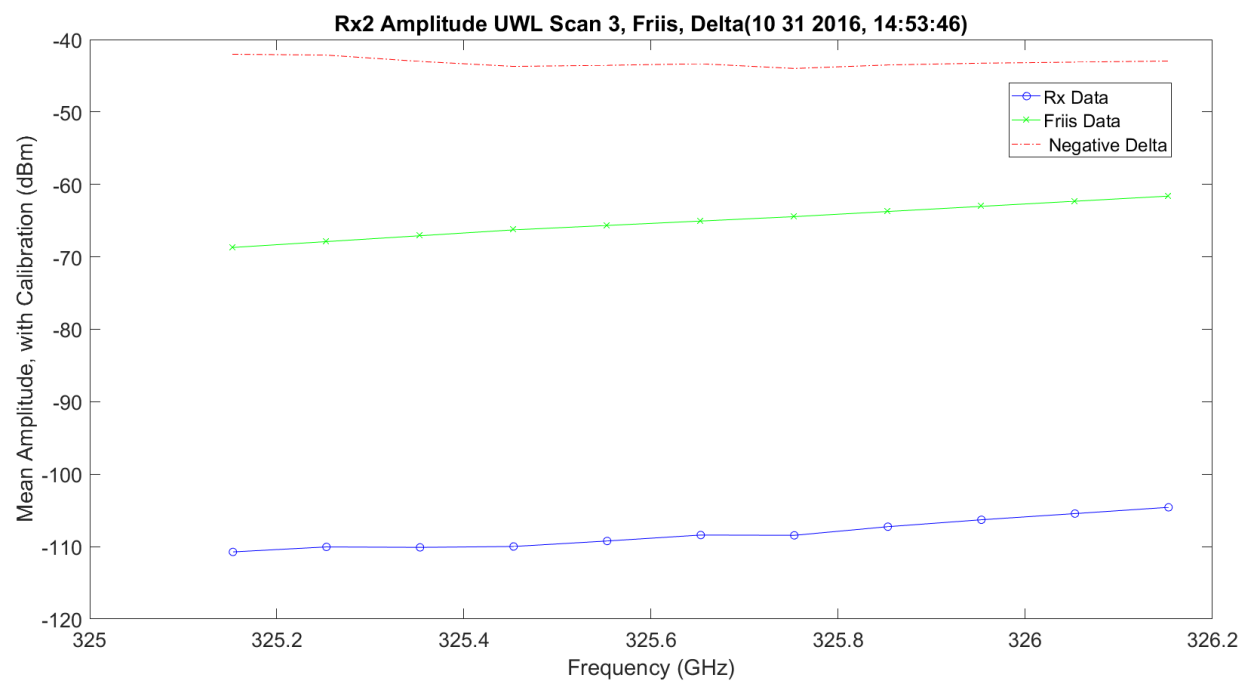


Figure 3.259. UWL / Friis Absorption Scan 3 for Rx2 – 11012016_145401.

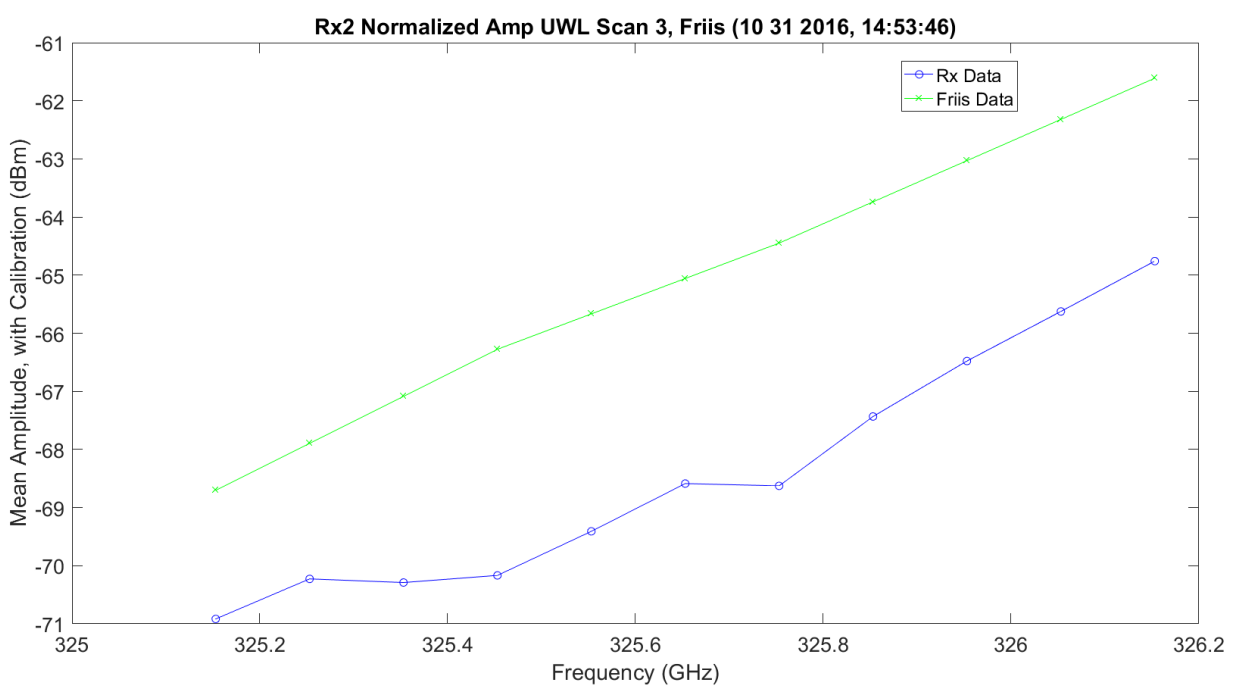


Figure 3.260. UWL / Friis Normalized Absorption Scan 3 for Rx2 – 11012016_145401.

The following images (Figure 3.261 – Figure 3.269) are the second set of identical scans: WB, LWL and UWL. They each scan 11 different frequencies. They are included for completeness, but they look identical to the first 33 scanned frequencies in Rx1. They are included here for completeness. The LWLs and UWLs have very different wing jugs.

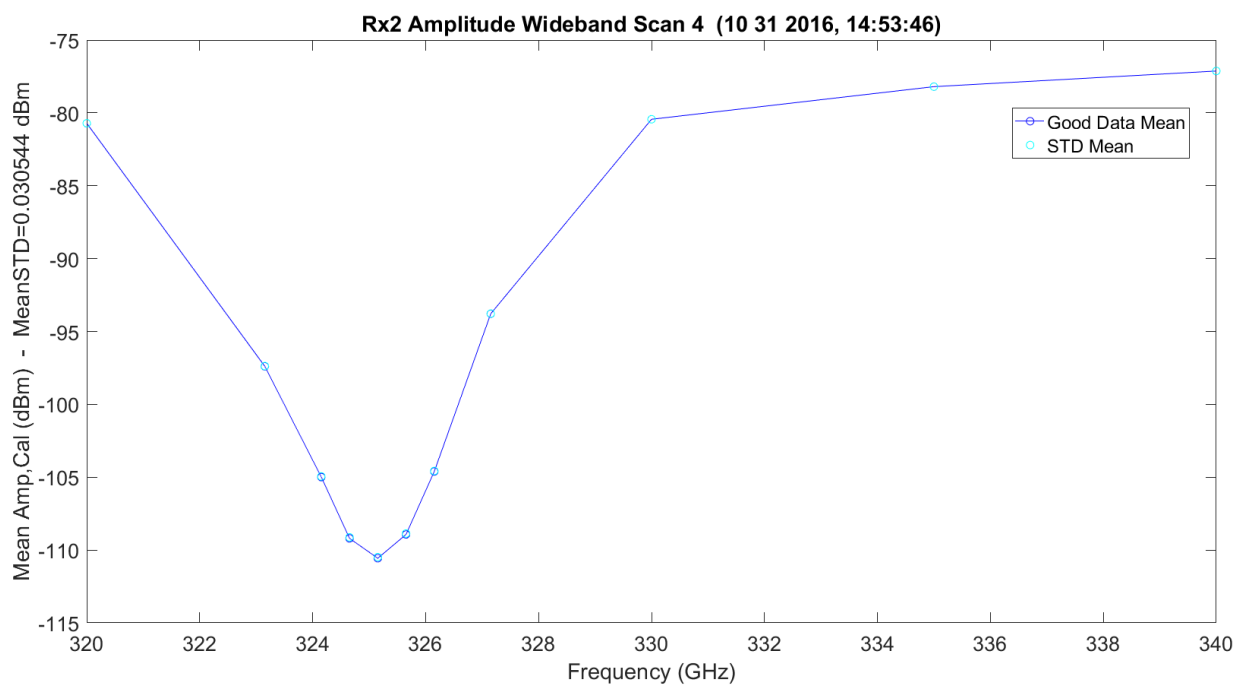


Figure 3.261. WB Scan 4 for Rx2 – 11012016_145401.

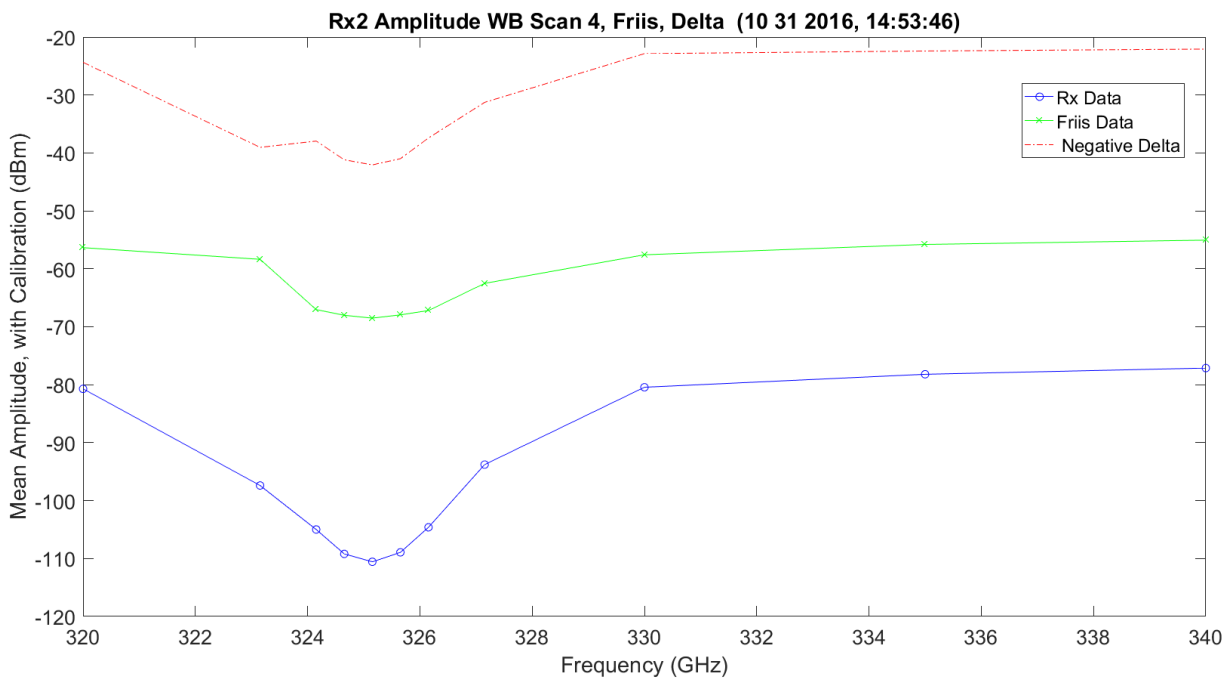


Figure 3.262. WB/Friis Normalized Scan 4 for Rx2 – 11012016_145401.

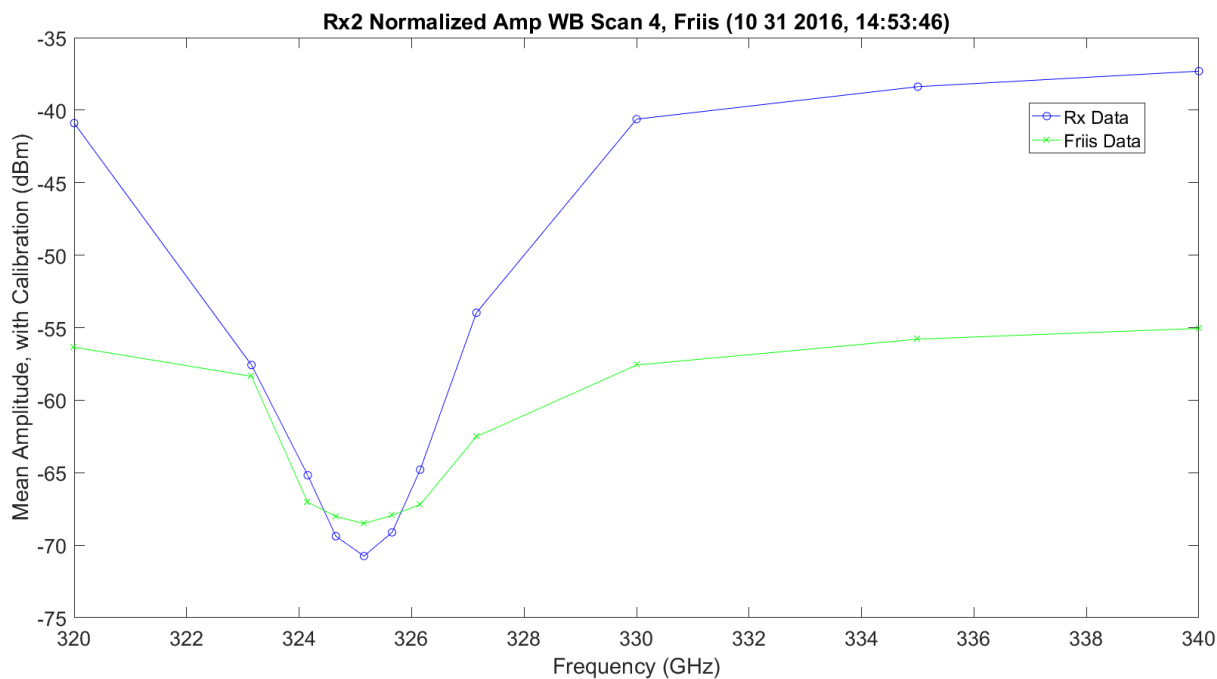


Figure 3.263. WB Absorption Scan 4 for Rx2 – 11012016_145401.

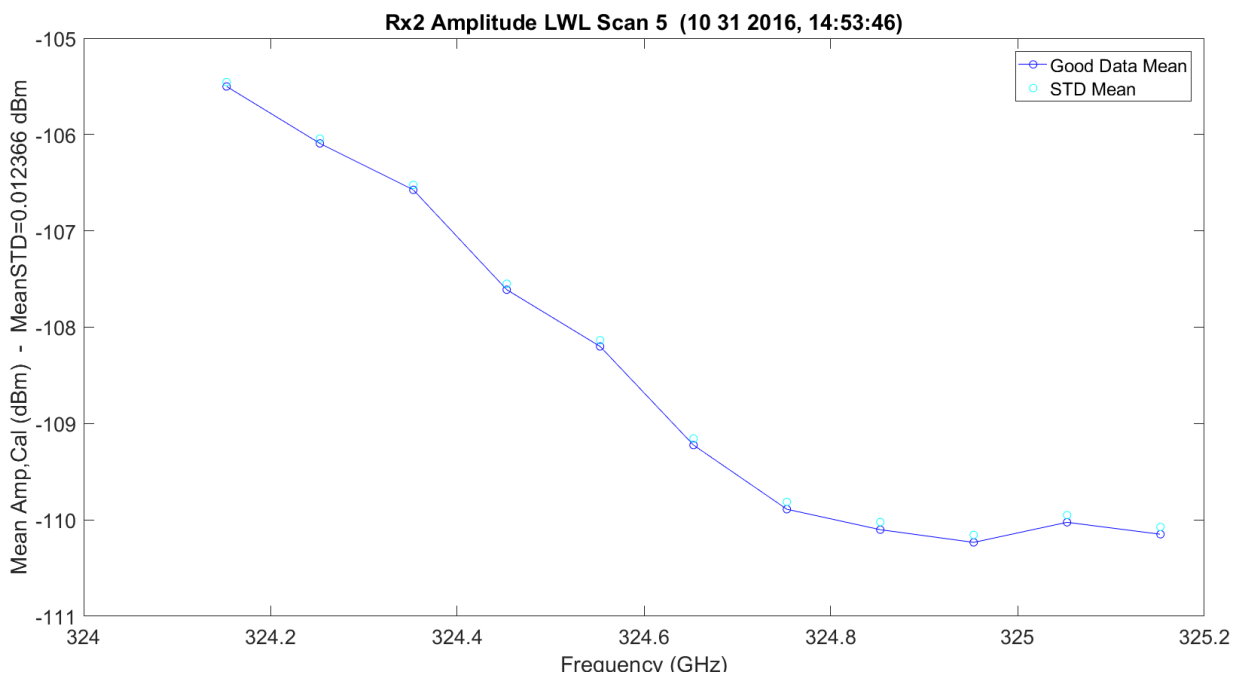


Figure 3.264. LWL / Friis Absorption Scan 5 for Rx2 – 11012016_145401.

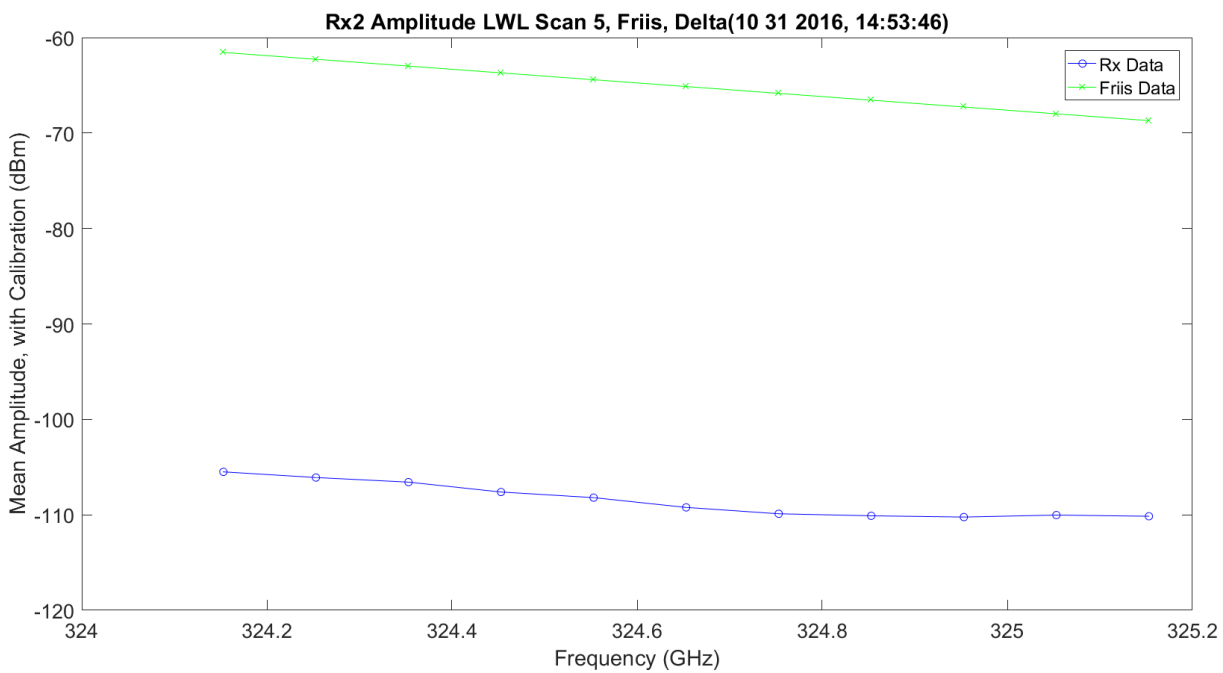


Figure 3.265. LWL / Friis Normalized Absorption Scan 5 for Rx2 – 11012016_145401.

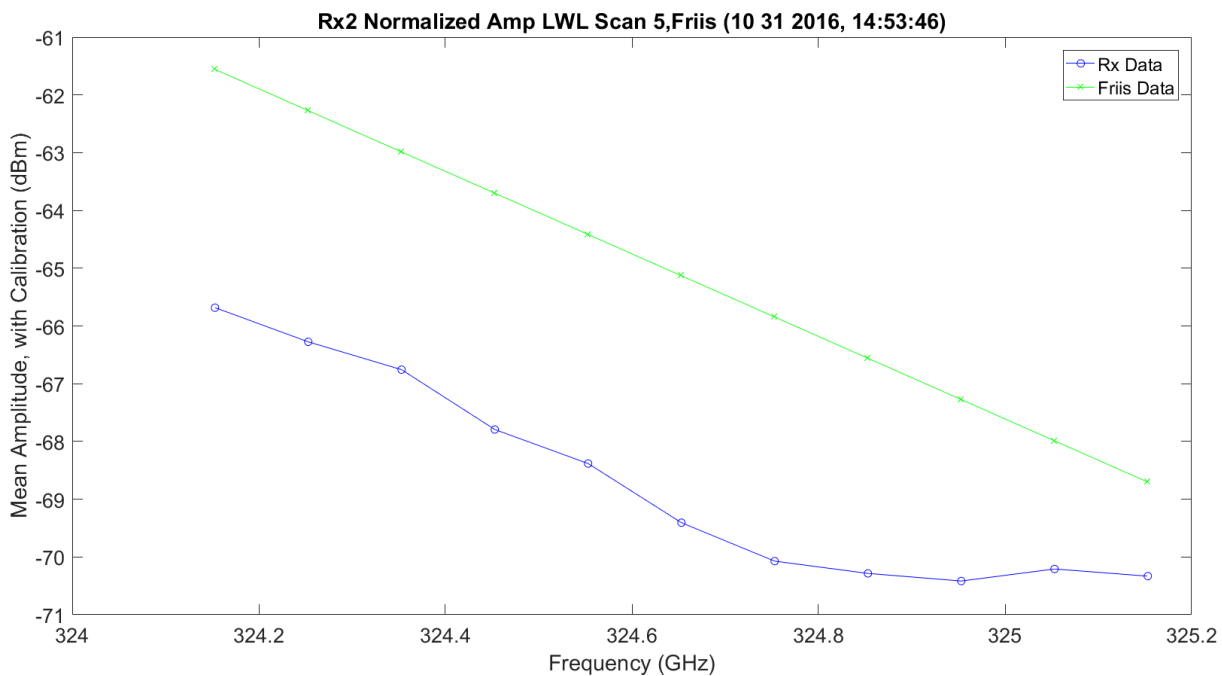


Figure 3.266. LWL Absorption Scan 3 for Rx2 – 11012016_145401.

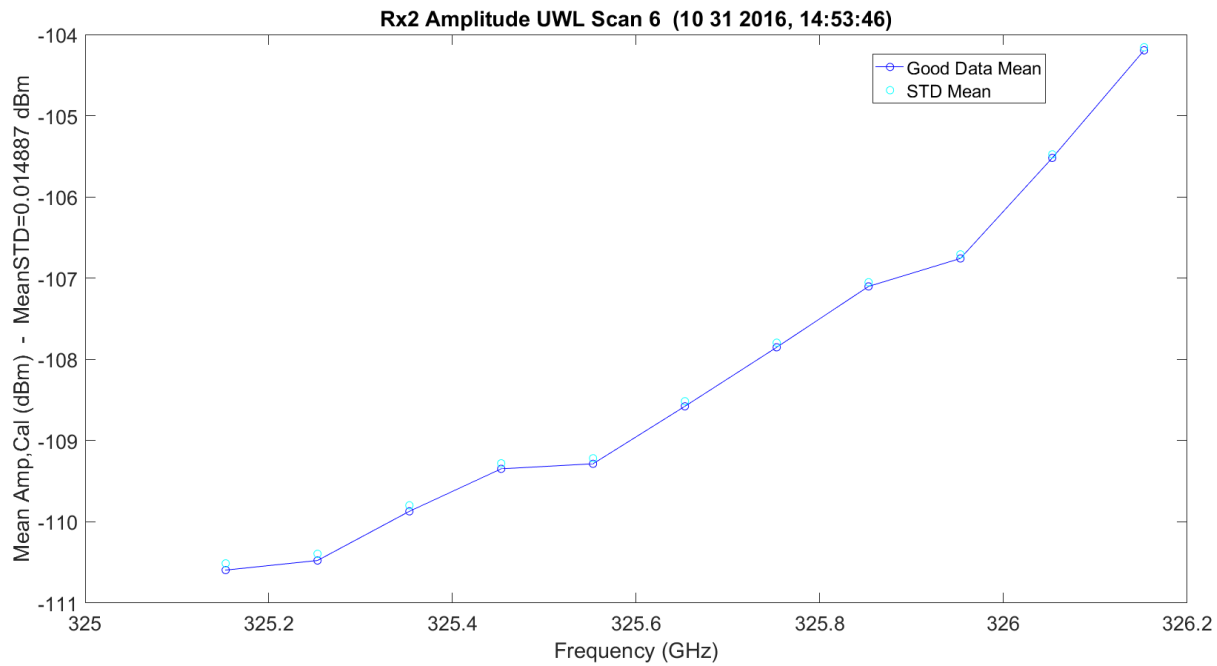


Figure 3.267. UWL / Friis Absorption Scan 6 for Rx2 – 11012016_145401.

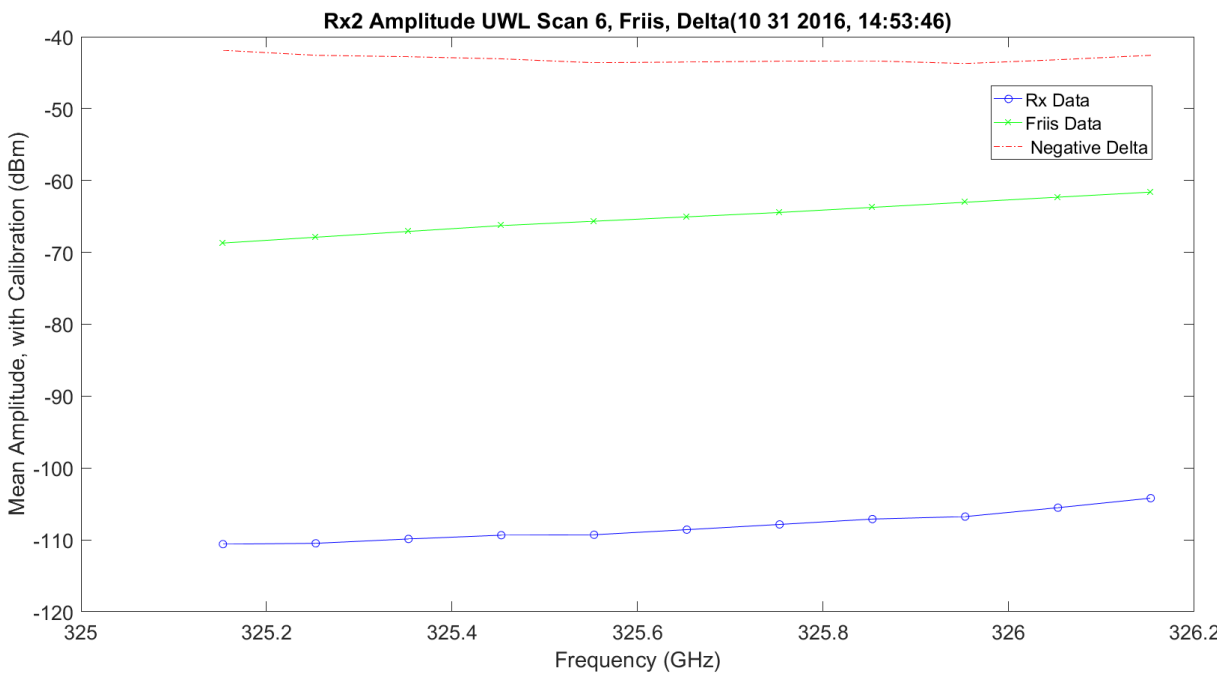


Figure 3.268. UWL / Friis Normalized Absorption Scan 6 for Rx2 – 11012016_145401.

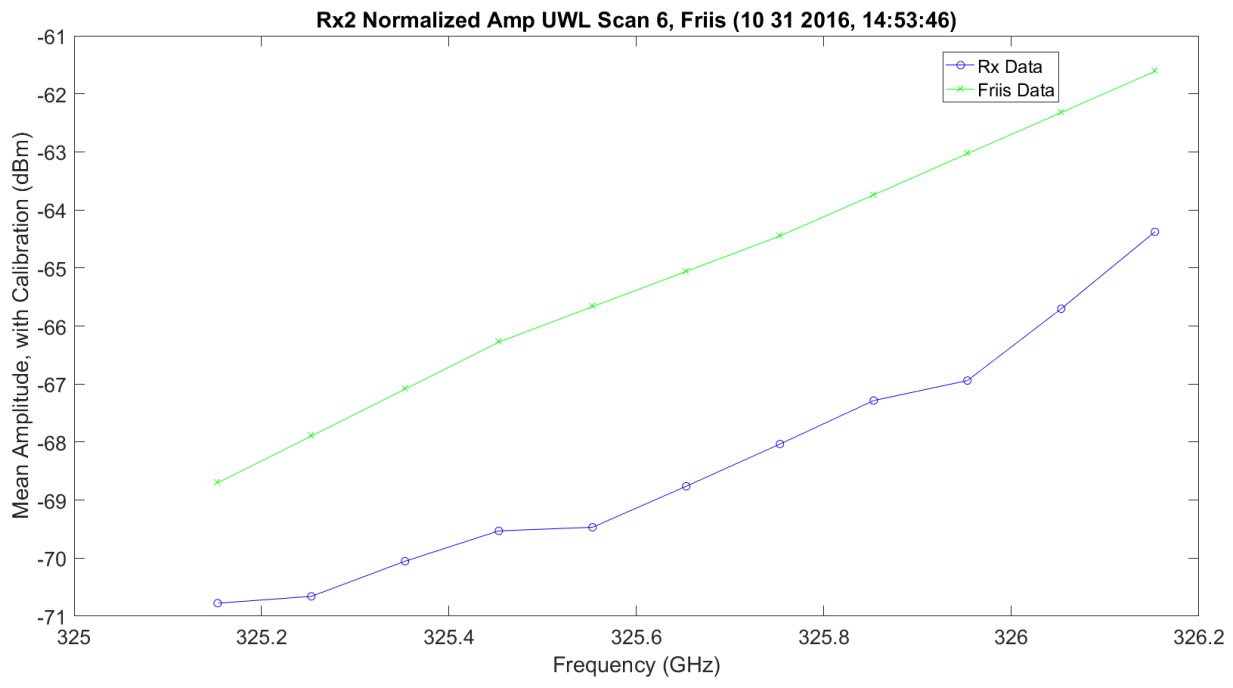


Figure 3.269. UWL / Friis Normalized Absorption Scan 6 for Rx2 – 11012016_145401.

Figure 3.270 shows both LWL and UWL, two scans each, on the same plot with the UWL flipped on top of the LWL for comparison. The LWL and UWL are about 4-5 dB lower than the Friis. The two scans each for UWL and LWL are compared. The shape of the LWL vs. UWL is significantly different at a frequency range of ~324.9 GHz (UWL reflected) to 325 GHz.

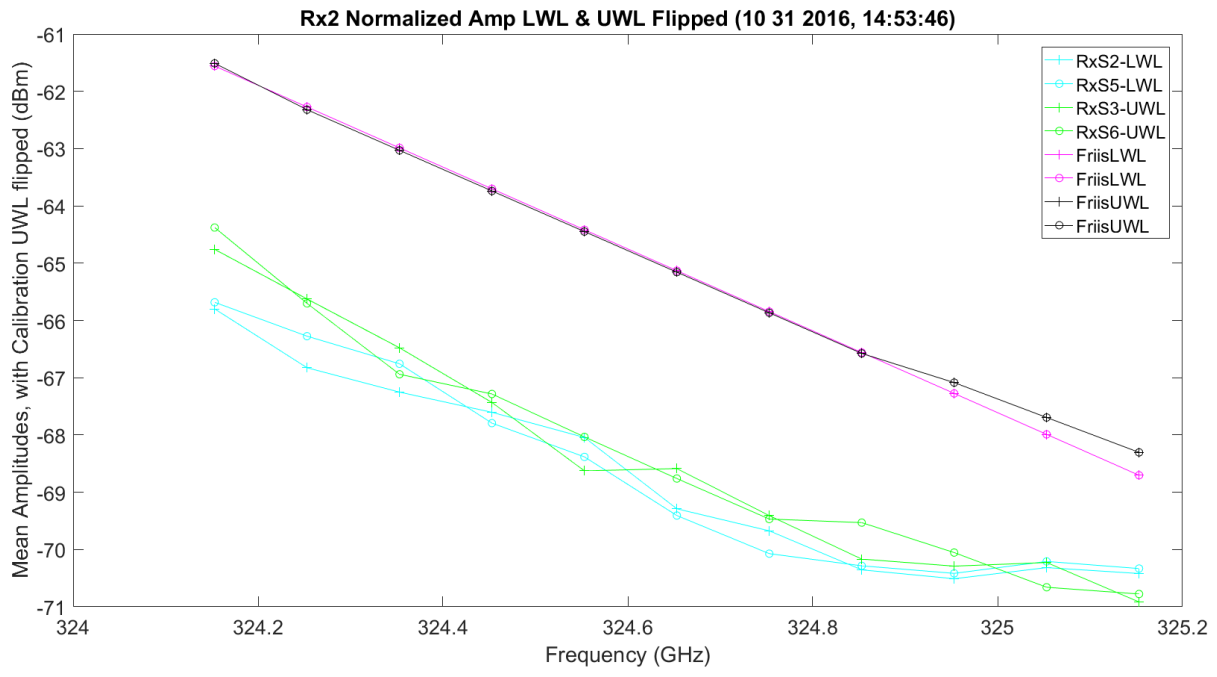


Figure 3.270. LWL & UWL Flipped Amp / Friis Normalized Absorption – 11012016_145401.

Figure 3.271 – Figure 3.273 show SNR plots for WB, LWL, and UWL, respectively. The WB SNR drops 10 dB around the peak on both the Friis and real data. The simulation vs. the real data has much higher signals, but very similar SNR. The WB SNR shows that the shape of the SNR going down vs. up the peak has different curves; the SNR gaining on the UWL is slower. It is easy to see that Rx1 has much worse SNR; it even has a result of offset in frequency for the peak of absorption and more absorption.

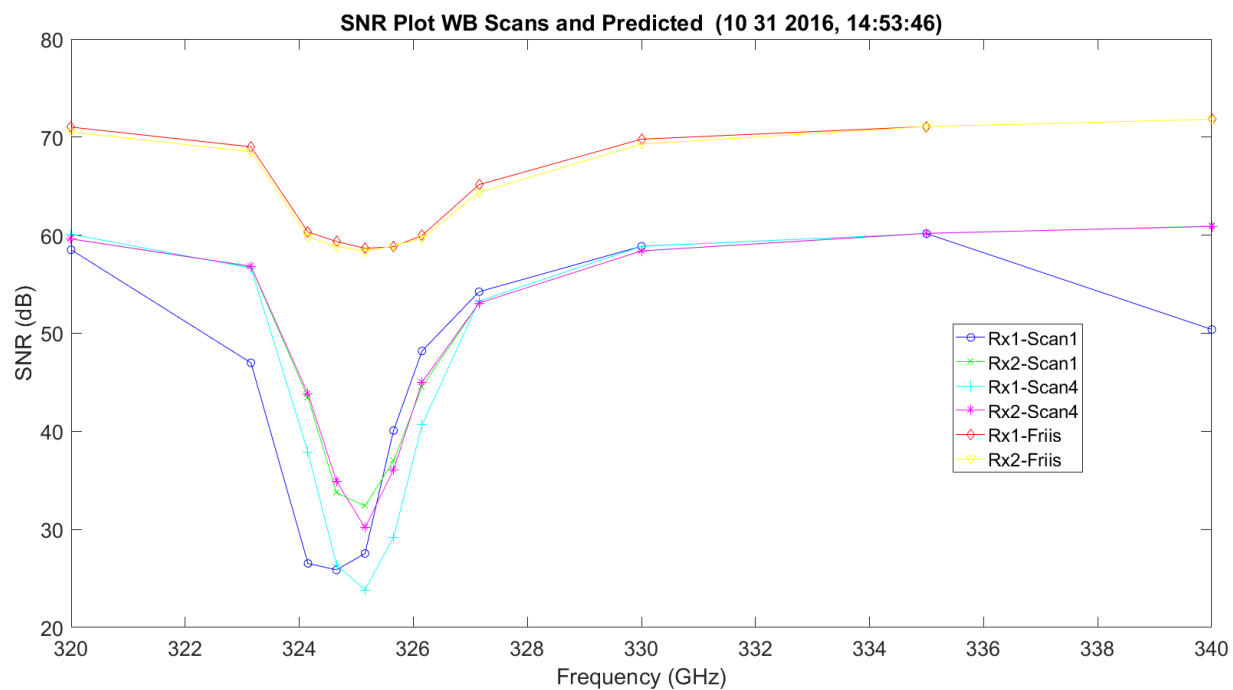


Figure 3.271. WB SNR and Predicted Friis – 11012016_145401.

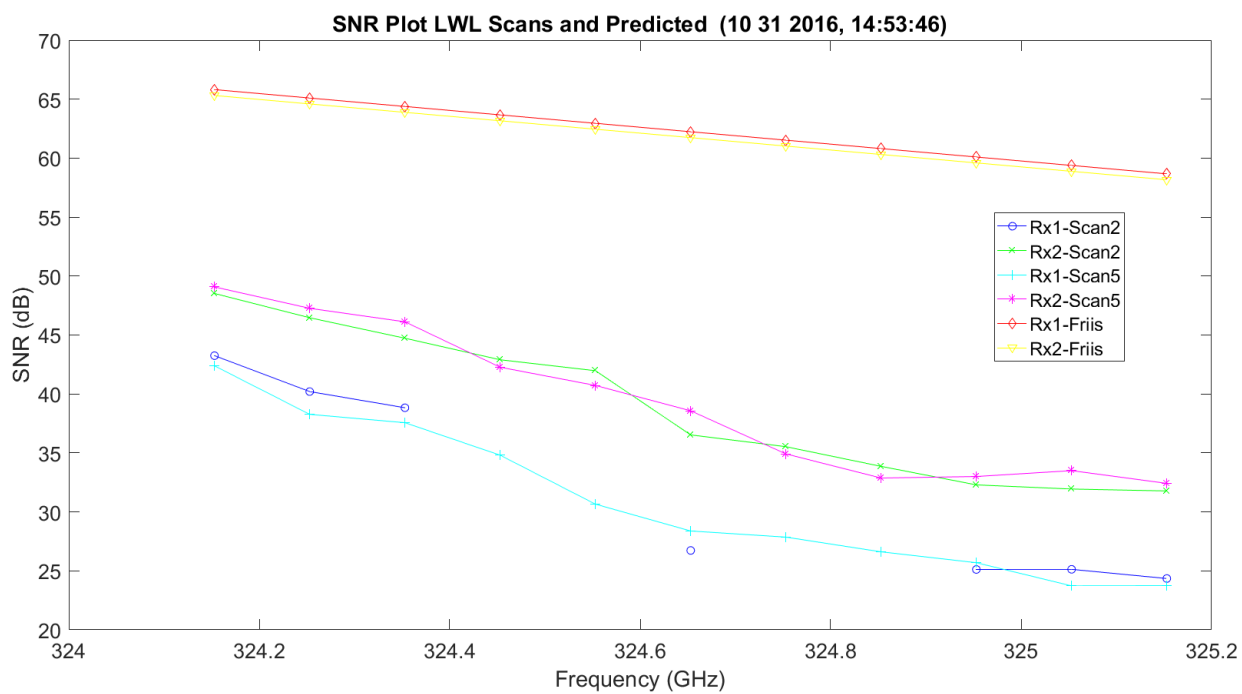


Figure 3.272. LWL SNR and Predicted Friis – 11012016_145401.

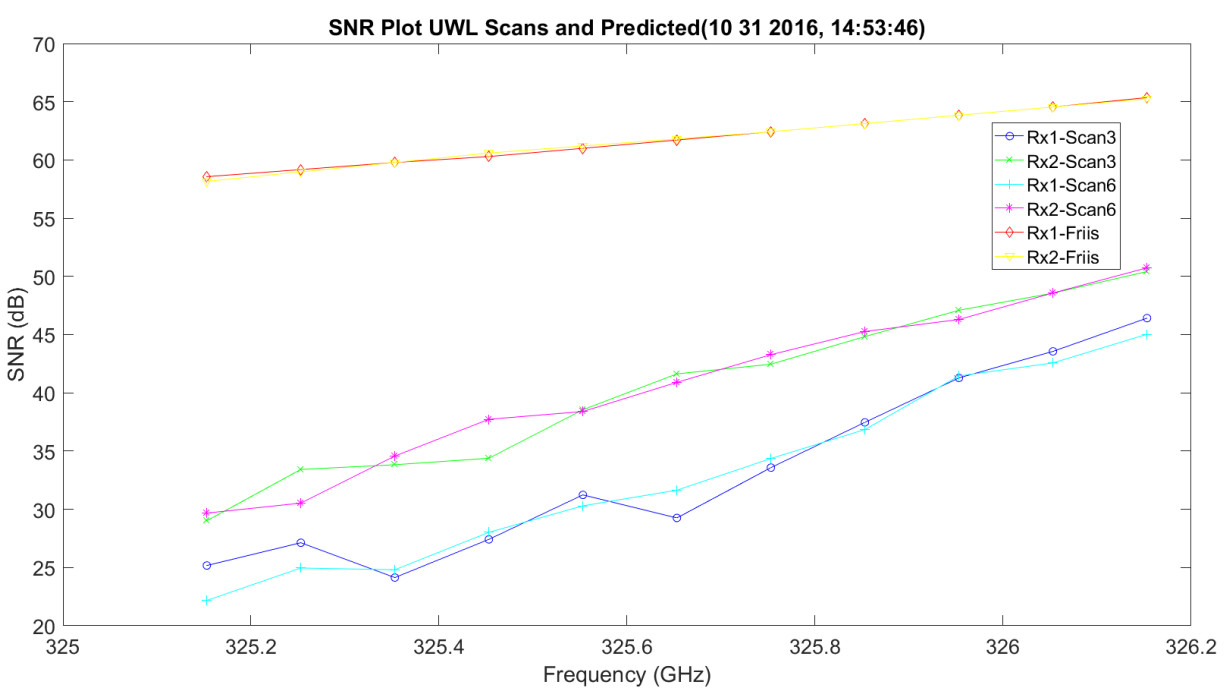


Figure 3.273. UWL SNR and Predicted Friis – 11012016_145401.

Figure 3.274 is a plot of C_n^2 . The $\times 10^{-13}$ is exactly what NIST was recording. The variation of the mantissa is not significant: 1 to 1.5. The mean value is shown in the title. Figure 3.275 shows the FFT of the C_n^2 . This shows there is no significant distortion on the measurement.

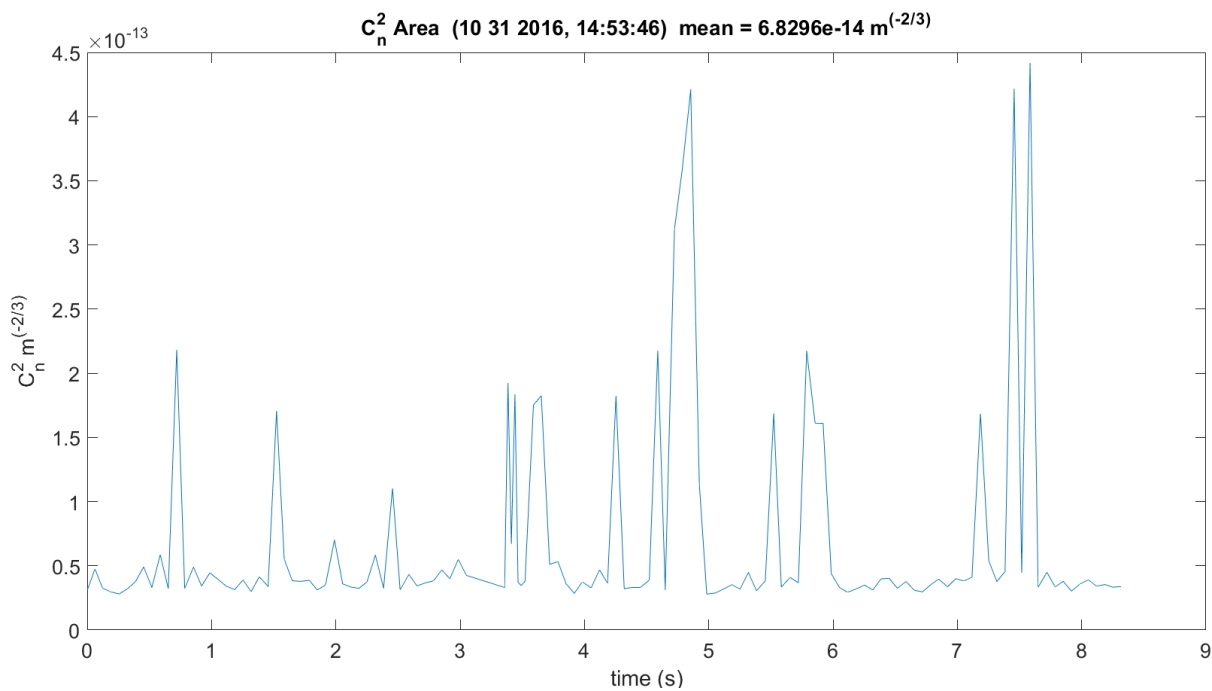


Figure 3.274. C_n^2 – 11012016_145401.

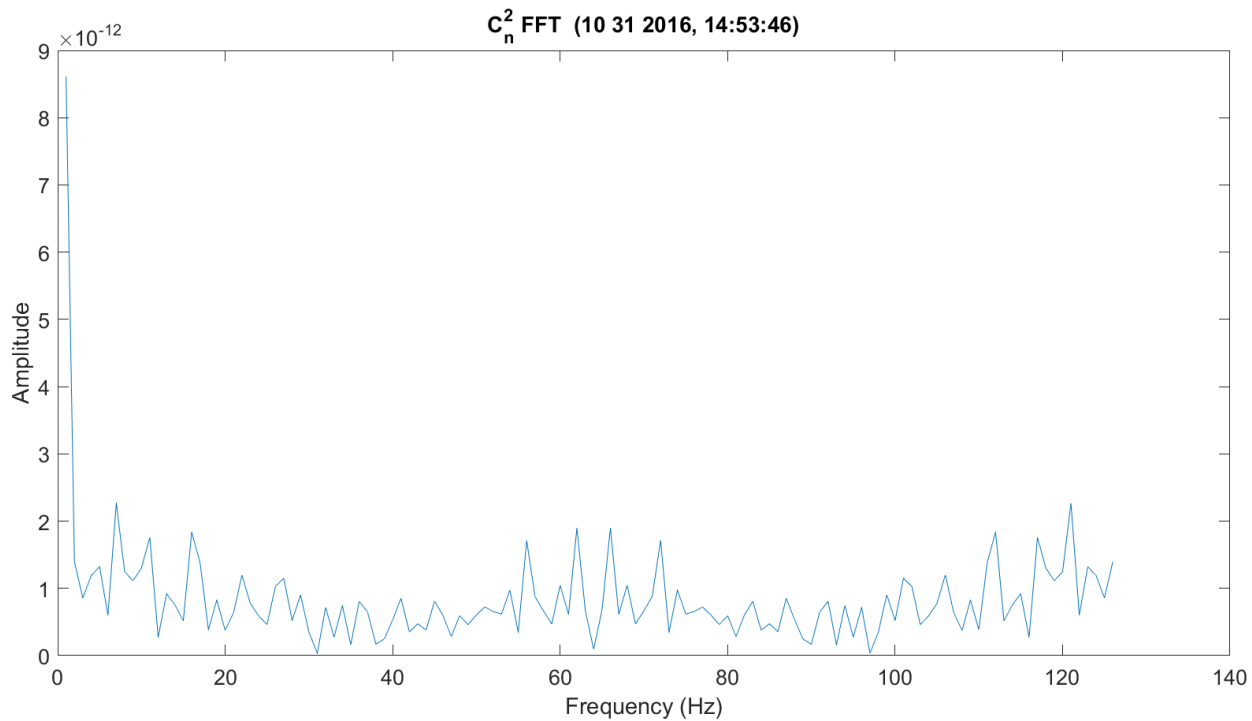


Figure 3.275. FFT of C_n^2 – 11012016_145401.

Figure 3.276 shows the transmit and receive anemometer temperatures. As expected, since the receiver is on the Mesa, the temperature is lower. The wind speed was very low during this sample.

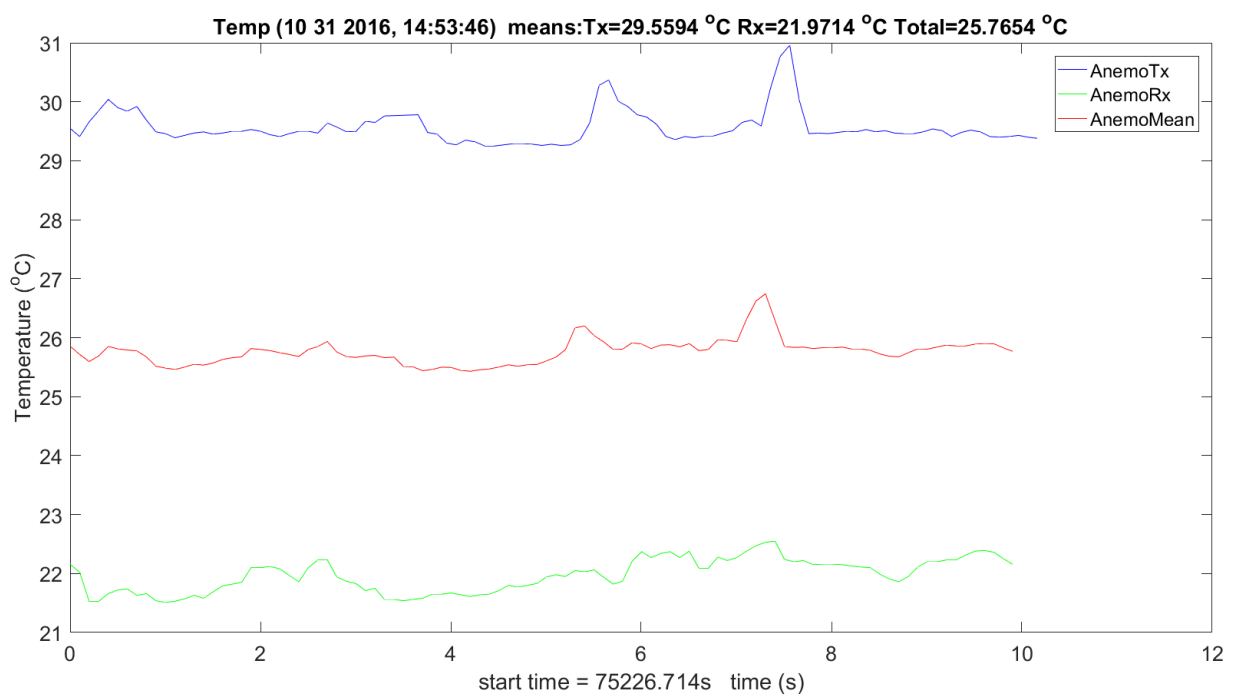


Figure 3.276. Transmit & Receiver Temp – 11012016_145401.

Figure 3.277 - Figure 3.279 show the wind information for *U*, *V* and *W*. *U* is the most critical for eddy formation. The receiver up on the mesa has higher negative or positive frequencies compared to the CU EE building.

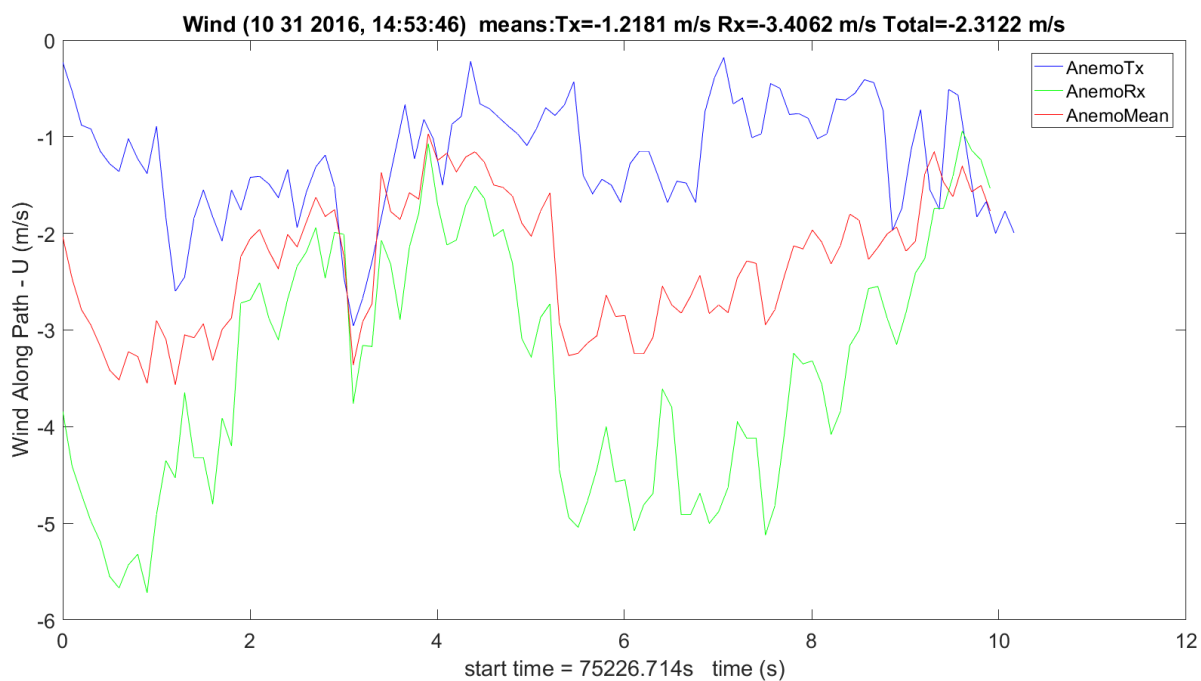


Figure 3.277. Wind *U* Transmit & Receiver - 11012016_145401.

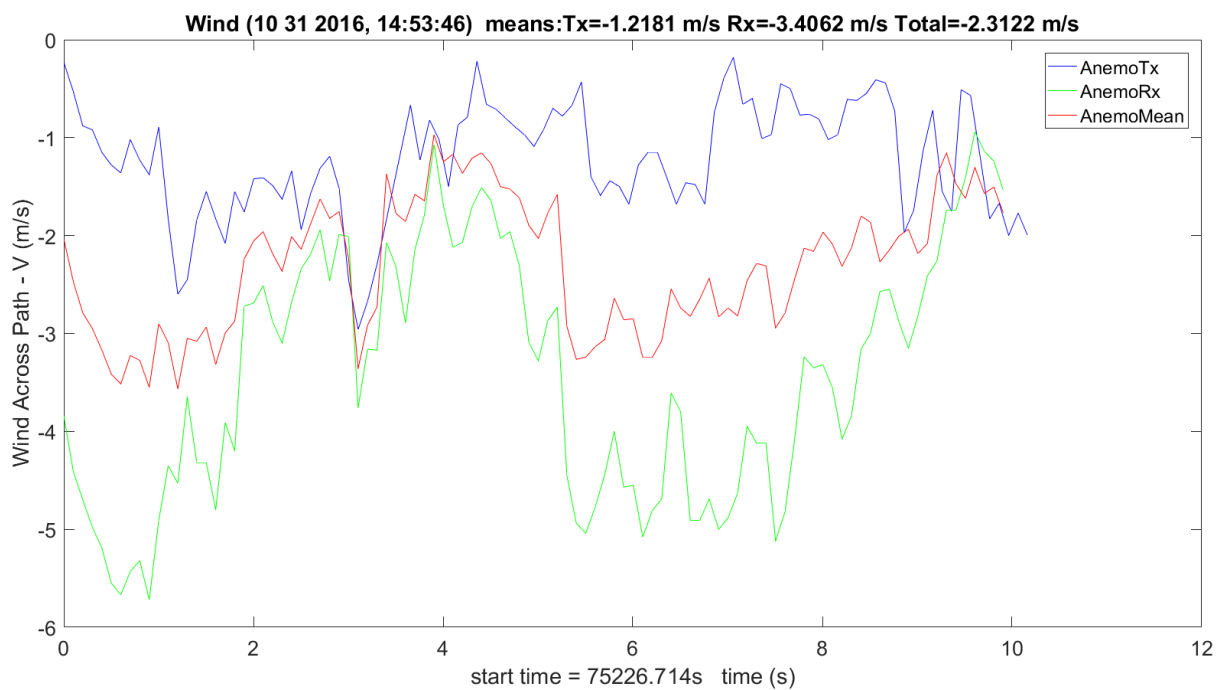


Figure 3.278. Wind *V* Transmit & Receiver - 11012016_145401.

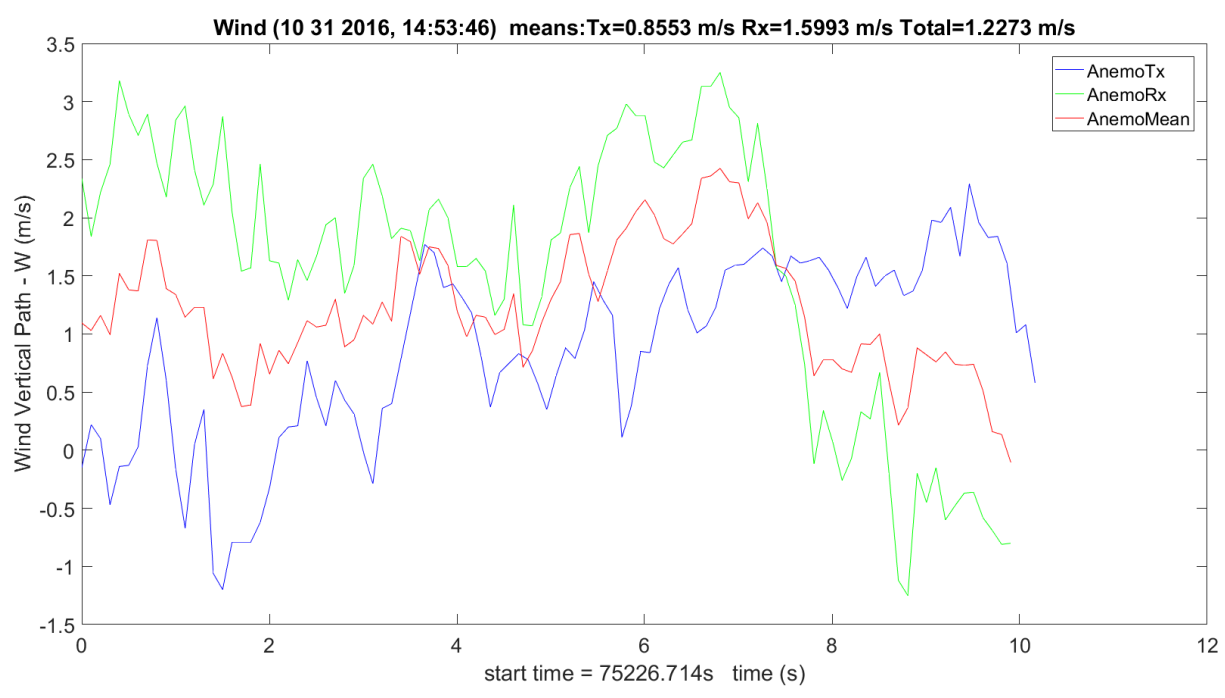


Figure 3.279. Wind *W* Transmit & Receiver – 11012016_145401.

Figure 3.280 shows the transmit and receive hygrometers. The dry and wet differences are small and the dry, since it has no moisture, is the optimal measurement. The humidity at the Mesa is significantly lower than the transmit: about 2.5 g/m^3 .

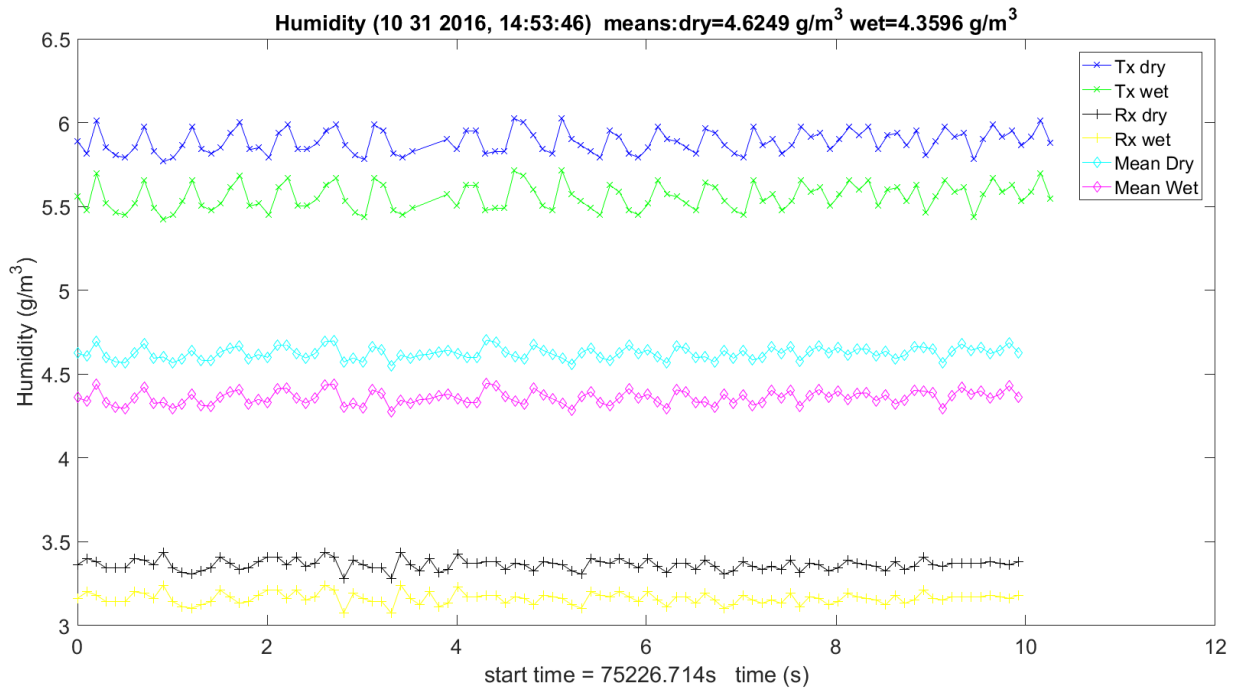


Figure 3.280. Humidity Transmit, Receiver & Mean – 11012016_145401.

Figure 3.281 – Figure 3.83 show the MCF for WB, LWL and UWL. Two same frequency scans are included for MCF-phase and the phase structure function. It is more dynamic around the 325.1529 GHz absorption peak. Outside of this time it is much more constant — this is on the WB. The LWL and UWL are only in the peak, so they always change.

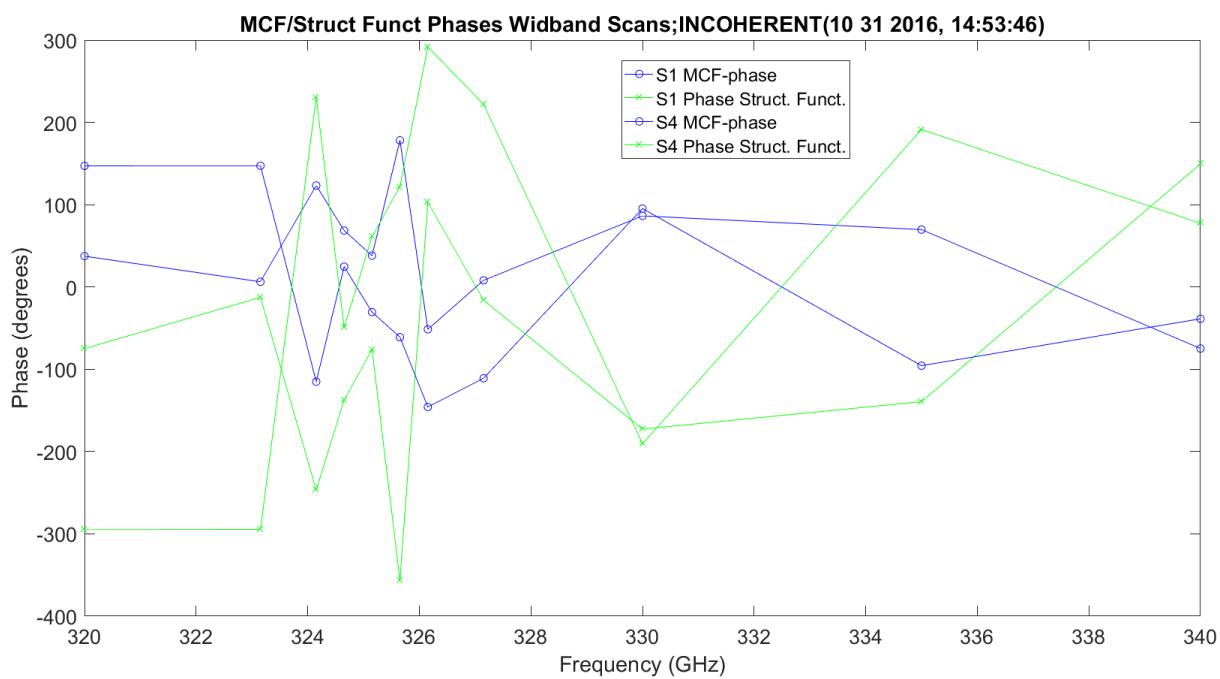


Figure 3.281. MCF – 11012016_145401.

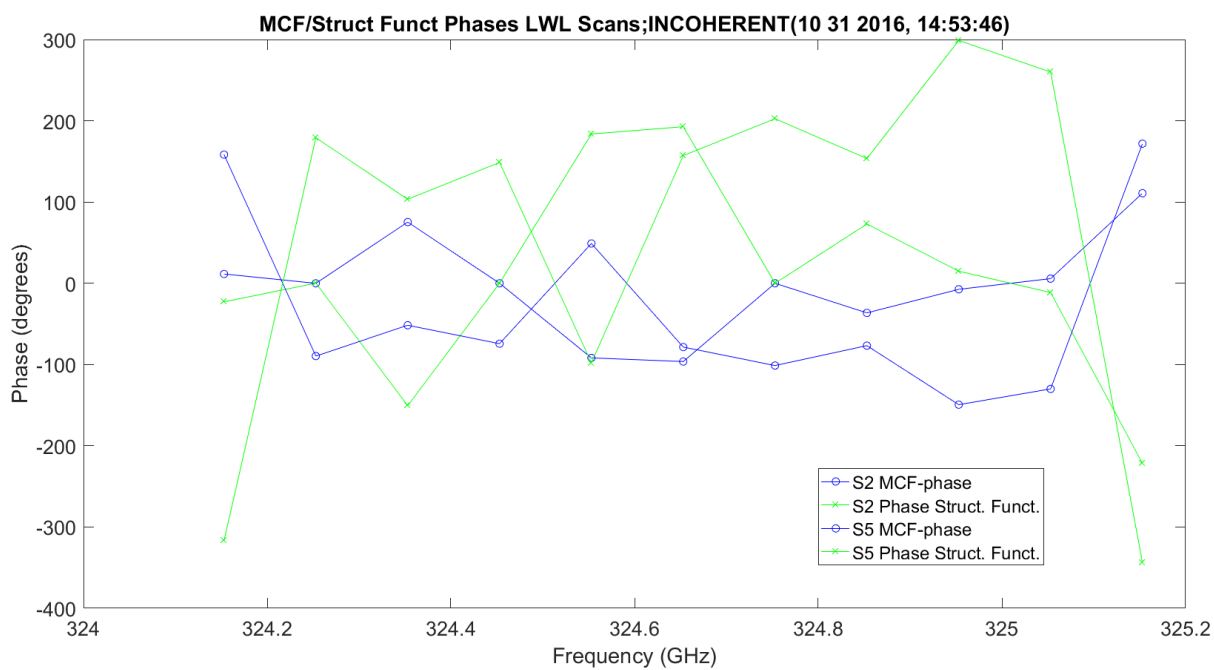


Figure 3.282. MCF – 11012016_145401.

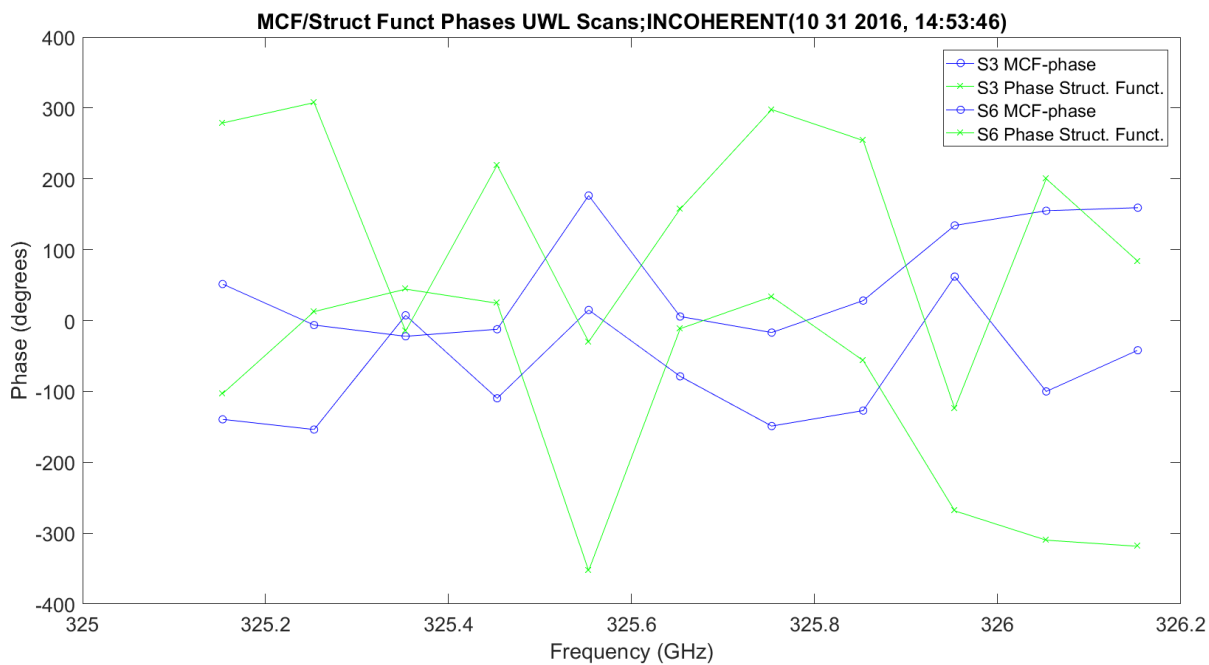


Figure 3.283. MCF – 11012016_145401.

Figure 3.284 shows the WB scans amplitude scintillation variance. It is easy to see how it peaks at the absorption peak; it is almost an identical shape. Rx1 has much lower offsets. This shows both receivers and prediction.

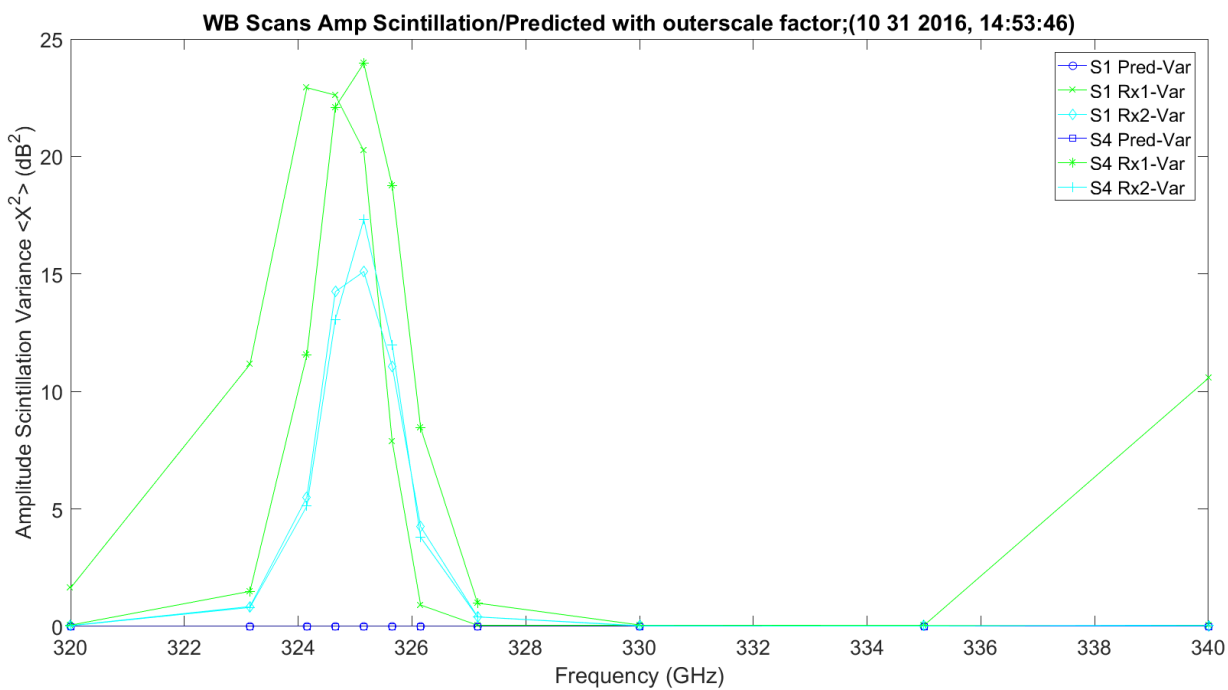


Figure 3.284. WB Amplitude Scintillation Variance and Predicted – 11012016_145401.

Figure 3.285 shows the LWL scans amplitude scintillation variance. It is a linear increase over frequency; Rx1 disappears for obvious reasons. Rx1 has much lower offsets (~7 dB). This shows both receivers and prediction.

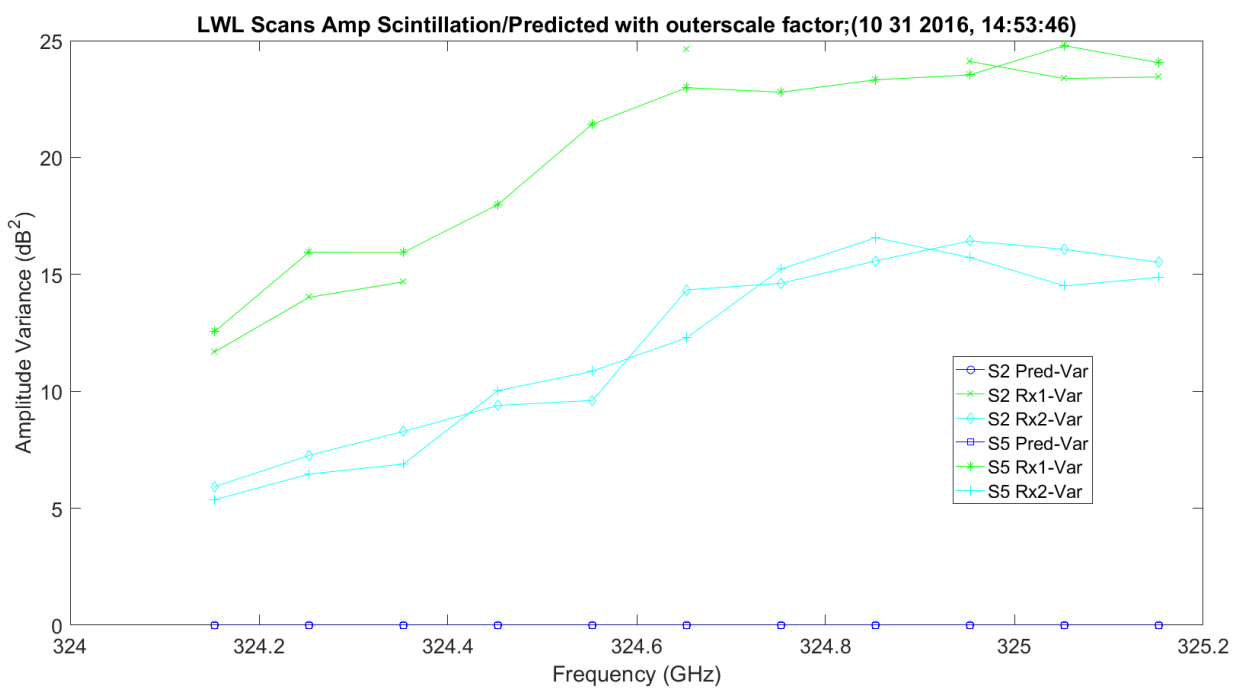


Figure 3.285. LWL Amplitude Scintillation Variance and Predicted – 11012016_145401.

Figure 3.286 shows the UWL scans amplitude scintillation variance. It is a linear increase over frequency; Rx1 disappears for obvious reasons. Rx1 has much lower offsets (~7 dB). This shows both receivers and prediction.

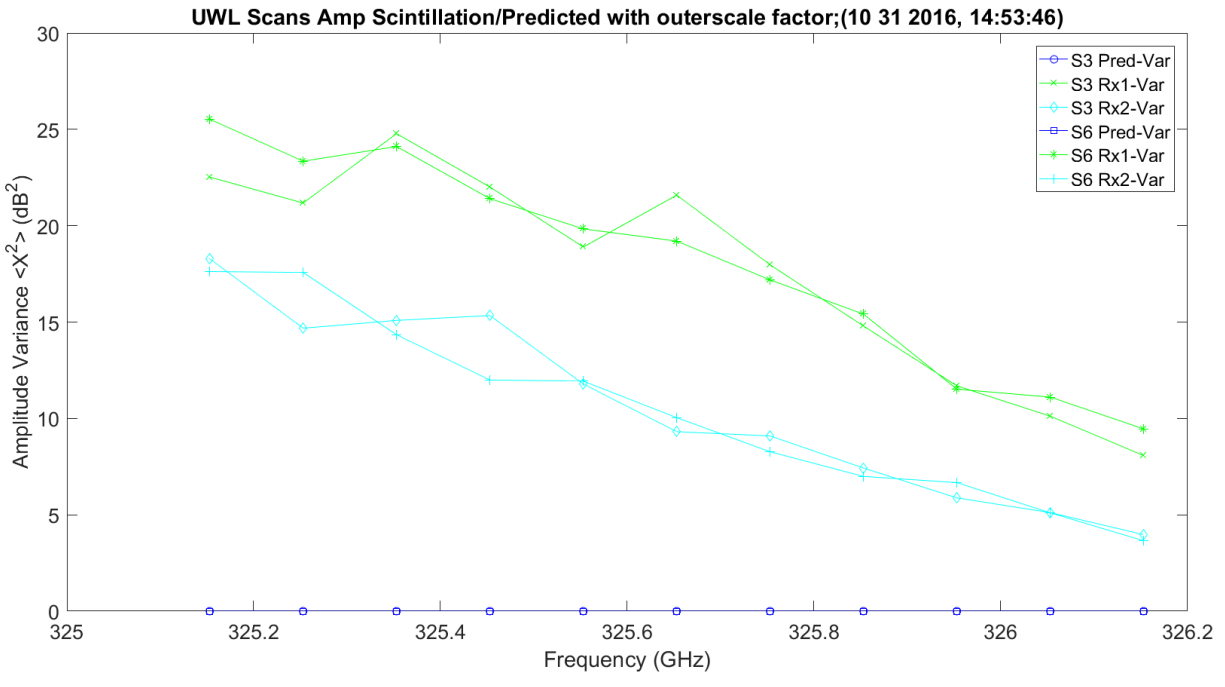


Figure 3.286. UWL Amplitude Scintillation Variance and Predicted – 11012016_145401.

Figure 3.287 shows the WB scans phase scintillation variance. The variance is around 180 degrees. It is fairly stable for both receivers, except when it is over the large absorption pulse.

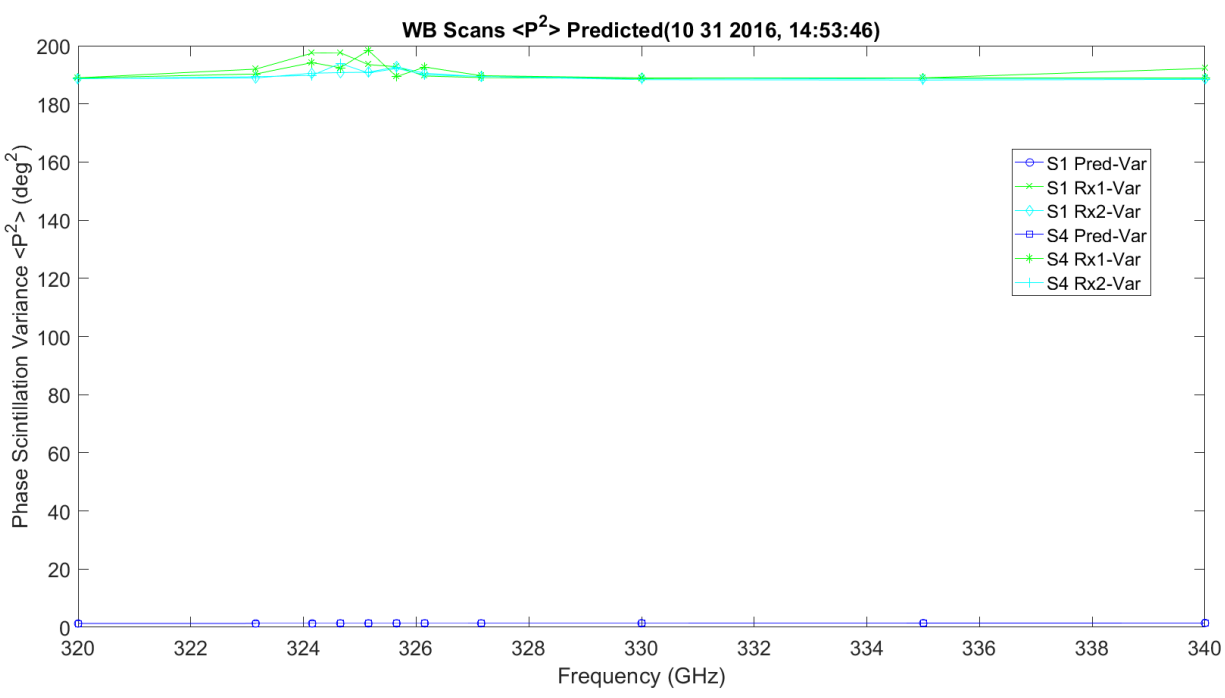


Figure 3.287. WB Phase Scintillation Variance and Predicted – 11012016_145401.

Figure 3.288 shows the LWL scans phase scintillation variance. The variance is around 180 degrees. Everything looks stable except for the green trances for Rx1. This is very dynamic over the absorption pulse.

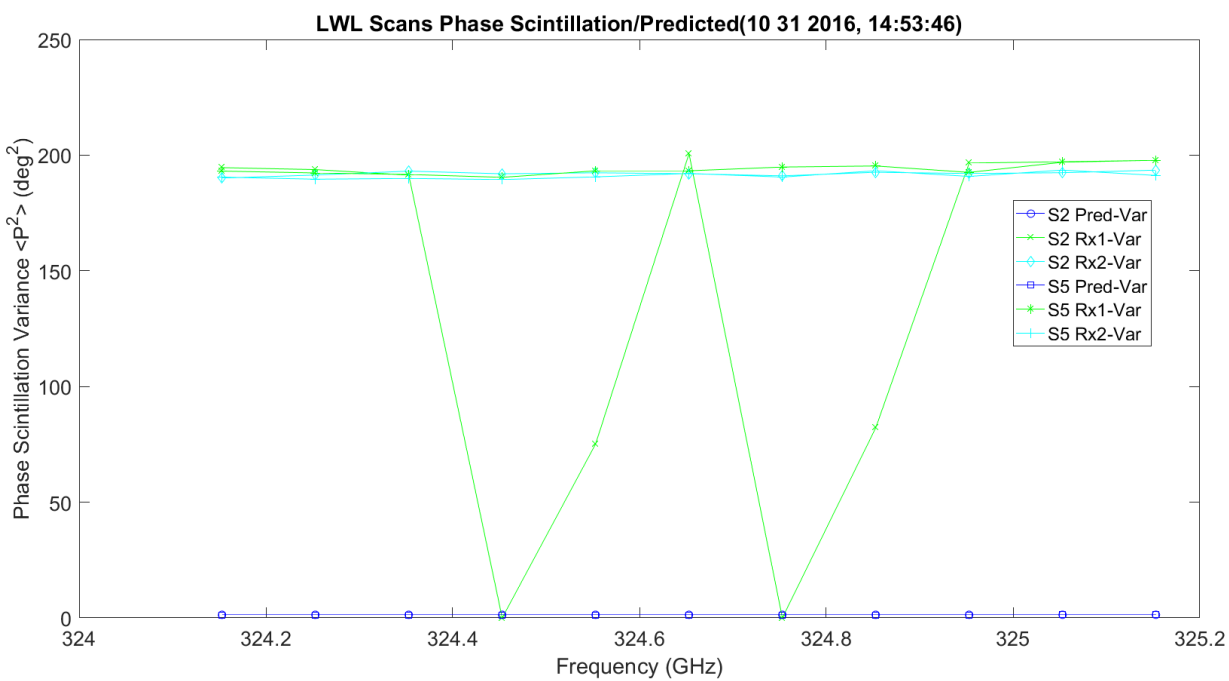


Figure 3.288. LWL Phase Scintillation Variance and Predicted – 11012016_145401.

Figure 3.289 shows the UWL scans phase scintillation variance. The variance is around 180 degrees. Everything looks stable, including Rx1. This is very dynamic over the absorption pulse.

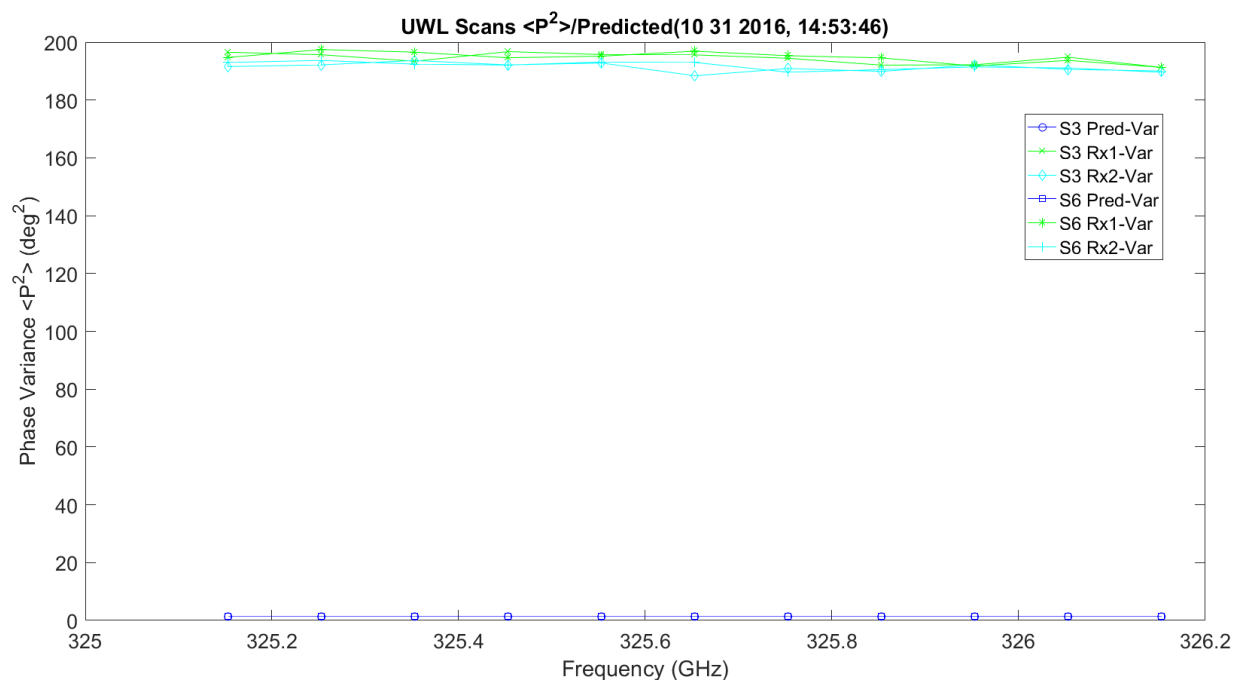


Figure 3.289. UWL Phase Scintillation Variance and Predicted – 11012016_145401.

Figure 3.290 shows the WB scans phase scintillation STD. The STD variance is around 14°, much higher than the prediction. It has linear growth with frequency.

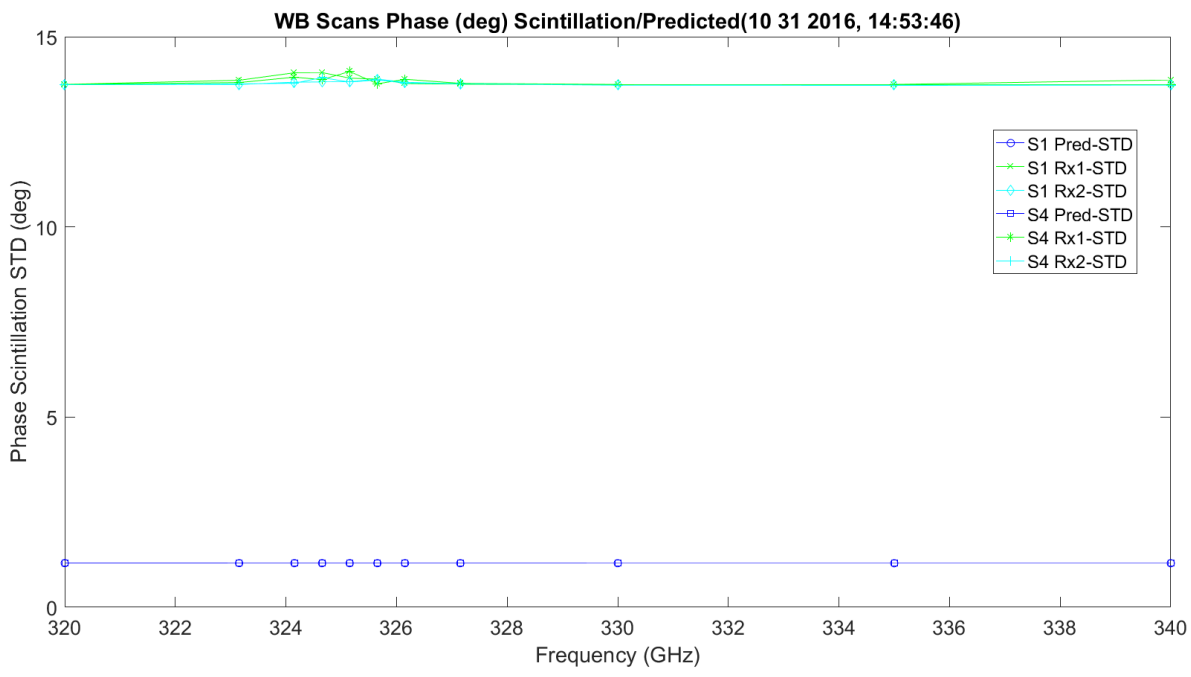


Figure 3.290. WB Phase Scintillation STD and Predicted Deg. – 11012016_145401.

Figure 3.291 shows the LWL scans phase scintillation STD. The STD variance is around 14°, much higher than the prediction. This is not true around some points on Rx1 where it goes to zero. It has linear growth with frequency.

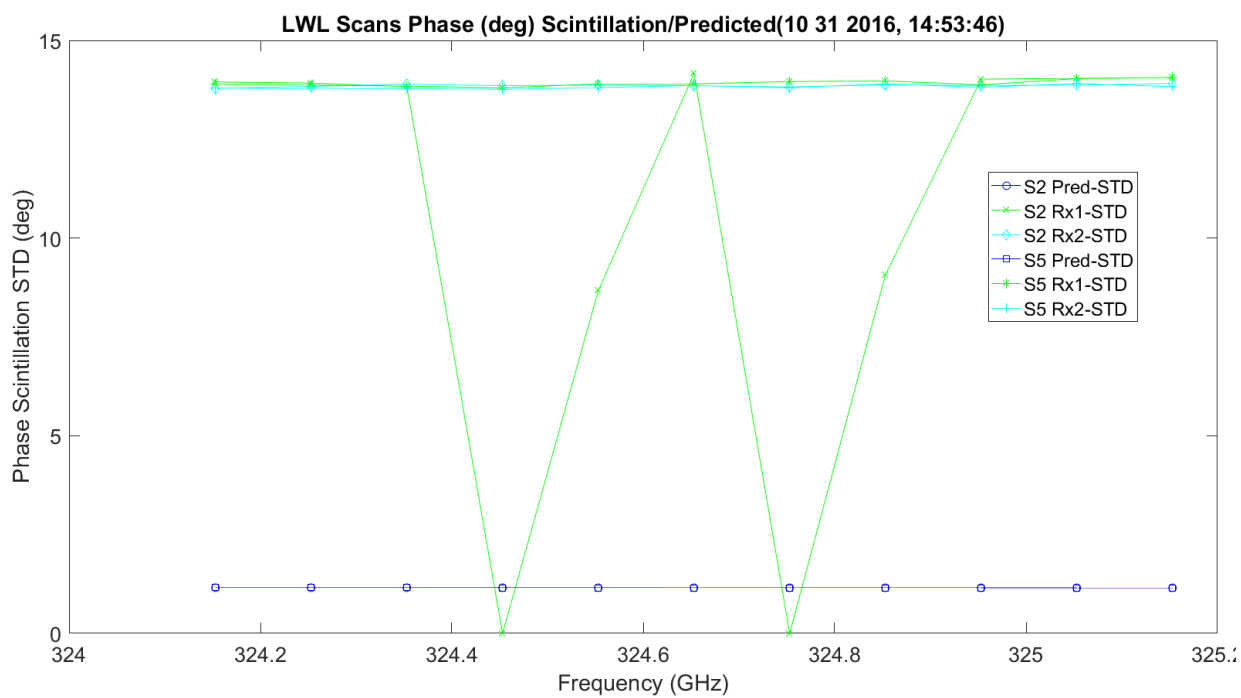


Figure 3.291. LWL Phase Scintillation STD and Predicted Deg. – 11012016_145401.

Figure 3.292 shows the UWL scans phase scintillation STD. The STD variance is around 14°, much higher than the prediction. This is not true around some points on Rx1. It has linear growth with frequency.

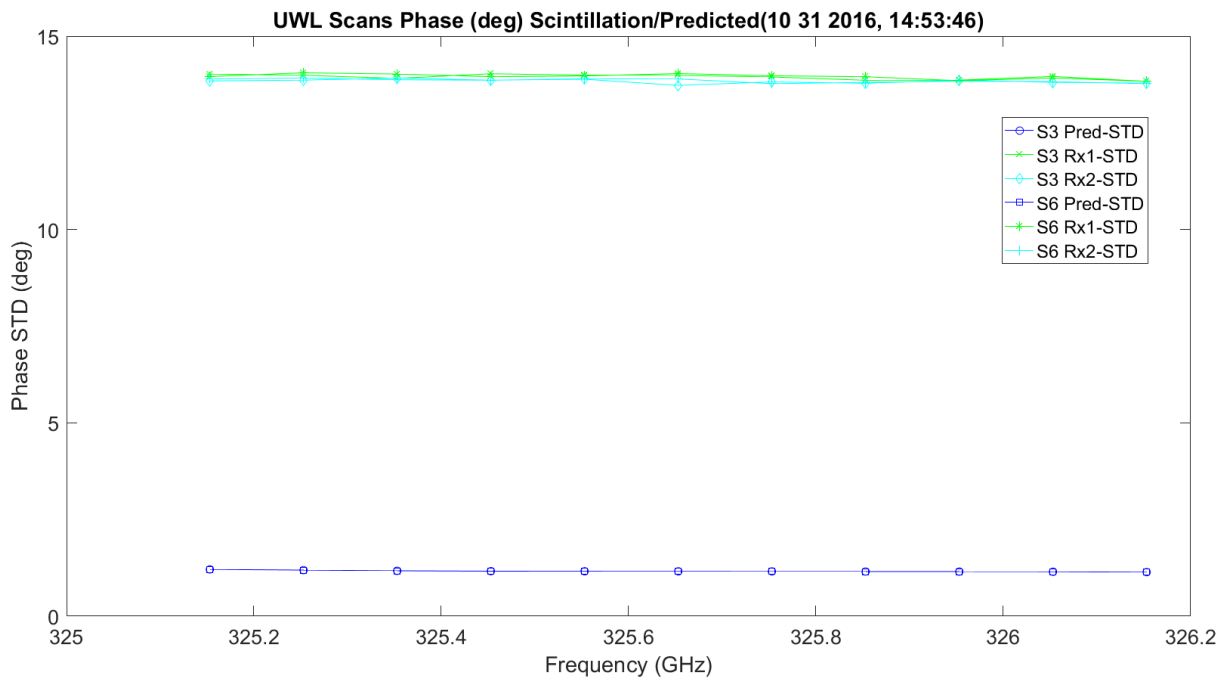


Figure 3.292. UWL Phase Scintillation STD and Predicted Deg. – 11012016_145401.

Figure 3.293 shows the WB scans phase scintillation STD. The STD variance is around 0.035 millimeters, much higher than the prediction shown in Figure 3.168. It has linear growth with frequency.

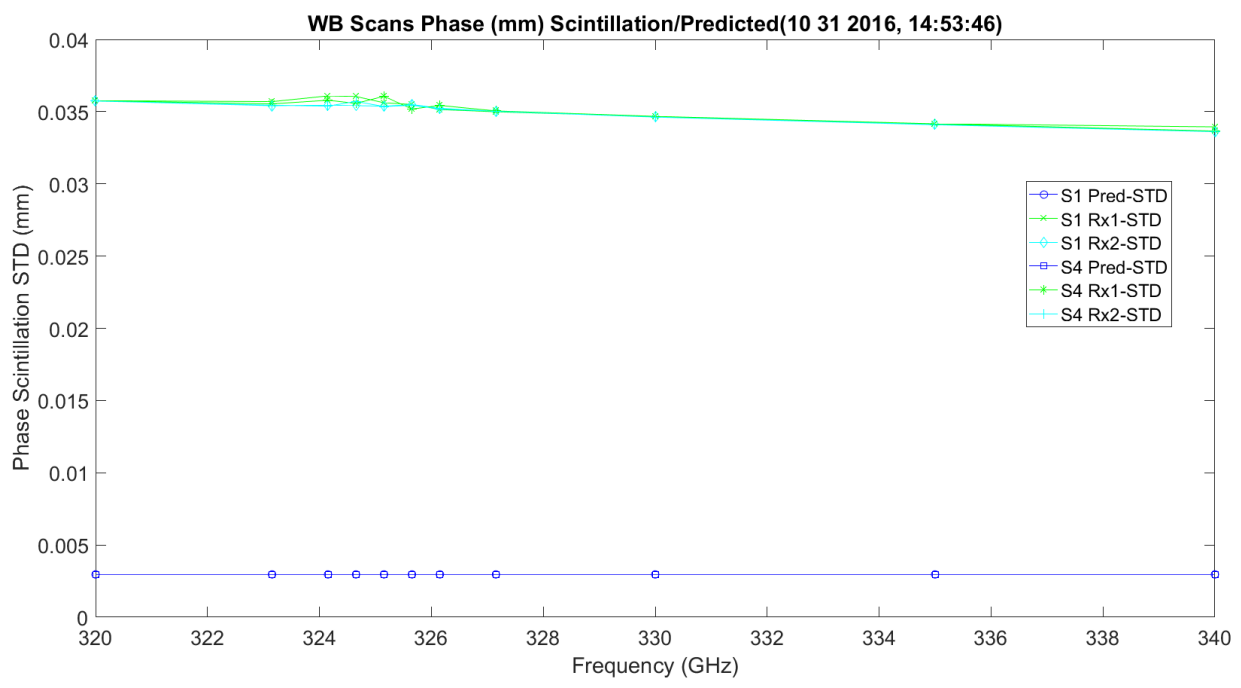


Figure 3.293. WB Phase Scintillation STD and Predicted MM – 11012016_145401.

Figure 3.294 shows the LWL scans phase scintillation STD. The STD variance is around 0.035 millimeters, much higher than the prediction which is shown in Figure 3.170. It has linear growth with frequency.

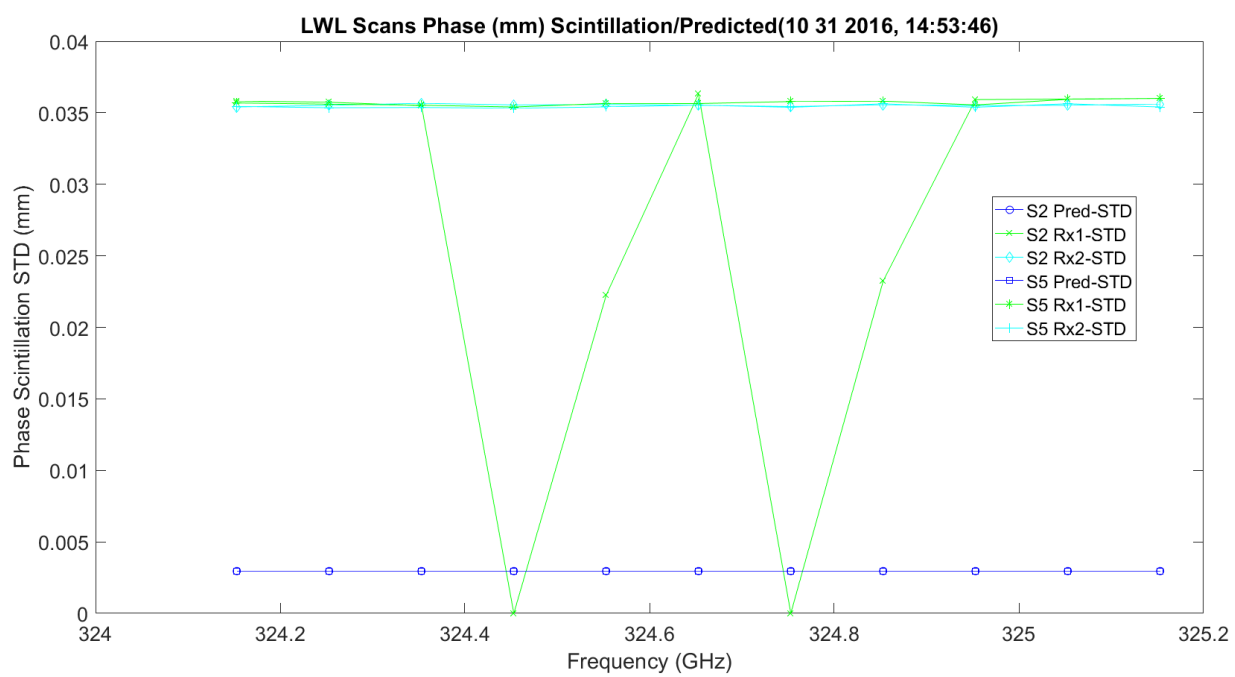


Figure 3.294. LWL Phase Scintillation STD and Predicted MM – 11012016_145401.

Figure 3.295 shows the UWL scans phase scintillation STD. The STD variance is around 0.035 millimeters, much higher than the prediction shown in Figure 3.167. It has linear growth with frequency.

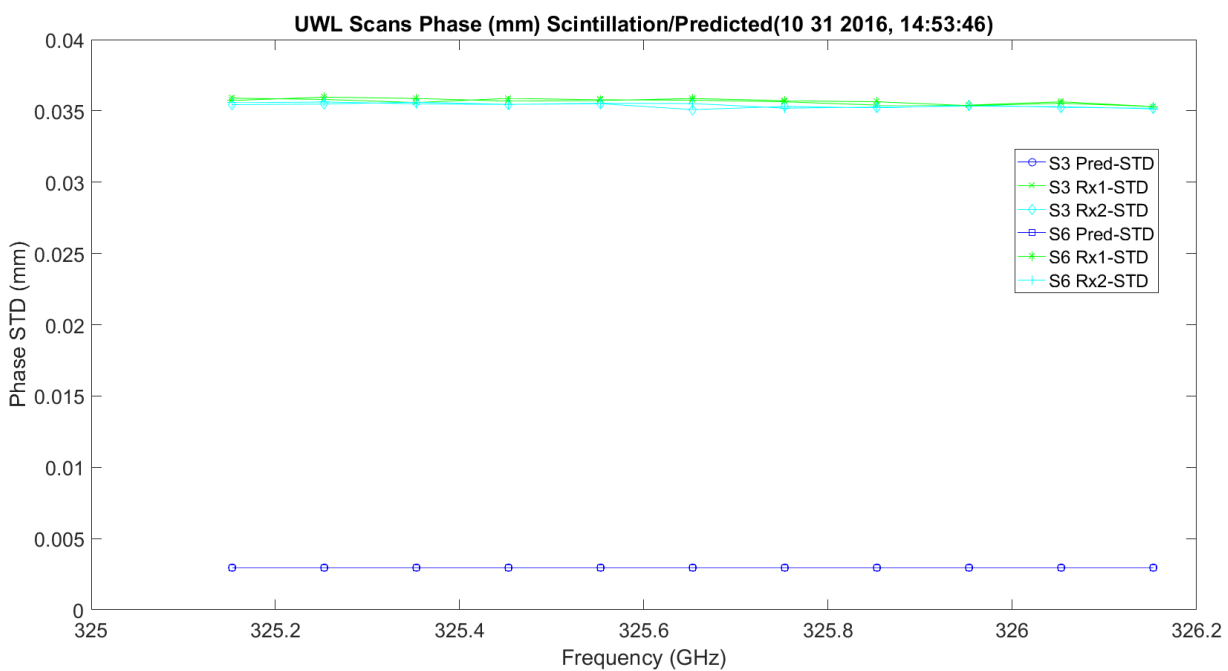


Figure 3.295. UWL Phase Scintillation STD and Predicted MM – 11012016_145401.

Figure 3.296 – Figure 3.298 show the same above in picosecond units. The differences are small numbers.

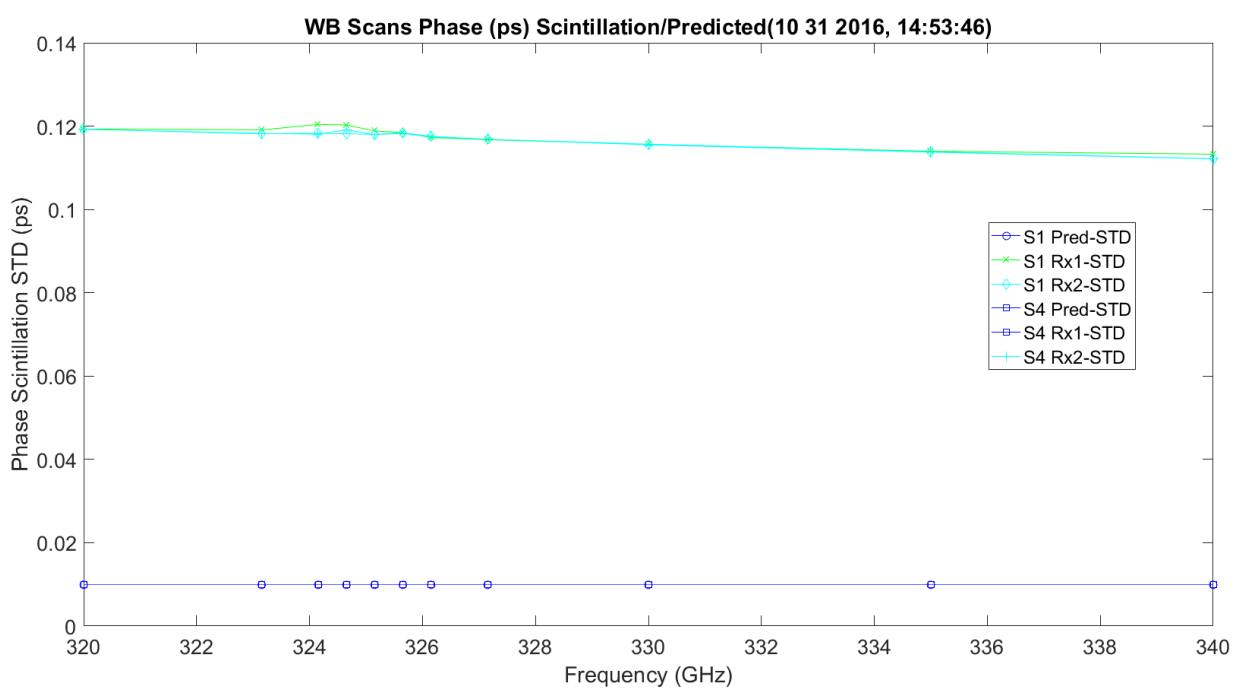


Figure 3.296. WB Phase Scintillation STD and Predicted ps – 11012016_145401.

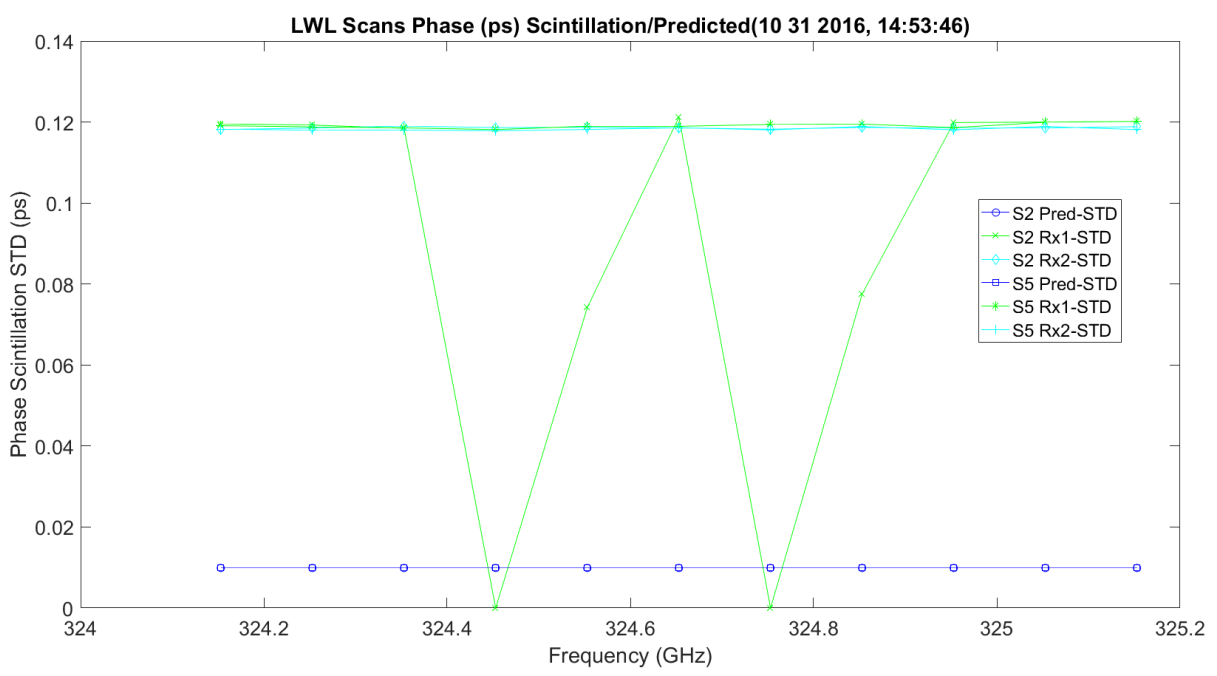


Figure 3.297. LWL Phase Scintillation STD and Predicted ps -- 11012016_145401.

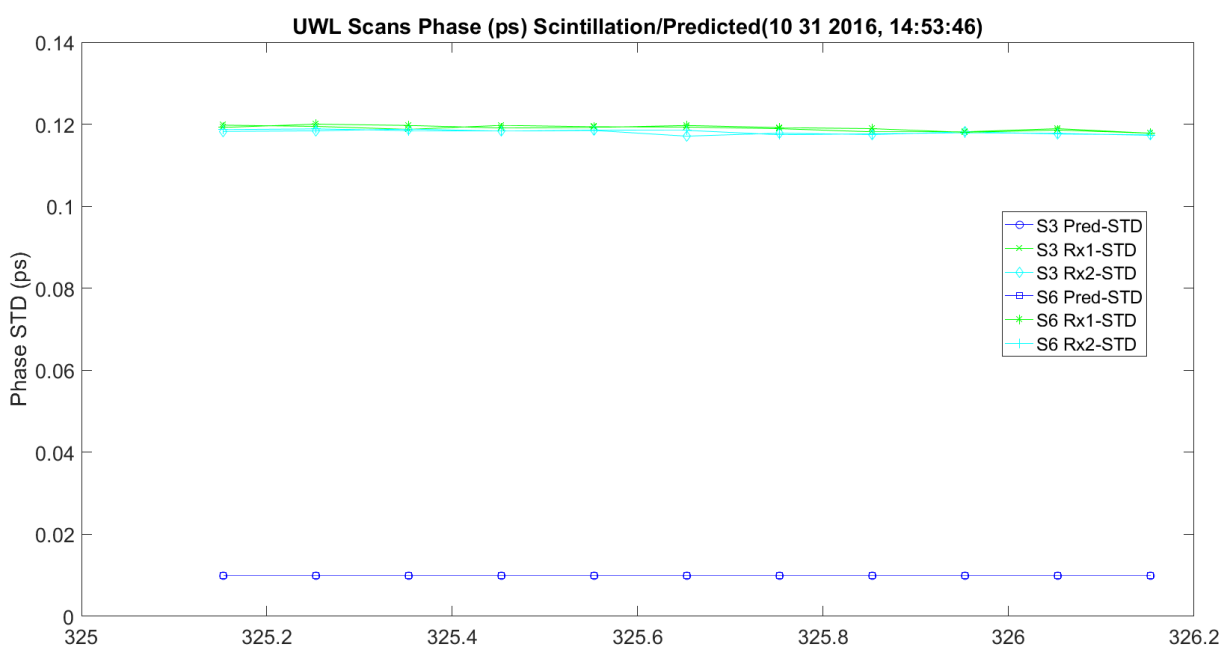


Figure 3.298. UWL Phase Scintillation STD and Predicted ps – 11012016_145401.

Figure 3.299 – Figure 3.301 show the WB, LWL and UWL amplitude and phase scintillation correlation. This is compared to prediction by Fresnel and Fraunhofer; these have the most significant correlation. Both receivers are very close to each other, but much lower on correlation. The UWL gets much closer at the start and works less correlated with increased frequency.

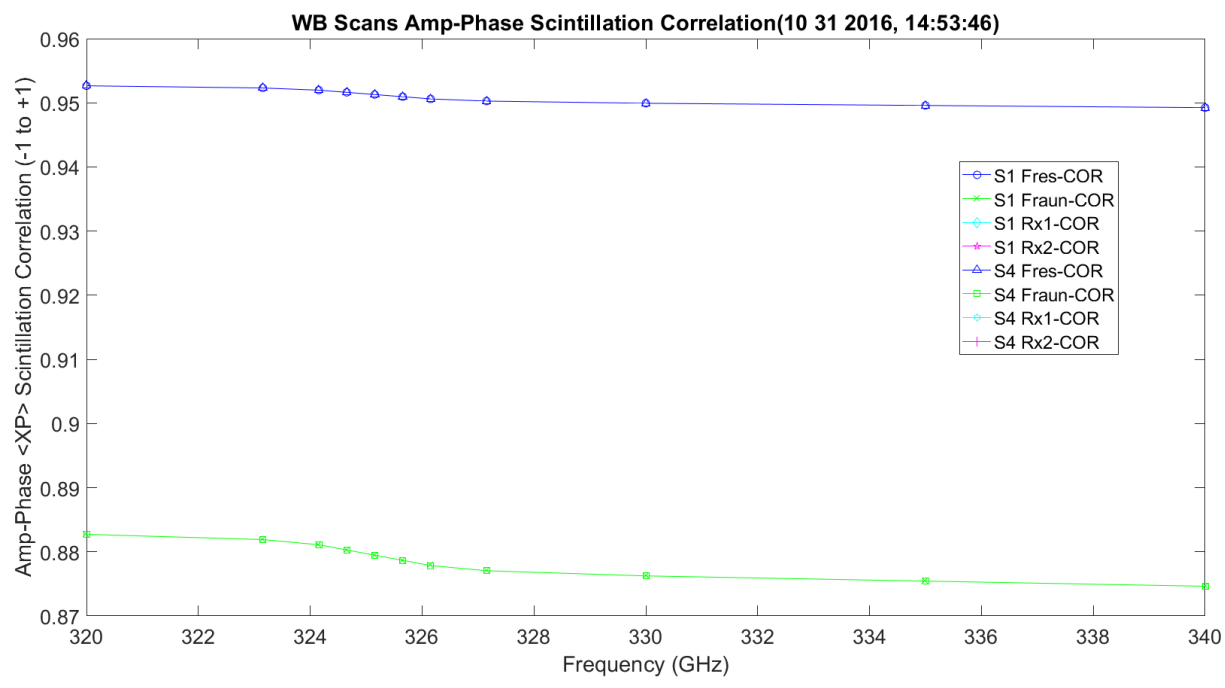


Figure 3.299. WB Amp/Phase Scintillation Correlation and Predicted – 11012016_145401.

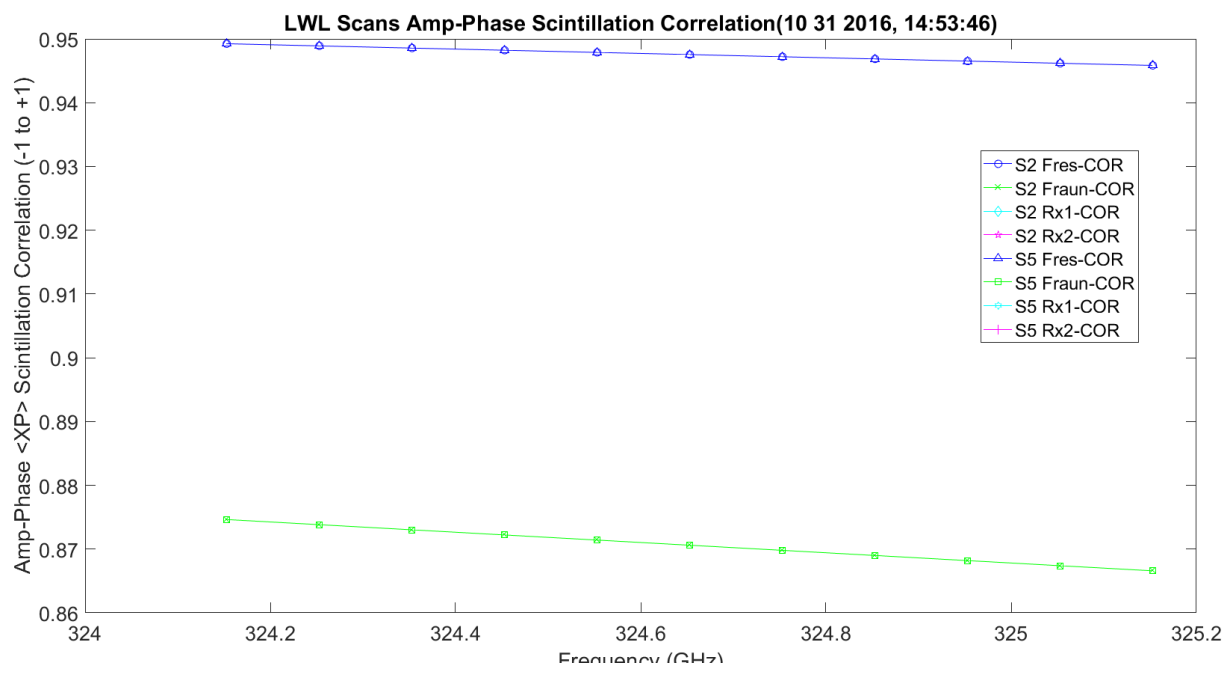


Figure 3.300. LWL Amp/Phase Scintillation Correlation and Predicted – 1012016_145401.

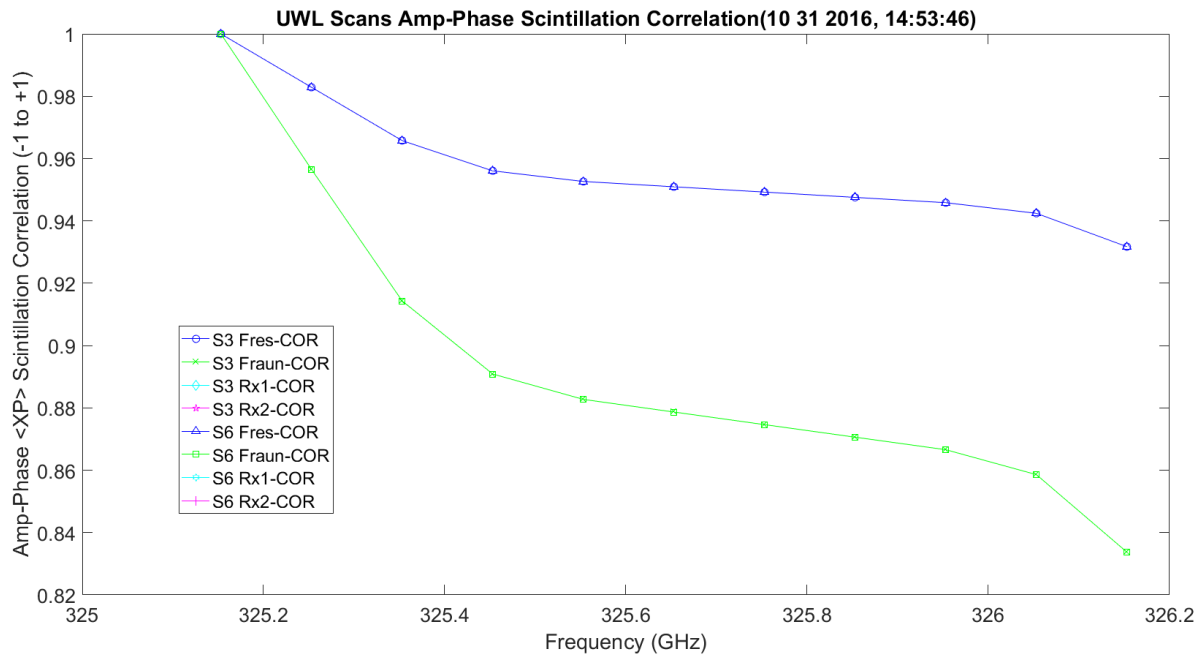


Figure 3.301. UWL Amp/Phase Scintillation Correlation and Predicted – 1012016_145401.

Figure 3.302 shows C_T^2 . This is the merge of Tx and Rx anemometers.

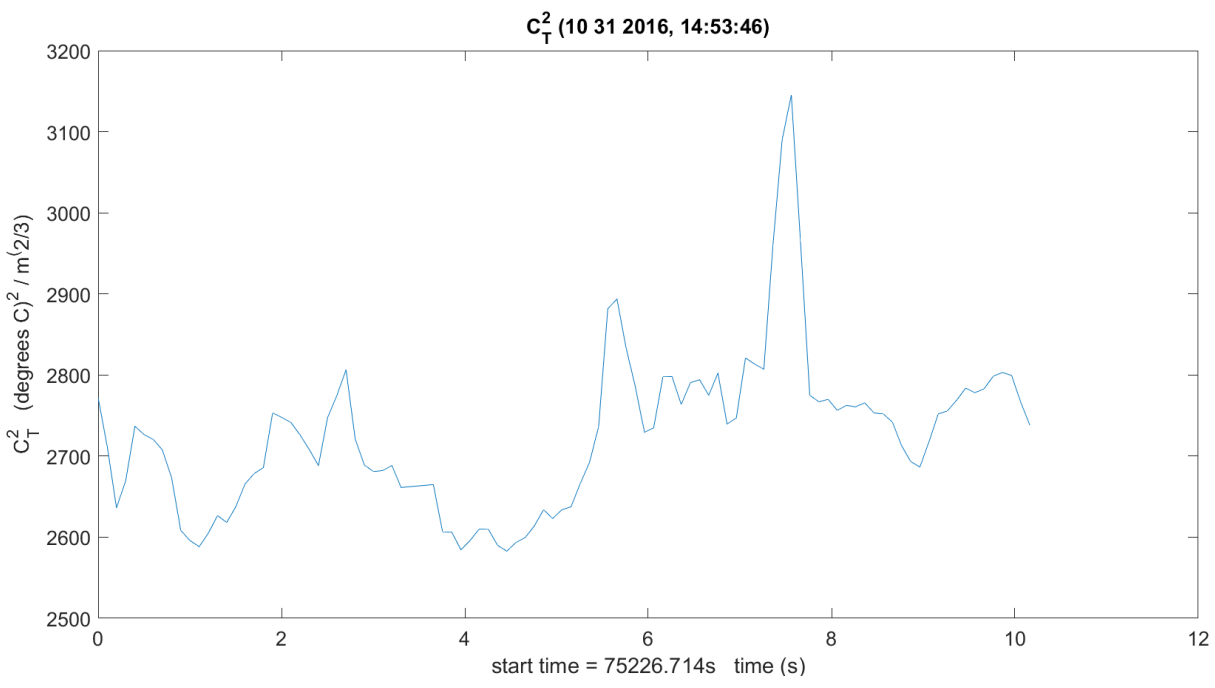


Figure 3.302. C_T^2 – 11012016_145401.

Figure 3.303 shows C_Q^2 . This includes transmit and receive hygrometer sensors averaged.

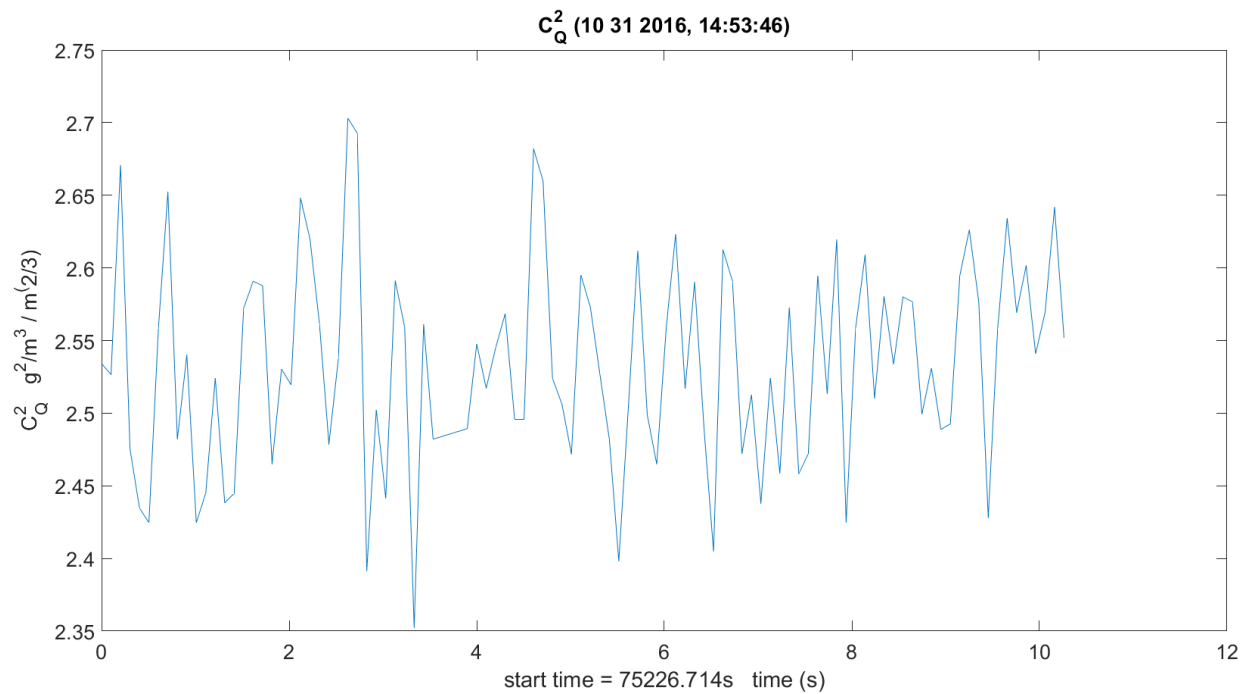


Figure 3.303. C_Q^2 – 11012016_145401.

Figure 3.304 shows C_{TQ} . This includes transmit and receive hygrometer sensors averaged and temperature.

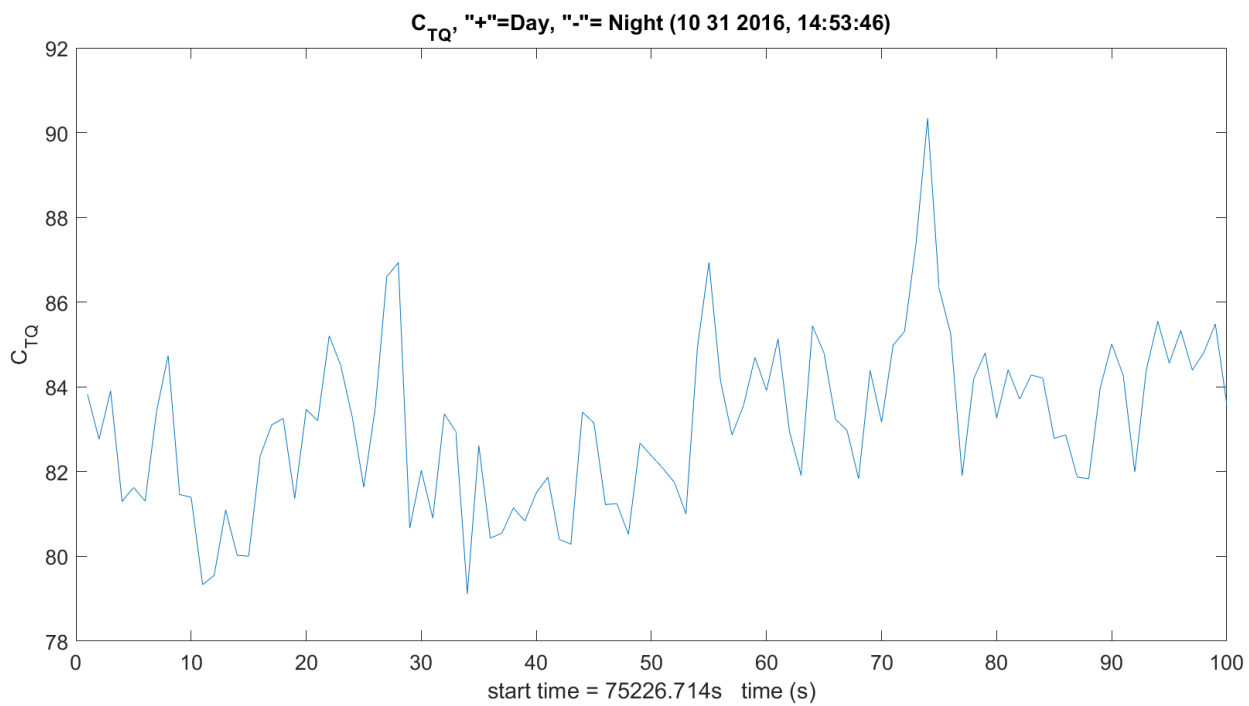


Figure 3.304. C_{TQ} – 11012016_145401.

Figure 3.305 shows C_n^2 variance compared to amplitude variance.

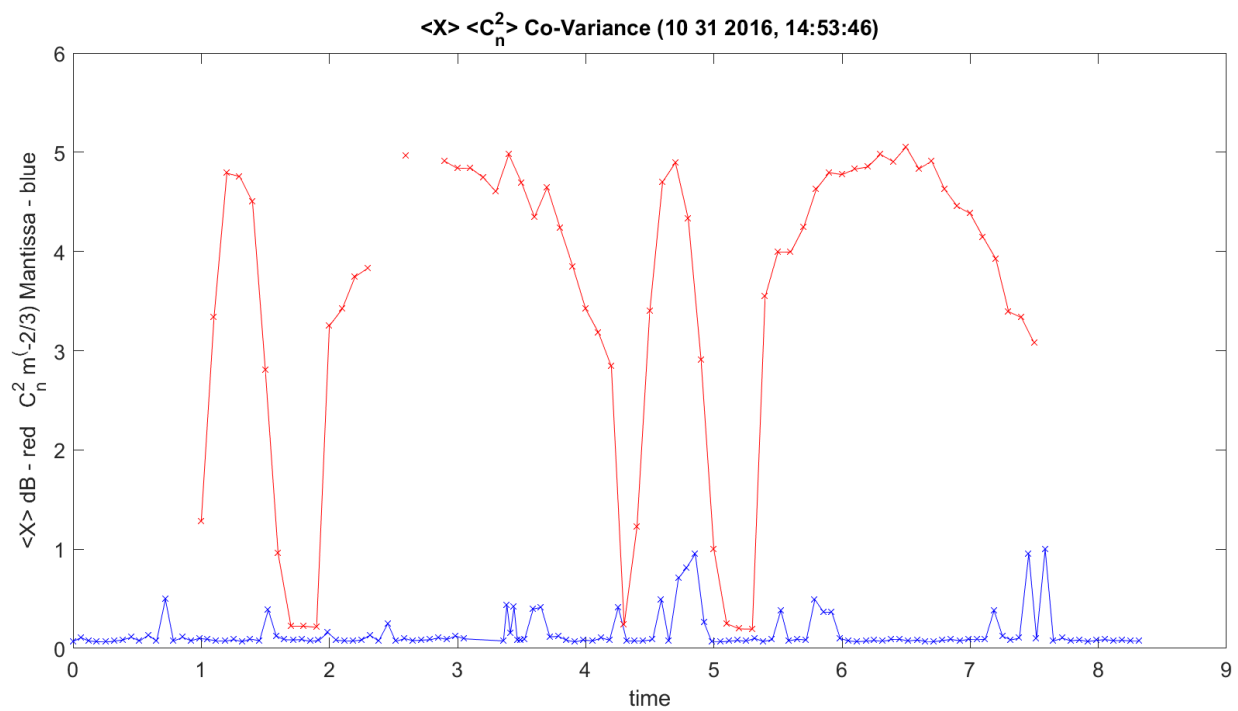


Figure 3.305. $\langle C_n^2 \rangle$ Construction and $\langle X \rangle$ Amplitude – 11012016_145401.

Figure 3.306 shows amplitude STD and C_7^2 variance relation.

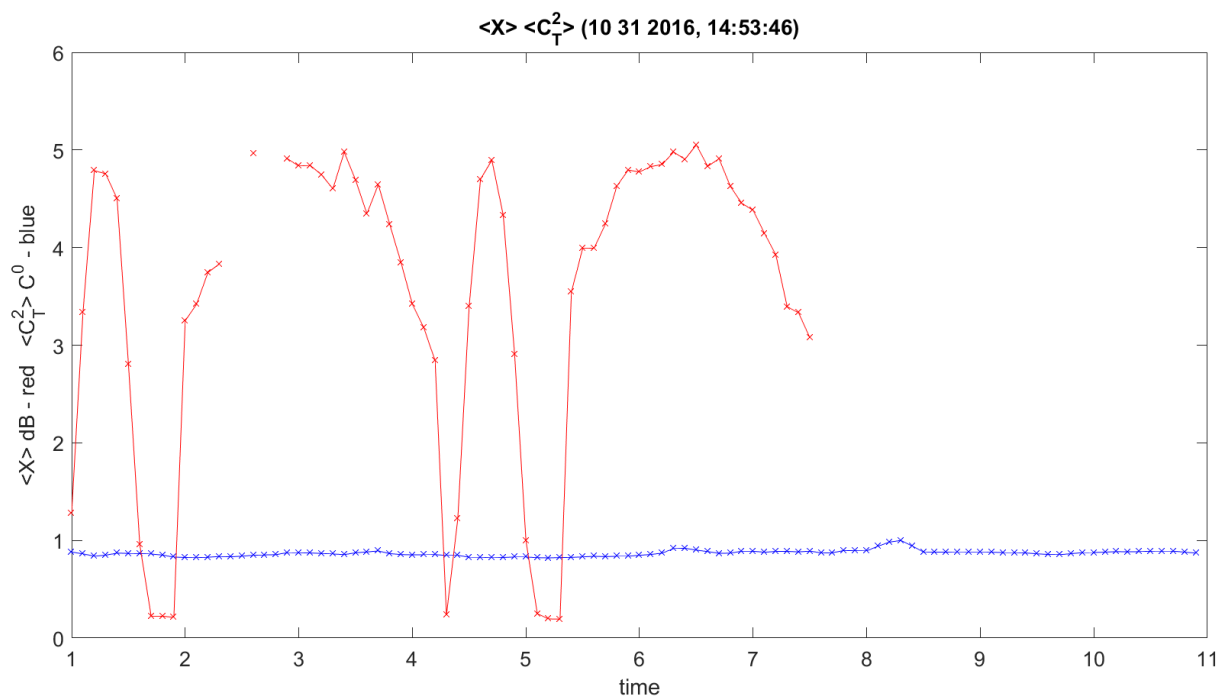


Figure 3.306. $\langle C_n^2 \rangle$ Temp Construction and Amplitude Variance – 11012016_145401.

Figure 3.307 shows amplitude STD and C_n^2 relation on two plots.

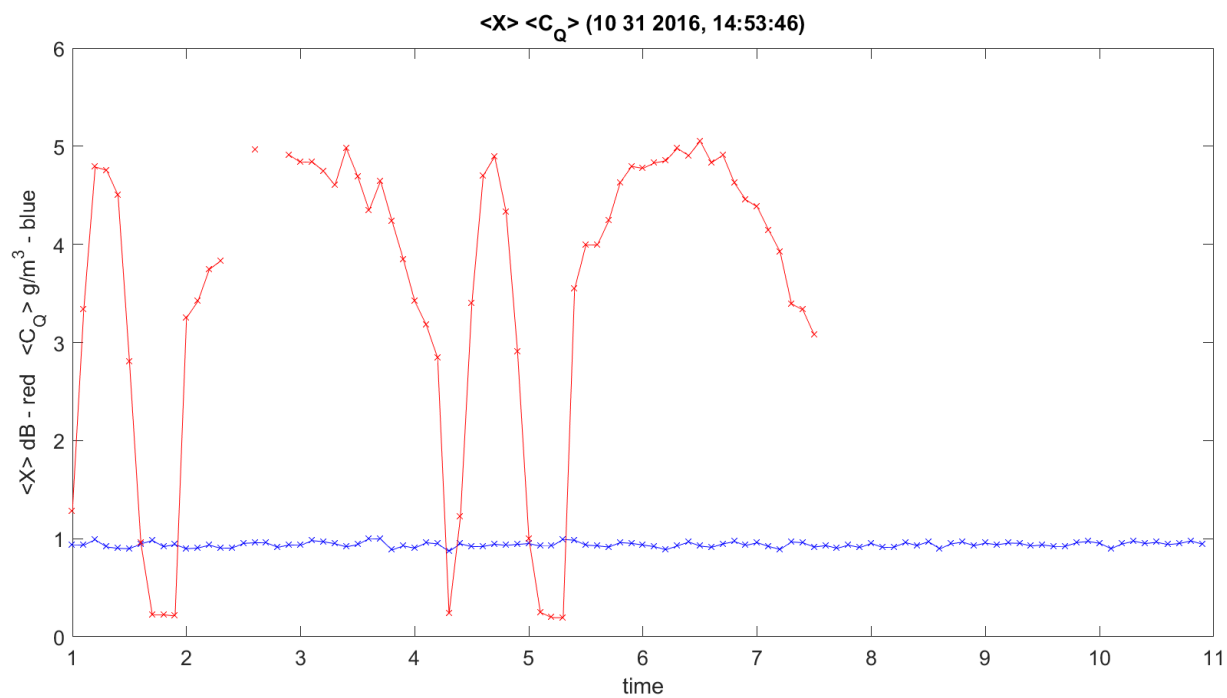


Figure 3.307. $\langle C_Q^2 \rangle$ Construction Temp and Amplitude Variance – 11012016_145401.

Figure 3.308 shows phase STD and $\langle C_n^2 \rangle$ relation on two plots.

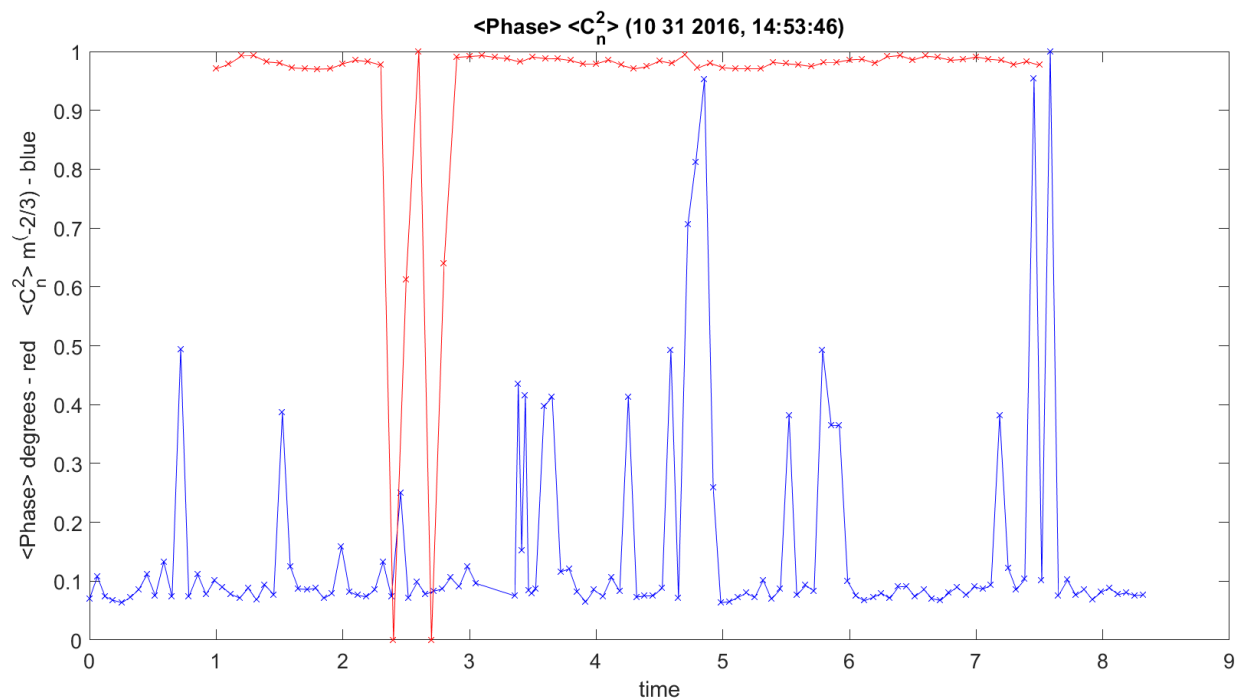


Figure 3.308. $\langle C_n^2 \rangle$ Temp Variance and Phase Variance – 11012016_145401.

Figure 3.309 shows phase STD and $\langle C_T^2 \rangle$ relation on two plots.

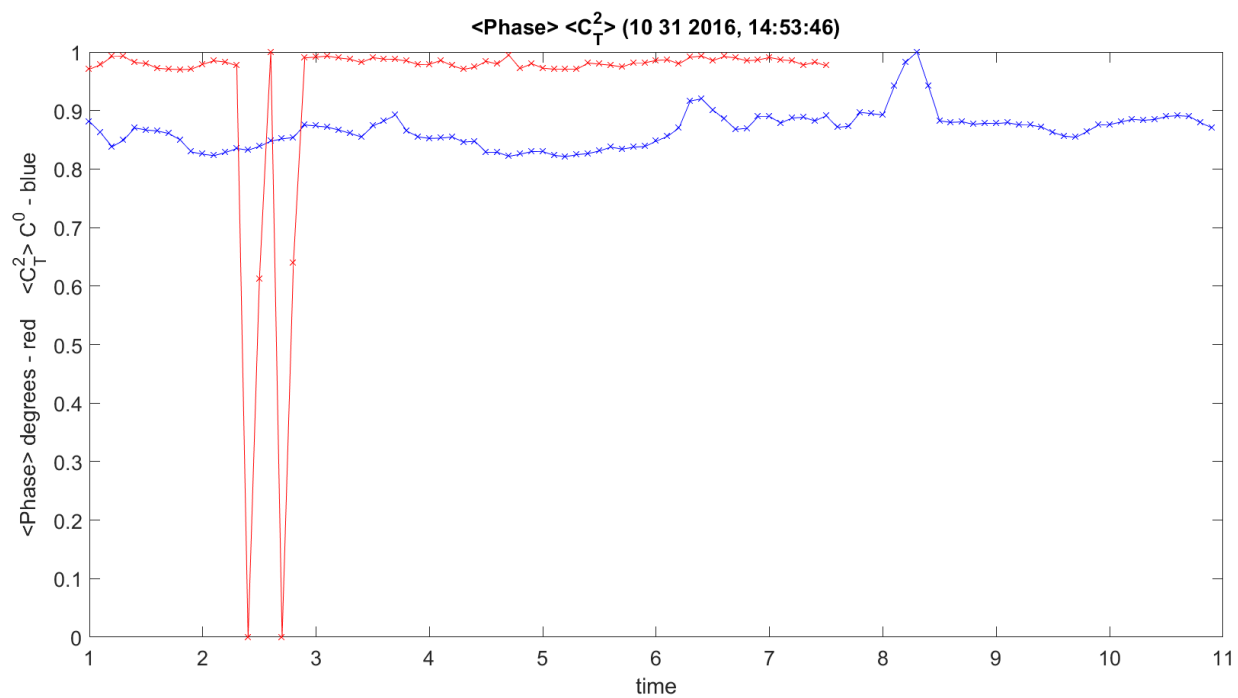


Figure 3.309. $\langle C_T^2 \rangle$ Temp Variance and Phase Variance – 11012016_145401.

Figure 3.310 shows phase STD and $\langle C_Q^2 \rangle$ relation on two plots.

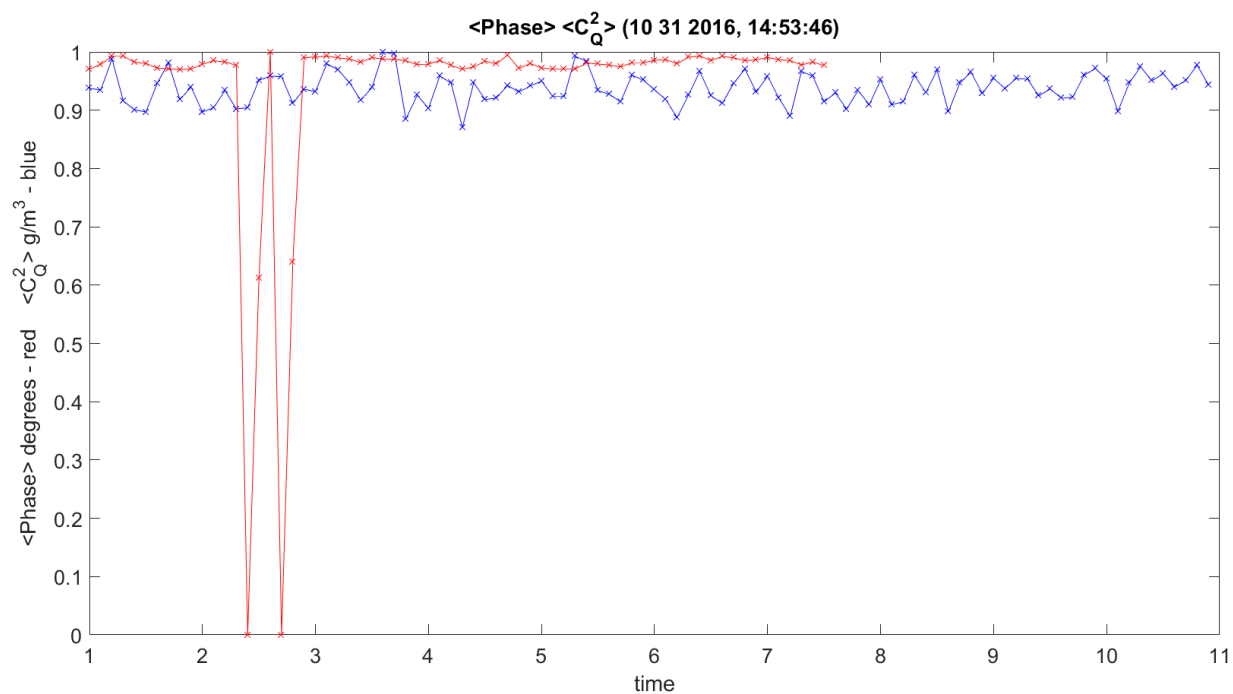


Figure 3.310. $\langle C_Q^2 \rangle$ Humidity Variance and Phase Variance – 11012016_145401.

Figure 3.311 shows $\langle C_T^2 \rangle$ and $\langle C_n^2 \rangle$ relation on two plots.

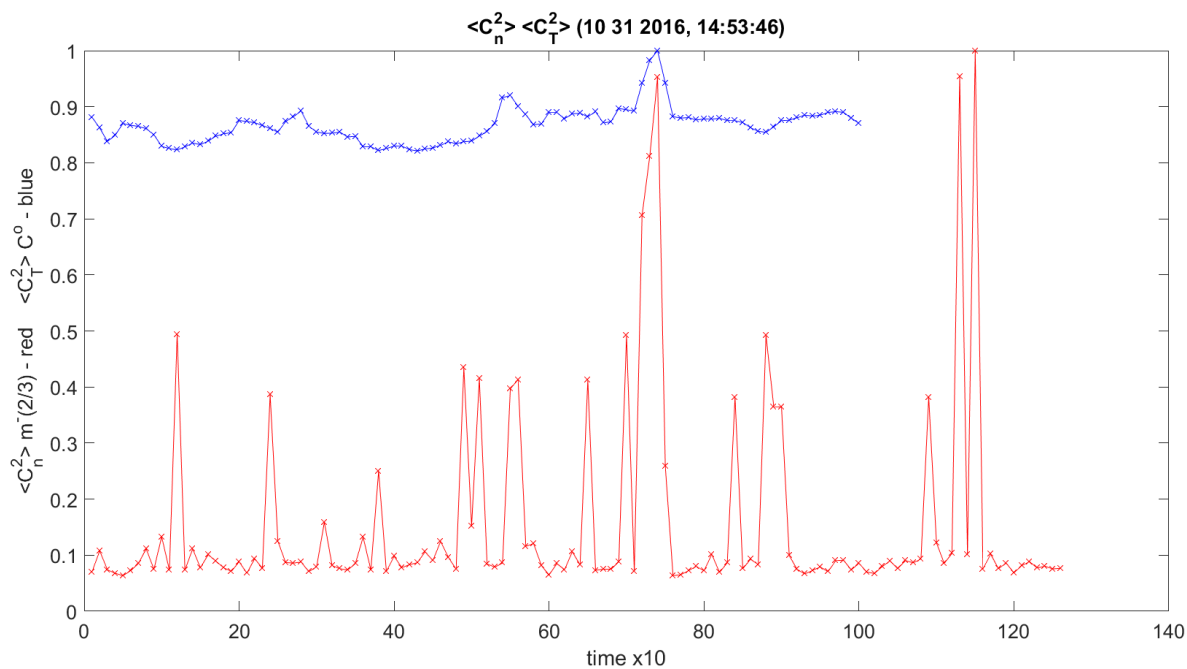


Figure 3.311. $\langle C_n^2 \rangle$ and $\langle C_T^2 \rangle$ Variance – 11012016_145401.

Figure 3.312 shows $\langle C_Q^2 \rangle$ and $\langle C_n^2 \rangle$ relation on two plots.

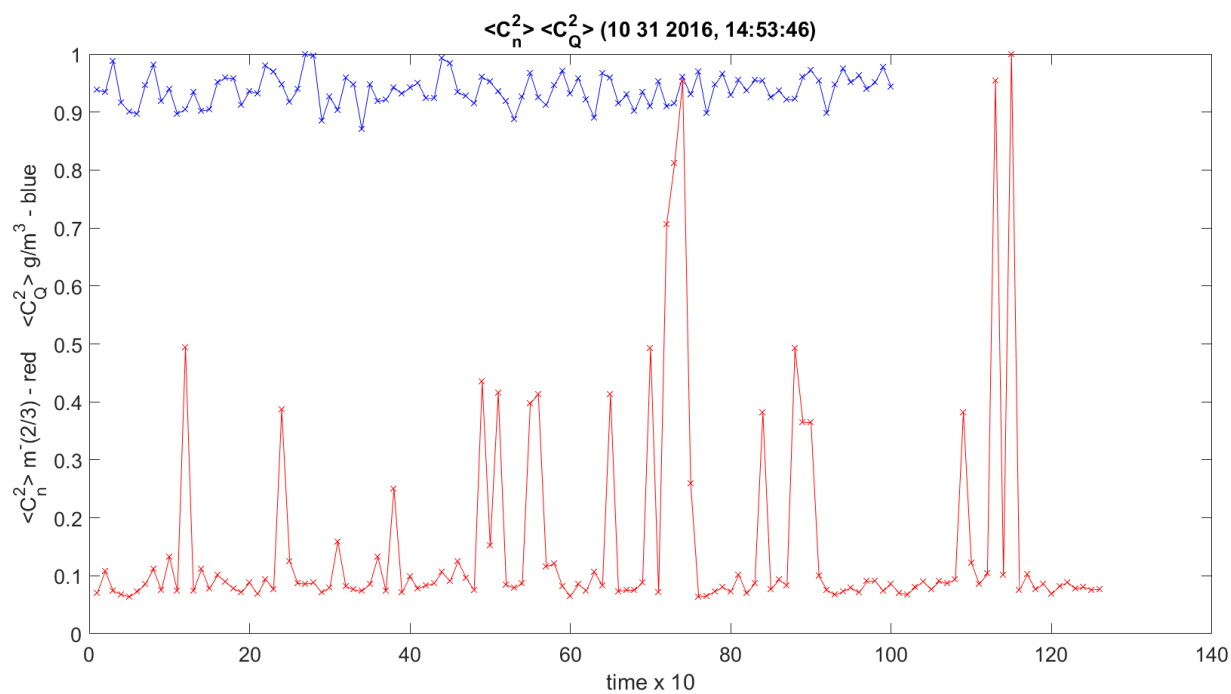


Figure 3.312. $\langle C_Q^2 \rangle$ Humidity Variance and $\langle C_n^2 \rangle$ Construction Variance – 1012016_145401.

Figure 3.313 shows $\langle C_T^2 \rangle$ and $\langle C_Q^2 \rangle$ relation on two plots.

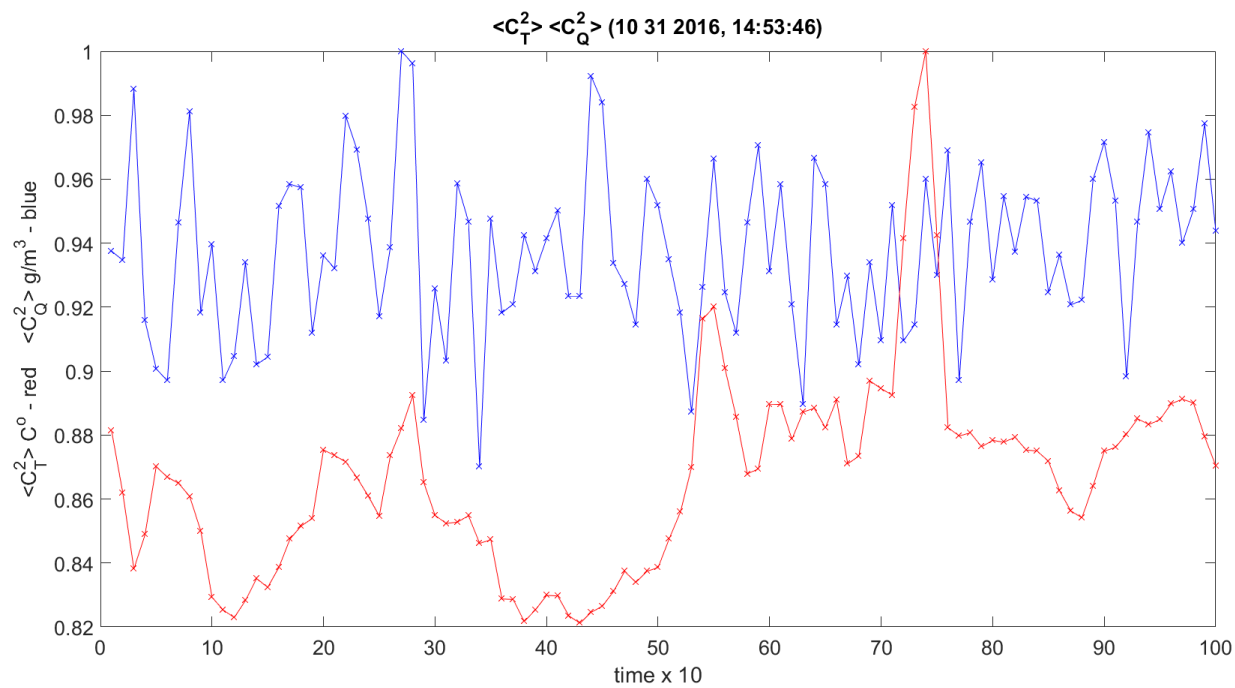


Figure 3.313. $\langle C_Q^2 \rangle$ Humidity Variance and $\langle C_T^2 \rangle$ Temp Variance – 11012016_145401.

Figure 3.314 shows amplitude/phase variance STD and U wind variance STD relation on two plots.

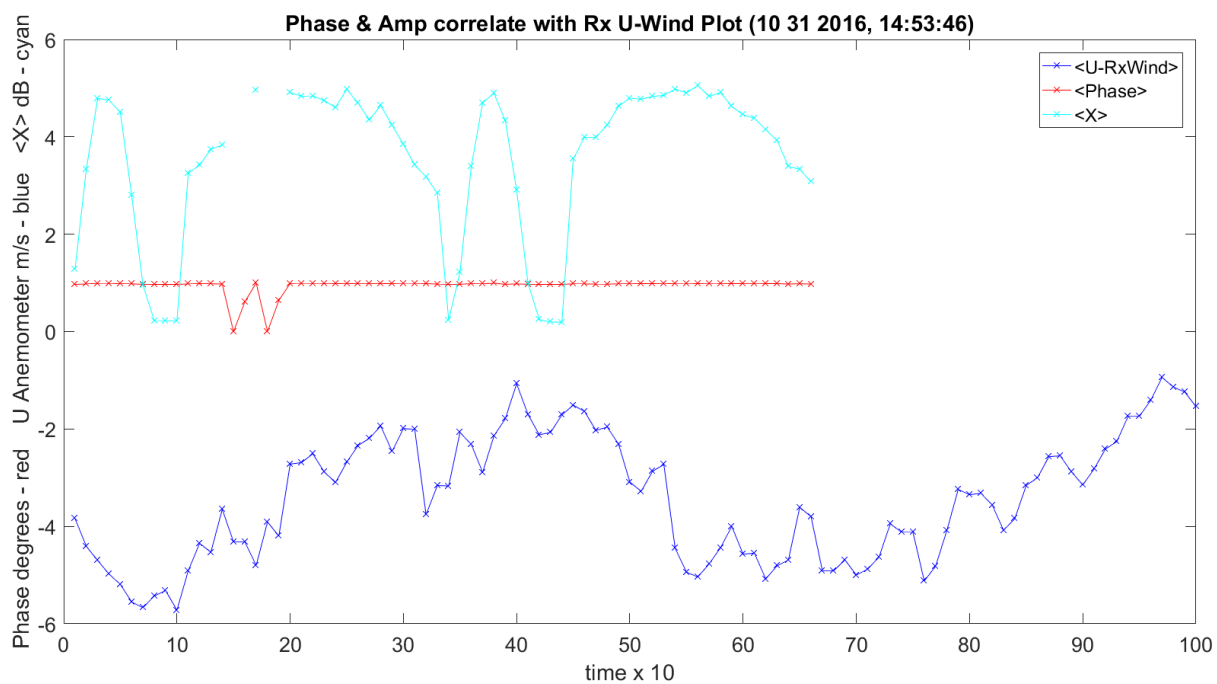


Figure 3.314. Phase, *U* Wind and Amplitude Variance – 11012016_145401.

Figure 3.315 shows amplitude/phase variance STD and *V* wind variance STD relation on two plots.

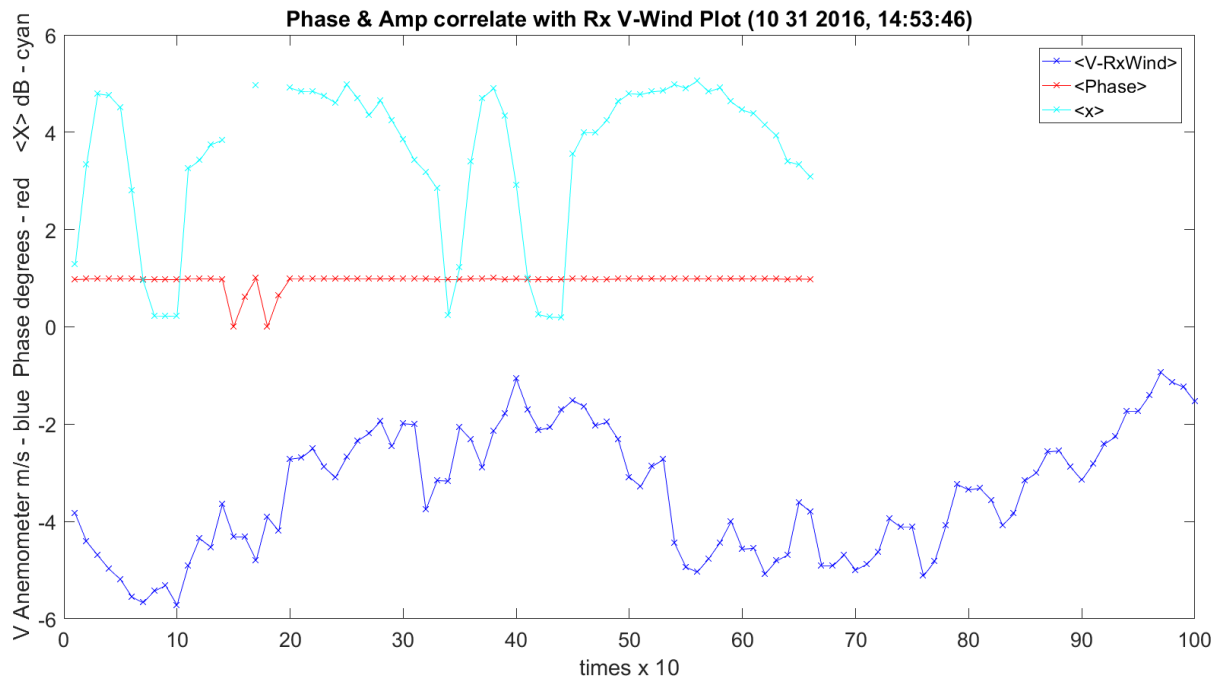


Figure 3.315. Phase, V Wind and Amplitude Variance – 11012016_145401.

Figure 3.316 shows amplitude/phase variance STD and W wind variance STD relation on two plots.

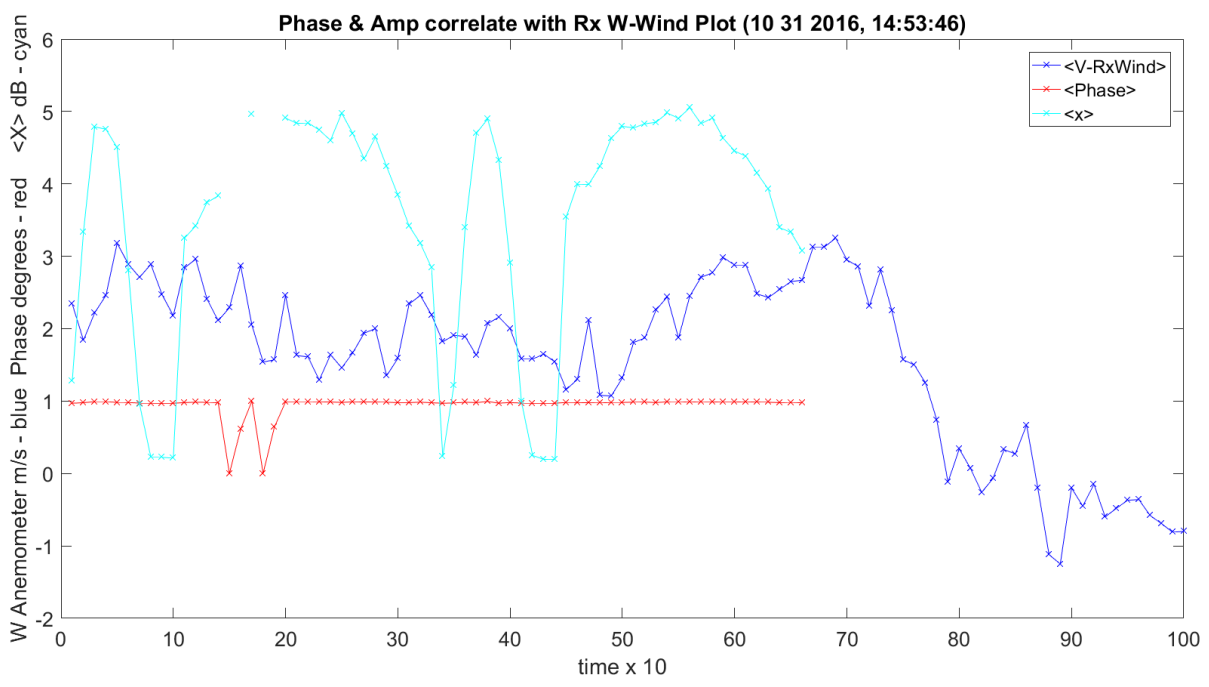


Figure 3.316. Phase, W Wind and Amplitude Variance – 11012016_145401.

Figure 3.317 and Figure 3.317 show the histogram for the 320 GHz frequency. Many of these can be done for every frequency in MATLAB selection at the top of the code.

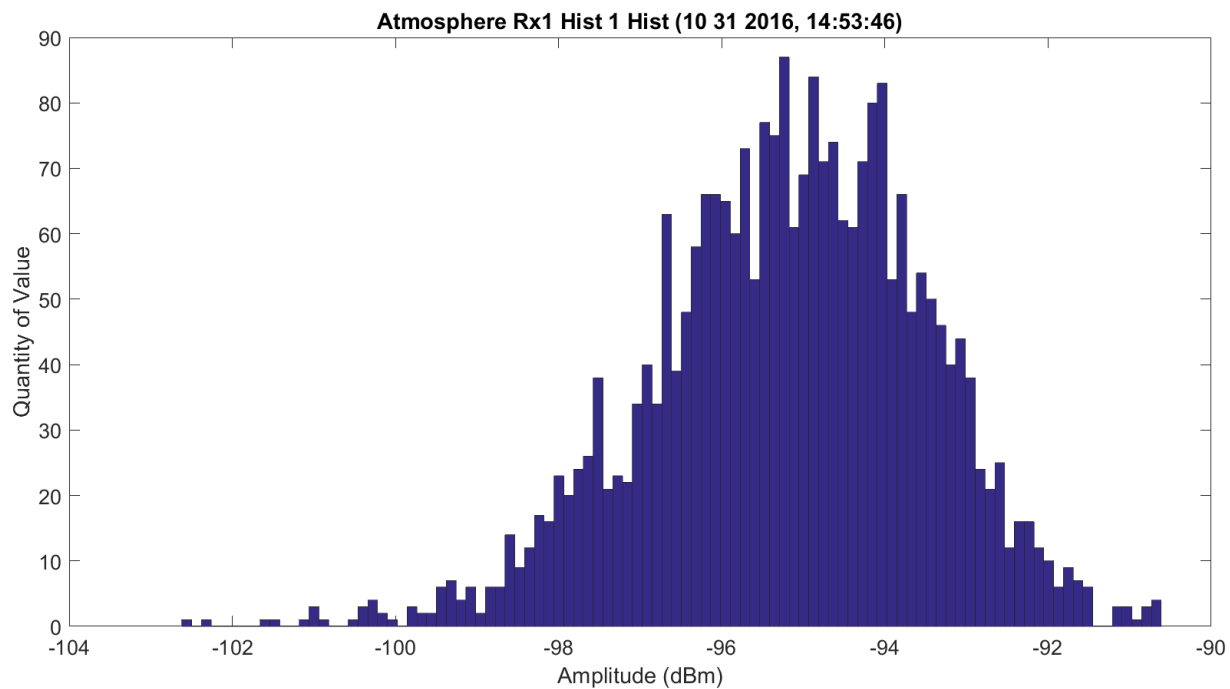


Figure 3.317. Hardware Excluded Histogram – 11012016_145401.

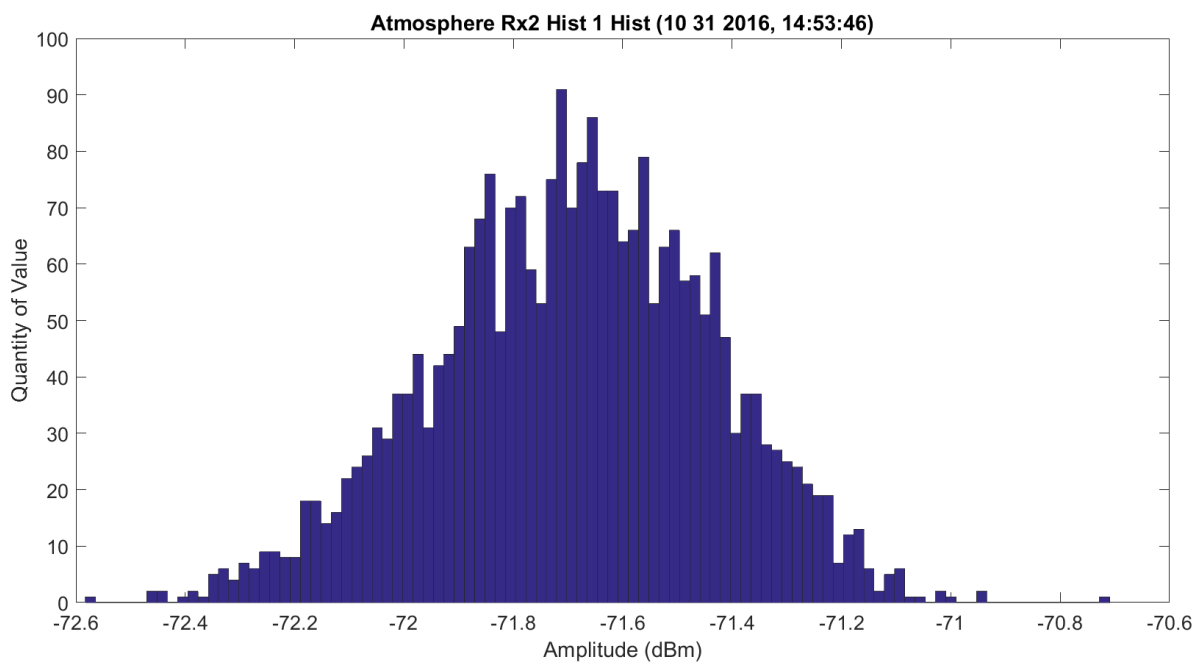


Figure 3.318. Hardware Excluded Histogram – 11012016_145401.

Figure 3.319 shows the WB mean amplitude for each frequency. This is Rx1 and looks like similar distortion.

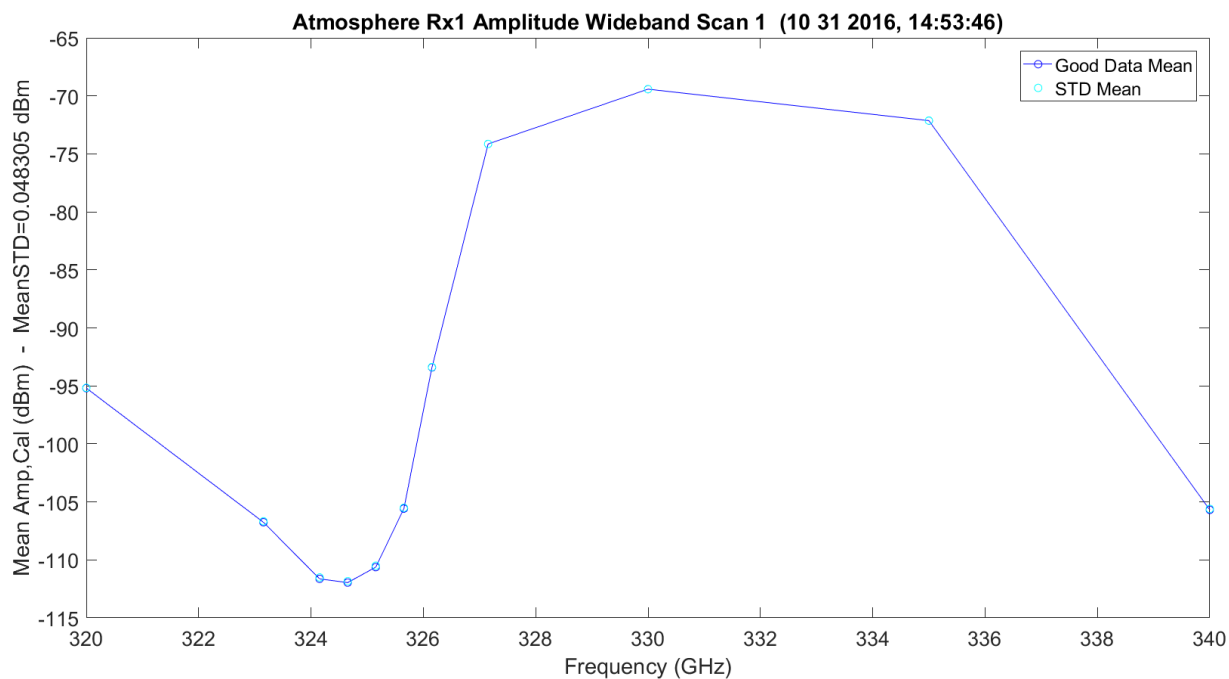


Figure 3.319. WB Amplitude No Hardware – 11012016_145401.

Figure 3.320 shows the WB mean amplitude with Friis and difference for each frequency.

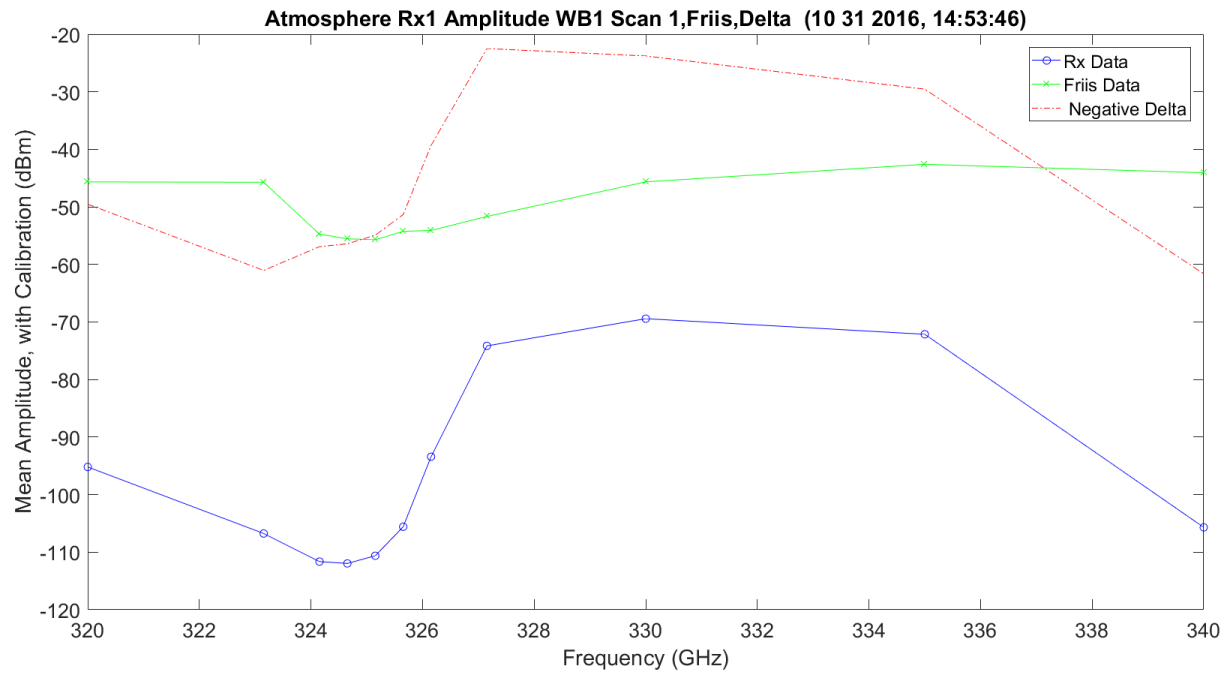


Figure 3.320. WB Amplitude No Hardware, Friis and Difference – 11012016_145401.

Figure 3.321 shows the WB mean amplitude normalized with Friis. In Rx1, the signal is lost for WB in this plot due to low SNR.

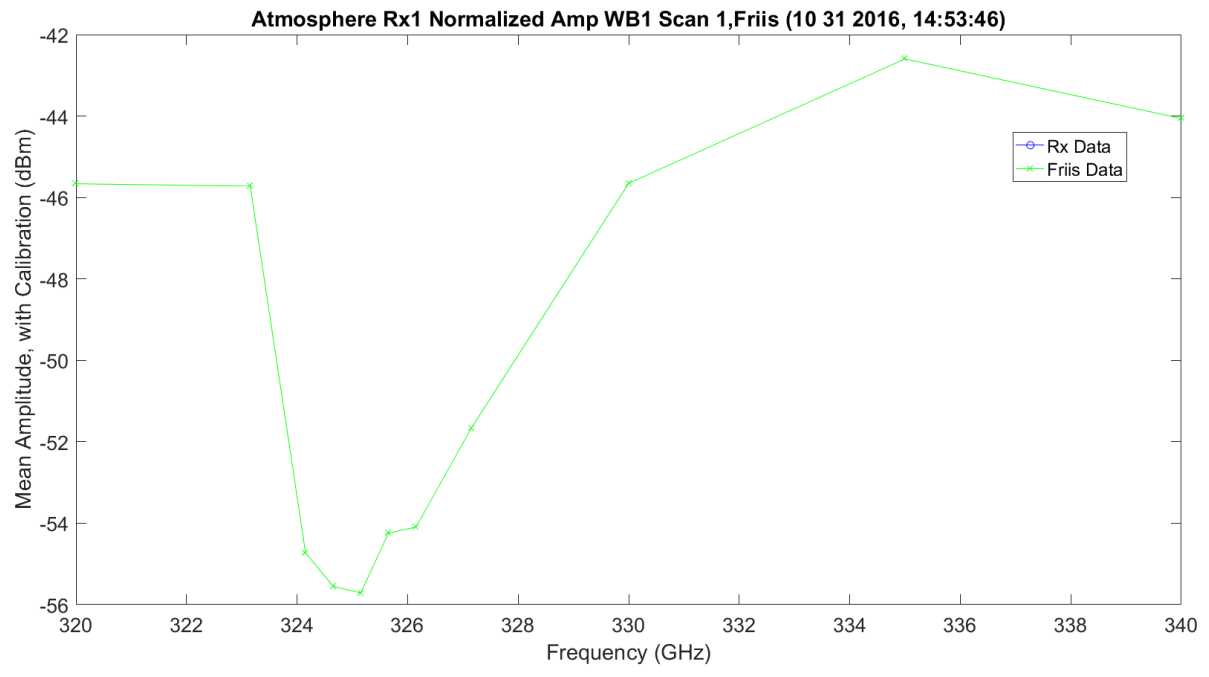


Figure 3.321. WB Normalized Amplitude No Hardware, Friis and Difference – 11012016_145401.

Figure 3.322 shows the LWL mean amplitude for each frequency.

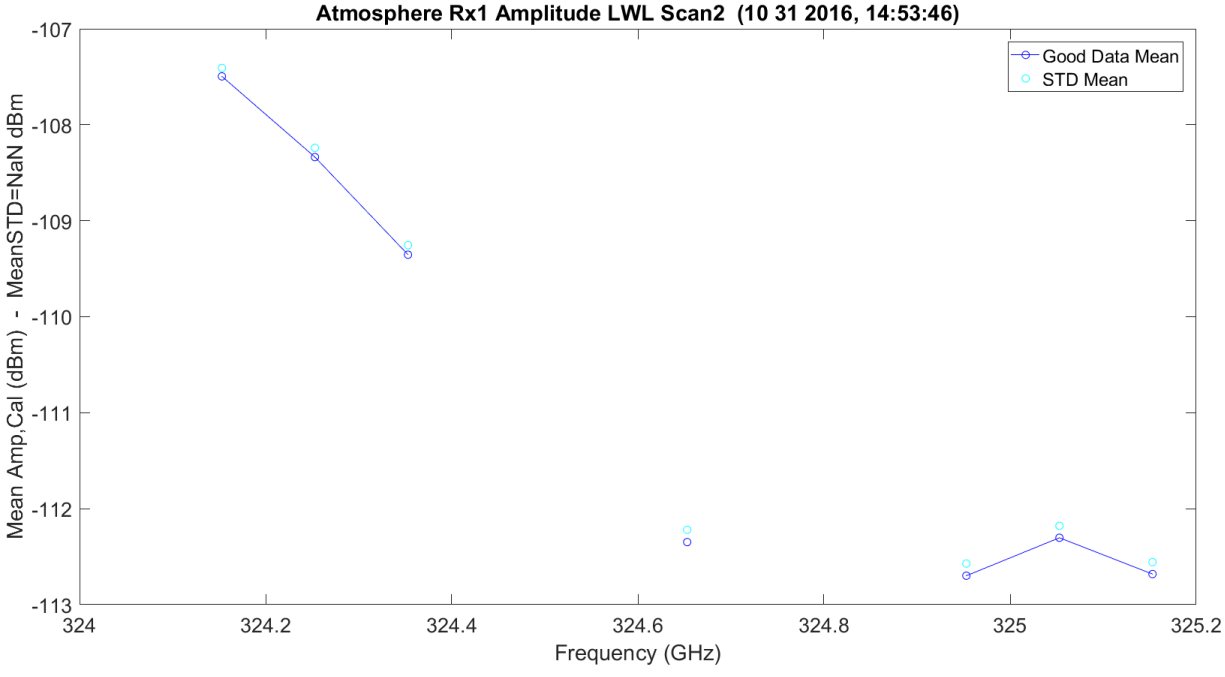


Figure 3.322. LWL Amplitude No Hardware – 11012016_145401.

Figure 3.323 shows the LWL mean amplitude with Friis and difference for each frequency.

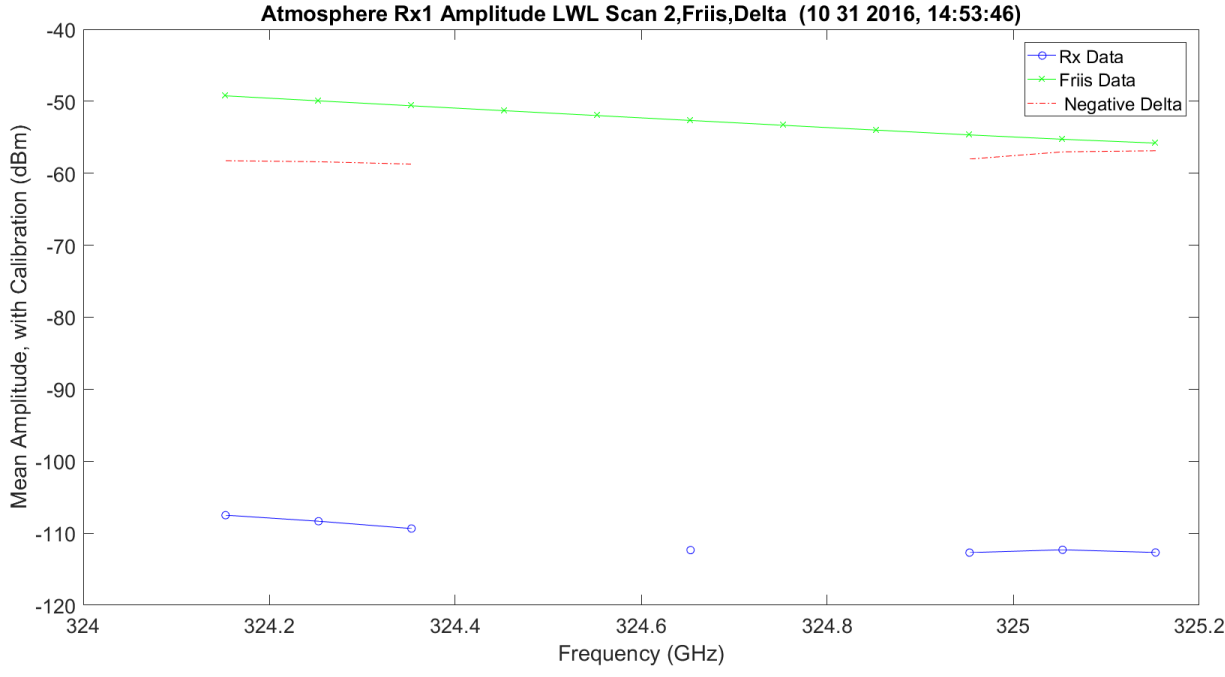


Figure 3.323. LWL Amplitude No Hardware, Friis and Difference – 11012016_145401.

Figure 3.324 shows the LWL mean amplitude normalized with Friis. The amplitude has a normalized linear difference. Again, Rx1, due to SNR, drops sometimes.

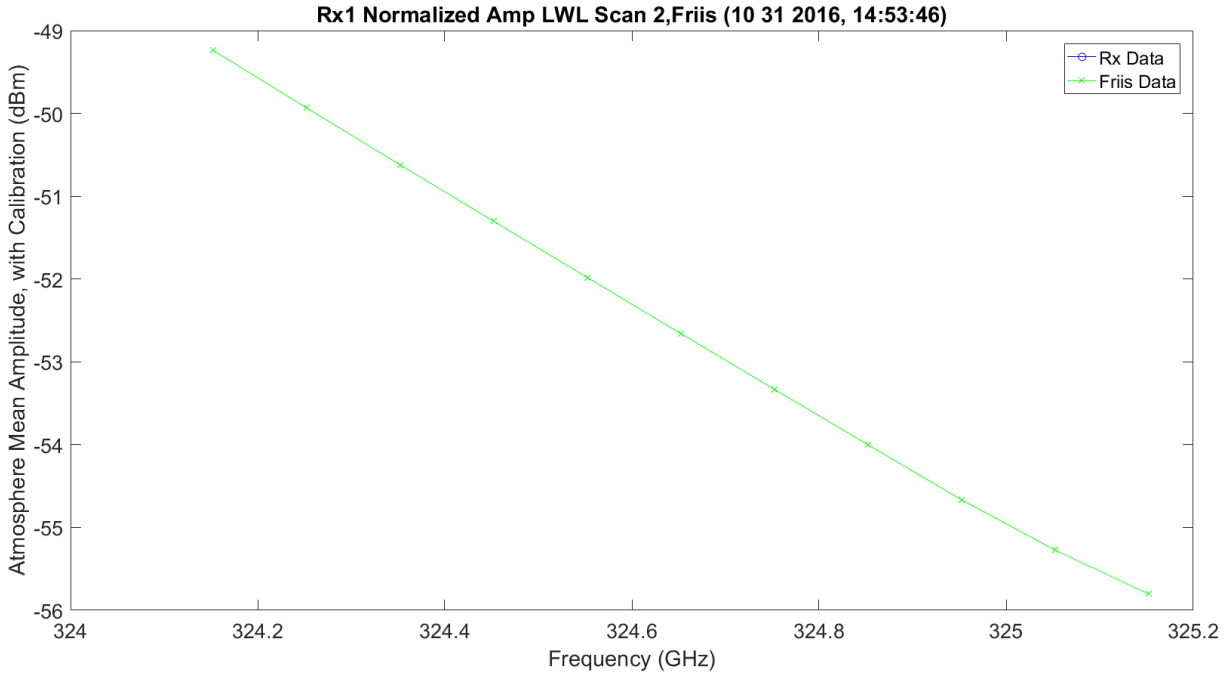


Figure 3.324. LWL Normalized Amplitude No Hardware, Friis and Difference – 1012016_145401.

Figure 3.325 shows the UWL mean amplitude for each frequency.

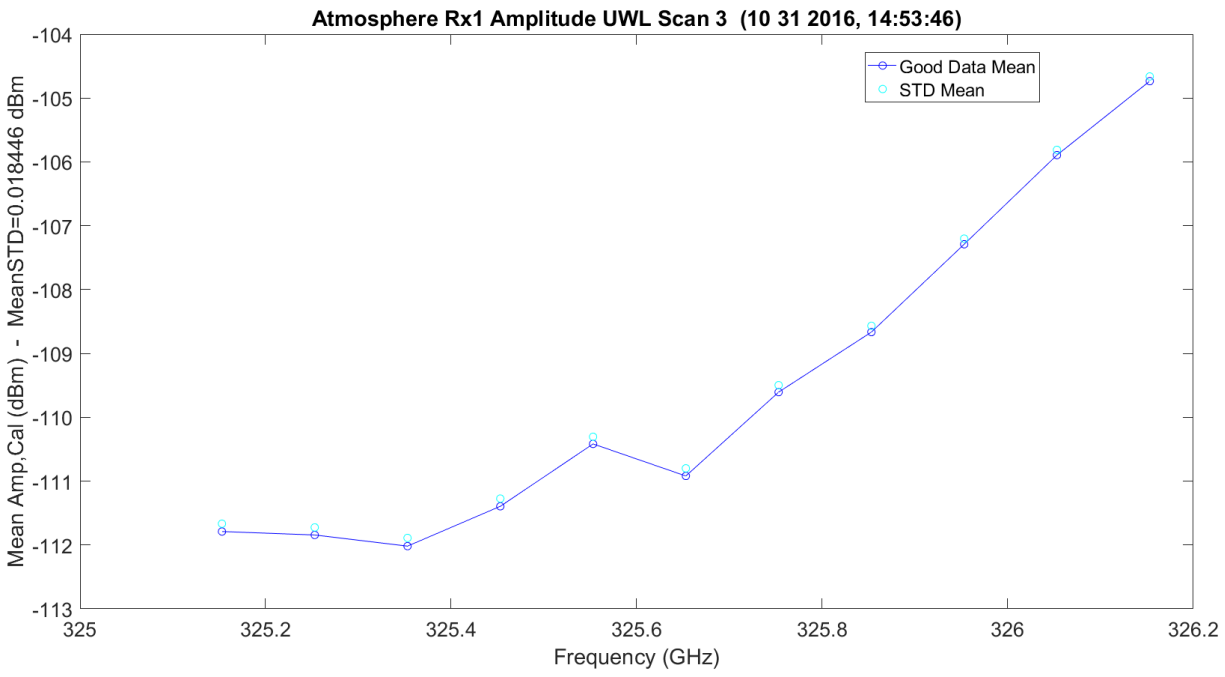


Figure 3.325. UWL Amplitude No Hardware – 11012016_145401.

Figure 3.326 shows the UWL mean amplitude with Friis and difference for each frequency.

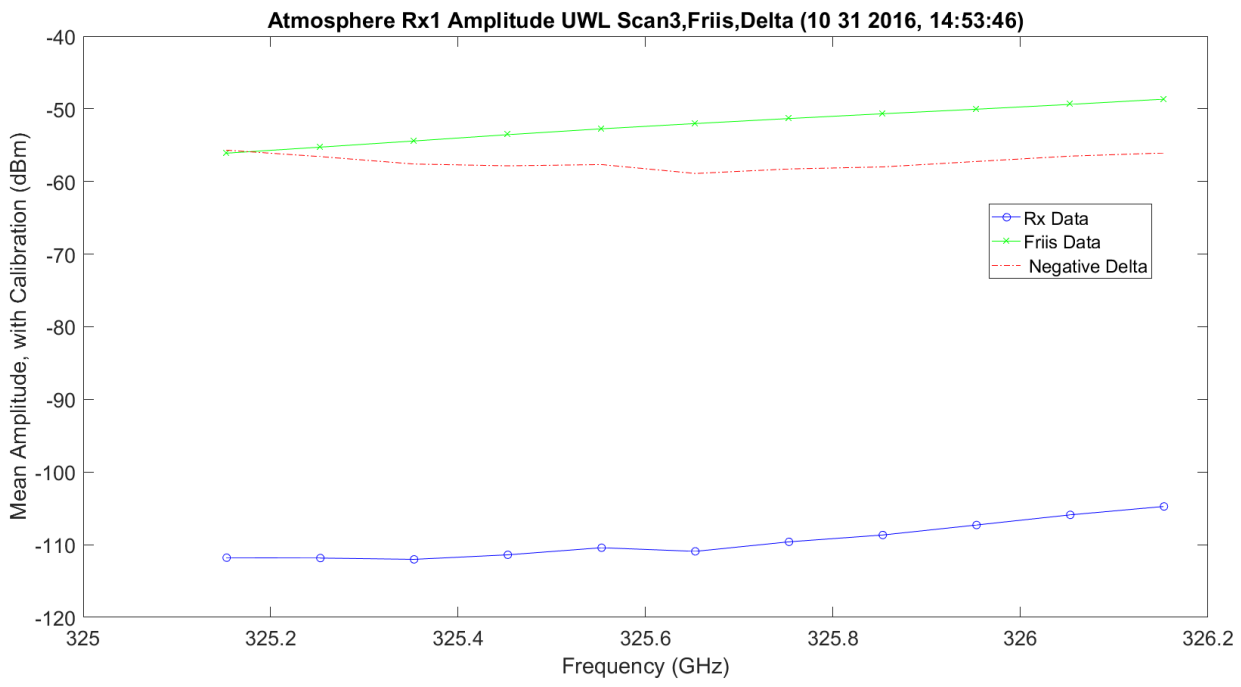


Figure 3.326. UWL Amplitude No Hardware, Friis and Difference – 11012016_145401.

Figure 3.327 shows the UWL mean amplitude normalized with Friis. The amplitude has a normalized linear difference.

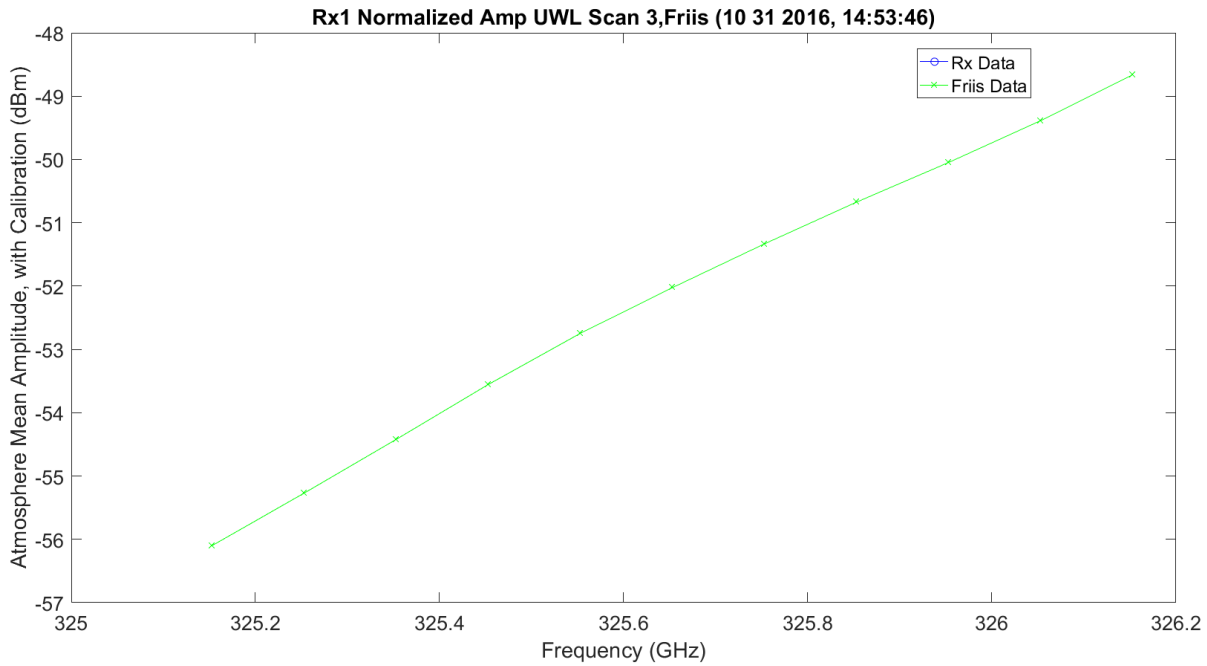


Figure 3.327. UWL Amplitude No Hardware, Friis and Difference – 11012016_145401.

Figure 3.328 – Figure 3.336 shows the same plots for Rx1 for the second set of three-11 frequency scans; these are the last 33 frequency changes on the total 66 frequencies.

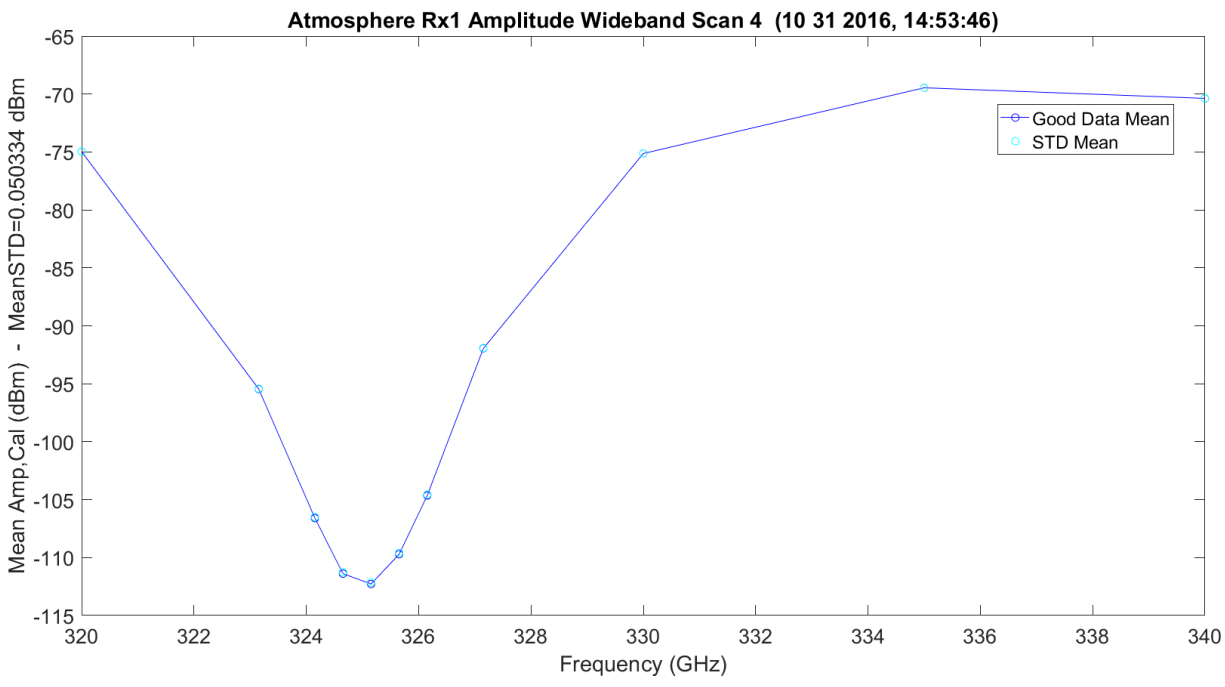


Figure 3.328. WB Scan 4 Amplitude No Hardware – 11012016_145401.

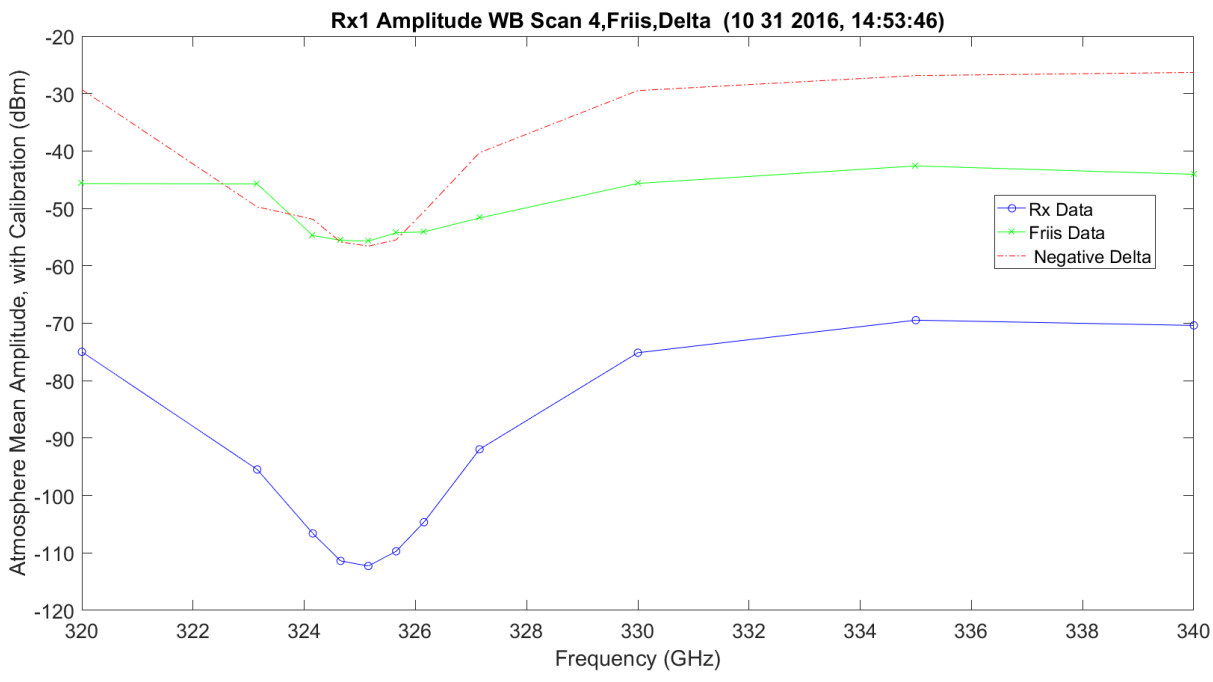


Figure 3.329. WB Scan 4 Amplitude No Hardware, Friis and Difference – 11012016_145401.

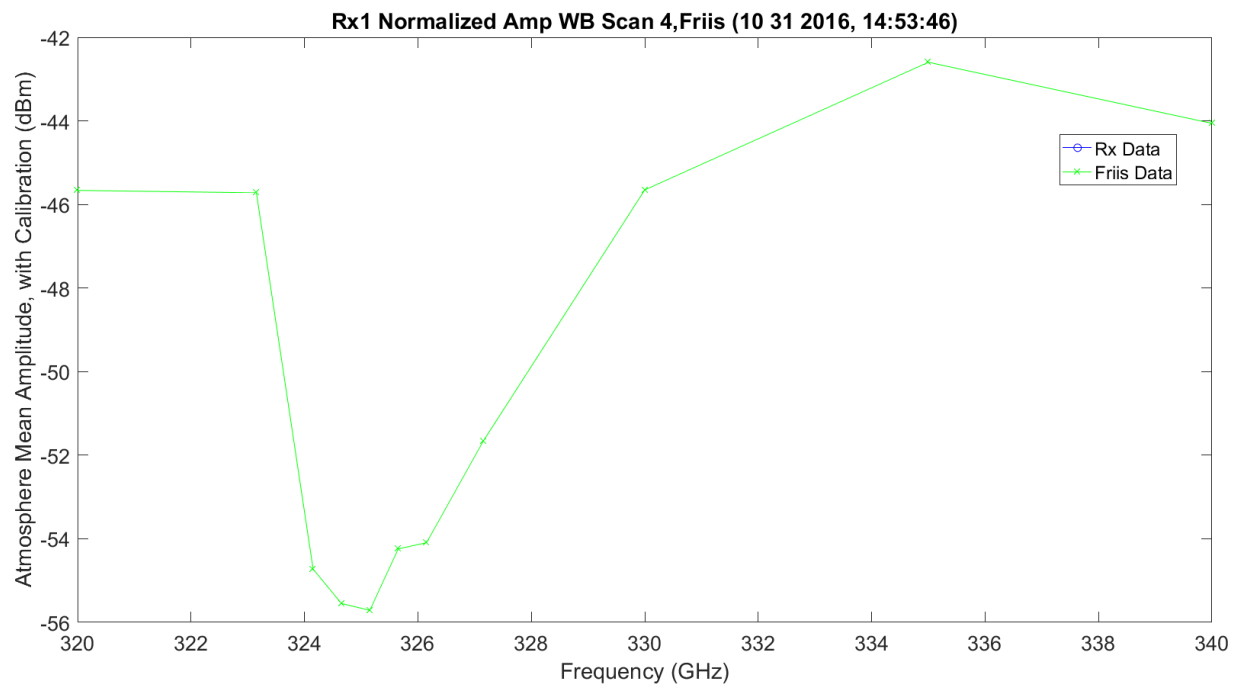


Figure 3.330. WB Scan 4 Amplitude No Hardware, Friis and Difference – 11012016_145401.

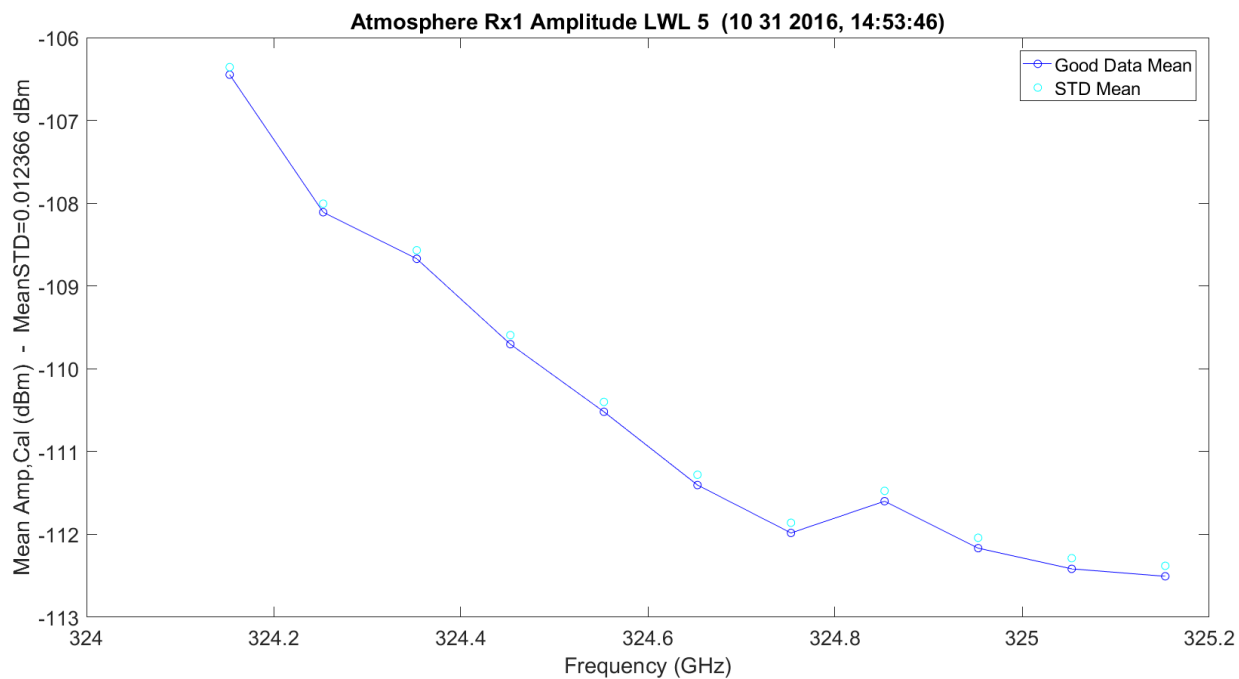


Figure 3.331. LWL Scan 5 Amplitude No Hardware – 11012016_145401.

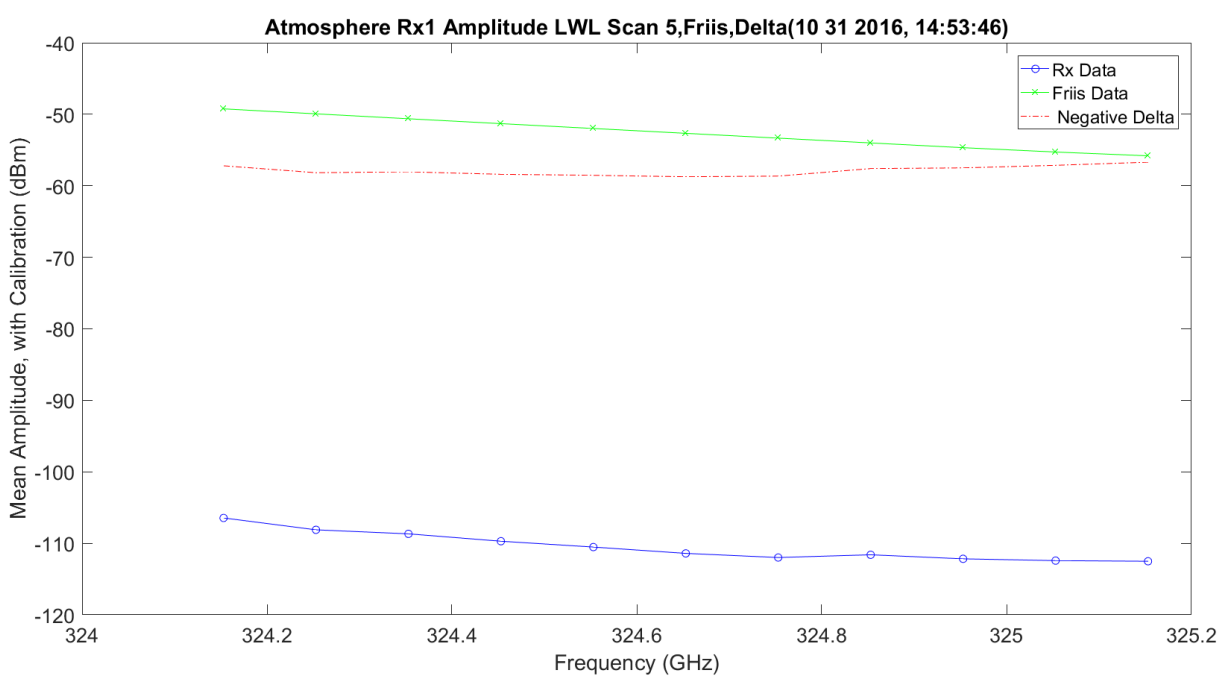


Figure 3.332. LWL Scan 5 Amplitude No Hardware, Friis and Difference – 11012016_145401.

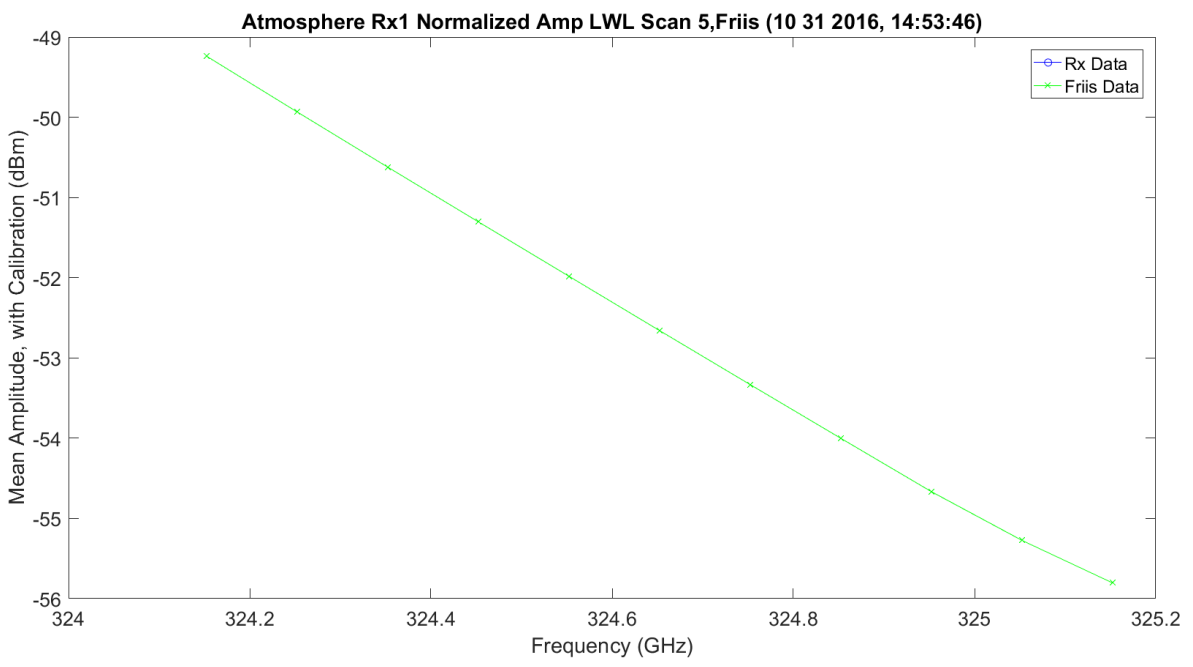


Figure 3.333. LWL Scan 5 Amplitude No Hardware, Friis and Difference – 11012016_145401.

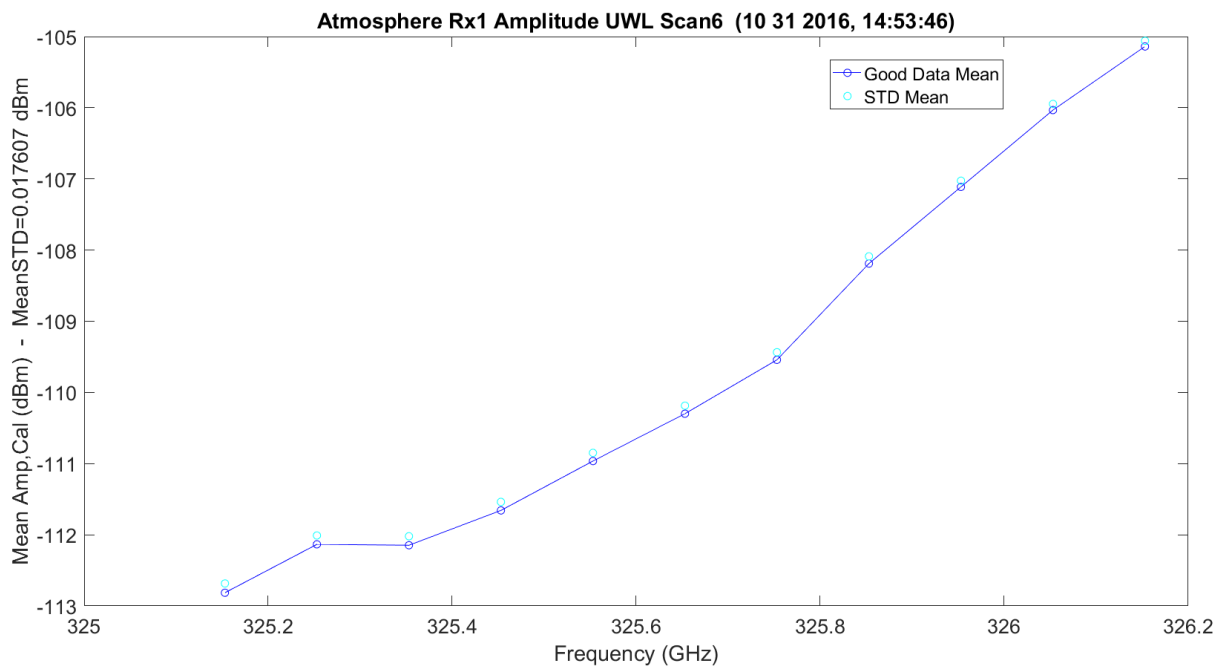


Figure 3.334. UWL Scan 6 Amplitude No Hardware – 11012016_145401.

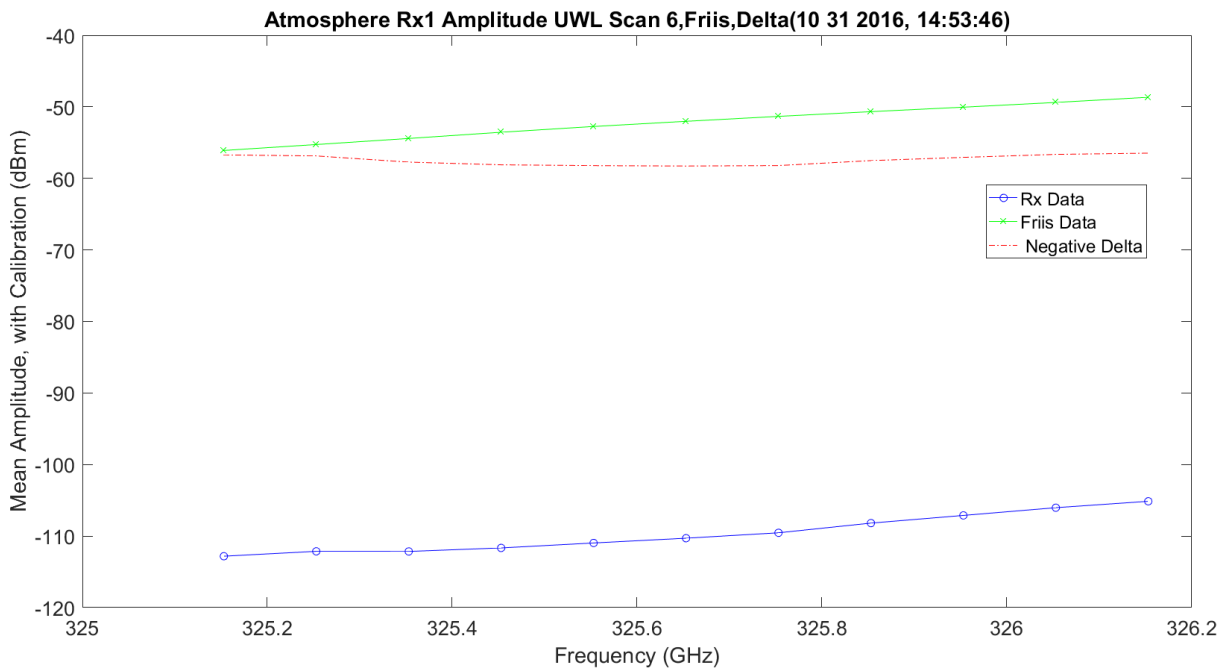


Figure 3.335. UWL Scan 6 Amplitude No Hardware, Friis and Difference – 11012016_145401.

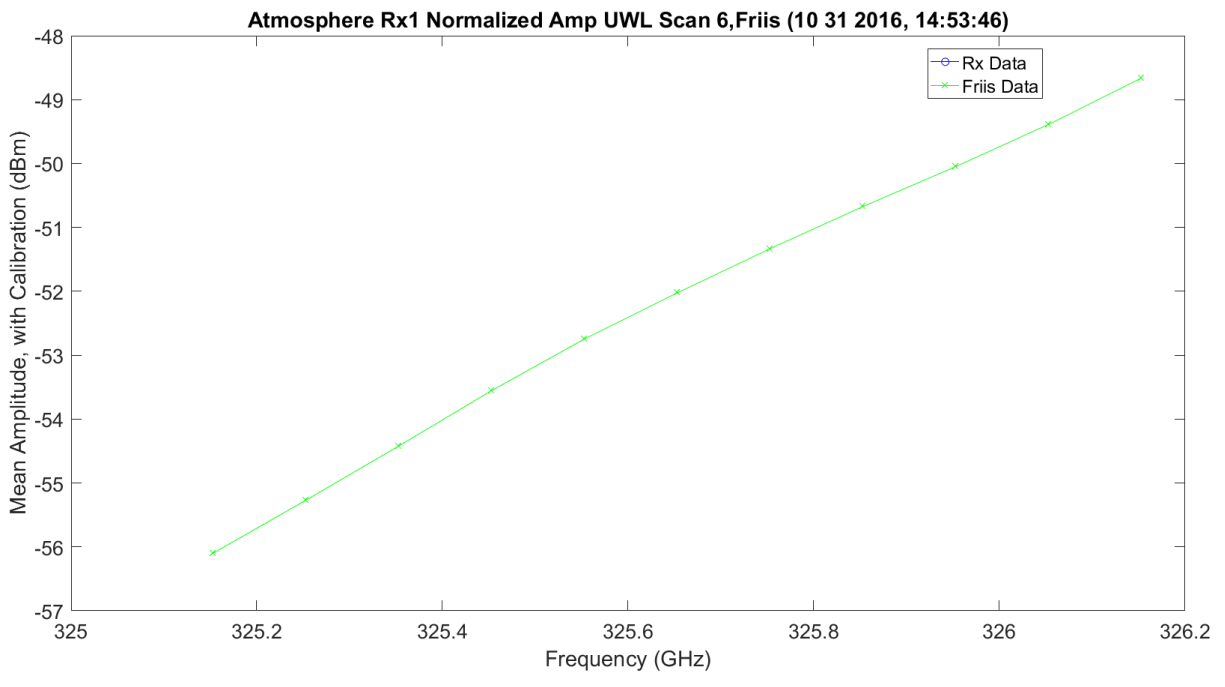


Figure 3.336. UWL Scan 6 Amplitude No Hardware, Friis and Difference – 11012016_145401.

Figure 3.337 shows the normalized and predicted plots with Friis vs. the LWL and UWL flipped to compare the two slopes. These are very similar to earlier plots.

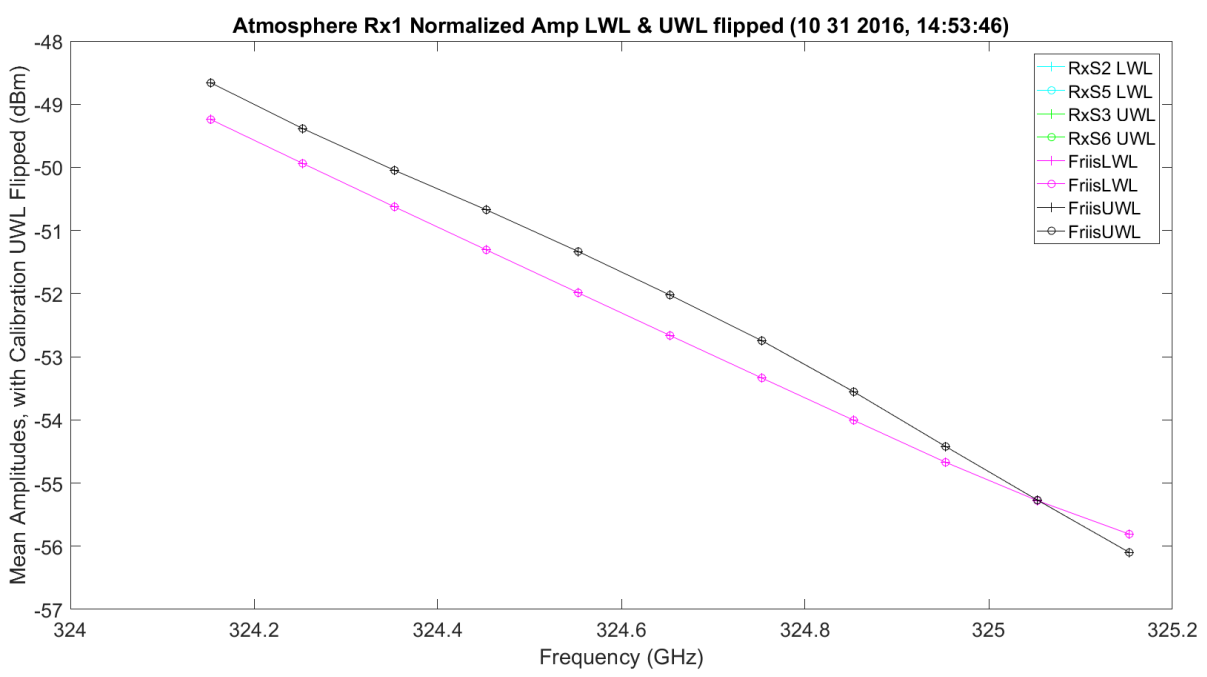


Figure 3.337. LWL & UWL Flipped Mean Amplitude No Hardware – 11012016_145401.

Figure 3.338 shows the WB mean amplitude for each frequency for Rx2. This matches all the above, only with better data due to the larger SNR. Figure 3.339 - Figure 3.339 are much better data, but match the Rx1 in the description above.

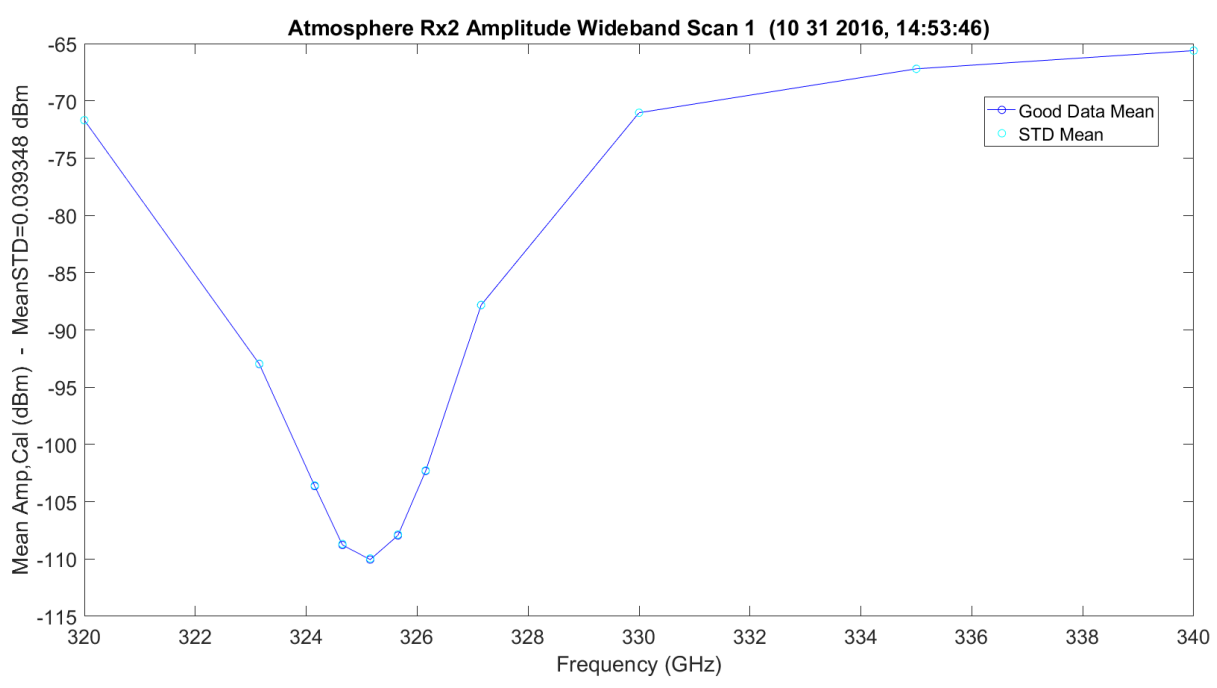


Figure 3.338. WB Amplitude No Hardware – 11012016_145401.

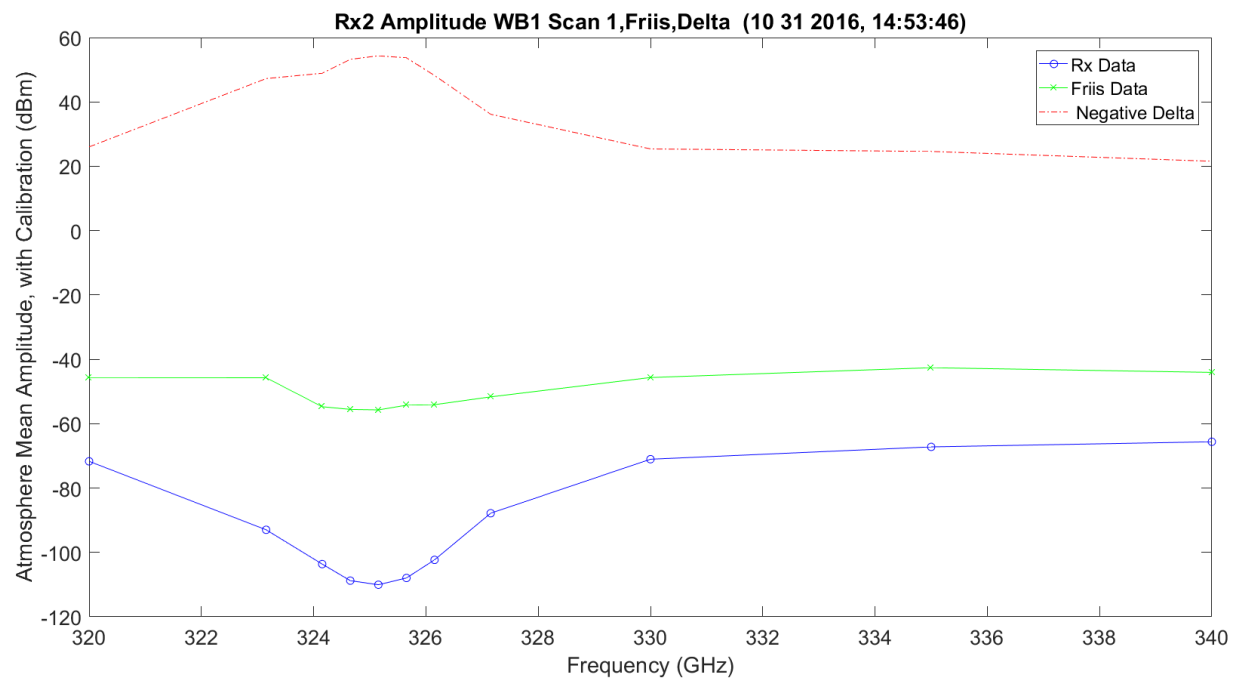


Figure 3.339. WB Amplitude No Hardware, Friis and Difference – 11012016_145401.

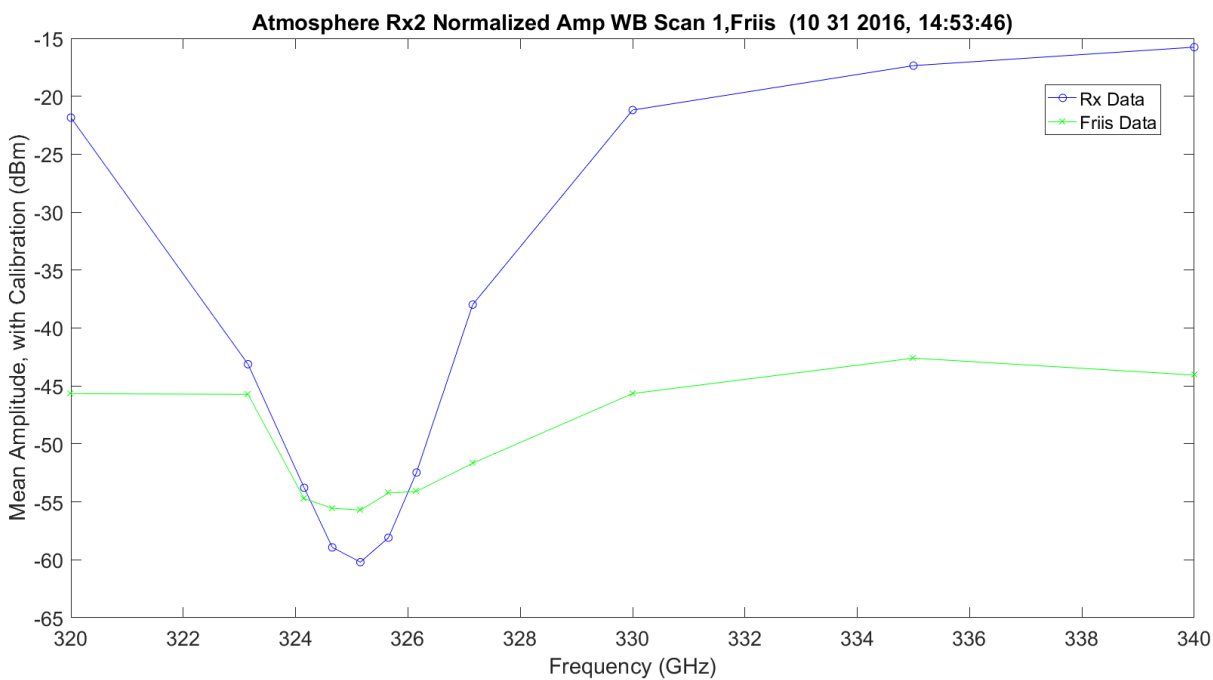


Figure 3.340. WB Normalized Amplitude No Hardware, Friis and Difference – 11012016_145401.

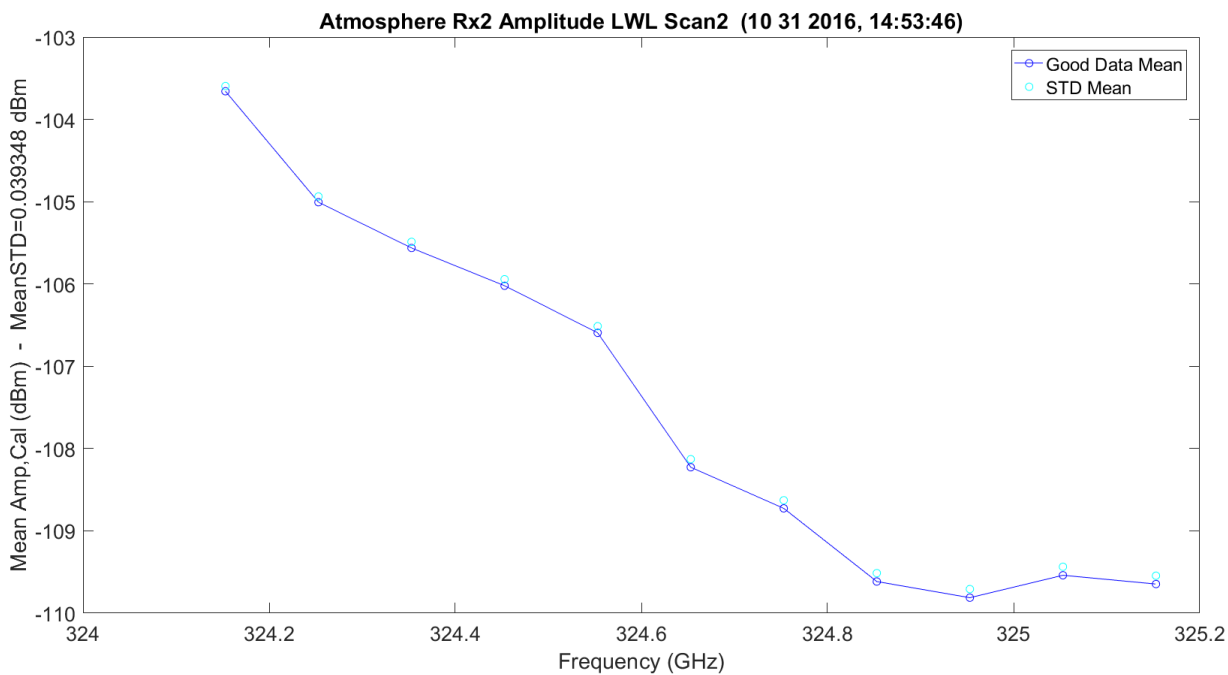


Figure 3.341. LWL Amplitude No Hardware – 11012016_145401.

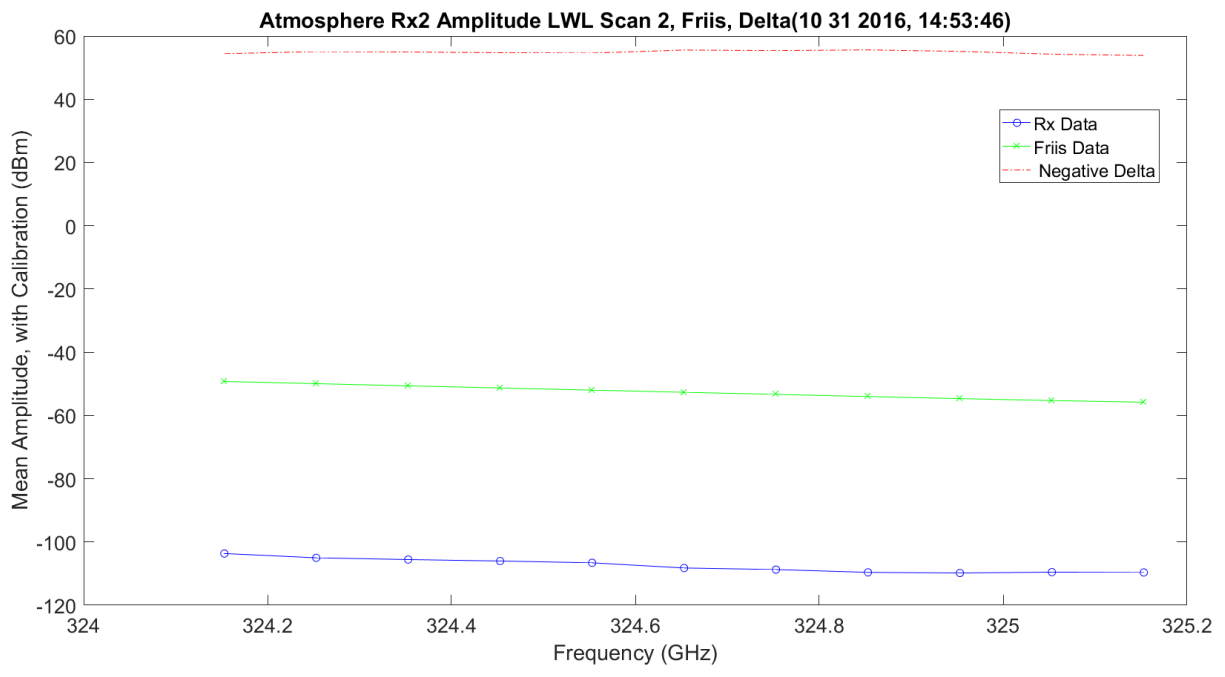


Figure 3.342. LWL Amplitude No Hardware, Friis and Difference – 11012016_145401.

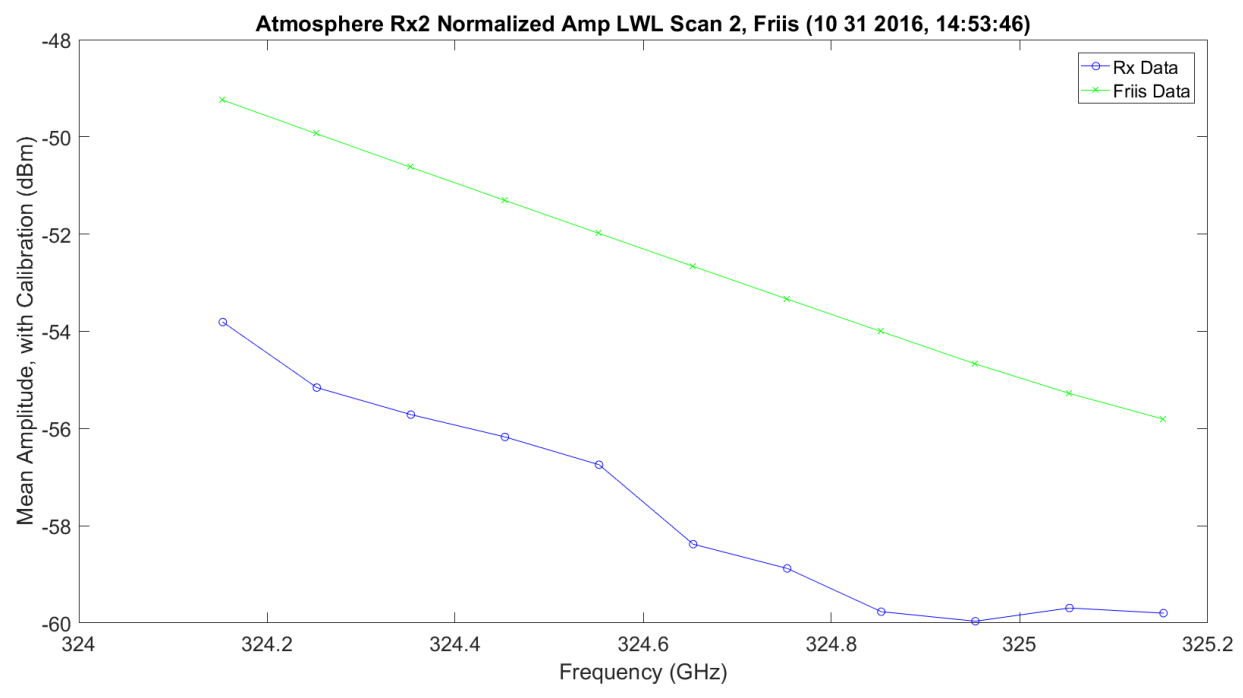


Figure 3.343. LWL Normalized Amplitude No Hardware, Friis and Difference – 11012016_145401.

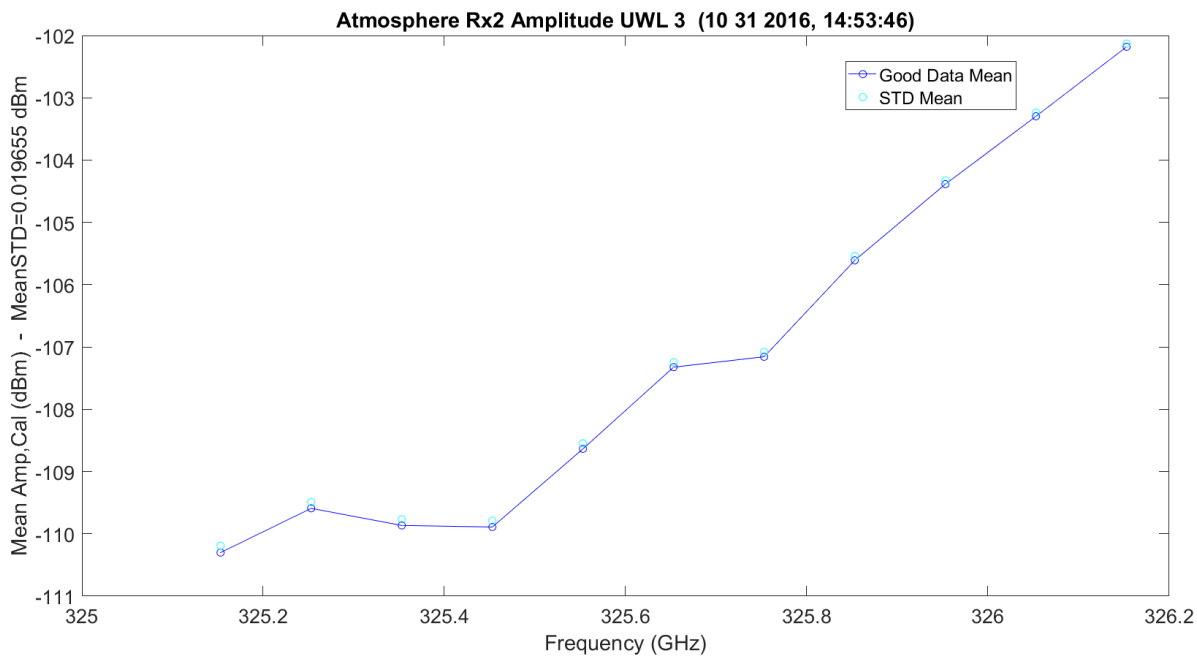


Figure 3.344. UWL Amplitude No Hardware – 11012016_145401.

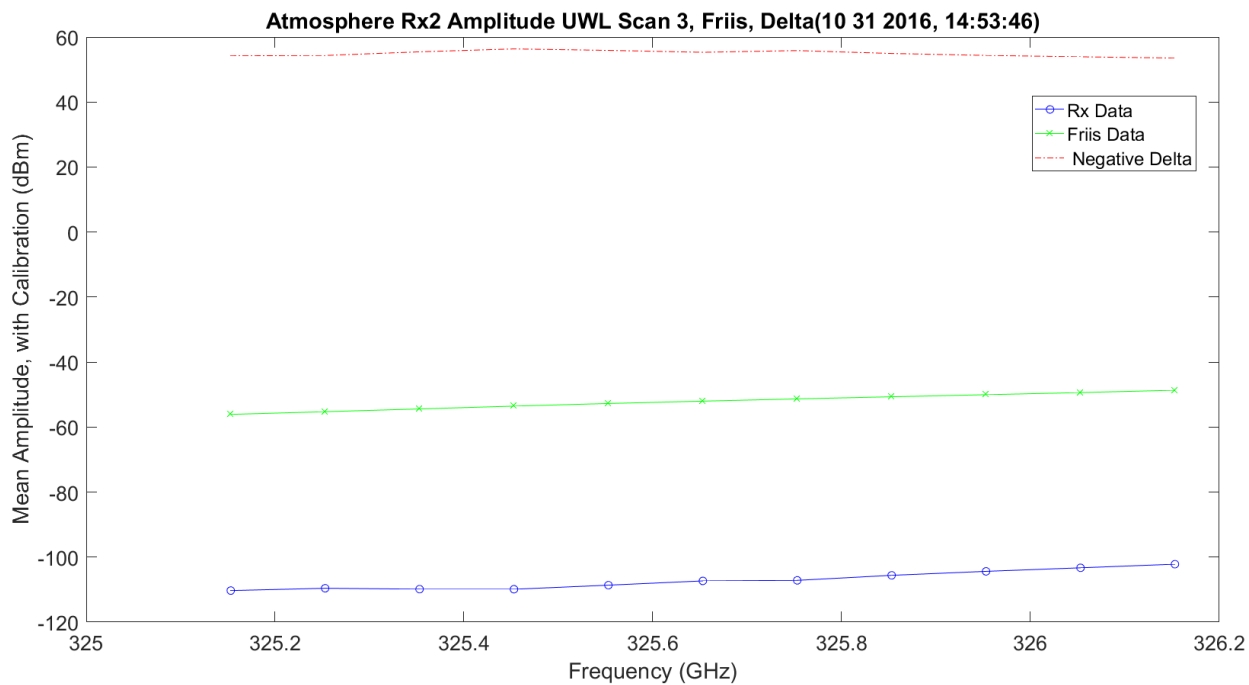


Figure 3.345. UWL Amplitude No Hardware, Friis and Difference – 11012016_145401.

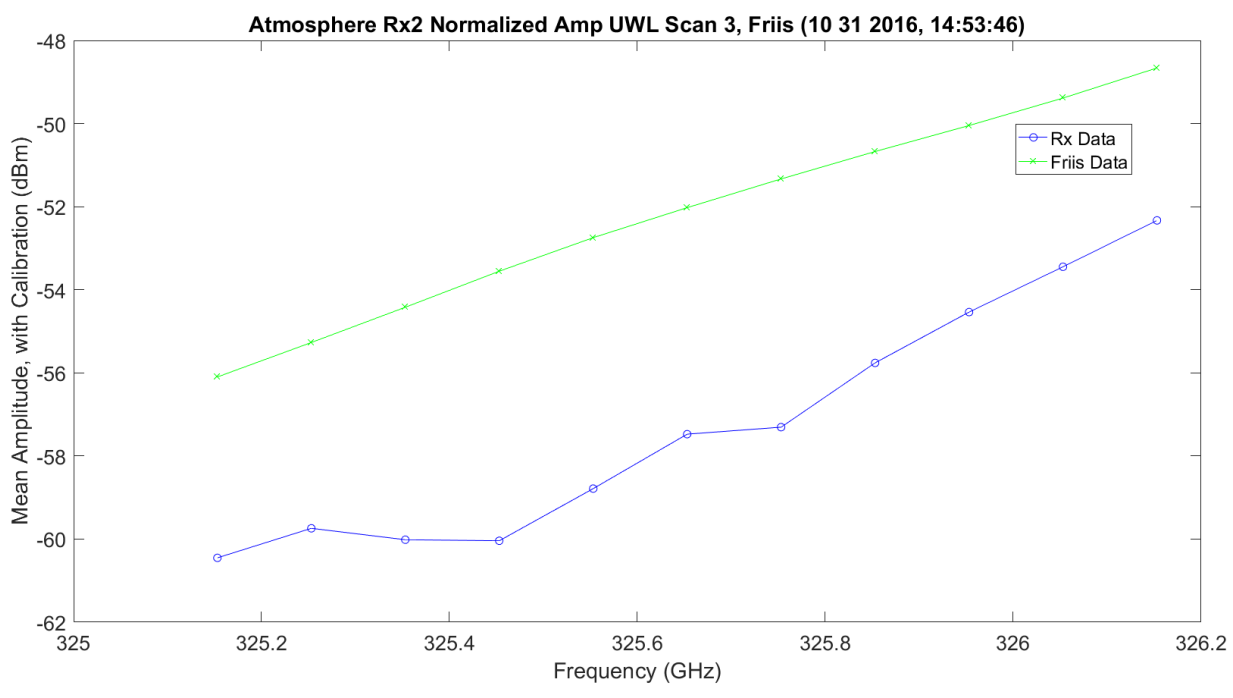


Figure 3.346. UWL Amplitude No Hardware, Friis and Difference – 11012016_145401.

Figure 3.347 – Figure 3.347 show the same plots for the second set of three-11 frequency scans; these are the last 33 frequency changes on the 66 total frequencies. Rx2 has very good data.

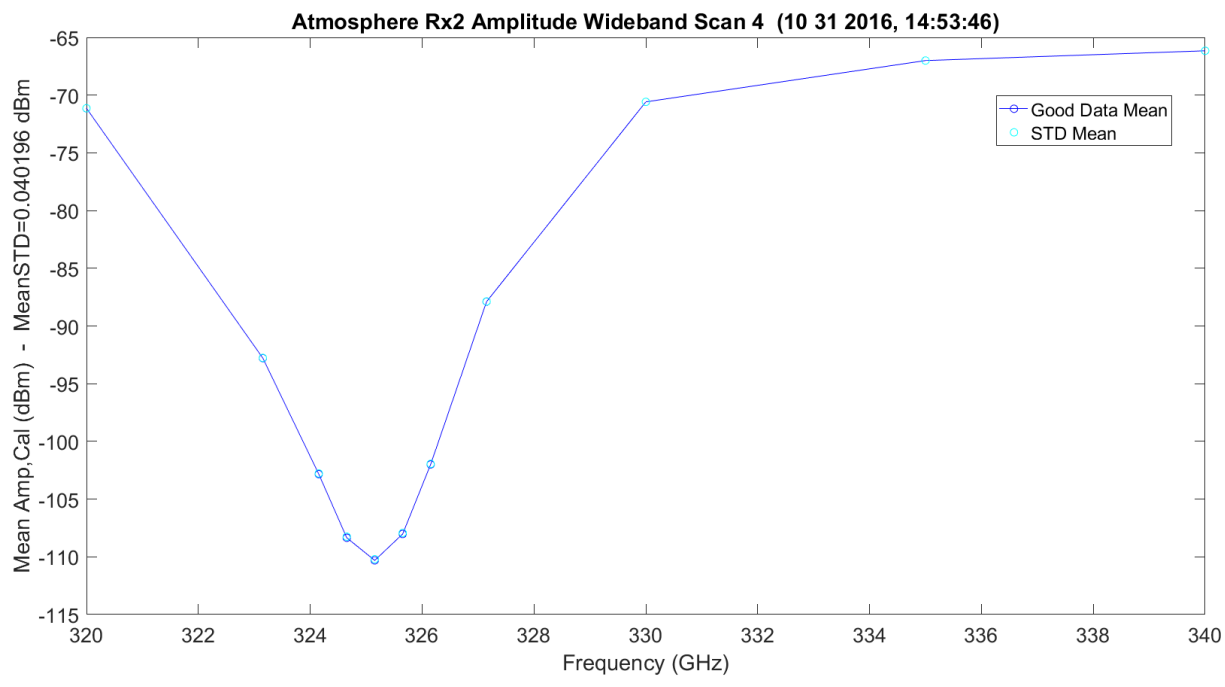


Figure 3.347. WB Scan 4 Amplitude No Hardware – 11012016_145401.

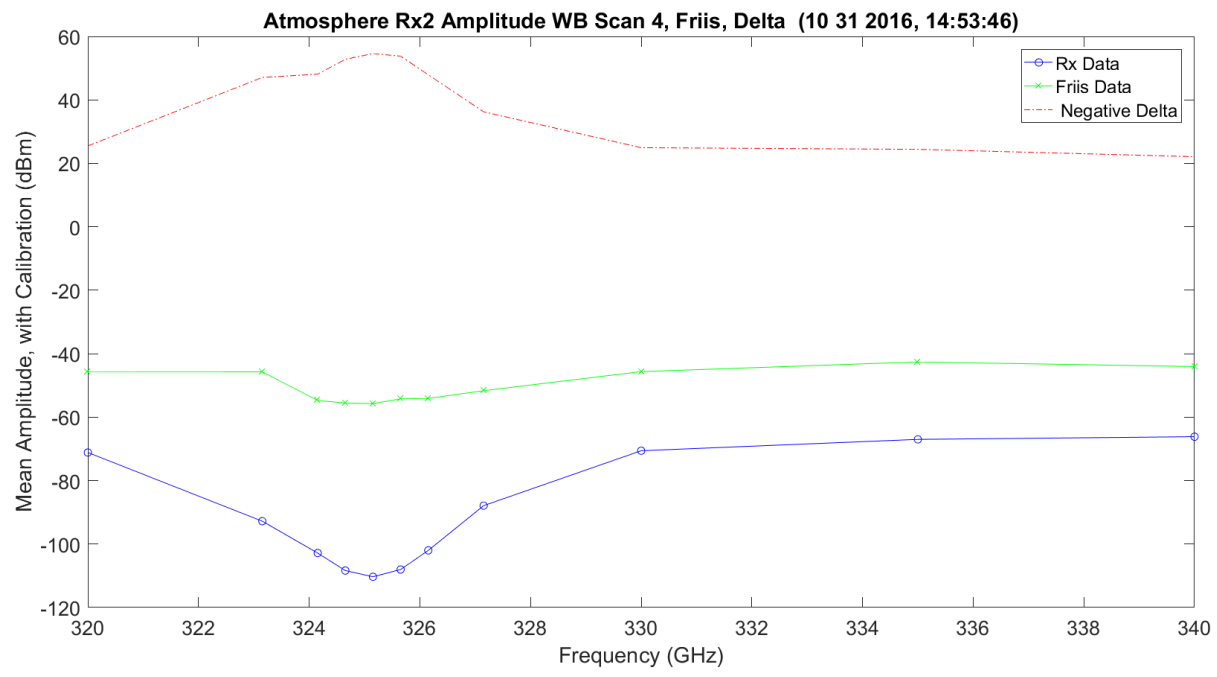


Figure 3.348. WB Scan 4 Amplitude No Hardware, Friis and Difference – 11012016_145401.

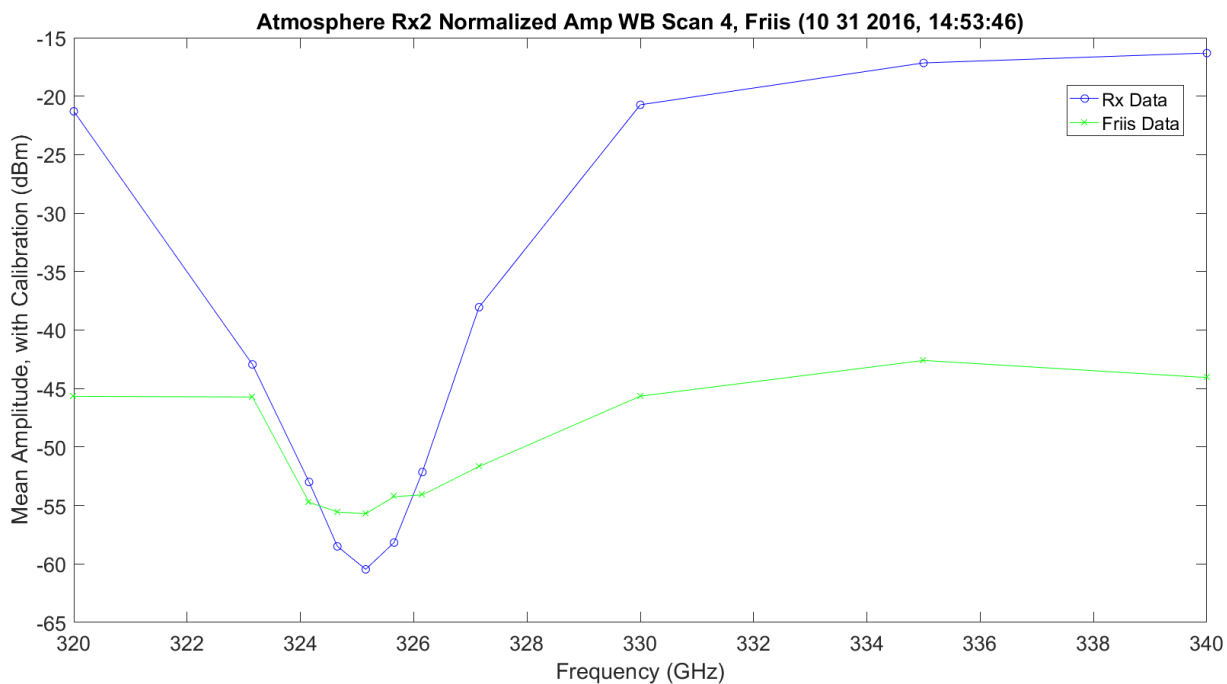


Figure 3.349. WB Scan 4 Amplitude No Hardware, Friis and Difference - 11012016_145401.

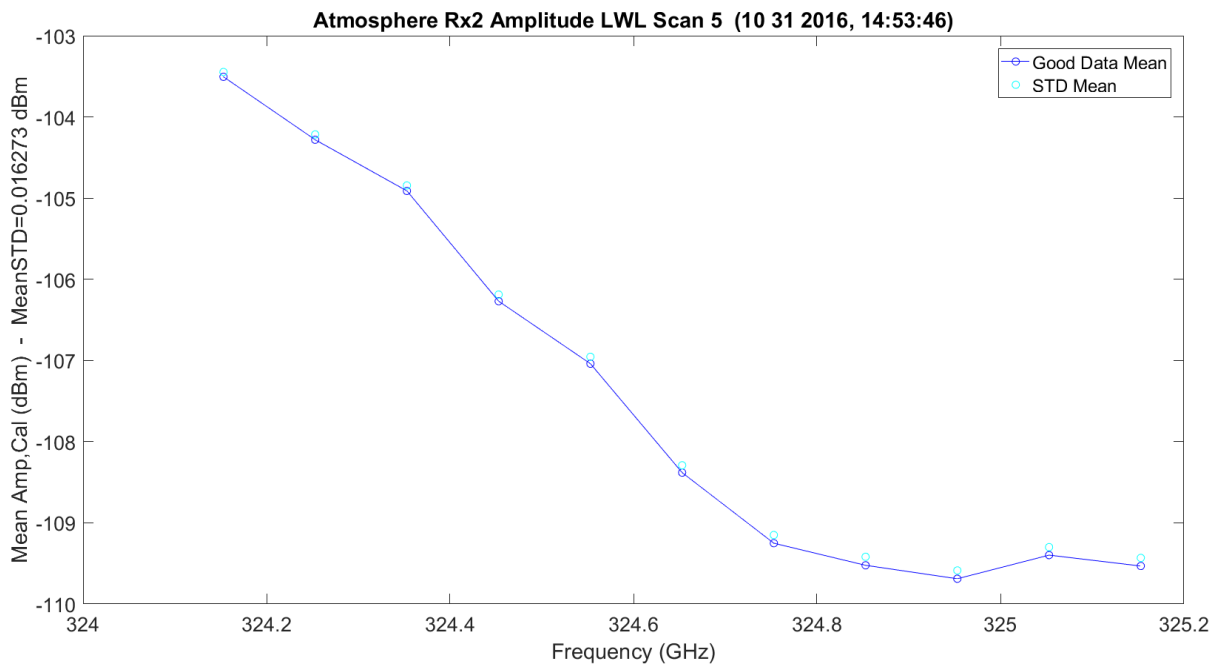


Figure 3.350. LWL Scan 5 Amplitude No Hardware – 11012016_145401.

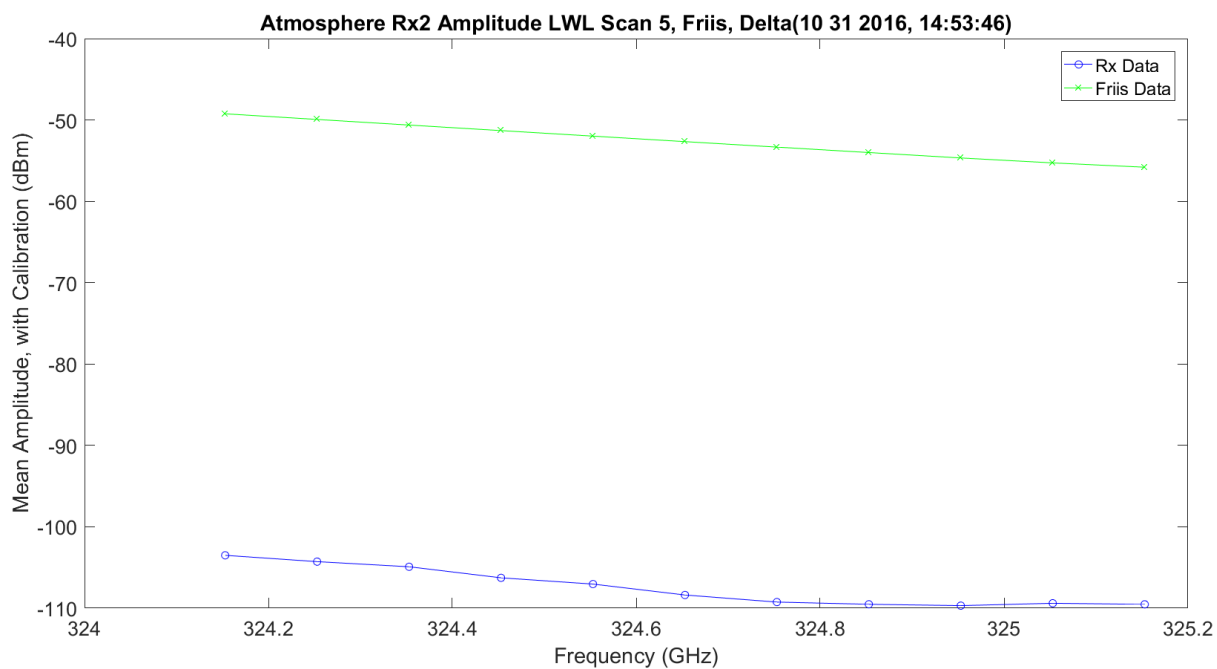


Figure 3.351. LWL Scan 5 Amplitude No Hardware, Friis and Difference – 11012016_145401.

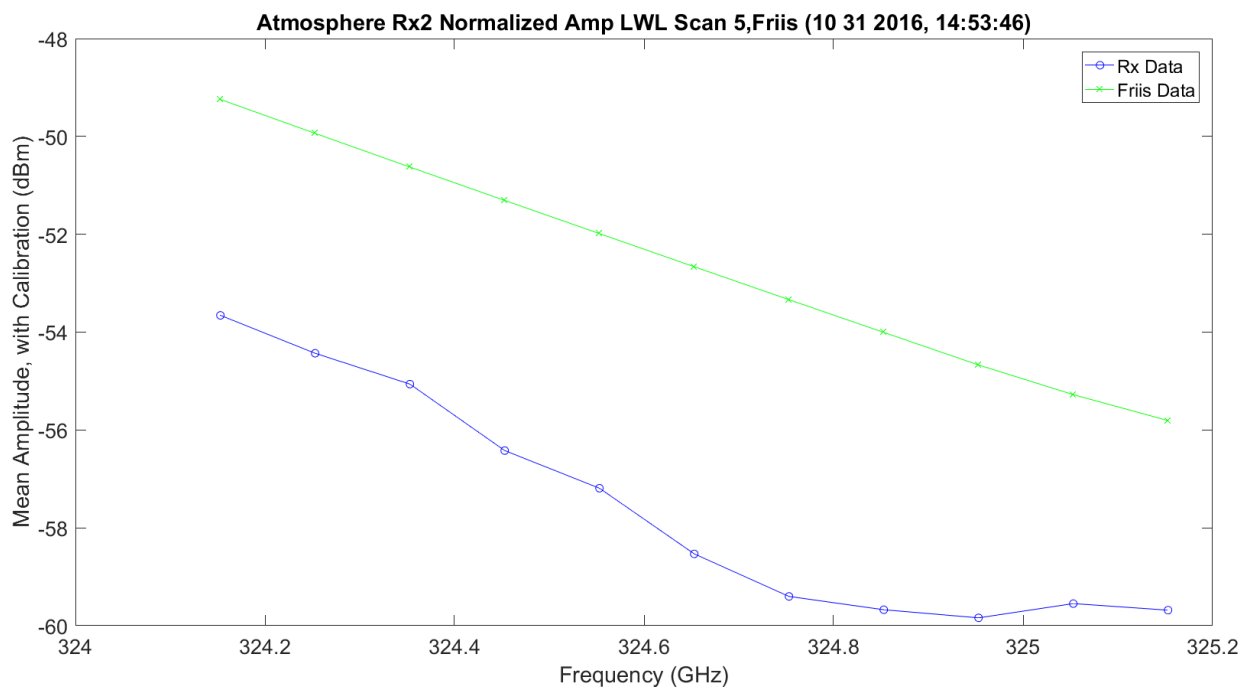


Figure 3.352. LWL Scan 5 Amplitude No Hardware, Friis and Difference – 11012016_145401.

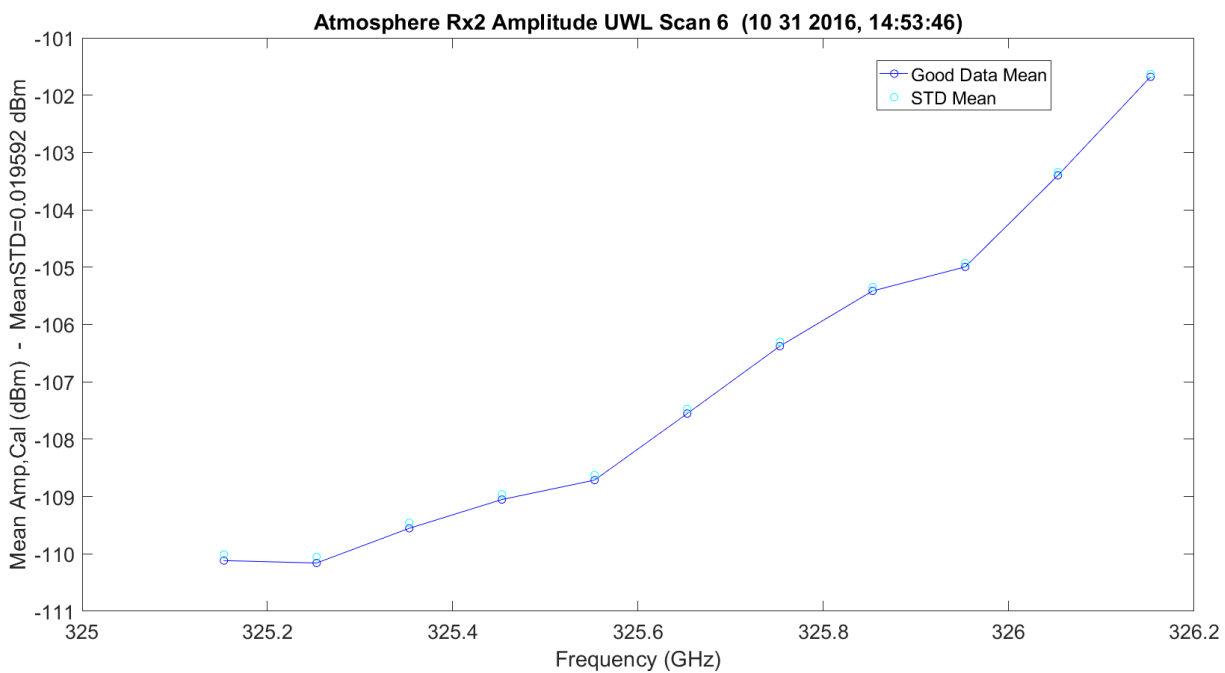


Figure 3.353. UWL Scan 6 Amplitude No Hardware – 11012016_145401.

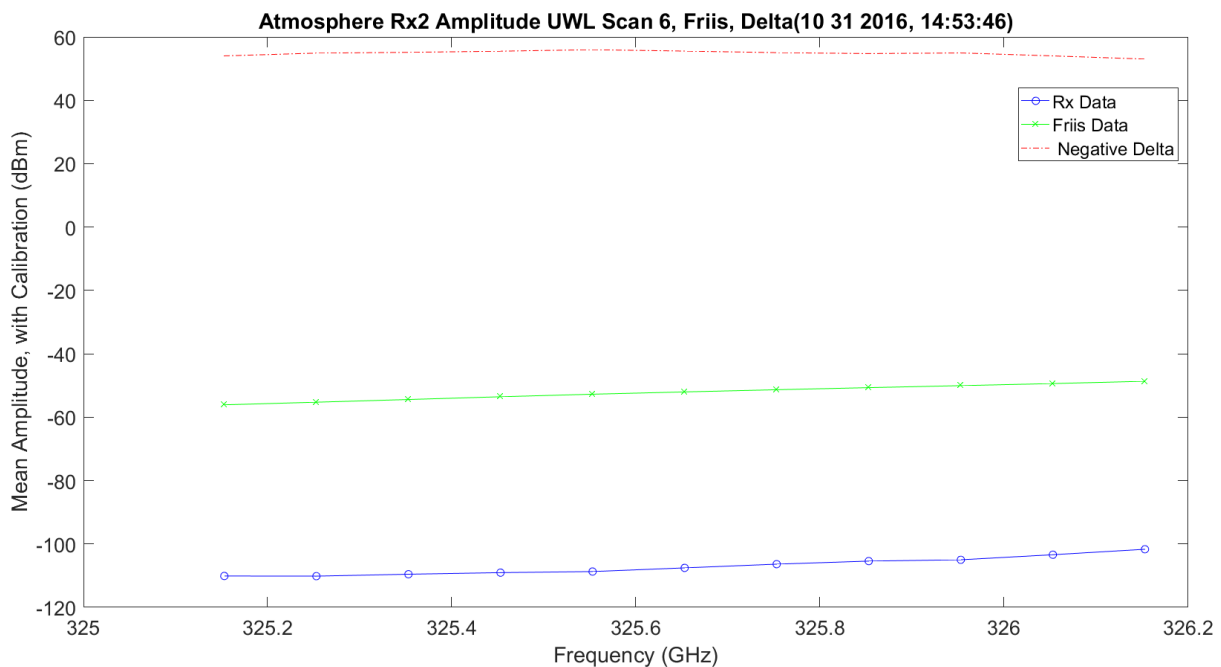


Figure 3.354. UWL Scan 6 Amplitude No Hardware, Friis and Difference – 11012016_145401.

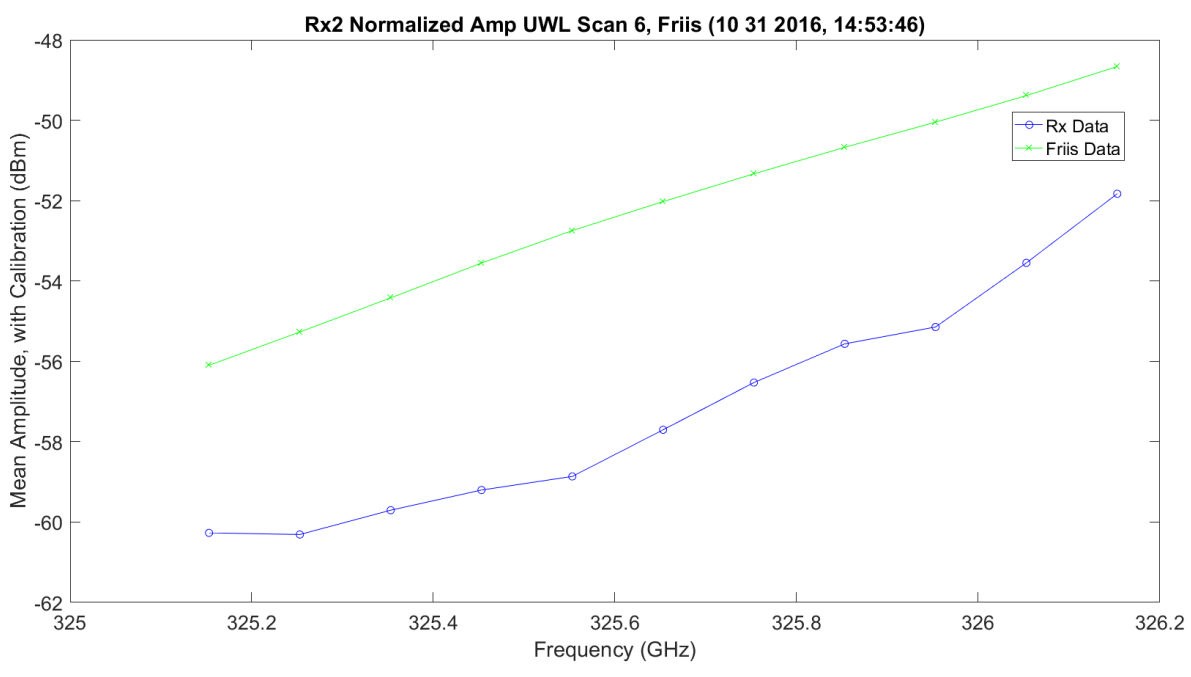


Figure 3.355. UWL Scan 6 Amplitude No Hardware, Friis and Difference – 11012016_145401.

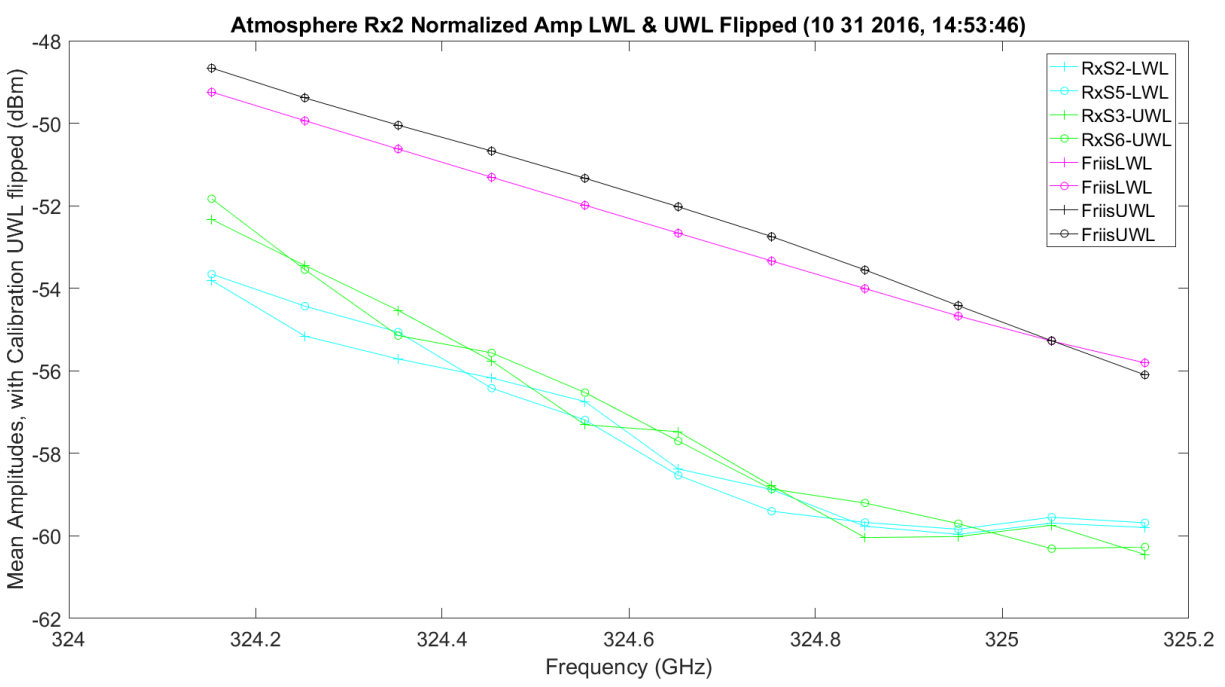


Figure 3.356. LWL & UWL Flipped Mean Amplitude No Hardware – 11012016_145401.

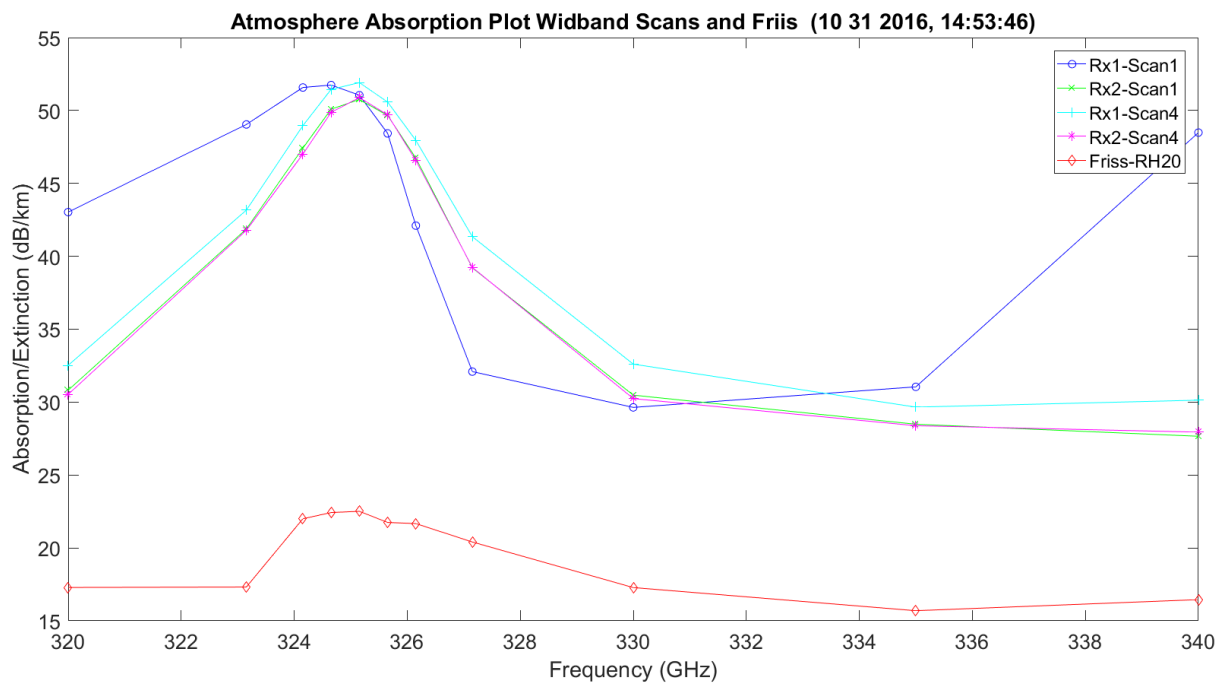


Figure 3.357. WB Extinction with No Hardware – 11012016_145401.

Figure 3.358 shows the LWL absorption plot. The red plot represents the Friis view at 20% RH. The data from TAIPAS was approximately at 30%+ RH, but is still higher.

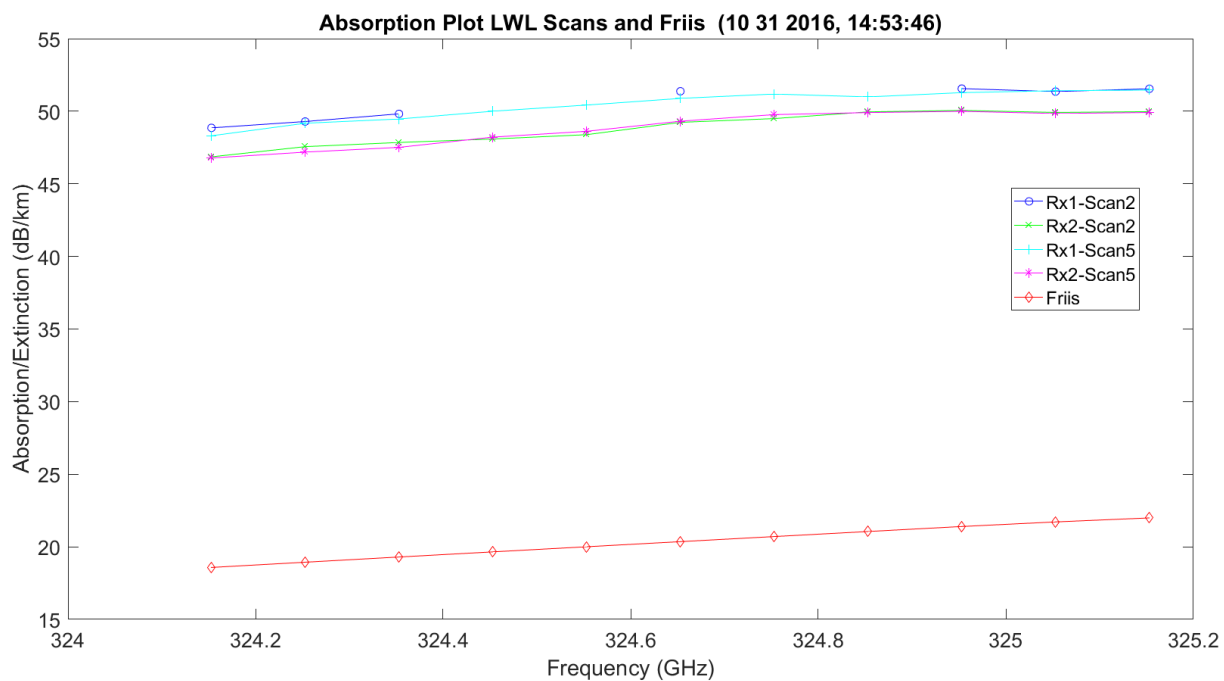


Figure 3.358. LWL Extinction with No Hardware – 11012016_145401.

Figure 3.359 shows the UWL absorption plot. The red plot represents the Friis view at 20% RH. The data from TAIPAS was approximately at 30%+ RH, but is still higher.

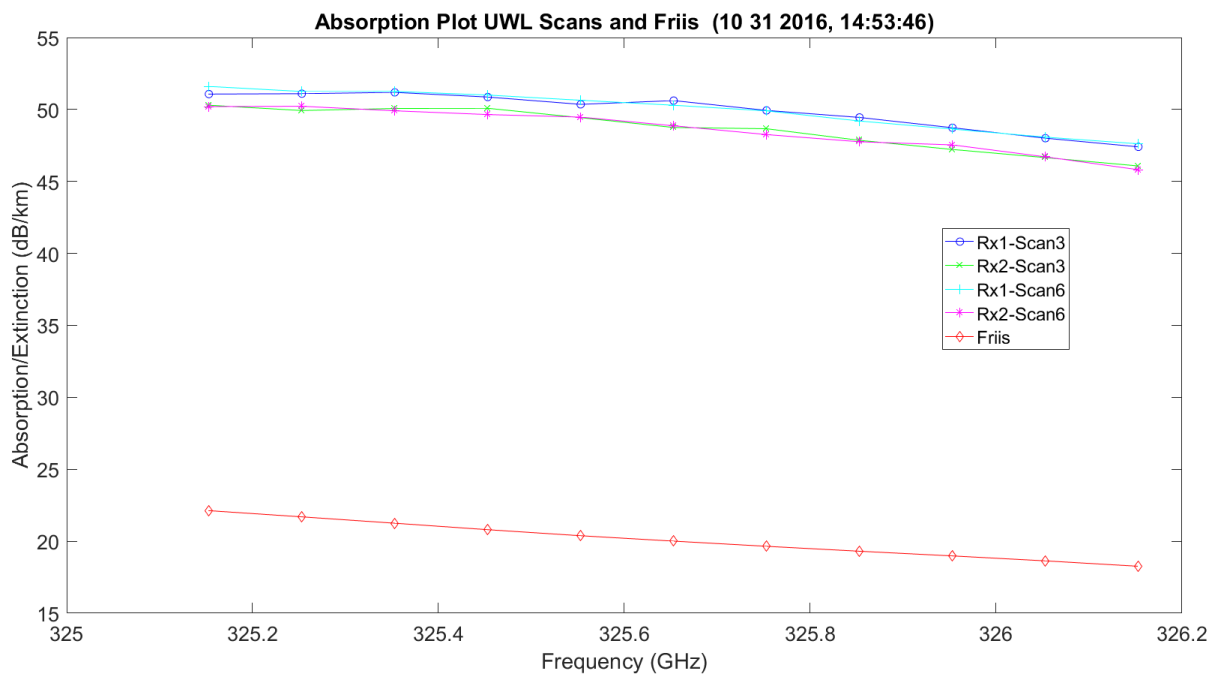


Figure 3.359. UWL Extinction with No Hardware – 11012016_145401.

Figure 3.360 shows the LWL and UWL flipped absorption plots. The red plot represents the Friis view at 20% RH. The data from TAIPAS was approximately at 30%+ RH, but is still higher.

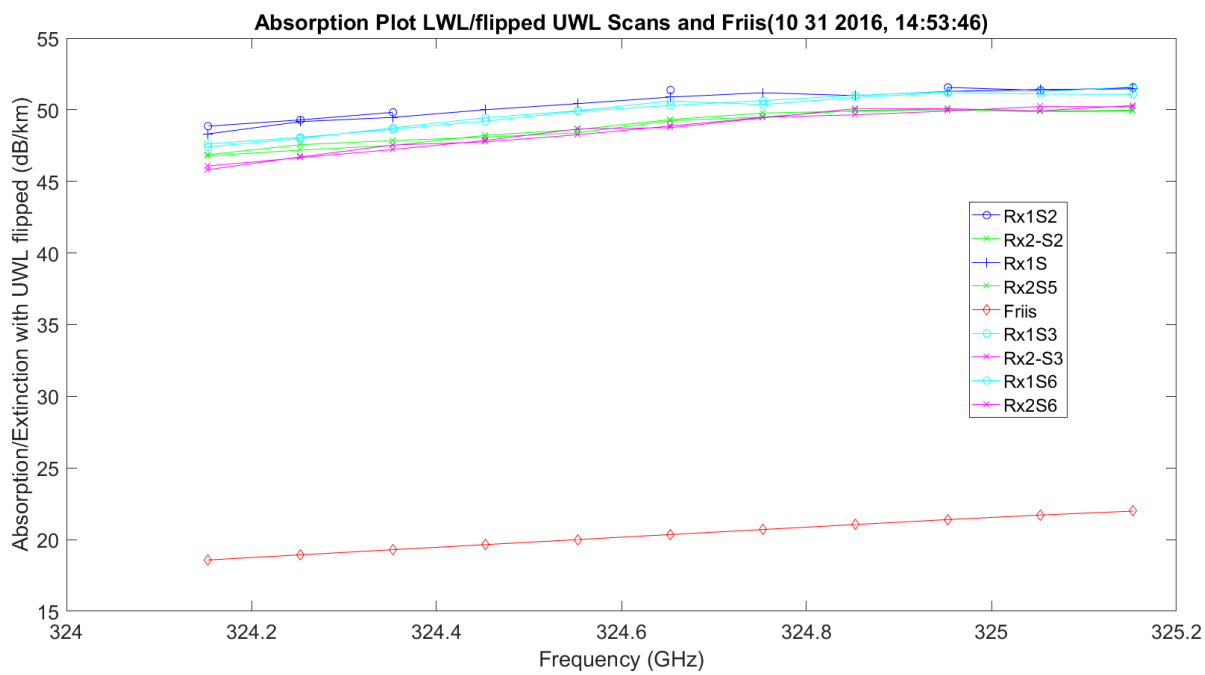


Figure 3.360. LWL & UWL Flipped Mean Amplitude No Hardware – 11012016_145401.

Chapter 4

Propagation in Aerosols

4.1 Introduction

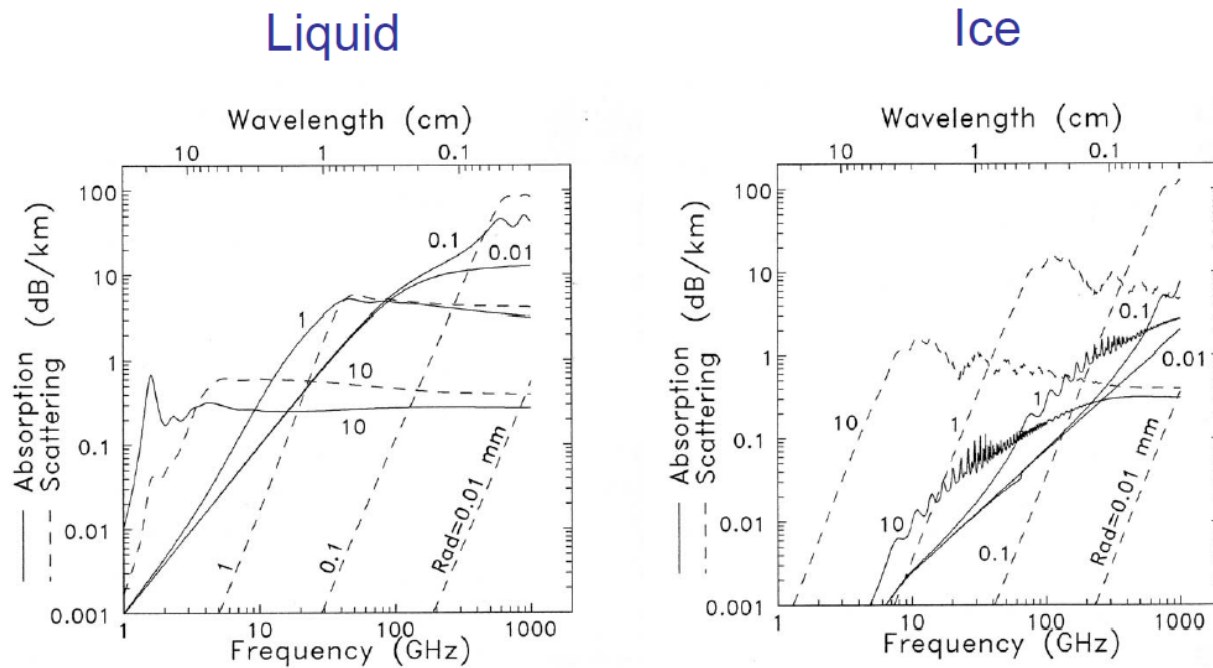
SMMW tropospheric extinction in clouds, fog, rain, snow and other aerosols is a capability of the TAIPAS system and will provide valuable scientific data that could aid in the improvement of current propagation models. This area of study entails the analysis of THz propagation through naturally-generated aerosols and hydrometeors that are available through regular data collection during the operation of the transmissometer. In Colorado, these events occur sporadically, so there is a reasonable probability that no aerosol data will be collected during the short operation time of the system after deployment on the open path prior to the thesis publication. This data will be collected over at least the next two years during further TAIPAS and model development. In the future, the extinction coefficient will be measured for varied aerosol and hydrometeor states — types, sizes and rates — and compared with expected values from existing models and data obtained by rain gauges and coincident optical extinction measurements. It is expected that some refinement and validation of models used to predict THz extinction in a non-clear atmosphere will be achieved. Analysis will be implemented on the effects on attenuation and refractivity coefficients under conditions of rain and clouds. This task will require novel and precise means of absolute clear-air calibration of the transmissometer, including radiometric, humidity reference, and beam wave diffraction methods. The results of this analysis will be a validated model for absorption and scattering by hydrometeors along an open path.

Please note, in the time TAIPAS was available, no aerosols existed, so this chapter has all theory and modeling.

4.2 Aerosol Scattering and Absorption

Aerosol scattering, due to rain, snow, dust, fog and sand, can break the Rytov approximation model when diffraction is significant and requires movement to a Markov model. The Markov model utilizes differential equations for moments of the electric field strength or quantum physics, based on adaptation of the path integral or Monte Carlo statistical method. When EM hits aerosols, it causes the spreading and contracting of the rays that make up the beam; this causes significant amplitude scintillation - $\langle \chi^2 \rangle$. Figure 4.1 [39] shows plots of a mono-dispersion with 1 g/m^3 . This will not be leveraged in understanding the aerosol effects of rain and ice, but it shows the evolution to Figure 4.2 [39], which shows the effect of poly-dispersive liquid and ice aerosols on the extinction coefficient: scattering, the real component, absorption, and the imaginary component. These are Mie spherical particles with liquid assuming a Marshall-Palmer particle size distribution and ice assuming Sekhon-Srivastava distribution. The plots show ice dominates the scattering component and liquid dominates absorption. Figure 4.3 shows the rain and snow absorption and scattering based on precipitation rates; snow scattering and rain absorption dominate. Absorption and scattering are added to the propagation losses to account for total losses per km. Figure 4.4 [64] shows particle sizes in terms of diameters and distributions for different types of materials.

Microwave Scattering & Absorption

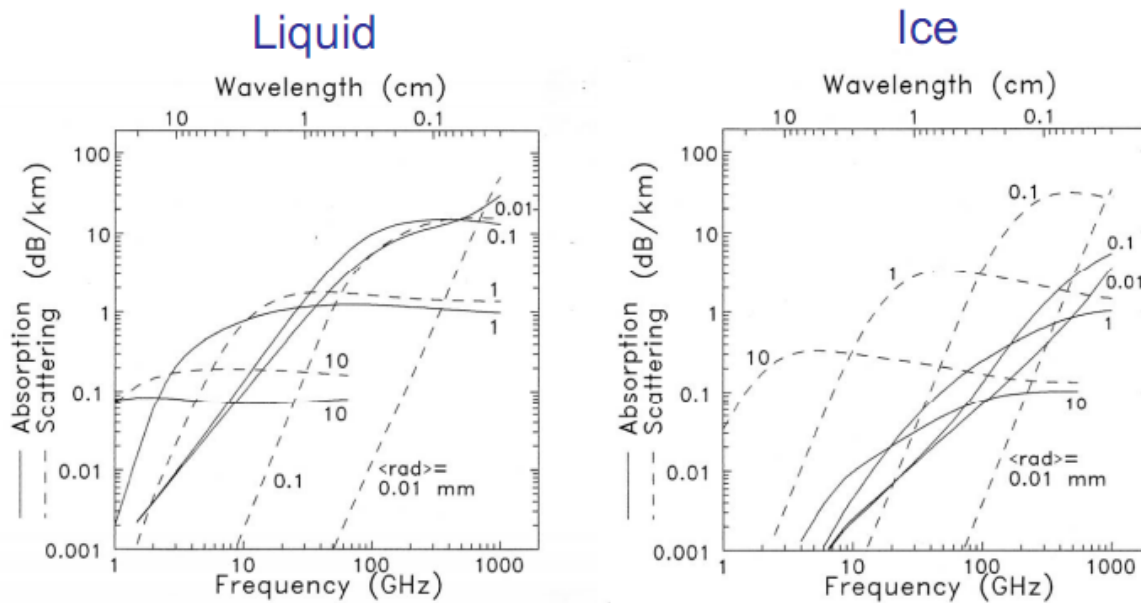


Above curves are for monodispersions of net 1 g/m^3 equivalent water density and indicated radii a

From Janssen (ed.) 1992, Ch 3 by A.J. Gasiewski

Figure 4.1. Liquid and Ice Mono-dispersions Absorption and Scattering Plots [39].

Polydispersive Scattering & Absorption

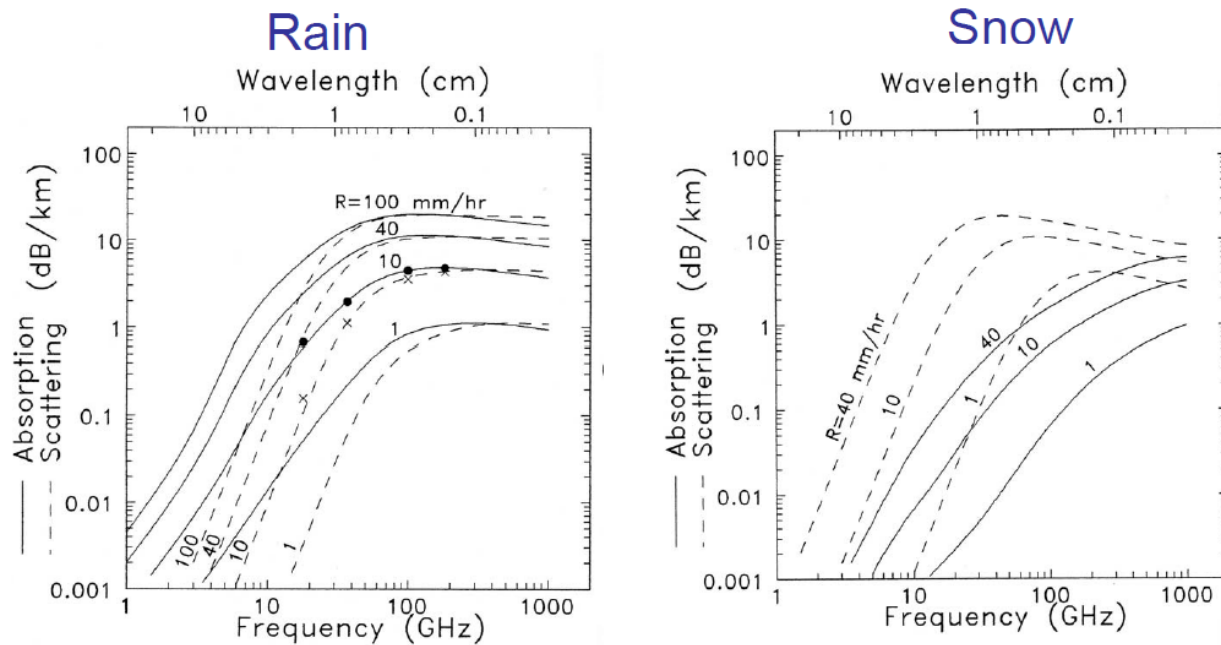


Above curves for exponential polydispersions of net 1 g/m^3 equivalent water density and indicated average radii $\langle a \rangle$

From Janssen (ed.) 1992, Ch 3 by A.J. Gasiewski

Figure 4.2. Liquid and Ice Poly-dispersions Absorption and Scattering Plots [39].

Rain/Snow Scattering & Absorption

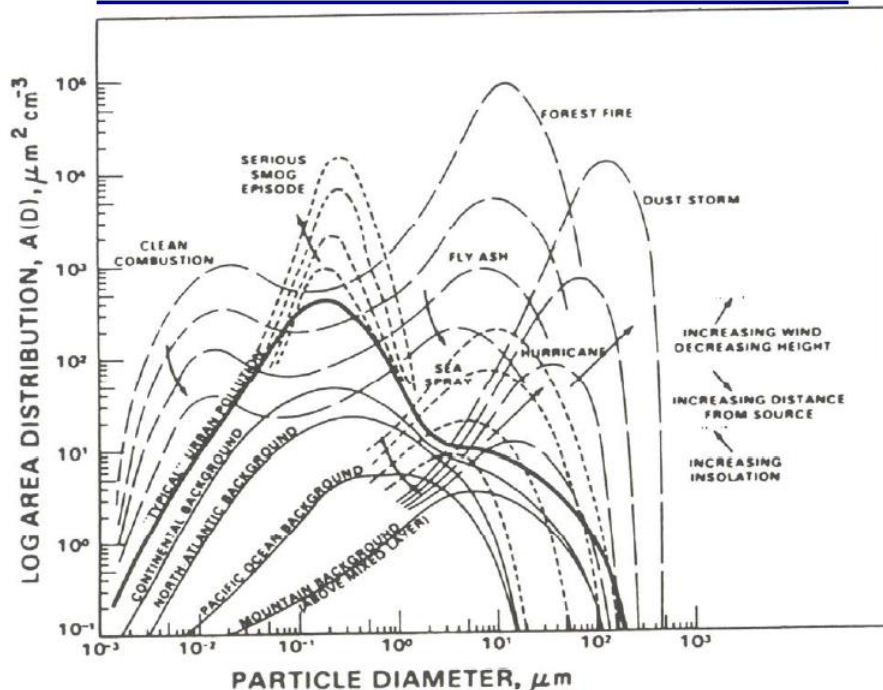


Above curves for a Marshall Palmer (rain) and Sekhon-Srivastava (snow) size dispersion for the indicated precipitation rates R

From Janssen (ed.) 1992, Ch 3 by A.J. Gasiewski

Figure 4.3. Rain and Snow Absorption and Scattering Plots [39].

Aerosol Size Distributions



Idealized aerosol spectra, showing typical ground-level background distributions and the general dependence of the spectra on height, wind speed, distance from source, and surface heating (From Slinn, 1975).

Figure 4.4. Smaller Diameter Aerosol Distributions with Wind Speeds [64].

Since aerosols can very quickly become larger than the 325.1529 GHz wavelength, ~ 1 mm, the relative polarization of the EM field has a significant impact; ice is more vertical in shape and can have a greater scattering effect with V-pol and raindrops that become oblate, more horizontally dominated, and can have greater scattering H-pol effects. Also, the constructive and destructive refraction is a significant component that drives scintillation of the scattering effects if objects are not perfectly spherical; this is the case for all objects, but it facilitates the math. In other words, real scatterers are not uniform in shape or distribution.

Figure 4.5 shows the cross section, σ , plot. Since the object is spherical, the angle of incidence is inconsequential; cross section is equal from all directions. The simplification of utilizing a sphere also removes effects of polarization in all regions and frequency in the optical region. In the optical region, the effects are more a function of the shape than projected area. The scintillation, constructive and destructive, caused by surface traveling waves, does not occur with a sphere. Resistive material will dampen the surface traveling waves. The logarithm vertical axis is the sphere cross section divided by the area of the center slice of the sphere (Equation 4.1). The logarithm horizontal scale is the circumference in wavelengths (Equation 4.2). The first section, called the Rayleigh region, covers particles with a spherical conference equal to or less than one wavelength. The cross section in this linear region is a function of frequency and radius (Equation 4.3). The Mie or resonance region is the damping oscillation section with a period of the wavelength: Mie normalized cross section nulls at wavelength boundaries. The optical region begins when the circumference of the sphere is ten wavelengths.

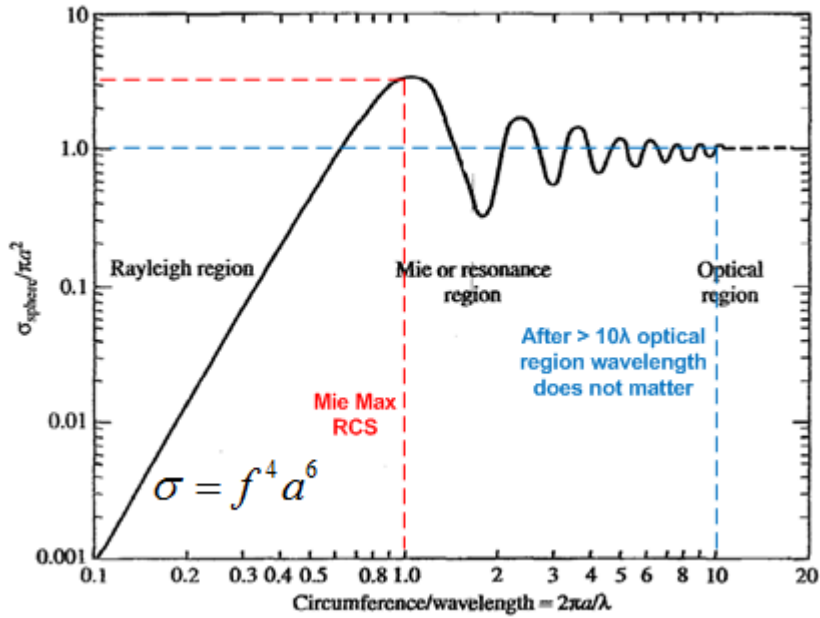


Figure 4.5. Spherical Cross Section Plot [65].

$$\sigma_{normalized} = \frac{\sigma_{sphere}}{\pi a^2} \quad (4.1)$$

$$Circumference_in_Wavelengths = \frac{2\pi a}{\lambda} \quad (4.2)$$

$$\sigma_{sphere_Rayleigh} = f^4 a^6 \quad (4.3)$$

Leveraging the absorption peak frequency of 325.1529 GHz, the region boundaries are calculated. The Rayleigh region, wavelength large compared to aerosol geometry, stops when the vertical axis cross section to sphere slice area equals one and the circumference is one wavelength; it equals one on the horizontal axis. The radius at the peak of the Rayleigh region occurs around 0.6 of a wavelength (Equation 4.4), wavelength of 0.922 mm. The cross section divided by the area of the sphere slice equals one at this point. Therefore, the maximum cross

section (Equation 4.5) in the Rayleigh region is 24.33 mm^2 (-76.14 dBsm). The Mie region starts at this point and peaks approximately when the circumference is one wavelength and the normalized cross section is approximately equal to three; this is the largest normalized cross section. The one wavelength is critical, since the wave wraps around the sphere and backscatters; this is the maximum at wavelength increments, with the peak at one wavelength. The radius (Equation 4.6) and the maximum cross section (Equation 4.7) value for the end Mie region is 0.203 mm^2 (-66.92 dBsm). The Mie region ends and the optical region starts when the circumference is ten wavelengths and the normalized cross section is one; the wavelength no longer matters, since the cross section is the area of the sphere. In the optical region, the circumference of the sphere in wavelengths no longer matters; the normalized cross section is always one. These boundaries are important to understand when considering the size of smoke or dust particles versus rain or snow. The boundaries of the regions as a function of the radius of the aerosol are presented in Equation 4.8 through Equation 4.10.

$$a = (0.6) \left(\frac{\lambda}{2\pi} \right) = 0.088 \text{ mm} \quad (4.4)$$

$$\sigma_{Max_sphere_Rayleigh} = \pi(.088 \text{ mm})^2 = .0243 \text{ mm}^2 = -76.14 \text{ dBsm} \quad (4.5)$$

$$a = \left(\frac{\lambda}{2\pi} \right) = 0.147 \text{ mm} \quad (4.6)$$

$$\sigma_{Max_sphere_Mie} = 3\pi(.147 \text{ mm})^2 = 0.203 \text{ mm}^2 = -66.92 \text{ dBsm} \quad (4.7)$$

$$a = \left(\frac{10\lambda}{2\pi} \right) = 1.47 \text{ mm} \quad (4.8)$$

$$\sigma_{sphere_optical_start} = \pi(1.47 \text{ mm})^2 = 2.15 \text{ mm}^2 = -28.34 \text{ dBsm} \quad (4.9)$$

$$\textit{Rayleigh} : a \leq 88 \mu\text{m} \quad (4.10)$$

$$\textit{Mie} : .088 \text{mm} < a < 1.47 \text{mm} \quad (4.11)$$

$$\textit{Optical} : a \geq 1.47 \text{mm} \quad (4.12)$$

The scattering toward the emitter source from the cross section causes a loss of forward propagating power. Also, as discussed above, the backscatter can cause constructive or destructive effects on the wave propagating forward. These aerosols can add to refraction that will cause angular changes. The aerosols will add to absorption; this power is absorbed due to conduction, permittivity and permeability losses. The total of absorption and scattering makes up the complex extinction of the signal; scattering is the real part and absorption is the imaginary part.

Figure 4.6 and Figure 4.7 are larger versions of the plots for rain and snow with markings for the TAIPAS frequencies. For rain at TAIPAS frequencies at all millimeter per hour rates, the attenuation due to scattering is equal to the absorption. For example, at 100 mm/hr of rain, there is a 40 dB/km of extinction. Table 4.1 and Table 4.1 show the rain Friis analyses, and, even at this rain rate, the SNR is 12.7 dB. The rain rates covered include 1, 10, 40 and 100 mm/hr. The snow scattering and absorption have separation even at the high TAIPAS frequency; the scattering bumps as the absorption flattens and they don't become closer, unlike rain, until 1 THz. For example, for the max snow rate of 40 mm/hr, scattering is 12 dB/km and absorption is 4.5 dB/km. Table 4.3 and Figure 4.4 show the snow Friis analysis with the max snow rate driving a healthy SNR of 57 dB. The yellow fields on Table 4.1 and Table 4.3 are inputs and absorption and scattering are derived from Figure 4.6 and Figure 4.7.

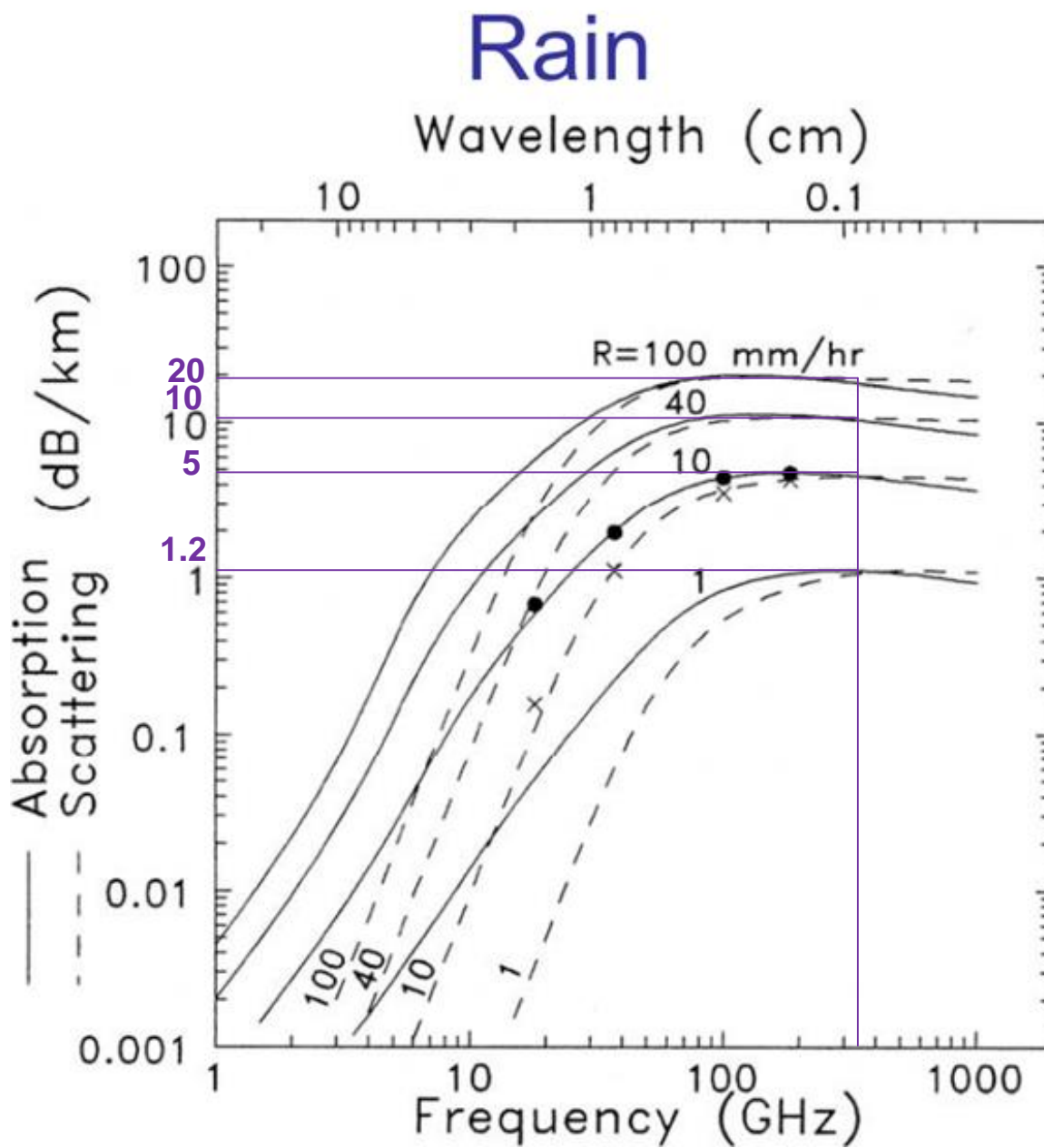


Figure 4.6. TAIPAS Rain Extinction [39].

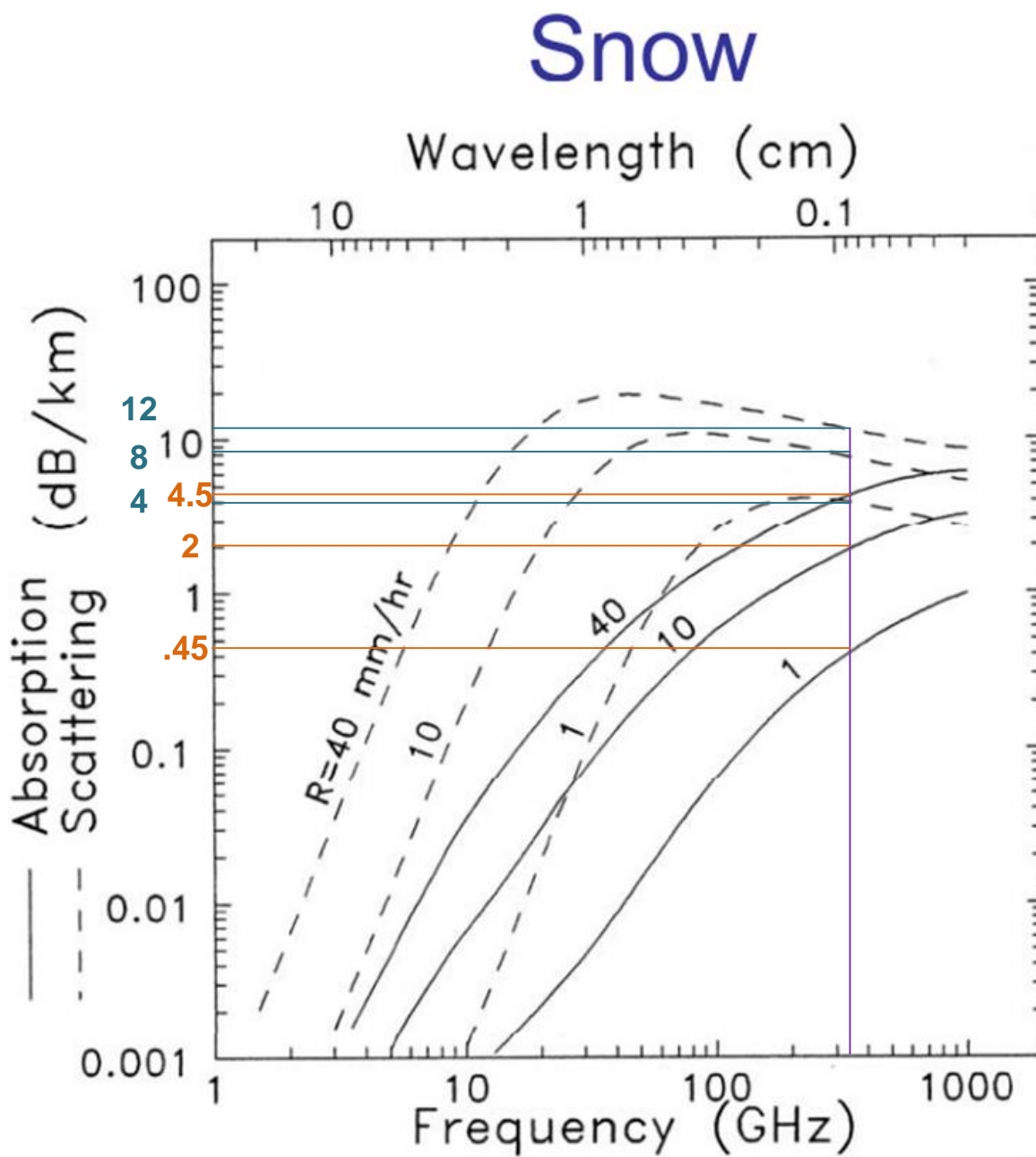


Figure 4.7. TAIPAS Snow Extinction [39].

Table 4.1. TAIPAS Rain Friis – 1924 m Path.

TAIPAS THz Rain System Calculations (340GHz)											
				Available Test Site Ranges (m)							
				CUTWR	NIST	NCAR	DoC	NOAA			
				520	1920	3370	6520	22570			
				Range							
				1920 (m)							
				Ref. Coef.							
				0.316							
				$\Gamma = \frac{Z_L - Z_0}{Z_L + Z_0} = .316$							
				Plot #1	$VSWR = \frac{1+ \Gamma }{1- \Gamma } = 1.926$						
				$c = 2.998 \times 10^8 \text{ m/s}$							
				$\lambda = \frac{c}{f}$							
				$P_{r_Circ_Aperture} = \frac{\pi^2 P_t \text{Dia}_t^2 \text{Dia}_r^2}{(4R\lambda)^2} e^{-\kappa_e R}$							
				$\kappa_e = \kappa_a + \kappa_s$							
				$1Np = 4.3429 \text{ dB}$							
Power Received											
Rain Rate	f	λ	$P_{t_exciter}$	P_{t_Horn}	Plot #2 Absorpt.	Plot #2 Scatter.	κ_e Extict.	κ_e Extict.	P_r Rx Power	P_r Rx Power	
1 (mm/hr)	340 (GHz)	0.882 (mm)	19 (mw)	12.996 (mw)	1.2 (dB/km)	1.2 (dB/km)	2.4 (dB/km)	0.5526 (Np/km)	6.35E-05 (mW)	-41.97 (dBm)	
10 (mm/hr)	340 (GHz)	0.882 (mm)	19 (mw)	12.996 (mw)	5 (dB/km)	5 (dB/km)	10 (dB/km)	2.3026 (Np/km)	2.21E-06 (mW)	-56.56 (dBm)	
40 (mm/hr)	340 (GHz)	0.882 (mm)	19 (mw)	12.996 (mw)	10 (dB/km)	10 (dB/km)	20 (dB/km)	4.6052 (Np/km)	2.65E-08 (mW)	-75.76 (dBm)	
100 (mm/hr)	340 (GHz)	0.882 (mm)	19 (mw)	12.996 (mw)	20 (dB/km)	20 (dB/km)	40 (dB/km)	9.2103 (Np/km)	3.83E-12 (mW)	-114.16 (dBm)	

Table 4.2. TAIPAS Rain SNR – 1924 m Path.

SNR			
B	0.01 (MHz)	NF	7.11 (dB)
T_0	290 (K)	P_n	2.06E-13 (mw)
τ_{int}	1 (sec)		-126.87 dBm
T_{rec}	1200 (K)	∂T_{rms}	2.910 K
		$NF = 10 \log \left(\frac{T_{rec}}{T_0} \right)$	
		$P_n = kTB ; k = 1.38 \times 10^{-23} \text{ J/K}$	
		$\partial T_{rms} = \frac{T}{\sqrt{B\tau_{int}}}$	
			$SNR = 10 \log \left(\frac{P_r}{P_n} \right)$
			84.9 (dB)
			70.3 (dB)
			51.1 (dB)
			12.7 (dB)

Table 4.3. TAIPAS Snow Friis – 1924 m path.

TAIPAS THz Snow System Calculations (340GHz)											
				Available Test Site Ranges (m)							
				CUTWR	NIST	NCAR	DoC	NOAA			
				520	1924	3370	6520	22570			
				Range							
				1924 (m)							
				Ref. Coef.							
				0.316							
				$\Gamma = \frac{Z_L - Z_0}{Z_L + Z_0} = .316$							
				Plot #1	$VSWR = \frac{1+ \Gamma }{1- \Gamma } = 1.926$						
				$c = 2.998 \times 10^8 \text{ m/s}$							
				$\lambda = \frac{c}{f}$							
				$P_{r_Circ_Aperture} = \frac{\pi^2 P_t \text{Dia}_t^2 \text{Dia}_r^2}{(4R\lambda)^2} e^{-\kappa_e R}$							
				$\kappa_e = \kappa_a + \kappa_s$							
				$1Np = 4.3429 \text{ dB}$							
Power Received											
Rain Rate	f	λ	$P_{t_exciter}$	P_{t_Horn}	Plot #2 Absorpt.	Plot #2 Scatter.	κ_e Extict.	κ_e Extict.	P_r Rx Power	P_r Rx Power	
1 (mm/hr)	340 (GHz)	0.882 (mm)	19 (mw)	12.996 (mw)	0.45 (dB/km)	4 (dB/km)	4.45 (dB/km)	1.0247 (Np/km)	2.54E-05 (mW)	-45.94 (dBm)	
10 (mm/hr)	340 (GHz)	0.882 (mm)	19 (mw)	12.996 (mw)	2 (dB/km)	8 (dB/km)	10 (dB/km)	2.3026 (Np/km)	2.18E-06 (mW)	-56.62 (dBm)	
40 (mm/hr)	340 (GHz)	0.882 (mm)	19 (mw)	12.996 (mw)	4.5 (dB/km)	12 (dB/km)	16.5 (dB/km)	3.7993 (Np/km)	1.22E-07 (mW)	-69.13 (dBm)	

Table 4.4. TAIPAS Snow SNR – 1924 m Path.

SNR	B	NF	$NF = 10 \log \left(\frac{T_{rec}}{T_0} \right)$	SNR	$SNR = 10 \log \left(\frac{P_r}{P_n} \right)$
	0.01 (MHz)	7.11 (dB)			
	T_0	P_n	70.2 (dB)		
	290 (K)	2.06E-13 (mw)	57.7 (dB)		
	τ_{int}	$P_n = kTB ; k = 1.38 \times 10^{-23} J/K$			
	1 (sec)	-126.87 dBm			
	T_{rec}	∂T_{rms}	$\partial T_{rms} = \frac{T}{\sqrt{B\tau_{int}}}$		
	1200 (K)	2.910 K			

4.3 LEEDR Model

Figure 4.8 shows the rain extinction in dB/km predicted by the AFIT LEEDR model performed at the Boulder location. The attenuation with 25 mm of rain per hour has approximately 45 dB/km attenuation. This is significantly higher attenuation than shown in Figure 4.6 with a 40-mm rain attenuation of 20 dB/km and 100 mm rain attenuation of 40 dB/km. At the higher altitude, it would be expected that the LEEDR location dependent model would be less than the general all-encompassing ones in Figure 4.3.

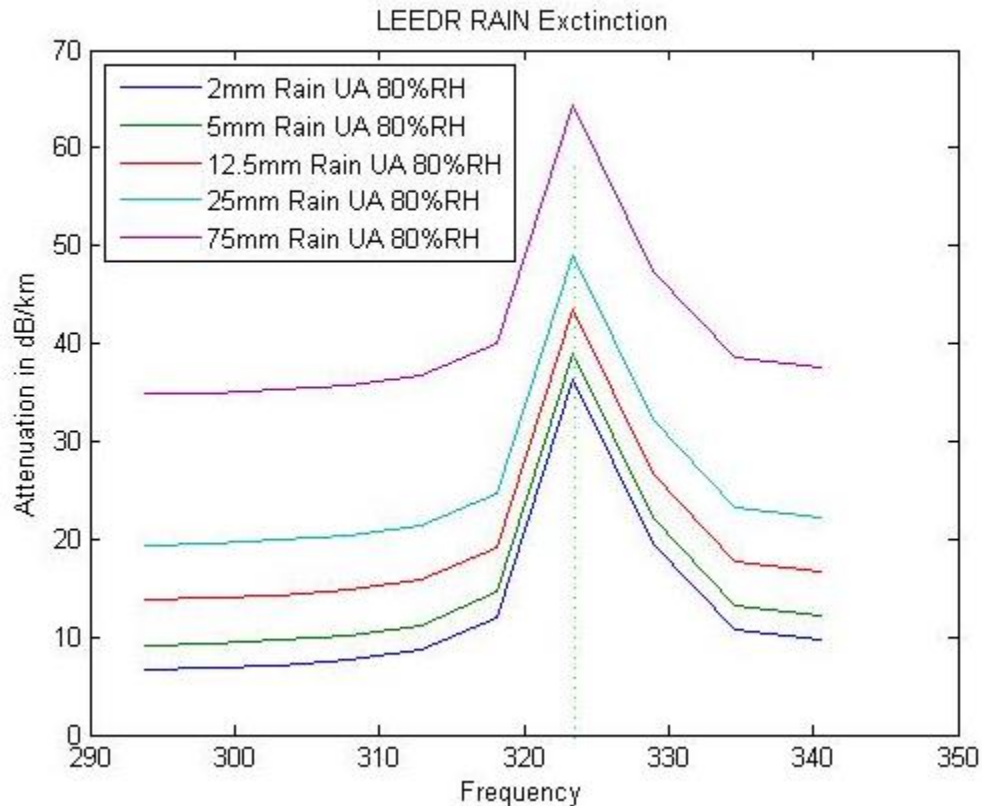


Figure 4.8. LEEDR Rain Extinction.

The LEEDR model has significant sand aerosol prediction capabilities, since this was a driving concern for the U.S. government. With 20% RH in Boulder, LEEDR in a sand environment predicts C_n^2 ranges fairly linear from $2.57 \times 10^{-18} \text{ m}^{-2/3}$ at 14 m altitude to $2.57 \times 10^{-18} \text{ m}^{-2/3}$ at 140 m altitude. Sand distribution density did not affect the linear curve. An RH of 95% with rain 2 mm to 75 mm yielded a single line of $2.385 \times 10^{-18} \text{ m}^{-2/3}$ at 14 m altitude to $2.295 \times 10^{-18} \text{ m}^{-2/3}$ at 140 m altitude. Figure 4.9 shows the extinction for sand with dielectric of $2.34 + j.08$, radius sizes from 1 μm to 500 μm , and cubic meter concentrations of 10^{10} , 10^{11} and 10^{12} . As the concentrations increase by an order of magnitude, the attenuation in dB/km increases significantly. Figure 4.10 shows an example input of one of the sand models. Table

4.5 shows the summary of the setup; latitude and longitude are located in Boulder. For example, turbulence is based on Tatarski. Path model results are shown in Figure 4.11 and 4.12. The sand causes significant attenuation after the 325.1529 GHz peak at higher frequencies. Table 4.6 shows the inputs and outputs for an order of magnitude concentration increase. Figure 4.13 shows the inputs and outputs for an order of magnitude concentration increase. Figure 4.13 shows the output and Figure 4.14 shows the attenuation plot in dB/km. The peak at 325.1529 GHz is almost removed as higher frequencies increase attenuation; the curve is approximately linear.

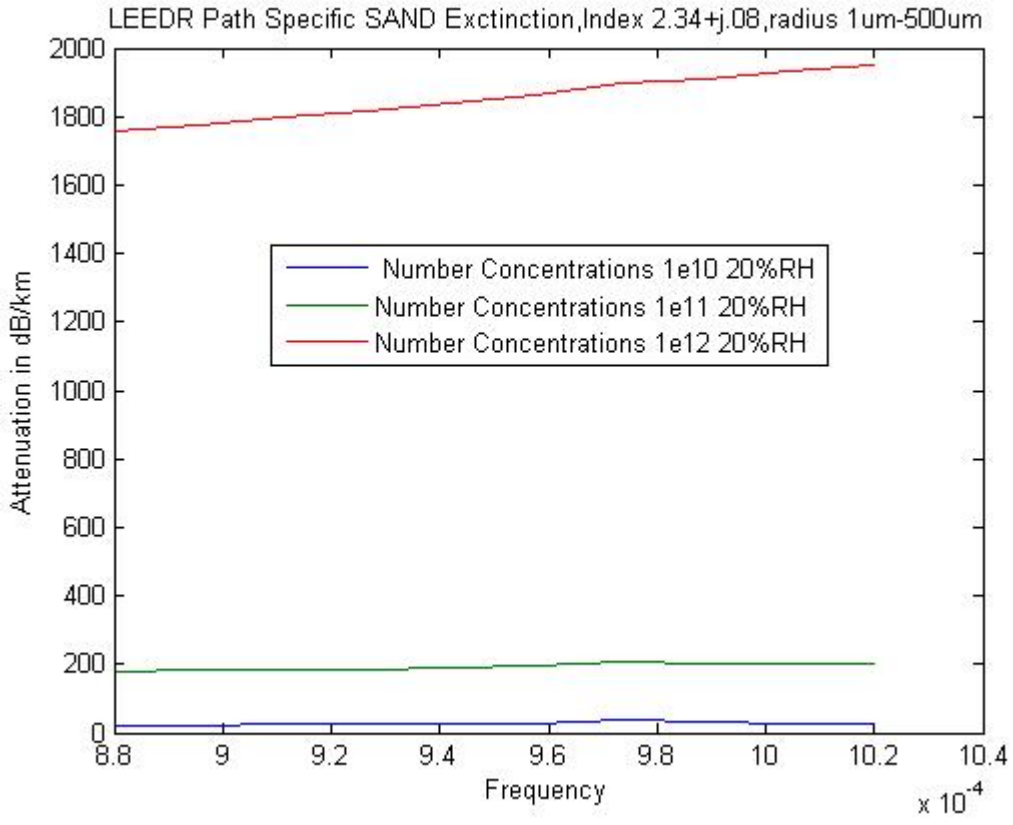


Figure 4.9. LEEDR Sand Extinction.

Aerosols

Standard

Volcanic

Model:

None
Summer Moderate
Summer High
Summer Extreme
Winter Moderate
Winter High
Winter Extreme

Maritime (MODTRAN)
Navy Aerosol Model
Advanced Navy Aerosol Model
Brownout Desert
Brownout MidLat

Index Real Portion:	2.34
Index Imaginary Portion	0.08
Number Concentrations	1e+11
Particle Min Radius (um)	1
Particle Max Radius (um)	500

Figure 4.10. LEEDR Aerosol Input Selection.

Table 4.5. LEEDR Sand Tabular Inputs and Results.

LEEDR Profile	
Time	3/24/2016 18:35
Name	3/24/2016 18:35
Wavelength (m)	0.000922
Latitude	40.0274
Longitude	-105.2519
PATH	
Path Type	Slant
Platform Altitude (m)	14
Target Altitude (m)	135
Path Length (m)	1920
Path Transmittance	1.15E-41
Path Extinction (1/km)	49.0972
Path Specific Attenuation (db/km)	213.2263
ATMOSPHERE	
Atmosphere	ExPERT
- ExPERT Site	BUCKLEY AFB
- Relative Humidity Percentile	20%
- Time of Day	15->18
- Atmosphere Standard Type	Midlatitude North
- Site Altitude	1769
- High Ozone Latitude	40.0274
Aerosols	Standard
- Aerosols Standard Type	Brownout Desert
Volcanic	None
Molecular	Calculation
Turbulence	Calculations - Tatarski
- Multiplier	1
Wind	Climatological
Season	Summer
Boundary Layer (m)	1524
GROUND LEVEL	

Path Results	
Path Transmittance:	1.14949e-41
Path Extinction (1/km):	49.0972
Path Specific Attenuation (dB/km):	213.226
Surface Visibility (km):	0.00853072
Slant Path Visibility (km):	0.00853072
Wavelength (m):	0.000922

Figure 4.11. LEEDR Sand Path Results.

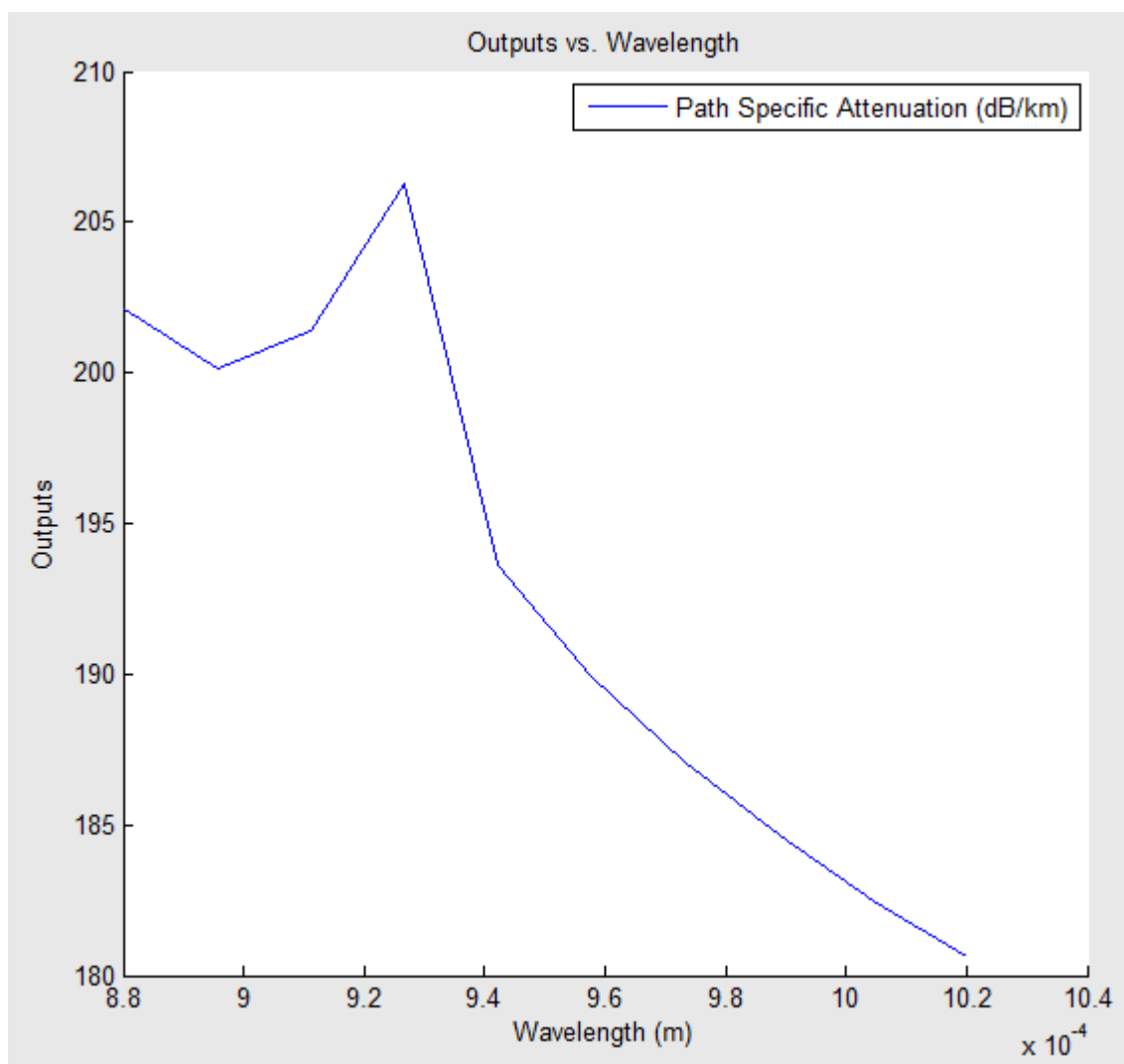


Figure 4.12. LEEDR Sand Path Attenuation in dB/km.

Table 4.6. LEEDR Sand Tabular Inputs and Results with Increased Concentration.

LEEDR Profile	
Time	3/24/2016 18:47
Name	3/24/2016 18:47
Wavelength (m)	0.000922
Latitude	40.0274
Longitude	-105.2519
PATH	
Path Type	Slant
Platform Altitude (m)	14
Target Altitude (m)	135
Path Length (m)	1920
Path Transmittance	0
Path Extinction (1/km)	439.3588
Path Specific Attenuation (db/km)	1908.109
ATMOSPHERE	
Atmosphere	ExPERT
- ExPERT Site	BUCKLEY AFB
- Relative Humidity Percentile	20%
- Time of Day	15->18
- Atmosphere Standard Type	Midlatitude North
- Site Altitude	1769
- High Ozone Latitude	40.0274
Aerosols	Standard
- Aerosols Standard Type	Brownout Desert
Volcanic	None
Molecular	Calculation
Turbulence	Calculations - Tatarski
- Multiplier	1
Wind	Climatological
Season	Summer
Boundary Layer (m)	1524
GROUND LEVEL	

Path Results	
Path Transmittance:	0
Path Extinction (1/km):	439.359
Path Specific Attenuation (dB/km):	1908.11
Surface Visibility (km):	0.00104635
Slant Path Visibility (km):	0.00104635
Wavelength (m):	0.000922

Figure 4.13. LEEDR Sand Path Results with Increased Concentration.

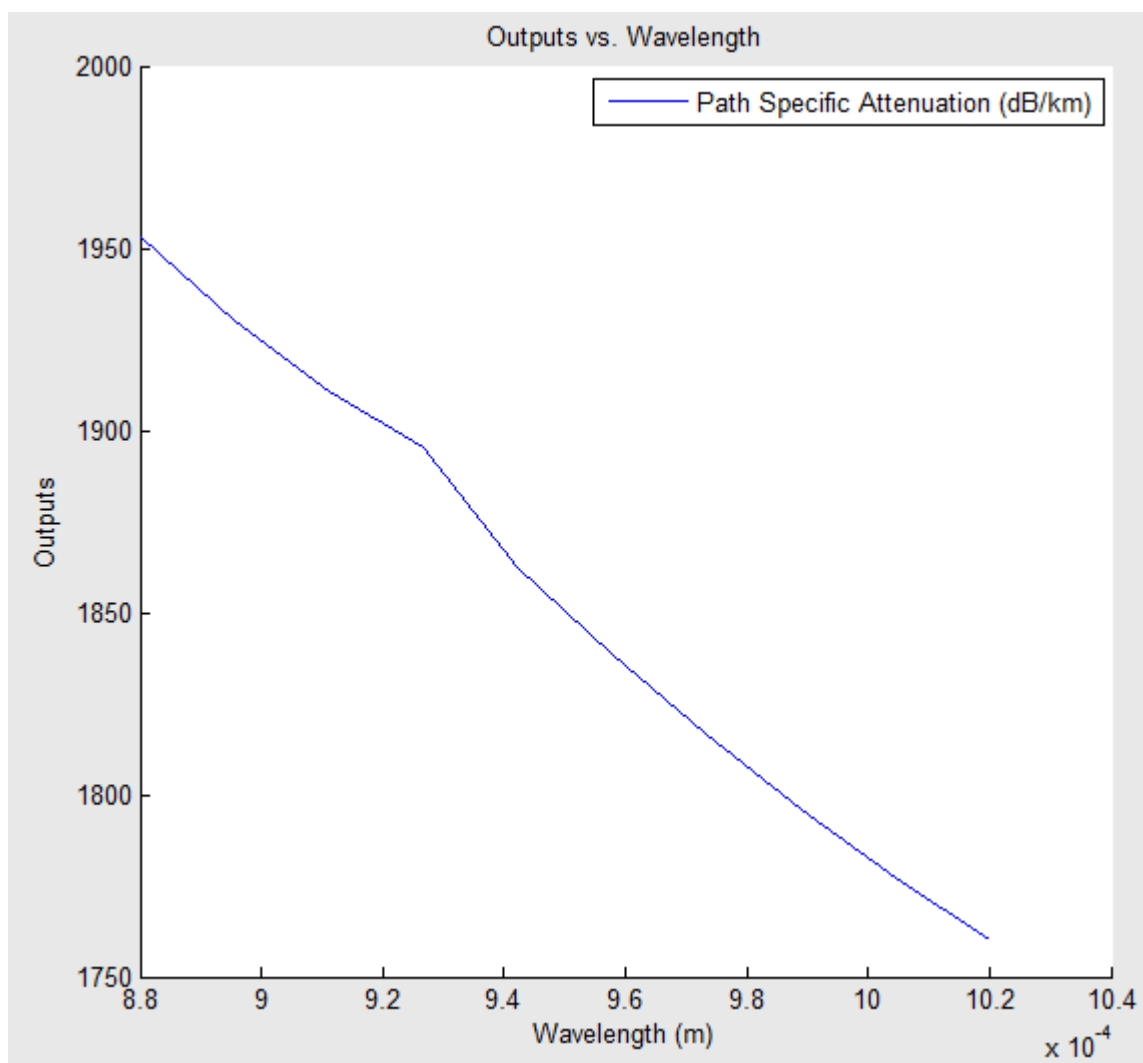


Figure 4.14. LEEDR Sand Path Attenuation in dB/km with Increased Concentration.

Chapter 5

Corroboration of Manning Beam Wave Complex Refractive Model

5.1 Introduction

SMMW signals, unlike optical, are affected heavily by both temperature and humidity, the first of which affects phase and the latter of which causes attenuation. This chapter corroborates the Manning beam wave complex refractive model [30]. The exploration is of the Manning beam wave statistical propagation model for complex refracting and absorbing media and its corroboration over a band encompassing the 325 GHz water vapor resonance in the anomalous dispersion region and the 340 GHz transmission window. Techniques are explored to separate the effects caused by C_T^2 and C_Q^2 by using on- and off-line measurements of relevant fluctuation statistics. The re-derivation of Manning's solution for a beam wave propagating in a complex turbulence medium [30] is implemented. While Wheelon [31, 32] covers microwave propagation, in Volume 1 his analysis focuses on optical propagation for which fluctuations in the imaginary part of the index of refraction are insignificant which covers phase and AoA variations. Volume 2 extensively covers RF with Rytov low scattering environments and addresses high scattering atmosphere as well; he does limit C_n^2 dependence only on temperature. Analysis is required, utilizing the full Lorentzian line shapes implementation, to determine how temperature and moisture fluctuations affect the real and imaginary components of the index-of-refraction. Due to the lack of operational time and data collection time on TAIPAS, this chapter covers the theory only.

5.2 Lorentz

The real and imaginary relations for functions in the upper half-plane (positive imaginary component) can be implemented mathematically with Kramers-Kronig (KK) relations; it allows the real part to be a function of the imaginary part or vice versa. The absorption driven imaginary part — even function — is always positive; real refractive component is an odd function. This works for a linear and time-invariant system. The KK relations for real as a function of imaginary permittivity and imaginary as a function of real permittivity are shown in Equation 5.1 and Equation 5.2, essentially Hilbert and inverse Hilbert transforms. These drive the derivation of the Lorentzian permittivity with separate imaginary and real components as a function of frequency and atomic resonance.

$$\epsilon'(\omega) - \epsilon_{\infty} = \frac{1}{\pi} \int_{-\infty}^{\infty} \frac{\epsilon''(\omega')}{\omega' - \omega} d\omega' \quad (5.1)$$

$$\epsilon''(\omega) = -\frac{1}{\pi} \int_{-\infty}^{\infty} \frac{\epsilon'(\omega') - \epsilon_{\infty}}{\omega' - \omega} d\omega' \quad (5.2)$$

Figure 5.1 shows plots of the permittivity imaginary and real components during resonance period and beyond: Lorentz. The permittivity has a peak in the imaginary absorption section and dynamic change in the real refraction index component; this is the anomalous dispersion region. During the peak and cross over time, there is anomalous and negative dispersion. However, temperature and absolute humidity density variations perturb the down-range beam phase and amplitude characteristics differently near absorption line centers and line wings, as evidenced by the following full Lorentzian model for the complex permittivity for a collection of lines

(Equations 5.3 and Equation 5.4). The τ component is the collision time at the atomic level; this is driven primarily by temperature, so $\tau \sim T^{0.8}$ [6]. The humidity factor is driven by the molecular content. At the peak is the anomalous dispersion and crossing point of refractive-index where $\omega_0 = \omega$; the real permittivity transverses zero and inverts setting around the absorption peak — imaginary. Equation 5.5 through Equation 5.10 show the anomalous point, which demonstrates that there is a common frequency and temperature related cross-correlation between the refractivity and the absorption, based on frequency and temperature. That appears to be true until anomalous dispersion points with $\omega \gg 1$; this is definitely true at TAIPAS's 325.1529 GHz resonant frequency. This extrapolates the derivation (Equation 5.11 – Equation 5.14) to show that the real or refractivity part is a function inversely proportional to frequency only and the imaginary or absorption is equal to the collision rate ($T^{0.8}$) function of temperature only, both during this dynamic anomalous time. The refractivity real part is close to zero for large frequencies, which coincides with the inversion plot in Figure 5.1. In this case, the only commonality or correlation between refractivity and absorption is due to humidity. That being said, microscale temperature variations affect the overall air density, which impact both density and dry air density, so temperature has some low correlation effects. Finally, the effects of absorption fluctuations caused by absolute humidity variations also affect the down-range beam characteristics, particularly near strong water vapor line centers.

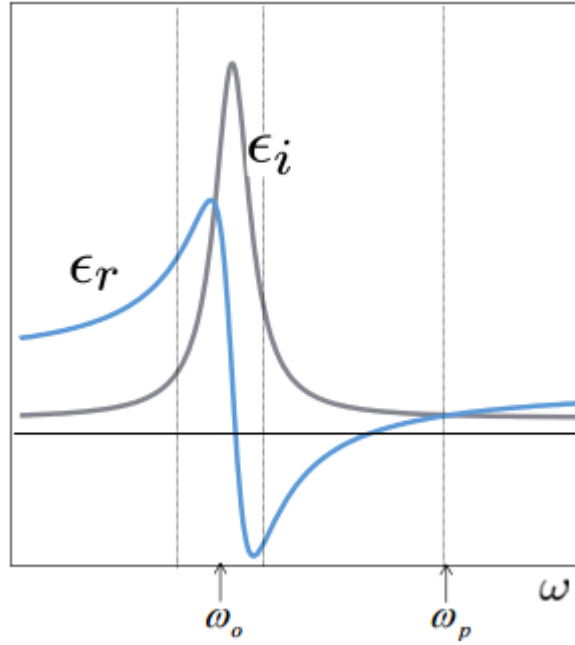


Figure 5.1. Permittivity Real and Imaginary Components Including Resonance.

$$\epsilon_{g(\omega)} = \sum_{\text{species } k,n} \sum \left(\frac{n_o e^{-\frac{E_2}{kT}}}{Z} \left[1 - e^{-\frac{\hbar\omega_0}{kT}} \right] \left(\frac{|\bar{\mu}_{12}|^2}{3\hbar} \right) \right) \times \quad (5.3)$$

$$\left[\frac{\omega_0 - \omega}{(\omega_0 - \omega)^2 + (1/\tau)^2} + \frac{\omega_0 + \omega}{(\omega_0 + \omega)^2 + (1/\tau)^2} + i \left\{ \frac{1/\tau}{(\omega_0 - \omega)^2 + (1/\tau)^2} + \frac{1/\tau}{(\omega_0 + \omega)^2 + (1/\tau)^2} \right\} \right]$$

$$Z \triangleq \sum_i e^{-\frac{E_i}{kT}} \quad (5.4)$$

$$\epsilon_{g(\omega)} = \sum_{\text{species } k,n} \sum \left(\frac{n_o e^{-\frac{E_2}{kT}}}{Z} \left[1 - e^{-\frac{\hbar\omega_0}{kT}} \right] \left(\frac{|\bar{\mu}_{12}|^2}{3\hbar} \right) \right) \times \quad (5.5)$$

$$\left[\frac{2\omega}{4\omega^2 + (1/\tau)^2} + i \left\{ \tau + \frac{1/\tau}{4\omega^2 + (1/\tau)^2} \right\} \right]; \omega_0 = \omega$$

$$\epsilon_{g(\omega)} = \sum_{\text{species } k,n} \sum \left(\frac{n_o e^{-\frac{E_2}{kT}}}{Z} \left[1 - e^{-\frac{\hbar\omega_0}{kT}} \right] \left(\frac{|\bar{\mu}_{12}|^2}{3\hbar} \right) \right) \times \quad (5.6)$$

$$\left[\frac{2\omega\tau^2}{4\omega^2\tau^2 + 1} + i \left\{ \tau + \frac{\tau}{4\omega^2\tau^2 + 1} \right\} \right]; \omega_0 = \omega$$

$$\epsilon_{g(\omega)} = \sum_{\text{species } k,n} \sum \left(\frac{n_o e^{-\frac{E_2}{kT}}}{Z} \left[1 - e^{-\frac{\hbar\omega_0}{kT}} \right] \left(\frac{|\bar{\mu}_{12}|^2}{3\hbar} \right) \right) \times \quad (5.7)$$

$$\left[\frac{2\omega\tau^2}{4\omega^2\tau^2 + 1} + i \left\{ \tau + \frac{\tau(4\omega^2\tau^2 + 1)}{4\omega^2\tau^2 + 1} \right\} \right]; \omega_0 = \omega$$

$$\epsilon_{g(\omega)} = \sum_{\text{species } k,n} \left(\frac{n_o e^{-\frac{E_2}{kT}}}{Z} \left[1 - e^{-\frac{\hbar\omega_0}{kT}} \right] \left(\frac{|\bar{\mu}_{12}|^2}{3\hbar} \right) \right) \times \left[\frac{2\omega\tau^2}{4\omega^2\tau^2 + 1} + i \left\{ \frac{\tau^2 + \tau(4\omega^2\tau^2 + 1)}{4\omega^2\tau^2 + 1} \right\} \right]; \omega_0 = \omega \quad (5.8)$$

$$\epsilon_{g(\omega)} = \sum_{\text{species } k,n} \left(\frac{n_o e^{-\frac{E_2}{kT}}}{Z} \left[1 - e^{-\frac{\hbar\omega_0}{kT}} \right] \left(\frac{|\bar{\mu}_{12}|^2}{3\hbar} \right) \right) \times \left[\frac{2\omega\tau^2}{4\omega^2\tau^2 + 1} + i \left\{ \frac{2\tau(2\omega^2\tau^2 + 1)}{4\omega^2\tau^2 + 1} \right\} \right]; \omega_0 = \omega \quad (5.9)$$

$$\epsilon_{g(\omega)} = \sum_{\text{species } k,n} \left(\frac{n_o e^{-\frac{E_2}{kT}}}{Z} \left[1 - e^{-\frac{\hbar\omega}{kT}} \right] \left(\frac{|\bar{\mu}_{12}|^2}{3\hbar} \right) \right) \times \left(\frac{2\tau}{4\omega^2\tau^2 + 1} \right) \times \left[\omega\tau + i(2\omega^2\tau^2 + 1) \right]; \omega_0 = \omega \quad (5.10)$$

$$\epsilon_{g(\omega)} = \sum_{\text{species } k,n} \left(\frac{n_o e^{-\frac{E_2}{kT}}}{Z} \left[1 - e^{-\frac{\hbar\omega}{kT}} \right] \left(\frac{|\bar{\mu}_{12}|^2}{3\hbar} \right) \right) \times \left(\frac{2\tau}{4\omega^2\tau^2} \right) \times \left[\omega\tau + i(2\omega^2\tau^2) \right]; \omega \gg 1; \omega_0 = \omega \quad (5.11)$$

$$\epsilon_{g(\omega)} = \sum_{\text{species } k,n} \left(\frac{n_o e^{-\frac{E_2}{kT}}}{Z} \left[1 - e^{-\frac{\hbar\omega}{kT}} \right] \left(\frac{|\bar{\mu}_{12}|^2}{3\hbar} \right) \right) \left(\frac{2\omega\tau^2}{4\omega^2\tau^2} \right) [1 + i(2\omega\tau)]; \omega \gg 1; \omega_0 = \omega \quad (5.12)$$

$$\epsilon_{g(\omega)} = \sum_{\text{species } k,n} \sum \left(\frac{n_o e^{-\frac{E_2}{kT}}}{Z} \left[1 - e^{-\frac{\hbar\omega}{kT}} \right] \left(\frac{|\bar{\mu}_{12}|^2}{3\hbar} \right) \right) \left(\frac{1}{2\omega} \right) [1 + i(2\omega\tau)]; \omega \gg 1; \omega_0 = \omega \quad (5.13)$$

$$\epsilon_{g(\omega)} = \sum_{\text{species } k,n} \sum \left(\frac{n_o e^{-\frac{E_2}{kT}}}{Z} \left[1 - e^{-\frac{\hbar\omega}{kT}} \right] \left(\frac{|\bar{\mu}_{12}|^2}{3\hbar} \right) \right) \left[\frac{1}{2\omega} + i(\tau) \right]; \omega \gg 1; \omega_0 = \omega \quad (5.14)$$

5.3 Spatial Wave Types

The plane wave is an infinite set of parallel rays, while the spherical wave is a set of diverging rays — lines out from a point. Focused beams are converging rays. A beam wave or collimated beams are a spatially limited bundle of parallel rays; spatial subset of a planar beam. Figure 5.2 shows this pictorially. For planar or beam waves, the ray trajectory reduces to a straight line and the permittivity remains isotropic over the path; this is usually true over a terrestrial propagation experiment or link. Beam wave requires significant directivity or high gain antennas and the best achieved is a Gaussian shaped beam wave. Wheelon [31, 32] only considers that collimated or beam waves can be produced over ranges by a laser. As seen in earlier chapters, the THz signal spot size grows, but not very much relative to the path length; even the alignment laser grows to a large spots size, even with a pinhole aperture in front of the laser. If receivers are set close to the LoS, like TAIPAS, beam waves and plane waves are

equivalent in a relatively small area. Beam wave shapes don't work for significantly separated receivers to implement the MCF. They are highly focused propagation, but with the Gaussian shape, some coverage may be possible. A plane wave covers the displaced receivers.

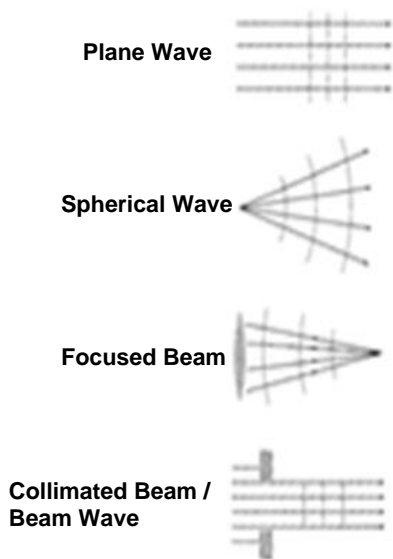


Figure 5.2. EM Wave Types [31].

The phase structure function is dominated by large scale turbulence — large eddies — and amplitude structure function is driven by small scale turbulence — small eddies; it has been proven that large eddies are much less symmetrical than small eddies. In a Gaussian beam wave system, the beam width needs to be large enough to cover the receive aperture with maximum AoA errors and support MCF measurements. Assume the beam spread due to diffraction is not significant.

5.4 Manning

In a CA environment, random fluctuations are only caused by the complex permittivity. The first Rytov approximation is the model approach in a weak scattering environment. Manning [30] focusses on the Gaussian beam wave to derive structure functions, log amplitude scintillation, phase scintillation and MCF. The Von Karman model covers fluctuations in both components of the complex refractive-index with their cross-correlation. Manning focuses on millimeter and near millimeter wave propagation, which is perfect for covering the TAIPAS system. The higher frequency drives larger gain for a given aperture, which drives the system to a Gaussian beam wave. Thermal fluctuations drive permittivity variations that drive intensity and AoA; the stochastic portion of EM propagation dominates. Manning's thesis fills the holes of absorption with small eddy sizes compared to 1 mm inner scale lengths; TAIPAS falls in this area, but the beam on the open path never passes turbulent structures this small. Normally, propagation derivations require that the wavelength has to be significantly smaller than the inner scale length; Manning deviates from this focus on the millimeter wavelength or relatively equal, smaller inner scale lengths. Manning's approach is that this is a boundary between much larger and significantly smaller than inner scale length; this will not occur on an open path like TAIPAS. The complex permittivity effects are maintained: real part affects refractivity or reducing and increasing speed of the wave, and the imaginary part, which drives the absorption and is significant at SMMW RF. The complex permittivity is driven by temperature, humidity and pressure in-homogeneities, which causes the stochastic components of the complex permittivity. Manning considers the beam wave as the EM spatial representation due to the small wavelengths for a given aperture size and the shape of the phase front on a similar receive aperture; there is high gain in both directions, which fits the TAIPAS system. Leveraging

Maxwell's equations, just like Wheelon, the vector wave equation is derived with a complex permittivity with randomness in both space and time. Manning states that this neglects the depolarization component when λ is assumed to be much smaller than the inner scale length; this induces errors in the derivation. Manning assumes that even with millimeter wavelengths, the depolarized field component is negligible relative to the scattering component.

Manning presents a transformation-perturbation approach, the Rytov method, to solve the stochastic parameter wave equation. The approach also assumes that the second order Rytov can be ignored, which is true in any low scattering environment. The first order solution containing stochastic components can only be solved with statistical parameters.

Manning implements the derivation of the stochastic wave equation. This is implemented by taking the curl of both sides of the Faraday law and applying the vector identity; the curl of the curl equals the gradient of the divergence and substitutes it into Amperes law. The Laplace of E and curl of B on the right-side inserts into the derivative, with respect to time, and allows Ampere's law to be substituted. Since the E field is harmonic, the solution can be represented by exponential. The third term of the vector wave equation contains the interaction terms of the orthogonal components of the field; it describes the depolarization due to the spatial variations of permittivity. The depolarization term of the wave equation is negligible for the wavelength approximately equal to the inner scale length, TAIPAS, which decouples the vector wave equation into three scalar wave equations. This yields a stochastic parameter wave equation, so a statistical approach is required: the Rytov method of the transformation perturbation technique. Rytov takes the approach leveraging permittivity's mean values and fluctuating parts

representing delta permittivity's with average fluctuating parts equal to zero. This complex permittivity is substituted into the scalar wave equations that yield three scalar equations; a direction can be assumed, so only one of these needs to be considered. The parametric nature of the equation is addressed with defining a complex phase that is a function of a space vector, such that the solution of E is an exponent to the phase power. This is substituted into the scale wave equation. A complex phase (Eikonal) is defined for the E field. The inhomogeneous wave equation solution in terms of the Green Function solution, which is not in closed form, must be solved iteratively: first and second Rytov, which is ample for first order permittivity stochastic part. A spectral representation can represent real and imaginary fluctuations of the index-of-refraction. The first Rytov model is for low scattering environment, single scattering approximation. The scattering produces a conical shape forward with fields given by the Fresnel approximation, all scattering in the forward direction for diffusion.

Manning's single Gaussian beam wave propagation source representation changes the variable to include a focusing effect with a radius of the curvature of the wave front. This occurs at the aperture and varies with range: $R < 0$, focused beam wave; $R > 0$, collimated beam wave; and R going to infinity represents a plane wave or spherical wave changing the beam radius at the aperture.

Manning drives the representation of derivation of the spatial correlation and structure functions for log amp and phase first Rytov equation. The index-of-refraction is representing the permittivity and its variances in a three-dimensional (3D) spatial spectrum. Rytov is a single scatter, so one only requires correlating the plane transverse to the direction of propagation. An

approach to form a complex random function is deriving the covariance function between two points in space. Two points in space can generate a complex random function with a constancy of statistics: homogeneity and spatial positions are independent of spatial position. Refractive index random variances are statistically homogeneous for local views. The Gaussian beam wave has a complex radius of curvature. Structure functions of the log-amplitude and phase fluctuations are utilized to construct correlation and covariance functions. The small spatial distances allow the assumption of turbulence homogeneity of a random function with constant mean; this is true for isotropy/local isotropy as well. If large separations of two points exist, these assumptions cannot be utilized; it requires the utilization of structure functions, which account for changes in mean over large spatial distances.

Manning addresses the MCF of a beam wave propagation in a randomly refracting / dispersing and absorbing atmosphere. MCF leverages the cross correlation of the complex field in a plane transverse to the direction of propagation. It measures the degree of coherence of spatially separated apertures: amplitude/intensity, phase and AoA. If depolarization can be ignored, then the MCF results are scalar. The central limit theorem drives the first Rytov approximation to a normal distribution; the averages of amplitude and phase are zero.

The complex permittivity fluctuations caused by turbulence are homogeneous and isotropic locally. The spatial frequency spectrum of fluctuations / structure function of isotropic refractive-index fluctuations — atmospheric turbulence — are defined by von Karman; this covers the inertial region only, since the energy input region, outer scale length, is the largest turbulent inhomogeneity. Manning drives the solution for the propagation equations for von

Karman's spectra of refractive-index fluctuations. Structure function and cross correlation for amplitude can be measured by leveraging two receivers placed in the transverse plane; TAIPAS supports this capability. Variance in amplitude can be measured by a single receiver; phase variance is not easily measured in his thesis. TAIPAS will be able to measure the phase variance since the transmitter and two receivers are coherent. The broken-down spectrum component refractive-index fluctuations, as a function of the spatial wavenumber and the construction constant, real, imaginary and cross correlation for index-of-refraction, varies with range and are broken into real components (Equation 5.15), imaginary components (Equation 5.17) and correlation between real and imaginary components (Equation 5.16). The index-of-refraction constant (C_n^2) does not change significantly over a constant level path, but does change with altitude changes, the smaller at the higher the altitude. For TAIPAS, the C_n^2 does change in the mantissa slightly; there are no order of magnitude effects. The C_n^2 is broken into the same three-component structure parameters of refractive-index fluctuations: real (Equation 5.18), imaginary (Equation 5.19) and a correlation of the two (Equation 5.20). The T is the absolute temperature, Q is absolute humidity and A_s and B_s are spectroscopically determined, wavelength dependent coefficients. These constants can be determined spectroscopically with multiple equations. The spectral sensitivity to temperature and humidity is determined by the Lorentzian. This states that the real and imaginary component of the construction coefficient are wavelength dependent, but this has been proven false in future findings; this allows an optical scintillometer to provide C_n^2 for any RF frequency. Manning's top references include Wheelon and Tatarski. The way to utilize Equation 5.20 is to leverage the A_T fluctuations in B_T fluctuations in temperature and humidity for the real and imaginary part; this required leveraging Jacobians mathematics. The

correlations of $A_T B_T$ and $A_Q B_Q$ both must leverage Jacobians as well. This is discussed extensively in Chapter 1.

$$\Phi_{RR}(\kappa) = .033 C_{n_R}^2(r) \left(\kappa^2 + \frac{1}{L_0^2} \right)^{-11/6} e^{-\kappa^2/\kappa_m^2}; \kappa_m \equiv 5.92/\ell_0 \quad (5.15)$$

$$\Phi_{RI}(\kappa) = .033 C_{n_R n_I}^2(r) \left(\kappa^2 + \frac{1}{L_0^2} \right)^{-11/6} e^{-\kappa^2/\kappa_m^2}; \kappa_m \equiv 5.92/\ell_0 \quad (5.16)$$

$$\Phi_{II}(\kappa) = .033 C_{n_I}^2(r) \left(\kappa^2 + \frac{1}{L_0^2} \right)^{-11/6} e^{-\kappa^2/\kappa_m^2}; \kappa_m \equiv 5.92/\ell_0 \quad (5.17)$$

$$C_{n_R}^2(r) = \frac{A_T^2}{\langle T \rangle^2} C_T^2(r) + \frac{A_Q^2}{\langle Q \rangle^2} C_Q^2(r) + 2 \frac{A_T A_Q}{\langle T \rangle \langle Q \rangle} C_{TQ}(r) \quad (5.18)$$

$$C_{n_I}^2(r) = \frac{B_T^2}{\langle T \rangle^2} C_T^2(r) + \frac{B_Q^2}{\langle Q \rangle^2} C_Q^2(r) + 2 \frac{B_T B_Q}{\langle T \rangle \langle Q \rangle} C_{TQ}(r) \quad (5.19)$$

$$C_{n_R n_I}^2(r) = \frac{A_T B_T}{\langle T \rangle^2} C_T^2(r) + \frac{A_Q B_Q}{\langle Q \rangle^2} C_Q^2(r) + \frac{B_T A_Q + A_T B_Q}{\langle T \rangle \langle Q \rangle} C_{TQ}(r) \quad (5.20)$$

Chapter 6

Anomalous Refractivity Validation

6.1 Introduction

The selection of the TAIPAS frequency band resulted from the THz band's significant absorption peak at the 325.1529 GHz water vapor resonance. This chapter investigates the hypotheses that there can be anomalous, negative trending/down linear significant slope, refractivities required by the KK relations around this large absorption peak. Figure 6.1 shows the refractivity, ϵ_r , and the absorption, ϵ_i , for the Lorentzian line shapes. The KK relations, along with the Lorentzian line shape, should produce a low refractivity region above, coming out of the peak absorption at higher frequencies, the line center and a high refractivity region below the line center, and coming into the absorption peak at lower frequencies. This refractivity difference will be studied to determine the potential for measurable effects on amplitude and phase scintillations. Also, the shape of the imaginary absorption component will be explored to verify the symmetry of the shape around the peak. The transmissometer was utilized to measure these effects at the upper and lower wing frequencies of 325.153 ± 1.0 GHz. The 1 GHz scans are shown in Table 6.1 and Table 6.2. There was a limited amount of time for acquiring multiple sets of data, so no conclusions were made at the time of this thesis.

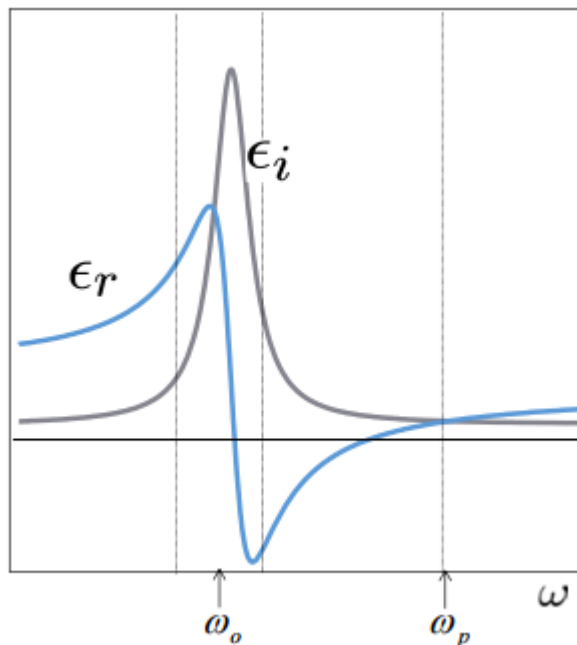


Figure 6.1. Permittivity Real and Imaginary Components including Resonance.

Table 6.1. Narrow Band, Absorption LWL Frequency Scan.

Narrow Band (NB) Scan (5 GHz)
Lower Wing Line (LWL) of Absorption Peak (USAP)

<i>Freq Name</i> →	<i>Synth Freq</i> →	<i>RF</i> →	<i>Peak Offset</i>
f_1	13.506375000	324.153	-1.000
f_2	13.510541667	324.253	-.900
f_3	13.514708333	324.353	-.800
f_4	13.518875000	324.453	-.700
f_5	13.523041667	324.553	-.600
f_6	13.527208333	324.653	-.500
f_7	13.531375000	324.753	-.400
f_8	13.535541667	324.853	-.300
f_9	13.539708333	324.953	-.200
f_{10}	13.543875000	325.053	-.100
f_{11}	13.548041667	325.153	0.000 <i>H₂O Line Center</i>

Table 6.2. Narrow Band, Absorption UWL Frequency Scan.

Narrow Band (NB) Scan (5 GHz)			
Upper Wing Line (UWL) of Absorption Peak (DSAP)			
<i>Freq Name</i> →	<i>Synth Freq</i> →	<i>RF</i> →	<i>Peak Offset</i>
f_1	13.548041667	325.153	0.000 <i>H₂O Line Center</i>
f_2	13.552208333	325.253	.100
f_3	13.556375000	325.353	.200
f_4	13.560541667	325.453	.300
f_5	13.564708333	325.553	.400
f_6	13.568875000	325.653	.500
f_7	13.573041667	325.753	.600
f_8	13.577208333	325.853	.700
f_9	13.581375000	325.953	.800
f_{10}	13.585541667	326.053	.900
f_{11}	13.589708333	326.153	1.000

6.2 Lorentz / Kramers-Kronig

The real and imaginary relations for functions in the upper half-plane — positive imaginary component — can be implemented mathematically with KK relations; it allows the real to be a function of the imaginary part or vice versa. The absorption driven imaginary part — even function — is always positive; real refractive component is an odd function. This works for a linear and time-invariant system. The KK relations for real as a function of imaginary permittivity and imaginary as a function of real permittivity are shown in Equation 6.1 and Equation 6.2, essentially, Hilbert and inverse Hilbert transforms. These drive the derivation of the Lorentzian permittivity with separate imaginary and real components as a function of frequency and atomic resonance (Figure 6.1).

$$\epsilon'(\omega) - \epsilon_\infty = \frac{1}{\pi} \int_{-\infty}^{\infty} \frac{\epsilon''(\omega')}{\omega' - \omega} d\omega' \quad (6.1)$$

$$\epsilon''(\omega) = -\frac{1}{\pi} \int_{-\infty}^{\infty} \frac{\epsilon'(\omega') - \epsilon_\infty}{\omega' - \omega} d\omega' \quad (6.2)$$

Figure 6.1 shows plots of the permittivity imaginary and real components during resonance period and beyond: Lorentz. The permittivity has a peak in the imaginary absorption section and dynamic change in the real refraction index component; this is the anomalous dispersion region. During the peak and cross over time, there is anomalous and negative dispersion. However, temperature and absolute humidity density variations perturb the down-range beam phase and amplitude characteristics differently near absorption line centers and line wings, as evidenced by the following full Lorentzian model for the complex permittivity for a collection of lines (Equation 6.3). The τ component is the collision time at the atomic level; this is driven primarily by temperature, so $\tau \sim T^{0.8}$ [6]. The humidity factor is driven by the molecular content of n_0 . At the peak are the anomalous dispersion and crossing point of refractive index where $\omega_0 = \omega$; the real permittivity goes across zero and inverts setting around the absorption peak — imaginary.

$$\epsilon_{g(\omega)} = \sum_{\text{species } k,n} \sum \left(\frac{n_o e^{-\frac{E_2}{kT}}}{Z} \left[1 - e^{-\frac{h\omega_0}{kT}} \right] \left(\frac{|\bar{\mu}_{12}|^2}{3\hbar} \right) \right) \times \quad (6.3)$$

$$\left[\frac{\omega_0 - \omega}{(\omega_0 - \omega)^2 + (1/\tau)^2} + \frac{\omega_0 + \omega}{(\omega_0 + \omega)^2 + (1/\tau)^2} + i \left\{ \frac{1/\tau}{(\omega_0 - \omega)^2 + (1/\tau)^2} + \frac{1/\tau}{(\omega_0 + \omega)^2 + (1/\tau)^2} \right\} \right]$$

6.3 TAIPAS Hallway – 40 m Indoor Path

The absorption imaginary component symmetry is compared by MATLAB fold-over of the LWL and UWL of the absorption on top of each other. The UWL scan, Table 6.2, is reflected about the 325.1529 GHz peak to overlay on top of the LWL scan, Table 6.1.

The following figures show the LWL and UWL absorption slope scans utilizing a mean value for each frequency scan amplitude. In the case of the hallway path of ~40 m, the plots can be off due to errors in calibration and are not expected on the much longer path of the destination (1924 m); real data will dominate the atmospheric response and calibration will be in the noise. Figure 6.2 shows the LWL of absorption; it looks inverted of the expected due to calibration since it is only over a ~1.5 dB amplitude swing. Figure 6.3 shows the Figure 6.1 plot with the Friis expectation plot in green and the difference in red. The amplitudes are exaggerated off due to the lack of power tuning; no perfect gain adjustments will be done until TAIPAS is deployed on the open path. Figure 6.4 shows an amplitude normalized Friis plot overlaid with the short path collected LWL. The Friis shows the UWL of received power of ~0.25 dB. Figure 6.5 -

Figure 6.5 show similar plots for the UWL absorption plot or LWL of power attenuation. The amplitude range it covers is ~ 0.6 dB, which is very small, but it still has an inverted result from expectations. Figure 6.8 shows the fold over of the UWL on top of the LWL and normalized. There are two sets of scans down for each and they fall fairly on top of one another. Friis LWL and UWL are the red and black plots that are even slightly off. The green is the UWL and the blue is the LWL; the UWL falls closer to predicted, but the LWL is an acceptable amount off.

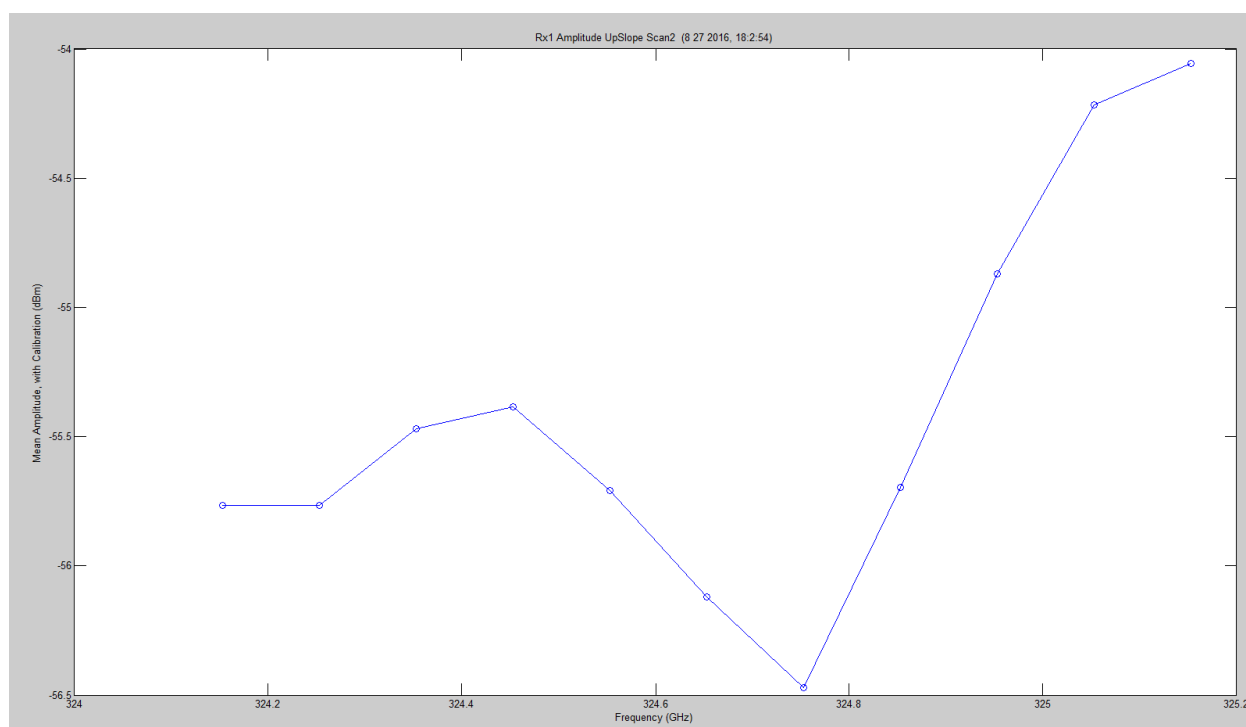


Figure 6.2. TAIPAS LWL Hallway Scan.

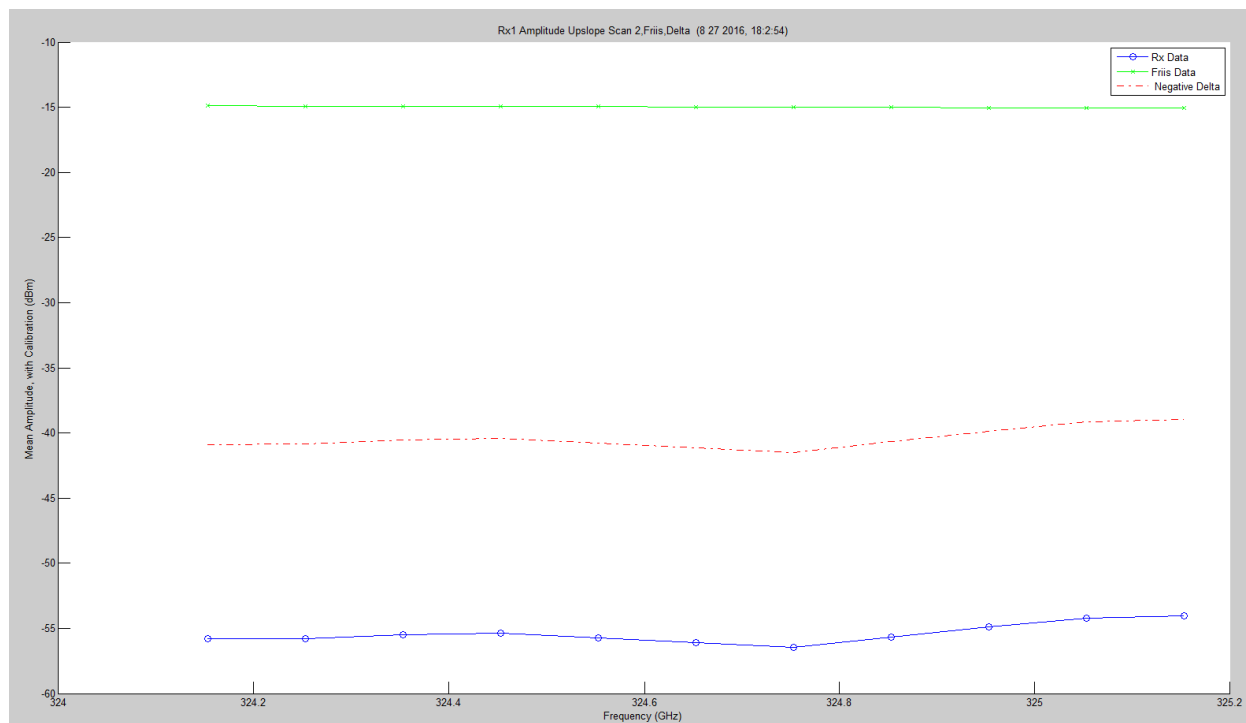


Figure 6.3. TAIPAS LWL Hallway Scan with Friis.

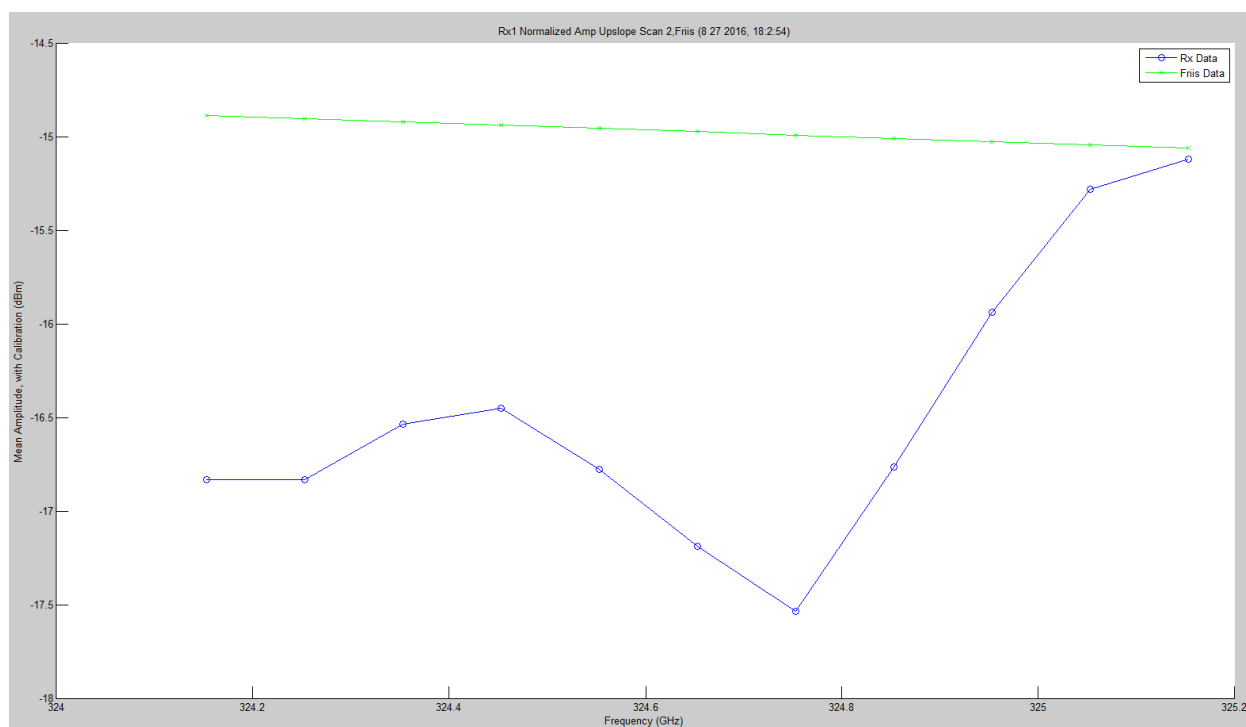


Figure 6.4. TAIPAS LWL Hallway Scan Normalized with Friis.

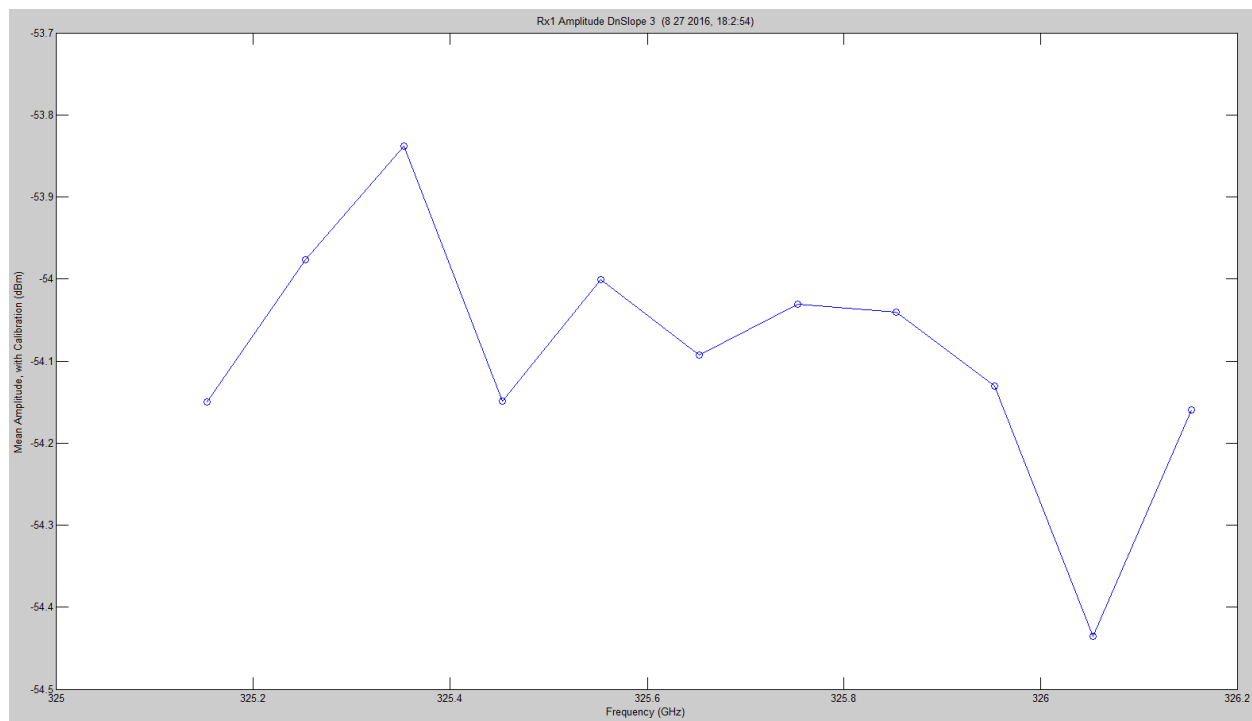


Figure 6.5. TAIPAS UWL Hallway Scan.

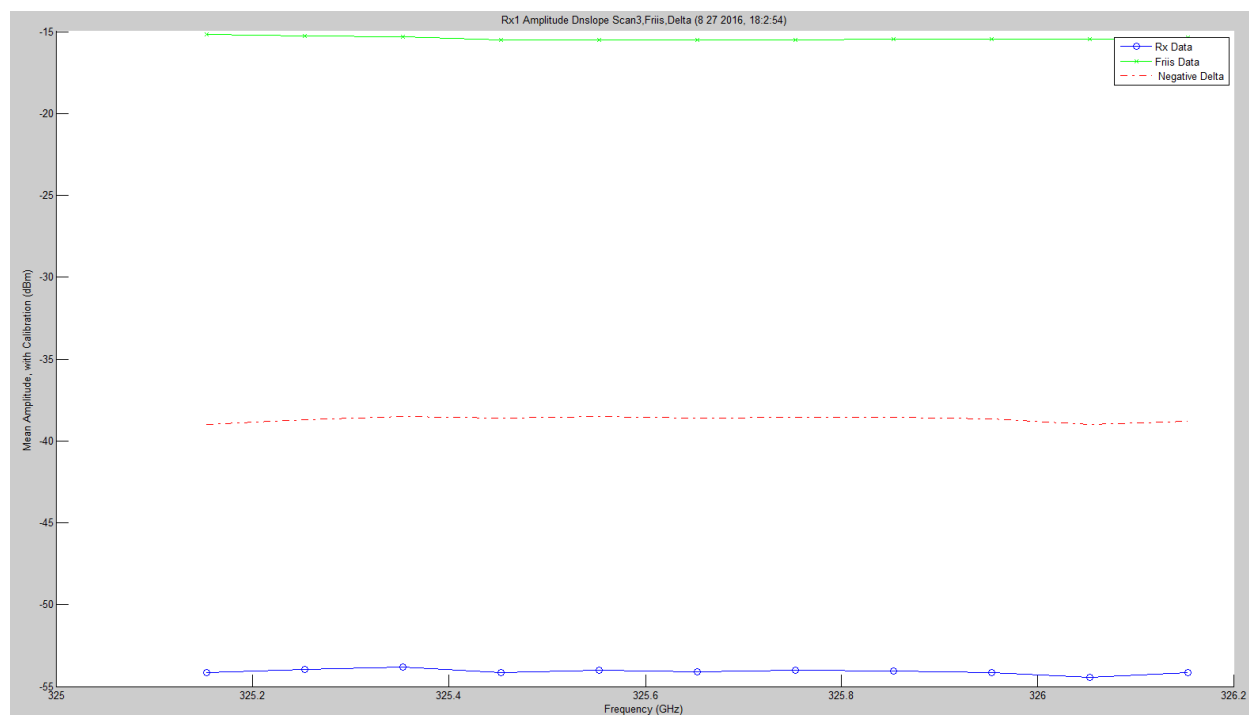


Figure 6.6. TAIPAS UWL Hallway Scan with Friis.

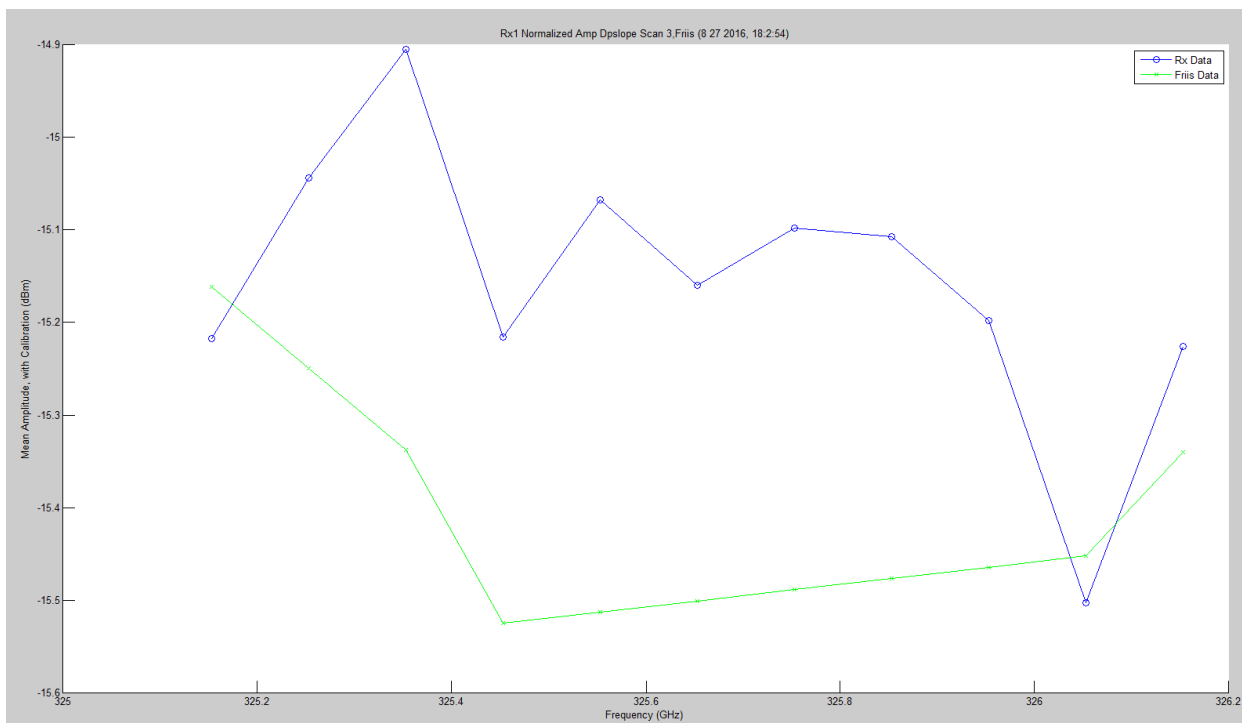


Figure 6.7. TAI PAS UWL Hallway Scan Normalized with Friis.

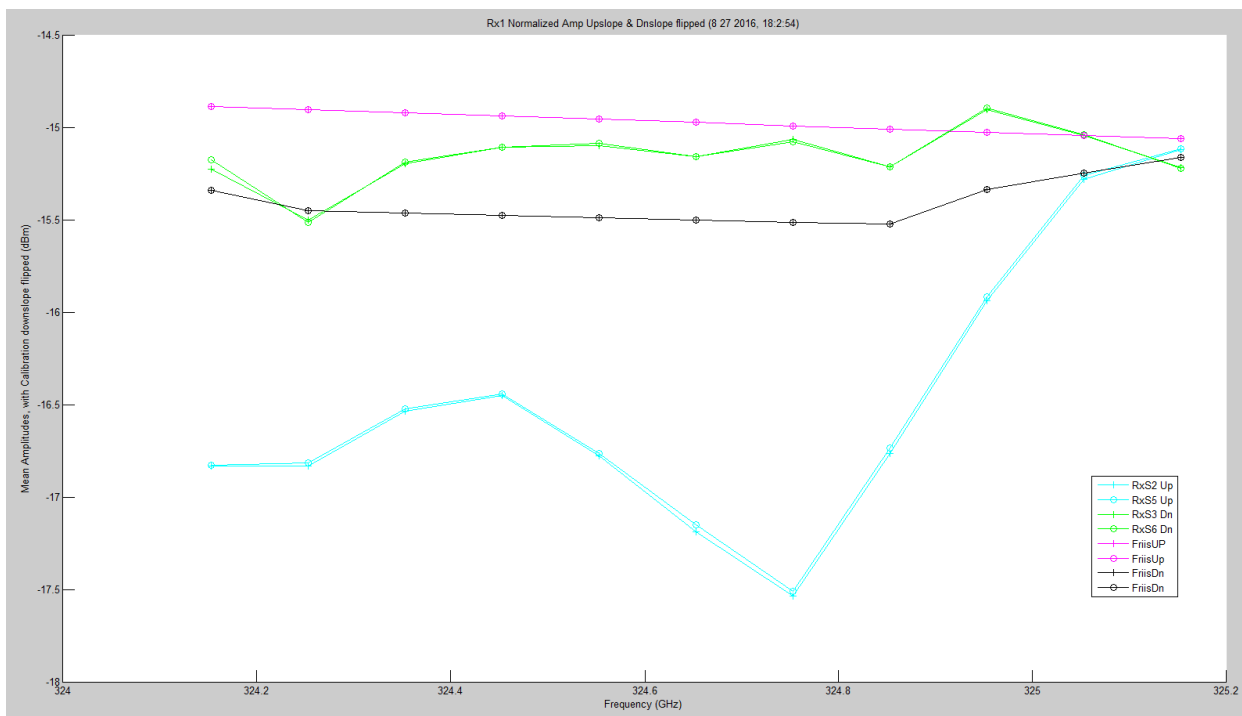


Figure 6.8. TAI PAS LWL and UWL Flipped Hallway Scan Normalized with Friis.

Figure 6.9 – Figure 6.11 show the extinction plots for the absorption LWL and UWL scans. Since two receivers could not fit in the hallway, nor was the spot size large enough over 40 m to cover them, the Rx1 equals Rx2. The Friis calculation is at the bottom of the plot. The large attenuation per km is due to the lack of alignment in the hallway. Figure 6.11 shows the same LWL and Friis plot with the UWL flipped. This allows comparison of the LWL and UWL absorption shapes.

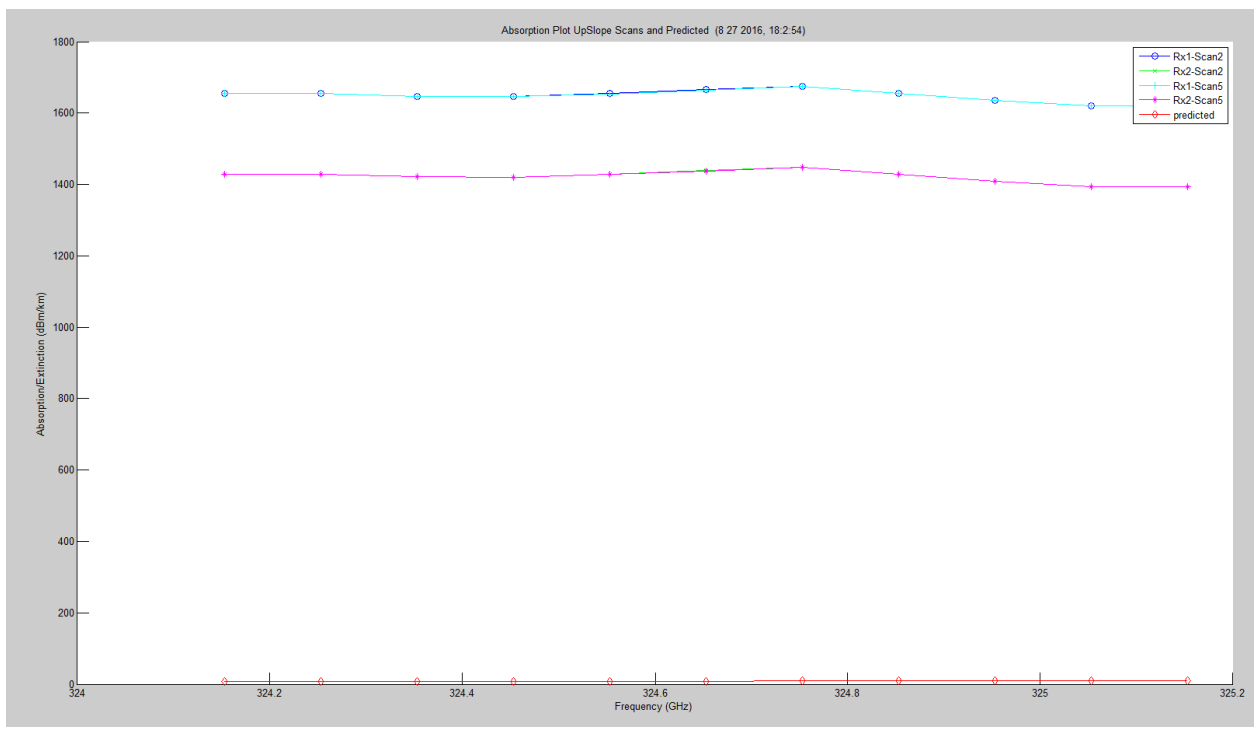


Figure 6.9. Hallway LWL and Friis Extinction Plots.

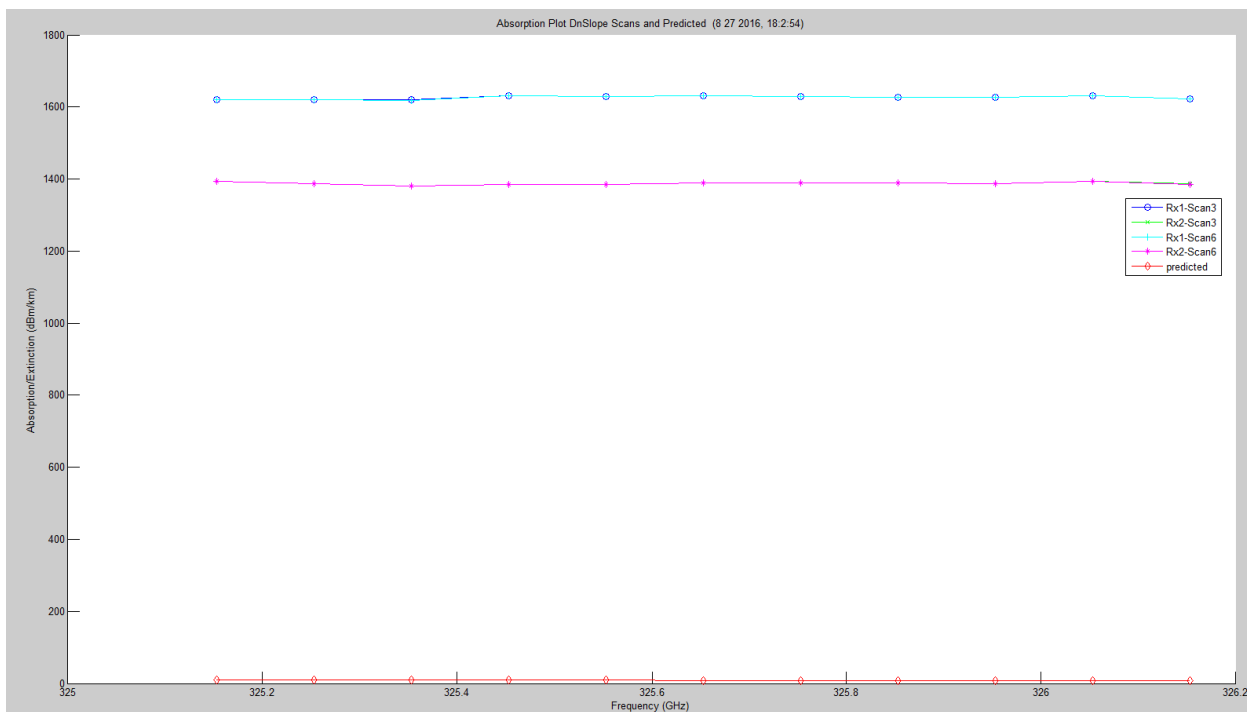


Figure 6.10. Hallway UWL and Friis Extinction Plots.

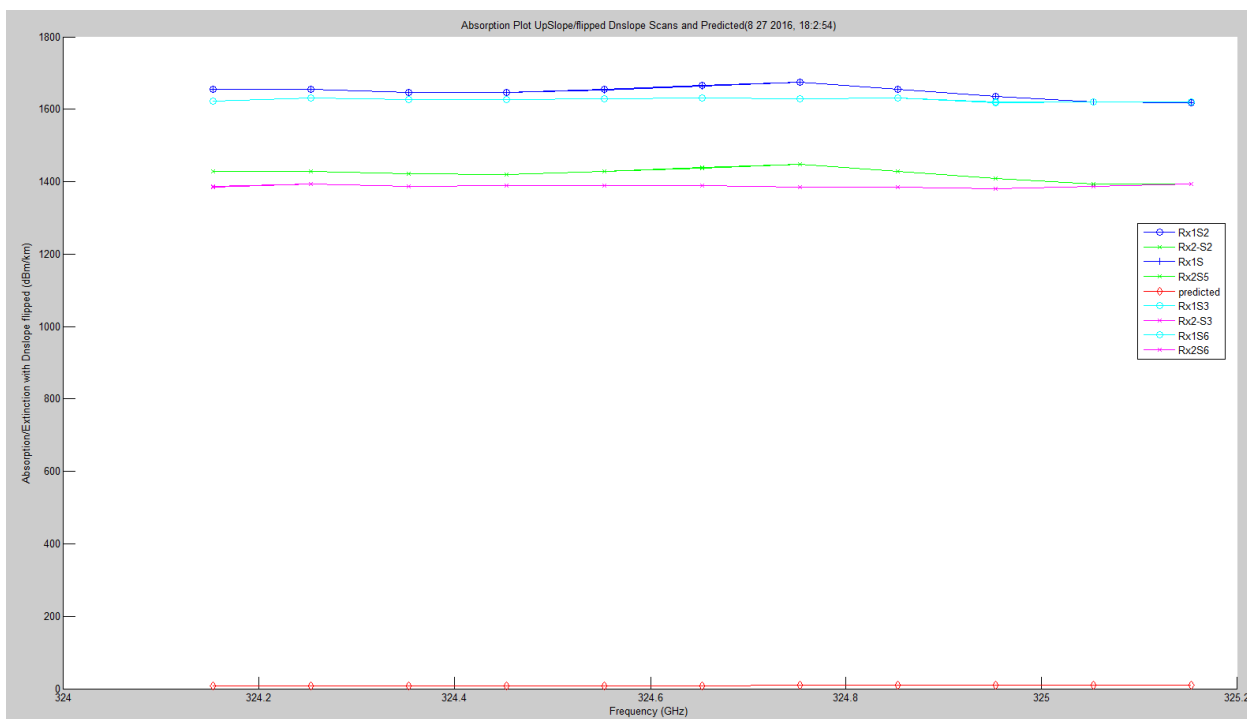


Figure 6.11. Hallway LWL, Flipped UWL and Friis Extinction Plots.

Figure 6.12 – Figure 6.14 show the MCF and phase structure functions for the WB, LWL and UWL scans. The WB is included to show the dynamics under the absorption peak. The phase structure function is just minus two times the MCF. The blue plots in this case represent the two sets of identical frequency scans (e.g. WB 1 and 4). These are close for all scans. The maximum phase range is $\sim 0.15^\circ$.

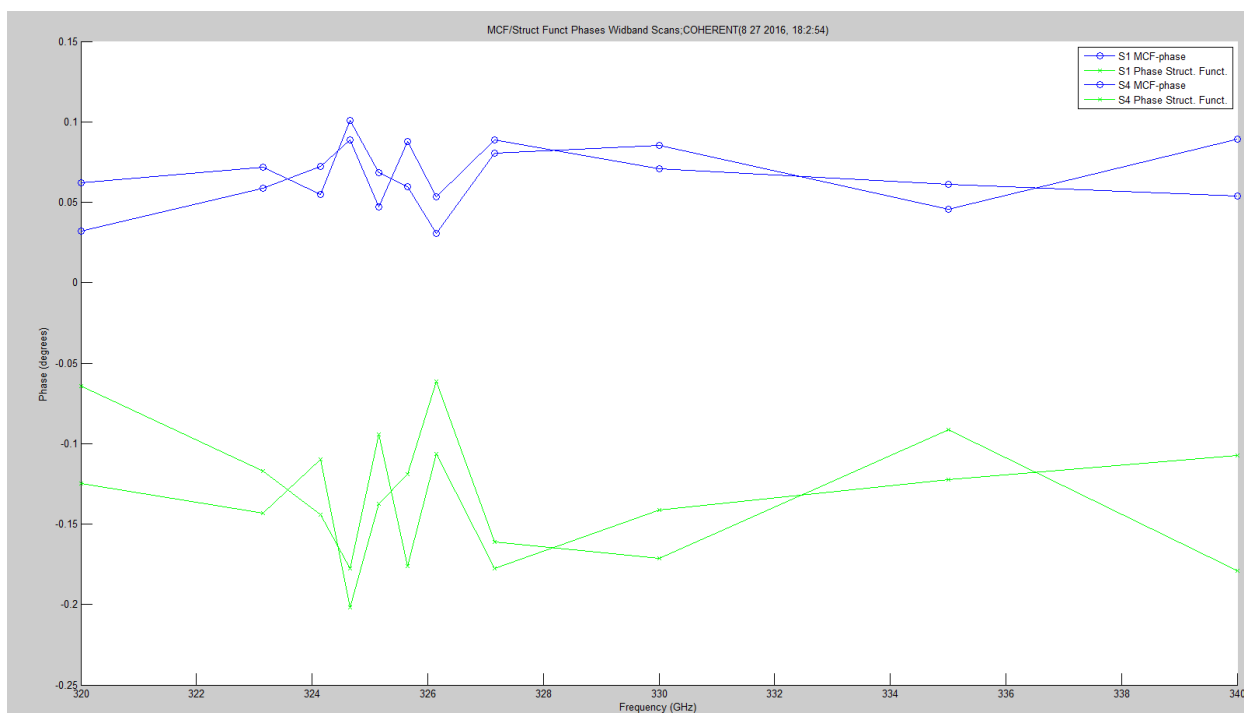


Figure 6.12. WB MCF/Structure Function Plots.

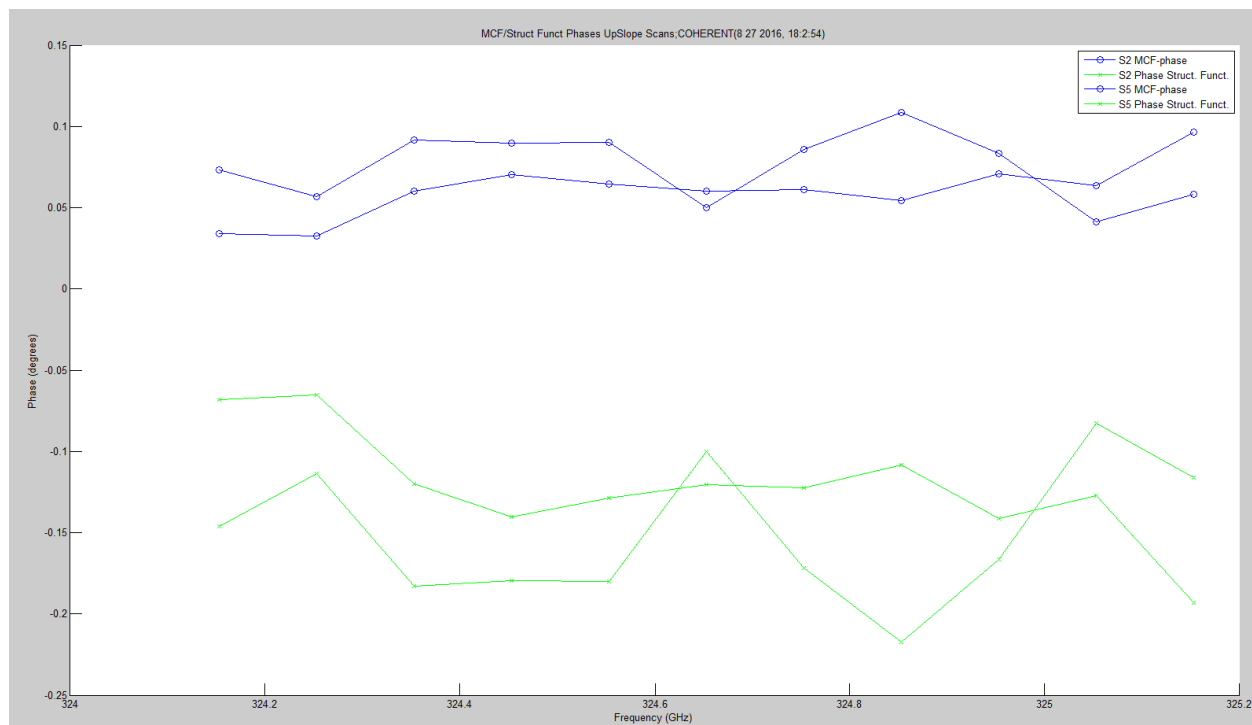


Figure 6.13. LWL MCF/Structure Function Plots.

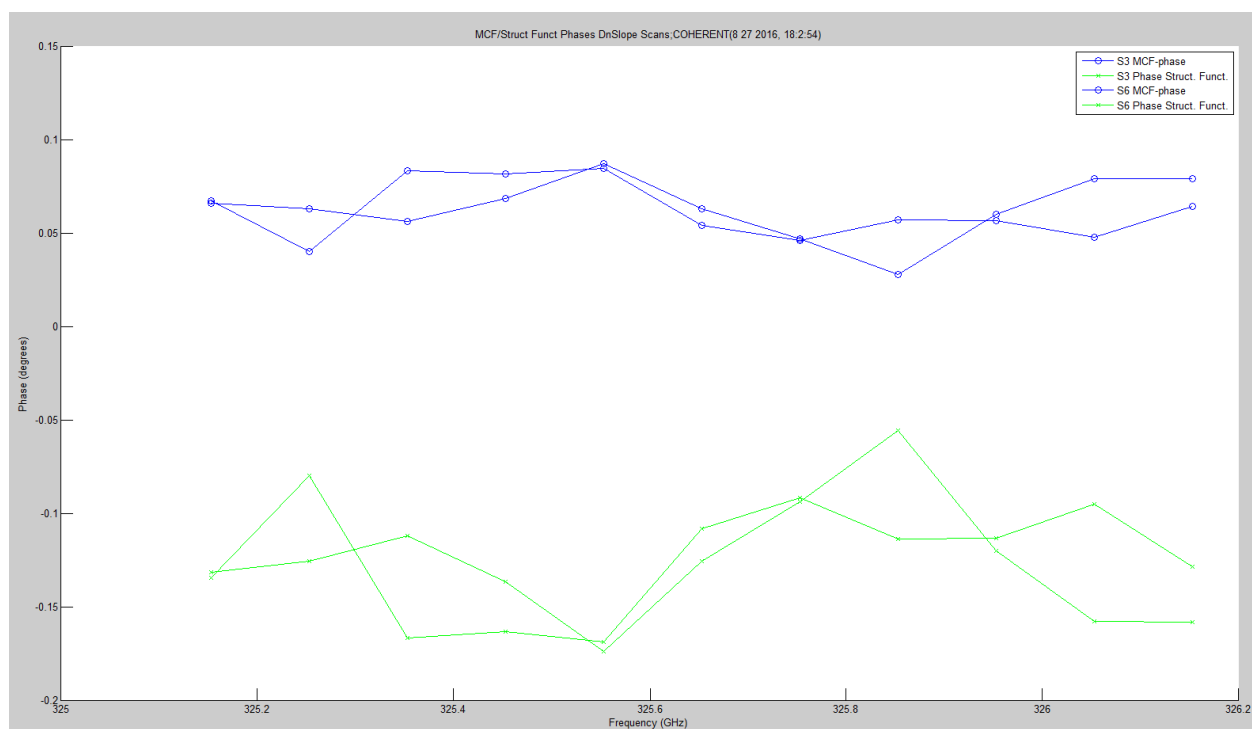


Figure 6.14. UWL MCF/Structure Function Plots.

Figure 6.15 – Figure 6.17 show the amplitude scintillation, $\langle \chi^2 \rangle$, for all the scans — two each — compared to the predicted valued utilizing Kolmogorov with outer scale. The WB is included for the same reasons as above. The predicted values are very flat and there are more dynamics in real data; it could be accentuated by calibration errors. The largest dynamics occur around the peak of absorption. The LWL and UWL are not the same, but are very similar.

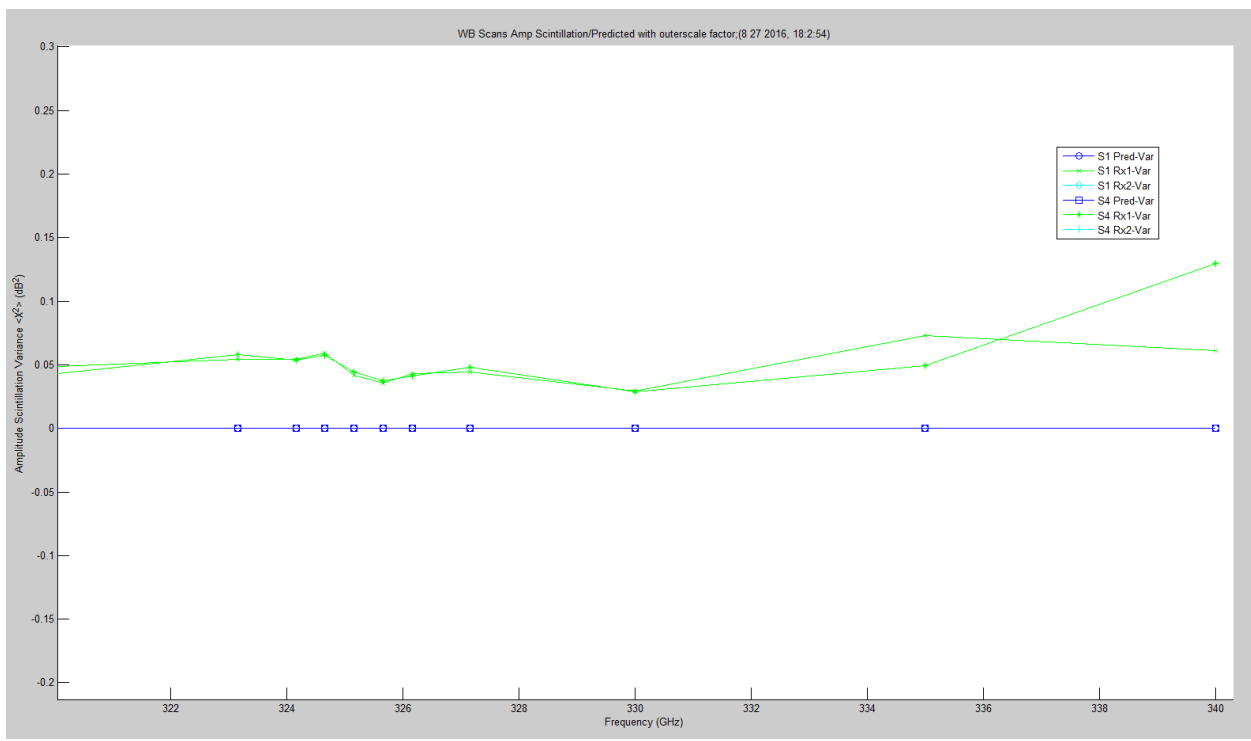


Figure 6.15. WB Amplitude Scintillation with Outer Scale Factor Prediction.

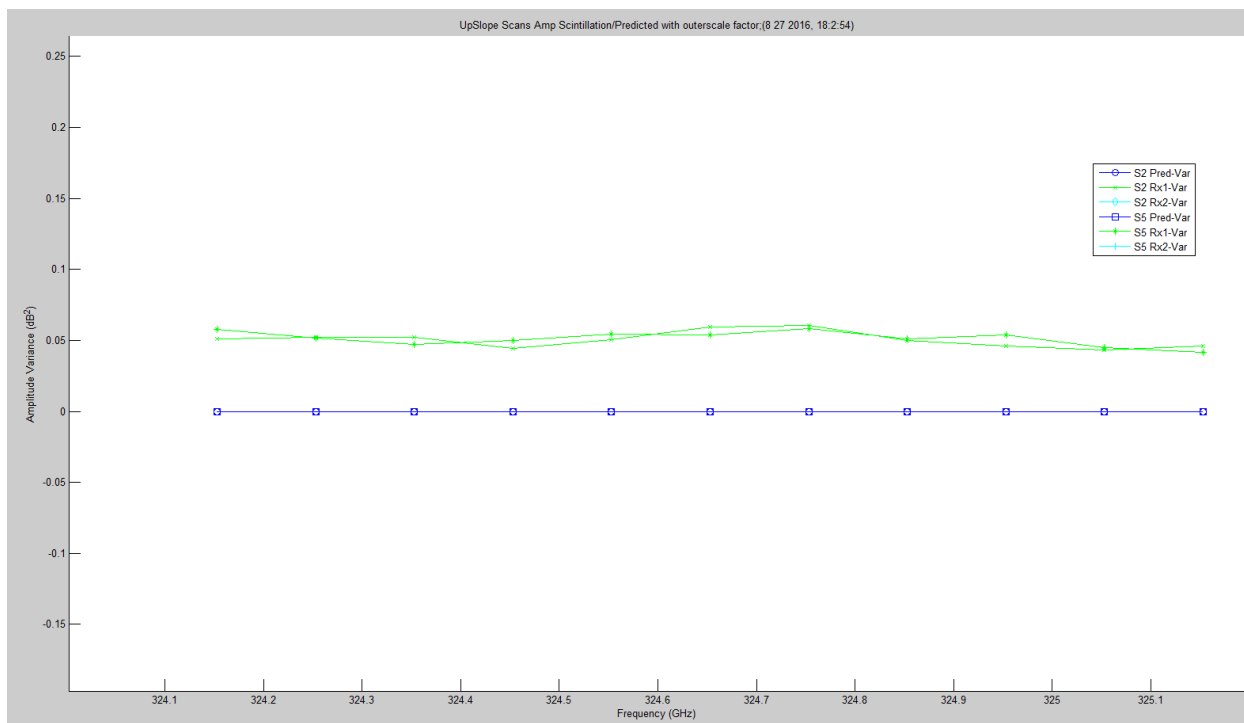


Figure 6.16. LWL Amplitude Scintillation with Outer Scale Factor Prediction.

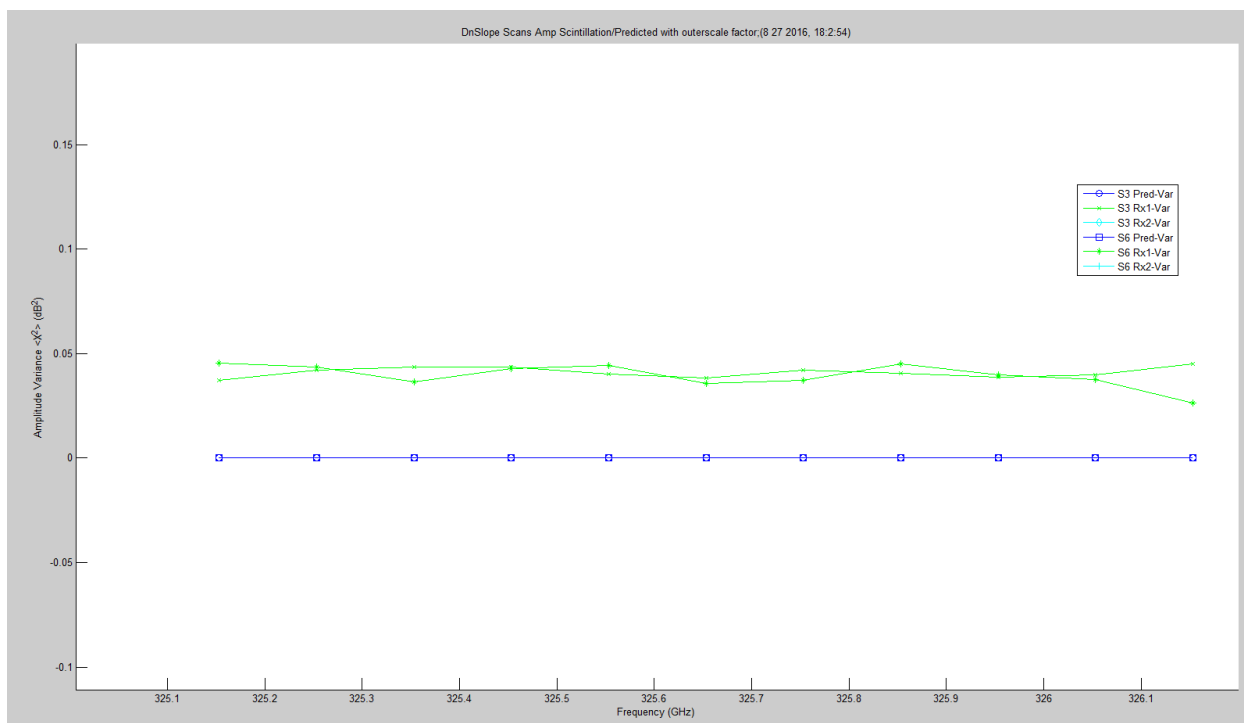


Figure 6.17. UWL Amplitude Scintillation with Outer Scale Factor Prediction.

Figure 6.18 – Figure 6.21 show the phase scintillation, $\langle \phi^2 \rangle$, for all the up and down scans — two each — compared to the predicted values utilizing the GO von Karman Model. Each set of plots shows the collected data for both receivers, with minor differences for both scans, and the predicted value. This is repeated for both LWL and UWL scans for phase in degrees, millimeters and picoseconds. In Figure 6.22, WB phase variance standard deviation is included to show that the dynamics of the phase occur at the resonant peak. The prediction is smooth, but changes at the peak in Figure 6.23. Figure 6.24 – Figure 6.27 show the same phase scintillation for LWL and UWL absorption slopes. Figure 6.28 – Figure 6.35 show the same data in different units: millimeters and picoseconds.

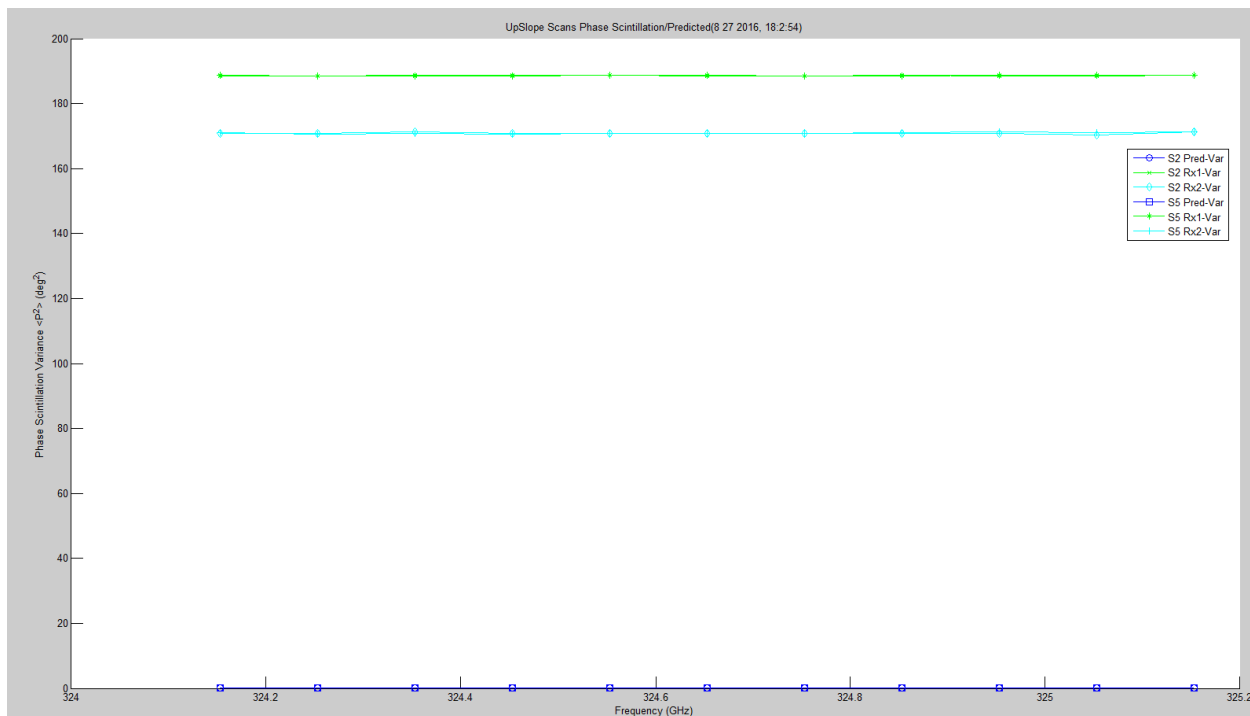


Figure 6.18. LWL Phase Scintillation with Prediction.

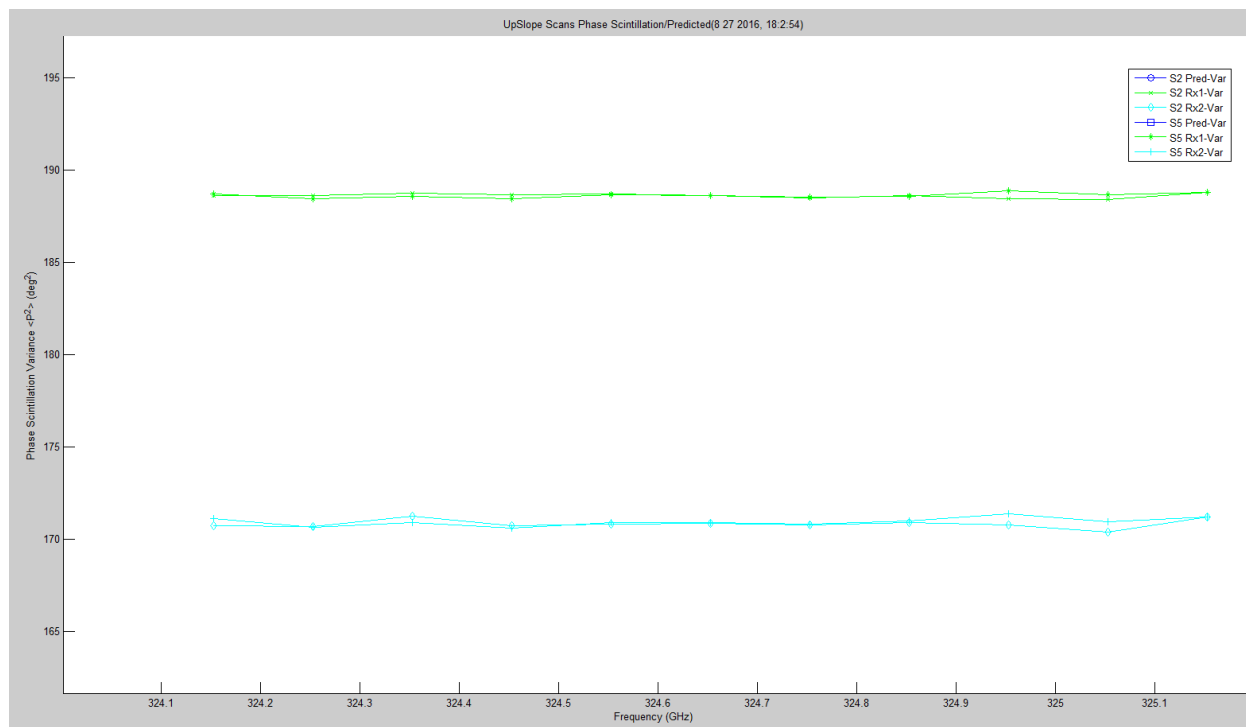


Figure 6.19. LWL Phase Scintillation.

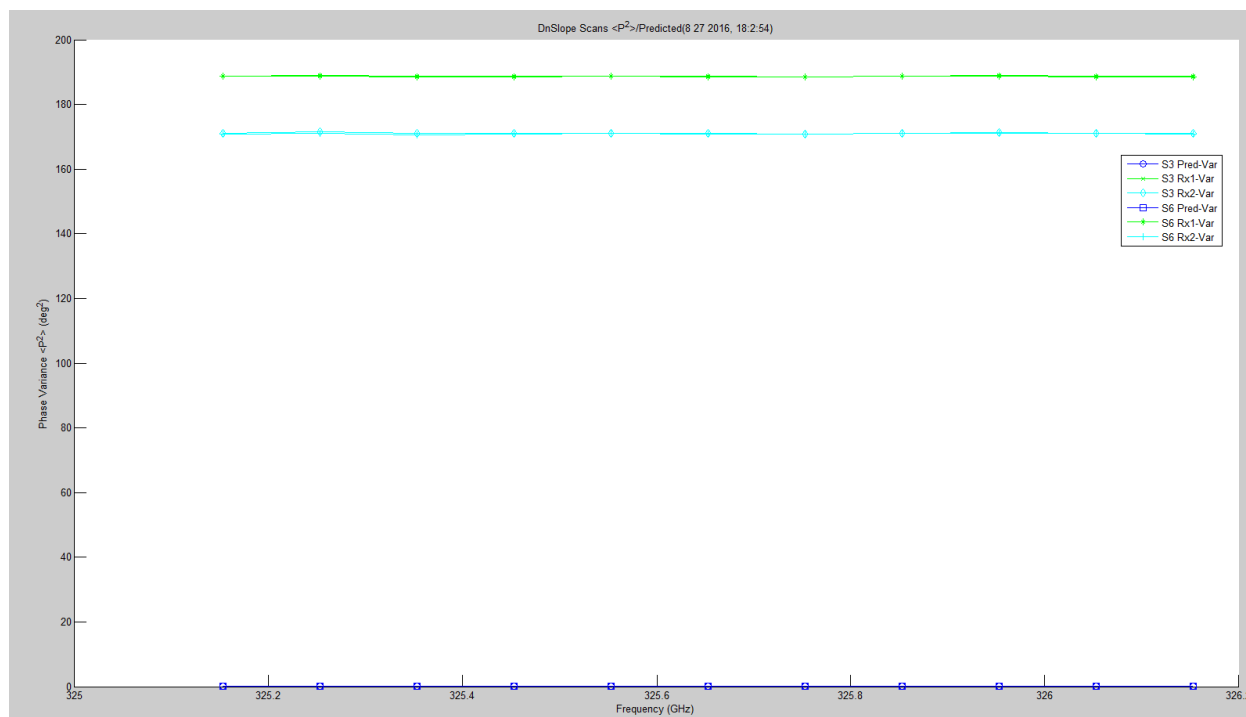


Figure 6.20. UWL Phase Scintillation with Prediction.

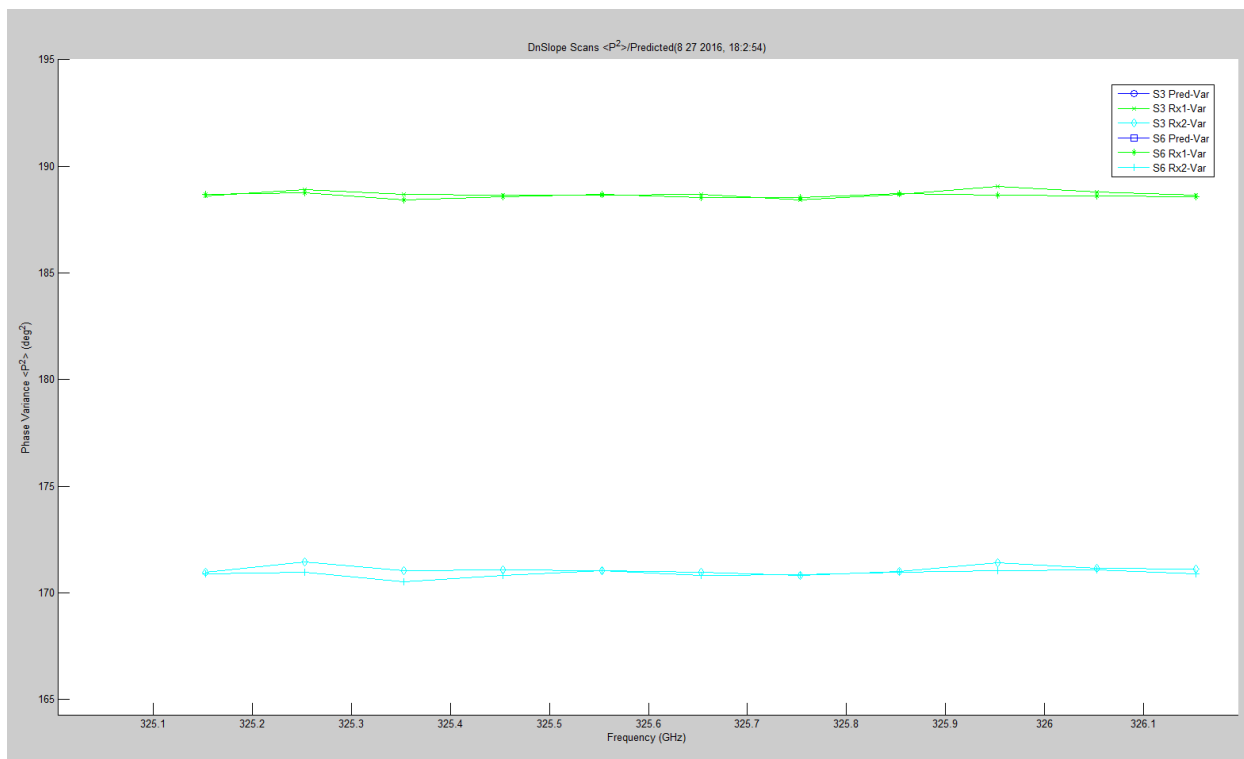


Figure 6.21. UWL Phase Scintillation.

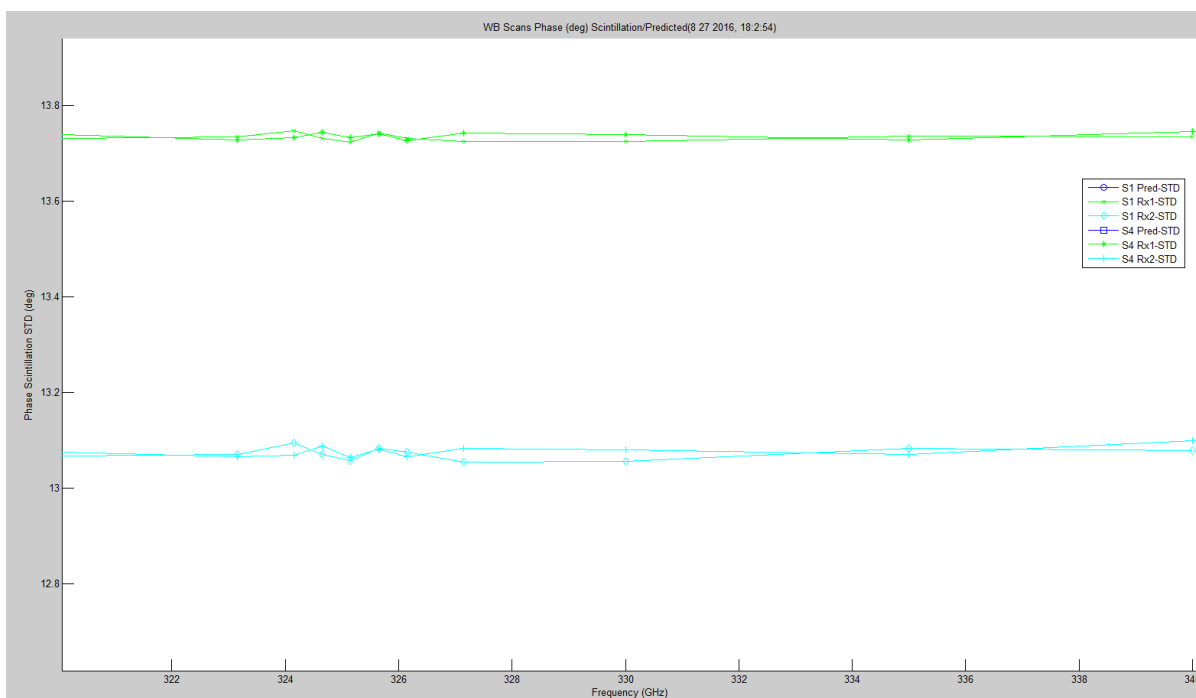


Figure 6.22. WB Phase Scintillation STD Degrees.

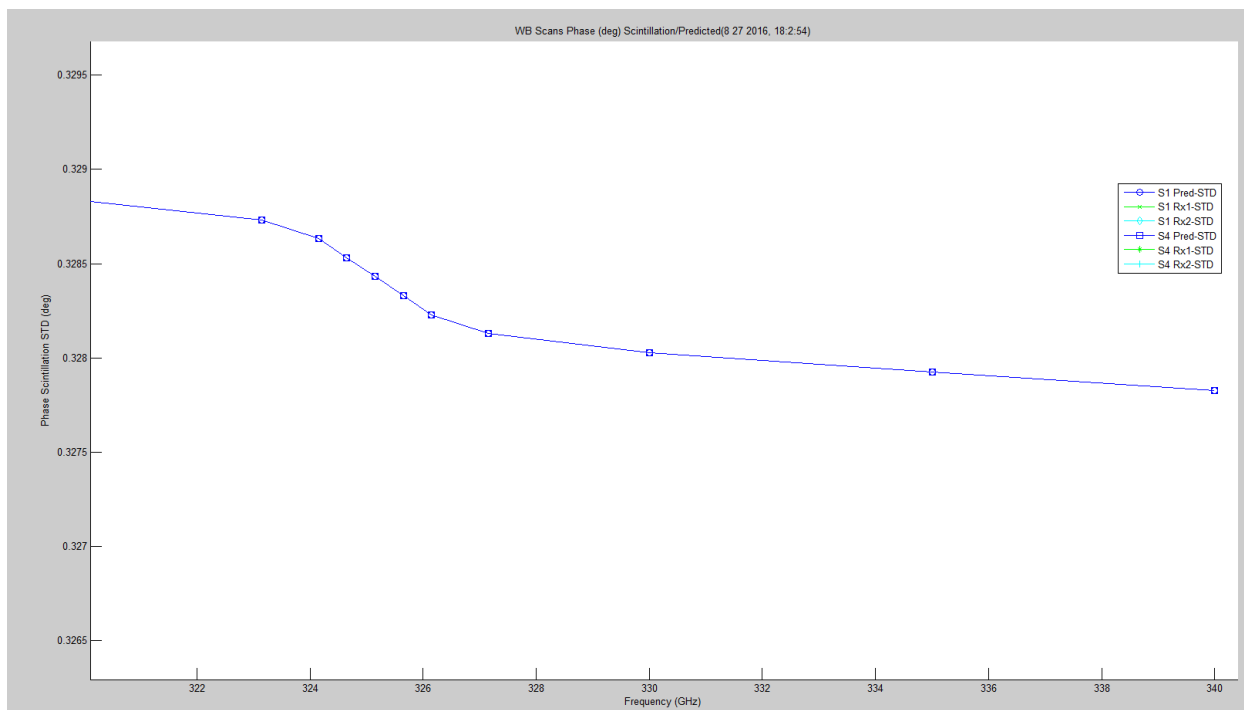


Figure 6.23. WB Phase Scintillation STD Prediction Degrees.

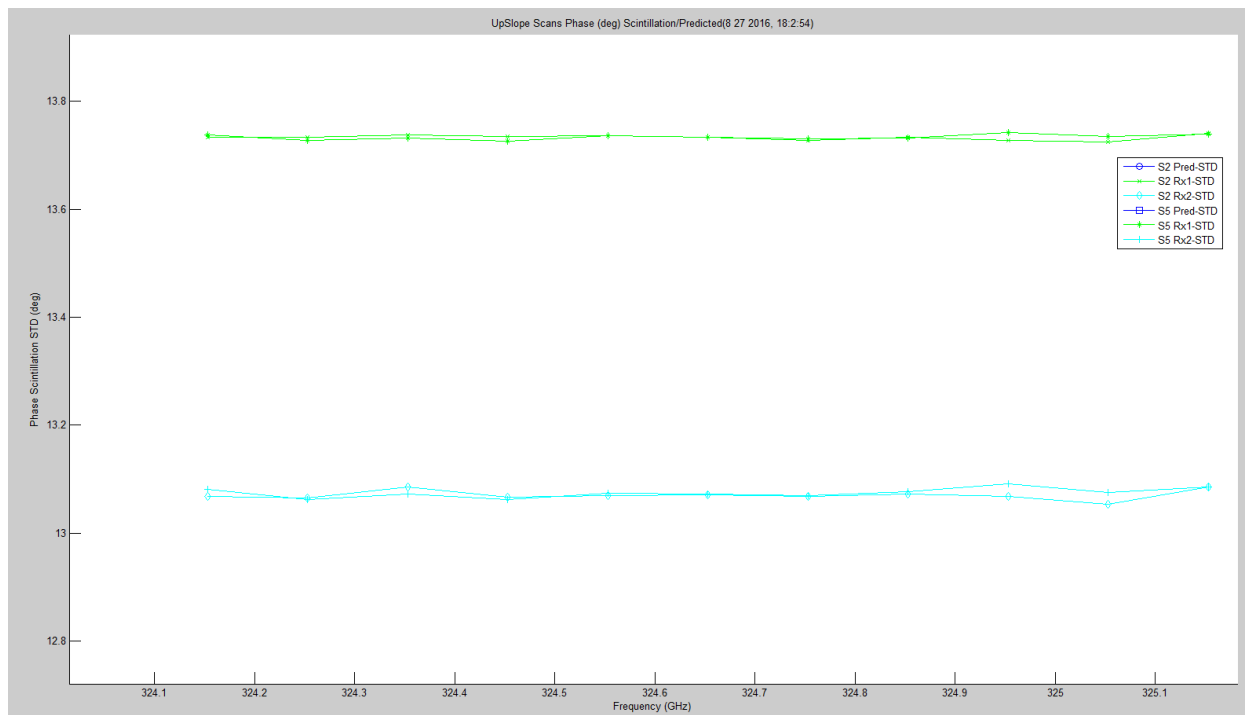


Figure 6.24. LWL Phase Scintillation STD Degrees.

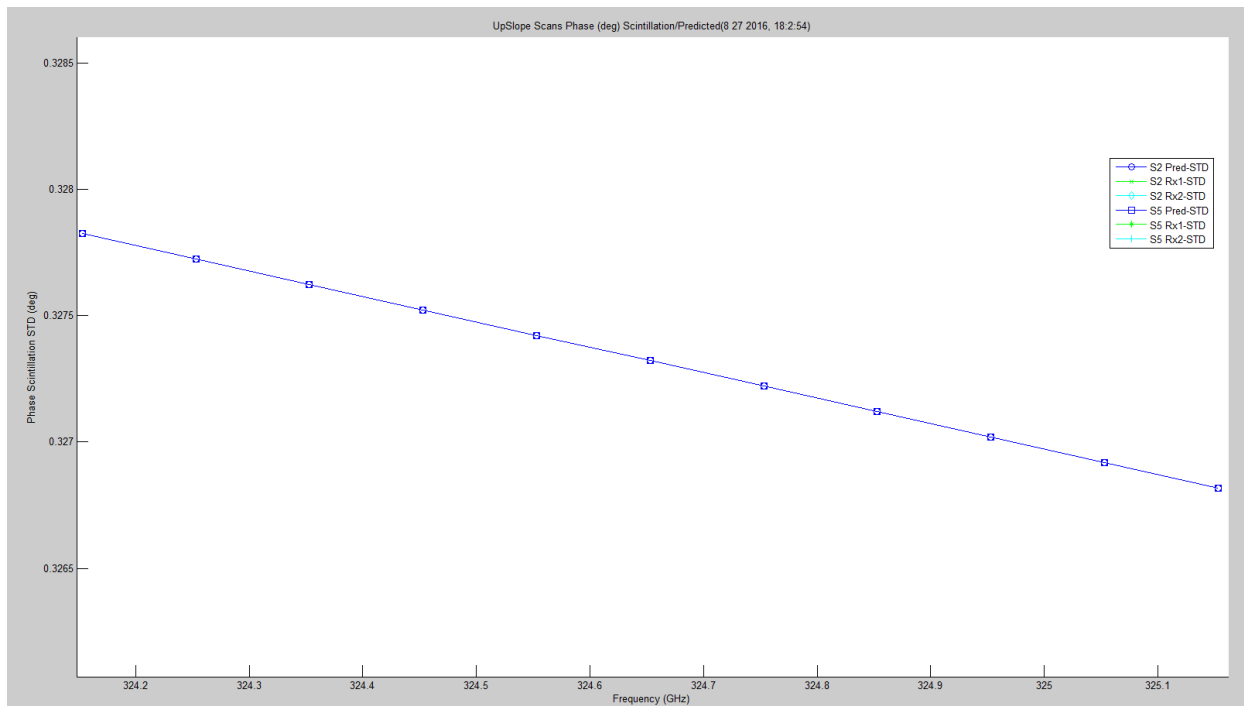


Figure 6.25. LWL Phase Scintillation STD Prediction Degrees.

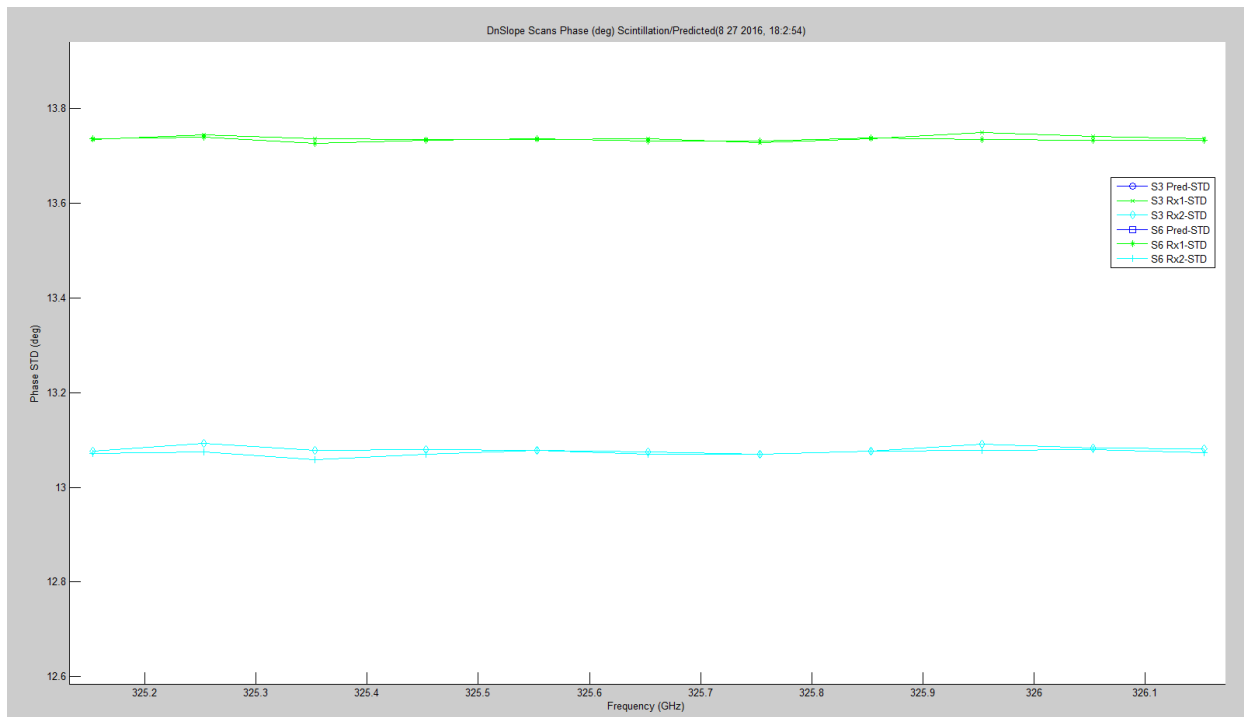


Figure 6.26. UWL Phase Scintillation STD Degrees.

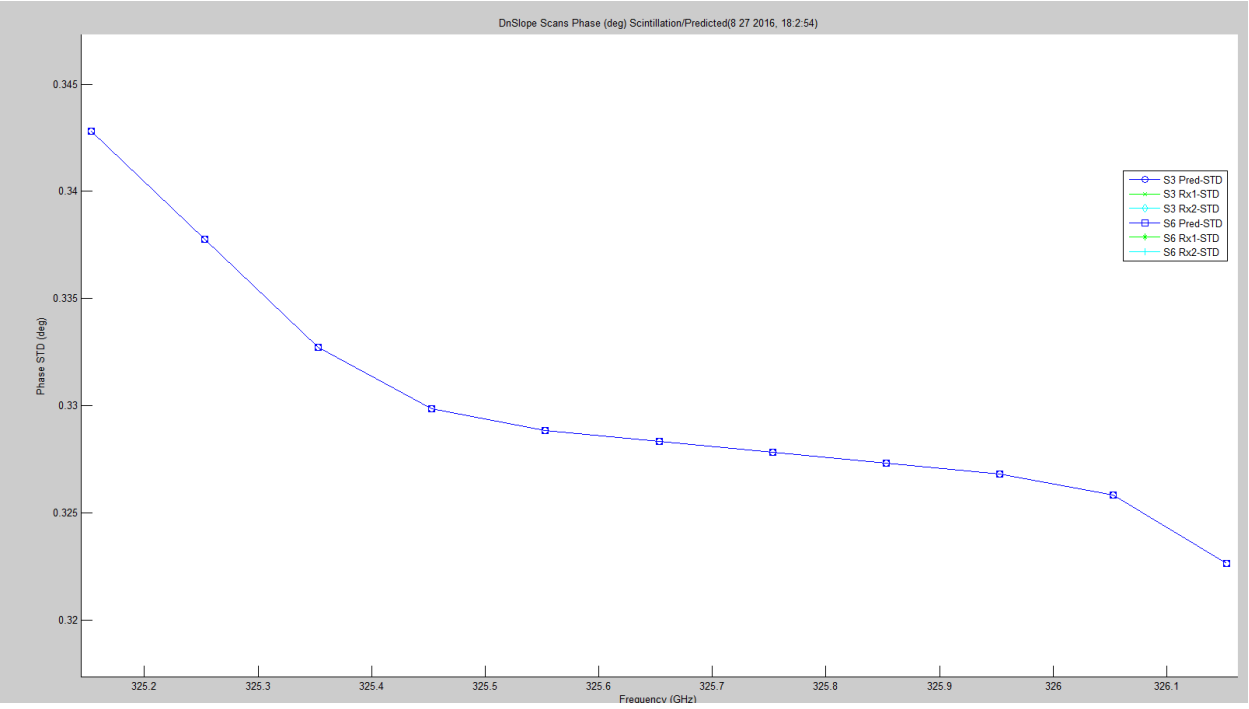


Figure 6.27. UWL Phase Scintillation STD Prediction Degrees.

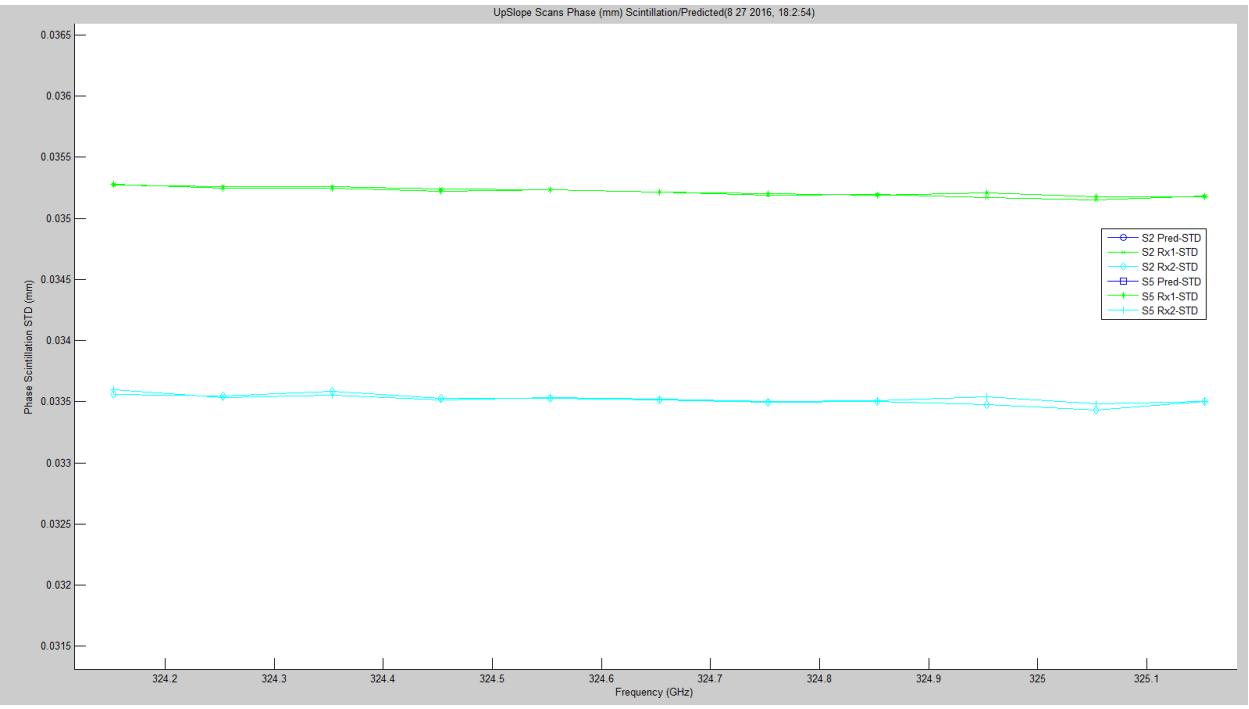


Figure 6.28. LWL Phase Scintillation STD Millimeters.

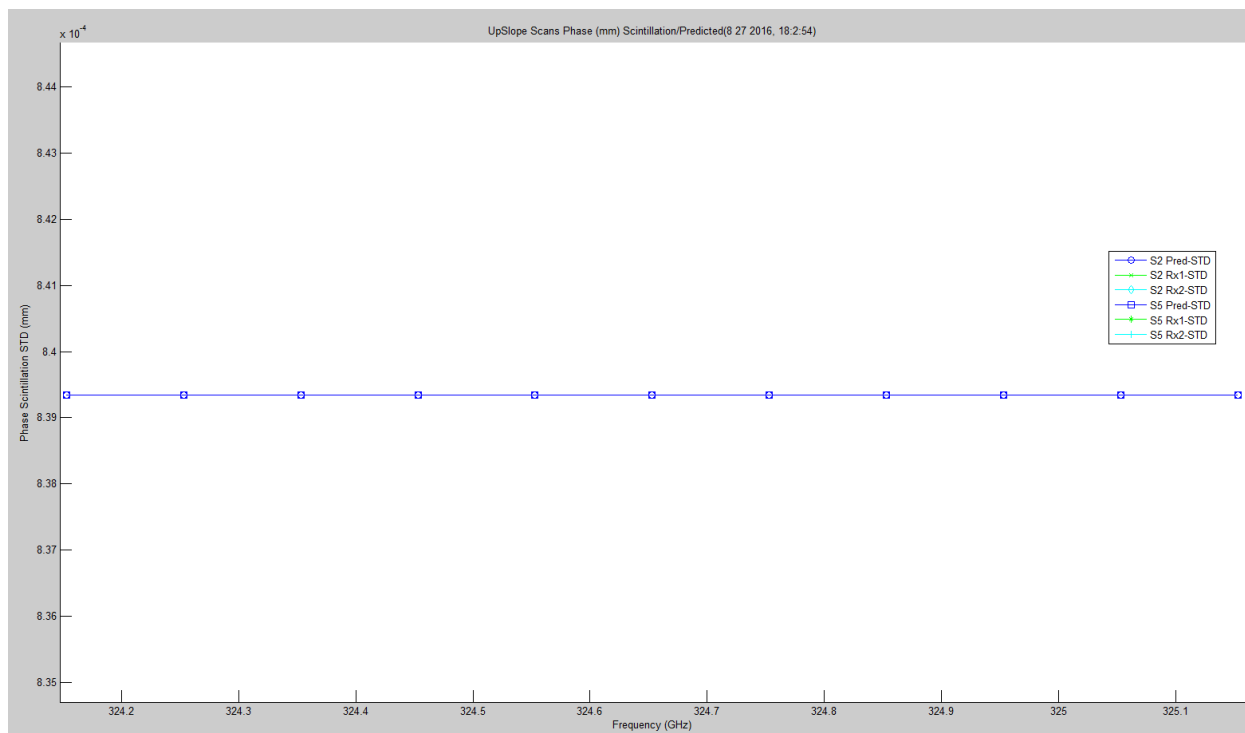


Figure 6.29. LWL Phase Scintillation STD Prediction Millimeters.

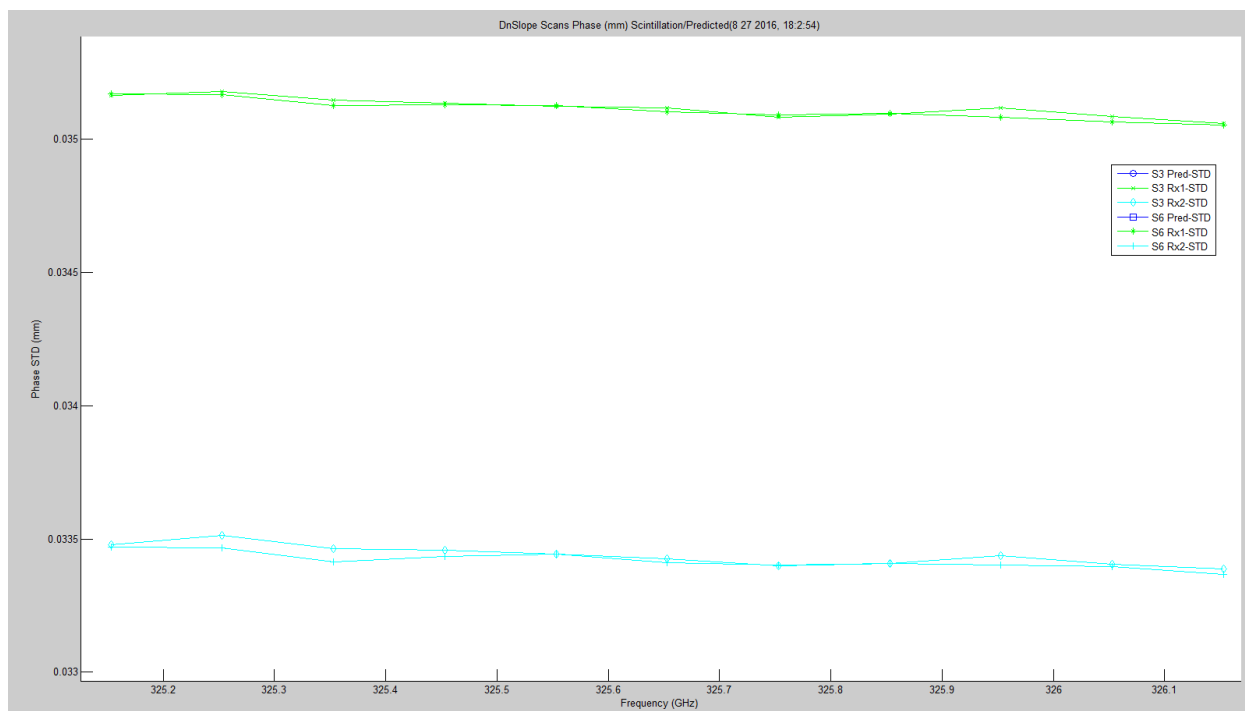


Figure 6.30. UWL Phase Scintillation STD Millimeters.

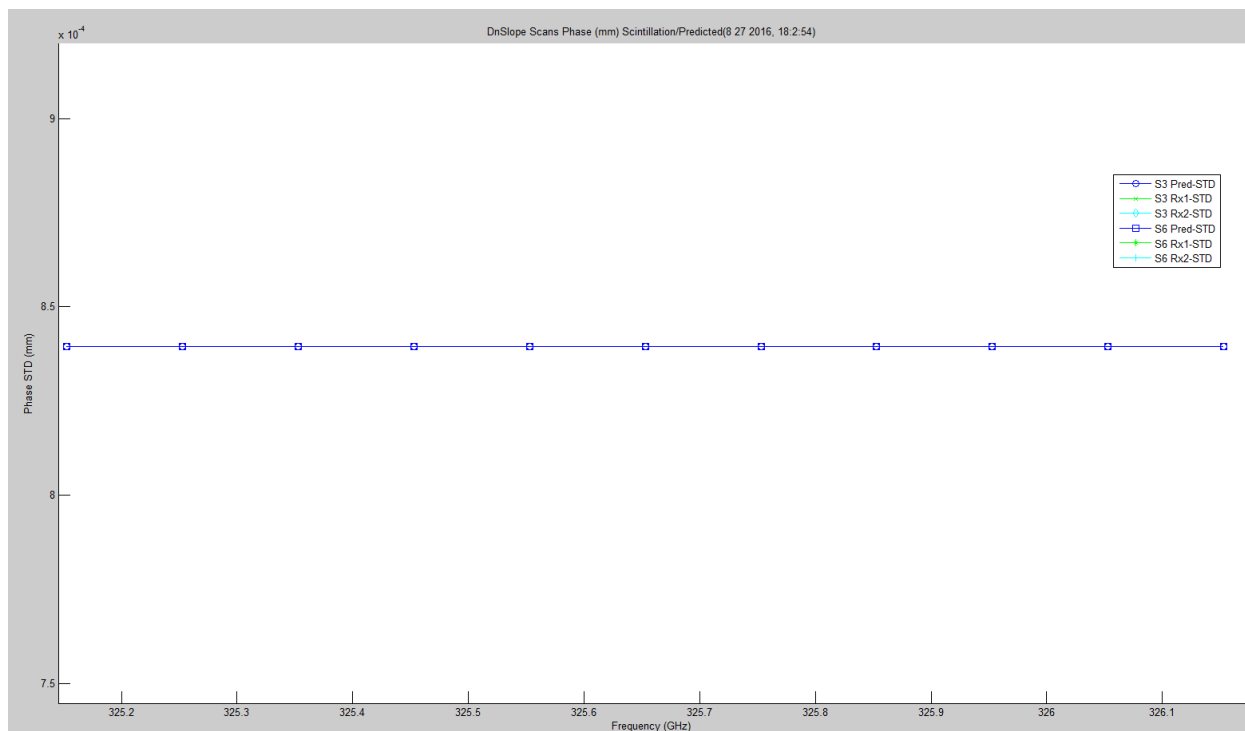


Figure 6.31. UWL Phase Scintillation STD Prediction Millimeters.

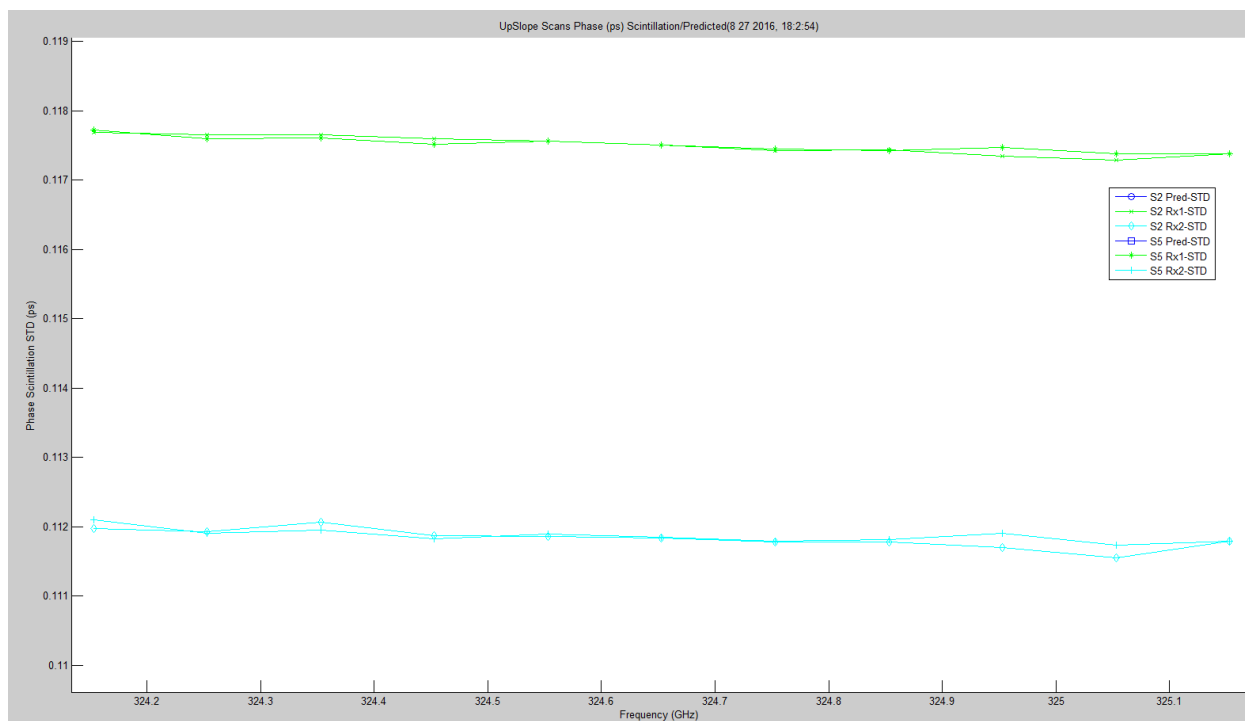


Figure 6.32. LWL Phase Scintillation STD Picoseconds.

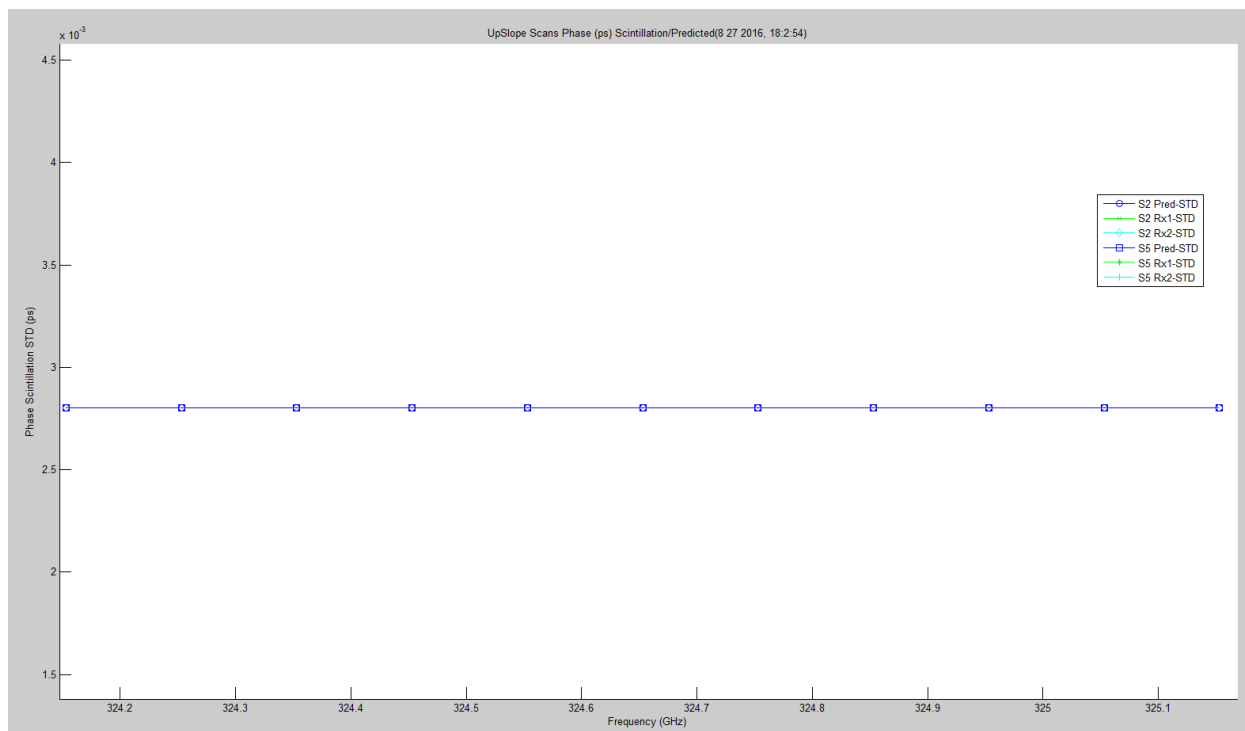


Figure 6.33. LWL Phase Scintillation STD Prediction Picoseconds.

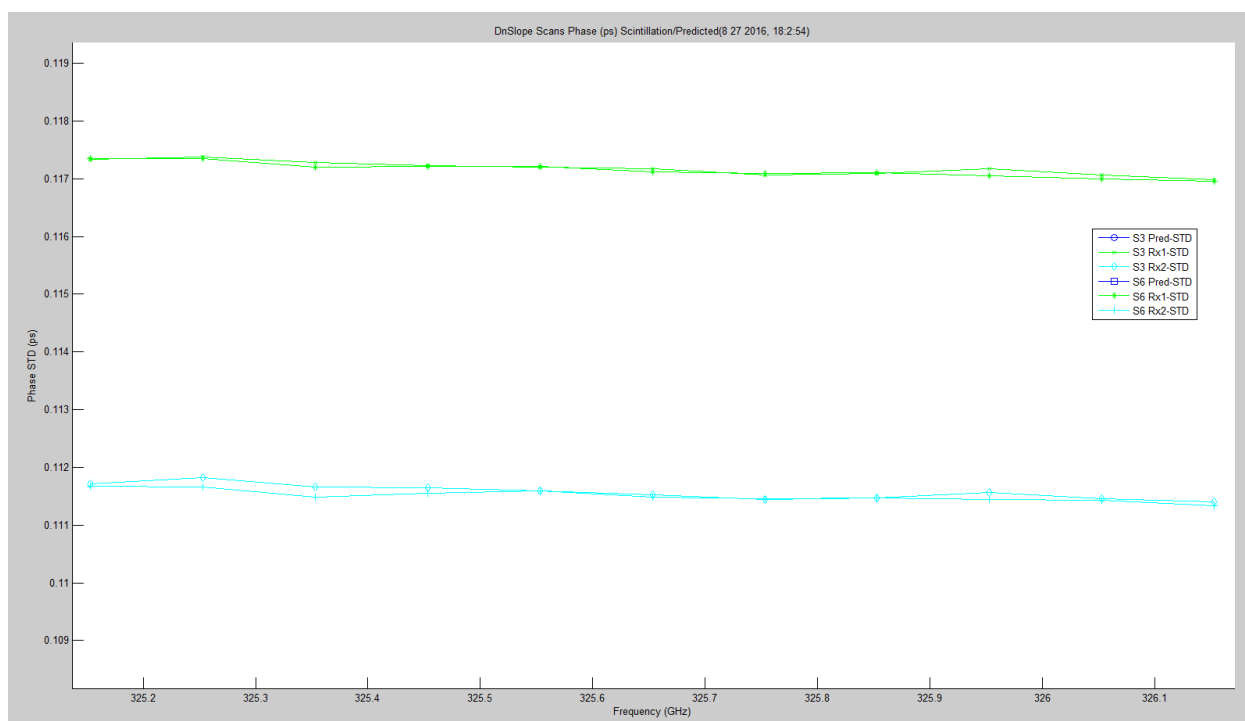


Figure 6.34. UWL Phase Scintillation STD Picoseconds.

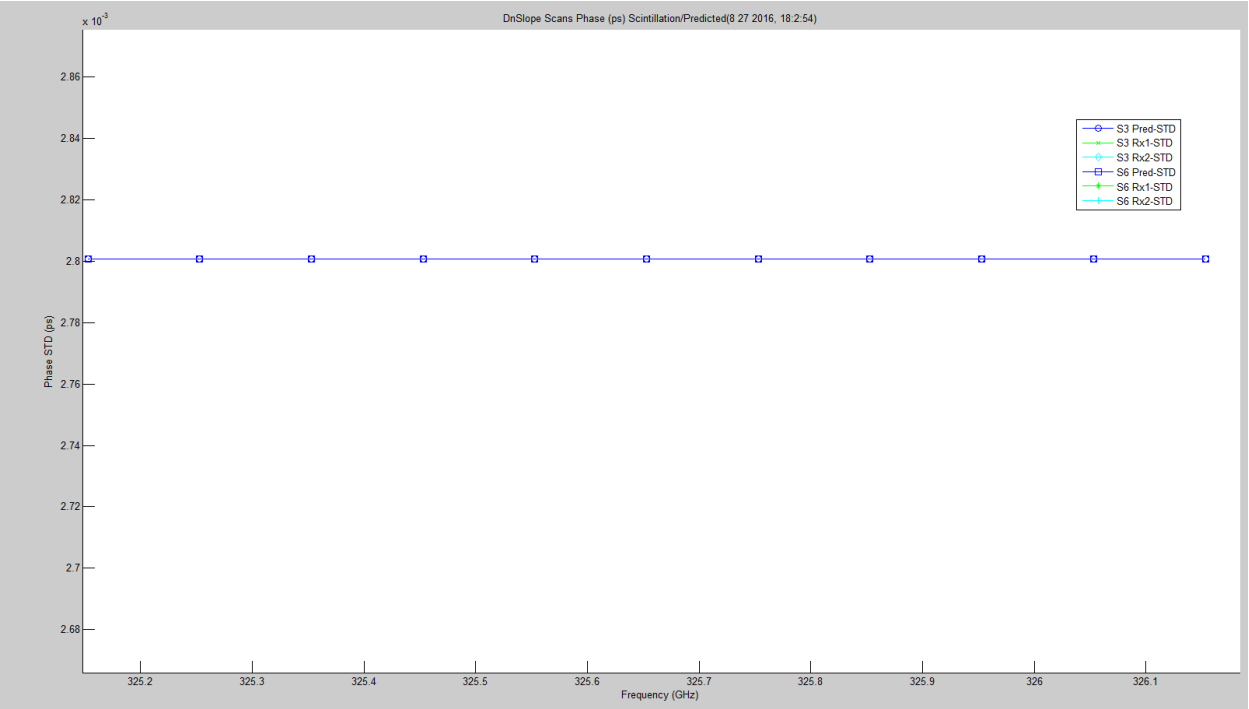


Figure 6.35. UWL Phase Scintillation STD Prediction Picoseconds.

Figure 6.36 – Figure 6.43 show the amplitude and phase scintillation correlation, $\langle \chi\phi \rangle$, for all the scans — three each: total view of predicted and hallway data; view of predicted data; and view of hallway data. WB was left in to show the big picture. The prediction utilizes the Rytov, Fresnel and Fruanhofer versions. In the case of the real data, the correlation becomes stronger as frequency is increased, especially around the absorption peak.

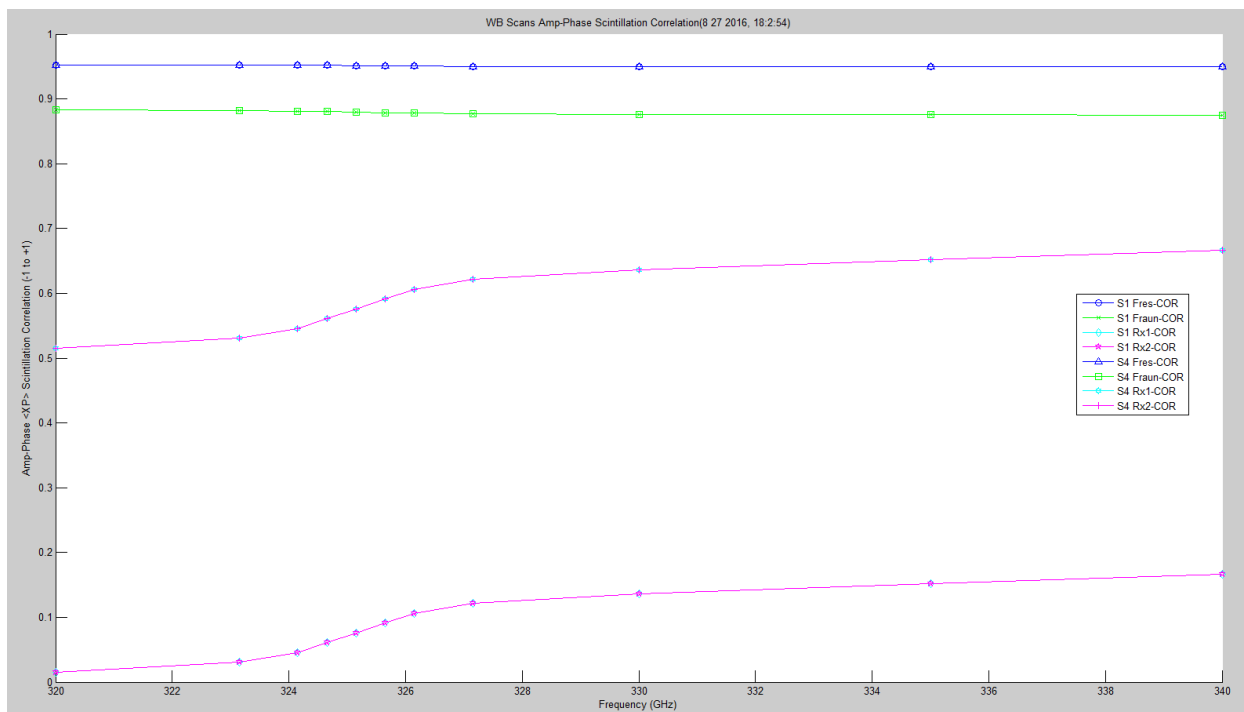


Figure 6.36. WB Amplitude/Phase Scintillation Cross Correlation with Prediction.

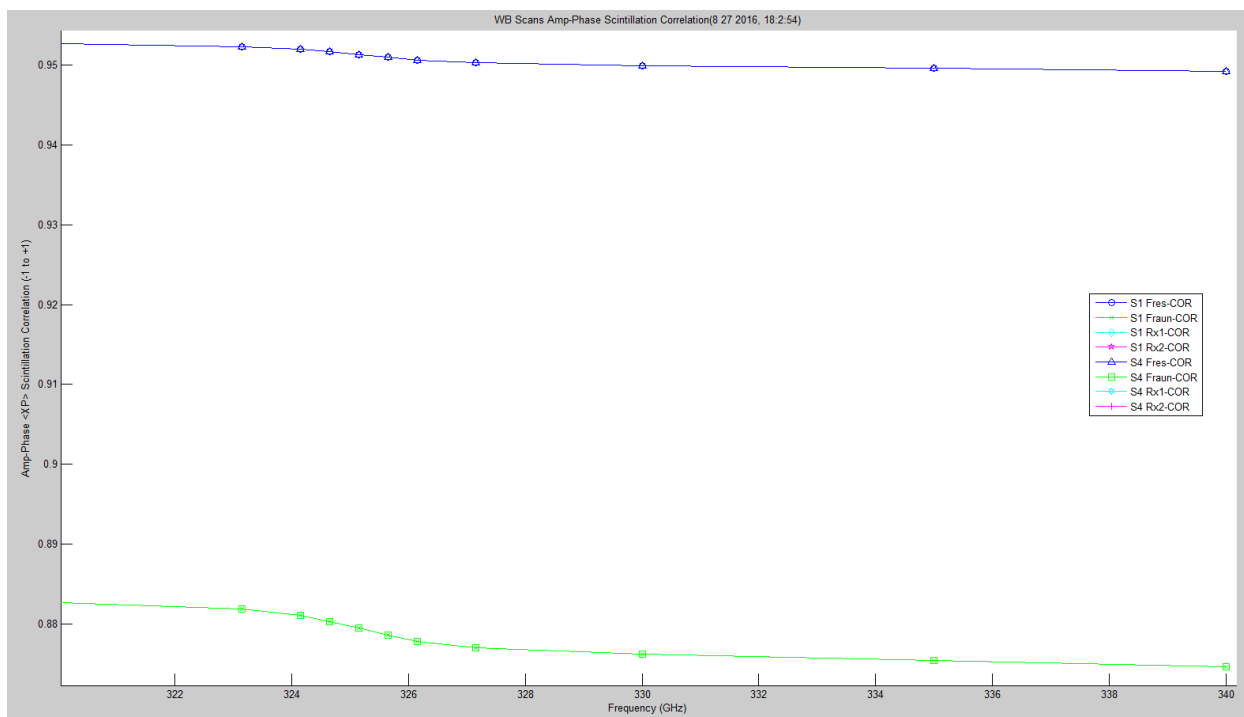


Figure 6.37. WB Amplitude/Phase Scintillation Cross Correlation with Prediction.

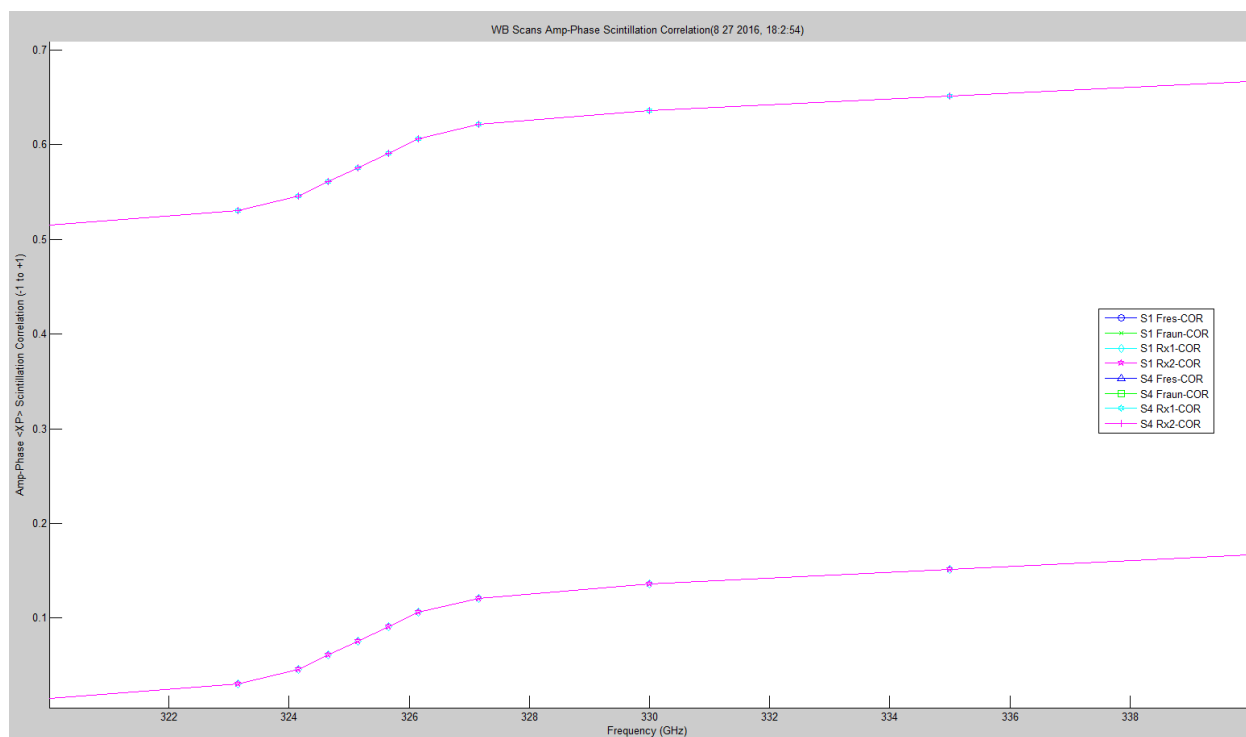


Figure 6.38. WB Amplitude/Phase Scintillation Cross Correlation Hallway Data.

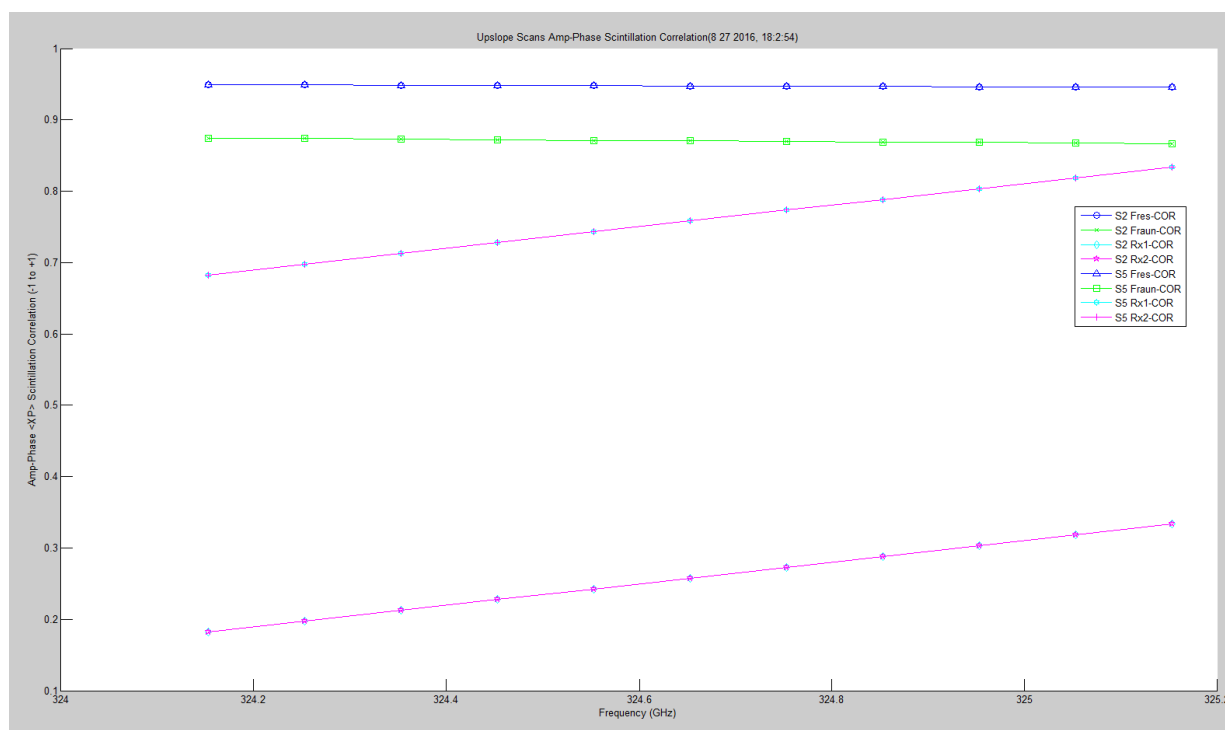


Figure 6.39. LWL Amplitude/Phase Scintillation Cross Correlation with Prediction.

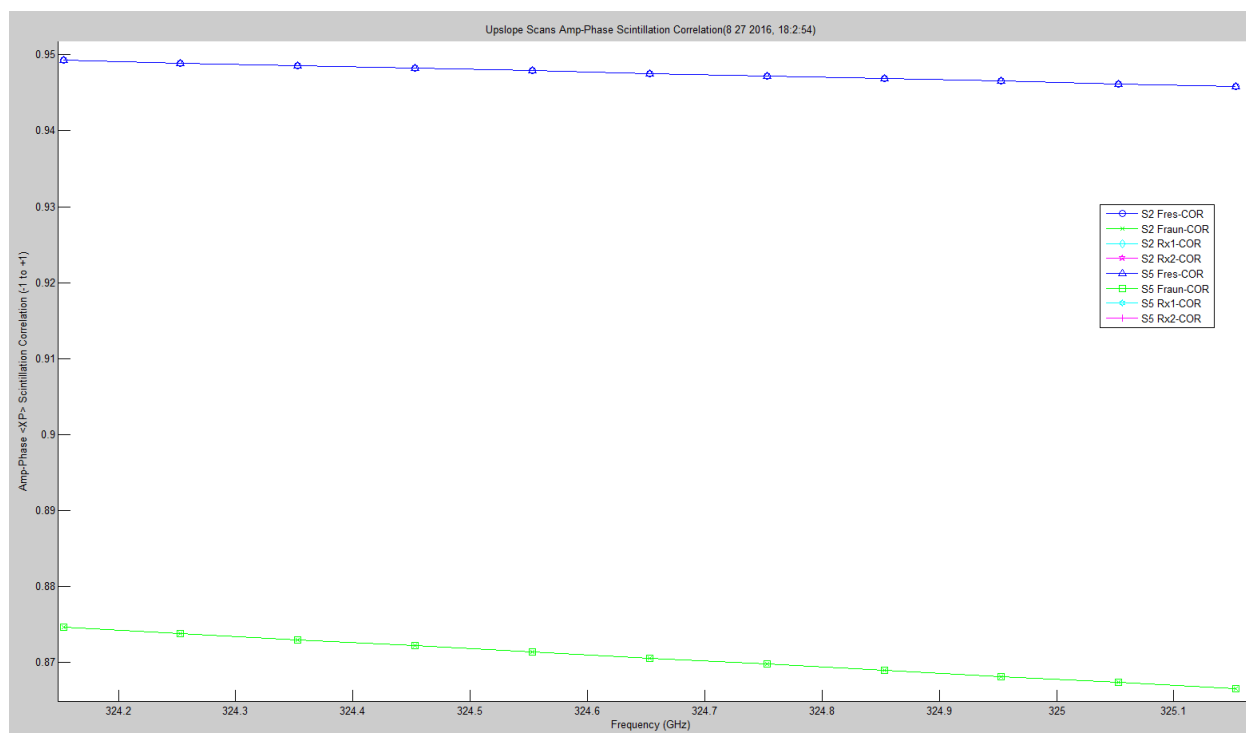


Figure 6.40. LWL Amplitude/Phase Scintillation Cross Correlation Prediction Data.

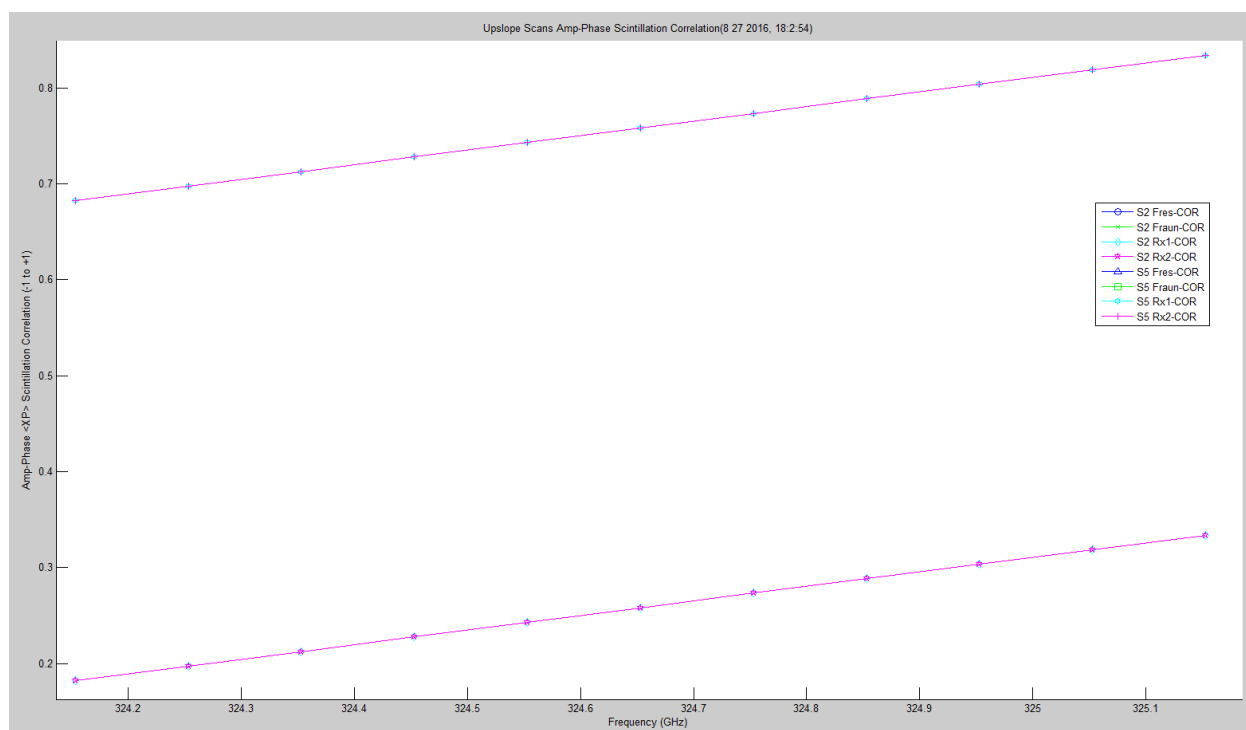


Figure 6.41. LWL Amplitude/Phase Scintillation Cross Correlation Hallway Data.

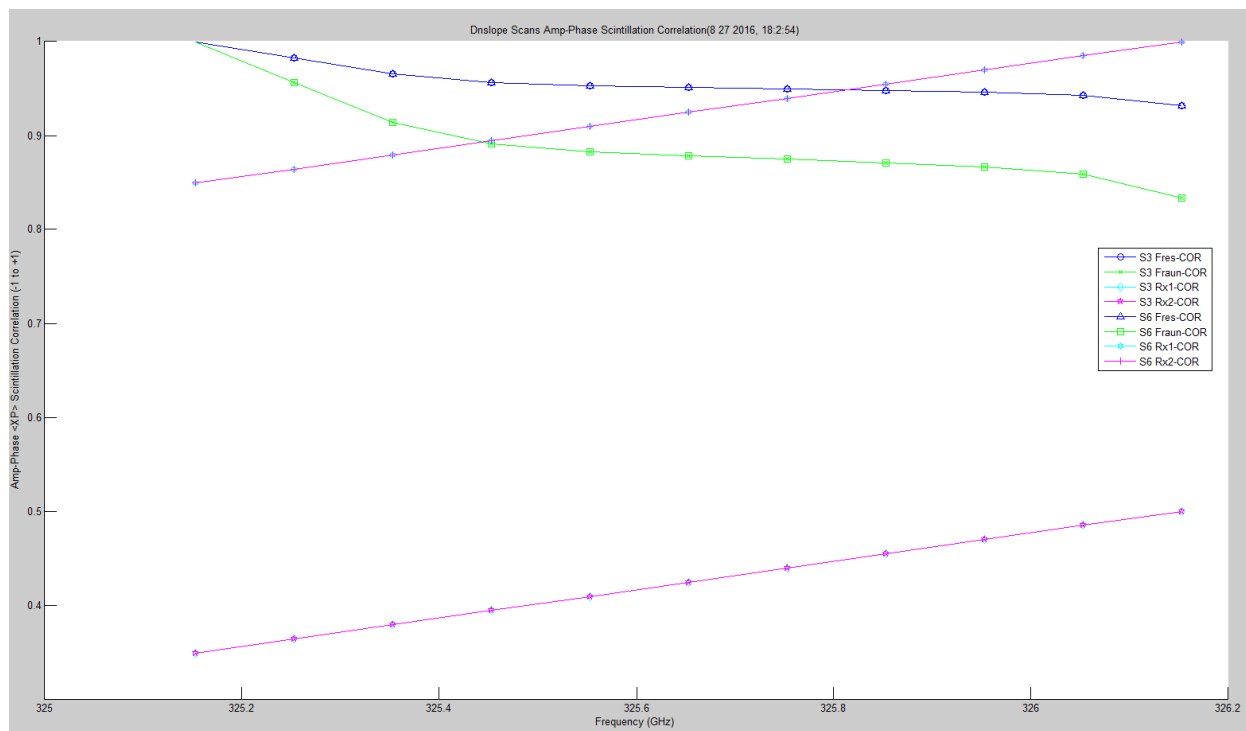


Figure 6.42. UWL Amplitude/Phase Scintillation Cross Correlation with Prediction.

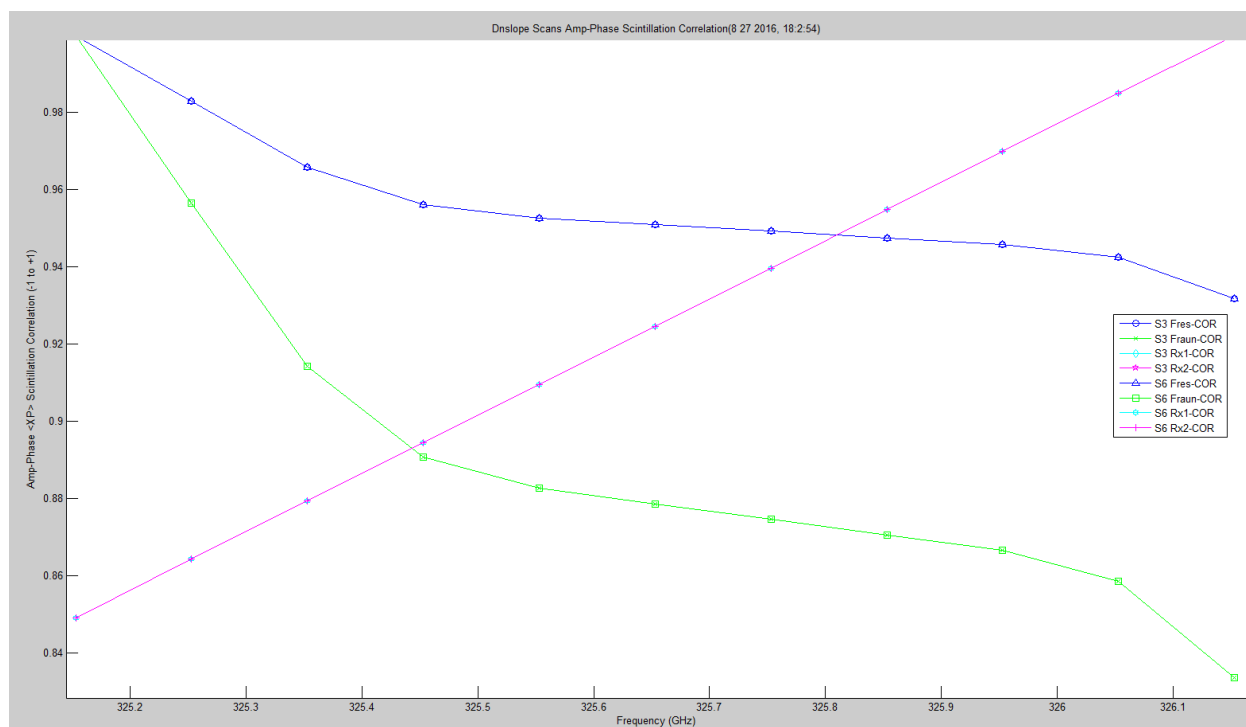


Figure 6.43. UWL Amplitude/Phase Scintillation Cross Correlation Prediction Data.

Figure 6.44 shows an FFT of a single-tuned frequency for the hallway test case. It is in the 15 kHz carrier range due to the offset of the synthesizers on the transmitter and receiver. The sampling after the DDC is 40 kHz; this is the limit on the FFT plot scale. The broadening of the frequency's base is due to phase noise, atmospheric effects of phase and the fact in the hallway that Coho phase lock is not implemented, but will be implemented on the open path. Figure 6.45 shows a histogram of the single frequency. In the case of the open path, this will be implemented for the 11 LWL and 11 UWL frequencies each. This will allow another observation of refractivity effects at each frequency, phase spread at base of frequency tone.

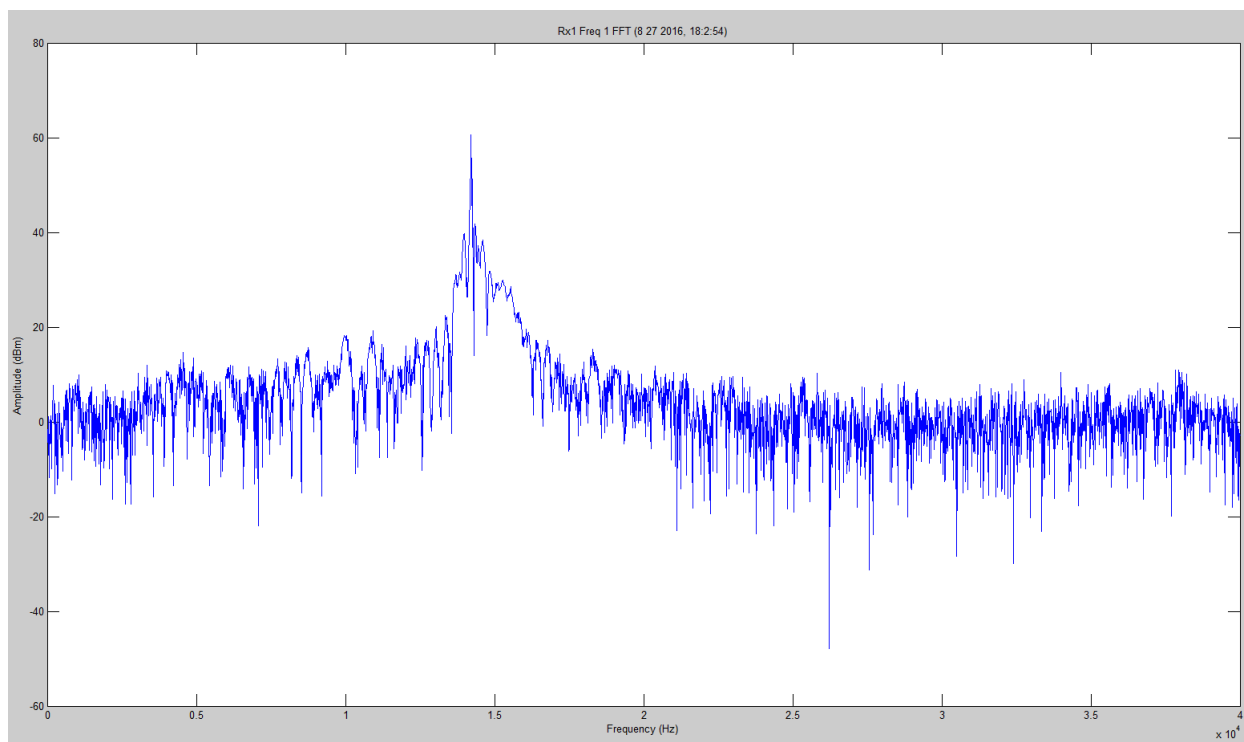


Figure 6.44. TAIPAS Single Scan FFT of Tuned Data.

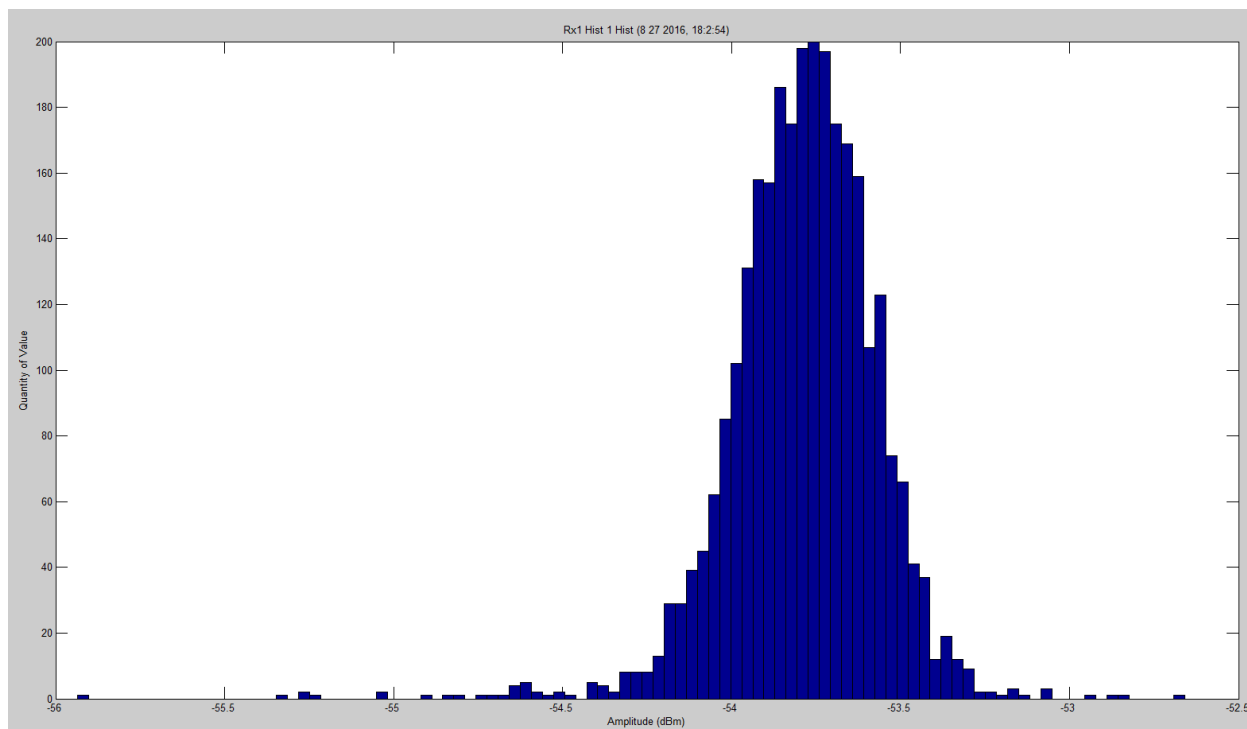


Figure 6.45. TAIPAS Single Scan Histogram of Tuned Data.

6.4 TAIPAS 1924 m Open Path

There were several hundred test implementations over the system just running with two receivers. The example discussed is a full system with two receivers, however, the SNR on Rx1 is much less than Rx2. The FFT plots shown in Figure 6.46 and Figure 6.47 show the difference in SNR.

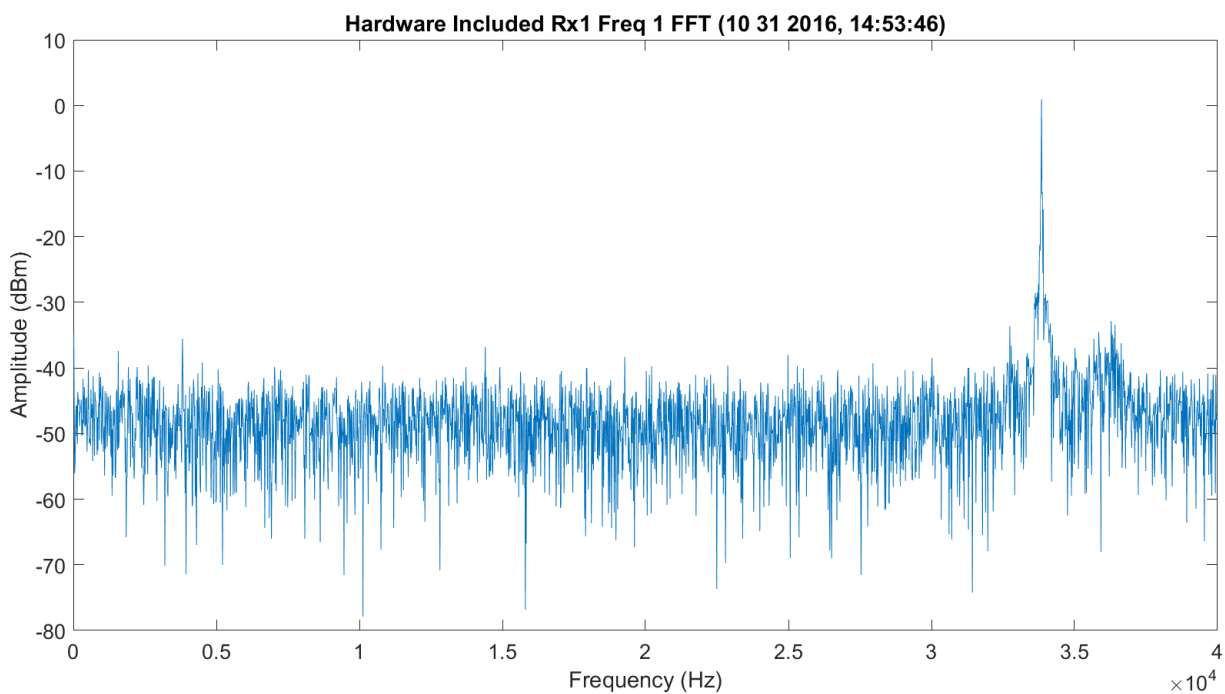


Figure 6.46. FFT of First WB Frequency (320 GHz) after DDC for Rx1 - 1012016_145401.

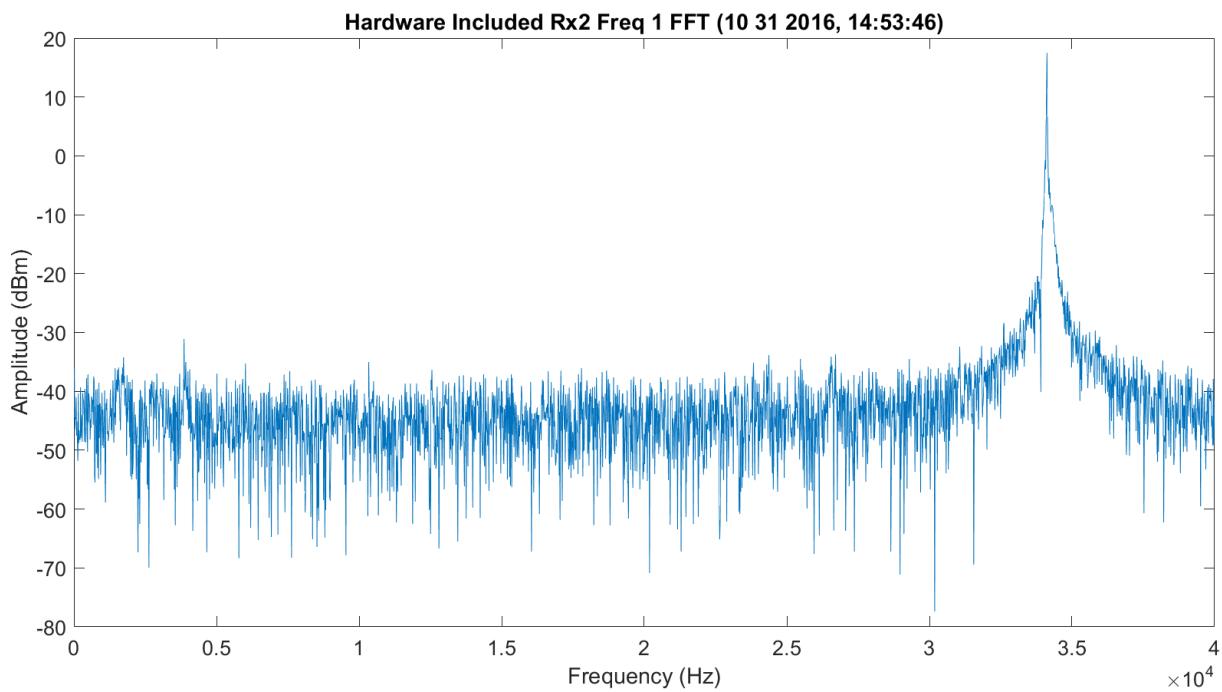


Figure 6.47. FFT of first WB Frequency (320 GHz) after DDC for Rx2 - 1012016_145401.

The following figures show the LWL, scans 2 and 5 frequency set; and the UWL, scans 3 and 6 frequency set, absorption scans utilizing a mean value for each frequency scan amplitude. This is implemented on the 1924 m open path between the EE building at CU and the mesa at NIST. Figure 6.48 shows the LWL absorption; this looks good in amplitude, but since it is Rx1 with low SNR, some points are missing on the downward slope. Figure 6.49 shows the Figure 6.48 plot with the Friis expectation plot in green and the difference in red. In future scans like 5 and Rx2, the ripple in the slopes will be more visible. The frequencies are 100 MHz, and while the calibration on the transmitter and receivers may be slightly different, there are significant differences that show the slope lines are not as smooth as presented before.

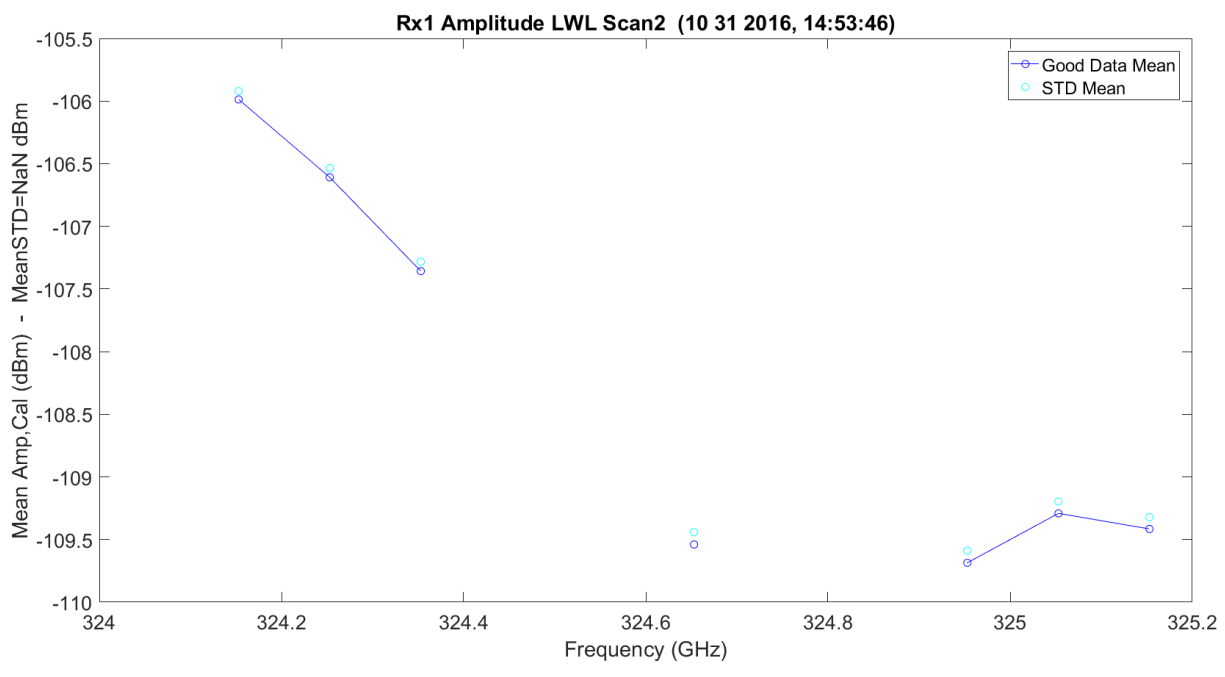


Figure 6.48. LWL Absorption Scan 2 for Rx1 - 11012016_145401.

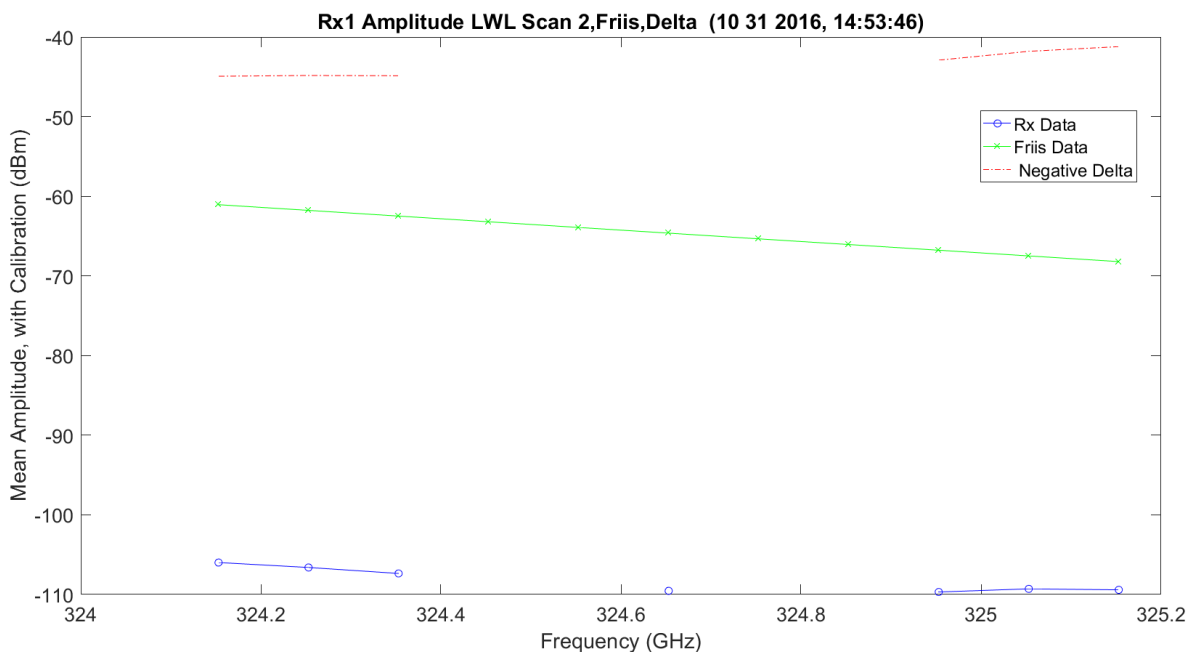


Figure 6.49. LWL / Friis Absorption Scan 2 for Rx1 - 11012016_145401.

Figure 6.50 shows an absorption UWL scan 3 frequency. There is more ripple in the finely spaced frequencies of 100 MHz, which could be due to the calibration of the data on transmit and receive; the values can change minor in dB from point-to-point. It looks like the high sample of the UWL does show some atmospheric ripples on the EM. Figure 6.51 shows the data with the Friis prediction and the difference. The ripples on the collected data become less obvious, due to the larger scale, and the wings of the two look approximately the same, but, they have approximately 48 dB offset difference in amplitude. This UWL performed much better than the above LWL.

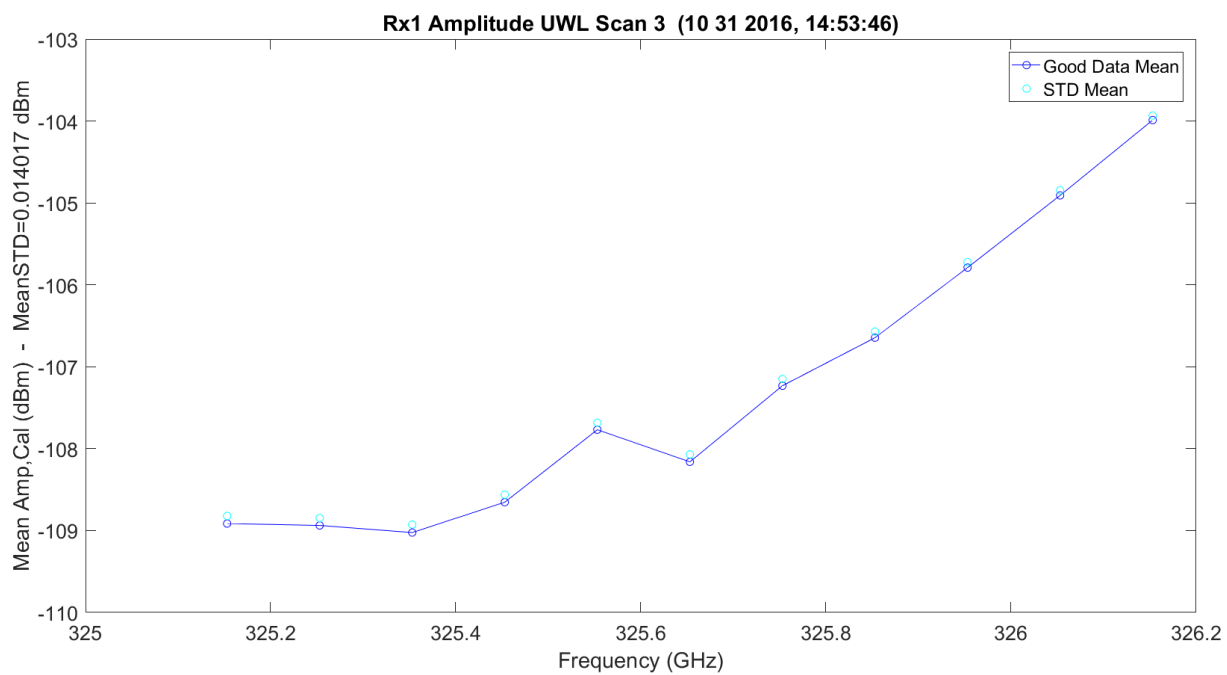


Figure 6.50. UWL Absorption Scan 3 for Rx1 - 11012016_145401.

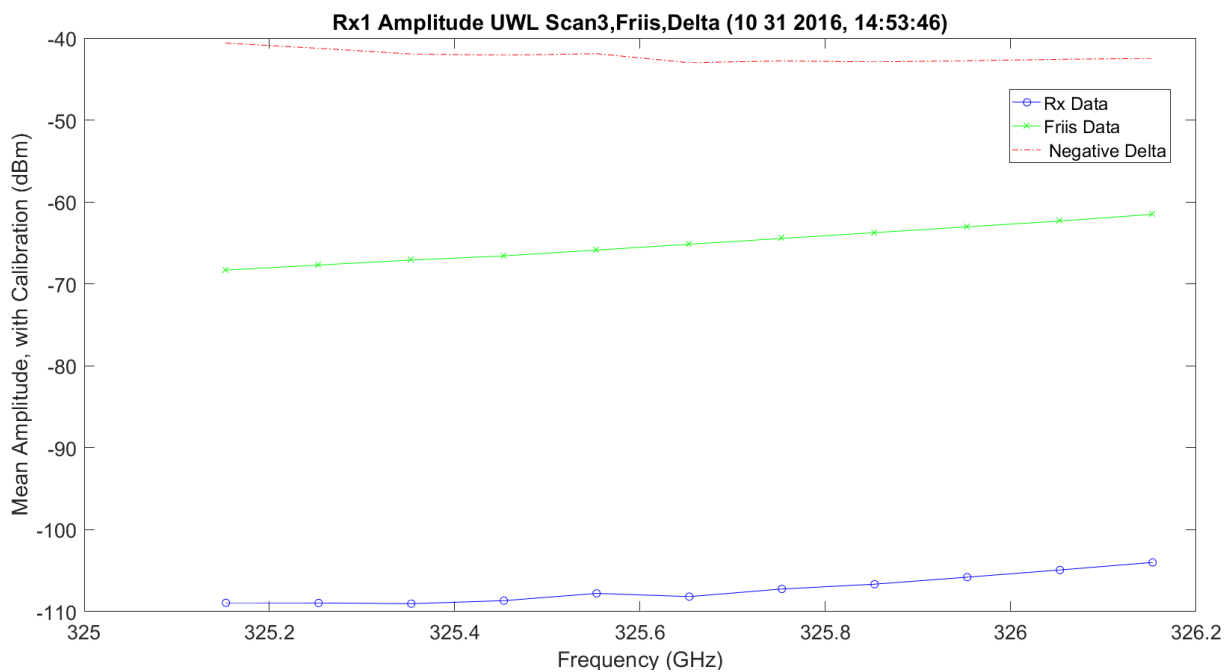


Figure 6.51. UWL / Friis Absorption Scan 3 for Rx1 - 11012016_145401.

Figure 6.52 shows the LWL in scan 5, which has low SNR, but much better performance. In this case, the variations in the slope with 100 MHz steps are very high compared to earlier predicted perfect smoothness. Figure 6.53 shows the plot in the context of Friis. At this precision, comparing LWL and Friis looks the same for slope and smoothness.

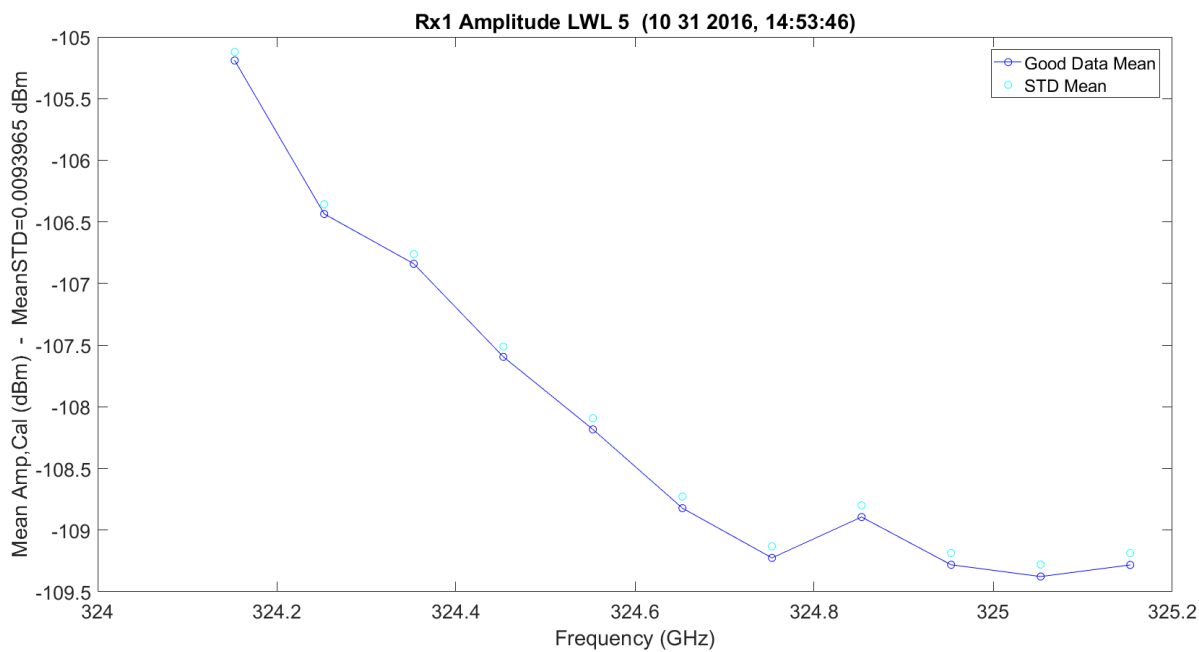


Figure 6.52. LWL / Friis Absorption Scan 5 for Rx1 - 11012016_145401.

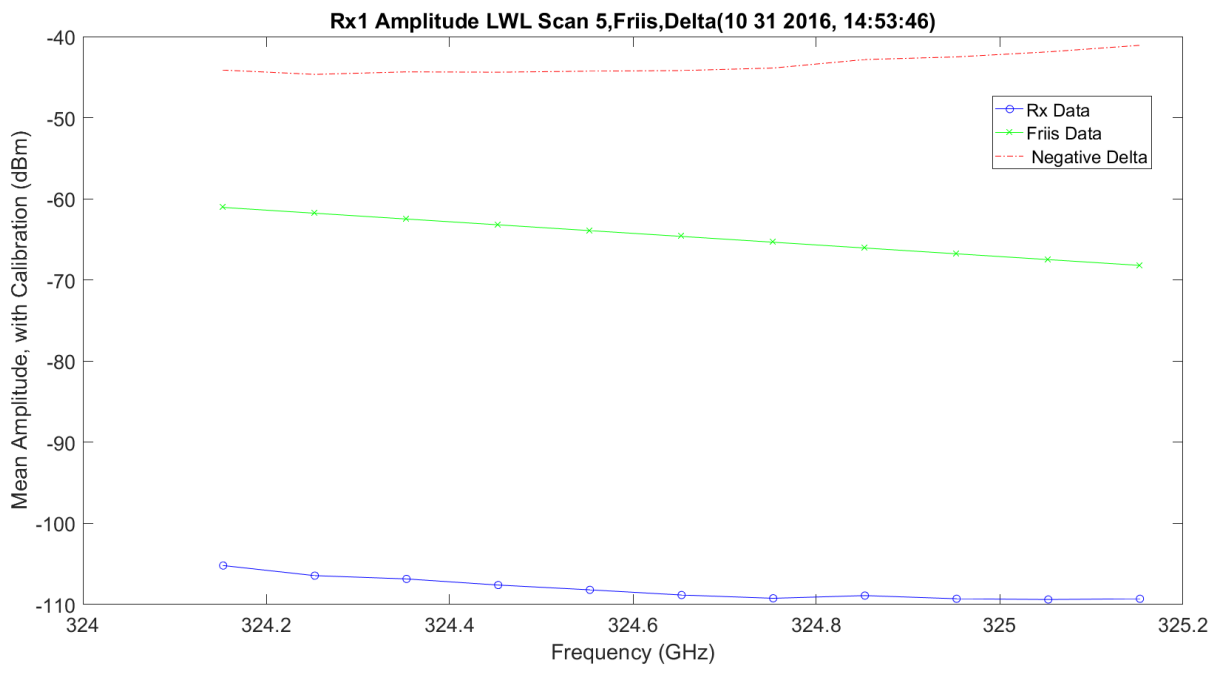


Figure 6.53. LWL / Friis Normalized Absorption Scan 5 for Rx1 - 11012016_145401.

Figure 6.54 shows the UWL in scan 6, which has much higher SNR and compares to scan 3. In this case, the variations in the slope with 100 MHz steps are still high, but do not have as much ripple as scan 3. This drives the conclusion of the ripple cause away from calibration and more toward atmospheric changes. Figure 6.55 shows the plot in the context of Friis. At this precision, comparing LWL to Friis yields the same slope and smoothness.

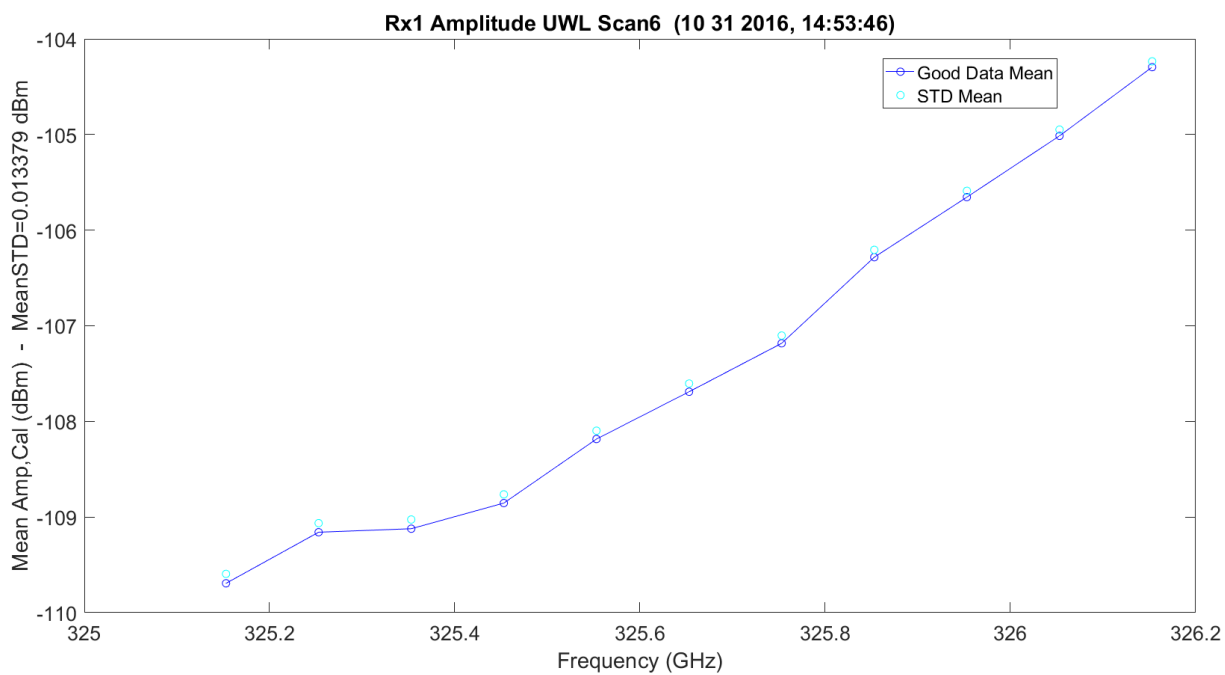


Figure 6.54. UWL / Friis Absorption Scan 6 for Rx1 - 11012016_145401.

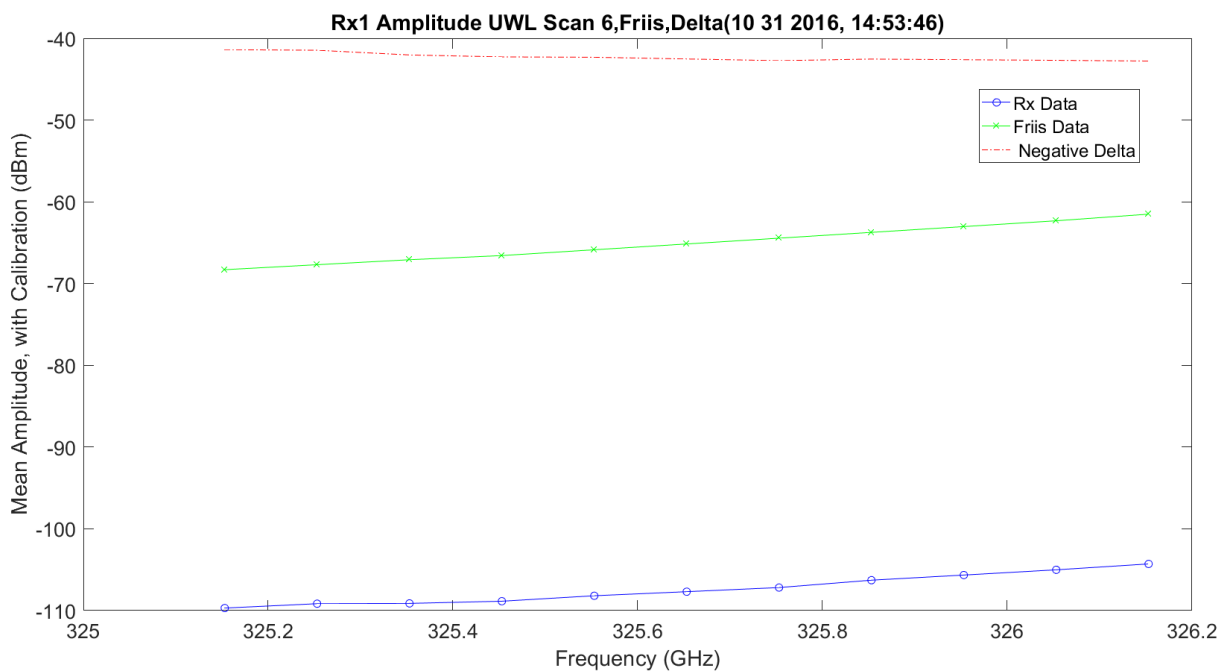


Figure 6.55. UWL / Friis Normalized Absorption Scan 6 for Rx1 - 11012016_145401.

Figure 6.56 shows an absorption LWL scan 2 frequency on Rx2. There is more ripple in the finally spaced frequencies of 100 MHz, which could be due to the calibration of the data on transmit and receive; the values can change minor in dB from point-to-point. It looks like the high sample of the LWL does show some atmospheric ripples on the EM. Figure 6.57 shows the data with the Friis prediction and the difference. The ripples on the collected data become less obvious and the wings of the two look approximately the same, but, they have approximately 40 dB of difference in amplitude. Figure 6.58 shows the normalization of the Friis and collected data. As expected, this shows the rippling on the collected, but the Friis response is flat. The real data is less flat and the wing is flatter than the Friis prediction.

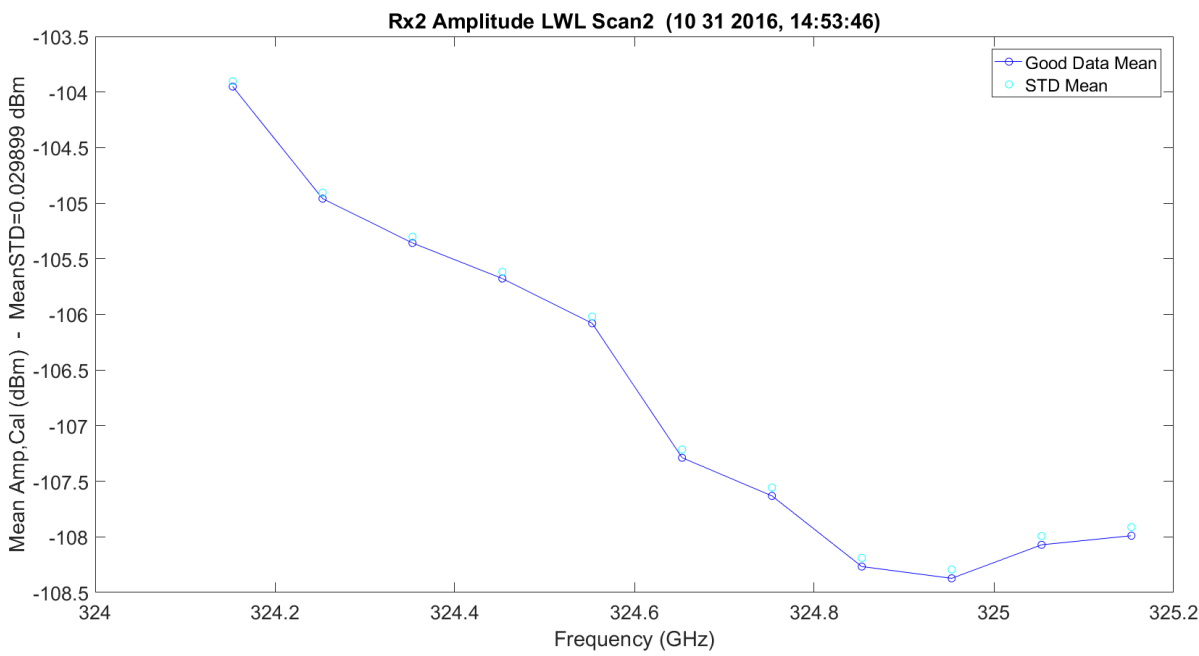


Figure 6.56. LWL Absorption Scan 2 for Rx2 - 11012016_145401.

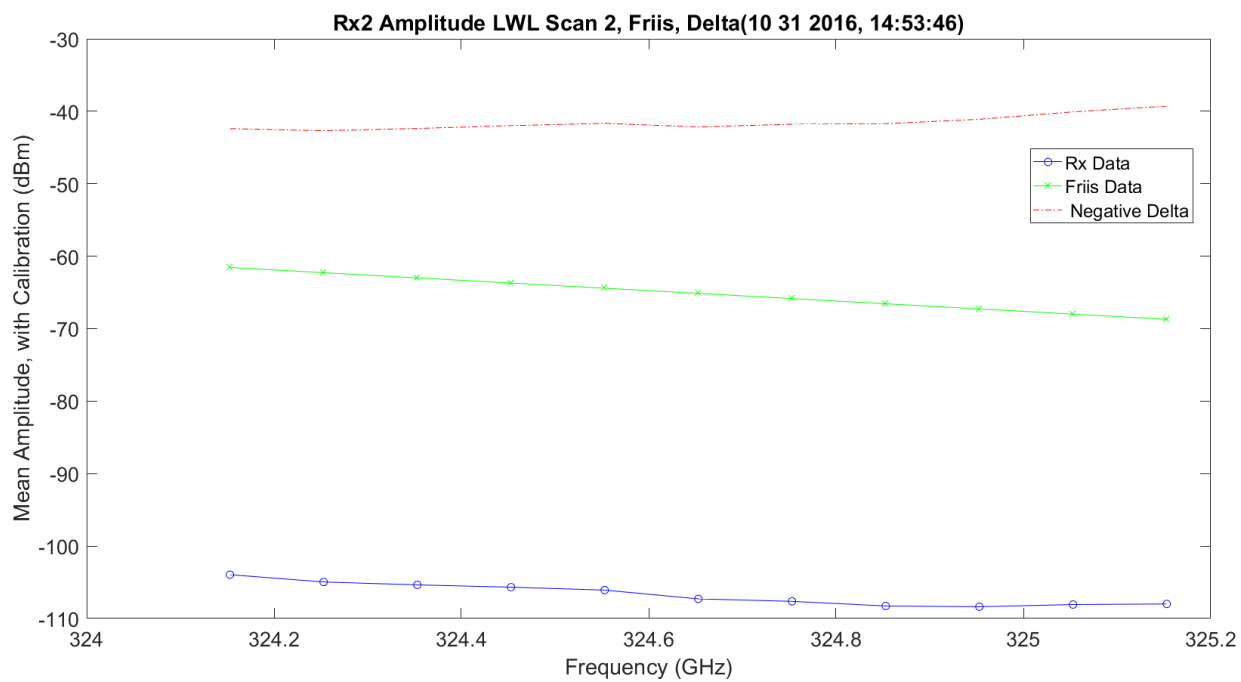


Figure 6.57. LWL / Friis Absorption Scan 2 for Rx1 - 11012016_145401.

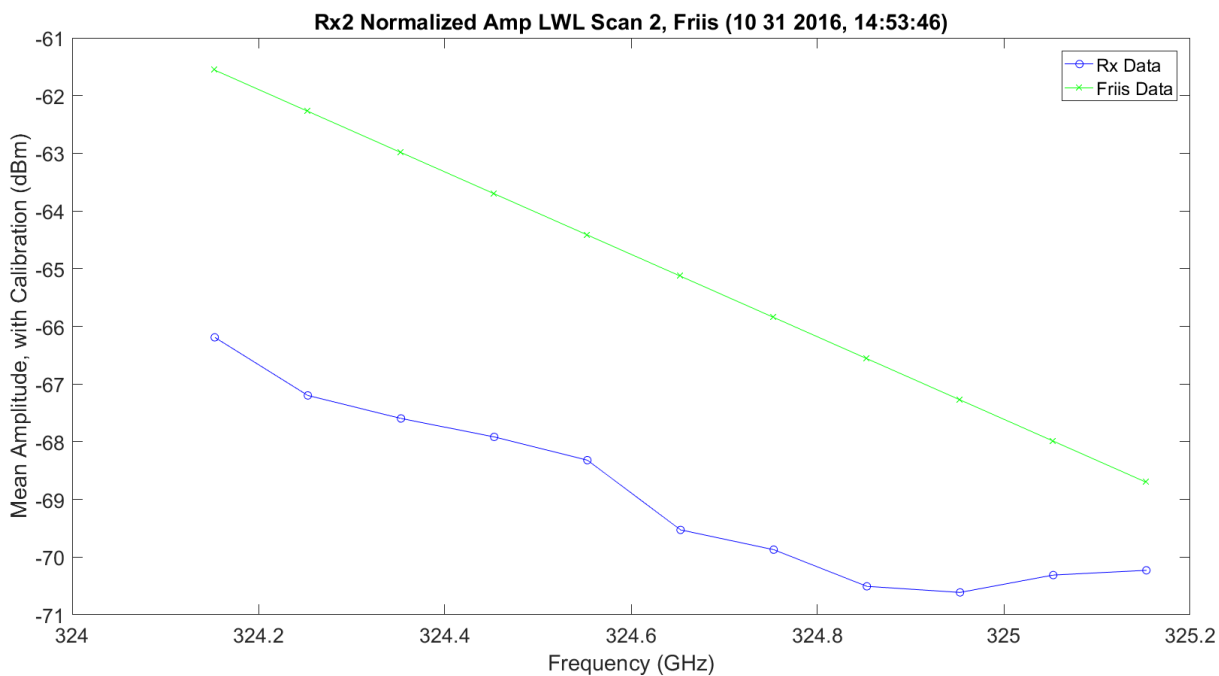


Figure 6.58. LWL / Friis Normalized Absorption Scan 2 for Rx1 - 11012016_145401.

Figure 6.59 shows an absorption UWL scan 3 frequency. There is more ripple in the finely spaced frequencies of 100 MHz, which could be due to the calibration of the data on transmit and receive; the values can change minor in dB from point-to-point. It looks like the high sample of the UWL does show some atmospheric ripples on the EM. Figure 6.60 shows the data with the Friis prediction and the difference. The ripples on the collected data become less obvious and the wings of the two look approximately the same, but, they have approximately 40 dB of difference in amplitude. Figure 6.61 shows the normalization of the Friis and collected data. As expected, this shows the rippling on the collected, but the Friis response is flat. The real data is less flat and the wing is flatter than the Friis prediction. In this figure, the parallelization of the Friis and real data looks close, with offset and some ripple hits.

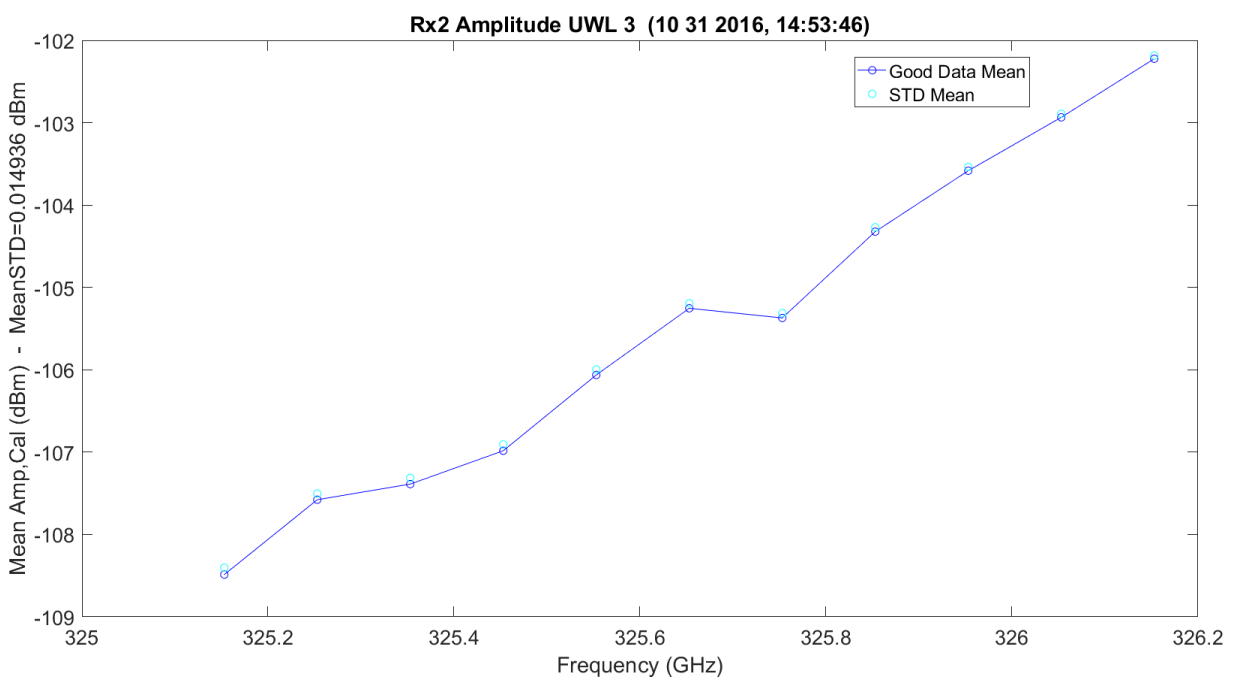


Figure 6.59. UWL Absorption Scan 3 for Rx1 - 11012016_145401.

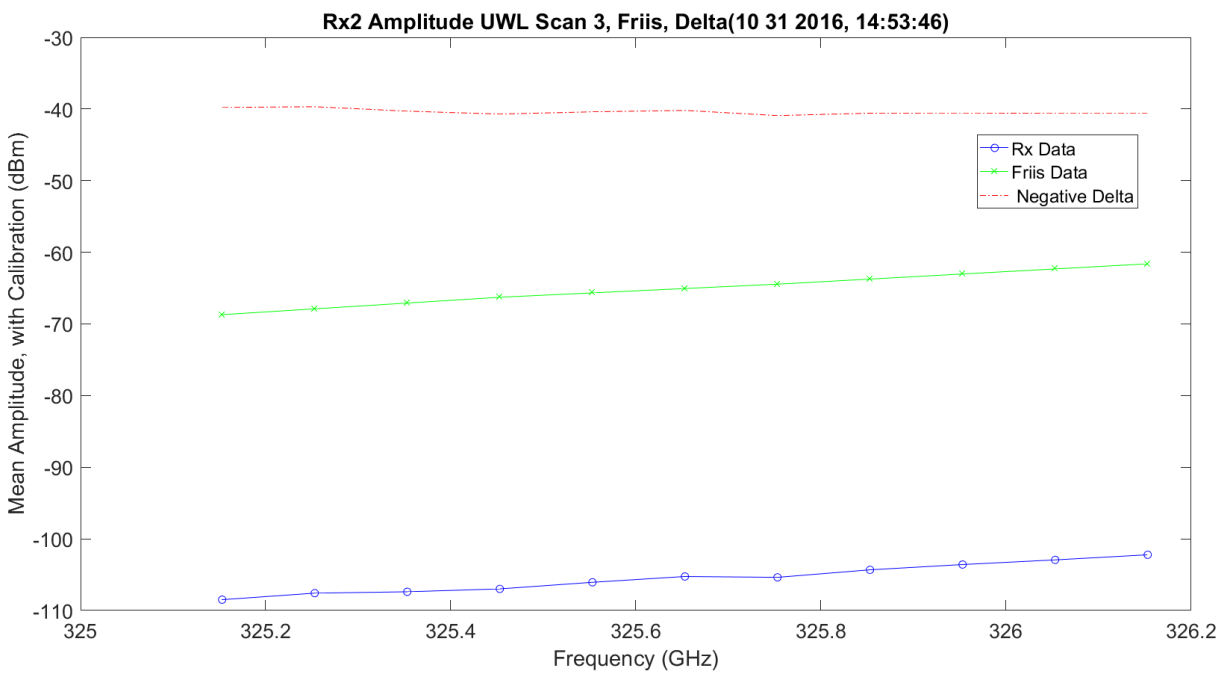


Figure 6.60. UWL / Friis Absorption Scan 3 for RX1 - 11012016_145401.

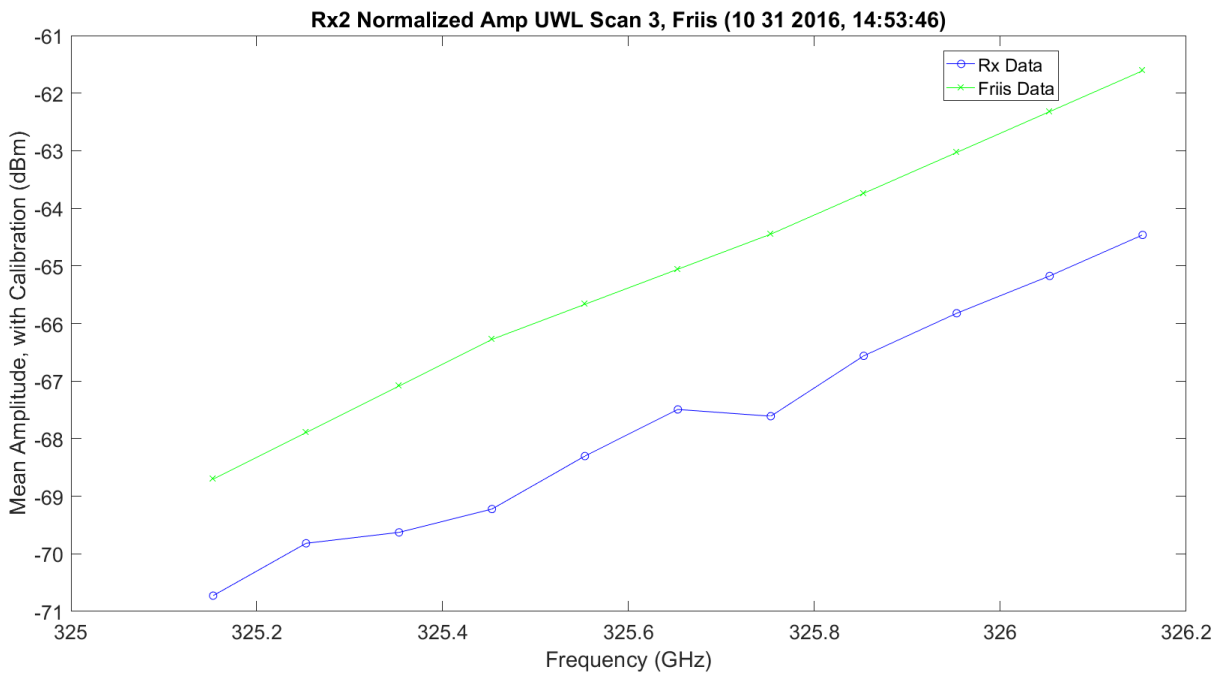


Figure 6.61. UWL / Friis Normalized Absorption Scan 3 for Rx1 - 11012016_145401.

The following images (Figure 6.62 - Figure 6.67) are the second set of identical scans: WB, LWL and UWL. They each scan 11 different frequencies. They are included for completeness, but they look identical to the first 33 scanned frequencies in Rx2. The LWLs and UWLs have very different wing jugs where assumed, due to calibration on Tx an Rx.

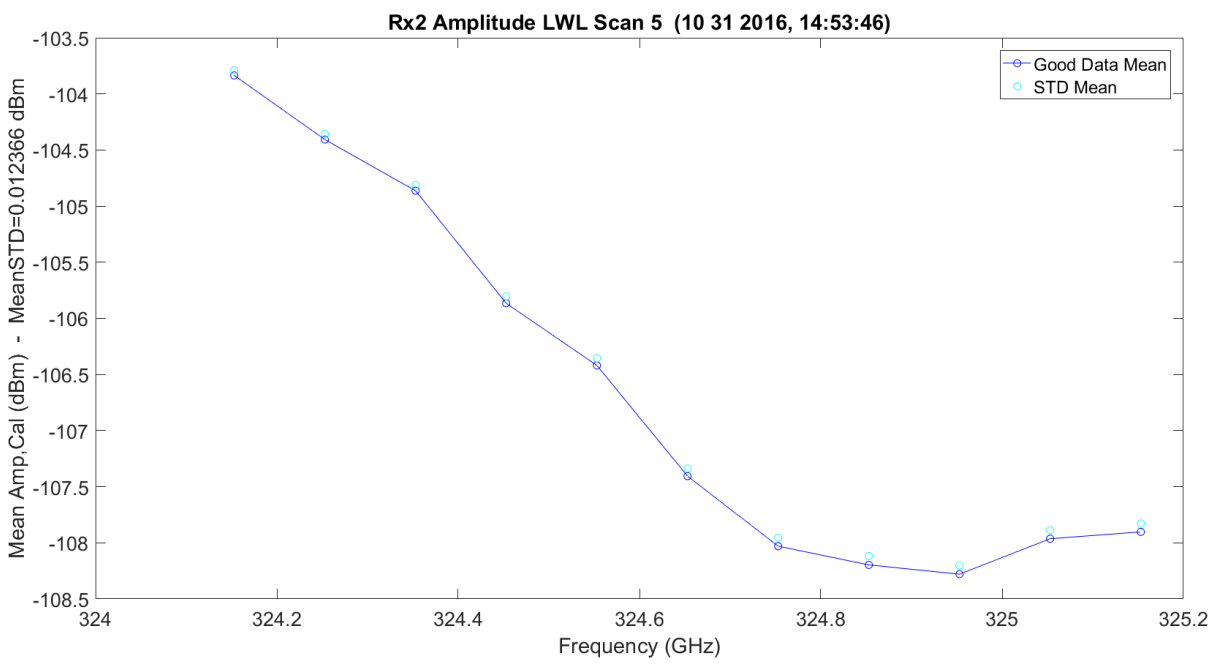


Figure 6.62. LWL / Friis Absorption Scan 5 for Rx2 - 11012016_145401.

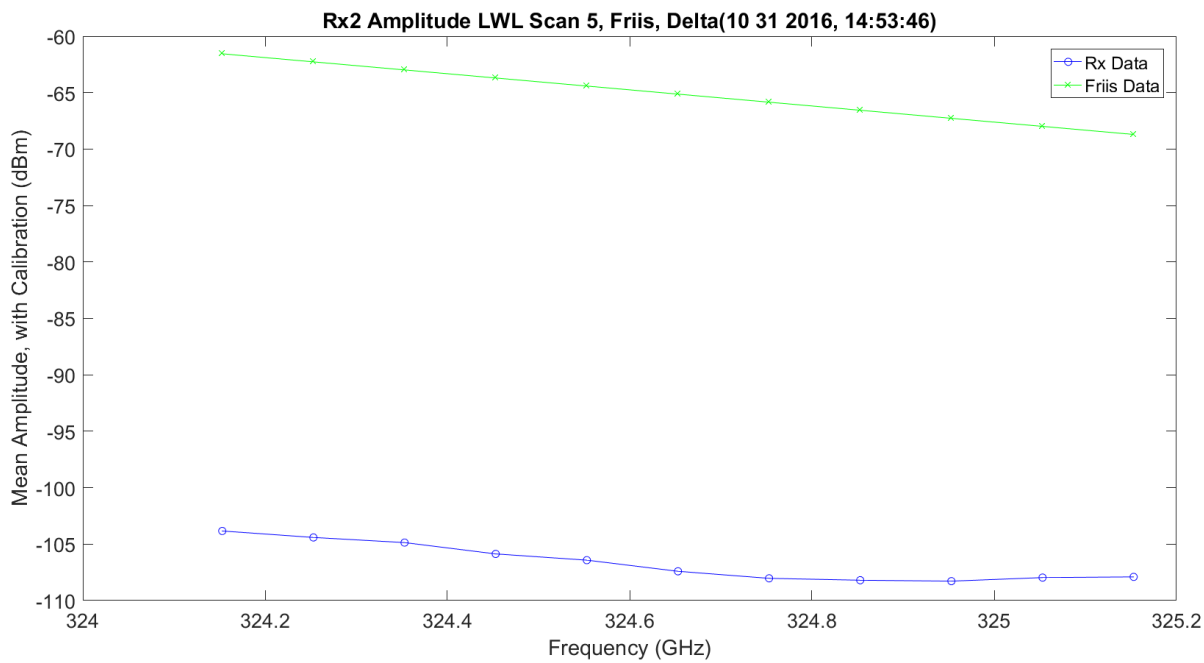


Figure 6.63. LWL / Friis Normalized Absorption Scan 5 for Rx2 - 11012016_145401.

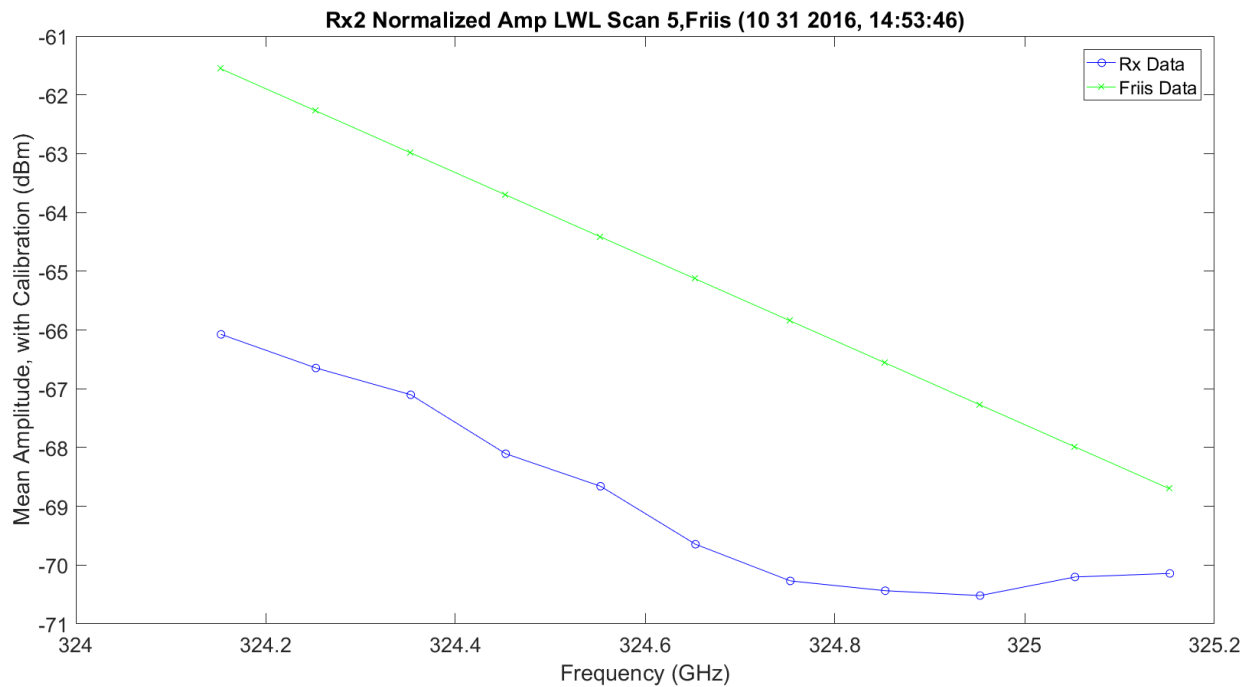


Figure 6.64. LWL Absorption Scan 3 for Rx2 - 11012016_145401.

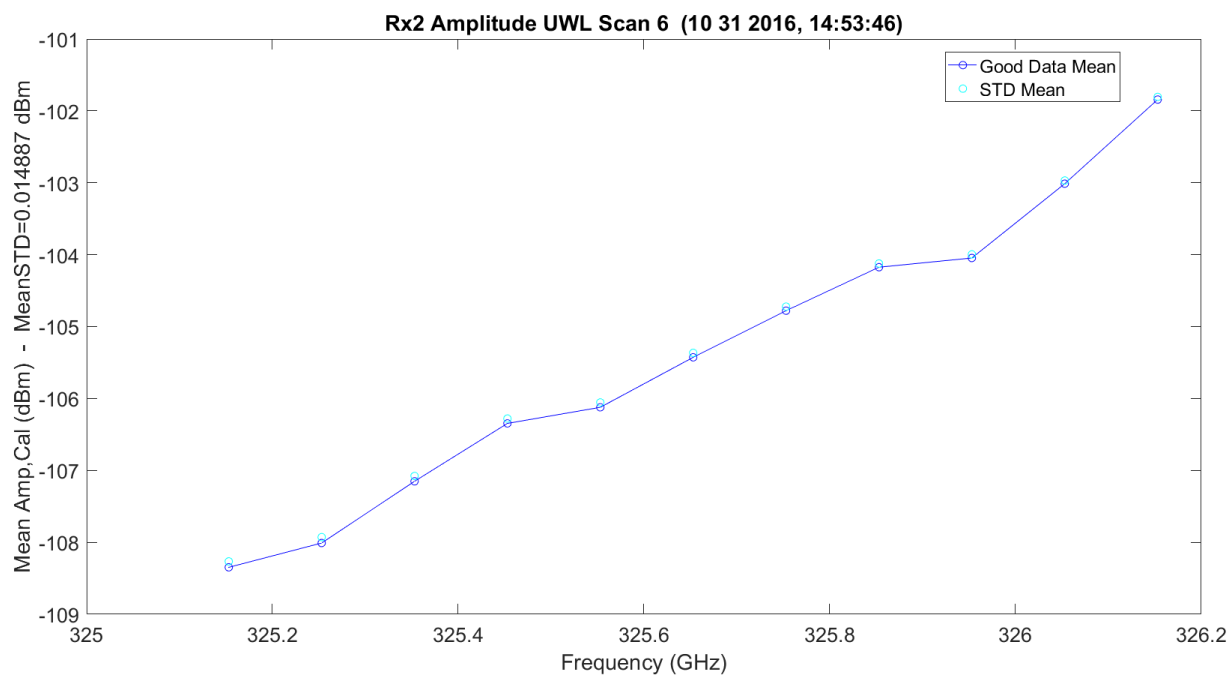


Figure 6.65. UWL / Friis Absorption Scan 6 for Rx2 - 11012016_145401.

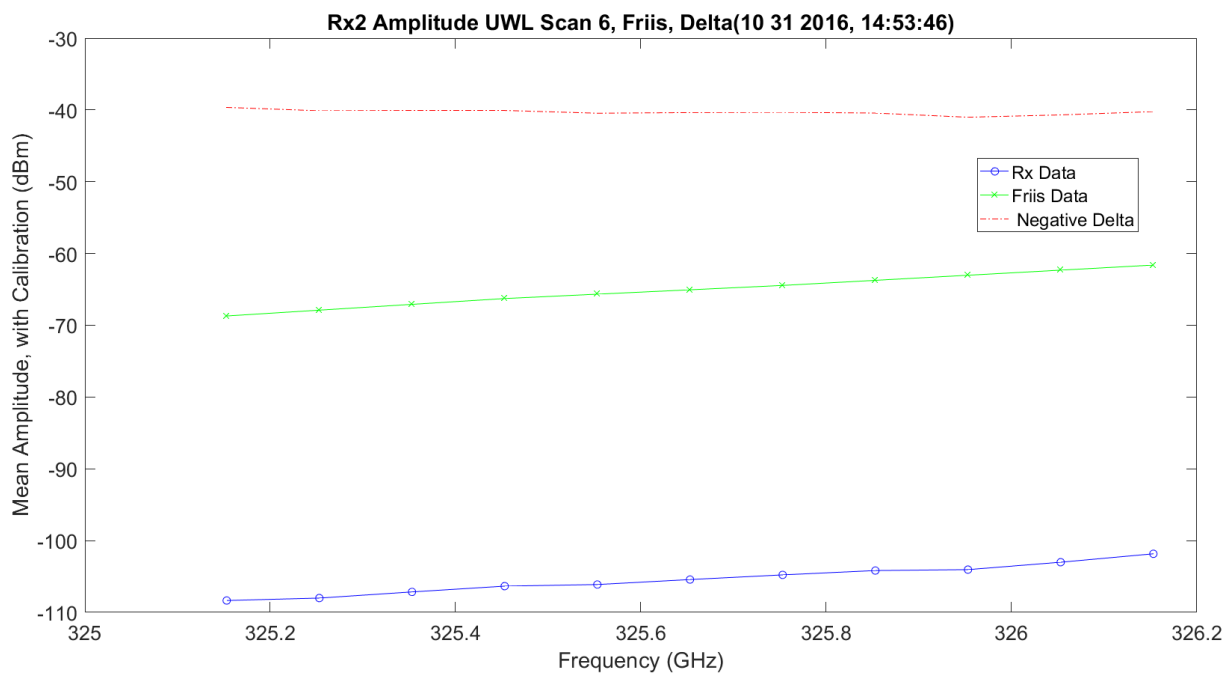


Figure 6.66. UWL / Friis Normalized Absorption Scan 6 for Rx2 - 11012016_145401.

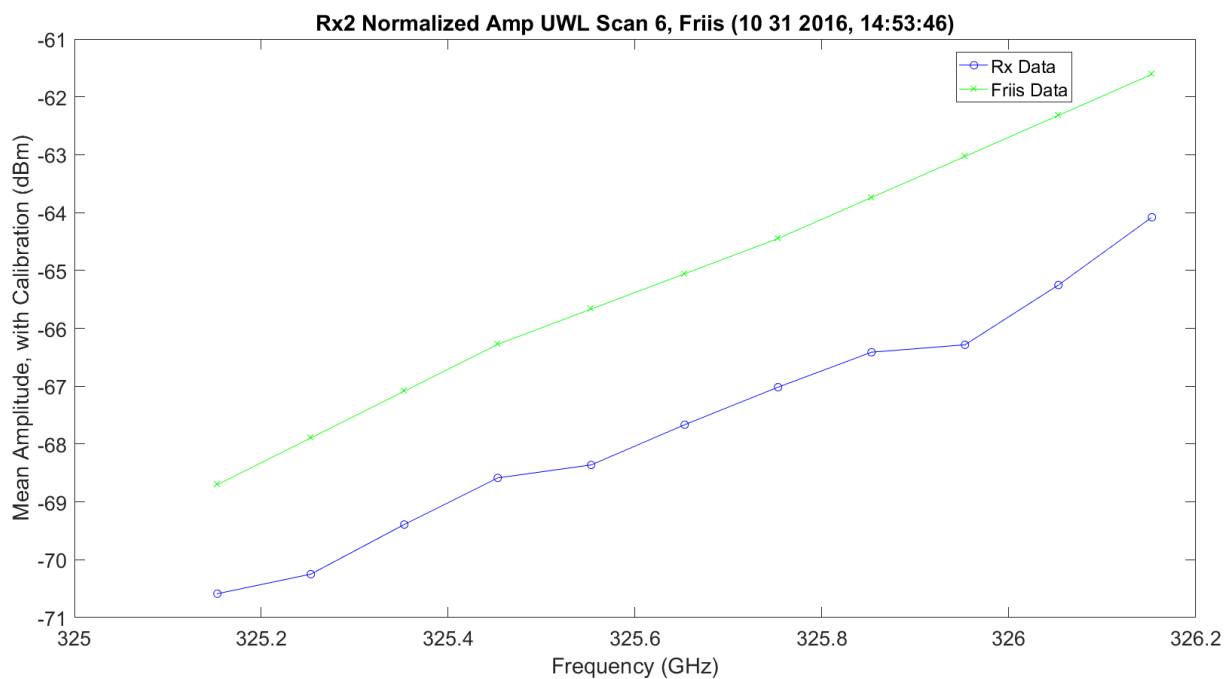


Figure 6.67. UWL / Friis Normalized Absorption Scan 6 for Rx2 - 11012016_145401.

Figure 6.68 shows both LWL and UWL— two scans each — on the same plot with the UWL reflected on top of the LWL for comparison. The two scans for UWL and LWL compared to each are similar, but with significant ripple compared to the Friis prediction. The shape of the LWL vs. UWL is significantly different at a frequency range of approximately 324.9 GHz to 325 GHz.

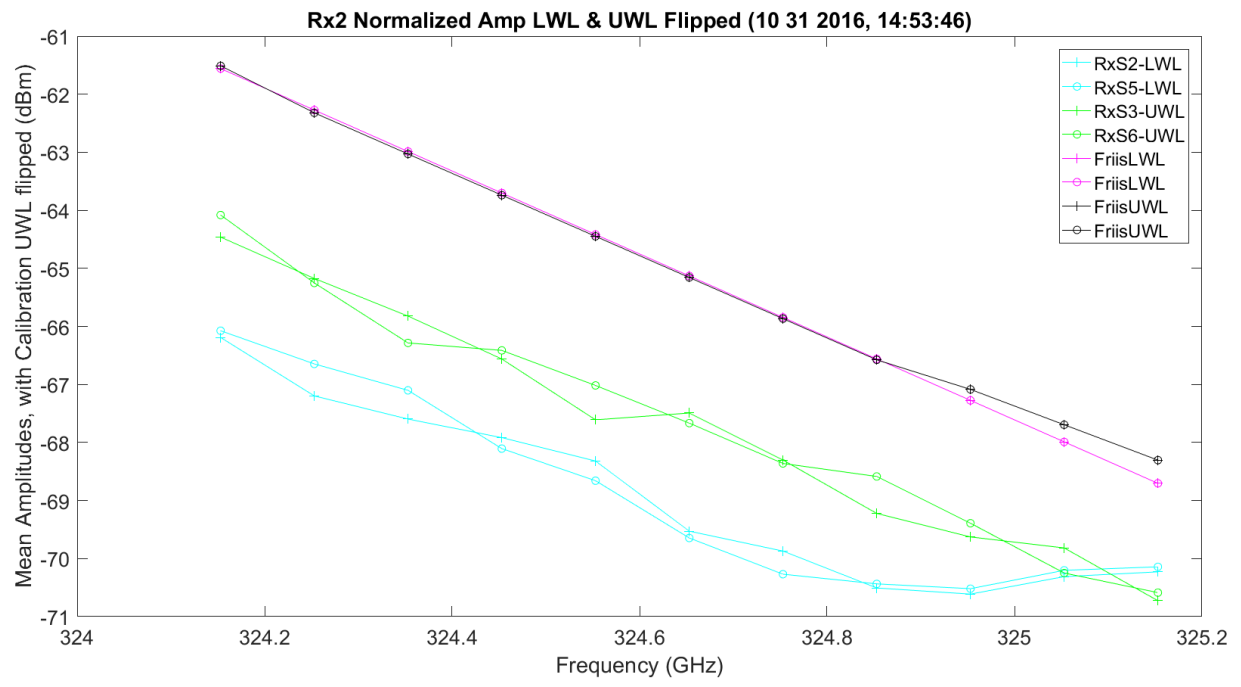


Figure 6.68. LWL & UWL Flipped Amp / Friis Normalized Absorption - 11012016_145401.

The SNR plots, Figure 6.69 and 6.70 below, show the same ripple relationship in amplitude. It can be seen from above and, for the SNR plots, even for the same channel with a 3.5 s difference in acquisition, the variation changes.

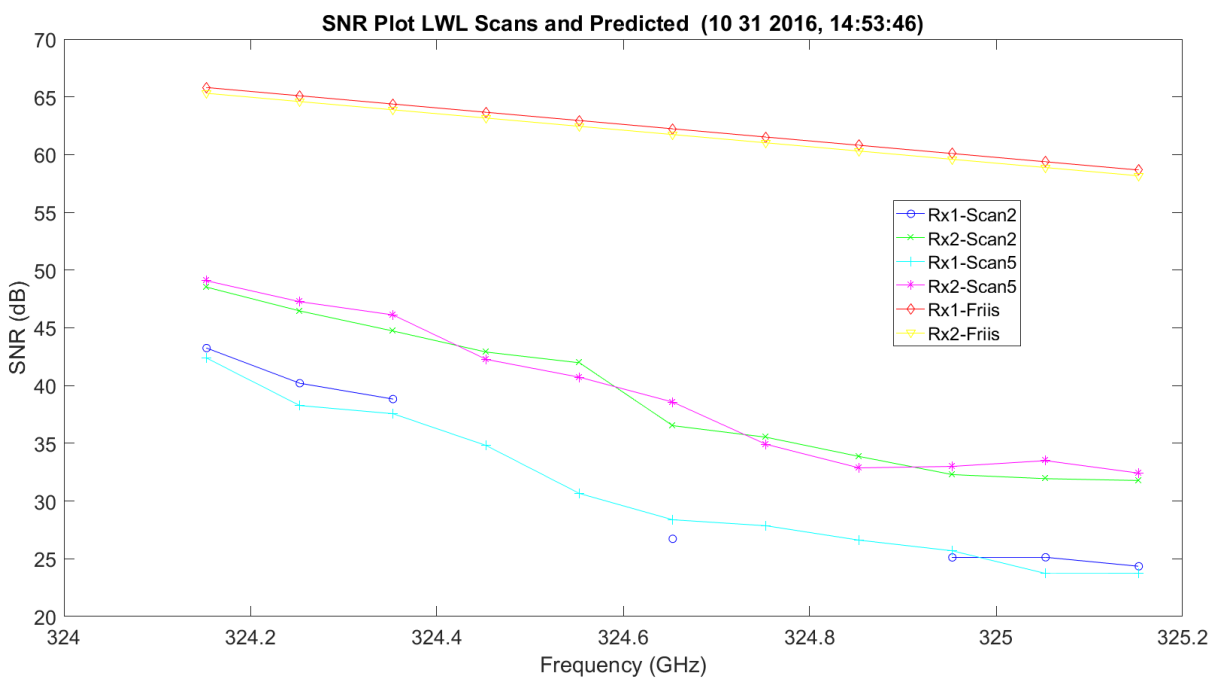


Figure 6.69. LWL SNR and Predicted Friis - 11012016_145401.

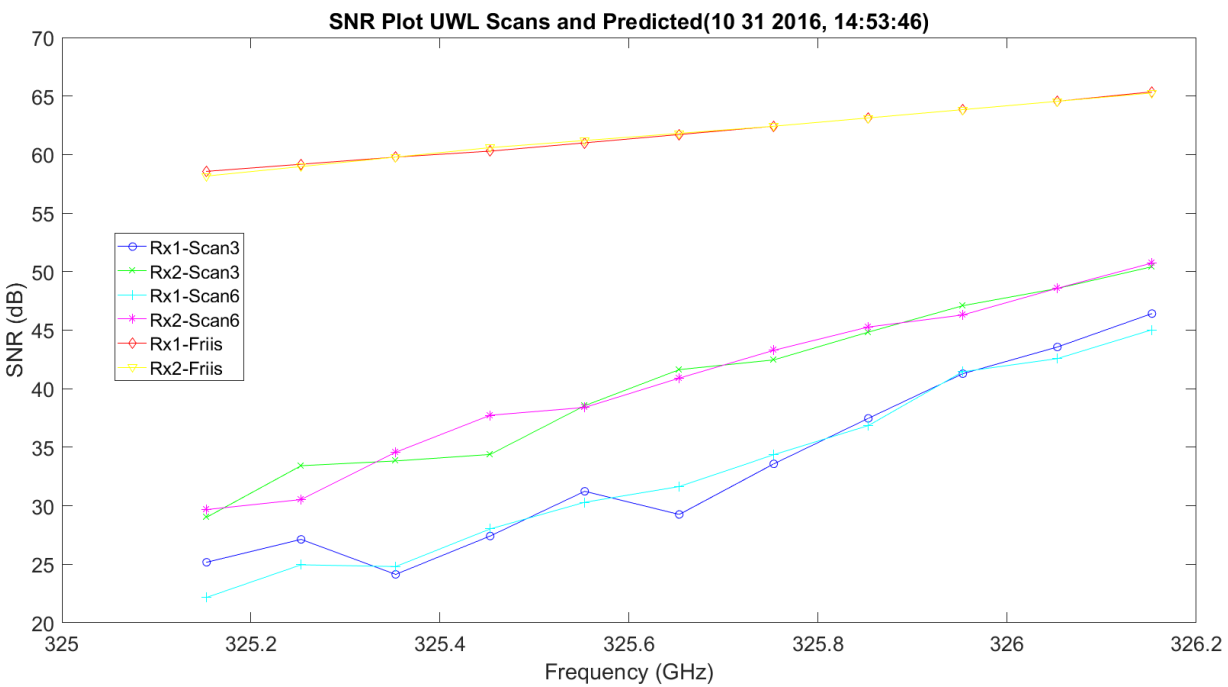


Figure 6.70. UWL SNR and Predicted Friis - 11012016_145401.

Figure 6.71 - Figure 6.72 show the MCF and phase structure functions for LWL and UWL for both receivers. Two frequency scans are included for MCF-phase and the phase structure function. It is more dynamic around the 325.1529 GHz absorption pulse. The LWL and UWL only cover the pulse, so they always change. The phase structure function is just minus two times the MCF. The blue plots in this case represent the two sets of identical frequency scans.

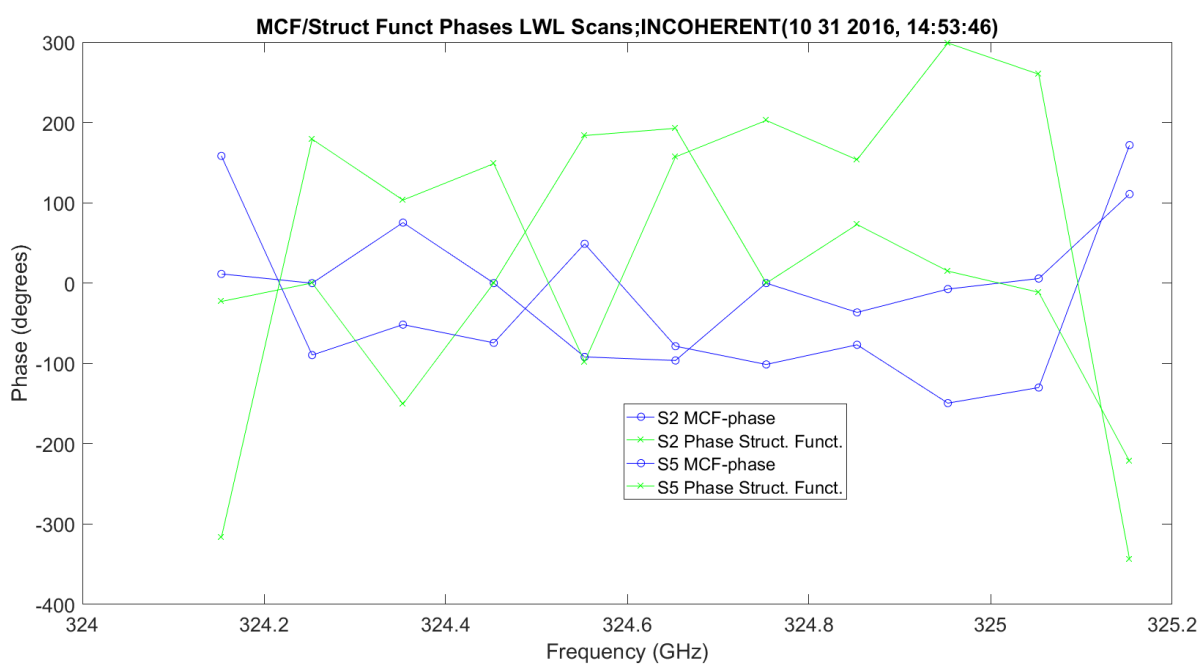


Figure 6.71. MCF - 11012016_145401.

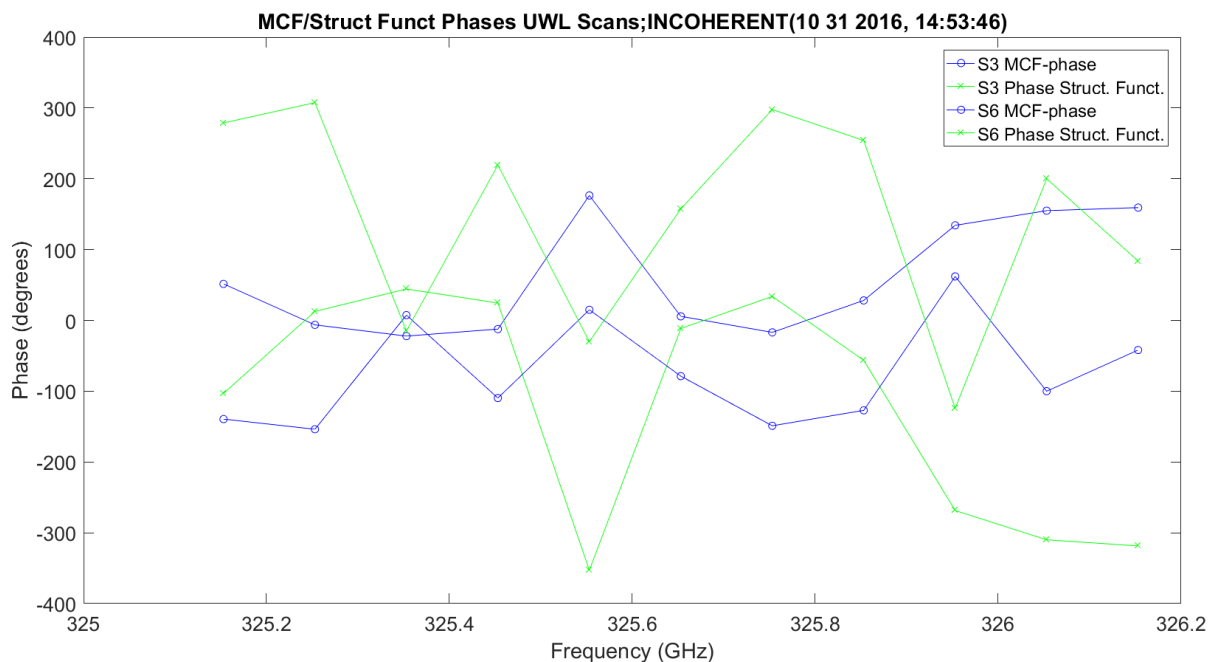


Figure 6.72. MCF - 11012016_145401.

Figure 6.73 shows the LWL scans amplitude scintillation variance: $\langle \chi^2 \rangle$. It is a linear increase over frequency with a fixed range; Rx1 disappears for obvious reasons. Rx2 has much lower offsets — ~7 dB. This shows both receivers and predicted values utilizing Kolmogorov with outer scale values. The predicted values are very flat at the bottom and there are more dynamics in the real data; it could be accentuated by calibration errors. The largest dynamics occur around the peak of absorption. The LWL and UWL are not the same, but are very similar.

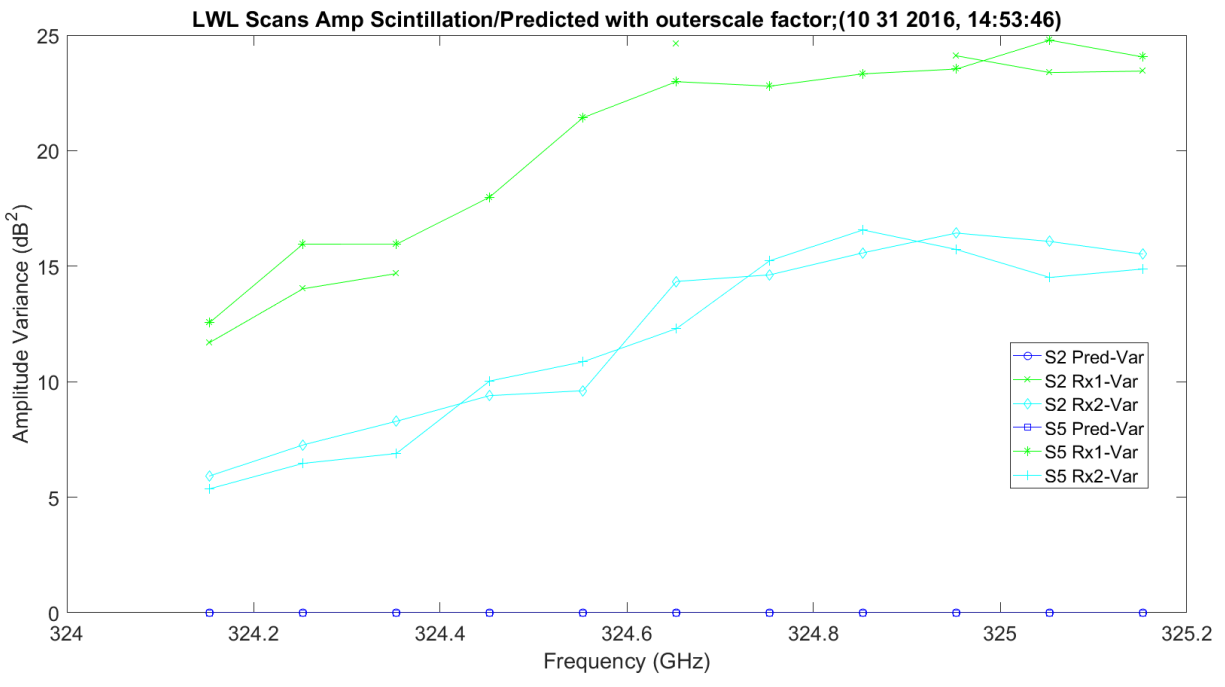


Figure 6.73. LWL Amplitude Scintillation Variance and Predicted - 11012016_145401.

Figure 6.74 shows the UWL scans amplitude scintillation variance. It is a linear increase over frequency with a fixed range; Rx1 disappears for obvious reasons. Rx2 has much lower offsets (~7 dB). This shows both receivers and prediction.

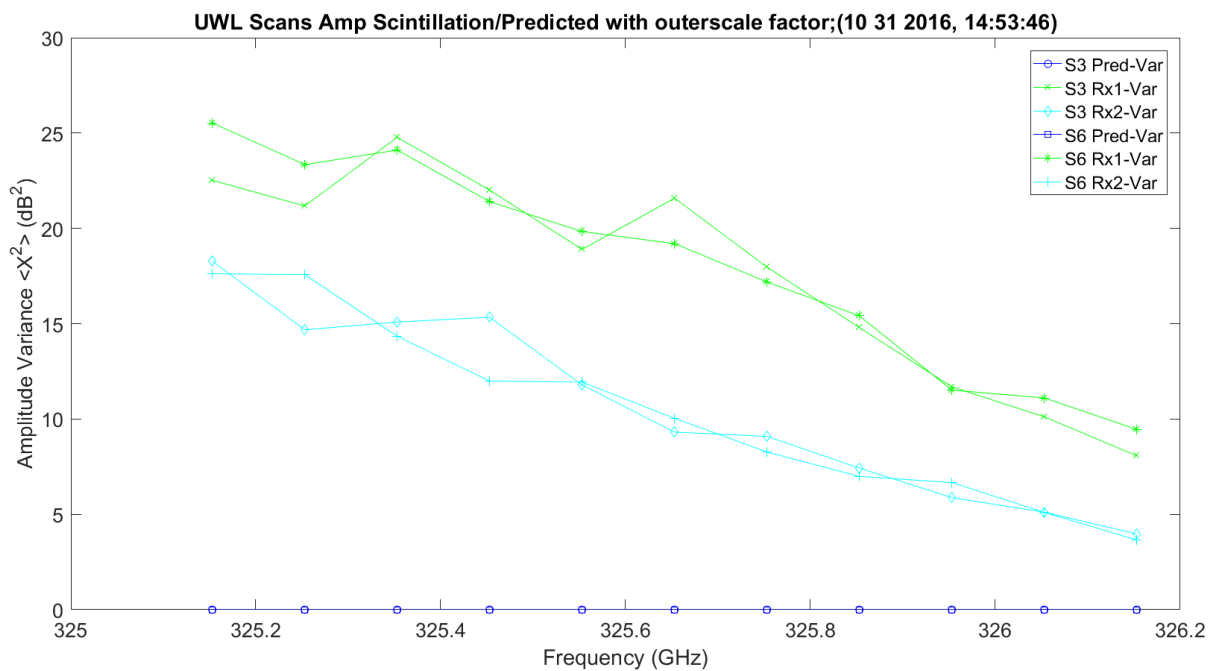


Figure 6.74. LWL Amplitude Scintillation Variance and Predicted - 11012016_145401.

Figure 6.75 shows the LWL scans phase scintillation variance. The offset is $\sim 180^\circ$. Everything looks stable except for the green traces for Rx1, which vary $\sim 180^\circ$. This is very dynamic over the absorption pulse.

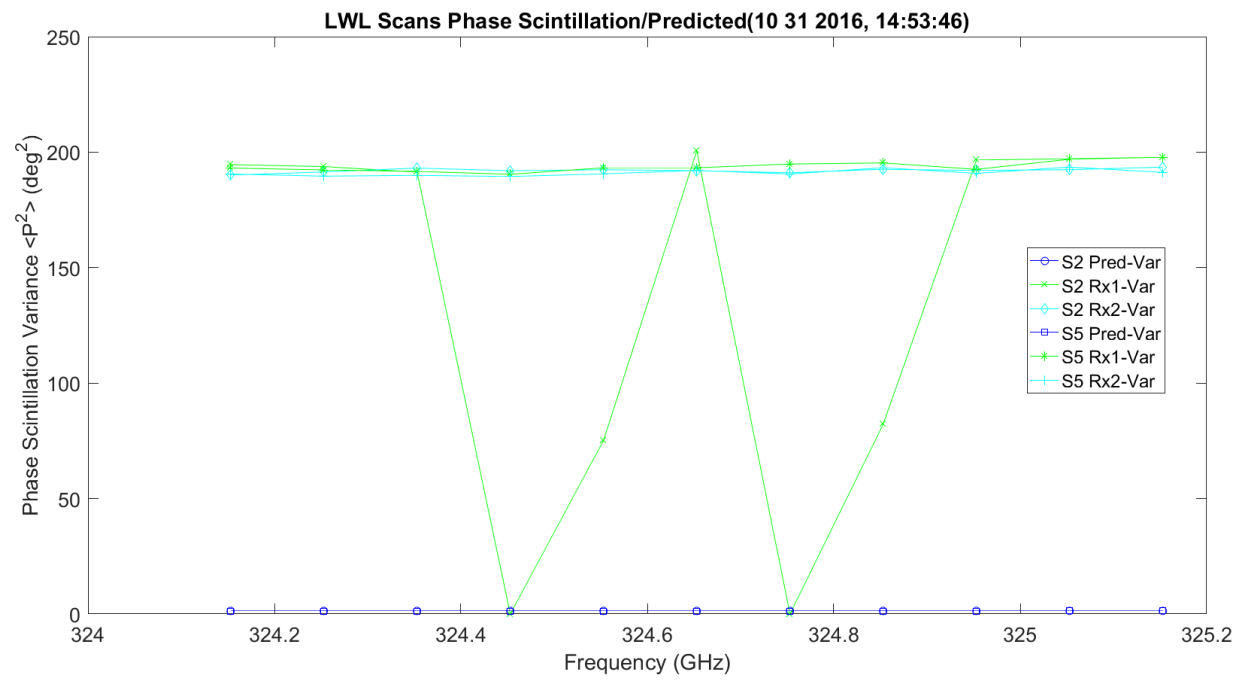


Figure 6.75. LWL Phase Scintillation Variance and Predicted - 11012016_145401.

Figure 6.76 shows the UWL scans phase scintillation variance. The offset is $\sim 180^\circ$. Everything looks stable, including Rx1. This is very dynamic over the absorption pulse.

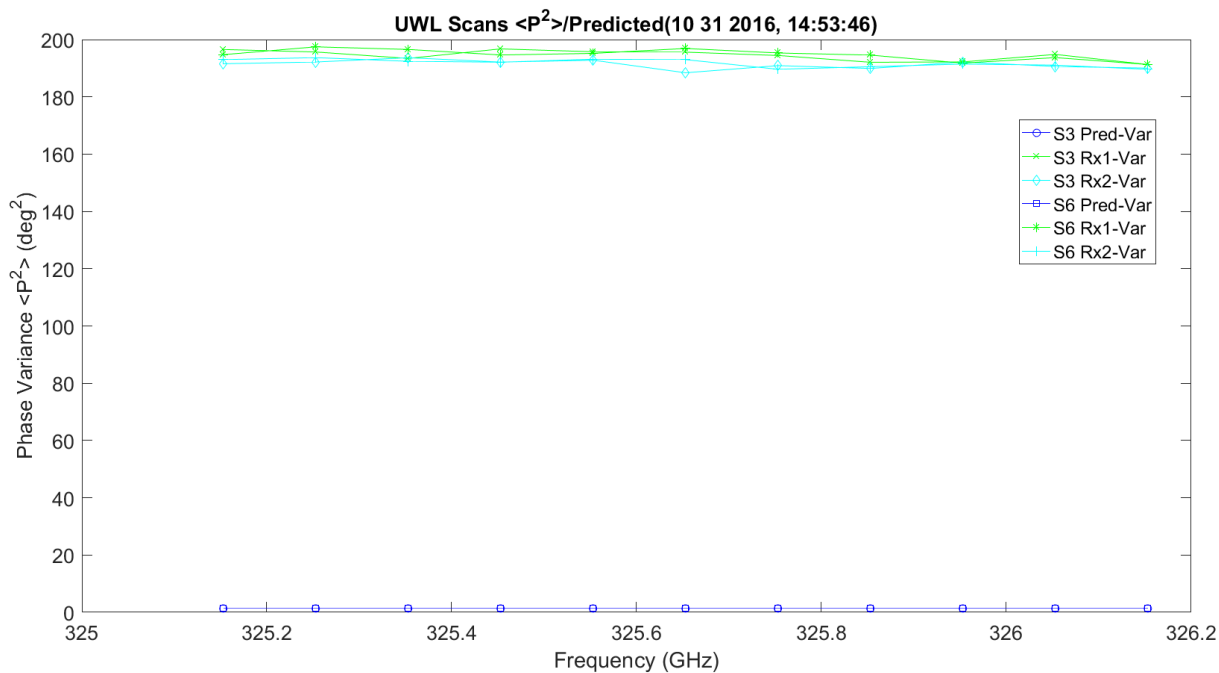


Figure 6.76. UWL Phase Scintillation Variance and Predicted - 11012016_145401.

Figure 6.77 and Figure 6.78 show the phase scintillation, $\langle \phi^2 \rangle$, for all the up and down scans — two each — compared to the predicted value utilizing the GO von Karman Model. Each set of plots shows the collected data for both receivers, with minor difference for both scans, and the predicted value.

Figure 6.77 shows the LWL scans phase scintillation STD. The STD variance is around 14° , much higher than the prediction. This is not true around some points on Rx1 where it goes to zero. It has linear growth with frequency.

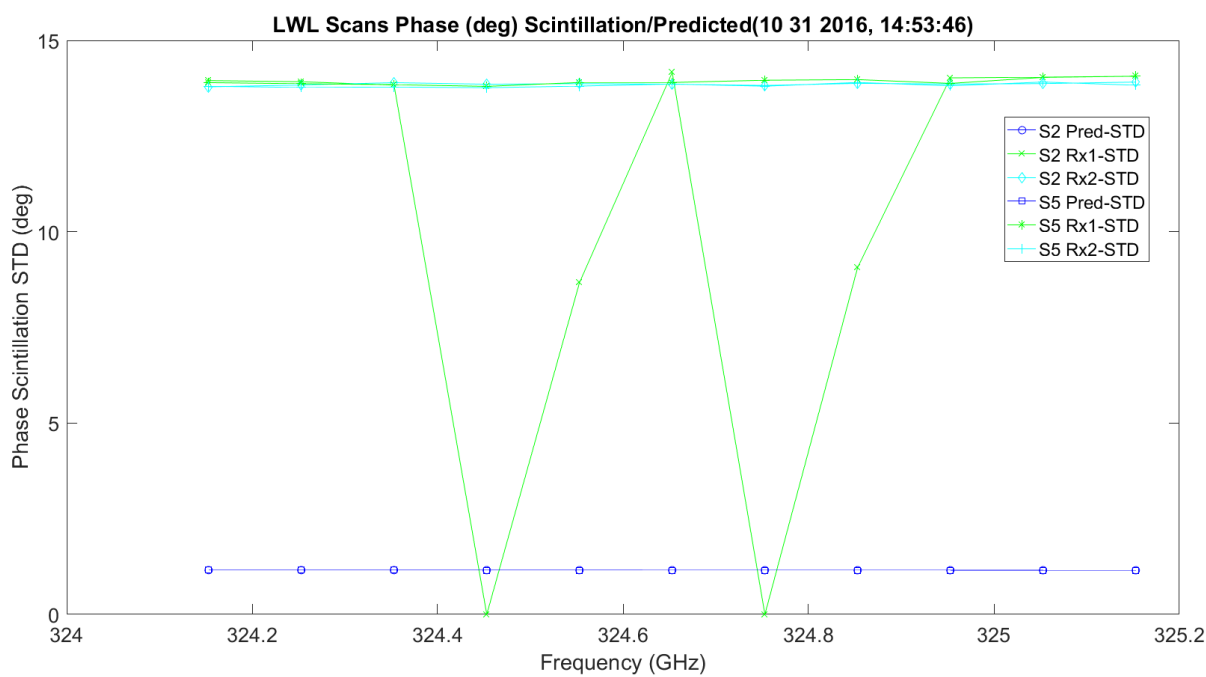


Figure 6.77. LWL Phase Scintillation STD and Predicted Deg. - 11012016_145401.

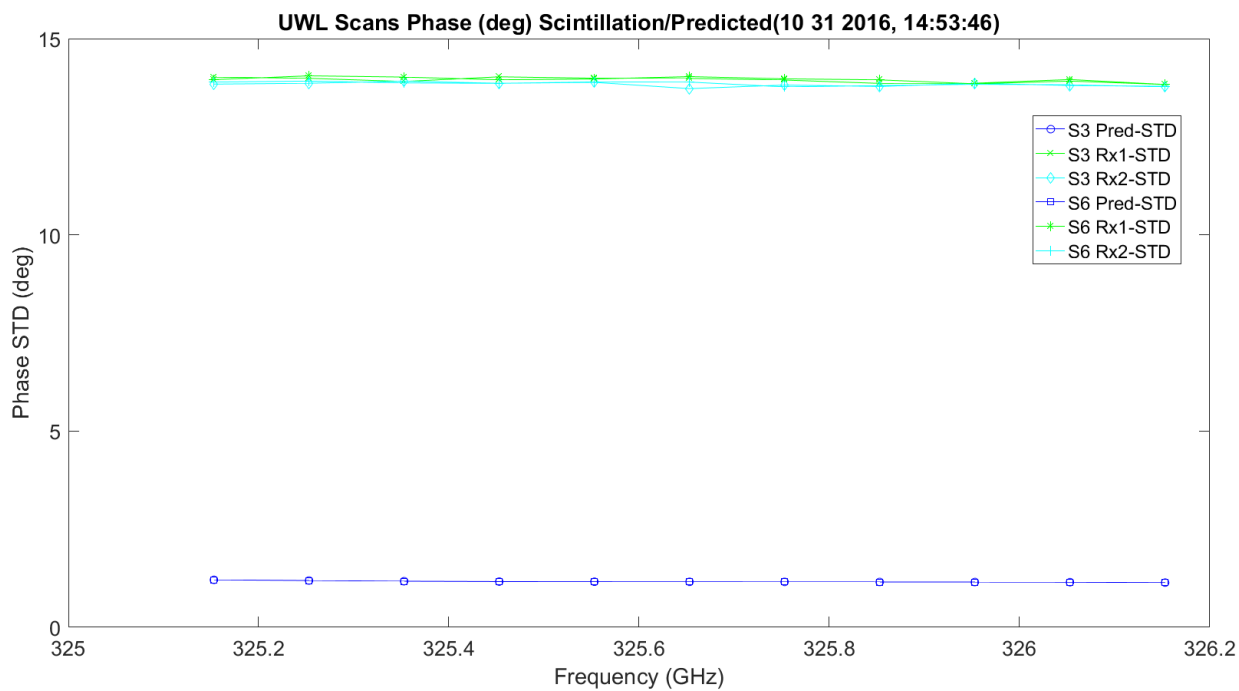


Figure 6.78. UWL Phase Scintillation STD and Predicted Deg. - 11012016_145401.

Figure 6.79 and Figure 6.80 show the amplitude and phase scintillation correlation, $\langle\chi\phi\rangle$, for all the scans — three each: total view of predicted open path data; view of predicted data; and view of open path data. WB was left in to show the big frequency picture. The prediction utilizes the Rytov, Fresnel and Fruanhofer versions. In the real data, the correlation becomes stronger as frequency is increased, especially around the absorption peak. The shapes of the predicted values for the LWL linear with small slope and the UWL, where there is much more change on a curve, match very well.

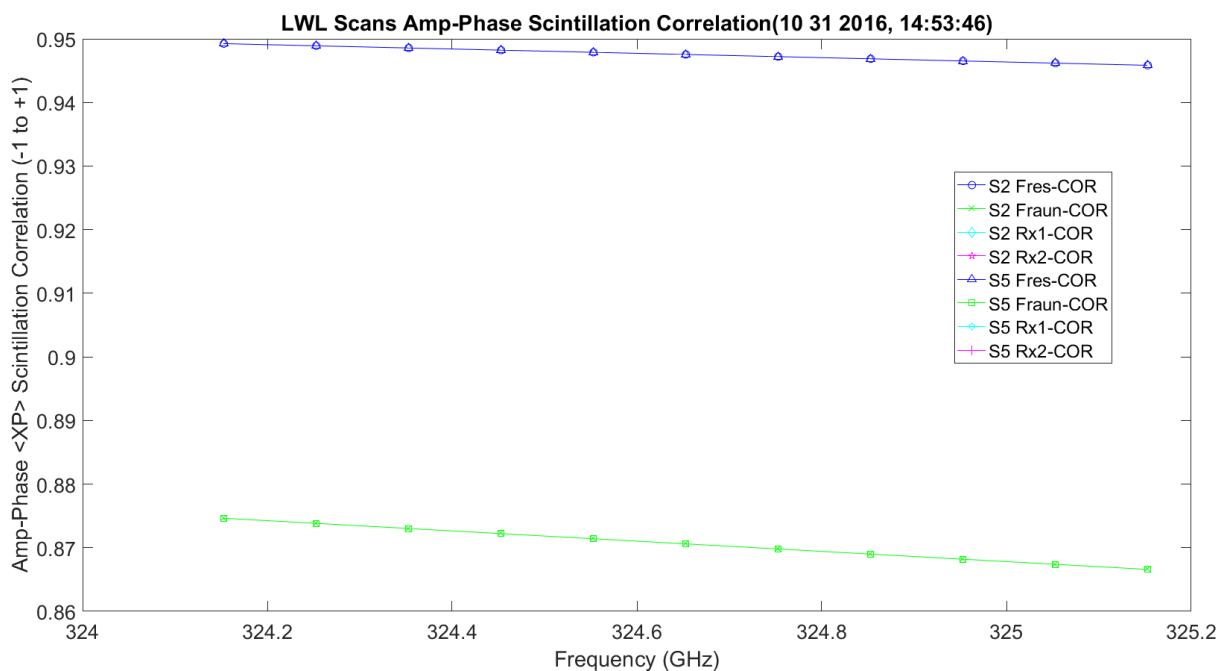


Figure 6.79. LWL Amp/Phase Scintillation Correlation and Predicted - 11012016_145401.

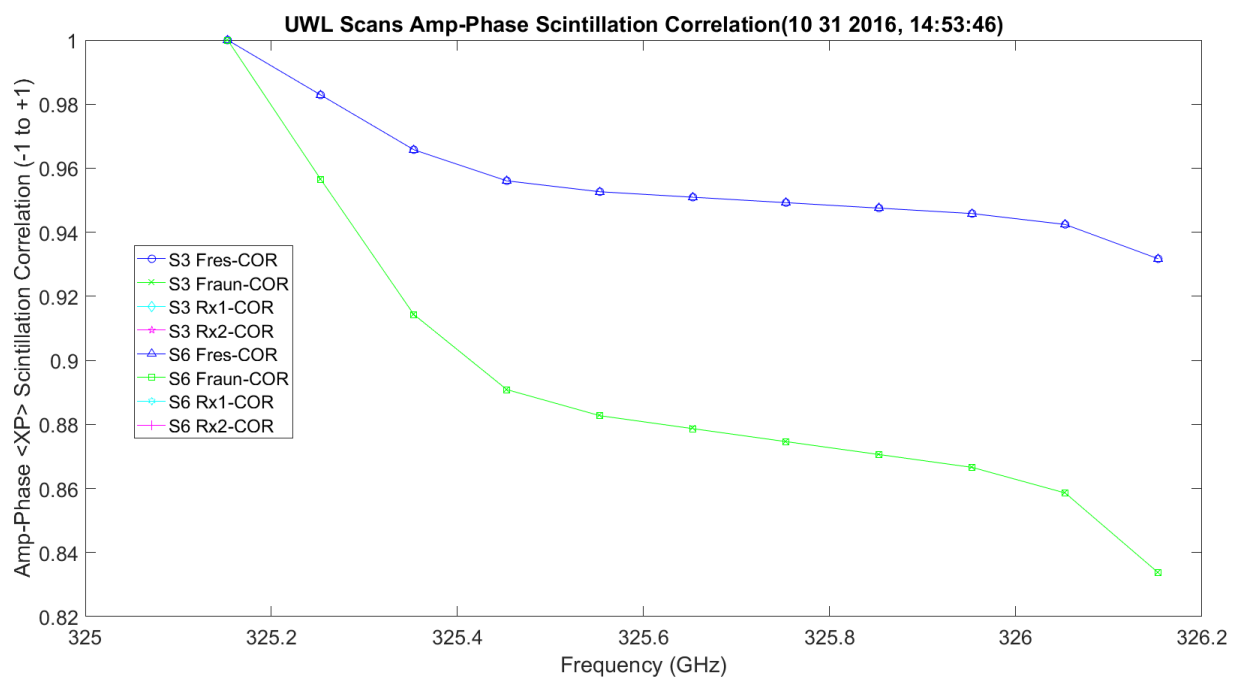


Figure 6.80. UWL Amp/Phase Scintillation Correlation and Predicted - 11012016_145401.

Figure 6.81 shows the LWL absorption plot. The red plot represents the Friis view at 20% RH. The data from TAIPAS was approximately at 30%+ RH. Note that all these have smoother lines, including Friis, and the vertical range is much larger.

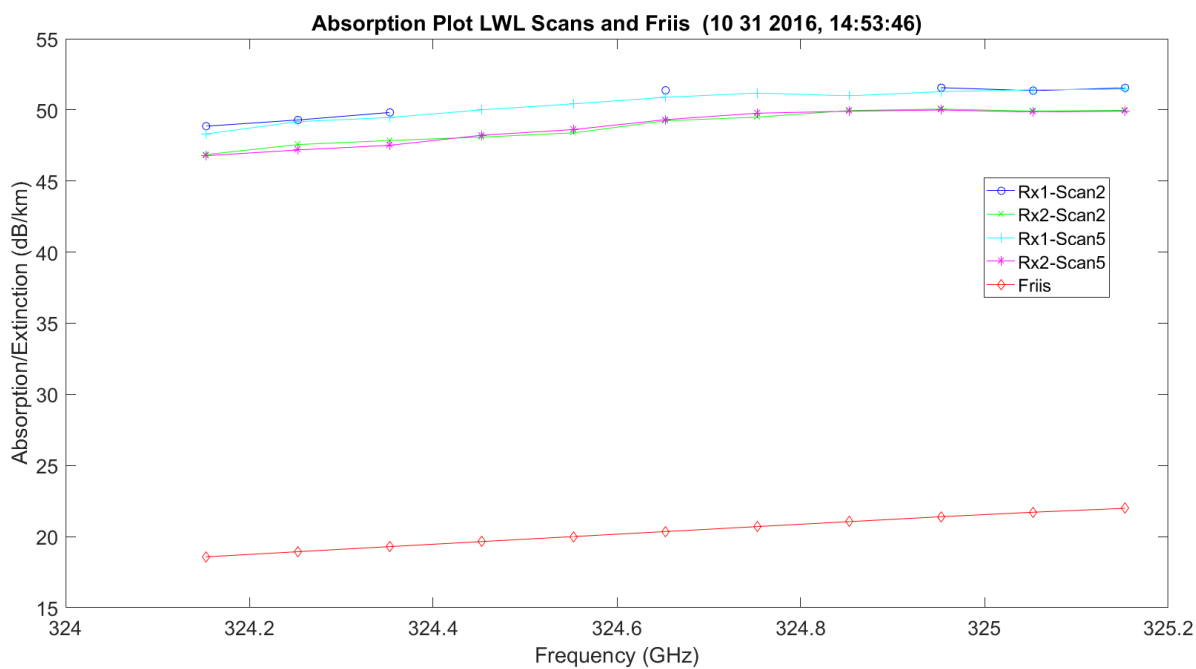


Figure 6.81. LWL Extinction with No Hardware - 11012016_145401.

Figure 6.82 shows the UWL absorption plot. The red plot represents the Friis view at 20% RH. The data from TAIPAS was approximately at 30%+ RH.

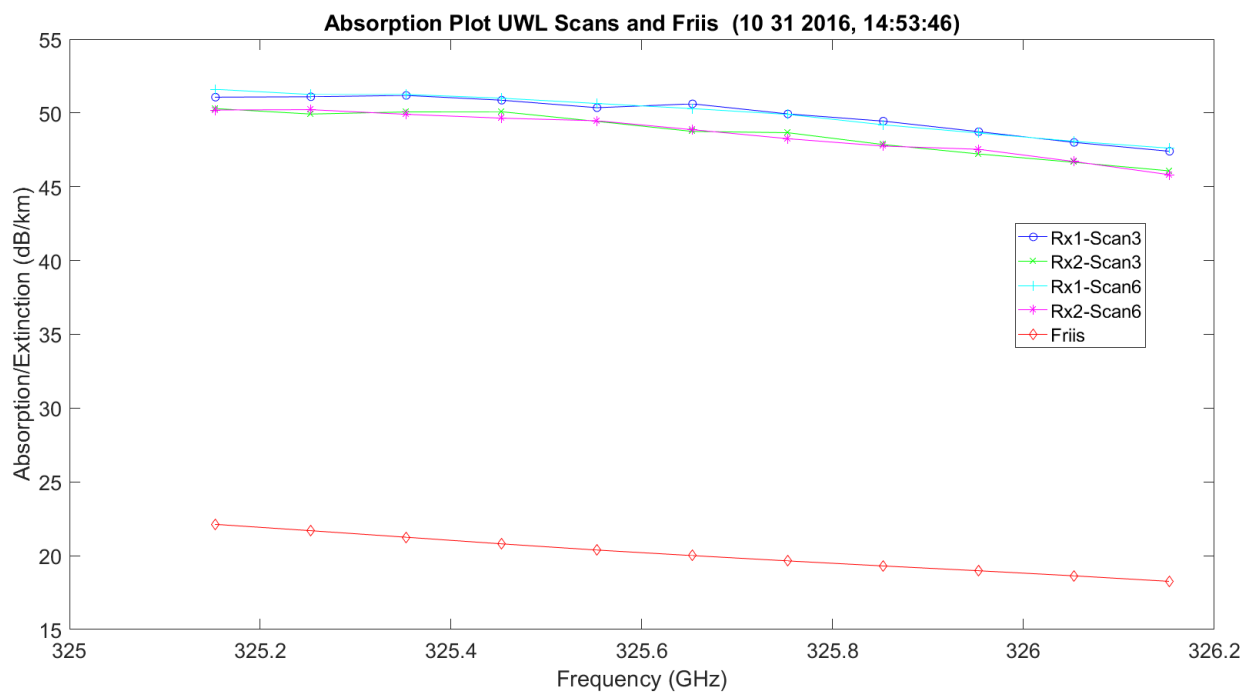


Figure 6.82. UWL Extinction with No Hardware - 11012016_145401.

Figure 6.83 shows the LWL and UWL flipped absorption plots. The red plot represents the Friis view at 20% RH. The data from TAI PAS was approximately at 30%+ RH.

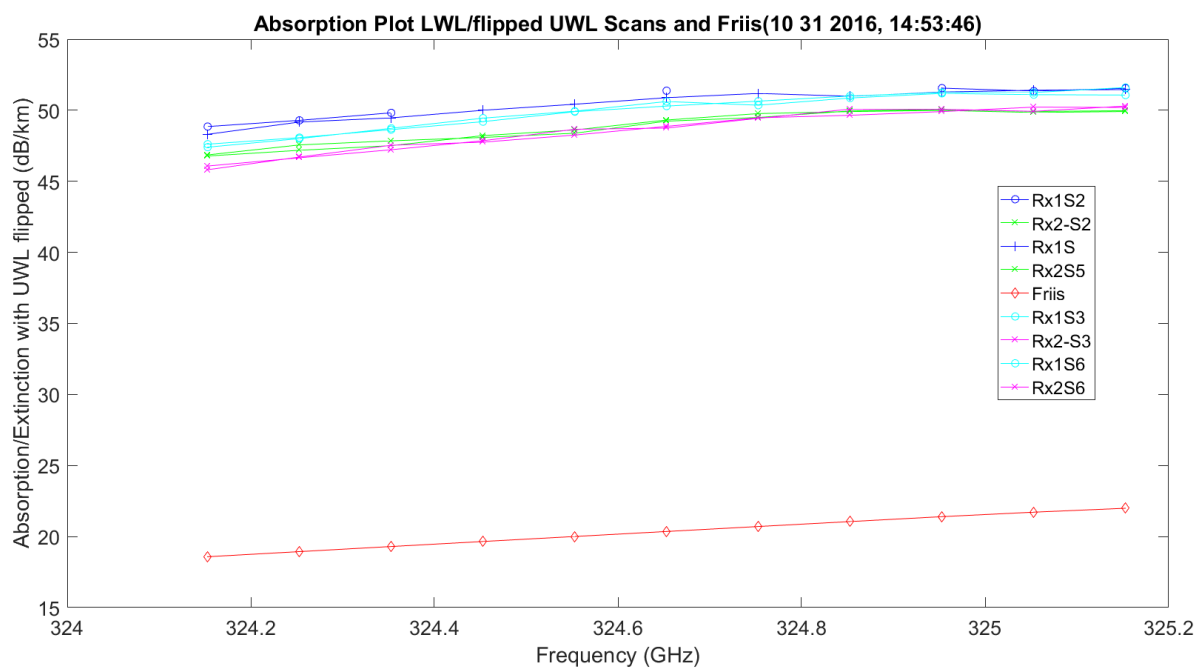


Figure 6.83. LWL & UWL Flipped Mean Amplitude No Hardware- 11012016_145401.

Chapter 7

IR/Thz Beam Co-Propagation

7.1 Introduction

The investigation under this chapter will be: “Under what conditions can a THz IR and SMMW beam co-propagate closely enough to satisfy double resonance sensing criteria?” Papers written by De Lucia, Petkie and Everitt [1] identify a double resonance, remote spectroscopic sensing technique utilizing high intensity IR pump beams to rotationally repopulate gases, along with a THz radar to sense this repopulation. Such remote spectroscopy is hindered in the lower atmosphere, compared to the upper atmosphere, due to the random turbulent medium. This thesis researched the single area to be studied for successful implementation of a double resonance spectroscopy technique, that is, whether the necessary co-collimation of the IR and THz beams holds for anticipated levels of atmospheric turbulence. Co-collimation of a temperature sensitive IR beamwave and a temperature and humidity-dependent THz beam wave is critical to the implementation of the double resonance, remote sensing technique. Use of the Manning beam wave model [30] will permit statistical studies of the cross-frequency propagation statistics at THz and IR frequencies. Previous analyses have provided equations for the phase and AoA variances that are only frequency dependent as a function of C_n^2 . The Manning solution will be extended to provide beamwave cross-frequency statistics at both IR and THz bands.

In a recent paper by de Lucia et al. [1], the possibility of remotely sensing a variety of organic and inorganic trace gases by their perturbed terahertz (THz) absorption spectrum was explored. In this double resonance spectroscopy technique, a strong IR exciter pulse alters the

thermal distribution of rotational states of asymmetric top molecules while a THz probe beam measures the differential absorption resulting from the short-lived state repopulation. To be successful, it is critical that the IR and THz pulses propagate within the same volume of gas in rapid succession at low tropospheric levels. Such beam waves will undergo significant levels of random drift, relative to the antenna boresight, while propagating in a scintillating, low altitude atmosphere. In order to understand the conditions under which such beams remain co-collimated along a path that ranges up to several km, this study examines the propagation characteristics of THz and IR beam waves in a fluctuating atmosphere, with specific emphasis on the mutual cross-frequency coherence function that describes the alignment of the beams.

The double resonance techniques leverage the spectral region and molecular rotational fingerprint for point detection of the gas; pressure reduction of the sample to linewidths at the Doppler limit, well below average spacing of spectral lines, is required. The molecular species and separation of molecular signatures from random and systemic variations are represented in these fine spectral lines. There are many issues with the implementation of this type of system: range dependence due to atmospheric propagation, frequency dependent power variations, temporal fluctuations — 1 sec time scale — of attenuation, water concentration variation, spatial variation of temperature and water along ray paths, time varying clutter, etc. All affect the SNR and co-collimation of the beams. The SNR problem is challenging, but this chapter will focus on the co-collimation problem. In order to assure beam co-collimation, the relative divergence of the two beams must be well understood. This will allow adjustments in beam size and/or transmit points to ensure that the beams are collimated at the appropriate range. The double resonance technique depends on rapid molecular collision relaxation time at atmospheric

pressure and temperature: 100 ps IR laser pulses are utilized. The rapid collisional relaxation-modulate the THz emission or absorption on a time scale much faster than the 1 s temporal atmospheric fluctuations. The beams must stay co-collimated for this duration of time at the range of interest to allow for averaging.

The desire is to have detections at a range up to 1 km. The IR beam is a column beam for this duration. If it is assumed that the THz antenna has a 1 m diameter, its beam will be in the near field where there is no divergence: flux tube / collimated. This is valid for a 300 GHz, THz beam, up to 2 km. Key parameters required for calculations, including the near field of the antenna, are calculated (Equation 7.1 – Equation 7.3).

$$\lambda_{THz} = \frac{c}{f} = \frac{2.977 \times 10^8 \text{ m/s}}{300 \times 10^9 \text{ cycles/s}} \approx 1 \text{ mm} \quad (7.1)$$

$$R_{near_field} \leq \frac{2D^2}{\lambda} = \frac{2(1\text{m})^2}{1\text{mm}} = 2 \text{ km} \quad (7.2)$$

$$Round_Trip_time_1\text{km} = \frac{2R}{c} = \frac{2(1\text{km})}{2.977 \times 10^8 \text{ m/s}} = 7 \text{ us} \quad (7.3)$$

In this experiment, at the range of interest, both beams are column beams: spatially limited bundle of parallel rays. Turbulence, temperature and humidity variations in the atmosphere can cause refraction of the beams, causing them to dance throughout the duration of the ray path. If this dancing error from the boresight of both beams is significant, it could cause the beams to lose spatial coincidence at the sensing range of interest. Broadband THz generation and detection measure changes in the amplitude and phase, which allow for determination of

absorption and dispersion of the sample: Time Domain Spectroscopy (TDS). For co-collimation of the beams, amplitude variations are lightly explored; the focus is on phase and their relations to AoA variations.

7.2 Co-Collimation Theory

The co-collimation requirement of double resonance spectroscopy requires two beams of significantly spanned frequency, one at THz frequencies and two to three orders-of-magnitude higher in frequency in the infrared band, to be overlapped at the range of interest. The close-to-ground tropospheric propagation in random media causes EM scintillation: amplitude and phase variations. The lower atmosphere has the largest effects on phase and ray path. Turbulence in the atmosphere varies the ray path of the beams due to refraction. Refraction causes bending due to change in speed driven by dielectric changes; Fresnel equations are derived from Snell's law of boundary conditions. The trajectories are determined by the dielectric constant and antenna pattern — collimated beam. Refraction and diffraction are not taken into account in ME; they assume a constant media and approximate the ray paths by straight lines. The co-locating of these two beams is not related to amplitude; phase and AoA are the two driving factors in understanding the path taken by the beams. This will allow absorption to be ignored. The sensing application being addressed requires a close-to-the-surface atmospheric condition, which will be a driving force in the determination of the co-collimation. The experiment will also assume a clear air — aerosol free and non-ionized — atmospheric condition where there are random weak fluctuations —turbulence irregularities — of complex permittivity; the permeability will be assumed to be one close to the surface — *Lower Atmosphere*: $\varepsilon = n^2$; $\mu \approx 1$. The random atmospheric water vapor spatial and temporal — $t = 1$ s — permittivity fluctuations

are caused by velocity turbulence induced by thermal, pressure and humidity in-homogeneities. It should be noted that the temperature and humidity components also have a cross-correlation dependence. The permittivity has an average component that is a function of space and a stochastic component that is a function of space and time; the stochastic part causes scintillation. These fluctuations have a direct impact on localized temperature and humidity conditions in the ray path. Since absorption is not a driving factor in the ray path, the permittivity will be assumed to be real, zero imaginary portion. The atmosphere becomes less absorptive at higher elevations and higher frequencies. It is well established that THz frequencies are highly absorptive, primarily due to water vapor content, but also atomic oxygen. This will affect the maximum range and signal intensity of the radar, but it does not affect the co-collimation requirement.

There are multiple ways to attack solutions for the stochastic scalar wave equation derived from MEs. The first Rytov transformation-perturbation approximation can be utilized and is a good path when accuracy of amplitude with diffraction is a critical parameter. Rytov utilizes volume integrals of change in permittivity along the path. Log amplitude variance/scintillations, due to the bunching and diverging of rays / energy, is proportional to the third power of distance and fifth moment of the turbulent spectrum. Therefore, it is most affected by small turbulent structures which occur closer to the ground. So amplitude scintillation will definitely occur, it is just not an important factor in co-collimation. GO is a very reasonable approach, due to its use of line integrals to represent change in permittivity along the path, when phase and AoA are the key parameters of interest and amplitude is not required; amplitude is possible for turbulent structure sizes longer than Fresnel length ($\sqrt{R\lambda}$). It assumes the medium changes gradually and cannot describe the scattering of objects comparable to the wavelength. The wavelength is

assumed to be very small, so diffraction is also ignored. If the environment is a heavy scattering context, then second order Rytov — first order only single scattering in forward direction — or Markov models for strong scattering regime must be explored. Since these models are derived from a stochastic wave equation with random variables, they yield statistical solutions for parameters of interest: structure functions — log amplitude, phase, spatial correlation, MCF, etc. For this case, the GO approach is more than sufficient and much more straight-forward to yield accurate ray path information; this is verified against experimental data in Wheelon [31, 32]. Since the EM field is harmonic, the solution to the wave equation can be an exponential. The depolarization term of the wave equation is negligible for $\lambda = \ell_0$ — inner scale length; this occurs at the lower atmosphere where turbulent structures are smaller. Rytov and GO take the approach that the permittivity has mean and fluctuating components. The average of the fluctuating parts is zero. The end goal is to have a spectral representation expression for the random fluctuations of the index-of-refraction. At the IR band and above, the index-of-refraction is driven by temperature. For THz frequencies, it is driven by temperature and humidity.

Understanding the index-of-refraction is the primary component of the structure of the atmosphere, which is critical in order to predict with high probability the ray paths of the two signals; its primary cause is due to the mean value of the real part of the complex permittivity. This is necessary in understanding how independent variables — frequency, distance, zenith angle, etc. — drive measured quantities. The primary driver of dielectric variations is due to internal re-arrangement of turbulent structure and the movement caused by wind as a result of thermal and humidity differences. Fluctuations of the real and imaginary parts of the index-of-

refraction and their cross correlation are predicted in a series of models of the spatial frequency spectrum: Kolmogorov, von Karman and Greenwood-Tarazono. These models are all based on the eddies — turbulent structures — from their time of formation through their breakdown and eventual dissipation through release of thermals. The eddy sizes are based on the process of breakdown from the insertion of energy phase where a small fraction of kinetic energy — ~10% in the ambient wind field is converted into turbulence energy at large outer scale lengths (L_0), through the cascading/redistribution of energy subdividing inertial phase or turbulent energy decay down to the smallest scale length through the dissipation phase where eddies disappear. Large, elongated/elliptical/misshaped eddies are created by instability produced in ambient wind field, then subdivided into more rounded eddies down to the millimeter range as they get closer to the surface; isotropy is a function of height with lower levels being more isotropic and higher altitudes being anisotropic. The inner scale eddy length, (ℓ_0), is the smallest eddy size or permittivity fluctuation. It is assumed that the wavelength (λ) is much smaller than the inner scale length, which at 300 GHz is not true. The atmosphere has a typical inner scale length of 1 mm. The IR signal will have no problem meeting this requirement, but it would be ideal if the THz frequency was larger than 300GHz. It is a convention to relate the eddy size to wavenumber (κ); these relations are the general wavenumber (Equation 7.3), the inner scale wavenumber (Equation 7.4) and the outer scale wavenumber (Equation 7.5).

$$\kappa = \frac{2\pi}{l} \quad (7.3)$$

$$\kappa_s = \frac{2\pi}{\ell_0} \quad (7.4)$$

$$\kappa_0 = \frac{2\pi}{L_0} \quad (7.5)$$

The wavenumber increases as the eddy size decreases; this is useful in understanding the turbulence processes. Energy cascade starts at the outer scale wavenumber and decays down to the inner scale wavenumber, below this dissipation through viscosity as heat occurs. These same processes are believed to cause the creation, subdivision and decay of fluctuations of temperature, humidity and refractive-index — passive scalars. The turbulent velocity agitates passive scalars to create random structures.

As shown later, phase and refraction, which drive AoA and ray path, are related, so phase variances will be a starting point in understanding the dielectric structure of the atmosphere. Phase correlation is generally measured as a function of a dual receiver separation (ρ). For LoS propagation, phase variance is proportional to distance and the first moment of the spectrum of turbulent irregularities; therefore, phase depends on large eddies and diffraction can be disregarded. GO also describes the many small random refractive bending or AoA variance, which is proportional to the distance traveled and the third moment of the spectrum of turbulent irregularities or small eddies dependence.

Atmospheric fluctuations, 1 ms frozen time, are slower than EM frequency, so they can be condensed into a single relationship: wave equation for random media. ME are modified for dielectric constants having small changes; the derived scalar wave equation is away from the antenna (Equation 7.6) in free atmosphere. The equation is scalar since most of the affective turbulence or wind is in the horizontal direction, along the path. The equation was derived taking

the curl of Faraday's law and substituting Ampere's law. The result is a stochastic function of position and time. It is required to define how the dielectric fluctuations at a single point vary with time and correlate fluctuations of separate points in space; turbulence theory describes these fluctuations. Tropospheric turbulence parameters are non-dispersive over large frequency bands, with not a lot of wave velocity dependence over frequency. This will make it promising to co-collimate diverse frequency beams.

$$\nabla^2 E(\vec{r}) + k^2 \left[1 + \Delta\varepsilon(\vec{r}, t) \right] E(\vec{r}) = 0 \quad (7.6)$$

7.3 Structure Functions

The atmospheric turbulence needs to be characterized for insertion into propagation equations. This is implemented through the structure function, which is a statistical distribution; permittivity changes along the path of interest. There is a need to describe the change in permittivity in range and time, $\Delta\varepsilon(r, t)$, in random media and relate this mathematically to atmospheric measurements. This is approached from phase, then AoA, through the end requirement for co-collimation of ray path variations. It should be noted that fluctuations, temperature and humidity change at a single point in space daily, yearly and with weather. Whether these are considered gradual evolution or low frequency fluctuations, they will not be utilized as drivers due to the short operation/pulse time of the sensor. Temperature fluctuations change over a 1.5° span in 1-2 seconds and are generally a stationary process; statistics don't depend on measurement time. This translates directly into statistical averages of change in permittivity, which are not dependent on position. The covariance between two receivers depends on the separation distance and not the placement points, so the atmosphere is

homogeneous. The covariance can be replaced by correlation by dividing by the mean-square value: normalized covariance. The spatial correlation function, relating to variations in permittivity, is unity for zero separation and decreases as separation increases. When receivers are placed vertically or perpendicular to the wind vector, correlation drops quickly due to elliptical eddy shape with elongation in horizontal direction. As expected, the correlation in the horizontal direction, parallel to wind, lasts over longer distances in the downwind direction — advection. Through experimentation, it was determined that temperature and permittivity distribution functions both follow a $2/3$ scaling law — turbulence theory — based on separation (ρ), and, for large separations, approach a constant value. The temperature structure function (Equation 7.7) is an estimate magnitude of stochastic temperature and permittivity variation from taking the mean squared of difference readings; this removes trend terms and leaves the stochastic component.

The decay of eddy sizes from large to small structures influences the spatial covariance; eddies that are smaller than ρ cannot influence the measurement of spatial covariance. Kolmogorov found a robust solution through the velocity characteristics that are transportable to index-of-refraction and refractive-index spectra for the linear inertial region with sharp cutoffs at the inner scale and outer scale lengths. Equivocation of the turbulence spectrum and the structure function through the velocity spectrum was implemented. The index-of-refraction structure function (Equation 7.8) is identical to the temperature structure function. Index-of-refraction is utilized instead of permittivity: $n = \sqrt{\epsilon}$. The refractive-index structure/distribution function and constant (C_n^2) for random media are different for THz and IR frequencies at the

same point and time. These also don't take humidity or the correlation between humidity and temperature into account, which will influence the THz refractive-index distributions; this is especially critical in the lower atmosphere. Assume that it is isotropic, since it is close to the surface and homogeneous since the sensors separation is small. There is also a wavenumber spectrum of irregularities ($\Phi_n(\vec{\kappa})$) description called the Turbulence Spectrum, which completely describes the medium. If isotropic, the wavenumber is a scalar, which is the average length of an eddy. The Fourier transform is utilized to relate power spectrum and the covariance function, which show that turbulence theory describes atmospheric irregularities and is governed by the physics of atmospheric hydrodynamics. Von Karman extended this model to include the energy input region and will be primarily used from this point forward. The energy input region has a large effect on estimates for the average scale length and refractive-index variance since they are proportional to the first two moments of the spectrum. The energy loss region affects the amplitude scintillation for optical signals since the Fresnel length is close to the inner scale length; amplitude is not a concern for co-collimation, so the von Karman model, which is best for close to the ground applications, will suffice. It assumes isotropic or spherical eddy structure, which is a good model for close to the ground operation; experimental data for the horizontal and vertical correlation lengths are equivalent. The von Karman model has good agreement with experimental data for optical and microwave links. Optical is less isotropic at the surface, but it still yields optimal results. It is important to note that troposphere irregularities near the surfaces are correlated over longer distances in the horizontal than the vertical dimension; horizontal is the dimension of interest for the co-collimated application. The von Karman model refractive-

index fluctuations (Equation 7.8), spectrum from the energy release to inner scale lengths/average lengths (Equation 7.9) and structure function (Equation 7.10) are important.

$$D_T(\rho) = C_T^2 |\rho|^{\frac{2}{3}} \quad (7.7)$$

$$\langle \delta n^2 \rangle = .523 C_n^2 (\kappa_0)^{-\frac{2}{3}} \quad (7.8)$$

$$\Phi_n(\kappa) = .033 C_n^2 (\kappa^2 + \kappa_0^2)^{-\frac{1}{6}} ; 0 < \kappa < \kappa_s \quad (7.9)$$

$$D_n(\rho) = .8294 C_n^2 \rho^{\frac{2}{3}} \int_{\kappa_0 \rho}^{\infty} x^{-\frac{5}{3}} \left(1 - \frac{\sin(x)}{x} \right) dx \quad (7.10)$$

The average eddy size is approximately 0.476 times the outer scale length. It is easier to establish turbulent irregularities in the lower atmosphere, since direct measurements of temperature, humidity and refractive-index do not require moving platforms.

The index-of-refraction structure constant (Equation 7.11) is the key parameter in all the derived structure equations for tropospheric propagation: temperature in Kelvin and pressure in millibars. The refractive-index is independent of frequency for frequencies ranging from 1-30 GHz. It is a function of temperature, humidity and pressure. These equations were derived utilizing Taylor's hypothesis, stating eddies are frozen in time during measurement and wind carries past the instrument at a constant speed.

$$\text{Microwave: } n = 1 + \frac{77.6}{T} \left(p + 4810 \frac{e}{T} \right) 10^{-6} \quad (7.11)$$

The refractive-index is dependent on frequency for optical frequencies IR and up. However, it is no longer a function of humidity and pressure; pressure still correlates with temperature, so it is indirectly driven by pressure. The index-of-refraction covariance structure function constant, at optical frequencies, can be derived from the temperature covariance structure constant (Equation 7.12 and Equation 7.13) with wavelength in micrometers.

$$n = 1 + \frac{77.6p}{T} \left(1 + \frac{7.52 \times 10^{-3}}{\lambda^2} \right) 10^{-6} \quad (7.12)$$

$$C_n^2 = C_T^2 \left[\frac{77.6p}{T^2} \left(1 + \frac{7.52 \times 10^{-3}}{\lambda^2} \right) \right]^2 10^{-12} \quad (7.13)$$

For the optical version, the index-of-refraction decreases as temperature and frequency increase. Since water vapor decreases with increases in altitude in the troposphere, the microwave index-of-refraction migrates to only temperature dependence and is equal to the optical version. The THz band index-of-refraction lays somewhere between these two; at current 300 GHz radar frequencies, it is likely much closer to the microwave index-of-refraction. As hardware becomes available to build much higher frequency radars, it could migrate toward the optical index-of-refraction. These coefficients change dynamically over small periods — instantly — and long periods of time. It can change by three orders of magnitude throughout the day. Thermal plumes can occur instantly near the surface. Microwave / THz signals can be affected by columns of water vapor in the convective boundary layer. The optimal method is to utilize a scintillometer to measure these values in real-time during experiments or operation of real-time systems. The co-collimation application has very short time periods of data collection

which allow for more stability of the index-of-refraction. Example values for structure constants derived from large samples (Equation 7.14 – Equation 7.16) show that for optical and microwave, much lower than the radar frequency of 300 GHz, are approximately equal; index-of-refraction structure constant changes, but negligibly over the bands.

$$\text{Microwave } 36\text{GHz} - \text{avg. Stable Conditions} : \bar{C}_n^2 = 1.2 \times 10^{-14} \text{ m}^{-2/3} \quad (7.14)$$

$$\text{Microwave } 36\text{GHz} - \text{avg. Convective Conditions} : \bar{C}_n^2 = 6.6 \times 10^{-14} \text{ m}^{-2/3} \quad (7.15)$$

$$\text{Optical} - \text{avg. Stable Conditions} : \bar{C}_n^2 = 1.0 \times 10^{-14} \text{ m}^{-2/3} \quad (7.16)$$

The turbulence spectrum is difficult to pin down since both defining parameters are intermittent random functions: inner scale length and index-of-refraction structure coefficient; dependent on frequency (minimal), temperature and humidity. The inner scale varies from 3.5 mm at the surface to about 12 mm at a height of 1 km. Near the surface, the outer scale length is approximately 0.46 times the height.

7.4 Ray Path / Phase / AoA

Now that the structure of the permittivity in the turbulent atmosphere is understood, phase and AoA, which will yield measures of the ray path, need to be defined through GO. The approximate solution for the EM field equations for wavelength, less than other dimensions, dielectric constant and boundary conditions, don't change much over one wavelength and ignoring diffraction and polarization produces the scalar wave equation. A solution to the scalar wave equation with zero source — free space — is exponential (Equation 7.17). This can be written as a function of range with the phase equal to the wavenumber times the eikonal (ψ)

(Equation 7.18). The eikonal is defined by the dielectric constant and the type of wave transmitted and represents the central result of geometrical optics (Equation 7.19). The ray path or trajectory of the signal and phase, or surface/geometric wave front, descriptions depend on the solution to the eikonal equation, which is a line integral (Equation 7.20). The solution is unique, since the propagation vector is perpendicular to the surface of constant phase; ray path trajectories are orthogonal to geometric wave-fronts. The eikonal is perturbed due to the random fluctuations of the dielectric constant. The ray paths correspond to the direction of the Poynting vector along an isotropic medium. The resulting equation for the bending of the ray trajectory path, which is only a start toward understanding co-collimation (weak identifier) with α the initial angle of elevation, is shown in Equation 7.21.

$$E = E_0 e^{jkz} \quad (7.17)$$

$$E(r) = A(r) e^{jk\Psi(r)} \quad (7.18)$$

$$(\nabla\Psi)^2 = \varepsilon(r) \quad (7.19)$$

$$\Psi(R) = \oint_T^R ds \sqrt{\varepsilon(s)} \quad (7.20)$$

$$x = \int_0^{z(x)} du \frac{\cos \alpha_0 \sqrt{\varepsilon(0)}}{[\varepsilon(u) - \varepsilon(0) \cos^2 \alpha_0]^{1/2}} \quad (7.21)$$

This is dependent on understanding the permittivity profile along the path, which in the troposphere depends on altitude. This only considers changes in the z dimension or the progressive bending of a ray driven by the dielectric constant. Ray trajectories become a straight

line for constant dielectric. This assumes on x and z movement with the y dimension constant. Incremental movement in all dimensions needs to be understood to assure co-collimation.

This leads to getting an understanding of the progressive phase variation along the path in order to understand the movement of the beam. The total phase shift is the eikonal multiplied by the wavenumber (Equation 7.22). This phase shift will relate the distributions of the two permittivity profiles and be an indicator of the path taken. For co-collimation, changes in phase will relate to ray trajectory travel and will be a measure of the dancing of the beam columns. In other words, the total phase shift will relate the distributions of the two permittivity profiles for the IR and THz beams. If the two beams traveled the same path, their eikonals will be identical and the phase shifts will be off by the difference in frequency (Equation 7.23). The phase shift transverses many radians for atmospheric paths. The required component is the small changes in the dielectric along the ray path: average component and stochastic random component as a function of space and time. If the permittivity is limited to only change as a function of height, the total phase shift equation reduces to Equation 7.24 and Equation 7.25 with $\epsilon(z)$ equal to a constant. Unfortunately, the co-collimation problem is not that simple. The phase changes as a function of time over the entire path, which transverses all dimensions (Equation 7.26). If the path is assumed to be primarily horizontal, which is possible for the co-collimation applications, the phase for microwave through optical reduces to Equation 7.27. Fluctuations in the dielectric constant, which can be related by the two-phase shifts of the beams, causes the ray path to wander in two dimensions as it propagates. This is affected by the small refractive bendings causing angular errors in the tangent vector relative to the nominal ray path. The 2D equations for cross plane/orthogonal angular error and in plane angular error with perturbed dielectric are

functions of integrals over distance (Equation 7.28 and Equation 7.29). Combining the two equations yields a total angular error vector to the normal component of the gradient of the dielectric variations integrated along the ray path (Equation 7.30). As shown in the equation, the total angle error is related to the phase (Equation 7.31).

$$S = k\Psi = k\oint ds\sqrt{\varepsilon(s)} \quad (7.22)$$

$$|S_{THz} - S_{IR}| = \Psi \left(\frac{|\omega_{THz} - \omega_{IR}|}{c} \right) \quad (7.23)$$

$$S = k \int_0^h dz \frac{\varepsilon(z)}{[\varepsilon(z) - \varepsilon(0) \cos^2 \alpha_0]^{1/2}} \quad (7.24)$$

$$S = kh \csc \alpha_0 \quad (7.25)$$

$$\varphi(t) = \frac{k}{2} \int_0^R ds \frac{1}{\sqrt{\varepsilon(z)}} \Delta\varepsilon(x, y, z; t) \quad (7.26)$$

$$\varphi(t) = \frac{k}{2} \int_0^R dx \Delta\varepsilon(x; t) \quad (7.27)$$

$$\delta\theta_{\perp} = \frac{dy}{ds} = \frac{1}{2\sqrt{\varepsilon(R)}} \int_T^R ds \frac{1}{\sqrt{\varepsilon(s)}} \frac{\partial}{\partial y} \Delta\varepsilon(s, t) \quad (7.28)$$

$$\delta\theta_n = \frac{1}{2\sqrt{\varepsilon(R)}} \int_T^R ds \frac{1}{\sqrt{\varepsilon(s)}} \frac{\partial}{\partial n} \Delta\varepsilon(x, y, z; t) \quad (7.29)$$

$$\delta\theta = \frac{1}{2\sqrt{\varepsilon(R)}} \int_T^R ds \frac{1}{\sqrt{\varepsilon(s)}} \nabla_{\perp} \Delta\varepsilon(x, y, z; t) \quad (7.30)$$

$$\delta\theta = \frac{1}{k\sqrt{\varepsilon}} \nabla_{\perp} \varphi \quad (7.31)$$

It is important to note that the phase shifts are a function of frequency, but the AoA is not a function of frequency. This is promising for the co-collimation of frequency diverse waveforms. It does not guarantee co-collimation, since the dielectric for the THz frequency achievable with hardware still has a significant humidity permittivity dependence, where the IR signal will not. As long as the IR pulse is closely spaced with the THz pulse such that the stochastic portion of the dielectric does not vary significantly, the beams will dance together.

There are limited validity conditions that need to be considered when looking at phase and angle errors in random media. The first condition is that the random medium be smooth: dielectric constant cannot change substantially over a wavelength. This allows the solution to the wave equation to be eikonal and transport equations with the medium is considered smooth under a condition in Equation 7.32 and Equation 7.33. The second condition is dependent on the caustic behavior of the rays in a beam and is primarily a driver of amplitude variations. It is not accurate to use ray theory where rays are converging or diverging rapidly in a beam; rays will combine within beam under these conditions. This is why GO is not optimal for predicting amplitude fluctuations. This would be exacerbated in a high scattering medium. The third condition deals with diffraction. If diffraction is to be ignored, the spreading of rays in a collimated beam has to be significantly less than the diameter of the ray bundle. This also requires the Fresnel length to be much less than the inner scale length.

$$C_n^2 \lambda^2 (\kappa_m)^{4/3} \ll 1 \quad (7.32)$$

$$\kappa_m = \frac{5.91}{\ell_0} = 0.9406(\kappa_s) \quad (7.33)$$

Phase variance has strong large eddy dependence, so influential sizes are close to the outer scale length. Since for most optical and microwave propagation, the Fresnel length is much less than the outer scale length, GO is very applicable for estimating phase fluctuations. In order to yield good phase structure function measurements, receiver separation must be much larger than Fresnel length. Angular variance is dependent on the third moment of the spectrum; therefore, small eddies are also important. Most angular measurements of aperture size, considering aperture averaging, replace the smallest eddies as the most critical parameter: the Fresnel length must be much less than the aperture size to bring in the inner scale length. This is easily achieved for optical frequencies, but, for most cases, yields too large of aperture sizes for practical microwave systems. Diffraction theory needs to be utilized for microwave frequencies; this may be true for THz depending on what part of the T-gap band is utilized. Amplitude variation is proportional to the fifth moment of the wavenumber spectrum, so very small eddies are important for measurements. This forces diffraction theory to describe amplitude scintillation as well.

Phase variance is utilized heavily in single path propagation experiments as a primary benchmarking parameter. It is proportional to the first moment of the wavenumber spectrum of irregularities, which forces a large eddy dependence. Phase is significantly affected by the energy input phase of the turbulent cascade process. Phase fluctuation is a stochastic function of

time, since it is a linear function of the stochastic change in permittivity parameter. Random functions of time need to be described by moments and correlation functions. When the scale lengths are small, like close to the surface, phase variance scales linearly with range. Phase fluctuations of optical signals are much larger than those at microwave frequencies. In the case of horizontal propagation close to the surface, assumed for the co-collimation application, turbulent dynamics are relatively constant. Since the outer scale lengths for eddies at the surface are much smaller than path lengths, the following phase variance — second moment — Equation 7.34 can be utilized with Equation 7.35, a von Karman Model.

$$\langle \varphi^2 \rangle = 4\pi^2 Rk^2 \int_0^{\infty} d\kappa \kappa \Phi_n(\kappa); \kappa_0 R \gg 1 \quad (7.34)$$

$$\langle \varphi^2 \rangle = .782 Rk^2 C_n^2 \kappa_0^{-5/3} \quad (7.35)$$

The von Karman model is utilized since it defines the energy input region: eddy formation and large eddy region. The dissipation region, below the inner scale, can be ignored since the inner scale wavenumber (κ_s) is much greater than the outer scale wavenumber (κ_0). The index-of-refraction structure coefficient can be determined utilizing a scintillometer; the outer scale length can be assumed to equal .4 times the height above the ground (Tatarski). When the path is not greater than the outer scale length, increased altitude in the troposphere, anisotropic needs to be applied. The sample length effect also comes into play when measuring phase influenced by random variations of refractive-index; when using a finite data sample, it is impossible to distinguish between the effects of large eddies and atmospheric trends throughout the day, year, etc. Temperature and water vapor dominate refractive-index in the lower troposphere;

irregularities are caused by the turbulent motion of the wind. The horizontal portion of the wind can be considered a constant, so normal wind vectors will be the primary influence to phase variance. When wind is not present, self-motion becomes the dominant factor in generating refractive irregularities. This could also be caused by vertical convection due to temperature gradients.

The primary driving influence for co-collimation comes down to AoA fluctuations along the path due to a stochastic permittivity component that forces a quivering, dancing or jittering of the beams. The covariance matrix relating these beams is needed in future propagation experiments at the frequencies of interest in IR and THz. Measuring the angular dancing is relatively easy at the surface, since the level of turbulence is approximately constant. The eddies, in this case, that are responsible for the angular errors are nearly isotropic, making the two-phase error components equal. The AoA variance for closely spaced receivers is proportional to the third moment of the wavenumber turbulence spectrum and will increase linearly with the path length; primarily dependent on small eddies which is the opposite of phase errors. For this case, the von Karman model is not required since characterization is required only at the small wavenumber portion of the spectrum. Influence primarily falls in the inertial range of the spectrum; therefore, the Kolmogorov model can be utilized. The collimated beam Equation 7.36 for AoA error and, more importantly, Equation 7.37 for the co-collimation causing the spot wandering variance are important: ω_0 is the transmit beam-width in meters.

$$\langle \delta\theta^2 \rangle_{col_beam} = 2.914RC_n^2(\omega_0)^{-1/3} \quad (7.36)$$

$$\langle p^2 \rangle_{col_beam} = .971R^3 C_n^2 (\omega_0)^{-1/3} \quad (7.37)$$

These errors will be larger in a propagation link experiment due to aperture smoothing; this is not a consideration for the co-collimation application, since there is not aperture at the time of the beam overlap requirement. In the past, descriptions of beam wander and AoA fluctuations were developed from diffraction theory utilizing the Markov approximation. It has been found that GO is a much simpler description for beamwaves. The spot wandering equation is very close to the calculations derived using Markov approximations, which include diffraction and strong scattering effects; therefore, ray theory can even work for a variety of scattering conditions. Manning [30] utilized Rytov first order approximation to yield the relevant statistical parameters of an EM field propagating in a randomly dispersing and absorbing atmosphere utilizing the von Karman model for the spectrum of the refractive-index fluctuations. The first order is a single scattering forward; the second order was dropped with no effect. The wavenumber spectrum fluctuations are very close to Equation 7.9. Manning derived the equations for absorption, or the imaginary portion of the spectrum and cross correlation between the real and imaginary parts; this is not a concern for the co-collimation, so it was excluded. The real part affects the refractivity (Equation 7.38). Manning also derived the index-of-refraction structure coefficient as a function of path length with humidity included (Equation 7.39). The A parameter is spectroscopically determined. The equation takes water vapor into account and ignores oxygen, ozone and carbon dioxide. T is the absolute temperature and Q is absolute humidity. If this new value is plugged into the equation above for the structure coefficient, assuming the co-collimation requirement is fixed at some measurement point R , the new spot

variance equation is as follows for the THz (Equation 7.40) and IR (Equation 7.41) signals. The error between the two beams is easily derived as a function of only humidity (Equation 7.42). As expected, the longer the range, the more the spot variance delta grows to the third power, and, as expected, the smaller the THz beamwidth, the larger the delta to the divided cubed root. For a given range, the beam width of the THz radar should be large to increase the probability of the overlap of the co-propagation; unfortunately gain is reduced. The delta spot variance of the two beams could be calculated and utilized as a parameter of merit for co-collimation. For example, 2 km requires a very small beam width to yield a small variance difference. It is most likely required to have a much larger THz beam to encompass the IR beam, even when both vary. The chemical molecular resonance processing can pull out the desired results of the radar. The other alternative is to have a very short range, which defeats the use of the long-range spectrometer.

$$\Phi_{RR}(\kappa) = .033C_{n_R}^2(r) \left(\kappa^2 + \frac{1}{L_0^2} \right)^{-11/6} e^{-\kappa^2/\kappa_m^2} \quad (7.38)$$

$$C_{n_R}^2(r) = \frac{A_T^2}{\langle T \rangle^2} C_T^2(r) + \frac{A_Q^2}{\langle Q \rangle^2} C_Q^2(r) + 2 \frac{A_T A_Q}{\langle T \rangle \langle Q \rangle} C_{TQ}(r) \quad (7.39)$$

$$\langle p^2 \rangle_{col_beam_THz} = .971R^3 \left(\frac{A_T^2}{\langle T \rangle^2} C_T^2(R) + \frac{A_Q^2}{\langle Q \rangle^2} C_Q^2(R) + 2 \frac{A_T A_Q}{\langle T \rangle \langle Q \rangle} C_{TQ}(R) \right) (\omega_0)^{-1/3} \quad (7.40)$$

$$\langle p^2 \rangle_{col_beam_IR} = .971R^3 \left(\frac{A_T^2}{\langle T \rangle^2} C_T^2(R) + 2 \frac{A_T A_Q}{\langle T \rangle \langle Q \rangle} C_{TQ}(R) \right) (\omega_0)^{-1/3} \quad (7.41)$$

$$\Delta \langle p^2 \rangle_{col_beam_IR_THz} = .971R^3 \left(\frac{A_Q^2}{\langle Q \rangle^2} C_Q^2(R) \right) (\omega_0)^{-1/3} \quad (7.42)$$

$$\Delta \langle p^2 \rangle_{col_beam_IR_THz_2km} = \frac{(7.68 \times 10^9 m^3) \left(\frac{A_Q^2}{\langle Q \rangle^2} C_Q^2(R) \right)}{\sqrt[3]{\omega_0}} \quad (7.43)$$

7.5 Conclusion

The phase is a weak correlation measure for co-collimation due to its heavy dependence on large eddy sizes. Small eddies are going to be the driving factor, due to the AoA; therefore, spot wander dependence is on them. There are a lot more physics of the atmosphere that can be applied, including effects on pressure and how that affects the temperature / humidity cross correlation version of the structure constant. Part of the correlation between humidity and temperature at the surface is due to evaporation; it causes cooling that decreases T as Q increases. Also, the heat capacity changes with humidity; water in the vapor phase has different thermal conductivity. Co-collimation of two frequency diverse beams is very possible, but requires detailed design analysis and real-time readings of the appropriate parameters. If a large enough THz beam can be generated to cover all spot wandering variance at all ranges, the co-collimation will be a success with no critical real-time atmospheric measurements required. This will require high SNR to pull out the desired resonance frequencies. This is easier in SNR if the IR beam can be larger than the smaller THz beam, but this is difficult to implement.

Chapter 8

Conclusions

Chapter 2 described TAIPAS's new coherent, dual receiver, open path transmissometer. It has many new features: coherency, advanced hardware, and a range of 1924 m on an open slanted path. This was much more complex than the earlier work. It was also implemented in Colorado, which allows for a huge variation of atmospheric conditions. The last time a program was implemented in the early 1980s for over \$2M in funding and more than five Ph.D. researchers, the Net Present Future Value (NPFV) was approximately \$30M. Dr. McMillan, who worked at the Army as they awarded \$750K, stated that the program would be impossible to complete. External companies and universities added approximately \$200K, which increased the total budget to \$950K; the Ph.D. student on this program did not charge the contract. The scintillometer was advanced under this program with new math for a single LED and design of a future convolution-based, Barker-coded, multi-LED system, which will improve resolution and will be implemented on future Army work. An alignment system was designed for a system that had an unacceptable path due to altitude and the building and houses below. This system allowed for alignment resolution of 2.5 m when the beam spot size was ~24 m. The THz transmit and receive antennas were built out of Rexolite Lens and highly sensitive calipers for precise resolution to optimize gain; the power on this system was very low, since no tubes were leveraged. The system was permanently installed for 24/7 operation, accessible from anywhere in the world via VPN.

Chapter 3 delves into advanced analysis of the propagation. This includes data to fill the covariance matrix between amplitude, phase, temperature, index-of-refraction and humidity. There were wideband scans and LWL and UWL scans in much higher resolution than the past. Close to ten thousand lines of MATLAB were written to process all the data from a single acquisition pass that occurred in less than seven seconds. The plotting and comparisons were extensive.

Chapter 4 has shown the system is available to analyze any type of aerosol-based atmosphere: rain, snow, smoke, dust, bugs, etc. Unfortunately, these conditions did not exist during the operation of TAIPAS and the research. Future funding will allow these to be accomplished over the next couple of years.

Chapter 5 dives into the Manning thesis and the approach he came up with for a scintillation structure constant that can be analyzed significantly with relationships of temperature, humidity and the cross correlation of both.

Chapter 6 dives into light analyzing of the LWL and UWL signals; more data than collected at the time of the thesis is required to draw conclusions. The resolution of the frequency samples had never been implemented before. This first set of data shows that the previously smooth, perfectly symmetrical wing lines may not be true. This chapter shows that there is variation, even on the same channel within 3.5 seconds, to LWL and UWL plots. This will require more studying on the future program to determine the exact drivers of these variations. These variations far exceed any transmitter or receiver calibration that is driven by the variation in

power. It is very difficult to understand in any physics situation the belief that the LWL and UWL are perfectly matched and smooth. TAIPAS, and common sense, are driving future work to make a conclusion on these varying slopes.

Chapter 7 shows the dependence to implement IR and THz co-propagation. While techniques for implementing this co-propagation — funded by the Army solely for this purpose — look very promising, more work will be done on a future program.

The total system success and deployment, and the advanced early data implemented in clear-air, were lead and driven by Professor Albin Gasiewski, the advisor for the Ph.D. The results in advances leveraging TAIPAS will continue for decades. For example, a large commercial company has approached the team for advanced bandwidth cell communication systems; this can extend to 150 GHz. This will obviously drive cell systems and phones / modems toward the TAIPAS program. The team utilized the same approach on another Army program for implementing 3D imaging of the ground at 210 GHz; TAIPAS knowledge will continue to drive the needs for implementation.

References

- [1] De Lucia, F., Petkie, D. and Everitt, H., "A Double Resonance Approach to Submillimeter / Terahertz Remote Sensing at Atmospheric Pressure", 2006.
- [2] Cooper, K.B., R. J. Dengler, N. Llombart, B. Thomas, G. Chattopadhyay, and P.H. Siegel, "THz Imaging Radar for Standoff Personnel Screening," *IEEE Trans. Terahertz Sci. Tech.*, vol. 1, no. 1, pp. 169-182, September 2011.
- [3] Colavita, M.M., M. Shao, and D.H. Staelin, "Atmospheric Phase Measurements with the Mark III Stellar Interferometer," *Appl. Optics*, vol. 26, no. 19, pp. 4106 -4112, October 1987.
- [4] Schaffer, K.K., T.M. Crawford, K.A. Aird, B.A. Benson, L.E. Bleem, J.E. Carlstrom, C.L. Chang, H.M. Cho, A.T. Crites, T. deHaan, M.A. Dobbs, E.M. George, N.W. Halverson, G.P. Holder, W.L. Holzapfel, S. Hoover, J.D. Hrubes, M. Joy, R. Keisler, L. Knox, A.T. Lee, E.M. Leitch, M. Lueker, D. Luong-Van, J.J. McMahon, J. Mehl, S.S. Meyer, J.J. Mohr, T.E. Montroy, S. Padin, T. Plagge, C. Pryke, C.L. Reichardt, J.E. Ruhl, E. Shirokoff, H.G. Spieler, B. Stalder, Z. Staniszewski, A.A. Stark, K. Story, K. Vanderlinde, J.D. Vieira, and R. Williamson, "The First Public Release of South Pole Telescope Data: Maps of a 95 deg² Field From 2008 Observations," *Astroph. J.*, vol. 743:90, pp. 1-18, December 2011.
- [5] A. Wootten and A.R. Thompson, "The Atacama Large Millimeter/Submillimeter Array," *Proc. IEEE.*, vol. 97, Issue 8, pp. 1463-1471. August 2009.
- [6] Gasiewski, A.J., "Electromagnetic Absorption, Propagation and Scattering," ECEN 5264 course notes, University of Colorado, Spring 2011.
- [7] Liebe, H.J., "A Contribution to Modeling Atmospheric Millimeter-wave Properties," *Frequenz*, vol. 41, no 31, 1987.
- [8] Liebe, H. J., "MPM: an atmospheric millimeter wave propagation model," *Int. J. Infrared and Millimeter Waves*, 10, 631-650, 1989.
- [9] Rosenkranz, P. W., "Water vapor microwave continuum absorption: a comparison of measurements and models," *Radio Sci.*, vol. 33, pp. 919-928, 1998.
- [10] Foldy, L.L., "The Multiple Scattering of Waves," *Phys. Rev.*, 67, 107, 1948.
- [11] Tsang, L., J.A. Kong, and R.T. Shin, *Theory of Microwave Remote Sensing*, New York: John Wiley and Sons, 1985.

- [12] Bohren, C.F., and D.R. Huffman, Absorption and Scattering of Light by Small Particles, New York: John Wiley and Sons, 1983.
- [13] Budden, K.G., Radio Waves in the Ionosphere, Cambridge University Press, 1961.
- [14] Kneizys, F. X., Shettle, E. P., Abreu, L. W., Chetwynd, J. H, Anderson, G. P., "Users Guide to LOWTRAN 7," Air Force Geophysics Laboratory, Hanscom AFB, MA, 16 August 1988.
- [15] NICT 2009: see http://act.nict.go.jp/thz/en/3/research3_e.html
- [16] Pickett, H., R. Poynter, E. Cohen, M. Delitsky, J. Pearson, and H.Mueller, "Submillimeter, millimeter, and microwave spectral line catalog," J. Quant. Spectrosc. Radiat. Transfer, vol. 60, pp. 883-890, 1998.
- [17] Rothman L.S., Jacquemart D., Barbe A., Benner D.C., Birk M., Brown L.R., Carleer M.R., Chackerian C., Chance K., Coudert L.H., Dana V., Devi V.M., Flaud J.M., Gamache R.R., Goldman A., Hartmann J.M., Jucks K.W., Maki A.G., Mandin J.Y., Massie S.T., Orphal J., Perrin A., Rinsland C.P., Smith M.A.H., Tennyson J., Tolchenov R.N., Toth R.A., Vander Auwera J., Varanasi P., Wagner G., "The HITRAN 2004 molecular spectroscopic database," J. Quant. Spectroscopy Rad. Transfer, vol. 96, no. 2, pp. 139-204, 2005.
- [18] Liebe, H.J., G.G. Gimmetstad, and J.D. Hopponen, "Atmospheric Oxygen Microwave Spectrum - Experiment versus Theory," IEEE Trans. Ant. Prop., vol. AP-25, pp. 327, 1977.
- [19] Wiltse, J.C. "Near-millimeter waves" Proc. IEEE vol. 73, no. 1, pp. 45-48, 1985.
- [20] Galm, J.M., Merat, F.L. and Claspy, P.C., "Estimates of atmospheric attenuation sensitivity with respect to absolute humidity at 337 GHz," IEEE Trans. Ant. Propagation, vol. 38, no. 7, pp. 982-986, July 1990.
- [21] Sitterle, J.J., P.C. Claspy, and F.L. Merat, "A procedure for calculating the atmospheric mutual coherence function via the statistical Fourier-optical method," IEEE Trans. Ant. Propagation, vol. 37, no. 1, pp. 131-134, Jan. 1989.
- [22] Gasiewski, A.J., "Atmospheric Propagation Loss Measurements in the Spectral Window Near 337 GHz," M.S. dissertation, Case Western Reserve University, Advisor: P.C. Claspy, August, 1983.
- [23] Liebe, H.J., "An Atmospheric Millimeter Wave Propagation Model", NTIA report 83-137, U.S. Dept. of Commerce, 1983.

- [24] Anderson, K.D., "94-GHz Propagation in the Evaporation Duct," vol. 38, no. 5, pp. 746-753, May 1990.
- [25] R. J. Hill, W. P. Schoenfeld, J. P. Riley, J. T. Priestley, S. F. Clifford, S. P. Eckes, R. A. Bohlander, and R. W. McMillan, "Data analysis of the NOAA-GIT millimeter-wave propagation experiment near Flatville, Illinois," NOAA Tech. Rep. ERL 429-WP260, 1985.
- [26] Hill, Reginald J., Bohlander, Ronald A., Clifford, Steven F., McMillan, Robert W., Priestley, Joseph T., and Schoenfeld, W. P., "Turbulence-Induced Millimeter-Wave Scintillation Compared With Micrometeorological Measurements", Trans. Geosci. Remote Sensing, vol. 26, No. 3, pp. 330-342, May 1988.
- [27] Bohlander, Ronald A., McMillan, Robert W., Patterson, E. M., Clifford, Steven F., Hill, Reginald J., Priestley, Joseph T., and Schoenfeld, W. P., "Fluctuations in Millimeter-Wave Signals Propagated Through Inclement Weather", Trans. Geosci. Remote Sensing, vol. 26, No. 3, pp. 343-354, May 1988.
- [28] Churnside, J., and Lataitis, R., "Wander of an Optical Beam in the Turbulent Atmosphere", Applied Optics, vol. 29, Issue 7, pp. 926-930, 1990.
- [29] Rytov, S.M. "Diffraction of Light by Ultrasonic Waves," *Izv. Akad. Nauk SSSR, ser. fiz.* no. 2, p. 223, 1937.
- [30] Manning, R.M., "Stochastic Electromagnetic Wave Propagation in a Dispersing and Absorbing Clear Atmosphere", M.S. Thesis, Case Western Reserve University, Advisor: P.C. Claspy, 1982.
- [31] Wheelon, Albert D., "Electromagnetic Scintillation", Geometrical Optics, Vol. 1, Cambridge, UK: Cambridge University Press (2001).
- [32] Wheelon, Albert D., "Electromagnetic Scintillation", Weak Scattering, Vol. 2, Cambridge, UK: Cambridge University Press (2003).
- [33] Tartarski, V.I., "The Effects of the Turbulent Atmosphere on Wave Propagation", (translated from Russian by the Israel Program for Scientific Translations Ltd., ISBN 0 7065 0680 4), reproduced by National Technical Service, U.S. Department of Commerce, Springfield, Va. 22151, 1971.
- [34] Obukhov, A.M., "Some Specific Features of Atmospheric Turbulence," *J. Geophys. Res.*, vol. 67, no. 8, pp. 3011-3014, July 1962.
- [35] Gasiewski, A.J., "Atmospheric Temperature Sounding and Precipitation Cell Parameter Estimation Using Passive 118 GHz O2 Observations", Ph.D. Thesis, Massachusetts Institute of Technology. Advisor: Professor David H. Staelin, December 1988.

- [36] Gasiewski, A.J. "Numerical Sensitivity Analysis of Passive EHF and SMMW Channels to Tropospheric Water Vapor, Clouds, and Precipitation," *IEEE Trans. Geosci. Remote Sensing*, vol. 30, no. 5, pp. 859-870, September 1992.
- [37] Klein, M., and A.J. Gasiewski, "The Sensitivity of Millimeter and Sub-millimeter Frequencies to Atmospheric Temperature and Water Vapor Variations," *J. Geophys. Res. - Atmospheres*, vol. 13, pp. 17481-17511, July 16, 2000.
- [38] Rosenkranz, P. W. 1993, "Absorption of microwaves by atmospheric gases," Chapter 2 in *Atmospheric Remote Sensing by Microwave Radiometry*, M. A. Janssen (ed). New York: Wiley.
- [39] Gasiewski, A.J., "Microwave Radiative Transfer in Hydrometeors," Chapter 3 in "Atmospheric Remote Sensing by Microwave Radiometry", (M.A. Janssen, ed.), New York: John Wiley and Sons (1993).
- [40] Liljegren, J.C., S.-A. Boukabara, K.C. Pereira, and S.A. Clough, "The Effect of the Half-Width of the 22-GHz Water Vapor Line on Retrievals of Temperature and Water Vapor Profiles With a 12-Channel Microwave Radiometer," *IEEE Trans. Geosci. Remote Sensing*, vol. 43, no. 5, May 2005.
- [41] Clough, S. A., M. W. Shephard, E. J. Mlawer, J. S. Delamere, M. J. Iacono, K. Cady-Pereira, S. Boukabara, and P. D. Brown, "Atmospheric radiative transfer modeling: a summary of the AER codes," Short Communication, *J. Quant. Spectrosc. Radiat. Transfer*, 91, pp. 233-244, 2005.
- [42] Strohbehn, J.W., and S.F. Clifford, "Polarization and Angle of Arrival Fluctuations for a Plane Wave Propagated through a Turbulent Medium," *IEEE Trans Ant. Propagation*, AP-15, pp. 416-421, 1967.
- [43] Rosenkranz, P.W., and D.H. Staelin, "Polarized Thermal Microwave Emission from Oxygen in the Mesosphere," *Radio Sci.*, vol. 23, pp. 721-729, 1988.
- [44] Budden, K.G., Radio Waves in the Ionosphere, Cambridge University Press, 1961.
- [45] GAIM 2009: see <http://iono.jpl.nasa.gov/gaim/intro.html>
- [46] Taylor, G.I., "The Spectrum of Turbulence," *Proc. Royal Soc.*, vol. 164, no. A 919, pp. 476-490, February, 1938.
- [47] Bohlander, R.A., R.W. McMillan, E. M. Patterson, S.F. Clifford, R.J. HILL, J.T. Priestley, and W.P. Schoenfeld, "Fluctuations in Millimeter-Wave Signals Propagated Through Inclement Weather," *IEEE Trans. Geosci. Rem. Sensing*, vol. 26, no. 3, pp. 343-354, May 1988.

- [48] R.J. Hill, R.A., Bohlander, S.F. Clifford, R.W. McMillan, J.T. Priestly, and W.P. Schoenfeld, "Turbulence-Induced Millimeter-Wave Scintillation Compared with Micrometeorological Measurements," *IEEE Trans. Geosci. Rem. Sensing*, vol. 26, no. 3, pp. 330-342, May 1988.
- [49] Van Vleck, J.H., "The Absorption of Microwaves by Uncondensed Water Vapor," *Phys. Rev.*, vol. 7f, no. 7, pp. 425-433, April, 1947.
- [50] Payne, V.H., E.J. Mlawer, K.E. Cady-Pereira, and J.-L. Moncet, "Water Vapor Continuum Absorption in the Microwave," *IEEE Trans. Geosci. Rem. Sensing.*, vol. 49, no. 6, pp. 2194-2208, June 2011.
- [51] Bohlander, Ronald A., McMillan, Robert W., and Gallagher, James J., "Atmospheric Effects on Near-Millimeter-Wave Propagation (Invited Paper)", *Proceedings of the IEEE*, vol. 73, No. 1, pp. 49-60, January 1985.
- [52] A. D. Wheelon, "Skewed Distribution of Irradiance Predicted by the Second-Order Rytov Approximation", *JOSA A* 18 (11), pp. 2789-2798 (2001).
- [53] T. W. Crowe, W. L. Bishop, D. W. Porterfield, J. L. Hesler, and R. M. Weikle, II, "Opening the terahertz window with integrated diode circuits," *IEEE Journal of Solid-State Circuits*, vol. 40, no. 10, pp. 2104, 2005.
- [54] U. R. Pfeiffer, E. Ojefors, A. Lissauskas, and H. G. Roskos, "Opportunities for silicon at mmWave and Terahertz frequencies," in *IEEE Bipolar/BiCMOS Circuits and Technology Meeting*, pp. 149-156, 2008.
- [55] Golio, M., "RF and Microwave Applications and Systems", CRC press, 2008.
- [56] S. Tichkulel and A. Muschinski, "Optical anemometry based on the temporal cross-correlation of Angle-of-arrival fluctuations obtained from spatially separated light sources," *IEEE IGARSS*, pp. 1980-1983, 2012.
- [57] S. Alquaddoomi, and R.A. Scholtz, *IEEE Trans. Inform. Theory*, "On the Nonexistence of Barker Arrays and Related Matters", VOL. 35, NO. 5, September 1989.
- [58] Potvin. G., D. Dion, J. Clavierie, P.A. Frederickson, K.L. Davidson, and J.L. Forand, "An Empirical Analysis of Bulk Cn^2 Models over Water," *J. Appl. Meteor. Climat.*, vol. 47, pp. 3044-3060, December, 2008.
- [59] R. M. Manning, "Theoretical Investigation of Millimeter Wave Propagation Through a Clear Atmosphere", *Proc. SPIE 410, Laser Beam Propagation in the Atmosphere*, J. C. Leader, ed., pp. 119-136 (1983).

- [60] R. M. Manning, "Beam Wave Propagation within the Second Rytov Perturbation Approximation", *Radiophysics and Quantum Electron.* 39 (4), pp. 287-295 (1996).
- [61] Nastrom, G.D., and F.D. Eaton, "The Coupling of Gravity Waves and Turbulence at White Sands, New Mexico, from VHF Radar Observations," *J. Appl. Meteor.*, vol. 32, no. 1, pp. 81-87, 1983.
- [62] R. A. Torrealba, "The design and construction of a long-distance atmospheric propagation test chamber", Calhoun: The NPS Institutional Archive, Naval Postgraduate School, 2015.
- [63] Brussaard, G, and Watson, P.A., "Atmospheric Modelling and Millimeter Wave Propagation", 1995.
- [64] Slinn, W., "Atmospheric aerosol particles in surface-level air," *Atmospheric Environment*, vol. 9, Issue 8, pp. 763-764, 1975.
- [65] Skolnik, M.I., "Introduction to Radar Systems", 3rd edition, 2001.
- [66] S. T. Fiorino, R. J. Bartell, M. J. Krizo, G. L. Caylor, K. P. Moore, T. R. Harris et al, "A first principles atmospheric propagation & characterization tool – the laser environmental effects definition and reference (LEEDR), *SPIE*, 6878 (68780B), 2008.
- [67] S. T. Fiorino, "The laser environmental effects definition and reference (LEEDR) [Online]. Available: <http://www.afit.edu/CDE/page.cfm?page=329&tabname=Tab5A>, 2013.
- [68] Tartarski, V.I., "Wave Propagation in Turbulent Medium, McGraw-Hill, 1961.
- [69] Gasiewski, A.J., University of Colorado at Boulder, ECEN 5264, "Electromagnetic Absorption, Scattering and Propagation", Slides & Book, 2009.
- [70] Kursinski, E. R., Ward, D., Stovern, M., Otarola, A. C., Young, A., Wheelwright, B., ... & Hainsworth, J. (2012). Development and testing of the Active Temperature, Ozone and Moisture Microwave Spectrometer (ATOMMS) cm and mm wavelength occultation instrument. *Atmospheric Measurement Techniques*, 5(2), 439-456.
- [71] Cohen, Jean, Captain USAF, "Demonstration and Verification of a Broad Spectrum Anomalous Dispersion Effects Tool for Index of Refraction and Optical Turbulence Calculations", Air Force Institute of Technology Thesis, WPAFB, Ohio.
- [72] Wang, T., Ochs, G.R., and Clifford, S.F., "A Saturation-Resistant Optical Scintillometer to Measure Cn^2 ".

- [73] A. Ishimaru, "Fluctuations of a Beam Wave Propagating Through a Locally Homogeneous Medium", *Radio Sci.* 4 (4), pp. 295-305 (1969).
- [74] A. Ishimaru, *Wave Propagation and Scattering in Random Media*, Academic Press, New York. Vol. 2, 1978.
- [75] Sasiela, Richard J., "Electromagnetic Wave Propagation in Turbulence: Evaluation and Application of Mellin Transforms (Second Edition)," Bellingham, Washington: The Society of Photo-Optical Instrumentation Engineers (SPIE) Press (2007).
- [76] Lee, Yun-Shik, "Principles of Terahertz Science and Technology," New York: Springer Science+Business Media, LLC (2009).

Appendix A: MATLAB Diffraction Source Code

```

% Compute Fresnel zone link power Diffraction

close all
clear
clc

%Part I: Calculation of on-axis field power ratio for uniform plane wave
illumminating circular aperture od diameter D=2a...
%This calculation provides on-axis power flux density diffracted through a
%circular aperture illuminated by a uniform field. Far zone distances are
%calculated and shown to clearly delineate the transition to 1/R^2 power
%flux loss. In the near zone field diffraction amplitudes up to a factor of
%twice above that of a plane wave are observed, resulting in up to 6 dB
%power flux increases above that of the illuminating uniform plane wave.
%Note: The aperture field is considered uniform, and thus does not consider
%aperture edge currents that modify the UPW aperture fields. These currents
%effectively backscatter the incident field for electrically small
%apertures. A result is that the field decays faster than 1/R^2 for small
%(<lambda/10) apertures in the immediate vicinity of the aperture. This
%effect is not expected to be observed, rather, Rayleigh scattering by the
small hole is
%anticipated.

adz=logspace(-3,2,20000)'; %ratio of aperture radius a to boresite
distance z
D=[1/30,1/10,1/3,1,3,10,30]; %aperture diameter D =
0.033,0.1,1,3,10,30 wavelenghts
ka=2*pi*D/2; %electrical aperture size parameter ka

adz2=adz.*adz;
eta_la_all=[];
eta_la_ii=[];
for kk=1:length(ka)
    eta_la=(1+adz2/2)./sqrt(1+adz2)-cos(ka(kk)*(sqrt(1+1./adz2)-1./adz));
    eta_la=2*eta_la./sqrt(1+adz2);
    eta_la_all=[eta_la_all,eta_la];
    [mm,ii]=min(abs(adz-1/(4/pi*ka(kk))));
    eta_la_ii=[eta_la_ii,eta_la(ii)];
    [ii,eta_la(ii)]
end

figure('NumberTitle','off','Name','Fresnel Zone Power','Color',[1,1,1]);
semilogx(repmat(1./adz,1,length(ka)),eta_la_all); hold on
semilogx(4/pi*ka',eta_la_ii','*');
grid on
xlabel('z/a (-)');
ylabel('\eta_{la}')
title('Fresnel Zone Power: UPW/Circular Aperture (* z_f=2D^2/\lambda)');
legend('D=2a=\lambda/30','D=2a=\lambda/10','D=2a=\lambda/3','D=2a=\lambda','D
=2a=3\lambda','D=2a=10\lambda','D=2a=30\lambda');

```

```

figure('NumberTitle','off','Name','Fresnel Zone Power','Color',[1,1,1]);
semilogx(repmat(1./adz,1,length(ka)),10*log10(eta_la_all)); hold on
semilogx(4/pi*ka,10*log10(eta_la_ii),'*k');
grid on
xlabel('z/a (-)');
ylabel('\eta_{la} (dB)')
title('Fresnel Zone Power: UPW/Circular Aperture (* z_f=2D^2/\lambda)');
legend('D=2a=\lambda/30','D=2a=\lambda/10','D=2a=\lambda/3','D=2a=\lambda','D
=2a=3\lambda','D=2a=10\lambda','D=2a=30\lambda');

%Part I.a: Same calculation as part I for uniform plane wave, except rendered
for a range of
%aperture sizes for aperture-observation point distances R-za.

close all
clear
clc

f=325e9;           %Frequency in Hz (TAIPAS)
%R=1924;           %Path length in m (TAIPAS)
R=0.1;            %Path length in m
c=299792458;      %Speed of light (m/s)
lambda=c/f;       %Wavelength in m
kR=2*pi*R/lambda; %Phase delay along path boresite
Flmax=sqrt(lambda*R)/2; %First Fresnel zone maximum radius (for grid
specification)

tic
%Set rendering parameters...
Nza=4001;          %Number of path aperture locations
Na=4001;          %Number of aperture radius values
Nf=100000;        %Approximate maximum aperture size in
number of full Fresnel zones
%Nf=7;           %Approximate maximum aperture size in
number of full Fresnel zones
zadR=linspace(0,1,Nza)'; %Fractional locations of aperture
along propagation path
%zadR=linspace(0.9985,1,Nza)'; %Fractional locations of aperture
along propagation path
%ellipse_factor=1-zadR; %Fresnel ellipse factor
%ellipse_factor=2*sqrt(zadR.*(1-zadR)); %Fresnel ellipse factor
%ellipse_factor(1:floor(end/2))=1;
%ellipse_factor(end)=ellipse_factor(2)/2; %Arbitrarily add
Fresnel zones to path endpoints
ellipse_factor=ones(size(zadR)); %Fresnel ellipse
factor
adR=ellipse_factor*linspace(0,sqrt(2*Nf),Na)*Flmax/R; %scaled aperture radii
along propagation path
adR2=adR.*adR;
zadR=repmat(zadR,1,Na);
onemzadR=(1-zadR);
onemzadR2=onemzadR.*onemzadR;
sqrtonemzadR2padR2=sqrt(onemzadR2+adR2);

```

```

eta_la_all=onemzadR.*exp(-j*kR*(sqrtonemzadR2padR2-
onemzadR))./sqrtonemzadR2padR2;
eta_la_all=(1-eta_la_all).*conj((1-eta_la_all));
toc

%Render link efficiency data...
h=figure('NumberTitle','off','Color',[1,1,1],'name','Fresnel Zone Link
Efficiency');
pcolor(R*zadR',R*adR',eta_la_all');
shading interp
axis('square','xy');
%axis('image');
caxis([0,4]);
xlabel('Path Distance z_a (m)');
ylabel('Aperture Radius a (m)');
title(['Fresnel Zone Link Efficiency \eta_l: UPW/CA at f=',num2str(f/1e9),'
GHz and R=',num2str(R/1000),' km']);
colormap(jet);
hc=colorbar;

%Render link efficiency data...
h=figure('NumberTitle','off','Color',[1,1,1],'name','Fresnel Zone Link
Efficiency');
pcolor(zadR',adR',eta_la_all');
shading interp
axis('square','xy');
%axis('image');
caxis([0,4]);
xlabel('Relative Path Distance z_a/R (-)');
ylabel('Normalized Aperture Radius a/R (-)');
title(['Fresnel Zone Link Efficiency \eta_l: UPW/CA for
\lambda=',num2str(lambda*1000,'%0.3f'),' mm and
R/\lambda=',num2str(R/lambda,'%8.3e')]);
colormap(jet);
hc=colorbar;

%Part II: Calculation of on-axis field power ratio for spherical wave
illumminating circular path aperture of radius a...
%This calculation provides link efficiency relative to free-space Friis
formula for received power.
%Note: Specific link parameters are solely to determine proper rendering
%grid range and resolution. The expression for relative link efficiency is
%dependent only on the following parameters:
% kR = path boresite phase delay (radians)
% a/R = scaled aperture radius (dimensionless)
% za/R = along-path fractional aperture location (dimensionless)
%Note that in this example where the beam cross-sectional area is not
%included in the calculation the amplitude factor does not diminish the
%efficiency oscillations until enough Fresnel zones are included to warrant
%geometric amplitude decay. Depending on the first Fresnel zone radius for
%the path this can be a very large number, and this produce extreme numbers
%of oscillations on MMW paths.

close all

```

```

clear
clc

f=325e9;           %Frequency in Hz (TAIPAS)
R=1924;           %Path length in m (TAIPAS)
c=299792458;      %Speed of light (m/s)
lambda=c/f;       %Wavelength in m
kR=2*pi*R/lambda; %Phase delay along path boresite
Flmax=sqrt(lambda*R)/2; %First Fresnel zone maximum radius (for grid
specification)

tic
%Rendering parameters...
Nza=4001;           %Number of path aperture locations
Na=4001;           %Number of aperture radius values
Nf=500;           %Approximate maximum aperture size in
number of full Fresnel zones
zadR=linspace(0,1,Nza)'; %Fractional locations of aperture
along propagation path
ellipse_factor=2*sqrt(zadR.*(1-zadR)); %Fresnel ellipse factor
ellipse_factor([1,end])=ellipse_factor(2)/2; %Arbitrarily add
Fresnel zones to path endpoints
adR=ellipse_factor*linspace(0,sqrt(2*Nf),Na)*Flmax/R; %scaled aperture radii
along propagation path
adR2=adR.*adR;
zadR=repmat(zadR,1,Na);
zadR2=zadR.*zadR;
onemzadR2=(1-zadR).*(1-zadR);

eta_ls_all=sqrt(onemzadR2+adR2).*(sqrt(onemzadR2+adR2)+sqrt(zadR2+adR2));
eta_ls_all=(1-zadR)./eta_ls_all;
eta_ls_all=eta_ls_all.*exp(-j*kR*(sqrt(onemzadR2+adR2)+sqrt(zadR2+adR2)-1));
eta_ls_all=(1-eta_ls_all).*conj((1-eta_ls_all));
toc

%Render link efficiency data...
h=figure('NumberTitle','off','Color',[1,1,1],'name','Fresnel Zone Link
Efficiency');
pcolor(R*zadR',R*adR',eta_ls_all');
shading interp
axis('square','xy');
%axis('image');
caxis([0,4]);
xlabel('Path Distance z_a (m)');
ylabel('Aperture Radius a (m)')
title(['Fresnel Zone Link Efficiency \eta_l: SW/CA at f=',num2str(f/1e9),'
GHz and R=',num2str(R/1000),' km']);
colormap(jet);
hc=colorbar;

%Render link efficiency data...
h=figure('NumberTitle','off','Color',[1,1,1],'name','Fresnel Zone Link
Efficiency');
pcolor(zadR',adR',eta_ls_all');

```

```

shading interp
axis('square','xy');
%axis('image');
caxis([0,4]);
xlabel('Relative Path Distance z_a/R (-)');
ylabel('Normalized Aperture Radius a/R (-)')
title(['Fresnel Zone Link Efficiency \eta_1: SW/CA for
\lambda=',num2str(lambda*1000,'%0.3f'),' mm and
R/\lambda=',num2str(R/lambda,'%8.3e')]);
colormap(jet);
hc=colorbar;

% %Part III: Calculation of on-axis field power ratio for Gaussian
transmitter beam wave illuminating a circular path aperture of radius a.
% %The Gaussian beam is specified by the aperture phase radius of curvature
and waist
% %radius, and thus this case serves to illustrate effects of focussed
Gaussian
% %transmitter beam and circular aperture stop on the on-axis field at the
receiver.
% %This calculation provides link efficiency relative to free-space Friis
formula for received power.
% %Note: Specific link parameters are solely to determine proper rendering
% %grid range and resolution. The expression for relative link efficiency is
% %dependent only on the following parameters:
% % kR = path boresite phase delay (radians)
% % a/R = scaled aperture radius (dimensionless)
% % za/R = along-path fractional aperture location (dimensionless)
% % Wo/lambda = Transverse beam waist radius in wavelengths at aperture
(dimensionless)
% % Ro/R = Phase radius of curvature in aperture (dimensionless)
% %Note: The integrals in this part (Part III) did not converge well!!!
%
% f=325e9; %Frequency in Hz (TAIPAS)
% R=1924; %Path length in m (TAIPAS)
% c=299792458; %Speed of light (m/s)
% lambda=c/f; %Wavelength in m
% k=2*pi/lambda; %Wavenumber in m-1
% kR=k*R; %Phase delay along path boresite
% Flmax=sqrt(lambda*R)/2; %First Fresnel zone maximum radius (for grid
specification)
% ao=0.05; %TAIPAS near-equivalent beam parameters
% Wo=0.6435*ao; %Wylde (1984) GB approximation of corrugated horn of
aperture radus a
% Ro=inf;
%
% %Set rendering parameters...
% incl_int=3; %Testing switch to include/exclude
complex integral (option 3 is preferred based on accuracy studies of
integration)
% Nza=4001; %Number of path aperture locations
% Na=4001; %Number of aperture radius values
% Nf=500; %Approximate maximum aperture size
in number of full Fresnel zones

```

```

% Nppw=200; %Number of panels per wavelength for
radial aperture integration in variable t
% zadR=linspace(0,1,Nza)'; %Fractional locations of aperture
along propagation path
% ellipse_factor=2*sqrt(zadR.*(1-zadR)); %Fresnel ellipse factor
% ellipse_factor([1,end])=ellipse_factor(2)/2; %Arbitrarily add
Fresnel zones to path endpoints
% adR=ellipse_factor*linspace(0,sqrt(2*Nf),Na)*Flmax/R; %Scaled aperture
radii along propagation path
% adR2=adR.*adR;
% Ap=1./((1+R*zadR/Ro).^2 + 4*((R*zadR).^2)/((Wo^4)*(k^2)));
% App=(2*R*zadR/((Wo^4)*k) + (k/(2*Ro))*(1+R*zadR/Ro)).*Ap;
% Ap=Ap/(Wo^2);
% Ap=repmat(Ap,1,Na);
% App=repmat(App,1,Na);
% zadR=repmat(zadR,1,Na);
% onemzadR=(1-zadR);
% onemzadR2=onemzadR.*onemzadR;
% R2=R*R;
% k2=k*k;
% kR2=kR*kR;
% alpha=(1/(Wo*Wo))+j*(k/(2*Ro));
%
% switch incl_int
% case 0 %Neglecting complex integral on page 16 of notes...
% fprintf('Excluding integral from efficiency solution on page 16 of
notes...\n');
% eta_bl_all=onemzadR.*(1+(2*kR/(k*k))*App.*onemzadR);
%
eta_bl_all=eta_bl_all./(sqrt(onemzadR2+adR2).*(1+(2*kR/(k*k))*App.*sqrt(onemz
adR2+adR2)));
% eta_bl_all=eta_bl_all.*exp(-((R*R)*(adR.^2)).*Ap);
% eta_bl_all=eta_bl_all.*exp(-j*kR*(sqrt(onemzadR2+adR2)-
onemzadR+App.*((R*R)*(adR.^2))/kR));
%
% case 1 %Complicated integral, from page 16 of notes, questionable
accuracy...
% fprintf('Including integral from page 16 of notes...\n');
% eta_bl_all=onemzadR.*(1+(2*kR/(k*k))*App.*onemzadR);
%
eta_bl_all=eta_bl_all./(sqrt(onemzadR2+adR2).*(1+(2*kR/(k*k))*App.*sqrt(onemz
adR2+adR2)));
% eta_bl_all=eta_bl_all.*exp(-((R*R)*(adR.^2)).*Ap);
% eta_bl_all=eta_bl_all.*exp(-j*kR*(sqrt(onemzadR2+adR2)-
onemzadR+App.*((R*R)*(adR.^2))/kR));
% int=zeros(size(adR));
% for zz=1:Nza
% fprintf('za/R distance = %0.5f \n',zadR(zz,1));
% llim=kR*onemzadR(zz,1);
% twoAppdk2=2*App(zz,1)/(k*k);
% ApdApp=Ap(zz,1)/App(zz,1);
% R2onemzadR2=R2*onemzadR2(zz,1);
% k2d2App=k2/(2*App(zz,1));
% k2d4App2=k2/(4*(App(zz,1)*App(zz,1)));
% for aa=2:Na

```

```

%
ulim=kR*(sqrt(onemzadR2(zz,1)+adR(zz,aa))+(R/k)*App(zz,1)*(adR(zz,aa)^2));
%
    Npanels=ceil(Nppw*(ulim-llim)/(2*pi));
%
    deltat=(ulim-llim)/Npanels;
%
    %Trapezoidal rule: Sum over 1+Npanels t point evaluations,
add only half at endpoints...
%
    tgrid=linspace(llim,ulim,Npanels+1);
%
    root1=k*sqrt(tgrid/App(zz,1) + k2d4App2 + R2onemzadR2);
%
    term1=tgrid + k2d2App - root1;
%
    term2=k*sqrt(R2onemzadR2 + term1/App(zz,1));
%
    term3=1 + twoAppdk2*term2;
%
    intgrid=exp(-j*tgrid).*exp(-ApdApp*term1);
%
    intgrid=intgrid./(term3.^2);
%
    intgrid=intgrid.*((twoAppdk2 - 1./root1)./term2 -
ApdApp*term3./root1);
%
    int(zz,aa)=int(zz,aa-1) +
(deltat*kR*onemzadR(zz,1))*(intgrid(1)/2+sum(intgrid(2:end-
1))+intgrid(end)/2);
%
    llim=ulim;
%
    end
%
end
%
eta_bl_all=eta_bl_all-int;
%
%
%
case 2 %Neglecting complex integral on page 11 of notes...
%
fprintf('Excluding integral from efficiency solution on page 11 of
notes...\n');
%
term1=-1./((k2/alpha)-j*(2*zadR*kR));
%
eta_bl_all=onemzadR./sqrt(onemzadR2+adR2);
%
eta_bl_all=eta_bl_all.*exp(kR2*(adR.^2).*term1);
%
eta_bl_all=eta_bl_all.*exp(-j*kR*(sqrt(onemzadR2+adR2)-onemzadR));
%
%
case 3 %Easier integral, from page 11 of notes, seemingly accurate...
%
fprintf('Including integral from page 11 of notes...\n');
%
term1=-1./((k2/alpha)-j*(2*zadR*kR));
%
eta_bl_all=onemzadR./sqrt(onemzadR2+adR2);
%
eta_bl_all=eta_bl_all.*exp(kR2*(adR.^2).*term1);
%
eta_bl_all=eta_bl_all.*exp(-j*kR*(sqrt(onemzadR2+adR2)-onemzadR));
%
int=zeros(size(adR));
%
for zz=1:Nza
%
    fprintf('za/R distance = %0.5f \n',zadR(zz,1));
%
    llim=kR*onemzadR(zz,1);
%
    for aa=2:Na
%
        ulim=kR*sqrt(onemzadR2(zz,1)+adR(zz,aa));
%
        Npanels=ceil(Nppw*(ulim-llim)/(2*pi));
%
        deltat=(ulim-llim)/Npanels;
%
        %Trapezoidal rule: Sum over 1+Npanels t point evaluations,
add only half at endpoints...
%
        tgrid=linspace(llim,ulim,Npanels+1);
%
        intgrid=exp(-j*tgrid).*exp(term1(zz)*(tgrid.^2));
%
        int(zz,aa)=int(zz,aa-1) +
deltat*(intgrid(1)/2+sum(intgrid(2:end-1))+intgrid(end)/2);
%
        llim=ulim;
%
    end
%
end

```

```

%
int (zz, :) = int (zz, :) * 2 * kR * onemzadR (zz, 1) * term1 (zz) * exp (kR2 * onemzadR2 (zz, 1) * term1 (zz) + j * kR * onemzadR (zz, 1));
%           end
%           eta_bl_all = eta_bl_all - int;
%
% end
% eta_bl_all = (1 - eta_bl_all) .* conj ((1 - eta_bl_all));

```

```

%Part IV: Calculation of on-axis field power ratio for Gaussian transmitter
beam wave illuminating a circular path aperture of radius a
%and received by a Gaussian-beam receiver. This problem has a very simple
%and elegant closed form expression for the link efficiency etl_1.
%The Gaussian beams are specified by the aperture phase radii of curvature
and waist

```

```

%radii at the transmitter and receiver (respectively), and thus serve to
illustrate effects of focussed Gaussian
%transmitter and receiver beams and a circular aperture stop on the received
signal amplitude.

```

```

%This calculation provides link efficiency relative to the free-space Friis
formula for received Gaussian beam power.

```

```

%Note: Specific link parameters are solely to determine proper rendering
%grid range and resolution. The expression for relative link efficiency is
%dependent only on the following parameters:

```

```

% kR   = path boresite phase delay (radians)
% a/R  = scaled aperture radius (dimensionless)
% za/R = along-path fractional aperture location (dimensionless)
% Wot/lambda = Transverse beam waist radius in wavelengths at transmitter
aperture (dimensionless)
% Wor/lambda = Transverse beam waist radius in wavelengths at receiver
aperture (dimensionless)
% Rot/R = Phase radius of curvature in transmitter aperture (dimensionless)
% Ror/R = Phase radius of curvature in receiver aperture (dimensionless)

```

```

close all
clear
clc

```

```

f=325e9;           %Frequency in Hz (TAIPAS)
R=1924;           %Path length in m (TAIPAS)
c=299792458;      %Speed of light (m/s)
lambda=c/f;       %Wavelength in m
k=2*pi/lambda;    %Wavenumber in m-1
kR=k*R;           %Phase delay along path boresite
Flmax=sqrt(lambda*R)/2; %First Fresnel zone maximum radius (for grid
specification)
aot=0.05;         %TAIPAS near-equivalent beam parameters
aor=0.05;         %Case with TAPIAS receiver aperture same diameter as
transmitter aperture
%aor=0.01;        %Case with TAIPAS receiver aperture stopped down by 5x to
2 cm diameter
Wot=0.6435*aot;   %Wylde (1984) GB approximation of corrugated horn of
aperture radius a

```

```

Wor=0.6435*aor;
Rot=inf;
Ror=inf;
deta=[0.01,0.0001,0.000001];           %Power variation thresholds due to CA
blockage (e.g., -20,-40,-60 dB down fluctuations)
%TAIPAS physical path parameters:
PathR=[0,100,200,300,400,500,600,700,800,900,1000,1100,1200,1300,1400,1500,16
00,1700,1800,1900,1920];
PathH=[3.0,8.1,10.2,12.3,33.4,21.5,43.6,49.7,39.8,39.8,58.9,50.0,54.1,53.2,56
.3,68.4,65.5,47.6,36.7,29.8,2.0];

tic
%Set rendering parameters...
Nza=4001;                               %Number of path aperture locations
Na=8001;                                 %Number of aperture radius values
Nf=500;                                  %Approximate maximum aperture size in
number of full Fresnel zones
zadR=linspace(0,1,Nza)';                %Fractional locations of aperture
along propagation path
ellipse_factor=2*sqrt(zadR.*(1-zadR)); %Fresnel ellipse factor
ellipse_factor([1,end])=ellipse_factor(2)/2; %Arbitrarily add
Fresnel zones to path endpoints
adR=ellipse_factor*linspace(0,sqrt(2*Nf),Na)*Flmax/R; %Scaled aperture radii
along propagation path
za=R*zadR;
alphan=(1/(Wot*Wot))+j*(k/(2*Rot));
alphan=(1/(Wor*Wor))+j*(k/(2*Ror));
A=(1./(1/alphan-j*2*za/k)) + (1./(1/alphan-j*2*(R-za)/k));
amin=(1./sqrt(real(A)))*sqrt(-log(sqrt(1+deta)-1));
A=repmat(A,1,Na);
deltaeta=exp(-(R*R)*(real(A).*adR.*adR));
deltaeta=2*deltaeta+deltaeta.*deltaeta;
eta_btrl_all=exp(-(R*R)*(A.*adR.*adR));
V_nb=1-eta_btrl_all;
eta_btrl_all=(1-eta_btrl_all).*conj((1-eta_btrl_all));
toc

%Render link efficiency data...
h=figure('NumberTitle','off','Color',[1,1,1],'name','Fresnel Zone Link
Efficiency');
pcolor(R*zadR',R*adR',eta_btrl_all');
shading interp
axis('square','xy');
caxis([0,4]);
xlabel('Path Distance z_a (m)');
ylabel('Aperture Radius a (m)');
title(['Fresnel Zone Link Efficiency \eta_1: GBTR/CA at f=',num2str(f/1e9),'
GHz, R=',num2str(R/1000),' km,
W_o=[' ,num2str(Wot*100),' ',' ,num2str(Wor*100),' ] cm, R_o=[\infty,\infty]']);
colormap(jet(256));
hc=colorbar;

h=figure('NumberTitle','off','Color',[1,1,1],'name','Fresnel Zone Link
Efficiency');

```

```

pcolor(R*zadR',R*adR',10*log10(eta_btrl_all)');
shading interp
axis('square','xy');
caxis([-20,6]);
xlabel('Path Distance z_a (m)');
ylabel('Aperture Radius a (m)')
title(['Fresnel Zone Link Efficiency \eta_1 (dB): GBTR/CA at
f=',num2str(f/1e9),' GHz, R=',num2str(R/1000),' km,
W_o=[' ,num2str(Wot*100),' ',' ',num2str(Wor*100),' ' ] cm, R_o=[\infty,\infty]']);
colormap(jet(256));
hc=colorbar;

%Render link efficiency deviation data to illustrate impact of circular
clearance aperture...
h=figure('NumberTitle','off','Color',[1,1,1],'name','Fresnel Zone Link
Efficiency');
pcolor(R*zadR',R*adR',10*log10(abs(eta_btrl_all-1))');
shading interp
axis('square','xy');
caxis([-30,5]);
xlabel('Path Distance z_a (m)');
ylabel('Aperture Radius a (m)')
title(['Fresnel Zone Link Efficiency \delta\eta_1 (dB): GBTR/CA at
f=',num2str(f/1e9),' GHz, R=',num2str(R/1000),' km,
W_o=[' ,num2str(Wot*100),' ',' ',num2str(Wor*100),' ' ] cm, R_o=[\infty,\infty]']);
colormap(jet(256));
hc=colorbar;

%Render link efficiency maximum deviation data to illustrate impact of
circular clearance aperture...
h=figure('NumberTitle','off','Color',[1,1,1],'name','Fresnel Zone Link
Efficiency');
pcolor(R*zadR',R*adR',10*log10(deltaeta)');
shading interp
axis('square','xy');
caxis([-30,5]);
xlabel('Path Distance z_a (m)');
ylabel('Aperture Radius a (m)')
title(['Fresnel Zone Link Efficiency \delta\eta_1 (dB): GBTR/CA at
f=',num2str(f/1e9),' GHz, R=',num2str(R/1000),' km,
W_o=[' ,num2str(Wot*100),' ',' ',num2str(Wor*100),' ' ] cm, R_o=[\infty,\infty]']);
colormap(jet(256));
hc=colorbar;

%Render normalized link efficiency data...
h=figure('NumberTitle','off','Color',[1,1,1],'name','Fresnel Zone Link
Efficiency');
pcolor(zadR',adR',eta_btrl_all');
shading interp
axis('square','xy');
caxis([0,4]);
xlabel('Relative Path Distance z_a/R (-)');
ylabel('Normalized Aperture Radius a/R (-)')

```

```

title(['Fresnel Zone Link Efficiency \eta_1: GBTR/CA at f=',num2str(f/1e9), '
GHz, R=',num2str(R/1000), ' km,
W_o=[' ,num2str(Wot*100), ', ', num2str(Wor*100), ', ] cm, R_o=[\infty,\infty]']);
colormap(jet(256));
hc=colorbar;

%Render link clearance data...
h=figure('NumberTitle','off','Color',[1,1,1],'name','Fresnel Zone Link
Efficiency');
plot(R*zadR,amin(:,1),'b',R*zadR,amin(:,2),'m',R*zadR,amin(:,3),'g',PathR,Pat
hH,'o-r');
grid on
xlabel('Path Distance z_a (m)');
ylabel('Clearance Radius (m)');
title(['Fresnel Zone Link Clearance: GBTR/CA at f=',num2str(f/1e9), ' GHz,
R=',num2str(R/1000), ' km, W_o=[' ,num2str(Wot*100), ', ', num2str(Wor*100), ', ] cm,
R_o=[\infty,\infty]']);
legend('\delta\eta_1<1% (-20 dB)', '\delta\eta_1<0.01% (-40
dB)', '\delta\eta_1<0.0001% (-60 dB)', 'Estimated Path Clearance');

%Render complex normalized voltage data for key z_a planes...
h=figure('NumberTitle','off','Color',[1,1,1],'name','Communications Link
Efficiency');
plot(real(V_nb(ceil(end/2),:)),imag(V_nb(ceil(end/2),:)), 'b',real(V_nb(ceil(0
.1*end/2),:)),imag(V_nb(ceil(0.1*end/2),:)), 'r',real(V_nb(ceil(0.01*end/2),:))
),imag(V_nb(ceil(0.01*end/2),:)), 'g');
grid on
axis('equal','xy');
xlabel('Re{V_n}');
ylabel('Im{V_n}');
legend('z_a=R/2','z_a=R/20','z_a=R/200');
title(['Communications Link Efficiency V_n=V/V_{max} for a=[0..\infty]:
GBTR/CA at f=',num2str(f/1e9), ' GHz, R=',num2str(R/1000), ' km,
W_o=[' ,num2str(Wot*100), ', ', num2str(Wor*100), ', ] cm, R_o=[\infty,\infty]']);

%Part V: Calculation of on-axis field power ratio for truncated power-law
transmitter beam wave illuminating a circular path aperture of radius a
%and received by a truncated power-law receiving aperture.
%The transmitter and receiver beams are specified by the aperture phase
%radii of curvature, power law decay parameter, and truncation radius. The
%calculation serves to illustrate effects of a realistic transmitter and
receiver antenna pair and a circular aperture stop on the
%received signal amplitude.
%This calculation provides link efficiency relative to the free-space Friis
formula for received T-R power.
%Note: Specific link parameters are solely to determine proper rendering
%grid range and resolution. The expression for relative link efficiency is
%dependent only on the following parameters:
% kR = path boresite phase delay (radians)
% a/R = scaled aperture radius (dimensionless)
% za/R = along-path fractional aperture location (dimensionless)

```

```

%Transmitter and receiver antenna parameters

close all
clear
clc

f=325e9;           %Frequency in Hz (TAIPAS)
R=1924;           %Path length in m (TAIPAS)
c=299792458;      %Speed of light (m/s)
lambda=c/f;       %Wavelength in m
k=2*pi/lambda;    %Wavenumber in m-1
kR=k*R;           %Phase delay along path boresite
Flmax=sqrt(lambda*R)/2; %First Fresnel zone maximum radius (for grid
specification)
%Assumed aperture lens antenna field distributions:
% E_x(rho,theta,z=0)=E_o(1-(rho/rhoo)^2)^P for rho<ao
%for each transmitter and receiver
rhoot=0.05;       %TAIPAS near-equivalent aperture lens antenna parameters
rhoor=0.05;       %Case with TAPIAS receiver aperture same diameter as
transmitter aperture
Rot=inf;          %Focused lens phase correction (not used due to
introduction of quadratic phase term in T/R aperture integrals).
Ror=inf;
Pt=1;             %Quadratic field taper within aperture
(HPBW=1.27*lambda/D)
Pr=1;
deta=[0.01,0.0001,0.000001]; %Power variation thresholds due to CA
blockage (e.g., -20,-40,-60 dB down fluctuations)
%TAIPAS physical path parameters:
PathR=[0,100,200,300,400,500,600,700,800,900,1000,1100,1200,1300,1400,1500,16
00,1700,1800,1900,1920];
PathH=[3.0,8.1,10.2,12.3,33.4,21.5,43.6,49.7,39.8,39.8,58.9,50.0,54.1,53.2,56
.3,68.4,65.5,47.6,36.7,29.8,2.0];

tic
%Set rendering parameters...
Nza=4001;         %Number of path aperture locations
Na=8001;         %Number of aperture radius values
Nf=500;          %Approximate maximum aperture size in
number of full Fresnel zones
Nppw=200;        %Number of panels per wavelength for
radial aperture integration in variable rho
%Nza=1001;       %Number of path aperture locations
%Na=2001;        %Number of aperture radius values
%Nf=500;         %Approximate maximum aperture size in
number of full Fresnel zones
%Nppw=100;       %Number of panels per wavelength for
radial aperture integration in variable rho
Rft=2*(2*rhoot*rhoot)/lambda; %Far zone distance from transmitter
and receiver, respectively
Rfr=2*(2*rhoor*rhoor)/lambda;
if (Rft+Rfr)<R
    fprintf('Integrating per page 6 of notes...\n');

```

```

    zadR=linspace (Rft/R,1-Rfr/R,Nza)';      %Fractional locations of aperture
along propagation path
    ellipse_factor=2*sqrt (zadR.*(1-zadR)); %Fresnel ellipse factor
    ellipse_factor(1)=ellipse_factor(2)/2;   %Arbitrarily add Fresnel
zones to path endpoints
    ellipse_factor(end)=ellipse_factor(end-1)/2; %Arbitrarily add Fresnel
zones to path endpoints
    adR=ellipse_factor*linspace(0,sqrt(2*Nf),Na)*Flmax/R; %Scaled aperture
radii along propagation path
    V_nJ1=zeros(size(adR));
    for zz=1:Nza
        fprintf('za/R distance = %0.7f \n',zadR(zz,1));
        llim=0;
        for aa=2:Na
            %Trapezoidal rule: Sum over 1+Npanels evaluations, add only half
at endpoints...
            ulim=R*adR(zz,aa);
            za=R*zadR(zz);
            Rmza=R-za;
            Npanels=ceil(Nppw*(ulim-llim)/lambda);
            deltarhodza=(ulim-llim)/Npanels/za;
            rhogrid=linspace(llim,ulim,Npanels+1);
            if aa==2, rhogrid(1)=2*eps; end
            rhodza=rhogrid/za;
            rhodza2=rhodza.*rhodza;
            sqrtoneprhodza2=sqrt(1+rhodza2);
            rhodRmza=rhogrid/Rmza;
            rhodRmza2=rhodRmza.*rhodRmza;
            sqrtoneprhodRmza2=sqrt(1+rhodRmza2);

            integrand=(1+1./sqrtoneprhodza2).*(1+1./sqrtoneprhodRmza2).*exp((-
j*k*za)*sqrtoneprhodza2+(-j*k*Rmza)*sqrtoneprhodRmza2);

            integrand=((integrand./sqrtoneprhodza2)./sqrtoneprhodRmza2).*rhodza;
            bjargza=(k*rhoot)*rhodza./sqrtoneprhodza2;
            bjargRmza=(k*rhoor)*rhodRmza./sqrtoneprhodRmza2;
            integrand=integrand.*besselj(Pt+1,bjargza)./(bjargza.^(Pt+1));

            integrand=integrand.*besselj(Pr+1,bjargRmza)./(bjargRmza.^(Pr+1));
            V_nJ1(zz,aa)=V_nJ1(zz,aa-1) +
deltarhodza*(integrand(1)/2+sum(integrand(2:end-1))+integrand(end)/2);
            llim=ulim;
        end
        V_nJ1(zz,:)=V_nJ1(zz,:)/V_nJ1(zz,end);
    end
    eta_J1_all=V_nJ1.*conj(V_nJ1);
    toc
else
    fprintf('Parameter error: Transmitter plus/or receiver far zone distances
Rft=%0.4f m or Rfr=%0.4f m exceeds total path length R=%0.4f
km.\n',Rft,Rfr,R/1000);
    fprintf('Fresnel link efficiencies inapplicable for close-coupled T/R
antennas.\n');
end

```

```

%Render link efficiency data...
h=figure('NumberTitle','off','Color',[1,1,1],'name','Fresnel Zone Link
Efficiency');
pcolor(R*zadR',R*adR',eta_J1_all');
shading interp
axis('square','xy');
v=axis; axis([0,R,v(3),v(4)]);
caxis([0,4]);
xlabel('Path Distance z_a (m)');
ylabel('Aperture Radius a (m)');
title(['Fresnel Zone Link Efficiency \eta_l: CAQTTR/CA at
f=',num2str(f/1e9),' GHz, R=',num2str(R/1000),' km,
a_o=[' ,num2str(rhoot*100),' ,',num2str(rhoor*100),' ] cm,
R_o=[\infty,\infty]']);
colormap(jet(256));
hc=colorbar;

%Render link efficiency data...
h=figure('NumberTitle','off','Color',[1,1,1],'name','Fresnel Zone Link
Efficiency');
pcolor(R*zadR',R*adR',10*log10(eta_J1_all)');
shading interp
axis('square','xy');
v=axis; axis([0,R,v(3),v(4)]);
caxis([-20,6]);
xlabel('Path Distance z_a (m)');
ylabel('Aperture Radius a (m)');
title(['Fresnel Zone Link Efficiency \eta_l (dB): CAQTTR/CA at
f=',num2str(f/1e9),' GHz, R=',num2str(R/1000),' km,
a_o=[' ,num2str(rhoot*100),' ,',num2str(rhoor*100),' ] cm,
R_o=[\infty,\infty]']);
colormap(jet(256));
hc=colorbar;

%Render link efficiency deviation data to illustrate impact of circular
clearance aperture...
deltaeta=eta_J1_all-1;
h=figure('NumberTitle','off','Color',[1,1,1],'name','Fresnel Zone Link
Efficiency');
pcolor(R*zadR',R*adR',10*log10(abs(deltaeta))');
shading interp
axis('square','xy');
v=axis; axis([0,R,v(3),v(4)]);
caxis([-30,5]);
xlabel('Path Distance z_a (m)');
ylabel('Aperture Radius a (m)');
title(['Fresnel Zone Link Efficiency \delta\eta_l (dB): CAQTTR/CA at
f=',num2str(f/1e9),' GHz, R=',num2str(R/1000),' km,
a_o=[' ,num2str(rhoot*100),' ,',num2str(rhoor*100),' ] cm,
R_o=[\infty,\infty]']);
colormap(jet(256));
hc=colorbar;

%Render normalized link efficiency data...

```

```

h=figure('NumberTitle','off','Color',[1,1,1],'name','Fresnel Zone Link
Efficiency');
pcolor(zadR',adR',eta_J1_all');
shading interp
axis('square','xy');
v=axis; axis([0,1,v(3),v(4)]);
caxis([0,4]);
xlabel('Relative Path Distance z_a/R (-)');
ylabel('Normalized Aperture Radius a/R (-)')
title(['Fresnel Zone Link Efficiency \eta_l: CAQTTR/CA at
f=',num2str(f/1e9),' GHz, R=',num2str(R/1000),' km,
a_o=['',num2str(rhoot*100),' ','',num2str(rhoor*100),' ']' cm,
R_o=[\infty,\infty]']);
colormap(jet(256));
hc=colorbar;

%Render complex normalized voltage data for key z_a planes...
h=figure('NumberTitle','off','Color',[1,1,1],'name','Communications Link
Efficiency');
plot(real(V_nJ1(ceil(end/2),:)),imag(V_nJ1(ceil(end/2),:)), 'b',real(V_nJ1(cei
l(0.1*end/2),:)),imag(V_nJ1(ceil(0.1*end/2),:)), 'r',real(V_nJ1(ceil(0.01*end/
2),:)),imag(V_nJ1(ceil(0.01*end/2),:)), 'g');
grid on
axis('equal','xy');
xlabel('Re{V_n}');
ylabel('Im{V_n}');
legend('z_a=R/2','z_a=R/20','z_a=R/200');
title(['Communications Link Efficiency V_n=V/V_{max} for a=[0..\infty]:
CAQTTR/CA at f=',num2str(f/1e9),' GHz, R=',num2str(R/1000),' km,
a_o=['',num2str(rhoot*100),' ','',num2str(rhoor*100),' ']' cm,
R_o=[\infty,\infty]']);

%Note: Need to re-run above case for Na=8001 points, re-print figures (AJG
022417)

%Part V.a: Calculation of on-axis field power ratio for truncated power-law
transmitter beam wave illuminating a circular path aperture of radius a
%and received by a truncated power-law receiving aperture where the path
%length is long and only the end of the path through the bulk of the
%troposphere is relevant.
%The transmitter and receiver beams are specified by the aperture phase
%radii of curvature, power law decay parameter, and truncation radius. The
%calculation serves to illustrate effects of a realistic space-to-earth
transmitter and receiver antenna pair and a circular aperture stop on the
%received signal amplitude.
%This calculation provides link efficiency relative to the free-space Friis
formula for received T-R power.
%Note: Specific link parameters are solely to determine proper rendering
%grid range and resolution. The expression for relative link efficiency is
%dependent only on the following parameters:
% kR = path boresite phase delay (radians)
% a/R = scaled aperture radius (dimensionless)
% za/R = along-path fractional aperture location (dimensionless)

```

```

%Transmitter and receiver antenna parameters

close all
clear
clc

f=73.5e9;           %Frequency in Hz (VW-band communications study, downlink
frequency)
R=35786e3;         %Path length in m (VW-band communications study,
geostationary transmitter)
Ha=20e3;           %Height of attenuating portion of atmosphere in m
c=299792458;       %Speed of light (m/s)
lambda=c/f;        %Wavelength in m
k=2*pi/lambda;     %Wavenumber in m-1
kR=k*R;            %Phase delay along path boresite
Flmax=sqrt(lambda*R)/2; %First Fresnel zone maximum radius (for grid
specification)
%Assumed aperture lens antenna field distributions:
% E_x(rho,theta,z=0)=E_o(1-(rho/rhoo)^2)^P for rho<ao
%for each transmitter and receiver
rhoot=0.15;        %VW band communications study transmitter aperture antenna
parameters
rhoor=0.60;        %VW band communications study receiver aperture antenna
parameters
Rot=inf;           %Focused lens phase correction (not used due to
introduction of quadratic phase term in T/R aperture integrals).
Ror=inf;
Pt=1;              %Quadratic field taper within aperture
(HPBW=1.27*lambda/D)
Pr=1;
deta=[0.01,0.0001,0.000001]; %Power variation thresholds due to CA
blockage (e.g., -20,-40,-60 dB down fluctuations)

tic
%Set rendering parameters...
Nza=4001;          %Number of path aperture locations
Na=8001;           %Number of aperture radius values
Nf=2000;           %Approximate maximum aperture size in
number of full Fresnel zones
Nppw=200;          %Number of panels per wavelength for
radial aperture integration in variable rho
%Nza=1001;         %Number of path aperture locations
%Na=1001;          %Number of aperture radius values
%Nf=2000;          %Approximate maximum aperture size in
number of full Fresnel zones
%Nppw=100;         %Number of panels per wavelength for
radial aperture integration in variable rho
Rft=2*(2*rhoot*rhoot)/lambda; %Far zone distance from transmitter
and receiver, respectively
Rfr=2*(2*rhoor*rhoor)/lambda;
if (Rft+Rfr)<R
    fprintf('Integrating per page 6 of notes...\n');
    zadR=linspace((R-Ha)/R,1-Rfr/R,Nza)'; %Fractional locations of
aperture along propagation path for VW-communications study

```

```

    ellipse_factor=2*sqrt(zadR.*(1-zadR));           %Fresnel ellipse factor
    ellipse_factor(1)=ellipse_factor(2)/2;         %Arbitrarily add Fresnel
zones to path endpoints
    ellipse_factor(end)=ellipse_factor(end-1)/2;   %Arbitrarily add Fresnel
zones to path endpoints
    adR=ellipse_factor*linspace(0,sqrt(2*Nf),Na)*Flmax/R; %Scaled aperture
radii along propagation path
    V_nJ1Ha=zeros(size(adR));
    for zz=1:Nza
        fprintf('za/R distance = %0.7f \n',zadR(zz,1));
        llim=0;
        for aa=2:Na
            %Trapezoidal rule: Sum over 1+Npanels evaluations, add only half
at endpoints...
            ulim=R*adR(zz,aa);
            za=R*zadR(zz);
            Rmza=R-za;
            Npanels=ceil(Nppw*(ulim-llim)/lambda);
            deltarhodza=(ulim-llim)/Npanels/za;
            rhogrid=linspace(llim,ulim,Npanels+1);
            if aa==2, rhogrid(1)=2*eps; end
            rhodza=rhogrid/za;
            rhodza2=rhodza.*rhodza;
            sqrtoneprhodza2=sqrt(1+rhodza2);
            rhodRmza=rhogrid/Rmza;
            rhodRmza2=rhodRmza.*rhodRmza;
            sqrtoneprhodRmza2=sqrt(1+rhodRmza2);

integrand=(1+1./sqrtoneprhodza2).*(1+1./sqrtoneprhodRmza2).*exp((-
j*k*za)*sqrtoneprhodza2+(-j*k*Rmza)*sqrtoneprhodRmza2);

integrand=((integrand./sqrtoneprhodza2)./sqrtoneprhodRmza2).*rhodza;
    bjargza=(k*rhoot)*rhodza./sqrtoneprhodza2;
    bjargRmza=(k*rhoor)*rhodRmza./sqrtoneprhodRmza2;
    integrand=integrand.*besselj(Pt+1,bjargza)./(bjargza.^(Pt+1));

integrand=integrand.*besselj(Pr+1,bjargRmza)./(bjargRmza.^(Pr+1));
    V_nJ1Ha(zz,aa)=V_nJ1Ha(zz,aa-1) +
deltarhodza*(integrand(1)/2+sum(integrand(2:end-1))+integrand(end)/2);
    llim=ulim;
    end
    %Note: Need to be cautious in normalizing before integration has
proceeded out to a large enough radius, otherwise normalization may be done
to
    %a value of Vn not representative of full received power. However,
limit of diffraction integral seems to be unable to be found analytically, so
numerical
    %normalization is be required. A solution is to integrate out in
radius a to a greater number of fesnel zones.
    V_nJ1Ha(zz,:)=V_nJ1Ha(zz,:)/V_nJ1Ha(zz,end);
    end
    eta_J1Ha_all=V_nJ1Ha.*conj(V_nJ1Ha);
    toc
else

```

```

    fprintf('Parameter error: Transmitter plus/or receiver far zone distances
Rft=%0.4f m or Rfr=%0.4f m exceeds total path length R=%0.4f
km.\n',Rft,Rfr,R/1000);
    fprintf('Fresnel link efficiencies inapplicable for close-coupled T/R
antennas.\n');
end

%Render link efficiency data...
h=figure('NumberTitle','off','Color',[1,1,1],'name','Fresnel Zone Link
Efficiency');
pcolor((R*zadR'-R)/1000,R*adR',eta_J1Ha_all');
shading interp
axis('square','xy');
v=axis; axis([-Ha/1000,0,v(3),v(4)]);
caxis([0,4]);
xlabel('Path Distance z_a (km)');
ylabel('Aperture Radius a (m)');
title(['Fresnel Zone Link Efficiency \eta_1: CAQTTR/CA at
f=',num2str(f/1e9),' GHz, R=',num2str(R/1000),' km,
a_o=[' ,num2str(rhoot*100),' ,',num2str(rhoor*100),' ] cm,
R_o=[\infty,\infty]']);
colormap(jet(256));
hc=colorbar;

%Render link efficiency data...
h=figure('NumberTitle','off','Color',[1,1,1],'name','Fresnel Zone Link
Efficiency');
pcolor((R*zadR'-R)/1000,R*adR',10*log10(eta_J1Ha_all)');
shading interp
axis('square','xy');
v=axis; axis([-Ha/1000,0,v(3),v(4)]);
caxis([-20,6]);
xlabel('Path Distance z_a (km)');
ylabel('Aperture Radius a (m)');
title(['Fresnel Zone Link Efficiency \eta_1 (dB): CAQTTR/CA at
f=',num2str(f/1e9),' GHz, R=',num2str(R/1000),' km,
a_o=[' ,num2str(rhoot*100),' ,',num2str(rhoor*100),' ] cm,
R_o=[\infty,\infty]']);
colormap(jet(256));
hc=colorbar;

%Render link efficiency deviation data to illustrate impact of circular
clearance aperture...
deltaetaHa=eta_J1Ha_all-1;
h=figure('NumberTitle','off','Color',[1,1,1],'name','Fresnel Zone Link
Efficiency');
pcolor((R*zadR'-R)/1000,R*adR',10*log10(abs(deltaetaHa))');
shading interp
axis('square','xy');
v=axis; axis([-Ha/1000,0,v(3),v(4)]);
caxis([-30,5]);
xlabel('Path Distance z_a (km)');
ylabel('Aperture Radius a (m)');

```

```

title(['Fresnel Zone Link Efficiency \delta\eta_1 (dB): CAQTTR/CA at
f=',num2str(f/1e9),' GHz, R=',num2str(R/1000),' km,
a_o=[' ,num2str(rhoot*100),' ,',num2str(rhoor*100),' ] cm,
R_o=[\infty,\infty]']);
colormap(jet(256));
hc=colorbar;

%Render normalized link efficiency data...
h=figure('NumberTitle','off','Color',[1,1,1],'name','Fresnel Zone Link
Efficiency');
pcolor(zadR',adR',eta_J1Ha_all');
shading interp
axis('square','xy');
v=axis; axis([zadR(1),1,v(3),v(4)]);
caxis([0,4]);
xlabel('Relative Path Distance z_a/R (-)');
ylabel('Normalized Aperture Radius a/R (-)')
title(['Fresnel Zone Link Efficiency \eta_1: CAQTTR/CA at
f=',num2str(f/1e9),' GHz, R=',num2str(R/1000),' km,
a_o=[' ,num2str(rhoot*100),' ,',num2str(rhoor*100),' ] cm,
R_o=[\infty,\infty]']);
colormap(jet(256));
hc=colorbar;

%Render complex normalized voltage data for key z_a planes...
h=figure('NumberTitle','off','Color',[1,1,1],'name','Communications Link
Efficiency');
plot(real(V_nJ1Ha(1,:)),imag(V_nJ1Ha(1,:)),'b',real(V_nJ1Ha(ceil(end/2),:)),i
mag(V_nJ1Ha(ceil(end/2),:)),'r',real(V_nJ1Ha(end-1,:)),imag(V_nJ1Ha(end-
1,:)),'g');
grid on
axis('equal','xy');
xlabel('Re{V_n}');
ylabel('Im{V_n}');
legend('z_a=R-H_a','z_a=R-R_{fr}-H_a/2','z_a=R-R_{fr}');
title(['Communications Link Efficiency V_n=V/V_{max} for a=[0..\infty]:
CAQTTR/CA at f=',num2str(f/1e9),' GHz, R=',num2str(R/1000),' km,
a_o=[' ,num2str(rhoot*100),' ,',num2str(rhoor*100),' ] cm,
R_o=[\infty,\infty]']);

%Part VI: Calculation of on-axis field power ratio for Gaussian transmitter
beam wave illuminating a half-space knife-edge aperture of offset xa
%and received by a Gaussian-beam receiver. This problem has a very simple
%and elegant closed form expression for the link efficiency etl_1 in terms of
the complex error function.
%The Gaussian beams are specified by the aperture phase radii of curvature
and waist
%radii at the transmitter and receiver (respectively), and thus serve to
illustrate effects of focussed Gaussian
%transmitter and receiver beams and a circular aperture stop on the received
signal amplitude.

```

```

%This calculation provides link efficiency relative to the free-space Friis
formula for received Gaussian beam power.
%Note: Specific link parameters are solely to determine proper rendering
%grid range and resolution. The expression for relative link efficiency is
%dependent only on the following parameters:
% kR = path boresite phase delay (radians)
% a/R = scaled aperture radius (dimensionless)
% za/R = along-path fractional aperture location (dimensionless)
% Wot/lambda = Transverse beam waist radius in wavelengths at transmitter
aperture (dimensionless)
% Wor/lambda = Transverse beam waist radius in wavelengths at receiver
aperture (dimensionless)
% Rot/R = Phase radius of curvature in transmitter aperture (dimensionless)
% Ror/R = Phase radius of curvature in receiver aperture (dimensionless)

close all
clear
clc

f=325e9;           %Frequency in Hz (TAIPAS)
R=1924;           %Path length in m (TAIPAS)
c=299792458;     %Speed of light (m/s)
lambda=c/f;      %Wavelength in m
k=2*pi/lambda;   %Wavenumber in m-1
kR=k*R;          %Phase delay along path boresite
Flmax=sqrt(lambda*R)/2; %First Fresnel zone maximum radius (for grid
specification)
aot=0.05;        %TAIPAS near-equivalent beam parameters
aor=0.05;        %Case with TAPIAS receiver aperture same diameter as
transmitter aperture
%aor=0.01;       %Case with TAIPAS receiver aperture stopped down by 5x to
2 cm diameter
Wot=0.6435*aot;  %Wylde (1984) GB approximation of corrugated horn of
aperture radius a
Wor=0.6435*aor;
Rot=inf;
Ror=inf;
deta=[0.01,0.0001,0.000001]; %Power variation thresholds due to CA
blockage (e.g., -20,-40,-60 dB down fluctuations)
%TAIPAS physical path parameters:
PathR=[0,100,200,300,400,500,600,700,800,900,1000,1100,1200,1300,1400,1500,16
00,1700,1800,1900,1920];
PathH=[3.0,8.1,10.2,12.3,33.4,21.5,43.6,49.7,39.8,39.8,58.9,50.0,54.1,53.2,56
.3,68.4,65.5,47.6,36.7,29.8,2.0];

tic
%Set grid parameters...
Nza=4001;        %Number of path aperture locations
Na=8001;        %Number of aperture radius values
Nf=500;         %Approximate maximum aperture size in
number of full Fresnel zones
zadR=linspace(0,1,Nza)'; %Fractional locations of aperture
along propagation path
ellipse_factor=2*sqrt(zadR.*(1-zadR)); %Fresnel ellipse factor

```

```

ellipse_factor([1,end])=ellipse_factor(2)/2;           %Arbitrarily add
Fresnel zones to path endpoints
xadR=ellipse_factor*linspace(0,sqrt(2*Nf),Na)*Flmax/R; %Scaled aperture
radii along propagation path
za=R*zadR;
alphan=(1/(Wot*Wot))+j*(k/(2*Rot));
alphan=(1/(Wor*Wor))+j*(k/(2*Ror));
A=(1./(1/alphan-j*2*za/k)) + (1./(1/alphan-j*2*(R-za)/k));
A=repmat(A,1,Na);
ApdAdp=real(A)./imag(A);
alphaminus=ApdAdp-sqrt(ApdAdp.*ApdAdp+1);
alphaminus2=alphaminus.*alphaminus;
sqrtA=sqrt(A);
eta_hsebtrl_all=sqrt(real(A).*(1-alphaminus2)-2*imag(A).*alphaminus).*((1-
j*alphaminus)./(1+alphaminus2))./sqrtA;
sqrtARxadR=sqrtA.*(R*xadR);
eta_hsebtrl_all=eta_hsebtrl_all.*erfz(sqrtARxadR);
V_nhse=[1-eta_hsebtrl_all(:,end:-1:2),1+eta_hsebtrl_all]/2;
eta_hsebtrl_mii_all=[1-eta_hsebtrl_all(:,end:-
1:2),1+eta_hsebtrl_all].*conj([1-eta_hsebtrl_all(:,end:-
1:2),1+eta_hsebtrl_all]);
eta_hsebtrl_all=(1+eta_hsebtrl_all).*conj((1+eta_hsebtrl_all))/4;
toc

%Render link efficiency data...
h=figure('NumberTitle','off','Color',[1,1,1],'name','Communications Link
Efficiency');
pcolor(R*zadR,R*xadR,eta_hsebtrl_all);
shading interp
axis('square','xy');
caxis([0,1.5]);
xlabel('Path Distance z_a (m)');
ylabel('Aperture Edge Distance x_a (m)')
title(['Communications Link Efficiency \eta_l: GBTR/HSE at
f=',num2str(f/1e9),' GHz, R=',num2str(R/1000),' km,
W_o=[',num2str(Wot*100),' ',num2str(Wor*100),' ] cm, R_o=[\infty,\infty]']);
colormap(jet(256));
hc=colorbar;

h=figure('NumberTitle','off','Color',[1,1,1],'name','Communications Link
Efficiency');
pcolor(R*zadR,R*xadR,10*log10(eta_hsebtrl_all));
shading interp
axis('square','xy');
caxis([-20,3]);
xlabel('Path Distance z_a (m)');
ylabel('Aperture Edge Distance x_a (m)')
title(['Communications Link Efficiency \eta_l (dB): GBTR/HSE at
f=',num2str(f/1e9),' GHz, R=',num2str(R/1000),' km,
W_o=[',num2str(Wot*100),' ',num2str(Wor*100),' ] cm, R_o=[\infty,\infty]']);
colormap(jet(256));
hc=colorbar;

```

```

%Render link efficiency deviation data to illustrate impact of half space
edge aperture...
h=figure('NumberTitle','off','Color',[1,1,1],'name','Communications Link
Efficiency');
pcolor(R*zadR',R*xadR',10*log10(abs(eta_hsebtrl_all-1))');
shading interp
axis('square','xy');
caxis([-30,3]);
xlabel('Path Distance z_a (m)');
ylabel('Aperture Edge Distance x_a (m)')
title(['Communications Link Efficiency \delta\eta_l (dB): GBTR/HSE at
f=',num2str(f/1e9),' GHz, R=',num2str(R/1000),' km,
W_o=['',num2str(Wot*100),' ','',num2str(Wor*100),' ']' cm, R_o=[\infty,\infty]']);
colormap(jet(256));
hc=colorbar;

% %Render link efficiency maximum deviation data to illustrate impact of half
space aperture...
% h=figure('NumberTitle','off','Color',[1,1,1],'name','Fresnel Zone Link
Efficiency');
% pcolor(R*zadR',R*xadR',10*log10(deltaeta)');
% shading interp
% axis('square','xy');
% caxis([-30,5]);
% xlabel('Path Distance z_a (m)');
% ylabel('Aperture Edge Distance x_a (m)')
% title(['Fresnel Zone Link Efficiency \delta\eta_l (dB): GBTR/HSE at
f=',num2str(f/1e9),' GHz, R=',num2str(R/1000),' km,
W_o=['',num2str(Wot*100),' ','',num2str(Wor*100),' ']' cm, R_o=[\infty,\infty]']);
% colormap(jet(256));
% hc=colorbar;
%
%Render normalized link efficiency data...
h=figure('NumberTitle','off','Color',[1,1,1],'name','Communications Link
Efficiency');
pcolor(zadR',xadR',eta_hsebtrl_all');
shading interp
axis('square','xy');
caxis([0,1.5]);
xlabel('Relative Path Distance z_a/R (-)');
ylabel('Normalized Aperture Edge Distance x_a/R (-)')
title(['Communications Link Efficiency \eta_l: GBTR/HSE at
f=',num2str(f/1e9),' GHz, R=',num2str(R/1000),' km,
W_o=['',num2str(Wot*100),' ','',num2str(Wor*100),' ']' cm, R_o=[\infty,\infty]']);
colormap(jet(256));
hc=colorbar;

% %Render link clearance data...
% h=figure('NumberTitle','off','Color',[1,1,1],'name','Communications Link
Efficiency');
%
% plot(R*zadR,amin(:,1),'b',R*zadR,amin(:,2),'m',R*zadR,amin(:,3),'g',PathR,Pat
hH,'o-r');
% grid on
% xlabel('Path Distance z_a (m)');

```

```
% ylabel('Edge Clearance Distance (m)')
% title(['Fresnel Zone Link Clearance: GBTR/HSE at f=',num2str(f/1e9),' GHz,
R=',num2str(R/1000),' km, W_o=[' ,num2str(Wot*100),' ,',num2str(Wor*100),' ] cm,
R_o=[\infty,\infty]']);
% legend('\delta\eta_1<1% (-20 dB)', '\delta\eta_1<0.01% (-40
dB)', '\delta\eta_1<0.0001% (-60 dB)', 'Estimated Path Clearance');
```

```
%Render link efficiency data...
```

```
h=figure('NumberTitle','off','Color',[1,1,1],'name','Communications Link
Efficiency');
pcolor(R*xadR, [-R*xadR(:,end:-1:2),R*xadR]', eta_hsebtrl_mii_all');
shading interp
axis('square','xy');
caxis([0,1.5]);
xlabel('Path Distance z_a (m)');
ylabel('Aperture Edge Distance x_a (m)')
title(['Communications Link Efficiency \eta_1: GBTR/HSE at
f=',num2str(f/1e9),' GHz, R=',num2str(R/1000),' km,
W_o=[' ,num2str(Wot*100),' ,',num2str(Wor*100),' ] cm, R_o=[\infty,\infty]']);
colormap(jet(256));
hc=colorbar;
```

```
%Render link efficiency data...
```

```
h=figure('NumberTitle','off','Color',[1,1,1],'name','Communications Link
Efficiency');
pcolor(R*xadR, [-R*xadR(:, (ceil(end/2)+1):-
1:2),R*xadR(:,1:(ceil(end/2)+1))]', ...
10*log10(abs(eta_hsebtrl_mii_all(:, (Na-1)/2:end+1-(Na-1)/2)-
[zeros(Nza, (Na+1)/2), ones(Nza,1)/4, ones(Nza, (Na+1)/2)]))');
shading interp
axis('square','xy');
caxis([-30,3]);
xlabel('Path Distance z_a (m)');
ylabel('Aperture Edge Distance x_a (m)')
title(['Communications Link Efficiency \eta_1 (dB): GBTR/HSE at
f=',num2str(f/1e9),' GHz, R=',num2str(R/1000),' km,
W_o=[' ,num2str(Wot*100),' ,',num2str(Wor*100),' ] cm, R_o=[\infty,\infty]']);
colormap(jet(256));
hc=colorbar;
```

```
% h=figure('NumberTitle','off','Color',[1,1,1],'name','Communications Link
Efficiency');
% plot(R*xadR(ceil(end/2),:), eta_hsebtrl_all(ceil(end/2),:));
% grid on
% xlabel('Aperture Edge Distance x_a (m)')
% ylabel('\eta_1 (-)');
% title(['Communications Link Efficiency \eta_1: GBTR/HSE at
f=',num2str(f/1e9),' GHz, R=',num2str(R/1000),' km,
W_o=[' ,num2str(Wot*100),' ,',num2str(Wor*100),' ] cm, R_o=[\infty,\infty]']);
```

```
h=figure('NumberTitle','off','Color',[1,1,1],'name','Communications Link
Efficiency');
plot([-R*xadR(ceil(end/2),end:-
1:2),R*xadR(ceil(end/2),:)], eta_hsebtrl_mii_all(ceil(end/2),:));
```

```

grid on
xlabel('Aperture Edge Distance x_a (m)')
ylabel('\eta_l (-)');
title(['Communications Link Efficiency \eta_l: GBTR/HSE at
f=',num2str(f/1e9),' GHz, R=',num2str(R/1000),' km,
W_o=['',num2str(Wot*100),'','',num2str(Wor*100),''] cm, R_o=[\infty,\infty]']);

%Render complex normalized voltage data for key z_a planes (Euler spiral)...
h=figure('NumberTitle','off','Color',[1,1,1],'name','Communications Link
Efficiency');
plot(real(V_nhse(ceil(end/2),:)),imag(V_nhse(ceil(end/2),:)),'b',real(V_nhse(
ceil(0.1*end/2),:)),imag(V_nhse(ceil(0.1*end/2),:)),'r',real(V_nhse(ceil(0.01
*end/2),:)),imag(V_nhse(ceil(0.01*end/2),:)),'g');
grid on
axis('equal','xy');
xlabel('Re{V_n}');
ylabel('Im{V_n}');
legend('z_a=R/2','z_a=R/20','z_a=R/200');
title(['Communications Link Efficiency V_n=V/V_{max} for x_a=[-
\infty..\infty]: GBTR/HSE at f=',num2str(f/1e9),' GHz, R=',num2str(R/1000),'
km, W_o=['',num2str(Wot*100),'','',num2str(Wor*100),''] cm,
R_o=[\infty,\infty]']);

%Compare complex normalized voltage data for key z_a planes versus aperture
sizes for circular aperture and half space edge...
if exist('V_nb')
    h=figure('NumberTitle','off','Color',[1,1,1],'name','Communications Link
Efficiency');
    plot(R*adR(ceil(end/2),:),abs(V_nb(ceil(end/2),:)),'b',[-
R*xadR(ceil(end/2),end:-
1:2),R*xadR(ceil(end/2),:)],abs(V_nhse(ceil(end/2),:)),'r');
    grid on
    xlabel('Off-Boresite Aperture Edge Distance (m)');
    ylabel('\eta_l (-)');
    legend('Circular Aperture','Half Space Edge Aperture');
    title(['Communications Link Efficiency V_n=V/V_{max} for Aperture Edge
Distances: GBTR/CA,HSE at f=',num2str(f/1e9),' GHz, R=',num2str(R/1000),' km,
W_o=['',num2str(Wot*100),'','',num2str(Wor*100),''] cm, R_o=[\infty,\infty]']);

    h=figure('NumberTitle','off','Color',[1,1,1],'name','Communications Link
Efficiency');
    plot(R*adR(ceil(end/2),:),10*log10(abs(V_nb(ceil(end/2),:))),'b',[-
R*xadR(ceil(end/2),end:-
1:2),R*xadR(ceil(end/2),:)],10*log10(abs(V_nhse(ceil(end/2),:))),'r');
    grid on
    v=axis; axis([v(1),v(2),-35,5]);
    xlabel('Off-Boresite Aperture Edge Distance (m)');
    ylabel('\eta_l (-)');
    legend('Circular Aperture','Half Space Edge Aperture');
    title(['Communications Link Efficiency V_n=V/V_{max} for Aperture Edge
Distances: GBTR/CA,HSE at f=',num2str(f/1e9),' GHz, R=',num2str(R/1000),' km,
W_o=['',num2str(Wot*100),'','',num2str(Wor*100),''] cm, R_o=[\infty,\infty]']);
end

```

%Note: Need to find minima-seeking and interpolation method to bound half
%space edge aperture link degradation - analogous to case for circular
%aperture, but numerical since analytic expression for minima of Euler
%Cornu spiral seems impractical.

%Note: Would be useful to develop section to calculate half space aperture
%link budget for case of quadratic taper circular aperture. However, this
%would entail a two-dimensional numerical diffraction integral over Bessel
%functions, and may be impractical.

Appendix B: Datasheets

Micro Lambda Wireless
Wenzel Associates
Applied Technologies, Inc. Anemometer
Campbell Scientific Hygrometer
Ubiquiti airGrid
Point Grey Chameleon CCD
Sony CCD
Mead Telescope
Edmund Optics Bandpass Filter
METAR / SPECI Data
Quarton Inc. Laser Diode

MLSN PERFORMANCE SPECIFICATIONS

(Operating Case Temperature: 0° to +60° C Baseplate)

Model No.	MLSN-1012	MLSN-1214	MLSN-1416
RF Specifications			
Output Frequency	10-12 GHz	12-14 GHz	14-16 GHz
Output Power Min.	+8 dBm	+8 dBm	+8 dBm
Po Variation over Freq/Temp	4 dB	4 dB	4 dB
Step Size, Min.	1 Hz	1 Hz	1 Hz
Switching Speed, 100 MHz Step, Typ.	10 mS	10 mS	10 mS
1000 MHz Step, Typ.	11 mS	11 mS	11 mS
Full Band Step, Typ.	12 mS	12 mS	12 mS
Warm-up Time ("Lock") @ DC (Minutes)	3.0	3.0	3.0
Output Impedance	50 Ohms	50 Ohms	50 Ohms
Load VSWR	2.0:1	2.0:1	2.0:1
Harmonics	-20 dBc	-25 dBc	-30 dBc
Non-Harmonic Spurious			
100 Hz ≤ f off ≤ 10 kHz	-60 dBc	-60 dBc	-60 dBc
10 kHz ≤ f off ≤ 100 kHz	-60 dBc	-60 dBc	-60 dBc
f off > 100 kHz	-60 dBc	-60 dBc	-60 dBc
Phase Noise @ 100 Hz Offset			
@ 1 kHz Offset	-96 dBc/Hz	-95 dBc/Hz	-94 dBc/Hz
@ 10 kHz Offset	-103 dBc/Hz	-102 dBc/Hz	-101 dBc/Hz
@ 100 kHz Offset	-115 dBc/Hz	-113 dBc/Hz	-110 dBc/Hz
@ 1 MHz Offset	-137 dBc/Hz	-136 dBc/Hz	-135 dBc/Hz
External Ref. Osc. - Fixed Freq.	10 MHz	10 MHz	10 MHz
(Unit is not Phase Coherent to External Reference)			
External Ref. Osc. Input Power	0 +/- 6 dBm	0 +/- 6 dBm	0 +/- 6 dBm
Supply Voltage & Current			
+15 Vdc (+10% -5%)	900 mA	1000 mA	1200 mA
+5 Vdc (+10% -5%)	700 mA	700 mA	700 mA
Supply Voltage Ripple			
(Pk-Pk from 2 kHz to 3 MHz)	10 mV	10 mV	10 mV
Digital Control Format			
Phase Lock Alarm (Programmable)	High=Locked	High=Locked	High=Locked
Connections			
Control/Alarm (J1)	AMP-103166-8	AMP-103166-8	AMP-103166-8
RF Connectors (J2 - J5)	SMA-F	SMA-F	SMA-F
Case Style	161-001	161-001	161-001



Wenzel Associates, Inc.
"Quietly the Best"



Crystal Oscillators > 4 to 30 MHz > Streamline OCXO

Features:

- Very Low Phase Noise
- Very Good Frequency Stability over Temperature
- PCB Mount and SMA Packages Available
- Internal Voltage Regulator
- Low Aging Rate

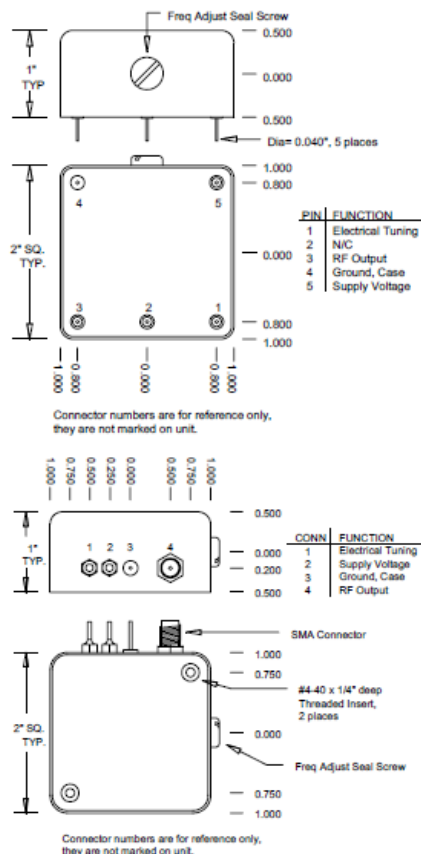
Applications:

- High Performance General Purpose OCXO
- GPS Receivers
- Synthesizers

The Streamline oscillators offer excellent overall performance at a modest cost. Industry standard packaging is available with various connector and pin styles. Please let us know your custom packaging needs. SC-cut crystals provide aging to 1×10^{-10} per day and phase noise floors to -165 dBc. Includes an internal voltage regulator and high performance oven.



Typical Specifications:				
Frequency (Specify)		4 to 30 MHz		
Frequency		5	10	MHz
Output Level		+13		
Output Level		dBm		
Aging		$\pm 1 \times 10^{-9}$ to $\pm 5 \times 10^{-10}$		
Phase Noise	10 Hz	-130	-135	-120
	100 Hz	-155	-160	-155
	1 kHz	-165	-165	-165
	10 kHz	-165	-165	-165
				dBc/Hz
Temperature Stability (Specify)				
Range A	0 to +50C			
Range B	0 to +65C			
Range C	0 to +70C	$\pm 1.5 \times 10^{-8}$ to	$\pm 1.5 \times 10^{-8}$ to	
Range D	-20 to +70C	$\pm 2 \times 10^{-9}$	$\pm 5 \times 10^{-9}$	
Range E	-40 to +70C			
Range F	-55 to +85C			
Spurious		-80		
Spurious		dBc		
Harmonics		-30		
Harmonics		dBc		
Electrical Tuning Range (Specify)				
Tuning A	0 to +10 VDC	$\pm 2 \times 10^{-7}$ to $\pm 2 \times 10^{-6}$		
Tuning B	± 5 VDC			
Supply Voltage (Specify)		+12 or +15		
Supply Voltage (Specify)		VDC		
Warm-up Power		5		
Warm-up Power		Watts		
Total Power typical		2.2		
Total Power typical		Watts		
Crystal Type		SC		
Dimensions		51 x 51 x 25.4		
Dimensions		mm		
Dimensions		2.0 x 2.0 x 1.0		
Dimensions		inches		
Connectors	Style A	Solder pins on base		
	Style B	SMA and Feedthrus		



Anemometer: Applied Technologies, Inc.

Summary of Features

- Single component wind velocity
- Fast response temperature
- Extreme accuracy
- Microprocessor based
- Solid-state digital operation
- No moving parts
- Unattended operation
- Ease of mounting
- Rugged construction
- Low power
- DC powered

Summary of Functions

- Ability to do remote commands through the serial port
- Perform internal calibration to maintain accuracy
- User programmable data rates and averaging, from 5 min. to 200 Hz
- Select data averaging or median filter
- Select from several output formats
- Select from several baud rates
- Synchronize sonic operation to external trigger
- Ability to output a trigger pulse for other instruments
- Select the output Speed of Sound and/or Temperature
- Enter RH value for more accurate temperature output
- User adjustments to temperature calculations
- Change horizontal velocity to wind speed & direction, while retaining vertical and temperature
- Select data quality algorithm (to remove spikes)
- User adjustments to data quality calculations
- Ability to provide data quality status word in output format
- Turn flow distortion correction on or off
- User adjustments to flow distortion calculations

Specifications

Measurement Range:	
Wind velocity (V)	±15 m/sec
Wind velocity (Vx)	±20 m/sec
Wind velocity (K, Sx)	±30 m/sec
Wind velocity (A)	±65 m/sec
Temperature	-50 to +60°C
Wind Direction	0 – 359 Degrees
Path Length:	
"V" Circular Probe	10 cm
"Vx" Probe	15 cm
"K" Kaimal Probe	15 cm
"Sx" Basic Probe	15 cm
"A" Non-orthogonal Probe	15 cm
Accuracy:	
Wind Speed	±0.01 m/sec
Orthogonality	±0.1 degrees
Temperature (absolute)	2°C
Sonic Temperature	±0.1°C
Resolution:	
Wind Speed	0.01 m/sec (normal) 0.001 m/sec (optional)
Wind Direction	0.1 degrees
Temperature	0.01°C
Output:	
Data Rate	<1 Hz to 200 Hz - Variable
Digital	Serial RS-232C compatible
Baud Rate	4800 or 115,200
Speed of Sound	Operator Optional
Operating Temperature Range:	
-50°C to +60°C	
Power Requirements:	
+12 VDC@ 100 mA, (9 – 32 VDC)	
Probe Array:	
"V" - Three Axis	17.8cm x 17.8cm x 17.8cm
"Vx" - Three Axis	25.4cm x 25.4cm x 25.4cm
"K" - Three Axis	25.4cm x 33.0cm x 40.6cm
"Sx" - Three Axis	25.4cm x 35.6cm x 35.6cm
"Sx" - Two Axis	25.4cm x 25.4cm x 17.8cm
"Sx" - Single Axis	2.54cm x 15.9cm x 17.8cm
"A" - Non-Orthogonal	12.6cm x 22.6cm x 19.6cm
Weight	<1.0kg
Mounting (All Probe Styles):	3.175 cm square tube

Hygrometer: Campbell Scientific

General Description

The KH20 is a krypton hygrometer for measuring water vapor fluctuations in the air. The name KH20 (KH-twenty) was derived from KH₂O (K-H₂O), and the sensor has been known with this name since 1985. It is typically used with the CSAT3 3-D sonic anemometer for measuring latent heat flux (LE), using Eddy Covariance technique. Please refer to the Open Path Eddy Covariance System operator's manual for details on flux measurements using the KH20 sensor.

The KH20 sensor uses a krypton lamp that emits two absorption lines: major line at 123.58 nm and minor line at 116.49 nm. Both of these lines are absorbed by water vapor, and a small amount of the minor line is absorbed by oxygen. The KH20 is not suitable for absolute water vapor concentration measurements due to its signal offset drift.

The KH20 heads are sealed and will not suffer damage should they get wet. In addition, the electronics box and the connectors are housed inside a rain shield (CSI p/n 14113) that protects them from moisture. The KH20 is suitable for long-term continuous outdoor applications.

The KH20 sensor is comprised of two main parts: the sensor head and the electronics box. The sensor head comes with cables with 6 ft of lead length that connect the sensor to the electronics box. It is shipped with a rain shield (CSI p/n 14113) to protect the electronics box and the connectors from moisture, a 20 inch 3/4 IPS threaded aluminium pipe (CSI p/s 3874), a 3/4" x 3/4" Nu-Rail (CSI p/n 1017), and a 5/32 inch Allen wrench (CSI p/n 4697) for mounting. The sensor comes with a signal/power cable which has 25 ft lead length. If a longer cable is desired, the customer can order a replacement cable (p/n KH20CBL-L) and specify the desired lead length after -L.

Specifications

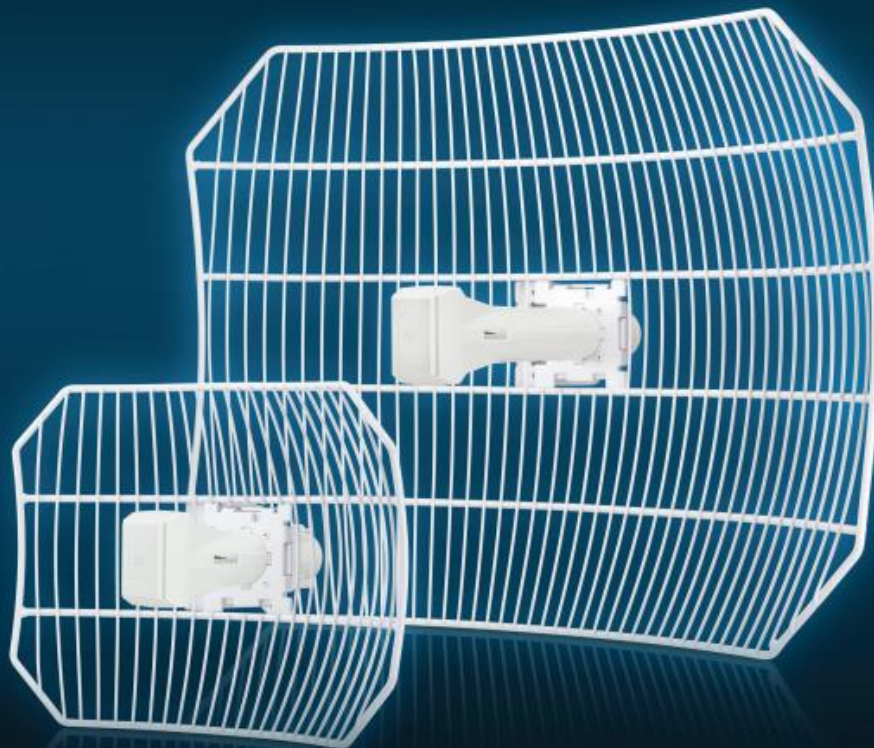
2.1 Measurements

Calibration Range:	1.7 to 19.5 g/m ³ (nominal)
Frequency Response:	100 Hz
Operating Temperature Range:	-30 to +50°C

2.2 Electrical

Supply Voltage:	10 V to 16 Vdc
Current Consumption:	20 mA max at 12 Vdc
Power Consumption:	0.24 Watts
Output Signal Range:	0 to 5Vdc

DATASHEET



*air*Grid[®] *M*

airMAX[®] Wireless Broadband CPE

Models: AG-HP-2G16, AG-HP-2G20, AG-HP-5G23, AG-HP-5G27

High Performance, Long Range

Integrated InnerFeed[®] CPE

Easy Assembly and Installation

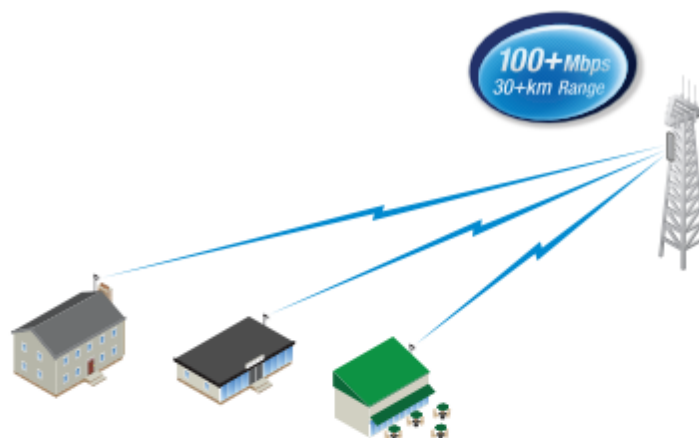


airGrid[®] M

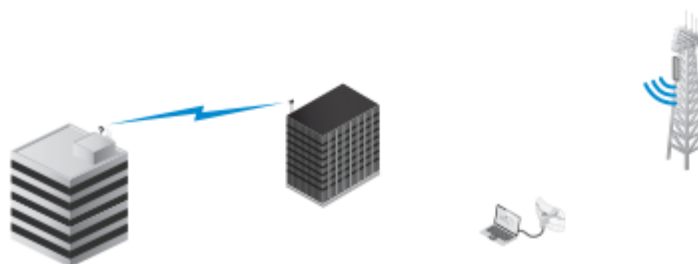
Utilizing InnerFeed technology, the new airGrid[®] M HP Series from Ubiquiti Networks represents the latest evolution of outdoor wireless broadband devices. The revolutionary InnerFeed technology integrates the entire radio system into the feedhorn of the antenna. airGrid M combines Ubiquiti's InnerFeed and airMAX[®] (TDMA protocol) technologies to create a simple, yet extremely powerful and robust wireless CPE (Customer Premises Equipment).

Complete antenna and radio system integration provides affordable cost/performance solutions to the wireless broadband industry. airGrid M operates in the worldwide, license-free frequency range of either 2 GHz or 5 GHz, and features breakthrough performance of up to 100+ Mbps in real outdoor throughput and incredible range of up to 30+ km.

The low-cost, high-performance, robust "all-in-one" design and light weight of airGrid M make it versatile and ideal in several different applications.



airGrid M as a cost-effective CPE in an airMAX Point-to-Multi-Point network.



Use an airGrid M on each side of a Point-to-Point link to create a reliable connection.

airGrid M as a powerful wireless client.

Integrated airMAX Technology

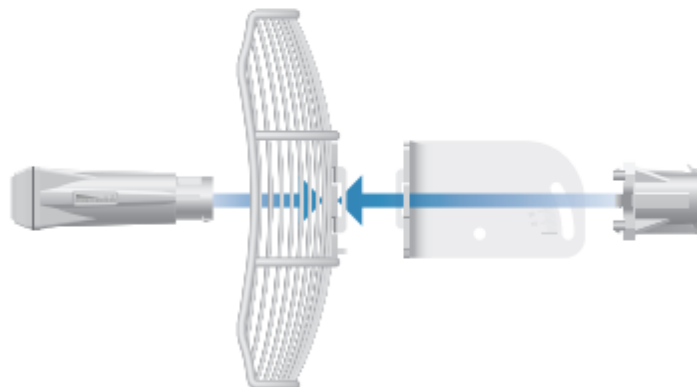
Unlike standard Wi-Fi protocol, the exclusive Ubiquiti Networks[®] airMAX Time Division Multiple Access (TDMA) protocol allows each client to send and receive data using pre-designated time slots managed by an intelligent AP controller. This "time slot" method eliminates hidden node collisions and maximizes airtime efficiency.

Compared to other systems in its class, the airGrid M delivers superior performance in reduced latency, throughput, and scalability.

- **Intelligent QoS** Priority is given to voice/video for seamless access.
- **Scalability** High capacity and scalability.
- **Long Distance** Capable of high-speed, 30+ km links.

Easy, No-Tool Assembly

With its updated mechanical design, assembling and disassembling the airGrid M is literally a snap. No tools are required.



You simply snap the feed, antenna, mounting bracket and rear housing together for a secure, solid assembly.

Models

airGrid M2 HP

Model: AG-HP-2G16

- 2412 - 2462 MHz
- 16 dBi
- Antenna Size: 370 x 270 mm



Front View



Side View

airGrid M2 HP

Model: AG-HP-2G20

- 2412 - 2462 MHz
- 20 dBi
- Antenna Size: 620 x 460 mm



Front View



Side View

Models

airGrid M5 HP

Model: AG-HP-5G23

- Worldwide: 5170 – 5875 MHz
- India: 5825 – 5875 MHz
- USA: 5725 – 5850 MHz
- 23 dBi
- Antenna Size: 370 x 270 mm



Front View



Side View

airGrid M5 HP

Model: AG-HP-5G27

- Worldwide: 5170 – 5875 MHz
- India: 5825 – 5875 MHz
- USA: 5725 – 5850 MHz
- 27 dBi
- Antenna Size: 620 x 460 mm



Front View



Side View

Specifications

System Information	
Processor Specs	Atheros MIPS 74Kc, 560 MHz
Memory Information	64 MB DDR2, 8 MB Flash
Networking Interface	(1) 10/100 Ethernet Port

Regulatory / Compliance Information	
Wireless Approvals	FCC Part 15.247, IC RS210, CE
RoHS Compliance	Yes

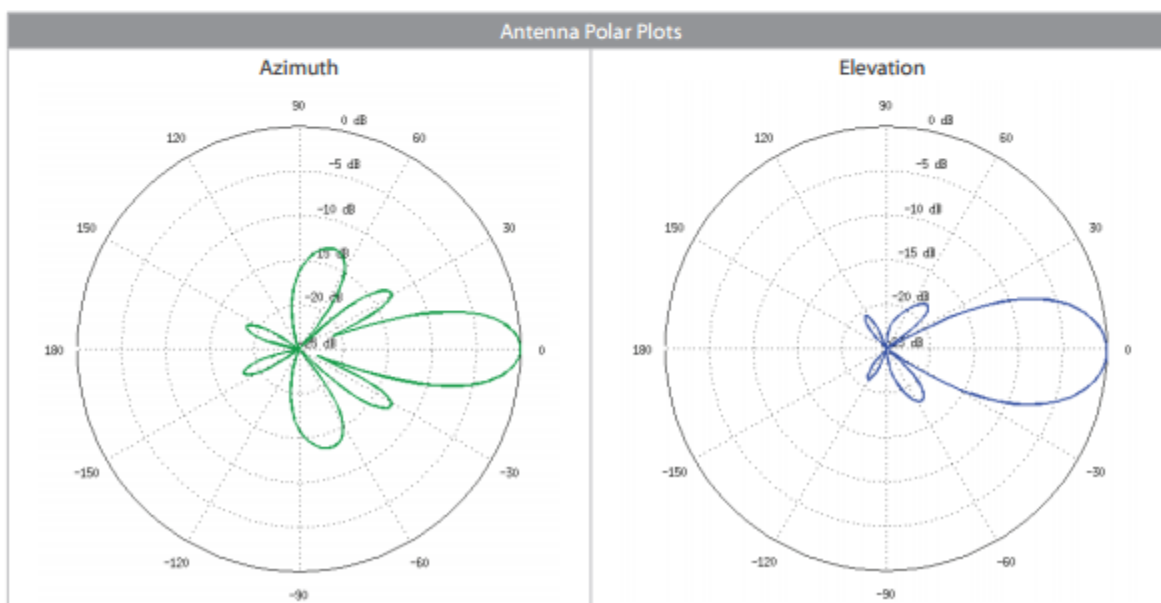
Physical / Electrical / Environmental	
Enclosure Characteristics	Outdoor UV Stabilized Plastic
Mounting Kit	Pole Mounting Kit (Included)
Max. Power Consumption	3W
Power Supply	24V, 0.5A PoE Adapter (Included)
Power Method	Passive Power over Ethernet (Pairs 4, 5+; 7, 8 Return)
Operating Temperature	-30 to 75° C (-22 to 167° F)
Operating Humidity	5 to 95% Condensing
Shock and Vibration	ETSI300-019-1.4
ETSI Specification	EN 302 326 DN2



Specifications

AG-HP-2G16	
Dimensions (Mount Included)	370 x 270 x 270 mm (14.57 x 10.63 x 10.63")
Weight (Mount Included)	1478 g (3.258 lb)
Wind Survivability	200 km/h (125 mph)
Wind Loading	58 N @ 200 km/h (13 lbf @ 125 mph)
Operating Frequency	2412 - 2462 MHz
Max. VSWR	1.5:1
Gain	16 dBi

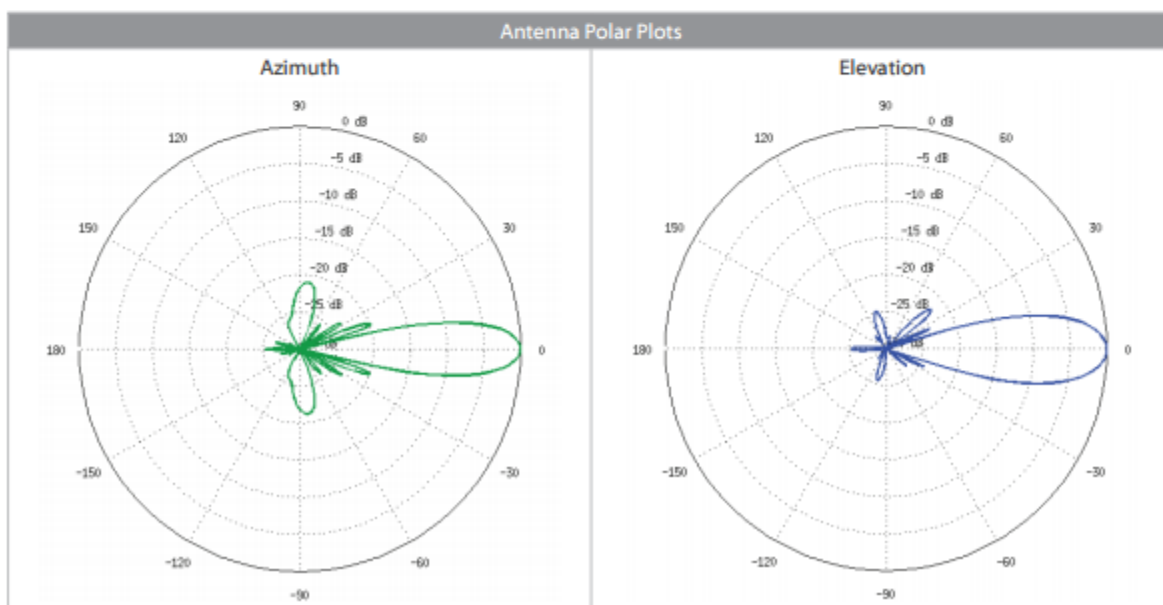
AG-HP-2G16 Output Power: 28 dBm							
TX Power Specifications				RX Power Specifications			
Modulation	Data Rate	Avg. TX	Tolerance	Modulation	Data Rate	Sensitivity	Tolerance
11g	1 - 24 Mbps	28 dBm	± 2 dB	11g	1 - 24 Mbps	-97 dBm min.	± 2 dB
	36 Mbps	26 dBm	± 2 dB		36 Mbps	-80 dBm	± 2 dB
	48 Mbps	25 dBm	± 2 dB		48 Mbps	-77 dBm	± 2 dB
	54 Mbps	24 dBm	± 2 dB		54 Mbps	-75 dBm	± 2 dB
11n / airMAX	MCS0	28 dBm	± 2 dB	11n / airMAX	MCS0	-96 dBm	± 2 dB
	MCS1	28 dBm	± 2 dB		MCS1	-95 dBm	± 2 dB
	MCS2	28 dBm	± 2 dB		MCS2	-92 dBm	± 2 dB
	MCS3	28 dBm	± 2 dB		MCS3	-90 dBm	± 2 dB
	MCS4	27 dBm	± 2 dB		MCS4	-86 dBm	± 2 dB
	MCS5	25 dBm	± 2 dB		MCS5	-83 dBm	± 2 dB
	MCS6	23 dBm	± 2 dB		MCS6	-77 dBm	± 2 dB
	MCS7	22 dBm	± 2 dB		MCS7	-74 dBm	± 2 dB



Specifications

AG-HP-2G20	
Dimensions (Mount Included)	620 x 460 x 390 mm (24.41 x 18.11 x 15.35")
Weight (Mount Included)	2603 g (5.739 lb)
Wind Survivability	200 km/h (125 mph)
Wind Loading	102 N @ 200 km/h (23 lbf @ 125 mph)
Operating Frequency	2412 - 2462 MHz
Max. VSWR	1.5:1
Gain	20 dBi

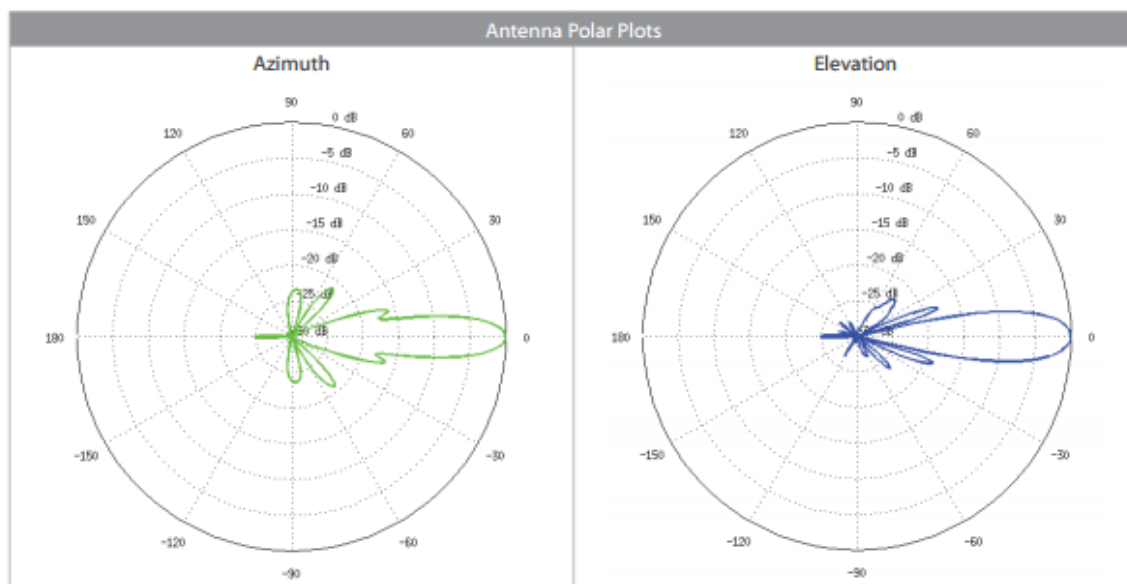
AG-HP-2G20 Output Power: 28 dBm							
TX Power Specifications				RX Power Specifications			
Modulation	Data Rate	Avg. TX	Tolerance	Modulation	Data Rate	Sensitivity	Tolerance
11g	1 - 24 Mbps	28 dBm	± 2 dB	11g	1 - 24 Mbps	-97 dBm min.	± 2 dB
	36 Mbps	26 dBm	± 2 dB		36 Mbps	-80 dBm	± 2 dB
	48 Mbps	25 dBm	± 2 dB		48 Mbps	-77 dBm	± 2 dB
	54 Mbps	24 dBm	± 2 dB		54 Mbps	-75 dBm	± 2 dB
11n / airMAX	MCS0	28 dBm	± 2 dB	11n / airMAX	MCS0	-96 dBm	± 2 dB
	MCS1	28 dBm	± 2 dB		MCS1	-95 dBm	± 2 dB
	MCS2	28 dBm	± 2 dB		MCS2	-92 dBm	± 2 dB
	MCS3	28 dBm	± 2 dB		MCS3	-90 dBm	± 2 dB
	MCS4	27 dBm	± 2 dB		MCS4	-86 dBm	± 2 dB
	MCS5	25 dBm	± 2 dB		MCS5	-83 dBm	± 2 dB
	MCS6	23 dBm	± 2 dB		MCS6	-77 dBm	± 2 dB
	MCS7	22 dBm	± 2 dB		MCS7	-74 dBm	± 2 dB



Specifications

AG-HP-5G23	
Dimensions (Mount Included)	370 x 270 x 260 mm (14.57 x 10.63 x 10.24")
Weight (Mount Included)	1452 g (3.201 lb)
Wind Survivability	200 km/h (125 mph)
Wind Loading	58 N @ 200 km/h (13 lbf @ 125 mph)
Operating Frequency	Worldwide: 5170 – 5875 MHz USA: 5725 – 5850 MHz
Max. VSWR	1.5:1
Gain	23 dBi

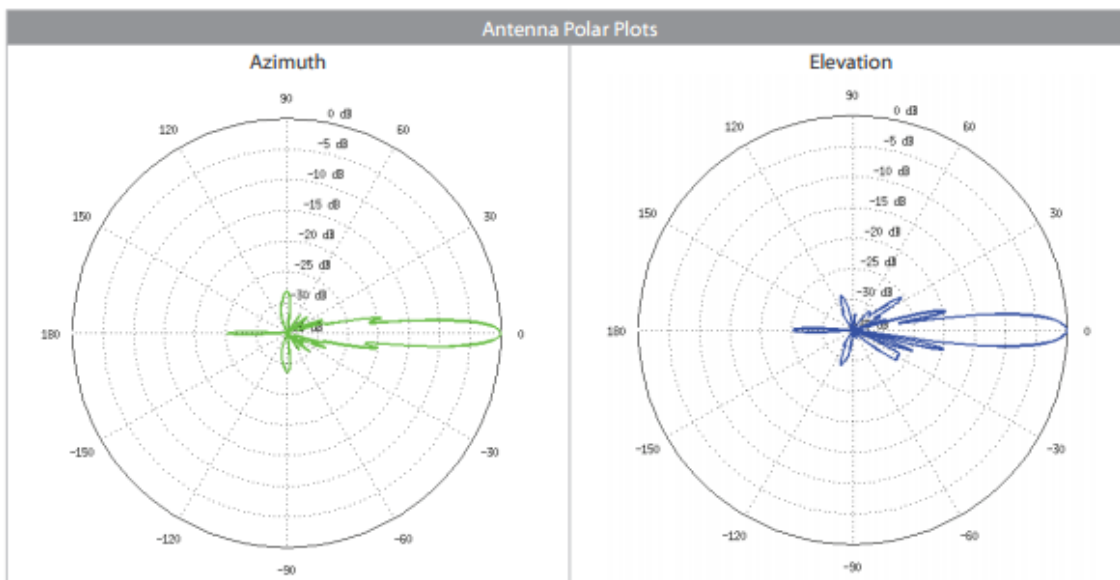
AG-HP-5G23 Output Power: 25 dBm							
TX Power Specifications				RX Power Specifications			
Modulation	Data Rate	Avg. TX	Tolerance	Modulation	Data Rate	Sensitivity	Tolerance
11a	1 - 24 Mbps	25 dBm	± 2 dB	11a	1 - 24 Mbps	-97 dBm min.	± 2 dB
	36 Mbps	24 dBm	± 2 dB		36 Mbps	-90 dBm	± 2 dB
	48 Mbps	22 dBm	± 2 dB		48 Mbps	-86 dBm	± 2 dB
	54 Mbps	21 dBm	± 2 dB		54 Mbps	-84 dBm	± 2 dB
11n /airMAX	MCS0	25 dBm	± 2 dB	11n /airMAX	MCS0	-97 dBm	± 2 dB
	MCS1	25 dBm	± 2 dB		MCS1	-96 dBm	± 2 dB
	MCS2	25 dBm	± 2 dB		MCS2	-93 dBm	± 2 dB
	MCS3	24 dBm	± 2 dB		MCS3	-91 dBm	± 2 dB
	MCS4	23 dBm	± 2 dB		MCS4	-87 dBm	± 2 dB
	MCS5	22 dBm	± 2 dB		MCS5	-84 dBm	± 2 dB
	MCS6	21 dBm	± 2 dB		MCS6	-78 dBm	± 2 dB
	MCS7	19 dBm	± 2 dB		MCS7	-75 dBm	± 2 dB



Specifications

AG-HP-5G27	
Dimensions (Mount Included)	620 x 460 x 360 mm (24.41 x 18.11 x 14.17")
Weight (Mount Included)	2585 g (5.699 lb)
Wind Survivability	200 km/h (125 mph)
Wind Loading	102 N @ 200 km/h (23 lbf @ 125 mph)
Operating Frequency	Worldwide: 5170 – 5875 MHz USA: 5725 – 5850 MHz
Max. VSWR	1.5:1
Gain	27 dBi

AG-HP-5G27 Output Power: 25 dBm							
TX Power Specifications				RX Power Specifications			
Modulation	Data Rate	Avg. TX	Tolerance	Modulation	Data Rate	Sensitivity	Tolerance
11a	1 - 24 Mbps	25 dBm	± 2 dB	11a	1 - 24 Mbps	-97 dBm min.	± 2 dB
	36 Mbps	24 dBm	± 2 dB		36 Mbps	-90 dBm	± 2 dB
	48 Mbps	22 dBm	± 2 dB		48 Mbps	-86 dBm	± 2 dB
	54 Mbps	21 dBm	± 2 dB		54 Mbps	-84 dBm	± 2 dB
11n / airMAX	MCS0	25 dBm	± 2 dB	11n / airMAX	MCS0	-97 dBm	± 2 dB
	MCS1	25 dBm	± 2 dB		MCS1	-96 dBm	± 2 dB
	MCS2	25 dBm	± 2 dB		MCS2	-93 dBm	± 2 dB
	MCS3	24 dBm	± 2 dB		MCS3	-91 dBm	± 2 dB
	MCS4	23 dBm	± 2 dB		MCS4	-87 dBm	± 2 dB
	MCS5	22 dBm	± 2 dB		MCS5	-84 dBm	± 2 dB
	MCS6	21 dBm	± 2 dB		MCS6	-78 dBm	± 2 dB
	MCS7	19 dBm	± 2 dB		MCS7	-75 dBm	± 2 dB



Specifications are subject to change. Ubiquiti products are sold with a limited warranty described at: www.ubnt.com/support/warranty
 ©2013-2016 Ubiquiti Networks, Inc. All rights reserved. Ubiquiti, Ubiquiti Networks, the Ubiquiti U logo, the Ubiquiti beam logo, airGrid, airMAX, airOS, and InnerFeed are trademarks or registered trademarks of Ubiquiti Networks, Inc. in the United States and in other countries. All other trademarks are the property of their respective owners.

Chameleon™

1.3 MP CCD + USB INTERFACE + COMPACT

POINT GREY
Innovation in Imaging

- **USB 2.0 480 Mb/s digital video camera**
- **High quality 1.3 MP Sony® EXview HAD CCD®**
- **Ultra-compact and lightweight**
- **General purpose I/O for trigger and strobe**
- **Imaging and control software included**

The Chameleon™ USB 2.0 digital video camera from Point Grey Research is a complete, cost effective and reliable imaging solution. A high sensitivity Sony EXview HAD CCD sensor, combined with a hi-speed USB 2.0 digital interface, makes the Chameleon an ideal choice for demanding imaging applications such as object and gesture tracking, test and measurement, life science and bioscience, augmented reality, multitouch display, security and biometrics, and robot guidance.



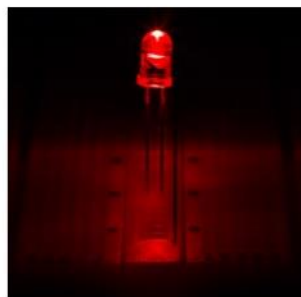
Specification	CMLN-13S2M/C
Image Sensor Type	Sony progressive scan interline transfer CCD's with square pixels and global shutter
Image Sensor Model	ICX445 1/3" EXview HAD CCD™
Maximum Resolution	1296(H) x 964(V)
Pixel Size	3.75µm x 3.75µm
Analog-to-Digital Converter	Analog Devices 12-bit ADC
Video Data Output	8, and 16-bit digital data
Image Data Formats	Y8, Y16 (monochrome), 8-bit and 16-bit raw Bayer data (color models)
Digital Interface	5-pin Mini-B USB 2.0 digital interface for camera control, video data transmission, and power
Transfer Rates	480 Mbit/s
Maximum Frame Rate	1296x964 Y8 at 18 FPS
Partial Image Modes	pixel binning and region of interest modes via Format_7
General Purpose I/O Ports	7-pin JST GPIO connector, 4 pins for trigger and strobe, 1 pin +3.3 V, 1 VEXT pin for external power
Gain Control	automatic / manual / one-push gain modes, programmable via software, 0 dB to 24 dB in 0.04 dB increments
Shutter Speed	automatic / manual / one-push modes, programmable via software, 0.01 ms to greater than 10 s (extended shutter mode)
Synchronization	via external trigger
External Trigger Modes	DCAM v1.31 Trigger Modes 0, 1 (bulb trigger), 3, and 14 (overlapped trigger and transfer)
Voltage Requirements	4.745 to 5.25 V via the Mini B USB 2.0 interface or JST 7-pin GPIO connector
Power Consumption	2 W (max) at 5 V
Dimensions (W x D x H)	44 mm x 25.5 mm x 41 mm (excluding optics)
Mass	37 grams (including tripod mounting bracket)
Memory Storage	3 memory channels for custom camera settings
Lens Mount	CS-mount (5mm C-mount adapter included)
Emissions Compliance	Complies with CE rules and Part 15 Class B of FCC Rules
Operating Temperature	0° to 45°C
Storage Temperature	-30° to 60°C
Warranty	1 year

Sony CCD

Resolution	1296 x 964
Frame Rate	18 FPS
Megapixels	1.3 MP
Chroma	Mono
Sensor Name	Sony ICX445
Sensor Type	CCD
Readout Method	Global shutter
Sensor Format	1/3"
Pixel Size	3.75 μm
Lens Mount	CS-mount
ADC	12-bit
Quantum Efficiency (% at 525 nm)	64
Temporal Dark Noise (e-)	8.82
Absolute Sensitivity Threshold (γ)	6421
Dynamic Range (dB)	56.77
Gain Range	0 dB to 24 dB
Exposure Range	0.01 ms to 10 seconds
Trigger Modes	Standard, bulb, skip frames, overlapped
Partial Image Modes	Pixel binning, ROI
Image Processing	Color/Greyscale conversion, gamma, white balance
User Sets	2 memory channels for custom camera settings
Flash Memory	256 KB non-volatile memory
Non-isolated I/O Ports	2 bi-directional
Serial Port	1 (over non-isolated I/O)
Auxiliary Output	3.3 V, 150 mA maximum
Interface	USB 2.0
Power Requirements	4.745 to 5.25 V via Mini-B USB 2.0 interface or JST 7-pin GPIO connector
Power Consumption (Maximum)	2 W
Dimensions	25.5 mm x 44 mm x 41 mm
Mass	37 grams
Machine Vision Standard	IIDC v1.31
Compliance	CE, FCC, KCC, RoHS
Temperature (Operating)	0° to 45°C
Temperature (Storage)	-30° to 60°C
Humidity (Operating)	20 to 80% (no condensation)
Humidity (Storage)	20 to 95% (no condensation)
Warranty	1 year

Mead Telescope

	6 inch SC	8 inch SC	10 inch SC	80mm APO	115mm APO	SolarMax™ II 60	SolarMax™ II 90
Product Number	0610-08-01	0810-08-01	1010-08-01	0306-08-01	4507-08-01	SMT60-10-LX80	SMT90-15-LX80
UPC	7 09942 38132 0	7 09942 38121 4	7 09942 38122 1	7 09942 38127 6	7 09942 38128 3	7 09942 38129 0	7 09942 38130 6
Optical Design	Schmidt-Cassegrain			Apochromatic Refractor		Refractor	
Aperture	6 inch	8 inch	10 inch	80mm	115mm	60mm	90mm
Focal Length and Focal Ratio	1524mm, f/10	2034mm, f/10	2540mm, f/10	480mm, f/6	805mm, f/7	400mm, f/6.6	800mm, f/8.8
Optical Coatings	UHTC			Fully Multi-Coated		Fully Coated	
Resolving Power (Dawes Limit)	0.760 arcseconds	0.570 arcseconds	0.456 arcseconds	1.45 arcseconds	1.01 arcseconds	1.93 arcseconds	1.29 arcseconds
Secondary Obstruction (% by area)	21.18	13.65	11.9	N/A	N/A	N/A	N/A
Viewfinder	8x50mm with cross-hair reticle			Red Dot	8x50mm with cross-hair reticle	Sol-ranger projection type	
Eyepiece	26mm Series 4000 Super Plössl					25mm Cemax	
Diagonal	1.25 inch diagonal			2 inch with 99% reflectivity		1.25 inch blocking filter 10	1.25 inch blocking filter 15
Materials							
Primary and Secondary Mirrors	Low-expansion borosilicate glass			N/A			
Correcting Plate/Lens	Aspheric high-spectral transmission Borofloat glass from Schott AG Germany			FPL53 extra-low dispersion glass	FK61 extra-low dispersion glass	BK-7	
Optical Tube	Aluminum						



5mm Red LED - 627 nm - T1 3/4 LED w/ 8 Degree Viewing Angle

[Write a Review](#)

Part Number: RL5-R12008

UPC: 847781012101



Product Description

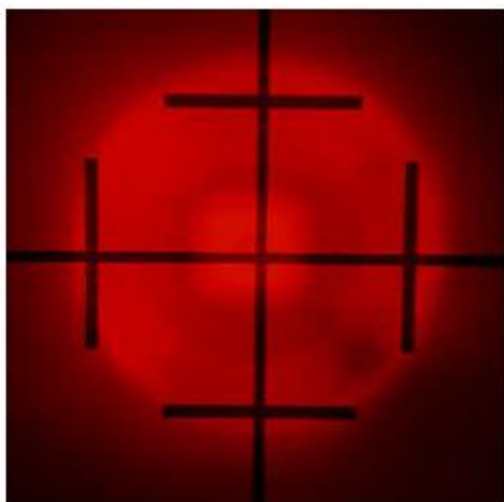
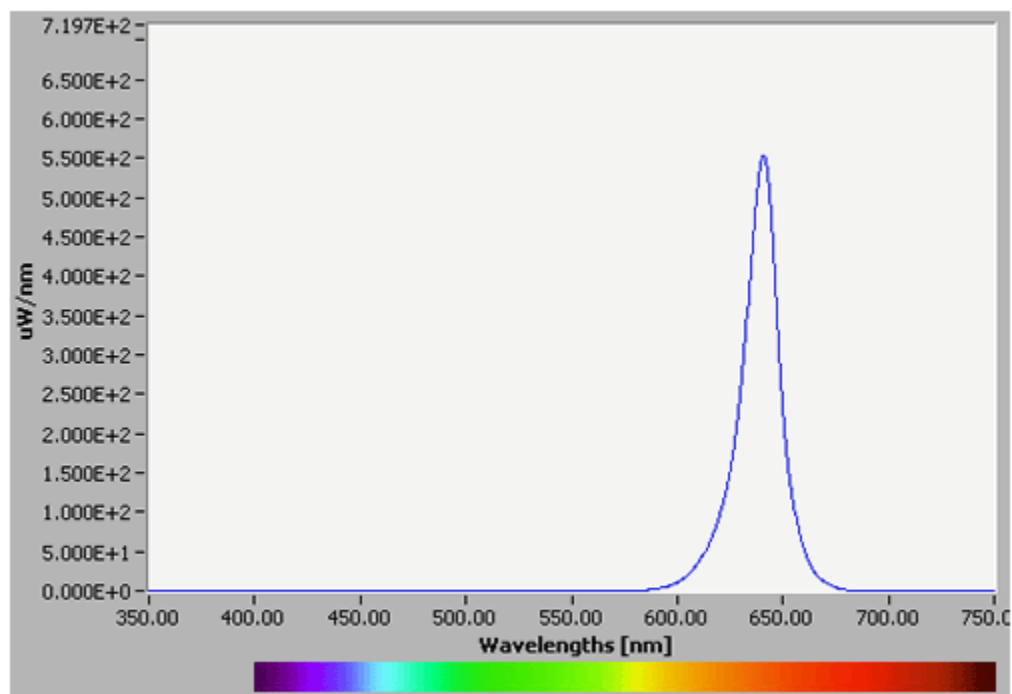
Red 5mm through hole LED featuring a 627nm wavelength, 12,000mcd. with 8 degree viewing angle. Component LEDs are sensitive electronic devices and require some knowledge of electronic circuits to operate them. Price listed is per unit, however, bulk discounts are available and are automatically applied to your order.

Specifications

Continuous Forward Current	50 mA	Forward Voltage	2.3
LED Color	Red	LED Package	5 mm (T-1 3/4)
Lens	Clear	Lumen	0.2 Lumen
Maximum Forward Voltage	2.4V	Millicandela	12000mcd
Operating Temperature	-40~+85 °C	Peak Forward Current	200mA
Power Dissipation	125mW	Reverse Current	10µA
Reverse Voltage	5V	Storage Temperature	-40~+85 °C
Total Power Consumption	0.11 Watts	Tube Diameter	T1-3/4
Viewing Angle	8 degree	Wavelength	627 nm

Package Dimensions: 0.39" (1cm) x 0.24" (1cm) x 0.24" (1cm)

Package Weight: 0.01oz (0kg)



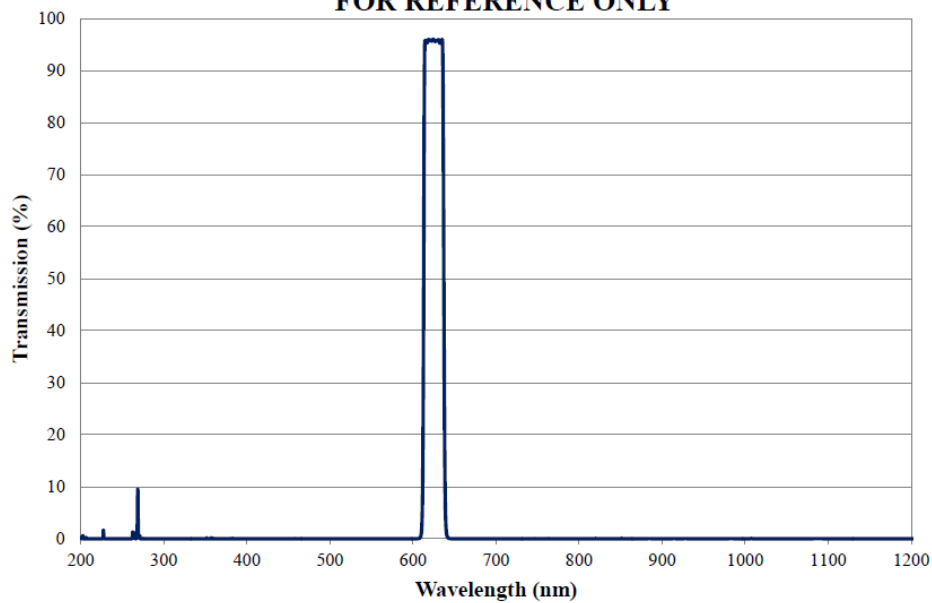
625 nm CWL, 25 mm Dia. Hard Coated OD 4 25 nm Bandpass Filter



Coating Curve

Edmund Optics Inc.
USA | Asia | Europe

625nm Hard Coated Bandpass Interference Filter: 25nm FWHM OD >4.0 Coating Performance FOR REFERENCE ONLY

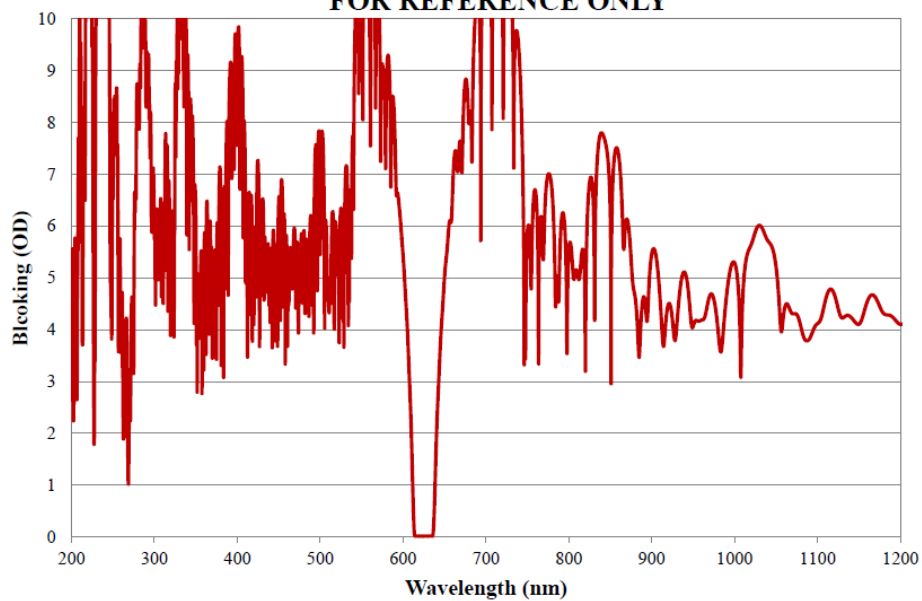


EO Edmund
optics | worldwide
www.edmundoptics.com

Coating Curve

Edmund Optics Inc.
USA | Asia | Europe

625nm Hard Coated Bandpass Interference Filter OD >4.0 Coating Performance FOR REFERENCE ONLY



 **Edmund**
optics | worldwide
www.edmundoptics.com

METAR/SPECI from KCOS, Colorado Springs, City Of Colorado Springs Municipal Airport (United States).

SA	13/08/2015 18:54->	METAR KCOS 131854Z 00000KT 10SM SCT090 SCT200 30/08 A3033 RMK AO2 SLP167 T03000078=
SA	13/08/2015 17:54->	METAR KCOS 131754Z VRB06KT 10SM FEW080 SCT200 30/08 A3035 RMK AO2 SLP173 T03000083 10300 20194 58003=
SA	13/08/2015 16:54->	METAR KCOS 131654Z 10007KT 10SM FEW080 SCT200 29/08 A3036 RMK AO2 SLP174 T02940078=
SA	13/08/2015 15:54->	METAR KCOS 131554Z VRB06KT 10SM FEW080 SCT150 29/08 A3036 RMK AO2 SLP173 T02940078=
SA	13/08/2015 14:54->	METAR KCOS 131454Z 33007KT 10SM SCT140 27/09 A3036 RMK AO2 SLP180 T02720094 51007=
SA	13/08/2015 13:54->	METAR KCOS 131354Z 33005KT 10SM BKN130 23/10 A3036 RMK AO2 SLP185 ACC S-W T02330100=
SA	13/08/2015 12:54->	METAR KCOS 131254Z 34005KT 10SM BKN130 21/11 A3035 RMK AO2 SLP188 ACC SW T02060106=
SA	13/08/2015 11:54->	METAR KCOS 131154Z 00000KT 10SM FEW130 BKN160 BKN250 21/10 A3034 RMK AO2 SLP175 T02060100 10228 20200 56002=
SA	13/08/2015 10:54->	METAR KCOS 131054Z 35004KT 10SM SCT120 BKN140 BKN220 21/11 A3034 RMK AO2 SLP171 T02060106=
SA	13/08/2015 09:54->	METAR KCOS 130954Z 33007KT 10SM FEW110 SCT130 BKN220 21/11 A3033 RMK AO2 SLP169 T02110106=
SA	13/08/2015 08:54->	METAR KCOS 130854Z 31009KT 10SM SCT110 BKN140 22/09 A3034 RMK AO2 SLP171 T02220094 58009=
SA	13/08/2015 07:54->	METAR KCOS 130754Z 30011KT 10SM FEW080 BKN130 22/10 A3035 RMK AO2 PK WND 31027/0700 SLP173 T02220100=
SA	13/08/2015 06:54->	METAR KCOS 130654Z 30019G27KT 10SM BKN140 BKN160 22/10 A3037 RMK AO2 PK WND 30027/0653 SLP181 CB DSIPTD T02220100 403170150=
SA	13/08/2015 05:54->	METAR KCOS 130554Z 36009KT 10SM SCT090 BKN120 22/11 A3038 RMK AO2 TSB14E52 SLP186 OCNL LTGICCG DSNT W CB DSNT W MOV NE 60000 T02170111 10283 20217 51008=
SP	13/08/2015 05:17->	<i>SPECI KCOS 130517Z 36011KT 10SM TS SCT090CB BKN120 23/11 A3038 RMK AO2 TSB14 OCNL LTGICCG VC N TS VC N MOV NE T02280111=</i>
SA	13/08/2015 04:54->	METAR KCOS 130454Z 02005KT 10SM SCT090 BKN120 23/12 A3039 RMK AO2 SLP189 OCNL LTGICCG DSNT W-NW CB DSNT W-NW MPV NE T02330117=
SA	13/08/2015 03:54->	METAR KCOS 130354Z 29008KT 10SM FEW090 BKN120 BKN200 24/11 A3035 RMK AO2 SLP182 OCNL LTGICCG DSNT W-NW CB DSNT W-NW MOV E T02390106=
SA	13/08/2015 02:54->	METAR KCOS 130254Z 31007KT 10SM FEW090 SCT110 BKN250 23/12 A3034 RMK AO2 SLP183 OCNL DSNT W CB DSNT W MOV E 60000 T02330117 51006=
SA	13/08/2015 01:54->	METAR KCOS 130154Z 31010KT 10SM SCT095 BKN120 BKN250 24/12 A3032 RMK AO2 RAE25 SLP183 P0000 T02390117=
SA	13/08/2015 00:54->	METAR KCOS 130054Z COR 28009G25KT 10SM -RA SCT075 BKN100

[Product Index](#) > [Optoelectronics](#) > [Laser Diodes](#) > [Quarton Inc. VLM-635-01-LPA](#)



Product Overview	
Digi-Key Part Number	VLM-635-01-LPA-ND
Quantity Available	204 Can ship immediately
Manufacturer	Quarton Inc.
Manufacturer Part Number	VLM-635-01-LPA
Description	Laser Diode 635nm 3mW 3V 40mA Cylinder (10.4mm Dia)
Lead Free Status / RoHS Status	Lead free / RoHS Compliant
Manufacturer Standard Lead Time	4 Weeks

Documents & Media	
Datasheets	VLM-635-01 LPA , VLM-650-01 LPA
Online Catalog	Red Laser Beam Diode Module

Product Attributes		Select All	<input type="checkbox"/>
Category	Optoelectronics		<input checked="" type="checkbox"/>
Family	Laser Diodes		<input checked="" type="checkbox"/>
Manufacturer	Quarton Inc.		<input type="checkbox"/>
Series	-		<input type="checkbox"/>
Part Status	Active		<input type="checkbox"/>
Wavelength	635nm		<input type="checkbox"/>
Voltage - Input	3V		<input type="checkbox"/>
Current Rating	40mA		<input type="checkbox"/>
Power (Watts)	3mW		<input type="checkbox"/>
Package / Case	Cylinder (10.4mm Dia)		<input type="checkbox"/>

Appendix C: XML Code

XML Example File

```

<?xml version="1.0"?>

<!-- taipas frequency sweep and adc_capture (I and Q) -->

<!-- start-time="30" for relative time start in 30 seconds -->

<test-instructions start_time="30">

<!-- port is optional. default= 9450 -->

<jobs_hostname="taipas-tx"><command time_offset="00.020"> /home/taipas/taipas_install/bin/FreqSynthController -
f320.000000000 </command><command time_offset="00.040"> /home/taipas/taipas_install/bin/FreqSynthController -
f323.153000000 </command><command time_offset="00.060"> /home/taipas/taipas_install/bin/FreqSynthController -
f324.153000000 </command><command time_offset="00.080"> /home/taipas/taipas_install/bin/FreqSynthController -
f324.653000000 </command><command time_offset="00.100"> /home/taipas/taipas_install/bin/FreqSynthController -
f325.153000000 </command><command time_offset="00.120"> /home/taipas/taipas_install/bin/FreqSynthController -
f325.653000000 </command><command time_offset="00.140"> /home/taipas/taipas_install/bin/FreqSynthController -
f326.153000000 </command><command time_offset="00.160"> /home/taipas/taipas_install/bin/FreqSynthController -
f327.153000000 </command><command time_offset="00.180"> /home/taipas/taipas_install/bin/FreqSynthController -
f330.000000000 </command><command time_offset="00.200"> /home/taipas/taipas_install/bin/FreqSynthController -
f335.000000000 </command><command time_offset="00.220"> /home/taipas/taipas_install/bin/FreqSynthController -
f340.000000000 </command>

<!--section-demarc-->

<command time_offset="00.240"> /home/taipas/taipas_install/bin/FreqSynthController -
f324.153000000 </command><command time_offset="00.260">
/home/taipas/taipas_install/bin/FreqSynthController -f324.253000000 </command><command
time_offset="00.280"> /home/taipas/taipas_install/bin/FreqSynthController -f324.353000000
</command><command time_offset="00.300">
/home/taipas/taipas_install/bin/FreqSynthController -f324.453000000 </command><command

```

```

time_offset="00.320"> /home/taipas/taipas_install/bin/FreqSynthController -f324.553000000
</command><command time_offset="00.340">
/home/taipas/taipas_install/bin/FreqSynthController -f324.653000000 </command><command
time_offset="00.360"> /home/taipas/taipas_install/bin/FreqSynthController -f324.753000000
</command><command time_offset="00.380">
/home/taipas/taipas_install/bin/FreqSynthController -f324.853000000 </command><command
time_offset="00.400"> /home/taipas/taipas_install/bin/FreqSynthController -f324.953000000
</command><command time_offset="00.420">
/home/taipas/taipas_install/bin/FreqSynthController -f325.053000000 </command><command
time_offset="00.440"> /home/taipas/taipas_install/bin/FreqSynthController -f325.153000000
</command>
<!--section-demarc-->
<command time_offset="00.460"> /home/taipas/taipas_install/bin/FreqSynthController -
f325.153000000 </command><command time_offset="00.480">
/home/taipas/taipas_install/bin/FreqSynthController -f325.253000000 </command><command
time_offset="00.500"> /home/taipas/taipas_install/bin/FreqSynthController -f325.353000000
</command><command time_offset="00.520">
/home/taipas/taipas_install/bin/FreqSynthController -f325.453000000 </command><command
time_offset="00.540"> /home/taipas/taipas_install/bin/FreqSynthController -f325.553000000
</command><command time_offset="00.560">
/home/taipas/taipas_install/bin/FreqSynthController -f325.653000000 </command><command
time_offset="00.580"> /home/taipas/taipas_install/bin/FreqSynthController -f325.753000000
</command><command time_offset="00.600">

```

```

/home/taipas/taipas_install/bin/FreqSynthController -f325.853000000 </command><command
time_offset="00.620"> /home/taipas/taipas_install/bin/FreqSynthController -f325.953000000
</command><command time_offset="00.640">
/home/taipas/taipas_install/bin/FreqSynthController -f326.053000000 </command><command
time_offset="00.660"> /home/taipas/taipas_install/bin/FreqSynthController -f326.153000000
</command></jobs><jobs hostname="taipas-rx"><command time_offset="00.010">
/home/taipas/adc_write_data.sh </command><command time_offset="00.020">
/home/taipas/taipas_install/bin/FreqSynthController -f320.001000000 </command><command
time_offset="00.040"> /home/taipas/taipas_install/bin/FreqSynthController -f323.154000000
</command><command time_offset="00.060">
/home/taipas/taipas_install/bin/FreqSynthController -f324.154000000 </command><command
time_offset="00.080"> /home/taipas/taipas_install/bin/FreqSynthController -f324.654000000
</command><command time_offset="00.100">
/home/taipas/taipas_install/bin/FreqSynthController -f325.154000000 </command><command
time_offset="00.120"> /home/taipas/taipas_install/bin/FreqSynthController -f325.654000000
</command><command time_offset="00.140">
/home/taipas/taipas_install/bin/FreqSynthController -f326.154000000 </command><command
time_offset="00.160"> /home/taipas/taipas_install/bin/FreqSynthController -f327.154000000
</command><command time_offset="00.180">
/home/taipas/taipas_install/bin/FreqSynthController -f330.001000000 </command><command
time_offset="00.200"> /home/taipas/taipas_install/bin/FreqSynthController -f335.001000000
</command><command time_offset="00.220">
/home/taipas/taipas_install/bin/FreqSynthController -f340.001000000 </command>

```

```

<!--section-demarc-->

<command time_offset="00.240"> /home/taipas/taipas_install/bin/FreqSynthController -
f324.154000000 </command><command time_offset="00.260">
/home/taipas/taipas_install/bin/FreqSynthController -f324.254000000 </command><command
time_offset="00.280"> /home/taipas/taipas_install/bin/FreqSynthController -f324.354000000
</command><command time_offset="00.300">
/home/taipas/taipas_install/bin/FreqSynthController -f324.454000000 </command><command
time_offset="00.320"> /home/taipas/taipas_install/bin/FreqSynthController -f324.554000000
</command><command time_offset="00.340">
/home/taipas/taipas_install/bin/FreqSynthController -f324.654000000 </command><command
time_offset="00.360"> /home/taipas/taipas_install/bin/FreqSynthController -f324.754000000
</command><command time_offset="00.380">
/home/taipas/taipas_install/bin/FreqSynthController -f324.854000000 </command><command
time_offset="00.400"> /home/taipas/taipas_install/bin/FreqSynthController -f324.954000000
</command><command time_offset="00.420">
/home/taipas/taipas_install/bin/FreqSynthController -f325.054000000 </command><command
time_offset="00.440"> /home/taipas/taipas_install/bin/FreqSynthController -f325.154000000
</command>

<!--section-demarc-->

<command time_offset="00.460"> /home/taipas/taipas_install/bin/FreqSynthController -
f325.154000000 </command><command time_offset="00.480">
/home/taipas/taipas_install/bin/FreqSynthController -f325.254000000 </command><command
time_offset="00.500"> /home/taipas/taipas_install/bin/FreqSynthController -f325.354000000

```

```

</command><command                                time_offset="00.520">
/home/taipas/taipas_install/bin/FreqSynthController -f325.454000000 </command><command
time_offset="00.540"> /home/taipas/taipas_install/bin/FreqSynthController -f325.554000000
</command><command                                time_offset="00.560">
/home/taipas/taipas_install/bin/FreqSynthController -f325.654000000 </command><command
time_offset="00.580"> /home/taipas/taipas_install/bin/FreqSynthController -f325.754000000
</command><command                                time_offset="00.600">
/home/taipas/taipas_install/bin/FreqSynthController -f325.854000000 </command><command
time_offset="00.620"> /home/taipas/taipas_install/bin/FreqSynthController -f325.954000000
</command><command                                time_offset="00.640">
/home/taipas/taipas_install/bin/FreqSynthController -f326.054000000 </command><command
time_offset="00.660"> /home/taipas/taipas_install/bin/FreqSynthController -f326.154000000
</command></jobs></test-instructions>

```

XML File Instructions

FINAL XML FILE FOR COLLECTION

```
<?xml version="1.0"?>
```

```
<!-- taipas frequency sweep and adc_capture (I and Q) -->
```

```
<!-- start-time="2" for relative time start (start in 2 seconds) -->
```

```
<!-- the start-time allows all commands to be pushed to and queued in the
JobController_Server -->
```

```
<test-instructions start_time="2">
```

```

<!-- port is optional. default= 9450 -->

<!-- -->

<!-- -->

<!-- -->

<!-- THIS CONTROLS THE TX BOX COMPUTER -->

<!-- -->

<!-- -->

<!-- -->

<jobs hostname="taipas-tx"><command time_offset="00.100"> echo "Sending Commands
to Tx computer now..." </command>

<!--Turn on data collection for other sensors -->

<!-- blank line -->

<!-- Hygrometer samples -->

<command time_offset="00.250">
/home/taipas/0_RunTaipas/get_hygro_dataTx1733_10hz10sec.sh </command>

<!-- Anemometer samples -->

<command time_offset="00.500">
/home/taipas/0_RunTaipas/get_anemo_dataTx_10hz10sec.sh </command>

<!-- Scintillation samples -->

<command time_offset="00.750">
/home/taipas/0_RunTaipas/get_scintillometer_dataTx_10seconds.sh </command>

<!-- Change frequencies in synch with the receiver according to this schedule -->

<!-- Don't forget that the receiver ADCs don't start collection until 0.900 seconds -->

```

```

<command time_offset="01.000"> /home/taipas/taipas_install/bin/FreqSynthController -L
/home/taipas/tmp/freqlim_Tx_522.txt -
F330.000000000,325.000000000,320.000000000,319.000000000,320.000000000,323.15300000
0,324.153000000,324.653000000,325.153000000,325.653000000,326.153000000,327.15300000
0,330.000000000,335.000000000,340.000000000,324.153000000,324.253000000,324.35300000
0,324.453000000,324.553000000,324.653000000,324.753000000,324.853000000,324.95300000
0,325.053000000,325.153000000,325.153000000,325.253000000,325.353000000,325.45300000
0,325.553000000,325.653000000,325.753000000,325.853000000,325.953000000,326.05300000
0,326.153000000,320.000000000,323.153000000,324.153000000,324.653000000,325.15300000
0,325.653000000,326.153000000,327.153000000,330.000000000,335.000000000,340.00000000
0,324.153000000,324.253000000,324.353000000,324.453000000,324.553000000,324.65300000
0,324.753000000,324.853000000,324.953000000,325.053000000,325.153000000,325.15300000
0,325.253000000,325.353000000,325.453000000,325.553000000,325.653000000,325.75300000
0,325.853000000,325.953000000,326.053000000,326.153000000 -t 50 </command>

<!-- Take a picture immediately after data collection -->

<command time_offset="09.300"> /home/taipas/0_RunTaipas/make_snapshot_Tx.sh
</command>

<!-- Make a video of duration 1 -THIS DOES NOT WORK -->

<!--command time_offset="09.000"-->

<!--/home/taipas/0_RunTaipas/make_video_Tx.sh 1-->

<!--/command-->

<!-- Move Tx data files to the data directory from tmp directory-->

```

```

<!-- The Tx data directory is actually remotely mapped to the Tx /home/taipas/data_store/tx/
directory -->

<command time_offset="14.750"> echo "Moving data now..." </command><command
time_offset="15.000"> /home/taipas/0_RunTaipas/move_Tx_data.sh </command>

<!-- tell me I'm done-->

<command time_offset="20.000"> echo "Transmitter script is Done. Hit Enter to
continue..." </command></jobs>

<!-- -->

<!-- -->

<!-- -->

<!-- THIS CONTROLS THE RX BOX COMPUTER -->

<!-- -->

<!-- -->

<!-- -->

<jobs hostname="taipas-rx"><command time_offset="00.100"> echo "Sending Commands
to Rx computer now..." </command>

<!--Turn on data collection for other sensors -->

<!-- Hygrometer samples -->

<command time_offset="00.250">
/home/taipas/0_RunTaipas/get_hygro_dataRx1729_10hz10sec.sh </command>

<!-- Anemometer samples -->

<command time_offset="00.500">
/home/taipas/0_RunTaipas/get_anemo_dataRx_10hz10sec.sh </command>

```

```

<!-- This starts the ADC logger for the THz link; Duration must be adjusted by choosing the
correct get_adc_data_file-->

<!-- Calculate minimum duration by taking the frequency change interval time x # of
frequencies plus time before & after plus any Rx-Tx start offset time -->

<!-- For this example with 70 frequencies -->

<!-- 70 frequencies x 0.070 = 4.900 seconds -->

<!-- plus 0.100 seconds before changing frequencies to allow ADC and computers to settle -
->

<!-- plus at least 0.100 seconds after changing frequencies to allow us to easily see the end
of the data -->

<!-- plus 0.020 seconds offset to account for the Tx and Rx offset start times for changing
frequencies -->

<!-- EQUALS 5.120 seconds -->

<!-- So, select the appropriate get_adc_data_ApBCseconds.sh file where A.BC equals the
seconds of data collection-->

<command>                                time_offset="00.900">
/home/taipas/0_RunTaipas/get_adc_data_5p20seconds.sh </command>

<!-- Change frequencies in synch with the receiver according to this schedule -->

<!-- Tweaked the received frequencies so we have a measured 1MHz offset, measured at the
receiver on spectrum analyzer -->

<!-- Frequencies may be 'tweaked' by adjusting the offset, currently optimized at
325.000000000 GHz -->

```

<!-- NOTE: The time offset below is 00ms later than the transmitter to account for the transmitter response time (delay) and can be adjusted -->

<!-- The best way to determine the transmitter delay is to run a 200ms frequency change interval and determine the smallest delay in the ADC data -->

```
<command time_offset="01.020"> /home/taipas/taipas_install/bin/FreqSynthController -s
FTE4OYEV -L /home/taipas/tmp/freqtim_RxFTE4OYEV_522Short.txt -
F330.001021500,325.001021500,320.001021500,319.001021500,320.001021500,323.15402150
0,324.154021500,324.654021500,325.154021500,325.654021500,326.154021500,327.15402150
0,330.001021500,335.001021500,340.001021500,324.154021500,324.254021500,324.35402150
0,324.454021500,324.554021500,324.654021500,324.754021500,324.854021500,324.95402150
0,325.054021500,325.154021500,325.154021500,325.254021500,325.354021500,325.45402150
0,325.554021500,325.654021500,325.754021500,325.854021500,325.954021500,326.05402150
0,326.154021500,320.001021500,323.154021500,324.154021500,324.654021500,325.15402150
0,325.654021500,326.154021500,327.154021500,330.001021500,335.001021500,340.00102150
0,324.154021500,324.254021500,324.354021500,324.454021500,324.554021500,324.65402150
0,324.754021500,324.854021500,324.954021500,325.054021500,325.154021500,325.15402150
0,325.254021500,325.354021500,325.454021500,325.554021500,325.654021500,325.75402150
0,325.854021500,325.954021500,326.054021500,326.154021500 -t 50 </command><command
time_offset="01.021"> /home/taipas/taipas_install/bin/FreqSynthController -s FTE4OYF6V -L
/home/taipas/tmp/freqtim_RxFTE4OYF6_522Short.txt -
F330.001021500,325.001021500,320.001021500,319.001021500,320.001021500,323.15402150
0,324.154021500,324.654021500,325.154021500,325.654021500,326.154021500,327.15402150
0,330.001021500,335.001021500,340.001021500,324.154021500,324.254021500,324.35402150
```

```

0,324.454021500,324.554021500,324.654021500,324.754021500,324.854021500,324.95402150
0,325.054021500,325.154021500,325.154021500,325.254021500,325.354021500,325.45402150
0,325.554021500,325.654021500,325.754021500,325.854021500,325.954021500,326.05402150
0,326.154021500,320.001021500,323.154021500,324.154021500,324.654021500,325.15402150
0,325.654021500,326.154021500,327.154021500,330.001021500,335.001021500,340.00102150
0,324.154021500,324.254021500,324.354021500,324.454021500,324.554021500,324.65402150
0,324.754021500,324.854021500,324.954021500,325.054021500,325.154021500,325.15402150
0,325.254021500,325.354021500,325.454021500,325.554021500,325.654021500,325.75402150
0,325.854021500,325.954021500,326.054021500,326.154021500 -t 50 </command>

<!-- Take a picture immediately after data collection -->

<command time_offset="09.300"> /home/taipas/0_RunTaipas/make_snapshot_Rx.sh
</command>

<!-- Make a video of duration 10 - THIS DOES NOT WORK -->

<!--command time_offset="09.000"-->

<!--/home/taipas/0_RunTaipas/make_video_Rx.sh 10 -->

<!--/command-->

<!-- Move Rx data files to the data directory from tmp directory-->

<!-- The Rx data directory is actually remotely mapped to the Tx /home/taipas/data_store/rx/
directory -->

<command time_offset="14.750"> echo "Moving data now..." </command><command
time_offset="15.000"> /home/taipas/0_RunTaipas/move_Rx_data.sh </command>

<!-- tell me I'm done-->

```

```
<command time_offset="20.000"> echo "Receiver script is Done. Hit Enter to continue....."  
</command></jobs></test-instructions>
```

Appendix D: MATLAB LEEDR Source Code

```

% TAIPAS MATLAB Code for LEEDR MODEL
%%
% *Plot LEEDR Path Specific Extinction Data*

% Boulder, CO LAT 40.0274   LONG -105.2519
%% Convert Wavelength into Frequency in GHz
c = 2.997e8;
% calculate frequency and flip column about x-axis
freq=flipud(c./Wavelength/1e9);

%% Plot LEEDR Path Specific CLEAR AIR Data *****

% Build Matrices CA for wavelength and frequency plots
% - the freq plot needs columns to be flipped
CA_Matrix=[CA_1RH,CA_5RH,CA_10RH,CA_20RH,CA_50RH,CA_80RH,CA_90RH,...
           CA_95RH,CA_99RH]; % Wavelength Matrix

%flip Columns about X axis to convert order from wavelnght to frequency
CA_1RH_F=flipud(CA_1RH);
CA_5RH_F=flipud(CA_5RH);
CA_10RH_F=flipud(CA_10RH);
CA_20RH_F=flipud(CA_20RH);
CA_50RH_F=flipud(CA_50RH);
CA_80RH_F=flipud(CA_80RH);
CA_90RH_F=flipud(CA_90RH);
CA_95RH_F=flipud(CA_95RH);
CA_99RH_F=flipud(CA_99RH);

CA_Matrix_F=[CA_1RH_F,CA_5RH_F,CA_10RH_F,CA_20RH_F,CA_50RH_F,...
             CA_80RH_F,CA_90RH_F,CA_95RH_F,CA_99RH_F]; % Frequency Matrix

%% Create Wavelength Plot
figure1 = figure('Name','LEEDR Path Specific Clear Air Extinction');

% Create axes
axes1 = axes('Parent',figure1);
box(axes1,'on');
hold(axes1,'all');

% Create multiple lines using matrix input to plot
plot1 = plot(Wavelength,CA_Matrix,'Parent',axes1);
set(plot1(1),'DisplayName','CA 1% RH');
set(plot1(2),'DisplayName','CA 5% RH');
set(plot1(3),'DisplayName','CA 10% RH');
set(plot1(4),'DisplayName','CA 20% RH');
set(plot1(5),'DisplayName','CA 50% RH');
set(plot1(6),'DisplayName','CA 80% RH');

```

```

set(plot1(7), 'DisplayName', 'CA 90% RH');
set(plot1(8), 'DisplayName', 'CA 95% RH');
set(plot1(9), 'DisplayName', 'CA 99% RH');

% Create xlabel
xlabel('Wavelength');

% Create ylabel
ylabel('Attenuation in dB/km');

% Create title
title('LEEDR Clear Air Exctinction');

% Create legend
legend(axes1, 'show');

% Create line
annotation(figure1, 'line', [0.354131534569983 0.354131534569983], ...
    [0.90625 0.111979166666667], 'LineStyle', ':', 'Color', [0 1 0]);

%% Create Frequency Plot
figure1 = figure('Name', 'LEEDR Path Specific Clear Air Extinction');

% Create axes
axes1 = axes('Parent', figure1);
box(axes1, 'on');
hold(axes1, 'all');

% Create multiple lines using matrix input to plot
plot1 = plot(freq, CA_Matrix_F, 'Parent', axes1);
set(plot1(1), 'DisplayName', 'CA 1% RH');
set(plot1(2), 'DisplayName', 'CA 5% RH');
set(plot1(3), 'DisplayName', 'CA 10% RH');
set(plot1(4), 'DisplayName', 'CA 20% RH');
set(plot1(5), 'DisplayName', 'CA 50% RH');
set(plot1(6), 'DisplayName', 'CA 80% RH');
set(plot1(7), 'DisplayName', 'CA 90% RH');
set(plot1(8), 'DisplayName', 'CA 95% RH');
set(plot1(9), 'DisplayName', 'CA 99% RH');

% Create xlabel
xlabel('Frequency');

% Create ylabel
ylabel('Attenuation in dB/km');

% Create title
title('LEEDR Clear Air Exctinction');

% Create legend

```

```

legend(axes1, 'location', 'northwest');

% Create line
annotation(figure1, 'line', [0.563237774030354 0.563237774030354], ...
    [0.7854583333333333 0.1067708333333333], 'LineStyle', ':', 'Color', [0 1 0]);

%% Plot LEEDR Path Specific RAIN Air Data *****
% note: relative humidity in rain can range from 60%-100%

% Build Matrices for wavelength and frequency plots
% - the freq plot needs columns to be flipped
RAIN_Matrix=[Rain2mm_UrbanAerosols_80RH,Rain5mm_UrbanAerosols_80RH,...
    Rain12_5mm_UrbanAerosols_80RH,Rain25mm_UrbanAerosols_80RH,...
    Rain75mm_UrbanAerosols_80RH]; % Wavelength Matrix

%flip Columns about X axis to convert order from wavelength to frequency
Rain2mm_UrbanAerosols_80RH_F=flipud(Rain2mm_UrbanAerosols_80RH);
Rain5mm_UrbanAerosols_80RH_F=flipud(Rain5mm_UrbanAerosols_80RH);
Rain12_5mm_UrbanAerosols_80RH_F=flipud(Rain12_5mm_UrbanAerosols_80RH);
Rain25mm_UrbanAerosols_80RH_F=flipud(Rain25mm_UrbanAerosols_80RH);
Rain75mm_UrbanAerosols_80RH_F=flipud(Rain75mm_UrbanAerosols_80RH);

% Frequency Matrix
RAIN_Matrix_F=[Rain2mm_UrbanAerosols_80RH_F,...
    Rain5mm_UrbanAerosols_80RH_F,Rain12_5mm_UrbanAerosols_80RH_F,...
    Rain25mm_UrbanAerosols_80RH_F,Rain75mm_UrbanAerosols_80RH_F];

%% Create Wavelength Plot
figure1 = figure('Name', 'LEEDR Path Specific RAIN Extinction');

% Create axes
axes1 = axes('Parent', figure1);
box(axes1, 'on');
hold(axes1, 'all');

% Create multiple lines using matrix input to plot
plot1 = plot(Wavelength,RAIN_Matrix,'Parent',axes1);
set(plot1(1), 'DisplayName', '2mm Rain UA 80%RH');
set(plot1(2), 'DisplayName', '5mm Rain UA 80%RH');
set(plot1(3), 'DisplayName', '12.5mm Rain UA 80%RH');
set(plot1(4), 'DisplayName', '25mm Rain UA 80%RH');
set(plot1(5), 'DisplayName', '75mm Rain UA 80%RH');

% Create xlabel
xlabel('Wavelength');

% Create ylabel
ylabel('Attenuation in dB/km');

% Create title
title('LEEDR RAIN 95% RH Exctinction');

```

```

% Create legend
legend(axes1, 'show');

% Create line
annotation(figure1, 'line', [0.354131534569983 0.354131534569983], ...
    [0.90625 0.111979166666667], 'LineStyle', ':', 'Color', [0 1 0]);

%% Create Frequency Plot
figure1 = figure('Name', 'LEEDR Path Specific RAIN Extinction');

% Create axes
axes1 = axes('Parent', figure1);
box(axes1, 'on');
hold(axes1, 'all');

% Create multiple lines using matrix input to plot
plot1 = plot(freq, RAIN_Matrix_F, 'Parent', axes1);
set(plot1(1), 'DisplayName', '2mm Rain UA 80%RH');
set(plot1(2), 'DisplayName', '5mm Rain UA 80%RH');
set(plot1(3), 'DisplayName', '12.5mm Rain UA 80%RH');
set(plot1(4), 'DisplayName', '25mm Rain UA 80%RH');
set(plot1(5), 'DisplayName', '75mm Rain UA 80%RH');

% Create xlabel
xlabel('Frequency');

% Create ylabel
ylabel('Attenuation in dB/km');

% Create title
title('LEEDR RAIN Extinction');

% Create legend
legend(axes1, 'location', 'northwest');

% Create line
annotation(figure1, 'line', [0.563237774030354 0.563237774030354], ...
    [0.785458333333333 0.106770833333333], 'LineStyle', ':', 'Color', [0 1 0]);

%% Plot LEEDR Path Specific SAND Air Data *****
%
% Build Matrices for wavelength and frequency plots
%- the freq plot needs columns to be flipped
% Wavelength Matrix
SAND_Matrix=[Sand_Low_20RH, Sand_Med_20RH, Sand_High_20RH];

%flip Columns about X axis to convert order from wavelength to frequency
Sand_Low_20RH_F=flipud(Sand_Low_20RH);
Sand_Med_20RH_F=flipud(Sand_Med_20RH);
Sand_High_20RH_F=flipud(Sand_High_20RH);

```

```

% Frequency Matrix
SAND_Matrix_F=[Sand_Low_20RH_F,Sand_Med_20RH_F,Sand_High_20RH_F];

%% Create Wavelength Plot
figure1 = figure('Name','LEEDR Path Specific SAND Extinction');

% Create axes
axes1 = axes('Parent',figure1);
box(axes1,'on');
hold(axes1,'all');

% Create multiple lines using matrix input to plot
plot1 = plot(Wavelength,SAND_Matrix,'Parent',axes1);
set(plot1(1),'DisplayName','Number Concentrations 1e10 20%RH');
set(plot1(2),'DisplayName','Number Concentrations 1e11 20%RH');
set(plot1(3),'DisplayName','Number Concentrations 1e12 20%RH');

% Create xlabel
xlabel('Wavelength');

% Create ylabel
ylabel('Attenuation in dB/km');

% Create title
title(...
    'LEEDR SAND Path Specific Extinction, Index 2.34+j.08, radius 1um-500um');

% Create legend
legend(axes1,'location','Best');

%% Create Frequency Plot
figure1 = figure('Name','LEEDR Path Specific SAND Extinction');

% Create axes
axes1 = axes('Parent',figure1);
box(axes1,'on');
hold(axes1,'all');

% Create multiple lines using matrix input to plot
plot1 = plot(Wavelength,SAND_Matrix_F,'Parent',axes1);
set(plot1(1),'DisplayName','Number Concentrations 1e10 20%RH');
set(plot1(2),'DisplayName','Number Concentrations 1e11 20%RH');
set(plot1(3),'DisplayName','Number Concentrations 1e12 20%RH');

% Create xlabel
xlabel('Frequency');

% Create ylabel
ylabel('Attenuation in dB/km');

% Create title

```

```
title(...  
    'LEEDR Path Specific SAND Extinction, Index 2.34+j.08,radius 1um-500um');  
  
% Create legend  
legend(axes1,'location', 'Best');
```



```

%CCCCCCCCCCCCCCCCCCCCCCCCCCCCCCCCCCCCCCCCCCCCCCCCCCCCCCCCCCCCCCCCCCCCCCCCCCCCCCCCCCCCCCCC
% Adjustments to file before running
% Naming should be as below
% The deletions are done automatically if you run strip_hash.sh on the TX
% computer, this is a Bash script file or by hand
% Delete top text and bottom text of ADC file
% Delete text at top of Hygrometer files
% Delete Text at top of Anemometer file
% no changes to Scintillometer file
% no changes to Freq_select/tim files
% These file names are auto generated by XML file.
% File NAMES
% adc_          .txt
% hygro_Tx_     .txt
% hygro_Rx_     .txt
% anemo_Tx_     .txt
% anemo_Rx_     .txt
% scint_        .txt
% these two files are used to check synchronous operation of synthesizers
% looking at the transition from up to down slope tells synchronization too
% These are usually between 3 ms and 8 ms
% freqtim_Tx_   .txt
% freqtim_Rx_   .txt
%CCCCCCCCCCCCCCCCCCCCCCCCCCCCCCCCCCCCCCCCCCCCCCCCCCCCCCCCCCCCCCCCCCCCCCCCCCCCCCCCCCCCCCCC

%% CCCCCCCCCCCCCCCCCCCCCCCCCCCCCCCCCCCCCCCCCCCCCCCCCCCCCCCCCCCCCCCCCCCCCCCCCCCCCCCCCCCCC
% SPECIAL SYSTEM ADJUSTMENT DATA
%
% THIS WILL NEED TO BE adjusted ~80 dB when the ADC Gain box is installed
% on a longer link
% when the receiver has a loss like in the lab test set up a positive
% number will get added back into the data received.  If the receiver has a
% positive gain, when the IF gain amplifier box is in on the long path,
% or a short path with Pads, the gain needs to be adjusted - subtract
% receiver added gain prior to ADC
%
% lab set up, 6 dB splitter and 10 dB pad into ADC - use - 16 dB
% receiver gain adjustment with IF amplifier box = 80 dB with pads in the
% hall at CU/CET
%CHANGE THIS WHEN PATH CHANGES !!!!! - since Gain is variable in hardware
% Receiver_GAIN_adj_dB = 95;  % Minus Pads on subharmonic mixer and ADC

Receiver_GAIN_adj_dB = 95 - 6 - 9;  % Gain box-subhar pad - pads at ADC
%Receiver_GAIN_adj_dB = 40;  % Gain box-subhar pad - pads at ADC

% Friis / EM calculation inputs
Path_Length_m = 1924;  % CHANGE THIS ON DIFFERENT PATHS !!!!!
% Path_Length_m = 40;  % CHANGE THIS ON DIFFERENT PATHS !!!!!

10_m = .001;  % Turbulence Inner Scale Length (10 = 1 mm)
Reflection_Coefficient = .316;  % reflection coefficient of horn
Lens_D_m = .09;  % diameter of the lens

```



```

% forces Rx#2 to get the same data as Rx#1 - disable with a 1

% This equals 1 for hallway
Rx2_disable = 0;

% Disable the Rx1 channel when it is not in the beam, no data taken, this
% forces Rx#1 to get the same data as Rx#2 - disable with a 1
Rx1_disable = 0;

% Enable and Disable Filtering mode
Filter = 0; % disabled =0, enabled =1

% Disable histogram plots with a 1
disable_Hist_plots = 0;

% FFT plot disable / enable - FFT of each frequency scan sample set,
% disable with a 1
disable_fft_plots = 0;

% Matlab crashes with too many FFT plots, this allows plot a scan range
% this range is used for the FFT plots and the histogram plots
FFT_plot_start = 1; % this gives the start range of the quantity FFT plots
FFT_plot_end = 1; % this is the end range of the quantity of FFT plot

%%%%%%%%%%%%%%%%%%%%%%%%%%%%%%%%%%%%%%%%%%%%%%%%%%%%%%%%%%%%%%%%%%%%%%%%

%*****
% End of CONFIGURATION CHANGES
%*****

%% #####
% Constants
c_mpers = 2.997*10^8; % speed of light in atmosphere
k_JperK = 1.38*10^(-23); % Boltzman's constant
% #####

%% ##### INPUT FILE NAMES #####
% the file name loaded must be the middle of the name
% Prefix = adc_, hygro_Tx_, hygro_Rx_, anemo_Tx_, anemo_Rx_,
%          scint_, freqtim_Rx, freqtim_Tx

% the core is the constant middle section of the file name between .txt and
% the underscore after the prefix
prompt='Enter the core (prefix_core.txt) file name (in current directory)';
% Input file Name
file_name_core = input(prompt, 's');

% Generate all data file names
ADC_file = ['adc_',file_name_core, '.txt'];
% Hygrometer files
Hygrom_Tx_file = ['hygro_Tx_',file_name_core, '.txt'];
Hygrom_Rx_file = ['hygro_Rx_',file_name_core, '.txt'];
% Anemometer files

```

```

Anemom_Tx_file = ['anemo_Tx_',file_name_core, '.txt'];
Anemom_Rx_file = ['anemo_Rx_',file_name_core, '.txt'];
%Scintillometer files
Scint_file = ['scint_',file_name_core, '.txt'];
% these two files are used to check synchronous operation of synthesizers
Freqtim_Tx = ['freqtim_Tx_',file_name_core, '.txt'];
Freqtim_Rx = ['freqtim_Rx_',file_name_core, '.txt'];
#####

%% ##### LOAD DATA FROM ACQUISITION FILES #####

% THZ DATA - 3 scans of all frequencies each (all GHz) - nearest 24 Hz
% 100 ms separation between frequency selects 1.1 s total scan per 11 freq.
% Three scans in 3.1 s, 6 scans in 6.2 s depending on tune time. The
% receiver synthesizer is programmed 1 MHz off from the transmit to
% generate the 1 MHz IF frequency at the ADC

% Wide Band (WB) Tx Scan - 20 GHz - Entire Absorption Peak (EAP)
% Synthesizer to RF out = X24 Multiplier - 576 Hz error possible
% FREQ Name          Synth Freq          RF          Peak Offset
% 01  f1             13.3333333333    320.000     -5.153
% 02  f2             13.4647083333    323.153     -2.000
% 03  f3             13.5063750000    324.153     -1.000
% 04  f4             13.5272083333    324.653     -0.500
% 05  f5             13.5480416667    325.153     0.000
% 06  f6             13.5688750000    325.653     0.500
% 07  f7             13.5897083333    326.153     1.000
% 08  f8             13.6313750000    327.153     2.000
% 09  f9             13.7500000000    330.000     4.847
% 10  f10            13.9583333333    335.000     9.847
% 11  f11            13.1666666667    340.000    14.847

% Narrow Band (NB) Tx Scan - 5 GHz
% Lower Wing Line (LWL) of Absorption Peak (USAP)
% Synthesizer to RF out = X24 Multiplier- 576 Hz error possible
% FREQ Name          Synth Freq          RF          Peak Offset
% 12  f1             13.5063750000    324.153     -1.000
% 13  f2             13.5105416667    324.253     -0.900
% 14  f3             13.5147083333    324.353     -0.800
% 15  f4             13.5188750000    324.453     -0.700
% 16  f5             13.5230416667    324.553     -0.600
% 17  f6             13.5272083333    324.653     -0.500
% 18  f7             13.5313750000    324.753     -0.400
% 19  f8             13.5355416667    324.853     -0.300
% 20  f9             13.5397083333    324.953     -0.200
% 21  f10            13.5438750000    325.053     -0.100
% 22  f11            13.5480416667    325.153     0.000

% Narrow Band (NB) Tx Scan - 5 GHz
% Upper Wing Line (UWL) of Absorption Peak (DSAP)
% Synthesizer to RF out = X24 Multiplier - 576 Hz error possible
% FREQ Name          Synth Freq          RF          Peak Offset
% 23  f1             13.5480416667    325.153     0.000
% 24  f2             13.5422083333    325.253     0.100

```

```

% 25 f3          13.556375000    325.353    0.200
% 26 f4          13.560541667    325.453    0.300
% 27 f5          13.564708333    325.553    0.400
% 28 f6          13.568875000    325.653    0.500
% 29 f7          13.573041667    325.753    0.400
% 30 f8          13.577208333    325.853    0.600
% 31 f9          13.581375000    325.953    0.700
% 32 f10         13.585541667    326.053    0.800
% 33 f11         13.589708333    326.153    1.000

% set up scan column vectors
Scan_WB_Frequencies = [320.000;323.153;324.153;324.653;325.153;...
    325.653;326.153;327.153;330.000;335.000;340.000];

Scan_LWL_Frequencies = [324.153;324.253;324.353;324.453;324.553;...
    324.653;324.753;324.853;324.953;325.053;325.153];

Scan_UWL_Frequencies = [325.153;325.253;325.353;325.453;325.553;...
    325.653;325.753;325.853;325.953;326.053;326.153];

% the total XML scan is of two full scans = total of 66 valid frequencies
Scan_Entire_Frequencies = [Scan_WB_Frequencies;Scan_LWL_Frequencies;...
    Scan_UWL_Frequencies;Scan_WB_Frequencies;...
    Scan_LWL_Frequencies;Scan_UWL_Frequencies];

% read THz data from ADC_file - two receivers I/Q data in Volts
% Column Format: Timestamp Rx1_I Rx1_Q Rx2_I Rx2_Q
THz_data = load(ADC_file);

THz_time = THz_data(:,1);
THz_Rx1_I = THz_data(:,2);
THz_Rx1_Q = THz_data(:,3);
THz_Rx2_I = THz_data(:,4);
THz_Rx2_Q = THz_data(:,5);

% If Rx2 is not aligned with the Tx beam and provides bad data, make Rx2
% the same as Rx1 in order not to process bad data
if Rx2_disable == 1
    read = 'Rx2 channel is disabled';
    % if the Rx2 channel is not present, set it equal to Rx1 - multiply to
    % change the phase relationship to allow the mutual coherence function
    % to work somewhat correctly with slightly different amplitude and phase
    % multiply I by 2 and Q by 4 - randomly picked
    THz_Rx2_I = THz_Rx1_I ;
    THz_Rx2_Q = THz_Rx1_Q ;
end

if Rx1_disable == 1
    read = 'Rx2 channel is disabled';
    % if the Rx2 channel is not present, set it equal to Rx1 - multiply to
    % change the phase relationship to allow the mutual coherence function
    % to work somewhat correctly with slightly different amplitude and phase
    % multiply I by 2 and Q by 4 - randomly picked

```

```

THz_Rx1_I = THz_Rx2_I;
THz_Rx1_Q = THz_Rx2_Q;
end

% read Hygrometer data from Tx and Rx Hygrometers
% the Hygrometers each require a calibration file as noted

% Tx Hygrometer
% Version: 1.0_7b8455dadeba Built on: Mar 22 2016 @ 13:20:53
% Serial Number: 1729
% Calibration Data - built into software
% Clean Full Range Calibration data (Xkw:ln(Vo)) = -0.2 / 8.49
%# Clean Dry Range Calibration data (Xkw:ln(Vo)) = -0.21 / 8.538
% Clean Wet Range Calibration data (Xkw:ln(Vo)) = -0.198 / 8.458
% Scaled Full Range Calibration data (Xkw:ln(Vo)) = -0.201 / 8.15
% Scaled Dry Range Calibration data (Xkw:ln(Vo)) = -0.216 / 8.219
% Scaled Wet Range Calibration data (Xkw:ln(Vo)) = -0.198 / 8.103
% File Column format
%           Clean    Clean    Clean    Scaled    Scaled    Scaled
% Time      Full     Dry     Wet     Full     Dry     Wet
% for Colorado, the scaled values are not necessary
% the two primary values required are Clean Dry and Clean Wet in g/m^3

Hygrometer_data_Tx = load(Hygrom_Tx_file);

Hygrometer_Tx_time = Hygrometer_data_Tx(:,1);
Hygrometer_Tx_dry  = Hygrometer_data_Tx(:,3);
Hygrometer_Tx_wet  = Hygrometer_data_Tx(:,4);

% Rx Hygrometer
% Version: 1.0_7b8455dadeba Built on: Mar 22 2016 @ 13:20:53
% Serial Number: 1733
% Calibration - built into software
% Clean Full Range Calibration data (Xkw:ln(Vo)) = -0.184 / 8.695
% Clean Dry Range Calibration data (Xkw:ln(Vo)) = -0.199 / 8.776
% Clean Wet Range Calibration data (Xkw:ln(Vo)) = -0.177 / 8.588
% Scaled Full Range Calibration data (Xkw:ln(Vo)) = -0.187 / 8.077
% Scaled Dry Range Calibration data (Xkw:ln(Vo)) = -0.201 / 8.151
% Scaled Wet Range Calibration data (Xkw:ln(Vo)) = -0.181 / 7.985
% File Column format
%           Clean    Clean    Clean    Scaled    Scaled    Scaled
% Time      Full     Dry     Wet     Full     Dry     Wet
% for Colorado, the scaled values are not necessary
% the two primary values required are Clean Dry and Clean Wet in g/m^3

Hygrometer_data_Rx = load(Hygrom_Rx_file);

Hygrometer_Rx_time = Hygrometer_data_Rx(:,1);
Hygrometer_Rx_dry  = Hygrometer_data_Rx(:,3);
Hygrometer_Rx_wet  = Hygrometer_data_Rx(:,4);

```

```

% read Anemometer data from Tx and Rx Anemometers
% Column Format: # Timestamp ms      U m/s      V m/s      W m/s      Temp (C degrees)

Anemometer_data_Tx = load(Anemom_Tx_file);

Anemometer_Tx_time = Anemometer_data_Tx(:,1);
Anemometer_Tx_U = Anemometer_data_Tx(:,2);
Anemometer_Tx_V = Anemometer_data_Tx(:,3);
Anemometer_Tx_W = Anemometer_data_Tx(:,4);
Anemometer_Tx_Temp = Anemometer_data_Tx(:,5);

Anemometer_data_Rx = load(Anemom_Rx_file);

Anemometer_Rx_time = Anemometer_data_Rx(:,1);
Anemometer_Rx_U = Anemometer_data_Rx(:,2);
Anemometer_Rx_V = Anemometer_data_Rx(:,3);
Anemometer_Rx_W = Anemometer_data_Rx(:,4);
Anemometer_Rx_Temp = Anemometer_data_Rx(:,5);

% read Scintillometer Data
% Timestamp      X location      Y location      angle      AREA
% Units = #Pixels

Scintillometer_data = load(Scint_file);

Scintillometer_time = Scintillometer_data(:,1);
Scintillometer_Xloc = Scintillometer_data(:,2);
Scintillometer_Yloc = Scintillometer_data(:,3);
Scintillometer_Angle = Scintillometer_data(:,4);
Scintillometer_Area = Scintillometer_data(:,5);

% read Tx / Rx Synchronization Data
% Time      RF Frequency Selected (GHz) Text
% remove third column of text - have to handle as text file

% Tx and Rx Synchronization files
% Read in Tx Time      RF_Freq
fileID = fopen(Freqtim_Tx);
Frequency_select_Tx = textscan(fileID, '%f %f %s');
fclose(fileID);
Select_Tx_Time = Frequency_select_Tx{1};
Select_Tx_Freq = Frequency_select_Tx{2};

% Read in Rx Time      RF_Freq
fileID=fopen(Freqtim_Rx);
Frequency_select_Rx = textscan(fileID, '%f %f %s');
fclose(fileID);
Select_Rx_Time = Frequency_select_Rx{1};
Select_Rx_Freq = Frequency_select_Rx{2};
#####

%% ##### DATE & TIME #####
% Create Date and time from THz time record and

```

```

% record milli-second pointer for all data

% Obtain Date and time from THz Receiver EPOCH time data

THz_time_vector = cdflib.epochBreakdown(THz_time);

THz_year = THz_time_vector(1,1)+1970; % started at 1970
THz_month = THz_time_vector(2,1);
THz_day = THz_time_vector(3,1);
% this assumes we are on MDT, MST=7

THz_hour = THz_time_vector(4,1)- 6 - daylight_adjust;
if THz_hour < 0
    THz_hour = 24 + THz_hour; % adjust time at 0 crossing
end

THz_minute = THz_time_vector(5,1);
THz_second = THz_time_vector(6,1);

% cacluate all millisecond pointers for all sensors
% THz Receiver Link ms Time
THz_ms = THz_time_vector(7,:);

% Hygrometer ms Time at Tx and Rx
Hygrometer_time_vector_Tx = cdflib.epochBreakdown(Hygrometer_Tx_time);
Hygrometer_ms_Tx = Hygrometer_time_vector_Tx(7,:);
Hygrometer_time_vector_Rx = cdflib.epochBreakdown(Hygrometer_Rx_time);
Hygrometer_ms_Rx = Hygrometer_time_vector_Rx(7,:);

% Anemometer ms Time at Tx and Rx
Anemometer_time_vector_Tx = cdflib.epochBreakdown(Anemometer_Tx_time);
Anemometer_ms_Tx = Anemometer_time_vector_Tx(7,:);
Anemometer_time_vector_Rx = cdflib.epochBreakdown(Anemometer_Rx_time);
Anemometer_ms_Rx = Anemometer_time_vector_Tx(7,:);

% Scintillometer ms Time
Scintillometer_time_vector = cdflib.epochBreakdown(Scintillometer_time);
Scintillometer_ms = Scintillometer_time_vector(7,:);

% Select frequency Tx / Rx control ms time vector
Select_time_vector_Tx = cdflib.epochBreakdown(Select_Tx_Time);
Select_time_ms_Tx = Select_time_vector_Tx(7,:);
Select_time_vector_Rx = cdflib.epochBreakdown(Select_Rx_Time);
Select_time_ms_Rx = Select_time_vector_Rx(7,:);
#####

% ##### Rx/Tx COMPUTER TIME SYNC #####
% Check Synchronization of Tx and Rx computers first
% plot the freq timing freqtim_Tx_ .txt and freqtim_Rx_ .txt
% this shows the time synchronization between the Tx and Rx
% if this time is greater than 10 ms skew more time should be allowed for
% synchronization or take new data

```

```

% Tx Time
% Obtain Date and time from System Timing Tx and Rx EPOCH time data
FreqTim_time_vector_Tx = cdflib.epochBreakdown(Select_Tx_Time);

FreqTim_year = FreqTim_time_vector_Tx(1,1) + 1970; % started at 1970
FreqTim_month = FreqTim_time_vector_Tx(2,1);
FreqTim_day = FreqTim_time_vector_Tx(3,1);
% this assumes we are on MDT, MST=7
FreqTim_hour_Tx = FreqTim_time_vector_Tx(4,1) - 6 - daylight_adjust;

if FreqTim_hour_Tx < 0
    FreqTim_hour_Tx = 24 + FreqTim_hour_Tx; % adjust time at 0 crossing
end

FreqTim_minute_Tx = FreqTim_time_vector_Tx(5,1);
FreqTim_second_Tx = FreqTim_time_vector_Tx(6,1);

% Rx Time
% Obtain Date and time from Anemometer Tx and Rx EPOCH time data
FreqTim_time_vector_Rx = cdflib.epochBreakdown(Select_Rx_Time);
% year, month and day will be identical to Tx
% this assumes we are on MDT, MST=7, MDT = 6
FreqTim_hour_Rx = FreqTim_time_vector_Rx(4,1) - 6 - daylight_adjust;

if FreqTim_hour_Rx < 0
    FreqTim_hour_Rx = 24 + FreqTim_hour_Rx; % adjust time at 0 crossing
end

FreqTim_minute_Rx = FreqTim_time_vector_Rx(5,1);
FreqTim_second_Rx = FreqTim_time_vector_Rx(6,1);

% Tx cacluate all second pointers
% FreqTim Tx ms Time
FreqTim_ms_Tx = FreqTim_time_vector_Tx(7,:);
% add minutes, seconds and ms
FreqTim_time_s_Tx = (FreqTim_time_vector_Tx(4,:).*(60*60) + ...
    FreqTim_time_vector_Tx(5,:).*60 + FreqTim_time_vector_Tx(6,:) + ...
    FreqTim_ms_Tx./1000)';

% record the start time of the Frequency Timing collection
FreqTim_Start_time_s_Tx = FreqTim_time_s_Tx(1,1);
% start Freq time from zero - subtract start time from all times
FreqTim_time_zero_s_Tx = FreqTim_time_s_Tx - FreqTim_Start_time_s_Tx;

% FreqTime Rx ms Time
FreqTim_ms_Rx = FreqTim_time_vector_Rx(7,:);
% add minutes, seconds and ms
FreqTim_time_s_Rx = (FreqTim_time_vector_Rx(4,:).*(60*60) + ...
    FreqTim_time_vector_Rx(5,:).*60 + FreqTim_time_vector_Rx(6,:) + ...
    FreqTim_ms_Rx./1000)';

% record the start time of the Frequency Timing collection
FreqTim_Start_time_s_Rx = FreqTim_time_s_Rx(1,1);

```

```

% start Freq time from zero - subtract start time from all times
FreqTim_time_zero_s_Rx = FreqTim_time_s_Rx - FreqTim_Start_time_s_Rx;

% Calculate the Difference time between Tx and Rx timing
Time_Delta_Tx_Rx_ms = ...
    (FreqTim_time_zero_s_Rx - FreqTim_time_zero_s_Tx).*1000;

figure01 = figure('Color',[1,1,1], 'Name', 'Tx Rx Freq Timing Plot');

% Create axes
axes1 = axes('Parent',figure01);
hold(axes1, 'on');
box(axes1, 'on');

    hold on; % plot multiple graphs on single plot

% Plot with lines between points and "o" on points
plot(FreqTim_time_zero_s_Tx,Select_Tx_Freq, '- b x');

% plot Rx on same plot in green
plot(FreqTim_time_zero_s_Rx,Select_Rx_Freq, '- k +');

hold off

% Create xlabel
label_for_X = ['start time = ', num2str(THz_ms(1,1)), ...
    's time (s)'];
xlabel(label_for_X);
% Create ylabel
ylabel('Frequency (GHz), Tx Baseband, Rx = 1MHz IF');
Title = ['Frequency Select Timing - one of two scans (', ...
    num2str(FreqTim_month), ' ', num2str(FreqTim_day), ' ', ...
    num2str(FreqTim_year), ' ', num2str(FreqTim_hour_Tx), ...
    ':', num2str(FreqTim_minute_Tx), ':', num2str(FreqTim_second_Tx), ')'];
% Create title
title(Title);

    legend('Tx Freq Sel Tim', 'Rx Freq Sel Tim');

box(axes1, 'on');
% Set the remaining axes properties
set(axes1, 'FontSize', 16);

% plot time difference between Tx and Rx

figure02 = figure('Color',[1,1,1], ...
    'Name', 'Tx Rx Freq Timing delta Plot');

% Create axes
axes1 = axes('Parent',figure02);
hold(axes1, 'on');

```

```

box(axes1, 'on');

plot(FreqTim_time_zero_s_Tx, Time_Delta_Tx_Rx_ms, '- r d');

% Create xlabel
label_for_X = ['start time = ', num2str(THz_ms(1,1)), ...
              's   time (s)'];
xlabel(label_for_X);
% Create ylabel
ylabel('Time Delta (ms)');
Title = ['Frequency Select Time Delta (', num2str(FreqTim_month), ' ', ...
        num2str(FreqTim_day), ' ', num2str(FreqTim_year), ' ', ...
        num2str(FreqTim_hour_Tx), ':', num2str(FreqTim_minute_Tx), ':', ...
        num2str(FreqTim_second_Tx), ')'];
% Create title
title(Title);

box(axes1, 'on');
% Set the remaining axes properties
set(axes1, 'FontSize', 16);
#####

%% ##### FIR Filter Function #####
if Filter == 1;

% calculate the AC voltage amplitude
THz_Rx1_VAC = complex(THz_Rx1_I, THz_Rx1_Q);

% set up sampling fequency
fs = 40000;

% get teh filter coefficients for the band around KHz
h = fir1(13001, [1.30e4/(fs/2) 1.400e4/(fs/2)]);

% plot filter response in the Filter tool
freqz(h);

Filter_Signal = filter(h, 1, THz_Rx1_VAC);

figure;

hold on;

plot((abs(THz_Rx1_VAC) - Receiver_GAIN_adj_dB), 'g');

plot(abs(Filter_Signal), 'r');

hold off;

end

%% ##### RAW DATA AMP #####

```

```

% Create Raw Data Amplitude Plot in Samples vs. dBm
% of the Entire Amplitude Sample(3 scans, 11 freq. each for total
% of 33 frequency changes) - this is done twice in the XML for 66 Freqs

% Create Amplitude from I and Q (could do with abs() function)

Amp_Rx1_Volts = sqrt(THz_Rx1_I.^2+THz_Rx1_Q.^2);

Amp_Rx2_Volts = sqrt(THz_Rx2_I.^2+THz_Rx2_Q.^2);

% Amplitude power in dBm with receiver gain adjustment, 50 Ohm input
% impedance and converting to RMS voltage from AC
Amp_Rx1_dBm = 10.*(log10(((Amp_Rx1_Volts*.707).^2)./(50 *.001)))...
              - Receiver_GAIN_adj_dB;

Amp_Rx2_dBm = 10.*(log10(((Amp_Rx2_Volts*.707).^2)./(50 *.001)))...
              - Receiver_GAIN_adj_dB;

%PLOT Rx1
figure03 = figure('Color',[1,1,1], 'Name', 'Rx1 Raw Data Amplitude Plot');

% Develop X Axis
% Determine the number of rows, columns in Amp to plot
Amp_Dimensions_Rx1 = size(Amp_Rx1_dBm);

Number_Amp_Rows_Rx1 = Amp_Dimensions_Rx1(1); % Determine the number of Rows

% Make x equal to a sequence from 1 to the number of rows (# samples)
x = 1:Number_Amp_Rows_Rx1;

time = x./40e3; % convert samples to time based on sample rate = 40 KHz
% after decimation starting with 40 MHz clock, get 40 KHz

% Create axes
axes1 = axes('Parent',figure03);
hold(axes1, 'on');
box(axes1, 'on');

% Convert Voltage to Power in dBm and Plot - into a 50 Ohm load
plot(time,Amp_Rx1_dBm)

% Create xlabel
xlabel('Time (s)');

% Create ylabel
ylabel('Amplitude (dBm)');

Title = [...
'Hardware Included Raw Rx 1 Amplitude 2 X 3 Scans = 66 Freq Changes(',...
num2str(THz_month), ' ', num2str(THz_day), ' ', num2str(THz_year), ...
', ', num2str(THz_hour), ':', num2str(THz_minute), ...
':', num2str(THz_second), ')'];

```

```

% Create title
title(Title);

box(axes1, 'on');
% Set the remaining axes properties
set(axes1, 'FontSize', 16);

%PLOT Rx2
figure04 = figure('Color', [1,1,1], 'Name', 'Rx2 Raw Data Amplitude Plot');

% Develop X Axis
% Determine the number of rows, columns in Amp to plot
Amp_Dimensions_Rx2 = size(Amp_Rx2_dBm);

Number_Amp_Rows_Rx2 = Amp_Dimensions_Rx2(1); % Determine the number of Rows

% Make x equal to a sequence from 1 to the number of rows (# samples)
x = 1:Number_Amp_Rows_Rx2;

time = x./40e3; % convert samples to time based on sample rate =40 KHz
% after decimation starting with 40 MHz clock, get 40 KHz

% Create axes
axes1 = axes('Parent', figure04);
hold(axes1, 'on');
box(axes1, 'on');

% Convert Voltage to Power in dBm and Plot
plot(time, Amp_Rx2_dBm); % plot Amplitude Data in dBm

% Create xlabel
xlabel('Time (s)');

% Create ylabel
ylabel('Amplitude (dBm)');

Title = [
'Hardware Included Raw Rx 2 Amplitude 2 X 3 Scans = 66 Freq Changes ('...
, num2str(THz_month), ' ', num2str(THz_day), ' ', num2str(THz_year), ...
', ', num2str(THz_hour), ':', num2str(THz_minute), ':', ...
num2str(THz_second), ')'];

% Create title
title(Title);

box(axes1, 'on');
% Set the remaining axes properties
set(axes1, 'FontSize', 16);
#####

% ##### FILTERED AMPLITUDE (AVG) #####

```

```

% Filter Amplitude Scans to remove noise data to allow for easy detection
% of transition from good and bad data areas
% plot that low pass filtered data

% The total data collection is made of up two of the following:
%     Wideband           (WB)  scan  (11 frequencies)
%     Lower Wing Line (LWL) scan  (11 frequencies)
%     Upper Wing Line (UWL) scan  (11 frequencies)
% For a total of 66 valid frequencies

% scan file from the end forward and save valid frequency data
% collect all samples from each frequency
% start with collect of right most frequency 66 = UWL 11

% First smooth power amplitude data with a sliding average
% Low Pass Filter to reduce noise to allow for determining good from
% bad data

% Rx1 CHANNEL
% Starting sum of 80 points (2.5 ms) - last point in file
Amp_Rx1_dBm_avg(Number_Amp_Rows_Rx1) = ...
    mean(Amp_Rx1_dBm((Number_Amp_Rows_Rx1-80:Number_Amp_Rows_Rx1)));

% work from right to left in plot (bottom to beginnning of file)
% don't need to take care of first four frequencies
for i=1:(Number_Amp_Rows_Rx1-200)

    % sliding a 80 sample window and taking the mean at each sample
    % increment
    Amp_Rx1_dBm_avg(Number_Amp_Rows_Rx1-i) = ...
        mean(Amp_Rx1_dBm((Number_Amp_Rows_Rx1-80-i:Number_Amp_Rows_Rx1-i)));
end

%Transpose into a column from row vector
Amp_Rx1_dBm_avg = Amp_Rx1_dBm_avg';

%PLOT Rx1_Average
figure05 = figure('Color',[1,1,1],'Name','Rx1 Sliding Avg Amplitude Plot');

% Develop X Axis
% Determine the number of rows, columns in Amp to plot
Amp_Dimensions_Rx1_avg = size(Amp_Rx1_dBm_avg);

% Determine the number of Rows
Number_Amp_Rows_Rx1_avg = Amp_Dimensions_Rx1_avg(1);

% Make x equal to a sequence from 1 to the number of rows (# samples)
x = 1:Number_Amp_Rows_Rx1_avg;

time = x./40e3; % convert samples to time based on sample rate =40 KHz
% after decimatation starting with 40 MHz clock, get 40 KHz

```

```

% Create axes
axes1 = axes('Parent',figure05);
hold(axes1,'on');
box(axes1,'on');

% Convert Voltage to Power in dBm and Plot
plot(time,Amp_Rx1_dBm_avg); % plot Amplitude Data in dBm

% Create xlabel
xlabel('Time (s)');

% Create ylabel
ylabel('Amplitude (dBm)');

Title = [...
'Hardware Included Rx1 Sliding-AVG Amplitude 2 X 3 Scans= 66 Freq ('...
    ,num2str(THz_month),' ', num2str(THz_day),' ', num2str(THz_year),...
    ', ', num2str(THz_hour),':',num2str(THz_minute),':',...
    num2str(THz_second),')'];

% Create title
title(Title);

box(axes1,'on');
% Set the remaining axes properties
set(axes1,'FontSize',16);

% Rx2 CHANNEL
% Starting sum of 80 points (2.5 ms) - last point in file
Amp_Rx2_dBm_avg(Number_Amp_Rows_Rx2) = ...
    mean(Amp_Rx2_dBm(Number_Amp_Rows_Rx2-80:Number_Amp_Rows_Rx2));

% work from right to left in plot (bottom to beginning of file)
% don't need to take care of first four frequencies
for i=1:(Number_Amp_Rows_Rx2-200)

    % sliding a 80 sample window and taking the mean at each sample
    % increment
    Amp_Rx2_dBm_avg(Number_Amp_Rows_Rx2-i) = ...
        mean(Amp_Rx2_dBm(Number_Amp_Rows_Rx2-80-i:Number_Amp_Rows_Rx2-i));
end

% Transpose the vector
Amp_Rx2_dBm_avg = Amp_Rx2_dBm_avg';

%PLOT Rx2 Average
figure06 = figure('Color',[1,1,1],'Name','Rx2 Sliding Avg Amplitude Plot');

% Develop X Axis
% Determine the number of rows, columns in Amp to plot
Amp_Dimensions_Rx2_avg = size(Amp_Rx2_dBm_avg);

```

```

% Determine the number of Rows
Number_Amp_Rows_Rx2_avg = Amp_Dimensions_Rx2_avg(1);

% Make x equal to a sequence from 1 to the number of rows (# samples)
x = 1:Number_Amp_Rows_Rx2_avg;

time = x./40e3; % convert samples to time based on sample rate =40 KHz
% after decimatation starting with 40 MHz clock, get 40 KHz

% Create axes
axes1 = axes('Parent',figure06);
hold(axes1,'on');
box(axes1,'on');

% Convert Voltage to Power in dBm and Plot
plot(time,Amp_Rx2_dBm_avg); % plot Amplitude Data in dBm

% Create xlabel
xlabel('Time (s)');

% Create ylabel
ylabel('Amplitude (dBm)');

Title = [...
    'Hardware Included Rx2 Sliding-AVG Amplitude 2 X 3 Scans= 66 Freq ('...
    ,num2str(THz_month),' ', num2str(THz_day),' ', num2str(THz_year),...
    ', ', num2str(THz_hour),':',num2str(THz_minute),':',...
    num2str(THz_second),')'];

% Create title
title(Title);

box(axes1,'on');
% Set the remaining axes properties
set(axes1,'FontSize',16);
#####

%% ##### Retrieve Good Data #####
% Separate out good data into a matrix of 66 frequency columns
% Good data is when the Tx and Rx synthesizers are in sync and stable

% Intialize Rx1&2 Good Data Matrix and Header
% create a sequence of headers for 66 sample sets
Rx1_THz_Header = strseq('THz_Rx1_C_freq',1:66);
Rx2_THz_Header = strseq('THz_Rx2_C_freq',1:66);

% Create the Rx1&2 complex data matrix and initialize it to zero
Rx1_THz_Data_c(1:40000,1:66) = 0;
Rx2_THz_Data_c(1:40000,1:66) = 0;

Rx1_THz_temp_c(1:40000,1) = 0;
Rx2_THz_temp_c(1:40000,1) = 0;

```

```

%% Implement Rx1 - Cannot do both at the same time, since code is
% searching for edges

% Initialize the data count
Rx1_data_count = 1;

% combine I&Q into one complex vector
% this array is for the entire 66 data collections

Rx1_THz_c = complex(THz_Rx1_I,THz_Rx1_Q);

% note - start at end of the collection and work forward to the first-66-1
% take 400 samples back in time (10 ms) in the valid area - of the last
% collection (66) - this is the initial valid data
Rx1_Valid_Sample = abs(Amp_Rx1_dBm_avg(Number_Amp_Rows_Rx1_avg - 400));

for Rx1_j = 1:66 %% dividing up 66 frequencies into separate columns
% Collect Valid Data and discard data during out of tune phases
% create a temp array to allow the time reversal in the final matrix
% zero out temporary array

Rx1_bad_data_count = 0;

% Rx1_frequency_count = 66-Rx1_j+1 %Test statement

% SINGLE FREQUENCY GOOD DATA EXTRACTION
% note last frequency (66) will be >10X the samples of all other freq
% Freq 66 will have approximately 38K samples - sits collecting
% good data should be about 80ms-90ms for all others = 3200 samples
% four frequencies at beginning of entire data set doesn't matter, so -10
% won't hurt - put here not to let it go to a negative index

% test statement => Vsample_before_validdata_loop = Valid_Sample

% notice data_count counts from 1 up, but is going right to left in data =
% opposite time of collection

% for number of samples - 10
for Rx1_i = Rx1_data_count : Number_Amp_Rows_Rx1_avg-10

% if the difference of the data to the valid sample
% is < 5 dB, save - looking for dip - UWL
% collect good data - if change is less than 5 dBm
% use absolute value since still noise riding on averaged data
if (abs(Rx1_Valid_Sample - ...
        abs(Amp_Rx1_dBm_avg(Number_Amp_Rows_Rx1_avg - Rx1_i,1)))...
    < Rx1_Threshold_Good_to_Bad_Data_dB)

```

```

% save complex good samples for individual frequency
% cannot use i after second loop for good data pointer, need to
% subtract off the current data_count: where you are in the data
Rx1_data_valid_increment = Rx1_i - Rx1_data_count + 1;
Rx1_THz_temp_c(Rx1_data_valid_increment) = ...
    Rx1_THz_c(Number_Amp_Rows_Rx1_avg - Rx1_i,1);

else

% Rx1_good_data_Count = Rx1_i - Rx1_data_count + 1 % test code

% Invalid Sample will be a few ms further into the data set, the
% total invalid time is 10 - 20 ms, so go forward 2 ms - this gets
% down the falling slope (~2 ms)- moving left to
% right in the dataset

Rx1_Invalid_Sample = ...
    abs(Amp_Rx1_dBm_avg(Number_Amp_Rows_Rx1_avg -(Rx1_i+120)));

% keep track of data count for bad data extraction and skip
% down slope by 2.5ms
Rx1_data_count = Rx1_i + 120;

% re-order in time (flip) the samples into the data matrix for each
% of the 66 frequencies to start at earliest time to the latest
% time = end of collection

Rx1_THz_Data_c(:,66-Rx1_j+1) = flipud(Rx1_THz_temp_c);

% end 'i' "for" loop
break;
end % end of if/else statement for good data
end % end of i for loop for good data

% SINGLE FREQUENCY BAD DATA EXTRACTION
% Discard InValid Data
% find next valid frequency data set LWL
for Rx1_i = Rx1_data_count:(Number_Amp_Rows_Rx1_avg - 10)

% initialize variable for embedded for loop
% if the difference of samples two samples is < 5 dBm,
% discard - look for rising edge (right to left, but
% scanning right to left - down in time)
if (abs(Rx1_Invalid_Sample - ...
    abs(Amp_Rx1_dBm_avg(Number_Amp_Rows_Rx1_avg - Rx1_i, 1)))...
    < Rx1_Threshold_Good_to_Bad_Data_dB)

```

```

% test statement
% Rx1_count_to_rising_edge_bad_data = Rx1_i - Rx1_data_count

else
    % before ending the loop - keep the i value for use in special case
    Rx1_bad_data_count = Rx1_i - Rx1_data_count;

    % update data_count and add 2 ms (80 samples) to get up the slope
    Rx1_data_count = Rx1_i + 80;

    break; % end 'i' "for" loop
end % end if for testing for good data
end % end of 'i' for loop for finding good data

% if don't meet the special case below - jump down to end of 'j' for loop

%SPECIAL CASE OF DISCARD BAD DATA - back to back same frequencies
% the transition from 56 to 55 and 23 to 22 frequencies has no change
% in the synthesizer wich causes two lows during the bad data time -
% during the programming of the synthesizers which is out of sync by ~
% 36 ms - therefore a special qualifier is needed
% This is the value (160) that needs to possibly be tuned dependent on
% how synchronized the Tx and Rx clocks become
if (Rx1_bad_data_count < 160)

    % start a for loop to go through the first part of the special case
    % find the next down slope
    for Rx1_k = Rx1_data_count:(Number_Amp_Rows_Rx1_avg - 10)

        % detect next falling edge, second synthesizer program period
        if (abs(Rx1_Valid_Sample - ...
            abs(Amp_Rx1_dBm_avg(Number_Amp_Rows_Rx1_avg - Rx1_k, 1))) ...
            < Rx1_Threshold_Good_to_Bad_Data_dB)

            else
                %increase the baddata count value
                Rx1_bad_data_count = Rx1_bad_data_count + ...
                    (Rx1_k - Rx1_data_count);

                % save the data_count / pointer
                % move pointer down slope fully to bottom, add 2 ms
                Rx1_data_count = Rx1_k + 80;

                break; % end for loop
            % finished discarded high valid time between two invalid
            % synthesizer programming times
        end % end if for down slop detection
    end % end of 'k' for loop for detection of down slop of bad data

```

```

% start a for loop to go through the last part of the special case
% find the next up slope
for Rx1_x = Rx1_data_count:(Number_Amp_Rows_Rx1_avg - 10)

% Continue to throw away data until detect next rising edge
if (abs(Rx1_Invalid_Sample - ...
        abs(Amp_Rx1_dBm_avg(Number_Amp_Rows_Rx1_avg - Rx1_x,1))) ...
    < Rx1_Threshold_Good_to_Bad_Data_dB)

else

    %increase the bad data count value
    Rx1_bad_data_count = Rx1_bad_data_count + ...
                        (Rx1_x - Rx1_data_count);

    % save the data_count / pointer, to
    % remove time during synthesizer settling, move up slope 2ms
    % (80 samples)
    Rx1_data_count = Rx1_x + 80;

    break; % end for loop
    % finished discarded of last low, synthesizer programming times
    % end or if for finding the final rising edge in bad
    % data special case
end
% end or 'x' for loop for finding the final rising edge in
% bad data special case
end

else

    % This was not a special case, so end and just move on to next
    % frequency , increment the j loop
end % end of if <160 special bad data case

% Update valid sample to the latest set of good data, move along 10 ms
%(400 samples) past synthesizer stabilization time
Rx1_Valid_Sample = abs(Amp_Rx1_dBm_avg(Number_Amp_Rows_Rx1_avg - ...
                                     (Rx1_data_count + 400)));

% test statement
% Rx1_Total_bad_data_count = Rx1_bad_data_count

% clear out the temp data valid collection vector before starting a new
% collection
Rx1_THz_temp_c(:,1) = 0;

end % end of j for loop

%% Implement Rx2 - Cannot do both at the same time, since code

```

```

% is searching for edges
% Note: this is the same as the Rx1 Code

% Initialize a data count
Rx2_data_count = 1;

% combine I&Q into one complex vector
% this array is for the entire 66 data collections
Rx2_THz_c = complex(THz_Rx2_I,THz_Rx2_Q);

% note - start at end of the collection and work forward to the first-66-1
% take 400 samples back in time (10 ms) in the valid area - of the last
% collection (66)
Rx2_Valid_Sample = abs(Amp_Rx2_dBm_avg(Number_Amp_Rows_Rx2_avg - 400));

for Rx2_j = 1:66 %% dividing up 66 frequencies into separate columns
% Collect Valid Data and discard data during out of tune phases
% create a temp array to allow the time reversal in the final matrix
% zero out temporary array

Rx2_bad_data_count = 0;

% Rx2_frequency_count = 66-Rx2_j+1 %Test statement

% SINGLE FREQUENCY GOOD DATA EXTRACTION
% note last frequency (66) will be >10X the samples of all other freq
% Freq 66 will have approximately 38K samples
% good data should be about 80ms for all others = 3200 samples
% four frequencies at beginning of entire data set don't matter, so -10
% won't hurt - put here not to let it go to a negative index
% test statment = Vsample_before_validdata_loop = Valid_Sample

% for number of samples - 10
for Rx2_i = Rx2_data_count : Number_Amp_Rows_Rx2_avg-10

% if the difference of the data to the valid sample
% is < 5 dB, save - looking for dip - down slope
% collect good data - if change is less than 5 dBm
% use absolute value since still noise riding on averaged data
if (abs(Rx2_Valid_Sample - ...
        abs(Amp_Rx2_dBm_avg(Number_Amp_Rows_Rx2_avg - Rx2_i,1)))...
    < Rx2_Threshold_Good_to_Bad_Data_dB)

% save complex good samples for individual frequency
% cannot use i after second loop for good data pointer, need to
% subtract off the current data_count: where you are in the data
Rx2_data_valid_increment = Rx2_i - Rx2_data_count + 1;

Rx2_THz_temp_c(Rx2_data_valid_increment) = ...
    Rx2_THz_c(Number_Amp_Rows_Rx2_avg - Rx2_i,1);

else

```

```

% Rx2_good_data_Count = Rx2_i - _Rx2_data_count + 1 % test code

% Invalid Sample will be a few ms further into the data set, the
% total invalid time is 20 ms, so go forward 2 ms - this gets you
% down the falling slope (~1 ms)- moving left to right
% in the dataset

Rx2_Invalid_Sample = ...
abs(Amp_Rx2_dBm_avg(Number_Amp_Rows_Rx2_avg - (Rx2_i+120)));

% keep track of data count for bad data extraction and skip
% down slope by 2.5 ms
Rx2_data_count = Rx2_i + 120;

% re-order in time (flip) the samples into the data matrix for
% each of the 66 frequencies to start at earliest time to the
% latest time = end of collection
Rx2_THz_Data_c(:,66-Rx2_j+1) = flipud(Rx2_THz_temp_c);

% end 'i' "for" loop
break;
end % end of if/else statement for good data
end % end of i for loop for good data

% SINGLE FREQUENCY BAD DATA EXTRACTION
% Discard InValid Data
% find next valid frequency data set LWL
for Rx2_i = Rx2_data_count:(Number_Amp_Rows_Rx2_avg - 10)

% initialize variable for embedded for loop
% if the difference of samples two samples is < 5 dBm, discard
% - look for rising edge
if (abs(Rx2_Invalid_Sample - ...
        abs(Amp_Rx2_dBm_avg(Number_Amp_Rows_Rx2_avg - Rx2_i, 1)))...
    < Rx2_Threshold_Good_to_Bad_Data_dB)

% test statement
% Rx2_count_to_rising_edge_bad_data_Rx2 = Rx2_i - Rx2_data_count

else
% before ending the loop - keep the i value for use in special case
Rx2_bad_data_count = Rx2_i - Rx2_data_count;

% update data_count and add 2 ms (80 samples) to get up the slop
Rx2_data_count = Rx2_i + 80;

break; % end 'i' "for" loop
end % end if for testing for good data

```

```

end % end of 'i' for loop for finding good data

% if don't meet the special case below - jump down to end of 'j' for loop

%SPECIAL CASE OF DISCARD BAD DATA - back to back same frequencies
% the transition from 56 to 55 and 23 to 22 frequencies has no change
% in the synthesizer wich causes two lows during the bad data time -
% during the programming of the synthesizers which is out of sync by ~
% 36 ms - therefore a special qualifier is needed
% This is the value (160) that needs to possibly be tuned dependent on
% how synchronized the Tx and Rx clocks become
if (Rx2_bad_data_count < 160)

    % start a for loop to go through the first part of the special case
    % find the next down slope
    for Rx2_k = Rx2_data_count:(Number_Amp_Rows_Rx2_avg - 10)

        % detect next falling edge, second synthesizer program period
        if (abs(Rx2_Valid_Sample - ...
            abs(Amp_Rx2_dBm_avg(Number_Amp_Rows_Rx2_avg - Rx2_k, 1)))...
            < Rx2_Threshold_Good_to_Bad_Data_dB)

            else
                %increase the bad data count value
                Rx2_bad_data_count = Rx2_bad_data_count + ...
                    (Rx2_k - Rx2_data_count);

                % save the data_count / pointer
                % move pointer down slope fully to bottom, add 2 ms
                Rx2_data_count = Rx2_k + 80;

                break; % end for loop
            % finished discared high valid time between two invalid
            % synthesizer programming times
            end % end if for down slop detection
        end % end of 'k' for loop for detection of down slop of bad data

        % start a for loop to go through the last part of the special case
        % find the next up slope
        for Rx2_x = Rx2_data_count:(Number_Amp_Rows_Rx2_avg - 10)

            % Continue to throw away data until detect next rising edge
            if (abs(Rx2_Invalid_Sample - ...
                abs(Amp_Rx2_dBm_avg(Number_Amp_Rows_Rx2_avg - Rx2_x, 1)))...
                < Rx2_Threshold_Good_to_Bad_Data_dB)

            else

                %increase the bad data count value

```

```

Rx2_bad_data_count = Rx2_bad_data_count + ...
                    (Rx2_x - Rx2_data_count);

% save the data_count / pointer, to
% remove time during synthesizer settling, move up slope 2ms
% (80 samples)
Rx2_data_count = Rx2_x + 80;

break; % end for loop
% finished discarded of last low, synthesizer programming times
% end or if for finding the final rising edge in bad data
% special case
end
% end or 'x' for loop for finding the final rising edge in bad
% data special case
end

else

% This was not a special case, so end and just move on to next
% frequency , increment the j loop
end % end of if <160 special bad data case

% Update valid sample to the latest set of good data, move along 10 ms
%(400 samples) past synthesizer stabilization time
Rx2_Valid_Sample = abs(Amp_Rx2_dBm_avg(Number_Amp_Rows_Rx2_avg - ...
                    (Rx2_data_count + 400)));

% test statment
% Total_bad_data_count = bad_data_count

% clear out the temp data valid collection vector before starting a new
% collection
Rx2_THz_temp_c(:,1) = 0;
end % end of j for loop

%% ##### Shorten / clean Valid Data Matrix #####
% Shorten the overall THz data matrix to remove all zero values for Rx1&2,
% Freq 66 is the longest, since it is the last tuned frequency
% (~40K samples), all others are in the ~3K range, starting point
% at sample 37,112.
%
% Truncate the data matrix to remove all zeros (approximately ~80ms per
% freq)

% initialize new truncated matrix without any zeros
Rx1_THz_Complex_Data(1:(Good_Data), 1:66) = 0;

Rx2_THz_Complex_Data(1:(Good_Data), 1:66) = 0;

```

```

for j = 1:66
    for i = 1:(Good_Data) % this is where all are VALID!!!

        % Make new non-zero matrix
        Rx1_THz_Complex_Data(i,j) = Rx1_THz_Data_c(i+40000 - Good_Data,j);

        Rx2_THz_Complex_Data(i,j) = Rx2_THz_Data_c(i+40000 - Good_Data,j);
    end
end

#####

% ##### FFT of Each Frequency Scan #####
% For each Scan frequency - Frequency Conversion and Plot
% use flag to enable and disable 66 frequency plots - top of file
% also the range of FFT plots for Rx1 and Rx2 is defined up at the top of
% the file, too many crashes MATLAB

if disable_fft_plots == 0;

% This is for test purposes to confirm frequency is approximately 40 KHz
% current offset/ miss is about 2.5 KHz to 3 KHz
Rx1_THz_FFT_Data(1:(Good_Data),1:66) = 0;

Rx2_THz_FFT_Data(1:(Good_Data),1:66) = 0;

for j = 1:66

Rx1_THz_FFT_Data(:,j) = ...
    10.*(log10((abs(fft(Rx1_THz_Complex_Data(:,j))))).^2).*707 ...
    ./ (50 *.001)) - Receiver_GAIN_adj_dB;
Rx2_THz_FFT_Data(:,j) = ...
    10.*(log10((abs(fft(Rx2_THz_Complex_Data(:,j))))).^2).*707 ...
    ./ (50 *.001)) - Receiver_GAIN_adj_dB;
end
% make a vector x as long as the number of samples in the FFT !!

for j = FFT_plot_start:FFT_plot_end;

%PLOT Rx1 & Rx2, Freq j FFT

j_string = num2str(j); % convert Freq number to string for plot title

plot_title_Rx1 = ['Hardware Included Rx1 Freq ', j_string, ' FFT '];
plot_title_Rx2 = ['Hardware Included Rx2 Freq ', j_string, ' FFT '];

figure07 = figure('Color',[1,1,1], 'Name',plot_title_Rx1);

```

```

% make a vector x as long as the number of samples in the FFT
x = 1:(Good_Data);

% multiply each x index by the FFT bin size (Ws/N)
freq = x.*(40e3/Good_Data);

% Create axes
axes1 = axes('Parent',figure07);
hold(axes1,'on');
box(axes1,'on');

% Plot Frequency vs. Mean Amplitude in dBm
plot(freq, Rx1_THz_FFT_Data(:,j));

% Create xlabel
xlabel('Frequency (Hz)');

% Create ylabel
ylabel('Amplitude (dBm)');

Title = [ plot_title_Rx1, '(' ,num2str(THz_month), ' ',...
          num2str(THz_day), ' ', num2str(THz_year), ', ', ' ', num2str(THz_hour), ...
          ': ', num2str(THz_minute), ': ', num2str(THz_second), ') '];

% Create title
title(Title);

box(axes1,'on');
% Set the remaining axes properties
set(axes1,'FontSize',16);

figure08 = figure('Color',[1,1,1],'Name',plot_title_Rx2);

% Plot Frequency vs. Mean Amplitude in dBm

% Create axes
axes1 = axes('Parent',figure08);
hold(axes1,'on');

plot(freq, Rx2_THz_FFT_Data(:,j));

% Create xlabel
xlabel('Frequency (Hz)');

% Create ylabel
ylabel('Amplitude (dBm)');

Title = [ plot_title_Rx2, '(' ,num2str(THz_month), ' ',...
          num2str(THz_day), ' ', num2str(THz_year), ', ', ' ', num2str(THz_hour), ...
          ': ', num2str(THz_minute), ': ', num2str(THz_second), ') '];

```

```

% Create title
title(Title);

box(axes1, 'on');
% Set the remaining axes properties
set(axes1, 'FontSize',16);

end % end of for plot FFT for loop
end % end of if statement to enable to disable plotting of 66 FFT plots

#####

% #####
%          DATA PROCESSING AT INCLUDES HARDWARE AND PHYSICS
% #####

% ##### Tx/Rx CALIBRATION #####
%# 50 dBi on each side cancels and power is common miniumu on each sweep##

% Make a matrix of the amplitude with CALIBRATION, calculate
% the mean, calibrate and plot one point for each frequency

% TRANSMIT CALIBRATION
% Calibration, frequency in column one and power in column two in mW
VDI_Tx_Cal_Points_mW = [319.22,15.16;... % 1
                        319.50,15.74;... % 2
                        320.00,17.50;... % 3
                        320.50,18.55;... % 4
                        321.00,21.77;... % 5
                        321.50,26.18;... % 6
                        322.00,24.71;... % 7
                        322.50,22.73;... % 8
                        323.00,22.16;... % 9
                        323.50,21.19;... % 10
                        324.00,21.07;... % 11
                        324.50,21.35;... % 12
                        325.00,21.89;... % 13
                        325.50,25.03;... % 14
                        326.00,23.47;... % 15
                        326.50,21.21;... % 16
                        327.00,17.50;... % 17
                        327.50,19.12;... % 18
                        328.00,20.68;... % 19
                        330.00,20.19;... % 20
                        335.00,22.83;... % 21
                        340.00,17.92]; % 22

% Lower Wing Line (LWL) Tx Calibration
% from the above known values implement a spline curve fit to figure out
% the power numbers in mW from the exact frequencies

```

```

TxLWL_Interp_324_153_mW = spline(VDI_Tx_Cal_Points_mW(10:12,1),...
                                VDI_Tx_Cal_Points_mW(10:12,2),324.153);

TxLWL_Interp_324_253_mW = spline(VDI_Tx_Cal_Points_mW(10:12,1),...
                                VDI_Tx_Cal_Points_mW(10:12,2),324.253);

TxLWL_Interp_324_353_mW = spline(VDI_Tx_Cal_Points_mW(10:12,1),...
                                VDI_Tx_Cal_Points_mW(10:12,2),324.353);

TxLWL_Interp_324_453_mW = spline(VDI_Tx_Cal_Points_mW(10:12,1),...
                                VDI_Tx_Cal_Points_mW(10:12,2),324.453);

TxLWL_Interp_324_553_mW = spline(VDI_Tx_Cal_Points_mW(11:13,1),...
                                VDI_Tx_Cal_Points_mW(11:13,2),324.553);

TxLWL_Interp_324_653_mW = spline(VDI_Tx_Cal_Points_mW(11:13,1),...
                                VDI_Tx_Cal_Points_mW(11:13,2),324.653);

TxLWL_Interp_324_753_mW = spline(VDI_Tx_Cal_Points_mW(11:13,1),...
                                VDI_Tx_Cal_Points_mW(11:13,2),324.753);

TxLWL_Interp_324_853_mW = spline(VDI_Tx_Cal_Points_mW(11:13,1),...
                                VDI_Tx_Cal_Points_mW(11:13,2),324.853);

TxLWL_Interp_324_953_mW = spline(VDI_Tx_Cal_Points_mW(11:13,1),...
                                VDI_Tx_Cal_Points_mW(11:13,2),324.953);

TxLWL_Interp_325_053_mW = spline(VDI_Tx_Cal_Points_mW(12:14,1),...
                                VDI_Tx_Cal_Points_mW(12:14,2),325.053);

TxLWL_Interp_325_153_mW = spline(VDI_Tx_Cal_Points_mW(12:14,1),...
                                VDI_Tx_Cal_Points_mW(12:14,2),325.153);

TAIPAS_Tx_Cal_Points_LWL_mW = [TxLWL_Interp_324_153_mW;...
                              TxLWL_Interp_324_253_mW;TxLWL_Interp_324_353_mW;...
                              TxLWL_Interp_324_453_mW;TxLWL_Interp_324_553_mW;...
                              TxLWL_Interp_324_653_mW;TxLWL_Interp_324_753_mW;...
                              TxLWL_Interp_324_853_mW;TxLWL_Interp_324_953_mW;...
                              TxLWL_Interp_325_053_mW;TxLWL_Interp_325_153_mW];

% convert to dBm
TAIPAS_Tx_Cal_Points_LWL_dBm = ...
    10*log10(TAIPAS_Tx_Cal_Points_LWL_mW);

% Calculate the minimum
TAIPAS_Tx_Cal_Points_LWL_min_dBm = ...
    min(TAIPAS_Tx_Cal_Points_LWL_dBm);

% Upper Wing Line (UWL)Tx Calibration
% from the above known values implement a spline curve fit to figure out
% the power numbers in mW from the exact frequencies

```

```

TxUWL_Interp_325_153_mW = spline(VDI_Tx_Cal_Points_mW(12:14,1),...
                                VDI_Tx_Cal_Points_mW(12:14,2),325.153);

TxUWL_Interp_325_253_mW = spline(VDI_Tx_Cal_Points_mW(12:14,1),...
                                VDI_Tx_Cal_Points_mW(12:14,2),325.253);

TxUWL_Interp_325_353_mW = spline(VDI_Tx_Cal_Points_mW(12:14,1),...
                                VDI_Tx_Cal_Points_mW(12:14,2),325.353);

TxUWL_Interp_325_453_mW = spline(VDI_Tx_Cal_Points_mW(12:14,1),...
                                VDI_Tx_Cal_Points_mW(12:14,2),325.453);

TxUWL_Interp_325_553_mW = spline(VDI_Tx_Cal_Points_mW(13:15,1),...
                                VDI_Tx_Cal_Points_mW(13:15,2),325.553);

TxUWL_Interp_325_653_mW = spline(VDI_Tx_Cal_Points_mW(13:15,1),...
                                VDI_Tx_Cal_Points_mW(13:15,2),325.653);

TxUWL_Interp_325_753_mW = spline(VDI_Tx_Cal_Points_mW(13:15,1),...
                                VDI_Tx_Cal_Points_mW(13:15,2),325.753);

TxUWL_Interp_325_853_mW = spline(VDI_Tx_Cal_Points_mW(13:15,1),...
                                VDI_Tx_Cal_Points_mW(13:15,2),325.853);

TxUWL_Interp_325_953_mW = spline(VDI_Tx_Cal_Points_mW(13:15,1),...
                                VDI_Tx_Cal_Points_mW(13:15,2),325.953);

TxUWL_Interp_326_053_mW = spline(VDI_Tx_Cal_Points_mW(14:16,1),...
                                VDI_Tx_Cal_Points_mW(14:16,2),326.053);

TxUWL_Interp_326_153_mW = spline(VDI_Tx_Cal_Points_mW(14:16,1),...
                                VDI_Tx_Cal_Points_mW(14:16,2),326.153);

TAIPAS_Tx_Cal_Points_UWL_mW = [TxUWL_Interp_325_153_mW;...
                              TxUWL_Interp_325_253_mW;TxUWL_Interp_325_353_mW;...
                              TxUWL_Interp_325_453_mW;TxUWL_Interp_325_553_mW;...
                              TxUWL_Interp_325_653_mW;TxUWL_Interp_325_753_mW;...
                              TxUWL_Interp_325_853_mW;TxUWL_Interp_325_953_mW;...
                              TxUWL_Interp_326_053_mW;TxUWL_Interp_326_153_mW];

% convert to dBm
TAIPAS_Tx_Cal_Points_UWL_dBm = ...
                                10*log10(TAIPAS_Tx_Cal_Points_UWL_mW);

% Calculate the minimum
TAIPAS_Tx_Cal_Points_UWL_min_dBm = ...
                                min(TAIPAS_Tx_Cal_Points_UWL_dBm);

% Wideband Tx Calibration
% Calibration, frequency in column one and power in column two in mW
% from the above known values implement a spline curve fit to figure out
% the power numbers in mW from the exact frequencies

```

```

TxWB_Interp_320_000_mW = VDI_Tx_Cal_Points_mW(3,2);

TxWB_Interp_323_153_mW = spline(VDI_Tx_Cal_Points_mW(8:10,1),...
                                VDI_Tx_Cal_Points_mW(8:10,2),323.153);

TxWB_Interp_324_153_mW = spline(VDI_Tx_Cal_Points_mW(10:12,1),...
                                VDI_Tx_Cal_Points_mW(10:12,2),324.153);

TxWB_Interp_324_653_mW = spline(VDI_Tx_Cal_Points_mW(11:13,1),...
                                VDI_Tx_Cal_Points_mW(11:13,2),324.653);

TxWB_Interp_325_153_mW = spline(VDI_Tx_Cal_Points_mW(12:14,1),...
                                VDI_Tx_Cal_Points_mW(12:14,2),325.153);

TxWB_Interp_325_653_mW = spline(VDI_Tx_Cal_Points_mW(13:15,1),...
                                VDI_Tx_Cal_Points_mW(13:15,2),325.653);

TxWB_Interp_326_153_mW = spline(VDI_Tx_Cal_Points_mW(14:16,1),...
                                VDI_Tx_Cal_Points_mW(14:16,2),326.153);

TxWB_Interp_327_153_mW = spline(VDI_Tx_Cal_Points_mW(16:18,1),...
                                VDI_Tx_Cal_Points_mW(16:18,2),327.153);

TxWB_Interp_330_000_mW = VDI_Tx_Cal_Points_mW(20,2);

TxWB_Interp_335_000_mW = VDI_Tx_Cal_Points_mW(21,2);

TxWB_Interp_340_000_mW = VDI_Tx_Cal_Points_mW(22,2);

TAIPAS_Tx_Cal_Points_wb_mW = [TxWB_Interp_320_000_mW;...
    TxWB_Interp_323_153_mW;TxWB_Interp_324_153_mW;...
    TxWB_Interp_324_653_mW;TxWB_Interp_325_153_mW;...
    TxWB_Interp_325_653_mW;TxWB_Interp_326_153_mW;...
    TxWB_Interp_327_153_mW;TxWB_Interp_330_000_mW;...
    TxWB_Interp_335_000_mW;TxWB_Interp_340_000_mW];

% convert to dBm
TAIPAS_Tx_Cal_Points_wb_dBm = 10*log10(TAIPAS_Tx_Cal_Points_wb_mW);

% Calculate the minimum
TAIPAS_Tx_Cal_Points_wb_min_dBm = min(TAIPAS_Tx_Cal_Points_wb_dBm);

% find the minimum of all three scans to use as a common adjustment for
% all scans, make a row of mins for the three scans and find a common min
TAIPAS_Tx_Cal_scans_mins_dBm = [TAIPAS_Tx_Cal_Points_wb_min_dBm,...
    TAIPAS_Tx_Cal_Points_LWL_min_dBm,...
    TAIPAS_Tx_Cal_Points_UWL_min_dBm];

```

```

% calculate the minimum of each scan minimum to find common minimum
TAIPAS_Tx_Cal_dBm = min(TAIPAS_Tx_Cal_scans_mins_dBm);

% Calculate the adjustments necessary relative to the minimum
TAIPAS_Tx_Cal_Points_LWL_adjustments_dBm = ...
    TAIPAS_Tx_Cal_Points_LWL_dBm - TAIPAS_Tx_Cal_dBm;

% Calculate the adjustments necessary relative to the minimum
TAIPAS_Tx_Cal_Points_UWL_adjustments_dBm = ...
    TAIPAS_Tx_Cal_Points_UWL_dBm - TAIPAS_Tx_Cal_dBm;

% Calculate the adjustments necessary relative to the minimum
TAIPAS_Tx_Cal_Points_wb_adjustments_dBm = ...
    TAIPAS_Tx_Cal_Points_wb_dBm - TAIPAS_Tx_Cal_dBm;

% make a 66 long row of Tx adjustments
TAIPAS_Tx_Cal_adjustments_dBm = ...
    [TAIPAS_Tx_Cal_Points_wb_adjustments_dBm', ...
    TAIPAS_Tx_Cal_Points_LWL_adjustments_dBm', ...
    TAIPAS_Tx_Cal_Points_UWL_adjustments_dBm', ...
    TAIPAS_Tx_Cal_Points_wb_adjustments_dBm', ...
    TAIPAS_Tx_Cal_Points_LWL_adjustments_dBm', ...
    TAIPAS_Tx_Cal_Points_UWL_adjustments_dBm'];

% RECEIVER CALIBRATION

% minimal information on LWL, 6.5 dB Conversion loss + 3 dB for SSB
% no data from 320-325
TAIPAS_Rx1_139_Cal_Points_LWL_dB = [8.5;8.5;8.5;8.5;8.5;8.5;8.5;...
    8.5;8.5;8.5;8.5];

% Calculate the minimum
TAIPAS_Rx1_139_Cal_Points_LWL_min_dB = ...
    min(TAIPAS_Rx1_139_Cal_Points_LWL_dB);

TAIPAS_Rx2_138_Cal_Points_LWL_dB = [9;9;9;9;9;9;9;9;9;9;9];
% Calculate the minimum
TAIPAS_Rx2_138_Cal_Points_LWL_min_dB = ...
    min(TAIPAS_Rx2_138_Cal_Points_LWL_dB);

% minimal information on UWL, dB Conversion loss + 3 dB for SSB
TAIPAS_Rx1_139_Cal_Points_UWL_dB = [8.6;8.7;8.8;9;9;9;9;9;9;9;8.9];

% Calculate the minimum
TAIPAS_Rx1_139_Cal_Points_UWL_min_dB = ...
    min(TAIPAS_Rx1_139_Cal_Points_UWL_dB);

TAIPAS_Rx2_138_Cal_Points_UWL_dB = [9;8.9;8.8;8.7;8.8;8.9;9;9;9;9;9];

% Calculate the minimum

```

```

TAIPAS_Rx2_138_Cal_Points_UWL_min_dB = ...
    min (TAIPAS_Rx2_138_Cal_Points_UWL_dB);

% minimal information on wideband, dB Conversion loss + 3 dB for SSB
TAIPAS_Rx1_139_Cal_Points_wb_dB = ...
    [8.5;8.5;8.5;8.5;8.6;9;8.8;8.4;8.5;9.2;9.1];

% Calculate the minimum
TAIPAS_Rx1_139_Cal_Points_wb_min_dB = min(TAIPAS_Rx1_139_Cal_Points_wb_dB);

TAIPAS_Rx2_138_Cal_Points_wb_dB = [9;9;9;9;8.9;8.9;9.1;9.2;9;9.2;9.1];

% Calculate the minimum
TAIPAS_Rx2_138_Cal_Points_wb_min_dB = min(TAIPAS_Rx2_138_Cal_Points_wb_dB);

% used for calculating the minimum to know how to normalize the data
TAIPAS_Rx_Cal_scans_mins_dB = [TAIPAS_Rx1_139_Cal_Points_wb_min_dB,...
    TAIPAS_Rx1_139_Cal_Points_LWL_min_dB,...
    TAIPAS_Rx1_139_Cal_Points_UWL_min_dB,...
    TAIPAS_Rx2_138_Cal_Points_wb_min_dB,...
    TAIPAS_Rx2_138_Cal_Points_LWL_min_dB,...
    TAIPAS_Rx2_138_Cal_Points_UWL_min_dB];

% calculate the minimum of each scan minimum to find common minimum
TAIPAS_Rx_Cal_dB = min(TAIPAS_Rx_Cal_scans_mins_dB);

% calculate the differences from the minimum insertion loss to add to
% signal
TAIPAS_Rx1_139_Cal_LWL_adjustment_dB = ...
    TAIPAS_Rx1_139_Cal_Points_LWL_dB - TAIPAS_Rx_Cal_dB;

% calculate the differences from the minimum insertion loss to add to
% signal
TAIPAS_Rx2_138_Cal_LWL_adjustment_dB = ...
    TAIPAS_Rx2_138_Cal_Points_LWL_dB - TAIPAS_Rx_Cal_dB;

% calculate the differences from the minimum insertion loss to add to
% signal
TAIPAS_Rx1_139_Cal_UWL_adjustment_dB = ...
    TAIPAS_Rx1_139_Cal_Points_UWL_dB - TAIPAS_Rx_Cal_dB;

% calculate the differences from the minimum insertion loss to add to
% signal
TAIPAS_Rx2_138_Cal_UWL_adjustment_dB = ...
    TAIPAS_Rx2_138_Cal_Points_UWL_dB - TAIPAS_Rx_Cal_dB;

% calculate the differences from the minimum insertion loss to add to
% signal
TAIPAS_Rx1_139_Cal_wb_adjustment_dB = ...
    TAIPAS_Rx1_139_Cal_Points_wb_dB - TAIPAS_Rx_Cal_dB;

```

```

% calculate the differences from the minimum insertion loss to add to
% signal
TAIPAS_Rx2_138_Cal_wb_adjustment_dB = ...
    TAIPAS_Rx2_138_Cal_Points_wb_dB - TAIPAS_Rx_Cal_dB;

% note that LWL does not have any variation information so no
% adjustments will be made to LWL - subtract from itself = 0
% vector is 66 long (rows) for the total adjustments
TAIPAS_Rx1_139_Cal_adjustments_dB = ...
    [TAIPAS_Rx1_139_Cal_wb_adjustment_dB',...
    TAIPAS_Rx1_139_Cal_LWL_adjustment_dB',...
    TAIPAS_Rx1_139_Cal_UWL_adjustment_dB',...
    TAIPAS_Rx1_139_Cal_wb_adjustment_dB',...
    TAIPAS_Rx1_139_Cal_LWL_adjustment_dB',...
    TAIPAS_Rx1_139_Cal_UWL_adjustment_dB'];

TAIPAS_Rx2_138_Cal_adjustments_dB = ...
    [TAIPAS_Rx2_138_Cal_wb_adjustment_dB',...
    TAIPAS_Rx2_138_Cal_LWL_adjustment_dB',...
    TAIPAS_Rx2_138_Cal_UWL_adjustment_dB',...
    TAIPAS_Rx2_138_Cal_wb_adjustment_dB',...
    TAIPAS_Rx2_138_Cal_LWL_adjustment_dB',...
    TAIPAS_Rx2_138_Cal_UWL_adjustment_dB'];

% make all numbers relative to the lowest number; lowest number has no
% effect, don't need to call until after mean - will just give a DC offset
% of the Cal value to the mean - lower to the minimum level

Rx1_THz_Complex_Data_Amp_dBm(1:(Good_Data), 1:66) = 0;
Rx2_THz_Complex_Data_Amp_dBm(1:(Good_Data), 1:66) = 0;

% convert each freq data to magnitude and adjust for Tx and Rx calibrations
for j = 1:66
    for i = 1:(Good_Data)

        % Channel #1
        % covert to Amplitude in dBm and AC to RMS
        Rx1_THz_Complex_Data_Amp_dBm(i,j) = ...
        10.*(log10(((abs(Rx1_THz_Complex_Data(i,j)).*.707).^2)./(50 *.001))));

        % add back in test set up pads and splitters
        Rx1_THz_Complex_Data_Amp_dBm(i,j) = ...
            Rx1_THz_Complex_Data_Amp_dBm(i,j) - Receiver_GAIN_adj_dB;

        % Adjust for Tx and Rx variations
        Rx1_THz_Complex_Data_Amp_dBm(i,j) = ...
            Rx1_THz_Complex_Data_Amp_dBm(i,j) - ...
            TAIPAS_Tx_Cal_adjustments_dBm(j) - ...
            TAIPAS_Rx1_139_Cal_adjustments_dB(j);

        % Channel #2
        % covert to Amplitude in dBm and AC to RMS
        Rx2_THz_Complex_Data_Amp_dBm(i,j) = ...

```

```

10.*(log10(((abs(Rx2_THz_Complex_Data(i,j)).*.707).^2)./(50 *.001))));

% add back in test set up pads and splitters
Rx2_THz_Complex_Data_Amp_dBm(i,j) = ...
    Rx2_THz_Complex_Data_Amp_dBm(i,j) - Receiver_GAIN_adj_dB;

% Adjust for Tx and Rx variations
Rx2_THz_Complex_Data_Amp_dBm(i,j) = ...
    Rx2_THz_Complex_Data_Amp_dBm(i,j) - ...
    TAIPAS_Tx_Cal_adjustments_dBm(j) - ...
    TAIPAS_Rx2_138_Cal_adjustments_dB(j);

end
end

% calculate the mean of every frequency column and store in a single row
% (66 values - one for each frequency)
Rx1_THz_Mean_Amp_Cal_dBm = mean(Rx1_THz_Complex_Data_Amp_dBm);

Rx2_THz_Mean_Amp_Cal_dBm = mean(Rx2_THz_Complex_Data_Amp_dBm);

% Calculate STD for use on plots- there is on STD in row for each 66
% frequency selection
Rx1_THz_Mean_Amp_STD_dBm = ...
    std(Rx1_THz_Complex_Data_Amp_dBm)/sqrt(Good_Data);

Rx2_THz_Mean_Amp_STD_dBm = ...
    std(Rx2_THz_Complex_Data_Amp_dBm)/sqrt(Good_Data);

% calculate variance for noise calculation
Rx1_THz_Variance_Amp_Cal_dBsq = var(Rx1_THz_Complex_Data_Amp_dBm);

Rx2_THz_Variance_Amp_Cal_dBsq = var(Rx2_THz_Complex_Data_Amp_dBm);

#####

%% ##### HISTOGRAM #####
% Make a HISTOGRAM Plot of each Scan

% For each Scan frequency - Histogram Conversion and Plot
% use flag to enable and disable 66 frequency plots - top of file
% also the range of plots for Rx1 and Rx2 is defined up at the top of
% the file, too many crashes MATLAB
% the range used will be the FFT plot range defined in the top of the file
if disable_Hist_plots == 0;
% This is for test purposes to view distribution of data

for j = FFT_plot_start:FFT_plot_end;

    %PLOT Histogram Rx1 & Rx2

j_string = num2str(j); % convert Freq number to string for plot title

```

```

plot_title_Rx1 = ['Hardware Included Rx1 Hist ', j_string, ' Hist '];

plot_title_Rx2 = ['Hardware Included Rx2 Hist ', j_string, ' Hist '];

% Plot Rx1
figure09 = figure('Color',[1,1,1], 'Name',plot_title_Rx1);

% Create axes
axes1 = axes('Parent',figure09);
hold(axes1, 'on');
box(axes1, 'on');
% Plot Hist in dBm

hist(Rx1_THz_Complex_Data_Amp_dBm(:,j),100);

% Create xlabel
xlabel('Amplitude (dBm)');

% Create ylabel
ylabel('Quantity of Value');

Title = [ plot_title_Rx1, '(' ,num2str(THz_month), ' ',...
          num2str(THz_day), ' ', num2str(THz_year), ', ', num2str(THz_hour), ...
          ':', num2str(THz_minute), ':', num2str(THz_second), ') '];

% Create title
title(Title);

box(axes1, 'on');
% Set the remaining axes properties
set(axes1, 'FontSize',16);

% Plot Rx2
figure10 = figure('Color',[1,1,1], 'Name',plot_title_Rx2);

% Create axes
axes1 = axes('Parent',figure10);
hold(axes1, 'on');
box(axes1, 'on');

% Plot Hist in dBm
hist(Rx2_THz_Complex_Data_Amp_dBm(:,j),100);

% Create xlabel
xlabel('Amplitude (dBm)');

% Create ylabel
ylabel('Quantity of Value');

Title = [ plot_title_Rx2, '(' ,num2str(THz_month), ' ',...
          num2str(THz_day), ' ', num2str(THz_year), ', ', num2str(THz_hour), ...

```

```

    ':' , num2str(THz_minute), ':' , num2str(THz_second), ' '];

% Create title
title(Title);

box(axes1, 'on');
% Set the remaining axes properties
set(axes1, 'FontSize', 16);
end
end

#####

%% ##### FRIIS #####
% Calculate the mathematical and physics based predicted values using Friis

% the first 33 frequencies, since the last 33 frequencies in an exact
% repeat
Frequency_Scan_33_GHz = [Scan_WB_Frequencies; Scan_LWL_Frequencies; ...
    Scan_UWL_Frequencies];

% calculate the wavelength - lamda=c/f
Wavelength_Scan_33_m = c_mpers ./ (Frequency_Scan_33_GHz .* 10^9);

% Exciter Power at the horn output using interpolated data from VDI power
% data and the reflection coefficient of the horn

% Exciter Power - interpolated from VDI power data
Power_Exciter_33_mW = [TAIPAS_Tx_Cal_Points_wb_mW; ...
    TAIPAS_Tx_Cal_Points_LWL_mW; TAIPAS_Tx_Cal_Points_UWL_mW];

% Power out of the horn - Exciter less S11 (return loss)
Power_Horn_Tx_33_mW = (1- Reflection_Coefficient) * Power_Exciter_33_mW;

% XXXXXXXXXXXXXXXXXXXXXXXXXXXXXXXX
% Liebe absorption and scattering with Al Gasiewski adds - looked up from
% plot at this point
% Extinction Coefficient Calculation in dB/km - absorption + Scattering
Extinction_Coeff_dBperkm = CA_Humidity_20Percent_Absorption_dBperkm + ...
    CA_Scatter_dBperkm;

% Extinction Coefficient convert to Np/km, 1Np=1/e = 4.3429 dB = 8.685/2
Extinction_Coeff_Npperkm = Extinction_Coeff_dBperkm ./ (8.685889638/2);

% XXXXXXXXXXXXXXXXXXXXXXXXXXXXXXXX

% Develop effective diameter of the lens for the different scan frequencies
Effective_Lens_D_m = Lens_D_m * 325.153 ./ Frequency_Scan_33_GHz;

% Power received at the Antenna/Horn - Friis equation
Power_received_mW = Power_Horn_Tx_33_mW .* ...

```

```

((pi .* Effective_Lens_D_m.^2)./ ...
(4*Path_Length_m .* Wavelength_Scan_33_m)).^2 .* ...
exp(-Extinction_Coef_Npperkm ./ 1000 .* Path_Length_m);

%Power received after the Antenna/Horn
Power_received_Horn_output33_mW = ...
    (1 - Reflection_Coefficient) * Power_received_mW;

% Convert received power at Horn to dBm
Power_received_Horn_output33_dBm = ...
    10*log10(Power_received_Horn_output33_mW);

% 6 dB insertion loss on the mixer and add 3 dB for SSB and Rx calibration
Insertion_loss33_Rx1_139_dB = [TAIPAS_Rx1_139_Cal_Points_wb_dB;...
    TAIPAS_Rx1_139_Cal_Points_LWL_dB;...
    TAIPAS_Rx1_139_Cal_Points_UWL_dB];

% 6 dB insertion loss on the mixer and add 3 dB for SSB and Rx calibration
Insertion_loss33_Rx2_138_dB = [TAIPAS_Rx2_138_Cal_Points_wb_dB;...
    TAIPAS_Rx2_138_Cal_Points_LWL_dB;...
    TAIPAS_Rx2_138_Cal_Points_UWL_dB];

% make a 33 long row of Tx adjustments
TAIPAS_Tx_Cal_adj_33_dBm = [TAIPAS_Tx_Cal_Points_wb_adjustments_dBm',...
    TAIPAS_Tx_Cal_Points_LWL_adjustments_dBm',...
    TAIPAS_Tx_Cal_Points_UWL_adjustments_dBm'];

% Power received on Rx1 for 33 frequencies
Pwr_rec_Rx1_139_Insertion_Loss33_dBm = ...
    Power_received_Horn_output33_dBm - Insertion_loss33_Rx1_139_dB ...
    - TAIPAS_Tx_Cal_adj_33_dBm';

% Power received on Rx1 for 66 frequencies
Pwr_rec_Rx1_139_Insertion_Loss_dBm = ...
    [Pwr_rec_Rx1_139_Insertion_Loss33_dBm; ...
    Pwr_rec_Rx1_139_Insertion_Loss33_dBm];

% Difference in power between Friis and actual Rx1
Delta_Rx1_rec_Friis = Pwr_rec_Rx1_139_Insertion_Loss_dBm - ...
    Rx1_THz_Mean_Amp_Cal_dBm';

% normalize mean Rx data to expected Friis - remove DC separation, if
% prediction is accurate, not much normalization

%YYYYYY
Rx1_THz_Normal_dBm = ...
    Rx1_THz_Mean_Amp_Cal_dBm' + abs(mean(Delta_Rx1_rec_Friis));

```

```

% Power received on Rx2
Pwr_rec_Rx2_138_Insertion_Loss33_dBm = ...
    Power_received_Horn_output33_dBm - Insertion_loss33_Rx2_138_dB ...
    - TAIPAS_Tx_Cal_adj_33_dBm';

% Power received on Rx2 for 66 frequencies
Pwr_rec_Rx2_138_Insertion_Loss_dBm = ...
    [Pwr_rec_Rx2_138_Insertion_Loss33_dBm;...
    Pwr_rec_Rx2_138_Insertion_Loss33_dBm];

% Difference in power between Friis and actual Rx1
Delta_Rx2_rec_Friis = Pwr_rec_Rx2_138_Insertion_Loss_dBm - ...
    Rx2_THz_Mean_Amp_Cal_dBm';

% normalize mean Rx data to expected Friis - remove DC separation
Rx2_THz_Normal_dBm = ...
    Rx2_THz_Mean_Amp_Cal_dBm' + abs(mean(Delta_Rx2_rec_Friis));

% plot on same amplitude plot as received data for comparison

#####

% ##### MEAN Data with CALIBRATION #####
% Plot Mean data from both receivers with calibration for every
% 11 points (Scans), a total of 6 scans, also add the predicted FRIIS
% value data

% RECEIVER #1

if Rx1_disable == 0

% PLOT Rx1, Scan 1 ONLY (wideband)
figure11 = ...
    figure('Color',[1,1,1], 'Name', 'Rx1 Scan1 Mean Amp Cal Plot only');

% Create axes
axes1 = axes('Parent',figure11);
hold(axes1, 'on');
box(axes1, 'on');

hold on;

% Plot Frequency vs. Mean Amplitude in dBm
plot(Scan_WB_Frequencies, Rx1_THz_Mean_Amp_Cal_dBm(1:11), '-o b');

% Plot Frequency vs. STD of Mean Amplitude in dBm - cyan color
plot(Scan_WB_Frequencies, ...
    (Rx1_THz_Mean_Amp_Cal_dBm(1:11) + Rx1_THz_Mean_Amp_STD_dBm(1:11)), 'o c');

% Add all Calibration to see if it affects the signal

```

```

Tx_Calibration_wb = (TAIPAS_Tx_Cal_Points_wb_dBm' + ...
                    mean(Rx1_THz_Mean_Amp_Cal_dBm(1:11)));
% Plot Frequency vs. calibration Amplitude in tx and rx dBm
plot(Scan_WB_Frequencies,Tx_Calibration_wb, '-o g');

Rx1_Calibration_wb = (TAIPAS_Rx1_139_Cal_Points_wb_dB' + ...
                    mean(Rx1_THz_Mean_Amp_Cal_dBm(1:11)));
% Plot Frequency vs. calibration Amplitude in tx and rx dBm
plot(Scan_WB_Frequencies, Rx1_Calibration_wb, '-o r');

hold off;

% Display the mean of the 11 STD values
Mean_STD = std(Rx1_THz_Mean_Amp_STD_dBm(1:11));

% Convert the mean STD number to string
Mean_STD_Number = num2str(Mean_STD);

% Y label
Y_Axis_label = ...
    ['Mean Amp,Cal (dBm) - ', 'MeanSTD=', Mean_STD_Number, ' dBm'];

% Create xlabel
xlabel('Frequency (GHz)');

% Create ylabel
ylabel(Y_Axis_label);

Title = ['Hardware Included Rx1 Amplitude Wideband Scan 1 (',...
        num2str(THz_month), ' ', ...
        num2str(THz_day), ' ', num2str(THz_year), ' ', num2str(THz_hour), ...
        ':', num2str(THz_minute), ':', num2str(THz_second), ')'];

% Create title
title(Title);

% Legend of Standard deviations on each cyan point
legend('Good Data Mean', 'STD Mean', 'Tx-Cal', 'Rx1-Cal');

box(axes1, 'on');
% Set the remaining axes properties
set(axes1, 'FontSize', 16);

% PLOT Rx1, Scan 1 with Friis and delta (wideband)
figure12 = ...
    figure('Color', [1,1,1], 'Name', 'Rx1 Scan1 Mean Amp - Friis - Delta Plot');

% Create axes
axes1 = axes('Parent', figure12);
hold(axes1, 'on');

```

```

box(axes1, 'on');

hold on

% Plot Frequency vs. Mean Amplitude in dBm
plot(Scan_WB_Frequencies, Rx1_THz_Mean_Amp_Cal_dBm(1:11), '-o b');

% plot predicted via Friis received data on Rx1
plot(Scan_WB_Frequencies, Pwr_rec_Rx1_139_Insertion_Loss_dBm(1:11), '-x g');

% plot delta of Friis vs. received data on Rx1
plot(Scan_WB_Frequencies, -Delta_Rx1_rec_Friis(1:11), '-. r');

hold off

% Create xlabel
xlabel('Frequency (GHz)');

% Create ylabel
ylabel('Mean Amplitude, with Calibration (dBm)');
Title = ['Rx1 Amplitude WB1 Scan 1, Friis, Delta (' , num2str(THz_month), ...
        ' ', num2str(THz_day), ' ', num2str(THz_year), ', ', num2str(THz_hour), ...
        ':', num2str(THz_minute), ':', num2str(THz_second), ') '];

% Create title
title(Title);

% creat legend
legend('Rx Data', 'Friis Data', ' Negative Delta');

box(axes1, 'on');
% Set the remaining axes properties
set(axes1, 'FontSize', 16);

%PLOT Rx1, Scan 1 and Friis absolutes - normalize to Friis DC (wideband)
figure13 = figure('Color', [1,1,1], ...
                 'Name', 'Rx1 Scan1 Mean Amp - Friis - DC Normalize');

% Create axes
axes1 = axes('Parent', figure13);
hold(axes1, 'on');
box(axes1, 'on');

hold on

% Plot Frequency vs. Mean Amplitude in dBm
plot(Scan_WB_Frequencies, Rx1_THz_Normal_dBm(1:11), '-o b');

```

```

% plot predicted via Friis received data on Rx1
plot(Scan_WB_Frequencies,Pwr_rec_Rx1_139_Insertion_Loss_dBm(1:11), '-x g');

hold off

% Create xlabel
xlabel('Frequency (GHz)');

% Create ylabel
ylabel('Mean Amplitude, with Calibration (dBm)');
Title =['Rx1 Normalized Amp WB1 Scan 1,Friis (' ,num2str(THz_month), ' ',...
        num2str(THz_day), ' ', num2str(THz_year), ' ', ' ', num2str(THz_hour),...
        ':',num2str(THz_minute), ':',num2str(THz_second), ') '];

% Create title
title(Title);

% creat legend
legend('Rx Data','Friis Data');

box(axes1,'on');
% Set the remaining axes properties
set(axes1,'FontSize',16);

%PLOT Rx1,Scan 2 - Lower Wing Line (LWL)
figure14 = figure('Color',[1,1,1],'Name','Rx1 Scan2 Mean Amp Cal Plot');

% Create axes
axes1 = axes('Parent',figure14);
hold(axes1,'on');
box(axes1,'on');

hold on;

% Plot Frequency vs. Mean Amplitude in dBm
plot(Scan_LWL_Frequencies,Rx1_THz_Mean_Amp_Cal_dBm(12:22), '-o b');

% Plot Frequency vs. STD of Mean Amplitude in dBm - cyan color
plot(Scan_LWL_Frequencies, ...
     (Rx1_THz_Mean_Amp_Cal_dBm(12:22) + Rx1_THz_Mean_Amp_STD_dBm(12:22)), 'o c')

% Add all Calibration to see if it affects the signal
Tx_Calibration_LWL = (TAIPAS_Tx_Cal_Points_LWL_dBm' + ...
                    mean(Rx1_THz_Mean_Amp_Cal_dBm(12:22)));
% Plot Frequency vs. calibration Amplitude in tx and rx dBm
plot(Scan_LWL_Frequencies,Tx_Calibration_LWL, '-o g');

Rx1_Calibration_LWL = (TAIPAS_Rx1_139_Cal_Points_LWL_dB' + ...
                    mean(Rx1_THz_Mean_Amp_Cal_dBm(12:22)));
% Plot Frequency vs. calibration Amplitude in tx and rx dBm

```

```

plot(Scan_LWL_Frequencies, Rx1_Calibration_LWL, '-o r');

hold off;

% Display the mean of the 11 STD values
Mean_STD = std(Rx1_THz_Mean_Amp_STD_dBm(12:22));

% Convert the mean STD number to string
Mean_STD_Number = num2str(Mean_STD);

% Y label
Y_Axis_label = ...
    ['Mean Amp, Cal (dBm) - ', 'MeanSTD=', Mean_STD_Number, ' dBm'];

% Create xlabel
xlabel('Frequency (GHz)');

% Create ylabel
ylabel(Y_Axis_label);

Title = ['Rx1 Amplitude LWL Scan2 (', num2str(THz_month), ' ', ...
    num2str(THz_day), ' ', num2str(THz_year), ' ', num2str(THz_hour), ...
    ':', num2str(THz_minute), ':', num2str(THz_second), ')'];

% Create title
title(Title);

% Legend of Standard deviations on each cyan point
legend('Good Data Mean', 'STD Mean', 'Tx-Cal', 'Rx1-Cal');

box(axes1, 'on');
% Set the remaining axes properties
set(axes1, 'FontSize', 16);

%PLOT Rx1, Scan 2 with Friis and delta (LWL)
figure15 = figure('Color', [1,1,1], 'Name', ...
    'Rx1 Scan2 Mean Amp - Friis - Delta Plot');

% Create axes
axes1 = axes('Parent', figure15);
hold(axes1, 'on');
box(axes1, 'on');

hold on

% Plot Frequency vs. Mean Amplitude in dBm
plot(Scan_LWL_Frequencies, Rx1_THz_Mean_Amp_Cal_dBm(12:22), '-o b');

% plot predicted via Friis received data on Rx1
plot(Scan_LWL_Frequencies, Pwr_rec_Rx1_139_Insertion_Loss_dBm(12:22), ...
    '-x g');

```

```

% plot delta of Friis vs. received data on Rx1
plot(Scan_LWL_Frequencies, -Delta_Rx1_rec_Friis(12:22), '-. r');

hold off

% Create xlabel
xlabel('Frequency (GHz)');

% Create ylabel
ylabel('Mean Amplitude, with Calibration (dBm)');

Title = ['Rx1 Amplitude LWL Scan 2,Friis,Delta (',...
        num2str(THz_month), ' ', num2str(THz_day), ' ', num2str(THz_year), ', ', ' ',...
        num2str(THz_hour), ':', num2str(THz_minute), ':', num2str(THz_second), ')'];

% Create title
title(Title);

% creat legend
legend('Rx Data', 'Friis Data', ' Negative Delta');

box(axes1, 'on');
% Set the remaining axes properties
set(axes1, 'FontSize', 16);

%PLOT Rx1, Scan 2 and Friis absolutes - normalize to Friis DC (LWL)
figure16 = figure('Color', [1,1,1], 'Name', ...
                 'Rx1 Scan2 Mean Amp - Friis - DC Normalize');

% Create axes
axes1 = axes('Parent', figure16);
hold(axes1, 'on');
box(axes1, 'on');

hold on

% Plot Frequency vs. Mean Amplitude in dBm
plot(Scan_LWL_Frequencies, Rx1_THz_Normal_dBm(12:22), '-o b');

% plot predicted via Friis received data on Rx1
plot(Scan_LWL_Frequencies, Pwr_rec_Rx1_139_Insertion_Loss_dBm(12:22), ...
     '-x g');

hold off

% Create xlabel
xlabel('Frequency (GHz)');

% Create ylabel
ylabel('Mean Amplitude, with Calibration (dBm)');
Title = ['Rx1 Normalized Amp LWL Scan 2,Friis (' , num2str(THz_month), ...
        ' ', num2str(THz_day), ' ', num2str(THz_year), ', ', ' ', num2str(THz_hour), ...

```

```

    ':' , num2str(THz_minute), ':' , num2str(THz_second), ') '];

% Create title
title(Title);

% creat legend
legend('Rx Data', 'Friis Data');

box(axes1, 'on');
% Set the remaining axes properties
set(axes1, 'FontSize', 16);

%PLOT Rx1, Scan 3 Upper Wing Line (UWL)
figure17 = figure('Color', [1,1,1], 'Name', 'Rx1 Scan3 Mean Amp Cal Plot');

% Create axes
axes1 = axes('Parent', figure17);
hold(axes1, 'on');
box(axes1, 'on');

hold on;

% Plot Frequency vs. Mean Amplitude in dBm
plot(Scan_UWL_Frequencies, Rx1_THz_Mean_Amp_Cal_dBm(23:33), '-o b');

% Plot Frequency vs. STD of Mean Amplitude in dBm - cyan color
plot(Scan_UWL_Frequencies, ...
     (Rx1_THz_Mean_Amp_Cal_dBm(23:33) + Rx1_THz_Mean_Amp_STD_dBm(23:33)), 'o c')

% Add all Calibration to see if it affects the signal
Tx_Calibration_UWL = (TAIPAS_Tx_Cal_Points_UWL_dBm' + ...
                    mean(Rx1_THz_Mean_Amp_Cal_dBm(23:33)));
% Plot Frequency vs. calibration Amplitude in tx and rx dBm
plot(Scan_UWL_Frequencies, Tx_Calibration_UWL, '-o g');

Rx1_Calibration_UWL = (TAIPAS_Rx1_139_Cal_Points_UWL_dB' + ...
                    mean(Rx1_THz_Mean_Amp_Cal_dBm(23:33)));
% Plot Frequency vs. calibration Amplitude in tx and rx dBm
plot(Scan_UWL_Frequencies, Rx1_Calibration_UWL, '-o r');

hold off;

% Display the mean of the 11 STD values
Mean_STD = std(Rx1_THz_Mean_Amp_STD_dBm(23:33));

% Convert the mean STD number to string
Mean_STD_Number = num2str(Mean_STD);

% Y label
Y_Axis_label = ...

```

```

    ['Mean Amp, Cal (dBm) - ', 'MeanSTD=', Mean_STD_Number, ' dBm'];

% Create xlabel
xlabel('Frequency (GHz)');

% Create ylabel
ylabel(Y_Axis_label);

Title = ['Rx1 Amplitude UWL Scan 3 (' , num2str(THz_month), ' ', ...
        num2str(THz_day), ' ', num2str(THz_year), ' ', num2str(THz_hour), ...
        ':', num2str(THz_minute), ':', num2str(THz_second), ')'];

% Legend of Standard deviations on each cyan point
legend('Good Data Mean', 'STD Mean', 'Tx-Cal', 'Rx1-Cal');

% Create title
title(Title);

box(axes1, 'on');
% Set the remaining axes properties
set(axes1, 'FontSize', 16);

%PLOT Rx1, Scan 3 with Friis and delta (UWL)
figure18 = figure('Color', [1,1,1], 'Name', ...
    'Rx1 Scan3 Mean Amp - Friis - Delta Plot');

% Create axes
axes1 = axes('Parent', figure18);
hold(axes1, 'on');
box(axes1, 'on');

hold on

% Plot Frequency vs. Mean Amplitude in dBm
plot(Scan_UWL_Frequencies, Rx1_THz_Mean_Amp_Cal_dBm(23:33), '-o b');

% plot predicted via Friis received data on Rx1
plot(Scan_UWL_Frequencies, Pwr_rec_Rx1_139_Insertion_Loss_dBm(23:33), ...
    '-x g');

% plot delta of Friis vs. received data on Rx1
plot(Scan_UWL_Frequencies, -Delta_Rx1_rec_Friis(23:33), '-. r');

hold off

% Create xlabel
xlabel('Frequency (GHz)');

% Create ylabel
ylabel('Mean Amplitude, with Calibration (dBm)');

```

```

Title = ['Rx1 Amplitude UWL Scan3,Friis,Delta (' ,num2str(THz_month),...
        ' ',num2str(THz_day), ' ', num2str(THz_year), ' ', ' ', num2str(THz_hour),...
        ':' ,num2str(THz_minute), ':' ,num2str(THz_second), ' ')];

% Create title
title(Title);

% creat legend
legend('Rx Data','Friis Data',' Negative Delta');

box(axes1,'on');
% Set the remaining axes properties
set(axes1,'FontSize',16);

%PLOT Rx1, Scan 3 and Friis absolutes - normalize to Friis DC (UWL)
figure19 = figure('Color',[1,1,1],...
                 'Name','Rx1 Scan3 Mean Amp - Friis - DC Normalize');

% Create axes
axes1 = axes('Parent',figure19);
hold(axes1,'on');
box(axes1,'on');

hold on

% Plot Frequency vs. Mean Amplitude in dBm
plot(Scan_UWL_Frequencies,Rx1_THz_Normal_dBm(23:33), '-o b');

% plot predicted via Friis received data on Rx1
plot(Scan_UWL_Frequencies,Pwr_rec_Rx1_139_Insertion_Loss_dBm(23:33),...
     '-x g');

hold off

% Create xlabel
xlabel('Frequency (GHz)');

% Create ylabel
ylabel('Mean Amplitude, with Calibration (dBm)');
Title = ['Rx1 Normalized Amp UWL Scan 3,Friis (' ,num2str(THz_month),...
        ' ',num2str(THz_day), ' ', num2str(THz_year), ' ', ' ', num2str(THz_hour),...
        ':' ,num2str(THz_minute), ':' ,num2str(THz_second), ' ')];

% Create title
title(Title);

% creat legend
legend('Rx Data','Friis Data');

box(axes1,'on');
% Set the remaining axes properties
set(axes1,'FontSize',16);

```

```

%PLOT Rx1, Scan 4 (wideband)
figure20 = figure('Color',[1,1,1],'Name','Rx1 Scan4 Mean Amp Cal Plot');

% Create axes
axes1 = axes('Parent',figure20);
hold(axes1,'on');
box(axes1,'on');

hold on;

% Plot Frequency vs. Mean Amplitude in dBm
plot(Scan_WB_Frequencies,Rx1_THz_Mean_Amp_Cal_dBm(34:44), '-o b');

% Plot Frequency vs. STD of Mean Amplitude in dBm -cyan color
plot(Scan_WB_Frequencies, ...
     (Rx1_THz_Mean_Amp_Cal_dBm(34:44)+Rx1_THz_Mean_Amp_STD_dBm(34:44)), 'o c');

% Add all Calibration to see if it affects the signal
Tx_Calibration_wb = (TAIPAS_Tx_Cal_Points_wb_dBm' + ...
                    mean(Rx1_THz_Mean_Amp_Cal_dBm(34:44)));
% Plot Frequency vs. calibration Amplitude in tx and rx dBm
plot(Scan_WB_Frequencies,Tx_Calibration_wb, '-o g');

Rx1_Calibration_wb = (TAIPAS_Rx1_139_Cal_Points_wb_dB' + ...
                    mean(Rx1_THz_Mean_Amp_Cal_dBm(34:44)));
% Plot Frequency vs. calibration Amplitude in tx and rx dBm
plot(Scan_WB_Frequencies, Rx1_Calibration_wb, '-o r');

hold off;

% Display the mean of the 11 STD values
Mean_STD = std(Rx1_THz_Mean_Amp_STD_dBm(34:44));

% Convert the mean STD number to string
Mean_STD_Number = num2str(Mean_STD);

% Y label
Y_Axis_label = ...
    ['Mean Amp,Cal (dBm) - ', 'MeanSTD=',Mean_STD_Number, ' dBm'];

% Create xlabel
xlabel('Frequency (GHz)');

```

```

% Create ylabel
ylabel(Y_Axis_label);

Title = ['Rx1 Amplitude Wideband Scan 4 (' ,num2str(THz_month), ' ',...
      num2str(THz_day), ' ', num2str(THz_year), ', ', ' ', num2str(THz_hour), ...
      ':', num2str(THz_minute), ':', num2str(THz_second), ') '];

% Create title
title(Title);

% Legend of Standard deviations on each cyan point
legend('Good Data Mean', 'STD Mean', 'Tx-Cal', 'Rx1-Cal');

box(axes1, 'on');
% Set the remaining axes properties
set(axes1, 'FontSize', 16);

%PLOT Rx1, Scan 4 with Friis and delta - (wideband)
figure21 = figure('Color', [1,1,1],...
      'Name', 'Rx1 Scan4 Mean Amp - Friis - Delta Plot');

% Create axes
axes1 = axes('Parent', figure21);
hold(axes1, 'on');
box(axes1, 'on');

hold on

% Plot Frequency vs. Mean Amplitude in dBm
plot(Scan_WB_Frequencies, Rx1_THz_Mean_Amp_Cal_dBm(34:44), '-o b');

% plot predicted via Friis received data on Rx1
plot(Scan_WB_Frequencies, Pwr_rec_Rx1_139_Insertion_Loss_dBm(34:44), '-x g');

% plot delta of Friis vs. received data on Rx1
plot(Scan_WB_Frequencies, -Delta_Rx1_rec_Friis(34:44), '-. r');

hold off

% Create xlabel
xlabel('Frequency (GHz)');

% Create ylabel
ylabel('Mean Amplitude, with Calibration (dBm)');

Title = ['Rx1 Amplitude WB Scan 4, Friis, Delta (' ,num2str(THz_month), ...
      ' ', num2str(THz_day), ' ', num2str(THz_year), ', ', ' ', num2str(THz_hour), ...
      ':', num2str(THz_minute), ':', num2str(THz_second), ') '];

```

```

% Create title
title(Title);

% creat legend
legend('Rx Data','Friis Data',' Negative Delta');

box(axes1,'on');
% Set the remaining axes properties
set(axes1,'FontSize',16);

%PLOT Rx1, Scan 4 and Friis absolutes - normalize to Friis DC (wb)
figure22 = figure('Color',[1,1,1],'Name','Rx1 Scan4 Mean Amp - Friis - DC
Normalize');

% Create axes
axes1 = axes('Parent',figure22);
hold(axes1,'on');
box(axes1,'on');

hold on

% Plot Frequency vs. Mean Amplitude in dBm
plot(Scan_WB_Frequencies,Rx1_THz_Normal_dBm(34:44), '-o b');

% plot predicted via Friis received data on Rx1
plot(Scan_WB_Frequencies,Pwr_rec_Rx1_139_Insertion_Loss_dBm(34:44),'-x g');

hold off

% Create xlabel
xlabel('Frequency (GHz)');

% Create ylabel
ylabel('Mean Amplitude, with Calibration (dBm)');

Title = ['Rx1 Normalized Amp WB Scan 4,Friis (' ,num2str(THz_month),' ',...
        num2str(THz_day),' ', num2str(THz_year),' ', num2str(THz_hour),...
        ':',num2str(THz_minute),':',num2str(THz_second),')'];

% Create title
title(Title);

% creat legend
legend('Rx Data','Friis Data');

box(axes1,'on');
% Set the remaining axes properties
set(axes1,'FontSize',16);

```

```

%PLOT Rx1, Scan 5 - Lower Wing Line (LWL)
figure23 = figure('Color',[1,1,1],'Name','Rx1 Scan5 Mean Amp Cal Plot');

% Create axes
axes1 = axes('Parent',figure23);
hold(axes1,'on');
box(axes1,'on');

hold on;

% Plot Frequency vs. Mean Amplitude in dBm
plot(Scan_LWL_Frequencies,Rx1_THz_Mean_Amp_Cal_dBm(45:55), '-o b');

% Plot Frequency vs. STD of Mean Amplitude in dBm - cyan color
plot(Scan_LWL_Frequencies, ...
     (Rx1_THz_Mean_Amp_Cal_dBm(45:55)+Rx1_THz_Mean_Amp_STD_dBm(45:55)), 'o c');

% Add all Calibration to see if it affects the signal
Tx_Calibration_LWL = (TAIPAS_Tx_Cal_Points_LWL_dBm' + ...
                    mean(Rx1_THz_Mean_Amp_Cal_dBm(45:55)));
% Plot Frequency vs. calibration Amplitude in tx and rx dBm
plot(Scan_LWL_Frequencies,Tx_Calibration_LWL, '-o g');

Rx1_Calibration_LWL = (TAIPAS_Rx1_139_Cal_Points_LWL_dB' + ...
                    mean(Rx1_THz_Mean_Amp_Cal_dBm(45:55)));
% Plot Frequency vs. calibration Amplitude in tx and rx dBm
plot(Scan_LWL_Frequencies, Rx1_Calibration_LWL, '-o r');

hold off;

% Display the mean of the 11 STD values
Mean_STD = std(Rx1_THz_Mean_Amp_STD_dBm(45:55));

% Convert the mean STD number to string
Mean_STD_Number = num2str(Mean_STD);

% Y label
Y_Axis_label = ...
    ['Mean Amp,Cal (dBm) - ', 'MeanSTD=',Mean_STD_Number, ' dBm'];

% Create xlabel
xlabel('Frequency (GHz)');

% Create ylabel
ylabel(Y_Axis_label);

```

```

Title = ['Rx1 Amplitude LWL 5 (' ,num2str(THz_month), ' ',...
        num2str(THz_day), ' ', num2str(THz_year), ', ', num2str(THz_hour), ...
        ':', num2str(THz_minute), ':', num2str(THz_second), ')'];

% Create title
title(Title);

% Legend of Standard deviations on each cyan point
legend('Good Data Mean', 'STD Mean', 'Tx-Cal', 'Rx1-Cal');

box(axes1, 'on');
% Set the remaining axes properties
set(axes1, 'FontSize', 16);

%PLOT Rx1, Scan 5 with Friis and delta (LWL)
figure24 = figure('Color', [1,1,1],...
                 'Name', 'Rx1 Scan5 Mean Amp - Friis - Delta Plot');

% Create axes
axes1 = axes('Parent', figure24);
hold(axes1, 'on');
box(axes1, 'on');

hold on

% Plot Frequency vs. Mean Amplitude in dBm
plot(Scan_LWL_Frequencies, Rx1_THz_Mean_Amp_Cal_dBm(45:55), '-o b');

% plot predicted via Friis received data on Rx1
plot(Scan_LWL_Frequencies, Pwr_rec_Rx1_139_Insertion_Loss_dBm(45:55), ...
     '-x g');

% plot delta of Friis vs. received data on Rx1
plot(Scan_LWL_Frequencies, -Delta_Rx1_rec_Friis(45:55), '-. r');

hold off

% Create xlabel
xlabel('Frequency (GHz)');

% Create ylabel
ylabel('Mean Amplitude, with Calibration (dBm)');

Title = ['Rx1 Amplitude LWL Scan 5, Friis, Delta(' ,num2str(THz_month), ...
        ' ', num2str(THz_day), ' ', num2str(THz_year), ', ', num2str(THz_hour), ...
        ':', num2str(THz_minute), ':', num2str(THz_second), ')'];

% Create title
title(Title);

```

```

% creat legend
legend('Rx Data','Friis Data',' Negative Delta');

box(axes1,'on');
% Set the remaining axes properties
set(axes1,'FontSize',16);

%PLOT Rx1, Scan 5 and Friis absolutes - normalize to Friis DC (LWL)
figure25 = figure('Color',[1,1,1],...
    'Name','Rx1 Scan5 Mean Amp - Friis - DC Normalize');

% Create axes
axes1 = axes('Parent',figure25);
hold(axes1,'on');
box(axes1,'on');

hold on

% Plot Frequency vs. Mean Amplitude in dBm
plot(Scan_LWL_Frequencies,Rx1_THz_Normal_dBm(45:55), '-o b');

% plot predicted via Friis received data on Rx1
plot(Scan_LWL_Frequencies,Pwr_rec_Rx1_139_Insertion_Loss_dBm(45:55),...
    '-x g');

hold off

% Create xlabel
xlabel('Frequency (GHz)');

% Create ylabel
ylabel('Mean Amplitude, with Calibration (dBm)');

Title = ['Rx1 Normalized Amp LWL Scan 5,Friis (' ,num2str(THz_month),...
    ' ',num2str(THz_day),' ', num2str(THz_year),' ', num2str(THz_hour),...
    ':' ,num2str(THz_minute),' ':' ,num2str(THz_second),' ')'];

% Create title
title(Title);

% creat legend
legend('Rx Data','Friis Data');

box(axes1,'on');
% Set the remaining axes properties
set(axes1,'FontSize',16);

%PLOT Rx1, Scan 6 (UWL)
figure26 = figure('Color',[1,1,1],'Name','Rx1 Scan6 Mean Amp Cal Plot');

```

```

% Create axes
axes1 = axes('Parent',figure26);
hold(axes1,'on');
box(axes1,'on');

hold on;

% Plot Frequency vs. Mean Amplitude in dBm
plot(Scan_UWL_Frequencies,Rx1_THz_Mean_Amp_Cal_dBm(56:66), '-o b');

% Plot Frequency vs. STD of Mean Amplitude in dBm - cyan color
plot(Scan_UWL_Frequencies, ...
     (Rx1_THz_Mean_Amp_Cal_dBm(56:66)+Rx1_THz_Mean_Amp_STD_dBm(56:66)), 'o c');

% Add all Calibration to see if it affects the signal
Tx_Calibration_UWL = (TAIPAS_Tx_Cal_Points_UWL_dBm' + ...
                    mean(Rx1_THz_Mean_Amp_Cal_dBm(56:66)));
% Plot Frequency vs. calibration Amplitude in tx and rx dBm
plot(Scan_UWL_Frequencies,Tx_Calibration_UWL, '-o g');

Rx1_Calibration_UWL = (TAIPAS_Rx1_139_Cal_Points_UWL_dB' + ...
                    mean(Rx1_THz_Mean_Amp_Cal_dBm(45:55)));
% Plot Frequency vs. calibration Amplitude in tx and rx dBm
plot(Scan_UWL_Frequencies, Rx1_Calibration_UWL, '-o r');

hold off;

% Display the mean of the 11 STD values
Mean_STD = std(Rx1_THz_Mean_Amp_STD_dBm(56:66));

% Convert the mean STD number to string
Mean_STD_Number = num2str(Mean_STD);

% Y label
Y_Axis_label = ...
    ['Mean Amp, Cal (dBm) - ', 'MeanSTD=', Mean_STD_Number, ' dBm'];

% Create xlabel
xlabel('Frequency (GHz)');

% Create ylabel
ylabel(Y_Axis_label);

Title = ['Rx1 Amplitude UWL Scan6 (' , num2str(THz_month), ' ', ...
        num2str(THz_day), ' ', num2str(THz_year), ' ', num2str(THz_hour), ...
        ':', num2str(THz_minute), ':', num2str(THz_second), ')'];

% Create title
title(Title);

```

```

% Legend of Standard deviations on each cyan point
legend('Good Data Mean', 'STD Mean', 'Tx-Cal', 'Rx1-Cal');

box(axes1, 'on');
% Set the remaining axes properties
set(axes1, 'FontSize', 16);

%PLOT Rx1, Scan 6 with Friis and delta (UWL)
figure27 = figure('Color', [1,1,1], ...
                 'Name', 'Rx1 Scan6 Mean Amp - Friis - Delta Plot');

% Create axes
axes1 = axes('Parent', figure27);
hold(axes1, 'on');
box(axes1, 'on');

hold on

% Plot Frequency vs. Mean Amplitude in dBm
plot(Scan_UWL_Frequencies, Rx1_THz_Mean_Amp_Cal_dBm(56:66), '-o b');

% plot predicted via Friis received data on Rx1
plot(Scan_UWL_Frequencies, Pwr_rec_Rx1_139_Insertion_Loss_dBm(56:66), ...
     '-x g');

% plot delta of Friis vs. received data on Rx1
plot(Scan_UWL_Frequencies, -Delta_Rx1_rec_Friis(56:66), '-. r');

hold off

% Create xlabel
xlabel('Frequency (GHz)');

% Create ylabel
ylabel('Mean Amplitude, with Calibration (dBm)');
Title = ['Rx1 Amplitude UWL Scan 6, Friis, Delta(', num2str(THz_month), ...
        ' ', num2str(THz_day), ' ', num2str(THz_year), ', ', num2str(THz_hour), ...
        ':', num2str(THz_minute), ':', num2str(THz_second), ')'];

% Create title
title(Title);

% creat legend
legend('Rx Data', 'Friis Data', ' Negative Delta');

box(axes1, 'on');
% Set the remaining axes properties
set(axes1, 'FontSize', 16);

```

```

%PLOT Rx1, Scan 6 and Friis absolutes - normalize to Friis DC (UWL)
figure28 = figure('Color',[1,1,1],...
                 'Name','Rx1 Scan6 Mean Amp - Friis - DC Normalize');

% Create axes
axes1 = axes('Parent',figure28);
hold(axes1,'on');
box(axes1,'on');

hold on

% Plot Frequency vs. Mean Amplitude in dBm
plot(Scan_UWL_Frequencies,Rx1_THz_Normal_dBm(56:66), '-o b');

% plot predicted via Friis received data on Rx1
plot(Scan_UWL_Frequencies,Pwr_rec_Rx1_139_Insertion_Loss_dBm(56:66),...
     '-x g');

hold off

% Create xlabel
xlabel('Frequency (GHz)');

% Create ylabel
ylabel('Mean Amplitude, with Calibration (dBm)');

Title = ['Rx1 Normalized Amp UWL Scan 6,Friis (',num2str(THz_month),...
        ', ',num2str(THz_day),', ', num2str(THz_year),', ', num2str(THz_hour),...
        ':',num2str(THz_minute),':',num2str(THz_second),')'];

% Create title
title(Title);

% create legend
legend('Rx Data','Friis Data');

box(axes1,'on');
% Set the remaining axes properties
set(axes1,'FontSize',16);

% PLOT Rx1, Foldover (flip UWL) of up and UWL plots this
% allows the LWL and UWL to be overlaid on each other to see
% differences easier

figure29 = ...
    figure('Color',[1,1,1],...
          'Name','Rx1 Foldover LWL/UWL - Friis - DC Normalize');

% Create axes
axes1 = axes('Parent',figure29);
hold(axes1,'on');

```

```

box(axes1, 'on');

hold on

% Plot Frequency vs. Mean Amplitude in dBm
plot(Scan_LWL_Frequencies,Rx1_THz_Normal_dBm(12:22), '-+ c');

% Plot Frequency vs. Mean Amplitude in dBm
plot(Scan_LWL_Frequencies,Rx1_THz_Normal_dBm(45:55), '-o c');

% note folding of frequencies for plot
% Plot Frequency vs. Mean Amplitude in dBm
plot(Scan_LWL_Frequencies,flipud(Rx1_THz_Normal_dBm(23:33)), '-+ g');

% Plot Frequency vs. Mean Amplitude in dBm
plot(Scan_LWL_Frequencies,flipud(Rx1_THz_Normal_dBm(56:66)), '-o g');

% plot predicted via Friis received data on Rx1
plot(Scan_LWL_Frequencies,Pwr_rec_Rx1_139_Insertion_Loss_dBm(12:22),...
                                           '-+ m');
% plot predicted via Friis received data on Rx1
plot(Scan_LWL_Frequencies,Pwr_rec_Rx1_139_Insertion_Loss_dBm(45:55),...
                                           '-o m');
% note folding of frequencies for plot
% plot predicted via Friis received data on Rx1
plot(Scan_LWL_Frequencies,flipud...
     (Pwr_rec_Rx1_139_Insertion_Loss_dBm(23:33)), '-+ k');

% plot predicted via Friis received data on Rx1
plot(Scan_LWL_Frequencies,flipud...
     (Pwr_rec_Rx1_139_Insertion_Loss_dBm(56:66)), '-o k');

hold off

% Create xlabel
xlabel('Frequency (GHz)');

% Create ylabel
ylabel('Mean Amplitudes, with Calibration UWL Flipped (dBm)');

Title = ['Rx1 Normalized Amp LWL & UWL flipped (',...
        num2str(THz_month), ' ', num2str(THz_day), ' ', num2str(THz_year), ', ', '...',
        num2str(THz_hour), ':', num2str(THz_minute), ':', num2str(THz_second), ')'];

% Create title
title(Title);

% creat legend
legend('RxS2 LWL', 'RxS5 LWL', 'RxS3 UWL', 'RxS6 UWL', 'FriisLWL',...
      'FriisLWL', 'FriisUWL', 'FriisUWL');

box(axes1, 'on');

```

```

% Set the remaining axes properties
set(axes1, 'FontSize', 16);

end

%% RECEIVER #2
if Rx2_disable == 0

%PLOT Rx2, Scan 1 ONLY (wideband)
figure30 = figure('Color', [1,1,1], ...
                 'Name', 'Rx2 Scan1 Mean Amp Cal Plot only');

% Create axes
axes1 = axes('Parent', figure30);
hold(axes1, 'on');
box(axes1, 'on');

hold on;

% Plot Frequency vs. Mean Amplitude in dBm
plot(Scan_WB_Frequencies, Rx2_THz_Mean_Amp_Cal_dBm(1:11), '-o b');

% Plot Frequency vs. STD of Mean Amplitude in dBm - cyan color
plot(Scan_WB_Frequencies, ...
     (Rx2_THz_Mean_Amp_Cal_dBm(1:11) + Rx2_THz_Mean_Amp_STD_dBm(1:11)), 'o c');

% Add all Calibration to see if it affects the signal
Tx_Calibration_wb = (TAIPAS_Tx_Cal_Points_wb_dBm' + ...
                    mean(Rx2_THz_Mean_Amp_Cal_dBm(1:11)));
% Plot Frequency vs. calibration Amplitude in tx and rx dBm
plot(Scan_WB_Frequencies, Tx_Calibration_wb, '-o g');

Rx2_Calibration_wb = (TAIPAS_Rx2_138_Cal_Points_wb_dB' + ...
                    mean(Rx2_THz_Mean_Amp_Cal_dBm(1:11)));
% Plot Frequency vs. calibration Amplitude in tx and rx dBm
plot(Scan_WB_Frequencies, Rx2_Calibration_wb, '-o r');

hold off;

% Display the mean of the 11 STD values
Mean_STD = std(Rx2_THz_Mean_Amp_STD_dBm(1:11));

% Convert the mean STD number to string
Mean_STD_Number = num2str(Mean_STD);

% Y label

```

```

Y_Axis_label = ...
    ['Mean Amp, Cal (dBm) - ', 'MeanSTD=', Mean_STD_Number, ' dBm'];

% Create xlabel
xlabel('Frequency (GHz)');

% Create ylabel
ylabel(Y_Axis_label);

Title = ['Rx2 Amplitude Wideband Scan 1 (', num2str(THz_month), ' ', ...
    num2str(THz_day), ' ', num2str(THz_year), ' ', num2str(THz_hour), ...
    ':', num2str(THz_minute), ':', num2str(THz_second), ')'];

% Create title
title(Title);

% Legend of Standard deviations on each cyan point
legend('Good Data Mean', 'STD Mean', 'Tx-Cal', 'Rx2-Cal');

box(axes1, 'on');
% Set the remaining axes properties
set(axes1, 'FontSize', 16);

%PLOT Rx2, Scan 1 with Friis and delta (wideband)
figure31 = figure('Color', ...
    [1,1,1], 'Name', 'Rx2 Scan1 Mean Amp - Friis - Delta Plot');

% Create axes
axes1 = axes('Parent', figure31);
hold(axes1, 'on');
box(axes1, 'on');

hold on

% Plot Frequency vs. Mean Amplitude in dBm
plot(Scan_WB_Frequencies, Rx2_THz_Mean_Amp_Cal_dBm(1:11), '-o b');

% plot predicted via Friis received data on Rx2
plot(Scan_WB_Frequencies, Pwr_rec_Rx2_138_Insertion_Loss_dBm(1:11), '-x g');

% plot delta of Friis vs. received data on Rx2
plot(Scan_WB_Frequencies, -Delta_Rx2_rec_Friis(1:11), '-. r');

hold off

% Create xlabel
xlabel('Frequency (GHz)');

```

```

% Create ylabel
ylabel('Mean Amplitude, with Calibration (dBm)');
Title = ['Rx2 Amplitude WB1 Scan 1,Friis,Delta (' ,num2str(THz_month),...
        ' ',num2str(THz_day), ' ', num2str(THz_year), ' ', num2str(THz_hour),...
        ':' ,num2str(THz_minute), ':' ,num2str(THz_second), ') '];

% Create title
title(Title);

% creat legend
legend('Rx Data','Friis Data',' Negative Delta');

box(axes1,'on');
% Set the remaining axes properties
set(axes1,'FontSize',16);

%PLOT Rx2, Scan 1 and Friis absolutes - normalize to Friis DC (wideband)
figure32 = figure('Color',[1,1,1],...
                 'Name','Rx2 Scan1 Mean Amp - Friis - DC Normalize');

% Create axes
axes1 = axes('Parent',figure32);
hold(axes1,'on');
box(axes1,'on');

hold on

% Plot Frequency vs. Mean Amplitude in dBm
plot(Scan_WB_Frequencies,Rx2_THz_Normal_dBm(1:11), '-o b');

% plot predicted via Friis received data on Rx2
plot(Scan_WB_Frequencies,Pwr_rec_Rx2_138_Insertion_Loss_dBm(1:11),'-x g');

hold off

% Create xlabel
xlabel('Frequency (GHz)');

% Create ylabel
ylabel('Mean Amplitude, with Calibration (dBm)');

Title = ['Rx2 Normalized Amp WB Scan 1,Friis (' ,num2str(THz_month),...
        ' ',num2str(THz_day), ' ', num2str(THz_year), ' ', num2str(THz_hour),...
        ':' ,num2str(THz_minute), ':' ,num2str(THz_second), ') '];

% Create title
title(Title);

% creat legend
legend('Rx Data','Friis Data');

```

```

box(axes1, 'on');
% Set the remaining axes properties
set(axes1, 'FontSize', 16);

%PLOT Rx2, Scan 2 Lower Wing Line (LWL)
figure33 = figure('Color', [1,1,1], ...
                 'Name', 'Rx2 Scan2 Mean Amp Cal Plot');

% Create axes
axes1 = axes('Parent', figure33);
hold(axes1, 'on');
box(axes1, 'on');

hold on

% Plot Frequency vs. Mean Amplitude in dBm
plot(Scan_LWL_Frequencies, Rx2_THz_Mean_Amp_Cal_dBm(12:22), '-o b');

% Plot Frequency vs. STD of Mean Amplitude in dBm - cyan color
plot(Scan_LWL_Frequencies, ...
     (Rx2_THz_Mean_Amp_Cal_dBm(12:22) + Rx2_THz_Mean_Amp_STD_dBm(12:22)), 'o c');

% Add all Calibration to see if it affects the signal
Tx_Calibration_LWL = (TAIPAS_Tx_Cal_Points_LWL_dBm' + ...
                    mean(Rx2_THz_Mean_Amp_Cal_dBm(12:22)));
% Plot Frequency vs. calibration Amplitude in tx and rx dBm
plot(Scan_LWL_Frequencies, Tx_Calibration_LWL, '-o g');

Rx2_Calibration_LWL = (TAIPAS_Rx2_138_Cal_Points_LWL_dBm' + ...
                    mean(Rx2_THz_Mean_Amp_Cal_dBm(12:22)));
% Plot Frequency vs. calibration Amplitude in tx and rx dBm
plot(Scan_LWL_Frequencies, Rx2_Calibration_LWL, '-o r');

hold off

% Display the mean of the 11 STD values
Mean_STD = std(Rx2_THz_Mean_Amp_STD_dBm(1:11));

% Convert the mean STD number to string
Mean_STD_Number = num2str(Mean_STD);

% Y label
Y_Axis_label = ...
    ['Mean Amp, Cal (dBm) - ', 'MeanSTD=', Mean_STD_Number, ' dBm'];

```

```

% Create xlabel
xlabel('Frequency (GHz)');

% Create ylabel
ylabel(Y_Axis_label);

Title = ['Rx2 Amplitude LWL Scan2 (' ,num2str(THz_month), ' ',...
      num2str(THz_day), ' ', num2str(THz_year), ', ', num2str(THz_hour), ...
      ':', num2str(THz_minute), ':', num2str(THz_second), ')'];

% Create title
title(Title);

% Legend of Standard deviations on each cyan point
legend('Good Data Mean', 'STD Mean', 'Tx-Cal', 'Rx2-Cal');

box(axes1, 'on');
% Set the remaining axes properties
set(axes1, 'FontSize', 16);

%PLOT Rx2, Scan 2 with Friis and delta (LWL)
figure34 = figure('Color',...
      [1,1,1], 'Name', 'Rx2 Scan2 Mean Amp - Friis - Delta Plot');

% Create axes
axes1 = axes('Parent', figure34);
hold(axes1, 'on');
box(axes1, 'on');

hold on

% Plot Frequency vs. Mean Amplitude in dBm
plot(Scan_LWL_Frequencies, Rx2_THz_Mean_Amp_Cal_dBm(12:22), '-o b');

% plot predicted via Friis received data on Rx2
plot(Scan_LWL_Frequencies, Pwr_rec_Rx2_138_Insertion_Loss_dBm(12:22), ...
      '-x g');

% plot delta of Friis vs. received data on Rx2
plot(Scan_LWL_Frequencies, -Delta_Rx2_rec_Friis(12:22), '-. r')

hold off

% Create xlabel
xlabel('Frequency (GHz)');

% Create ylabel
ylabel('Mean Amplitude, with Calibration (dBm)');

```

```

Title = ['Rx2 Amplitude LWL Scan 2, Friis, Delta(',num2str(THz_month),...
        ' ',num2str(THz_day),' ', num2str(THz_year),' ', num2str(THz_hour),...
        ':',num2str(THz_minute),':',num2str(THz_second),')'];

% Create title
title(Title);

% creat legend
legend('Rx Data','Friis Data',' Negative Delta');

box(axes1,'on');
% Set the remaining axes properties
set(axes1,'FontSize',16);

% PLOT Rx2, Scan 2 and Friis absolutes - normalize to Friis DC (LWL)
figure35 = figure('Color',[1,1,1],...
                 'Name','Rx2 Scan2 Mean Amp - Friis - DC Normalize');

% Create axes
axes1 = axes('Parent',figure35);
hold(axes1,'on');
box(axes1,'on');

hold on

% Plot Frequency vs. Mean Amplitude in dBm
plot(Scan_LWL_Frequencies,Rx2_THz_Normal_dBm(12:22), '-o b');

% plot predicted via Friis received data on Rx2
plot(Scan_LWL_Frequencies,Pwr_rec_Rx2_138_Insertion_Loss_dBm(12:22),...
     '-x g');

hold off

% Create xlabel
xlabel('Frequency (GHz)');

% Create ylabel
ylabel('Mean Amplitude, with Calibration (dBm)');

Title = ['Rx2 Normalized Amp LWL Scan 2, Friis (',num2str(THz_month),...
        ' ',num2str(THz_day),' ', num2str(THz_year),' ', num2str(THz_hour),...
        ':',num2str(THz_minute),':',num2str(THz_second),')'];

% Create title
title(Title);

% creat legend
legend('Rx Data','Friis Data');

```

```

box(axes1, 'on');
% Set the remaining axes properties
set(axes1, 'FontSize', 16);

%PLOT Rx2, Scan 3 Upper Wing Line (UWL)
figure36 = figure('Color', [1,1,1], ...
                 'Name', 'Rx2 Scan2 Mean Amp Cal Plot');

% Create axes
axes1 = axes('Parent', figure36);
hold(axes1, 'on');
box(axes1, 'on');

hold on;

% Plot Frequency vs. Mean Amplitude in dBm
plot(Scan_UWL_Frequencies, Rx2_THz_Mean_Amp_Cal_dBm(23:33), '-o b');

% Plot Frequency vs. STD of Mean Amplitude in dBm - cyan color
plot(Scan_UWL_Frequencies, ...
     (Rx2_THz_Mean_Amp_Cal_dBm(23:33)+Rx2_THz_Mean_Amp_STD_dBm(23:33)), 'o c');

% Add all Calibration to see if it affects the signal
Tx_Calibration_UWL = (TAIPAS_Tx_Cal_Points_UWL_dBm' + ...
                    mean(Rx2_THz_Mean_Amp_Cal_dBm(23:33)));
% Plot Frequency vs. calibration Amplitude in tx and rx dBm
plot(Scan_UWL_Frequencies, Tx_Calibration_UWL, '-o g');

Rx2_Calibration_UWL = (TAIPAS_Rx2_138_Cal_Points_UWL_dBm' + ...
                    mean(Rx2_THz_Mean_Amp_Cal_dBm(23:33)));
% Plot Frequency vs. calibration Amplitude in tx and rx dBm
plot(Scan_UWL_Frequencies, Rx2_Calibration_UWL, '-o r');

hold off;

% Display the mean of the 11 STD values
Mean_STD = std(Rx2_THz_Mean_Amp_STD_dBm(23:33));

% Convert the mean STD number to string
Mean_STD_Number = num2str(Mean_STD);

% Y label
Y_Axis_label = ...
    ['Mean Amp, Cal (dBm) - ', 'MeanSTD=', Mean_STD_Number, ' dBm'];

```

```

% Create xlabel
xlabel('Frequency (GHz)');

% Create ylabel
ylabel(Y_Axis_label);

Title = ['Rx2 Amplitude UWL 3 (' ,num2str(THz_month), ' ',...
      num2str(THz_day), ' ', num2str(THz_year), ', ', ' ', num2str(THz_hour), ...
      ':', num2str(THz_minute), ':', num2str(THz_second), ')'];

% Create title
title(Title);

% Legend of Standard deviations on each cyan point
legend('Good Data Mean', 'STD Mean', 'Tx-Cal', 'Rx2-Cal');

box(axes1, 'on');
% Set the remaining axes properties
set(axes1, 'FontSize', 16);

%PLOT Rx2, Scan 3 with Friis and delta (UWL)
figure37 = figure('Color', [1,1,1],...
      'Name', 'Rx2 Scan3 Mean Amp - Friis - Delta Plot');

% Create axes
axes1 = axes('Parent', figure37);
hold(axes1, 'on');
box(axes1, 'on');

hold on

% Plot Frequency vs. Mean Amplitude in dBm
plot(Scan_UWL_Frequencies, Rx2_THz_Mean_Amp_Cal_dBm(23:33), '-o b');

% plot predicted via Friis received data on Rx2
plot(Scan_UWL_Frequencies, Pwr_rec_Rx2_138_Insertion_Loss_dBm(23:33), ...
      '-x g');

% plot delta of Friis vs. received data on Rx2
plot(Scan_UWL_Frequencies, -Delta_Rx2_rec_Friis(23:33), '-. r');

hold off

% Create xlabel
xlabel('Frequency (GHz)');

% Create ylabel
ylabel('Mean Amplitude, with Calibration (dBm)');

```

```

Title = ['Rx2 Amplitude UWL Scan 3, Friis, Delta(',num2str(THz_month),...
        ' ',num2str(THz_day),' ', num2str(THz_year),' ', num2str(THz_hour),...
        ':',num2str(THz_minute),':',num2str(THz_second),')'];

% Create title
title(Title);

% creat legend
legend('Rx Data','Friis Data',' Negative Delta');

box(axes1,'on');
% Set the remaining axes properties
set(axes1,'FontSize',16);

%PLOT Rx2, Scan 3 and Friis absolutes - normalize to Friis DC (UWL)
figure38 = figure('Color',[1,1,1],...
                 'Name','Rx2 Scan3 Mean Amp - Friis - DC Normalize');

% Create axes
axes1 = axes('Parent',figure38);
hold(axes1,'on');
box(axes1,'on');

hold on

% Plot Frequency vs. Mean Amplitude in dBm
plot(Scan_UWL_Frequencies,Rx2_THz_Normal_dBm(23:33), '-o b');

% plot predicted via Friis received data on Rx2
plot(Scan_UWL_Frequencies,Pwr_rec_Rx2_138_Insertion_Loss_dBm(23:33),...
     '-x g');

hold off

% Create xlabel
xlabel('Frequency (GHz)');

% Create ylabel
ylabel('Mean Amplitude, with Calibration (dBm)');

Title = ['Rx2 Normalized Amp UWL Scan 3, Friis (',num2str(THz_month),...
        ' ',num2str(THz_day),' ', num2str(THz_year),' ', num2str(THz_hour),...
        ':',num2str(THz_minute),':',num2str(THz_second),')'];

% Create title
title(Title);

% create legend
legend('Rx Data','Friis Data');

box(axes1,'on');

```

```

% Set the remaining axes properties
set(axes1, 'FontSize', 16);

%PLOT Rx2, Scan 4 (wideband)
figure39 = figure('Color', [1,1,1], 'Name', 'Rx2 Scan4 Mean Amp Cal Plot');

% Create axes
axes1 = axes('Parent', figure39);
hold(axes1, 'on');
box(axes1, 'on');

hold on;

% Plot Frequency vs. Mean Amplitude in dBm
plot(Scan_WB_Frequencies, Rx2_THz_Mean_Amp_Cal_dBm(34:44), '-o b');

% Plot Frequency vs. STD of Mean Amplitude in dBm - cyan color
plot(Scan_WB_Frequencies, ...
     (Rx2_THz_Mean_Amp_Cal_dBm(34:44)+Rx2_THz_Mean_Amp_STD_dBm(34:44)), 'o c');

% Add all Calibration to see if it affects the signal
Tx_Calibration_wb = (TAIPAS_Tx_Cal_Points_wb_dBm' + ...
                    mean(Rx2_THz_Mean_Amp_Cal_dBm(34:44)));
% Plot Frequency vs. calibration Amplitude in tx and rx dBm
plot(Scan_WB_Frequencies, Tx_Calibration_wb, '-o g');

Rx2_Calibration_wb = (TAIPAS_Rx2_138_Cal_Points_wb_dB' + ...
                    mean(Rx2_THz_Mean_Amp_Cal_dBm(34:44)));
% Plot Frequency vs. calibration Amplitude in tx and rx dBm
plot(Scan_WB_Frequencies, Rx2_Calibration_wb, '-o r');

hold off;

% Display the mean of the 11 STD values
Mean_STD = std(Rx2_THz_Mean_Amp_STD_dBm(34:44));

% Convert the mean STD number to string
Mean_STD_Number = num2str(Mean_STD);

% Y label
Y_Axis_label = ...
    ['Mean Amp, Cal (dBm) - ', 'MeanSTD=', Mean_STD_Number, ' dBm'];

% Create xlabel

```

```

xlabel('Frequency (GHz)');

% Create ylabel
ylabel(Y_Axis_label);

Title = ['Rx2 Amplitude Wideband Scan 4 (' , num2str(THz_month), ' ', ...
      num2str(THz_day), ' ', num2str(THz_year), ' ', num2str(THz_hour), ...
      ':', num2str(THz_minute), ':', num2str(THz_second), ')'];

% Create title
title(Title);

% Legend of Standard deviations on each cyan point
legend('Good Data Mean', 'STD Mean', 'Tx-Cal', 'Rx2-Cal');

box(axes1, 'on');
% Set the remaining axes properties
set(axes1, 'FontSize', 16);

%PLOT Rx2, Scan 4 with Friis and delta (wideband)
figure40 = figure('Color', [1,1,1], ...
      'Name', 'Rx2 Scan4 Mean Amp - Friis - Delta Plot');

% Create axes
axes1 = axes('Parent', figure40);
hold(axes1, 'on');
box(axes1, 'on');

hold on

% Plot Frequency vs. Mean Amplitude in dBm
plot(Scan_WB_Frequencies, Rx2_THz_Mean_Amp_Cal_dBm(34:44), '-o b');

% plot predicted via Friis received data on Rx2
plot(Scan_WB_Frequencies, Pwr_rec_Rx2_138_Insertion_Loss_dBm(34:44), '-x g');

% plot delta of Friis vs. received data on Rx2
plot(Scan_WB_Frequencies, -Delta_Rx2_rec_Friis(34:44), '-. r');

hold off

% Create xlabel
xlabel('Frequency (GHz)');

% Create ylabel
ylabel('Mean Amplitude, with Calibration (dBm)');

```

```

Title = ['Rx2 Amplitude WB Scan 4, Friis, Delta (' ,num2str(THz_month),...
        ' ',num2str(THz_day), ' ', num2str(THz_year), ', ', num2str(THz_hour),...
        ':' ,num2str(THz_minute), ':' ,num2str(THz_second), ') '];

% Create title
title(Title);

% creat legend
legend('Rx Data', 'Friis Data', ' Negative Delta');

box(axes1, 'on');
% Set the remaining axes properties
set(axes1, 'FontSize', 16);

%PLOT Rx2, Scan 4 and Friis absolutes - normalize to Friis DC (wb)
figure41 = figure('Color', [1,1,1],...
                 'Name', 'Rx2 Scan4 Mean Amp - Friis - DC Normalize');

% Create axes
axes1 = axes('Parent', figure41);
hold(axes1, 'on');
box(axes1, 'on');

hold on

% Plot Frequency vs. Mean Amplitude in dBm
plot(Scan_WB_Frequencies, Rx2_THz_Normal_dBm(34:44), '-o b');

% plot predicted via Friis received data on Rx2
plot(Scan_WB_Frequencies, Pwr_rec_Rx2_138_Insertion_Loss_dBm(34:44), '-x g');

hold off

% Create xlabel
xlabel('Frequency (GHz)');

% Create ylabel
ylabel('Mean Amplitude, with Calibration (dBm)');

Title = ['Rx2 Normalized Amp WB Scan 4, Friis (' ,num2str(THz_month),...
        ' ',num2str(THz_day), ' ', num2str(THz_year), ', ', num2str(THz_hour),...
        ':' ,num2str(THz_minute), ':' ,num2str(THz_second), ') '];

% Create title
title(Title);

% creat legend
legend('Rx Data', 'Friis Data');

box(axes1, 'on');
% Set the remaining axes properties

```

```

set(axes1,'FontSize',16);

%PLOT Rx2, Scan 5 Lower Wing Line(LWL)
figure42 = figure('Color',[1,1,1],'Name','Rx2 Scan5 Mean Amp Cal Plot');

% Create axes
axes1 = axes('Parent',figure42);
hold(axes1,'on');
box(axes1,'on');

hold on;

% Plot Frequency vs. Mean Amplitude in dBm
plot(Scan_LWL_Frequencies,Rx2_THz_Mean_Amp_Cal_dBm(45:55), '-o b');

% Plot Frequency vs. STD of Mean Amplitude in dBm - cyan color
plot(Scan_LWL_Frequencies, ...
     (Rx2_THz_Mean_Amp_Cal_dBm(45:55)+Rx2_THz_Mean_Amp_STD_dBm(45:55)), 'o c');

% Add all Calibration to see if it affects the signal
Tx_Calibration_LWL = (TAIPAS_Tx_Cal_Points_LWL_dBm' + ...
                    mean(Rx2_THz_Mean_Amp_Cal_dBm(45:55)));
% Plot Frequency vs. calibration Amplitude in tx and rx dBm
plot(Scan_LWL_Frequencies,Tx_Calibration_LWL, '-o g');

Rx2_Calibration_LWL = (TAIPAS_Rx2_138_Cal_Points_LWL_dB' + ...
                    mean(Rx2_THz_Mean_Amp_Cal_dBm(45:55)));
% Plot Frequency vs. calibration Amplitude in tx and rx dBm
plot(Scan_LWL_Frequencies, Rx2_Calibration_LWL, '-o r');

hold off;

% Display the mean of the 11 STD values
Mean_STD = std(Rx2_THz_Mean_Amp_STD_dBm(45:55));

% Convert the mean STD number to string
Mean_STD_Number = num2str(Mean_STD);

% Y label
Y_Axis_label = ...
    ['Mean Amp, Cal (dBm) - ', 'MeanSTD=', Mean_STD_Number, ' dBm'];

```

```

% Create xlabel
xlabel('Frequency (GHz)');

% Create ylabel
ylabel(Y_Axis_label);

Title = ['Rx2 Amplitude LWL Scan 5  (' ,num2str(THz_month), ' ',...
        num2str(THz_day), ' ', num2str(THz_year), ', ', ' ', num2str(THz_hour), ...
        ':', num2str(THz_minute), ':', num2str(THz_second), ')'];

% Create title
title(Title);

% Legend of Standard deviations on each cyan point
legend('Good Data Mean', 'STD Mean', 'Tx-Cal', 'Rx2-Cal');

box(axes1, 'on');
% Set the remaining axes properties
set(axes1, 'FontSize', 16);

%PLOT Rx2, Scan 5 with Friis and delta (LWL)
figure43 = figure('Color', [1,1,1], ...
                 'Name', 'Rx2 Scan5 Mean Amp - Friis - Delta Plot');

% Create axes
axes1 = axes('Parent', figure43);
hold(axes1, 'on');
box(axes1, 'on');

hold on
% Plot Frequency vs. Mean Amplitude in dBm
plot(Scan_LWL_Frequencies, Rx2_THz_Mean_Amp_Cal_dBm(45:55), '-o b');

% plot predicted via Friis received data on Rx2
plot(Scan_LWL_Frequencies, Pwr_rec_Rx2_138_Insertion_Loss_dBm(45:55), ...
     '-x g');

% plot delta of Friis vs. received data on Rx2

hold off

% Create xlabel
xlabel('Frequency (GHz)');

% Create ylabel
ylabel('Mean Amplitude, with Calibration (dBm)');

```

```

Title = ['Rx2 Amplitude LWL Scan 5, Friis, Delta(', num2str(THz_month), ...
        ' ', num2str(THz_day), ' ', num2str(THz_year), ' ', num2str(THz_hour), ...
        ':', num2str(THz_minute), ':', num2str(THz_second), ')'];

% Create title
title(Title);

% creat legend
legend('Rx Data', 'Friis Data', ' Negative Delta');

box(axes1, 'on');
% Set the remaining axes properties
set(axes1, 'FontSize', 16);

%PLOT Rx2, Scan 5 and Friis absolutes - normalize to Friis DC (LWL)
figure44 = figure('Color', [1,1,1], ...
    'Name', 'Rx2 Scan5 Mean Amp - Friis - DC Normalize');

% Create axes
axes1 = axes('Parent', figure44);
hold(axes1, 'on');
box(axes1, 'on');

hold on
% Plot Frequency vs. Mean Amplitude in dBm
plot(Scan_LWL_Frequencies, Rx2_THz_Normal_dBm(45:55), '-o b');

% plot predicted via Friis received data on Rx2
plot(Scan_LWL_Frequencies, Pwr_rec_Rx2_138_Insertion_Loss_dBm(45:55), ...
    '-x g');

hold off

% Create xlabel
xlabel('Frequency (GHz)');

% Create ylabel
ylabel('Mean Amplitude, with Calibration (dBm)');

Title = ['Rx2 Normalized Amp LWL Scan 5, Friis (', num2str(THz_month), ...
        ' ', num2str(THz_day), ' ', num2str(THz_year), ' ', num2str(THz_hour), ...
        ':', num2str(THz_minute), ':', num2str(THz_second), ')'];

% Create title
title(Title);

% creat legend
legend('Rx Data', 'Friis Data');

box(axes1, 'on');
% Set the remaining axes properties

```

```

set(axes1,'FontSize',16);

%PLOT Rx2, Scan 6 Upper Wing Line(UWL)
figure45 = figure('Color',[1,1,1],'Name','Rx2 Scan6 Mean Amp Cal Plot');

% Create axes
axes1 = axes('Parent',figure45);
hold(axes1,'on');
box(axes1,'on');

hold on;

% Plot Frequency vs. Mean Amplitude in dBm
plot(Scan_UWL_Frequencies,Rx2_THz_Mean_Amp_Cal_dBm(56:66), '-o b');

% Plot Frequency vs. STD of Mean Amplitude in dBm - cyan color
plot(Scan_UWL_Frequencies, ...
     (Rx2_THz_Mean_Amp_Cal_dBm(56:66)+Rx2_THz_Mean_Amp_STD_dBm(56:66)), 'o c');

% Add all Calibration to see if it affects the signal
Tx_Calibration_UWL = (TAIPAS_Tx_Cal_Points_UWL_dBm' + ...
                    mean(Rx2_THz_Mean_Amp_Cal_dBm(56:66)));
% Plot Frequency vs. calibration Amplitude in tx and rx dBm
plot(Scan_UWL_Frequencies,Tx_Calibration_UWL, '-o g');

Rx2_Calibration_UWL = (TAIPAS_Rx2_138_Cal_Points_UWL_dBm' + ...
                    mean(Rx2_THz_Mean_Amp_Cal_dBm(56:66)));
% Plot Frequency vs. calibration Amplitude in tx and rx dBm
plot(Scan_UWL_Frequencies, Rx2_Calibration_UWL, '-o r');

hold off;

% Display the mean of the 11 STD values
Mean_STD = std(Rx2_THz_Mean_Amp_STD_dBm(56:66));

% Convert the mean STD number to string
Mean_STD_Number = num2str(Mean_STD);

% Y label
Y_Axis_label = ...
    ['Mean Amp, Cal (dBm) - ', 'MeanSTD=',Mean_STD_Number, ' dBm'];

```

```

% Create xlabel
xlabel('Frequency (GHz)');

% Create ylabel
ylabel(Y_Axis_label);

Title = ['Rx2 Amplitude UWL Scan 6  (' ,num2str(THz_month), ' ',...
      num2str(THz_day), ' ', num2str(THz_year), ', ', ' ', num2str(THz_hour), ...
      ':', num2str(THz_minute), ':', num2str(THz_second), ') '];

% Create title
title(Title);

% Legend of Standard deviations on each cyan point
legend('Good Data Mean', 'STD Mean', 'Tx-Cal', 'Rx2-Cal');

box(axes1, 'on');
% Set the remaining axes properties
set(axes1, 'FontSize', 16);

%PLOT Rx2, Scan 6 with Friis and delta  (UWL)
figure46 = figure('Color', [1,1,1], ...
      'Name', 'Rx2 Scan6 Mean Amp - Friis - Delta Plot');

% Create axes
axes1 = axes('Parent', figure46);
hold(axes1, 'on');
box(axes1, 'on');

hold on

% Plot Frequency vs. Mean Amplitude in dBm
plot(Scan_UWL_Frequencies, Rx2_THz_Mean_Amp_Cal_dBm(56:66), '-o b');

% plot predicted via Friis received data on Rx2
plot(Scan_UWL_Frequencies, Pwr_rec_Rx2_138_Insertion_Loss_dBm(56:66), ...
      '-x g');

% plot delta of Friis vs. received data on Rx2
plot(Scan_UWL_Frequencies, - Delta_Rx2_rec_Friis(56:66), '-. r');

hold off

% Create xlabel
xlabel('Frequency (GHz)');

% Create ylabel

```

```

ylabel('Mean Amplitude, with Calibration (dBm)');

Title = ['Rx2 Amplitude UWL Scan 6, Friis, Delta(', num2str(THz_month), ...
        ' ', num2str(THz_day), ' ', num2str(THz_year), ' ', num2str(THz_hour), ...
        ':', num2str(THz_minute), ':', num2str(THz_second), ')'];

% Create title
title(Title);

% creat legend
legend('Rx Data', 'Friis Data', ' Negative Delta');

box(axes1, 'on');
% Set the remaining axes properties
set(axes1, 'FontSize', 16);

%PLOT Rx2, Scan 6 and Friis absolutes - normalize to Friis DC (UWL)
figure47 = figure('Color', [1,1,1], ...
                 'Name', 'Rx2 Scan6 Mean Amp - Friis - DC Normalize');

% Create axes
axes1 = axes('Parent', figure47);
hold(axes1, 'on');
box(axes1, 'on');

hold on

% Plot Frequency vs. Mean Amplitude in dBm
plot(Scan_UWL_Frequencies, Rx2_THz_Normal_dBm(56:66), '-o b');

% plot predicted via Friis received data on Rx2
plot(Scan_UWL_Frequencies, Pwr_rec_Rx2_138_Insertion_Loss_dBm(56:66), ...
     '-x g');

hold off

% Create xlabel
xlabel('Frequency (GHz)');

% Create ylabel
ylabel('Mean Amplitude, with Calibration (dBm)');

Title = ['Rx2 Normalized Amp UWL Scan 6, Friis (', num2str(THz_month), ...
        ' ', num2str(THz_day), ' ', num2str(THz_year), ' ', num2str(THz_hour), ...
        ':', num2str(THz_minute), ':', num2str(THz_second), ')'];

% Create title
title(Title);

```

```

% create legend
legend('Rx Data','Friis Data');

box(axes1,'on');
% Set the remaining axes properties
set(axes1,'FontSize',16);

% PLOT Rx2, Foldover (flip UWL) of up and UWL plots this
% allows the LWL and UWL to be overlaid on each other to see
% differences easier

figure48 = ...
    figure('Color',[1,1,1],...
          'Name','Rx2 Foldover LWL/UWL - Friis - DC Normalize');

% Create axes
axes1 = axes('Parent',figure48);
hold(axes1,'on');
box(axes1,'on');

hold on
% Plot Frequency vs. Mean Amplitude in dBm
plot(Scan_LWL_Frequencies,Rx2_THz_Normal_dBm(12:22), '-+ c');

% Plot Frequency vs. Mean Amplitude in dBm
plot(Scan_LWL_Frequencies,Rx2_THz_Normal_dBm(45:55), '-o c');

% note folding of frequencies for plot
% Plot Frequency vs. Mean Amplitude in dBm
plot(Scan_LWL_Frequencies,flipud(Rx2_THz_Normal_dBm(23:33)), '-+ g');

% Plot Frequency vs. Mean Amplitude in dBm
plot(Scan_LWL_Frequencies,flipud(Rx2_THz_Normal_dBm(56:66)), '-o g');

% plot predicted via Friis received data on Rx2
plot(Scan_LWL_Frequencies,Pwr_rec_Rx2_138_Insertion_Loss_dBm(12:22),...
     '-+ m');
% plot predicted via Friis received data on Rx2
plot(Scan_LWL_Frequencies,Pwr_rec_Rx2_138_Insertion_Loss_dBm(45:55),...
     '-o m');

% note folding of frequencies for plot
% plot predicted via Friis received data on Rx2
plot(Scan_LWL_Frequencies,flipud...
     (Pwr_rec_Rx1_139_Insertion_Loss_dBm(23:33)), '-+ k');

% plot predicted via Friis received data on Rx2
plot(Scan_LWL_Frequencies,flipud...
     (Pwr_rec_Rx1_139_Insertion_Loss_dBm(56:66)), '-o k');

hold off

```

```

% Create xlabel
xlabel('Frequency (GHz)');

% Create ylabel
ylabel('Mean Amplitudes, with Calibration UWL flipped (dBm)');

Title = ['Rx2 Normalized Amp LWL & UWL Flipped (',...
        num2str(THz_month), ' ', num2str(THz_day), ' ', num2str(THz_year), ', ', ',...
        num2str(THz_hour), ':', num2str(THz_minute), ':', num2str(THz_second), ')'];

% Create title
title(Title);

% creat legend
legend('RxS2-LWL', 'RxS5-LWL', 'RxS3-UWL', 'RxS6-UWL', 'FriisLWL', ...
        'FriisLWL', 'FriisUWL', 'FriisUWL');

box(axes1, 'on');
% Set the remaining axes properties
set(axes1, 'FontSize', 16);

end % end of if statement to disable Rx2

#####

%% ##### SNR #####
% SNR Calculation vs. Friis - Pwr received divided by noise power
% must of the 80 dB gain ADC conditioner box in place to have Anti-aliasing
% filter
% SIGNAL - Power received 66 column
% NOISE - row of variances for 66 scans

Rx1_SNR_dB = ...
    Pwr_rec_Rx1_139_Insertion_Loss_dBm - Rx1_THz_Variance_Amp_Cal_dBsq';

Rx2_SNR_dB = ...
    Pwr_rec_Rx2_138_Insertion_Loss_dBm - Rx2_THz_Variance_Amp_Cal_dBsq';

% calculate Friis predicted version of the SNR
Friis_Noise_dBm = ...
    10*log10(k_JperK * (T0_K + Trec_peak_k) * (B_MHz * 10^6)*1000);

% calculate Friis predicted version of the SNR

Rx1_Friis_SNR_dB = Pwr_rec_Rx1_139_Insertion_Loss_dBm - Friis_Noise_dBm;

Rx2_Friis_SNR_dB = Pwr_rec_Rx2_138_Insertion_Loss_dBm - Friis_Noise_dBm;

```

```

% PLOT SNR for Wideband Scans vs. Friis predicted - anti-aliasing
% figure in 80 dB gain box is extremely important

%PLOT Rx1&2, Scans 1 & 4 and predicted (wideband)
figure61 = figure('Color',[1,1,1],...
                 'Name','SNR Plot Widband Scans and Predicted');

% Create axes
axes1 = axes('Parent',figure61);
hold(axes1,'on');
box(axes1,'on');

hold on;
% Plot Frequency vs. Absorption in dBm/km
plot(Scan_WB_Frequencies, 116+Rx1_SNR_dB(1:11), '-o b')

plot(Scan_WB_Frequencies, 116+Rx2_SNR_dB(1:11), '-x g')

plot(Scan_WB_Frequencies, 116+Rx1_SNR_dB(34:44), '+ c')

plot(Scan_WB_Frequencies, 116+Rx2_SNR_dB(34:44), '-* m')

plot(Scan_WB_Frequencies, Rx1_Friis_SNR_dB(1:11), '-d r')

plot(Scan_WB_Frequencies, Rx2_Friis_SNR_dB(1:11), '-v y')

hold off;

% Create xlabel
xlabel('Frequency (GHz)');

% Create ylabel
ylabel('SNR (dB)');

Title = ['SNR Plot WB Scans and Predicted (',...
        num2str(THz_month),' ', num2str(THz_day),' ',...
        num2str(THz_year),' ', num2str(THz_hour),...
        ':',num2str(THz_minute),':',num2str(THz_second),')'];

% Create title
title(Title);

% create Legend
legend('Rx1-Scan1','Rx2-Scan1','Rx1-Scan4','Rx2-Scan4',...
      'Rx1-Friis','Rx2-Friis');

box(axes1,'on');
% Set the remaining axes properties
set(axes1,'FontSize',16);

```

```

%PLOT Rx1&2, Scans 2 & 5 and Friis predicted (LWL)
figure62 = figure('Color',[1,1,1],...
    'Name','Absorption Plot LWL Scans and Friis Predicted');

% Create axes
axes1 = axes('Parent',figure62);
hold(axes1,'on');
box(axes1,'on');
hold on;

% Plot Frequency vs. Absorption in dBm/km

plot(Scan_LWL_Frequencies, 116+Rx1_SNR_dB(12:22), '-o b')

plot(Scan_LWL_Frequencies, 116+Rx2_SNR_dB(12:22), '-x g')

plot(Scan_LWL_Frequencies, 116+Rx1_SNR_dB(45:55), '-+ c')

plot(Scan_LWL_Frequencies, 116+Rx2_SNR_dB(45:55), '-* m')

plot(Scan_LWL_Frequencies, Rx1_Friis_SNR_dB(12:22), '-d r')

plot(Scan_LWL_Frequencies, Rx2_Friis_SNR_dB(12:22), '-v y')

hold off;

% Create xlabel
xlabel('Frequency (GHz)');

% Create ylabel
ylabel('SNR (dB)');

Title = ['SNR Plot LWL Scans and Predicted (' , ...
    num2str(THz_month), ' ', num2str(THz_day), ' ', num2str(THz_year), ', ', ' , ...
    num2str(THz_hour), ': ', num2str(THz_minute), ': ', num2str(THz_second), ') '];

% Create title
title(Title);

% create Legend
legend('Rx1-Scan2', 'Rx2-Scan2', 'Rx1-Scan5', 'Rx2-Scan5', ...
    'Rx1-Friis', 'Rx2-Friis');

box(axes1,'on');
% Set the remaining axes properties
set(axes1,'FontSize',16);

```

```

%PLOT Rx1&2, Scans 3 & 6 and FRIIS predicted (UWL)
figure63 = figure('Color',[1,1,1],...
                 'Name','Absorption Plot UWL Scans and Predicted');

% Create axes
axes1 = axes('Parent',figure63);
hold(axes1,'on');
box(axes1,'on');

hold on
% Plot Frequency vs. Absorption in dBm/km

plot(Scan_UWL_Frequencies, 116+Rx1_SNR_dB(23:33), '-o b');
plot(Scan_UWL_Frequencies, 116+Rx2_SNR_dB(23:33), '-x g');
plot(Scan_UWL_Frequencies, 116+Rx1_SNR_dB(56:66), '-+ c');
plot(Scan_UWL_Frequencies, 116+Rx2_SNR_dB(56:66), '-* m');
plot(Scan_UWL_Frequencies, Rx1_Friis_SNR_dB(23:33), '-d r');
plot(Scan_UWL_Frequencies, Rx2_Friis_SNR_dB(23:33), '-v y');

hold off;

% Create xlabel
xlabel('Frequency (GHz)');

% Create ylabel
ylabel('SNR (dB)');

Title = ['SNR Plot UWL Scans and Predicted(',num2str(THz_month),' ',...
        num2str(THz_day),' ', num2str(THz_year),' ', num2str(THz_hour),...
        ':',num2str(THz_minute),':',num2str(THz_second),')'];

% Create title
title(Title);

% create Legend
legend('Rx1-Scan3','Rx2-Scan3','Rx1-Scan6','Rx2-Scan6', ...
      'Rx1-Friis','Rx2-Friis');

box(axes1,'on');
% Set the remaining axes properties
set(axes1,'FontSize',16);

#####

% ##### Cn2 #####

```

```

% Calculate and Plot Integrated Cn2 - Two ways:area and displacement

% SINGLE LED - area calculation - shutter speed > 1 ms

Diameter_m = .152; % diameter of telescope = 6" from data sheet

Pixel_size_m = 3.75 * 10^(-6); % from data sheet - convert um to m

Focal_Length_m = 1.524; % from telescope data sheet

number_of_pixels = Scintillometer_Area; % area is number of pixels

% cacluate Cn2
Cn2 = .009788 * Path_Length_m^(-1) * Diameter_m^(1/3) * ...
      Focal_Length_m^(-1)* Pixel_size_m^(2).* number_of_pixels;

% calculate the mean of Cn2
Cn2_SingleLED_Mean = mean(Cn2);

% Obtain Date and time from Scintillometer Receiver EPOCH time data
scint_time_vector = cdflib.epochBreakdown(Scintillometer_time);

scint_year = scint_time_vector(1,1)+1970; % started at 1970

scint_month = scint_time_vector(2,1);

scint_day = scint_time_vector(3,1);

% this assumes we are on MDT=6, MST=7
scint_hour = scint_time_vector(4,1)- 6 - daylight_adjust;

if scint_hour < 0
    scint_hour = 24 + scint_hour; % adjust time at 0 crossing
end

scint_minute = scint_time_vector(5,1);

scint_second = scint_time_vector(6,1);

% cacluate all millisecond pointers for all sensors
% Scint Receiver Link ms Time
scint_ms = scint_time_vector(7,:);

% add minutes, seconds and ms
scint_s = scint_time_vector(4,:).* (60*60) + ...
          scint_time_vector(5,:).*60 + scint_time_vector(6,:) + scint_ms./1000;

% Get the size vector for the time dimension vector
scint_Time_Dimensions = size(scint_s);

% pick out the number of rows out of the size vector

```

```

Number_scint_Time_Rows = scint_Time_Dimensions(1);

% record the start time of the scint collection
scint_Start_time_s = scint_s(1,1);

% start anemometer time from zero - subtract start time from all times
scint_time_zero_s = scint_s - scint_Start_time_s;

%PLOT Cn2
figure49 = figure('Color',[1,1,1], 'Name', 'C_n^2 Plot - based on Area');

% Create axes
axes1 = axes('Parent',figure49);
hold(axes1, 'on');
box(axes1, 'on');

% Plot Cn2 m^(-2/3)
plot(scint_time_zero_s, Cn2, '-');

% Create xlabel
xlabel('time (s)');

% Create ylabel
ylabel('C_n^2 m^(^-2/^3^)');

Title = ['C_n^2 Area (' , num2str(scint_month), ' ', ...
        num2str(scint_day), ' ', num2str(scint_year), ' ', ...
        num2str(scint_hour), ':', num2str(scint_minute), ':', ...
        num2str(scint_second), ')', ' mean = ', ...
        num2str(Cn2_SingleLED_Mean), ' m^(^-2/^3^)'];

% Create title
title(Title);

box(axes1, 'on');
% Set the remaining axes properties
set(axes1, 'FontSize', 16);

% frequency domain analysis of Cn2

Cn2_Freq = abs(fft(Cn2));

x = 1:134; % make a vector x as long as the number of samples in the FFT
freq_Cn2 = x.*(1 /.06) ; % FFT bin size (Ws/N)

figure50 = figure('Color',[1,1,1], 'Name', 'C_n^2, FFT');

% Create axes
axes1 = axes('Parent',figure50);
hold(axes1, 'on');

```

```

box(axes1, 'on');

% Plot Frequency vs. Mean Amplitude in dBm
plot(Cn2_Freq, '- ');

% Create xlabel
xlabel('Frequency (Hz)');

% Create ylabel
ylabel('Amplitude');

Title = ['C_n^2 FFT (' , num2str(scint_month), ' ', ...
        num2str(scint_day), ' ', num2str(scint_year), ', ', ...
        num2str(scint_hour), ':', num2str(scint_minute), ':', ...
        num2str(scint_second), ')'];

% Create title
title(Title);

box(axes1, 'on');
% Set the remaining axes properties
set(axes1, 'FontSize', 16);

% Multiple LED - Barker Cross - displacement calculation -
% shutter speed < 1 ms - use the delta LED equation

% calculate the standard deviation in the X direction - X is in # of Pixels
% so Centriod is displacement times pixel size
Total_Displacement = sqrt(Scintillometer_Xloc.^2 + Scintillometer_Yloc.^2);

Centriod_m = std(Total_Displacement .* Pixel_size_m);

% Calculate Cn2 with displacement
Cn2_Barker = Centriod_m^2 / (2.838 * Path_Length_m * Diameter_m^(-1/3) * ...
                            Focal_Length_m);

Cn2_Barker_Mean = mean(Cn2_Barker); % Find the mean of Cn2

%PLOT Cn2
figure51 = figure('Color', [1,1,1], ...
                 'Name', 'C_n^2 Plot - based on displacement');

% Create axes
axes1 = axes('Parent', figure51);
hold(axes1, 'on');
box(axes1, 'on');

% Plot Cn2 m^(-2/3)
plot(scint_time_zero_s, Cn2_Barker, '- o b');

```

```

% Create xlabel
xlabel('time (s)');

% Create ylabel
ylabel('C_n^2  m^(-^2/^3^)');

Title = ['C_n^2 AoA (' ,num2str(scint_month), ' ',...
        num2str(scint_day), ' ', num2str(scint_year), ' ', ' ',...
        num2str(scint_hour), ':', num2str(scint_minute), ':', ' ',...
        num2str(scint_second), ')', ' ', ...
        ' mean = ', num2str(Cn2_Barker_Mean), ' m^(-^2/^3^)'];

% Create title
title(Title);

box(axes1, 'on');
% Set the remaining axes properties
set(axes1, 'FontSize', 16);
#####

% ##### ANEMOMETER #####
%      Anemometer Processing and Plotting
% Format: # Timestamp    U m/s    V m/s    W m/s    Temp (C degrees)
% calculate the means for all data

% U along wind component - parallel the THz path
% V across wind component - perpendicular the THz path
% W vertical wind component - below to above THz path
% Tx means

Anemometer_Tx_U_mean_m_per_s = mean(Anemometer_Tx_U);

Anemometer_Tx_V_mean_m_per_s  = mean(Anemometer_Tx_V);

Anemometer_Tx_W_mean_m_per_s  = mean(Anemometer_Tx_W);

Anemometer_Tx_Temp_mean_C = mean(Anemometer_Tx_Temp);

% Rx
Anemometer_Rx_U_mean_m_per_s = mean(Anemometer_Rx_U);

Anemometer_Rx_V_mean_m_per_s  = mean(Anemometer_Rx_V);

Anemometer_Rx_W_mean_m_per_s  = mean(Anemometer_Rx_W);

Anemometer_Rx_Temp_mean_C = mean(Anemometer_Rx_Temp);

% Tx time
Anemometer_Tx_time = Anemometer_data_Tx(:,1);

% Obtain Date and time from Anemometer Tx and Rx EPOCH time data

```

```

Anemo_time_vector_Tx = cdflib.epochBreakdown(Anemometer_Tx_time);

Anemo_year = Anemo_time_vector_Tx(1,1)+1970; % started at 1970

Anemo_month = Anemo_time_vector_Tx(2,1);

Anemo_day = Anemo_time_vector_Tx(3,1);

% this assumes we are on MDT=6, MST=7
Anemo_hour_Tx = Anemo_time_vector_Tx(4,1) - 6 - daylight_adjust;

if Anemo_hour_Tx < 0

    Anemo_hour_Tx = 24 + Anemo_hour_Tx; % adjust time at 0 crossing

end

Anemo_minute_Tx = Anemo_time_vector_Tx(5,1);

Anemo_second_Tx = Anemo_time_vector_Tx(6,1);

% Rx Time
Anemometer_Rx_time = Anemometer_data_Rx(:,1);

% Obtain Date and time from Anemometer Tx and Rx EPOCH time data
Anemo_time_vector_Rx = cdflib.epochBreakdown(Anemometer_Rx_time);

% year, month and day will be identical to Tx
% this assumes we are on MDT, MST=7
Anemo_minute_Rx = Anemo_time_vector_Rx(5,1);

Anemo_second_Rx = Anemo_time_vector_Rx(6,1);

% Tx cacluate all second pointers for Anemometer
% Anemo Tx ms Time
Anemo_ms_Tx = Anemo_time_vector_Tx(7,:);

% add minutes, seconds and ms
Anemo_time_s_Tx = Anemo_time_vector_Tx(4,:).*(60*60) + ...
Anemo_time_vector_Tx(5,:).*60 + Anemo_time_vector_Tx(6,:) + ...
    Anemo_ms_Tx./1000;

% record the start time of the anaomometer collection
Anemo_Start_time_s_Tx = Anemo_time_s_Tx(1,1);

% start anemometer time from zero - subtract start time from all times
Anemo_time_zero_s_Tx = Anemo_time_s_Tx - Anemo_Start_time_s_Tx;

% Rx cacluate all second pointers for Anemometer

```

```

% don't need to line up Tx and Rx vectors in Time, since the frequency
% samples are stagared by 100ms increments. These times are off in the 40
% ms range
% Anemo Rx ms Time
Anemo_ms_Rx = Anemo_time_vector_Rx(7,:);

% add minutes, seconds and ms
Anemo_time_s_Rx = Anemo_time_vector_Rx(4,:).*(60*60) + ...
    Anemo_time_vector_Rx(5,:).*60 + Anemo_time_vector_Rx(6,:) + ...
    Anemo_ms_Rx./1000;

% record the start time of the anaomometer collection
Anemo_Start_time_s_Rx = Anemo_time_s_Rx(1,1);

% start anemometer time from zero - subtract start time from all times
Anemo_time_zero_s_Rx = Anemo_time_s_Rx - Anemo_Start_time_s_Rx;

% calculate the Tx + Rx mean vector
Anemometer_mean_Temp = (Anemometer_Tx_Temp + Anemometer_Rx_Temp)./2;

% calculate the mean value of the mean vector
Anemometer_mean_Temp_value = mean(Anemometer_mean_Temp);

% plot Tx and Rx Temperatures vs. Time
figure52 = figure('Color',[1,1,1],'Name','Temperature Plot');

    % Create axes
    axes1 = axes('Parent',figure52);
    hold(axes1,'on');
    box(axes1,'on');

    hold on; % plot multiple graphs on single plot

    % Plot with lines between points and "o" on points
    plot(Anemo_time_zero_s_Tx,Anemometer_Tx_Temp, '- b');

    % plot Rx on same plot in green
    plot(Anemo_time_zero_s_Rx,Anemometer_Rx_Temp, '- g');

    % plot mean in red
    plot(Anemo_time_zero_s_Rx,Anemometer_mean_Temp, '- r');

    hold off

    % Create xlabel
    label_for_X = ['start time = ',num2str(Anemo_Start_time_s_Tx),...
        's time (s)'];
    xlabel(label_for_X);

    % Create ylabel
    ylabel('Temperature (^oC)');

```

```

Title = ['Temp (',num2str(Anemo_month),' ',...
        num2str(Anemo_day),' ', num2str(Anemo_year),' ',...
        num2str(Anemo_hour_Tx),':',num2str(Anemo_minute_Tx),...
        ':',num2str(Anemo_second_Tx),')', ...
        ' means:', 'Tx=',num2str(Anemometer_Tx_Temp_mean_C),' ^oC',...
        ' Rx=',num2str(Anemometer_Rx_Temp_mean_C),' ^oC',' Total=',...
        num2str(Anemometer_mean_Temp_value),' ^oC'];

% Create title
title(Title);

% legend
legend('AnemoTx','AnemoRx','AnemoMean');

box(axes1,'on');
% Set the remaining axes properties
set(axes1,'FontSize',16);

% U wind along Path
% calculate the Tx + Rx mean vector
Anemometer_mean_U = (Anemometer_Tx_U + Anemometer_Rx_U)./2;

% calculate the mean value of the mean vector
Anemometer_mean_U_value = mean(Anemometer_mean_U);

% Plot Wind components for Tx and Rx together vs time

% plot U along path wind
figure53 = figure('Color',[1,1,1],'Name','U Wind along path Plot');

% Create axes
axes1 = axes('Parent',figure53);
hold(axes1,'on');
box(axes1,'on');

hold on; % plot multiple graphs on single plot

% Plot with lines between points and "o" on points
plot(Anemo_time_zero_s_Tx,Anemometer_Tx_U, '- b');

% plot Rx on same plot in green
plot(Anemo_time_zero_s_Rx,Anemometer_Rx_U, '- g');

% plot mean in red
plot(Anemo_time_zero_s_Rx,Anemometer_mean_U, '- r');

hold off
% Create xlabel

```

```

label_for_X = ['start time = ', num2str(Anemo_Start_time_s_Tx), ...
              's time (s)'];
xlabel(label_for_X);

% Create ylabel
ylabel('Wind Along Path - U (m/s)');

Title = ['Wind (', num2str(Anemo_month), ' ', ...
        num2str(Anemo_day), ' ', num2str(Anemo_year), ' ', ...
        num2str(Anemo_hour_Tx), ':', num2str(Anemo_minute_Tx), ':', ...
        num2str(Anemo_second_Tx), ')', ...
        ' means:', 'Tx=', num2str(Anemometer_Tx_U_mean_m_per_s), ' m/s', ...
        ' Rx=', num2str(Anemometer_Rx_U_mean_m_per_s), ' m/s', ' Total=', ...
        num2str(Anemometer_mean_U_value), ' m/s'];

% Create title
title(Title);

% legend
legend('AnemoTx', 'AnemoRx', 'AnemoMean');

box(axes1, 'on');
% Set the remaining axes properties
set(axes1, 'FontSize', 16);

% V wind along Path
% calculate the Tx + Rx mean vector
Anemometer_mean_V = (Anemometer_Tx_V + Anemometer_Rx_V) ./ 2;

% calculate the mean value of the mean vector
Anemometer_mean_V_value = mean(Anemometer_mean_V);

% plot V across path wind
figure54 = figure('Color', [1, 1, 1], 'Name', 'V Wind across path Plot');

% Create axes
axes1 = axes('Parent', figure54);
hold(axes1, 'on');
box(axes1, 'on');

hold on; % plot multiple graphs on single plot

% Plot with lines between points and "o" on points
plot(Anemo_time_zero_s_Tx, Anemometer_Tx_V, '- b');

% plot Rx on same plot in green
plot(Anemo_time_zero_s_Rx, Anemometer_Rx_V, '- g');

% plot mean in red

```

```

plot(Anemo_time_zero_s_Rx,Anemometer_mean_V, '- r');

hold off

% Create xlabel
label_for_X = ['start time = ',num2str(Anemo_Start_time_s_Tx),...
              's time (s)'];
xlabel(label_for_X);

% Create ylabel
ylabel('Wind Across Path - V (m/s)');

Title = ['Wind (',num2str(Anemo_month),' ',...
        num2str(Anemo_day),' ', num2str(Anemo_year),',', ' ',...
        num2str(Anemo_hour_Tx),':',num2str(Anemo_minute_Tx),':',...
        num2str(Anemo_second_Tx),')', ' means:', 'Tx=',...
        num2str(Anemometer_Tx_V_mean_m_per_s), ' m/s',...
        ' Rx=',num2str(Anemometer_Rx_V_mean_m_per_s),...
        ' m/s', ' Total=',num2str(Anemometer_mean_V_value), ' m/s'];

% Create title
title(Title);

% legend('Anemometer-Tx-Temp','Anemometer-Rx-Temp', ...
% 'location','northwest');
legend('AnemoTx','AnemoRx','AnemoMean');

box(axes1,'on');
% Set the remaining axes properties
set(axes1,'FontSize',16);

% W wind Vertical to path
% calculate the Tx + Rx mean vector
Anemometer_mean_W = (Anemometer_Tx_W + Anemometer_Rx_W)./2;

% calculate the mean value of the mean vector
Anemometer_mean_W_value = mean(Anemometer_mean_W);

% plot W vertical wind path
figure55 = figure('Color',[1,1,1],'Name','W Wind vertical path Plot');

% Create axes
axes1 = axes('Parent',figure55);
hold(axes1,'on');
box(axes1,'on');

hold on; % plot multiple graphs on single plot

% Plot with lines between points and "o" on points
plot(Anemo_time_zero_s_Tx,Anemometer_Tx_W, '- b');

```

```

% plot Rx on same plot in green
plot(Anemo_time_zero_s_Rx,Anemometer_Rx_W, '- g');

% plot mean in red
plot(Anemo_time_zero_s_Rx,Anemometer_mean_W, '- r');

hold off

% Create xlabel
label_for_X = ['start time = ',num2str(Anemo_Start_time_s_Tx),...
              's time (s)'];
xlabel(label_for_X);

% Create ylabel
ylabel('Wind Vertical Path - W (m/s)');

Title = ['Wind (',num2str(Anemo_month),' ',...
        num2str(Anemo_day),' ', num2str(Anemo_year),' ',...
        num2str(Anemo_hour_Tx),':',num2str(Anemo_minute_Tx),':',...
        num2str(Anemo_second_Tx),')', ' means:', 'Tx=',...
        num2str(Anemometer_Tx_W_mean_m_per_s), ' m/s',...
        ' Rx=',num2str(Anemometer_Rx_W_mean_m_per_s), ' m/s',...
        ' Total=',num2str(Anemometer_mean_W_value), ' m/s'];

% Create title
title(Title);

% legend('Anemometer-Tx-Temp','Anemometer-Rx-Temp',...
% 'location','northwest');
legend('AnemoTx','AnemoRx','AnemoMean');

box(axes1,'on');
% Set the remaining axes properties
set(axes1,'FontSize',16);
#####

%% ##### HYGROMETER #####
% Plot Hygrometer data at Tx and Rx together
% make an Array of the average of the two
% Units are g/m^3

Boulder_Altitude_m = 1655; % Boulder altitude in Meters

Boulder_pressure_psi = 12.2;

Boulder_sat_hum_kPH = 86;

% read Hygrometer data from Tx and Rx Hygrometers
% the Hygrometers each require a calibration file as noted, the calibration
% is applied in the TAIPAS software

```

```

% Tx Hygrometer
% Version: 1.0_7b8455dadeba Built on: Mar 22 2016 @ 13:20:53
% Serial Number: 1729
% Clean Full Range Calibration data (Xkw:ln(Vo)) = -0.2 / 8.49
%# Clean Dry Range Calibration data (Xkw:ln(Vo)) = -0.21 / 8.538
% Clean Wet Range Calibration data (Xkw:ln(Vo)) = -0.198 / 8.458
% Scaled Full Range Calibration data (Xkw:ln(Vo)) = -0.201 / 8.15
% Scaled Dry Range Calibration data (Xkw:ln(Vo)) = -0.216 / 8.219
% Scaled Wet Range Calibration data (Xkw:ln(Vo)) = -0.198 / 8.103
%           Clean      Clean      Clean      Scaled      Scaled      Scaled
% Time           Full      Dry      Wet      Full      Dry      Wet
% for Colorado, the scaled values are not necessary
% the two primary values required are Clean Dry and Clean Wet in g/m^3

% cacluate mean

Hygrometer_Tx_dry_mean_g_per_m3 = mean(Hygrometer_Tx_dry);

Hygrometer_Tx_wet_mean_g_per_m3 = mean(Hygrometer_Tx_wet);

% Rx Hygrometer
% Version: 1.0_7b8455dadeba Built on: Mar 22 2016 @ 13:20:53
% Serial Number: 1733
% Clean Full Range Calibration data (Xkw:ln(Vo)) = -0.184 / 8.695
% Clean Dry Range Calibration data (Xkw:ln(Vo)) = -0.199 / 8.776
% Clean Wet Range Calibration data (Xkw:ln(Vo)) = -0.177 / 8.588
% Scaled Full Range Calibration data (Xkw:ln(Vo)) = -0.187 / 8.077
% Scaled Dry Range Calibration data (Xkw:ln(Vo)) = -0.201 / 8.151
% Scaled Wet Range Calibration data (Xkw:ln(Vo)) = -0.181 / 7.985
%           Clean      Clean      Clean      Scaled      Scaled      Scaled
% Time           Full      Dry      Wet      Full      Dry      Wet
% for Colorado, the scaled values are not necessary
% the two primary values required are Clean Dry and Clean Wet in g/m^3

% cacluate mean

Hygrometer_Rx_dry_mean_g_per_m3 = mean(Hygrometer_Rx_dry);

Hygrometer_Rx_wet_mean_g_per_m3 = mean(Hygrometer_Rx_wet);

% Tx Time
% Obtain Date and time from Anemometer Tx and Rx EPOCH time data
Hygro_time_vector_Tx = cdflib.epochBreakdown(Hygrometer_Tx_time);

Hygro_year = Hygro_time_vector_Tx(1,1)+1970; % started at 1970

Hygro_month = Hygro_time_vector_Tx(2,1);

Hygro_day = Hygro_time_vector_Tx(3,1);

% this assumes we are on MDT, MST=7

```

```

Hygro_hour_Tx = Hygro_time_vector_Tx(4,1) - 6 - daylight_adjust;

if Hygro_hour_Tx < 0

    Hygro_hour_Tx = 24 + Hygro_hour_Tx; % adjust time at 0 crossing

end

Hygro_minute_Tx = Hygro_time_vector_Tx(5,1);

Hygro_second_Tx = Hygro_time_vector_Tx(6,1);

% Rx Time
% Obtain Date and time from Anemometer Tx and Rx EPOCH time data
Hygro_time_vector_Rx = cdflib.epochBreakdown(Hygro_meter_Rx_time);

% year, month and day will be identical to Tx
% this assumes we are on MDT, MST=7
Hygro_hour_Rx = Hygro_time_vector_Rx(4,1) - 6 - daylight_adjust;

if Hygro_hour_Rx < 0

    Hygro_hour_Rx = 24 + Hygro_hour_Rx; % adjust time at 0 crossing

end

Hygro_minute_Rx = Hygro_time_vector_Rx(5,1);

Hygro_second_Rx = Hygro_time_vector_Rx(6,1);

% Tx calculate all second pointers for Anemometer
% Anemo Tx ms Time
Hygro_ms_Tx = Hygro_time_vector_Tx(7,:);

% add minutes, seconds and ms
Hygro_time_s_Tx = Hygro_time_vector_Tx(4,:).* (60*60) + ...
    Hygro_time_vector_Tx(5,:).*60 + Hygro_time_vector_Tx(6,:)...
    + Hygro_ms_Tx./1000;

% record the start time of the anemometer collection
Hygro_Start_time_s_Tx = Hygro_time_s_Tx(1,1);

% start anemometer time from zero - subtract start time from all times
Hygro_time_zero_s_Tx = Hygro_time_s_Tx - Hygro_Start_time_s_Tx;

% Rx calculate all second pointers for Anemometer
% don't need to line up Tx and Rx vectors in Time, since the frequency
% samples are staggered by 100ms increments. These times are off in the 40
% ms range
% Anemo Rx ms Time

```

```

Hygro_ms_Rx = Hygro_time_vector_Rx(7,:);

% add minutes, seconds and ms
Hygro_time_s_Rx = Hygro_time_vector_Rx(4,:).*(60*60) + ...
    Hygro_time_vector_Rx(5,:).*60 + Hygro_time_vector_Rx(6,:) + ...
    Hygro_ms_Rx./1000;

% record the start time of the anaomometer collection
Hygro_Start_time_s_Rx = Hygro_time_s_Rx(1,1);

% start anemometer time from zero - subtract start time from all times
Hygro_time_zero_s_Rx = Hygro_time_s_Rx - Hygro_Start_time_s_Rx;

% calculate the Tx + Rx mean vectors
Hygro_mean_dry = (Hygrometer_Tx_dry + Hygrometer_Rx_dry)./2;

Hygro_mean_wet = (Hygrometer_Tx_wet + Hygrometer_Rx_wet)./2;

% calculate the mean value of the mean vector
Hygro_mean_dry_value = mean(Hygro_mean_dry);

Hygro_mean_wet_value = mean(Hygro_mean_wet);

% plot Tx and Rx humidities vs. Time

figure56 = figure('Color',[1,1,1],'Name','Humidity Plot');

% Create axes
axes1 = axes('Parent',figure56);
hold(axes1,'on');
box(axes1,'on');

    hold on; % plot multiple graphs on single plot

    % Plot with lines between points and "o" on points
plot(Hygro_time_zero_s_Tx,Hygrometer_Tx_dry, '- b x');

plot(Hygro_time_zero_s_Tx,Hygrometer_Tx_wet, '- g x');

    % plot Rx on same plot in green
plot(Hygro_time_zero_s_Rx,Hygrometer_Rx_dry, '- k +');

plot(Hygro_time_zero_s_Rx,Hygrometer_Rx_wet, '- y +');

    % plot mean
plot(Hygro_time_zero_s_Rx,Hygro_mean_dry, '- c d');

plot(Hygro_time_zero_s_Rx,Hygro_mean_wet, '- m d');

    hold off

```

```

% Create xlabel
label_for_X = ['start time = ', num2str(Anemo_Start_time_s_Tx), ...
              's time (s)'];
xlabel(label_for_X);

% Create ylabel
ylabel('Humidity (g/m^3)');

Title = ['Humidity (', num2str(Hygro_month), ' ', ...
        num2str(Hygro_day), ' ', num2str(Hygro_year), ' ', ...
        num2str(Hygro_hour_Tx), ':', num2str(Hygro_minute_Tx), ':', ...
        num2str(Hygro_second_Tx), ')', ' means:', 'dry=', ...
        num2str(Hygro_mean_dry_value), ' g/m^3', ...
        ' wet=', num2str(Hygro_mean_wet_value), ' g/m^3'];

% Create title
title(Title);

legend('Tx dry', 'Tx wet', 'Rx dry', 'Rx wet', 'Mean Dry', 'Mean Wet');

box(axes1, 'on');
% Set the remaining axes properties
set(axes1, 'FontSize', 16);
#####

%% ##### MUTUAL COHERENCE FUNCTION (MCF) #####
% MUTUAL COHERENCE FUNCTION (MCF) = <Rx1 x Rx2*>
% variance of the Conjugate of Rx2 times Rx1

% Amplitude Spatial Covariance with Aperture averaging is close to one for
% all cases for for .5 m = 1, 1 m = 1, 2 m = .98 and 3 m = .92; no
% adjustments where made here - does not affect phase at all.

% conjugate Rx2
Conj_Rx2_THz_Complex_Data = conj(Rx2_THz_Complex_Data);

% multiply Rx1 and conjugate Rx2 - and get expected value for each
% frequency
MCF = mean(Rx1_THz_Complex_Data .* Conj_Rx2_THz_Complex_Data);

% compute the tan-1 of the complex number (imaginary over real)
MCF_Phase_rad = angle(MCF);
MCF_Phase_deg = (180/pi) .* MCF_Phase_rad;

% Amplitude Spatial Covariance with Aperture averaging is close to one for
% all cases without aperture averaging (.5 m = 1, 1 m = 1, 2 m = .98 and
% 3 m = .92 - does not affect phase at all. With aperture averaging, see
% below equation
Amp_sp_cov_apert_avg_range = [1, .99, .94, .88];

Amp_Spatial_Cov_Apert_Avg = ...

```

```

        Amp_sp_cov_apert_avg_range(Rx_separation_Rho_m + 1);

MCF_Amp_squared = (abs(MCF).* Amp_Spatial_Cov_Apert_Avg).^2;

% the phase structure function MCF = <E1E2*> = |E|^2 exp[-1/2 D(rho)]
Phase_Structure_Function_rad = -2 .* MCF_Phase_rad;

% if phase structure function <1, then coherent
% Phase in Degrees
Phase_Structure_Function_deg = (180/pi).* Phase_Structure_Function_rad;

% Amplitude power in dBm with receiver gain adjustment
MCF_W_dBm = ...
    10.*(log10((MCF_Amp_squared)./(50 *.001))) - Receiver_GAIN_adj_dB;

% Test if the distance allows the two receivers to behave as Coherent
for i=1:66

    if Phase_Structure_Function_rad(i) >= 1;
        Coho = 'INCOHERENT';

    else

        Coho = 'COHERENT';

    end
end

% plot variances against frequency
%PLOT MCF Scans 1 & 4 (wideband)
figure64 = figure('Color',[1,1,1],'Name','MCF Wideband Scans');

% Create axes
axes1 = axes('Parent',figure64);
hold(axes1,'on');
box(axes1,'on');

hold on;

% Plot Frequency vs. MCF
plot(Scan_WB_Frequencies, MCF_Phase_deg(1:11), '-o b');

plot(Scan_WB_Frequencies, Phase_Structure_Function_deg(1:11), '-x g');

plot(Scan_WB_Frequencies, MCF_Phase_deg(34:44), '-o b');

plot(Scan_WB_Frequencies, Phase_Structure_Function_deg(34:44), '-x g');

hold off;

% Create xlabel

```

```

xlabel('Frequency (GHz)');

% Create ylabel
ylabel('Phase (degrees)');

Title = ['MCF/Struct Funct Phases Widband Scans;',Coho,'(',...
        num2str(THz_month),' ',num2str(THz_day),' ', num2str(THz_year),' ',...
        num2str(THz_hour),':',num2str(THz_minute),':',num2str(THz_second),')'];

% Create title
title(Title);

% create Legend
legend('S1 MCF-phase','S1 Phase Struct. Funct.','S4 MCF-phase',...
        'S4 Phase Struct. Funct.');
```

```

box(axes1,'on');
    % Set the remaining axes properties
    set(axes1,'FontSize',16);

%PLOT MCF Scans 2 & 5 (LWL)
figure66 = figure('Color',[1,1,1],'Name','MCF LWL Scans');
```

```

% Create axes
    axes1 = axes('Parent',figure66);
    hold(axes1,'on');
    box(axes1,'on');
```

```

hold on;
```

```

% Plot Frequency vs. MCF
plot(Scan_LWL_Frequencies, MCF_Phase_deg(12:22), '-o b');
```

```

plot(Scan_LWL_Frequencies, Phase_Structure_Function_deg(12:22),'-x g');
```

```

plot(Scan_LWL_Frequencies, MCF_Phase_deg(45:55), '-o b');
```

```

plot(Scan_LWL_Frequencies, Phase_Structure_Function_deg(45:55),'-x g');
```

```

hold off;
```

```

% Create xlabel
xlabel('Frequency (GHz)');
```

```

% Create ylabel
ylabel('Phase (degrees)');
```

```

Title = ['MCF/Struct Funct Phases LWL Scans;',Coho,'(',...
        num2str(THz_month),' ',num2str(THz_day),' ', num2str(THz_year),' ',...
        num2str(THz_hour),':',num2str(THz_minute),':',num2str(THz_second),')'];
```

```

% Create title
title(Title);

% create Legend
legend('S2 MCF-phase','S2 Phase Struct. Funct.','S5 MCF-phase', ...
       'S5 Phase Struct. Funct.');
```

```

box(axes1,'on');
% Set the remaining axes properties
set(axes1,'FontSize',16);

%PLOT MCF Scans 2 & 5 (UWL)
figure67 = figure('Color',[1,1,1],'Name','MCF UWL Scans');
```

```

% Create axes
axes1 = axes('Parent',figure67);
hold(axes1,'on');
box(axes1,'on')

hold on;
% Plot Frequency vs. MCF
plot(Scan_UWL_Frequencies, MCF_Phase_deg(23:33), '-o b')

plot(Scan_UWL_Frequencies, Phase_Structure_Function_deg(23:33),'-x g')

plot(Scan_UWL_Frequencies, MCF_Phase_deg(56:66), '-o b')

plot(Scan_UWL_Frequencies, Phase_Structure_Function_deg(56:66),'-x g')

hold off;

% Create xlabel
xlabel('Frequency (GHz)');

% Create ylabel
ylabel('Phase (degrees)');

Title = ['MCF/Struct Funct Phases UWL Scans;',Coho,'(', ...
        num2str(THz_month),' ',num2str(THz_day),' ', num2str(THz_year),' ', ...
        num2str(THz_hour),':',num2str(THz_minute),':',num2str(THz_second),')'];

% Create title
title(Title);

% create Legend
legend('S3 MCF-phase','S3 Phase Struct. Funct.','S6 MCF-phase', ...
       'S6 Phase Struct. Funct.');
```

```

box(axes1,'on');
% Set the remaining axes properties
set(axes1,'FontSize',16);
```

```

#####

%% ##### AMPLITUDE SCINTILLATION #####
% AMPLITUDE SCINTILLATION THEORY vs Data

% PLANEWAVE - since the receive point is very far and the sample window
% (Lens) is very small, the phase front will be constant other than AoA
% wavenumber = 2pi/lambda
% Amplitude Plane Wave - special case Kolmogorov; inertial,
% derived from first Rytov Approximation.
% special case = innerscale length going to zero
% Amplitude Variance
% Figure lambda for all frequencies scanned lambda=c/f
lambda_Scan_m = c_mpers ./ (Scan_Entire_Frequencies .* 10^9);

% if the variance of the amplitude < 1 then weak scattering
Amp_Variance_Kolmogorov_Npsq = .307.*(2*pi./lambda_Scan_m).^ (7/6).* ...
    (Path_Length_m^(11/6)*Cn2_SingleLED_Mean);

% 1Np^2= 75.44 dB^2, STD = sqrt of variance
Amp_STD_dB = sqrt(Amp_Variance_Kolmogorov_Npsq .* 75.44);

% since most of the propagation is closer to the outer scale factor, can
% make an outscale factor adjustment using Tatarski outer scale
% factor approximation of L0=.4h - Tatarski
% outer scale factor parameter = (2piR)lambda/L0^2
% figure average height
Height_avg_m = mean(Heights);

% calculate the outscale length - Tatarski estimate
L0_m = .4 * Height_avg_m;

% calculate the outscale factor parameter - function of frequency
Outer_scale_factor_param = (2*pi*Path_Length_m .*lambda_Scan_m ./ (L0_m^2));

% amplitude variance with outscale Factor Parameter adjustment
Amp_Var_Kolm_Outscale_Npsq = ...
    Amp_Variance_Kolmogorov_Npsq .* Outer_scale_factor_param;

% 1Np^2 = 75.44 dB^2
Amp_Var_Kolm_Outscale_dBsq = Amp_Var_Kolm_Outscale_Npsq.*75.44;

% Since this was a function of lambda- need to reverse order for frequency
Amp_Var_Kolm_Outscale_freq_dBsq = flipud(Amp_Var_Kolm_Outscale_dBsq);

% STD = sqrt of variance
Amp_STD_Kolm_Outscale_dB = sqrt(Amp_Var_Kolm_Outscale_dBsq);

% note since the Kolmogorov prediction is lambda - need to reverse order
% for frequency
Amp_STD_Kolm_Outscale_freq_dB = fliplr(Amp_STD_Kolm_Outscale_dB');

```

```

% since the fresnel length (sqrt(lamda*pathlength)) > (7 X(innerscale
% lengths), then there is no need to account for amplitude spatial
% covariance with Inner-Scale Influence
% Amplitude Wave Averaging Gain Factor Adjustment =1, since the Fresnel
% length is greater than the radius of the lens

% Collected TAIPAS data
% cacluate the STD of the data by taking the square root of the variance
Rx1_THz_STD_Amp_Cal_dB = sqrt(Rx1_THz_Variance_Amp_Cal_dBsq);

Rx2_THz_STD_Amp_Cal_dB = sqrt(Rx2_THz_Variance_Amp_Cal_dBsq);

% plot variances, STD against frequency
% note since the Kolmogorov prediction is lambda - need to reverse order

% PLOT Variance vs. Frequency

%PLOT Variance Amplitude Scintillation Scans 1 & 4 (wideband)
figure68 = figure('Color',[1,1,1],'Name','Variance Wideband Scans');

% Create axes
    axes1 = axes('Parent',figure68);
    hold(axes1,'on');
    box(axes1,'on')

hold on;

% Plot Frequency vs. STD
plot(Scan_WB_Frequencies, Amp_Var_Kolm_Outerscale_freq_dBsq(1:11), '-o b')

plot(Scan_WB_Frequencies, Rx1_THz_Variance_Amp_Cal_dBsq(1:11), '-x g')

plot(Scan_WB_Frequencies, Rx2_THz_Variance_Amp_Cal_dBsq(1:11), '-d c')

plot(Scan_WB_Frequencies, Amp_Var_Kolm_Outerscale_freq_dBsq(34:44),'-s b')

plot(Scan_WB_Frequencies, Rx1_THz_Variance_Amp_Cal_dBsq(34:44), '-* g')

plot(Scan_WB_Frequencies, Rx2_THz_Variance_Amp_Cal_dBsq(34:44), '-+ c')

hold off;

% Create xlabel
xlabel('Frequency (GHz)');

% Create ylabel
ylabel('Amplitude Scintillation Variance <X^2> (dB^2)');

```

```

Title = ['WB Scans Amp Scintillation/Predicted with outerscale factor;',...
        '(' , num2str(THz_month), ' ', num2str(THz_day), ' ', num2str(THz_year), ...
        ', ', num2str(THz_hour), ':', num2str(THz_minute), ':', ...
        num2str(THz_second), ')'];

% Create title
title(Title);

% create Legend
legend('S1 Pred-Var', 'S1 Rx1-Var', 'S1 Rx2-Var', 'S4 Pred-Var', ...
        'S4 Rx1-Var', 'S4 Rx2-Var');

box(axes1, 'on');
% Set the remaining axes properties
set(axes1, 'FontSize', 16);

%PLOT Amplitude Scintillation Variance Scans 2 & 5 (LWL)
figure69 = figure('Color', [1,1,1], 'Name', 'Variance LWL Scans');

% Create axes
axes1 = axes('Parent', figure69);
hold(axes1, 'on');
box(axes1, 'on')

hold on;
% Plot Frequency vs. STD
plot(Scan_LWL_Frequencies, ...
      Amp_Var_Kolm_Outerscale_freq_dBs(12:22), '-o b')

plot(Scan_LWL_Frequencies, ...
      Rx1_THz_Variance_Amp_Cal_dBs(12:22), '-x g')

plot(Scan_LWL_Frequencies, ...
      Rx2_THz_Variance_Amp_Cal_dBs(12:22), '-d c')

plot(Scan_LWL_Frequencies, ...
      Amp_Var_Kolm_Outerscale_freq_dBs(45:55), '-s b')

plot(Scan_LWL_Frequencies, ...
      Rx1_THz_Variance_Amp_Cal_dBs(45:55), '-* g')
plot(Scan_LWL_Frequencies, ...
      Rx2_THz_Variance_Amp_Cal_dBs(45:55), '-+ c')

hold off;

% Create xlabel
xlabel('Frequency (GHz)');

% Create ylabel
ylabel('Amplitude Variance (dB^2)');

```

```

Title = ...
    ['LWL Scans Amp Scintillation/Predicted with outerscale factor;', ...
    '(', num2str(THz_month), ' ', num2str(THz_day), ' ', num2str(THz_year), ...
    ', ', num2str(THz_hour), ':', num2str(THz_minute), ':', ...
    num2str(THz_second), ')'];

% Create title
title(Title);

% create Legend
legend('S2 Pred-Var', 'S2 Rx1-Var', 'S2 Rx2-Var', 'S5 Pred-Var', ...
       'S5 Rx1-Var', 'S5 Rx2-Var');

box(axes1, 'on');
    % Set the remaining axes properties
    set(axes1, 'FontSize', 16);

%PLOT Amplitude Scintillation Variance Scans 3 & 6 (UWL)
figure70 = figure('Color', [1,1,1], 'Name', 'Variance UWL Scans');

% Create axes
    axes1 = axes('Parent', figure70);
    hold(axes1, 'on');
    box(axes1, 'on')

hold on;
% Plot Frequency vs. STD
plot(Scan_UWL_Frequencies, ...
     Amp_Var_Kolm_Outerscale_freq_dBsq(23:33), '-o b')

plot(Scan_UWL_Frequencies, ...
     Rx1_THz_Variance_Amp_Cal_dBsq(23:33), '-x g')

plot(Scan_UWL_Frequencies, ...
     Rx2_THz_Variance_Amp_Cal_dBsq(23:33), '-d c')

plot(Scan_UWL_Frequencies, ...
     Amp_Var_Kolm_Outerscale_freq_dBsq(56:66), '-s b')

plot(Scan_UWL_Frequencies, ...
     Rx1_THz_Variance_Amp_Cal_dBsq(56:66), '-* g')

plot(Scan_UWL_Frequencies, ...
     Rx2_THz_Variance_Amp_Cal_dBsq(56:66), '-+ c')

hold off;

% Create xlabel
xlabel('Frequency (GHz)');

% Create ylabel

```

```

ylabel('Amplitude Variance <X^2> (dB^2)');

Title = ...
    ['UWL Scans Amp Scintillation/Predicted with outerscale factor;',...
    '(' ,num2str(THz_month), ' ', num2str(THz_day), ' ', num2str(THz_year), ...
    ', ', num2str(THz_hour), ':', num2str(THz_minute), ':', ...
    num2str(THz_second), ')'];

% Create title
title(Title);

% create Legend
legend('S3 Pred-Var', 'S3 Rx1-Var', 'S3 Rx2-Var', 'S6 Pred-Var', ...
       'S6 Rx1-Var', 'S6 Rx2-Var');

    box(axes1, 'on');
    % Set the remaining axes properties
    set(axes1, 'FontSize', 16);

% PLOT STD vs. Frequency

%PLOT STD Amplitude Scintillation Scans 1 & 4 (wideband)
figure71 = figure('Color', [1,1,1], 'Name', 'STD Wideband Scans');

% Create axes
    axes1 = axes('Parent', figure71);
    hold(axes1, 'on');
    box(axes1, 'on')

hold on;

% Plot Frequency vs. STD
plot(Scan_WB_Frequencies, Amp_STD_Kolm_Outscale_freq_dB(1:11), '-o b')

plot(Scan_WB_Frequencies, Rx1_THz_STD_Amp_Cal_dB(1:11), '-x g')

plot(Scan_WB_Frequencies, Rx2_THz_STD_Amp_Cal_dB(1:11), '-d c')

plot(Scan_WB_Frequencies, Amp_STD_Kolm_Outscale_freq_dB(34:44), '-s b')

plot(Scan_WB_Frequencies, Rx1_THz_STD_Amp_Cal_dB(34:44), '-* g')

plot(Scan_WB_Frequencies, Rx2_THz_STD_Amp_Cal_dB(34:44), '-+ c')

hold off

% Create xlabel
xlabel('Frequency (GHz)');

% Create ylabel
ylabel('Amplitude Scintillation Standard Deviations <X> (dB)');

```

```

Title = ['WB Scans Amp Scintillation/Predicted with outerscale factor;',...
        '(', num2str(THz_month), ' ', num2str(THz_day), ' ', num2str(THz_year), ...
        ', ', num2str(THz_hour), ':', num2str(THz_minute), ':', ...
        num2str(THz_second), ')'];

% Create title
title(Title);

% create Legend
legend('S1 Pred-STD', 'S1 Rx1-STD', 'S1 Rx2-STD', 'S4 Pred-STD', ...
       'S4 Rx1-STD', 'S4 Rx2-STD');

box(axes1, 'on');
% Set the remaining axes properties
set(axes1, 'FontSize', 16);

%PLOT Amplitude Scintillation STD Scans 2 & 5 (LWL)
figure72 = figure('Color', [1,1,1], 'Name', 'STD LWL Scans');

% Create axes
axes1 = axes('Parent', figure72);
hold(axes1, 'on');
box(axes1, 'on')

hold on

% Plot Frequency vs. STD
plot(Scan_LWL_Frequencies, ...
     Amp_STD_Kolm_Outscale_freq_dB(12:22), '-o b')

plot(Scan_LWL_Frequencies, Rx1_THz_STD_Amp_Cal_dB(12:22), '-x g')

plot(Scan_LWL_Frequencies, Rx2_THz_STD_Amp_Cal_dB(12:22), '-d c')

plot(Scan_LWL_Frequencies, Amp_STD_Kolm_Outscale_freq_dB(45:55), '-s b')

plot(Scan_LWL_Frequencies, Rx1_THz_STD_Amp_Cal_dB(45:55), '-* g')

plot(Scan_LWL_Frequencies, Rx2_THz_STD_Amp_Cal_dB(45:55), '-+ c')

hold off

% Create xlabel
xlabel('Frequency (GHz)');

% Create ylabel
ylabel('Amplitude Standard Deviations <X> (dB)');

Title = ...

```

```

    ['LWL Scans Amp Scintillation/Predicted with outerscale factor;',...
    '(' ,num2str(THz_month), ' ', num2str(THz_day), ' ', num2str(THz_year), ...
    ', ', num2str(THz_hour), ':', num2str(THz_minute), ':', ...
    num2str(THz_second), ')'];

% Create title
title(Title);

% create Legend
legend('S2 Pred-STD', 'S2 Rx1-STD', 'S2 Rx2-STD', 'S5 Pred-STD', ...
       'S5 Rx1-STD', 'S5 Rx2-STD');

box(axes1, 'on');
    % Set the remaining axes properties
    set(axes1, 'FontSize', 16);

%PLOT Amplitude Scintillation STD Scans 3 & 6 (UWL)
figure73 = figure('Color', [1,1,1], 'Name', 'STD UWL Scans');

% Create axes
axes1 = axes('Parent', figure73);
hold(axes1, 'on');
box(axes1, 'on')

hold on

% Plot Frequency vs. STD
plot(Scan_UWL_Frequencies, Amp_STD_Kolm_Outscale_freq_dB(23:33), '-o b')

plot(Scan_UWL_Frequencies, Rx1_THz_STD_Amp_Cal_dB(23:33), '-x g')

plot(Scan_UWL_Frequencies, Rx2_THz_STD_Amp_Cal_dB(23:33), '-d c')

plot(Scan_UWL_Frequencies, Amp_STD_Kolm_Outscale_freq_dB(56:66), '-s b')

plot(Scan_UWL_Frequencies, Rx1_THz_STD_Amp_Cal_dB(56:66), '-* g')

plot(Scan_UWL_Frequencies, Rx2_THz_STD_Amp_Cal_dB(56:66), '-+ c')

hold off

% Create xlabel
xlabel('Frequency (GHz)');

% Create ylabel
ylabel('Amplitude Standard Deviations <X> (dB)');

Title = ...
    ['UWL Scans Amp Scintillation/Predicted with outerscale factor;',...
    '(' ,num2str(THz_month), ' ', num2str(THz_day), ' ', num2str(THz_year), ...
    ', ', num2str(THz_hour), ':', num2str(THz_minute), ':', ...
    num2str(THz_second), ')'];

```

```

% Create title
title(Title);

% create Legend
legend('S3 Pred-STD', 'S3 Rx1-STD', 'S3 Rx2-STD', 'S6 Pred-STD', ...
      'S6 Rx1-STD', 'S6 Rx2-STD');

box(axes1, 'on');
    % Set the remaining axes properties
    set(axes1, 'FontSize', 16);
#####

%% ##### PHASE SCINTILLATION #####
% PHASE SCINTILLATION - Path Phase Variance/STD

% PLANEWAVE - since the receive point is very far and the sample window
% (Lens) is very small, the phase front will be constant other than AoA
% lambda wavenumber = 2pi/lambda
% outerscale wavenumber = 2pi/L0
% Phase Plane Wave - special case Geometric Optics (GO)

% Phase Variance - von Karman Model
Phase_Variance_GO_radsq = (.728*Path_Length_m).* ...
    (2*pi./lambda_Scan_m).^2.*Cn2_SingleLED_Mean.*(2*pi/L0_m)^(-5/3);

% Phase Variance in degrees squared
Phase_Variance_GO_degsq = Phase_Variance_GO_radsq.*(180/pi);

% Phase STD in degrees
Phase_STD_GO_deg = sqrt(Phase_Variance_GO_degsq);

% Phase STD in mm - divide degrees by 360 gives fraction of wavelength then
% multiply by wavelength
Phase_STD_GO_mm = (Phase_STD_GO_deg./360).* lambda_Scan_m .* 1000;

% calculate phase STD in picoseconds with T=lambda/C
Phase_STD_GO_ps = (Phase_STD_GO_mm./1000)./c_mpers.*1e12;

% Collected TAIPAS data
% cacluate the STD of the data by taking the square root of the variance

Phase_Rx1_rad= angle(Rx1_THz_Complex_Data);

Phase_Rx2_rad = angle(Rx2_THz_Complex_Data);

% Calculate variance in degrees squared
Phase_Rx1_Var_degsq = var(Phase_Rx1_rad).(180/pi);

Phase_Rx2_Var_degsq = var(Phase_Rx2_rad).(180/pi);

% Calculate STD in degrees - transpose to column vector
Phase_Rx1_STD_deg = sqrt(Phase_Rx1_Var_degsq)';

```

```

Phase_Rx2_STD_deg = sqrt(Phase_Rx2_Var_degsq)';

% Convert to mm
Phase_Rx1_STD_mm = (Phase_Rx1_STD_deg./360).* lambda_Scan_m .* 1000;

Phase_Rx2_STD_mm = (Phase_Rx2_STD_deg./360).* lambda_Scan_m .* 1000;

% Convert to ps
Phase_Rx1_STD_ps = (Phase_Rx1_STD_mm./1000)./c_mpers.*1e12;

Phase_Rx2_STD_ps = (Phase_Rx2_STD_mm./1000)./c_mpers.*1e12;

% note since the lambda is used in the equations,need to reverse order or
% flip for frequency plot
Phase_Variance_GO_freq_degsq = fliplr(Phase_Variance_GO_degsq);

Phase_STD_GO_freq_deg = flipud(Phase_STD_GO_deg);

Phase_STD_GO_freq_mm = flipud(Phase_STD_GO_mm);

Phase_STD_GO_freq_ps = flipud(Phase_STD_GO_ps);

% don't need to flip real data - already a function of freq
Phase_Rx1_Var_freq_degsq = (Phase_Rx1_Var_degsq);

Phase_Rx2_Var_freq_degsq = (Phase_Rx2_Var_degsq);

Phase_Rx1_STD_freq_deg = (Phase_Rx1_STD_deg);

Phase_Rx2_STD_freq_deg = (Phase_Rx2_STD_deg);

Phase_Rx1_STD_freq_mm = (Phase_Rx1_STD_mm);

Phase_Rx2_STD_freq_mm = (Phase_Rx2_STD_mm);

Phase_Rx1_STD_freq_ps = (Phase_Rx1_STD_ps);

Phase_Rx2_STD_freq_ps = (Phase_Rx2_STD_ps);

% plot phase variances, STD vs frequency for all units

%PLOT Variance Phase Scintillation Scans 1 & 4 (wideband)
figure74 = figure('Color',[1,1,1],'Name','Variance Wideband Scans');

% Create axes
axes1 = axes('Parent',figure74);
hold(axes1,'on');
box(axes1,'on')

```

```

hold on

% Plot Frequency vs. Variance
plot(Scan_WB_Frequencies, Phase_Variance_GO_freq_degsq(1:11), '-o b')

plot(Scan_WB_Frequencies, Phase_Rx1_Var_freq_degsq(1:11), '-x g')

plot(Scan_WB_Frequencies, Phase_Rx2_Var_freq_degsq(1:11), '-d c')

plot(Scan_WB_Frequencies, Phase_Variance_GO_freq_degsq(34:44), '-s b')

plot(Scan_WB_Frequencies, Phase_Rx1_Var_freq_degsq(34:44), '-* g')

plot(Scan_WB_Frequencies, Phase_Rx2_Var_freq_degsq(34:44), '-+ c')

hold off

% Create xlabel
xlabel('Frequency (GHz)')

% Create ylabel
ylabel('Phase Scintillation Variance <P^2> (deg^2)')

Title = ['WB Scans <P^2> Predicted', '(', ...
        num2str(THz_month), ' ', num2str(THz_day), ' ', num2str(THz_year), ' ', ...
        num2str(THz_hour), ':', num2str(THz_minute), ':', num2str(THz_second), ')'];

% Create title
title(Title);

% create Legend
legend('S1 Pred-Var', 'S1 Rx1-Var', 'S1 Rx2-Var', 'S4 Pred-Var', ...
      'S4 Rx1-Var', 'S4 Rx2-Var');

box(axes1, 'on');
    % Set the remaining axes properties
    set(axes1, 'FontSize', 16);

%PLOT Variance Phase Scintillation Scans 2 & 5 (LWL)
figure75 = figure('Color', [1,1,1], 'Name', 'Variance LWL Scans');

% Create axes
axes1 = axes('Parent', figure75);
hold(axes1, 'on');
box(axes1, 'on')

hold on;
% Plot Frequency vs. Variance

```

```

plot(Scan_LWL_Frequencies, Phase_Variance_GO_freq_degsq(12:22), '-o b')

plot(Scan_LWL_Frequencies, Phase_Rx1_Var_freq_degsq(12:22), '-x g')

plot(Scan_LWL_Frequencies, Phase_Rx2_Var_freq_degsq(12:22), '-d c')

plot(Scan_LWL_Frequencies, Phase_Variance_GO_freq_degsq(45:55), '-s b')

plot(Scan_LWL_Frequencies, Phase_Rx1_Var_freq_degsq(45:55), '-* g')

plot(Scan_LWL_Frequencies, Phase_Rx2_Var_freq_degsq(45:55), '+ c')

hold off

% Create xlabel
xlabel('Frequency (GHz)')

% Create ylabel
ylabel('Phase Scintillation Variance <P^2> (deg^2)')

Title = ['LWL Scans Phase Scintillation/Predicted', '(', ...
        num2str(THz_month), ' ', num2str(THz_day), ' ', num2str(THz_year), ' ', ...
        num2str(THz_hour), ':', num2str(THz_minute), ':', num2str(THz_second), ')'];

% Create title
title(Title);

% create Legend
legend('S2 Pred-Var', 'S2 Rx1-Var', 'S2 Rx2-Var', 'S5 Pred-Var', ...
        'S5 Rx1-Var', 'S5 Rx2-Var');

box(axes1, 'on');
% Set the remaining axes properties
set(axes1, 'FontSize', 16);

%PLOT Variance Phase Scintillation Scans 3 & 6 (UWL)
figure76 = figure('Color', [1,1,1], 'Name', 'Variance UWL Scans');

% Create axes
axes1 = axes('Parent', figure76);
hold(axes1, 'on');
box(axes1, 'on')

hold on

% Plot Frequency vs. Variance
plot(Scan_UWL_Frequencies, Phase_Variance_GO_freq_degsq(23:33), '-o b')

plot(Scan_UWL_Frequencies, Phase_Rx1_Var_freq_degsq(23:33), '-x g')

```

```

plot(Scan_UWL_Frequencies, Phase_Rx2_Var_freq_degsq(23:33), '-d c')

plot(Scan_UWL_Frequencies, Phase_Variance_GO_freq_degsq(56:66), '-s b')

plot(Scan_UWL_Frequencies, Phase_Rx1_Var_freq_degsq(56:66), '-* g')

plot(Scan_UWL_Frequencies, Phase_Rx2_Var_freq_degsq(56:66), '-+ c')

hold off

% Create xlabel
xlabel('Frequency (GHz)')

% Create ylabel
ylabel('Phase Variance <P^2> (deg^2)')

Title = ['UWL Scans <P^2>/Predicted', '(' , ...
        num2str(THz_month), ' ', num2str(THz_day), ' ', num2str(THz_year), ' ', ' ', ...
        num2str(THz_hour), ':', num2str(THz_minute), ':', num2str(THz_second), ')'];

% Create title
title(Title);

% create Legend
legend('S3 Pred-Var', 'S3 Rx1-Var', 'S3 Rx2-Var', 'S6 Pred-Var', ...
      'S6 Rx1-Var', 'S6 Rx2-Var');

box(axes1, 'on');
% Set the remaining axes properties
set(axes1, 'FontSize', 16);

%PLOT STD in degrees Phase Scintillation Scans 1 & 4 (wideband)
figure77 = figure('Color', [1,1,1], 'Name', 'STD Degrees Wideband Scans');

% Create axes
axes1 = axes('Parent', figure77);
hold(axes1, 'on');
box(axes1, 'on')

hold on

% Plot Frequency vs. STD
plot(Scan_WB_Frequencies, Phase_STD_GO_freq_deg(1:11), '-o b')

plot(Scan_WB_Frequencies, Phase_Rx1_STD_freq_deg(1:11), '-x g')

plot(Scan_WB_Frequencies, Phase_Rx2_STD_freq_deg(1:11), '-d c')

```

```

plot(Scan_WB_Frequencies, Phase_STD_GO_freq_deg(34:44), '-s b')

plot(Scan_WB_Frequencies, Phase_Rx1_STD_freq_deg(34:44), '-* g')

plot(Scan_WB_Frequencies, Phase_Rx2_STD_freq_deg(34:44), '-+ c')

hold off

% Create xlabel
xlabel('Frequency (GHz)')

% Create ylabel
ylabel('Phase Scintillation STD (deg)')

Title = ['WB Scans Phase (deg) Scintillation/Predicted','(', ...
        num2str(THz_month),', ',num2str(THz_day),', ', num2str(THz_year),', ',', ...
        num2str(THz_hour),':',num2str(THz_minute),':',num2str(THz_second),')'];

% Create title
title(Title);

% create Legend
legend('S1 Pred-STD','S1 Rx1-STD','S1 Rx2-STD','S4 Pred-STD', ...
        'S4 Rx1-STD','S4 Rx2-STD');

box(axes1,'on');
    % Set the remaining axes properties
    set(axes1,'FontSize',16);

%PLOT STD Degrees Phase Scintillation Scans 2 & 5 (LWL)
figure78 = figure('Color',[1,1,1],'Name','STD Degrees LWL Scans');

% Create axes
    axes1 = axes('Parent',figure78);
    hold(axes1,'on');
    box(axes1,'on')

hold on

% Plot Frequency vs. STD
plot(Scan_LWL_Frequencies, Phase_STD_GO_freq_deg(12:22), '-o b')

plot(Scan_LWL_Frequencies, Phase_Rx1_STD_freq_deg(12:22), '-x g')

plot(Scan_LWL_Frequencies, Phase_Rx2_STD_freq_deg(12:22), '-d c')

plot(Scan_LWL_Frequencies, Phase_STD_GO_freq_deg(45:55), '-s b')

plot(Scan_LWL_Frequencies, Phase_Rx1_STD_freq_deg(45:55), '-* g')

```

```

plot(Scan_LWL_Frequencies, Phase_Rx2_STD_freq_deg(45:55), '-+ c')

hold off

% Create xlabel
xlabel('Frequency (GHz)')

% Create ylabel
ylabel('Phase Scintillation STD (deg)')

Title = ['LWL Scans Phase (deg) Scintillation/Predicted','(', ...
        num2str(THz_month),', ',num2str(THz_day),', ', num2str(THz_year),', ',', ...
        num2str(THz_hour),':',num2str(THz_minute),':',num2str(THz_second),')'];

% Create title
title(Title);

% create Legend
legend('S2 Pred-STD','S2 Rx1-STD','S2 Rx2-STD','S5 Pred-STD', ...
        'S5 Rx1-STD','S5 Rx2-STD');

box(axes1,'on');
    % Set the remaining axes properties
    set(axes1,'FontSize',16);

%PLOT STD Degrees Phase Scintillation Scans 3 & 6 (UWL)
figure79 = figure('Color',[1,1,1],'Name','STD Degrees UWL Scans');

% Create axes
    axes1 = axes('Parent',figure79);
    hold(axes1,'on');
    box(axes1,'on')

hold on

% Plot Frequency vs. STD
plot(Scan_UWL_Frequencies, Phase_STD_GO_freq_deg(23:33), '-o b')

plot(Scan_UWL_Frequencies, Phase_Rx1_STD_freq_deg(23:33), '-x g')

plot(Scan_UWL_Frequencies, Phase_Rx2_STD_freq_deg(23:33), '-d c')

plot(Scan_UWL_Frequencies, Phase_STD_GO_freq_deg(56:66), '-s b')

plot(Scan_UWL_Frequencies, Phase_Rx1_STD_freq_deg(56:66), '-* g')

plot(Scan_UWL_Frequencies, Phase_Rx2_STD_freq_deg(56:66), '-+ c')

hold off

```

```

% Create xlabel
xlabel('Frequency (GHz)');

% Create ylabel
ylabel('Phase STD (deg)');

Title = ['UWL Scans Phase (deg) Scintillation/Predicted','(', ...
        num2str(THz_month), ' ', num2str(THz_day), ' ', num2str(THz_year), ' ', '...',
        num2str(THz_hour), ':', num2str(THz_minute), ':', num2str(THz_second), ')'];

% Create title
title(Title);

% create Legend
legend('S3 Pred-STD', 'S3 Rx1-STD', 'S3 Rx2-STD', 'S6 Pred-STD', ...
        'S6 Rx1-STD', 'S6 Rx2-STD');

box(axes1, 'on');
    % Set the remaining axes properties
    set(axes1, 'FontSize', 16);

%PLOT STD in millimeters Phase Scintillation Scans 1 & 4 (wideband)
figure80 = figure('Color', [1,1,1], 'Name', 'STD mm Wideband Scans');

% Create axes
    axes1 = axes('Parent', figure80);
    hold(axes1, 'on');
    box(axes1, 'on')

hold on

% Plot Frequency vs. STD
plot(Scan_WB_Frequencies, Phase_STD_GO_freq_mm(1:11), '-o b')

plot(Scan_WB_Frequencies, Phase_Rx1_STD_freq_mm(1:11), '-x g')

plot(Scan_WB_Frequencies, Phase_Rx2_STD_freq_mm(1:11), '-d c')

plot(Scan_WB_Frequencies, Phase_STD_GO_freq_mm(34:44), '-s b')

plot(Scan_WB_Frequencies, Phase_Rx1_STD_freq_mm(34:44), '-* g')

plot(Scan_WB_Frequencies, Phase_Rx2_STD_freq_mm(34:44), '-+ c')

hold off

% Create xlabel
xlabel('Frequency (GHz)')

% Create ylabel

```

```

ylabel('Phase Scintillation STD (mm)')

Title = ['WB Scans Phase (mm) Scintillation/Predicted','(', ...
        num2str(THz_month),', ',num2str(THz_day),', ', num2str(THz_year),', ',', ...
        num2str(THz_hour),':',num2str(THz_minute),':',num2str(THz_second),')'];

% Create title
title(Title);

% create Legend
legend('S1 Pred-STD','S1 Rx1-STD','S1 Rx2-STD','S4 Pred-STD', ...
        'S4 Rx1-STD','S4 Rx2-STD');

box(axes1,'on');
    % Set the remaining axes properties
    set(axes1,'FontSize',16);

%PLOT STD mm Phase Scintillation Scans 2 & 5 (LWL)
figure81 = figure('Color',[1,1,1],'Name','STD mm LWL Scans');

% Create axes
    axes1 = axes('Parent',figure81);
    hold(axes1,'on');
    box(axes1,'on')

hold on

% Plot Frequency vs. STD
plot(Scan_LWL_Frequencies, Phase_STD_GO_freq_mm(12:22), '-o b')

plot(Scan_LWL_Frequencies, Phase_Rx1_STD_freq_mm(12:22), '-x g')

plot(Scan_LWL_Frequencies, Phase_Rx2_STD_freq_mm(12:22), '-d c')

plot(Scan_LWL_Frequencies, Phase_STD_GO_freq_mm(45:55), '-s b')

plot(Scan_LWL_Frequencies, Phase_Rx1_STD_freq_mm(45:55), '-* g')

plot(Scan_LWL_Frequencies, Phase_Rx2_STD_freq_mm(45:55), '-+ c')

hold off

% Create xlabel
xlabel('Frequency (GHz)')

% Create ylabel
ylabel('Phase Scintillation STD (mm)')

Title = ['LWL Scans Phase (mm) Scintillation/Predicted','(', ...

```

```

    num2str(THz_month), ' ', num2str(THz_day), ' ', num2str(THz_year), ', ', ' ', ...
    num2str(THz_hour), ':', num2str(THz_minute), ':', num2str(THz_second), ') '];

% Create title
title(Title);

% create Legend
legend('S2 Pred-STD', 'S2 Rx1-STD', 'S2 Rx2-STD', 'S5 Pred-STD', ...
       'S5 Rx1-STD', 'S5 Rx2-STD');

box(axes1, 'on');
    % Set the remaining axes properties
    set(axes1, 'FontSize', 16);

%PLOT STD mm Phase Scintillation Scans 3 & 6 (UWL)
figure82 = figure('Color', [1,1,1], 'Name', 'STD mm UWL Scans');

% Create axes
    axes1 = axes('Parent', figure82);
    hold(axes1, 'on');
    box(axes1, 'on')

hold on

% Plot Frequency vs. STD
plot(Scan_UWL_Frequencies, Phase_STD_GO_freq_mm(23:33), '-o b')

plot(Scan_UWL_Frequencies, Phase_Rx1_STD_freq_mm(23:33), '-x g')

plot(Scan_UWL_Frequencies, Phase_Rx2_STD_freq_mm(23:33), '-d c')

plot(Scan_UWL_Frequencies, Phase_STD_GO_freq_mm(56:66), '-s b')

plot(Scan_UWL_Frequencies, Phase_Rx1_STD_freq_mm(56:66), '-* g')

plot(Scan_UWL_Frequencies, Phase_Rx2_STD_freq_mm(56:66), '-+ c')

hold off

% Create xlabel
xlabel('Frequency (GHz)')

% Create ylabel
ylabel('Phase STD (mm)')

Title = ['UWL Scans Phase (mm) Scintillation/Predicted', '(', ...
        num2str(THz_month), ' ', num2str(THz_day), ' ', num2str(THz_year), ', ', ' ', ...
        num2str(THz_hour), ':', num2str(THz_minute), ':', num2str(THz_second), ') '];

% Create title

```

```

title(Title);

% create Legend
legend('S3 Pred-STD', 'S3 Rx1-STD', 'S3 Rx2-STD', 'S6 Pred-STD', ...
       'S6 Rx1-STD', 'S6 Rx2-STD');
box(axes1, 'on');
% Set the remaining axes properties
set(axes1, 'FontSize', 16);

%PLOT STD in picoseconds Phase Scintillation Scans 1 & 4 (wideband)
figure83 = figure('Color', [1,1,1], 'Name', 'STD ps Wideband Scans');

% Create axes
axes1 = axes('Parent', figure83);
hold(axes1, 'on');
box(axes1, 'on')

hold on

% Plot Frequency vs. STD
plot(Scan_WB_Frequencies, Phase_STD_GO_freq_ps(1:11), '-o b')

plot(Scan_WB_Frequencies, Phase_Rx1_STD_freq_ps(1:11), '-x g')

plot(Scan_WB_Frequencies, Phase_Rx2_STD_freq_ps(1:11), '-d c')

plot(Scan_WB_Frequencies, Phase_STD_GO_freq_ps(34:44), '-s b');

plot(Scan_WB_Frequencies, Phase_STD_GO_freq_ps(34:44), '-s b')

plot(Scan_WB_Frequencies, Phase_Rx2_STD_freq_ps(34:44), '-+ c')

hold off

% Create xlabel
xlabel('Frequency (GHz)')

% Create ylabel
ylabel('Phase Scintillation STD (ps)')

Title = ['WB Scans Phase (ps) Scintillation/Predicted', '(', ...
        num2str(THz_month), ', ', num2str(THz_day), ', ', num2str(THz_year), ', ', ...
        num2str(THz_hour), ':', num2str(THz_minute), ':', num2str(THz_second), ')'];

% Create title
title(Title);

% create Legend
legend('S1 Pred-STD', 'S1 Rx1-STD', 'S1 Rx2-STD', 'S4 Pred-STD', ...

```

```

'S4 Rx1-STD', 'S4 Rx2-STD');

box(axes1, 'on');
    % Set the remaining axes properties
    set(axes1, 'FontSize', 16);

%PLOT STD mm Phase Scintillation Scans 2 & 5 (LWL)
figure84 = figure('Color', [1,1,1], 'Name', 'STD ps LWL Scans');

% Create axes
    axes1 = axes('Parent', figure84);
    hold(axes1, 'on');
    box(axes1, 'on')

hold on

% Plot Frequency vs. STD
plot(Scan_LWL_Frequencies, Phase_STD_GO_freq_ps(12:22), '-o b')

plot(Scan_LWL_Frequencies, Phase_Rx1_STD_freq_ps(12:22), '-x g')

plot(Scan_LWL_Frequencies, Phase_Rx2_STD_freq_ps(12:22), '-d c')

plot(Scan_LWL_Frequencies, Phase_STD_GO_freq_ps(45:55), '-s b')

plot(Scan_LWL_Frequencies, Phase_Rx1_STD_freq_ps(45:55), '-* g')

plot(Scan_LWL_Frequencies, Phase_Rx2_STD_freq_ps(45:55), '-+ c')

hold off

% Create xlabel
xlabel('Frequency (GHz)')

% Create ylabel
ylabel('Phase Scintillation STD (ps)')

Title = ['LWL Scans Phase (ps) Scintillation/Predicted', '(' , ...
    num2str(THz_month), ' ', num2str(THz_day), ' ', num2str(THz_year), ' ', ' , ...
    num2str(THz_hour), ':', num2str(THz_minute), ':', num2str(THz_second), ') '];

% Create title
title(Title);

% create Legend
legend('S2 Pred-STD', 'S2 Rx1-STD', 'S2 Rx2-STD', 'S5 Pred-STD', ...
    'S5 Rx1-STD', 'S5 Rx2-STD');

box(axes1, 'on');
    % Set the remaining axes properties

```

```

set(axes1, 'FontSize',16);

%PLOT STD mm Phase Scintillation Scans 3 & 6 (UWL)
figure85 = figure('Color',[1,1,1], 'Name', 'STD ps UWL Scans');

% Create axes
axes1 = axes('Parent',figure85);
hold(axes1, 'on');
box(axes1, 'on')

hold on

% Plot Frequency vs. STD
plot(Scan_UWL_Frequencies, Phase_STD_GO_freq_ps(23:33), '-o b')
plot(Scan_UWL_Frequencies, Phase_Rx1_STD_freq_ps(23:33), '-x g')
plot(Scan_UWL_Frequencies, Phase_Rx2_STD_freq_ps(23:33), '-d c')
plot(Scan_UWL_Frequencies, Phase_STD_GO_freq_ps(56:66), '-s b')
plot(Scan_UWL_Frequencies, Phase_Rx1_STD_freq_ps(56:66), '-* g')
plot(Scan_UWL_Frequencies, Phase_Rx2_STD_freq_ps(56:66), '-+ c')

hold off

% Create xlabel

% Create ylabel
ylabel('Phase STD (ps)')

Title = ['UWL Scans Phase (ps) Scintillation/Predicted', '(' , ...
        num2str(THz_month), ' ', num2str(THz_day), ' ', num2str(THz_year), ' ', ' ', ...
        num2str(THz_hour), ':', num2str(THz_minute), ':', num2str(THz_second), ') '];

% Create title
title(Title);

% create Legend
legend('S3 Pred-STD', 'S3 Rx1-STD', 'S3 Rx2-STD', 'S6 Pred-STD', ...
        'S6 Rx1-STD', 'S6 Rx2-STD');

box(axes1, 'on');
% Set the remaining axes properties
set(axes1, 'FontSize',16);
#####

% ##### AMP/PHASE SCINT CROSS CORRELATION #####

```

```

% RYTOV Cross Correlation of Amplitude and Phase for Plane Wave
% similarity between -1 to +1
% FRESNEL = Planer <phase amp> = 3.732 * Variance or
%  $1.146R^{(11/6)}k^{(7/6)}Cn^2$ 
Rytov_Plane_Cross_Correl_Fresnel = 3.732 .* Amp_Variance_Kolmogorov_Npsq;

% flip to make a function of frequency
Rytov_Plane_Cross_Correl_Fresnel_Freq = ...
    flipud(Rytov_Plane_Cross_Correl_Fresnel);

% find the max of the vector to normalize
Rytov_Plane_CC_Fres_Freq_max = max(Rytov_Plane_Cross_Correl_Fresnel_Freq);

% normalize the vector
Rytov_Plane_CC_Fres_Freq_Norm = ...
    Rytov_Plane_Cross_Correl_Fresnel_Freq ./ Rytov_Plane_CC_Fres_Freq_max;

% FRAUNHOFER = Planer <phase amp> = .58<amp^2>(R*lambda ... * Variance
Rytov_Plane_Cross_Correl_Fraunhofer = ...
    .58 .* Amp_Variance_Kolmogorov_Npsq .* ...
    (Path_Length_m * (2*pi/L0_m)^2 /2 /pi .* lambda_Scan_m).^(-11/6);

% flip the vector to make a function of frequency
Rytov_Plane_Cross_Correl_Fraunhofer_Freq = ...
    flipud(Rytov_Plane_Cross_Correl_Fraunhofer);

% find the max of the vector to normalize
Rytov_Plane_CC_Fraun_Freq_max = ...
    max(Rytov_Plane_Cross_Correl_Fraunhofer_Freq);

% normalize the vector by dividing by the maximum value
Rytov_Plane_CC_Fraun_Freq_Norm = ...
    Rytov_Plane_Cross_Correl_Fraunhofer_Freq ./ ...
    Rytov_Plane_CC_Fraun_Freq_max;

% TAIPAS real received data
% convert data to Np
Rx1_THz_STD_Amp_Cal_Np = Rx1_THz_STD_Amp_Cal_dB ./ 4.3429;

Rx2_THz_STD_Amp_Cal_Np = Rx2_THz_STD_Amp_Cal_dB ./ 4.3429;

% calculate phase angle in radians
Phase_Rx1_rad = angle(Rx1_THz_Complex_Data);

Phase_Rx2_rad = angle(Rx2_THz_Complex_Data);

% calculate STD
Phase_Rx1_STD_rad = sqrt(var(Phase_Rx1_rad));

Phase_Rx2_STD_rad = sqrt(var(Phase_Rx2_rad));

% calculate cross correction

```

```

Rx1_Amp_Phase_Cross_Correl = ...
    xcorr(Rx1_THz_STD_Amp_Cal_Np,Phase_Rx1_STD_rad,'coeff');

Rx2_Amp_Phase_Cross_Correl = ...
    xcorr(Rx2_THz_STD_Amp_Cal_Np,Phase_Rx2_STD_rad,'coeff');

% plot cross correlations

%PLOT Amp/Phase Scintillation Cross Correlation Scans 1 & 4 (wideband)
figure86 = figure('Color',[1,1,1],'Name',...
    'Amp-Phase Cross Correlation Wideband Scans');

% Create axes
    axes1 = axes('Parent',figure86);
    hold(axes1,'on');
    box(axes1,'on')

hold on

% Plot Frequency vs. Variance
plot(Scan_WB_Frequencies, Rytov_Plane_CC_Fres_Freq_Norm(1:11), '-o b')

plot(Scan_WB_Frequencies, Rytov_Plane_CC_Fraun_Freq_Norm(1:11), '-x g')

plot(Scan_WB_Frequencies, Rx1_Amp_Phase_Cross_Correl(1:11), '-d c')

plot(Scan_WB_Frequencies, Rx1_Amp_Phase_Cross_Correl(1:11), '-p m')

plot(Scan_WB_Frequencies, Rytov_Plane_CC_Fres_Freq_Norm(34:44), '-^ b')

plot(Scan_WB_Frequencies, Rytov_Plane_CC_Fraun_Freq_Norm(34:44), '-s g')

plot(Scan_WB_Frequencies, Rx1_Amp_Phase_Cross_Correl(34:44), '-h c')

plot(Scan_WB_Frequencies, Rx1_Amp_Phase_Cross_Correl(34:44), '-+ m')

hold off

% Create xlabel
xlabel('Frequency (GHz)')

% Create ylabel
ylabel('Amp-Phase <XP> Scintillation Correlation (-1 to +1)')

Title = ['WB Scans Amp-Phase Scintillation Correlation','(', ...
    num2str(THz_month),' ',num2str(THz_day),' ', num2str(THz_year),' ', ...
    num2str(THz_hour),':',num2str(THz_minute),':',num2str(THz_second),')'];

% Create title
title(Title);

```

```

% create Legend
legend('S1 Fres-COR','S1 Fraun-COR','S1 Rx1-COR','S1 Rx2-COR', ...
       'S4 Fres-COR','S4 Fraun-COR','S4 Rx1-COR','S4 Rx2-COR');

box(axes1,'on');
% Set the remaining axes properties
set(axes1,'FontSize',16);

%PLOT Amp/Phase Scintillation Cross Correlation Scans 2 & 5 (LWL)
figure87 = figure('Color',[1,1,1],...
                 'Name','Amp-Phase Cross Correlation LWL Scans');

% Create axes
axes1 = axes('Parent',figure87);
hold(axes1,'on');
box(axes1,'on')

hold on

% Plot Frequency vs. Variance
plot(Scan_LWL_Frequencies, ...
     Rytov_Plane_CC_Fres_Freq_Norm(12:22), '-o b')

plot(Scan_LWL_Frequencies, ...
     Rytov_Plane_CC_Fraun_Freq_Norm(12:22), '-x g')

plot(Scan_LWL_Frequencies, Rx1_Amp_Phase_Cross_Correl(12:22), '-d c')

plot(Scan_LWL_Frequencies, Rx1_Amp_Phase_Cross_Correl(12:22), '-p m')

plot(Scan_LWL_Frequencies, ...
     Rytov_Plane_CC_Fres_Freq_Norm(45:55), '-^ b')

plot(Scan_LWL_Frequencies, ...
     Rytov_Plane_CC_Fraun_Freq_Norm(45:55), '-s g')

plot(Scan_LWL_Frequencies, Rx1_Amp_Phase_Cross_Correl(45:55), '-h c')

plot(Scan_LWL_Frequencies, Rx1_Amp_Phase_Cross_Correl(45:55), '-+ m')

hold off

% Create xlabel
xlabel('Frequency (GHz)')

% Create ylabel
ylabel('Amp-Phase <XP> Scintillation Correlation (-1 to +1)')

Title = ['LWL Scans Amp-Phase Scintillation Correlation',...
        '(', num2str(THz_month), ', ', num2str(THz_day), ', ', num2str(THz_year), ...
        ', ', num2str(THz_hour), ': ', num2str(THz_minute), ': ', ...

```

```

    num2str(THz_second), ' ');

% Create title
title(Title);

% create Legend
legend('S2 Fres-COR', 'S2 Fraun-COR', 'S2 Rx1-COR', 'S2 Rx2-COR', ...
       'S5 Fres-COR', 'S5 Fraun-COR', 'S5 Rx1-COR', 'S5 Rx2-COR');

box(axes1, 'on');
    % Set the remaining axes properties
    set(axes1, 'FontSize', 16);

%PLOT Amp/Phase Scintillation Cross Correlation Scans 3 & 6 (UWL)
figure88 = figure('Color', [1,1,1], 'Name', ...
                 'Amp-Phase Cross Correlation UWL Scans');

% Create axes
    axes1 = axes('Parent', figure88);
    hold(axes1, 'on');
    box(axes1, 'on')

hold on

% Plot Frequency vs. Variance
plot(Scan_UWL_Frequencies, ...
     Rytov_Plane_CC_Fres_Freq_Norm(23:33), '-o b')

plot(Scan_UWL_Frequencies, ...
     Rytov_Plane_CC_Fraun_Freq_Norm(23:33), '-x g')

plot(Scan_UWL_Frequencies, Rx1_Amp_Phase_Cross_Correl(23:33), '-d c')

plot(Scan_UWL_Frequencies, Rx1_Amp_Phase_Cross_Correl(23:33), '-p m')

plot(Scan_UWL_Frequencies, ...
     Rytov_Plane_CC_Fres_Freq_Norm(56:66), '-^ b')

plot(Scan_UWL_Frequencies, ...
     Rytov_Plane_CC_Fraun_Freq_Norm(56:66), '-s g')

plot(Scan_UWL_Frequencies, Rx1_Amp_Phase_Cross_Correl(56:66), '-h c')

plot(Scan_UWL_Frequencies, Rx1_Amp_Phase_Cross_Correl(56:66), '-+ m')

hold off

% Create xlabel
xlabel('Frequency (GHz)')

```

```

% Create ylabel
ylabel('Amp-Phase <XP> Scintillation Correlation (-1 to +1)')

Title = ['UWL Scans Amp-Phase Scintillation Correlation', ...
        '(', num2str(THz_month), ' ', num2str(THz_day), ' ', num2str(THz_year), ...
        ', ', num2str(THz_hour), ':', num2str(THz_minute), ':', ...
        num2str(THz_second), ')'];

% Create title
title(Title);

% create Legend
legend('S3 Fres-COR', 'S3 Fraun-COR', 'S3 Rx1-COR', 'S3 Rx2-COR', ...
       'S6 Fres-COR', 'S6 Fraun-COR', 'S6 Rx1-COR', 'S6 Rx2-COR');

    box(axes1, 'on');
    % Set the remaining axes properties
    set(axes1, 'FontSize', 16);
#####

%% ##### ANGLE OF ARRIVAL (AoA) #####
% calculate and plot Angle of Arrival (AoA)
% Future - not testing AoA

% TBD - This will be implemented in the next phase of TAIPAS

% #####

%% #####
% Cx^2, x = T, Q Calculations

% Calculate Ct2 - construction coefficient of temperature =
%
% (delta T txrx)^2/|path_length|^2/3
% this was implemented with potential time offsets between tx and rx with a
% max of 8 ms, so it won't be perfect until the next phase of TAIPAS
% CT2 is 100 x 1

Ct2=((Anemometer_Tx_Temp.*Anemometer_Rx_Temp).^2)/abs(Path_Length_m^(2/3));

figure89 = figure('Color',[1,1,1], 'Name', 'Ct2 Plot');

% Create axes
axes1 = axes('Parent', figure89);
hold(axes1, 'on');
box(axes1, 'on')

```

```

% Plot with lines between points and "o" on points
plot(Anemo_time_zero_s_Tx,Ct2, '-');

% Create xlabel
label_for_X = ['start time = ',num2str(Anemo_Start_time_s_Tx),...
              's   time (s)'];
xlabel(label_for_X)

% Create ylabel
ylabel('C_T^2   (degrees C)^2 / m^(2/3)')

Title = ['C_T^2 (' ,num2str(Anemo_month), ' ',...
        num2str(Anemo_day), ' ', num2str(Anemo_year), ', ', ' ',...
        num2str(Anemo_hour_Tx), ':', num2str(Anemo_minute_Tx), ...
        ':', num2str(Anemo_second_Tx), ') '];

% Create title
title(Title);

    box(axes1, 'on');
% Set the remaining axes properties
set(axes1, 'FontSize', 16);

%%
%
% Calculate Cq2 - construction coefficient of humidity =
%                               (delta Q txrx)^2/|path_length|^2/3

% this was implemented with potential time offsets between tx and rx with a
% max of 8 ms - next gen TAIPAS hardware will allow increase
% synchronization

Cq2 = ((Hygrometer_Tx_dry.*Hygrometer_Rx_dry).^2)/Path_Length_m^(2/3);

figure90 = figure('Color',[1,1,1], 'Name', 'Cq2 Plot');

% Create axes
axes1 = axes('Parent',figure90);
hold(axes1, 'on');
box(axes1, 'on')

% Plot with lines between points and "o" on points
plot(Hygro_time_zero_s_Tx,Cq2, '-');

% Create xlabel
label_for_X = ['start time = ',num2str(Anemo_Start_time_s_Tx),...
              's   time (s)'];
xlabel(label_for_X)

% Create ylabel
ylabel('C_Q^2   g^2/m^3 / m^(2/3)')

```

```

Title = ['C_Q^2 (' ,num2str(Anemo_month), ' ',...
        num2str(Anemo_day), ' ', num2str(Anemo_year), ', ', ' ',...
        num2str(Anemo_hour_Tx), ':', num2str(Anemo_minute_Tx), ...
        ':', num2str(Anemo_second_Tx), ') '];

% Create title
title(Title);

box(axes1, 'on');
% Set the remaining axes properties
set(axes1, 'FontSize', 16);
% #####
%#% #####
% Cacluate CTQ
% Calculate Ctq = sqrt(Ct2Ctq2) = <CqCt>=<CtCq>, +=day, -=night
% Matrix 5, 6 and 6, 5

% this was implemented with potential time offsets between tx and rx with a
% max of 8 ms

Ctq = sqrt(Ct2 .* Cq2);

figure91 = figure('Color', [1,1,1], 'Name', 'Ctq Plot');

% Create axes
axes1 = axes('Parent', figure91);
hold(axes1, 'on');
box(axes1, 'on')

% Plot with lines between points and "o" on points
plot(1:100, Ctq, '-o');

% Create xlabel
label_for_X = ['start time = ', num2str(Anemo_Start_time_s_Tx), ...
              's time (s)'];
xlabel(label_for_X);

% Create ylabel
ylabel('C_T_Q');

Title = ['C_T_Q, "+"=Day, "-"= Night (' ,num2str(Anemo_month), ' ',...
        num2str(Anemo_day), ' ', num2str(Anemo_year), ', ', ' ',...
        num2str(Anemo_hour_Tx), ':', num2str(Anemo_minute_Tx), ...
        ':', num2str(Anemo_second_Tx), ') '];

% Create title
title(Title);

box(axes1, 'on');
% Set the remaining axes properties
set(axes1, 'FontSize', 16);

```

```

% #####
%% Implement cross covariance terms !!!!!!!!
%% amplitude phase - implemented above - sum matrix = 1,2 and 2,1
% #####

%% amplitude -X Cn2 - sum matrix = 1,4 and 4,1
% this was implemented with potential time offsets between tx and rx with a
% max of 8 ms -
%
% convert dB variance to standard deviation; this is a
% matrix of 1 x 66 - these is the variance of the mean samples of each
% tuned frequency

% Cn2 only has 134 x 1 points, need to reduce down to 66 to cover the mean
% samples of every frequency tune

% make X variance data match matrix dimension - convert 66 x 1

% <X> <Cn2> - plot the relationship of the variances
% Cn2 variance - THIS NEEDS TO BE CHANGED DEPENDING ON X10 exponent

Cn2_variance = Cn2 ./ max(Cn2);

% line up amplitude in time
time_amp(1:66,1) = 1;

for i = 1:66

    if i == 1
time_amp(i,1) = time_amp(i,1);
    else
time_amp(i,1) = time_amp(i-1,1) + .1;
    end
end

figure92 = figure('Color',[1,1,1], 'Name', '<X> Cn2 Plot');

% Create axes
axes1 = axes('Parent',figure92);
hold(axes1, 'on');
box(axes1, 'on')

hold on
% Plot with lines between points and "o" on points

plot(scint_time_zero_s,Cn2_variance, 'x- b');

plot(time_amp(1:66,1) , Rx1_THz_STD_Amp_Cal_dB, 'x- r' )

```

```

hold off

% Create xlabel
label_for_X = 'time';

xlabel(label_for_X)

% Create ylabel
ylabel('<X> dB - red   C_n^2 m^(-2/3) Mantissa - blue')

Title = ['<X> <C_n^2> Co-Variance (' ,num2str(Anemo_month), ' ',...
        num2str(Anemo_day), ' ', num2str(Anemo_year), ', ', ' ',...
        num2str(Anemo_hour_Tx), ':', num2str(Anemo_minute_Tx), ...
        ':', num2str(Anemo_second_Tx), ') '];

% Create title
title(Title);

box(axes1, 'on');
% Set the remaining axes properties
set(axes1, 'FontSize', 16);
% #####

%% amplitude-X Ct2 - sum matrix = 1,5 and 5,1

% this was implemented with potential time offsets between tx and rx with a
% max of 8 ms -

% Temperature from anemometer only as 100 samples
% convert dB variance to standard deviation and then to volts; this is a
% matrix of Good_Data x 66, CT2 is 100 x 1

% XCt2 = xcorr(Ct2(1:66,1), Rx1_THz_Variance_Amp_Cal_dBsq');

% line up amplitude in time
time_Ct2(1:100,1) = 1;

for i = 1:100

    if i == 1
time_Ct2(i,1) = time_Ct2(i,1);
    else
time_Ct2(i,1) = time_Ct2(i-1,1) + .1;
    end
end

figure93 = figure('Color', [1,1,1], 'Name', '<X> <CT^2> Plot');

% Create axes
axes1 = axes('Parent', figure93);

```

```

hold(axes1, 'on');
box(axes1, 'on')

Ct2_max = max(Ct2);

hold on
% Plot with lines between points and "o" on points

plot(time_Ct2(1:100,1), (Ct2./Ct2_max), 'x- b');

plot(time_amp(1:66,1), Rx1_THz_STD_Amp_Cal_dB, 'x- r' )

hold off

% Create xlabel
label_for_X = 'time';

xlabel(label_for_X)

% Create ylabel
ylabel('<X> dB - red   <C_T^2> C^0 - blue')

Title = ['<X> <C_T^2> (' , num2str(Anemo_month), ' ', ...
        num2str(Anemo_day), ' ', num2str(Anemo_year), ' ', ' ', ...
        num2str(Anemo_hour_Tx), ':', num2str(Anemo_minute_Tx), ...
        ':', num2str(Anemo_second_Tx), ') '];

% Create title
title(Title);

box(axes1, 'on');
% Set the remaining axes properties
set(axes1, 'FontSize', 16);

% #####

%% amplitude-X Cq2 - sum matrix = 1,6 and 6,1

% this was implemented with potential time offsets between tx and rx with a
% max of 8 ms -

% Temperature from anemometer only as 100 samples, Mean of amplitude
% frequency tunes 66 long

% XCq2 = xcorr(Cq2(1:66,1), Rx1_THz_Variance_Amp_Cal_dBsq');

figure94 = figure('Color', [1,1,1], 'Name', '<XCq> Plot');

% Create axes
axes1 = axes('Parent', figure94);

```

```

hold(axes1, 'on');
box(axes1, 'on')

Cq2_max = max(Cq2);

hold on
% Plot with lines between points and "o" on points

plot(time_Ct2(1:100,1), (Cq2./Cq2_max), 'x- b');

plot(time_amp(1:66,1), Rx1_THz_STD_Amp_Cal_dB, 'x- r' )

hold off

% Create xlabel
label_for_X = 'time';

xlabel(label_for_X);

% Create ylabel
ylabel('<X> dB - red   <C_Q> g/m^3 - blue');

Title = ['<X> <C_Q> (' , num2str(Anemo_month), ' ', ...
        num2str(Anemo_day), ' ', num2str(Anemo_year), ' ', ' ', ...
        num2str(Anemo_hour_Tx), ':', num2str(Anemo_minute_Tx), ...
        ':', num2str(Anemo_second_Tx), ') '];
% Create title
title(Title);

    box(axes1, 'on');
    % Set the remaining axes properties
    set(axes1, 'FontSize', 16);
% #####

%% Phase-P Cn2 - sum matrix = 2,4 and 4,2

% this was implemented with potential time offsets between tx and rx with a
% max of 8 ms -

% Cn2 only has 130 points, can only stradle threw the matrix twice for all
% the good data
P_max = max(Phase_Rx1_STD_deg);

figure95 = figure('Color', [1,1,1], 'Name', '<PCn2> Plot');

% Create axes
axes1 = axes('Parent', figure95);
hold(axes1, 'on');

```

```

box(axes1, 'on')

hold on
% Plot with lines between points and "o" on points

plot(scint_time_zero_s, Cn2_variance, 'x- b');

plot(time_amp(1:66,1), (Phase_Rx1_STD_deg./P_max), 'x- r' )

hold off

% Create xlabel
label_for_X = 'time';

xlabel(label_for_X)

% Create ylabel
ylabel('<Phase> degrees - red    <C_n^2> m^(-2/3) - blue')

Title = ['<Phase> <C_n^2> (' , num2str(Anemo_month), ' ', ...
        num2str(Anemo_day), ' ', num2str(Anemo_year), ' ', ' ', ...
        num2str(Anemo_hour_Tx), ':', num2str(Anemo_minute_Tx), ...
        ':', num2str(Anemo_second_Tx), ') '];

% Create title
title(Title);

box(axes1, 'on');
% Set the remaining axes properties
set(axes1, 'FontSize', 16);
% #####

%% Phase-P Ct2 - sum matrix = 2,5 and 5,2

% this was implemented with potential time offsets between tx and rx with a
% max of 8 ms -

% Temperature from anemometer only as 100 samples

figure96 = figure('Color', [1,1,1], 'Name', '<Pct> Plot');

% Create axes
axes1 = axes('Parent', figure96);
hold(axes1, 'on');
box(axes1, 'on')

hold on
% Plot with lines between points and "o" on points

```

```

plot(time_Ct2(1:100,1), (Ct2./Ct2_max), 'x- b');

plot(time_amp(1:66,1), (Phase_Rx1_STD_deg./P_max), 'x- r' )

hold off

% Create xlabel
label_for_X = 'time';

xlabel(label_for_X)

% Create ylabel
ylabel('<Phase> degrees - red    <C_T^2> C^0 - blue')

Title = ['<Phase> <C_T^2> (' ,num2str(Anemo_month), ' ',...
        num2str(Anemo_day), ' ', num2str(Anemo_year), ' ',...
        num2str(Anemo_hour_Tx), ':', num2str(Anemo_minute_Tx),...
        ':', num2str(Anemo_second_Tx), ') '];

% Create title
title(Title);

box(axes1, 'on');
% Set the remaining axes properties
set(axes1, 'FontSize', 16);
% #####

%% Phase-P Cq2 - sum matrix = 2,6 and 6,2

% this was implemented with potential time offsets between tx and rx with a
% max of 8 ms -

% Temperature from anemometer only as 100 samples

figure97 = figure('Color', [1,1,1], 'Name', '<PCq^2> Plot');

% Create axes
axes1 = axes('Parent', figure97);
hold(axes1, 'on');
box(axes1, 'on')

hold on
% Plot with lines between points and "o" on points

plot(time_Ct2(1:100,1), (Cq2./Cq2_max), 'x- b');

plot(time_amp(1:66,1), (Phase_Rx1_STD_deg./P_max), 'x- r' )

hold off

% Create xlabel

```

```

label_for_X = 'time';

xlabel(label_for_X)

% Create ylabel
ylabel('<Phase> degrees - red    <C_Q^2> g/m^3 - blue')

Title = ['<Phase> <C_Q^2> (' , num2str(Anemo_month), ' ', ...
        num2str(Anemo_day), ' ', num2str(Anemo_year), ' ', ' ', ...
        num2str(Anemo_hour_Tx), ':', num2str(Anemo_minute_Tx), ...
        ':', num2str(Anemo_second_Tx), ') '];

% Create title
title(Title);

box(axes1, 'on');
% Set the remaining axes properties
set(axes1, 'FontSize', 16);

% #####

%% Cn2 Ct2 - sum matrix = 4,5 and 5,4

% this was implemented with potential time offsets between tx and rx with a
% max of 8 ms -
%

figure98 = figure('Color', [1,1,1], 'Name', '<Ct2><Cn2> Plot');

% Create axes
axes1 = axes('Parent', figure98);
hold(axes1, 'on');
box(axes1, 'on')

hold on
% Plot with lines between points and "o" on points

plot((Ct2./Ct2_max), 'x- b');

plot((Cn2_variance), 'x- r' )

hold off

% Create xlabel
label_for_X = 'time x10';

xlabel(label_for_X)

% Create ylabel
ylabel('<C_n^2> m^-(2/3) - red    <C_T^2> C^o - blue')

```

```

Title = ['<C_n^2> <C_T^2> (' ,num2str(Anemo_month), ' ',...
        num2str(Anemo_day), ' ', num2str(Anemo_year), ' ',...
        num2str(Anemo_hour_Tx), ':',num2str(Anemo_minute_Tx),...
        ':',num2str(Anemo_second_Tx), ') '];

% Create title
title(Title);

box(axes1, 'on');
% Set the remaining axes properties
set(axes1, 'FontSize',16);

% #####

%% Cn2 Cq2 - sum covariance matrix = 4,6 and 6,4

% this was implemented with potential time offsets between tx and rx with a
% max of 8 ms -
%

figure99 = figure('Color',[1,1,1], 'Name', '<Cq2><Cn2> Plot');

% Create axes
axes1 = axes('Parent',figure99);
hold(axes1, 'on');
box(axes1, 'on')

hold on
% Plot with lines between points and "o" on points

plot((Cq2./Cq2_max), 'x- b');

plot((Cn2_variance), 'x- r' )

hold off

% Create xlabel
label_for_X = 'time x 10';

xlabel(label_for_X)

% Create ylabel
ylabel('<C_n^2> m^-(2/3) - red <C_Q^2> g/m^3 - blue')

Title = ['<C_n^2> <C_Q^2> (' ,num2str(Anemo_month), ' ',...
        num2str(Anemo_day), ' ', num2str(Anemo_year), ' ',...
        num2str(Anemo_hour_Tx), ':',num2str(Anemo_minute_Tx),...
        ':',num2str(Anemo_second_Tx), ') '];

% Create title
title(Title);

```

```

box(axes1, 'on');
% Set the remaining axes properties
set(axes1, 'FontSize', 16);

%% Ct2 Cq2 -
% this is implemented outside the matrix
% this was implemented with potential time offsets between tx and rx with a
% max of 8 ms -

figure100 = figure('Color', [1,1,1], 'Name', '<Cq2><Ct2> Plot');

% Create axes
axes1 = axes('Parent', figure100);
hold(axes1, 'on');
box(axes1, 'on')

hold on
% Plot with lines between points and "o" on points

plot((Cq2./Cq2_max), 'x- b');

plot((Ct2./Ct2_max), 'x- r' )

hold off

% Create xlabel
label_for_X = 'time x 10';

xlabel(label_for_X)

% Create ylabel
ylabel('<C_T^2> C^o - red    <C_Q^2> g/m^3 - blue')

Title = ['<C_T^2> <C_Q^2> (' , num2str(Anemo_month), ' ', ...
        num2str(Anemo_day), ' ', num2str(Anemo_year), ' ', ...
        num2str(Anemo_hour_Tx), ':', num2str(Anemo_minute_Tx), ...
        ':', num2str(Anemo_second_Tx), ') '];

% Create title
title(Title);

box(axes1, 'on');
% Set the remaining axes properties
set(axes1, 'FontSize', 16);
% #####

%% Tx and Rx Wind Correlations with amplitude and phase
% Calculate and plot the correlation between phase and Rx U-wind
% and amplitude and Rx U-wind
% PU = xcorr(Anemometer_Rx_U(1:66,1), Phase_Rx1_STD_deg);
% XU = xcorr(Anemometer_Rx_U(1:66,1), Rx1_THz_Variance_Amp_Cal_dBsq');

```

```

Phase_max = max(Phase_Rx1_STD_deg);
Phase_Variance = Phase_Rx1_STD_deg ./ Phase_max;

figure101 = figure('Color',[1,1,1],'Name','PhaseAmpUWind');

% Create axes
axes1 = axes('Parent',figure101);
hold(axes1,'on');
box(axes1,'on')

hold on
% Plot with lines between points and "o" on points

plot(Anemometer_Rx_U, 'x- b');

plot(Phase_Variance,'x- r' );

plot(Rx1_THz_STD_Amp_Cal_dB,'x- c' );

hold off

% Create xlabel
label_for_X = 'time x 10';

xlabel(label_for_X)

% Create ylabel
ylabel('Phase degrees - red      U Anemometer m/s - blue      <X> dB - cyan')

Title = ['Phase & Amp correlate with Rx U-Wind Plot (',...
num2str(Anemo_month),' ',...
num2str(Anemo_day),' ', num2str(Anemo_year),' ', ',...
num2str(Anemo_hour_Tx),':',num2str(Anemo_minute_Tx),...
':',num2str(Anemo_second_Tx),' ')'];

% Create title
title(Title);

legend('<U-RxWind>','<Phase>', '<X>');

box(axes1,'on');
% Set the remaining axes properties
set(axes1,'FontSize',16);

%% Calculate and plot the correlation between phase and X Rx V-wind
% and amplitude and Rx V-wind
% PV = xcorr(Anemometer_Rx_V(1:66,1),Phase_Rx1_STD_deg);
% XV = xcorr(Anemometer_Rx_V(1:66,1),Rx1_THz_Variance_Amp_Cal_dBsq');

```

```

figure102 = figure('Color',[1,1,1], 'Name', 'PhaseAmpVWind');

% Create axes
axes1 = axes('Parent',figure102);
hold(axes1, 'on');
box(axes1, 'on')

    hold on
% Plot with lines between points and "o" on points

plot(Anemometer_Rx_V, 'x- b');

plot(Phase_Variance, 'x- r' );

plot(Rx1_THz_STD_Amp_Cal_dB, 'x- c' );

hold off

% Create xlabel
label_for_X = 'times x 10';

xlabel(label_for_X)

% Create ylabel
ylabel('V Anemometer m/s - blue Phase degrees - red <X> dB - cyan')

    Title = ['Phase & Amp correlate with Rx V-Wind Plot (',...
num2str(Anemo_month), ' ',...
num2str(Anemo_day), ' ', num2str(Anemo_year), ', ', ' ',...
num2str(Anemo_hour_Tx), ':', num2str(Anemo_minute_Tx), ...
':', num2str(Anemo_second_Tx), ') '];

% Create title
title(Title);

legend('<V-RxWind>', '<Phase>', '<x>');

box(axes1, 'on');
% Set the remaining axes properties
set(axes1, 'FontSize', 16);

%% Calculate and plot the correlation between phase and Rx W-wind
% and amplitude and Rx W-wind
% PW = xcorr(Anemometer_Rx_W(1:66,1),Phase_Rx1_STD_deg);
% XW = xcorr(Anemometer_Rx_W(1:66,1),Rx1_THz_Variance_Amp_Cal_dBsqr');

figure103 = figure('Color',[1,1,1], 'Name', 'PhaseAmpWWind');

```

```

% Create axes
axes1 = axes('Parent',figure103);
hold(axes1,'on');
box(axes1,'on')

    hold on
% Plot with lines between points and "o" on points

plot(Anemometer_Rx_W, 'x- b');

plot(Phase_Variance,'x- r' );

plot(Rx1_THz_STD_Amp_Cal_dB,'x- c' );

hold off

% Create xlabel
label_for_X = 'time x 10';

xlabel(label_for_X)

% Create ylabel
ylabel('W Anemometer m/s - blue Phase degrees - red <X> dB - cyan')

    Title = ['Phase & Amp correlate with Rx W-Wind Plot (',...
num2str(Anemo_month),' ',...
num2str(Anemo_day),' ', num2str(Anemo_year),' ',...
num2str(Anemo_hour_Tx),':',num2str(Anemo_minute_Tx),...
':',num2str(Anemo_second_Tx),')'];

% Create title
title(Title);

legend('<V-RxWind>','<Phase>','<x>');

box(axes1,'on');
% Set the remaining axes properties
set(axes1,'FontSize',16);

%% #####
%           DATA PROCESSING PHYSICS without Hardware except Tx Pwr removed
%#####

%% ##### Tx/Rx CALIBRATION and Hardware Losses removed #####
%% ##### Tx/Rx CALIBRATION #####

```

```

%# 50 dBi on each side cancels and power is common minimum on each sweep##

% Make a matrix of the amplitude with CALIBRATION, calculate
% the mean, calibrate and plot one point for each frequency

% TRANSMIT CALIBRATION
% Calibration, frequency in column one and power in column two in mW
VDI_Tx_Cal_Points_mW = [319.22,15.16;... % 1
                        319.50,15.74;... % 2
                        320.00,17.50;... % 3
                        320.50,18.55;... % 4
                        321.00,21.77;... % 5
                        321.50,26.18;... % 6
                        322.00,24.71;... % 7
                        322.50,22.73;... % 8
                        323.00,22.16;... % 9
                        323.50,21.19;... % 10
                        324.00,21.07;... % 11
                        324.50,21.35;... % 12
                        325.00,21.89;... % 13
                        325.50,25.03;... % 14
                        326.00,23.47;... % 15
                        326.50,21.21;... % 16
                        327.00,17.50;... % 17
                        327.50,19.12;... % 18
                        328.00,20.68;... % 19
                        330.00,20.19;... % 20
                        335.00,22.83;... % 21
                        340.00,17.92]; % 22

% Lower Wing Line (LWL) Tx Calibration
% from the above known values implement a spline curve fit to figure out
% the power numbers in mW from the exact frequencies

TxLWL_Interp_324_153_mW = spline(VDI_Tx_Cal_Points_mW(10:12,1),...
                                VDI_Tx_Cal_Points_mW(10:12,2),324.153);

TxLWL_Interp_324_253_mW = spline(VDI_Tx_Cal_Points_mW(10:12,1),...
                                VDI_Tx_Cal_Points_mW(10:12,2),324.253);

TxLWL_Interp_324_353_mW = spline(VDI_Tx_Cal_Points_mW(10:12,1),...
                                VDI_Tx_Cal_Points_mW(10:12,2),324.353);

TxLWL_Interp_324_453_mW = spline(VDI_Tx_Cal_Points_mW(10:12,1),...
                                VDI_Tx_Cal_Points_mW(10:12,2),324.453);

TxLWL_Interp_324_553_mW = spline(VDI_Tx_Cal_Points_mW(11:13,1),...
                                VDI_Tx_Cal_Points_mW(11:13,2),324.553);

TxLWL_Interp_324_653_mW = spline(VDI_Tx_Cal_Points_mW(11:13,1),...
                                VDI_Tx_Cal_Points_mW(11:13,2),324.653);

TxLWL_Interp_324_753_mW = spline(VDI_Tx_Cal_Points_mW(11:13,1),...

```

```

        VDI_Tx_Cal_Points_mW(11:13,2),324.753);

TxLWL_Interp_324_853_mW = spline(VDI_Tx_Cal_Points_mW(11:13,1),...
        VDI_Tx_Cal_Points_mW(11:13,2),324.853);

TxLWL_Interp_324_953_mW = spline(VDI_Tx_Cal_Points_mW(11:13,1),...
        VDI_Tx_Cal_Points_mW(11:13,2),324.953);

TxLWL_Interp_325_053_mW = spline(VDI_Tx_Cal_Points_mW(12:14,1),...
        VDI_Tx_Cal_Points_mW(12:14,2),325.053);

TxLWL_Interp_325_153_mW = spline(VDI_Tx_Cal_Points_mW(12:14,1),...
        VDI_Tx_Cal_Points_mW(12:14,2),325.153);

TAIPAS_Tx_Cal_Points_LWL_mW = [TxLWL_Interp_324_153_mW;...
        TxLWL_Interp_324_253_mW;TxLWL_Interp_324_353_mW;...
        TxLWL_Interp_324_453_mW;TxLWL_Interp_324_553_mW;...
        TxLWL_Interp_324_653_mW;TxLWL_Interp_324_753_mW;...
        TxLWL_Interp_324_853_mW;TxLWL_Interp_324_953_mW;...
        TxLWL_Interp_325_053_mW;TxLWL_Interp_325_153_mW];

% convert to dBm
TAIPAS_Tx_Cal_Points_LWL_dBm = ...
        10*log10(TAIPAS_Tx_Cal_Points_LWL_mW);

% Calculate the minimum
TAIPAS_Tx_Cal_Points_LWL_min_dBm = ...
        min(TAIPAS_Tx_Cal_Points_LWL_dBm);

% Upper Wing Line (UWL)Tx Calibration
% from the above known values implement a spline curve fit to figure out
% the power numbers in mW from the exact frequencies

TxUWL_Interp_325_153_mW = spline(VDI_Tx_Cal_Points_mW(12:14,1),...
        VDI_Tx_Cal_Points_mW(12:14,2),325.153);

TxUWL_Interp_325_253_mW = spline(VDI_Tx_Cal_Points_mW(12:14,1),...
        VDI_Tx_Cal_Points_mW(12:14,2),325.253);

TxUWL_Interp_325_353_mW = spline(VDI_Tx_Cal_Points_mW(12:14,1),...
        VDI_Tx_Cal_Points_mW(12:14,2),325.353);

TxUWL_Interp_325_453_mW = spline(VDI_Tx_Cal_Points_mW(12:14,1),...
        VDI_Tx_Cal_Points_mW(12:14,2),325.453);

TxUWL_Interp_325_553_mW = spline(VDI_Tx_Cal_Points_mW(13:15,1),...
        VDI_Tx_Cal_Points_mW(13:15,2),325.553);

TxUWL_Interp_325_653_mW = spline(VDI_Tx_Cal_Points_mW(13:15,1),...
        VDI_Tx_Cal_Points_mW(13:15,2),325.653);

TxUWL_Interp_325_753_mW = spline(VDI_Tx_Cal_Points_mW(13:15,1),...

```

```

VDI_Tx_Cal_Points_mW(13:15,2),325.753);

TxUWL_Interp_325_853_mW = spline(VDI_Tx_Cal_Points_mW(13:15,1),...
VDI_Tx_Cal_Points_mW(13:15,2),325.853);

TxUWL_Interp_325_953_mW = spline(VDI_Tx_Cal_Points_mW(13:15,1),...
VDI_Tx_Cal_Points_mW(13:15,2),325.953);

TxUWL_Interp_326_053_mW = spline(VDI_Tx_Cal_Points_mW(14:16,1),...
VDI_Tx_Cal_Points_mW(14:16,2),326.053);

TxUWL_Interp_326_153_mW = spline(VDI_Tx_Cal_Points_mW(14:16,1),...
VDI_Tx_Cal_Points_mW(14:16,2),326.153);

TAIPAS_Tx_Cal_Points_UWL_mW = [TxUWL_Interp_325_153_mW;...
TxUWL_Interp_325_253_mW;TxUWL_Interp_325_353_mW;...
TxUWL_Interp_325_453_mW;TxUWL_Interp_325_553_mW;...
TxUWL_Interp_325_653_mW;TxUWL_Interp_325_753_mW;...
TxUWL_Interp_325_853_mW;TxUWL_Interp_325_953_mW;...
TxUWL_Interp_326_053_mW;TxUWL_Interp_326_153_mW];

% convert to dBm
TAIPAS_Tx_Cal_Points_UWL_dBm = ...
10*log10(TAIPAS_Tx_Cal_Points_UWL_mW);

% Calculate the minimum
TAIPAS_Tx_Cal_Points_UWL_min_dBm = ...
min(TAIPAS_Tx_Cal_Points_UWL_dBm);

% Wideband Tx Calibration
% Calibration, frequency in column one and power in column two in mW
% from the above known values implement a spline curve fit to figure out
% the power numbers in mW from the exact frequencies

TxWB_Interp_320_000_mW = VDI_Tx_Cal_Points_mW(3,2);

TxWB_Interp_323_153_mW = spline(VDI_Tx_Cal_Points_mW(8:10,1),...
VDI_Tx_Cal_Points_mW(8:10,2),323.153);

TxWB_Interp_324_153_mW = spline(VDI_Tx_Cal_Points_mW(10:12,1),...
VDI_Tx_Cal_Points_mW(10:12,2),324.153);

TxWB_Interp_324_653_mW = spline(VDI_Tx_Cal_Points_mW(11:13,1),...
VDI_Tx_Cal_Points_mW(11:13,2),324.653);

TxWB_Interp_325_153_mW = spline(VDI_Tx_Cal_Points_mW(12:14,1),...
VDI_Tx_Cal_Points_mW(12:14,2),325.153);

TxWB_Interp_325_653_mW = spline(VDI_Tx_Cal_Points_mW(13:15,1),...
VDI_Tx_Cal_Points_mW(13:15,2),325.653);

TxWB_Interp_326_153_mW = spline(VDI_Tx_Cal_Points_mW(14:16,1),...

```

```

                                VDI_Tx_Cal_Points_mW(14:16,2),326.153);

TxWB_Interp_327_153_mW = spline(VDI_Tx_Cal_Points_mW(16:18,1),...
                                VDI_Tx_Cal_Points_mW(16:18,2),327.153);

TxWB_Interp_330_000_mW = VDI_Tx_Cal_Points_mW(20,2);

TxWB_Interp_335_000_mW = VDI_Tx_Cal_Points_mW(21,2);

TxWB_Interp_340_000_mW = VDI_Tx_Cal_Points_mW(22,2);

TAIPAS_Tx_Cal_Points_wb_mW = [TxWB_Interp_320_000_mW;...
    TxWB_Interp_323_153_mW;TxWB_Interp_324_153_mW;...
    TxWB_Interp_324_653_mW;TxWB_Interp_325_153_mW;...
    TxWB_Interp_325_653_mW;TxWB_Interp_326_153_mW;...
    TxWB_Interp_327_153_mW;TxWB_Interp_330_000_mW;...
    TxWB_Interp_335_000_mW;TxWB_Interp_340_000_mW];

% convert to dBm
TAIPAS_Tx_Cal_Points_wb_dBm = 10*log10(TAIPAS_Tx_Cal_Points_wb_mW);

% Calculate the minimum
TAIPAS_Tx_Cal_Points_wb_min_dBm = min(TAIPAS_Tx_Cal_Points_wb_dBm);

% find the minimum of all three scans to use as a common adjustment for
% all scans, make a row of mins for the three scans and find a common min
TAIPAS_Tx_Cal_scans_mins_dBm = [TAIPAS_Tx_Cal_Points_wb_min_dBm,...
    TAIPAS_Tx_Cal_Points_LWL_min_dBm,...
    TAIPAS_Tx_Cal_Points_UWL_min_dBm];

% calculate the minimum of each scan minimum to find common minimum
TAIPAS_Tx_Cal_dBm = min(TAIPAS_Tx_Cal_scans_mins_dBm);

% Calculate the adjustments necessary relative to the minimum
TAIPAS_Tx_Cal_Points_LWL_adjustments_dBm = ...
    TAIPAS_Tx_Cal_Points_LWL_dBm - TAIPAS_Tx_Cal_dBm;

% Calculate the adjustments necessary relative to the minimum
TAIPAS_Tx_Cal_Points_UWL_adjustments_dBm = ...
    TAIPAS_Tx_Cal_Points_UWL_dBm - TAIPAS_Tx_Cal_dBm;

% Calculate the adjustments necessary relative to the minimum
TAIPAS_Tx_Cal_Points_wb_adjustments_dBm = ...
    TAIPAS_Tx_Cal_Points_wb_dBm - TAIPAS_Tx_Cal_dBm;

% make a 66 long row of Tx adjustments
TAIPAS_Tx_Cal_adjustments_dBm = ...
    [TAIPAS_Tx_Cal_Points_wb_adjustments_dBm',...
    TAIPAS_Tx_Cal_Points_LWL_adjustments_dBm',...

```

```

    TAIPAS_Tx_Cal_Points_UWL_adjustments_dBm',...
    TAIPAS_Tx_Cal_Points_wb_adjustments_dBm',...
    TAIPAS_Tx_Cal_Points_LWL_adjustments_dBm',...
    TAIPAS_Tx_Cal_Points_UWL_adjustments_dBm'];

% RECEIVER CALIBRATION

% minimal information on LWL, 6.5 dB Conversion loss + 3 dB for SSB
% no data from 320-325
TAIPAS_Rx1_139_Cal_Points_LWL_dB = [8.5;8.5;8.5;8.5;8.5;8.5;8.5;...
                                     8.5;8.5;8.5;8.5];
TAIPAS_Rx2_138_Cal_Points_LWL_dB = [9;9;9;9;9;9;9;9;9;9;9];

% minimal information on UWL, dB Conversion loss + 3 dB for SSB
TAIPAS_Rx1_139_Cal_Points_UWL_dB = [8.6;8.7;8.8;9;9;9;9;9;9;9;8.9];

TAIPAS_Rx2_138_Cal_Points_UWL_dB = [9;8.9;8.8;8.7;8.8;8.9;9;9;9;9];

% minimal information on wideband, dB Conversion loss + 3 dB for SSB
TAIPAS_Rx1_139_Cal_Points_wb_dB = ...
                                     [8.5;8.5;8.5;8.5;8.6;9;8.8;8.4;8.5;9.2;9.1];

TAIPAS_Rx2_138_Cal_Points_wb_dB = [9;9;9;9;8.9;8.9;9.1;9.2;9;9.2;9.1];

% vector is 66 long (rows) for the total adjustments
TAIPAS_Rx1_139_Cal_adjustments_dB = ...
    [TAIPAS_Rx1_139_Cal_Points_wb_dB',...
    TAIPAS_Rx1_139_Cal_Points_LWL_dB',...
    TAIPAS_Rx1_139_Cal_Points_UWL_dB',...
    TAIPAS_Rx1_139_Cal_Points_wb_dB',...
    TAIPAS_Rx1_139_Cal_Points_LWL_dB',...
    TAIPAS_Rx1_139_Cal_Points_UWL_dB'];

TAIPAS_Rx2_138_Cal_adjustments_dB = ...
    [TAIPAS_Rx2_138_Cal_Points_wb_dB',...
    TAIPAS_Rx2_138_Cal_Points_LWL_dB',...
    TAIPAS_Rx2_138_Cal_Points_UWL_dB',...
    TAIPAS_Rx2_138_Cal_Points_wb_dB',...
    TAIPAS_Rx2_138_Cal_Points_LWL_dB',...
    TAIPAS_Rx2_138_Cal_Points_UWL_dB'];

% The above adjustment vectors are the variable losses due to the
% subharmonic mixer SSB plus 3 dB for DSB and variations. These values are
% available to add to the received signal to tell what was received after
% the horn. In the future, the return loss of the horn still needs to be
% included.

Rx1_THz_Complex_Data_Amp_dBm(1:(Good_Data), 1:66) = 0;

Rx2_THz_Complex_Data_Amp_dBm(1:(Good_Data), 1:66) = 0;

```

```

% Calibrate each data and develop the extinction data as well
% convert each freq data to magnitude and adjust for Tx and Rx calibrations
for j = 1:66
    for i = 1:(Good_Data)
        % Receiver #1
        % This section cacluates the propagation path with everything
        % removed except the 50 dBi of gain of the lens and horn gain
        % combination. Cancels at Tx and Rx. Don't need to subtract from Rx
        % since, not adding to Tx.
        % covert to Amplitude in dBm and AC to RMS, and add back in
        % Rx horn losses, this will yield the exact data
        % adjustments for 50 Ohm load and dBm are last
        % First cacluate the received data

        Rx1_THz_Complex_Data_Amp_dBm(i,j) = ...
            10.*(log10(((abs(Rx1_THz_Complex_Data(i,j)).*.707).^2)...
                ./(50 *.001)));

        % Add back in horn losses Rx estimated at reflection coefficient
        Rx1_THz_Complex_Data_Amp_dBm(i,j) = ...
            Rx1_THz_Complex_Data_Amp_dBm(i,j) + ...
            (Reflection_Coefficient .* Rx1_THz_Complex_Data_Amp_dBm(i,j));

        % add back in test set up pads and remove gain box data
        Rx1_THz_Complex_Data_Amp_dBm(i,j) = ...
            Rx1_THz_Complex_Data_Amp_dBm(i,j) - Receiver_GAIN_adj_dB;

        % Adjust for Tx and Rx calibration variations, remove receive
        % lossess and add increases in Tx above minimum Tx power. Note the
        % data is negative, so adjustments are opposite to expected
        % Tx POWER is uniform after adjustments WB=12.4 dBm, LWL = 13.5
        % dBm, UWL=13.53 dBm
        Rx1_THz_Complex_Data_Amp_dBm(i,j) = ...
            Rx1_THz_Complex_Data_Amp_dBm(i,j) - ...
            TAIPAS_Tx_Cal_adjustments_dBm(j) + ...
            TAIPAS_Rx1_139_Cal_adjustments_dB(j);

        % Receiver #2
        % This section cacluates the propagation path with everything
        % removed except the 50 dBi of gain of the lens and horn gain
        % combination. Cancels at Tx and Rx. Don't need to subtract from Rx
        % since, not adding to Tx.
        % covert to Amplitude in dBm and AC to RMS, and add back in
        % Rx horn losses, this will yield the exact data
        % adjustments for 50 Ohm load and dBm are last
        % First cacluate the received data

        Rx2_THz_Complex_Data_Amp_dBm(i,j) = ...

```

```

10.*(log10(((abs(Rx2_THz_Complex_Data(i,j)).*.707).^2)...
./ (50 *.001)));

% Add back in horn losses Rx estimated at reflection coefficient
Rx2_THz_Complex_Data_Amp_dBm(i,j) = ...
    Rx2_THz_Complex_Data_Amp_dBm(i,j) + ...
    (Reflection_Coefficient .* Rx2_THz_Complex_Data_Amp_dBm(i,j));

% add back in test set up pads and remove gain box data
Rx2_THz_Complex_Data_Amp_dBm(i,j) = ...
    Rx2_THz_Complex_Data_Amp_dBm(i,j) - Receiver_GAIN_adj_dB;

% Adjust for Tx and Rx calibration variations, remove receive
% lossess and add increases in Tx above minimum Tx power. Note the
% data is negative, so adjustments are opposite to expected
% Tx POWER is uniform after adjustments WB=12.4 dBm, LWL = 13.5
% dBm, 13.53 dBm
Rx2_THz_Complex_Data_Amp_dBm(i,j) = ...
    Rx2_THz_Complex_Data_Amp_dBm(i,j) - ...
    TAIPAS_Tx_Cal_adjustments_dBm(j) + ...
    TAIPAS_Rx2_138_Cal_adjustments_dB(j);

end
end
% calculate the mean of every frequency column and store in a single row
% (66 values - one for each frequency)
Rx1_THz_Mean_Amp_Cal_dBm = mean(Rx1_THz_Complex_Data_Amp_dBm);

Rx2_THz_Mean_Amp_Cal_dBm = mean(Rx2_THz_Complex_Data_Amp_dBm);

% calculate variance for noise calculation
Rx1_THz_Variance_Amp_Cal_dBsq = var(Rx1_THz_Complex_Data_Amp_dBm);

Rx2_THz_Variance_Amp_Cal_dBsq = var(Rx2_THz_Complex_Data_Amp_dBm);

% Calculate STD for use on plots- there is on STD in row for each 66
% frequency selection
Rx1_THz_Mean_Amp_STD_dBm = ...
    std(Rx1_THz_Complex_Data_Amp_dBm)/sqrt(Good_Data);

Rx2_THz_Mean_Amp_STD_dBm = ...
    std(Rx2_THz_Complex_Data_Amp_dBm)/sqrt(Good_Data);

#####

%% ##### HISTOGRAM and Hardware Losses removed #####
%# 50 dBi on each side cancels and power is common miniumu on each sweep##

% Make a HISTOGRAM Plot of each Scan

```

```

% For each Scan frequency - Histogram Conversion and Plot
% use flag to enable and disable 66 frequency plots - top of file
% also the range of plots for Rx1 and Rx2 is defined up at the top of
% the file, too many crashes MATLAB
% the range used will be the FFT plot range defined in the top of the file
if disable_Hist_plots == 0;
% This is for test purposes to view distribution of data

for j = FFT_plot_start:FFT_plot_end;

    %PLOT Histogram Rx1 & Rx2

j_string = num2str(j); % convert Freq number to string for plot title

plot_title_Rx1 = ['Atmosphere Rx1 Hist ', j_string, ' Hist '];

plot_title_Rx2 = ['Atmosphere Rx2 Hist ', j_string, ' Hist '];

% Plot Rx1
figure09 = figure('Color',[1,1,1], 'Name',plot_title_Rx1);

% Create axes
axes1 = axes('Parent',figure09);
hold(axes1, 'on');
box(axes1, 'on');
% Plot Hist in dBm

hist(Rx1_THz_Complex_Data_Amp_dBm(:,j),100);

% Create xlabel
xlabel('Amplitude (dBm)');

% Create ylabel
ylabel('Quantity of Value');

Title = [ plot_title_Rx1, '(', num2str(THz_month), ' ', ...
        num2str(THz_day), ' ', num2str(THz_year), ' ', num2str(THz_hour), ...
        ':', num2str(THz_minute), ':', num2str(THz_second), ') '];

% Create title
title(Title);

box(axes1, 'on');
% Set the remaining axes properties
set(axes1, 'FontSize',16);

% Plot Rx2
figure10 = figure('Color',[1,1,1], 'Name',plot_title_Rx2);

% Create axes
axes1 = axes('Parent',figure10);

```

```

hold(axes1, 'on');
box(axes1, 'on');

% Plot Hist in dBm
hist(Rx2_THz_Complex_Data_Amp_dBm(:,j),100);

% Create xlabel
xlabel('Amplitude (dBm)');

% Create ylabel
ylabel('Quantity of Value');

Title = [ plot_title_Rx2, '(' , num2str(THz_month), ' ', ...
          num2str(THz_day), ' ', num2str(THz_year), ' ', ' ', num2str(THz_hour), ...
          ':', num2str(THz_minute), ':', num2str(THz_second), ') '];

% Create title
title(Title);

box(axes1, 'on');
% Set the remaining axes properties
set(axes1, 'FontSize',16);
end
end

#####

%% ##### FRIIS with Hardware Losses removed #####
%% 50 dBi on each side cancels and power is common miniumu on each sweep##

% Calculate the mathematical and physics based predicted values using Friis
% note commmented equations to calculate Friis with system losses

% the first 33 frequencies, since the last 33 frequencies in an exact
% repeat

Frequency_Scan_33_GHz = [Scan_WB_Frequencies;Scan_LWL_Frequencies;...
                        Scan_UWL_Frequencies];

% calculate the wavelength - lamda=c/f
Wavelength_Scan_33_m = c_mpers ./ (Frequency_Scan_33_GHz .* 10^9);

% Exciter Power at the horn output using interpolated data from VDI power
% data and the reflection coefficient of the horn

% Exciter Power - interpolated from VDI power data
Power_Exciter_33_mW = [TAIPAS_Tx_Cal_Points_wb_mW;...
                      TAIPAS_Tx_Cal_Points_LWL_mW;TAIPAS_Tx_Cal_Points_UWL_mW];

```

```

% Power out of the horn - Exciter less S11 (return loss)
Power_Horn_Tx_33_mW = (1- Reflection_Coefficient) * Power_Exciter_33_mW;

% XXXXXXXXXXXXXXXXXXXXXXXXXXXXXXX -280 has start of H2O
% Liebe absorption and scattering with Al Gasiewski adds - looked up from
% plot at this point

% IMPORTANT TO NOTE: 20 RH weather conditions for dB/km Extinction
% Extinction Coefficient Calculation in dB/km - absorption + Scattering
Extinction_Coef_dBperkm = CA_Humidity_20Percent_Absorption_dBperkm + ...
    CA_Scatter_dBperkm;

% Extinction Coefficient convert to Np/km, 1Np=1/e = 4.3429 dB = 8.685/2
Extinction_Coef_Npperkm = Extinction_Coef_dBperkm ./ (8.685889638/2);

% XXXXXXXXXXXXXXXXXXXXXXXXXXXXXXX

% Develop effective diameter of the lens for the different scan frequencies
Effective_Lens_D_m = Lens_D_m * 325.153 ./ Frequency_Scan_33_GHz;

%Power received at the Antenna/Horn - Friis equation
Power_received_mW = Power_Horn_Tx_33_mW .* ...
    ((pi .* Effective_Lens_D_m.^2) ./ ...
    (4*Path_Length_m .* Wavelength_Scan_33_m)).^2 .* ...
    exp(-Extinction_Coef_Npperkm ./ 1000 .* Path_Length_m);

%Power received after the received Antenna/Horn
% Power_received_Horn_output33_mW = ...
%
%     (1 - Reflection_Coefficient) * Power_received_mW;

% Don't take the loss of the hardware as above
Power_received_Horn_output33_mW = ...
    Power_received_mW;

% This is the power received at the horn (no loss of the horn taken out),
% both lens gains are included, this is the power received assuming the Tx
% lens and rx lens cancel andTx power is different for each frequency
% around 10-12 dBm - the adjustments will normalize to the same point
Power_received_Horn_output33_dBm = ...
    10*log10(Power_received_Horn_output33_mW);

% make a 33 long row of Tx adjustments, assumes power is constant of
% WB=12.4 dBm, LWL = 13.5 dBm, 13.53 dBm
TAIPAS_Tx_Cal_adj_33_dBm = [TAIPAS_Tx_Cal_Points_wb_adjustments_dBm',...
    TAIPAS_Tx_Cal_Points_LWL_adjustments_dBm',...
    TAIPAS_Tx_Cal_Points_LWL_adjustments_dBm'];

Power_received_Horn_output33_dBm = Power_received_Horn_output33_dBm + ...
    TAIPAS_Tx_Cal_adj_33_dBm';

```

```

% Change in analysis from calculations in Excel to finding the propagation
% path values, not all the losses of the system. Getting based on transmit
% base, what is received at the Rx lens

% This can be replaced if desired to verify function to Excel Table.
% Power received on Rx1 for 33 frequencies
% Pwr_rec_Rx1_139_Insertion_Loss33_dBm = ...
%   Power_received_Horn_output33_dBm - Insertion_loss33_Rx1_139_dB ...
%                                     + TAIPAS_Tx_Cal_adj_33_dBm' ;
% This calculates the propagation path and does not look beyond hardware
% losses

Pwr_rec_Rx1_139_Insertion_Loss33_dBm = ...
    Power_received_Horn_output33_dBm;

% Power received on Rx1 for 66 frequencies
Pwr_rec_Rx1_139_Insertion_Loss_dBm = ...
    [Pwr_rec_Rx1_139_Insertion_Loss33_dBm; ...
     Pwr_rec_Rx1_139_Insertion_Loss33_dBm];

% Difference in power between Friis and actual Rx1
Delta_Rx1_rec_Friis = - Pwr_rec_Rx1_139_Insertion_Loss_dBm + ...
    Rx1_THz_Mean_Amp_Cal_dBm';

% normalize mean Rx data to expected Friis - remove DC separation, if
% prediction is accurate, not much normalization
Rx1_THz_Normal_dBm = ...
    Rx1_THz_Mean_Amp_Cal_dBm' + abs(mean(Delta_Rx1_rec_Friis));

% Power received on Rx2
%Pwr_rec_Rx2_138_Insertion_Loss33_dBm = ...
%   Power_received_Horn_output33_dBm - Insertion_loss33_Rx2_138_dB ...
%                                     + TAIPAS_Tx_Cal_adj_33_dBm';
Pwr_rec_Rx2_138_Insertion_Loss33_dBm = ...
    Power_received_Horn_output33_dBm ;

% Power received on Rx2 for 66 frequencies
Pwr_rec_Rx2_138_Insertion_Loss_dBm = ...
    [Pwr_rec_Rx2_138_Insertion_Loss33_dBm;...
     Pwr_rec_Rx2_138_Insertion_Loss33_dBm];

% Difference in power between Friis and actual Rx1
Delta_Rx2_rec_Friis = Pwr_rec_Rx2_138_Insertion_Loss_dBm - ...
    Rx2_THz_Mean_Amp_Cal_dBm';

% normalize mean Rx data to expected Friis - remove DC separation
Rx2_THz_Normal_dBm = ...
    Rx2_THz_Mean_Amp_Cal_dBm' + abs(mean(Delta_Rx2_rec_Friis));

```

```

% plot on same amplitude plot as received data for comparison

#####

%% ##### MEAN Data with CALIBRATION and Hardware Loss Removed #####
%# 50 dBi on each side cancels and power is common minimum on each sweep##

%% ##### MEAN Data with CALIBRATION and Hardware Loss Removed #####
%# 50 dBi on each side cancels and power is common minimum on each sweep##

% Plot Mean data from both receivers with calibration for every
% 11 points (Scans), a total of 6 scans, also add the predicted FRIIS
% value data

% RECEIVER #1

if Rx1_disable == 0

% PLOT Rx1, Scan 1 ONLY (wideband)
figure11 = ...
    figure('Color',[1,1,1], 'Name', 'Rx1 Scan1 Mean Amp Cal Plot only');

% Create axes
axes1 = axes('Parent',figure11);
hold(axes1, 'on');
box(axes1, 'on');

hold on;

% Plot Frequency vs. Mean Amplitude in dBm
plot(Scan_WB_Frequencies, ...
    Rx1_THz_Mean_Amp_Cal_dBm(1:11), '-o b');

% Plot Frequency vs. STD of Mean Amplitude in dBm - cyan color
plot(Scan_WB_Frequencies, ...
    (Rx1_THz_Mean_Amp_Cal_dBm(1:11) + Rx1_THz_Mean_Amp_STD_dBm(1:11)), 'o c');

hold off;

% Display the mean of the 11 STD values
Mean_STD = std(Rx1_THz_Mean_Amp_STD_dBm(1:11));

% Convert the mean STD number to string
Mean_STD_Number = num2str(Mean_STD);

% Y label
Y_Axis_label = ...
    ['Mean Amp, Cal (dBm) - ', 'MeanSTD=', Mean_STD_Number, ' dBm'];

```

```

% Create xlabel
xlabel('Frequency (GHz)');

% Create ylabel
ylabel(Y_Axis_label);

Title = ['Atmosphere Rx1 Amplitude Wideband Scan 1 (',...
        num2str(THz_month),' ',...
        num2str(THz_day),' ', num2str(THz_year),' ', num2str(THz_hour),...
        ':',num2str(THz_minute),':',num2str(THz_second),')'];

% Create title
title(Title);

% Legend of Standard deviations on each cyan point
legend('Good Data Mean','STD Mean');

box(axes1,'on');
% Set the remaining axes properties
set(axes1,'FontSize',16);

% PLOT Rx1, Scan 1 with Friis and delta (wideband)
figure12 = ...
    figure('Color',[1,1,1],'Name','Rx1 Scan1 Mean Amp - Friis - Delta Plot');

% Create axes
axes1 = axes('Parent',figure12);
hold(axes1,'on');
box(axes1,'on');

hold on

% Plot Frequency vs. Mean Amplitude in dBm
plot(Scan_WB_Frequencies, Rx1_THz_Mean_Amp_Cal_dBm(1:11), '-o b');

% plot predicted via Friis received data on Rx1
plot(Scan_WB_Frequencies, Pwr_rec_Rx1_139_Insertion_Loss_dBm(1:11),'-x g');

% plot delta of Friis vs. received data on Rx1
plot(Scan_WB_Frequencies, Delta_Rx1_rec_Friis(1:11), '-. r');

hold off

% Create xlabel
xlabel('Frequency (GHz)');

% Create ylabel
ylabel('Mean Amplitude, with Calibration (dBm)');
Title = ['Atmosphere Rx1 Amplitude WB1 Scan 1,Friis,Delta (',...

```

```

    num2str(THz_month), ...
    ' ', num2str(THz_day), ' ', num2str(THz_year), ', ', num2str(THz_hour), ...
    ':', num2str(THz_minute), ':', num2str(THz_second), ')']];

% Create title
title(Title);

% creat legend
legend('Rx Data', 'Friis Data', ' Negative Delta');

box(axes1, 'on');
% Set the remaining axes properties
set(axes1, 'FontSize', 16);

%PLOT Rx1, Scan 1 and Friis absolutes - normalize to Friis DC (wideband)
figure13 = figure('Color', [1,1,1], ...
    'Name', 'Rx1 Scan1 Mean Amp - Friis - DC Normalize');

% Create axes
axes1 = axes('Parent', figure13);
hold(axes1, 'on');
box(axes1, 'on');

hold on

% Plot Frequency vs. Mean Amplitude in dBm
plot(Scan_WB_Frequencies, Rx1_THz_Normal_dBm(1:11), '-o b');

% plot predicted via Friis received data on Rx1
plot(Scan_WB_Frequencies, Pwr_rec_Rx1_139_Insertion_Loss_dBm(1:11), '-x g');

hold off

% Create xlabel
xlabel('Frequency (GHz)');

% Create ylabel
ylabel('Mean Amplitude, with Calibration (dBm)');

Title = ['Atmosphere Rx1 Normalized Amp WB1 Scan 1, Friis (' , ...
    num2str(THz_month), ' ', ...
    num2str(THz_day), ' ', num2str(THz_year), ', ', num2str(THz_hour), ...
    ':', num2str(THz_minute), ':', num2str(THz_second), ')']];

% Create title
title(Title);

% creat legend
legend('Rx Data', 'Friis Data');

box(axes1, 'on');

```

```

% Set the remaining axes properties
set(axes1, 'FontSize', 16);

%PLOT Rx1, Scan 2 - Lower Wing Line (LWL)
figure14 = figure('Color', [1,1,1], 'Name', 'Rx1 Scan2 Mean Amp Cal Plot');

% Create axes
axes1 = axes('Parent', figure14);
hold(axes1, 'on');
box(axes1, 'on');

hold on;

% Plot Frequency vs. Mean Amplitude in dBm
plot(Scan_LWL_Frequencies, Rx1_THz_Mean_Amp_Cal_dBm(12:22), '-o b');

% Plot Frequency vs. STD of Mean Amplitude in dBm - cyan color
plot(Scan_LWL_Frequencies, ...
     (Rx1_THz_Mean_Amp_Cal_dBm(12:22) + Rx1_THz_Mean_Amp_STD_dBm(12:22)), 'o c')

hold off;

% Display the mean of the 11 STD values
Mean_STD = std(Rx1_THz_Mean_Amp_STD_dBm(12:22));

% Convert the mean STD number to string
Mean_STD_Number = num2str(Mean_STD);

% Y label
Y_Axis_label = ...
    ['Mean Amp, Cal (dBm) - ', 'MeanSTD=', Mean_STD_Number, ' dBm'];

% Create xlabel
xlabel('Frequency (GHz)');

% Create ylabel
ylabel(Y_Axis_label);

Title = ['Atmosphere Rx1 Amplitude LWL Scan2 ', num2str(THz_month), ' ', ...
        num2str(THz_day), ' ', num2str(THz_year), ' ', num2str(THz_hour), ...
        ': ', num2str(THz_minute), ': ', num2str(THz_second), ''];

% Create title
title(Title);

% Legend of Standard deviations on each cyan point
legend('Good Data Mean', 'STD Mean');

box(axes1, 'on');
% Set the remaining axes properties

```

```

set(axes1, 'FontSize',16);

%PLOT Rx1, Scan 2 with Friis and delta (LWL)
figure15 = figure('Color',[1,1,1], 'Name',...
                 'Rx1 Scan2 Mean Amp - Friis - Delta Plot');

% Create axes
axes1 = axes('Parent',figure15);
hold(axes1, 'on');
box(axes1, 'on');

hold on

% Plot Frequency vs. Mean Amplitude in dBm
plot(Scan_LWL_Frequencies, Rx1_THz_Mean_Amp_Cal_dBm(12:22), '-o b');

% plot predicted via Friis received data on Rx1
plot(Scan_LWL_Frequencies, Pwr_rec_Rx1_139_Insertion_Loss_dBm(12:22),...
     '-x g');

% plot delta of Friis vs. received data on Rx1
plot(Scan_LWL_Frequencies, Delta_Rx1_rec_Friis(12:22), '-. r');

hold off

% Create xlabel
xlabel('Frequency (GHz)');

% Create ylabel
ylabel('Mean Amplitude, with Calibration (dBm)');

Title = ['Atmosphere Rx1 Amplitude LWL Scan 2, Friis, Delta (',...
         num2str(THz_month), ' ', num2str(THz_day), ' ', num2str(THz_year), ' ', ' ',...
         num2str(THz_hour), ':', num2str(THz_minute), ':', num2str(THz_second), ')'];

% Create title
title(Title);

% creat legend
legend('Rx Data', 'Friis Data', ' Negative Delta');

box(axes1, 'on');
% Set the remaining axes properties
set(axes1, 'FontSize',16);

%PLOT Rx1, Scan 2 and Friis absolutes - normalize to Friis DC (LWL)
figure16 = figure('Color',[1,1,1], 'Name',...
                 'Rx1 Scan2 Mean Amp - Friis - DC Normalize');

% Create axes
axes1 = axes('Parent',figure16);

```

```

hold(axes1, 'on');
box(axes1, 'on');

hold on

% Plot Frequency vs. Mean Amplitude in dBm
plot(Scan_LWL_Frequencies, Rx1_THz_Normal_dBm(12:22), '-o b');

% plot predicted via Friis received data on Rx1
plot(Scan_LWL_Frequencies, Pwr_rec_Rx1_139_Insertion_Loss_dBm(12:22), ...
      '-x g');

hold off

% Create xlabel
xlabel('Frequency (GHz)');

% Create ylabel
ylabel('Atmosphere Mean Amplitude, with Calibration (dBm)');
Title = ['Rx1 Normalized Amp LWL Scan 2, Friis (' , num2str(THz_month), ...
        ' ', num2str(THz_day), ' ', num2str(THz_year), ' ', num2str(THz_hour), ...
        ':', num2str(THz_minute), ':', num2str(THz_second), ') '];

% Create title
title(Title);

% creat legend
legend('Rx Data', 'Friis Data');

box(axes1, 'on');
% Set the remaining axes properties
set(axes1, 'FontSize', 16);

%PLOT Rx1, Scan 3 Upper Wing Line (UWL)
figure17 = figure('Color', [1,1,1], 'Name', 'Rx1 Scan3 Mean Amp Cal Plot');

% Create axes
axes1 = axes('Parent', figure17);
hold(axes1, 'on');
box(axes1, 'on');

hold on;

% Plot Frequency vs. Mean Amplitude in dBm
plot(Scan_UWL_Frequencies, Rx1_THz_Mean_Amp_Cal_dBm(23:33), '-o b');

% Plot Frequency vs. STD of Mean Amplitude in dBm - cyan color
plot(Scan_UWL_Frequencies, ...
      (Rx1_THz_Mean_Amp_Cal_dBm(23:33) + Rx1_THz_Mean_Amp_STD_dBm(23:33)), 'o c')

hold off;

```

```

% Display the mean of the 11 STD values
Mean_STD = std(Rx1_THz_Mean_Amp_STD_dBm(23:33));

% Convert the mean STD number to string
Mean_STD_Number = num2str(Mean_STD);

% Y label
Y_Axis_label = ...
    ['Mean Amp, Cal (dBm) - ', 'MeanSTD=', Mean_STD_Number, ' dBm'];

% Create xlabel
xlabel('Frequency (GHz)');

% Create ylabel
ylabel(Y_Axis_label);

Title = ['Atmosphere Rx1 Amplitude UWL Scan 3 (' , num2str(THz_month), ...
    ' ', ...
    num2str(THz_day), ' ', num2str(THz_year), ' ', num2str(THz_hour), ...
    ':', num2str(THz_minute), ':', num2str(THz_second), ')'];

% Legend of Standard deviations on each cyan point
legend('Good Data Mean', 'STD Mean');

% Create title
title(Title);

box(axes1, 'on');
% Set the remaining axes properties
set(axes1, 'FontSize', 16);

%PLOT Rx1, Scan 3 with Friis and delta (UWL)
figure18 = figure('Color', [1,1,1], 'Name', ...
    'Rx1 Scan3 Mean Amp - Friis - Delta Plot');

% Create axes
axes1 = axes('Parent', figure18);
hold(axes1, 'on');
box(axes1, 'on');

hold on

% Plot Frequency vs. Mean Amplitude in dBm
plot(Scan_UWL_Frequencies, Rx1_THz_Mean_Amp_Cal_dBm(23:33), '-o b');

% plot predicted via Friis received data on Rx1
plot(Scan_UWL_Frequencies, Pwr_rec_Rx1_139_Insertion_Loss_dBm(23:33), ...
    '-x g');

% plot delta of Friis vs. received data on Rx1
plot(Scan_UWL_Frequencies, Delta_Rx1_rec_Friis(23:33), '-. r');

```

```

hold off

% Create xlabel
xlabel('Frequency (GHz)');

% Create ylabel
ylabel('Mean Amplitude, with Calibration (dBm)');

Title = ['Atmosphere Rx1 Amplitude UWL Scan3,Friis,Delta (',...
        num2str(THz_month),...
        ' ',num2str(THz_day),' ', num2str(THz_year),' ', ' ', num2str(THz_hour),...
        ':' ,num2str(THz_minute), ':' ,num2str(THz_second),')'];

% Create title
title(Title);

% creat legend
legend('Rx Data','Friis Data',' Negative Delta');

box(axes1,'on');
% Set the remaining axes properties
set(axes1,'FontSize',16);

%PLOT Rx1, Scan 3 and Friis absolutes - normalize to Friis DC (UWL)
figure19 = figure('Color',[1,1,1],...
                 'Name','Rx1 Scan3 Mean Amp - Friis - DC Normalize');

% Create axes
axes1 = axes('Parent',figure19);
hold(axes1,'on');
box(axes1,'on');

hold on

% Plot Frequency vs. Mean Amplitude in dBm
plot(Scan_UWL_Frequencies,Rx1_THz_Normal_dBm(23:33), '-o b');

% plot predicted via Friis received data on Rx1
plot(Scan_UWL_Frequencies,Pwr_rec_Rx1_139_Insertion_Loss_dBm(23:33),...
     '-x g');

hold off

% Create xlabel
xlabel('Frequency (GHz)');

% Create ylabel
ylabel('Atmosphere Mean Amplitude, with Calibration (dBm)');
Title = ['Rx1 Normalized Amp UWL Scan 3,Friis (' ,num2str(THz_month),...
        ' ',num2str(THz_day),' ', num2str(THz_year),' ', ' ', num2str(THz_hour),...
        ':' ,num2str(THz_minute), ':' ,num2str(THz_second),')'];

```

```

% Create title
title(Title);

% creat legend
legend('Rx Data','Friis Data');

box(axes1,'on');
% Set the remaining axes properties
set(axes1,'FontSize',16);

%PLOT Rx1, Scan 4 (wideband)
figure20 = figure('Color',[1,1,1],'Name','Rx1 Scan4 Mean Amp Cal Plot');

% Create axes
axes1 = axes('Parent',figure20);
hold(axes1,'on');
box(axes1,'on');

hold on;

% Plot Frequency vs. Mean Amplitude in dBm
plot(Scan_WB_Frequencies,Rx1_THz_Mean_Amp_Cal_dBm(34:44), '-o b');

% Plot Frequency vs. STD of Mean Amplitude in dBm - cyan color
plot(Scan_WB_Frequencies, ...
     (Rx1_THz_Mean_Amp_Cal_dBm(34:44)+Rx1_THz_Mean_Amp_STD_dBm(34:44)), 'o c');

hold off;

% Display the mean of the 11 STD values
Mean_STD = std(Rx1_THz_Mean_Amp_STD_dBm(34:44));

% Convert the mean STD number to string
Mean_STD_Number = num2str(Mean_STD);

% Y label
Y_Axis_label = ...
    ['Mean Amp, Cal (dBm) - ', 'MeanSTD=', Mean_STD_Number, ' dBm'];

% Create xlabel
xlabel('Frequency (GHz)');

% Create ylabel
ylabel(Y_Axis_label);

Title = ['Atmosphere Rx1 Amplitude Wideband Scan 4 (' , num2str(THz_month), '
', ...
    num2str(THz_day), ' ', num2str(THz_year), ', ', num2str(THz_hour), ...
    ': ', num2str(THz_minute), ': ', num2str(THz_second), ') '];

% Create title

```

```

title(Title);

% Legend of Standard deviations on each cyan point
legend('Good Data Mean', 'STD Mean');

box(axes1, 'on');
% Set the remaining axes properties
set(axes1, 'FontSize', 16);

%PLOT Rx1, Scan 4 with Friis and delta - (wideband)
figure21 = figure('Color', [1,1,1], ...
                 'Name', 'Rx1 Scan4 Mean Amp - Friis - Delta Plot');

% Create axes
axes1 = axes('Parent', figure21);
hold(axes1, 'on');
box(axes1, 'on');

hold on

% Plot Frequency vs. Mean Amplitude in dBm
plot(Scan_WB_Frequencies, Rx1_THz_Mean_Amp_Cal_dBm(34:44), '-o b');

% plot predicted via Friis received data on Rx1
plot(Scan_WB_Frequencies, Pwr_rec_Rx1_139_Insertion_Loss_dBm(34:44), '-x g');

% plot delta of Friis vs. received data on Rx1
plot(Scan_WB_Frequencies, Delta_Rx1_rec_Friis(34:44), '-. r');

hold off

% Create xlabel
xlabel('Frequency (GHz)');

% Create ylabel
ylabel('Atmosphere Mean Amplitude, with Calibration (dBm)');

Title = ['Rx1 Amplitude WB Scan 4, Friis, Delta (' , num2str(THz_month), ...
        ' ', num2str(THz_day), ' ', num2str(THz_year), ', ', num2str(THz_hour), ...
        ':', num2str(THz_minute), ':', num2str(THz_second), ') '];

% Create title
title(Title);

% creat legend
legend('Rx Data', 'Friis Data', ' Negative Delta');

box(axes1, 'on');
% Set the remaining axes properties
set(axes1, 'FontSize', 16);

```

```

%PLOT Rx1, Scan 4 and Friis absolutes - normalize to Friis DC (wb)
figure22 = figure('Color',[1,1,1],'Name','Rx1 Scan4 Mean Amp - Friis - DC
Normalize');

% Create axes
axes1 = axes('Parent',figure22);
hold(axes1,'on');
box(axes1,'on');

hold on

% Plot Frequency vs. Mean Amplitude in dBm
plot(Scan_WB_Frequencies,Rx1_THz_Normal_dBm(34:44), '-o b');

% plot predicted via Friis received data on Rx1
plot(Scan_WB_Frequencies,Pwr_rec_Rx1_139_Insertion_Loss_dBm(34:44),'-x g');

hold off

% Create xlabel
xlabel('Frequency (GHz)');

% Create ylabel
ylabel('Atmosphere Mean Amplitude, with Calibration (dBm)');

Title = ['Rx1 Normalized Amp WB Scan 4,Friis (' ,num2str(THz_month),' ',...
num2str(THz_day),' ', num2str(THz_year),' ', num2str(THz_hour),...
':',num2str(THz_minute),':',num2str(THz_second),'')'];

% Create title
title(Title);

% creat legend
legend('Rx Data','Friis Data');

box(axes1,'on');
% Set the remaining axes properties
set(axes1,'FontSize',16);

%PLOT Rx1, Scan 5 - Lower Wing Line (LWL)
figure23 = figure('Color',[1,1,1],'Name','Rx1 Scan5 Mean Amp Cal Plot');

% Create axes
axes1 = axes('Parent',figure23);
hold(axes1,'on');
box(axes1,'on');

hold on;

% Plot Frequency vs. Mean Amplitude in dBm

```

```

plot(Scan_LWL_Frequencies,Rx1_THz_Mean_Amp_Cal_dBm(45:55), '-o b');

% Plot Frequency vs. STD of Mean Amplitude in dBm - cyan color
plot(Scan_LWL_Frequencies, ...
     (Rx1_THz_Mean_Amp_Cal_dBm(45:55)+Rx1_THz_Mean_Amp_STD_dBm(45:55)), 'o c');

hold off;

% Display the mean of the 11 STD values
Mean_STD = std(Rx1_THz_Mean_Amp_STD_dBm(45:55));

% Convert the mean STD number to string
Mean_STD_Number = num2str(Mean_STD);

% Y label
Y_Axis_label = ...
    ['Mean Amp, Cal (dBm) - ', 'MeanSTD=', Mean_STD_Number, ' dBm'];

% Create xlabel
xlabel('Frequency (GHz)');

% Create ylabel
ylabel(Y_Axis_label);

Title = ['Atmosphere Rx1 Amplitude LWL 5 (' , num2str(THz_month), ' ', ...
        num2str(THz_day), ' ', num2str(THz_year), ' ', num2str(THz_hour), ...
        ':', num2str(THz_minute), ':', num2str(THz_second), ')'];

% Create title
title(Title);

% Legend of Standard deviations on each cyan point
legend('Good Data Mean', 'STD Mean');

box(axes1, 'on');
% Set the remaining axes properties
set(axes1, 'FontSize', 16);

%PLOT Rx1, Scan 5 with Friis and delta (LWL)
figure24 = figure('Color', [1,1,1], ...
                 'Name', 'Rx1 Scan5 Mean Amp - Friis - Delta Plot');

% Create axes
axes1 = axes('Parent', figure24);
hold(axes1, 'on');
box(axes1, 'on');

hold on

% Plot Frequency vs. Mean Amplitude in dBm
plot(Scan_LWL_Frequencies, Rx1_THz_Mean_Amp_Cal_dBm(45:55), '-o b');

```

```

% plot predicted via Friis received data on Rx1
plot(Scan_LWL_Frequencies,Pwr_rec_Rx1_139_Insertion_Loss_dBm(45:55),...
      '-x g');

% plot delta of Friis vs. received data on Rx1
plot(Scan_LWL_Frequencies, Delta_Rx1_rec_Friis(45:55), '-. r');

hold off

% Create xlabel
xlabel('Frequency (GHz)');

% Create ylabel
ylabel('Mean Amplitude, with Calibration (dBm)');

Title = ['Atmosphere Rx1 Amplitude LWL Scan 5,Friis,Delta(',...
        num2str(THz_month),...
        ' ',num2str(THz_day),' ', num2str(THz_year),', ', num2str(THz_hour),...
        ':',num2str(THz_minute),':',num2str(THz_second),')'];

% Create title
title(Title);

% creat legend
legend('Rx Data','Friis Data',' Negative Delta');

box(axes1,'on');
% Set the remaining axes properties
set(axes1,'FontSize',16);

%PLOT Rx1, Scan 5 and Friis absolutes - normalize to Friis DC (LWL)
figure25 = figure('Color',[1,1,1],...
    'Name','Rx1 Scan5 Mean Amp - Friis - DC Normalize');

% Create axes
axes1 = axes('Parent',figure25);
hold(axes1,'on');
box(axes1,'on');

hold on

% Plot Frequency vs. Mean Amplitude in dBm
plot(Scan_LWL_Frequencies,Rx1_THz_Normal_dBm(45:55), '-o b');

% plot predicted via Friis received data on Rx1
plot(Scan_LWL_Frequencies,Pwr_rec_Rx1_139_Insertion_Loss_dBm(45:55),...
      '-x g');

hold off

% Create xlabel
xlabel('Frequency (GHz)');

```

```

% Create ylabel
ylabel('Mean Amplitude, with Calibration (dBm)');

Title = ['Atmosphere Rx1 Normalized Amp LWL Scan 5,Friis (',...
        num2str(THz_month),...
        ' ',num2str(THz_day),' ', num2str(THz_year),' ', num2str(THz_hour),...
        ':',num2str(THz_minute),':',num2str(THz_second),'')'];

% Create title
title(Title);

% creat legend
legend('Rx Data','Friis Data');

box(axes1,'on');
% Set the remaining axes properties
set(axes1,'FontSize',16);

%PLOT Rx1, Scan 6 (UWL)
figure26 = figure('Color',[1,1,1],'Name','Rx1 Scan6 Mean Amp Cal Plot');

% Create axes
axes1 = axes('Parent',figure26);
hold(axes1,'on');
box(axes1,'on');

hold on;

% Plot Frequency vs. Mean Amplitude in dBm
plot(Scan_UWL_Frequencies,Rx1_THz_Mean_Amp_Cal_dBm(56:66), '-o b');

% Plot Frequency vs. STD of Mean Amplitude in dBm - cyan color
plot(Scan_UWL_Frequencies, ...
     (Rx1_THz_Mean_Amp_Cal_dBm(56:66)+Rx1_THz_Mean_Amp_STD_dBm(56:66)), 'o c');

hold off;

% Display the mean of the 11 STD values
Mean_STD = std(Rx1_THz_Mean_Amp_STD_dBm(56:66));

% Convert the mean STD number to string
Mean_STD_Number = num2str(Mean_STD);

% Y label
Y_Axis_label = ...
    ['Mean Amp,Cal (dBm) - ', 'MeanSTD=',Mean_STD_Number, ' dBm'];

% Create xlabel
xlabel('Frequency (GHz)');

```

```

% Create ylabel
ylabel(Y_Axis_label);

Title = ['Atmosphere Rx1 Amplitude UWL Scan6 (' ,num2str(THz_month), ' ',...
        num2str(THz_day), ' ', num2str(THz_year), ', ', num2str(THz_hour), ...
        ':', num2str(THz_minute), ':', num2str(THz_second), ') '];

% Create title
title(Title);

% Legend of Standard deviations on each cyan point
legend('Good Data Mean', 'STD Mean');

box(axes1, 'on');
% Set the remaining axes properties
set(axes1, 'FontSize', 16);

%PLOT Rx1, Scan 6 with Friis and delta (UWL)
figure27 = figure('Color', [1,1,1], ...
                 'Name', 'Rx1 Scan6 Mean Amp - Friis - Delta Plot');

% Create axes
axes1 = axes('Parent', figure27);
hold(axes1, 'on');
box(axes1, 'on');

hold on

% Plot Frequency vs. Mean Amplitude in dBm
plot(Scan_UWL_Frequencies, Rx1_THz_Mean_Amp_Cal_dBm(56:66), '-o b');

% plot predicted via Friis received data on Rx1
plot(Scan_UWL_Frequencies, Pwr_rec_Rx1_139_Insertion_Loss_dBm(56:66), ...
     '-x g');

% plot delta of Friis vs. received data on Rx1
plot(Scan_UWL_Frequencies, Delta_Rx1_rec_Friis(56:66), '-. r');

hold off

% Create xlabel
xlabel('Frequency (GHz)');

% Create ylabel
ylabel('Mean Amplitude, with Calibration (dBm)');
Title = ['Atmosphere Rx1 Amplitude UWL Scan
6, Friis, Delta (' ,num2str(THz_month), ...
            ' ', num2str(THz_day), ' ', num2str(THz_year), ', ', num2str(THz_hour), ...
            ':', num2str(THz_minute), ':', num2str(THz_second), ') '];

% Create title

```

```

title(Title);

% creat legend
legend('Rx Data','Friis Data',' Negative Delta');

box(axes1,'on');
% Set the remaining axes properties
set(axes1,'FontSize',16);

%PLOT Rx1, Scan 6 and Friis absolutes - normalize to Friis DC (UWL)
figure28 = figure('Color',[1,1,1],...
                 'Name','Rx1 Scan6 Mean Amp - Friis - DC Normalize');

% Create axes
axes1 = axes('Parent',figure28);
hold(axes1,'on');
box(axes1,'on');

hold on

% Plot Frequency vs. Mean Amplitude in dBm
plot(Scan_UWL_Frequencies,Rx1_THz_Normal_dBm(56:66), '-o b');

% plot predicted via Friis received data on Rx1
plot(Scan_UWL_Frequencies,Pwr_rec_Rx1_139_Insertion_Loss_dBm(56:66),...
     '-x g');

hold off

% Create xlabel
xlabel('Frequency (GHz)');

% Create ylabel
ylabel('Mean Amplitude, with Calibration (dBm)');

Title = ['Atmosphere Rx1 Normalized Amp UWL Scan 6,Friis (',...
        num2str(THz_month),...
        ' ',num2str(THz_day),' ', num2str(THz_year),' ', ' ', num2str(THz_hour),...
        ':',num2str(THz_minute),':',num2str(THz_second),')'];

% Create title
title(Title);

% create legend
legend('Rx Data','Friis Data');

box(axes1,'on');
% Set the remaining axes properties
set(axes1,'FontSize',16);

% PLOT Rx1, Foldover (flip UWL) of up and UWL plots this

```

```

% allows the LWL and UWL to be overlaid on each other to see
% differences easier

figure29 = ...
    figure('Color',[1,1,1],...
        'Name','Rx1 Foldover LWL/UWL - Friis - DC Normalize');

% Create axes
axes1 = axes('Parent',figure29);
hold(axes1,'on');
box(axes1,'on');

hold on

% Plot Frequency vs. Mean Amplitude in dBm
plot(Scan_LWL_Frequencies,Rx1_THz_Normal_dBm(12:22), '-+ c');

% Plot Frequency vs. Mean Amplitude in dBm
plot(Scan_LWL_Frequencies,Rx1_THz_Normal_dBm(45:55), '-o c');

% note folding of frequencies for plot
% Plot Frequency vs. Mean Amplitude in dBm
plot(Scan_LWL_Frequencies,flipud(Rx1_THz_Normal_dBm(23:33)), '-+ g');

% Plot Frequency vs. Mean Amplitude in dBm
plot(Scan_LWL_Frequencies,flipud(Rx1_THz_Normal_dBm(56:66)), '-o g');

% plot predicted via Friis received data on Rx1
plot(Scan_LWL_Frequencies,Pwr_rec_Rx1_139_Insertion_Loss_dBm(12:22),...
    '-+ m');
% plot predicted via Friis received data on Rx1
plot(Scan_LWL_Frequencies,Pwr_rec_Rx1_139_Insertion_Loss_dBm(45:55),...
    '-o m');
% note folding of frequencies for plot
% plot predicted via Friis received data on Rx1
plot(Scan_LWL_Frequencies,flipud...
    (Pwr_rec_Rx1_139_Insertion_Loss_dBm(23:33)), '-+ k');

% plot predicted via Friis received data on Rx1
plot(Scan_LWL_Frequencies,flipud...
    (Pwr_rec_Rx1_139_Insertion_Loss_dBm(56:66)), '-o k');

hold off

% Create xlabel
xlabel('Frequency (GHz)');

% Create ylabel
ylabel('Mean Amplitudes, with Calibration UWL Flipped (dBm)');

Title = ['Atmosphere Rx1 Normalized Amp LWL & UWL flipped (',...
    num2str(THz_month), ' ', num2str(THz_day), ' ', num2str(THz_year), ', ', ',...

```

```

    num2str(THz_hour), ':' , num2str(THz_minute), ':' , num2str(THz_second), ') '];

% Create title
title(Title);

% creat legend
legend('RxS2 LWL', 'RxS5 LWL', 'RxS3 UWL', 'RxS6 UWL', 'FriisLWL', ...
       'FriisLWL', 'FriisUWL', 'FriisUWL');

box(axes1, 'on');
% Set the remaining axes properties
set(axes1, 'FontSize', 16);

end

%% RECEIVER #2
if Rx2_disable == 0

%PLOT Rx2, Scan 1 ONLY (wideband)
figure30 = figure('Color', [1,1,1], ...
                 'Name', 'Rx2 Scan1 Mean Amp Cal Plot only');

% Create axes
axes1 = axes('Parent', figure30);
hold(axes1, 'on');
box(axes1, 'on');

hold on;

% Plot Frequency vs. Mean Amplitude in dBm
plot(Scan_WB_Frequencies, Rx2_THz_Mean_Amp_Cal_dBm(1:11), '-o b');

% Plot Frequency vs. STD of Mean Amplitude in dBm - cyan color
plot(Scan_WB_Frequencies, ...
     (Rx2_THz_Mean_Amp_Cal_dBm(1:11) + Rx2_THz_Mean_Amp_STD_dBm(1:11)), 'o c');

hold off;

% Display the mean of the 11 STD values
Mean_STD = std(Rx2_THz_Mean_Amp_STD_dBm(1:11));

% Convert the mean STD number to string
Mean_STD_Number = num2str(Mean_STD);

% Y label
Y_Axis_label = ...
    ['Mean Amp, Cal (dBm) - ', 'MeanSTD=', Mean_STD_Number, ' dBm'];

% Create xlabel
xlabel('Frequency (GHz)');

% Create ylabel

```

```

ylabel(Y_Axis_label);

Title = ['Atmosphere Rx2 Amplitude Wideband Scan 1 (',...
        num2str(THz_month),' ',...
        num2str(THz_day),' ', num2str(THz_year),' ', num2str(THz_hour),...
        ':' ,num2str(THz_minute), ':' ,num2str(THz_second), ')'];

% Create title
title(Title);

% Legend of Standard deviations on each cyan point
legend('Good Data Mean', 'STD Mean');

box(axes1, 'on');
% Set the remaining axes properties
set(axes1, 'FontSize', 16);

%PLOT Rx2, Scan 1 with Friis and delta (wideband)
figure31 = figure('Color',...
                [1,1,1], 'Name', 'Rx2 Scan1 Mean Amp - Friis - Delta Plot');

% Create axes
axes1 = axes('Parent', figure31);
hold(axes1, 'on');
box(axes1, 'on');

hold on

% Plot Frequency vs. Mean Amplitude in dBm
plot(Scan_WB_Frequencies, Rx2_THz_Mean_Amp_Cal_dBm(1:11), '-o b');

% plot predicted via Friis received data on Rx2
plot(Scan_WB_Frequencies, Pwr_rec_Rx2_138_Insertion_Loss_dBm(1:11), '-x g');

% plot delta of Friis vs. received data on Rx2
plot(Scan_WB_Frequencies, Delta_Rx2_rec_Friis(1:11), '-. r');

hold off

% Create xlabel
xlabel('Frequency (GHz)');

% Create ylabel
ylabel('Atmosphere Mean Amplitude, with Calibration (dBm)');
Title = ['Rx2 Amplitude WB1 Scan 1, Friis, Delta (' , num2str(THz_month), ...
        ' ', num2str(THz_day), ' ', num2str(THz_year), ' ', num2str(THz_hour), ...
        ':' , num2str(THz_minute), ':' , num2str(THz_second), ')'];

% Create title
title(Title);

```

```

% creat legend
legend('Rx Data','Friis Data',' Negative Delta');

box(axes1,'on');
% Set the remaining axes properties
set(axes1,'FontSize',16);

%PLOT Rx2, Scan 1 and Friis absolutes - normalize to Friis DC (wideband)
figure32 = figure('Color',[1,1,1],...
                 'Name','Rx2 Scan1 Mean Amp - Friis - DC Normalize');

% Create axes
axes1 = axes('Parent',figure32);
hold(axes1,'on');
box(axes1,'on');

hold on

% Plot Frequency vs. Mean Amplitude in dBm
plot(Scan_WB_Frequencies,Rx2_THz_Normal_dBm(1:11), '-o b');

% plot predicted via Friis received data on Rx2
plot(Scan_WB_Frequencies,Pwr_rec_Rx2_138_Insertion_Loss_dBm(1:11), '-x g');

hold off

% Create xlabel
xlabel('Frequency (GHz)');

% Create ylabel
ylabel('Mean Amplitude, with Calibration (dBm)');

Title = ['Atmosphere Rx2 Normalized Amp WB Scan 1,Friis (',...
        num2str(THz_month),...
        ' ',num2str(THz_day),' ', num2str(THz_year),' ', ' ', num2str(THz_hour),...
        ':'',num2str(THz_minute),' ':'',num2str(THz_second),' ')'];

% Create title
title(Title);

% creat legend
legend('Rx Data','Friis Data');

box(axes1,'on');
% Set the remaining axes properties
set(axes1,'FontSize',16);

%PLOT Rx2,Scan 2 Lower Wing Line(LWL)
figure33 = figure('Color',[1,1,1],...
                 'Name','Rx2 Scan2 Mean Amp Cal Plot');

```

```

% Create axes
axes1 = axes('Parent',figure33);
hold(axes1,'on');
box(axes1,'on');

hold on

% Plot Frequency vs. Mean Amplitude in dBm
plot(Scan_LWL_Frequencies,Rx2_THz_Mean_Amp_Cal_dBm(12:22), '-o b');

% Plot Frequency vs. STD of Mean Amplitude in dBm - cyan color
plot(Scan_LWL_Frequencies, ...
     (Rx2_THz_Mean_Amp_Cal_dBm(12:22)+Rx2_THz_Mean_Amp_STD_dBm(12:22)), 'o c');

hold off

% Display the mean of the 11 STD values
Mean_STD = std(Rx2_THz_Mean_Amp_STD_dBm(1:11));

% Convert the mean STD number to string
Mean_STD_Number = num2str(Mean_STD);

% Y label
Y_Axis_label = ...
    ['Mean Amp, Cal (dBm) - ', 'MeanSTD=', Mean_STD_Number, ' dBm'];

% Create xlabel
xlabel('Frequency (GHz)');

% Create ylabel
ylabel(Y_Axis_label);

Title = ['Atmosphere Rx2 Amplitude LWL Scan2  (' ,num2str(THz_month), ' ', ...
        num2str(THz_day), ' ', num2str(THz_year), ', ', num2str(THz_hour), ...
        ': ', num2str(THz_minute), ': ', num2str(THz_second), ') '];

% Create title
title(Title);

% Legend of Standard deviations on each cyan point
legend('Good Data Mean', 'STD Mean');

box(axes1,'on');
% Set the remaining axes properties
set(axes1,'FontSize',16);

%PLOT Rx2, Scan 2 with Friis and delta (LWL)
figure34 = figure('Color',...
    [1,1,1], 'Name', 'Rx2 Scan2 Mean Amp - Friis - Delta Plot');

```

```

% Create axes
axes1 = axes('Parent',figure34);
hold(axes1,'on');
box(axes1,'on');

hold on

% Plot Frequency vs. Mean Amplitude in dBm
plot(Scan_LWL_Frequencies, Rx2_THz_Mean_Amp_Cal_dBm(12:22), '-o b');

% plot predicted via Friis received data on Rx2
plot(Scan_LWL_Frequencies,Pwr_rec_Rx2_138_Insertion_Loss_dBm(12:22),...
     '-x g');

% plot delta of Friis vs. received data on Rx2
plot(Scan_LWL_Frequencies, Delta_Rx2_rec_Friis(12:22), '-. r')

hold off

% Create xlabel
xlabel('Frequency (GHz)');

% Create ylabel
ylabel('Mean Amplitude, with Calibration (dBm)');

Title = ['Atmosphere Rx2 Amplitude LWL Scan 2, Friis, Delta(',...
        num2str(THz_month),...
        ' ',num2str(THz_day),' ', num2str(THz_year),', ', num2str(THz_hour),...
        ':',num2str(THz_minute),':',num2str(THz_second),')'];

% Create title
title(Title);

% creat legend
legend('Rx Data','Friis Data',' Negative Delta');

box(axes1,'on');
% Set the remaining axes properties
set(axes1,'FontSize',16);

% PLOT Rx2, Scan 2 and Friis absolutes - normalize to Friis DC (LWL)
figure35 = figure('Color',[1,1,1],...
                 'Name','Rx2 Scan2 Mean Amp - Friis - DC Normalize');

% Create axes
axes1 = axes('Parent',figure35);
hold(axes1,'on');
box(axes1,'on');

hold on

```

```

% Plot Frequency vs. Mean Amplitude in dBm
plot(Scan_LWL_Frequencies,Rx2_THz_Normal_dBm(12:22), '-o b');

% plot predicted via Friis received data on Rx2
plot(Scan_LWL_Frequencies,Pwr_rec_Rx2_138_Insertion_Loss_dBm(12:22),...
      '-x g');
hold off

% Create xlabel
xlabel('Frequency (GHz)');

% Create ylabel
ylabel('Mean Amplitude, with Calibration (dBm)');

Title = ['Atmosphere Rx2 Normalized Amp LWL Scan 2, Friis (',...
        num2str(THz_month),...
        ' ',num2str(THz_day),' ', num2str(THz_year),' ', ' ', num2str(THz_hour),...
        ':',num2str(THz_minute),'::',num2str(THz_second),')'];

% Create title
title(Title);

% creat legend
legend('Rx Data','Friis Data');

box(axes1,'on');
% Set the remaining axes properties
set(axes1,'FontSize',16);

%PLOT Rx2, Scan 3 Upper Wing Line (UWL)
figure36 = figure('Color',[1,1,1],...
                  'Name','Rx2 Scan2 Mean Amp Cal Plot');

% Create axes
axes1 = axes('Parent',figure36);
hold(axes1,'on');
box(axes1,'on');

hold on;

% Plot Frequency vs. Mean Amplitude in dBm
plot(Scan_UWL_Frequencies,Rx2_THz_Mean_Amp_Cal_dBm(23:33), '-o b');

% Plot Frequency vs. STD of Mean Amplitude in dBm - cyan color
plot(Scan_UWL_Frequencies, ...
      (Rx2_THz_Mean_Amp_Cal_dBm(23:33)+Rx2_THz_Mean_Amp_STD_dBm(23:33)), 'o c');

hold off;

% Display the mean of the 11 STD values
Mean_STD = std(Rx2_THz_Mean_Amp_STD_dBm(23:33));

```

```

% Convert the mean STD number to string
Mean_STD_Number = num2str(Mean_STD);

% Y label
Y_Axis_label = ...
    ['Mean Amp, Cal (dBm) - ', 'MeanSTD=', Mean_STD_Number, ' dBm'];

% Create xlabel
xlabel('Frequency (GHz)');

% Create ylabel
ylabel(Y_Axis_label);

Title = ['Atmosphere Rx2 Amplitude UWL 3 (' , num2str(THz_month), ' ', ...
    num2str(THz_day), ' ', num2str(THz_year), ', ', num2str(THz_hour), ...
    ': ', num2str(THz_minute), ': ', num2str(THz_second), ') '];

% Create title
title(Title);

% Legend of Standard deviations on each cyan point
legend('Good Data Mean', 'STD Mean');

box(axes1, 'on');
% Set the remaining axes properties
set(axes1, 'FontSize', 16);

%PLOT Rx2, Scan 3 with Friis and delta (UWL)
figure37 = figure('Color', [1,1,1], ...
    'Name', 'Rx2 Scan3 Mean Amp - Friis - Delta Plot');

% Create axes
axes1 = axes('Parent', figure37);
hold(axes1, 'on');
box(axes1, 'on');

hold on

% Plot Frequency vs. Mean Amplitude in dBm
plot(Scan_UWL_Frequencies, Rx2_THz_Mean_Amp_Cal_dBm(23:33), '-o b');

% plot predicted via Friis received data on Rx2
plot(Scan_UWL_Frequencies, Pwr_rec_Rx2_138_Insertion_Loss_dBm(23:33), ...
    '-x g');

% plot delta of Friis vs. received data on Rx2
plot(Scan_UWL_Frequencies, Delta_Rx2_rec_Friis(23:33), '-. r');

hold off

% Create xlabel

```

```

xlabel('Frequency (GHz)');

% Create ylabel
ylabel('Mean Amplitude, with Calibration (dBm)');

Title = ['Atmosphere Rx2 Amplitude UWL Scan 3, Friis, Delta(',...
        num2str(THz_month),...
        ' ',num2str(THz_day), ' ', num2str(THz_year), ', ', num2str(THz_hour),...
        ':',num2str(THz_minute), ':',num2str(THz_second), ')'];

% Create title
title(Title);

% creat legend
legend('Rx Data','Friis Data',' Negative Delta');

box(axes1,'on');
% Set the remaining axes properties
set(axes1,'FontSize',16);

%PLOT Rx2, Scan 3 and Friis absolutes - normalize to Friis DC (UWL)
figure38 = figure('Color',[1,1,1],...
                 'Name','Rx2 Scan3 Mean Amp - Friis - DC Normalize');

% Create axes
axes1 = axes('Parent',figure38);
hold(axes1,'on');
box(axes1,'on');

hold on

% Plot Frequency vs. Mean Amplitude in dBm
plot(Scan_UWL_Frequencies,Rx2_THz_Normal_dBm(23:33), '-o b');

% plot predicted via Friis received data on Rx2
plot(Scan_UWL_Frequencies,Pwr_rec_Rx2_138_Insertion_Loss_dBm(23:33),...
     '-x g');

hold off

% Create xlabel
xlabel('Frequency (GHz)');

% Create ylabel
ylabel('Mean Amplitude, with Calibration (dBm)');

Title = ['Atmosphere Rx2 Normalized Amp UWL Scan 3, Friis (',...
        num2str(THz_month),...
        ' ',num2str(THz_day), ' ', num2str(THz_year), ', ', num2str(THz_hour),...
        ':',num2str(THz_minute), ':',num2str(THz_second), ')'];

% Create title

```

```

title(Title);

% create legend
legend('Rx Data','Friis Data');

box(axes1,'on');
% Set the remaining axes properties
set(axes1,'FontSize',16);

%PLOT Rx2, Scan 4 (wideband)
figure39 = figure('Color',[1,1,1],'Name','Rx2 Scan4 Mean Amp Cal Plot');

% Create axes
axes1 = axes('Parent',figure39);
hold(axes1,'on');
box(axes1,'on');

hold on;

% Plot Frequency vs. Mean Amplitude in dBm
plot(Scan_WB_Frequencies,Rx2_THz_Mean_Amp_Cal_dBm(34:44), '-o b');

% Plot Frequency vs. STD of Mean Amplitude in dBm - cyan color
plot(Scan_WB_Frequencies, ...
     (Rx2_THz_Mean_Amp_Cal_dBm(34:44)+Rx2_THz_Mean_Amp_STD_dBm(34:44)), 'o c');

hold off;

% Display the mean of the 11 STD values
Mean_STD = std(Rx2_THz_Mean_Amp_STD_dBm(34:44));

% Convert the mean STD number to string
Mean_STD_Number = num2str(Mean_STD);

% Y label
Y_Axis_label = ...
    ['Mean Amp, Cal (dBm) - ', 'MeanSTD=', Mean_STD_Number, ' dBm'];

% Create xlabel
xlabel('Frequency (GHz)');

% Create ylabel
ylabel(Y_Axis_label);

Title = ['Atmosphere Rx2 Amplitude Wideband Scan 4 (',...
        num2str(THz_month), ' ', ...
        num2str(THz_day), ' ', num2str(THz_year), ' ', num2str(THz_hour), ...
        ':', num2str(THz_minute), ':', num2str(THz_second), ')'];

% Create title
title(Title);

```

```

% Legend of Standard deviations on each cyan point
legend('Good Data Mean','STD Mean');

box(axes1,'on');
% Set the remaining axes properties
set(axes1,'FontSize',16);

%PLOT Rx2, Scan 4 with Friis and delta (wideband)
figure40 = figure('Color',[1,1,1],...
    'Name','Rx2 Scan4 Mean Amp - Friis - Delta Plot');

% Create axes
axes1 = axes('Parent',figure40);
hold(axes1,'on');
box(axes1,'on');

hold on

% Plot Frequency vs. Mean Amplitude in dBm
plot(Scan_WB_Frequencies, Rx2_THz_Mean_Amp_Cal_dBm(34:44), '-o b');

% plot predicted via Friis received data on Rx2
plot(Scan_WB_Frequencies,Pwr_rec_Rx2_138_Insertion_Loss_dBm(34:44),'-x g');

% plot delta of Friis vs. received data on Rx2
plot(Scan_WB_Frequencies, Delta_Rx2_rec_Friis(34:44), '-. r');

hold off

% Create xlabel
xlabel('Frequency (GHz)');

% Create ylabel
ylabel('Mean Amplitude, with Calibration (dBm)');

Title = ['Atmosphere Rx2 Amplitude WB Scan 4, Friis, Delta (',...
    num2str(THz_month),...
    ' ',num2str(THz_day),' ', num2str(THz_year),' ', num2str(THz_hour),...
    ':' ,num2str(THz_minute), ':' ,num2str(THz_second),')'];

% Create title
title(Title);

% creat legend
legend('Rx Data','Friis Data',' Negative Delta');

box(axes1,'on');
% Set the remaining axes properties
set(axes1,'FontSize',16);

```

```

%PLOT Rx2, Scan 4 and Friis absolutes - normalize to Friis DC (wb)
figure41 = figure('Color',[1,1,1],...
                 'Name','Rx2 Scan4 Mean Amp - Friis - DC Normalize');

% Create axes
axes1 = axes('Parent',figure41);
hold(axes1,'on');
box(axes1,'on');

hold on

% Plot Frequency vs. Mean Amplitude in dBm
plot(Scan_WB_Frequencies,Rx2_THz_Normal_dBm(34:44), '-o b');

% plot predicted via Friis received data on Rx2
plot(Scan_WB_Frequencies,Pwr_rec_Rx2_138_Insertion_Loss_dBm(34:44),'-x g');

hold off

% Create xlabel
xlabel('Frequency (GHz)');

% Create ylabel
ylabel('Mean Amplitude, with Calibration (dBm)');

Title = ['Atmosphere Rx2 Normalized Amp WB Scan 4, Friis (',...
        num2str(THz_month),...
        ' ',num2str(THz_day),' ', num2str(THz_year),' ', num2str(THz_hour),...
        ':' ,num2str(THz_minute), ':' ,num2str(THz_second),')'];

% Create title
title(Title);

% creat legend
legend('Rx Data','Friis Data');

box(axes1,'on');
% Set the remaining axes properties
set(axes1,'FontSize',16);

%PLOT Rx2, Scan 5 Lower Wing Line(LWL)
figure42 = figure('Color',[1,1,1],'Name','Rx2 Scan5 Mean Amp Cal Plot');

% Create axes
axes1 = axes('Parent',figure42);
hold(axes1,'on');
box(axes1,'on');

hold on;

```

```

% Plot Frequency vs. Mean Amplitude in dBm
plot(Scan_LWL_Frequencies,Rx2_THz_Mean_Amp_Cal_dBm(45:55), '-o b');

% Plot Frequency vs. STD of Mean Amplitude in dBm - cyan color
plot(Scan_LWL_Frequencies, ...
     (Rx2_THz_Mean_Amp_Cal_dBm(45:55)+Rx2_THz_Mean_Amp_STD_dBm(45:55)), 'o c');

hold off;

% Display the mean of the 11 STD values
Mean_STD = std(Rx2_THz_Mean_Amp_STD_dBm(45:55));

% Convert the mean STD number to string
Mean_STD_Number = num2str(Mean_STD);

% Y label
Y_Axis_label = ...
    ['Mean Amp, Cal (dBm) - ', 'MeanSTD=', Mean_STD_Number, ' dBm'];

% Create xlabel
xlabel('Frequency (GHz)');

% Create ylabel
ylabel(Y_Axis_label);

Title = ['Atmosphere Rx2 Amplitude LWL Scan 5 (',...
        num2str(THz_month), ' ', ...
        num2str(THz_day), ' ', num2str(THz_year), ', ', num2str(THz_hour), ...
        ': ', num2str(THz_minute), ': ', num2str(THz_second), ')'];

% Create title
title(Title);

% Legend of Standard deviations on each cyan point
legend('Good Data Mean', 'STD Mean');

box(axes1, 'on');
% Set the remaining axes properties
set(axes1, 'FontSize', 16);

%PLOT Rx2, Scan 5 with Friis and delta (LWL)
figure43 = figure('Color', [1,1,1], ...
                 'Name', 'Rx2 Scan5 Mean Amp - Friis - Delta Plot');

% Create axes
axes1 = axes('Parent', figure43);
hold(axes1, 'on');
box(axes1, 'on');

hold on

```

```

% Plot Frequency vs. Mean Amplitude in dBm
plot(Scan_LWL_Frequencies, Rx2_THz_Mean_Amp_Cal_dBm(45:55), '-o b');

% plot predicted via Friis received data on Rx2
plot(Scan_LWL_Frequencies, Pwr_rec_Rx2_138_Insertion_Loss_dBm(45:55), ...
     '-x g');

% plot delta of Friis vs. received data on Rx2

hold off

% Create xlabel
xlabel('Frequency (GHz)');

% Create ylabel
ylabel('Mean Amplitude, with Calibration (dBm)');

Title = ['Atmosphere Rx2 Amplitude LWL Scan 5, Friis, Delta(', ...
        num2str(THz_month), ...
        ' ', num2str(THz_day), ' ', num2str(THz_year), ', ', num2str(THz_hour), ...
        ':', num2str(THz_minute), ':', num2str(THz_second), ')'];

% Create title
title(Title);

% creat legend
legend('Rx Data', 'Friis Data', ' Negative Delta');

box(axes1, 'on');
% Set the remaining axes properties
set(axes1, 'FontSize', 16);

%PLOT Rx2, Scan 5 and Friis absolutes - normalize to Friis DC (LWL)
figure44 = figure('Color', [1,1,1], ...
    'Name', 'Rx2 Scan5 Mean Amp - Friis - DC Normalize');

% Create axes
axes1 = axes('Parent', figure44);
hold(axes1, 'on');
box(axes1, 'on');

hold on
% Plot Frequency vs. Mean Amplitude in dBm
plot(Scan_LWL_Frequencies, Rx2_THz_Normal_dBm(45:55), '-o b');

% plot predicted via Friis received data on Rx2
plot(Scan_LWL_Frequencies, Pwr_rec_Rx2_138_Insertion_Loss_dBm(45:55), ...
     '-x g');

hold off

% Create xlabel
xlabel('Frequency (GHz)');

```

```

% Create ylabel
ylabel('Mean Amplitude, with Calibration (dBm)');

Title = ['Atmosphere Rx2 Normalized Amp LWL Scan 5,Friis (',...
        num2str(THz_month),...
        ' ',num2str(THz_day),' ', num2str(THz_year),' ', num2str(THz_hour),...
        ':',num2str(THz_minute),':',num2str(THz_second),')'];

% Create title
title(Title);

% creat legend
legend('Rx Data','Friis Data');

box(axes1,'on');
% Set the remaining axes properties
set(axes1,'FontSize',16);

%PLOT Rx2, Scan 6 Upper Wing Line(UWL)
figure45 = figure('Color',[1,1,1],'Name','Rx2 Scan6 Mean Amp Cal Plot');

% Create axes
axes1 = axes('Parent',figure45);
hold(axes1,'on');
box(axes1,'on');

hold on;

% Plot Frequency vs. Mean Amplitude in dBm
plot(Scan_UWL_Frequencies,Rx2_THz_Mean_Amp_Cal_dBm(56:66), '-o b');

% Plot Frequency vs. STD of Mean Amplitude in dBm - cyan color
plot(Scan_UWL_Frequencies, ...
     (Rx2_THz_Mean_Amp_Cal_dBm(56:66)+Rx2_THz_Mean_Amp_STD_dBm(56:66)), 'o c');

hold off;

% Display the mean of the 11 STD values
Mean_STD = std(Rx2_THz_Mean_Amp_STD_dBm(56:66));

% Convert the mean STD number to string
Mean_STD_Number = num2str(Mean_STD);

% Y label
Y_Axis_label = ...
    ['Mean Amp,Cal (dBm) - ', 'MeanSTD=',Mean_STD_Number, ' dBm'];

% Create xlabel
xlabel('Frequency (GHz)');

```

```

% Create ylabel
ylabel(Y_Axis_label);

Title = ['Atmosphere Rx2 Amplitude UWL Scan 6 (',...
        num2str(THz_month), ' ',...
        num2str(THz_day), ' ', num2str(THz_year), ', ', ' ', num2str(THz_hour),...
        ':', num2str(THz_minute), ':', num2str(THz_second), ')'];

% Create title
title(Title);

% Legend of Standard deviations on each cyan point
legend('Good Data Mean', 'STD Mean');

box(axes1, 'on');
% Set the remaining axes properties
set(axes1, 'FontSize', 16);

%PLOT Rx2, Scan 6 with Friis and delta (UWL)
figure46 = figure('Color', [1,1,1],...
                 'Name', 'Rx2 Scan6 Mean Amp - Friis - Delta Plot');

% Create axes
axes1 = axes('Parent', figure46);
hold(axes1, 'on');
box(axes1, 'on');

hold on

% Plot Frequency vs. Mean Amplitude in dBm
plot(Scan_UWL_Frequencies, Rx2_THz_Mean_Amp_Cal_dBm(56:66), '-o b');

% plot predicted via Friis received data on Rx2
plot(Scan_UWL_Frequencies, Pwr_rec_Rx2_138_Insertion_Loss_dBm(56:66),...
     '-x g');

% plot delta of Friis vs. received data on Rx2
plot(Scan_UWL_Frequencies, Delta_Rx2_rec_Friis(56:66), '-. r');

hold off

% Create xlabel
xlabel('Frequency (GHz)');

% Create ylabel
ylabel('Mean Amplitude, with Calibration (dBm)');

Title = ['Atmosphere Rx2 Amplitude UWL Scan 6, Friis, Delta(',...
        num2str(THz_month),...
        ' ', num2str(THz_day), ' ', num2str(THz_year), ', ', ' ', num2str(THz_hour),...
        ':', num2str(THz_minute), ':', num2str(THz_second), ')'];

```

```

% Create title
title(Title);

% creat legend
legend('Rx Data', 'Friis Data', ' Negative Delta');

box(axes1, 'on');
% Set the remaining axes properties
set(axes1, 'FontSize', 16);

%PLOT Rx2, Scan 6 and Friis absolutes - normalize to Friis DC (UWL)
figure47 = figure('Color', [1,1,1], ...
    'Name', 'Rx2 Scan6 Mean Amp - Friis - DC Normalize');

% Create axes
axes1 = axes('Parent', figure47);
hold(axes1, 'on');
box(axes1, 'on');

hold on

% Plot Frequency vs. Mean Amplitude in dBm
plot(Scan_UWL_Frequencies, Rx2_THz_Normal_dBm(56:66), '-o b');

% plot predicted via Friis received data on Rx2
plot(Scan_UWL_Frequencies, Pwr_rec_Rx2_138_Insertion_Loss_dBm(56:66), ...
    '-x g');

hold off

% Create xlabel
xlabel('Frequency (GHz)');

% Create ylabel
ylabel('Mean Amplitude, with Calibration (dBm)');

Title = ['Rx2 Normalized Amp UWL Scan 6, Friis (' , num2str(THz_month), ...
    ' ', num2str(THz_day), ' ', num2str(THz_year), ' ', num2str(THz_hour), ...
    ':', num2str(THz_minute), ':', num2str(THz_second), ') '];

% Create title
title(Title);

% create legend
legend('Rx Data', 'Friis Data');

box(axes1, 'on');
% Set the remaining axes properties
set(axes1, 'FontSize', 16);

% PLOT Rx2, Foldover (flip UWL) of up and UWL plots this
% allows the LWL and UWL to be overlaid on each other to see

```

```

% differences easier

figure48 = ...
    figure('Color',[1,1,1],...
          'Name','Rx2 Foldover LWL/UWL - Friis - DC Normalize');

% Create axes
axes1 = axes('Parent',figure48);
hold(axes1,'on');
box(axes1,'on');

hold on
% Plot Frequency vs. Mean Amplitude in dBm
plot(Scan_LWL_Frequencies,Rx2_THz_Normal_dBm(12:22), '-+ c');

% Plot Frequency vs. Mean Amplitude in dBm
plot(Scan_LWL_Frequencies,Rx2_THz_Normal_dBm(45:55), '-o c');

% note folding of frequencies for plot
% Plot Frequency vs. Mean Amplitude in dBm
plot(Scan_LWL_Frequencies,flipud(Rx2_THz_Normal_dBm(23:33)), '-+ g');

% Plot Frequency vs. Mean Amplitude in dBm
plot(Scan_LWL_Frequencies,flipud(Rx2_THz_Normal_dBm(56:66)), '-o g');

% plot predicted via Friis received data on Rx2
plot(Scan_LWL_Frequencies,Pwr_rec_Rx2_138_Insertion_Loss_dBm(12:22),...
     '-+ m');
% plot predicted via Friis received data on Rx2
plot(Scan_LWL_Frequencies,Pwr_rec_Rx2_138_Insertion_Loss_dBm(45:55),...
     '-o m');

% note folding of frequencies for plot
% plot predicted via Friis received data on Rx2
plot(Scan_LWL_Frequencies,flipud...
     (Pwr_rec_Rx1_139_Insertion_Loss_dBm(23:33)), '-+ k');

% plot predicted via Friis received data on Rx2
plot(Scan_LWL_Frequencies,flipud...
     (Pwr_rec_Rx1_139_Insertion_Loss_dBm(56:66)), '-o k');

hold off

% Create xlabel
xlabel('Frequency (GHz)');

% Create ylabel
ylabel('Mean Amplitudes, with Calibration UWL flipped (dBm)');

Title = ['Atmosphere Rx2 Normalized Amp LWL & UWL Flipped (',...
        num2str(THz_month), ' ', num2str(THz_day), ' ', num2str(THz_year), ', ', ',...
        num2str(THz_hour), ':', num2str(THz_minute), ':', num2str(THz_second), ')'];

```

```

% Create title
title(Title);

% creat legend
legend('RxS2-LWL','RxS5-LWL','RxS3-UWL','RxS6-UWL','FriisLWL',...
       'FriisLWL','FriisUWL','FriisUWL');

box(axes1,'on');
% Set the remaining axes properties
set(axes1,'FontSize',16);

end % end of if statement to disable Rx2

#####

%% ##### Propagation Loss #####
% PLOT ABSORPTION / SCATTERING LOSS = Extinction and propagation loss

% Calculate real absorption.
% note calibrations have occurred, so
% Tx POWER is uniform after adjustments WB=12.4 dBm, LWL = 13.5
% dBm, UWL = 13.53 dBm
% calculate the power at the horn output on Tx
Pwr_at_Horn_output_dBm = ...
    [12.4;12.4;12.4;12.4;12.4;12.4;12.4;12.4;12.4;12.4;12.4;...
     13.5;13.5;13.5;13.5;13.5;13.5;13.5;13.5;13.5;13.5;13.5;...
     13.53;13.53;13.53;13.53;13.53;13.53;13.53;13.53;13.53;13.53;13.53];

% make this for two scans = total of 66
Total_Pwr_at_Horn_output_dBm = ...
    [Pwr_at_Horn_output_dBm;Pwr_at_Horn_output_dBm];

% Calculate the total power absorption in the atmosphere
Total_Pwr_absorption_Rx1_dBm = ...
    -1.*(Total_Pwr_at_Horn_output_dBm + Rx1_THz_Mean_Amp_Cal_dBm');

Total_Pwr_absorption_Rx2_dBm = ...
    -1.*(Total_Pwr_at_Horn_output_dBm + Rx2_THz_Mean_Amp_Cal_dBm');

% cacluate the total power absorption in the Friis
Power_received_Horn_output66_dBm = ...
    [Power_received_Horn_output33_dBm;Power_received_Horn_output33_dBm];

Total_Friis_Pwr_absorption_dBm = ...
    -1.*(Total_Pwr_at_Horn_output_dBm + Power_received_Horn_output66_dBm);

% Calculate extinction / km - note mostly due to absorption
Rx1_Pwr_absorption_dbperkm = ...
    Total_Pwr_absorption_Rx1_dBm ./ (Path_Length_m /1000);
Rx2_Pwr_absorption_dbperkm = ...
    Total_Pwr_absorption_Rx2_dBm ./ (Path_Length_m /1000);

```

```

Friis_Pwr_absorption_dbperkm = ...
    Total_Friis_Pwr_absorption_dBm ./ (Path_Length_m /1000);

% Plot Extinction data from both receivers and predicted for all scans
% of 6 scans

%PLOT Rx1&2, Scans 1 & 4 and predicted (wideband)
figure57 = figure('Color',[1,1,1],'Name',...
    'Absorption Plot Widband Scans and Friis');

% Create axes
axes1 = axes('Parent',figure57);
hold(axes1,'on');
box(axes1,'on');

hold on
% Plot Frequency vs. Absorption in dBm/km
plot(Scan_WB_Frequencies, Rx1_Pwr_absorption_dbperkm(1:11), '-o b')

plot(Scan_WB_Frequencies, Rx2_Pwr_absorption_dbperkm(1:11), '-x g')

plot(Scan_WB_Frequencies, Rx1_Pwr_absorption_dbperkm(34:44), '-+ c')

plot(Scan_WB_Frequencies, Rx2_Pwr_absorption_dbperkm(34:44), '-* m')

plot(Scan_WB_Frequencies, Friis_Pwr_absorption_dbperkm(1:11), '-d r')

hold off

% Create xlabel
xlabel('Frequency (GHz)');

% Create ylabel
ylabel('Absorption/Extinction (dB/km)');

Title = ['Atmosphere Absorption Plot Widband Scans and Friis (',...
    num2str(THz_month),' ',num2str(THz_day),' ', num2str(THz_year),' ',',...
    num2str(THz_hour),':',num2str(THz_minute),':',num2str(THz_second),')'];

% Create title
title(Title);

% create Legend
legend('Rx1-Scan1','Rx2-Scan1','Rx1-Scan4','Rx2-Scan4','Friss-RH20');

box(axes1,'on');
% Set the remaining axes properties
set(axes1,'FontSize',16);

```

```

%PLOT Rx1&2, Scans 2 & 5 and predicted (LWL)
figure58 = figure('Color',[1,1,1],...
                 'Name','Absorption Plot LWL Scans and Friis');

% Create axes
axes1 = axes('Parent',figure58);
hold(axes1,'on');
box(axes1,'on');

hold on

% Plot Frequency vs. Absorption in dBm/km
plot(Scan_LWL_Frequencies, Rx1_Pwr_absorption_dbperkm(12:22), '-o b')

plot(Scan_LWL_Frequencies, Rx2_Pwr_absorption_dbperkm(12:22), '-x g')

plot(Scan_LWL_Frequencies, Rx1_Pwr_absorption_dbperkm(45:55), '-+ c')

plot(Scan_LWL_Frequencies, Rx2_Pwr_absorption_dbperkm(45:55), '-* m')

plot(Scan_LWL_Frequencies, Friis_Pwr_absorption_dbperkm(12:22),'-d r')

hold off

% Create xlabel
xlabel('Frequency (GHz)')

% Create ylabel
ylabel('Absorption/Extinction (dB/km)')

Title = ['Absorption Plot LWL Scans and Friis (' , ...
        num2str(THz_month), ' ', num2str(THz_day), ' ', num2str(THz_year), ' ', ' ', ...
        num2str(THz_hour), ':', num2str(THz_minute), ':', num2str(THz_second), ')'];

% Create title
title(Title);

% create Legend
legend('Rx1-Scan2', 'Rx2-Scan2', 'Rx1-Scan5', 'Rx2-Scan5', 'Friis');

box(axes1,'on');
% Set the remaining axes properties
set(axes1,'FontSize',16);

%PLOT Rx1&2, Scans 3 & 6 and predicted (UWL)
figure59 = figure('Color',[1,1,1],...
                 'Name','Absorption Plot UWL Scans and Friis');

% Create axes

```

```

axes1 = axes('Parent',figure59);
hold(axes1,'on');
box(axes1,'on');

hold on

% Plot Frequency vs. Absorption in dBm/km
plot(Scan_UWL_Frequencies, Rx1_Pwr_absorption_dbperkm(23:33), '-o b')

plot(Scan_UWL_Frequencies, Rx2_Pwr_absorption_dbperkm(23:33), '-x g')

plot(Scan_UWL_Frequencies, Rx1_Pwr_absorption_dbperkm(56:66), '-+ c')

plot(Scan_UWL_Frequencies, Rx2_Pwr_absorption_dbperkm(56:66), '-* m')

plot(Scan_UWL_Frequencies, Friis_Pwr_absorption_dbperkm(23:33),'-d r')

hold off

% Create xlabel
xlabel('Frequency (GHz)')

% Create ylabel
ylabel('Absorption/Extinction (dB/km)')

Title = ['Absorption Plot UWL Scans and Friis (' , ...
        num2str(THz_month), ' ', num2str(THz_day), ' ', num2str(THz_year), ' ', ' , ...
        num2str(THz_hour), ':', num2str(THz_minute), ':', num2str(THz_second), ') '];

% Create title
title(Title);

% create Legend
legend('Rx1-Scan3', 'Rx2-Scan3', 'Rx1-Scan6', 'Rx2-Scan6', 'Friis');

box(axes1,'on');
% Set the remaining axes properties
set(axes1,'FontSize',16);

%%

% Plot the flip of the UWL so it overlays on the LWW
% PLOT Rx, Foldover (flip UWL) of LWL/UWL plots this
% allows the LWL/UWL to be overlaid on each other to see
% differences easier

%PLOT Rx1&2, Scans 2 & 5 and predicted (LWL/UWL)
figure60 = figure('Color',[1,1,1],'Name',...
        'Absorption Plot LWL flip UWL Scans and Friis');

% Create axes
axes1 = axes('Parent',figure60);

```

```

hold(axes1, 'on');
box(axes1, 'on');

hold on

% Plot Frequency vs. Absorption in dBm/km
plot(Scan_LWL_Frequencies, Rx1_Pwr_absorption_dbperkm(12:22), '-o b')

plot(Scan_LWL_Frequencies, Rx2_Pwr_absorption_dbperkm(12:22), '-x g')

plot(Scan_LWL_Frequencies, Rx1_Pwr_absorption_dbperkm(45:55), '-+ b')

plot(Scan_LWL_Frequencies, Rx2_Pwr_absorption_dbperkm(45:55), '-x g')

plot(Scan_LWL_Frequencies, Friis_Pwr_absorption_dbperkm(12:22), '-d r')

plot(Scan_LWL_Frequencies, flipud(Rx1_Pwr_absorption_dbperkm(23:33)), ...
                                           '-o c')

plot(Scan_LWL_Frequencies, flipud(Rx2_Pwr_absorption_dbperkm(23:33)), ...
                                           '-x m')

plot(Scan_LWL_Frequencies, flipud(Rx1_Pwr_absorption_dbperkm(56:66)), ...
                                           '-o c')

plot(Scan_LWL_Frequencies, flipud(Rx2_Pwr_absorption_dbperkm(56:66)), ...
                                           '-x m')

hold off

% Create xlabel
xlabel('Frequency (GHz)')

% Create ylabel
ylabel('Absorption/Extinction with UWL flipped (dB/km)')

Title = ['Absorption Plot LWL/flipped UWL Scans and Friis(', ...
        num2str(THz_month), ', ', num2str(THz_day), ', ', num2str(THz_year), ', ', ...
        num2str(THz_hour), ': ', num2str(THz_minute), ': ', num2str(THz_second), ')'];

% Create title
title(Title);

% create Legend
legend('Rx1S2', 'Rx2-S2', 'Rx1S', 'Rx2S5', 'Friis', 'Rx1S3', 'Rx2-S3', ...
      'Rx1S6', 'Rx2S6');

box(axes1, 'on');
% Set the remaining axes properties
set(axes1, 'FontSize', 16);

```

```
%%#####
```

```
% Plot Extinction vs. Humidity- need to implement this over many different  
% humidity conditions for each frequency - this is a standard plot
```